RADIO COMMUNICATION SERIES

DISCARDED

DISCARDED

DISCARDED

RADIO COMMUNICATION SERIES

BEVERLY DUDLEY, CONSULTING EDITOR

SHORT-WAVE RADIATION PHENOMENA

RADIO COMMUNICATION SERIES

BEVERLY DUDLEY, Consulting Editor

Bond—RADIO DIRECTION FINDERS

Bronwell and Beam—THEORY AND APPLICATION OF MICROWAVES

Frank—PULSED LINEAR NETWORKS

Goldman—FREQUENCY ANALYSIS, MODULATION AND NOISE

Hund—FREQUENCY MODULATION

Hund—SHORT-WAVE RADIATION PHENOMENA

King—ELECTROMAGNETIC ENGINEERING

I. FUNDAMENTALS

Moreno—MICROWAVE TRANSMISSION DESIGN DATA

Preisman—GRAPHICAL CONSTRUCTIONS FOR VACUUM TUBE CIRCUITS

Selgin—ELECTRICAL TRANSMISSION IN STEADY STATE

SHORT-WAVE RADIATION PHENOMENA

by

AUGUST HUND
Scientific and Technical Radio Consultant,
Fellow of the Institute of Radio Engineers

VOLUME II
FIRST EDITION

McGRAW-HILL BOOK COMPANY, INC.
New York Toronto London
1952

SHORT-WAVE RADIATION PHENOMENA

Copyright, 1952, by the McGraw-Hill Book Company, Inc. Printed in the United States of America. All rights reserved. This book, or parts thereof, may not be reproduced in any form without permission of the publishers.

Library of Congress Catalog Card Number: 51-12619

THE MAPLE PRESS COMPANY, YORK, PA.

University of Southern California

CONTENTS FOR VOLUME II

CHAPTER VII. SPACE RADIATION IN THE PRESENCE OF ELECTROMAGNETIC OBSTRUCTIONS 789

Application of the Optical Fresnel Relations on Reflection and Refraction of Electromagnetic Waves—Remarks on the Phase Factor of an Electromagnetic Wave Refracted into a General Medium—The Pseudo Brewster Angle of a Wave Medium with Dissipation—Magnitude of the Brewster Angle of Incidence and Actual Values of the Coefficient of Reflection for Vertically and Horizontally Polarized Electromagnetic Waves—Magnitude of the Generalized Index of Refraction of a Medium—Magnitude and Phase of the Complex Coefficient of Reflection for Vertical and Horizontal Polarization—Reflection and Time Phase Characteristics of an Electromagnetic Ray Reflected from a Plane Surface of the General Medium—Useful Concepts for Reflections on a Generalized Medium and Significance of the Pseudo Brewster Angle Effect—Remarks on the Reflection Coefficient for Vertical Polarization of the General Medium and Curves for the Pseudo Brewster Angle and the Brewster Dip—Vertical Field Pattern of a Linear Radiator Standing Normal to a Metal Plane—Relations for the Ray Theory of Wave Reception over Actual Ground—Comparison of Horizontally Polarized Waves with Vertically Polarized Waves over Flat Ground—Effect of the Height of the Mid-point of a Linear Antenna over Actual Ground for Different Angles of Wave Incidence and General Polarization—Notes on Wave Spread for Plane and Curved Earth—Effects of Multiple Reflections from Ground on the Space Field—Wave Reflections on Metal Plates and Planes of the General Medium—Remarks on Actual Electromagnetic Wave Conditions on Either Side of the Earth Surface (for Vertical Polarization)—Radiation Patterns over Perfect and Actual Ground—Effect of Radiator and Receiver Antenna Location with Respect to the Actual Ground on the Received Electromagnetic Field—Numerical Data of the Effect of the Transmitter Antenna Location on the Resultant Space Field for Comparatively Short Ranges—Numerical Examples of the Resultant Space Field for Large Angles of Wave Incidence—Numerical Data on Vertical Radiation Patterns over Actual Ground—Possibility of Stratum Waves in the Lower Atmosphere and Separation of Stratum, or "Close-to-ground," Waves from Space Waves—Wave-guide Action in the Dielectric Space between Boundary Planes—The Dielectric Constant of the Troposphere—The Foundations of the Classic Clausius-Mossoti Relation and of the Lorentz-Lorenz Law for Molar Refraction—Physical Properties of the Atmospheric Index of Refraction—Remarks on the Dielectric Constant and the Index of Refraction of the Ionosphere—General Remarks on the Effect of the Refractive Index Variations in the Troposphere on Radiation Beams—Remarks on the Path of an Electro-

magnetic Wave in the Lower Atmosphere—Possible Gradients and Interpretations of Curved Paths and Concept of the Equivalent Earth Radius—Modified Electromagnetic Wave Paths for an Equivalent Flat Earth and for Oblique Coordinates—Modified Wave Paths for Equivalent Flat Earth with Rectangular Coordinates—Concluding Remarks on Ray Traces—Effect of a Perfectly Conducting Plane Reflector on the Gain in a Preferred Direction of a Radiator That Is in Front of the Reflector—Effect of a Perfectly Conducting Plane Reflector on a Parallel Receiving Half-wave Dipole—Radiation Resistance of Antenna Arrays over a Perfect Reflector—Notes on the Form Factor of Linear Radiators over a Perfect Reflector.

CHAPTER VIII. ELECTROMAGNETIC DIFFRACTION 1018

Basic Concepts of Diffraction—Huygens' Principle, Fresnel Wave Interference, and Imaginary Radiation Surfaces—Remarks on Fresnel Zones (Applied to Electromagnetic Waves)—Exact and Approximate Magnitudes of Zonal Areas and Other Zonal Parameters—Magnitudes of Zonal Areas and Dimensions for Plane Wave Fronts—Application of the Wavelet Concept to a Parabolic Electromagnetic Projector—Notes on the Beam Width of a Plane Wave Front with Wavelets—Wave Propagation through Apertures—Diffraction from a Sharp Edge (Optical Straight-edge Approximation)—The Cornu Spiral Procedure for Interpreting Fresnel Integrals—Application of Cornu's Spiral and Tables for Fresnel Integrals—The Cornu Spiral Procedure for Sharp-wedge Diffraction—Electromagnetic Diffraction Due to Wedge-shaped Mountains for Short Waves—Notes on the Numerical Evaluation of the Resultant Field Diffracted into the Geometrical Shadow as Well as into the Unobstructed Region behind Wedge-shaped Mountains—Numerical Application of the Cornu Spiral Method to Diffraction into the Geometrical Shadow Zone—Numerical Application of the Cornu Spiral Method to Diffraction into the Unobstructed Region above the Geometrical Shadow Zone—Notes on Experimental Confirmation of Fresnel Diffraction Effects of Mountain Ridges—Notes on the Kirchhoff Diffraction Theory—Notes on the Sommerfeld Diffraction Theory—Proof that Eq. (897*a*) Satisfies Maxwell's Theory—Cornu Spiral for the Case of Diffraction of Electromagnetic Waves around the Earth Surface—The Burrows-Gray Diffraction Formula and Curves—Remarks on the Application of the Classic Theory of Apertures in Optics to Diffraction of Electromagnetic Waves—Electromagnetic Huygens Wavelet Radiators in the Primary Wave Front—Radiation Effect of a Slot Radiator (Wave-front Radiator of Finite Rectangular Area)—Diffractivity Tables and Curves—Remarks on the $D_{\theta\varphi}$ Formula for Computing Diffraction Patterns of Rectangular Slot Radiators—Relations for Several Parallel-slot Radiators—Comparisons of Radiation Effects of Electromagnetic Huygens Wavelet Center Radiators with Normal and Inclined Primary Rectangular Wave-front Incidence—Possible Applications of Parallel-slot Radiators and Field Patterns—The Diffraction Pattern of the Electromagnetic Wave Escaping from a Rectangular Wave Guide—Notes on the Actual Field Amplitude and Energy Pattern Escaping from an Open-ended Rectangular Wave Guide for $TE_{m,0}$ Waves—Classic and Electromagnetic Radiation

from a Circular Plane Primary Wave Front—Remarks on Plane wave-front Radiators of Any Contour—Arrays of Circular Wave-front Radiators—The Fresnel Diffraction Patterns—Distant Radiation Region Effect Due to a Wave-front Radiator of Any Contour—Application to Fresnel Diffraction of an Electromagnetic Rectangular Primary Wave-front Radiator—Significance of Fresnel Zones When Applied to Circular Electromagnetic Wave-front Radiators—Notes on Complementary Wave-front Radiators—Rectangular and Circular Gate Radiators—Circular Gate Radiator with a Spherical Wave Front.

CHAPTER IX. WAVE GUIDES AND CAVITIES 1185

Possible Waves in Guides Due to Boundary Conditions—Notes on Surface Conduction Currents and Displacement Current of Guides—Internal Impedance of a Plane Conductor—Remarks on the Power Flow along a Wave Guide—Power Dissipation and Attenuation in Wave Guides Due to the Finite Conductivity of the Metal Walls—Dielectric Energy Dissipation and Attenuation in Wave Guides Due to an Imperfect Dielectric within the Guide—Significant Properties of Waves in Guides, Characteristic Curves, and Formulas for Attenuation—Notes on Wave Transmission in Coaxial Lines—Essentials on Cavity Resonators—Basic Propagation Theory of Low-level Atmospheric Wave-guide Action (Low-level Wave Ducts)—Remarks on Electromagnetic Reflectors and Lenses Based on Wave-guide Action.

APPENDIX 1243

Systems of Units—List of Customary Symbols—Classic and MKS Units Compared—Notes on the Relation of the Modified Index M of Atmospheric Refraction to Electromagnetic Wave Propagation—Notes on Lommel's Expressions for Fresnel Integral Evaluations—Gauss and Gamma Functions—Notes on Si x and Ci x Functions—Notes on Bessel Functions—Notes on Scalar and Vector Relations in Cartesian, Cylindrical, and Spherical Coordinates—Hertzian Doublet Oscillator as a Special Case of the General Wave Equation—Notes on the Usefulness of the Equivalence Principle—Additional Expressions Used in Electromagnetic Wave Problems—Booker's Application of the Babinet Principle to Slot Radiators and Complementary Wire Radiators—Green Function, Green Theorem, and Their Relation to Electromagnetic Diffraction—Notes on Radiation Directivities of Slots in Metal Cylinders—Half-wave Dipole and Folded Dipole Values.

LIST OF REFERENCES 1288

NAME INDEX 1303

SUBJECT INDEX 1309

CHAPTER VII

SPACE RADIATION IN THE PRESENCE OF ELECTROMAGNETIC OBSTRUCTIONS

Space radiation, as commercially used, meets many obstacles that either partially or completely change the direction of wave propagation. Quite often not only the direction of propagation is changed but also the speed at which the electromagnetic field is moving. There may be also a change in polarization. An arriving plane wave front is often also changed to one that is no longer plane upon electromagnetic reflection. We often deal then with an incident electromagnetic ray, a reflected ray, and a refracted ray. The last ray penetrates into the obstacle. Even in atmosphere itself, a radiation beam that follows a refracted law often occurs, since the effective dielectric constant of the atmosphere may undergo small changes and cause the wave front to move along a beam that is curved. This is a text on short waves, and it does not take a large obstacle to cause conditions of the type mentioned. A 100-Mc wave corresponds to a free-space wavelength of only 3 m, while a 500-Mc wave has a wavelength of 0.6 m, and a 1,000-Mc wave a wavelength of only 0.3 m, etc. Since most commercial propagation passes through air, the above wavelengths are essentially the values that hold for air also. It is the largest cross dimension of an obstacle in terms of the wavelength that gives an idea of what the obstacle is apt to do to an arriving wave. Naturally, the electromagnetic properties of the obstacle are of first importance. By electromagnetic properties, we mean the dielectric constant κ in farads per meter, the permeability μ in henrys per meter, and the specific conductivity σ in mhos per meter. Since the largest cross dimension of the obstacle of known electromagnetic properties has to be compared with the wavelength, it is convenient to use the electrical length $\beta = 2\pi/\lambda$ per meter travel in air as a reference. Strictly taken, the electrical length per unit distance is $\alpha + j\beta$; but for air, the attenuation constant α due to the medium property vanishes. Then when an obstacle has dimensions smaller than $1/\beta$, it will interfere little with an incident wave, just as a thin stick in water has little effect on water waves started when a stone is thrown into a lake. Electromagnetically, the most potent obstacle consists of a good conductor such as copper. When, therefore, its dimensions are smaller than $1/\beta$,

it acts almost like an infinitesimal reradiator when struck by an arriving electromagnetic wave. Such a radiator has no appreciable radiation resistance, and any reflected waves from such a small body can hardly interfere with the arriving wave energy. As the obstacle gets larger and larger, it becomes more and more a noticeable reradiator when struck by an impinging wave and causes *diffraction* effects with maxima and minima in different direction. This means that wave interference sets in. But if the dimensions become much larger than $1/\beta$, the *optical ray theory* seems to give the best confirmation to what happens in the space field owing to the presence of an obstacle. This is the reason why, in this chapter, we assume that a metal as well as a general reflector is large compared with the operating wavelength. Experience shows that a few wavelengths of extensions in all directions make a fairly good electromagnetic mirror if the metal reflector is used, for instance, in connection with a half-wave dipole in order either to increase the reception gain or to cause a gain in a desired direction in the case of a transmitting half-wave dipole. It is subjects of this type that are analyzed in this chapter.

148. Application of the Optical Fresnel Relations on Reflection and Refraction of Electromagnetic Waves. The object of this section is to derive expressions for electromagnetic waves traveling from a medium 1 into a medium 2, where each medium is assumed isotropic but such that it may also exhibit a certain conductivity σ in mhos per meter in addition to the dielectric constant κ in farads per meter and permeability μ in henrys per meter. If the general medium is nonferromagnetic, the permeability is equal to $\mu_0 = 1.257 \times 10^{-6}$ henry/m. The derivation *assumes plane waves* and also that the boundary separating respective mediums is plane. The angle of wave incidence is taken for plane waves and for an incidence under any angle from 0 to 180 deg with respect to the plane of separation. The angle of incidence θ_1 is, however, expressed with respect to the normal to the plane of medium separation.

It is necessary to distinguish between the polarizations of the incident electromagnetic wave, since we have to meet the boundary conditions at the plane of medium separation. For medium 1, we have the electromagnetic properties μ_1, κ_1, σ_1 and for the medium 2 the properties μ_2, κ_2, σ_2. This means that across the boundary, we have sudden changes of these factors. We have, therefore, also corresponding *discontinuities* at the boundary for the electric $\mathcal{E}$ and magnetic H vector of the electromagnetic field. Now Maxwell's equations hold at any space point where the electromagnetic fields change *continuously*. Therefore, if we have a surface of *dis*continuity, we must satisfy the boundary conditions. A discontinuity is then the limiting condition of a more rapid continuous change. The boundary conditions require that the tangential electric field component be continuous. This means that on either side of the plane of separation (which is the boundary) and *tangent* to this plane, the electric field components must be the same. Therefore, if air is one medium and a perfect

conductor is the other medium, we *cannot* have a tangential $\mathcal{E}$ field along the boundary, because along the inside wall of a perfect conductor $\mathcal{E} = 0$ volts/m and, therefore, there *cannot* also be an electric field in air tangent to the copper surface. The boundary condition also requires that the *normal* component $B_n = \mu H_n$ of the magnetic *flux density* be continuous (the same on either side of the boundary). For a discontinuity of the tangential magnetic field component, we must have a surface current density; while for a discontinuity of the normal component $D_n = \kappa \mathcal{E}_n$ of the

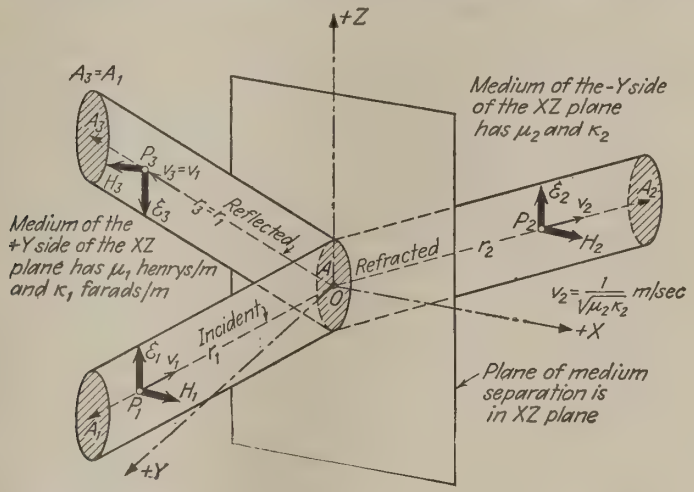

Locations: P_1 at x_1, y_1, z_1
P_2 at x_2, y_2, z_2
P_3 at x_3, y_3, z_3

$$v_1 = \frac{1}{\sqrt{\mu_1 \kappa_1}} \text{ m/sec}$$

Distances: r_1, r_2, and r_3 are from origin O, and

$$r_1 = x_1 \cos \alpha_1 + y_1 \cos \beta_1 + z_1 \cos \gamma_1$$
$$r_2 = x_2 \cos \alpha_2 + y_2 \cos \beta_2 + z_2 \cos \gamma_2$$
$$r_3 = x_3 \cos \alpha_3 + y_3 \cos \beta_3 + z_3 \cos \gamma_3$$

where α is the angle of r against X, β of r against Y, and γ of r against Z axis

FIG. 218. Field energy tubes shown for $\mathcal{E}_1$, $\mathcal{E}_2$, and $\mathcal{E}_3$ in the plane of wave incidence. Planes of constant phase are in the $\mathcal{E}$, H wave fronts and *normal* to respective velocities v_1, v_2, and v_3 m/sec, while planes of constant amplitude are parallel with the plane of medium separation.

electric flux density, we must have an equal surface charge density of $\kappa \mathcal{E}_n$ coulombs per square meter. Therefore, at the boundary between two dielectric mediums, *both* the tangential electric $\mathcal{E}$ and magnetic H fields are continuous; while for a perfectly conducting boundary, the tangential $\mathcal{E}$ field vanishes.

Let us take first two mediums 1 and 2, respectively, as in Fig. 218, that are *purely* dielectric with respective constants μ_1, κ_1 and μ_2, κ_2. Let us also take a distant field region for the location of the arriving electromagnetic wave. The respective field associations of $\mathcal{E}_1$ volts per meter and H_1 amperes per meter of the arriving incident wave are then a plane

wave front in space quadrature and in time phase as far as the obstacle is concerned. The arriving wave then travels with a speed of $v_1 = 1/\sqrt{u_1\kappa_1}$ meters per second. We can then take the propagation of electromagnetic field energy (along the normal to the plane wave front) as a ray and apply physical optics. Inasmuch as we deal with the transfer of electromagnetic energy in the case of wave propagation, it is convenient to start with energy relations and define the coefficient ρ of reflection as the square root of a power ratio by dividing the reflected energy per second leaving a reflecting surface A by the energy per second incident to the same surface A. If the two energies are of equal magnitude, we have perfect reflection, *i.e.*, $\rho = 1$. If the reflected energy is smaller than the incident energy, the difference is either dissipated at said surface (if also σ mhos per meter is effective), or partially dissipated at the surface and partially passed on into medium 2 as a refracted ray. According to optics, the incident, reflected, and refracted beams form the plane of incidence. Therefore, whatever electromagnetic field energy enters through cross section A_1 must be equal to the sum of respective field energies crossing areas A_2 and A_3. This is the case, since the arriving electromagnetic field energy flowing to the common area A in the plane of separation of the respective mediums splits up along the energy tube of reflection and the energy tube of refraction. In reality, the points P_1, P_2, and P_3 with respective cross sections are next to the area A at which reflected and refracted energy separation sets in, and we have the conditions of Fig. 219. The XY plane in this figure coincides with the plane of wave incidence. The YZ plane is the surface at which electromagnetic field energy divides into reflected and refracted energy. The electric field vectors $\mathcal{E}_1$, $\mathcal{E}_2$, and $\mathcal{E}_3$ are as shown in Fig. 219. They are in the plane of incidence. These electric polarizations can also be normal to the plane of incidence. When both the polarizations as shown in Fig. 219 and the polarizations that are normal to the plane of incidence are superimposed, we have the *general* case of polarization for plane electromagnetic waves. In Fig. 219, the associated magnetic field vectors are then parallel with the Z axis (perpendicular to the paper). According to optics, the planes of constant phase for the incident, transmitted (refracted), and reflected waves are perpendicular to the plane of incidence (XY plane). Therefore, areas A_1, A_2, and A_3 are the wave fronts next to the plane of separation with the corresponding common area A, for the indicated energy tubes. According to Snell, we have the reflection law $\theta_3 = \theta_1$, which means that the angle of *reflection* is equal to the angle of incidence. We have, for dielectrics 1 and 2, the *refraction* law $\sin\theta_1/\sin\theta_2 = v_1/v_2$ for the velocities v_1 and v_2 in medium 1 and medium 2, respectively. For the energy

tubes of Fig. 218, the electric and magnetic field associations are related to each other as in

$$\mathcal{E}_1/H_1 = Z_1/k_1; \qquad \mathcal{E}_2/H_2 = Z_2/k_2; \qquad \mathcal{E}_3/H_3 = Z_1/k_3$$

for the unit vectors k_1, k_2, and k_3 along the r_1, r_2, and r_3 directions and the characteristic space impedances $Z_1 = \sqrt{\mu_1/\kappa_2}$ and $Z_2 = \sqrt{\mu_2/\kappa_2}$ ohms.

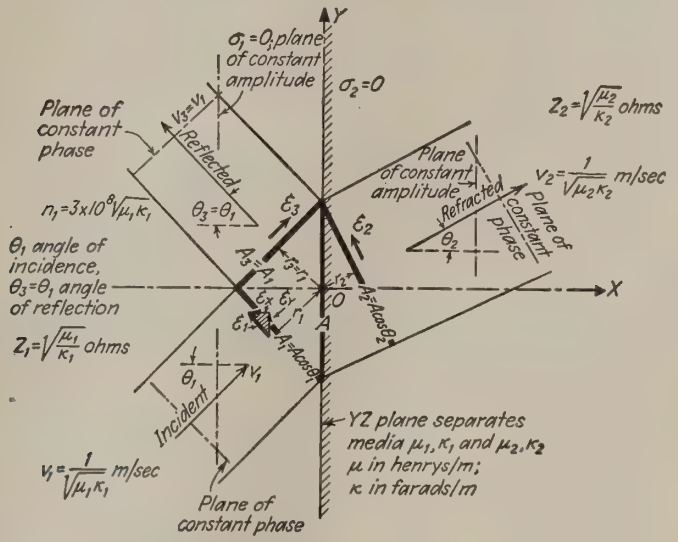

$$n = \frac{\sin\theta_1}{\sin\theta_2} = \frac{n_2}{n_1} = \frac{v_1}{v_2}$$

n is relative index of refraction.
YX plane (plane of paper) is plane of wave incidence

$$n_2 = \frac{c}{v_2} = \frac{1/\sqrt{\mu_0\kappa_0}}{1/\sqrt{\mu_2\kappa_2}} = 3 \times 10^8\sqrt{\mu_2\kappa_2}$$

θ_2 is angle of refraction for $\mathcal{E}$ vectors in plane of wave incidence.
Cross sections of wave front perpendicular to XY plane

$$A_1 = A\cos\theta_1; \qquad A_2 = A\cos\theta_2 \text{ sq m}$$

FIG. 219. Effective cross sections A_1, A_2, and A_3 of elementary energy tubes of incident, refracted, and reflected beams next to the common cross section A in the plane of medium separation.

If $\mathcal{E}$ and H denote the *effective* field values in volts per meter and amperes per meter, respectively, the power flow across A square meters is $P = A \cdot \mathcal{E} \cdot H$ watts. In Fig. 219, we have, for the energy tubes of the incident and the reflected beams, a cross section $A\cos\theta_1$ in each case; and for the refracted (transmitted) beam, we have a cross section $A\cos\theta_2$. In each case, the respective cross sections have their bases on the common area A.

For plane waves, we have, for the characteristic space impedance Z_0 and effective field values $\mathcal{E}$ and H, the relations $p = \mathcal{E}H = \mathcal{E}^2/Z_0 = Z_0H^2$ watts per square meter. For each second, we find that the power transfers P_1, P_2, and P_3 of the incident, refracted, and reflected beams for the $\mathcal{E}_1$, $\mathcal{E}_2$, and $\mathcal{E}_3$ values at $x = 0$ (at the boundary) are

$$\left.\begin{aligned} P_1 &= \frac{A\mathcal{E}_1^2 \cos\theta_1}{Z_1} \text{ watts}; \qquad P_2 = \frac{A\mathcal{E}_2^2 \cos\theta_2}{Z_2} \text{ watts} \\ P_3 &= \frac{A\mathcal{E}_3^2 \cos\theta_1}{Z_1} \text{ watts}; \qquad Z_1 = \sqrt{\frac{\mu_1}{\kappa_1}} \text{ ohms}; \qquad Z_2 = \sqrt{\frac{\mu_2}{\kappa_2}} \text{ ohms} \end{aligned}\right\} \tag{868}$$

The ratio of reflected to incident power results in

$$\frac{P_3}{P_1} = \frac{P_1 - P_2}{P_1} = 1 - \frac{P_2}{P_1} = 1 - \frac{Z_1\mathcal{E}_2^2 \cos\theta_2}{Z_2\mathcal{E}_1^2 \cos\theta_1}$$

$$\frac{P_3}{P_1} = 1 - \frac{\cos\theta_2}{\cos\theta_1}\sqrt{\frac{\mu_1\kappa_2}{\mu_2\kappa_1}}\frac{\mathcal{E}_2^2}{\mathcal{E}_1^2} = 1 - \frac{\mu_1 \cos\theta_2}{\mu_2 \cos\theta_1}\sqrt{\frac{\mu_2\kappa_2}{\mu_1\kappa_1}}\frac{\mathcal{E}_2^2}{\mathcal{E}_1^2}$$

The reflection coefficient ρ for any angle of incidence θ_1 is the ratio of the reflected field intensity $\mathcal{E}_3$ to the incident intensity $\mathcal{E}_1$ and, according to (868), is equal to $\sqrt{P_3/P_1}$, yielding the alternate formulas for the pure dielectric mediums 1 and 2 as

$$\left.\begin{aligned} \rho &= \sqrt{1 - \frac{Z_1 \cos\theta_2}{Z_2 \cos\theta_1}\frac{\mathcal{E}_2^2}{\mathcal{E}_1^2}} \\ \rho &= \sqrt{1 - \frac{\mu_1 \cos\theta_2}{\mu_2 \cos\theta_1}\frac{v_1}{v_2}\frac{\mathcal{E}_2^2}{\mathcal{E}_1^2}} \\ \rho &= \sqrt{1 - n\frac{\mu_1 \cos\theta_2}{\mu_2 \cos\theta_1}\frac{\mathcal{E}_2^2}{\mathcal{E}_1^2}} \end{aligned}\right\} \quad ; \quad \left.\begin{aligned} n_1 &= 3 \times 10^8\sqrt{\mu_1\kappa_1} \\ n_2 &= 3 \times 10^8\sqrt{\mu_2\kappa_2} \end{aligned}\right\} \text{ relative indexes referred to vacuum}$$

$$n = \frac{n_2}{n_1} \quad \text{relative index of medium 2 with respect to medium 1}$$

$$n_1 \sin\theta_1 = n_2 \sin\theta_2 \tag{868a}$$

where n denotes the relative index of refraction of dielectric mediums μ_1, κ_1 and μ_2, κ_2 for the indexes n_1 and n_2 for mediums 1 and 2, respectively.

We must distinguish between horizontal and vertical polarizations. In radio engineering, it has become common practice to signify the polarizations of waves by means of the *electric* polarization.[1] Figure 220*a* and *b* shows how the field associations are oriented for vertically and horizontally polarized electromagnetic waves. By *vertical* polarization, then, is meant the polarization caused by a vertical linear radiator. Horizontal polarization is produced by a horizontal linear radiator. There is quite a difference between vertical and horizontal polarization

[1] For an *elliptically* polarized plane wave progressing in the $+Z$ direction, we have the radiation

$$\mathcal{E} = \underset{\cdot}{v}_x\mathcal{E}_1\epsilon^{j(\omega t - \beta z)} + \underset{\cdot}{v}_y\mathcal{E}_2\epsilon^{j(\omega t - \beta z + \varphi)} \qquad \text{volts/m}$$

where, as on pp. 785–786, $\mathcal{E}_1$ and $\mathcal{E}_2$ are the orthogonal linear primary polarizations in the XY plane and $\underset{\cdot}{v}_x$ and $\underset{\cdot}{v}_y$ are unit vectors along the X and Z directions. For the

as far as the total radiation effects are concerned in the case of electromagnetic obstacles, which cause reflection and refraction effects. The resultant space field is then due to the direct ray (a ray as in unobstructed radiation space) and generally due to indirect rays (reflected rays). Inasmuch as the XY plane for either polarization of Fig. 220 is made to coincide with the plane of incidence, the incident, the transmitted (refracted), and the reflected rays must lie in this plane. The perpendicular YZ plane is such that it represents the plane of medium separation between the isotropic dielectrics μ_1, κ_1 and μ_2, κ_2, respectively. Therefore, by taking the $\mathcal{E}$ vector in Fig. 220*a* everywhere in the plane of incidence, we have the case of one fundamental polarization. The vertical polarization is then a special case of the above-mentioned $\mathcal{E}$ orientation. In Fig. 220*b*, the electric $\mathcal{E}$ vector is everywhere perpendicular to the XY plane (the other fundamental polarization). Table 44 gives the application of formula (868*a*) for vertically and horizontally polarized electromagnetic waves. This table leads, then, to the electromagnetic Fresnel relations, which are well known in optics. We have already found in this text that ground represents a general medium (μ, κ, and σ effective). We have also found that the operating frequency

---

relative time phase $\varphi = \pm 90°$ and $\mathcal{E}_1 = \mathcal{E}_2$, we have right-handed and left-handed circular polarizations, respectively. W. Sichak and S. Milazzo (*op. cit.* on p. 787) have given the relation

$$\left.\begin{aligned} E &= K\sqrt{1 \mp a \cdot b + d \cdot e \cos(2\psi)}; \qquad a = \frac{2r_2}{1 + r_2^2} \\ b &= \frac{2r_1}{1 + r_1^2}; \qquad d = \frac{r_2^2 - 1}{r_2^2 + 1}; \qquad e = \frac{r_1^2 - 1}{r_1^2 + 1} \end{aligned}\right\}$$

for the *magnitude* of the induced voltage. K is a constant, and r_1 is the ratio of maximum and minimum amplitudes in the field pickup aerial system when rotated in a plane transverse to the propagation direction Z of a linearly polarized wave, initiated in the initial XY plane. This is also the ratio of maximum to minimum values of the field vector of an elliptically polarized wave which would be radiated by the receiving antenna (if used as a radiator). The quantity r_2 is the ratio of maximum to minimum amplitude values of the field vector of the incident elliptically polarized wave. The quantity ψ denotes the angle between the direction of maximum amplitude of the electric field vector in the incident elliptically polarized wave and the direction of maximum amplitude of $\mathcal{E}$ which would exist if the receiving antenna system would radiate. This requires that the $\mathcal{E}$ vector be always in the plane normal to the propagation direction of the incident wave.

In the case where an *incident* circularly polarized wave affects a circularly polarized wave pickup system, we have the simplifications $r_1 = r_2 = 1$ and $E = K\sqrt{1 \mp 1}$. Thus, for a circular polarization, which is clockwise for the incident wave and for the wave pickup system, the induced voltage in the pickup system is $E = K\sqrt{2}$ volts for the absolute magnitude and vanishes if the receiving pickup aerial system causes helical rotation opposite to the incident circularly polarized wave.

has much to do with whether the earth crust is in effect behaving like a dielectric, like a semiconductor, or like an apparent conductor.

149. Remarks on the Phase Factor of an Electromagnetic Wave Refracted into a General Medium. From Table 44, step 33, the phase factor in the relations for the field associations $\mathcal{E}_2$ and H_2, for $\mathcal{E}_0/H_0 = \sqrt{\mu_2/\kappa_e}$, is $F_2 = \epsilon^{j(\omega t - \beta n r)}$, if the relative index of refraction is $n = \sqrt{\kappa_r - jq}$ for $q = 1.8 \times 10^4(\sigma_2/f)$ and f in megacycles per second, $\kappa_r = \kappa_2/\kappa_0$, $\kappa_0 = 8.854 \times 10^{-12}$ farad/m, and σ_2 is in mhos per meter. The permeability

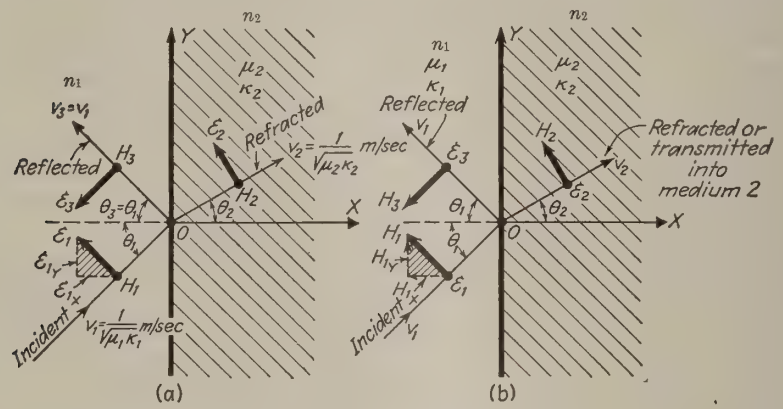

$$n = \frac{\sin\theta_1}{\sin\theta_2} = \frac{v_1}{v_2} = \frac{n_2}{n_1} = \sqrt{\frac{\mu_2\kappa_2}{\mu_1\kappa_1}} \text{ for pure dielectric mediums}$$

$$n_1 = 3 \times 10^8 \sqrt{\mu_1\kappa_1},\ \mu_1 \text{ henrys/m},\ \kappa_1 \text{ farads/m}$$

$$n_2 = \frac{c}{v_2} = c\sqrt{\mu_2\kappa_2} = 3 \times 10^8 \sqrt{\mu_2\kappa_2},\ \mu_2 \text{ henrys/m},\ \kappa_2 \text{ farads/m}$$

All $\mathcal{E}$ vectors in plane XY of incidence (corresponds to *vertical* polarization)

$$|H = H_z|; \qquad \mathcal{E} = \sqrt{|\mathcal{E}_x|^2 + |\mathcal{E}_y|^2}$$
$$\mathcal{E}_z = 0 = H_x = H_y$$

H_1, H_2, and H_3 are normal to the paper (along Z directions) and tangent to plane of separation.

All H vectors are in plane XY of wave incidence (*horizontal* polarization is an example)

$$|\mathcal{E} = \mathcal{E}_z|; \qquad H = \sqrt{|H_x|^2 + H_y|^2}$$
$$H_z = 0 = \mathcal{E}_x = \mathcal{E}_y$$

$\mathcal{E}_1$, $\mathcal{E}_2$, and $\mathcal{E}_3$ are normal to the paper and tangent to plane of separation.

FIG. 220. Cases for all electric vectors in the plane of wave incidence (220*a*) and all magnetic vectors in plane of wave incidence (220*b*). $\mathcal{E}_1$, $\mathcal{E}_2$, $\mathcal{E}_3$, H_1, H_2, and H_3 are taken at $x = 0$ in Fig. 219.

of medium 2 is then usually $\mu_2 = \mu_0 = 1.257 \times 10^{-6}$ henry/m. It is the space term $\epsilon^{-j\beta n r}$ that concerns us here, since the time factor $\epsilon^{j\omega t}$ does not differ from the time factor of an ideal dielectric medium 2, for which $\sigma_2 = 0$ mhos/m. The difference exists in the fact that the wavelength λ_2 in $\beta_2 = 6.28/\lambda_2$ differs from the value of a nondissipative dielectric. For the nondissipative dielectric $\Gamma_2 = j\beta = j\omega/v_2$, where $v_2 = 1/\sqrt{\mu_2\kappa_2}$ meters per second; while for the dissipative medium, we have $\Gamma_2 = j\omega\sqrt{\mu_2\kappa_e} = \alpha_2 + j\beta_2$, where $\kappa_e = \kappa_2 - j(\sigma/\omega)$ farads per meter and $v_2 = \omega/\beta_2$ meters per second.

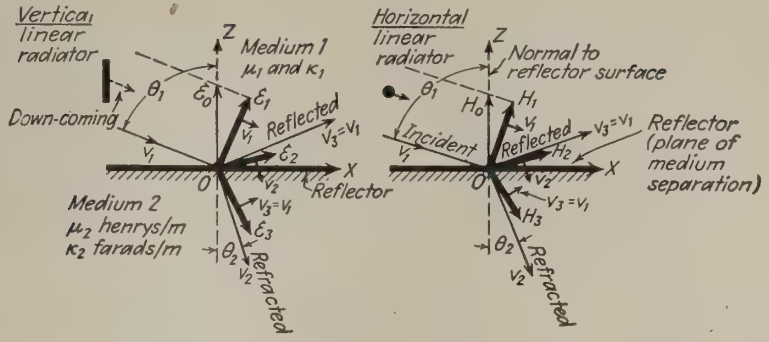

Reflected $\mathcal{E}_3 = \rho_v \mathcal{E}_1$
Incident $\mathcal{E}_1 = \mathcal{E}_0 \cos \theta_1$
$\mathcal{E}_0$ field parallel with linear radiator

Reflected $H_3 = \rho_h H_1 = \rho_h \sqrt{\frac{\kappa_1}{\mu_1}}\, \mathcal{E}_1$

$$H_2 = \sqrt{\frac{\kappa_2}{\mu_2}}\, \mathcal{E}_2$$

Incident $H_1 = H_0 \cos \theta_1$
H_0 field amplitude is normal to linear radiator

FIG. 221. Conditions for vertical and horizontal polarization in the presence of a reflecting surface of medium separation in a horizontal plane (XY plane). XY plane is reflecting surface; θ_1 is angle of incidence and angle of reflection with normal to reflector; θ_2 is angle of refraction with normal v_1, v_2, and v_3 velocities forming the plane of wave incidence. (*a*) Down-coming *vertical* polarization (all magnetic vectors point into the paper at O). (*b*) Down-coming *horizontal* polarization (all electric vectors point into paper at O).

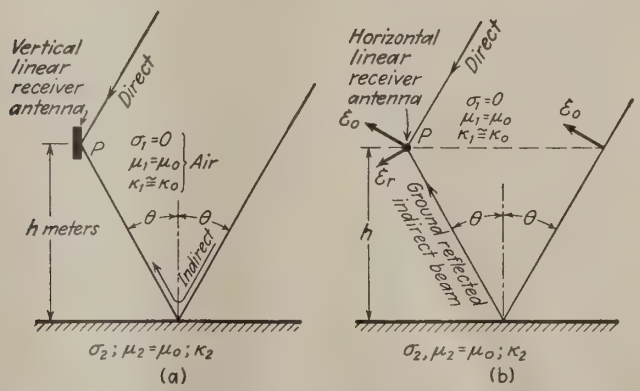

FIG. 222. Resultant wave effect of down-coming waves due to a direct and ground-reflected ray. θ is angle of wave incidence and wave reflection. (*a*) For a vertically polarized arriving down-coming wave (vertical receiver antenna). (*b*) For a horizontally polarized arriving down-coming wave (horizontal receiver antenna). $\delta = (4\pi h \cos \theta)/\lambda$; $\lambda \cong 300/f^{(\mathrm{Mc})}$ m. $\mathcal{E}_0$ is direct field in volts/m; $\mathcal{E}_r$ is reflected field in volts/m.

TABLE 44. ELECTROMAGNETIC REFLECTION AND REFRACTION

Steps	*Electric vector* $\mathcal{E}$ is *parallel* with XY plane or in XY plane (Fig. 220*a*), corresponds to *vertical polarization*	*Electric vector* $\mathcal{E}$ is *perpendicular* to XY plane (Fig. 220*b*), corresponds to *horizontal polarization*	Remarks
1	Figure 221*a* shows why $\mathcal{E}$ in the incident plane is identical with the polarization of a vertical radiator (ρ_v denotes the reflection coefficient for *vertical* polarization). $\rho_v = \mathcal{E}_3/\mathcal{E}_1 = H_3/H_1$, since the three-dimensional wave impedance $Z_1 = \sqrt{\mu_1/\kappa_1}$ ohms cancels	Figure 221*b* shows why $\mathcal{E}$ normal to the plane of incidence is identical with the polarization of a horizontal linear radiator (ρ_h denotes the coefficient for *horizontal* polarization); $\rho_h = \dfrac{H_3}{H_1} = \dfrac{\mathcal{E}_3}{\mathcal{E}_1}$	Applies to Fig. 220. XY plane is plane of incidence, and normal YZ plane is the plane of reflection. For plane waves in the distant radiation field, electric $\mathcal{E}$ and magnetic H fields are normal to each other and in time phase, for perfect dielectric mediums and $\mathcal{E}$ and H are normal to the direction of wave propagation. X is normal to the plane of reflection. Since $\mathcal{E}/H = \sqrt{\mu/\kappa}$, it does not matter whether we derive ρ with $\mathcal{E}$ or H vectors. The subscripts $\parallel$ for parallel and $\perp$ for perpendicular refer to polarizations where $\mathcal{E}$ is in the plane of incidence or normal to it, respectively
2	In Fig. 220*a* we note that for all $\mathcal{E}$ vectors (in any direction of the XY plane), it is possible to have $\mathcal{E}_x$ and $\mathcal{E}_y$ components (*elliptical* $\mathcal{E}$ polarization is possible). *Only* the H_z *magnetic vector* is *possible*	In Fig. 220*b*, for the same reason, elliptical H polarization is possible, since H can have x and y components, because H is entirely in the plane of incidence. *Only* the $\mathcal{E}_z$ *electric vector* is *possible*	
3	Since $\mathcal{E}$ vectors show up in the plane of incidence, we use $\mathcal{E}_1$, $\mathcal{E}_2$, and $\mathcal{E}_3$ for finding $\rho_v = \mathcal{E}_3/\mathcal{E}_1$ (reflection coefficient)	H vectors are in the plane of incidence, and H_1, H_2, and H_3 vectors are used for finding $\rho_h = H_3/H_1$ (reflection coefficient)	
4	Inasmuch as for this polarization at $x = 0$, the magnetic field intensities H_1, H_2, and H_3 are parallel with the Z axis (Fig. 220*a*), *i.e.*, perpendicular to the paper at O, they *must* be tangential to the YZ plane, which separates medium μ_1, κ_1 from medium μ_2, κ_2. This means that the resultant field $H_1 + H_3$ on the μ_1, κ_1 face must be equal to field H_2 on the μ_2, κ_2 face of separation. *Hence* $H_3 = H_2 - H_1$ and $\rho_v = H_3/H_1 = (H_2/H_1) - 1$	At $x = 0$, the *electric* $\mathcal{E}_1$, $\mathcal{E}_2$, and $\mathcal{E}_3$ field intensities are, according to Fig. 220*b*, parallel with the Z axis, *i.e.*, tangential to the plane of separation of medium 1 and medium 2. *Hence* $\mathcal{E}_1 + \mathcal{E}_3 = \mathcal{E}_2$ *must* be satisfied on the plane of medium separation. Therefore, $\rho_h = \mathcal{E}_3/\mathcal{E}_1 = (\mathcal{E}_2/\mathcal{E}_1) - 1$	

5	We have to deal with magnetic components, since *they* are directly tangent to the interface plane. The last expression of (868a) reads for $a = \frac{(n\mu_1 \cos \theta_2)}{(\mu_2 \cos \theta_1)}$, $\rho_v = \sqrt{1 - a(\varepsilon_2/\varepsilon_1)^2}$. But $\varepsilon_1 = Z_1 H_1$; $\varepsilon_2 = Z_2 H_2$ for $Z_1 = \sqrt{\mu_1/\kappa_1}$, $Z_2 = \sqrt{\mu_2/\kappa_2}$, and $\rho_v = \sqrt{1 - a(Z_2 H_2/Z_1 H_1)^2} = \sqrt{1 - b(H_2/H_1)^2}$ for $b = (n\kappa_1 \cos \theta_2)/(\kappa_2 \cos \theta_1)$. Hence, $H_2/H_1 = \sqrt{(1 - \rho_v^2)/b}$, which substituted in the result of step 4, yields $\rho_v = \left(\frac{H_2}{H_1}\right) - 1 = \sqrt{\frac{(1 - \rho_v^2)}{b}} - 1$ or $(1 + \rho_v)^2 = [(1 + \rho_v)(1 - \rho_v)/b]$ giving for *vertical* polarization $\rho_v = \frac{1 - b}{1 + b} = \frac{\kappa_2 \cos \theta_1 - n\kappa_1 \cos \theta_2}{\kappa_2 \cos \theta_1 + n\kappa_1 \cos \theta_2}$	Last expression of (868a) yields for $a = \frac{(n\mu_1 \cos \theta_2)}{\mu_2 \cos \theta_1}$, $\rho_h^2 = 1 - a\,\varepsilon_2^2/\varepsilon_1^2$, $\varepsilon_2/\varepsilon_1 = \sqrt{(1 - \rho_h^2)/a}$, which, substituted in the result of step 4, yields for $\rho_h = (\varepsilon_2/\varepsilon_1) - 1 = \sqrt{(1 - \rho_h^2)/a} - 1$ or $1 + \rho_h = \sqrt{\frac{(1 - \rho_h^2)}{a}}$, $(1 + \rho_h)^2 = [(1 + \rho_h)(1 - \rho_h)/a]$. This yields for horizontal polarization $\rho_h = \frac{1 - a}{1 + a} = \frac{\mu_2 \cos \theta_1 - n\mu_1 \cos \theta_2}{\mu_2 \cos \theta_1 + n\mu_1 \cos \theta_2}$ ρ_h (as well as ρ_v) holds for *pure* dielectric mediums $\mu_1, \kappa_1, \sigma_1 = 0$, $\mu_2, \kappa_2, \sigma_2 = 0$, and $\frac{v_1}{v_2} = \frac{(\sin \theta_1)}{(\sin \theta_2)}$ is *correct only* for *perfect* dielectrics $\rho_h = \frac{\cos \theta_1 - n \cos \theta_2}{\cos \theta_1 + n \cos \theta_2}$	The correspondence of vertical and horizontal polarization assumes that the plane of incidence is perpendicular to the horizon For any general orientation of the plane of incidence, we have $\rho_\parallel$ instead of ρ_v and $\rho_\perp$ instead of ρ_h for the respective coefficients of reflection. $v_1 = \frac{1}{\sqrt{\mu_1 \kappa_1}}$ and $v_2 = \frac{1}{\sqrt{\mu_2 \kappa_2}}$ m/sec velocity for perfect dielectric mediums where μ is in henrys/m and κ in farads/m. We also have $v_1/v_2 = n_2/n_1 = n$, which for nonferromagnetic mediums gives $\mu_1 = \mu_0 = \mu_2$, and yields the *relative* index n of refraction $n = \sqrt{\kappa_2/\kappa_1}$
6	$\frac{\sin \theta_1}{\sin \theta_2} = \frac{v_1}{v_2} = \frac{n_2}{n_1} = n$; $\cos \theta_2 = \sqrt{1 - \sin^2 \theta_2} = \sqrt{1 - \frac{\sin^2 \theta_1}{n^2}}$		
7	Elimination of the angle θ_2 of refraction, yields $\rho_v = \frac{\kappa_2 \cos \theta_1 - \kappa_1 \sqrt{n^2 - \sin^2 \theta_1}}{\kappa_2 \cos \theta_1 + \kappa_1 \sqrt{n^2 - \sin^2 \theta_1}}$	yields for horizontal polarization $\rho_h = \frac{\mu_2 \cos \theta_1 - \mu_1 \sqrt{n^2 - \sin^2 \theta_1}}{\mu_2 \cos \theta_1 + \mu_1 \sqrt{n^2 - \sin^2 \theta_1}}$	

TABLE 44. ELECTROMAGNETIC REFLECTION AND REFRACTION.—(*Continued*)

Steps	*Electric vector* $\mathcal{E}$ is *parallel* with XY plane or in XY plane (Fig. 220*a*), corresponds to *vertical polarization*	*Electric vector* $\mathcal{E}$ is *perpendicular* to XY plane (Fig. 220*b*), corresponds to *horizontal polarization*	Remarks
8	For $\mu_1 = \mu_0 = \mu_2$ as mostly the case, we have the same ρ_v relation as above, and in terms of the respective refraction indices for each medium $\underline{\rho_v} = \dfrac{\kappa_2 \cos\theta_1 - \kappa_1\sqrt{\left(\dfrac{n_2}{n_1}\right)^2 - \sin^2\theta_1}}{\kappa_2 \cos\theta_1 + \kappa_1\sqrt{\left(\dfrac{n_2}{n_1}\right)^2 - \sin^2\theta_1}}$ $= \dfrac{\kappa_2 \cos\theta_1 - \kappa_1\sqrt{\dfrac{\kappa_2}{\kappa_1} - \sin^2\theta_1}}{\kappa_2 \cos\theta_1 + \kappa_1\sqrt{\dfrac{\kappa_2}{\kappa_1} - \sin^2\theta_1}}$	For $\mu_1 = \mu_0 = \mu_2$ $\underline{\rho_h} = \dfrac{\cos\theta_1 - \sqrt{\left(\dfrac{n_2}{n_1}\right)^2 - \sin^2\theta_1}}{\cos\theta_1 + \sqrt{\left(\dfrac{n_2}{n_1}\right)^2 - \sin^2\theta_1}}$ $= \dfrac{\cos\theta_1 - \sqrt{\dfrac{\kappa_2}{\kappa_1} - \sin^2\theta_1}}{\cos\theta_1 + \sqrt{\dfrac{\kappa_2}{\kappa_1} - \sin^2\theta_1}}$	If the medium is air, we have $\kappa_1 = \kappa_0 = 8.854 \times 10^{-12}$ farad/m and a relative dielectric constant $\kappa_r = \kappa_2/\kappa_0$ for medium 2 referred to medium 1. Therefore, $n = \sqrt{\kappa_r}$, which for wave propagation from air (medium 1) into ocean (medium 2) yields $n = \sqrt{80} \cong 9$
9	If medium 1 is air, then we have practically $\mu_1 = \mu_0$ and $\kappa_1 = \kappa_0$; and for a nonferromagnetic perfectly dielectric medium 2, we have $\mu_2 = \mu_0$ and $\kappa_2 = \kappa_r\kappa_0$, if κ_r denotes the relative dielectric constant referred to empty space. We have then $\rho_\parallel = \underline{\rho_v} = \dfrac{\kappa_r \cos\theta_1 - \sqrt{\kappa_r - \sin^2\theta_1}}{\kappa_r \cos\theta_1 + \sqrt{\kappa_r - \sin^2\theta_1}}$	If an electromagnetic wave traveling in air strikes a perfect insulator $\mu_2 = \mu_0$, κ_2 (nonferromagnetic) $\rho_\perp = \underline{\rho_h} = \dfrac{\cos\theta_1 - \sqrt{\kappa_r - \sin^2\theta_1}}{\cos\theta_1 + \sqrt{\kappa_r - \sin^2\theta_1}}$	$\mu_0 = 1.257 \times 10^{-6}$ henry/m; $\kappa_0 = 8.854 \times 10^{-12}$ farad/m; θ_1 is the angle of incidence that an incident electromagnetic ray makes with normal to the plane of medium separation

10	If medium 2 is the earth crust such as ground, we *no longer* have $\sigma_2 = 0$ and, therefore, no pure dielectric reflector, but we have for nonferromagnetic ground $\mu_2 = \mu_0$, $\kappa_2 = \kappa_0\kappa_r$, and σ_2 mhos/m. The *relative equivalent* dielectric constant κ_e', which is *complex*, must then be used in place of the *real* relative dielectric constant κ_r. We obtain then $\underline{\rho_\parallel = \rho_v} = \dfrac{\kappa_e' \cos\theta_1 - \sqrt{\kappa_e' - \sin^2\theta_1}}{\kappa_e' \cos\theta_1 + \sqrt{\kappa_e' - \sin^2\theta_1}}$	For the same condition as for vertical polarization, but we obtain $\underline{\rho_\perp = \rho_h} = \dfrac{\cos\theta_1 - \sqrt{\kappa_e' - \sin^2\theta_1}}{\cos\theta_1 + \sqrt{\kappa_e' - \sin^2\theta_1}}$ for air against earth crust electromagnetic wave propagation (for ocean water $\sigma_2 \cong 4$ mhos/m) $\kappa_r \cong 80$, $\kappa_e = 80\kappa_0 - j(4/\omega)$, $\kappa_e' = \kappa_e/\kappa_0 = 80 - j(4/\omega\kappa_0)$ numeric; $\kappa_e' = 80 - j18{,}000 \times 4/f^{(\mathrm{Mc})} = 80 - j72{,}000/f^{(\mathrm{Mc})}$	$\kappa_e' = \kappa_e/\kappa_0$, $n = n_2/n_1 = \sqrt{\kappa_e'}$, $\kappa_e = \kappa_2 - j(\sigma_2/\omega)$, according to Eq. (3) on page 17 For details consult Secs. 11 and 12. $\omega = 6.28 \times 10^6 f^{(\mathrm{Mc})}$ $\dfrac{\sigma_2}{\omega\kappa_0} = 18{,}000\,\dfrac{\sigma}{f^{(\mathrm{Mc})}}$
11	From the general expression for the propagation constant Γ for μ, κ, *and* σ *effective*, we have $\Gamma = j\omega\sqrt{\mu\kappa_e} = j\omega\sqrt{\mu\left(\kappa - j\dfrac{\sigma}{\omega}\right)}$ instead of $\Gamma = j\omega\sqrt{\mu\kappa}$, holding for a perfectly insulating medium ($\sigma = 0$)		
12	We find in Fig. 222*a* $\rho_v = \dfrac{\kappa_e' \cos\theta - p}{\kappa_e' \cos\theta + p} = a + jb = \sqrt{a^2 + b^2}\,\epsilon^{j\varphi_v}$; $\varphi_v = \tan^{-1}(b/a)$ phase of reflection coefficient ρ_v, $p = \sqrt{\kappa_e' - \sin^2\theta}$, $\kappa_e' = \kappa_e/\kappa_0$	We find in Fig. 222*b* $\rho_h = \dfrac{\cos\theta - p}{\cos\theta + p} = c + jd$ $\varphi_h = \tan^{-1}(d/c)$ phase of reflection coefficient ρ_h; p is as to the left	θ is angle of incidence with respect to the normal to the plane of medium separation. For wave propagation against a plane surface with a complex medium (μ_2, κ_2, σ_2) behind it
13	Resultant field: $\mathcal{E} = \mathcal{E}_0[1 + \rho_v\epsilon^{-j(\delta+\varphi_v)}]$	Resultant field: $\mathcal{E} = \mathcal{E}_0[1 + \rho_h\epsilon^{-j(\delta+\varphi_h)}]$	
	Reflected field $\mathcal{E}_r = \rho\mathcal{E}_0\epsilon^{-j(\delta+\varphi)}$; direct field $\mathcal{E}_0$ volts/m; δ is phase delay, due to path difference of direct $\mathcal{E}_0$ ray and reflected $\mathcal{E}_r$ ray at reception point P of Fig. 222		

TABLE 44. ELECTROMAGNETIC REFLECTION AND REFRACTION.—(*Continued*)

Steps	*Electric vector* $\mathcal{E}$ is *parallel* with XY plane or in XY plane (Fig. 220*a*), corresponds to *vertical polarization*	*Electric vector* $\mathcal{E}$ is *perpendicular* to XY plane (Fig. 220*b*), corresponds to *horizontal polarization*	Remarks
14	If both mediums in Fig. 220 also have conductivities σ_1 and σ_2 in mhos/m, we have to use respective propagation constants Γ_1 and Γ_2, instead of the phase constants $j\beta_1$ and $j\beta_2$, since the medium attenuation constant α in $\Gamma = \alpha + j\beta$ is no longer zero. We then *no longer* have Snell's refraction law (holding for *perfect* dielectrics), which reads $$n = \frac{\sin\theta_1}{\sin\theta_2} = \frac{v_1}{v_2} = \frac{\omega/\beta_1}{\omega/\beta_2} = \frac{\beta_2}{\beta_1} = \frac{n_2}{n_1} = \frac{v_1 = \dfrac{1}{\sqrt{\mu_1\kappa_1}}}{v_2 = \dfrac{1}{\sqrt{\mu_2\kappa_2}}} = \sqrt{\frac{\mu_2\kappa_2}{\mu_1\kappa_1}} = \sqrt{\frac{\kappa_2}{\kappa_1}}, \text{ if } \mu_1 = \mu_0 = \mu_2$$ (for perfect dielectrics) *But* we have for two general mediums μ_1, κ_1, σ_1 and μ_2, κ_2, σ_2 $$n = \frac{\sin\theta_1}{\sin\theta_2} = \frac{\Gamma_2}{\Gamma_1} = \frac{\sqrt{\mu_2\left(\kappa_2 - j\dfrac{\sigma_2}{\omega}\right)}}{\sqrt{\mu_1\left(\kappa_1 - j\dfrac{\sigma_1}{\omega}\right)}} = \frac{\sqrt{\mu_2\kappa_{e_2}}}{\sqrt{\mu_1\kappa_{e_1}}} = \sqrt{\frac{\mu_2}{\mu_1}}\sqrt{\frac{\kappa_{e_2}}{\kappa_{e_1}}}$$ which may be called a *generalized* Snell refraction law. The quantity $n = n_2/n_1$ is again the relative index of refraction between respective mediums. For nonferromagnetic mediums, we have $\mu_1 = \mu_0 = \mu_2$ and $\sqrt{\mu_2/\mu_1}$ equal to unity, so that $n = \sqrt{\kappa_{e_2}/\kappa_{e_1}}$		Application to two general mediums 1 and 2, which possess also specific conductances σ_1 and σ_2 mhos/m, respectively. $n = n_2/n_1$ is the relative index of refraction of medium 2 with respect to medium 1. For two perfect dielectric mediums $$n_1 = \frac{3 \times 10^8}{v_1}$$ $$n_2 = \frac{3 \times 10^8}{v_2}$$ $$n = \frac{n_2}{n_1} = \frac{v_1}{v_2}$$
15	Since in Fig. 220*a*, the *tangential* boundary condition requires $H_1 + H_3 = H_2$, and $H_1 \cos\theta_1 - H_3 \cos\theta_1 = \left(\dfrac{\mu_2\Gamma_1}{\mu_1\Gamma_2}\right) H_2 \cos\theta_2$ for the continuity of the *perpendicular* magnetic field components *across* and *at* the surface of	In Fig. 220*b*, $\mathcal{E}_1 + \mathcal{E}_3 = \mathcal{E}_2$ satisfies the tangential boundary condition on either side and along the surface of medium separation (tangential components must be continuous). $\mathcal{E}_1 \cos\theta_1 - \mathcal{E}_3 \cos\theta_1 = (\mu_1\Gamma_2/\mu_2\Gamma_1)\mathcal{E}_2 \cos\theta_2$ satisfies that the perpendicular components *at* the	$H_3 = \rho H_1$ and $\mathcal{E}_3 = \rho\mathcal{E}_1$,

	medium separation, we can find the *reflection* coefficient from H_3/H_1, and the *refraction* coefficient from H_2/H_1. We have then for the coefficient of reflection $\rho_{\parallel} = \rho_v = \dfrac{H_3}{H_1} = \dfrac{\mu_1\Gamma_2 \cos\theta_1 - \mu_2\Gamma_1 \cos\theta_2}{\mu_1\Gamma_2 \cos\theta_1 + \mu_2\Gamma_1 \cos\theta_2}$ $= \dfrac{\mu_1\Gamma_2 \cos\theta_1 - \mu_2\Gamma_1 \sqrt{1 - \left(\dfrac{\Gamma_1}{\Gamma_2}\sin\theta_1\right)^2}}{\mu_1\Gamma_2 \cos\theta_1 + \mu_2\Gamma_1 \sqrt{1 - \left(\dfrac{\Gamma_1}{\Gamma_2}\sin\theta_1\right)^2}}$	surface of medium separation must be continuous. The coefficient of reflection is $\rho = \varepsilon_3/\varepsilon_1$, and the coefficient of refraction is found from $\varepsilon_2/\varepsilon_1$. Hence, $\rho_{\perp} = \rho_h = \dfrac{\varepsilon_3}{\varepsilon_1} = \dfrac{\mu_2\Gamma_1 \cos\theta_1 - \mu_1\Gamma_2 \cos\theta_2}{\mu_2\Gamma_1 \cos\theta_1 + \mu_1\Gamma_2 \cos\theta_2}$ $= \dfrac{\mu_2\Gamma_1 \cos\theta_1 - \mu_1\Gamma_2 \sqrt{p}}{\mu_2\Gamma_1 \cos\theta_1 + \mu_1\Gamma_2 \sqrt{p}}$ $p = 1 - \left(\dfrac{\Gamma_1}{\Gamma_2}\sin\theta_1\right)^2$	since $\cos\theta_2 = \sqrt{1 - \sin^2\theta_2}$ and, according to step 14, $\sin\theta_2 = \dfrac{\Gamma_1}{\Gamma_2}\sin\theta_1$
16	For perpendicular incidence on the plane of medium separation, we have $\theta_1 = 0°$ and *equal* numerical coefficients for ρ_v and ρ_h, since $\rho_{\parallel} = \rho_v = \dfrac{\mu_1\Gamma_2 - \mu_2\Gamma_1}{\mu_1\Gamma_2 + \mu_2\Gamma_1} = -\rho_h = -\rho_{\perp}$ The result is, however, of *opposite* sign, as also found by the theory of images, for which a radiator of electromagnetic waves is in effect just as much behind a reflector with its image radiator as the actual physical radiator is in front of the reflector. We have then *inphase* actual antenna currents and *inphase* image antenna currents for vertical and *antiphase* image currents for horizontal polarization. The reflector plane is then taken as the YZ plane of Fig. 220		Confirmation of the theory of electrical images
17	Coefficient of refraction $R_{\parallel} = R_v$ is found according to step 15 from the ratio H_2/H_1. Hence, $R_{\parallel} = R_v = \dfrac{H_2}{H_1}$ $= \dfrac{2\mu_1\Gamma_2 \cos\theta_1}{\mu_1\Gamma_2 \cos\theta_1 + \mu_2\Gamma_1 \cos\theta_2}$ $= \dfrac{2\mu_1\Gamma_2 \cos\theta_1}{\mu_1\Gamma_2 \cos\theta_1 + \mu_2\Gamma_1 \sqrt{p}}$ where $p = 1 - [(\Gamma_1/\Gamma_2)\sin\theta_1]^2$	$R_{\perp} = R_h$ found from $\varepsilon_2/\varepsilon_1$. Hence, $R_{\perp} = R_h = \dfrac{\varepsilon_2}{\varepsilon_1}$ $= \dfrac{2\mu_2\Gamma_1 \cos\theta_1}{\mu_2\Gamma_1 \cos\theta_1 + \mu_1\Gamma_2 \cos\theta_2}$ $= \dfrac{2\mu_2\Gamma_1 \cos\theta_1}{\mu_2\Gamma_1 \cos\theta_1 + \mu_1\Gamma_2 \sqrt{p}}$ where p is as to the left	Generalized refraction $H_2 = RH_1$, $\varepsilon_2 = R\varepsilon_1$. R is coefficient of *refraction*

TABLE 44. ELECTROMAGNETIC REFLECTION AND REFRACTION.—(*Continued*)

Steps	*Electric vector* $\mathfrak{E}$ is *parallel* with XY plane or in XY plane (Fig. 220*a*), corresponds to *vertical polarization*	*Electric vector* $\mathfrak{E}$ is *perpendicular* to XY plane (Fig. 220*b*), corresponds to *horizontal polarization*	Remarks
18	For perpendicular wave incidence ($\theta_1 = 0°$) $$R_{\parallel} = R_v = \frac{2\mu_1\Gamma_2}{\mu_1\Gamma_2 + \mu_2\Gamma_1} = R_h = R_{\perp}$$ we obtain not only the *same* magnitude for either type of polarization but also the *same* polarity		
19	The generalized expressions in steps 15 and 17 reduce to the corresponding values, holding for perfect dielectrics ($\sigma = 0$), as given in steps 5, 7, 8, 9, and 10 for the coefficient of reflection. The subscripts $\parallel$ and $\perp$ are used together with the subscripts v and h in formulas, since in texts on physical optics it is customary to speak of polarizations parallel and perpendicular to the plane of incidence, respectively. If an electromagnetic wave passes from a dielectric medium μ_1, κ_1 into a medium μ_2, κ_2 which also has no conductivity and for such a condition that the dielectric constant of medium 2 is smaller, we have for air as medium 2 and a nonferromagnetic medium 1 $$\mu_1 = \mu_0 = \mu_2; \qquad \kappa_2 \cong \kappa_0$$ $$n = \frac{n_2}{n_1} = \frac{\frac{v_2}{3 \times 10^8}}{\frac{v_1}{3 \times 10^8}} = \frac{\frac{1}{\sqrt{\mu_2\kappa_2}}}{\frac{1}{\sqrt{\mu_1\kappa_1}}} = \sqrt{\frac{\kappa_1}{\kappa_0}} = \sqrt{\kappa_r}$$ The relative index of refraction n between the two dielectric mediums is then equal to the square root of the relative numerical dielectric constant κ_r of medium 1 (which is the denser medium). But according to Snell, we have $n \sin \theta_2 = \sin \theta_1$ and for an angle θ_1 of incidence, resulting in a value $\sin \theta_1 = n$, we must have $$\sin \theta_1 = n = \sqrt{\kappa_r} = \underbrace{\sin \theta_1 = n \sin 90°}_{\text{Snell's refraction law}} = n \sin \theta_2$$	Special case in perfect dielectrics
	i.e., θ_2, which is the angle of refraction into the less electrically dense medium (air), must be 90 space degrees. The refracted ray, therefore, emerges at grazing angle, *i.e.*, tangent to the plane of medium separation. For angles θ_1 larger than the critical angle θ_c, *i.e.*,	*Total reflection; no electromagnetic power transfer from a denser me-*

$$\theta_1 = > \theta_c = \sin^{-1}(n) = \sin^{-1}(\sqrt{\kappa_r})$$

total reflection takes place, since the characteristic impedance into the medium μ_2, κ_2 for such incident waves becomes infinite. We note, therefore, that the abrupt dielectric change at the plane of separation can, for certain angles of incidence, render the medium a perfect obstacle, even though only a dielectric. For the critical incidence, we have likewise no power transmission into medium 2, but besides the reflected beam also a so-called "tangential" wave along the common interface

For angles of incidence $\theta_1 > \theta_c$, the relative index of refraction requires that $\sin \theta_2$ becomes larger than unity. We cannot realize such a condition except for imaginary values of $\cos \theta_2$, holding for $\sin \theta_1 > n$ (for details consult step 30)

dium into a less dense dium for

$$\sin \theta_1 \geqq \sqrt{\kappa_r} \geqq n$$

20 For both representations of Fig. 220, the phase factor F_2 of the refracted beam is

$$F_2 = \epsilon^{j\omega\left(t - \frac{y \sin \theta_2 + x \cos \theta_2}{v_2}\right)}$$

since $\mathcal{E}_2 = R\mathcal{E}_1 F_2$ is the expression of the electric field of the refracted beam in terms of the incident value, where R denotes the coefficient of refraction, which is different for vertical and horizontal polarizations. Since $R\mathcal{E}_1$ in this expression is the reduced amplitude at the surface of separation of respective mediums, when the refracted beam just enters medium μ_2, κ_2, it must be F_2, which accounts for all propagation properties. Even for a perfect dielectric, we may expect attenuation when an *imaginary* value for $\cos \theta_2$ is effective, since F_2 has y and x components, so that

Imaginary angles correspond to a decay of amplitude for perfect dielectrics

$$F_2 = \underbrace{\epsilon^{j\omega\left(t - \frac{\sin \theta_2}{v_2} y\right)}}_{\substack{\text{wave along } Y \text{ axis parallel to surface of separation}}} \underbrace{\epsilon^{-j\frac{\omega \cos \theta_2}{v_2} x}}_{\substack{\text{wave along } X \text{ axis, straight into medium } \mu_2,\ \kappa_2}}$$

But

$$\cos \theta_2 = \sqrt{1 - \sin^2 \theta_2} = \underbrace{\sqrt{1 - n^2 \sin^2 \theta_1}}_{\text{for real angles}}$$

$$\cos \theta_2 = -j \underbrace{\sqrt{n^2 \sin^2 \theta_1 - 1}}_{\text{for imaginary values}}$$

TABLE 44. ELECTROMAGNETIC REFLECTION AND REFRACTION.—(*Continued*)

Steps	*Electric vector* $\mathcal{E}$ is *parallel* with XY plane or in XY plane (Fig. 220*a*), corresponds to *vertical polarization*	*Electric vector* $\mathcal{E}$ is *perpendicular* to XY plane (Fig. 220*b*), corresponds to *horizontal polarization*	Remarks
	and the term along the X axis becomes $\epsilon^{-j\frac{\omega\cos\theta_2}{v_2}x} = \epsilon^{-\frac{\omega\sqrt{n^2\sin^2\theta_1-1}}{v_2}x}$ This result has a *real* negative exponent, and means a decay of the amplitude associated with this phase factor along the X direction		
21	The incident $\mathcal{E}_1$, H_1, transmitted (refracted) $\mathcal{E}_2$, H_2, and reflected $\mathcal{E}_3$, H_3 components, according to Fig. 220, have the phase factors $F_1 = \epsilon^{j\omega\left(t-\frac{y\sin\theta_1+x\cos\theta_1}{v_1}\right)}$ for incident waves; $F_2 = \epsilon^{j\omega\left(t-\frac{y\sin\theta_2+x\cos\theta_2}{v_2}\right)}$ for refracted (transmitted) waves; $F_3 = \epsilon^{j\omega\left(t-\frac{y\sin\theta_1-x\cos\theta_1}{v_1}\right)}$ for reflected waves. In an isotropic dielectric, we have a space impedance $Z = \sqrt{\mu/\kappa}$ ohms and a plane wave along the $\pm X$ direction, due to the reflection at the YZ plane of separation. For $\mathcal{E}_z$ and H_y field associations, we have $\mathcal{E}_z = \underbrace{Z_1 A\epsilon^{j\omega t-x\Gamma_1}}_{\text{incident}} - \underbrace{Z_1 B\epsilon^{j\omega t+x\Gamma_1}}_{\text{reflected}}$, $H_y = \underbrace{A\epsilon^{j\omega t-x\Gamma_1}}_{\text{incident}} + \underbrace{B\epsilon^{j\omega t+x\Gamma_1}}_{\text{reflected}}$; $\Gamma_1 = j\omega\sqrt{\mu_1\kappa_1}$. Hence, for vertical and horizontal polarizations (Fig. 220)		$\sigma_1 = 0$; $\sigma_2 = 0$; $v_1 = \frac{1}{\sqrt{\mu_1\kappa_1}}$ m/sec; $v_2 = \frac{1}{\sqrt{\mu_2\kappa_2}}$ m/sec; $Z_1 = \sqrt{\frac{\mu_1}{\kappa_1}}$ ohms; $Z_2 = \sqrt{\frac{\mu_2}{\kappa_2}}$ ohms; $\rho = B/A$ and $R = C/A$ are reflection and refraction coefficients
	Just as explained in detail to the right, we find: $H_1 = AF_1$ for incident wave; $H_3 = BF_3$ for reflected wave; $H_2 = CF_2$ for refracted wave } in medium μ_1, κ_1	$\mathcal{E}_1 = Z_1AF_1$ for incident wave; $\mathcal{E}_3 = -Z_1BF_3$ for reflected wave; $\mathcal{E}_2 = Z_2CF_2$ for refracted wave } in μ_1, κ_1. In medium 1, we have the total electric field	

In medium 1, we have the total tangential field $H'_x = AF_1 + BF_3$. In medium 2, the tangential field is $H''_x = H_2 = CF_2$. For the electric vector, we have

$$\mathcal{E} = \sqrt{\mathcal{E}_x^2 + \mathcal{E}_y^2} = \mathcal{E}\sqrt{\sin^2\theta + \cos^2\theta}.$$

For $\mathcal{E}_1$, we find

$$\left.\begin{aligned} \mathcal{E}_{1_x} &= Z_1 AF_1 \sin\theta_1 \\ \mathcal{E}_{1_y} &= -Z_1 AF_1 \cos\theta_1 \end{aligned}\right\} \text{incident in medium 1}$$

with the corresponding reflected components

$$\left.\begin{aligned} \mathcal{E}_{3_x} &= Z_1 BF_3 \sin\theta_1 \\ \mathcal{E}_{3_y} &= Z_1 BF_3 \cos\theta_1 \end{aligned}\right\} \text{reflected in medium 1}$$

For $\mathcal{E}_2$, we have the corresponding refracted components

$$\left.\begin{aligned} \mathcal{E}_{2_x} &= Z_2 CF_2 \sin\theta_2 \\ \mathcal{E}_{2_y} &= -Z_2 CF_2 \cos\theta_2 \end{aligned}\right\} \text{transmitted in medium 2}$$

We have then

$$\left.\begin{aligned} \mathcal{E}'_x &= (AF_1 + BF_3)Z_1 \sin\theta_1 \\ \mathcal{E}'_y &= (BF_3 - AF_1)Z_1 \cos\theta_1 \end{aligned}\right\} \text{total components in medium 1}$$

and

$$\left.\begin{aligned} \mathcal{E}''_x &= Z_2 CF_2 \sin\theta_2 \\ \mathcal{E}''_y &= -Z_2 CF_2 \cos\theta_2 \end{aligned}\right\} \text{total components in medium 2}$$

$\mathcal{E}'_x = \mathcal{E}_1 + \mathcal{E}_3 = Z_1(AF_1 - BF_3)$. In medium 2, we have only $\mathcal{E}''_x = \mathcal{E}_2 = Z_2 CF_2$. For the magnetic fields, we have x and y components for H_1, H_2, and H_3, where generally

$$H = \sqrt{H_x^2 + H_y^2}$$

for $H_x = H\sin\theta$ and $H_y = H\cos\theta$. For incident wave, H_1 has the components

$$\left.\begin{aligned} H_{1_x} &= -AF_1 \sin\theta_1 \\ H_{1_y} &= AF_1 \cos\theta_1 \end{aligned}\right\} \text{incident in medium } \mu_1, \kappa_1$$

The corresponding reflected components are

$$\left.\begin{aligned} H_{3_x} &= BF_3 \sin\theta_1 \\ H_{3_y} &= BF_3 \cos\theta_1 \end{aligned}\right\} \text{reflected in medium } \mu_1, \kappa_1$$

In medium μ_2, κ_2, we have only a refracted wave of resultant H_2, with components

$$\left.\begin{aligned} H_{2_x} &= -CF_2 \sin\theta_2 \\ H_{2_y} &= CF_2 \cos\theta_2 \end{aligned}\right\} \text{transmitted in medium 2}$$

In medium 1, we have the total components

$$H'_x = (BF_3 - AF_1)\sin\theta_1$$
$$H'_y = (BF_3 + AF_1)\cos\theta_1$$

In medium 2 we have

$$H''_x = -CF_2 \sin\theta_2$$
$$H''_y = CF_2 \cos\theta_2$$

22 In exactly the same manner as with energy tubes (Fig. 218), the coefficient of reflection and the coefficient of refraction can be derived by observing the boundary conditions for which Fig. 220*a* and *b* yields at $x = 0$

$$F_1 = F_3; \qquad F_1 = \epsilon^{j\omega\left(t - \frac{y\sin\theta_1}{v_1}\right)}; \qquad F_2 = \epsilon^{j\omega\left(t - \frac{y\sin\theta_2}{v_2}\right)}$$

since $x\cos\theta_1 = 0$ at the XZ plane

For dielectrics, R_v and R_h are the coefficients of *refraction* for vertical and horizontal polarizations, ρ_v and ρ_h are the corresponding co-

TABLE 44. ELECTROMAGNETIC REFLECTION AND REFRACTION.—(*Continued*)

Steps	*Electric vector* $\mathcal{E}$ is *parallel* with XY plane or in XY plane (Fig. 220*a*), corresponds to *vertical polarization*	*Electric vector* $\mathcal{E}$ is *perpendicular* to XY plane (Fig. 220*b*), corresponds to *horizontal polarization*	Remarks
	Tangential components $H_x' = H_x''$ or $(A + B)F_1 = CF_2$; $(1 + \rho_v)F_1 = R_vF_2$. If divided by A, tangential components $\mathcal{E}_y' = \mathcal{E}_y''$ or $Z_1F_1(B - A)\cos\theta_1 = -Z_2CF_2\cos\theta_2$ divided by A yields the other relation $Z_1(\rho_v - 1)F_1\cos\theta_1 + Z_2R_vF_2\cos\theta_2 = 0$ for finding ρ_v and R_v. Putting $a = Z_1\cos\theta_1$ and $b = Z_2\cos\theta_2$, we find $\rho_v = \dfrac{a-b}{a+b}$; $R_v = \dfrac{2a}{a+b}\dfrac{F_1}{F_2}$ where $\dfrac{F_1}{F_2} = \epsilon^{j\omega y\left(\frac{\sin\theta_2}{v_2} - \frac{\sin\theta_1}{v_1}\right)} = 1$ since $\dfrac{\sin\theta_2}{v_2} = \dfrac{\frac{v_2}{v_1}\sin\theta_1}{v_2}$ For any angle θ_1 of incidence $\underline{\rho_v} = \rho_\parallel = \dfrac{Z_1\cos\theta_1 - Z_2\cos\theta_2}{Z_1\cos\theta_1 + Z_2\cos\theta_2} = \dfrac{Z_1\sqrt{1 - \left(\frac{n_1}{n_2}\right)^2\sin^2\theta_1} - Z_2\cos\theta_1}{Z_1\sqrt{1 - \left(\frac{n_1}{n_2}\right)^2\sin^2\theta_1} + Z_2\cos\theta_1}$	Tangential components $\mathcal{E}_z' = \mathcal{E}_z''$, yield $Z_1F_1(A - B) = Z_2CF_2$ or $Z_1F_1(1 - \rho_h) = Z_2R_hF_2$, which is one equation for solving ρ_h and R_h values. Components $H_y' = H_y''$ yield $F_1(A + B)\cos\theta_1 = CF_2\cos\theta_2$ or $(1 + \rho_h)F_1\cos\theta_1 = R_hF_2\cos\theta_2$, which is the other equation with ρ_h and R_h terms. Putting $d = Z_1\cos\theta_2$ and $e = Z_2\cos\theta_1$, we find $\rho_h = \dfrac{d-e}{d+e}$ $R_h = \dfrac{2e}{d+e}\dfrac{Z_1}{Z_2}\dfrac{F_1}{F_2}$ where $F_1/F_2 = 1$ is as to the left. For any angle θ_1 of incidence $\underline{\rho_h} = \rho_\perp = \dfrac{Z_1\cos\theta_2 - Z_2\cos\theta_1}{Z_1\cos\theta_2 + Z_2\cos\theta_1} = \dfrac{Z_1\sqrt{1 - \frac{\sin^2\theta_1}{n^2}} - Z_2\cos\theta_1}{Z_1\sqrt{1 - \frac{\sin^2\theta_1}{n^2}} + Z_2\cos\theta_1}$ $R_h = R_\perp = \dfrac{2Z_1\cos\theta_1}{Z_1\sqrt{1 - \frac{\sin^2\theta_1}{n^2}} + Z_2\cos\theta_1}$	efficients of *reflection*. $\sigma_1 = 0 = \sigma_2$ $n_1 = \dfrac{3\times10^8}{v_1} = 3\times10^8\sqrt{\mu_1\kappa_1}$ $n_2 = \dfrac{3\times10^8}{v_2} = 3\times10^8\sqrt{\mu_2\kappa_2}$ and the relative index of refraction from medium 1 into medium 2 is $n = \dfrac{n_2}{n_1} = \dfrac{v_1}{v_2}$ since $\sigma_1 = 0 = \sigma_2$. For $\mu_1 = \mu_0 = \mu_2$, $n = \sqrt{\dfrac{\kappa_2}{\kappa_1}}$ $Z_1 = \sqrt{\dfrac{\mu_1}{\kappa_1}}$ ohms $Z_2 = \sqrt{\dfrac{\mu_2}{\kappa_2}}$ ohms ρ_v is a case of $\rho_\parallel$, and ρ_h is a case of $\rho_\perp$ and

	where $n = n_2/n_1$ and $R_v = R_\parallel = \dfrac{2Z_1 \cos\theta_1}{Z_1 \cos\theta_1 + Z_2\sqrt{1 - \dfrac{\sin^2\theta_1}{n^2}}}$		similarly for R_v and R_h
23	In medium 1, the incident electromagnetic wave arrives under a wave impedance $+Z_1 \cos\theta_1$, while the reflected wave experiences a value $-Z_1 \cos\theta_1$, and the refracted (transmitted) electromagnetic wave experiences an impedance $Z_2 \cos\theta_2$ as it leaves the plane of medium separation. Therefore, at the plane of separation, the incident beam experiences a medium 2 impedance $Z_2 \cos\theta_2$ ohms, which is *not matched* to the impedance $Z_1 \cos\theta_1$. The compensation is brought about by the impedance of the reflected wave	The arriving incident wave experiences an impedance $-Z_1/(\cos\theta_1)$ on the medium 1 side at the plane of separation, and the reflected wave an impedance $+Z_1/(\cos\theta_1)$, while the refracted (transmitted) wave experiences an impedance of $-Z_2/(\cos\theta_2)$ ohms Also here at the plane of separation, the impedance of the arriving incident wave is *not matched* with respect to the impedance of the wave leaving the other face of the plane of separation and moving in medium 2	Wave impedances at the plane of medium separation
24	These results show that for normal incidence, the second medium acts with the space impedance $Z_2 = \sqrt{\mu_2/\kappa_2}$ ohms and also cannot be matched against $Z_1 = \sqrt{\mu_1/\kappa_1}$ ohms unless the transmitted beam (refracted beam, which is now a straightforward beam into medium 2) carries all the field energy that is available from the incident beam. This can, however, happen only when both dielectrics are identical		
25	The correctness of the impedance expression $Z_1 \cos\theta_1$ for the incident wave under any angle θ_1 can also be found for general mediums where we deal with propagation constants Γ_1 and Γ_2 as in steps 10 to 18. Since for plane waves, the impedance is the ratio of the electric field di-	For Fig. 220*b*, the magnetic H_1 field has two components H_x and H_y of which only H_y is of interest, since it is parallel with the plane of medium separation. We have for this component $H_y = H_0 \cos\theta_1 \epsilon^{-r_1\Gamma_1}$ amp/m For the $\mathcal{E}_1$ field of the incident wave we have	General case σ_1, μ_1, κ_1 and σ_2, μ_2, κ_2. $\kappa_c = \kappa - j(\sigma_1/\omega)$ farads/m, according to Eq. (3)

TABLE 44. ELECTROMAGNETIC REFLECTION AND REFRACTION.—(*Continued*)

Steps	*Electric vector* $\mathcal{E}$ is *parallel* with XY plane or in XY plane (Fig. 220*a*), corresponds to *vertical polarization*	*Electric vector* $\mathcal{E}$ is *perpendicular* to XY plane (Fig. 220*b*), corresponds to *horizontal polarization*	Remarks
	vided by the associated perpendicular magnetic field, we have, for the incident wave of Fig. 219 and Fig. 220*a*, $\mathcal{E}_1 = \mathcal{E}_0\epsilon^{-r_1\Gamma_1}$, $H_1 = H_0\epsilon^{-r_1\Gamma_1}$, $\frac{\mathcal{E}_0}{H_0} = Z_1$, $Z_1 = \sqrt{\mu/\kappa_e}$. The omitted time factor $\epsilon^{j\omega t}$ is understood; $r_1 = y \sin\theta_1 - x\cos\theta_1$; r_1 is distance from origin O of the XYZ system along the wave normal; H_1 is normal to the plane of incidence (along the Z direction); and $H_z = H_0\epsilon^{-r_1\Gamma_1}$. $\mathcal{E}_1$ has an $\mathcal{E}_x$ and an $\mathcal{E}_y$ component of which $\mathcal{E}_y$ is parallel to the plane of separation as is H_z, and $\mathcal{E}_y = \mathcal{E}_0\epsilon^{-r_1\Gamma_1}\cos\theta_1$. Hence, impedance in the direction perpendicular to the plane of separation is $\frac{\mathcal{E}_y}{H_z} = \frac{\mathcal{E}_0\cos\theta_1}{H_0} = Z_1\cos\theta_1$ ohms	only a field $\mathcal{E}_z$, which is likewise parallel with the plane of separation and given by $\mathcal{E}_z = \mathcal{E}_0\epsilon^{-r_1\Gamma_1}$ volts/m Therefore, impedance in the direction perpendicular to the plane of separation is $\frac{\mathcal{E}_z}{H_y} = \frac{\mathcal{E}_0}{H_0\cos\theta_1} = \frac{Z_1}{\cos\theta_1}$ ohms	
	In exactly the same way the respective impedances for the reflected and refracted waves are confirmed		
26	Fresnel formulas as found in optics express the coefficients of *reflection* and *refraction* with the indices n_1 and n_2 eliminated. We find from step 5 and $n = \frac{n_2}{n_1} = \frac{\sin\theta_1}{\sin\theta_2}$		Fresnel formulas for *perfect* dielectric mediums $\sigma_1 = 0 = \sigma_2$ $\mu_1 = \mu_0 = \mu_2$

$$\rho_v = \frac{\kappa_2 \cos\theta_1 - n\kappa_1 \cos\theta_2}{\kappa_2 \cos\theta_1 + n\kappa_1 \cos\theta_2}$$

$$= \frac{\frac{\kappa_2}{\kappa_1}\cos\theta_1 - n\cos\theta_2}{\frac{\kappa_2}{\kappa_1}\cos\theta_1 + n\cos\theta_2}$$

$$= \frac{n^2\cos\theta_1 - n\cos\theta_2}{n^2\cos\theta_1 + n\cos\theta_2}$$

$$= \frac{n\cos\theta_1 - \cos\theta_2}{n\cos\theta_1 + \cos\theta_2}$$

$$= \frac{\frac{\sin\theta_1}{\sin\theta_2}\cos\theta_1 - \cos\theta_2}{\frac{\sin\theta_1}{\sin\theta_2}\cos\theta_1 + \cos\theta_2}$$

$$= \frac{\sin\theta_1\cos\theta_1 - \sin\theta_2\cos\theta_2}{\sin\theta_1\cos\theta_1 + \sin\theta_2\cos\theta_2}$$

$$= \frac{\sin(2\theta_1) - \sin(2\theta_2)}{\sin(2\theta_1) + \sin(2\theta_2)}$$

$$= \frac{2\sin(\theta_1 - \theta_2)\cos(\theta_1 + \theta_2)}{2\sin(\theta_1 + \theta_2)\cos(\theta_1 - \theta_2)}$$

$$= \frac{\tan(\theta_1 - \theta_2)}{\tan(\theta_1 + \theta_2)} = \rho_v = \rho_\parallel$$

This is the *first* Fresnel equation

$$\rho_h = \frac{\cos\theta_1 - n\cos\theta_2}{\cos\theta_1 + n\cos\theta_2}$$

$$= \frac{\cos\theta_1 - \frac{\sin\theta_1}{\sin\theta_2}\cos\theta_2}{\cos\theta_1 + \frac{\sin\theta_1}{\sin\theta_2}\cos\theta_2}$$

$$= \frac{\cos\theta_1\sin\theta_2 - \sin\theta_1\cos\theta_2}{\cos\theta_1\sin\theta_2 + \sin\theta_1\cos\theta_2}$$

$$= \frac{-(\sin\theta_1\cos\theta_2 - \cos\theta_1\sin\theta_2)}{\sin\theta_1\cos\theta_2 + \cos\theta_1\sin\theta_2}$$

$$= \frac{-\sin(\theta_1 - \theta_2)}{\sin(\theta_1 + \theta_2)}$$

$$= \frac{\sin(\theta_2 - \theta_1)}{\sin(\theta_2 + \theta_1)}$$

$$\rho_h = \rho_\perp = \frac{\sin(\theta_2 - \theta_1)}{\sin(\theta_2 + \theta_1)}$$

This is the *second* Fresnel equation

In the same way, we can derive the trigonometric Fresnel expressions for the coefficient R_v and R_h of *refraction*, by using relations in Step 22

$$n = \frac{n_2}{n_1} = \sqrt{\frac{\kappa_2}{\kappa_1}}$$

$$Z_1 = \sqrt{\frac{\mu_1}{\kappa_1}} \quad \text{ohms}$$

$$Z_2 = \sqrt{\frac{\mu_2}{\kappa_2}} \quad \text{ohms}$$

$$\frac{Z_1}{Z_2} = \sqrt{\frac{\mu_0\kappa_2}{\mu_0\kappa_1}}$$

$$= \sqrt{\frac{\kappa_2}{\kappa_1}} = n = \frac{\sin\theta_1}{\sin\theta_2}$$

Coefficients of reflection ρ and refraction R are *real* for $\sigma_1 = 0 = \sigma_2$, and both the reflected and refracted waves are either in phase or in antiphase with the incident wave. We must distinguish between the relative index n of refraction $n = n_{12}$

$= v_1/v_2 = n_2/n_1$

$= (\sin\theta_1)/(\sin\theta_2)$ for medium 2 with respect to medium 1, and $n' = n_{21} = 1/n$

$= (\sin\theta_2/\sin\theta_1)$ for medium 1 with respect to medium 2

TABLE 44. ELECTROMAGNETIC REFLECTION AND REFRACTION.—(*Continued*)

Steps	*Electric vector* $\mathcal{E}$ is *parallel* with XY plane or in XY plane (Fig. 220*a*), corresponds to *vertical polarization*	*Electric vector* $\mathcal{E}$ is *perpendicular* to XY plane (Fig. 220*b*), corresponds to *horizontal polarization*	Remarks
26 (*Cont.*)	$R_v = \dfrac{2a}{a+b}$	$R_h = \dfrac{2e}{d+e}\dfrac{Z_1}{Z_2}$	
	$= \dfrac{2Z_1 \cos\theta_1}{Z_1 \cos\theta_1 + Z_2 \cos\theta_2}$	$= \dfrac{2Z_2 \cos\theta_1}{Z_1 \cos\theta_2 + Z_2 \cos\theta_1}\dfrac{Z_1}{Z_2}$	
	$= \dfrac{2\dfrac{Z_1}{Z_2}\cos\theta_1}{\dfrac{Z_1}{Z_2}\cos\theta_1 + \cos\theta_2}$	$= \dfrac{2\dfrac{Z_1}{Z_2}\cos\theta_1}{\dfrac{Z_1}{Z_2}\cos\theta_2 + \cos\theta_1}$	
	$= \dfrac{2n\cos\theta_1}{n\cos\theta_1 + \cos\theta_2}$	$= \dfrac{2n\cos\theta_1}{n\cos\theta_2 + \cos\theta_1}$	
	$= \dfrac{2\dfrac{\sin\theta_1}{\sin\theta_2}\cos\theta_1}{\dfrac{\sin\theta_1}{\sin\theta_2}\cos\theta_1 + \cos\theta_2}$	$= \dfrac{2\dfrac{\sin\theta_1}{\sin\theta_2}\cos\theta_1}{\dfrac{\sin\theta_1}{\sin\theta_2}\cos\theta_2 + \cos\theta_1}$	
	$= \dfrac{2\sin\theta_1\cos\theta_1}{\sin\theta_1\cos\theta_1 + \sin\theta_2\cos\theta_2}$	$= \dfrac{2\sin\theta_1\cos\theta_1}{\sin\theta_1\cos\theta_2 + \cos\theta_1\sin\theta_2}$	
	$= \dfrac{\sin(2\theta_1)}{\frac{1}{2}[\sin(\theta_1+\theta_1) + \sin(\theta_1-\theta_1) + \sin(\theta_2+\theta_2) + \sin(\theta_2-\theta_2)]}$		
	$= \dfrac{2\sin(2\theta_1)}{\sin(2\theta_1) + \sin(2\theta_2)}$	$R_h = R_\perp = \dfrac{\sin(2\theta_1)}{\sin(\theta_1+\theta_2)}$	
	$= \dfrac{2\sin(2\theta_1)}{2\sin(\theta_1+\theta_2)\cos(\theta_1-\theta_2)}$	*from medium* 1 *into medium* 2	
	$= \dfrac{\sin(2\theta_1)}{\sin(\theta_1+\theta_2)\cos(\theta_1-\theta_2)} = R_v = R_\parallel$	$R_h' = \dfrac{2n'\cos\theta_1}{n'\cos\theta_2 + \cos\theta_1}$	

from medium 1 *into medium* 2;

$$R_v' = \frac{2n' \cos\theta_1}{n' \cos\theta_1 + \cos\theta_2} = \frac{2\dfrac{\sin\theta_2}{\sin\theta_1}\cos\theta_1}{\dfrac{\sin\theta_2}{\sin\theta_1}\cos\theta_1 + \cos\theta_2} = \frac{2\sin\theta_2\cos\theta_1}{\sin\theta_2\cos\theta_1 + \cos\theta_2\sin\theta_1} = \frac{2\cos\theta_1\sin\theta_2}{\sin(\theta_1+\theta_2)} = R_v' = R_\parallel'$$

from medium 2 *into medium* 1

$$= \frac{2\dfrac{\sin\theta_2}{\sin\theta_1}\cos\theta_1}{\dfrac{\sin\theta_2}{\sin\theta_1}\cos\theta_2 + \cos\theta_1} = \frac{2\sin\theta_2\cos\theta_1}{\sin\theta_2\cos\theta_2 + \sin\theta_1\cos\theta_1}$$

$$R_h' = R'_\perp = \frac{2\cos\theta_1\sin\theta_2}{\sin(\theta_1+\theta_2)\cos(\theta_1-\theta_2)}$$

from medium 2 *into medium* 1

The above relations can also be confirmed by means of the general propagation constant $\Gamma = j\omega\sqrt{\mu\kappa_e}$, $\kappa_e = \kappa - j(\sigma/\omega)$ farads/m, which for $\sigma_1 = 0 = \sigma_2$ mhos/m gives for respective mediums $\Gamma_1 = j\omega\sqrt{\mu_1\kappa_1} = j\beta_1$ and $\Gamma_2 = j\omega\sqrt{\mu_2\kappa_2} = j\beta_2$, where $\mu_1 = \mu_0 = \mu_2$, and from step 17

$$R_v = \frac{2\mu_0\omega\sqrt{\mu_0\kappa_2}\cos\theta_1}{\mu_0\omega\sqrt{\mu_0\kappa_2}\cos\theta_1 + \mu_0\omega\sqrt{\mu_0\kappa_1}\cos\theta_2} = \frac{2\sqrt{\kappa_2}\cos\theta_1}{\sqrt{\kappa_2}\cos\theta_1 + \sqrt{\kappa_1}\cos\theta_2} = \frac{2\sqrt{\dfrac{\kappa_2}{\kappa_1}}\cos\theta_1}{\sqrt{\dfrac{\kappa_2}{\kappa_1}}\cos\theta_1 + \cos\theta_2} = \frac{2n\cos\theta_1}{n\cos\theta_1 + \cos\theta_2}$$

as found above

$$R_h = \frac{2\mu_0\omega\sqrt{\mu_0\kappa_1}\cos\theta_1}{\mu_0\omega\sqrt{\mu_0\kappa_1}\cos\theta_1 + \mu_0\omega\sqrt{\mu_0\kappa_2}\cos\theta_2} = \frac{2\sqrt{\kappa_1}\cos\theta_1}{\sqrt{\kappa_1}\cos\theta_1 + \sqrt{\kappa_2}\cos\theta_2} = \frac{2\cos\theta_1}{\cos\theta_1 + \sqrt{\dfrac{\kappa_2}{\kappa_1}}\cos\theta_2} = \frac{2\cos\theta_1}{\cos\theta_1 + n\cos\theta_2}$$

TABLE 44. ELECTROMAGNETIC REFLECTION AND REFRACTION.—(*Continued*)

Steps	*Electric vector* $\mathcal{E}$ is *parallel* with XY plane or in XY plane (Fig. 220*a*), corresponds to *vertical polarization*	*Electric vector* $\mathcal{E}$ is *perpendicular* to XY plane (Fig. 220*b*), corresponds to *horizontal polarization*	Remarks
27	As angle θ_1 of incidence and angle θ_2 of refraction approach and become zero, the refraction law $(\sin\theta_1)/(\sin\theta_2) = n$ becomes $\theta_1 \cong n\theta_2$ for θ in radians (numeric) and we find $\rho_v = \dfrac{\theta_1 - n\theta_2}{\theta_1 + n\theta_2}$; $\rho_h = -\dfrac{\theta_1 - n\theta_2}{\theta_1 + n\theta_2} = -\rho_v$ yielding the same absolute magnitudes for respective coefficients ρ_v and ρ_h of reflection for an angle θ_1 of incidence equal to zero or close to it		
28	Fresnel formulas, as used in optics, express the coefficients of reflection and refraction without the use of the index of refraction, since the equivalent trigonometric relations are used and $(\sin\theta_1)/(\sin\theta_2)$ takes the place of $n = n_2/n_1$. It is especially the Fresnel relations for the coefficients of reflection that play a significant part as far as a decided distinction between vertical and horizontal polarization is concerned. We have then		*Perfect* dielectric mediums, *Brewster angle* for *total* transmission in the case of *vertical* polarization. $\rho = \dfrac{\mathcal{E}_3}{\mathcal{E}_1} = \dfrac{H_3}{H_1}$ $R = \dfrac{\mathcal{E}_2}{\mathcal{E}_1} = \dfrac{H_2}{H_1}$ $\mathcal{E}_1$ is incident, $\mathcal{E}_2$ is refracted (transmitted into medium μ_2, κ_2, $\sigma_2 = 0$). $\mathcal{E}_3$ is reflected back into medium μ_1, κ_1, $\sigma_1 = 0$. ρ_v and R_v apply to TM waves, and ρ_h and R_h to TE waves shows that for $\theta_1 = \theta_B$ we have com-
	Classic Fresnel formula $\rho_v = \rho_\parallel = \dfrac{\tan(\theta_1 - \theta_2)}{\tan(\theta_1 + \theta_2)}$ from step 26. In step 23 the quantity $Z_1 \cos\theta_1$ is the wave impedance of the incident wave in the direction perpendicular to the plane of medium separation, and $-Z_1 \cos\theta_1$ holds for the reflected wave. We have $Z_2 \cos\theta_2$ ohms for the refracted wave at the plane of separation, which is *not* matched against $Z_1 \cos\theta_1$ ohms. Therefore,	Classic Fresnel formula $\rho_h = \rho_\perp = \dfrac{\sin(\theta_2 - \theta_1)}{\sin(\theta_1 + \theta_2)}$ from step 26. In step 23 the quantities $-Z_1/(\cos\theta_1)$, $+Z_1/(\cos\theta_1)$, and $-Z_2/(\cos\theta_2)$ ohms are the respective wave impedances normal to interface of respective mediums for the incident, reflected, and refracted waves, respectively. Hence, the mismatch from medium 1 of the incident wave into medium 2 of the refracted wave causes the reflection coefficient	

$$\rho_v = \frac{Z_1 \cos\theta_1 - Z_2 \cos\theta_2}{Z_1 \cos\theta_1 + Z_2 \cos\theta_2}$$

which leads, according to step 26, to the classic Fresnel formula

If in the expression for ρ_v, we have $\theta_1 + \theta_2 = 90°$, then $\tan(\theta_1 + \theta_2) = \tan 90° = \infty$ and $\rho_v = 0$. This means that there is no field energy reflection back into medium 1, and the *entire incident wave energy passes into medium* 2. This is what is known as "total transmission into medium 2." The angle of incidence $\theta_1 = \theta_B$, for which the above condition happens, is known as the "Brewster angle" or "polarizing angle." The Brewster angle introduced into Snell's *refraction* law gives a means for obtaining the condition for this angle. We find then

$$\theta_B + \theta_2 = 90°$$

$$\underbrace{n_1 \sin\theta_B = n_2 \sin\theta_2}_{\text{Snell's law}}$$

$$\sin\theta_2 = \sin(90° - \theta_B) = \cos\theta_B$$

$$n_1 \sin\theta_B = n_2 \cos\theta_B$$

or

$$\tan\theta_B = \frac{n_2}{n_1} = n = \frac{\dfrac{3 \times 10^8}{v_2}}{\dfrac{3 \times 10^8}{v_1}} = \frac{v_1}{v_2}$$

$$= \frac{\sqrt{\mu_2 \kappa_2}}{\sqrt{\mu_1 \kappa_1}} = \sqrt{\frac{\kappa_2}{\kappa_1}}$$

$$\rho_h = \frac{\dfrac{Z_1}{\cos\theta_1} - \dfrac{Z_2}{\cos\theta_2}}{\dfrac{Z_1}{\cos\theta_1} + \dfrac{Z_2}{\cos\theta_2}}$$

$$= \frac{Z_1 \cos\theta_2 - Z_2 \cos\theta_1}{Z_1 \cos\theta_2 + Z_2 \cos\theta_1}$$

yielding the classic Fresnel formula

According to the ρ_h formula, there is *no* angle of incidence for horizontal polarization that causes total transmission into medium 2. Therefore, the Brewster angle θ_B is a characteristic feature in the case of *vertical* polarization. Therefore, when an electromagnetic wave is unpolarized and contains vertical and horizontal polarization components, we obtain, in medium 1, a horizontally polarized reflected wave, while the components with vertical polarization pass into medium 2, if incident under the Brewster angle θ_B. This means that we have polarization *separation*. This is the reason why this angle is also known as the polarization angle

plete *extinction* of the reflected wave and in medium 1 a condition of the free-field intensity in the case of *vertical* polarization (unobstructed radiation fields in medium μ_1, κ_1, $\sigma_1 = 0$)

TABLE 44. ELECTROMAGNETIC REFLECTION AND REFRACTION.—(*Continued*)

Steps	*Electric vector* $\mathfrak{E}$ is *parallel* with XY plane or in XY plane (Fig. 220*a*), corresponds to *vertical polarization*	*Electric vector* $\mathfrak{E}$ is *perpendicular* to XY plane (Fig. 220*b*), corresponds to *horizontal polarization*	Remarks
	for nonferromagnetic dielectrics ($\mu_1 = \mu_0 = \mu_2$) For medium 1 of air ($\mu_1 = \mu_0$, $\kappa_1 \cong \kappa_0$) we have $$n = \sqrt{\frac{\kappa_2}{\kappa_0}} = \sqrt{\kappa_r}$$ That we have complete electromagnetic transmission into medium 2 requires that the coefficient R_v of refraction becomes unity for the Brewster angle. We find, according to step 26, $$R_v = \frac{2n \cos \theta_1}{n \cos \theta_1 + \cos \theta_2}$$ which for $\theta_1 = \theta_B$ yields $$R_v = \frac{2 \tan \theta_B \cos \theta_B}{\tan \theta_B \cos \theta_B + \cos (90° - \theta_B)}$$ but $$\cos (90° - \theta_B) = \sin \theta_B$$ and $$R_v = \frac{2 \sin \theta_B}{\sin \theta_B + \sin \theta_B} = 1$$		

29	Inasmuch as an electromagnetic wave incident upon a plane of medium separation can be split up into components for which the electric field $\mathcal{E}$ is parallel or is normal to the plane of incidence, we have, for an angle $\theta_1 = \theta_B$ of incidence, a reflected wave, which is entirely a wave with a horizontal polarization. It is, therefore, possible to extinguish any reflection of the originally incident unpolarized wave by two *successive* reflections from two reflectors, both reflectors being oriented in such a way that respective beams enter under Brewster angles. The reflected beam from the first reflector returns only waves that are polarized with the $\mathcal{E}$ vector perpendicular to the plane of incidence. When, therefore, the second reflector is so oriented that the $\mathcal{E}_3$ vector of the reflected wave due to the first reflector is parallel to the plane of incidence and enters under the angle θ_B, the second reflector can cause no reflected electromagnetic beam but will transmit (refract) the entire wave energy into the medium behind the reflector. We have then total wave energy extinction as far as reflections are concerned from the second reflector	Generally polarized electromagnetic wave Entire reflected wave Energy extinction
30	We found in step 19 that for an electromagnetically denser medium 1 through which an incident wave moves toward a medium 2 (less dense), we have $n_2 < n_1$ and may expect total reflection If a UHF wave moves from a medium that is, for instance, porcelain ($\sigma_1 = 3 \times 10^{-13}$ mho/m, $\mu_1 = \mu_0 = 1.257 \times 10^{-6}$ henry/m, $\kappa_1 = 5.7\ \kappa_0$ farads/m), into a medium that is air ($\sigma_2 = 0$, $\mu_2 = \mu_0$ henrys/m, $\kappa_2 = \kappa_0 = 8.854 \times 10^{-12}$ farad/m), we may expect the above-mentioned condition, since the conductivity $\sigma_1 = 3 \times 10^{-13}$ mho/m can be ignored at UHF's, since $$\kappa_e = \kappa - j(\sigma/\omega) \cong \kappa \cong \kappa_1 \qquad \text{farads/m.}$$ We have then $n_1 = 3 \times 10^8 \sqrt{\mu_0 \kappa_1}$, $n_2 = 3 \times 10^8 \sqrt{\mu_0 \kappa_0}$, $n = \sqrt{\kappa_0/\kappa_1} = 1/\sqrt{\kappa_r} = 1/\sqrt{5.7}$, which is smaller than unity value If the electromagnetic beam advances normally toward the plane of medium separation in medium 1, we have some field energy passing squarely into medium 2 and some energy reflected back. For an angle of incidence θ_1 that is not zero but gradually increases toward the critical angle $\theta_1 = \theta_c$, we have for θ_c the case of total reflection, with no refracted beam passing into medium 2, since $\theta_2 = 90°$ (refracted beam along the surface of separation). According to step 19, we have then $\theta_c = \sin^{-1}(n)$. For $\theta_1 > \theta_c$ also no wave energy can pass into medium 2. For such larger angles of incidence, we find the following from steps 15 and 26:	Two dielectric mediums μ_1, κ_1, $\sigma_1 = 0$ and μ_2, κ_2, $\sigma_2 = 0$ for which the refractive index of medium 1 is $n_1 = \dfrac{3 \times 10^8}{v_1}$ $= 3 \times 10^8 \sqrt{\mu_1 \kappa_1}$ and of medium 2 $n_2 = 3 \times 10^8 \sqrt{\mu_2 \kappa_2}$ $n = \dfrac{\sqrt{\mu_2 \kappa_2}}{\sqrt{\mu_1 \kappa_1}} = \dfrac{n_2}{n_1}$ $= \sqrt{\dfrac{\kappa_2}{\kappa_1}}$ $\mu_1 = \mu_0 = \mu_2$; n is relative index of medium 2

TABLE 44. ELECTROMAGNETIC REFLECTION AND REFRACTION.—(*Continued*)

Steps	*Electric vector* $\mathcal{E}$ is *parallel* with XY plane or in XY plane (Fig. 220*a*), corresponds to *vertical polarization*	*Electric vector* $\mathcal{E}$ is *perpendicular* to XY plane (Fig. 220*b*), corresponds to *horizontal polarization*	Remarks
30 (*Cont.*)	We have $\rho_v = \dfrac{H_3}{H_1}$ $= \dfrac{\sqrt{\kappa_2}\cos\theta_1 - \sqrt{\kappa_1}\cos\theta_2}{\underbrace{\sqrt{\kappa_2}\cos\theta_1 + \sqrt{\kappa_1}\cos\theta_2}_{\text{from step 15 and } \mu_1 = \mu_0 = \mu_2}}$ $= \underbrace{\dfrac{\tan(\theta_1 - \theta_2)}{\tan(\theta_1 + \theta_2)}}_{\text{Fresnel (step 26)}} = \dfrac{p - q}{p + q} = \dfrac{\mathcal{E}_3}{\mathcal{E}_1}$ $p = \sin\theta_1\cos\theta_1$ $q = \sin\theta_2\cos\theta_2$	We have $\rho_h = \dfrac{\mathcal{E}_3}{\mathcal{E}_1}$ $= \dfrac{\sqrt{\kappa_1}\cos\theta_1 - \sqrt{\kappa_2}\cos\theta_2}{\underbrace{\sqrt{\kappa_1}\cos\theta_1 + \sqrt{\kappa_2}\cos\theta_2}_{\text{from step 15 and } \mu_1 = \mu_0 = \mu_2}}$ $= \underbrace{\dfrac{\sin(\theta_2 - \theta_1)}{\sin(\theta_2 + \theta_1)}}_{\text{Fresnel (step 26)}} = \dfrac{r - s}{r + s} = \dfrac{H_3}{H_1}$ $r = \cos\theta_1\sin\theta_2$ $s = \sin\theta_1\cos\theta_2$	with respect to medium 1. Case $n_1 > n_2$ $\cos\theta_2 = \sqrt{1 - \sin^2\theta_2}$ $= \sqrt{1 - \dfrac{\sin^2\theta_1}{n^2}}$ since $n_1\sin\theta_1 = n_2\sin\theta_2$ and $\sin\theta_2 = \dfrac{n_1}{n_2}\sin\theta_1$ $= \dfrac{\sin\theta_1}{n}$ For $\theta_1 = \theta_c$, $\sqrt{1 - \sin^2\theta_2}$ $= \sqrt{1 - \dfrac{\sin^2\theta_c}{n^2}}$ $= \sqrt{1 - \dfrac{n^2}{n^2}}$ $= 0 = \cos\theta_2$ $= \cos 90°$ or
	$\cos\theta_2 = \sqrt{1 - (\sin^2\theta_1/n^2)}$. For $\sin^2\theta_1 > n^2$, we have $\dfrac{\sin^2\theta_1}{n^2} > 1$ and $\underbrace{\cos\theta_2}_{\text{imaginary}} = j\sqrt{\dfrac{\sin^2\theta_1}{n^2} - 1}$ as the solution. But $\sin\theta_c = n$; and for angles of incidence θ_1 larger than θ_c, we have $q = jq$ and $s = js$ in the above relations		
	$\rho_v = \dfrac{p - jq}{p + jq}$ $= \dfrac{(p - jq)^2}{(p + jq)(p - jq)}$	In the same way for imaginary $\cos\theta_2$ values $\rho_h = \dfrac{r - js}{r + js} = d - je$ $d = \dfrac{r^2 - s^2}{r^2 + s^2}$; $e = \dfrac{2rs}{r^2 + s^2}$	

$$= \frac{p^2 - j2pq - q^2}{p^2 + q^2}$$

$$= \frac{p^2 - q^2}{p^2 + q^2} - j\frac{2pq}{p^2 + q^2} = a - jb$$

$$a = \frac{p^2 - q^2}{p^2 + q^2}; \qquad b = \frac{2pq}{p^2 + q^2}$$

$$\rho_v = \sqrt{a^2 + b^2}\, \epsilon^{-i\varphi_v}$$

$$\varphi_v = \tan^{-1}\frac{b}{a}$$

$$\rho_v = \sqrt{a^2 + b^2}\cos\varphi_v - j\sqrt{a^2 + b^2}\sin\varphi_v$$

$$\rho_h = \sqrt{d^2 + e^2}\cos\varphi_h - j\sqrt{d^2 + e^2}\sin\varphi_h$$

$$\varphi_h = \tan^{-1}\left(\frac{e}{d}\right)$$

$\theta_2 = 90°$ for $\theta_1 = \theta_c$; and for $\sin\theta_1 > n$, we have $\cos\theta_2$ *imaginary*

These results show that for angles of incidence $\theta_1 > \theta_c$, we have *complex* reflection coefficients, *even in dielectrics*

Inasmuch as ρ_v means the ratio of reflected field in volts/m to the incident field, we have the reflected field $\mathcal{E}_3 = p - jq$ volts/m and the incident field

$$\mathcal{E}_1 = p + jq \text{ volts/m}$$

and

$$\mathcal{E}_1 = \sqrt{p^2 + q^2}\, \epsilon^{j\frac{\varphi_v}{2}}$$

$$\mathcal{E}_3 = \sqrt{p^2 + q^2}\, \epsilon^{-j\frac{\varphi_v}{2}}$$

In the same way we have

$$\mathcal{E}_1 = \sqrt{r^2 + s^2}\, \epsilon^{j\frac{\varphi_h}{2}}$$

$$\mathcal{E}_3 = \sqrt{r^2 + s^2}\, \epsilon^{-j\frac{\varphi_h}{2}}$$

volts/m for the incident and the reflected waves at the plane of separation

Hence, $\mathcal{E}_1$ and $\mathcal{E}_3$ have again same absolute values but a relative phase difference of

$$\left(\frac{\varphi_h}{2}\right) - \left(-\frac{\varphi_h}{2}\right) = \varphi_h,$$

TABLE 44. ELECTROMAGNETIC REFLECTION AND REFRACTION.—(*Continued*)

Steps	*Electric vector* $\mathcal{E}$ is *parallel* with XY plane or in XY plane (Fig. 220*a*), corresponds to *vertical polarization*	*Electric vector* $\mathcal{E}$ is *perpendicular* to XY plane (Fig. 220*b*), corresponds to *horizontal polarization*	Remarks
	$\frac{\varphi_v}{2} = \tan^{-1}\left(\frac{q}{p}\right)$ $= \tan^{-1}\left(\frac{\sin\theta_2 \cos\theta_2}{\sin\theta_1 \cos\theta_1}\right)$ $= \tan^{-1}\left(\frac{\sin\theta_2 \sqrt{\frac{\sin^2\theta_1}{n^2} - 1}}{\sin\theta_1 \cos\theta_1}\right)$ $= \tan^{-1}\left(\frac{\sqrt{\frac{\sin^2\theta_1}{n^2} - 1}}{n\cos\theta_1}\right)$ and $\frac{\varphi_v}{2} = \tan^{-1}\left(\frac{\sqrt{\sin^2\theta_1 - n^2}}{n^2\cos\theta_1}\right)$	where $\frac{\varphi_h}{2} = \tan^{-1}\left(\frac{s}{r}\right)$ $= \tan^{-1}\left(\frac{\sin\theta_1 \cos\theta_2}{\cos\theta_1 \sin\theta_2}\right)$ $= \tan^{-1}\left(\frac{\sin\theta_1 \sqrt{\frac{\sin^2\theta_1}{n^2} - 1}}{\sin\theta_2 \cos\theta_1}\right)$ $= \tan^{-1}\left(\frac{n\sqrt{\frac{\sin^2\theta_1}{n^2} - 1}}{\cos\theta_1}\right)$ $\frac{\varphi_h}{2} = \tan^{-1}\left(\frac{\sqrt{\sin^2\theta_1 - n^2}}{\cos\theta_1}\right)$	

This shows that for the general case, where we have neither the condition of Fig. 220*a* nor the condition of Fig. 220*b* with respect to the plane of incidence (XY plane), we may expect due to total reflection angles ($\theta_1 > \theta_c$), total wave returns back into the more dense medium 1 with respective relative phase differences φ_v and φ_h referred to the phase of the incident field

As mentioned, this happens for wave travel from a denser into a less dense medium. Hence, we obtain *generally elliptically* polarized reflected waves

Fortunately, we work mostly from a less dense toward denser electromagnetic wave obstructions. For instance, air is the medium 1, where the electromagnetic wave is initiated and where we like to keep it. But many rays will strike the denser earth crust and partially bounce again away from it with no cases of total reflections (*but cases of total refraction*, in the case of vertical polarizations and the incidence θ_1 equal to the Brewster angle, if the earth crust acts at UHF's essentially as a dielectric). This is also true for any other electromagnetic wave obstacles, such as buildings, etc.

After the wave has entered such obstacles, we may in most cases (at UHF's) ignore the penetrated wave energy, since it is rapidly absorbed, and deal with the reflected wave energy and the wave energy of the direct ray, which meets no obstacles between radiation center and reception center. This is taken up in detail in following sections

31	For ideal distilled water, we should have $\sigma = 0$ mhos/m. Taking $\kappa = 80\kappa_0$ farads/m, the index of refraction with respect to vacuum is $$n = \frac{3 \times 10^8}{v} = \frac{\frac{1}{\sqrt{\mu_0\kappa_0}}}{\frac{1}{\sqrt{\mu_0 80\kappa_0}}}$$ $$= \sqrt{80} = 8.944$$ $$\theta_B = \tan^{-1}(n)$$ $$= \tan^{-1}(8.944) = 83.6°$$ Hence, when air is the medium from which a vertically polarized wave enters the surface of distilled water, the incident wave has to be $90° - 83.6° = 6.4°$ with respect to the plane surface of the distilled water to cause total wave energy penetration into the water	It is understood that values of the dielectric constant depend upon the temperature. This has nothing to do with polarization. For instance, the dielectric constant of ice is quite low as compared with the value of about 80 for water at room temperature. The dielectric constant of air is essentially the value holding for vacuum ($\cong \kappa_0$); the exact value at 0°C is $1.00059\kappa_0$ farads/m but is $1.0218\kappa_0$ under 40 atm Water vapor at 145°C has a value of $1.00705\kappa_0$ farads/m where $\kappa_0 = 8.854 \times 10^{-12}$ farad/m	Magnitude of the Brewster angle for perfect dielectrics. There are many other applications of this angle in some of the following sections. Consult also Figs. 226, 227, and 232–237
32	If a medium also has conductivity σ in mhos/m, besides μ henrys/m and κ farads/m, we have according to step 14 $$n = \frac{\Gamma}{\Gamma_0} = \frac{j\omega\sqrt{\mu\kappa_e}}{j\omega\sqrt{\mu_0\kappa_0}} = \frac{\sqrt{\mu\left(\kappa - j\frac{\sigma}{\omega}\right)}}{\sqrt{\mu_0\kappa_0}}$$ If we deal with a nonmagnetic medium, then $\mu = \mu_0$ henrys/m we have $$n = \sqrt{\frac{\kappa}{\kappa_0} - j\frac{\sigma}{\omega\kappa_0}} = \sqrt{\kappa_r - j1.8 \times 10^4 \frac{\sigma}{f}}$$		Index of refraction of a dissipative dielectric; σ mhos/m also present

TABLE 44. ELECTROMAGNETIC REFLECTION AND REFRACTION.—(*Continued*)

Steps	*Electric vector* $\mathcal{E}$ is *parallel* with XY plane or in XY plane (Fig. 220*a*), corresponds to *vertical polarization*	*Electric vector* $\mathcal{E}$ is *perpendicular* to XY plane (Fig. 220*b*), corresponds to *horizontal polarization*	Remarks
	where f is in Mc/sec, σ in mhos/m, and κ_r is the numeric relative dielectric constant of medium μ, κ, σ. We have then $n = \sqrt{\kappa'_e}$, where κ'_e is the relative numeric *complex* dielectric constant $\kappa_r - j1.8 \times 10^4(\sigma/f)$. Such complex cases were utilized in steps 10, 11, 12, and 33. We shall learn that vertically polarized waves entering into a dissipative medium under the Brewster angle will *not cause complete* wave energy transfer into the general medium, but nearly so, unless the conductivity effects in comparison to the dielectric displacement effects are very pronounced. We have then what is known as a "pseudo" Brewster angle effect. It is similar to customary circuit experience, where we only have pseudo resonance, since the resistance effect does not permit an infinite resonance current. In the same way, the conductivity effect in a dielectric does not permit total energy transmission into the dissipative medium. This also has a bearing on the image theory, where we have for the general medium, as it were, a "blurred" image effect instead of a sharp image effect		Bearing on theory of electric images
33	When an electromagnetic wave enters from air into a *general* medium, with conductivity effects besides the permeability and the dielectric constant, we have for the refracted beam $\mathcal{E}_2^{(\text{volts/m})} = \frac{\mathcal{E}_0}{r}\epsilon^{j\omega\left(t-\frac{nr}{c}\right)} = \frac{\mathcal{E}_0}{r}\epsilon^{j2\pi\left(ft-n\frac{r}{\lambda}\right)}$ $= \frac{\mathcal{E}_0}{r}\epsilon^{j\omega t}\epsilon^{-j\beta nr} = \frac{\mathcal{E}_0}{r}\epsilon^{j\omega t}\cos(\beta nr) - j\frac{\mathcal{E}_0}{r}\epsilon^{j\omega t}\sin(\beta nr) = \frac{\mathcal{E}_0}{r}(A - jB)$ where r is the distance in meters from the plane of medium separation in medium 2. The quantities σ_2, μ_2, and κ_2 are the electromagnetic properties, and $\mathcal{E}_0$ volts/m is the maximum time value of the electric field at the plane of medium separation. We now have to use for the relative index of refraction the general form $n = \sqrt{\kappa_r - jq}$, where κ_r is the actual relative numeric dielectric constant of the general medium 2 and $q = 1.8 \times 10^4(\sigma_2/f)$ with f in Mc/sec and σ_2 in mhos/m. The above relation is now of the form $(\mathcal{E}_0/r)F_2 = \mathcal{E}_2$. If the same ray were in air, we should have $n = 1$. The factor F_2 is now *no longer a pure* phase factor, as in the case of a perfect dielectric medium 2, but consists of a real part A and an imaginary part jB, since $\omega t - \beta nr = b + ja$. The part b accounts for the phase, and the part ja for the space absorption, which causes attenuation,		Refracted wave of the general medium with dissipation $v_2 = \frac{\omega}{\beta_2}$ $c = 3 \times 10^8$ m/sec; $\Gamma_2 = \alpha_2 + j\beta_2 = j\omega\sqrt{\mu_2\kappa_{e_2}}$ $\kappa_{e_2} = \kappa_2 - j\frac{\sigma_2}{\omega}$ farads/m; $n = \sqrt{\kappa'_{e_2}}$

due to medium heat losses, in addition to the amplitude decrease, due to wave spread (caused by the inverse r law in the factor $\mathcal{E}_0/r$). There is generally no amplitude change due to wave interference in refracted wave propagation, since the absorption term, as a rule, causes a rapid decay of the refracted energy. The main obstacle is the earth's crust, which may be solid ground or water like the ocean. For the surface of the earth, we have an actual relative numeric dielectric constant κ_r of values between 4 and 80, $\kappa_r = 80$ being about the value for ocean, lakes, and rivers. The range from 4 to 30 is for solid ground, the upper range holding for wet ground and the lower range for dry soil and rock. The ocean has a conductivity from 4 to 6 mhos/m. Fresh water has about 10^{-3} mho/m, while rivers and lakes have about six times this value as an average. Dry ground has from 10^{-4} to 10^{-5} mho/m, and 10^{-2} to 10^{-3} mho/m is the range for wet soil. Many details on electromagnetic properties are given in this text, and reference is made especially to Secs. 1, 12, 13, 14.

For *vertical* polarization, the refracted field associations are

$$\mathcal{E}_2 = \frac{\mathcal{E}_0}{r}(A - jB) = \frac{\mathcal{E}_0(\sin\theta_2 - \cos\theta_2)}{r} F_2$$

$$F_2 = \epsilon^{j2\pi\left(ft - n\frac{y\sin\theta_2 + x\cos\theta_2}{\lambda}\right)}$$

where $\mathcal{E}_0$ also includes the medium impedance effect. The impedance is upon normal incidence

$$Z_2 = \sqrt{\frac{j\omega\mu_2}{\sigma_2 + j\omega\kappa_2}} \qquad \text{complex ohms}$$

There is only one H component for such a polarization, namely, $H_z = H_2$, where

$$H_2 = \frac{\mathcal{E}_0}{rZ_2}\epsilon^{j[\omega t - \beta n(y\sin\theta_2 + x\cos\theta_2)]}$$

$$\beta = \frac{2\pi}{\lambda} = \frac{\omega}{c}; \qquad \frac{\mathcal{E}_0}{Z_2} = H_0$$

H_0 is the magnetic field intensity time maximum in amp/m at the surface of medium separation on the σ_2, μ_2, κ_2, side

For *horizontal* polarization, we have the phase factor

$$F_2 = \epsilon^{j[\omega t - \beta n(y\sin\theta_2 + x\cos\theta_2)]}$$

$$H_2 = \frac{\mathcal{E}_0 F_2}{rZ_2}(\cos\theta_2 - \sin\theta_2) \text{ amp/m}$$

with only an $\mathcal{E}_z = \mathcal{E}_2$ component, and

$$\mathcal{E}_2 = \frac{\mathcal{E}_0 F_2}{r} \qquad \text{volts/m}$$

$$\kappa'_{e_2} = \frac{\kappa_{e_2}}{\kappa_0} = \kappa_r - jk\frac{\sigma_2}{f}$$

$k = 1.8 \times 10^4$
where σ_2 is in mhos/m, f in Mc/sec

$$\kappa_r = \frac{\kappa_2}{8.854} \times 10^{12}$$

is the actual relative numeric dielectric constant; $\beta_2 = n\beta$;

$$n = \frac{\beta_2}{\beta} = \frac{\frac{\omega}{v_2}}{\frac{\omega}{3 \times 10^8}} = \frac{3 \times 10^8}{v_2}$$

TABLE 44. ELECTROMAGNETIC REFLECTION AND REFRACTION.—(*Continued*)

Steps	*Electric vector* $\mathcal{E}$ is *parallel* with XY plane or in XY plane (Fig. 220*a*), corresponds to *vertical polarization*	*Electric vector* $\mathcal{E}$ is *perpendicular* to XY plane (Fig. 220*b*), corresponds to *horizontal polarization*	Remarks
	To what extent we deal with a complex index of refraction and a corresponding complex equivalent dielectric constant depends upon the electromagnetic properties of the medium and greatly upon the frequency. This can be seen from the expression $n = \sqrt{\kappa_r - jq}$, where $q = 1.8 \times 10^4(\sigma_2/f)$ with f in Mc/sec. For average ground, we may take $\sigma_2 = 10^{-4}$ mho/m and the numeric relative dielectric constant $\kappa_r = 15$. Therefore, $q = 1.8 \times 10^{-4} \times 10^4/f$ or $q = 1.8/f$. Therefore, the relative equivalent dielectric constant $\kappa_e' = \kappa_r - j(1.8/f)$, yields for a 1-Mc wave, $\kappa_e' = 15 - j1.8$, which means the 1.8 value acts much smaller than 1.8 on the actual value 15, since in geometrical quadrature, due to the j factor. For a 100-Mc wave, we have only $-j0.018$ and for still higher frequencies, very small q values indeed. But for $q \ll \kappa_r$ as about above 100 Mc/sec, we may say that we deal in effect with the actual dielectric constant $\kappa_r = 15$ for average ground, in spite of its conductivity effect. The index of refraction n is then likewise a real quantity and equal to $n = \sqrt{15} = 3.873$. This would call for a Brewster angle of $\theta_B = \tan^{-1}(3.873) = 75.5°$ with respect to the normal to average ground. Therefore, when an electromagnetic wave for frequencies above 100 Mc/sec sweeps with $90° - 75.5° = 14.5°$ against level ground (for *vertical* polarization), the *entire* field energy is refracted into ground and lost (no reflected wave). For frequencies around 100 Mc/sec and lower, we still have considerable wave penetration into ground and a more or less weak reflected wave return in the case of *vertical* polarization. For ocean surface, we need quite a high frequency to expect the ocean to behave as an apparent pure dielectric (quasi dielectric) of relative dielectric constant of about 80, since the conductivity is about 5 mhos/m; and even at 1,150 Mc/sec, we find $q = 1.8 \times 10^4 \times 5/1{,}150 \cong 80$ and $\kappa_e' = \kappa_r - jq = 80 - j80$. This means that we have a semiconductor in effect, which is also a semidielectric, since just as much displacement current flows as conduction current in such a medium at 1,150 Mc/sec. It takes, therefore, an even higher frequency to obtain, in effect, a pure dielectric behavior of the ocean. This is followed up at other places of this text		Frequency effect on the behavior of the earth crust and a water surface

Inasmuch as the refraction law applies to the general medium (step 14 of Table 44), we find

$$\Gamma_1 \sin\theta_1 = \Gamma_2 \sin\theta_2; \qquad n = \frac{n_2}{n_1} = \frac{\sin\theta_1}{\sin\theta_2} = \frac{\Gamma_2}{\Gamma_1} = \frac{j\omega\sqrt{\mu_2\kappa_{e_2}}}{j\omega\sqrt{\mu_1\kappa_{e_1}}}$$

$$\sqrt{\mu_1\kappa_{e_1}} \cong \sqrt{\mu_0\kappa_0} \qquad \text{since medium 1 is air}$$

$$\sqrt{\mu_2\kappa_{e_2}} = \sqrt{\mu_0\left(\kappa_2 - j\frac{\sigma_2}{\omega}\right)} \qquad \text{for a nonmagnetic medium 2}$$

$$\kappa'_{e_2} = \frac{\kappa_2}{\kappa_0} - j\frac{\sigma_2}{\omega\kappa_0} = \kappa_r - j18{,}000\frac{\sigma_2}{f} = \kappa_r - jq \qquad \text{for } f \text{ in Mc/sec}$$

This is then the relative index of refraction n of medium 2 with respect to medium 1. Since medium 1 was taken as air and air behaves almost like vacuum (if the humidity

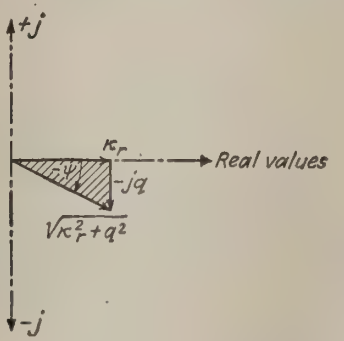

$$\tan\psi = \frac{q}{\kappa_r}; \qquad \sin\psi = \frac{q}{\sqrt{\kappa_r^2 + q^2}};$$

$$\cos\psi = \frac{\kappa_r}{\sqrt{\kappa_r^2 + q^2}}$$

$$\kappa_r = \frac{\kappa_2}{\kappa_0} = \frac{\kappa_2}{8.854}\,10^{12} \text{ numerical}$$

$$q = 1.8 \times 10^4\frac{\sigma_2}{f}$$

where σ_2 is in mhos/m, f in Mc/sec, q numerical

FIG. 223. Conditions for a general medium.

gradient is not taken into consideration), we have for the above result also the value for the relative index of refraction n_2 referred to vacuum. This means that $n_2 = \kappa_r - j1.8 \times 10^4\sigma_2/f^{(\mathrm{Mc})}$. We know that in medium 2, the velocity is $v_2 = \omega/\beta_2$, *i.e.*,

$$\beta_2 = \frac{\omega}{v_2} = \frac{6.28}{\lambda_2} = \beta n \qquad \text{for } \beta = \frac{6.28}{\lambda} \text{ and } \lambda = \frac{300}{f}$$

where f is in megacycles per second and the free-space wavelength λ is in meters.

We have, therefore,

$$\beta n = \frac{6.28n}{\lambda} = j\alpha_2 + \beta_2 = \beta n = \beta\sqrt{\kappa_r - jq}$$

$$= \beta\sqrt{\sqrt{\kappa_r^2 + q^2}}\,\Big/\underline{\frac{1}{2}\tan^{-1}\left(\frac{-q}{\kappa_r}\right)}$$

where, according to Fig. 223, we have

$$
\left.
\begin{aligned}
q &= 1.8 \times 10^4 \frac{\sigma_2}{f}; \quad \sqrt{\kappa_r^2 + q^2} = \frac{\kappa_r}{\cos \psi}; \quad \sqrt{\kappa_r^2 + q^2} = \frac{q}{\sin \psi} \\
\beta n &= \beta \sqrt{\frac{\kappa_r}{\cos \psi}}\, \epsilon^{-j\frac{\psi}{2}} = \beta \sqrt{\frac{\kappa_r}{\cos \psi}} \cos \frac{\psi}{2} - j\beta \sqrt{\frac{\kappa_r}{\cos \psi}} \sin \frac{\psi}{2} \\
\beta n &= \beta \sqrt{\frac{q}{\sin \psi}}\, \epsilon^{-j\frac{\psi}{2}} = \beta \sqrt{\frac{q}{\sin \psi}} \cos \frac{\psi}{2} - j\beta \sqrt{\frac{q}{\sin \psi}} \sin \frac{\psi}{2} \\
-j\beta n &= \underbrace{-j\beta \sqrt{\frac{\kappa_r}{\cos \psi}} \cos \frac{\psi}{2}}_{\beta_2} - \underbrace{\beta \sqrt{\frac{\kappa_r}{\cos \psi}} \sin \frac{\psi}{2}}_{\alpha_2} \\
-j\beta n &= -j\beta \sqrt{\frac{q}{\sin \psi}} \cos \frac{\psi}{2} - \beta \sqrt{\frac{q}{\sin \psi}} \sin \frac{\psi}{2} \\
F_2 &= \underbrace{\epsilon^{j(\omega t - \beta_2 r)}}_{\text{time and space phase}} \underbrace{\epsilon^{-\alpha_2 r}}_{\text{attenuation}}
\end{aligned}
\right\} \quad (869)
$$

where f is in megacycles per second, σ in mhos per meter, and r in meters. The expression for the attenuation constant α_2, in terms of the $q/\sin \psi$ ratio under the square root, has the advantage that for small arguments of ψ (angles of $\psi \leqq 10$ deg), the argument ψ, expressed in radians can be used in place of the sin of ψ, and

$$\alpha_2 = \beta \sqrt{\frac{q}{\sin \psi}} \sin \frac{\psi}{2} \cong \beta \sqrt{\frac{q}{\psi}} \frac{\psi}{2} = \frac{\beta}{2} \sqrt{q\psi}$$

In the phase factor F_2 of (869), the quantity r denotes the distance in meters along the refracted beam from the surface of medium separation. Step 33 of Table 44 gives an idea of how the surface of the earth behaves electromagnetically in the short-wave range of carrier frequencies, besides giving formulas for computing the relative index of refraction. It is seen that for many mediums, we have, in the short-wave range, in effect a pure dielectric, in spite of the conductivity of the medium. If this happens, n is a real value.

150. The Pseudo Brewster Angle of a Wave Medium with Dissipation. In Table 44, we learned that the Brewster angle of wave incidence is a characteristic feature for vertically polarized waves and that for an angle of incidence $\theta_B = \tan^{-1}(n)$, the *entire* arriving wave energy coming from medium 1 toward medium 2 passes into medium 2 if medium 2 is a perfect dielectric and n denotes the relative index of refraction of medium 2 with respect to medium 1. To find the generalized Brewster

angle θ_B, we use the generalized Snell refraction law

$$n = \frac{n_2}{n_1} = \frac{\sin \theta_1}{\sin \theta_2} = \frac{\Gamma_1}{\Gamma_2}$$

in the relation (step 15 of Table 44)

$$\rho_v = \frac{\mu_1\Gamma_2 \cos \theta_1 - \mu_2\Gamma_1 \cos \theta_2}{\mu_1\Gamma_2 \cos \theta_1 + \mu_2\Gamma_1 \cos \theta_2}$$

for a *minimum* value of the reflection coefficient ρ_v, holding for *vertical* polarization and for polarizations generally for which the electric $\mathcal{E}$ vector is oriented anywhere *in the plane* of incidence. In a dissipative dielectric, we can, at best, expect only a minimum value. For this value, the pseudo Brewster angle θ_B must satisfy the relation

$$\rho_{\min} = \frac{\Gamma_2 \cos \theta_B - \Gamma_1 \sqrt{1 - \left(\frac{\Gamma_1}{\Gamma_2} \sin \theta_B\right)^2}}{\Gamma_2 \cos \theta_B + \Gamma_1 \sqrt{1 - \left(\frac{\Gamma_1}{\Gamma_2} \sin \theta_B\right)^2}}$$

for $\mu_1 = \mu_0 = \mu_2$. Since for air $\kappa_1 \cong \kappa_0$, we find again $n = \Gamma_2/\Gamma_1 = \sqrt{\kappa_e'}$, where κ_e' is the *relative* dielectric constant $\kappa_e/\kappa_0 = \kappa_r - j1.8 \times 10^4\sigma_2/f$, for f in megacycles per second. Dividing the numerator and denominator by Γ_2, we find, for any angle θ_1 of wave incidence,

$$\rho_v = \frac{n \cos \theta_1 - \sqrt{1 - \frac{\sin^2 \theta_1}{n^2}}}{n \cos \theta_1 + \sqrt{1 - \frac{\sin^2 \theta_1}{n^2}}} = \frac{\kappa_e' \cos \theta_1 - \sqrt{\kappa_e' - \sin^2 \theta_1}}{\kappa_e' \cos \theta_1 + \sqrt{\kappa_e' - \sin^2 \theta_1}}$$

Taking medium 1 as a perfect dielectric, such as air, and medium 2 as a general medium, which in addition to $\mu_2 = \mu_0$ and κ_2 actions also has a σ_2 action, we find $\Gamma_1 = j\omega\sqrt{\mu_1\kappa_1} = j\beta_1$ and $\Gamma_2 = j\omega\sqrt{\mu_2\kappa_{e2}} = j\omega\sqrt{\mu_2[\kappa_2 - j(\sigma_2/\omega)]} = j\beta_e$. The equivalent complex phase constant β_e is, for the attenuation constant α_2, of the form $\beta_e = \beta_2 - j\alpha_2$, so that $\Gamma_2 = \alpha_2 + j\beta_2$ is satisfied. According to the generalized Snell refraction law, the angle θ_2 of refraction must be a complex sine function, and

$$\begin{aligned}\sin \theta_2 &= \frac{\Gamma_1}{\Gamma_2} \sin \theta_1 = \frac{j\beta_1}{\alpha_2 + j\beta_2} \sin \theta_1 = \frac{j\beta_1(\alpha_2 - j\beta_2)}{\alpha_2^2 + \beta_2^2} \sin \theta_1 \\ &= \frac{\beta_1(\beta_2 + j\alpha_2)}{\alpha_2^2 + \beta_2^2} \sin \theta_1 = \frac{\beta_1\beta_2}{\alpha_2^2 + \beta_2^2} \sin \theta_1 + j\frac{\alpha_2\beta_1}{\alpha_2^2 + \beta_2^2} \sin \theta_1 \\ &= (r + js) \sin \theta_1\end{aligned}$$

The cosine function of θ_2 is, therefore, also complex, because

$$\cos\theta_2 = \sqrt{1-\sin^2\theta_2} = \sqrt{1-(r+js)^2\sin^2\theta_1}$$
$$= \sqrt{1-(r^2-s^2)\sin^2\theta_1 - j2rs\sin^2\theta_1} = pe^{j\varphi}$$
$$1-(r^2-s^2)\sin^2\theta_1 - j2rs\sin^2\theta_1 = p^2\epsilon^{j2\varphi}$$
$$p^2\epsilon^{j2\varphi} = p^2[\cos(2\varphi) + j\sin(2\varphi)]$$

We have then

$$1-(r^2-s^2)\sin^2\theta_1 = p^2\cos(2\varphi); \qquad -2rs\sin^2\theta_1 = p^2\sin(2\varphi)$$
$$\tan(2\varphi) = \frac{-2rs\sin^2\theta_1}{1-(r^2-s^2)\sin^2\theta_1}$$

In exactly the same way, expressions for α_2 and β_2 are found by evaluating $\beta_e^2 = (\beta_2 - j\alpha_2)^2$ and equating in

$$\underbrace{\alpha_2^2+\beta_2^2}_{\text{real}} - j2\alpha_2\beta_2 = \underbrace{\omega^2\mu_2\kappa_2}_{\text{real}} - j\omega\sigma_2\mu_2$$

the real and imaginary terms

$$\alpha_2^2+\beta_2^2 = \omega^2\mu_2\kappa_2; \qquad 2\alpha_2\beta_2 = \omega\sigma_2\mu_2$$

The pseudo Brewster angle θ_B for a dissipative medium 2 is found for the complex relative dielectric constant $\kappa_e' = \kappa_r - jq$ by means of $\kappa_r = \kappa_2 10^{12}/8.854$ and $q = 18{,}000\,(\sigma_2/f)$ from the expression

$$\left.\begin{aligned}\cos\theta_B &= \sqrt{\frac{\kappa_r - 1 + \sqrt{(\kappa_r^2+q^2)^2(\kappa_r-1)^2 + q^2[(\kappa_r^2+q^2)^2-1]}}{(\kappa_r^2+q^2)^2-1}}\\ &\text{for a wave penetration into a dissipative medium } \sigma_2,\\ &\mu_2 = \mu_0,\ \kappa_2.\\ \cos\theta_B &= \frac{1}{\sqrt{1+\kappa_r}} \text{ for } q \ll \kappa_r;\ \cos\theta_B = \frac{1}{\sqrt{q}} \text{ for } q \gg \kappa_r\end{aligned}\right\} \quad (870)$$

where σ_2 is in mhos per meter, κ_r and q are numerical, f is in megacycles per second. There are many applications of this expression in sections that follow. Formula (870) must check the classic Brewster angle $\theta_B = \tan^{-1}(n)$ of incidence, holding for a perfect dielectric medium 2. We have then $\sigma_2 = 0$ and therefore also $q = 0$, which means $n = \sqrt{\kappa_r - jq} = \sqrt{\kappa_r}$ or $\kappa_r = n^2$. Therefore, for a perfect dielectric medium 2, formula (870) reads

$$\cos\theta_B = \sqrt{\frac{n^2-1+\sqrt{(n^4+0)^2(n^2-1)^2+0[(n^4+0)^2-1]}}{(n^4+0)^2-1}}$$
$$= \sqrt{\frac{n^2-1+\sqrt{n^8(n^2-1)^2}}{n^8-1}} = \sqrt{\frac{n^2-1+n^4(n^2-1)}{n^8-1}}$$
$$= \sqrt{\frac{(n^2-1)(1+n^4)}{(n^4+1)(n^4-1)}} = \sqrt{\frac{n^2-1}{n^4-1}} = \sqrt{\frac{n^2-1}{(n^2-1)(n^2+1)}}$$
$$= \frac{1}{\sqrt{1+n^2}}$$

But $\tan \theta_B = n$ holds also for a pure dielectric. Since $\tan \theta_B = n/1$, the hypotenuse of the rectangular triangle must be $\sqrt{1 + n^2}$ and the cosine of θ_B is $1/\sqrt{1 + n^2}$, which checks the pure dielectric Brewster angle. For vertical polarization, we have

$$\left.\begin{aligned} \rho = \rho_v &= \frac{n^2 \cos \theta_1 - m}{n^2 \cos \theta_1 + m} \\ \rho = \rho_h &= \frac{\cos \theta_1 - m}{\cos \theta_1 + m} \end{aligned}\right\} \begin{array}{l} \text{where } m = \sqrt{n^2 - \sin^2 \theta_1};\ n^2 = \kappa_r - jq = \\ \dfrac{\kappa_2}{\kappa_0} - j18{,}000 \dfrac{\sigma_2}{f^{(\text{Mc})}} \text{ if medium 1 is air and} \\ \text{medium 2 has } \mu_2 = \mu_0 \end{array}$$

in comparison with horizontal polarization. The angle $\theta_1 = \theta_B$, for a general medium 2, then causes *only* a *minimum* value of ρ_v. This means that the reflected field is likewise only a minimum for the pseudo Brewster angle θ_B. The time phase of the reflected field is then -90 deg with respect to the incident field.

151. Magnitude of the Brewster Angle of Incidence and Actual Values of the Coefficient of Reflection for Vertically and Horizontally Polarized Electromagnetic Waves. By vertical polarization is meant the electromagnetic field of a linear radiator that is vertical with respect to the plane of reflection. For horizontal polarization, the linear radiator, which causes the electromagnetic field, is parallel with the plane of reflection. Figure 224 shows *actual* and *image* linear radiators, for a plane metal reflector. According to the electrical image effect, the image current is in phase with the actual radiator current (Fig. 224*a*), in the case of a vertical radiator. The reason for this is that at a certain instant, the indicated half-wave radiator is charged negatively at the lower end and positively at the upper end. According to the image concept, equal and opposite charges occur just as far behind the reflector (in this case, ground is taken as the reflector) as in front of the reflector. Current then flows according to indicated directions. For a horizontal half-wave dipole (Fig. 224*b*), we note that for the same reason, we have antiphase *actual* and *image* currents. For the general orientation of linear radiator sections, we have then the conditions of Fig. 224*c*. It is mostly half-wave radiators and quarter-wave radiator tips that we apply in VHF and UHF work and with respect to perfect reflectors (practically so, since metal reference planes can be used for UHF's). For the general case such as actual ground, according to Table 44, the reflected wave is the value of the incident wave multiplied by the reflection coefficient ρ, which is generally complex, since we have, for vertical polarization, a coefficient $\rho_v = a - jb = \sqrt{a^2 + b^2}\, \epsilon^{j\varphi_v}$ and, for horizontal polarization, a coefficient of reflection $\rho_h = d - je = \sqrt{d^2 + e^2}\, \epsilon^{j\varphi_h}$ with respective time phase delays $\varphi_v = \tan^{-1}(-b/a)$ and $\varphi_h = \tan^{-1}(-e/d)$. For any

angle θ of incidence with respect to the normal to ground, we have respective coefficients of reflection

$$\left.\begin{aligned} &\text{Reflection coefficient } \rho = \rho_v = \frac{n^2 \cos\theta - m}{n^2 \cos\theta + m} \quad \text{for vertical polarization} \\ &\text{Reflection coefficient } \rho = \rho_h = \frac{\cos\theta - m}{\cos\theta + m} \quad \text{for horizontal polarization} \end{aligned}\right\} \tag{871}$$

where θ is the angle of wave incidence with the normal to the *plane* of medium separation, $m = \sqrt{n^2 - \sin^2\theta}$, $n^2 = \kappa_r - jq$, $q = 1.8 \times 10^4\sigma/f$,

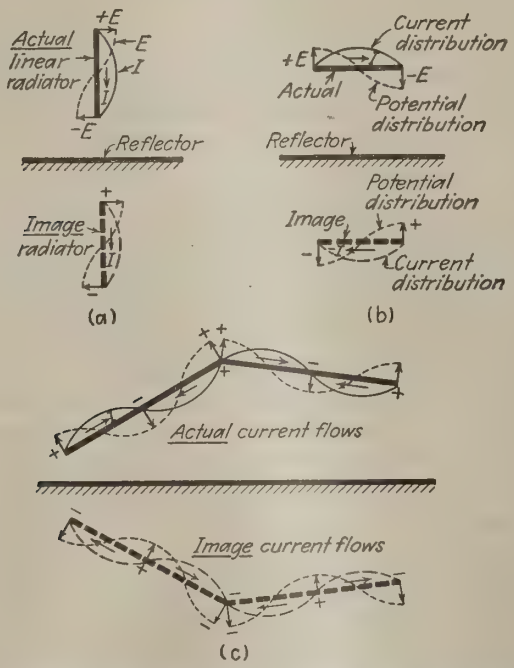

FIG. 224. Image effects just as far behind reflectors. (*a*) *Vertically* polarized (*in*phase actual and image currents). (*b*) *Horizontally* polarized (*anti*phase actual and image currents). (*c*) General orientation (can be decomposed into vertical and horizontal constituents).

σ is the conductivity of the reflector in mhos per meter, f is in megacycles per second; $\kappa_r = (\kappa/8.854) \times 10^{12}$ is the relative dielectric constant of a nonmagnetic reflector ($\mu = \mu_0 = 1.257 \times 10^{-6}$ henry/m), κ is the actual dielectric constant of the reflecting medium in farads per meter, and we have $\sigma = 5.8 \times 10^7$ mhos/m and $\kappa = 8.854 \times 10^{-12}$ farad/m for an annealed copper reflector. Figure 225 illustrates the case when a vertically polarized *plane* wave is incident to actual plane ground. Inasmuch as the incident as well as the reflected waves both proceed in air,

the respective wavelengths λ_1 and λ_3 are *identical* and essentially equal to the free-space wavelength $\lambda = 300/f$ meters, where f is in megacycles per second. The refracted wave progresses in the ground and depends on the velocity v_2 of propagation in ground. The wavelength λ_2 of the refracted wave is then relatively smaller, besides the fact that we have a rapid attenuation, so that only a few cycles can display themselves before the refracted beam becomes negligible. We are interested only

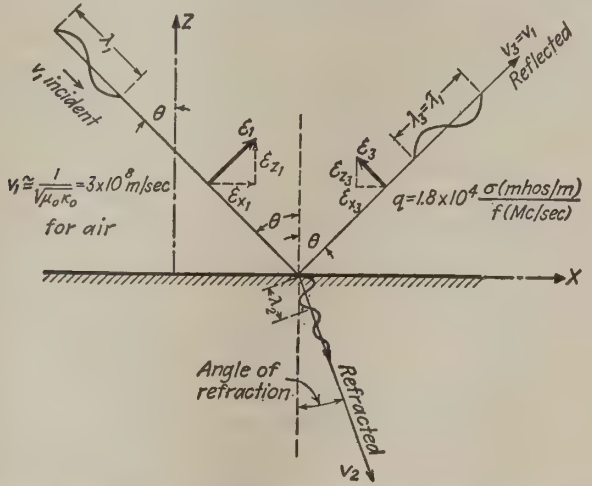

For $q \ll \kappa_r$, ground acts to reflections like a dielectric κ_r but as a dissipative medium to refracted waves. For $\beta = \omega\sqrt{\mu_0\kappa_0} = \omega/(3 \times 10^8)$; $\omega/6.28$ in cycles/sec; $\psi = \beta z \cos\theta$

$$\mathcal{E}_x = \mathcal{E}_{x_1} + \mathcal{E}_{x_2} = \mathcal{E}_0 \cos\theta \epsilon^{j(\omega t - \beta x \sin\theta)}[\epsilon^{j\psi} - \rho_v \epsilon^{-j(\varphi+\psi)}]$$

$$\mathcal{E}_z = \mathcal{E}_{z_1} + \mathcal{E}_{z_2} = \mathcal{E}_0 \sin\theta \epsilon^{j(\omega t - \beta x \sin\theta)}[\epsilon^{j\psi} + \rho_v \epsilon^{-j(\varphi+\psi)}]$$

$$\left.\begin{aligned} \mathcal{E}_{x_1} &= \mathcal{E}_0 \cos\theta \epsilon^{j[\omega t - \beta(x \sin\theta - z\cos\theta)]} \\ \mathcal{E}_{z_1} &= \mathcal{E}_0 \sin\theta \epsilon^{j[\omega t - \beta(x \sin\theta - z\cos\theta)]} \end{aligned}\right\} \text{incident}$$

$$\left.\begin{aligned} \mathcal{E}_{x_2} &= -\rho_v \epsilon^{-j\varphi_v} \mathcal{E}_0 \cos\theta \epsilon^{j[\omega t - \beta(x \sin\theta + z\cos\theta)]} \\ \mathcal{E}_{z_2} &= +\rho_v \epsilon^{-j\varphi_v} \mathcal{E}_0 \sin\theta \epsilon^{j[\omega t - \beta(x \sin\theta + z\cos\theta)]} \end{aligned}\right\} \text{reflected}$$

FIG. 225. Conditions for a vertically polarized electromagnetic wave incident on actual plane ground.

in the reflected beam, since it combines with the direct beam (the latter not shown in the figure) to yield the resultant space field. We deal, as far as the space propagation and the resultant space field are concerned, with a propagation constant $\Gamma = j\beta = j10^{-8}\omega/3$ for the frequency $\omega/6.28$ in cycles per second. For the Brewster angle θ_B, the reflection vector ρ_v becomes a minimum value, while the coefficient ρ_h, holding for horizontally polarized waves, is not affected by this angle of incidence. We found in Table 44, step 33, that at UHF's, the average ground acts, in effect (as far as wave reflections are concerned), like a quasi dielectric of relative numeric dielectric constant κ_r of about 15.

Hence, we can expect, in effect, an actual Brewster angle for which we have no reflected beam if $\theta_B = \tan^{-1}\sqrt{15} = \tan^{-1}(3.873) = 75.5$ deg is the angle of incidence with the normal to ground. For the angle of θ_B, the time phase of any reflected ray (if q is not negligible in comparison with κ_r) gives a minimum reflected ray with a relative time phase of minus 90 deg. For the angle of incidence $\theta < \theta_B$, the reflected $\mathcal{E}_3$ field is nearly in phase with the incident $\mathcal{E}_1$ field. For angles of incidence $\theta > \theta_B$, the reflected ray $\mathcal{E}_3$ is nearly in antiphase with the incident ray $\mathcal{E}_1$. It does not matter whether we think in terms of *electric* $\mathcal{E}$ fields or in terms of *magnetic H* fields when we refer to a ray or a beam, since the coefficient of reflection refers either to $\mathcal{E}$ fields or to H fields. Suppose we take a practical case, for instance, wet ground. The electromagnetic properties are then given by about the values $\sigma = 10^{-3}$ mho/m and $\kappa_r \cong 30$. For a 100-Mc wave, we have $q = 1.8 \times 10^4 \times 10^{-3}/100 = 0.18$ as against $\kappa_r = 30$. We have then only 0.6 per cent of the κ_r value and can neglect (at this frequency and higher) the q term in (871). The percentage effect is actually smaller than 0.6 per cent, since q acts in geometrical *quadrature* with respect to κ_r. We have then $\theta_B = \tan^{-1}(\sqrt{30}) = \tan^{-1}(5.4772) = 79.7$ deg. The values given in Table 45 hold for wet ground for frequencies above about 50 Mc/sec, and $n^2 = \kappa_r = 30$. This table as well as Fig. 226 shows how the reflection coefficients for vertical and horizontal polarizations vary with the angle of incidence θ. It will be noted that the reflected beam for horizontal polarization is always 180 time degrees behind the incident beam. For vertical polarization, the reflected beam is in phase with the incident beam from $\theta = 0$ deg (normal incidence) up to values close to the Brewster angle $\theta_B = 79.7$ deg, since at the incidence $\theta_B = 79.7$ deg of the Brewster angle, the reflection coefficient ρ_v becomes zero, and we have an abrupt phase jump from $\varphi_v = 0$ to $\varphi_v = -180$ deg, the Brewster angle corresponding to the between value of -90 deg. This means that between angles very little above 79.7 and 90 deg of incidence, the reflected beam is in antiphase with respect to the incident beam. We have for wet ground a quasi dielectric and therefore all the features of an ideal dielectric at UHF's. From these results, we note that horizontal polarization is more uniform, since, first, we always have antiphase reflection; and second, the reflection coefficient ρ_h varies only between the limits from -0.691 to -1. It is difficult to make a general statement with respect to the merits of respective polarizations, since they depend greatly on the service space zone. If the service zone is not more than about 10 deg with respect to the ground, then we have for vertical polarization also only antiphase reflections but a very rapid change of the ρ_v value with respect to the angle of incidence, which is also the angle of reflection.

TABLE 45. COMPUTATIONS FOR REFLECTION COEFFICIENTS FOR WET SOIL AND $\kappa_r = 30$

θ, deg	$\sin\theta$	$\cos\theta$	$\sin^2\theta$	$30 - \sin^2\theta$	m	$30\cos\theta$	$30\cos\theta - m$	$30\cos\theta + m$	ρ_v	$\cos\theta - m$	$\cos\theta + m$	ρ_h
0	0.000	1.000	0.000	30	5.475	30	24.525	35.475	0.691	−4.475	6.475	−0.691
10	0.174	0.985	0.029	29.971	5.47	29.5	24.03	34.97	0.69	−4.485	6.455	−0.695
20	0.342	0.939	0.116	29.884	5.46	28.1	22.64	33.56	0.675	−4.521	6.399	−0.705
30	0.5	0.867	0.25	29.75	5.45	25.9	20.45	31.35	0.65	−4.583	6.318	−0.725
40	0.643	0.766	0.412	29.588	5.435	23.0	17.565	28.435	0.62	−4.669	6.201	−0.75
50	0.766	0.6428	0.583	29.417	5.42	19.4	13.98	24.82	0.562	−4.777	6.063	−0.76
60	0.866	0.5	0.76	29.24	5.41	15.0	9.59	20.41	0.47	−4.41	5.91	−0.83
70	0.939	0.342	0.88	29.12	5.4	10.3	4.9	15.7	0.311	−5.058	5.742	−0.88
80	0.985	0.174	0.97	29.03	5.39	5.2	−0.19	10.59	−0.018	−5.216	5.564	−0.94
90	1.000	0.000	1.000	29.0	5.39	0.0	−5.39	5.39	−1.000	−5.39	5.39	−1.00

Remarks: $m = \sqrt{n^2 - \sin^2\theta} = \sqrt{30 - \sin^2\theta}$ uses formula (871). θ is the angle of incidence with respect to the normal to ground. $\theta = 90°$ is grazing incidence; at UHF for $q \ll \kappa_r$, $\kappa_r = 30$, $n^2 = \kappa_r$, $\rho_v = 0$, and $\varphi_v = -90°$ for 79.7° (Fig. 226).

Table 45 and Fig. 226 also show that for vertically and horizontally polarized waves, the respective reflection coefficients are always smaller than unity, except for grazing incidence ($\theta = 90$ deg). For dry ground, we have likewise a quasi-dielectric condition. Taking $\kappa_r = 10$ as an

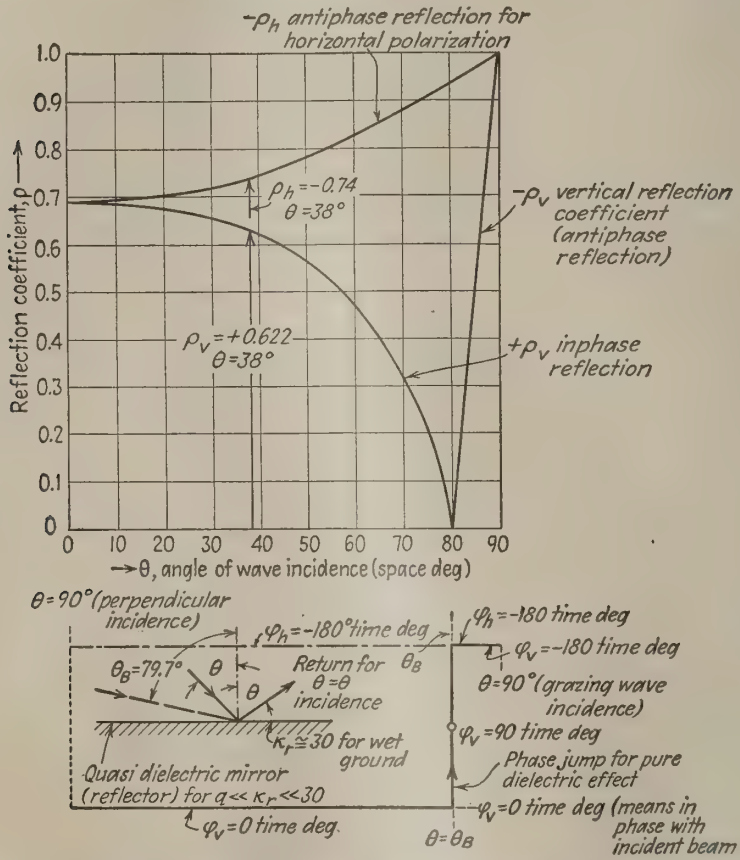

FIG. 226. Reflection coefficient and its time phase for vertical and horizontal polarization from plane wet ground above 40 Mc/sec. σ is in mhos/m; f in Mc/sec. These curves hold above 40 Mc/sec for reflections from wet ground, since $q = 1.8 \times 10^4 \sigma / f \ll \kappa_r \ll 30$. *Note:* Brewster angle θ_B refers only to vertically polarized waves (for which electric $\mathcal{E}$ vectors are parallel with plane of wave incidence). Brewster wave incidence ($\theta = \theta_B$), no reflection for a pure dielectric (and quasi-dielectric) plane obstacle. ρ_v is magnitude of reflection coefficient for vertical polarization; ρ_h is magnitude of reflection coefficient for horizontal polarization; φ_v is time phase for vertical and φ_h is time phase for horizontal polarization.

average value for the relative dielectric constant, we obtain a Brewster angle $\theta_B = \tan^{-1}(\sqrt{10}) = \tan^{-1}(3.16) = 72.5$ deg. The Brewster angle is, therefore, less grazing for dry ground. The computations of Table 46 refer to dry ground at UHF's. Since for dry ground, we have

a conductivity of about $\sigma = 10^{-4}$ to 10^{-5} mho/m, we have even for the highest conductivity value, even at 10 Mc/sec, a value of only $q = 1.8 \times 10^4 \times 10^{-4}/10 = 0.18$; and at 50 Mc/sec, we have $0.18/5 = 0.036$, which is negligible compared with the geometric quadrature component of 10. Hence, also in this case, Table 46 and the corresponding curves

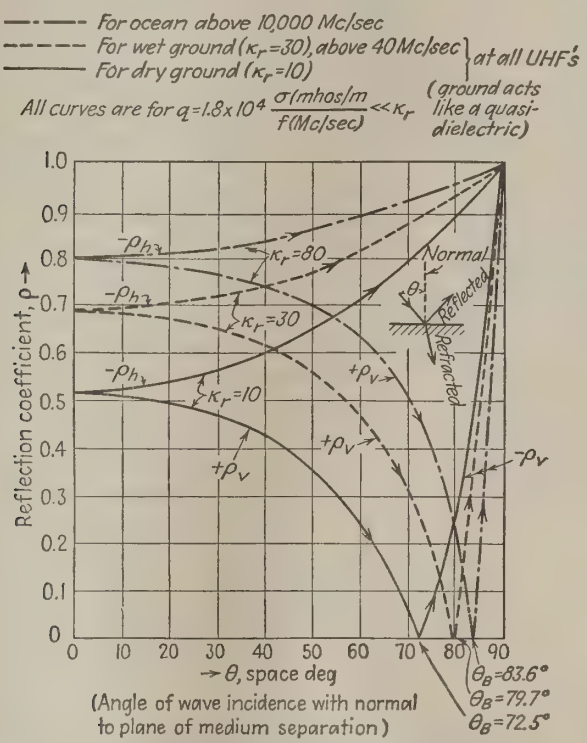

Fig. 227. Reflection coefficients for different ground conditions and vertical as well as horizontal polarization. All closed reflection coefficient patterns apply to VH and UH frequencies. $\mathcal{E}_1$ is incident field; $\mathcal{E}_3$ is reflected electric field. For *all* angles $\theta = 0$ to 90° of wave incidence $\mathcal{E}_3 = -\rho_h \mathcal{E}_1$ since $\varphi_h = 180$ time degrees. For $\theta < \theta_B$, we have $\mathcal{E}_3 = \rho_v \mathcal{E}_1$; for $\theta > \theta_B$, we have $\mathcal{E}_3 = -\rho_v \mathcal{E}_1$; generally $\mathcal{E}_3 = \rho \epsilon^{j\varphi}$.

of Fig. 227 hold well for frequencies above 50 Mc/sec. Table 47 gives the computations for a relative dielectric constant of $\kappa_r = 80$, which holds only when the frequency is very high (above 20,000 Mc/sec), since if we take $\sigma = 4$ mhos/m, we should have, at 100 Mc/sec, a value of q equal to $1.8 \times 10^4 \times \frac{4}{100} = 720$ as against $\kappa_r = 80$, which shows that the conductivity effect is *mostly* responsible for the reflections. Even for 1,000 Mc/sec, we have still a value $q = 72$ as against 80; while for frequencies equal to 10,000 Mc/sec, we have only 7.2 against 80. This would yield a magnitude for the relative equivalent dielectric constant

TABLE 46. COMPUTATIONS FOR THE REFLECTION COEFFICIENTS FOR DRY SOIL AND $\kappa_r = 10$

θ, deg	$10 - \sin^2\theta$	$m = \sqrt{10 - \sin^2\theta}$	$\cos\theta$	$10\cos\theta - m$	$10\cos\theta + m$	ρ_v	$\cos\theta - m$	$\cos\theta + m$	ρ_h
0	10	3.16	1.000	6.84	13.16	0.52	−2.16	4.16	−0.52
10	9.971	3.158	0.985	6.69	13.01	0.51	−2.17	4.143	−0.525
20	9.884	3.14	0.939	6.25	12.53	0.5	−2.201	4.079	−0.54
30	9.75	3.12	0.867	5.55	11.79	0.47	−2.26	3.987	−0.57
40	9.588	3.09	0.766	4.57	10.75	0.43	−2.32	3.856	−0.6
50	9.417	3.07	0.643	3.36	9.5	0.354	−2.43	3.713	−0.653
60	9.24	3.04	0.5	1.96	8.04	0.244	−2.54	3.54	−0.72
70	9.12	3.02	0.342	0.4	6.44	0.064	−2.68	3.36	−0.795
80	9.03	3.005	0.174	−1.265	4.745	−0.27	−2.83	3.18	−0.89
90	9	3.000	0.000	−3.000	3.000	−1.000	−3.00	3.000	−1.000

Remarks: Holds at VHF's and UHF's for dry soil and $\kappa_r = 10$. Uses (871). Figure 227 shows these coefficients. $\rho_v = 0$ and $\varphi_v = -90$ deg for $\theta_B = 72.5$ deg; $q \ll \kappa_r = 10 = n^2$.

TABLE 47. REFLECTION COEFFICIENTS FOR OCEAN SURFACE ABOVE 20,000 MC/SEC

θ, deg	$80 - \sin^2\theta$	$m = \sqrt{80 - \sin^2\theta}$	$\cos\theta$	$80 \times \cos\theta$	$80\cos\theta - m$	$80\cos\theta + m$	ρ_v	$\cos\theta - m$	$\cos\theta + m$	ρ_h
0	80	8.95	1.000	80	71.05	88.95	0.8	−7.95	9.95	−0.8
10	79.971	8.945	0.985	79	70.055	87.94	0.79	−7.96	9.93	−0.803
20	79.884	8.94	0.939	75	66.06	83.94	0.785	−8.001	9.879	−0.808
30	79.75	8.935	0.867	69.2	60.265	78.13	0.77	−8.068	9.802	−0.82
40	79.588	8.93	0.766	61.2	52.27	70.13	0.745	−8.164	9.696	−0.84
50	79.417	8.925	0.6428	51.5	42.575	60.425	0.705	−8.28	9.57	−0.867
60	79.24	8.915	0.5	40	31.085	48.915	0.64	−8.41	9.415	−0.895
70	79.12	8.91	0.342	27.4	18.49	36.31	0.51	−8.57	9.252	−0.925
80	79.03	8.905	0.174	13.9	4.995	22.805	0.217	−8.731	9.079	−0.96
90	79	8.9	0.000	0.0	−8.9	8.9	−1.000	−8.9	8.9	−1.000

Remarks: We have $q \ll \kappa_r$, $\kappa_r = 80$. Formula (871) is used and the coefficients of reflections are plotted in Fig. 227. Total refraction occurs for vertical polarization, at 83.6 deg of incidence with the normal to the ocean surface. We have then $\rho_v = 0$ and $\varphi_v = -90$ time degrees.

of $\kappa_e' = \sqrt{7.2^2 + 80^2} = 80.5$, instead of 80, which is quite close. The phase is $-\tan^{-1}(7.2/80) = -\tan^{-1}(0.09) = -5.1$ deg. Therefore, we can assume as a rough approximation that the ocean above 10,000 Mc/sec behaves like a dielectric. But if, for a very conservative approximation, we use a magnitude of q that is 2 per cent of the value of $\kappa_r = 80$, we have $q/\kappa_r = 0.02$, $q = 80 \times 0.02 = 1.6 = 7.2 \times 10^4/f$, and $f = 7.2 \times 10^4/1.6 = 45{,}000$ Mc/sec. This approximation is altogether too conservative, since we are not interested in the refracted field energy and its behavior in the dissipative ocean medium but in the reflection coefficient. We are concerned only with what happens at the *surface* of medium separation. We choose, therefore, frequencies of 20,000 Mc/sec and higher

as the criterion for quasi-dielectric behavior of the ocean. This means that we have to use a free-space wavelength in air of 1.5 cm or shorter, which is 0.59 in. or less for the free-space wavelength. Therefore, for frequencies of 20,000 Mc/sec and higher, we can assume $q \ll \kappa_r$. The absorption coefficient of the ocean then becomes independent of the frequency, directly proportional to the conductivity σ, and inversely proportional to $\sqrt{\kappa_r}$. But for frequencies below 100 Mc/sec, the absorption attenuation of the ocean water is inversely proportional to $\sqrt{f}$, independent of the dielectric constant, and directly proportional to $\sqrt{\sigma}$. This is then a condition for which $\kappa_r \ll q$. Figure 227 gives the curves for the respective reflection coefficients if $f \geqq 20{,}000$ Mc/sec, in comparison with UHF wave propagation over dry and wet ground. It is noted that the Brewster angle becomes more and more grazing as the dielectric constant increases and that vertical and horizontal reflection coefficients ρ_v and ρ_h, respectively, have the same magnitude for normal incidence but with respective phase angles of 0 and -180 deg. The magnitude of ρ increases if the relative dielectric constant increases, where the relative index of refraction is $n = \sqrt{\kappa_r}$, since these curves refer to a quasi-dielectric behavior of the ground. If we compute, for instance, for perpendicular incidence ($\rho_v = -\rho_h$) for dry rock, we find, for $\sigma = 10^{-5}$ mho/m and $\kappa_r = 4.7$, the values $q = 1.8 \times 10^4 \times 10^{-5}/f$, where f is in megacycles per second, making again $q \ll \kappa_r$ at VHF's and UHF's, and we have, according to formula (871),

$$\rho_v = -\rho_h = \frac{\kappa_r \cos\theta - \sqrt{\kappa_r - \sin^2\theta}}{\kappa_r \cos\theta + \sqrt{\kappa_r - \sin^2\theta}} = -\frac{\cos\theta - \sqrt{\kappa_r - \sin^2\theta}}{\cos\theta + \sqrt{\kappa_r - \sin^2\theta}}$$

for $\theta = 0$ deg, since

$$\rho = \rho_v = \frac{\kappa_r - \sqrt{\kappa_r}}{\kappa_r + \sqrt{\kappa_r}} = \frac{4.7 - 2.16}{4.7 + 2.16} = \frac{2.54}{6.86} = 0.367$$

$$\rho = \rho_h = \frac{1 - \sqrt{\kappa_r}}{1 + \sqrt{\kappa_r}} = \frac{1 - 2.16}{1 + 2.16} = \frac{-1.16}{3.16} = -0.367$$

Therefore, for vertical polarization, the reflected electric field $\mathcal{E}_3$ as well as the associated reflected magnetic field H_3 are only 36.7 per cent of the corresponding incident fields and in phase with these fields. However, antiphase condition exists for horizontally polarized waves. Therefore,

$$\mathcal{E}_3 = 0.367\mathcal{E}_1 \quad \text{for vertical polarization}$$
$$\mathcal{E}_3 = -0.367\mathcal{E}_1 \quad \text{for horizontal polarization}$$
$$H_3 = 0.367H_1 \quad \text{for vertical polarization}$$
$$H_3 = -0.367H_1 \quad \text{for horizontal polarization}$$

For *vertical* polarization, no ρ_v value exists for an angle of incidence $\theta_B = 65.2$ deg. This angle is now steeper than for the cases of Fig. 227. Several authors define the reflection coefficient as the ratio of the reflected wave *energy* to the incident wave *energy*, *i.e.*, as the ratios $(\mathcal{E}_3/\mathcal{E}_1)^2 = (H_3/H_1)^2$. In radio engineering, the definition of this text has become practice, and $\rho = \mathcal{E}_3/\mathcal{E}_1 = H_3/H_1$.

If we assume a salinity of the ocean such that $\sigma = 5$ mhos/m, we have at 100 Mc/sec a value of $q = 1.8 \times 10^4 \times \frac{5}{100} = 900$ and twice this value for 50 Mc/sec in comparison with $\kappa_r = 80$. The Brewster angle is, then, according to (870), found for the condition $\kappa_r \ll q$ and $\theta_B = \cos^{-1}(1/\sqrt{q}) = \cos^{-1}(1/\sqrt{900}) = \cos^{-1}(1/30) = 88.101$ deg for 100 Mc/sec and $\cos^{-1}(1/\sqrt{1{,}800}) = \cos^{-1}(1/42.5) = 88.7$ deg for 50 Mc/sec. Hence, the angle[1] for no vertically polarized reflection is almost 90 deg, *i.e.*, essentially a grazing angle with the ocean surface. For frequencies below 100 Mc/sec, we have then essentially only the term $-jq$ in $n = \sqrt{\kappa_r - jq}$, and

$$n \cong \sqrt{-jq} = \sqrt{-j}\sqrt{q} = \frac{1-j}{\sqrt{2}}\sqrt{q}$$

$$= (1-j)\sqrt{\frac{q}{2}} = \sqrt{\frac{q}{2}} - j\sqrt{\frac{q}{2}} = a - ja$$

This is again a complex index of refraction for

$$a = \sqrt{\frac{q}{2}} = 100\sqrt{0.9\left(\frac{\sigma}{f}\right)},$$

where σ is in mhos per meter and f in megacycles per second. Since the magnitude of the real as well as of the imaginary term is equal to $100\sqrt{0.9(\sigma/f)}$, the index of refraction n must have a phase angle ψ of 45 deg, because $\psi = \tan^{-1}(-a/a) = -45$ deg. This phase angle is *fixed* for *all frequencies below* 100 *Mc/sec* in the case of *ocean*. The magnitude of n is then, since $n = a - ja = \sqrt{a^2 + a^2}\,\epsilon^{-j45°} = 1.41a\epsilon^{-j45°}$ equal to $1.41a = 1.41 \times 100\sqrt{0.9(\sigma/f)} = 134\sqrt{\sigma/f} = 13.4\sqrt{\sigma}$ for $f = 100$ Mc/sec. Therefore, for a salinity giving $\sigma = 5$ mhos/m, we find at 100 Mc/sec for the reflecting ocean surface

$$n = 13.4\sqrt{5}\,\epsilon^{-j45°} = 2.24 \times 13.4\epsilon^{-j45°} = 30^{-j45°}$$

$$= 30\cos 45° - j30\sin 45° = 21.2 - j21.2$$

[1] Customary trigonometric handbook tables do not always go to such small values as 0.0333. It is then convenient to express the angle by its complementary value $90° - \theta_B$, for which $\cos\theta_B = \sin(90° - \theta_B) \cong 1.57 - \theta_B$, where θ_B is in radians. But 1 radian is 57.3 deg, and 0.0333 radian are $0.0333 \times 57.3 = 1.8909$ deg, rendering $\theta_B = 90 - 1.8909 = 88.109$ deg.

For a salinity yielding $\sigma = 4$ mhos/m, we have, for the ocean at 100 Mc/sec,

$$n = 13.4\sqrt{4}\,\epsilon^{-j45^\circ} = 26.8 \times 0.7071 - j26.8 \times 0.7071 = 18.98 - j18.98$$

At 50 Mc/sec, we have only one-quarter of these complex values, namely, $6.7\epsilon^{-j45^\circ}$ for $\sigma = 4$ mhos/m and $7.5\epsilon^{-j45^\circ}$ for $\sigma = 5$ mhos/m.

152. Magnitude of the Generalized Index of Refraction of a Medium. The general index of refraction of a medium $\mu = \mu_0 = 1.257 \times 10^{-6}$ henry/m, κ farads per meter, and σ mhos per meter is, for the relative numeric dielectric constant $\kappa_r = \kappa/\kappa_0 = 10^{12}(\kappa/8.854)$, given by

$$\left.\begin{aligned} n &= \sqrt{\kappa_r - jq}\,\epsilon^{j\psi} = \sqrt[4]{\kappa_r^2 + q^2}\cos\psi + j\sqrt[4]{\kappa_r^2 + q^2}\sin\psi \\ q &= 1.8 \times 10^4 \frac{\sigma}{f^{(\mathrm{Mc})}}; \qquad \psi = -\frac{1}{2}\tan^{-1}\left(\frac{q}{\kappa_r}\right) \end{aligned}\right\} \tag{872}$$

This is the relative index of refraction n of the medium referred to empty space, since

$$n = \frac{\Gamma}{\Gamma_0} = \frac{j\omega\sqrt{\mu\kappa_e}}{j\omega\sqrt{\mu_0\kappa_0}} = \sqrt{\frac{\kappa_e}{\kappa_0}} = \sqrt{\frac{\kappa - j(\sigma/\omega)}{\kappa_0}}$$
$$= \sqrt{\frac{\kappa}{\kappa_0} - j\frac{\sigma}{\omega\kappa_0}} = \sqrt{\kappa_r - jq}$$

It is also the relative index of refraction referred to air if we ignore the conditions of the gradient of the relative index of refraction in portions of the troposphere, especially next to ground, due to water vapor and temperature effect. We have already found that for land, we have the average value of $\kappa_r \cong 15$ while for lakes and ocean water, it is about 80. For a perfect conductor, the value of q is infinite; and for a perfect dielectric (a perfect insulator), $q = 0$. The ratio $\nu = q/\kappa_r$ is, therefore, a means of predicting to what extent we deal with a complex medium. For $\nu = 1$, *i.e.*, $q = \kappa_r$, we have $\psi = -22.5$ deg, and the magnitude of n becomes

$$|n| = \sqrt[4]{\kappa_r^2 + \kappa_r^2} = \sqrt[4]{2\kappa_r^2} = 1.19\sqrt{\kappa_r}$$

or

$$|n| = \sqrt[4]{2q^2} = 1.19\sqrt{q} = 1.19 \times 10^2\sqrt{1.8}\sqrt{\frac{\sigma}{f}} = 160\sqrt{\frac{\sigma^{(\mathrm{mhos/m})}}{f^{(\mathrm{Mc/sec})}}}$$

$$n = 160\overbrace{\cos(-22.5^\circ)}^{=\cos 22.5^\circ}\sqrt{\frac{\sigma}{f}} + j160\overbrace{\sin(-22.5^\circ)}^{=-\sin 22.5^\circ}\sqrt{\frac{\sigma}{f}}$$
$$= 160 \times 0.9239\sqrt{\frac{\sigma}{f}} - j160 \times 0.3827\sqrt{\frac{\sigma}{f}} = (147.6 - j61.6)\sqrt{\frac{\sigma}{f}}$$

In formulas (872), we note that the angle ψ refers *always* to *negative* numerical angles. The reason for this is that for a dielectric wave medium with medium dissipation due to a conductivity σ, we have an equivalent dielectric constant $\kappa_e = \kappa - j(\sigma/\omega)$ farads per meter. This constant is for an isotropic medium in effect such that it refers to 1 cu m of the general medium just as does σ. We know that σ denotes the conductivity in mhos across two parallel square-meter faces that are 1 m apart. These are then the opposite end faces of the cubic meter. In the same way, the actual dielectric constant κ refers to the capacitance in farads across the above-mentioned square-meter faces, since the faces are 1 m apart. This means that the general medium is, in effect, a "*leaky*" *condenser*, since it may be imagined as made up of infinitesimal cubical elements. If we add up all these differential cubes until they form 1 cu m of the general medium, we have across the above-mentioned opposite square-meter faces of the cube an equivalent capacitance of κ_e farads, since it is 1 m across the faces. Now when we have a leaky condenser, it must have an Amperian conduction current and a Maxwellian displacement current. This is exactly the case, and formula (1) on page 11 applies. It is the curl H relation, where J is the current in amperes across 1 sq m, since we deal with 1-cu-m medium in the place of differential cubical elements. But $J = \sigma\mathcal{E}$ amperes per square meter. The term $\partial(\kappa\mathcal{E})/\partial t$ in formula (1) is the Maxwellian displacement current, which for a harmonic field $\mathcal{E} = \mathcal{E}_0 e^{j\omega t}$ is equal to $j\omega\kappa\mathcal{E}$ amperes displacement current. We have then for our cubic meter a total current of $\sigma\mathcal{E} + j\omega\kappa\mathcal{E}$ amperes flowing through the square-meter face at which the field $\mathcal{E}$ acts. Since we have a dissipative medium, there must be a smaller $\mathcal{E}$ value after the electromagnetic wave has traveled through 1 m distance. Nevertheless, when we think in terms of a leaky cubical condenser across which we have a voltage of E volts, which is $\mathcal{E}$ volts per meter times 1 m, the applied voltage will supply the watt current $\sigma\mathcal{E}$ amperes and the wattless current $j\omega\kappa\mathcal{E}$ amperes. This is then equivalent to $j\omega\kappa_e\mathcal{E}$ amperes $= [j\omega\kappa - j\omega j(\sigma/\omega)]\mathcal{E} = (j\omega\kappa + \sigma)\mathcal{E}$ amperes. This is in agreement with the curl H relation of (1). The relation $\kappa_e = \kappa - j(\sigma/\omega)$ farads per meter, for a dielectric wave medium with dissipation, can have, in effect, three distinct forms. One form is as it stands and represents a leaky dielectric; the other form is the limit for which the ratio $\nu = q/\kappa_r$ is very large and $\kappa_e \cong -j(\sigma/\omega)$. For the third form, we have reached the limit from which one ν is very small and $\kappa_e \cong \kappa$. It is only the third form that can ever yield a real value for the relative index of refraction, since the second form, according to Sec. 151, also gives a complex index n of refraction, as does the form where neither q nor κ_r can be neglected with respect to the magnitude of κ_r and q, respectively.

Table 48 gives the absolute value and the corresponding phase angle for different values of $\nu = q/\kappa_r$. Figure 228 is a plot of the computed results. From these curves as well as Table 48, it is possible to compute, for a relative dielectric constant $\kappa_r = 15$ and 80, respectively, the conductivity for a given frequency f in megacycles per second. Since these κ_r values hold for average ground and ocean, as well as lakes, the curves of Fig. 228 should prove useful. The application is then as follows: Suppose we have ocean, with a value $\sigma = 5$ mhos/m, and we want to operate a 1,000-Mc wave over ocean. We have then $q = 1.8 \times 10^4$ 5/1,000 $= 90$, $\nu = q/\kappa_r = {}^{90}\!/_{80} = 1.125$. We find then, for the ν value on the curves, the magnitude n and the phase angle ψ and compute the complex

TABLE 48. MAGNITUDE OF THE INDEX n OF REFRACTION AND ITS PHASE FOR A DIELECTRIC MEDIUM WITH DISSIPATION

Phase $\psi°$ of index n	Ratio $\nu = \frac{q}{\kappa_r}$	$q = \nu\kappa_r$		Magnitude $n = \sqrt[4]{\kappa_r^2 + q^2}$	
		$\kappa_r = 15$ for average ground	$\kappa_r = 80$ for average ocean	$\kappa_r = 15$ for average ground	$\kappa_r = 80$ for average ocean
−0.0	0.0000	0.0000	0.0000	3.87	$n \cong \sqrt{\kappa_r}$: 8.94
−1	0.0349	0.54	2.79	3.87	8.94
−2	0.0699	1.05	5.59	3.87	8.94
−3	0.1051	1.58	8.8	3.87	8.94
−4	0.1405	2.1	11.25	3.87	8.94
−5	0.1763	2.64	14.1	3.9	9.0
−8	0.2867	4.3	23	3.95	9.11
−11	0.404	6.05	32.3	4.02	9.27
−14	0.5317	8	42.9	4.12	9.5
−17	0.6745	10.1	54	4.25	9.84
−20	0.8391	12.6	67	4.44	10.2
−22.5	1.0000	15	80	4.6	10.64
−26	1.2799	19.2	102	4.94	11.38
−29	1.6003	24	128	5.03	12.28
−32	2.0503	30.6	164	5.85	13.5
−35	2.7475	41.2	220	6.61	15.3
−38	4.0108	60.2	321	7.87	18.14
−41	7.1154	106.5	570	10.38	24.04
−41.5	8.1443	122.5	652	11.09	25.69
−42	9.5144	143	760	11.99	27.7
−42.5	11.43	172	915	13.14	30.35
−43	14.3	215	1144	14.68	33.75
−43.5	19.08	286	1530	16.91	$n \cong \sqrt{q}$: 39.2
−44	28.64	430	2290	20.74	47.6
−44.5	57.29	860	4600	29.32	67.8
−45	∞	∞	∞	∞	∞

Remarks: Results are plotted in Fig. 228. $n \cong \sqrt{\kappa_r}$. $q = 1.8 \times 10^4(\sigma/f)$, where σ is in mhos/m and f in Mc/sec. According to (872), $n = \sqrt[4]{\kappa_r^2 + q^2}\, \epsilon^{j\psi}$, $\psi = -\frac{1}{2} \tan^{-1}(q/\kappa_r)$, $\kappa_r = (\kappa/8.854)10^{12}$, where κ is in farads/m. A phase angle $\psi = -45$ deg indicates that for an infinite conductivity, $n \cong \sqrt{q}$ applies (practically large conductivity)

$$n = \sqrt{-jq} = \sqrt{-j}\,\sqrt{q} = (1 - j)\sqrt{\frac{q}{2}}.$$

For practical conditions $q \gg \kappa_r$, we have the approximation $n \cong \sqrt{q/2} - j\sqrt{q/2} \cong \sqrt{q}\,\epsilon^{-j45°}$; $q \ll \kappa_r$ yields $n \cong \sqrt{\kappa_r}$. From 0.0 to −4°, we have $n \cong \sqrt{\kappa_r}$. From −43.5 to −45°, we have $n \cong \sqrt{q}$.

value of n according to (872), similar to the numerical example that follows this formula.

153. Magnitude and Phase of the Complex Coefficient of Reflection for Vertical and Horizontal Polarization. According to (871), the coeffi-

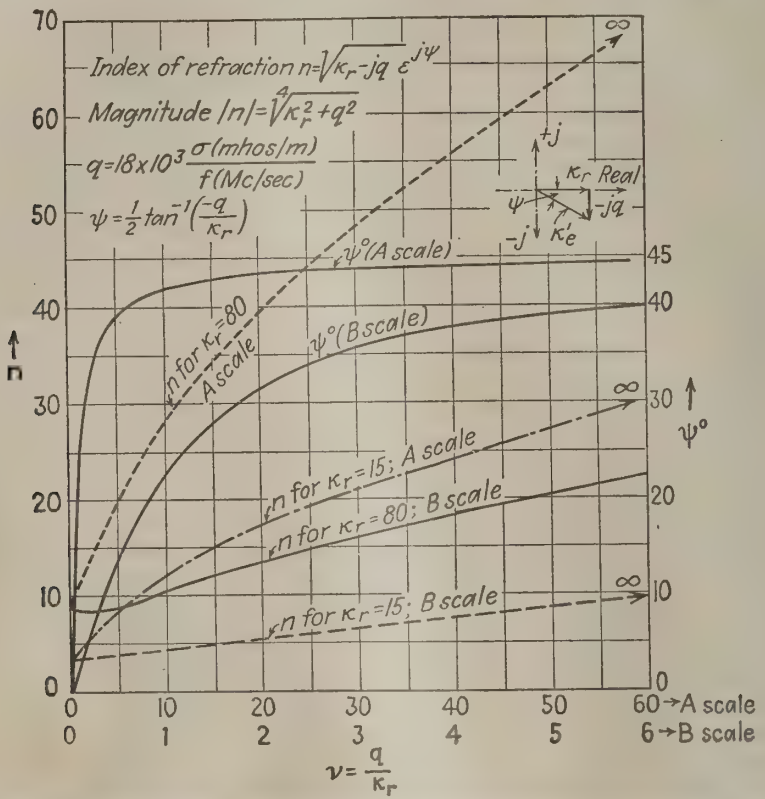

FIG. 228. Index of refraction curves for different earth crusts and phase angles. ($\kappa_r = 15$ refers to average ground; $\kappa_r = 80$ refers to ocean and lakes.)

cient of reflection is, for vertical and horizontal polarization,

$$\left.\begin{aligned} \rho = \rho_v &= \frac{n^2\cos\theta - m}{n^2\cos\theta + m}\,\epsilon^{j\varphi_v}; \qquad \rho = \rho_h = \frac{\cos\theta - m}{\cos\theta + m}\,\epsilon^{j\varphi_h} \\ m &= \sqrt{n^2 - \sin^2\theta} = \sqrt{n^2 + \cos^2\theta - 1} \end{aligned}\right\} \tag{873}$$

where n is the complex relative index of refraction of the general medium against which an electromagnetic wave is incident under an angle θ with the normal to the medium. Table 48 as well as the curves of Fig. 228 give a means of computing quickly the value of n, which is generally complex. Suppose we take the case of wave propagation over ocean

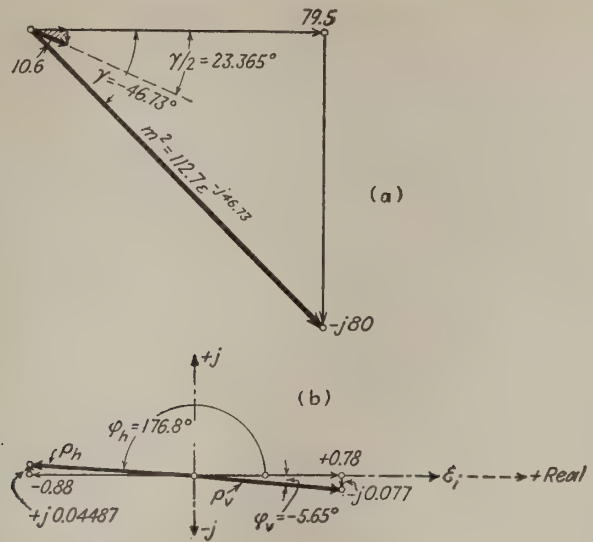

$\mathcal{E}_r$ is reflected field intensity; $\mathcal{E}_i$ is incident field intensity.

$$\mathcal{E}_r = \rho_v \epsilon^{j\varphi_v} \mathcal{E}_i \text{ for vertical polarization}$$
$$\mathcal{E}_r = \rho_h \epsilon^{j\varphi_h} \mathcal{E}_i \text{ for horizontal polarization}$$

FIG. 229. Magnitude and phase of the complex reflection coefficient for vertically and horizontally polarized waves incident on actual earth surface. For $\theta = 45°$, θ is angle of wave incidence and angle of wave reflection.

such that $\kappa_r = 80$ and we have an incidence of $\theta = 45$ deg. Let us further take the condition for which $\nu = 1$, *i.e.*, $q = \kappa_r = 80$ and $n^2 = 80 - j80$. Table 48 shows that we have then $\psi = -22.5$ deg. We have then $\cos\theta = \cos 45° = 0.7071$, $\cos^2 45° = 0.5$,

$$m = \sqrt{n^2 + \cos^2\theta - 1} = \sqrt{80 - j80 + 0.5 - 1} = \sqrt{79.5 - j80}$$

The graphical solution is given in Fig. 229*a*, with the shaded rectangular triangle, yielding the vector $10.6\epsilon^{-j23.365°}$. Hence

$$m^2 = \sqrt{79.5^2 + 80^2}\,\epsilon^{j\gamma} = 112.7\epsilon^{-j46.73°} \qquad \text{since } \gamma = \tan^{-1}\left(\frac{-80}{79.5}\right) = -46.73°$$

$$m = \sqrt{112.7}\,\epsilon^{j\frac{\gamma}{2}} = 10.6\epsilon^{-j23.365°} = 10.6\cos 23.365° - j10.6\sin 23.365°$$
$$= 10.6 \times 0.9178 - j10.6 \times 0.3971 = 9.7 - j4.2$$

We find then in respective expressions for the reflection coefficient

$$\rho_v = \frac{(80 - j80)0.7071 - 0.97 + j4.2}{(80 - j80)0.7071 + 0.97 - j4.2} = \frac{56.5 - j56.5 - 9.7 + j4.2}{56.5 - j56.5 + 9.7 - j4.2}$$
$$= \frac{46.8 - j52.3}{66.2 - j60.7} = \frac{a - jb}{c - jd}$$

$$\rho_h = \frac{0.7071 - 9.7 + j4.2}{0.7071 + 9.7 - j4.2} = \frac{j4.2 - 8.993}{10.41 - j4.2} = \frac{je - f}{g - jh}$$

$$\rho_v = \frac{(a - jb)(c + jd)}{c^2 + d^2} = \frac{(ac + bd) + j(ad - bc)}{c^2 + d^2}$$

$$= \frac{(3{,}100 + 3{,}160) + j(2{,}840 - 3{,}460)}{4{,}382.44 + 3{,}684.49} = \frac{6{,}260 - j620}{8{,}066.93}$$

$$\rho_h = \frac{(je - f)(g + jh)}{g^2 + h^2} = \frac{j(eg - fh) - (eh + fg)}{g^2 + h^2}$$

$$\rho_h = \frac{j(43.7 - 37.6) - (17.64 + 93.2)}{108.16 + 17.64} = \frac{j6.1 - 110.84}{125.8}$$

$$\rho_v = 0.78 - j0.077 = \sqrt{0.78^2 + 0.077^2}\,\epsilon^{j\varphi_v}$$

$$= 0.781 \angle -\tan^{-1}\left(\frac{0.077}{0.78}\right) = -5.65°$$

$$\rho_v = 0.781\epsilon^{-j5.65°}$$

$$\rho_h = j0.0487 - 0.88 = \sqrt{0.88^2 + 0.0487^2}\,\epsilon^{j\varphi_h}$$

$$= 0.881 \angle 180° - \tan^{-1}\left(\frac{0.0487}{0.88}\right) = 0.881\epsilon^{j176.8°}$$

From these numerical results as well as the corresponding vector diagrams of Fig. 229*b*, we note that the respective reflection coefficients have different values and are nearly in phase opposition. We have then, for the incident $\mathcal{E}_i$ and the reflected $\mathcal{E}_r$ electric fields,

$$\left.\begin{aligned} \mathcal{E}_r &= 0.781\epsilon^{-j5.65°}\mathcal{E}_i \quad \text{for vertical polarization} \\ \mathcal{E}_r &= 0.881\epsilon^{j176.8°}\mathcal{E}_i \quad \text{for horizontal polarization} \end{aligned}\right\} \text{ volts/m}$$

That phase opposition almost occurs for *horizontal* polarization can also be seen from the transformation

$$\rho_h = j0.04487 - 0.88 = -(0.88 - j0.04487) = -\sqrt{0.88^2 + 0.04487^2}$$

with a negative angle $\tan^{-1}$ (0.04487/0.88), since it is of the form $a - jb$. But the vector as a whole has a negative sign, which means antiphase condition, or 180 deg, and therefore, 180° − 3.2° with respect to the incident field. The resultant field next to the reflection location is then very different for respective polarizations. We find, for the real components of the reflected field, $0.781\mathcal{E}_i \cos 5.65° = 0.781 \times 0.9952\mathcal{E}_i = 0.78\mathcal{E}_i$ for vertical polarization. For horizontal polarization, we have $-0.881\mathcal{E}_i \times \cos 3.2° = -0.881 \times 0.998\mathcal{E}_i = -0.881\mathcal{E}_i$.

For the resultant field next to the surface of reflection, we have

$$\left.\begin{aligned} \mathcal{E}_R &= \mathcal{E}_i(1 + 0.78) = 1.78\mathcal{E}_i \quad \text{for } \textit{vertical} \text{ polarization} \\ \mathcal{E}_R &= \mathcal{E}_i(1 - 0.88) = 0.119\mathcal{E}_i \quad \text{for } \textit{horizontal} \text{ polarization} \end{aligned}\right\} \text{ volts/m}$$

showing clearly that *close to* the *reflecting surface, vertical polarization should be used.* It is now of interest to find out for which actual conditions such numerical reflection coefficients exist. This can be readily

found from the phase angle $\psi = -22.5$ deg of the index of refraction. Such a phase angle yields, according to Table 48, a value $\nu = 1 = q/\kappa_r$. Therefore, $q = 1.8 \times 10^4(\sigma/f) = \kappa_r = 80$, where κ_r applies to ocean. But such water has, according to its salinity, a conductivity σ ranging from 3 to 5.5 mhos/m. Assuming the value of 4 mhos/m, we find $1.8 \times 10^4 \times 4/f = 80$ and $f = 1.8 \times 10^4 \times \frac{4}{80} = 900$ Mc/sec. Therefore, by means of Table 48 as well as by means of the corresponding curves of Fig. 228, we can readily find the reflection coefficients, since the ratio $\nu = q/\kappa_r$ yields the significant complex n parameter.

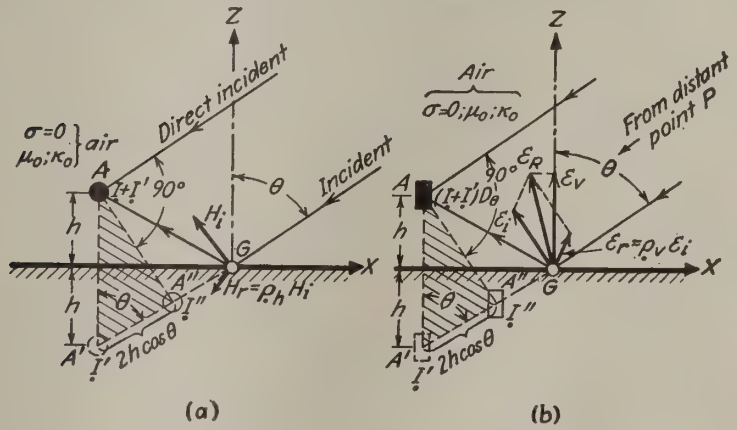

μ, κ, σ for electromagnetic properties of ground

μ, κ, σ medium constants of ground

FIG. 230. Received current in the actual linear antenna A is equal to the current I if no ground is present, and current I' is the image current in linear antenna A' in the presence of ground. A is actual linear antenna; A' is image linear antenna; A'' is fictitious linear antenna for zero path delay; path delay $\delta = 2\beta h \cos\theta$; $\beta = 2\pi/\lambda$ radians per unit height ($= 360/\lambda$ deg per unit height); G is point of reflection. (*a*) Horizontal polarization antennas and $\mathcal{E}$ vectors perpendicular to paper. (*b*) *Vertical* polarization antennas and $\mathcal{E}$ vectors in plane of paper; $\mathcal{E}_i$, H_i are incident and $\mathcal{E}_r$, H_r reflected fields. Current in image antenna A' is $I' = \rho I \epsilon^{j(\varphi-\delta)}\epsilon^{j\omega t}$. Current in fictitious antenna A'' is $I'' = \rho I \epsilon^{j\varphi}\epsilon^{j\omega t}$ for $\rho\epsilon^{j\varphi} = \rho_v\epsilon^{j\varphi_v}$ for vertical polarization, $\rho\epsilon^{j\varphi} = \rho_h\epsilon^{j\varphi_h}$ for horizontal polarization.

154. Reflection and Time Phase Characteristics of an Electromagnetic Ray Reflected from a Plane Surface of the General Medium. Inasmuch as the index of refraction n is complex, the coefficient of reflection must also be complex. This coefficient has then magnitude as well as a phase. Vertical and horizontal polarizations are special cases for the coefficients $\rho_\parallel$ and $\rho_\perp$, according to Table 44, since ρ_v denotes the reflection coefficient for a linear-radiator field for which the radiator is normal to the surface of reflection. For the radiator parallel with the plane of incidence, we have horizontal polarization and deal with the coefficient ρ_h. We have also, for normal wave incidence ($\theta = 0$ deg), the relation $\rho_v = 1 = -\rho_h$. For horizontal polarization, we have, in Fig. 230*a*, the

shaded antenna triangle $AA'A''$, where A represents the point projection of the actual antenna on the ZX plane and A' the point projection of the image linear antenna, which is just as far below the surface of the plane ground as the actual antenna is above it. The antenna triangle $AA'A''$ also includes the angle θ of incidence. Figure 230 represents the comparisons for an arriving down-coming electromagnetic wave in the case of a horizontal or of a vertical receiving linear antenna, respectively, in the presence of *actual* ground. We have then a direct ray PA and an indirect ray PGA, where PG is incident upon the ground, before a portion of it proceeds as ray GA to the reception center of the actual antenna. Point A'' is then such a location that PA'' is just as long as PA, and the field at both locations A and A'' must have the same phase as far as the geometric disposition goes. GA'' is *not* a refracted ray in this case. The image point A' cannot have the same phase condition as the actual point A, since the distance PA' is longer than the distance PA, where P is the radiation center of a distant source of electromagnetic waves. For this reason, we choose the expedient of an antenna triangle $AA'A''$ so that the geometrical distance $PA = PA'' < PA'$. As mentioned, the continuation GA'' as well as $A''A'$ have nothing to do with the refracted ray, since we deal in this section only with a direct ray PA and a ground-reflected ray PGA. But we can use fictitious reception centers A' and A'' to account for the resultant effect at the actual reception center A. Since A'' is just as far away from P as is A, the received fictitious current at A'' must have the same time phase delay as far as the distance PA'' is concerned as has the actual current at A due to the direct ray PA. Inasmuch as we have drawn the distance PA'' straight (since the ground continuation GA'' is in line with the air portion PG), we still have to satisfy what happens at the reflection point G. Equation (873) expresses what happens for either type of polarization. It is being taken care of by the complex reflection coefficient ρ, where ρ is either ρ_v or ρ_h, with a corresponding relative phase φ. Therefore, the fictitious current at A'' is at first of the same relative phase as the current at A due to the direct ray but must have, in addition, the phase φ due to the ground reflection. We have then at A'' a fictitious current $I'' = \rho I e^{j(\omega t+\varphi)}$, where I is the current in the actual antenna at A due to the direct ray. But now the image antenna is not located at A''. It is located at A'. This can be accounted for by just adding a phase delay due to the additional path $A''A'$, since $A''A'$ is the path difference between the direct ray $PA = PA''$ and the indirect path $PG + GA = PG + GA'$. This path difference is, according to Fig. 230, given by $A''A' = 2h \cos \theta$ with a corresponding time phase delay of $\beta 2h \cos \theta = (4\pi h \cos \theta)/\lambda$ radians. We have then the additional delay δ and the

image current I' at A'

$$\left.\begin{aligned} \delta &= 12.56\frac{h}{\lambda}\cos\theta \text{ radians} = 720\frac{h}{\lambda}\cos\theta \quad \text{deg} \\ I' &= I''\epsilon^{-j\delta} = \rho I\epsilon^{j\omega t}\epsilon^{j(\varphi-\delta)} \quad \text{amp} \end{aligned}\right\} \tag{874}$$

where we have ρ_v and φ_v for vertically polarized arriving electromagnetic waves and ρ_h and φ_h for horizontally polarized waves. But now the image antenna does not exist at all, and we have only the actual antenna at A. The resultant received current must then also be at location A, yielding the resultant current $\mathcal{I} + \mathcal{I}'$ in the actual antenna at A, since these currents must be added vectorially. This means that the received current is the vector sum of current I due to the direct incident ray and current I' due to the ground-reflected ray. We note that this formula also takes into account the height h of the location of the receiving center.

Now we must distinguish between the reception of vertically polarized waves and horizontally polarized waves, for two reasons. First, the magnitudes of ρ_v and φ_v differ from the corresponding magnitudes of ρ_h and φ_h, and one angle may be positive and the other negative. Second, we have to take into account the unobstructed space directivity of the antenna that receives. The space directivity is, of course, the same for an antenna whether used as a pickup expedient of electromagnetic waves or as a radiator. If we deal with a linear antenna, as would most likely be used at UHF's for vertical and horizontal polarizations, we know that we have a simplified space directivity pattern, since we have circular symmetry about a linear antenna, leaving only the directivity in any meridian plane of the linear antenna as a parameter to be taken care of. We work then mostly with half-wave antennas, although any other electrical length can be used. The meridian directivity may or may not play a part, depending on the orientation of the antenna with respect to ground, which causes reflected field energy. We orient the linear antenna according to the polarization of the arriving wave, since a linear antenna is, for the sake of good engineering practice, oriented so as to receive the strongest signal. This happens if the linear antenna is parallel with the electric vector of the arriving resultant field. We do not always have control of the direction of the resultant $\mathcal{E}$ field. This is especially the case when we receive in an airplane or receive on ground from a transmitter on a plane and is also the case if we receive on surface vessels with the linear receiving antenna waving in almost any orientation under adverse conditions. It is then good practice to orient the receiving antenna for the polarization used by the radiator. Therefore, vertical antennas will then generally be used for vertically polarized transmitted waves and horizontal receiving antennas for horizontally polarized transmitted waves and parallel with the arriving $\mathcal{E}$ vector. It is only for very weak arriving fields that we can change the orientation of the receiving antenna; also a diversity receiving antenna system may automatically always give optimum reception.

We have, for Fig. 230*a*, a reception effect $\mathcal{I} + \mathcal{I}'$ and, for Fig. 230*b*, an effect $(\mathcal{I} + \mathcal{I}')D_\theta$, where for a half-wave receiving dipole, we have $D_\theta = [\cos(90^\circ \cos\theta)]/\sin\theta$. This assumes that we use the indicated

vertical antenna in Fig. 230*b* and the horizontal linear antenna of Fig. 230*a* such that its length dimension is not only parallel to ground but also normal to the XZ plane. This condition is, no doubt, employed in practice, since it gives optimum signal-strength pickup. The reason why we do not require a directivity factor in Fig. 230*a* is that the directivity around the horizontal receiving antenna is constant and equal to maximum directivity (since $D = D_{\theta\max}$). We can use any other linear antenna whose length may differ from $\frac{1}{2}\lambda$ but must apply then the

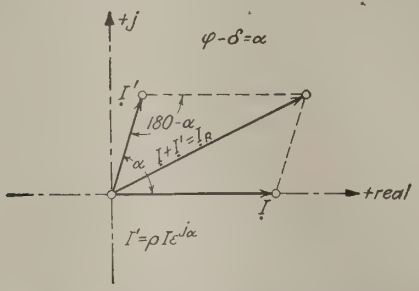

FIG. 231. Vector addition of actual and image currents for positive values of α. The time factor $\epsilon^{j\omega t}$ is understood, and I, I', and I_R denote the maximum time values; then absolute lengths of vectors I, I', and I_R are I, $I' = \rho I$ and $I_R = \sqrt{I^2 + \rho^2 I^2 - 2\rho I^2 \cos(180° - \alpha)}$ $= I\sqrt{1 + \rho^2 + 2\rho\cos\alpha} = I\sqrt{1 + (I'/I)^2 + 2(I'/I)\cos\alpha}$ amp.
If I, I', and I_R denote the corresponding effective values, this formula likewise applies.

appropriate D_θ formula, as explained on pages 529–547. The resultant received antenna current at A is then

$$\left.\begin{aligned} I_A^{(\text{amp})} &= D_\theta \epsilon^{j\omega t}[I + \rho_v I \epsilon^{j(\varphi_v - \delta)}] \quad \text{for vertical polarization} \\ I_A &= \epsilon^{j\omega t}[I + \rho_h I \epsilon^{j(\varphi_h - \delta)}] \quad \text{for horizontal polarization} \end{aligned}\right\} \tag{874a}$$

Putting $\varphi - \delta = \alpha$, where φ stands either for φ_v or φ_h, respectively, we generally have a vector addition as in Fig. 231 for the terms in the brackets. Whether α has positive or negative values depends upon the polarity and magnitude of the phase φ of the coefficient ρ of reflection. The magnitudes I_v and I_h of the received current are, for the respective polarizations,

$$\left.\begin{aligned} I_v &= D_\theta I\sqrt{1 + \rho_v^2 + 2\rho_v \cos\left(\varphi_v - \frac{720h\cos\theta}{\lambda}\right)} \\ I_v &= D_\theta I \quad \text{if no ground present (unobstructed)} \\ I_h &= I\sqrt{1 + \rho_h^2 + 2\rho_h \cos\left(\varphi_h - \frac{720h\cos\theta}{\lambda}\right)} \\ I_h &= I \quad \text{if no ground present} \end{aligned}\right\} \text{amp} \tag{874b}$$

where D_θ is the unobstructed free-field directivity of a linear radiator in any meridian plane of the radiator. The respective ratios I_v/I and I_h/I are then a measure for the effects due to *actual* ground (which is electromagnetically a general medium). We have then

$$\frac{I_v}{I} = D_\theta \sqrt{\text{holding for vertical polarization}}$$

and $I_h/I = \sqrt{\text{holding for horizontal polarization}}$, where the value under the square root is given in (874*b*). The relative image current I'/I, with

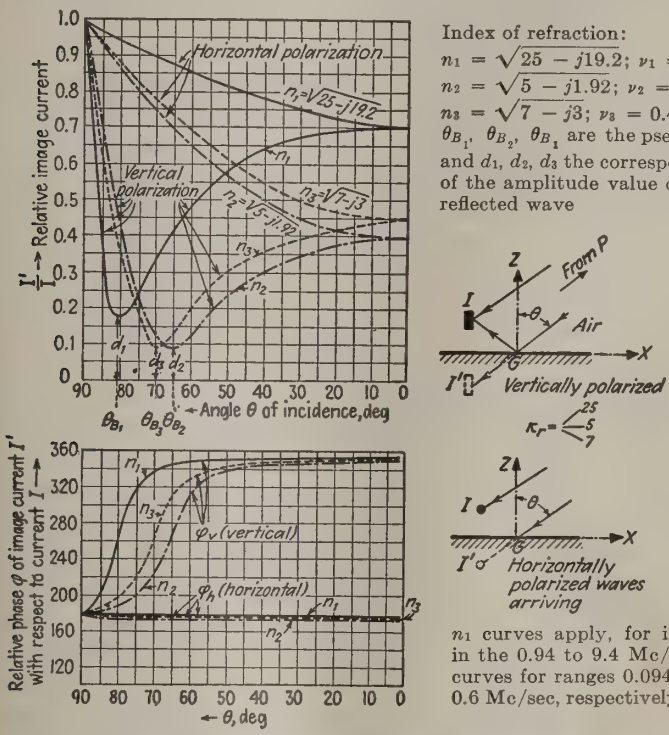
Horizontal polarization
Vertical polarization
$n_1=\sqrt{25-j19.2}$
$n_2=\sqrt{5-j1.92}$
$n_3=\sqrt{7-j3}$
$\frac{I'}{I}$ → Relative image current
θ_{B_1} θ_{B_2} θ_{B_3}
← Angle θ of incidence, deg
Relative phase φ of image current I' with respect to current I →
φ_v (vertical)
φ_h (horizontal)
← θ, deg
Index of refraction:
$n_1 = \sqrt{25 - j19.2}$; $\nu_1 = 0.77$
$n_2 = \sqrt{5 - j1.92}$; $\nu_2 = 0.384$
$n_3 = \sqrt{7 - j3}$; $\nu_3 = 0.429$
θ_{B_1}, θ_{B_2}, θ_{B_3} are the pseudo Brewster angles, and d_1, d_2, d_3 the corresponding Brewster dips of the amplitude value due to the dip in the reflected wave
From P
Air
Vertically polarized
$\kappa_r' = 25, 5, 7$
Horizontally polarized waves arriving
n_1 curves apply, for instance, to wet soil in the 0.94 to 9.4 Mc/sec range; n_2 and n_3 curves for ranges 0.094 to 0.94 and 0.06 to 0.6 Mc/sec, respectively, for dry soil

FIG. 232. Relative image current and its relativity phase with respect to the actual antenna current in absence of the reflecting surface of the earth.

respect to the actual antenna current I, due to the incident *direct* electromagnetic field (this is the field without the presence of ground), gives a measure for the reflection ability of the ground. Figure 232 shows applications of formulas (874*a*) for three different grounds, which have, respectively, the relative equivalent dielectric constants $\kappa_e' = 25 - j19.2$, $= 5 - j1.92$, and $= 7 - j3$. It will be noted that for angles of incidence θ_{B_1}, θ_{B_2}, and θ_{B^3}, respectively, we have *minimum* reflection conditions

instead of a complete extinction of the reflected indirect ray. The reason for this minimum reflected ray is that we have no quasi-dielectric ground effects for the given relative values of κ'_e, which are instrumental for the curves in Fig. 232. We have, therefore, only a *pseudo* Brewster angle effect and, as it were, can speak of a "blurred" image effect instead of a "sharp" image effect holding for a pure dielectric and causing complete transmission of the indirect ray into the ground for the Brewster angle. What is significant is that for horizontal polarization, we have essentially antiphase reflections as would be the case if the ground behaved electromagnetically like a perfect dielectric. We should also have antiphase reflections from a ground that would, in effect, behave like a good metal reflector, but with a complete field energy return. We also note in Fig. 232 that for vertical polarization, we have appreciable changes as the angle of θ varies. We have first a gradual decrease of I'/I as the angle of incidence increases from zero value (incidence perpendicular to ground) until for the Brewster angle θ_B a minimum reflection effect occurs. With a still further increase of the angle θ of incidence (beyond the Brewster angle), the ratio I'/I increases very rapidly, until at grazing incidence with the ground, we have complete (100 per cent) reflection. That this *must* happen for an incidence of $\theta = 90$ deg is evident, since the entire electromagnetic wave energy of the indirect ray PG of Fig. 230, if extended to the image point A', is then a ray PA' *along* the surface of the ground. Therefore, the field energy slips tangentially to ground. There is *some power lost, however,* since, owing to the finite conductivity of the ground, the arriving electromagnetic field has a *slight forward tilt* of the electric $\mathcal{E}$ vector, which resultant arriving vector can be decomposed into a true vertical $\mathcal{E}_v$ component and an $\mathcal{E}_t$ component that is *tangential* to ground and supplies the joulean heat losses dissipated in the ground. The reason why the curves in Fig. 232 give unity value for the reflection effect is that in formulas (874*a*), we compare only the incident indirect ray PG of Fig. 230 with the reflected ray GA. In reality, we generally have a *direct* incident ray (Fig. 230) as well as an indirect incident ray; both rays still hold generally for grazing incidence, and only for the normal component (normal to ground) the I'/I then holds. In other words, owing to the forward tilt only the component of $\mathcal{E}$ that is normal to ground constitutes the ρ_v coefficient, which is used in (874*a*). The energy extraction is, however, very small for short waves so that the forward tilt of the resultant $\mathcal{E}$ vector of the arriving incident wave for grazing incidence cannot be appreciable, and the normal component $\mathcal{E}_v$ with respect to ground is essentially equal to the resultant component $\mathcal{E}$.

The indexes of refraction in Fig. 232 show that we have, for the ratio $\nu = q/\kappa_r$ where $n_1 = \sqrt{25 - j19.2} = \sqrt{\kappa_r - jq}$, the ratio $\nu_1 = 19.2/25$

$= 0.77$; for $n_2 = \sqrt{5 - j1.92}$, we find $\nu_2 = 1.92/5 = 0.384$; and for $n_3 = \sqrt{7 - j3}$, we find $\nu_3 = 3/7 = 0.4286$. The magnitude of the index of refraction n can be found from $n = \sqrt[4]{\kappa_r^2 + q^2}$ and the phase from $\psi = \frac{1}{2} \tan^{-1}(-\nu)$, since $\nu = -q/\kappa_r$, if the polarity is also taken into account. We note that with increasing value of the ratio ν, the minimum of reflection, which is the Brewster dip, moves more toward grazing incidence with respect to the plane surface of the ground.

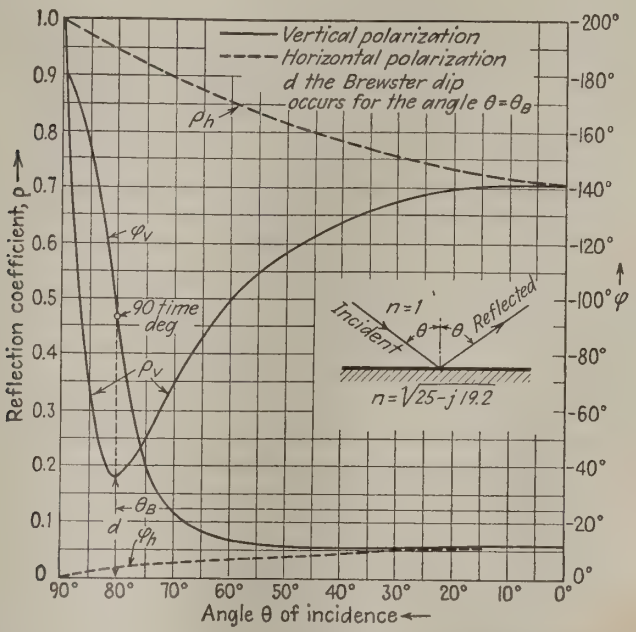

FIG. 233. Magnitude and phase of the reflection coefficient of the earth crust for an equivalent relative dielectric constant $\kappa_e' = 25 - j19.2$; magnitude is ρ and phase is φ. For

$$n = \sqrt[4]{25^2 - 19.2^2}\,\epsilon^{-j(\frac{1}{2}\tan^{-1}0.77)} = 5.6\epsilon^{-j18.8^\circ} \text{ since } \nu = \frac{19.2}{25} = 0.77$$

Polarity of φ is with respect to the phase of a perfect ground ($\varphi = \infty$); Brewster dip $d = 0.18$.

Inasmuch as the ground generally acts (depending very much on the frequency) as a space condenser with a dissipative dielectric, we deal with a capacitive impedance. Some writers refer to the phase φ of the reflection coefficient ρ with respect to the phase of a perfectly conducting reflector ($\sigma = \infty$). The angle φ is then the angle by which the reflected electromagnetic wave leads the phase of a perfect reflector. This, combined with the capacitive impedance concept, results in phase angles φ, which are always negative, so that in Eq. (874a), the phases φ_v as well as φ_h come out negative. This is equivalent to saying that we have the phase factor $\epsilon^{-j(\varphi_v+\delta)}$ for vertically polarized waves and $\epsilon^{-j(\varphi_h+\delta)}$ for hori-

zontally polarized waves. Doing this for an effective relative dielectric constant $\kappa_e' = 25 - j19.2$, we find the conditions of Fig. 233. The curves of Figs. 232 and 233 are quite useful and can be applied to many practical cases, since a fixed index n of refraction is basic. It should be borne in mind that not only the ratio $\nu = q/\kappa_r$ plays a part but also the magnitude of κ_r. The reason for this is that the actual relative dielectric constant κ_r selects the medium. In Fig. 233, it selects the medium with

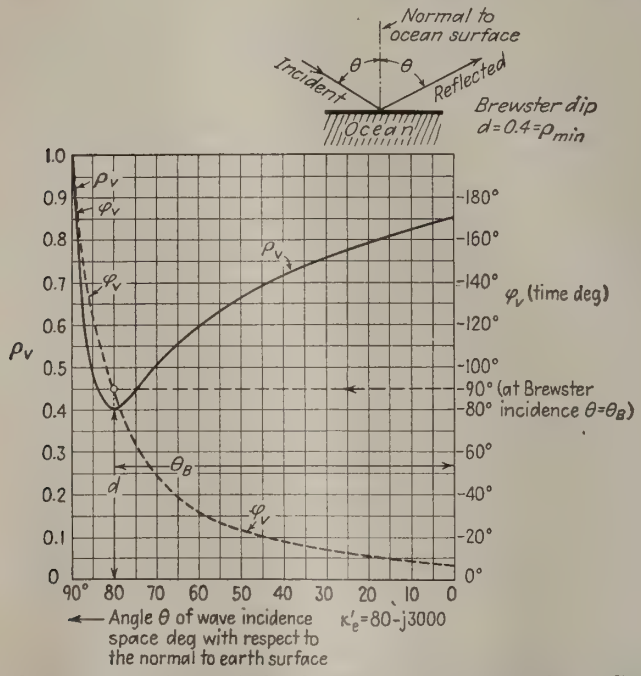

Fig. 234. Reflection curves for vertical polarization over ocean surface. Curves apply somewhere in the range of 18 to 30 Mc/sec for reflections from the ocean surface, the exact frequency depending on the degree of salinity and temperature. Index of refraction: $n = \sqrt{80 - j3000} = 54.8\epsilon^{-j44.24^\circ} = 39.5 - j38.4$; $n^2 = 3001 \cdot \epsilon^{-j88.48^\circ} = 3001 - j79$.

a value of $\kappa_r = 25$, which holds, for instance, for wet ground. Hence, a curve holding for a certain value of κ_r applies to many values of the conductivity σ as long as the frequency f is correspondingly chosen. This is then based upon the q term, which is equal to $1.8 \times 10^4(\sigma/f)$ for σ in mhos per meter and f in megacycles per second. Since, according to (873) and Fig. 233, we have $1.8 \times 10^4(\sigma/f) = 19.2 = q$, the frequency, for wet soil with a conductivity $\sigma = 10^{-2}$ mho/m, is found as $f = 1.8 \times 10^4 \times 10^{-2}/19.2 = 9.4$ Mc/sec. If we take the other limit of $\sigma = 10^{-3}$ mho/m, which also holds for wet soil, we find 0.94 Mc/sec. Therefore, for the average range from 0.94 to 9.4 Mc/sec, we can expect reflection

coefficients as given in Fig. 233. This range of frequencies is also covered by Fig. 232 for the n_1 values and the corresponding phase φ of the reflection coefficient. This frequency range is altogether too low for UHF's. Nevertheless, it brings out that by means of a single curve, we can cover quite a wide frequency range of ground conditions.

There are many other mediums on which electromagnetic reflections take place. They are not necessarily ground but may be buildings and structures of any kind. We deal with wave obstructions in this chapter, and it does not take a large object for short waves to cause reflections and a space interference pattern of the electromagnetic field. The curves of Figs. 232 and 233 may be of use then for many other purposes. Figure 234 gives curves for vertically polarized waves for an equivalent relative dielectric constant $\kappa_e' = 80 - j3{,}000$. Since we have $\kappa_r = 80$, these curves apply to wave propagation either over ocean or over lakes and rivers. For ocean water with $\sigma = 5$ mhos/m, we have then $f = 1.8 \times 10^4 \times 5/3{,}000 = 30$ Mc/sec.

155. Useful Concepts for Reflections on a Generalized Medium and Significance of the Pseudo Brewster Angle Effect. In previous sections, we learned that for the general medium, the equivalent relative dielectric constant is $\kappa_e' = \kappa_r - jq$, since not only the relative dielectric constant $\kappa_r = \kappa/\kappa_0$ but also the quadrature term $q = 1.8 \times 10^4(\sigma/f)$ play a part. It is this term which explains the joulean heat dissipation in the general medium. It also explains why, for the Brewster angle θ_B of wave incidence, we do *not* obtain a vertical reflection coefficient ρ_v that is not zero but only a $\rho_{\min}$ value. The Brewster angle dips for the general medium are marked as d_1, d_2, and d_3, respectively, in Fig. 232. We have then $\rho_{\min} = 0.18$ for d_1 and about a 0.09 value for both the d_2 and the d_3 values. These are the pseudo Brewster angle vertical reflection coefficients. According to Fig. 232, we have for the amplitude of the reflected field for the complex relative equivalent dielectric constant $\kappa_e' = 25 - j19.2$ (corresponding to the n_1 curves), only 18 per cent of the incident amplitude for either the $\mathcal{E}$ or the associated H vector of the electromagnetic field. Inasmuch as the energy transfer is proportional to the square of the field intensity, the energy reflection coefficient would be $0.18^2 = 0.0324$. This means that only 3.24 per cent of the incident field energy is reflected for the Brewster angle of incidence. There is much more to the significance of this particular polarization angle. We note, for instance, from the curves of Fig. 232 that for the respective minimum reflection coefficients d_1, d_2, and d_3, we have a phase angle $\varphi_v = 270$ deg. If this phase is expressed relative to the case of perfect reflection, it is $\varphi_v = -90$ deg. This is shown in Fig. 233 for an equivalent relative dielectric constant of value $25 - j19.2$. It is also -90 deg in Fig. 234

for a relative equivalent dielectric constant $80 - j3{,}000$. This means that the *Brewster angle amplitude dip occurs at minus* 90 *time degrees.*

For a pure dielectric medium, we have no joulean heat losses and the Brewster angle of dip goes straight to zero value. We have then an *abrupt* phase jump through the -90-deg angle from 0 to -180 deg for the φ_v value of the coefficient ρ_v of reflection. We have, in a general medium, electromagnetic properties that are similar to the properties in customary alternating-current networks. For a-c networks, we have an ohmic resistance the reciprocal of which is a conductivity in mhos. The conductivity σ in mhos per meter is the corresponding characteristic for the general medium. In a-c networks, we have the self-inductance in henrys as the second characteristic, in order to account for effects of variable magnetic fields. For the general medium, the permeability μ is the corresponding property in henrys per meter. The mutual inductance is only a generalization of the self-inductance. The third characteristic in an a-c network is the capacitance in farads, which accounts for variable electric field effects. The dielectric constant κ in farads per meter is the corresponding property for the general medium. We note that for the general medium, we deal with *gradients*, since all three characteristics are in mhos per meter, henrys per meter, and farads per meter, respectively. But we must realize that we also have to deal with voltage and current gradients, since $\mathcal{E}$ is in volts per meter and H in amperes per meter. We sometimes use gradients also in a-c networks. It is the case, for instance, for transmission lines, where we use capacitance per meter, inductance per meter, and resistance per meter. Since σ, μ, and κ are fundamental electromagnetic properties of space, we must retain *at least* the μ and κ properties under all conditions, just as in a-c networks, we can imagine that for an ideal network, we have also only L and C properties, since the conductivity is then infinite and there is no effective ohmic resistance. The corresponding case for a medium is a perfect dielectric with the vacuum as the very extreme case, for which we have $\mu = \mu_0 = 1.257 \times 10^{-6}$ henry/m and $\kappa = \kappa_0 = 8.854 \times 10^{-12}$ farad/m. If we were to lose either of these two properties, we could not have an electromagnetic field condition, *i.e.*, a motion of an electromagnetic field, since $1/\sqrt{\mu_0\kappa_0}$ meters per second $= 3 \times 10^8$ m/sec is the velocity of motion in empty space. The property μ_0 is then the never-vanishing value of empty volume accounting for the kinetic energy (inertia effect), and the property κ_0 the other never-vanishing value of empty volume accounting for the potential energy.

Since we have, for the general medium, in effect, a capacitive space impedance, we must have, for the Brewster angle of incidence, a minimum reflection effect from the surface of such a medium. We already have curves (Figs. 232 to 234) for what happens for smaller and larger angles of incidence than the Brewster angle θ_B. We have the formula (870) for the pseudo Brewster angle and formula (874*b*) for the I_v value in the case of vertically polarized waves sweeping against a general medium. If we plot the reflection coefficient ρ, as given in Fig. 233 by the ρ_v, ρ_h, φ_v, and φ_h curves, with respect to magnitude and phase, we obtain the vector display as given in Fig. 235. These vectors are drawn with respect to the phase and magnitude of the reflected field $\mathcal{E}_r$ equal to the magnitude $\mathcal{E}_i$ of the incident field in the case of a *perfectly conducting reflector* (infinite

mhos per meter). We have then $\mathcal{E}_r = \rho\mathcal{E}_i\epsilon^{j\varphi}$ volts per meter and $H_r = \rho H_i\epsilon^{j\varphi}$ amperes per meter, where we have ρ_v and φ_v for vertically polarized waves and ρ_h and φ_h for horizontally polarized waves. For a perfectly conducting reflector, we have then $\mathcal{E}_r = \rho_v\mathcal{E}_i = \mathcal{E}_i$, since $\rho_v = +1$ and $\varphi_v = 0$ deg. This is the case, since we have, for perfectly reflecting ground in Fig. 224, inphase actual and image currents of the same magnitude. However, for horizontally polarized electromagnetic waves, we have, for perfectly conducting ground (a perfect metal reflector), equal

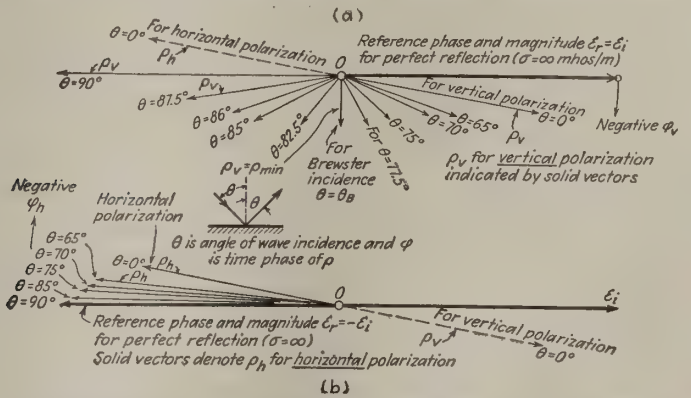

FIG. 235. Reflection coefficient ρ with respect to magnitude and time phase φ referred to the phase of the reflection coefficient for perfect reflection (metallic reflection comes closest to it). (*a*) and (*b*) are for wave propagation from air ($n \cong 1$) toward a medium

$$n = \sqrt{25 - j19.2};$$

θ space angles; $\varphi = \varphi_v = \varphi_h$ time angles; $\rho = \rho_v$ for vertical polarization $= \rho_h$ for horizontal polarization; ρ is coefficient of reflection. *Note:* (*a*) for *vertically* polarized waves the time phase angle $\varphi = \varphi_v$ time degrees covers 180 time degrees. For the Brewster wave incidence $\theta = \theta_B = 81$ space degrees, we have $\varphi = \varphi_v = 90$ time degrees and a minimum reflection coefficient $\rho_v = \rho_{min}$. (*b*) For *horizontally* polarized waves the time phase angle $\varphi = \varphi_h$ remains for the general medium at which surface wave reflections occur always negative and in the vicinity of antiphase condition. (There is *no* Brewster angle for *horizontal* polarization.)

antiphase actual and image currents. Hence, $\mathcal{E}_r = \rho_h\mathcal{E}_i = -\mathcal{E}_i$ volts per meter, since $\rho_h = -1$. This also means that $\mathcal{E}_r = \mathcal{E}_i\epsilon^{-j180°}$, $\varphi_h = -180$ deg, and $\epsilon^{-j180°} = \cos 180° - j \sin 180° = -1$. Such metallic ground action, however, does not exist but may be approximated in effect. But it can be used as in Fig. 235 as a reference condition, so that we can obtain an idea of how actual ground behaves for all angles of wave incidence. Since, for a perfect metallic reflector, we have $\rho = \pm 1$, depending upon the kinds of polarizations, the vectors of Fig. 235 either represent the reflection coefficients with respect to magnitude and phase, relative to perfect reflection coefficients, or can be taken as the values $\mathcal{E}_r$ in volts per meter of the reflected electric field if the incident $\mathcal{E}_i$ value is equal to 1 volt/m. We must distinguish between angle of wave inci-

dence θ and the relative time angle φ. The latter is the relative angle of the reflection coefficient ρ with respect to the ideal values $\rho = \pm 1$, *i.e.*, with respect to inphase and antiphase complete reflection conditions. This is the reason why the reference vector $\mathcal{E}_r$ in Fig. 235 is in phase with the incident vector $\mathcal{E}_i$ and drawn to the right for the case of vertically polarized waves. For horizontally polarized waves, it is drawn to the left in order to satisfy the condition $\mathcal{E}_r = -\mathcal{E}_i = -1$ volt/m. Since, in Fig. 233, the same reference condition is used, it was only necessary to use for a certain angle θ of incidence the corresponding phase angle φ of Fig. 233 as well as the corresponding magnitude ρ and draw in Fig. 235 the corresponding vector a length equal to ρ and with respect to the negative value of φ. Since the Brewster angle is $\theta_B = 81$ deg for these figures, we have to draw the corresponding vector for $\varphi_v = -90$ deg and make it equal to $d = 0.18$, because $\rho = \rho_{\min} = d$. This gives the vector $\rho_{\min}$ in the upper vector display of Fig. 235. For perpendicular incidence, Fig. 233 yields, for $\theta = 0$ deg, the respective relative phase angles $\varphi_v = \varphi_h = 10.5$ deg and the magnitudes $\rho_v = \rho_h = 0.705$. This means that for either polarization, we have vectors in Fig. 235 of the same length 0.705 but ρ_h lags 180 deg behind ρ_v for normal wave incidence. This can be readily seen by comparing the respective vectors of Fig. 235 in the upper and lower vector display for the $\theta = 0$ condition. Doing this for $\theta = 65$, 70 up to 90 deg, we find the vector displays of Fig. 235. We note that there is a great difference between vertical and horizontal polarization. For horizontal polarization (lower vector display), the various vectors are all crowded toward the reference vector with only a comparatively small relative change in magnitude. But for vertical polarization (upper vector display of Fig. 235), the various vectors are *all over*, covering a range of close to 170 deg, and the respective magnitudes vary *relatively greatly*. Therefore, for a relative equivalent dielectric constant $\kappa_e' = 25 - j19.2$, for which these vector displays hold, we have, for horizontally polarized waves, a relative phase delay that never exceeds 10.5 deg. This means that we have, in this case, roughly antiphase reflected fields with respect to the incident fields from 65 to 90 deg of wave incidence. We could have taken in all other angles of incidence and found this to hold true. We must realize that θ is the angle with respect to the *normal* to ground, and the 65- to 90-deg incidences are what we are most interested in, because 90 deg means grazing wave incidence. For vertical polarization, the relative time lag of ρ_v then covers a range from $\varphi_v = -10.5$ to -180 deg. We also obtain an idea from Fig. 235 of what we can expect when the polarization is still linearly polarized but with vertical *and* horizontal field components. The reflections are then made up of the components $\rho_v \mathcal{E}_i \epsilon^{-j\varphi_v}$ and $\rho_h \mathcal{E}_i \epsilon^{-j\varphi_h}$

for the respective angles of incidence. This means that *elliptical* polarization occurs in the reflected field, which is *different* from the elliptical polarization of the incident field for the various angles of incidence, since $\varphi_v - \varphi_h$ changes and does not vanish. For the Brewster angle of incidence ($\theta = \theta_B$), a small amount of the incident vertical polarization reflects and the resultant reflected wave is *mostly horizontally* polarized. But if we deal in the upper megacycle range of UHF's, the relative equivalent dielectric constant yields $\kappa_e' = \kappa_r - j\underline{q} \cong \kappa_r$, and the relative index of refraction becomes practically real; *i.e.*, $n \cong \sqrt{\kappa_r}$. The resultant reflected field at the Brewster angle $\theta_B = \tan^{-1}(n)$ is then entirely horizontally polarized, since the component of the incident vertical polarization is completely transmitted (refracted) into the ground. This happens, for instance, for wave propagation over mountain lakes with fresh water at 100 Mc/sec and higher, since $q = 1.8 \times 10^4(\sigma/f) = 1.8 \times 10^4 \times 5 \times 10^{-3}/100 = 0.9$ as against $\kappa_r = 80$. Therefore 0.9 is negligible as against the geometrical quadrature component of 80. It also happens for dry and wet ground in the UHF range of carrier frequencies.

Ground is not the only obstacle in electromagnetic wave propagation, and it is, therefore, necessary to have available curves that cover almost any condition for the ratio $\nu = q/\kappa_r$ in the relation $n = \sqrt{\kappa_r - j\underline{q}}$ for the complex relative index of refraction of almost any electromagnetic obstacle, such as buildings, etc. Table 48 is then of use with curves for fixed ν ratios as in Fig. 236, where the ν ratios of Table 48 are employed. Applying these curves to average ground with a conductivity range from $\sigma = 10^{-2}$ to 10^{-4} mho/m yields, for $\nu = 1$, the term $q = 15 = 1.8 \times 10^4(\sigma/f)$. For the limit of 10^{-2} mho/m, we find $f = 1.8 \times 10^4 \times 10^{-2}/15 = 12$ Mc/sec; while for the other limit, we have as low a frequency as 0.12 Mc/sec. The $\nu = 1$ curves, therefore, apply to a frequency band of about 0.12 to 12 Mc/sec. For the $\nu = 0.1$ curves, we find, for $\sigma = 10^{-2}$ mho/m a frequency of $f = 1.8 \times 10^4 \times 10^{-2}/1.5 = 120$ Mc/sec, which brings us into the VHF range of carrier frequencies. We also note from Fig. 236 that the Brewster angle θ_B of wave incidence moves all the more toward $\theta = 90$ deg the larger the ν ratio, *i.e.*, the larger the conduction term q with respect to the displacement term κ_r in the relation $n = \sqrt{\kappa_r - j\underline{q}}$. Only small ratios $\nu = q/\kappa_r (\leqq 0.1)$ can be of interest in UHF work for reflections from average ground. Moreover, for $\nu \ll 0.1$, the Brewster dip $d = \rho_{v_{\min}}$ approaches zero value as ν becomes smaller. This happens irrespective of the value of κ_r, since for $\nu = q/\kappa_r \ll 1$, we have $n = \sqrt{\kappa_r}\sqrt{1 + \nu^2}\underline{/-\tfrac{1}{2}\tan^{-1}(\nu)} \cong \sqrt{\kappa_r}$ as far as wave reflections are concerned. The values $3.87 - j0.196$, $4.27 - j1.77$, $9.1 - j8.2$, and $27.6 - j27.1$ are used for computing ρ_v and ρ_h as well as

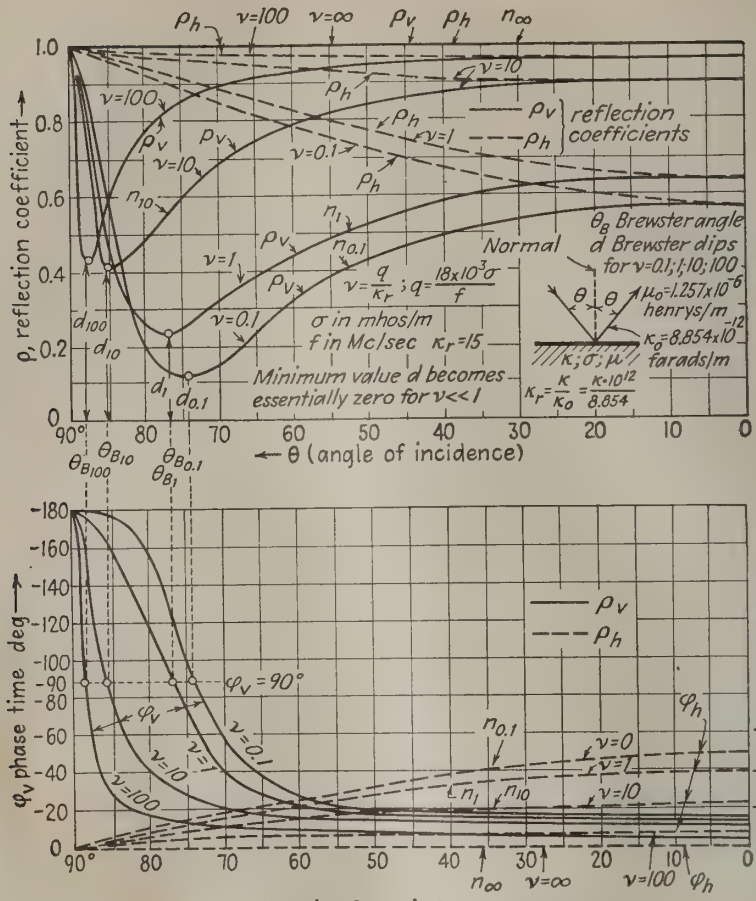

The time phases φ_v and φ_h deg are with respect to the phases, holding for ideal reflections ($\sigma = \infty$)

Holds for $\kappa_r = 15$ (average ground reflections)

$n = \sqrt{\kappa_r}\sqrt{1 - j\nu} = \sqrt{\kappa_r}\sqrt[4]{1 + \nu^2}\,\epsilon^{-j\frac{1}{2}\tan^{-1}(\nu)}$

n_1 is the index n for $\nu = 1$; n_{10} for $\nu = 10$; n_{100} for $\nu = 100$, etc.

$n = \sqrt{15 - jq} = 3.87\sqrt{1 - j\nu} = 3.87\sqrt[4]{1 + \nu^2}\,\epsilon^{-j\frac{1}{2}\tan^{-1}(\nu)}$

$n_{0.1} = 3.87\sqrt[4]{1.01}\,\epsilon^{-j\frac{1}{2}\tan^{-1}(0.1)} = 3.87\sqrt[2]{1.005}\,\epsilon^{-j8.9^\circ}$

$n_1 = 3.87\sqrt[4]{2}\,\epsilon^{-j\frac{1}{2}\tan^{-1}(1)} \cong 3.87\ (\cos 2.9^\circ - j \sin 2.9^\circ)$

$= 4.61\ (\cos 22.5^\circ - j \sin 22.5^\circ) = 3.87 - j0.196/\underline{-2.9^\circ}$

$= 4.27 - j1.77/\underline{-22.5^\circ}$

$n_{10} = 3.87\sqrt[4]{101}\,\epsilon^{-j\frac{1}{2}\tan^{-1}(10)}$

$= 12.26\epsilon^{-j42.1^\circ} = 9.1 - j8.2/\underline{-42.1^\circ}$

$n_{100} = 3.87\sqrt[4]{1 + 10^4}\,\epsilon^{-j\frac{1}{2}\tan^{-1}(100)}$

$= 38.7\epsilon^{-j44.6^\circ} = 27.6 - 27.1/\underline{-44.6^\circ}$

FIG. 236. Reflection coefficients and their phases for various useful values of the electromagnetic index of refraction $n = \sqrt{\kappa_r - jq}$, if $\kappa_r = 15$ (average ground condition).

φ_v and φ_h from formula (873). But for the phase, angles φ_v and φ_h (computed by this procedure) are then taken and the vectors drawn with respect to the phase for an ideal metallic reflector ($\sigma = \infty$), as in Fig. 235. The case for $\nu = 100$, yielding $n = 27.6 - j27.1$, is at about the beginning limit of the condition $\nu \gg 1$, for which $n = \sqrt{-jq} = \sqrt{q}\,\epsilon^{-j45°}$, since $n = \sqrt{\frac{1}{2}q} - j\sqrt{\frac{1}{2}q}$, and the general medium behaves electromagnetically as a good conductor. This must happen then for large values of σ and for customary conductivities of the earth's crust at lower frequencies, which is beyond the scope of this text. From the computations in Fig. 236, we note that the magnitude of the index n of refraction increases as the ratio ν increases. It is $|n| = 38.7$ for $\nu = 100$ and 3.87 for $\nu = 0.1$, which is the lowest value it can ever reach, since $n = \sqrt{\kappa_r} = \sqrt{15}$ is this value. However, if the medium causes reflections for $\nu \ll 1$ such that $n = \sqrt{\kappa_r}$ (equal to 3.87 in this case), then $\theta_B = \tan^{-1}(n) = \tan^{-1}(3.87) = 75.5$ deg, which about confirms the value for θ_B in Fig. 236 for $d_{0.1}$. Therefore, as far as the reflection coefficient is concerned, the ground behaves as a dielectric to reflections (depends also on the value of κ_r, besides the ratio $\nu = q/\kappa_r$). Taking the case for ocean water, we have $n = \sqrt{\kappa_r}\sqrt{1 - j\nu} = 8.944\sqrt{1 - j\nu}$, for conductivities ranging from about 3 to about 5.5 mhos/m. Using $\sigma = 4$ mhos/m, we find $q = 1.8 \times 10^4(4/f) = 7.2(10^4/f)$, giving for $\nu = 0.1$ a frequency $f = 7.2(10^4/8) = 9{,}000$ Mc/sec instead of 120 Mc/sec, which holds for average ground of $\kappa_r = 15$ and a conductivity of 10^{-2} mho/m. This brings us then to conditions that have been already discussed in connection with Fig. 227.

Since $n = \sqrt{\kappa_r}\sqrt{1 - j\nu}$, we note that the magnitude of ν indicates to what extent a reflecting obstacle behaves as a dielectric mirror to wave reflections. For $\nu \ll 1$, we have $n \cong \sqrt{\kappa_r}$; while for $\nu \gg 1$, we deal, in effect, with a conductive reflector or mirror, causing essentially inphase and antiphase reflections with respect to the incident wave for vertical and horizontal polarizations, respectively. Since, for the curves given in Fig. 237, we have $\sqrt{\kappa_r} = \sqrt{15} = 3.87$ for average ground and $\sqrt{80} = 8.944$ for ocean water, as well as for river and lake water, we can find the corresponding values for the index n of refraction of ocean for $\nu = 0.1$, 1, 10, and 100 by multiplying the values of n of Fig. 228 by $8.944/3.87 = 2.31$. This shows that the reflection coefficients are different for ocean. Only for the same values of κ_r and the same ratio ν for two different mediums can we expect the same reflection coefficients. The value of κ_r is fixed by a medium, while the ν ratio can be changed by choosing an appropriate frequency for a fixed conductivity σ of a medium.

From the reflection curves in Figs. 226, 227, 232, 233, 234, and 236, it can be seen that for actual ground conditions, we generally do *not* meet the condition of a perfect reflector (metallic mirror), for which we have $\rho_v = 1 = -\rho_h$, expressing that the reflected intensity is either *in* phase for vertical polarization or in *counter*phase for horizontal polarization, respectively, with regard to the incident field intensity. We have, for actual ground conditions, complete ($\rho = \pm 1$) reflections for either type of polarization if $\theta = 90$ deg, *i.e.*, grazing wave incidence, which would

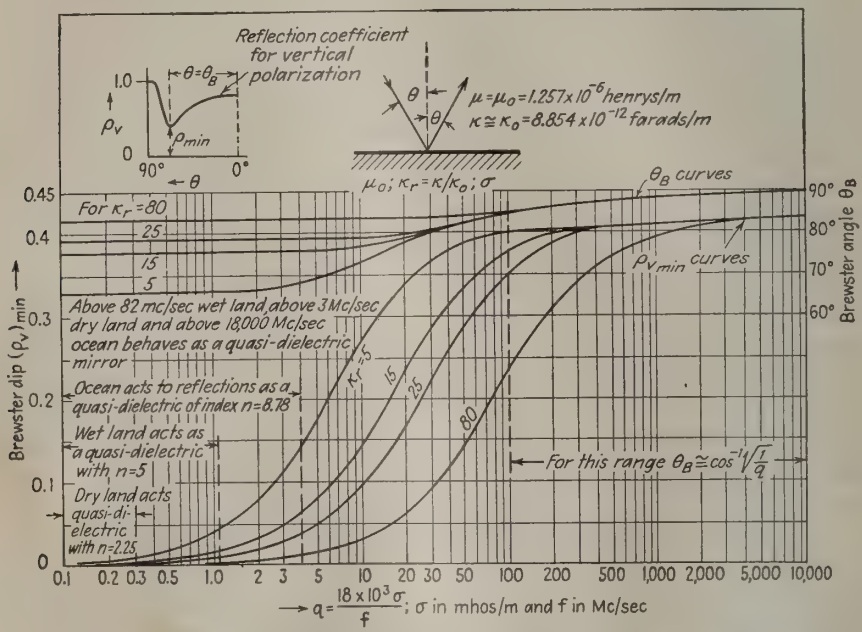

FIG. 237. Brewster angle of wave incidence θ_B on actual earth surface and Brewster dip ($\rho_{min} = \rho_v$).

be expected, since the arriving wave slides tangentially along the surface of the general medium and nothing hinders the motion. With respect to the phase of the reference reflected field from a perfect reflector ($\sigma = \infty$), there is a phase lag for both vertical and horizontal polarizations. The phase lag in the case of horizontal polarization is rather gradual from $\varphi_h = 0$ at $\theta = 90$ deg (grazing wave incidence) to a smaller value at $\theta = 0$ deg (perpendicular wave incidence), along a gradual somewhat curved decrease of ρ_h. For most angles of incidence, the reflected wave is in antiphase and only somewhat smaller than the incident wave, since, even for perpendicular wave incidence, the most extreme case shown in the figures still has a reflection coefficient as high as 0.4.

156. Remarks on the Reflection Coefficient for Vertical Polarization of the General Medium and Curves for the Pseudo Brewster Angle and the Brewster Dip. For vertically polarized electromagnetic waves, the relative phase φ_v changes over 180 deg as the angle θ of wave incidence varies from perpendicular incidence ($\theta = 0$ deg) to grazing incidence ($\theta = 90$ deg). At the same time, the magnitude ρ_v of the reflection coefficient changes over wide limits, besides passing through a minimum value (Brewster dip) at $\varphi_v = 90$ deg. The minimum value of ρ_v changes from a zero value, if $q = 0$ in $n = \sqrt{\kappa_r - jq}$, to about 0.4, for q much larger than κ_r, and the critical incidence θ_B is almost 90 deg (almost grazing or tangential incidence to the general medium). This limit requires q relatively large. For UHF's and wave propagation over land, the reflected field intensity $\mathcal{E}_r$ is nearly 180 deg out of phase with the incident intensity $\mathcal{E}_i$ for $\theta > \theta_B$ and nearly in phase for $\theta < \theta_B$. The Brewster angle θ_B can be computed from formula (870). For $q \gg \kappa_r$, we can use the approximation $\cos \theta_B = 1/\sqrt{q}$; and for $q \ll \kappa_r$, the approximation $\tan \theta_B = \sqrt{\kappa_r}$ can be used. The curves of Fig. 237 give the Brewster angle θ_B and the corresponding minimum value for the reflection coefficient ρ_v for different values of the relative dielectric constant κ_r and q. The range from $\kappa_r = 5$ to $\kappa_r = 80$ covers all earth surface conditions from dry land (rocky earth crust) to ocean water. The more a medium behaves like a pure dielectric the more the $\rho_{\min}$ curves (for vertical polarization) approach zero value. Calling 1 per cent, *i.e.*, $\rho_{\min} = 0.01$, practical zero reflection effect, *i.e.*, total electromagnetic energy transfer into the general medium, this will happen for ocean (Fig. 237) for a value $q = 4$, corresponding to a Brewster angle of $\theta_B = 83.5$ deg. For such a condition also, the approximation $\tan \theta_B = n$ holds. We have essentially a real index n of refraction found from $n = \sqrt{80} = 8.944$. This leads then essentially to the curves of Fig. 227 holding for $\kappa_r = 80$. We find, for such a condition, a frequency $f = 1.8 \times 10^4 \times 4/4 = 18{,}000$ Mc/sec, since $q = 1.8 \times 10^4 \sigma/f = 4$. Any still higher frequency will render the ocean surface still more a quasi-dielectric mirror. For dry earth crust, Fig. 237 shows that the ground acts as a quasi dielectric for a value of $q = 0.3$, since κ_r has a value of about 5. The value of q corresponds then to the Brewster angle $\theta_B = 66$ deg, yielding essentially a real index n of refraction, found as $n = \tan 66$ deg $= 2.25$. This checks again the relation $n = \sqrt{\kappa_r} = \sqrt{5} = 2.25$ holding for a perfect dielectric medium. For dry land, we have $\sigma = 10^{-4}$ to 10^{-5} mho/m. Using the average conductivity value of 5×10^{-5} mho/m, we find the frequency limit from which on with increasing value of f we approximate a dielectric mirror effect, as $f = 1.8 \times 10^4 \times 5 \times 10^{-5}/0.3 = 3$ Mc/sec. This means that we surely must have a dielectric mirror action for short

waves. It should be realized that the lowest limiting frequency values of 3 Mc/sec for rocky dry ground and 18,000 Mc/sec for ocean are very conservative, since we took 1 per cent reflection, with respect to the incident ray as the criterion. For wet soil, the $\kappa_r = 25$ curve of Fig. 237 represents the condition giving for $\rho_{min} = 0.01$ a value $q = 1.1$ and a Brewster angle $\theta_B = 78.5$ deg. We find then the relative index of refraction as $n = \tan 78.5 \text{ deg} = 5 = \sqrt{\kappa_r}$. Since, for wet soil, we have $\sigma = 10^{-2}$ to 10^{-3} mho/m, we find, for the average value $\sigma = 5 \times 10^{-3}$ mho/m, the lowest frequency, from which on upward we have quasi-dielectric behavior of the ground, as $f = 1.8 \times 10^4 \times 5 \times 10^{-3}/1.1 = 82$ Mc/sec. In exactly the same way, the other saturation limit of the S-shaped ρ_{min} curves can be evaluated. This limit is the region beyond the upper knee or bend, representing larger q values than corresponding κ_r values. We also note that the θ_B curves slide into a common curve from about $q = 100$ on and upward. The Brewster angle is, therefore, essentially independent of the dielectric constant and caused only by the conductivity σ and the frequency f. Therefore, for $q = 100$, irrespective of the κ_r values, we find $\cos \theta_B = 1/\sqrt{100} = 0.1$ and $\theta_B = 84.3$ deg. The region above $q = 100$ has then the following characteristics: For dry land, for which $\kappa_r \cong 5$, the corresponding frequency, for $\sigma = 5 \times 10^{-5}$ mho/m, is found from $f = 1.8 \times 10^4 \times 5 \times 10^{-5}/100 = 0.009$ Mc/sec, since we now use the value $q = 100$. This result is of no concern in this text, since it is in the very low high-frequency range. Applying the other extreme curve, holding for $\kappa_r = 80$ (ocean or any other water), we find, for ocean with a conductivity of $\sigma = 5$ mhos/m and $q = 100$, a frequency $f = 1.8 \times 10^4 \times 5/100 = 900$ Mc/sec. The phase angle of the relative equivalent dielectric constant $\kappa_e' = \kappa_r - jq = 80 - j100$ is then $\tan^{-1}(100/80) = 51.3$ deg, and a decided complex value for the relative index of refraction $n = \sqrt{80 - j100}$ then exists, since we find $n = \sqrt[4]{80^2 + 100^2}\, \epsilon^{-j25.65°} = 11.31 (\cos 25.65° - j \sin 25.65°) = 10.2 - j4.89 / -25.65°$. When the $\kappa_r = 80$ curve slides into the $\kappa_r = 5$ curve at about $q = 5{,}000$, we have the case where the Brewster dip ρ_{min} is affected only by σ and f. The dip is then no longer dependent upon the dielectric constant of the general medium. This must then be the case where $q \gg \kappa_r$. Such large relative values of q with respect to κ_r of the reflecting general medium can occur only for a highly conducting medium. It is also approached at very low frequencies for customary ground and low high-frequencies for ocean water. We have then $n \cong \sqrt{-jq} = (1 - j)\sqrt{\tfrac{1}{2}q}$, yielding again a complex index of refraction, but such that this index has a phase lag of 45 deg. Since for ocean, even at 100 Mc/sec, we have $q = 1.8 \times 10^4 \times 5/100 = 900$, we must have a

Brewster angle close to grazing wave incidence with respect to the surface of the ocean.

157. Vertical Field Pattern of a Linear Radiator Standing Normal to a Metal Plane. This has reference to practical short-wave radiators as shown in Fig. 238*a*. According to the electrical image theory, we have, in effect, the radiating system as in Fig. 238*b*, since the image antenna with equal inphase current also affects the radiation condition at the distant field point P. We have then at field point P, owing to the current element $i\,dz$ of the actual antenna, the associated field contributions

$$dH^{(\text{amp/m})} = \frac{\beta I \sin\theta_1}{r_1} \sin(\omega t - \beta r_1)\, dz$$

$$d\mathcal{E}^{(\text{volts/m})} = \frac{188.35 I \sin\theta_1}{r_1} \sin(\omega t - \beta r_1)\, dz$$

where the wavelength λ is $300/f^{(\text{Mc})}$ and expressed in meters as is the distance r_1 and I is in amperes. We can then use either relation to find the total field. We have

$$\mathcal{E}^{(\text{volts/m})} = \frac{188.35}{\lambda}\left[\int_0^l \frac{I \sin\theta_1}{r_1} \sin(\omega t - \beta r_1)\, dz + \int_{-l}^0 \frac{I \sin\theta_2}{r_2} \sin(\omega t - \beta r_2)\, dz\right]$$

$$\mathcal{E} \cong \frac{188.35 I_0 \sin\theta}{r\lambda}\left\{\int_0^l \sin[\beta(l-z)] \sin[\beta(r - z\cos\theta) - \omega t]\, dz + \int_{-l}^0 \sin[\beta(l+z)] \sin[\beta(r - z\cos\theta) - \omega t]\, dz\right\}$$

$$= \frac{376.7 I_0}{\beta r \lambda} P_\theta \sin(\omega t - \beta r)$$

and

$$\left.\begin{aligned} \mathcal{E} &= \frac{60 P_\theta I_0}{r} \sin(\omega t - \beta r) \quad \text{volts/m} \\ P_\theta &= \frac{\cos(\beta l \cos\theta) - \cos(\beta l)}{\sin\theta} \end{aligned}\right\} \tag{875}$$

where P_θ is the direction pattern in the presence of the metallic backup reflector in any meridian plane of the linear radiator, projecting through the central hole of the reflector. Theoretically, the reflector should extend to infinity. A few wavelengths for the diameter of the circular reflector seem, however, to give a satisfactory field pattern, according to (875). For short-wave work, the length l is about one-quarter of a

wavelength long. For $l = \frac{1}{4}\lambda$, we find $\beta l = 2\pi\lambda/4\lambda = \pi/2$ or 90 electrical degrees and $P_\theta = [\cos(90° \cos\theta)]/\sin\theta$, which happens to be the same meridian pattern as for a $\frac{1}{2}\lambda$ radiator in unobstructed space, except that there is no radiation below the metal reference plane. For $l = \frac{1}{2}\lambda$, we have $\beta l = 2\pi\lambda/2\lambda = \pi$, and

$$P_\theta = \frac{\cos(180° \cos\theta) + 1}{\sin\theta} \tag{875a}$$

On pages 920–922 in connection with Fig. 253, curves for $\sqrt{1 - \cos\delta}$ and $\sqrt{1 + \cos\delta}$ are given for $\delta = (720 \cos\theta)h/\lambda$, where h is the height of

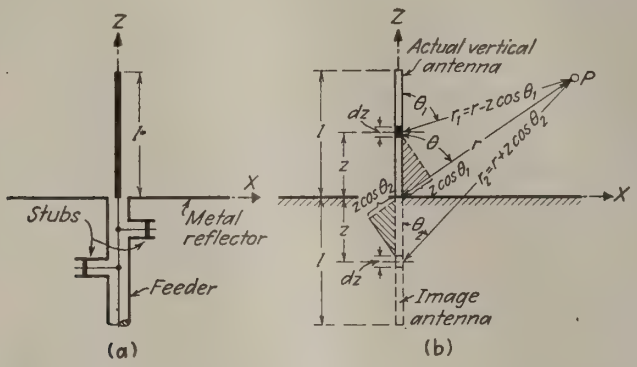

Such a back-up metal reflector can be readily used at VHF's and UHF's with only a few wavelengths' extensions in all directions in the XY plane.

l, r_1, r, r_2, and λ in meters. For $r >>> l$ we have $\theta_1 \cong \theta \cong \theta_2$. $i = I \cos\omega t$ is instantaneous current. $I = I_0 \sin[\beta(l - z)]$ at any distance z; I_0 is value at current loop.

$$\beta = \frac{2\pi}{\lambda} = \frac{\omega}{3 \times 10^8} \text{ if } \frac{\omega}{6.28} \text{ is in cycles/sec.}$$

FIG. 238. Linear radiator standing normal on a metallic reflector.

the mid-point of a linear antenna with respect to a perfectly reflecting ground or metal plane. The formula $P_\theta = D_\theta \sqrt{2}\sqrt{1 + \cos\delta}$ holds for an antenna that is normal to a perfect reflector (metal). Since $\sqrt{1 + \cos\delta} = \sqrt{2}\cos\delta/2$ and D_θ denotes the meridian directivity of a linear radiator in absence of the metal reflector, we have, for the mid-point of the linear radiator a distance h over the reflector,

$$P_\theta = 2D_\theta \cos\left(360\frac{h}{\lambda}\cos\theta\right) \tag{875b}$$

For a vertical $\frac{1}{2}\lambda$ linear radiator just clearing the metal reflector by means of a small circular opening in the reflector, as in Fig. 238*a*, we have $h = \frac{1}{4}\lambda$ and

$$P_\theta = 2D_\theta \cos (90° \cos \theta) = \frac{2 \cos (90° \cos \theta) \cos (90° \cos \theta)}{\sin \theta}$$

Since $\cos \alpha \cos \alpha = \frac{1}{2}[\cos (\alpha + \alpha) + \cos (\alpha - \alpha)] = \frac{1}{2}[\cos (2\alpha) + 1]$, we find again (875*a*). We can, therefore, use either the general formula (875*b*) or, more conveniently, the general formula (875) for finding the polar P_θ meridian pattern, since (875) does *not* require the knowledge of the unobstructed space directivity D_θ. In Eq. (875), the quantity I_0 is the current at the current antinode, which, for $l = \frac{1}{4}\lambda$, is equal to the feeder current. For $l = 0.1\lambda$, we have $\beta l = 36$ deg, and

$$P_\theta = P_{0.1} = \frac{\cos (36° \cos \theta) - 0.809}{\sin \theta} \tag{875c}$$

For $l = 0.125\lambda$, we find

$$P_{0.125} = \frac{\cos (45° \cos \theta) - 0.7071}{\sin \theta} \tag{875d}$$

For $l = 0.3\lambda$, we have

$$P_{0.3} = \frac{\cos (108° \cos \theta) + 0.309}{\sin \theta} \tag{875e}$$

since $\cos \beta l = \cos 108° = -\sin 18° = -0.309$. For $l = 0.4\lambda$, we find

$$P_{0.4} = \frac{\cos (144° \cos \theta) + 0.809}{\sin \theta} \tag{875f}$$

From formula (875), we can, therefore, find the vertical polar pattern for any length of electrical length βl, and Table 49 gives the evaluations for different radiator lengths l in terms of the operating wavelength λ. Evaluating the condition for $l = 0.64\lambda$, we find $\beta l = 230.4$ and

$$P_{0.64} = \frac{\cos (230.4° \cos \theta) + 0.6374}{\sin \theta} \tag{875g}$$

with the polar directivities as in Table 49 and Fig. 239. Only half patterns are shown ($\theta = 0$ to 90 deg), and the space pattern is simply the pattern of revolution about the $+Z$ axis. It is noted that the horizontal reach along the XY plane is *not* always twice the reference value (not always the conventional unity). We have, for $l = 0.5\lambda$, a value equal to 2; while for $l = 0.64\lambda$, we have only 1.6374, since, for such a wavelength distribution along the linear radiator, we have a portion along the vertical radiator for which, at a certain instant, the current flows upward and a portion for which the current flows downward. Therefore, we have a differential field due to these portions with reinforcements and counteractions, which also produce zero field zones. This is the reason why the $P_{0.64}$ pattern breaks up into two lobes. These lobes are marked $+P_{0.64}$

TABLE 49. POLAR MERIDIAN PATTERNS

θ, deg	sin θ	cos θ	Equation (875g), $l = 0.65\lambda$				Equation (875a), $l = 0.5\lambda$		
			a_0, deg	a	$P_{0.64} = \frac{a}{\sin\theta}$		b_0, deg	b	$P_{0.5} = \frac{b}{\sin\theta}$
0.0	0.0000	1.0000	230.4	0.0000	0.0000		180	0.0000	0.0000
5	0.0872	0.9962	228.5	−0.0239	−0.273				
10	0.1736	0.9848	226	−0.0573	−0.329		177.5	0.001	0.0057
15	0.2588	0.9659	222.5	−0.0999	−0.385				
20	0.342	0.9397	216	−0.1716	−0.503		169	0.0184	0.0536
25	0.4226	0.9063	208	−0.2455	−0.582				
30	0.5	0.866	199	−0.3081	−0.616	−lobe	156	0.0865	0.173
35	0.5736	0.8192	188	−0.3529	−0.616				
40	0.6428	0.766	176	−0.3602	−0.56		138	0.2569	0.4
45	0.7071	0.7071	162.5	−0.3163	−0.448				
50	0.766	0.6428	148	−0.2106	−0.276		116	0.5616	0.738
55	0.8192	0.5736	132.5	−0.156	−0.1905				
60	0.866	0.5	115.2	0.2116	0.245		90	1.0000	1.156
65	0.9063	0.4226	97	0.5155	0.57				
70	0.9397	0.342	78.7	0.8333	0.889		61.6	1.4756	1.57
75	0.9659	0.2588	59.7	1.1419	1.18	+lobe			
80	0.9848	0.1736	40	1.4034	1.425		31.25	1.855	1.88
85	0.9962	0.0872	20.1	1.5765	1.59				
90	1.0000	0.0000	0.0	1.6374	1.6374		0.00	1.0000	2.0000

θ, deg	Equation (875f), $l = 0.4\lambda$			Equation (875e), $l = 0.3\lambda$			$l = 0.25\lambda$ $P_\theta =$ D_θ of $\frac{\lambda}{2}$ free-space pattern	Equation (875d), $l = 0.125\lambda$		
	c_0, deg	c	$P_{0.4} = \frac{c}{\sin\theta}$	d_0, deg	d	$P_{0.3} = \frac{d}{\sin\theta}$		e_0	e	$P_{0.125} = \frac{e}{\sin\theta}$
0.0	144	0.0000	0.0000	108	0.0000	0.0000	0.0000	45	0.0000	0.000
10	142	0.021	0.121	106.4	0.0267	0.154	0.142	44.3	0.0086	0.05
20	135.7	0.0933	0.273	101.5	0.1096	0.321	0.28	42.4	0.0314	0.092
30	124.5	0.2426	0.486	93.5	0.248	0.496	0.417	39	0.07	0.14
40	110	0.467	0.725	82.5	0.4395	0.67	0.556	34.5	0.117	0.182
50	93	0.804	1.05	69.4	0.6608	0.865	0.693	29.0	0.1675	0.219
60	72	1.118	1.3	54	0.8968	1.03	0.816	22.5	0.2168	0.251
70	49.3	1.4611	1.56	37	1.1076	1.18	0.912	15.4	0.257	0.274
80	25	1.7153	1.74	18.8	1.2556	1.275	0.98	7.8	0.2836	0.288
90	0.0	1.809	1.809	0.0	1.309	1.309	1.000	0.0	0.293	0.293

Remarks: For a length $l > 0.5\lambda$, we obtain differential field action, for which reason we find, for instance, a negative lobe, marked $-P_{0.64}$ in Fig. 239, and negative values in this table and positive lobes $+P_{0.64}$. We have also $a_0 = 230.4 \cos\theta$; $b_0 = 180 \cos\theta$; $c_0 = 144 \cos\theta$; $d_0 = 108 \cos\theta$; $e_0 = 45 \times \cos\theta$; $a = \cos(230.4° \cos\theta) + 0.6374$; $b = \cos(180° \cos\theta) + 1$; $c = \cos(144° \cos\theta) + 0.809$; $d = \cos(108° \cos\theta) + 0.309$; $e = \cos(45° \cos\theta) + 0.707$.

and $-P_{0.64}$. The radiated power is proportional to the square of the field intensity, and the polarity signs of these patterns are, therefore, of no consequence. Moreover, it is seen that the horizontal reach is 1.809 for $l = 0.4\lambda$, 1.309 for $l = 0.3\lambda$, 1 for $l = 0.25\lambda$, and 0.293 for $l = 0.125\lambda$. We find then essentially a circular polar pattern for the latter wavelength distribution. For lengths still shorter in terms of the wavelength, the diameter of the circular pattern can be computed from $d = 1 - \cos \beta l$, which yields, for $l = 0.1\lambda$ and $\beta l = 36$ electrical degrees, a diameter $d = 1 - \cos 36 \text{ deg} = 1 - 0.809 = 0.191$. It is seen, therefore, that for wavelength distributions along the radiator length l, which does not exceed 0.5λ, we have only one lobe, and we have, by a suitable choice of

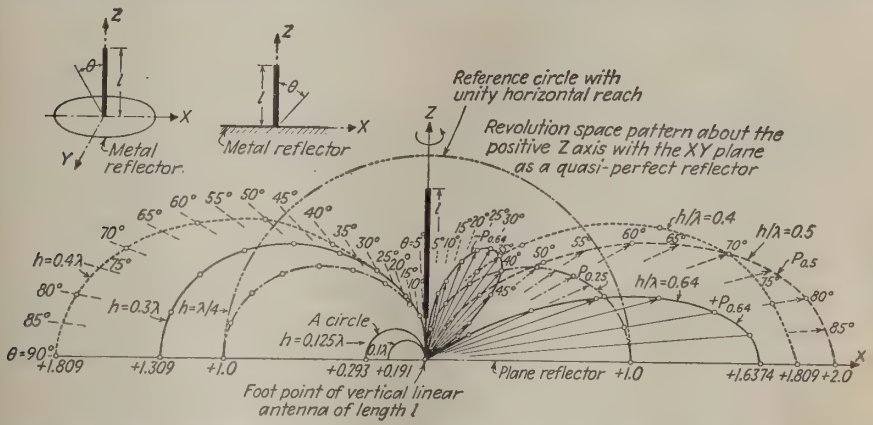

FIG. 239. Half meridian pattern of linear radiators standing perpendicular on a quasi-perfect reflector (metal reflector).

the distribution, a means of *diverting* some of the high-angle field energy with respect to the plane of the reflector toward the plane of the reflector. We have, then, for short waves, a ready means of actually meeting the conditions of a metallic reference reflector and with dimensions that are practical.

158. Relations for the Ray Theory of Wave Reception over Actual Ground. Discussing first the most complicated case for vertical polarization, for a plane ground, we have a path triangle *TGR* in Fig. 240. The space point T is the radiation center of a linear vertical radiator, and the space point R is the reception center. For an outward-moving electromagnetic wave initiated at T, we have, in any direction r_θ, for the tropospheric refractive index n, the free-space field intensity

$$\mathcal{E}_\theta = \frac{D_\theta \mathcal{E}}{r_\theta} \epsilon^{j\omega\left(t - n\frac{r_\theta}{v}\right)} \qquad \text{volts/m}$$

where $\mathcal{E}$ denotes the reference field intensity in the equatorial plane of the

vertical radiator at a distance of 1 m. This field $\mathcal{E}$ is then due to the *only* radiation field that can ever reach the distant radiation region. For this reason, we can also apply the inverse distance law even at 1 m distance from the radiator. By *free field intensity* is meant the field of the direct ray that passes, for instance, from point T to point R along the path $TR = r_0$. There is also a free-space field intensity arriving at R along the indirect path TGR. If it were not for the behavior of the ground, this indirect free-space field intensity would only be diminished owing to the inverse distance effect, where the distance is now $TG + GR = r$. This would also cause, with respect to the direct ray due to the path difference $r_0 - r$, a phase delay that is $\beta(r_0 - r)$ electrical degrees.

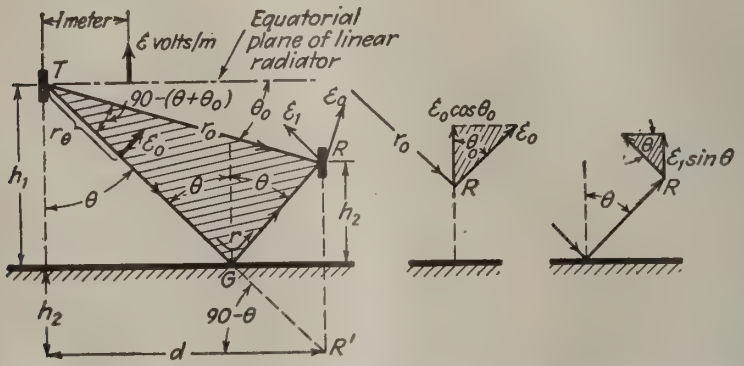

FIG. 240. Path triangle TGR for flat earth. θ angle of wave incidence with respect to ground; θ_0 vertical bearing on receiver antenna R; $r_0 = d/(\cos\theta_0)$; $r = d/(\sin\theta)$; $\tan(90° - \theta) = (h_1 + h_2)/d$; $\tan\theta_0 = (h_1 - h_2)/d$.
$TR = r_0 = \sqrt{(h_1 - h_2)^2 + d^2}$. $TG + GR = r = TR' = \sqrt{(h_1 + h_2)^2 + d^2}$. d, h_1, h_2, r, and r_0 are in meters.

In addition, we have to realize that at the reflection point G, a reflected wave is caused, which is generally smaller than the incident wave at G and has a relative phase with respect to the incident wave. This means that the field $\mathcal{E}_1$ at R, due to the indirect wave, is different in magnitude and phase from the direct arriving $\mathcal{E}_0$ wave, the phase difference being due to the path difference $r - r_0$ and the phase φ_v of the reflection coefficient ρ_v, due to the reflection at G. We also note that respective field vectors $\mathcal{E}_0$ and $\mathcal{E}_1$ are no longer vertical, so that it takes a resolution of this field along the vertical pickup antenna at R besides. For negligible atmospheric refraction, the index of refraction n in the above expression for the direct wave becomes unity. The quantity D_θ denotes the meridian directivity of the radiator. It is $[\cos(90° \cos\theta)]/\sin\theta$ for a vertical half-wave radiator. For the distances r and r_0 in meters and f in megacycles per second, the phase delay due to the path difference is

$\delta = 1.2(r_0 - r)f$ degrees and the field intensity of the indirect ray at R is

$$\mathcal{E}_1 = \rho_v \frac{D_\theta \mathcal{E}}{r} \epsilon^{j\psi} \quad \text{volts/m}$$

$$\psi = \omega\left(t - \frac{r}{3 \times 10^8}\right) + \varphi_v = \omega t - \beta r + \varphi_v$$

The field intensity of the direct ray at R is

$$\mathcal{E}_0 = \frac{D_{(90-\theta_0)}\mathcal{E}}{r_0} \epsilon^{j\psi_0} \quad \text{volts/m}$$

$$\psi_0 = \omega\left(t - \frac{r_0}{3 \times 10^8}\right) = \omega t - \beta r_0$$

since the directivities for the direct ray are with respect to angle $90° - \theta_0$ and for the indirect ray with respect to angle θ. In each case, the angle is referred to the direction of the vertical radiator at T. These relations then take all the above-mentioned conditions into account. Inasmuch as for vertically polarized waves the receiving antenna is usually also normal to ground, it is only the projections $\mathcal{E}_0 \cos \theta_0$ and $\mathcal{E}_1 \sin \theta$ tangential to the linear receiving antenna that will cause an induced current in the pickup antenna at R. The total vertical field $\mathcal{E}_v$ that will affect the receiving antenna at R is then

$$\mathcal{E}_v^{(\text{volts/m})} = \mathcal{E}_0 \cos \theta_0 + \mathcal{E}_1 \sin \theta = \underbrace{\frac{D_{(90°-\theta_0)}\mathcal{E} \cos \theta_0}{r_0} \epsilon^{j\psi_0}}_{\text{direct wave}} + \underbrace{\rho_v \frac{D_\theta \mathcal{E} \sin \theta}{r} \epsilon^{j\psi}}_{\text{indirect wave}}$$

$$= \frac{\mathcal{E}}{d}\left[D_{(90°-\theta_0)} \epsilon^{j\psi_0} \cos^2 \theta_0 + \rho_v D_\theta \epsilon^{j\psi} \sin^2 \theta\right] \quad (876)$$

since $r_0 = d/(\cos \theta_0)$ and $r = d/(\sin \theta)$ in terms of the horizontal separation of transmitter and receiver antennas. Putting

$$\frac{\mathcal{E}}{d} D_{(90°-\theta_0)} \cos^2 \theta_0 = a \qquad \text{and} \qquad \frac{\mathcal{E}}{d} \rho_v D_\theta \sin^2 \theta = b$$

and realizing that in $\mathcal{E}_v = a\epsilon^{j\psi_0} + b\epsilon^{j\psi}$, we deal with a geometric addition of respective vectors $A = a\epsilon^{j\psi_0}$ and $B = b\epsilon^{j\psi}$ and have the geometry of Fig. 241. The same result can be obtained by realizing that only the phase difference $\psi - \psi_0$ in the value under the bracket is of concern, and not the phase ψ' of the resultant, since only the magnitude of $\mathcal{E}_v$ plays a part. Hence, by multiplying the left and right sides of (876) by $\epsilon^{-j\psi_0}$, we find

$$\left.\begin{aligned}
\mathcal{E}_v\epsilon^{-j\psi_0} &= \frac{\mathcal{E}}{d}\left[D_{(90°-\theta_0)}\cos^2\theta_0 + \rho_v D_\theta \epsilon^{j(\psi-\psi_0)}\sin^2\theta\right] \\
&= \frac{\mathcal{E}}{d}\left[D_{(90°-\theta_0)}\cos^2\theta_0 + \rho_v D_\theta \epsilon^{j(\delta+\varphi_v)}\sin^2\theta\right] \qquad \text{volts/m} \\
\delta &= \frac{\omega(r_0 - r)}{3\times 10^8} = \frac{2\pi}{\lambda}(r_0 - r) = 1.2(r_0 - r)f^{(\text{Mc})}
\end{aligned}\right\} \qquad (876a)$$

This expression holds for any distance over plane ground, since it takes into consideration the angle θ of ground incidence as well as the angle θ_0 for different antenna heights. If the distance is in the line of sight, for curved ground, we have to multiply ρ_v by a factor C as we shall learn later. These general relations play a part in airplane-to-airplane

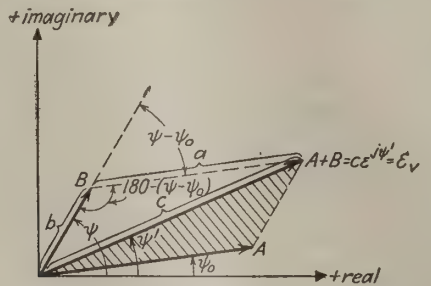

FIG. 241. Geometrical addition of vectors $A = a\epsilon^{j\psi_0}$ and $B = b\epsilon^{j\psi}$.

$$c = \sqrt{a^2 + b^2 - 2ab\cos[180° - (\psi - \psi_0)]} = \sqrt{a^2 + b^2 + 2ab\cos(\psi - \psi_0)}$$
$$= (\mathcal{E}/d)\sqrt{c^2 + d^2 + 2cd\cos(\psi - \psi_0)},$$

for $c = D_{(90°-\theta)}\cos^2\theta_0$; $d = \rho_v D_\theta \sin^2\theta$.

and airplane-to-ground-station communication, where θ_0 and θ have to be taken into account, since the horizontal separation d may be of the order of the vertical separation $h_1 - h_2$. Since the factor $\epsilon^{-j\psi_0}$, on the left side of (876a), represents only the time phase of the total vertical field at R, the factor $\mathcal{E}_v$ is the maximum value. We have then, for the effective values $\mathcal{E}_R = \mathcal{E}_v/\sqrt{2}$ and $\mathcal{E}_e = \mathcal{E}/\sqrt{2}$, the relation

$$\mathcal{E}_R^{(\text{volts/m})} = \frac{\mathcal{E}_e}{d}\left\{D_{(90°-\theta_0)}\cos^2\theta_0 + \rho_v D_\theta \epsilon^{j[1.2(r-r_0)f+\varphi_v]}\sin^2\theta\right\} \qquad (876b)$$

for the reference effective field $\mathcal{E}_e$ volts per meter anywhere at a meter's distance from the radiator in its equatorial plane, and r, r_0, and d are in meters and f in megacycles per second.

As mentioned, $\mathcal{E}_e$ is the reference effective field at 1 m distance in the equatorial plane. It is due only to the radiation portion of the field at this distance and has nothing to do with the induction field, which is wattless. Nevertheless, for short waves, there are many cases where we have only a radiation field at 1 m distance from the radiator. For instance at 1,000 Mc/sec, we have a free-space wavelength of 300/1,000 = 0.3 m, and 1 m from the radiator is in the radiation field. We have

to bear in mind, however, that the radiation formulas show that we have higher power inverse distance terms in addition to the $1/r$ term. Therefore, at 1 m distance, we could not confirm the reference value by a measurement, since the reference value is only a reference information and is *based* on the *distant* radiation field, where only the $1/r$ law essentially plays a part. We have, for a half-wave radiator at 1 mile's distance from the radiator and in the equatorial plane for a radiated power of 1 kw, an electric field of 0.1376 volt/m; while for the same radiated power for a quarter-wave radiator normal to a metal reference plane (backup plane), we have a field of 0.0973 volt/m. These are then free-space field values, and the quarter-wave linear radiator would be the case of Fig. 239 with the length $l = \lambda/4$. We can refer the above-mentioned theoretical free-space values (with no space dissipation, except the field amplitude decay due to wave spread) also to the reference distance of 1 m, since 1 mile = 1,609 m and the electric field is proportional to $\sqrt{P}/d$, where d is the distance in meters and P the radiated power in watts. For 1-kw radiation from a half-wave radiator, we have, at 1 meter's distance in the equatorial plane, $1{,}609 \times 0.1376 = 222$ volts/m. If the radiated power is only 10 watts instead of 1,000 watts, we have only $222/\sqrt{1{,}000/10} = 22.2$ volts/m at 1 m distance.

The application of formula (876*b*) is not difficult. Suppose we have a ground with an index of refraction of $n = 39.5 - j38.4$, yielding vertical coefficients ρ_v of reflection and phases φ_v as in Fig. 234. We find then, for an incidence of $\theta = 85$ deg from the ρ_v and φ_v curves of this figure, the values $\rho_v = 0.49$ and $\varphi_v = -122$ deg; while for the Brewster angle $\theta_B = 80.25$ deg, we have a Brewster dip of $\rho_{\min} = 0.4$ and $\varphi_v = -90$ deg, where the phase angles are relative with respect to the reflected field from a perfect metallic mirror. The time phase of -90 deg for the Brewster wave incidence then corresponds to $\varphi_v = -90$ deg, which is relative to the phase of the incident field to the medium of interest. Hence, -122 deg must also be the correct angle in (876*b*). This case refers to an equivalent relative dielectric constant $\kappa_e' = 80 - j3{,}000$. We have then $3{,}000 = 1.8 \times 10^4\sigma/f$, and the real part of 80 tells us that we deal with water, as, for instance, ocean, as a medium. For $\sigma = 5$ mhos/m, we then find a frequency $f = 1.8 \times 10^4 \times 5/3{,}000 = 30$ Mc/sec.

Before proceeding, we have to obtain a mental picture of what is meant by practical plane ground. Even for a smooth surface of the earth, the surface is roughly a portion of a sphere. A portion of a spherical surface can be made to coincide with a portion around the apex of a paraboloid. A portion along the path of a parabola can, therefore, be made to coincide with the path along a circle. Assuming, therefore, that the earth surface is about parabolic, at least for distances of about 100 miles, a path of 1 mile will have dropped at the end of 1 mile about 1 ft below the tangent through the starting point of the mile. At the end of 2 miles distance, the path has then curved down 4 ft; and at the end of 10 miles, the path along smooth ground would have dropped $10^2 = 100$ ft. This means that for 10 miles over smooth ground, a 101-ft tower could be seen only through field glasses as far as 1 ft length of the top of the tower is concerned. Even though a 100-ft drop in $10 \times 5{,}280 =$

52,800 ft is only $\frac{1}{528}$ of the distance, or 0.18 per cent, it makes a vertical height of 100 ft completely disappear. Therefore, if one antenna height is 100 ft or less, it would not be correct to apply flat-ground geometry to line-of-sight propagation unless atmospheric refraction and, for some conditions, diffraction is taken into account.

For the reflection condition depicted in Fig. 234 for a 30-Mc wave over ocean surface corresponding to a free-space wavelength of 10 m in air, we have many wavelengths for a separation of $d = 5{,}000$ m along respective paths r_0 and r in Fig. 240, since we should have 500 wavelengths for the horizontal separation of transmitter and receiver locations. This places the vertical pickup antenna at R well into the pure radiation field of the radiator that is located at T. We then find $\tan (90° - \theta) = (h_1 + h_2)/d$; and for an angle of ground incidence $\theta = 85$ deg, $\tan 5° = 0.0875$, and $h_1 + h_2 = 0.0875d$. Hence, $h_1 + h_2 = 0.0875 \times 5{,}000 = 437.5$ m for a horizontal separation of 5 km. But we have also $\tan \theta_0 = (h_1 - h_2)/d$, which, for a condition of $h_1 - h_2 = 200$ m, yields $\theta_\theta = \tan^{-1} (200/5{,}000) = 2.3$ deg. Therefore, $h_1 = 318.75$ m and $h_2 = h_1 - 200 = 118.75$ m. Both vertical antennas are then well within the line of sight, because a horizontal separation of $d = 5{,}000$ m corresponds to $5{,}000 \times 6.214 \times 10^{-4} = 3.11$ miles, which would give a vertical drop of $3.11^2 = 9.7$ ft, owing to a parabolic earth curvature. Hence, even the lowest center of the respective vertical antennas at T and R, respectively, is well above this value. This is true, since the lowest central height $h_2 = 118.75$ m $= 118.75 \times 3.281 = 390$ ft. For a half-wave radiator at 30 Mc/sec, the lowest point of the vertical antenna is $\lambda/4$ below the central height of h_2 or 2.5 m below 118.75 m, which is 116.25 m, or 382 ft, above ground. The flat earth requirement for Fig. 240 is, therefore, fully satisfied.

According to Fig. 234, the values for $\theta = 85$ deg are $\rho_v = 0.49$ and $\varphi_v = -122$ deg. We have also $\theta_0 = 2.3$ deg from the above evaluations. Moreover, $r = \sqrt{(h_1 + h_2)^2 + d^2} = \sqrt{437.5^2 + 5{,}000^2} = 5{,}192$ m; $r_0 = \sqrt{(h_1 - h_2)^2 + d^2} = \sqrt{200^2 + 5{,}000^2} \cong 5{,}000$; $r_0 - r = -192$ m is the path difference. The total time phase angle is

$$1.2(r_0 - r)f + \varphi_v = -(1.2 \times 192 \times 30 + 122) = -7{,}032°$$

Any time this angle has passed through 360 deg, it has again the same relative phase condition that it had before, causing a cycle of 360 deg. The equivalent delay angle of $-7{,}032$ deg is then $7{,}032/360 = 19.53$ negative cycles, which 19.53 cycles delay, since, as mentioned, a complete cycle is a mere repetition of the original phase condition. Therefore, only the fraction 0.53 plays a part. We have then a total time delay angle of $-0.53 \times 360 = -190.8$ deg, due to the path difference $r_0 - r$ of the direct and indirect wave as well as to the phase φ_v of the coefficient

ρ_v for vertical reflection at point G of the surface of the ground in Fig. 240. For a vertical Hertzian doublet at T, we have the directivity $D_\theta = \sin\theta$ and $D_{(90°-\theta_0)} = \sin(90° - \theta_0) = \cos\theta_0$. Formula (876b) yields

$$\mathcal{E}_R^{(\text{volts/m})} = \frac{\mathcal{E}_e}{d}(\cos^3\theta_0 + \rho_v\epsilon^{-j190.8°}\sin^3\theta)$$

$$= \frac{\mathcal{E}_e}{d}[\cos^3\theta_0 + \rho_v\sin^3\theta(\underbrace{\cos 190.8°}_{-\cos 10.8°} - j\underbrace{\sin 190.8°}_{-\sin 10.8°})]$$

$$= \frac{\mathcal{E}_e}{d}(\cos^3\theta_0 - \rho_v\sin^3\theta\cos 10.8° + j\rho_v\sin^3\theta\sin 10.8°)$$

$\cos\theta_0 = \cos 2.3° = 0.992$; $\quad \cos^3\theta_0 \cong 1$; $\quad \rho_v = 0.49$;
$\sin\theta = \sin 85° = 0.9962$; $\quad \sin^3\theta = 0.988$; $\quad \cos 10.8° = 0.9823$;
$\sin 10.8° = 0.1874$; $\quad \mathcal{E}_R = \mathcal{E}_e\dfrac{0.525 + j0.072}{5{,}000}\underline{/+7.8°}$ volts/m

A Hertzian doublet radiator has no practical value unless we understand by it only a very short dipole, so that a fixed current distribution exists. However, in either case, the radiation resistance is altogether too small. For short-wave work, a half-wave radiator is useful, and we find for it

$$D_\theta = \frac{\cos(90°\cos\theta)}{\sin\theta}$$

$$D_{(90°-\theta_0)} = \frac{\cos[90°\cos(90° - \theta_0)]}{\sin(90° - \theta_0)} = \frac{\cos(90°\sin\theta_0)}{\cos\theta_0}$$

$$\mathcal{E}_R^{(\text{volts/m})} = \frac{\mathcal{E}_e}{d}[\underbrace{\cos\theta_0\cos(90°\sin\theta_0)}_{a} + \underbrace{\rho_v\epsilon^{-j190.8°}\sin\theta\cos(90°\cos\theta)}_{b}]$$

$$= \frac{\mathcal{E}_e}{d}[a + b(j\sin 10.8° - \cos 10.8°)]$$

$$= \frac{\mathcal{E}_e}{d}(a - b\cos 10.8° + jb\sin 10.8°)$$

$$a = \cos\theta_0\cos(90°\sin\theta_0) = 0.992\cos\underbrace{(90° \times 0.0401)}_{3.61°}$$

$$= 0.992 \times 0.998 = 0.99$$

$$b = \rho_v\sin\theta\cos(90°\cos\theta) = 0.49 \times 0.9962\cos\underbrace{(90° \times 0.0872)}_{7.86°}$$

$b = 0.49 \times 0.9962 \times 0.9905 = 0.482$
$b\cos 10.8° = 0.482 \times 0.9823 = 0.474$
$b\sin 10.8° = 0.482 \times 0.1874 = 0.09$

$$\mathcal{E}_R = \mathcal{E}_e\frac{0.516 + j0.09}{5{,}000}\underline{/+9.9°} \quad \text{volts/m}$$

where the value in the parenthesis is not very different from the value found for a Hertzian doublet radiator (the same, in effect, as a differential

linear radiator), since for a half-wave radiator we have $0.516 + j0.09$ as against $0.525 + j0.072$. This is due to the fact that the direction polar diagram of an elementary radiator is not very different in shape from that of a half-wave radiator (see Fig. 103). It is to be borne in mind that the relative directivity D_θ is no measure for the actual radiated power. The value of $\mathcal{E}_e$ is considerable for a half-wave radiator, while it is vanishingly small for a differential radiator. We found, for instance, that for 10 watts radiated power from a half-wave radiator, we have an effective reference value $\mathcal{E}_e = 22.2$ volts/m. Therefore, at R of Fig. 240, we have an effective vertical field component

$$\mathcal{E}_R = \frac{22.5}{5{,}000}(0.516 + j0.09)$$

$$= \frac{22.5\sqrt{0.516^2 + 0.09^2}}{5{,}000}\epsilon^{j9.9°} = 2.36 \times 10^{-3}\epsilon^{j9.9°} \quad \text{volts/m}$$

yielding a real value of $2.36 \times 10^{-3} \cos 9.9° = 2.36 \times 10^{-3} \times 0.9851 = 2.32$ mv/m. If the receiving linear antenna has an effective length of 2 m, we shall have $2 \times 2.32 = 4.34$ mv induced across the dipole gap of the receiving antenna. We use mostly half-wave dipoles for receiving. The effective length is then $0.636l$ in unobstructed space, where l is the actual length in meters. For a frequency of 30 Mc/sec, we have $l = \lambda/2 = 10/2 = 5$ m and $l_e = 0.636 \times 5 = 3.18$ m with $3.18 \times 2.32 = 7.4$ mv induced across the gap of the half-wave dipole.

Equation (876*b*) is the expression for vertically polarized wave transmission and wave reception if flat earth is justified. In many cases, we have the transmitting and receiving antennas fairly close to ground, so that for larger horizontal separations ($d \gg h_1 + h_2$ in Fig. 240), we have θ_0 close to 0 deg and θ almost 90 deg, rendering $\cos\theta_0 \cong 1$ and $\sin\theta \cong 1$. For such conditions, we have $\theta \cong 90$ deg and $\rho_v \cong -1$. We have then, for Fig. 240,

$$r_0 = \sqrt{d^2 + (h_1 - h_2)^2} = d\sqrt{1 + \frac{(h_1 - h_2)^2}{d^2}}$$

$$r = \sqrt{d^2 + (h_1 + h_2)^2} = d\sqrt{1 + \frac{(h_1 + h_2)^2}{d^2}}$$

where $(h_1 + h_2)^2/d^2$ as well as $(h_1 - h_2)^2/d^2$ is very small compared with unity, so that the approximations $(1 + a)^m \cong 1 + ma$ can be applied for $a \ll 1$, where

$$a = \frac{(h_1 + h_2)^2}{d^2} \quad \text{or} \quad a = \frac{(h_1 - h_2)^2}{d^2} \quad \text{and} \quad m = \frac{1}{2}$$

Therefore,

$$r_0 \cong d\left[1 + \frac{1}{2}\frac{(h_1 - h_2)^2}{d^2}\right] = d + \frac{(h_1 - h_2)^2}{2d}; \qquad r \cong d + \frac{(h_1 + h_2)^2}{2d}$$

yielding the path difference

$$r - r_0 = \frac{(h_1 + h_2)^2 - (h_1 - h_2)^2}{2d} = \frac{2h_1h_2}{d}$$

Introducing this outcome into Eq. (876), the total vertical electric field becomes

$$\mathcal{E}_v^{(\text{volts/m})} = \mathcal{E}_0 \cos\theta_0 + \mathcal{E}_1 \sin\theta \cong \mathcal{E}_0 + \mathcal{E}_1 = \frac{D_{(90°-\theta_0)}\mathcal{E}}{r_0}\epsilon^{j\psi_0} + \rho_v\frac{D_\theta \mathcal{E}}{r}\epsilon^{j\psi}$$

But

$$D_{(90°-\theta_0)} = \frac{\cos(90° \sin\theta_0)}{\cos\theta_0} \cong 1; \qquad D_\theta = \frac{\cos(90°\cos\theta)}{\sin\theta} \cong 1; \qquad \rho_v \cong -1$$

where $\rho_v \cong -1$ for almost grazing angles with the ground means that

$$\rho_v = 1\epsilon^{-j180°}; \qquad \varphi_v = -180°$$

Hence,

$$\psi_0 = \omega t - \beta r_0 = 360 \times 10^6 ft - 1.2fr_0 \quad \text{deg}$$
$$\psi = 360 \times 10^6 ft - 1.2fr - 180°$$

for f in megacycles per second, t in seconds and r and r_0 in meters.

$$\mathcal{E}_v\epsilon^{-j\psi_0} = \frac{\mathcal{E}}{r_0} + \frac{\mathcal{E}}{r}\epsilon^{j(\psi-\psi_0)} \qquad \text{volts/m}$$

but

$$\theta \cong 90°; \qquad \theta_0 \cong 0°; \qquad r_0 = \frac{d}{\cos\theta_0} \cong d; \qquad r = \frac{d}{\sin\theta} \cong d$$

and

$$\mathcal{E}_v\epsilon^{-j\psi_0} = \frac{\mathcal{E}}{d}[1 + \epsilon^{j(\psi-\psi_0)}] = \frac{\mathcal{E}}{d}[1 + \epsilon^{j1.2(r_0-r)}\epsilon^{-j180°}] = \frac{\mathcal{E}}{d}[1 - \epsilon^{j1.2f(r_0-r)}]$$

$$= \frac{\mathcal{E}}{d}\left(1 - \epsilon^{-j2.4f\frac{h_1h_2}{d}}\right) \qquad \text{volts/m}$$

where $\mathcal{E}_v$ denotes the maximum value with an effective value $\mathcal{E}_R = \mathcal{E}_v/\sqrt{2}$ and the effective value $\mathcal{E}_e = \mathcal{E}/\sqrt{2}$ as the reference value at 1 m distance from the radiator along the equatorial plane. Therefore,

$$\mathcal{E}_R = \frac{\mathcal{E}_e}{d}\left(1 - \epsilon^{-j2.4f\frac{h_1h_2}{d}}\right)$$

Multiplying the term 1 as well as the factor $\epsilon^{-j2.4f\frac{h_1h_2}{d}}$ by the *same* phase factor $\epsilon^{j1.2f\frac{h_1h_2}{d}}$, nothing is changed, since the same relative phase still exists between both

terms. We find then

$$\mathcal{E}_R = \frac{\mathcal{E}_e}{d}\left(\epsilon^{j1.2f\frac{h_1h_2}{d}} - \epsilon^{-j1.2f\frac{h_1h_2}{d}}\right) = \frac{\mathcal{E}_e}{d}\left\{\cos\left(1.2f\frac{h_1h_2}{d}\right) + j\sin\left(1.2f\frac{h_1h_2}{d}\right) - \left[\cos\left(1.2f\frac{h_1h_2}{d}\right) - j\sin\left(1.2f\frac{h_1h_2}{d}\right)\right]\right\}$$

$$\mathcal{E}_R = j\frac{2\mathcal{E}_e}{d}\sin\left(1.2f\frac{h_1h_2}{d}\right) \quad \text{volts/m} \tag{876c}$$

where f is in megacycles per second and h_1, h_2, and d are in meters, for $\mathcal{E}_e$ volts per meter. It must be realized that the factor 1.2 carries with it the dimension degree · seconds per meter, since it is the outcome of $360° \times 10^6 f/(3 \times 10^8) = 1.2f$, corresponding to $\omega/c = \omega/(3 \times 10^8) = \beta$ and 3×10^8 is the velocity in free space in meters per second. The entire argument $1.2f(h_1h_2/d)$ is then in degrees. Formula (876) then holds for field intensities near ground, where both the T and the R locations are close enough to the surface of the earth so that the condition $h_1 + h_2 \ll d$ is satisfied, and we have the approximations $\theta_0 \cong 0$ and $\theta \cong 90$ deg. For relatively large distances, the sine function is equal to its argument expressed in radians, and we find

$$\mathcal{E}_R \cong 0.0419\frac{fh_1h_2}{d^2}\mathcal{E}_e = 12.56\frac{h_1h_2}{\lambda d^2}\mathcal{E}_e \quad \text{volts/m} \tag{876d}$$

where h_1, h_2, d, and λ are in meters and f is in megacycles per second, showing an inverse square distance law instead of the inverse distance relation holding, for instance, in the standard broadcast range for ground-to-ground transmissions. The inverse square distance condition is, therefore, due to the wave interference between direct and indirect rays, which interference cannot be significant at longer waves even such as 500 m in length (corresponding to 600 kc/sec). Moreover, (876d) shows that the effective vertical field at the reception center R of Fig. 240 is larger the higher the frequency f is chosen. This is, however, offset by the fact that in the case of a receiving half-wave dipole, at higher frequencies, the physical length $l = \lambda/2$ meters becomes shorter the higher the frequency is chosen, since $\lambda \times 300/f$ meters for f in megacycles per second. The induced voltage is $0.636l\mathcal{E}_R$ volts $= 0.313\lambda\mathcal{E}_R$ volts, because the equivalent length $l_e = 2l/\pi$ for a half-wave antenna. But if we use equal-phased half-wave sections, we can take advantage of the frequency proportionality.

It can be shown that (876c) also holds for horizontal polarization. For shorter distances, where the approximation of (876d) does not hold and (876c) must be used, we obtain maximum field values of magnitudes $2\mathcal{E}_e/d$ for such distances, which render $fh_1h_2/d = 75, 225, 5 \times 75, 7 \times 75, \cdots$, and minimum values (zeros) for $fh_1h_2/d = 150, 300, 450, \cdots$. These conditions are the outcome for the conditions that make $1.2fh_1h_2/d = 90$ deg, 270 deg, 5×90 deg, 7×90 deg, $\cdots$ for $\sin(1.2fh_1h_2/d) = \pm 1$, and $1.2fh_1h_2/d = 180$ deg, 2×180 deg, 3×180 deg, $\cdots$ for $\sin(1.2fh_1h_2/d) = 0$.

159. Comparison of Horizontally Polarized Waves with Vertically Polarized Waves over Flat Ground. As we have already found in the

theoretical derivations, the relations become less involved for horizontal polarizations, because in Fig. 242 the linear transmitter radiator T as well as the linear receiver antenna R are now parallel with the surface of reflection (surface of ground). We have then

$$\mathcal{E}_\theta^{(\text{volts/m})} = \frac{D_\theta \mathcal{E}}{r_\theta} \epsilon^{j(\omega t - \beta n r_\theta)} = \frac{\mathcal{E}}{r_\theta} \epsilon^{j(\omega t - \beta r_\theta)}$$

for the free-field intensity along any θ direction. Since the receiving linear antenna is oriented so as to give maximum pickup (parallel with the radiator and parallel to ground), we have the directivity $D_\theta = 1$ as

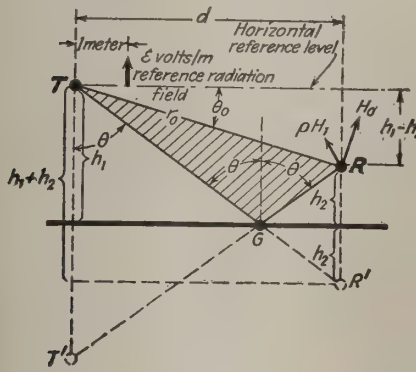

Linear antennas T and R point perpendicularly into the paper

$r = TG + GR = TR'$

$r = \dfrac{d}{\sin \theta}$; $r_0 = \dfrac{d}{\cos \theta_0}$

$\theta_0 = \tan^{-1}\left(\dfrac{h_1 - h_2}{d}\right)$

h_1, h_2, r_0, r, and d are in meters

FIG. 242. Path triangle for horizontally polarized waves.

well as the atmospheric index of refraction $n = 1$ if there is no change in the gradient of n. We have then respective time phase angles

$$\psi_0 = (360 \times 10^6 t - 1.2 r_0) f \quad \text{deg}$$
$$\psi = (360 \times 10^6 t - 1.2 r) f + \varphi_h \quad \text{deg}$$

for f in megacycles per second, r_0 and r in meters, and t in seconds. The quantity φ_h is the phase of the reflection coefficient ρ_h due to wave reflection at the surface of the ground in the case of horizontally polarized waves. For maximum reception orientation of the linear pickup antenna at R, we have

$$\mathcal{E}_h^{(\text{volts/m})} = \mathcal{E}_0 + \mathcal{E}_1 = \frac{\mathcal{E}}{r_0} \epsilon^{j\psi_0} + \rho_h \frac{\mathcal{E}}{r} \epsilon^{j\psi}$$
$$= \frac{\mathcal{E}}{d} (\epsilon^{j\psi_0} \cos \theta_0 + \rho_h \epsilon^{j\psi} \sin \theta)$$

since the $\mathcal{E}_0$ and $\mathcal{E}_1$ electric field vectors are perpendicular to the indicated H_0 and H_1 vectors and point into the paper. The $\mathcal{E}_0$ and $\mathcal{E}_1$ vectors are along the receiving antenna. By multiplying again both sides of the equation with the factor $\epsilon^{-j\psi_0}$ and calling $\mathcal{E}_R$ and $\mathcal{E}_e$ the effective electric

field values in volts per meter at R and $\mathcal{E}_e$ again the reference value at 1 m distance from the radiator in its equatorial plane, we find

$$\left.\begin{aligned} \mathcal{E}_R^{(\text{volts/m})} &= \frac{\mathcal{E}_e}{d}(\cos\theta_0 + \rho_h \epsilon^{j\delta_h}\sin\theta) && \text{for horizontal polarization (Fig. 242)} \\ \mathcal{E}_R^{(\text{volts/m})} &= \frac{\mathcal{E}_e}{d}[D_{(90°-\theta_0)}\cos^2\theta_\theta + \rho_v D_\theta \epsilon^{j\delta_v}\sin^2\theta] && \text{for vertical polarization (Fig. 240)} \\ \delta_h = \delta + \varphi_h; \qquad \delta_v &= \delta + \varphi_v; \qquad \delta = 1.2(r_0 - r)f \quad \text{deg} \end{aligned}\right\} \tag{876e}$$

where r and r_0 are in meters and f is in megacycles per second. It is now of interest to examine the order of magnitude for respective polarizations. Suppose we have a ground with an equivalent relative dielectric constant $\kappa_e' = 80 - j80$, yielding a relative index of refraction $n = \sqrt{80 - j80}$ of the ground with respect to air above it. We have already carried out the detailed computation for such a complex value and found $\rho_v = 0.781\epsilon^{-j5.65°}$ and $\rho_h = 0.881\epsilon^{j176.8°}$. Therefore, $\varphi_v = -5.65$ deg and $\varphi_h = +176.8$ deg for an angle of incidence $\theta = 45$ deg. The real value 80 of $80 - j80$ shows that we deal either with ocean surface, a lake, or a river, whatever may be the case. The value of the imaginary part jq is $q = 80 = 1.8 \times 10^4(\sigma/f)$ for the conductivity σ of the ground in mhos per meter and the frequency f in megacycles per second. Assuming ocean water with an average conductivity of $\sigma = 4$ mhos/m, we find a frequency $f = 1.8 \times 10^4 \times 4/80 = 900$ Mc/sec, which is well in the UHF range of carrier frequencies. Taking the horizontal separation of respective transmitting (T) and receiving (R) dipoles again as $d = 5{,}000$ m and the dipoles at altitudes $h_1 = 318.75$ m and $h_2 = 118.75$ m, we find

$$h_1 - h_2 = 200 \text{ m}; \qquad \theta_0 = \tan^{-1}\left(\frac{h_1 - h_2}{d}\right) = \tan^{-1}\left(\frac{200}{5{,}000}\right) = \tan^{-1}(0.04) = 2.3°$$

For the direct path TR, we find a length $r_0 = d/(\cos\theta_0) = 5{,}000/0.9992 \cong 5{,}000$ m. For the indirect path TGR, we have the same length as TR', where R' denotes the image point of the reception center for either type of polarization. Hence, $r = d/(\sin\theta) = 5{,}000/0.7071 = 7{,}072$ m. Therefore, we have a path difference between direct and indirect rays of $r_0 - r = -2{,}072$ m and find from (876e) the relative time delay

$$\delta = 1.2(r_0 - r)f = -1.2 \times 2{,}072 \times 900 = -2{,}237{,}760°$$

To this we must add the time angle φ degrees for the respective polarizations. We find then, according to (876e),

$$\delta_h = \delta + \varphi_h = -2{,}237{,}760 + 176.8 = -2{,}237{,}583.2°$$
$$\delta_v = \delta + \varphi_v = -2{,}237{,}760 - 5.65 = -2{,}237{,}765.65°$$

$\frac{\delta_h}{360} = \frac{-360k_h - 360p_h}{360}$ where k_h is the number of complete cycles (complete 360°) and p_h is the decimal number of complete cycles

$\frac{\delta_v}{360} = \frac{-360k_v - 360p_v}{360}$ where k_v is number of complete cycles and p_v is number of fractional cycles

$$\delta_h = -360k_h - 360p_h = -360k_h - 183.2° \quad \text{in effect } -183.2°$$
$$\delta_v = -360k_v - 360p_v = -360k_v - 5.65° \quad \text{in effect } -5.65°$$

In the above evaluations, only the values within a complete cycle, *i.e.*, within 360 deg, count, and the division by 360 deg has to be *accurate*, since only the portion after the decimal point is used. A slide rule *cannot* do this but can be used as follows: The first four places of the δ_h and δ_v values are within the division of a slide-rule setting, and we find, for instance, $2{,}240(10^3/360) \cong 6{,}200$, while the actual multiplication yields $6{,}200 \times 360 = 2{,}232{,}000$ and represents the exact value for 6,200 complete cycles. Subtracting this from the respective negative values for δ_h and δ_v, we find $2{,}237{,}583.2 - 2{,}232{,}000 = 5{,}583.2$ and $2{,}237{,}765.65 - 2{,}232{,}000 = 5{,}765.65$. The first reduced number yields the approximate slide-rule value $5{,}583.2/360 \cong 15$ complete cycles, while the second reduced number yields $5{,}765.65/360 \cong 16$ complete cycles, the exact values being $15 \times 360 = 5{,}400$ and $16 \times 360 = 5{,}760$ deg, respectively. Subtracting again these exact reduced values from respective reduced degrees 5,583.2 and 5,765.65, we find $5{,}765.65 - 5{,}760 = 5.65$ deg $= -\delta_v$ and $5{,}583.2 - 5{,}400 = 183.2$ deg $= -\delta_h$.

It is, therefore, *necessary* to carry out the division by 360 deg accurately, since it is the *decimal figure* that *counts*, as in the numerical example on page 872, where we found for a delay angle of −7,032 deg, a division $7{,}032/360 = 19.53$ negative cycles, and

$$\frac{\delta_v}{360} = \frac{-7{,}032}{360} = -19.53 = \underbrace{-19 - 0.53}_{-k_v - p_v} = \frac{-19 \times 360 - 0.53 \times 360}{360}$$

with $-0.53 \times 360 = -360p_v = -190.8$ deg that counts in effect.

We note that we have the respective phase delays $\delta_h = -183.2$ deg and $\delta_v = -5.65$ deg. For horizontal polarization (Fig. 242), we have $\cos \theta_0 = \cos 2.3° = 0.9992$ and $\sin \theta = \sin 45° = 0.7071$, yielding

$$\mathcal{E}_R^{(\text{volts/m})} = \mathcal{E}_e \frac{0.9992 + 0.881 \times 0.7071\epsilon^{-j183.2°}}{5{,}000}$$
$$= \mathcal{E}_e \frac{0.9992 + 0.65\epsilon^{-j183.2°}}{5{,}000}$$
$$= \frac{\mathcal{E}_e}{5{,}000}(0.9992 + 0.65 \cos 183.2° - j0.65 \sin 183.2°)$$
$$= \frac{\mathcal{E}_e}{5{,}000}\sqrt{(0.9992 - 0.65 \sin 3.2°)^2 + (-0.65 \cos 3.2°)^2}\,\epsilon^{j\alpha_h}$$

$$= \frac{\mathcal{E}_e}{5{,}000}\sqrt{0.9556^2 + (-0.645)^2}\,\epsilon^{j\alpha_h}$$

$$\alpha_h = \tan^{-1}\left(\frac{-0.65\cos 3.2^\circ}{0.9992 - 0.65\sin 3.2^\circ}\right)$$

$$= \tan^{-1}\left(\frac{-0.65 \times 0.9984}{0.9992 - 0.65 \times 0.0588}\right)$$

$$= \tan^{-1}(-0.675) = -34^\circ$$

$\cos(-34^\circ) = \cos(34^\circ) = 0.829;$ $\mathcal{E}_R = 23 \times 10^{-5}\mathcal{E}_e\epsilon^{-j34^\circ}$ volts/m

This gives then a real component of $23 \times 10^{-5}\ \mathcal{E}_e \cos 34^\circ = 19.1 \times 10^{-5}\mathcal{E}_e$ volts per meter, for horizontal polarization. For vertical polarization, we find

$$D_{(90^\circ-\theta_0)} = \frac{\cos[90^\circ\cos(90^\circ - \theta_0)]}{\sin(90^\circ - \theta_0)} = \frac{\cos(90^\circ \sin\theta_0)}{\cos\theta_0}$$

$$= \frac{\cos(90^\circ \sin 2.3^\circ)}{\cos 2.3^\circ} = \frac{\cos 3.61^\circ}{0.9992} = 0.998$$

$$\cos\theta_0 = 0.9992 \cong 1; \qquad \cos^2\theta_0 \cong 1$$

$$D_\theta = \frac{\cos(90^\circ\cos\theta)}{\sin\theta} = \frac{\cos(90^\circ\cos 45^\circ)}{\sin 45^\circ}$$

$$= \frac{\cos 63.5^\circ}{0.7071} = \frac{0.4462}{0.7071} = 0.633$$

$$\sin\theta = 0.7071; \qquad \sin^2\theta = 0.49985$$

$$\mathcal{E}_R^{(\text{volts/m})} = \frac{\mathcal{E}_e}{5{,}000}(0.998 + 0.781 \times 0.633 \times 0.49985\epsilon^{-j5.65^\circ})$$

$$= \frac{\mathcal{E}_e}{5{,}000}(0.998 + 0.246\cos 5.65^\circ - j0.246\sin 5.65^\circ)$$

$$= \frac{\mathcal{E}_e}{5{,}000}\sqrt{(0.998 + \underbrace{0.246\cos 5.65^\circ}_{0.245})^2 + (\underbrace{-0.246\sin 5.65^\circ}_{0.0242})^2}\,\epsilon^{j\alpha_v}$$

$$\alpha_v = \tan^{-1}\left(\frac{-0.246 \times 0.0984}{0.998 + 0.246 \times 0.9951}\right) = \tan^{-1}(-0.0195) = 1.15^\circ$$

This gives $\cos\alpha_v = 0.9998$, which is essentially an inphase condition, and

$$\mathcal{E}_R = \frac{\mathcal{E}_e}{5{,}000}\sqrt{1.243^2 + 0.0242^2} = 25\mathcal{E}_e\epsilon^{-j1.15^\circ}$$

Real component $= 25\mathcal{E}_e \cos 1.15^\circ = 25\mathcal{E}_e$ volts/m

For the real components, we have then the comparisons

$\mathcal{E}_R^{(\text{volts/m})} = 25\mathcal{E}_e$ for vertical polarization (Fig. 240)
$\mathcal{E}_R^{(\text{volts/m})} = 19.1\mathcal{E}_e$ for horizontal polarization (Fig. 242)

160. Effect of the Height of the Mid-point of a Linear Antenna over Actual Ground for Different Angles of Wave Incidence and General Polarization. This has reference to electromagnetic waves arriving from airplanes at land and offshore stations using, for instance, half-wave dipoles as a pickup expedient. By mid-point of a linear radiator or a receiving antenna is meant the symmetry point of the antenna. It is also known as the "radiation center" for a radiator and the "reception center" for a receiving antenna. For an array of several half-wave

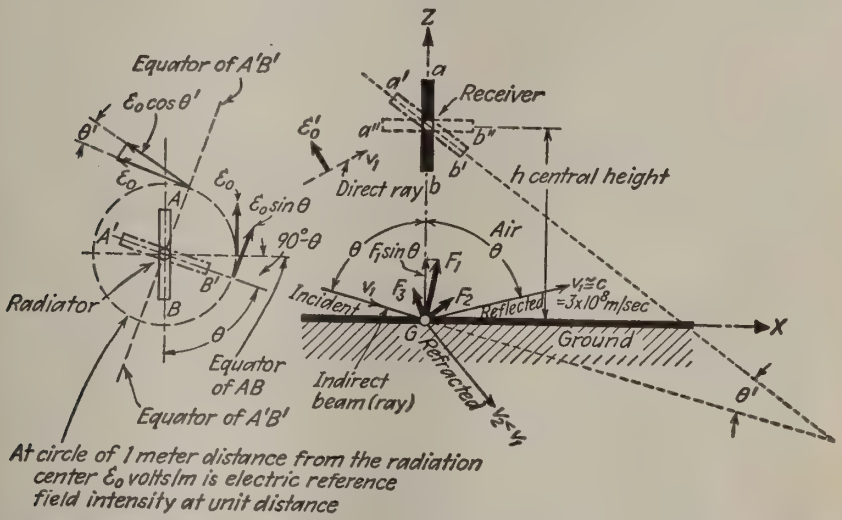

FIG. 243. General case for parallel and perpendicular polarization. (For parallel polarization the electric $\mathcal{E}$ vectors are in the plane of wave incidence and H vectors are normal to this plane; for perpendicular polarization the magnetic H vectors are in the plane of wave incidence and the $\mathcal{E}$ vectors normal to the plane.) F_1 is $\perp$ to v_1, F_2 is $\perp$ to v_2, and F_3 is $\perp$ to v_1 (leaving ground). All vectors refer to reflection point G. Reflected field $F_3 = \rho F_1 \epsilon^{j\varphi}$; refracted field $F_2 = RF_1\epsilon^{j\varphi'}$; ρ is the magnitude of reflection coefficient, φ phase (time) of reflection coefficient, R magnitude of refraction coefficient, φ' time phase of refraction coefficient. ZX plane is plane of wave incidence.

radiators or receiving antennas, we mean by mid-point the symmetry center of the array. The general case is shown in Fig. 243, where F_1 denotes the incident and $F_3 = \rho F_1$ the magnitude of the reflected field vector. It is also to be multiplied by the phase factor $\epsilon^{j\varphi}$ if the reflection coefficient ρ is complex. According to Table 44, we must distinguish between reflection coefficients $\rho_\parallel$ and $\rho_\perp$, respectively, depending upon whether the electric vector $\mathcal{E}$ is parallel with the plane of incidence or is normal to this plane. The plane of incidence in Fig. 243 is the ZX plane. This leads generally to three conditions as far as the effect on a receiving dipole is concerned. The reason for this is that for perpendicular electric polarization, there can be only *one* perpendicular direction of $\mathcal{E}$ to the

horizontal XY plane. For parallel polarization, the electric $\mathcal{E}$ vector can be normal to ground as for the $a - b$ orientation of the receiver dipole. If this dipole were a radiator, we should obtain a parallel polarization known as "vertical" polarization. The vector $\mathcal{E}$ can, however, still be parallel with the ZX plane, but also parallel with the X direction of the ground. This is *not* horizontal polarization (although the orientation $a'' - b''$ is horizontal). By *horizontal* polarization is meant the $a''' - b'''$ orientation of the dipole (if it were radiating), which is a dipole pointing perpendicular to the paper (along the Y axis). This must be the case since the paper is the plane of incidence. Having this definition in mind, we can put $\rho_v = \rho_{\parallel}$ and $\rho_h = \rho_{\perp}$ as is done in Table 44. Figure 243 then shows all three cases that can be expressed by such reflection coefficients.

We call $a' - b'$ a general orientation[1] of a linear receiving antenna for parallel polarization ($\mathcal{E}$ in the plane of ZX and inclined to both the Z and X axis). One arriving field vector is always normal to the direction of propagation and in the plane of incidence. This vector is shown as F_1 in Fig. 243. For parallel polarization, $F_1 = \mathcal{E}_1$, while the associated magnetic vector H_1 must be perpendicular to the ZX plane at G, which is the point of reflection on the surface of the ground. For perpendicular polarization, we have $F_1 = H_1$, $F_2 = H_2$, and $F_3 = H_3$, and the corresponding $\mathcal{E}$ associations are normal to the ZX plane at the reflection point G. Since, for parallel polarization, $a'b'$ is a general receiving dipole orientation, there exists a definite direction θ of the incident beam for which *no* incident or reflected beam can exist. This means that the *indirect* beam *cannot* occur. This happens for parallel polarization if a linear radiator is oriented as is dipole $A'B'$. For this radiator, the free-field intensity is $\mathcal{E}_0$ volts per meter and is the largest field effect at 1 m distance, since $\mathcal{E}_0$ is parallel with the $A'B'$ direction in the ZX plane. The field $\mathcal{E}_0 \sin \theta$ must be zero, since it is normal to radiator $A'B'$. Therefore, the indicated wave incidence is for the $A'B'$ radiator such that $F_1 = 0$ and $\mathcal{E}_1 = H_1 = 0$. Therefore, also $\mathcal{E}_2 = H_2 = 0 = \mathcal{E}_3 = H_3 = F_3 = F_2$. This then excludes the indirect wave. This is not true, however, for the direct wave, since a vector $\mathcal{E}_0'$ arrives whose component (parallel with $a'b'$) will induce a voltage, since for such relative orientations as $A'B'$ and $a'b'$ the free-field component $\mathcal{E}_0 \cos \theta'$ is effective at 1 m distance from the $A'B'$ radiator.

Suppose we have a radiator AB that radiates a vertically polarized wave. For an angle θ of incidence, the free-field intensity at unit distance is not $\mathcal{E}_0$ as in the equatorial plane of the AB radiator but is only

[1] With respect to general linear polarization and elliptical polarization, refer to pages 549–552 and 785–788.

$\mathcal{E}_0 \sin \theta$, since $\mathcal{E}_0 \sin \theta$ is perpendicular to the incident beam. At G, we have then a corresponding field component $F_1 = \mathcal{E}_1$ for the incident electric field vector and a component $\mathcal{E}_1 \sin \theta$ along the Z axis. The time phase of $\mathcal{E}_1 \sin \theta$ is zero, since we refer the phase of the reflected vector F_3 to the incident field F_1. Therefore, if the incident field component $\mathcal{E}_1 \sin \theta$ (along the Z axis) is taken at the mid-point elevation of h meters, the relative phase can no longer be zero but must be delayed at this altitude h by an angle $\beta h \cos \theta$, where $\beta = 1.2f$ degrees per meter, where f is in megacycles per second. This is the case, since $\beta = \omega/(3 \times 10^8) = 360 \times 10^6 f/(3 \times 10^8)$. The relation

$$\beta = 1.2f^{(\text{Mc})} \qquad \text{deg/m} \tag{877}$$

expresses that for each megacycle, an electromagnetic wave experiences a phase delay of 1.2 deg when progressing through 1 m distance. This is strictly true in empty space and practically so in air. Therefore, for a 300-Mc wave, we should have equal phase conditions at consecutive field points 1 m apart, because $360 = 1.2 \times 300$.

The relative phase of the incident field at a reception center h meters above the reflection point G is $-\beta h \cos \theta = -1.2fh \cos \theta = -\delta$ degrees, due to the time delay along the vertical distance of h meters. The incident field intensity at the reflection point G causes, therefore, at the reception center h meters above G, a vertical electric field component $\mathcal{E}_1 \sin \theta \epsilon^{j\delta}$ volts per meter. Since in dealing with parallel polarization the reflected amplitude is $\rho_\parallel \mathcal{E}_1 \epsilon^{j\varphi_\parallel} \sin \theta$ at G and at the reception center of dipole ab, it becomes $\rho_\parallel \mathcal{E}_1 \epsilon^{j\varphi_\parallel} \epsilon^{-j\delta} \sin \theta$, where $\rho_\parallel = \rho_v$ and $\varphi_\parallel = \varphi_v$. Figure 244 gives the vector situations at the reflection point G and at the reception center. We note that generally for an angle of incidence which is *not* $\theta = 90$ deg, the resultant field $\mathcal{E}_R$ at any altitude h above the reflection point G is no longer normal to ground but makes an angle

$$\gamma = \tan^{-1}\left[\frac{\epsilon^{j\delta} - \rho_v \epsilon^{j(\varphi_v - \delta)}}{\epsilon^{j\delta} + \rho_v \epsilon^{j(\varphi_v - \delta)}} \cot \theta\right]$$

$$= \tan^{-1}\left[\frac{1 - \rho_v \epsilon^{j(\varphi_v - 2\delta)}}{1 + \rho_v \epsilon^{j(\varphi_v - 2\delta)}} \cot \theta\right] \qquad \text{deg} \tag{877a}$$

The last form of angle γ is obtained by multiplying the numerator and denominator by $\epsilon^{-j\delta}$. We can, therefore, pick up field energy with a receiving dipole or any linear antenna in the vertical direction ab as shown in Fig. 244 or with such an antenna in a horizontal position in the plane of incidence (plane of the paper). From the vector triangle of the field components at the elevated reception center, we have the sum of the vertical field contributions

$$\begin{aligned}\mathcal{E}_v &= \mathcal{E}_1 e^{j\delta} \sin\theta + \rho_v \mathcal{E}_1 e^{j(\varphi_v - \delta)} \sin\theta \\ &= \mathcal{E}_1 \sin\theta[1 + \rho_v e^{j(\varphi_v - 2\delta)}] \qquad \text{volts/m} \qquad (877b)\end{aligned}$$

since the last form represents the same relative phase 2δ as the first form. We have, however, the *difference* of the horizontal field contributions (according to Fig. 244) and find the total horizontal field

$$\begin{aligned}\mathcal{E}_h &= \mathcal{E}_1 e^{j\delta} \cos\theta - \rho_h \mathcal{E}_1 e^{j(\varphi_h - \delta)} \cos\theta \\ &= \mathcal{E}_1 \cos\theta[1 - \rho_h e^{j(\varphi_h - 2\delta)}] \qquad \text{volts/m} \qquad (877c)\end{aligned}$$

Hence, for a linear receiving antenna, as indicated *ab* orientation, we measure the vertical component of $\mathcal{E}_R$ at the reception center. The

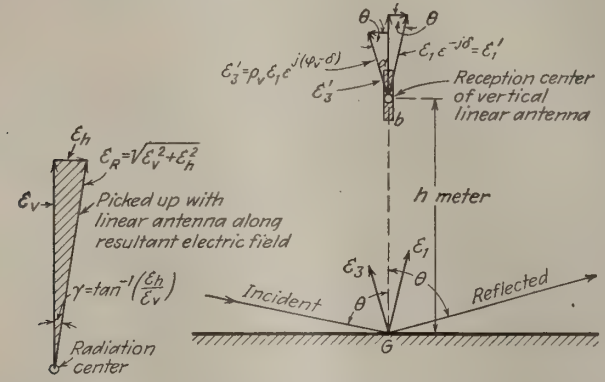

$\mathcal{E}_v = (\mathcal{E}_1' + \mathcal{E}_3')\sin\theta$ is field picked up with a vertical linear antenna.
$\mathcal{E}_h = (\mathcal{E}_1' - \mathcal{E}_3')\cos\theta$ is picked up with a horizontal linear antenna

f is in Mc/sec
$\delta = -1.2fhD_{(90-\theta)}$ deg
φ_v is time phase angle of reflection coefficient ρ_v in deg
$D_{(90°-\theta)} = \cos\theta$ for a receiving doublet
$D_{(90°-\theta)} = \dfrac{\cos(90°\sin\theta)}{\cos\theta}$ for a receiving half-wave dipole

FIG. 244. Incident and reflected electric field components at places above the reflection point G for parallel polarization.

horizontal orientation should not be confused with the horizontal orientation of a receiving antenna when horizontally polarized waves arrive, since, for such a polarization, the receiving antenna would point normal to the paper.

In exactly the same way, we can derive the expression for horizontal polarization ($\mathcal{E}$ is normal to the plane of incidence). We have then in Fig. 243 $F_1 = H_1$, $F_2 = H_2$, and $F_3 = H_3$, and $\mathcal{E}_1$, $\mathcal{E}_2$, and $\mathcal{E}_3$ are perpendicular to the paper. We have then only one $\mathcal{E}_R$ field (with no components), since it is normal to the plane of incidence. Since the amplitudes $\mathcal{E}_1$ and $\mathcal{E}_3 = \rho_h \mathcal{E}_1$ are parallel to ground and perpendicular to the plane of incidence (along Y axis), we have *no* sin θ and cos θ functions

in the final expression and find

$$\mathcal{E}_R = \mathcal{E}_1[1 + \rho_h e^{j(\varphi_h - 2\delta)}] \qquad \text{volts/m} \tag{877d}$$

since $\mathcal{E}_R = \mathcal{E}_h$. The receiving antenna then points perpendicularly into the paper in Fig. 243. The expressions (877*b*), (877*c*), and (877*d*) have the form

$$\mathcal{E} = p\mathcal{E}_1[1 \pm \rho e^{j(\varphi - 2\delta)}] \tag{877e}$$

where $p = \sin\theta$, $= \cos\theta$, $= 1$ for (877*b*), (877*c*), (877*d*) and $\mathcal{E}_1$ is the field intensity in volts per meter incident at the reflection point G. Magnitude ρ and phase φ of the reflection factor depend on the polarization. The real component of (877*e*) becomes

$$\mathcal{E} = p\mathcal{E}_1 \sqrt{[1 \pm \rho\cos(\varphi - 2\delta)]^2 + \rho^2 \sin^2(\varphi - 2\delta)}\cos\psi \qquad \text{volts/m}$$
$$\psi = \tan^{-1}\left[\frac{\sin(\varphi - 2\delta)}{1 \pm \rho\cos(\varphi - 2\delta)}\right]; \qquad \delta = -1.2fhD \tag{877f}$$

where D is the direction factor. For a vertical half-wave radiator, it is $D_\theta = [\cos(90^\circ \cos\theta)]/\sin\theta$, while it is unity for horizontally polarized waves with the receiving linear antenna lined up in parallel with the radiator.

161. Notes on Wave Spread for Plane and Curved Earth. In unobstructed radiation space, the electromagnetic field energy is propagated in all directions from a point source. For no conductivity effects in the wave medium (a pure dielectric like air), the same energy flux must cross the larger spherical surface S as streams perpendicular to the surface S_0 of Fig. 245. In the distant radiation field, $\mathcal{E}$ volts per meter and H amperes per meter (both effective values) cause a normal energy flux of $p = \mathcal{E}H$ watts per square meter. This is then the energy flux of $\mathcal{E}H$ joules across each square-meter normal surface during 1 sec. Hence, at the reference distance of $r_0 = 1$ m, p_0S_0 watts are streaming normal to S_0 square meters and pS watts is the same wattage through S square meters. It is taken for granted that S is in the distant radiation region, so that $\mathcal{E}$ and H form a plane wave front as far as 1-square-meter area is concerned. The quantities $\mathcal{E}$ and H are also in space quadrature and in time phase. The reference values $\mathcal{E}_0$ and H_0, at 1 m distance, are then the space quadrature field associations, which are likewise in time phase and such that $p_0S_0 = pS$ with values for respective Poynting vectors as in Fig. 245. The reference ratio $\mathcal{E}_0/H_0$ must then be equal to the ratio $\mathcal{E}/H = 376.7$ ohms, where also $p = 376.7H^2$ watts per square meter. For no medium losses (heat losses), the energy continuity requires $p_0S_0 = pS$ or $S_0\mathcal{E}_0^2 = S\mathcal{E}^2$, and

$$\mathcal{E} = \mathcal{E}_0 \sqrt{\frac{S_0}{S}} = \frac{r_0}{r}\,\mathcal{E}_0 \qquad \text{volts/m}\,, \tag{878}$$

since spherical surfaces are proportional to the squares of respective radii. Since r_0 is taken as unity distance, Eq. (878) is the well-known inverse distance law $\mathcal{E} = \mathcal{E}_0/r$, where $\mathcal{E}_0$ represents the electric field intensity at $r_0 = 1$ m. The ratio r_0/r is a measure for the *wave spread* or reduction in the field intensity when a wave travels through a distance of $r - r_0$ meters. Inasmuch as r/r_0 is, according to (878), equal to $\sqrt{S_0/S}$, we can compare such ratios for plane and spherical earth as in Fig. 246. Such a wave spread or dilution of the electromagnetic field energy across ever-growing spherical surfaces S (as the distance r grows from the radiation center) causes what is known as "geometrical" attenuation of the field intensity. Over plane ground, we have the ratio

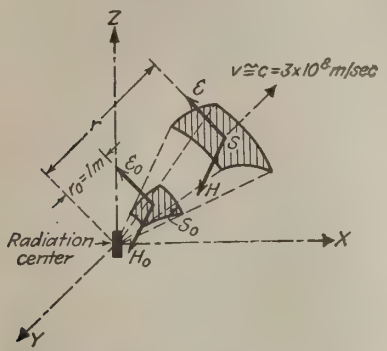

Fig. 245. Wave spread for spherical expanding wave fronts. Magnitudes of Poynting energy vectors $p_0 > p$; $p_0 = \mathcal{E}_0^2/377$ watts/m^2; $p = \mathcal{E}^2/377$ watts/m^2; $\mathcal{E}_0$ is the radiation reference value at unity distance from radiation center. r and r_0 are in meters, and S and S_0 in square meters; $\mathcal{E}_0$ and $\mathcal{E}$ are effective field values in volts/m; $\mathcal{E}_0/H_0 = \mathcal{E}/H \cong 377$ ohms for air.

$$\mathcal{E}/\mathcal{E}_0 = \sqrt{S_0/S} = \sqrt{S_0/S'} = r_0/r,$$

because in Fig. 246 the image spherical surface element S' at the image center location P_2' is exactly of same size as the actual surface element S at the receiving center P_2. This is *no longer true* for wave propagation over spherical earth, since $\mathcal{E}/\mathcal{E}_0 = \sqrt{S_0/S} = \sqrt{S_0/S'}\,\sqrt{S'/S}$ and $\mathcal{E}/\mathcal{E}_0 = (r_0/r)\,\sqrt{S'/S}$. The factor r_0/r is the inverse distance effect *due to wave spread*, while the factor $\sqrt{S'/S} = C$ is the *curvature effect*. This effect is given by the approximation

$$C \cong \frac{1}{\sqrt{1 + (2h_1'h_2' \tan^3\theta)/(Rd)}} \tag{878a}$$

showing that the curvature effect of the earth surface is unity for perpendicular wave incidence. When the incidence and the line of sight approach each other, the value of C approaches zero. The factor C must be used in the reflection term of Eqs. (876*a*) and (876*b*) by multiplying ρ by C. This applies then for curved earth (assumed spherical) for distances *within the line of sight*. It is also assumed that the index n of atmospheric refraction is unity so that rectilinear wave propagation prevails for both the direct and the indirect ground-reflected rays.

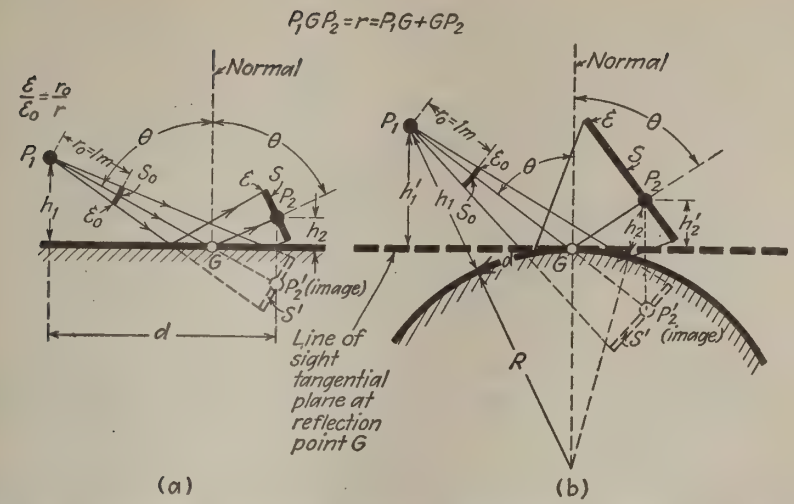

FIG. 246. Wave spread over flat and spherical earth surfaces. (*a*) For plane ground, P_1 and P_2 are actual antenna centers (symmetry points). (*b*) For spherical ground, $\mathcal{E}/\mathcal{E}_0 = r_0/r\sqrt{S'/S} \cong r_0/r\sqrt{1 + (2h_1'h_2' \tan^3\theta)/Rd}$.

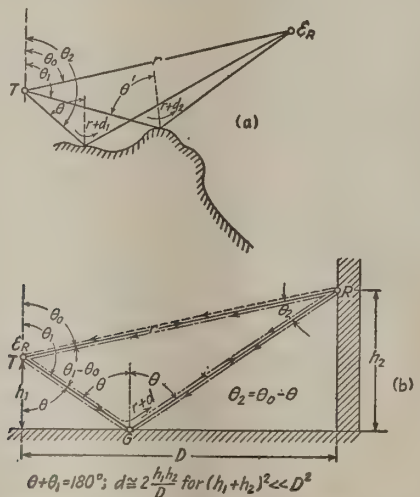

FIG. 247. Multiple reflections due to two different grounds. Reflections and paths for reception at the transmitting center. (*a*) Resultant field $\mathcal{E}_R$ in the distant radiation region. (*b*) Resultant field $\mathcal{E}_R$ at radiation center.

162. Effects of Multiple Reflections from Ground on the Space Field. We may have cases as in Fig. 247 for the radiation region. Matters are then no more difficult, since it is only necessary to add geometrically the various arriving component fields at the reception center R. Figure 247 shows the case where three arriving waves are instrumental at R.

One wave travels along the direct path r, and two indirect waves, upon reflection at the ground, travel along respective total paths $r + d_1$ and $r + d_2$ meters. We must then deal with different reflection coefficients ρ_1 and ρ_2 and corresponding phases φ_1 and φ_2, since the angles of incidence are θ and θ', where ρ and φ depend upon the polarization besides. If $\mathcal{E}_0$ denotes the true reference radiation portion in volts per meter at 1 m distance from the radiation center and in the equatorial plane of the radiator, we have at R of Fig. 247:

$$\mathcal{E}_R^{(\text{volts/m})} = \frac{D_{\theta_0}\mathcal{E}_0}{r}\epsilon^{j(\omega t-\beta r)} + \rho_1\frac{D_{\theta_1}\mathcal{E}_0}{r+d_1}\epsilon^{j[\omega t+\varphi_1-\beta(r+d_1)]} + \rho_2\frac{D_{\theta_2}\mathcal{E}_0}{r+d_2}\epsilon^{j[\omega t+\varphi_2-\beta(r+d_2)]}$$

where, for horizontal polarization, $D_{\theta_0} = D_{\theta_1} = D_{\theta_2} = 1$ if the linear pickup antenna at R is parallel with the radiator. For the abbreviations

$$a = \frac{D_{\theta_0}\mathcal{E}_0}{r}; \qquad b = \frac{\rho_1 D_{\theta_1}\mathcal{E}_0}{r+d_1}; \qquad e = \frac{\rho_2 D_{\theta_2}\mathcal{E}_0}{r+d_2}$$

we find

$$\left.\begin{aligned} \mathcal{E} &= \epsilon^{j(\omega t-\beta r)}[a + b\epsilon^{j(\varphi_1-\beta d_1)} + e\epsilon^{j(\varphi_2-\beta d_2)}] \\ &= \epsilon^{j(\omega t-\beta r)}(a + b\epsilon^{j\Delta_1} + e\epsilon^{j\Delta_2}) \qquad \text{volts/m} \\ \Delta_1 &= \varphi_1 - 1.2fd_1 \qquad \text{deg} \\ \Delta_2 &= \varphi_2 - 1.2fd_2 \qquad \text{deg} \end{aligned}\right\}. \tag{879}$$

where f is in megacycles per second, d_1 and d_2 are in meters, and Δ_1 and Δ_2 are the relative phases in degrees with respect to the direct field component. Hence, maxima effects result when a, b, and e are positive and Δ_1 as well as Δ_2 are $180k$ degrees, for $k = 0, 2, 4, 6, \cdots$. For the general case, a, b, and e depend on the respective directivities D_{θ_0}, D_{θ_1}, and D_{θ_2}. Inasmuch as we have three terms in (879), minima effects occur when one term is neutralized by the geometric sum of the other terms.

In Fig. 247*b*, the radiation and reception center is assumed at the same space point T. This means that a provision has to be made so that there are receiving times during which the transmitter *cannot* affect the sensitive receiving equipment. We have three confluent path triangles. A reflecting wall returns a resultant distant field at R to field point T as field $\mathcal{E}_R$, *i.e.*, to the location of the electromagnetic source, from whence it came. We have now two distinct reflection points, namely, G at the surface of the ground and R at the surface of the reflecting wall. If the obstructing wall through R were not a reflector, we should have at R a resultant field due to the components

$$\frac{D_{\theta_0}\mathcal{E}_0}{r}\epsilon^{j(\omega t-\beta r)} \quad \text{and} \quad \rho\frac{D_{\theta_1}\mathcal{E}_0}{r+d}\epsilon^{j[\omega t+\varphi-\beta(r+d)]} \quad \text{volts/m}$$

for the reflection coefficient ρ and its phase at G. This accounts for the full-line path triangle TRG with a direct path $TR = r$ and an indirect path $TG + GR = r + d$. For optimum reception orientation and a horizontal radiator, we have $D_{\theta_0} = D_{\theta_1} = 1$; while for a vertical radiator, the directivities D_{θ_0} and D_{θ_1} are generally different, since θ_0 and θ_1 differ in magnitude. If the wall were a perfect conductor, the image point R' of R and R itself would coincide at the surface of the wall at R. For horizontal polarization, we have at R a reflection coefficient -1, causing $-\mathcal{E}_0/r$ and $-\rho_h\mathcal{E}_0/(r + d)$ amplitudes of the reflected fields at R, where ρ_h is the complex reflection coefficient at G and the minus sign, or -1, is the reflection coefficient at R. Each component can then proceed along the direct path RT as well as along the indirect path $RG + GT$. This means that we have four waves returning to T, one starting with the amplitude $-\mathcal{E}_0/r$ along the dash-dash path $RT = r$, the second along the dash-dot-dash path along RT with initial amplitude $-\rho_h\mathcal{E}_0/(r + d)$, the third with the initial amplitude $-\mathcal{E}_0/r$ along the dash-dot-dot-dash path $RG + GT = r + d$, and the fourth with the initial amplitude $-\rho_h\mathcal{E}_0/(r + d)$ along the same path dash-dot-dash $RG + GT = r + d$. The resultant field at T, due to the reflections at R, is then subject to phase delays caused by the reflection coefficient -1 of a perfect metallic reflector at R, the phase factor $\epsilon^{j\varphi_h}$ due to ground reflection, and the respective phase delays due to the path difference. The values of the four returning electromagnetic waves right next to the reflection point R are, with respect to magnitude and phase, $(\mathcal{E}_0/r)\epsilon^{j(\omega t-\beta r)}\epsilon^{-j180^\circ}$ along the dash-dash path RT as well as RG, $\rho_h[\mathcal{E}_0/(r + d)]\epsilon^{j[\omega t+\varphi-\beta(r+d)]}\epsilon^{-j180^\circ}$ along dash-dot-dash path RT and RG, since the reflection causing phase reversal at R is taken care of by the factor ϵ^{-j180° with a real component cos 180 deg $= -1$. The corresponding arriving field values at T, after traveling respective paths RT and $RG + GT$, become, for the abbreviations $a = \mathcal{E}_0/r$ and $b = \rho_h\mathcal{E}_0/(r + d)$, equal to

$$\left.\begin{array}{ll}
\dfrac{a}{r}\,\epsilon^{j(\omega t-\beta r)}\epsilon^{-j180^\circ}\epsilon^{-j\beta r} & \text{along dash-dash path } RT \\
\dfrac{b}{r}\,\epsilon^{j[\omega t+\varphi_h-\beta(r+d)]}\epsilon^{-j180^\circ}\epsilon^{-j\beta r} & \text{along dash-dot-dash path } RT \\
\rho_h\epsilon^{j\varphi}\,\dfrac{a}{r+d}\,\epsilon^{j(\omega t-\beta r)}\epsilon^{-j180^\circ}\epsilon^{-j\beta(r+d)} & \text{along dash-dot-dot-dash path } RG + GT \\
\rho_h\epsilon^{j\varphi_h}\,\dfrac{b}{r+d}\,\epsilon^{j[\omega t+\varphi_h-\beta(r+d)]}\epsilon^{-j180^\circ}\epsilon^{-j\beta(r+d)} & \text{along dash-dot-dash path } RG + GT
\end{array}\right\} \text{at } T \qquad (879a)$$

The resultant field $\mathcal{E}_R$ at T then becomes

$$\mathcal{E}_R = \frac{a}{r}\epsilon^{j(\omega t-2\beta r-180°)} + \frac{b}{r}\epsilon^{j[\omega t+\varphi_h-2\beta(r+d)-180°]} + \rho_h\frac{a}{r+d}\epsilon^{j[\omega t+\varphi_h-2\beta(r+d)-180°]} + \rho_h\frac{b}{r+d}\epsilon^{j[\omega t+2\varphi_h-2\beta(r+d)-180°]}$$

$$= \epsilon^{j(\omega t-\beta r-180°)}\left[\frac{a}{r} + \frac{b}{r}\epsilon^{j(\varphi_h-\beta d)} + \frac{\rho_h a}{r+d}\epsilon^{j(\varphi_h-\beta d)} + \frac{\rho_h b}{r+d}\epsilon^{j2(\varphi-\beta d)}\right] \quad \text{volts/m} \qquad (879b)$$

The common phase factor $\exp[j(\omega t - \beta r - 180°)]$ cannot change the resultant value $\mathcal{E}_R$, since it is the same rotation for either vector term in the bracket. It can be ignored as far as the absolute value of $\mathcal{E}_R$ at T is concerned. As far as the inverse distance effect in the field amplitude value is concerned, we have $1/r \cong 1/(r+d)$, since $r \gg d$, and we can write in (879*b*)

$$\frac{a}{r} = \frac{\mathcal{E}_0}{r^2}; \qquad \frac{b}{r} = \frac{\rho_h\mathcal{E}_0}{(r+d)r} \cong \frac{\rho_h\mathcal{E}_0}{r^2}$$

$$\frac{\rho_h a}{r+d} = \frac{\rho_h\mathcal{E}_0}{(r+d)r} \cong \frac{\rho_h\mathcal{E}_0}{r^2}; \qquad \frac{\rho_h b}{r+d} = \frac{\rho_h^2\mathcal{E}_0}{(r+d)^2} \cong \frac{\rho_h^2\mathcal{E}_0}{r^2}$$

The absolute value of the resultant field due to the total wave return at T then becomes

$$\left.\begin{aligned} &\mathcal{E}_R = \frac{\mathcal{E}_0}{r^2}(1 + 2\rho_h\epsilon^{j\Delta} + \rho_h^2\epsilon^{j2\Delta}) = \frac{\mathcal{E}_0}{r^2}(1 + \rho_h\epsilon^{j\Delta})^2 \qquad \text{volts/m} \\ &\Delta = \varphi_h - 1.2fd \qquad \text{deg} \end{aligned}\right\} \qquad (879c)$$

where d and r are in meters and f is in megacycles per second. In this formula, d is the path difference in meters between the indirect and direct beams. We deal now with an inverse *square distance law* instead of an inverse distance law. Inasmuch as the returned wave energy is proportional to the field intensity in square, the returned energy must vary inversely as the *fourth* power of the distance r. Therefore, if at T another reflection were to occur, we should have at R a resultant field proportional to $1/r^3$; and for another perfect reflection at R, we should find a field at T that is proportional to $1/r^4$. This can be realized, since after an outward travel $\mathcal{E}_0/r$ is the arriving field of a beam. Therefore, the reference field for the returning wave is now $\mathcal{E}_0/r$ for the first arrival at R and not $\mathcal{E}_0$. Upon perfect reflection of a beam at R, the same beam will cause at T, according to the inverse distance law, a field that is the

reference field $\mathcal{E}_0/r$ divided by the distance r or $\mathcal{E}_0/r^2$, etc. Equation (879*c*) can also be written as

$$\left.\begin{aligned}
\mathcal{E}_R^{(\text{volts/m})} &= \frac{\mathcal{E}_0}{r^2}\,[1 + \rho_h(\cos\Delta + j\sin\Delta)]^2 \\
&= \frac{\mathcal{E}_0}{r^2}\,[\sqrt{(1 + \rho_h\cos\Delta)^2 + \rho_h^2\sin^2\Delta}]^2\,\epsilon^{j\psi} \\
&= \frac{\mathcal{E}_0}{r^2}\,(1 + 2\rho_h\cos\Delta + \rho_h^2)\epsilon^{j\psi} \\
\psi^\circ &= \tan^{-1}\left(\frac{\rho_h\sin\Delta}{1 + \rho_h\cos\Delta}\right)
\end{aligned}\right\} \qquad (879d)$$

Inasmuch as $\mathcal{E}_0$ and $\mathcal{E}_R$ are known, $\mathcal{E}_R$ can be measured, and r is known, the above equation must give a means of determining the reflection coefficient ρ_h and its phase φ_h for horizontal polarization. Equation (879*d*) also shows that the returned field at T must oscillate between minima and maxima values, since $\cos\Delta$ passes through ± 1 values for $\Delta = 0,\ 180,\ 360,\ \cdots$ degrees. The formula given in Fig. 247*b* holds only for the condition $(h_1 + h_2)^2 \ll D^2$, which should apply in many cases, while the path difference, for all other conditions, can be computed from

$$d = \sqrt{D^2 + (h_1 + h_2)^2} - \sqrt{D^2 + (h_1 - h_2)^2} \qquad (879e)$$

In each case, rectilinear space propagation is assumed (atmospheric index of refraction equal to unity). The path difference can be found *most quickly* by drawing to a reduced scale the path triangle $TRGT$ and scaling off the reduced lengths kr and $k(r + d)$ by means of a map measure. The factor k is the constant of scale reduction. This procedure is especially expedient when curved direct and indirect paths prevail (index of atmospheric refraction plays a part). For any kind of polarization for the arriving electromagnetic waves at the reception center R, we generally have the component fields

$$\left.\begin{aligned}
&\frac{D_{\theta_0}\mathcal{E}_0}{r}\,\epsilon^{j(\omega t - \beta n r)} && \text{volts/m for the direct wave} \\
&\frac{\rho D_{\theta_1}\mathcal{E}_0}{r + d}\,\epsilon^{j[\omega t + \varphi - \beta n(r+d)]} && \text{volts/m for the ground-reflected indirect wave}
\end{aligned}\right\} \qquad (879f)$$

The quantity n is then the atmospheric index of refraction with respect to vacuum. We deal with a gradient dn/dh, which means a change of $n = \sqrt{\kappa_r}$ with the elevation above ground. The quantity κ_r denotes the numeric relative dielectric constant $\kappa/(8.854 \times 10^{-12})$ of the air at a certain altitude of h meters above ground.

Matters are more involved for vertical polarization and a general medium (μ, κ, σ) of the reflecting wall with the surface point R of Fig. 247*b*. It is then customary to work with scattering coefficients, which are found experimentally by noting the field return from a particular surface. Such coefficients can be found for any curved surface of reflection in terms of an effective area and the wave energy return in a desired direction.

Matters are also involved, even in the case of a perfectly reflecting wall on which R is a surface point, if we deal with vertical polarization, since D_{θ_0} and D_{θ_1} in Eq. (879*f*), for $\rho = \rho_v$ and $\varphi = \varphi_v$ and $n = 1$, differ and are no longer equal to unity, even though for relatively large coverages (large distances), we have $\theta_0 \cong \theta_1$, and angles in the neighborhood of 90 deg are of concern. We have then, for a vertical half-wave radiator,

$$D_{\theta_0} = D_{\theta_1} = \frac{\cos\,(90^\circ \cos\,\theta_1)}{\sin\,\theta_1} \cong \sin\,\theta_1$$

for $\theta_1 = 90$ to 75 deg of incidence and D_{θ_1} equal to about unity, for angles of 90 to about 85 deg. For all other cases, the formula

$$D_{\theta_0} = D_{\theta_1} = \frac{\cos\,(90^\circ \cos\,\theta_1)}{\sin\,\theta_1}$$

must be used. For a perfect target at R, the reflection coefficient is now $+1$, *i.e.*, *inphase* wave returns occur, with initial values as given by (879*f*) for $\rho = \rho_v$ and $\varphi = \varphi_v$ and $n = 1$, as far as respective paths RT and RG of Fig. 247*b* are of concern. We have then, for the four initial values along the following four return paths and right next to reflection point R (for vertically polarized waves),

$$\left.\begin{array}{ll}
\dfrac{D_{\theta_0}\mathcal{E}_0}{r}\,\epsilon^{j(\omega t-\beta r)} & \text{along the dash-dash path } RT \\
\dfrac{D_{\theta_0}\mathcal{E}_0\cos\,\theta_2}{r}\,\epsilon^{j(\omega t-\beta r)} & \text{along the dash-dot-dot-dash path } RG \\
\dfrac{\rho_v D_{\theta_1}\mathcal{E}_0}{r+d}\,\epsilon^{j[\omega t+\varphi_v-\beta(r+d)]} & \text{along the dash-dot-dash path } RG \\
\dfrac{\rho_v D_{\theta_1}\mathcal{E}_0\cos\,\theta_2}{r+d}\,\epsilon^{j[\omega t+\varphi_v-\beta(r+d)]} & \text{along the dash-dot-dash path } RT
\end{array}\right\} \text{right next to } R \qquad (879g)$$

For the abbreviations $D_{\theta_0}\mathcal{E}_0/r = a$ and $\rho_v D_{\theta_1}\mathcal{E}_0/(r+d) = b$, we find the corresponding arriving field values at T

$$\left.\begin{array}{ll}
\dfrac{a}{r}\,\epsilon^{j(\omega t-\beta r)}\epsilon^{-j\beta r} & \text{along the dash-dash path } RT \\
\dfrac{b\cos\theta_2}{r}\,\epsilon^{j[\omega t+\varphi_v-\beta(r+d)]}\epsilon^{-j\beta r} & \text{along the dash-dot-dash path } RT \\
\rho_v\epsilon^{j\varphi_v}\dfrac{a\cos\theta_2}{r+d}\,\epsilon^{j(\omega t-\beta r)}\epsilon^{-j\beta(r+d)} & \text{along the dash-dot-dot-dash path } RG+GT \\
\rho_v\epsilon^{j\varphi_v}\dfrac{b}{r+d}\,\epsilon^{j[\omega t+\varphi_v-\beta(r+d)]} & \text{along the dash-dot-dash path } RG+GT
\end{array}\right\}\ \text{at } T \qquad (879h)$$

The resultant field $\mathcal{E}_R$ at the radiation center T, due to the four returned waves, is again the geometric addition of the above components, yielding

$$\mathcal{E}_R = \epsilon^{j(\omega t-2\beta r)}\left[\frac{a}{r}+\frac{b\cos\theta_2}{r}\,\epsilon^{j(\varphi_v-\beta d)} + \frac{\rho_v a\cos\theta_2}{r+d}\,\epsilon^{j(\varphi_v-\beta d)}+\frac{\rho_v b}{r+d}\,\epsilon^{j2(\varphi_v-\beta d)}\right] \quad \text{volts/m} \qquad (879i)$$

The common phase factor $\exp j(\omega t - 2\beta r)$ will again not change the value of the resultant field $\mathcal{E}_R$, since each term in the parenthesis is changed by it. We therefore ignore the common factor as far as the absolute value of $\mathcal{E}_R$ is concerned. For $r \gg d$ and $\gg \lambda$, the inverse distance effects for the justified approximation, $1/r \cong 1/(r+d)$; and in (879i), we can write

$$\frac{a}{r}=\frac{D_{\theta_0}\mathcal{E}_0}{r^2};\qquad \frac{b\cos\theta_2}{r}=\frac{\rho_v D_{\theta_1}\mathcal{E}_0\cos\theta_2}{(r+d)r}\cong\frac{\rho_v D_{\theta_1}\mathcal{E}_0\cos\theta_2}{r^2}$$

$$\frac{\rho_v a\cos\theta_2}{r+d}=\frac{\rho_v D_{\theta_0}\mathcal{E}_0\cos\theta_2}{r(r+d)}\cong\frac{\rho_v D_{\theta_0}\mathcal{E}_0\cos\theta_2}{r^2}$$

$$\frac{\rho_v b}{r+d}=\frac{\rho_v^2 D_{\theta_1}\mathcal{E}_0}{(r+d)^2}\cong\frac{\rho_v^2 D_{\theta_1}\mathcal{E}_0}{r^2}$$

The absolute value of the resultant field, due to the total wave return from R at the radiation center T, then becomes

$$\left.\begin{array}{l}
\mathcal{E}_R=\dfrac{\mathcal{E}_0}{r^2}\left(D_{\theta_0}+\rho_v D_{\theta_1}\epsilon^{j\Delta}\cos\theta_2+\rho_v D_{\theta_0}\epsilon^{j\Delta}\cos\theta_2+\rho_v^2 D_{\theta_1}\epsilon^{j2\Delta}\right) \quad \text{volts/m} \\
\Delta=\varphi_v-1.2fd \quad \text{deg}
\end{array}\right\} \qquad (879j)$$

where d and r are in meters and f is in megacycles per second. In Fig. 247b, we have $\theta+\theta_1 = 180° = \theta_2 + 2\theta + \theta_1 - \theta_0$, $\theta_2 = \theta_0 - \theta$. Therefore, when the back-scattering point R is a relatively large distance r away from the radiation center T, the paths TR and GR become essentially parallel and $\theta_2 \cong 0$. Therefore, $\theta_0 = \theta$. This holds in several practical applications, where h_1 is small compared with the direct path of

length r. We have then in (879j), $\cos \theta_2 = 1$. $D_{\theta_2} = D_\theta$, $D_{\theta_1} = D_{180°-\theta}$, since $\theta_1 + \theta = 180$ deg. Since $\sin (180° - \theta) = \sin \theta$ and $\cos [90° \times \cos (180° - \theta)] = \cos (-90° \cos \theta) = \cos (90° \cos \theta)$, we find, for a vertical half-wave radiator, $D_{\theta_1} = D_\theta$ and (879j) simplifies to

$$\mathcal{E}_R = \frac{D_\theta \mathcal{E}_0}{r^2} (1 + 2\rho_v \epsilon^{j\Delta} + \rho_v^2 \epsilon^{j2\Delta}) = \frac{D_\theta \mathcal{E}_0}{r^2} (1 + \rho \epsilon^{j\Delta})^2 \quad \text{volts/m} \qquad (879k)$$

We have then for a vertical and a horizontal half-wave radiator at T, for the respective returned field intensities

$$\left.\begin{aligned} \mathcal{E}_R^{(\text{volts/m})} &= \frac{D_\theta \mathcal{E}_0}{r^2} (1 + \rho_v \epsilon^{j\Delta_v})^2 \quad \text{for a vertical half-wave radiator at } T \\ \mathcal{E}_R^{(\text{volts/m})} &= \frac{\mathcal{E}_0}{r^2} (1 + \rho_h \epsilon^{j\Delta_h})^2 \quad \text{for a horizontal half-wave radiator at } T \end{aligned}\right\} \text{Fig. (247}b\text{)}$$

$$\left.\begin{aligned} \Delta = \Delta_v &= \varphi_v - 1.2fd \quad \text{deg}; \qquad D_\theta = \frac{\cos (90° \cos \theta)}{\sin \theta} \\ \Delta = \Delta_h &= \varphi_h - 1.2fd \quad \text{deg} \end{aligned}\right\} \qquad (879l)$$

where f is in megacycles per second and d and r are in meters. The result of (879l) can also be written in the form

$$\left.\begin{aligned} \mathcal{E}_R^{(\text{volts/m})} &= \frac{D_\theta \mathcal{E}_0}{r^2} (1 + 2\rho_v \cos \Delta_v + \rho_v^2) \epsilon^{j\psi_v} \\ \mathcal{E}_R^{(\text{volts/m})} &= \frac{\mathcal{E}_0}{r^2} (1 + 2\rho_h \cos \Delta_h + \rho_h^2) \epsilon^{j\psi_h} \\ \psi_v^0 &= \tan^{-1} \left(\frac{\rho_v \sin \Delta_v}{1 + \rho_v \cos \Delta_v} \right) \quad \text{for vertical } \frac{\lambda}{2} \text{ radiator at } T \\ \psi_h^0 &= \tan^{-1} \left(\frac{\rho_h \sin \Delta_h}{1 + \rho_h \cos \Delta_h} \right) \quad \text{for horizontal } \frac{\lambda}{2} \text{ radiator at } T \end{aligned}\right\} \qquad (879m)$$

For cases where h_1 or h_2 or both are relatively *not* small enough in comparison with the direct path r to make $\theta_2 \cong 0$, Eq. (879j) must be used for vertically polarized waves. When the backward wave return comes from a curved perfect reflector, the $\mathcal{E}_R$ result has to be multiplied by an empirical factor smaller than unity, in order to account for the scattering effect. It is then convenient to work with a semiempirical reduction factor, based on the concept of an equivalent reflecting plane surface,

that returns the same amount of wave energy as the actual curved target does.

163. Wave Reflections on Metal Plates and Planes of the General Medium. If a plane electromagnetic wave polarized along the Z axis of the ZX plane is stopped as in Fig. 248 by a surface of a medium with

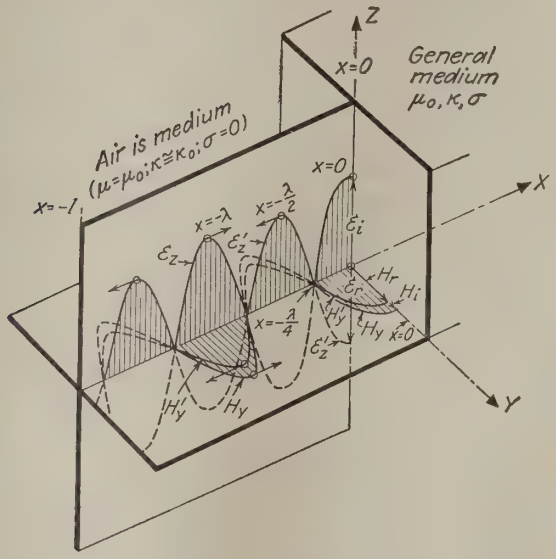

$$\left.\begin{aligned} \mathcal{E}_z &= \mathcal{E}_i \epsilon^{j(\omega t - \overrightarrow{\beta x})} \text{ volts/m} \\ H_y &= H_i \epsilon^{j(\omega t - \overrightarrow{\beta x})} \text{ amp/m} \end{aligned}\right\} \text{incident traveling EM waves}$$

$$\left.\begin{aligned} \mathcal{E}_{z'} &= -\mathcal{E}_r \epsilon^{j(\omega t + \overleftarrow{\beta x})} \\ H_{y'} &= H_r \epsilon^{j(\omega t + \overleftarrow{\beta x})} \end{aligned}\right\} \text{reflected traveling EM waves}$$

$$\left.\begin{aligned} \mathcal{E}_{\text{standing}} &= \mathcal{E}_i \epsilon^{j(\omega t - \beta x)} - \mathcal{E}_r \epsilon^{j(\omega t + \beta x)} = \epsilon^{j\omega t}(\mathcal{E}_i \epsilon^{-j\beta x} - \mathcal{E}_r \epsilon^{+j\beta x}) \\ H_{\text{standing}} &= \epsilon^{j\omega t}(H_i \epsilon^{-j\beta x} + H_r \epsilon^{+j\beta x}) \end{aligned}\right\} \text{standing or stationary waves}$$

$$\epsilon^{j(\omega t - \beta x)} = \epsilon^{j\omega\left(t - \frac{\beta}{\omega}x\right)} = \epsilon^{j\omega\left(t - \frac{x}{v}\right)}; \quad v = \frac{x}{t} = \frac{\omega}{\beta} \cong \frac{\omega}{\omega/(3 \times 10^8)} = 3 \times 10^8 \text{ m/sec for air}$$

FIG. 248. Wave reflections on planes of the general medium. ZX plane is plane of wave incidence, and $\theta = 0$.

a conductivity σ mhos per meter, a permeability μ henrys per meter, and a dielectric constant of κ farads per meter, we have indicated incident and reflected fields, which move in air in *opposite* directions with the *same* velocity. This causes standing space waves. The ratio $\mathcal{E}_r/\mathcal{E}_i = H_r/H_i$ defines the coefficient of reflection ρ, which is also given by $\rho = (Z_0 - Z_l)/(Z_l + Z_0)$, where $Z_0 = \mathcal{E}_i/H_i = \mathcal{E}_r/H_r = \sqrt{\mu_0/\kappa_0}$ ohms ($= 376.7$ ohms). The load impedance Z_l is for $\mathcal{E}$ in the plane of incidence equal to $Z \cos \theta$

ohms and for $\mathcal{E}$ normal to the plane of incidence $Z/(\cos\theta)$ ohms. For normal incidence, we have $\cos\theta = \cos 0° = 1$, and the load impedance Z_l is, for either type of polarization, equal to $Z = \sqrt{\mu/\kappa_\epsilon}$ complex ohms if the reflecting surface is part of a general medium with the electromagnetic properties μ, κ, and σ. The complex equivalent dielectric constant κ_ϵ is given by $\kappa_\epsilon = \kappa - j(\sigma/\omega)$ farads per meter for the frequency $\omega/6.28$ in cycles per second. The ratio $\mathcal{E}_r/\mathcal{E}_i$ must then also be complex, since the quantity Z in $\rho = (Z_0 - Z)/(Z_0 + Z)$, for normal wave incidence, causes a complex value of ρ. Complete reflection occurs if ρ has unity value and is real, which occurs strictly for a perfectly conducting obstructing medium ($\sigma = \infty$). At the surface of such a medium, we have a *complete* discontinuity as far as the conductivity is concerned. On one side of the surface of reflection, we have $\sigma = 0$ and, on the other side, $\sigma = \infty$. The tangential $\mathcal{E}$ component of medium $\sigma = \infty$ *must* then *vanish*, which, according to the boundary condition, also requires zero value of the tangential component on the side with $\sigma = 0$. Therefore, the total tangential $\mathcal{E}$ field at the surface of a perfectly conducting metal plate must vanish. According to the $\mathcal{E}$ relation, the total tangential field *at the boundary* is found for $x = 0$, and we have

$$\mathcal{E}_{\text{boundary}} = \epsilon^{j\omega t}(\mathcal{E}_i - \mathcal{E}_r) = 0 \text{ volts/m}$$
$$H_{\text{boundary}} = \epsilon^{j\omega t}(H_i + H_r) \quad \text{amp/m}$$

which means that the reflected field is equal in magnitude to the incident field. For the stationary fields in air, in front of the metal surface, we have

$$\mathcal{E}_{\text{standing}} = \mathcal{E}_z + \mathcal{E}'_z = \mathcal{E}_i\epsilon^{j\omega t}(\epsilon^{-j\beta x} - \epsilon^{j\beta x})$$
$$= -j2\mathcal{E}_i\epsilon^{j\omega t}\sin(\beta x) \quad \text{volts/m}$$
$$H_{\text{standing}} = H_y + H'_y = H_i\epsilon^{j\omega t}(\epsilon^{-j\beta x} + \epsilon^{j\beta x}) = 2H_i\epsilon^{j\omega t}\cos(\beta x) \quad \text{amp/m}$$

But

$$Z_0 = \frac{\mathcal{E}_i}{H_i} = 376.7 \text{ real ohms}$$

and

$$\left.\begin{aligned} \mathcal{E}_{\text{standing}} &= -j2\mathcal{E}_i\epsilon^{j\omega t}\sin(\beta x) \quad \text{volts/m} \\ H_{\text{standing}} &= \frac{2\mathcal{E}_i\epsilon^{j\omega t}}{376.7}\cos(\beta x) \quad \text{amp/m} \end{aligned}\right\} \tag{880}$$

This result shows that on account of the sin (βx) and cos (βx) functions, the associated fields of the standing space waves are still in space quadrature. However, on account of the j factor, the standing associated fields are in time quadrature, which is a characteristic for stationary (standing) electromagnetic waves (there is no motion, *i.e.*, no wave

propagation, for the resultant effect). Zero electric fields then exist whenever $\beta x = 0, 180, 360, \cdots$ deg since $\mathcal{E}_{\text{standing}}$ is a sin (βx) function. Zero magnetic fields exist whenever $\beta x = 90$ deg, 3×90 deg, 5×90 deg. Maximum field effects occur whenever the arguments are halfway between these angles, so that $H_{\max}$ effects go together with $\mathcal{E}_{\min} = 0$ effects and $\mathcal{E}_{\max}$ effects go together with $H_{\min} = 0$ effects. Therefore, at $x = 0$ (which is the surface of the perfect metal reflector), we have sin $(\beta x) = 0$ and $\mathcal{E} = 0$, *but* we have cos $(\beta x) = 1$ and

$$H = 2H_i = \frac{2\mathcal{E}_i}{376.7} \qquad \text{amp/m}$$

If we divide the numerator and the denominator in $\rho = (Z_0 - Z)/(Z_0 + Z)$ by Z_0, we find, for the abbreviation $r = Z/Z_0$, the ratio $\rho = (1 - r)/(1 + r)$, which, for a general medium, yields

$$\left.\begin{aligned} r &= \frac{Z}{Z_0} = \frac{\sqrt{\mu_0/\kappa_e}}{\sqrt{\mu_0/\kappa_0}} = \sqrt{\frac{\kappa_0}{\kappa_e}} = \frac{1}{\sqrt{\kappa_r - jq}} \\ \kappa_r &= \frac{\kappa}{\kappa_0} = \frac{10^{12}\kappa}{8.854}; \qquad q = 1.8 \times 10^4 \frac{\sigma}{f} \end{aligned}\right\} \tag{880a}$$

where σ is in mhos per meter, κ is in farads per meter, and f in megacycles per second. It is assumed that the general medium has a permeability equal to that holding for empty space and air. We have now a means of finding the complex value of ρ and also a means of finding out what reflection effect a copper plate with a *finite* conductivity $\sigma = 5.8 \times 10^7$ mhos/m and a probable dielectric constant $\kappa = \kappa_0 = 8.854 \times 10^{-12}$ farad/m will give for an arriving electromagnetic wave. We have then

$$q = 1.8 \times 10^4 \times 5.8 \frac{10^7}{f} = 1.042 \frac{10^{12}}{f}$$

as against $\kappa_r = \kappa_0/\kappa_0 = 1$. We have, therefore, even for a *mega*megacycle electromagnetic wave, still a value $q = 1.042 \times 10^6$, which is practically one *million* times larger than the $\kappa_r = 1$ value in $\sqrt{\kappa_r - jq}$, and we find

$$\left.\begin{aligned} r &\cong \frac{1}{\sqrt{-jq}} = \frac{1}{\sqrt{-j}\sqrt{q}} = \frac{1}{(1-j)\sqrt{q/2}} \\ &= \frac{1.4142\,(1+j)}{(1-j)(1+j)\sqrt{q}} = 1.4142\,\frac{1+j}{2\sqrt{q}} \\ &= 0.7071(1+j)\,\frac{\sqrt{f}}{\sqrt{1.042 \times 10^{12}}} \\ &= \frac{0.7071(1+j)\sqrt{f}}{1.02 \times 10^6} = 6.93 \times 10^{-7}\sqrt{f}\,(1+j) \end{aligned}\right\} \tag{880b}$$

Applying this formula to a 1,000-Mc wave, we find

$$r = 6.93 \times 10^{-7}\sqrt{1{,}000}\,(1 + j) = 6.93 \times 10^{-7} \times 31.62(1 + j) = 2.19 \times 10^{-5}(1 + j)$$

$$\rho = \frac{1 - r}{1 + r} = \frac{1 - 2.19 \times 10^{-5} - j2.19 \times 10^{-5}}{1 + 2.19 \times 10^{-5} + j2.19 \times 10^{-5}} = \frac{0.9999781 - j0.0000219}{1.0000219 + j0.0000219} \cong 1$$

Even for a *million*-megacycle wave, we find

$$r = 6.93 \times 10^{-7}\sqrt{10^6}\,(1 + j) = 6.93 \times 10^{-4}(1 + j)$$

$$\rho = \frac{1 - 6.93 \times 10^{-4} - j6.93 \times 10^{-4}}{1 + 6.93 \times 10^{-4} + j6.93 \times 10^{-4}} = \frac{0.999307 - j0.000693}{1.000693 + j0.000693} \cong 1$$

Therefore, in the case of such an extremely UHF wave, the tangential component of $\mathcal{E}$, at the surface of the copper plate, must be extremely small. It is this component which must cover the joulean heat loss at the surface skin of the copper obstacle, due to the finite conductivity of 5.8×10^7 mhos/m instead of an infinite conductivity. It is the *power that counts*. Since we have normal incidence in Fig. 248, the power flow across each square-meter area of the incident wave must be $\mathcal{E}_i H_i$ watts (for $\mathcal{E}_i$ and H_i effective values), which is also equal to $376.7H_i^2$ watts per square meter. The penetrating power for each square-meter surface is equal to $(2H_i)^2 Z$ watts, since, at the reflector surface (surface of the metal obstruction), the incident H_i and the reflected H_r fields are practically *equal* ($\rho = 1$) and *in phase*. The value $2H_i$ is, therefore, operative at the metal surface. The copper medium offers, to a 90-deg "head-on" electromagnetic wave arrival, an impedance

$$\left.\begin{aligned} Z = \sqrt{\frac{\mu_0}{\kappa_e}} &= \sqrt{\frac{\mu_0}{\kappa - j\frac{\sigma}{\omega}}} \cong \sqrt{\frac{\mu_0}{-j\frac{\sigma}{\omega}}} = \frac{\mu_0}{\sqrt{-j}\sqrt{\mu_0\frac{\sigma}{\omega}}} \\ &= \frac{\mu_0}{(1 - j)\sqrt{\mu_0\frac{\sigma}{2\omega}}} = \frac{\mu_0(1 + j)}{2\sqrt{\mu_0\frac{\sigma}{2\omega}}} = \frac{\mu_0(1 + j)}{\sqrt{\frac{2\mu_0\sigma}{\omega}}} \\ &= \frac{\mu_0}{\sqrt{\frac{2\mu_0\sigma}{\omega}}} + j\frac{\mu_0}{\sqrt{\frac{2\mu_0\sigma}{\omega}}} = A + jA; \qquad Z = A + jA \text{ ohms} \end{aligned}\right\} \quad (880c)$$

where A is the active inphase component and jA is reactive and *cannot* cause power loss. Therefore, the resistive component of the load impedance Z must account for the penetrating power through the plate metal surface, and we have

$$\left.\begin{aligned} \text{Penetrating power} &= 4H_i^2 \frac{\mu_0}{\sqrt{2\mu_0 \frac{\sigma}{\omega}}} \quad \text{watts/m}^2 \\ \frac{\text{Penetrating power}}{\text{Incident power}} &= \frac{4H_i^2 \dfrac{\mu_0}{\sqrt{2\mu_0 \dfrac{\sigma}{\omega}}}}{H_i^2 \sqrt{\dfrac{\mu_0}{\kappa_0}}} = \sqrt{\frac{8\omega\kappa_0}{\sigma}} \\ &= 2.109 \times 10^{-2} \sqrt{\frac{f^{(\text{Mc/sec})}}{\sigma^{(\text{mhos/m})}}} \end{aligned}\right\} \quad (880d)$$

Applying this result to a copper reflector, which experiences a perpendicular wave incidence for a 1,000-Mc excitation, we find

$$2.109 \times 10^{-2} \sqrt{\frac{1{,}000}{5.8 \times 10^7}} = 2.109 \times 10^{-2} \frac{1}{2.408 \times 10^2} = 8.75 \times 10^{-5}$$

and the penetrating power $P = 0.0000875P_i$ watts is the result, where P_i is the available incident power at the copper surface. This proves that the *reflection* at the surface of the metal obstruction is *practically complete.*

164. Remarks on Actual Electromagnetic Wave Conditions on Either Side of the Earth Surface (for Vertical Polarization). The general formula (876*b*) is used. It reads

$$\mathcal{E}_R = \frac{\mathcal{E}_s}{d} \{D_{(90°-\theta_0)} \cos^2 \theta_0 + \rho_v D_\theta C \epsilon^{j[\varphi_v - 1.2f(r-r_0)]} \sin^2 \theta\} \quad \text{volts/m}$$

if we also use the coefficient C for the curvature effect of the earth surface. For grazing incidence, we find

$$\begin{gathered} \theta_0 = 0; \qquad \theta = 90°; \qquad D_{(90°-\theta_0)} = D_\theta = D_{90°} = 1 \\ \sin 90° = 1 = \sin^2 90°; \qquad r - r_0 = 0; \qquad \rho_v = +1 \\ \exp j[\varphi_v - 1.2f(r - r_0)] = \exp j\varphi_v = \epsilon^{j180°} = \cos 180° + j \sin 180° = -1 \end{gathered}$$

and, therefore, $\mathcal{E}_R = 0$. This result does not quite agree with experience, since the above stipulation for $\theta = 90$ deg and $\theta_0 = 0$ deg requires that the vertical linear radiator at T of Fig. 240 and the linear receiving antenna at R are with their mid-points T and R at the surface of the ground. This means that the radiator penetrates with half its vertical length into ground, since $r - r_0 = 0$ and $h_1 = h_2 = 0$ requires such a condition. As far as the radiator is concerned, we have the condition of Fig. 249. Only the portion $ab = ab'$ with b' just clearing the ground is then the equivalent radiator, and the voltage is applied between b'

and ground. This subject matter has been treated elsewhere.[1] The general ground leads then *not only* to a forward tilt τ of the resultant electric vector $\mathcal{E}$, with respect to the normal to the ground, but also to an *elliptical* polarization, since the vertical $\mathcal{E}_z$ and the horizontal $\mathcal{E}_x$ components of $\mathcal{E}$ are generally not in time phase, because the index of refrac-

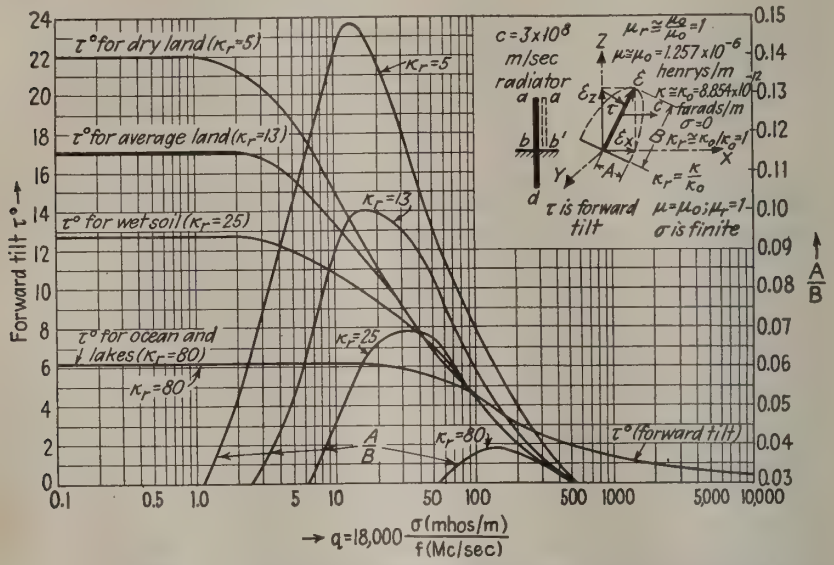

FIG. 249. Forward tilt at the earth surface and elliptical polarization at this surface. *Note:* The longitudinal $\mathcal{E}_x$ component along the direction of wave propagation causes guide action along the earth surface. Relative equivalent dielectric constant of a general medium is $\kappa_e' = \kappa_r - jq$; $q = (18 \times 10^3)/f$, σ is in mhos/m, f in Mc/sec, relative index of refraction is $n = \sqrt{\kappa_e'}$.

tion n of the ground is $n = \sqrt{\kappa_r - jq}$, for $q = 1.8 \times 10^4(\sigma/f)$ and f in megacycles per second. Calling ψ the time phase difference and using the abbreviation $\Omega = \omega t$, we have a resultant instantaneous field at a ground point, which is

$$\mathcal{E}_t = \sqrt{\mathcal{E}_z^2 \sin^2 \Omega + \mathcal{E}_x^2 \sin^2 (\Omega + \psi)}$$
$$= \sqrt{\tfrac{1}{2}\{\mathcal{E}_z^2 + \mathcal{E}_x^2 - \cos (2\Omega)[\mathcal{E}_z^2 + \mathcal{E}_x^2 \cos (2\psi)] + \sin (2\Omega)\mathcal{E}_x^2 \sin (2\psi)\}}$$

causing, during each cycle, a maximum and a minimum value for

$$2\Omega = \tan^{-1}\left(\frac{-\mathcal{E}_x^2 \sin (2\psi)}{\mathcal{E}_z^2 + \mathcal{E}_x^2 \cos (2\psi)}\right)$$

[1] HUND, A., "High-frequency Measurements," 1st ed., 1933, pp. 292–295; 2d ed., 1951, pp. 341–348, McGraw-Hill Book Company, Inc., New York.

The curves of Fig. 249 are based on Maxwell's equations, and we have

$$\mathcal{E}_x^{(\text{volts/m})} = \frac{\dfrac{\partial H_z}{\partial y} - \dfrac{\partial H_y}{\partial z}}{G}; \qquad \mathcal{E}_y = \frac{\dfrac{\partial H_x}{\partial z} - \dfrac{\partial H_z}{\partial x}}{G}$$

$$\mathcal{E}_z = \frac{\dfrac{\partial H_y}{\partial x} - \dfrac{\partial H_x}{\partial y}}{G}; \qquad \text{found from the curl relations Eq. (137)}$$

for the admittance gradient

$$\left.\begin{aligned} G &= j\omega\kappa_0 \qquad \text{above ground} \\ G &= \sigma + j\omega\kappa \qquad \text{below the surface of ground} \end{aligned}\right\} \text{mhos/m}$$

where κ_0 and κ are the dielectric constants of air and ground, respectively, in farads per meter. In addition, we find from Eq. (137)

$$H_x^{(\text{amp/m})} = \frac{\dfrac{\partial \mathcal{E}_y}{\partial z} - \dfrac{\partial \mathcal{E}_z}{\partial y}}{G'}; \qquad H_y = \frac{\dfrac{\partial \mathcal{E}_z}{\partial x} - \dfrac{\partial \mathcal{E}_x}{\partial z}}{G'}$$

$$H_z = \frac{\dfrac{\partial \mathcal{E}_x}{\partial y} - \dfrac{\partial \mathcal{E}_y}{\partial x}}{G'}$$

for the impedance gradient $G' = j\omega\mu = j\omega\mu_0$ ohms/m in air and in ground. The unit of $\dfrac{\partial H}{\partial} - \dfrac{\partial H}{\partial}$ is in amp/m^2 and the unit of $\dfrac{\partial \mathcal{E}}{\partial} - \dfrac{\partial \mathcal{E}}{\partial}$ relations in volts/m^2

According to (137), we have for time variations

$$\left.\begin{aligned} \sigma\mathcal{E}_x + \kappa\frac{\partial \mathcal{E}_x}{\partial t} &= \cancel{\frac{\partial H_z}{\partial y}} - \frac{\partial H_y}{\partial z} \\ \sigma\mathcal{E}_y + \kappa\cancel{\frac{\partial \mathcal{E}_y}{\partial t}} &= \cancel{\frac{\partial H_x}{\partial z}} - \cancel{\frac{\partial H_z}{\partial x}} \\ \sigma\mathcal{E}_z + \kappa\frac{\partial \mathcal{E}_z}{\partial t} &= \frac{\partial H_y}{\partial x} - \cancel{\frac{\partial H_x}{\partial y}} \end{aligned}\right\} \qquad (881a)$$

In Fig. 249 we have only $\mathcal{E}_z$, $\mathcal{E}_x$, and H_y fields and portions containing $\mathcal{E}_y$, H_x, and H_z vanish. We have left then only

$$\left.\begin{aligned} \sigma\mathcal{E}_x + \kappa\frac{\partial \mathcal{E}_x}{\partial t} &= -\frac{\partial H_y}{\partial z} \\ \sigma\mathcal{E}_z + \kappa\frac{\partial \mathcal{E}_z}{\partial t} &= \frac{\partial H_y}{\partial x} \end{aligned}\right\} \qquad (881b)$$

$$\left.\begin{aligned} \mu\cancel{\frac{\partial H_x}{\partial t}} &= \cancel{\frac{\partial \mathcal{E}_y}{\partial z}} - \frac{\partial \mathcal{E}_z}{\partial y} \\ \mu\frac{\partial H_y}{\partial t} &= \frac{\partial \mathcal{E}_z}{\partial x} - \frac{\partial \mathcal{E}_x}{\partial z} \\ \mu\cancel{\frac{\partial H_z}{\partial t}} &= \frac{\partial \mathcal{E}_x}{\partial y} - \cancel{\frac{\partial \mathcal{E}_y}{\partial x}} \end{aligned}\right\} \text{ reducing for the same reason to } \left\{ \mu\frac{\partial H_y}{\partial t} = \frac{\partial \mathcal{E}_z}{\partial x} - \frac{\partial \mathcal{E}_x}{\partial z} \right\} \qquad (881c)$$

University of Southern California

The relations are, therefore, greatly reduced. We find for variations that are harmonic functions with a time factor $\epsilon^{j\omega t}$ the reduced expressions

$$\left.\begin{aligned} &\mathcal{E}_x = \frac{-\dfrac{\partial H_y}{\partial z}}{G}; \qquad \mathcal{E}_z = \frac{+\dfrac{\partial H_y}{\partial x}}{G}; \qquad H_y = \frac{\dfrac{\partial \mathcal{E}_z}{\partial x} - \dfrac{\partial \mathcal{E}_x}{\partial z}}{G'} \\ &G' = j\omega\mu_0; \qquad G = j\omega\kappa_0 \text{ for air}; \qquad G = \sigma + j\omega\kappa \text{ for ground} \end{aligned}\right\} \tag{881d}$$

Differentiating (881c) with respect to t yields

$$\mu \frac{\partial^2 H_y}{\partial t^2} = \frac{\partial^2 \mathcal{E}_z}{\partial x\, \partial t} - \frac{\partial^2 \mathcal{E}_x}{\partial z\, \partial t} \tag{881e}$$

Differentiating the first of Eqs. (881b) with respect to z and the second equation with respect to x yields

$$\left.\begin{aligned} \sigma \frac{\partial \mathcal{E}_x}{\partial z} + \kappa \frac{\partial^2 \mathcal{E}_x}{\partial z\, \partial t} &= -\frac{\partial^2 H_y}{\partial z^2} \\ \sigma \frac{\partial \mathcal{E}_z}{\partial x} + \kappa \frac{\partial^2 \mathcal{E}_z}{\partial x\, \partial t} &= \frac{\partial^2 H_y}{\partial x^2} \end{aligned}\right\} \text{ or } \left\{\begin{aligned} \frac{\partial^2 \mathcal{E}_x}{\partial z\, \partial t} &= -\frac{1}{\kappa}\left(\frac{\partial^2 H_y}{\partial z^2} + \sigma \frac{\partial \mathcal{E}_x}{\partial z}\right) \\ \frac{\partial^2 \mathcal{E}_z}{\partial x\, \partial t} &= \frac{1}{\kappa}\left(\frac{\partial^2 H_y}{\partial x^2} - \sigma \frac{\partial \mathcal{E}_z}{\partial x}\right) \end{aligned}\right\} \tag{881f}$$

Introducing the expressions for $\partial^2 \mathcal{E}_x/(\partial z\, \partial t)$ and $\partial^2 \mathcal{E}_z/(\partial x\, \partial t)$ in (881e) yields

$$\mu\kappa \frac{\partial^2 H_y}{\partial t^2} = \frac{\partial^2 H_y}{\partial x^2} - \sigma \frac{\partial \mathcal{E}_z}{\partial x} + \frac{\partial^2 H_y}{\partial z^2} + \sigma \frac{\partial \mathcal{E}_x}{\partial z} = \frac{\partial^2 H_y}{\partial x^2} + \frac{\partial^2 H_y}{\partial z^2} + \sigma \underbrace{\left(\frac{\partial \mathcal{E}_x}{\partial z} - \frac{\partial \mathcal{E}_z}{\partial x}\right)}_{= -\mu \frac{\partial H_y}{\partial t}}$$

Hence,

$$\frac{\partial^2 H_y}{\partial x^2} + \frac{\partial^2 H_y}{\partial z^2} = \mu\left(\kappa \frac{\partial^2 H_y}{\partial t^2} + \sigma \frac{\partial H_y}{\partial t}\right) \tag{881g}$$

For the relative values $\mu_r = \mu/\mu_0$ and $\kappa_r = \kappa/\kappa_0$, we find

$$\frac{\partial^2 H_y}{\partial x^2} + \frac{\partial^2 H_y}{\partial z^2} = \mu_r\mu_0\left(\kappa_r\kappa_0 \frac{\partial^2 H_y}{\partial t^2} + \sigma \frac{\partial H_y}{\partial t}\right) \tag{881h}$$

Since we have only an H_y value and no other components, we can put $H_y = H$ amperes per meter. On the air side above the ground surface, we have $\sigma = 0$, $\kappa_r = \kappa_0/\kappa_0 = 1$, and $\mu_r = \mu_0/\mu_0 = 1$, and (881h) reads for air and ground *next* to the ground surface, for $H_y = H_{\text{ground}} = H_g$,

$$\left.\begin{aligned} &\frac{\partial^2 H}{\partial x^2} + \frac{\partial^2 H}{\partial z^2} = \frac{1}{c^2}\frac{\partial^2 H}{\partial t^2} && \text{above ground in air} \\ &\frac{\partial^2 H_g}{\partial x^2} + \frac{\partial^2 H_g}{\partial z^2} = \frac{\kappa_r}{c^2}\frac{\partial^2 H_g}{\partial t^2} + 1.257 \times 10^{-6}\sigma \frac{\partial H_g}{\partial t} && \text{below the surface of ground} \\ &c = 3 \times 10^8 \text{ m/sec} \end{aligned}\right\} \tag{881i}$$

The first of Eqs. (881*i*) shows that the magnetic H vector along the Y direction travels with the velocity 3×10^8 m/sec. For the second relation, we have *two* time functions, and $(3 \times 10^8)/\sqrt{\kappa_r}$ meters per sec is *not* the actual phase velocity, since the dissipation term $\mu_0\sigma(\partial H_g/\partial t)$ also affects the phase velocity.

Inasmuch as we have variations along the X as well as along the Z axis, there must occur a dual propagation for a tilted $\mathcal{E}$ vector in Fig. 249. This means that a wave motion occurs along the ground surface as well as perpendicular into the ground from the surface. The latter causes also a wave motion upward into air. These wave motions are subjected to different propagation constants $\Gamma_x = \Gamma_1$ and $\Gamma_z = \Gamma_2$ and Γ_3. These constants express that as the tilted $\mathcal{E}$ vector moves along the X direction, both the vertical $\mathcal{E}_z$ and the horizontal $\mathcal{E}_x$ components move with it. As far as the $\mathcal{E}_z$ field is concerned, we have a transverse wave motion, with the $\mathcal{E}_z$ and H_y vectors constituting the surface of the wave front, which is normal to the X direction and moves along this direction. As far as the $\mathcal{E}_x$ field component is concerned in Fig. 249, we have a *longitudinal* $\mathcal{E}_x$ wave but still a transverse H_y magnetic vector with respect to the surface wave along the ground. This is then a *guided* wave, since we deal with a longitudinal $\mathcal{E}_x$ wave, which may also be called a TM wave in comparison with the TEM wave with $\mathcal{E}_z$ and H_y field associations. The perpendicular $\mathcal{E}_x$ and H_y vectors form a surface that is parallel with the surface of the ground and slides, as it were, along the ground surface, as far as the initial values of $\mathcal{E}_x$ and H_y at the surface of the ground are concerned. The transverse wave motion perpendicular into the ground with $\mathcal{E}_x$ and H_y values rapidly decreases along the $-Z$ direction (into the ground) owing to the finite conductivity of the ground. The longitudinal $\mathcal{E}_x$ propagation is attenuated very little and under certain conditions may account for strong ground field intensities at relatively large distances. The reason for this is that a dissipative ground tilts the original vertical $\mathcal{E}$ polarization into a $(90° - \tau)$ direction with respect to ground (Fig. 249). This means that the conventional space wave diverts some of its field energy into the ground. This can be seen from the second of Eqs. (881*i*). We have then for a harmonic field excitation

$$\left.\begin{aligned} &\frac{\partial H_g}{\partial t} = j\omega H_g \qquad \text{and} \qquad \frac{\partial^2 H_g}{\partial t^2} = -\omega^2 H_g \\ &\text{resulting in} \\ &\frac{\partial^2 H_g}{\partial x^2} + \frac{\partial^2 H_g}{\partial z^2} = -\frac{\kappa_r \omega^2}{c^2} H_g + j\omega\mu_0\sigma H_g \\ &\qquad = (j7.9f\sigma - 4.36 \times 10^{-4} f^2 \kappa_r) H_g \end{aligned}\right\} \quad (881j)$$

where f is in megacycles per second and $\kappa_r = 10^{12}\kappa/8.854$. Since H_g is multiplied by a complex quantity, a relative time phase exists.

It is the order of magnitude that counts. The magnitude can be found from a knowledge of the respective propagation constants along the desired direction ($+X$ direction) of propagation and the directions $\pm Z$, which are the diverted directions of wave propagation. These propagation diversions account for the energy dissipation in the ground and the energy reflection perpendicularly upward from the ground. For customary grazing wave incidence along the ground, we have then a multiple-wave propagation, with a partial wave-guide action along the surface of the ground. Since we must satisfy the upper H and the lower H_g relation of (881*i*), we find

$$\left.\begin{aligned} H &= A\epsilon^{-x\Gamma_1 - z\Gamma_2 + j\omega t} && \text{for the field next to ground surface in air} \\ H_g &= A\epsilon^{-x\Gamma_1 + z\Gamma_3 + j\omega t} && \text{for the ground field} \end{aligned}\right\} \quad (881k)$$

From the first relation, we find, for $j\omega t - x\Gamma_1 - z\Gamma_2 = p$ in the first relation of (881*i*), the terms

$$\frac{\partial^2 H}{\partial x^2} = \Gamma_1^2 A\epsilon^p \qquad \text{and} \qquad \frac{\partial^2 H}{\partial z^2} = \Gamma_2^2 A\epsilon^p$$

$$\frac{\partial^2 H}{\partial t^2} = -\omega^2 H = \omega^2 A\epsilon^p \qquad \text{for an } \epsilon^{j\omega t} \text{ variation}$$

Using these results in (881*i*), the common factor $A\epsilon^p$ will cancel out, and the first of Eqs. (881*i*) reduces to

$$\Gamma_1^2 + \Gamma_2^2 = -\frac{\omega^2}{c^2} = -\beta^2 \quad (881l)$$

By the same reasoning, for the lower expression of (881*i*) and (881*k*) we have, for $p_1 = j\omega t - x\Gamma_1 + z\Gamma_3$, the terms

$$\frac{\partial^2 H_g}{\partial x^2} = \Gamma_1^2 A\epsilon^{p_1}; \qquad \frac{\partial^2 H_g}{\partial z^2} = \Gamma_2^2 A\epsilon^{p_1}$$

$$\frac{\partial H_g}{\partial t} = j\omega H_g = j\omega A\epsilon^{p_1}; \qquad \frac{\partial^2 H_g}{\partial t^2} = -\omega^2 A\epsilon^{p_1}$$

and the second of Eqs. (881*i*) reads

$$\Gamma_1^2 + \Gamma_3^2 = j1.257 \times 10^{-6}\sigma\omega - \beta^2\kappa_r; \qquad \beta = \frac{\omega}{c} \quad (881m)$$

where $\omega/6.28$ is in cycles per second. If f is expressed in megacycles per second, we find

$$\Gamma_1^2 + \Gamma_3^2 = j7.9\sigma f - 4.36 \times 10^{-4}\kappa_r f^2 \quad (881n)$$

We require another relation to find the values of the respective propagation constants Γ_1, Γ_2, and Γ_3. From the boundary condition

$$\left(\frac{\partial H}{\partial x}\right)_{z=0} = \left(\frac{\partial H_g}{\partial x}\right)_{z=0} = 0$$

and for tangential electric fields on either side of the ground surface, we have $\mathcal{E}_x = \mathcal{E}_{g_x}$, where $\mathcal{E}_x$ is *in air* and tangential to ground surface and $\mathcal{E}_{g_x}$ is tangential *but in ground*. From the first of Eqs. (881*k*) for air, we have $H_y = H$, $\sigma = 0$, $\kappa = \kappa_0 = 8.854 \times 10^{-12}$ farad/m, and

$$\kappa_0 \frac{\partial \mathcal{E}_x}{\partial t} = -\frac{\partial H}{\partial z} = -\frac{\partial (A\epsilon^{-x\Gamma_1 - z\Gamma_2 + j\omega t})}{\partial z} = +\Gamma_2 A\epsilon^p$$

Integrating yields

$$\kappa_0 \mathcal{E}_x = \frac{\Gamma_2 A\epsilon^p}{j\omega}; \qquad \mathcal{E}_x = \frac{\Gamma_2}{j\omega\kappa_0} A\epsilon^p \quad \text{volts/m} \tag{881o}$$

For ground, we find the only magnetic vector $H_y = H_g$ amperes per meter, and the first of Eqs. (881k) leads to

$$\sigma \mathcal{E}_{g_x} + \kappa \frac{\partial \mathcal{E}_{g_x}}{\partial t} = -\frac{\partial H_g}{\partial z} = -\frac{\partial (A\epsilon^{-x\Gamma_1 + z\Gamma_3 + j\omega t})}{\partial z} = -\Gamma_3 A\epsilon^{p_1} \tag{881p}$$

Integration yields

$$\left(\frac{\sigma}{j\omega} + \kappa\right) \mathcal{E}_{g_x} = -\frac{\Gamma_3 A\epsilon^{p_1}}{j\omega}; \qquad \mathcal{E}_{g_x} = -\frac{\Gamma_3}{\sigma + j\omega\kappa} A\epsilon^{p_1} \quad \text{volts/m} \tag{881q}$$

But at the surface of the ground, $\mathcal{E}_x = \mathcal{E}_{g_x}$ and $p = p_1$, since $p = j\omega t - x\Gamma_1 - z\Gamma_2$ and $p_1 = j\omega t - x\Gamma_1 + z\Gamma_3$; and for $z = 0$, we find $p = j\omega t - x\Gamma_1 = p_1$. On equating $\mathcal{E}_x$ and $\mathcal{E}_{g_x}$, the common factor $A\epsilon^{j\omega t - x\Gamma_1}$ cancels, and

$$\frac{\Gamma_2}{\Gamma_3} = -\frac{j\omega\kappa_0}{\sigma + j\omega\kappa} = -\frac{j\omega}{\sigma/(8.854 \times 10^{-12}) + j\omega\kappa_r} = -\frac{j\omega}{1.13 \times 10^{11}\sigma + j\omega\kappa_r} \tag{881r}$$

By means of (881l), (881m), and (881r), we can find expressions for Γ_1, Γ_2, and Γ_3. We have then for $a = 1.257 \times 10^{-6}$, $b = 1.13 \times 10^{11}$, and $c = 3 \times 10^8$, the relations

$$\Gamma_1^2 + \Gamma_2^2 = -\frac{\omega^2}{c^2} = -\beta^2; \qquad \Gamma_1^2 + \Gamma_3^2 = ja\sigma\omega - \frac{\omega^2\kappa_r}{c^2}$$

$$\Gamma_2 = -\frac{j\omega\Gamma_3}{b\sigma + j\omega\kappa_r} = -\frac{\Gamma_3}{\dfrac{b\sigma}{j\omega} + \kappa_r} = -\frac{\Gamma_3}{\kappa_r\left(1 - j\dfrac{b\sigma}{\omega\kappa_r}\right)}$$

$$\Gamma_2 = -\frac{\Gamma_3}{\kappa_r(1 - jd)}; \qquad d = \frac{b\sigma}{\omega\kappa_r}$$

It is the dissipation term d that has a great deal to do with the propagation due to ground effect, since, for $d \ll 1$, we have essentially $\Gamma_2 \cong -\Gamma_3/\kappa_r$. For any value of d, irrespective of its relative magnitude with respect to unity value, we find $\Gamma_3 = (jd - 1)\kappa_r\Gamma_2$; and for the abbreviations $e = jd - 1$ and $g = \omega^2/c^2 = \beta^2$, we find

$$\Gamma_1^2 + \Gamma_3^2 = -g\left(\kappa_r - j\frac{a\sigma\omega}{g}\right) = -g\kappa_r\left(1 - j\frac{ac^2\sigma}{\omega\kappa_r}\right)$$

$$= -g\kappa_r\left(1 - j\frac{b\sigma}{\omega\kappa_r}\right) = -g\kappa_r(1 - jd) = eg\kappa_r$$

Since $\Gamma_3 = e\kappa_r\Gamma_2$, we find for $\Gamma_1^2 + \Gamma_3^2$

$$\Gamma_1^2 + e^2\kappa_r^2\Gamma_2^2 = eg\kappa_r; \qquad \Gamma_1^2 + \Gamma_2^2 = -g \tag{881s}$$

yielding

$$\Gamma_2^2(e^2\kappa_r^2 - 1) = g(e\kappa_r + 1)$$

by subtracting the second of Eqs. (881s) from the first. Hence,

$$\Gamma_2^2 = g\frac{e\kappa_r + 1}{e^2\kappa_r^2 - 1} = \frac{g}{e\kappa_r - 1} \tag{881t}$$

Since

$$\Gamma_1^2 + \Gamma_2^2 = \Gamma_1^2 + \frac{g}{e\kappa_r - 1} = -g$$

we find

$$\left.\begin{aligned} \Gamma_1^2 &= -g\left(1 + \frac{1}{e\kappa_r - 1}\right) = -g\frac{e\kappa_r}{e\kappa_r - 1} = g\frac{e\kappa_r}{1 - e\kappa_r} \\ \Gamma_3^2 &= e^2\kappa_r^2\Gamma_2^2 = g\frac{e^2\kappa_r^2}{e\kappa_r - 1} \end{aligned}\right\} \tag{881u}$$

For f in megacycles per second, we have in the abbreviations

$$g = \beta^2 = \frac{\omega^2}{c^2} = \frac{4\pi^2 \times 10^{12}f^2}{9 \times 10^{16}} = 4.36 \times 10^{-4}f^2$$

$$\sqrt{g} = 0.0209f; \qquad d = \frac{b\sigma}{\omega\kappa_r} = \frac{1.13 \times 10^{11}}{6.28 \times 10^6}\frac{\sigma}{\kappa_r f} = 1.8 \times 10^4\frac{\sigma}{\kappa_r f}$$

$$e = j1.8 \times 10^4\frac{\sigma}{\kappa_r f} - 1 = j\frac{q}{\kappa_r} - 1; \qquad q \text{ and } \kappa_r \text{ in Fig. 249}$$

$$\left.\begin{aligned} \Gamma_1 &= 0.0209f\sqrt{\frac{jq - \kappa_r}{1 + \kappa_r - jq}} = \sqrt{\kappa_r - jq}\,\Gamma_2; \qquad q = 1.8 \times 10^4\frac{\sigma^{(\text{mhos/m})}}{f^{(\text{Mc/sec})}} \\ \Gamma_2 &= \frac{0.0209f}{\sqrt{jq - (1 + \kappa_r)}}; \qquad \Gamma_3 = \frac{0.0209(jq - \kappa_r)f}{\sqrt{jq - (1 + \kappa_r)}} = (jq - \kappa_r)\Gamma_2 \end{aligned}\right\} \tag{881v}$$

These expressions for respective propagation constants give data for the *longitudinal* surface (Γ_1 wave) and respective *cross-surface* (Γ_2 and Γ_3) waves. Suppose we have a frequency in the lower frequency range, say $f = 0.16$ Mc/sec, and we deal with dry ground of relative dielectric constant $\kappa_r = 4$ and a conductivity $\sigma = 10^{-4}$ mho/m. This yields $q = 1.8 \times 10^4(10^{-4}/0.16) = 11.25$ and $jq - \kappa_r = j11.25 - 4$. Therefore,

$$\sqrt{\frac{jq - \kappa_r}{1 + \kappa_r - jq}} = \sqrt{\frac{j11.25 - 4}{5 - j11.25}}\sqrt{\frac{(j11.25 - 4)(5 + j11.25)}{5^2 + 11.25^2}}$$

$$= \sqrt{\frac{j11 - 146.55}{151.55}} = \sqrt{\frac{\sqrt{11^2 + 146.55^2}/180° - \tan^{-1}(11/146.55)}{151.55}}$$

$$= \sqrt{\frac{146.7/+175.7°}{151.5}} = 0.99\,\epsilon^{j85.55°}$$

The angle under the square root is $180° - \tan^{-1}(11/146.55)$, since $j11$

points upward and -146.55 points normally to the left along the negative real axis. The angle is, therefore, in the second quadrant and an angle to 180 deg minus the tangent^{-1} of the value of the imaginary part to the real value. The above evaluation yields, according to (881v), the propagation constant Γ_1 of the surface wave as

$$\Gamma_1 = 0.0209 \times 0.16 \times 0.99\epsilon^{j87.85} = 33.1 \times 10^{-4}\epsilon^{j87.85}$$
$$= 33.1 \times 10^{-4}\underbrace{(\cos 87.85^\circ}_{0.0384} + j\underbrace{\sin 87.85^\circ)}_{0.999} = \underbrace{1.27 \times 10^{-4}}_{\text{neper/m}} + \underbrace{j33 \times 10^{-4}}_{\text{circular radian/m}}$$
$$= \alpha_1 + j\beta_1$$

We have then an attenuation constant of $\alpha_1 = 1.27 \times 10^{-4}$ neper/m and a phase constant of $\beta_1 = 3.3 \times 10^{-5}$ circular radian/m. The attenuation for the surface wave along the ground is then of the order found for telephone currents flowing in a cable. For the propagation constant Γ_2 for the wave propagation normal to ground but in air, we have

$$\sqrt{jq - (1 + \kappa_r)} = \sqrt{j11.25 - 5}$$
$$= \sqrt[4]{11.25^2 + 5^2}\Big/90^\circ - \frac{1}{2}\tan^{-1}\left(\frac{11.25}{5}\right) = 3.5\epsilon^{j57^\circ}$$

$$\frac{1}{\sqrt{jq - (1 + \kappa_r)}} = \frac{\epsilon^{-j57^\circ}}{3.5}$$

$$\Gamma_2 = \frac{0.0209 \times 0.16\epsilon^{-j57^\circ}}{3.5} = 9.55 \times 10^{-5}\epsilon^{-j57^\circ}$$

$$\Gamma_2 = 9.55 \times 10^{-5}(\cos 57^\circ - j \sin 57^\circ) = 9.55 \times 10^{-5}(0.545 - j0.839)$$
$$= 5.2 \times 10^{-4} - 7.9 \times 10^{-4} = \alpha_2 + j\beta_2; \qquad \alpha_2 = 5.2 \times 10^{-4} \text{ neper/m}$$

In the same way, we find for the propagation normal into ground

$$\Gamma_3 = 1.14 \times 10^{-2}\epsilon^{j52.8^\circ} = 6.9 \times 10^{-3} + j9.6 \times 10^{-3} = \alpha_3 + j\beta_3$$

If we inspect first the phase constants $\beta_1 = 33 \times 10^{-4}$,

$$\beta_2 = -7.9 \times 10^{-4}, \qquad \text{and} \qquad \beta_3 = 91 \times 10^{-4} \text{ circular radian/m},$$

where β_2 and β_3 correspond to *cross*-ground surface propagations, we have $\lambda_1 = 6.28(10^4/33) = 1{,}900$ m, $\lambda_2 = 6.28(10^4/7.9) = 7{,}920$ m, $\lambda_3 = 6.28(10^4/91) = 690$ m, $\lambda_0 = 300/f = 300/0.16 = 1{,}870$ m free-space λ. For the wave normal to ground and *in air*, we have a phase velocity $v_2 = f\lambda_2 = 0.16 \times 10^6 \times 7{,}920 = 12.65 \times 10^8$ m/sec, which is $12.65/3 = 4.217$ times the value of the velocity of light. For the cross-ground surface propagation *into ground*, we find a phase velocity v_3, which is $\lambda_3/\lambda_0 = 690/1{,}870 = 0.37$ times the free-space velocity. For the wave along the ground surface, we have $\lambda_1/\lambda_0 = 1{,}900/1{,}870 = 1.1016$ and a phase velocity $v_1 = 3.3 \times 10^8$ m/sec. These phase velocities are then larger and smaller than the free-space velocity 3×10^8 m/sec. These velocities should not be confused with the velocity at which energy is being transferred (consult Secs. 69, 70). If we compare respective attenuation constants $\alpha_1 = 1.27 \times 10^{-4}$, $\alpha_2 = 5.2 \times 10^{-4}$, and $\alpha_3 = 69 \times 10^{-4}$ neper/m, we note that the surface wave is the least attenuated while, of course, severe attenuation occurs for the wave passing normally into ground.

The above numerical example does not belong to the range of VHF's and UHF's. It was chosen only to bring out drastic numerical results. If we now take a VHF case, for which a 100-Mc wave moves along dry ground owing to a vertical radiator normal to ground, we find $q = 1.8 \times 10^4 \times 10^{-4}/100 = 0.018$, which is negligible in comparison with the geometric quadrature value $\kappa_r = 4$, and formulas (881v) simplify to

$$\left.\begin{aligned} \Gamma_1 &= +j0.0209f\sqrt{\frac{\kappa_r}{\kappa_r+1}}; \qquad \Gamma_2 = -j\frac{0.0209f}{\sqrt{\kappa_r+1}} \\ \Gamma_3 &= +j\frac{0.0209\kappa_r f}{\sqrt{\kappa_r+1}}; \qquad q = 1.8\times 10^4\frac{\sigma^{(\text{mhos/m})}}{f^{(\text{Mc/sec})}} \ll \kappa_r \end{aligned}\right\} \quad (881w)$$

We find then

$$\sqrt{\frac{\kappa_r}{\kappa_r+1}} = \sqrt{\frac{4}{5}} = 0.895; \qquad \sqrt{\kappa_r+1} = \sqrt{5} = 2.24$$

$$\Gamma_1 = j0.0209 \times 100 \times 0.895 = +j1.87 = j\beta_1$$

$$\Gamma_2 = -j0.0209\frac{100}{2.24} = -j0.932 = -j\beta_2$$

$$\Gamma_3 = j0.0209 \times 4\frac{100}{2.24} = +j3.74 = j\beta_3$$

The free-space wavelength is $\lambda_0 = 300/f = 300/100 = 3$ m; $\beta_1 = 1.87 = 6.28/\lambda_1$; $\lambda_1 = 3.35$ m; for a cross-surface wave in air, $\lambda_2 = 6.28/0.932 = 6.7$ m; for a wave penetrating perpendicularly into ground, $\lambda_3 = 6.28/3.74 = 1.68$ m. Since for such ground, if taken quasi-dielectric, $v_3 = 3 \times 10^8/\sqrt{4} = 1.5 \times 10^8$ m/sec, we find a wavelength in ground as $150/100 = 1.5$ m instead of 1.68 m.

Let us take up an application of formula (881v), for the condition $q \gg \kappa_r$, so that essentially $(1 + \kappa_r) \ll q$. We have then the approximations

$$\Gamma_1 = j0.0209f$$

$$\Gamma_2 = \frac{0.0209f}{\sqrt{jq}} = \frac{0.0209f}{\sqrt{j}\sqrt{q}} = \frac{0.0209\sqrt{j}\,f}{j\sqrt{q}} = -j\frac{0.0209\sqrt{j}\,f}{\sqrt{q}}$$

$$\Gamma_3 = j\frac{0.0209qf}{\sqrt{jq}} = \frac{0.0209\sqrt{j}\,qf}{\sqrt{q}}; \qquad \sqrt{j} = \frac{(1+j)}{\sqrt{2}}$$

hence,

$$\left.\begin{aligned} \Gamma_1 &= 0.0209f = j\beta_1; \qquad q = 1.8\times 10^4\sigma/f^{(\text{Mc/sec})} \gg \kappa_r \\ \Gamma_2 &= \frac{0.0209f(1-j)}{\sqrt{2q}} = \frac{0.0209f}{\sqrt{2q}} - j\frac{0.0209f}{\sqrt{2q}} = \alpha_2 + j\beta_2 \\ \Gamma_3 &= \frac{0.0209qf(1+j)}{\sqrt{2q}} = \frac{0.0209qf}{\sqrt{2q}} + j\frac{0.0209qf}{\sqrt{2q}} = \alpha_3 + j\beta_3 \end{aligned}\right\} \quad (881x)$$

The surface wave for such a relative magnitude of q with respect to κ_r shows that no attenuation effects occur, since $\alpha_1 = 0$. This may account for the fact that in some short-wave propagations, we find anomalous strong field values at quite large distances. For the perpendicular cross-ground wave in air, we have $\alpha_2 = -\beta_2$; and for the perpendicular cross-ground wave into ground, we find $\alpha_3 = \beta_3 = q\alpha_2$. This means that for the wave emerging from the surface of the ground into air under 90 deg and the wave emerging from this surface perpendicularly into ground, the dissipative attenuation constant is numerically equal to the β value of the corresponding Γ relation. Applying (881x) to vertically polarized electromagnetic waves over ocean surface, we have, for $\kappa_r = 80$, $\sigma = 4$ mhos/m, and a frequency as low as 0.48 Mc/sec, $q = 1.8 \times 10^4 \times 4/0.48 = 150{,}000$, which is large compared with $\kappa_r = 80$; $\Gamma_1 = 0.0209 \times 0.16 = j0.00335 = j\beta_1$; $6.28/\lambda_1 = 3.35 \times 10^{-3}$; $\lambda_1 = 6.28 \times 10^3/3.35 = 1{,}870$ m of the surface wave as against $300/0.48 = 625$ m in empty space. For the approximation of (881x), no attenuation value occurs for α_1. But if we use the accurate formula (881v), we have $\Gamma_1 = \alpha_1 + j\beta_1$ and $\alpha_1 = 5.9 \times 10^{-8}$ neper/m. This is, however, equivalent to a damping effect of the wave smaller than that experienced on a good communication line. We find from (881x) the other values

$$\alpha_2 = \frac{\beta_1}{\sqrt{2q}} = \frac{3.35 \times 10^{-3}}{\sqrt{30 \times 10^4}} = \frac{3.35 \times 10^{-3}}{5.48 \times 10^2} = 6.12 \times 10^{-6} \text{ neper/m}$$

$$= 8.686 \times 6.12 \times 10^{-6} = 5.31 \times 10^{-5} \text{ db/m}$$

$$\alpha_3 = q\alpha_2 = 15 \times 10^4 \times 5.31 \times 10^{-5} = 7.99 \text{ db/m} = 0.115 \times 7.99$$

$$= 0.92 \text{ neper/m}$$

Therefore, in ground normal to its surface, we have an attenuation as high as 7.99 db for each meter of wave passage. This corresponds to a loss as found in a very thin copper conductor. Moreover, from these results, we find

$$\lambda_2 = \frac{6.28 \times 10^6}{6.12} = 1.02 \times 10^6 \text{ m}$$

$$\lambda_3 = \frac{6.28}{0.92} = 6.8 \text{ m with phase velocities}$$

$$v_3 = 6.8 \times 0.48 \times 10^6 = 3.2 \times 10^6 \text{ m/sec}$$

$$v_2 = 1.02 \times 10^6 \times 0.48 \times 10^6 = 4.9 \times 10^{11} \text{ m/sec}$$

$$v_1 = 1{,}870 \times 0.48 \times 10^6 = 8.95 \times 10^8 \text{ m/sec}$$

for wave along ground surface

We note that even at frequencies as high as 100 Mc/sec, we have $q = 1.8 \times 10^4 \times \frac{4}{100} = 720$, which is still nine times the absolute value of $\kappa_r = 80$ and acts in geometrical quadrature. In Table 50, the evaluation is given for such a frequency and a frequency of 900 Mc/sec, for

TABLE 50. VERTICAL TRANSMITTER ANTENNA OVER OCEAN AND FORWARD TILT OF RESULTANT E VECTOR

Frequency f, Mc/sec	Conduction term q	Displacement term κ_r	$0.0209f$	$\kappa_r + 1$	$jq - \kappa_r$	$jq - (1 + \kappa_r)$
100	720	80	2.09	81	$j720 - 80$	$j720 - 81$
900	80	80	18.81	81	$j80 - 80$	$j80 - 81$
Frequency f, Mc/sec	$\dfrac{q}{1 + \kappa_r}$	$\tan^{-1}\left(\dfrac{q}{1 + \kappa_r}\right)$	$180° - \left[\tan^{-1}\left(\dfrac{q}{1 + \kappa_r}\right)\right]°$		$90° - \dfrac{1}{2}\left[\tan^{-1}\left(\dfrac{q}{1 + \kappa_r}\right)\right]°$ is the phase outside of the square root $\sqrt{jq - (1 + \kappa_r)}$	
100	8.89	83.6	96.4°		48.2°	
900	0.987	44.6	135.4°		67.7°	

Frequency f, Mc/sec

$$\sqrt{jq - (1 + \kappa_r)} = \sqrt[4]{q^2 + (1 + \kappa_r)^2} \Big/ 180° - \left[\tan^{-1}\left(\frac{q}{1 + \kappa_r}\right)\right]°$$

$$= \sqrt[4]{q^2 + (1 + \kappa_r)^2} \Big/ 90° - \left[\frac{1}{2}\tan^{-1}\left(\frac{q}{1 + \kappa_r}\right)\right]°$$

100

$$\sqrt[4]{720^2 + 81^2}\, \epsilon^{j48.2°} = 26.91(\underbrace{\cos 48.2°}_{0.6678} + j \underbrace{\sin 48.2°}_{0.7455})$$

$$= (17.9 + j20)/48.2°$$

900

$$\sqrt[4]{80^2 + 81^2}\, \epsilon^{j67.7°} = 10.65(\underbrace{\cos 67.7°}_{0.379} + j \underbrace{\sin 67.7°}_{0.925})$$

$$= (4.05 + j9.9)/67.7°$$

Frequency f, Mc/sec

$$\Gamma_2 = \frac{0.0209f}{\sqrt{jq - (1 + \kappa_r)}} = \alpha_2 + j\beta_2$$

100

$$\Gamma_2 = \frac{2.09}{26.91}\, \epsilon^{-j48.2} = 0.078(\cos 48.2 - j \sin 48.2) = 0.051 - j0.058$$

$\alpha_2 = 0.051$ neper/m; $\beta_2 = -0.058$ circular radians/m

$$\lambda_2 = \frac{6.28}{0.058} = 108 \text{ m as against } \lambda_0 = \frac{300}{100} = 3 \text{ m}$$

$$v_2 = f\lambda_2 = \underbrace{100 \times 10^6}_{\text{cycles/sec}} \times 108 = 108 \times 10^8 \text{ m/sec as against } 3 \times 10^8 \text{ m/sec}$$

900

$$\Gamma_2 = \frac{18.81}{10.65}\, \epsilon^{-j67.7°} = 1.76(\cos 67.7° - j \sin 67.7°) = 0.67 - j1.63$$

$\alpha_2 = 0.67$ neper/m; $\beta_2 = -1.63$ circular radians/m

$$\lambda_2 = \frac{6.28}{1.63} = 3.84 \text{ m as against } \lambda_0 = \frac{300}{900} = 0.333 \text{ m}$$

$v_2 = f\lambda_2 = 900 \times 10^6 \times 3.84 = 34.56 \times 10^8$ m/sec as against 3×10^8 m/sec

TABLE 50. VERTICAL TRANSMITTER ANTENNA OVER OCEAN AND FORWARD TILT OF RESULTANT $\mathcal{E}$ VECTOR.—(*Continued*)

Frequency f, Mc/sec	$\Gamma_3 = (jq - \kappa_r)\Gamma_2 = (\alpha_3 + j\beta_3) \Big/ \tan^{-1}\left(\frac{\beta_3}{\alpha_3}\right)$
100	$\Gamma_3 = (j720 - 80)(0.051 - j0.058)$ $= (37.675 + j41.4) \Big/ +47.6°$; $\alpha_3 = 37.67$ nepers/m; $\beta_3 = 41.4$ radians/m; $\lambda_3 = \frac{6.28}{41.4} = 0.152$ m as against $\lambda_0 = \frac{300}{100} = 3$ m; $v_3 = f\lambda_3 = 100 \times 10^6 \times 0.152 = 0.152 \times 10^8$ m/sec as against 3×10^8 m/sec
900	$\Gamma_3 = (j80 - 80)(0.67 - j1.63) = (77.2 + j184.8) \Big/ +67.4°$ $\alpha_3 = 77.2$ nepers/m; $\beta_3 = 184.8$ radians/m $\lambda_3 = \frac{6.28}{184.8} = 0.0338$ m as against $\lambda_0 = \frac{300}{900} = 0.333$ m $v_3 = f\lambda_3 = 900 \times 10^6 \times 0.0338 = 30.42 \times 10^6$ m/sec as against 3×10^8 m/sec

Frequency f, Mc/sec	$\sqrt{\kappa_r - jq} = \sqrt[4]{\kappa_r^2 + q^2} \Big/ -\frac{1}{2}\tan^{-1}\frac{q}{\kappa_r}$	$\Gamma_1 = \sqrt{\kappa_r - jq}\,\Gamma_2 = (\alpha_1 + j\beta_1) \Big/ \tan^{-1}\left(\frac{\beta_1}{\alpha_1}\right)$
100	$\sqrt[4]{80^2 + 720^2}\,\epsilon^{-j41.85°}$ $= 26.9(\cos 41.85° - j \sin 41.85°)$ $= 26.9(0.745 - j0.667)$ $= 20 - j18$	$\Gamma_1 = (20 - j18)(0.051 - j0.058)$ $= -0.02 - j2.08$ $\alpha_1 = -0.02$ neper/m $\beta_1 = -2.08$ radians/m $\lambda_1 = \frac{6.28}{2.08} = 3.01$ m as against $\lambda_0 = 3$ m $v_1 = f\lambda_1 = 100 \times 10^6 \times 3.01 \cong 3 \times 10^8$ m/sec
900	$\sqrt[4]{2 \times 80^2}\,\epsilon^{-j22.5°}$ $= 10.645(\cos 22.5° - j \sin 22.5°)$ $= 10.645(0.924 - j0.383)$ $= 9.85 - j4.07$	$\Gamma_1 = (9.85 - j4.07)(0.67 - j1.63)$ $= -0.03 - j18.77$ $\alpha_1 = -0.03$ neper/m $\beta_1 = -18.77$ radians/m $\lambda_1 = \frac{6.28}{18.77} = 0.334$ m as against $\lambda_0 = 0.333$ m $v_1 = f\lambda_1 \cong f\lambda_0 = 3 \times 10^8$ m/sec

Remarks: Relates to Fig. 249. Equation (881*v*) is used for a vertical radiator with its lower end next to the ocean surface. $\kappa_r = 80$, $\sigma = 4$ mhos/m, $\mu = \mu_0 = 1.257 \times 10^{-6}$ henry/m, $q = 1.8 \times 10^4(\sigma/f)$, where f is in Mc/sec, λ_1 and v_1 are wavelength and phase velocity of surface wave, α_1 and β_1 are the corresponding attenuation and phase constants $\Gamma = \alpha + j\beta$, λ_2 and λ_3, v_2 and v_3 hold for normal cross-ocean surface waves, proceeding into ocean and into air, respectively. Resultant $\mathcal{E}$ vector is not normal, *but* slightly tilted forward (Fig. 249). The $\Gamma_1 = \alpha_1 + j\beta_1$ is the wave sliding along the surface of the ground.

which $q = \kappa_r$, *i.e.*, the conduction term of the same magnitude as the displacement term. The outcome of this table shows that in the short-wave range of carrier frequencies, the wavelength of the propagation along the ocean surface (the surface wave) is essentially equal to the wavelength of the space wave that is not guided by the ocean surface.

In Fig. 249, the forward tilt τ, due to the action of the earth surface, is plotted against the characteristic term q. The range is such that it includes all actual conditions of the surface of the earth. Taking again ocean with an average salinity, we have $\sigma = 4$ mhos/m and $\kappa_r = 80$. For 100 Mc/sec, we find $q = 1.8 \times 10^4 \times \frac{4}{100} = 720$ and a forward tilt of about $\tau = 1.5$ deg, while for 900 Mc/sec, for which $q = 80$, we find about $\tau = 4.9$ deg on the $\kappa_r = 80$ curve. The τ curves for ocean and lakes show that over the entire radio-frequency range, we can never expect more than about 6.2-deg forward tilt. Assuming an average conductivity $\sigma = 5 \times 10^{-3}$ mho/m for mountain lakes, for a 100-Mc wave, we have $q = 1.8 \times 10^4 \times 5(10^{-3}/100) = 0.9$ and, for a 900-Mc wave, only one-ninth of this value, *i.e.*, $q = 0.1$. For each frequency, the curves of Fig. 249 give $\tau = 6.2$ deg. For dry ground, we have an average conductivity of 5×10^{-5} mho/m and $\kappa_r \cong 5$. At 100 Mc/sec, we find $q = 1.8 \times 10^4 \times 5(10^{-5}/100) = 0.009$ and, therefore, $q = 0.001$ for 900 Mc/sec. The curves of Fig. 249 do not extend to such small values but, if drawn, would give the maximum value of $\tau = 22$ deg as is indicated by the $\kappa_r = 5$ curve, which must be used. For wet ground, we deal essentially with the $\kappa_r = 25$ curve for τ degrees and find for an average conductivity $\sigma = 5 \times 10^{-3}$ mho/m the value $q = 0.9$ for 100 Mc/sec, since $q = 1.8 \times 10^4 \times 5(10^{-3}/100) = 0.9$ and $q = 0.1$ for 900 Mc/sec. In each case, the curve of Fig. 249 yields a forward tilt $\tau = 12.8$ deg.

Inasmuch as Eq. (876*b*) does not account for field intensities for grazing angles of incidence ($h_1 = 0 = h_2$ in Fig. 240), it must represent the field of the Sommerfeldian space wave, while the surface wave just discussed accounts for the field next to the earth surface. Therefore, for a grounded vertical radiator and a grounded vertical linear pickup antenna, it must be the surface wave that is instrumental.

165. Radiation Patterns over Perfect and Actual Ground. For short waves, a perfect reference plane is of just as much importance as plane ground. The antenna structures are small, and we can just as well use a metal reference "back-up" reflector for an artificial ground as the actual ground. Even though the metal should extend strictly to infinity, a reference metal plane of a few wavelengths' extension seems to give satisfactory service.

We found on page 848 that we can compare the received current for *vertically* polarized waves by means of the relations

$$\left.\begin{aligned} I_v^{(\text{amp})} &= D_\theta I \sqrt{1 + \rho_v^2 + 2\rho_v \cos\left(\varphi_v^\circ - \frac{720°h \cos\theta}{\lambda}\right)} \\ &\qquad \text{for any ground as plane reflector} \\ I_v^{(\text{amp})} &= D_\theta I \sqrt{2\left[1 + \cos\left(-\frac{720°h \cos\theta}{\lambda}\right)\right]} \\ &\text{for a perfect plane reflector } (\sigma = \infty \text{ mhos/m}) \text{ (a metal plane)} \\ I_v^{(\text{amp})} &= D_\theta I \qquad \text{no reflector present} \end{aligned}\right\} \quad (882)$$

In these relations, h meters denotes the height of the mid-point of a linear vertical pickup antenna above the reflector and θ is the angle of wave incidence with respect to the normal to the reflector. The quantity D_θ represents the directivity, which would be $[\cos(90° \cos\theta)]/\sin\theta$ for a half-wave linear antenna *normal* to the reflector. The quantity ρ_v is the coefficient of reflection of ground for a certain angle θ of wave incidence, and φ_v the phase due to reflection. For *horizontally* polarized waves, we employ horizontal linear antennas and have the comparisons

$$\left.\begin{aligned} I_h^{(\text{amp})} &= I \sqrt{1 + \rho_h^2 + 2\rho_h \cos\left(\varphi_h^\circ - \frac{720°h \cos\theta}{\lambda}\right)} \\ &\qquad \text{for any plane ground as a reflector} \\ I_h^{(\text{amp})} &= I \sqrt{2\left[1 + \cos\left(180° - \frac{720°h \cos\theta}{\lambda}\right)\right]} \\ &\text{for a plane perfect reflector (a metal plane, copper sheet)} \\ I_h^{(\text{amp})} &= I \qquad \text{(we have a circular pattern) with no reflector present} \end{aligned}\right\} \quad (882a)$$

In either case, the expressions for a perfect reflector are obtained by the substitution $\rho_v = +1 = |\rho_v|$, meaning that the phase factor $\epsilon^{j\varphi_v} = 1$ and $\varphi_v = 0$ deg. For horizontal polarization, we have $\rho_h = -1$ and a phase factor $\epsilon^{j\varphi_h} = \epsilon^{j180°} = \cos 180° + j \sin 180° = -1$. Let us apply these relations to the case where we have a half-wave linear radiator. The mid-point of the linear antenna is then h meters above the reflector. For a vertical half-wave antenna, h is then in the limit such that the lower end of the antenna just does not touch the reflector. Inasmuch as the current I, measured at the current antinode of the radiator, is the same for all three relations in (882) and (882a), the vertical polar pattern is

$$P_\theta = D_\theta \sqrt{1 + \rho^2 + 2\rho \cos\left(\varphi^\circ - \frac{720°h \cos\theta}{\lambda}\right)} \quad (882b)$$

with $D_\theta = 1$ for horizontal polarization, where it is understood that the pickup antenna is horizontal and so oriented that maximum signal is

received. For a vertical half-wave antenna with no reflector present, the value of the square root is unity; and for $\theta = 10$ deg wave incidence with respect to the linear antenna, we have $\cos 10° = 0.9848$, $\sin 10° = 0.1736$, $90° \cos 10° = 88.6$ deg, $\cos (90° \cos 10°) = \cos 88.6° = 0.0244$, $P_\theta = D_\theta = 0.0244/0.1736 = 0.142$. For vertical polarization, the meridian pattern of a linear $\lambda/2$ radiator must be the same, whether used as a pickup antenna or as a radiator. Therefore, the above directivity $D_\theta = 0.142$ holds also for a half-wave radiator in a $\theta = 10$ deg direction with respect to the radiator. Suppose we have a horizontal half-wave radiator, causing horizontally polarized waves, *i.e.*, waves with the electric $\mathcal{E}$ vector normal to the plane of incidence. If the radiator is h meters over a metal plane and parallel to it, so that $h = \lambda/4$, then we have $D_\theta = 1$ (since there is horizontal polarization with a circular fixed directivity in the plane of incidence), $\rho = |\rho_h| = 1$, $\varphi = \varphi_h = 180$ deg, and $h/\lambda = 0.25$. For $\theta = 10$ deg with respect to the normal of the metal reflector, we find then

$$720° \frac{h}{\lambda} \cos \theta = 720° \times 0.25 \cos 10° = 720° \times 0.25 \times 0.9848 = 177°$$

$$\cos \left(\varphi_h - \frac{720° h \cos \theta}{\lambda} \right) = \cos (180° - 177°) = \cos 3°$$

$$P_\theta = P_{10°} = \sqrt{1 + |\rho_h|^2 + 2|\rho_h| \cos 3°} = \sqrt{1 + 1 + 2 \cos 3°}$$
$$= \sqrt{2 + 2 \times 0.9986} = 1.99$$

We must realize that in (882*b*), by ρ_h we mean only the absolute positive value of the reflection coefficient, since its phase is taken care of by the φ term in the argument of the cosine function under the square root. It so happens that for a perfect reflector, $\rho_h = |\rho_h| \epsilon^{j180°} = 1 \cdot \epsilon^{j180°} = -1$. We can then use $\rho_h = -1$ but *must* omit the φ term in the argument of the cosine function and find

$$P_{10°} = \sqrt{1 + \rho^2 + 2\rho \cos (-177°)} = \sqrt{1 + 1 - 2 \cos (-177°)}$$
$$= \sqrt{2 - 2 \cos 177°} = \sqrt{2 - 2 \cos (180° - 3°)} = \sqrt{2 + 2 \cos 3°}$$
$$= 1.99$$

This confirms the 1.99 value found above.

For a vertical half-wave radiator over a metal reflector such that $h = \lambda/4$ of the mid-point of the radiator *just clears* the metal plane, we have

$$\rho = \rho_v = 1; \qquad \varphi = 0; \qquad D_\theta = D_{10} = 0.142$$

$$P_{10} = 0.142 \sqrt{1 + 1 + 2 \cos (-177°)} = 0.142 \sqrt{2 - 2 \cos 3°}$$
$$= 0.142 \sqrt{0.0028} = 0.0075$$

TABLE 51*

θ, deg	cos θ numeric	Directivity D_θ from Table 25	$\frac{720°h \cos\theta}{\lambda} = \delta° = \cos d$	*Horizontal* polarization over *perfect* ground, $\sigma = \infty$ mhos/m			
				cos d	2 cos d	2 + 2 cos d	$P_\theta = \sqrt{2 + 2\cos d}$
0.0	1.0000	0.000	180	1.0000	2.0000	4.0000	2.0000
10	0.9848	0.142	177	0.9986	1.9972	3.9972	1.999
20	0.9387	0.28	168.5	0.9799	1.9598	3.9598	1.9899
30	0.866	0.417	156	0.9135	1.8270	3.827	1.957
40	0.766	0.556	138	0.7431	1.4862	3.4862	1.868
50	0.6428	0.693	116	0.4384	0.8768	2.8768	1.697
60	0.5	0.816	90	0.0000	0.0000	2.0000	1.414
70	0.342	0.912	61.5	−0.4772	−0.9544	1.0456	1.0198
80	0.1736	0.98	31.4	−0.8536	−1.7072	0.2928	0.5385
85	0.0872	0.999	15.7				
90	0.0000	1.000	0.0	−1.0000	−2.0000	0.0000	0.0000

Remarks (Fig. 250): For vertical and horizontal half-wave antennas with their mid-points a distance $h = \frac{1}{4}\lambda$ above ground (actual), $\kappa_\epsilon' = 25 - j19.2$, $\kappa_r = \kappa/\kappa_0 = 25$, $q = 19.2$, $q = 1.8 \times 10^4(\sigma/f)$, where f is in Mc/sec and σ in mhos/m. We have also $d = 180° - \delta$.

θ, deg	*Vertical* polarization over *perfect* ground, $\sigma = \infty$ mhos/m					*Horizontal* polarization, *actual* ground, $n = \sqrt{25 - j19.2}$, $\Delta = \varphi_h - \delta°$			
	cos (−δ) = cos δ	2 cos δ	2 + 2 cos δ	$\sqrt{2 + 2\cos\delta}$	$P_\theta = D_\theta\sqrt{2 + 2\cos\delta}$	From Figs. 232, 233		$\varphi_h - \delta = \Delta$ deg	cos Δ
						ρ_h	$\varphi_h°$		
0.0	−1.0000	−2.0000	0.0000	0.0000	0.0000	0.7	176	−4	0.9976
10	−0.9986	−1.9972	0.0028	0.0529	0.0075	0.72	176.4	−0.6	0.9999
20	−0.9799	−1.9598	0.0402	0.2004	0.056	0.735	176.9	8.4	0.9893
30	−0.9135	−1.827	0.173	0.412	0.172	0.753	177.35	21.35	0.9314
40	−0.7431	−1.4862	0.5138	0.717	0.396	0.782	177.8	39.8	0.7683
50	−0.4384	−0.8768	1.1232	1.058	0.753	0.82	178.2	62.2	0.4664
60	0.0000	0.0000	2.0000	1.414	1.16	0.85	178.68	88.68	0.0238
70	0.4772	0.9544	2.9544	1.717	1.57	0.89	179.1	117.6	−0.4633
80	0.8536	1.7072	3.7072	1.926	1.89	0.94	179.55	148.15	−0.8494
90	1.0000	2.0000	4.0000	2.0000	2.0000	1.00	180	180	−1.0000

θ, deg	*Horizontal* polarization over *actual* ground, $n = \sqrt{25 - j19.2}$, $\Delta = (\varphi_h - \delta)$ deg, $A = 1 + \rho_h^2 + 2\rho_h \cos\theta$						*Vertical* polarization over *actual* ground, $\Delta = (\varphi_v - \delta)$ deg. $n = \sqrt{25 - j19.2}$			
	ρ_h^2	$1 + \rho_h^2$	$2\rho_h$	$2\rho_h \cos\Delta$	A	$P_\theta = \sqrt{A}$	From Figs. 232, 233		$\varphi_v - \delta$	cos Δ
							ρ_v	$\varphi_v°$		
0.0	0.49	1.49	1.4	1.39	2.88	1.697	0.7	360	180	−1.0000
10	0.518	1.518	1.44	1.44	2.958	1.72	0.699	358.5	181.5	−0.9997
20	0.5402	1.5402	1.47	1.46	3.0	1.732	0.695	358	189.5	−0.9863
30	0.567	1.567	1.506	1.41	2.977	1.726	0.68	357	201	−0.9336
40	0.6115	1.6115	1.564	1.2	2.811	1.676	0.65	356	218	−0.788
50	0.6724	1.6724	1.64	0.765	2.4374	1.562	0.598	354	238	−0.5299
60	0.7225	1.7225	1.7	0.0405	1.763	1.327	0.505	350	260	−0.1736
70	0.7921	1.7921	1.78	−0.825	0.9671	0.981	0.365	338	276.5	0.1132
80	0.8836	1.8836	1.88	−1.59	0.246	0.496	0.18	272	240.6	−0.4909
85	.....	.....	.....	.....	.....	.....	0.3	212	196.3	−0.9598
90	1.0000	2.0000	2.000	−2.0000	0.0000	0.000	1.000	180	180	−1.0000

* For $h = \frac{1}{4}\lambda$ above the reflector.

TABLE 51.*—(*Continued*)

θ, deg	*Vertical* polarization over *actual* ground, $n = \sqrt{25 - j19.2}$, $\Delta = \varphi_v - \delta°$, $A = 1 + \rho_v^2 + 2\rho_v \cos \Delta$						
	ρ_v^2	$1 + \rho_v^2$	$2\rho_v$	$2\rho_v \cos \Delta$	A	$\sqrt{A}$	$P_\theta = D_\theta \sqrt{A}$
0.0	0.49	1.49	1.4	−1.4	0.09	0.3	0.0000
10	0.4886	1.489	1.398	−1.398	0.091	0.301	0.0429
20	0.483	1.483	1.39	−1.37	0.113	0.335	0.094
30	0.4624	1.462	1.36	−1.27	0.192	0.436	0.182
40	0.4225	1.422	1.3	−1.02	0.402	0.632	0.352
50	0.3576	1.358	1.196	−0.632	0.726	0.852	0.592
60	0.255	1.255	1.01	−0.176	1.079	1.039	0.848
70	0.1332	1.133	0.73	0.0825	1.2155	1.102	1.02
80	0.0324	1.032	0.36	−0.187	0.845	0.9195	0.9000
85	0.09	1.09	0.6	−0.575	0.515	0.7176	0.7175
90	1.0000	2.000	2.00	−2.000	0.000	0.0000	0.0000

The quantity θ is the angle of wave incidence with respect to the normal to ground (or reflector). δ degrees $= 720°(h/\lambda) \cos \theta$. P_θ is the vertical polar pattern.

* For $h = \frac{1}{4}\lambda$ above the reflector.

which is essentially zero. We note already the *vast difference* between respective polarizations, even though the radiation center is, in each case, a quarter wavelength above the metal reflector. Suppose we have *actual* ground as a reflector, with an equivalent relative dielectric constant $\kappa_e' = 25 - j19.2$, where 25 is the actual relative dielectric constant $\kappa_r = \kappa/\kappa_0$ of the ground and $19.2 = q = 1.8 \times 10^4 \sigma/f$ with f in megacycles per second and σ in mhos per meter. The magnitude 25 shows that we deal with *wet* ground or soil, for which we find conductivity values of 10^{-2} to 10^{-3} mho/m. Taking $\sigma = 10^{-2}$ mho/m, we have $f = 1.8 \times 10^4(10^{-2}/19.2) = 9.4$ Mc/sec. In Fig. 232 on page 849, we have curves for the reflection coefficient ρ and its time phase φ for the index of refraction $n = \sqrt{25 - j19.2}$. For $\theta = 10$ deg, we find for *horizontal* polarization $\rho_h = 0.72$, $\varphi_h = 176$ deg. Since $D_\theta = 1$, we find from (882*b*)

$$P_{10} = \sqrt{1 + 0.72^2 + 2 \times 0.72 \cos (176° - 177°)}$$
$$= \sqrt{1.5184 + 1.44 \cos (-1°)} = \sqrt{1.5184 + 1.44 \cos 1°} = 1.72$$

in comparison with the value of 1.99 for a perfect ground reflector ($\sigma = \infty$). For *vertical* polarization, we find from Fig. 232, the values $\rho_v = 0.7$ and $\varphi_v \cong 360$ deg, *i.e.*, equal to 0 deg, and

$$P_{10} = 0.142 \sqrt{1 + 0.7^2 + 2 \times 0.7 \cos (0° - 177°)}$$
$$= 0.142 \sqrt{1.49 - 1.4 \cos 3°} = 0.142 \sqrt{0.09} = 0.142 \times 0.3 = 0.0426$$

as against 0.0075 for a perfect ground.

Table 51 gives the computations for every 10 deg of incidence θ with respect to the normal to ground. Figure 250 gives the results for the mid-point of the half-wave antenna a height $h = \frac{1}{4}\lambda$ above the reflector for vertical and horizontal orientation (for vertical orientation, the lower end of the half-wave antenna just clears the ground). We note that for

actual ground, the vertical radiation pattern, in the case of *vertical* polarization, no longer shows radiation as well as reception effects along the plane of the surface of the ground; while for a perfect ground, we have a decided ground surface radiation as well as reception effects. For horizontal linear antennas and *horizontal* polarization, the radiation patterns for actual and perfect grounds do not differ as much as would be expected

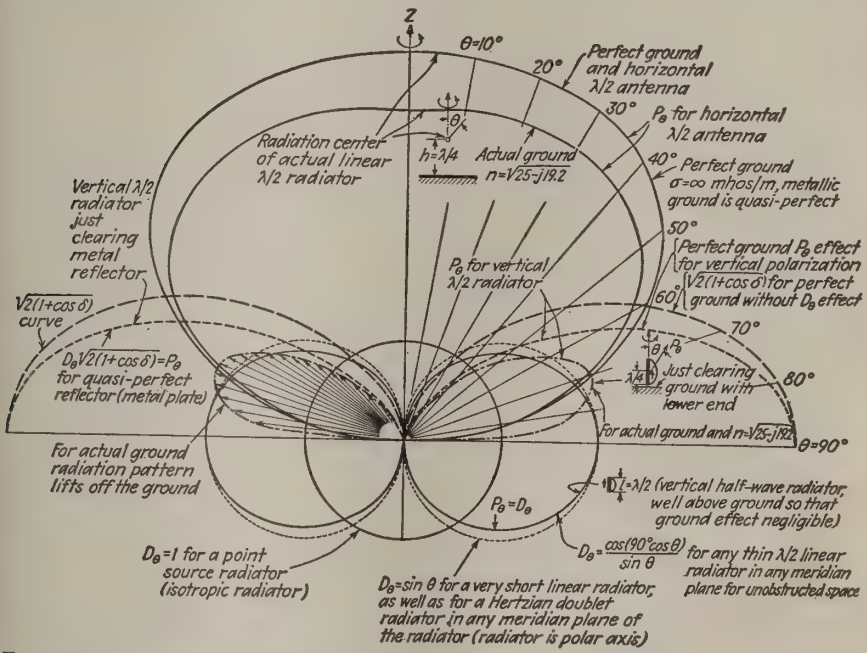
Z
θ=10°
20°
30°
40°
50°
60°
70°
80°
θ=90°
Perfect ground and horizontal λ/2 antenna
Pθ for horizontal λ/2 antenna
Perfect ground σ=∞ mhos/m, metallic ground is quasi-perfect
Perfect ground Pθ effect for vertical polarization √2(1+cos δ) for perfect ground without Dθ effect
Just clearing ground with lower end
Radiation center of actual linear λ/2 radiator
h=λ/4
Actual ground n=√25-j19.2
Vertical λ/2 radiator just clearing metal reflector
√2(1+cos δ) curve
Pθ for vertical λ/2 radiator
Dθ√2(1+cos δ)=Pθ for quasi-perfect reflector (metal plate)
For actual ground and n=√25-j19.2
For actual ground radiation pattern lifts off the ground
l=λ/2 (vertical half-wave radiator well above ground so that ground effect negligible)
Pθ=Dθ
Dθ=cos(90°cos θ)/sin θ for any thin λ/2 linear radiator in any meridian plane for unobstructed space
Dθ=1 for a point source radiator (isotropic radiator)
Dθ=sin θ for a very short linear radiator, as well as for a Hertzian doublet radiator in any meridian plane of the radiator (radiator is polar axis)

FIG. 250. This diagram applies, for instance, to wet soil from 0.94 to 9.4 Mc/sec and any obstructing wave medium, satisfying $\kappa_e' = 25 - j19.2$, where $19.2 = 18{,}000\sigma$ (mhos/m)/f(Mc/sec), and $25 = \kappa_r = \kappa/\kappa_0$; $\kappa_0 = 8.854 \times 10^{-12}$ farad/m, and κ farad/m for the obstructing wave medium; $\delta = 720(h/\lambda)\cos\theta$ degrees; $P_\theta = D_\theta\sqrt{2(1+\cos\delta)}$ for *vertical* antenna on metal reflector with $2(1+\cos\delta)$ as reflector effect; $P_\theta = \sqrt{2(1-\cos\delta)}$ for *horizontal* antenna parallel with metal reflecting surface.

from the reflection curves (Figs. 232, 233). For $h = \frac{1}{2}\lambda$, we find the evaluations of Table 52. Figures 251 and 252 give polar plots for vertical and horizontal $\lambda/2$ antennas with their mid-points either a quarter or a half wavelength above ground, for *perfect* ground ($\sigma = \infty$), as well as for *actual* ground, characterized by a relative index of electromagnetic refraction $n = \sqrt{25 - j19.2}$. Such an index refers to wet soil. From these illustrations, it will be noted that for a *horizontal* $\lambda/2$ antenna, a distance $h = \lambda/2$ above perfect ground, the vertical polar pattern looks about the same as for a *vertical* $\lambda/2$ antenna, which is $h = \lambda/4$ above actual ground. In each case, there is no radiation whatsoever along the

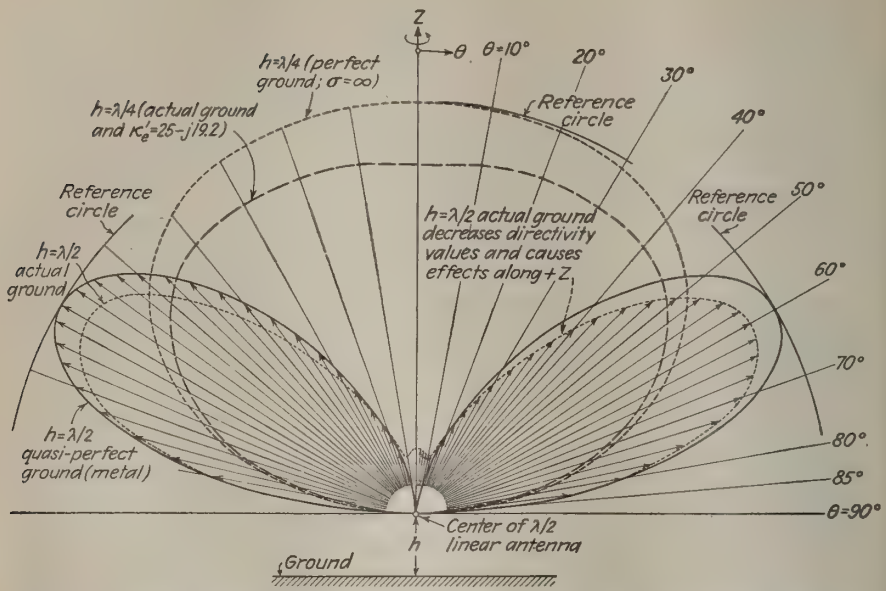

FIG. 251. Vertical pattern for horizontal $\lambda/2$ linear antenna for quasi-perfect ground and actual ground of $\kappa_e' = 25 - j19.2$.

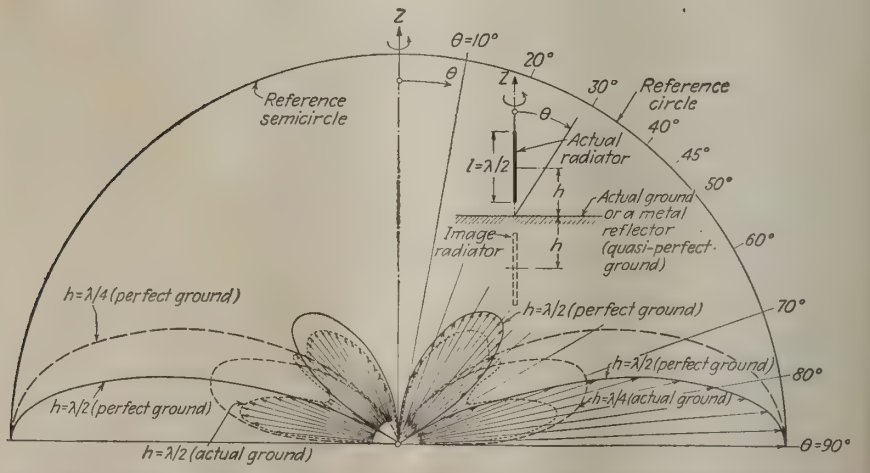

FIG. 252. Vertical pattern of vertical half-wave linear radiator over quasi-perfect ground and actual ground for $\kappa_e' = 25 - j19.2$.

horizon, since only elevated angle radiation up to a certain angle occurs. For still more elevation, we have no radiation. Therefore, actual ground causes the radiation pattern to lift away from the horizon. However, for $h = \lambda/2$ over actual ground and with a horizontal $\lambda/2$ antenna, there is no zero-radiation region on each side of the normal ($\theta = 0$); while for the $h = \lambda/4$ case over actual ground and a vertical $\lambda/2$ antenna, the no-radiation region around the normal ($\theta = 0$) is almost 40 deg, *i.e.*, 20 deg on either side of $\theta = 0$.

TABLE 52*

θ, deg	D_θ from Table 25	cos θ	$\frac{720° h \cos\theta}{\lambda} = \delta = 360° \cos\theta$	*Horizontal* $\frac{\lambda}{2}$ antenna over *perfect* ground, $\sigma = \infty$ mhos/m: $\Delta = 180° - \delta$	cos Δ	2 cos Δ	$2 + 2\cos\Delta$	$P_\theta = \sqrt{2 + 2\cos\Delta}$	*Vertical* $\frac{\lambda}{2}$ antenna over perfect ground, $\Delta = -\delta$: cos Δ	2 cos Δ
0.0	0.000	1.0000	360	−180	−1.0000	−2.0000	0.0000	0.0000	1.0000	2.0000
10	0.142	0.9848	354	−174	−0.9945	−1.989	0.011	0.1049	0.9945	1.989
20	0.28	0.9387	337	−157	−0.9202	−1.8404	0.1596	0.4	0.9202	1.8404
30	0.417	0.866	312	−132	−0.6691	−1.3382	0.6618	0.8124	0.6691	1.3382
35	0.485	0.8192	294	.....	.....	.....	.....	.....	0.4067	0.8134
40	0.556	0.766	276	−96	−0.1045	−0.209	1.791	1.338	0.1045	0.209
45	0.619	0.7071	254	.....	.....	.....	.....	.....	−0.2756	−0.551
50	0.693	0.6428	232	−52	0.6157	1.2314	3.2314	1.797	−0.6157	−1.231
55	0.76	0.5736	207	.....	.....	.....	.....	.....	−0.891	−1.782
60	0.816	0.5	180	0.0	1.0000	2.0000	4.0000	2.0000	−1.0000	−2.000
65	0.86	0.4226	152	.....	.....	.....	.....	.....	−0.8829	−1.766
70	0.912	0.342	123	57	0.5446	1.0892	3.0892	1.758	−0.5446	−1.089
75	0.942	0.2588	93	.....	.....	.....	.....	.....	−0.0523	−0.105
80	0.98	0.1736	62.8	117.2	−0.4571	−0.914	1.086	1.04	0.4571	0.914
85	0.99	0.0872	31.4	148.6	−0.8536	−1.7072	0.2928	0.5385	0.8536	1.707
87	0.999	0.0523	17.8	.....	.....	.....	.....	.....	0.9521	1.904
90	1.000	0.0000	0.0	180	−1.0000	−2.0000	0.0000	0.0000	1.0000	2.000

θ, deg	*Vertical* $\frac{\lambda}{2}$ antenna over *perfect* ground, $\sigma = \infty$ mhos/m, $\Delta = -\delta$: $2 + 2\cos\Delta$	$A = \sqrt{2(1 + \cos\Delta)}$	$P_\theta = AD_\theta$	*Vertical* $\frac{\lambda}{2}$ antenna over *actual* ground, $n = \sqrt{25 - j19.2}$, $\Delta = (\varphi_v - \delta)$ deg, $A = 1 + \rho_v^2 + 2\rho_v \cos\Delta$: From Figs. 232, 233 ρ_v	φ_v	$\varphi_v - \delta$ deg	cos Δ	$1 + \rho_v^2$	$2\rho_v$	$2\rho_v \cos\Delta$	A
0.0	4.0000	2.000	0.000	0.7	360	0.000	1.0000	1.49	1.4	1.4	2.89
10	3.989	1.997	0.284	0.699	358.5	4.5	0.9969	1.489	1.398	1.396	2.885
20	3.8404	1.959	0.55	0.695	358	21	0.9336	1.483	1.39	1.3	2.783
30	3.3382	1.827	0.763	0.68	357	45	0.7071	1.467	1.36	0.96	2.427
35	2.8134	1.676	0.812	0.67	356.1	62.1	0.4695	1.4489	1.34	0.629	2.078
40	2.209	1.487	0.829	0.65	356	80	0.1736	1.422	1.3	0.226	1.648
45	1.4488	1.204	0.741	0.625	355	101	−0.191	1.3908	1.25	−0.239	1.152
50	0.7686	0.877	0.608	0.598	354	122	−0.5299	1.358	1.196	−0.635	0.723
55	0.218	0.469	0.355	0.56	352	145	−0.8192	1.314	1.12	−0.915	0.399
60	0.0000	0.000	0.000	0.505	350	170	−0.9848	1.255	1.01	−0.995	0.26
65	0.2342	0.484	0.415	0.44	344	192	−0.9781	1.194	0.88	−0.86	0.344
70	0.9108	0.954	0.87	0.365	338	215	−0.8199	1.133	0.73	−0.6	0.533
75	1.8954	1.375	1.298	0.27	320	227	−0.682	1.073	0.54	−0.37	0.703
80	2.914	1.706	1.68	0.18	272	209.2	−0.8729	1.032	0.36	−0.315	0.717
85	3.7072	1.926	1.926	0.3	212	180.6	−0.9999	1.09	0.6	−0.6	0.49
87	3.9042	1.975	1.97	0.5	196	178.2	−0.9999	1.25	1.0	−1.0	0.25
90	4.0000	2.000	2.000	1.000	180	180	−1.0000	2.000	2.00	−2.000	0.000

* For $h = 0.5\lambda$ and perfect as well as actual ground with index $n = \sqrt{25 - j19.2}$.

TABLE 52.*—(*Continued*)

θ, deg	*Vertical* $\frac{\lambda}{2}$ antenna over *actual* ground, $n = \sqrt{25 - j19.2}$		*Horizontal* $\frac{\lambda}{2}$ antenna, over *actual* ground, $n = \sqrt{25 - j19.2}$, $\Delta = (\varphi_h - \delta)$ deg, $A = 1 + \rho_h^2 + 2\rho_h \cos \Delta$								
	$\sqrt{A}$	$P_\theta = D_\theta \sqrt{A}$	From Fig. 232		$(\varphi_h - \delta)$ deg	$\cos \Delta$	$2\rho_h$	$2\rho_h \cos \Delta$	$1 + \rho_h^2$	A	$P_\theta = \sqrt{A}$
			ρ_h	φ_h							
0.0	1.7	0.000	0.7	176	−184	−0.9976	1.4	−1.398	1.49	0.092	0.304
10	1.697	0.24	0.72	176.4	−177.6	−0.9991	1.44	−1.44	1.518	0.078	0.283
20	1.667	0.47	0.735	176.9	−160.1	−0.9403	1.47	−1.38	1.54	0.1602	0.4
30	1.559	0.65	0.753	177.35	−134.65	−0.6902	1.506	−1.04	1.567	0.527	0.728
35	1.442	0.7									
40	1.284	0.706	0.782	177.8	−98.2	−0.1426	1.564	−0.224	1.611	1.3875	1.18
45	1.072	0.66									
50	0.848	0.587	0.82	178.2	−53.8	0.5906	1.64	0.97	1.672	2.6424	1.625
55	0.632	0.48									
60	0.51	0.415	0.85	178.68	−1.32	0.9997	1.7	1.7	1.722	3.4225	1.849
65	0.5744	0.495									
70	0.728	0.662	0.89	179.1	56.1	0.5577	1.78	0.995	1.792	2.787	1.67
75	0.837	0.79									
80	0.848	0.83	0.94	179.55	116.75	−0.4501	1.88	−0.845	1.884	1.039	1.02
85	0.7	0.693									
87	0.5	0.5									
90	0.0000	0.000	1.000	180	180	−1.0000	2.000	−2.000	2.00	0.000	0.000

* For $h = 0.5\lambda$ and perfect as well as actual ground with index $n = \sqrt{25 - j19.2}$.

At UHF's the actual ground effect can be avoided by using a metal plate so as to simulate perfect ground, and we can use the reflection coefficients $\rho_v = +1$ and $\rho_h = -1$, respectively. We find then, for the vertical polar pattern, the simplified relations

$$\left.\begin{aligned} P_\theta &= D_\theta \sqrt{2(1 + \cos \delta)} && \left\{ \begin{array}{l} \text{for vertical polarization and} \\ \text{vertical linear antenna} \end{array} \right. \\ P_\theta &= \sqrt{2(1 - \cos \delta)} && \left\{ \begin{array}{l} \text{for horizontal polarization and} \\ \text{horizontal antenna} \end{array} \right. \\ \delta &= 720° \frac{h}{\lambda} \cos \theta \end{aligned}\right\} \qquad (882c)$$

which hold for any length of a linear antenna for an unobstructed directivity pattern D_θ in the meridian plane with the antenna as the polar axis. As far as the shape of these polar patterns is concerned, $D_\theta \sqrt{1 + \cos \delta}$ and $\sqrt{1 - \cos \delta}$, respectively, are the determining functions. Table 53 gives the numerical evaluations of these functions. As predicted by $\sqrt{1 + \cos \delta}$ and $\sqrt{1 - \cos \delta}$, we have symmetrical curves as in Fig. 253 with respect to 90, 3×90, 5×90, $\cdots$ of the variable δ. Any angle of δ can be read off on these curves, and the value of $\sqrt{1 - \cos \delta}$ gives directly the P_θ vertical polar directivity for a horizontal antenna and horizontal polarization if the unit of the scale is of no concern. For instance, for an angle of incidence $\theta = 70$ deg, $h = 0.25\lambda$, we

have $\delta = 720° \times 0.25 \cos 70° = 180° \times 0.342 = 61.5$ deg, and Fig. 253 yields $\sqrt{1 - \cos \delta} = 0.72$ for 61.5 deg. Inasmuch as in formula (882c) we have $P_\theta = \sqrt{2(1 - \cos \delta)}$, which is $\sqrt{2}\sqrt{1 - \cos \delta}$, we have to multiply 0.72 by 1.4142, yielding $P_{70} = 1.019$, as found in Table 51 for $\theta = 70$ deg for horizontal polarization over perfect ground. It is then an easy matter to compute the respective P_θ patterns for perfect

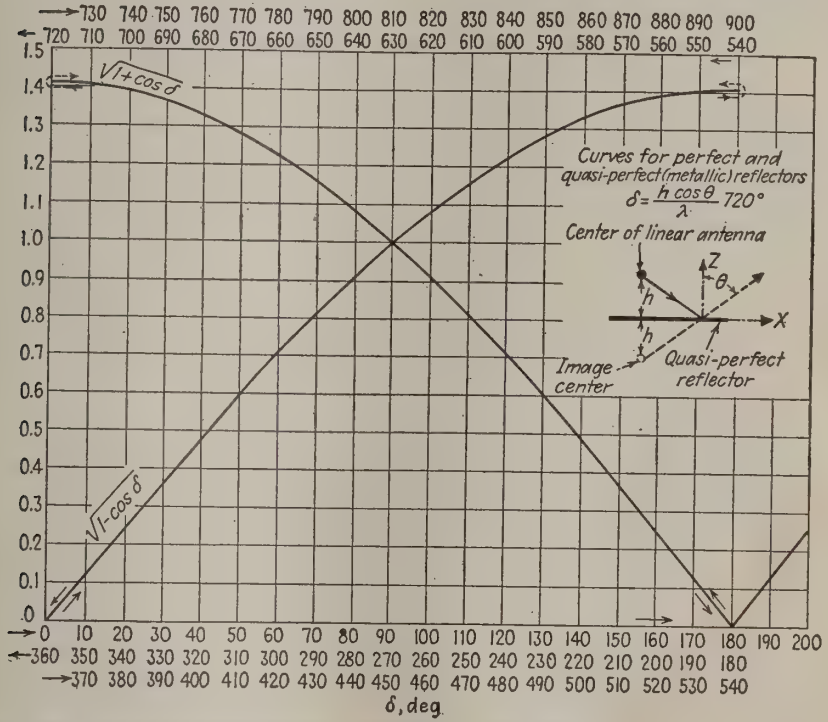

FIG. 253. Characteristic functions for vertical and horizontal polarization over quasi-perfect ground.

reflectors and either type of polarization and any h value. As mentioned, metal reflectors are used in short-wave work with extensions of only a few wavelengths. We found in Sec. 163 that such metal plates do exhibit practically a unity value for the coefficient of reflection, so that Table 53 and the curves of Fig. 253 should be useful in practical short-wave work. Table 54 gives the evaluations for quasi-perfect reflectors and half-wave radiators. For vertical linear radiators, the $\sqrt{1 + \cos \delta}$ value of Fig. 253 must be multiplied with the unobstructed space directivity D_θ of the linear radiator in order to yield the P_θ value for vertical polarization over metal reference planes. For vertical radiators (half-wave radiators), the height h must be larger than 0.25λ, since the extreme ends

of the half-wave radiator are high potential points. For this reason, the columns for $h = 0.1\lambda$ and $h = 0.05\lambda$ cannot give possible physical spacings. Figure 254 gives the shape of the vertical polar pattern P_θ in the vertical ZX plane if the half-wave radiator is parallel with the metal reflector. The radiator then causes horizontally polarized waves. The patterns given for $h/\lambda = 0.25$, 0.3, 0.4, 0.5, 0.6, 0.75, and $h = \lambda$,

TABLE 53. EVALUATION OF THE CHARACTERISTIC FUNCTIONS FOR VERTICAL AND HORIZONTAL POLARIZATIONS OVER PERFECT GROUND
($\sigma = \infty$ mhos/m)

δ, deg	$\cos \delta$	$1 + \cos \delta$	$\sqrt{1 + \cos \delta}$	$1 - \cos \delta$	$\sqrt{1 - \cos \delta}$
0.0	1.0000	2.0000	1.41	0.0000	0.0000
10	0.9848	1.9848	1.4088	0.0152	0.1233
20	0.9387	1.9387	1.3928	0.0613	0.2474
30	0.866	1.866	1.3675	0.134	0.3663
40	0.766	1.766	1.32885	0.234	0.4825
50	0.6428	1.6428	1.282	0.3572	0.5974
60	0.5	1.5	1.225	0.5	0.7071
70	0.342	1.342	1.158	0.658	0.811
80	0.1736	1.1736	1.0834	0.8264	0.9085
90	0.0000	1.0000	1.0000	1.0000	1.0000
100	−0.1736	0.8264	0.9085	1.1736	1.0834
110	−0.342	0.658	0.811	1.342	1.158
120	−0.5	0.5	0.7071	1.5	1.225
130	−0.6428	0.3572	0.5974	1.6428	1.282
140	−0.766	0.234	0.4825	1.766	1.32885
150	−0.866	0.134	0.3663	1.866	1.3675
160	−0.9397	0.0613	0.2474	1.9397	1.3928
170	−0.9848	0.0152	0.1233	1.9848	1.4088
180	−1.0000	0.0000	0.0000	2.0000	1.4142

respectively. It will be noted that all maxima effects lie on a semicircle with a radius that is twice as much as would be the case in the absence of the horizontal metal reflector. The shape of the polar pattern changes radically as the elevation h of the radiator above the reflector changes. For $h/\lambda = 0.25$, we have, for instance, maximum directivity along the Z axis ($\theta = 0$ deg) and no directivity along the $\pm X$ axis, since the P_θ pattern lifts away from the horizontal plane. For $h/\lambda = 0.4$, the directivity "dent" around the Z direction is rather pronounced; and at $\theta = \pm 50$ deg, we have maximum directivity, so that a pronounced downward dent exists between -50 and $+50$ deg. For $h/\lambda = 0.5$, the downward dent around $\theta = 0$ deg is so pronounced that the P_θ pattern *breaks up into two lobes* with maximum effects along ± 60 deg directions. We have then shadow zones around the Z axis as well as around the X axis, since

the respective lobes, which are symmetrical with respect to the Z axis, are lifted away from the horizontal plane with an upward inclination of 30 deg. For $h/\lambda = 0.6$, the two side lobes have an upward inclination of 25 deg, since maximum effects occur for $\theta = \pm 65$ deg. We have also a lobe with a maximum along the $+Z$ axis. This lobe would have a smaller maximum if $h = 0.55\lambda$ instead of 0.6λ. For $h = 0.75\lambda$, the central lobe broadens considerably and is tangent to the reference semicircle, while the other two symmetrical lobes have only 20-deg upward

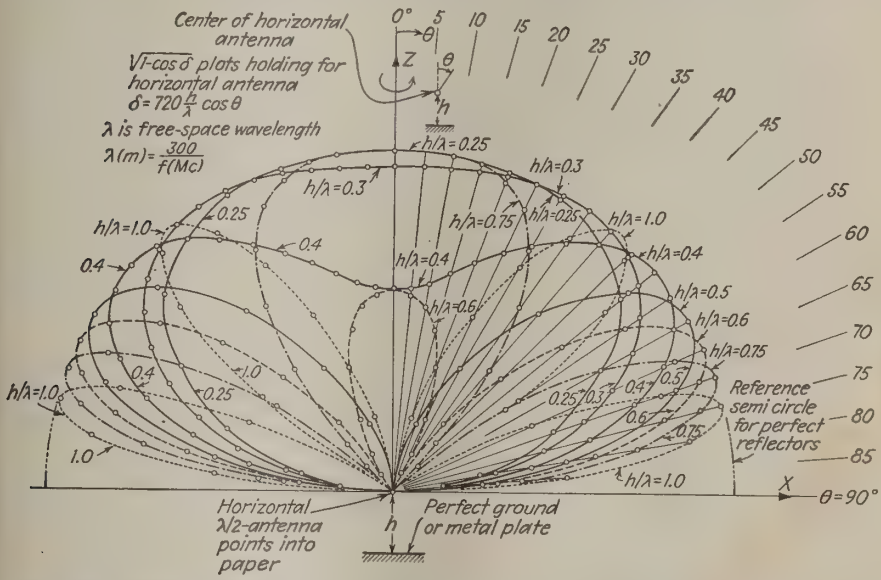

FIG. 254. Vertical patterns for a horizontal half-wave radiator over a metal plane in the XY plane.

inclinations and are more elongated, but still tangent to the reference semicircle. For $h = \lambda$, we have again no directivity along the Z axis. We have then four separate lobes at about 42.5 and 75 deg, upward inclination. Therefore, between $h = 0\lambda$ to $h = 0.5\lambda$, we deal with a single P_θ pattern; for $h > 0.5\lambda$ to $h < \lambda$, we have three lobes for the P_θ pattern; for $h = \lambda$ to $h < 1.5\lambda$, we have four lobes, with no directivities along the Z and X directions; for $h = 1.5\lambda$ to $h < 2\lambda$, we have five lobes, etc. Figure 255 compares vertical and horizontal orientations of half-wave radiators for different elevations h above a metal reference plane. Since each representation in this figure compares horizontal with vertical antenna orientation, only respective half patterns are shown for the sake of clearness. Each half pattern when rotated about the Z axis yields the space pattern in unobstructed radiation space. The

TABLE 54. FOR METAL REFLECTORS AND VERTICAL AND HORIZONTAL HALF-WAVE RADIATORS

θ, deg	cos θ	$h = 0.3\lambda$ yields $\delta = 216° \cos \theta$			$h = 0.4\lambda$ yields $\delta = 288° \cos \theta$			$h = 0.6\lambda$ yields $\delta = 432° \cos \theta$		
		δ, deg	From Fig. 253		δ, deg	$\sqrt{1 - \cos \delta}$	$D_\theta \sqrt{1 + \cos \delta}$	δ, deg	$\sqrt{1 - \cos \delta}$	$D_\theta \sqrt{1 + \cos \delta}$
			$\sqrt{1 - \cos \delta}$	$D_\theta \sqrt{1 + \cos \delta}$						
0.0	1.0000	216	1.342	0.0000	288	0.83	0.0000	432	0.83	0.0000
5	0.9962	215	1.346	0.0344	287	0.84	0.0905	430	0.81	0.093
10	0.9848	213	1.35	0.0568	284	0.865	0.158	426	0.765	0.1656
15	0.9659	209	1.365	0.0745	278	0.925	0.224	418	0.68	0.26
20	0.9387	202.5	1.387	0.0785	270	1.000	0.28	405	0.535	0.364
25	0.9063	198	1.398	0.077	261	1.08	0.32	386	0.315	0.484
30	0.866	187	1.408	0.0354	249	1.165	0.334	374	0.165	0.584
35	0.8192	177	1.41	0.0186	235	1.25	0.324	353.5	0.08	0.691
40	0.766	165.8	1.4	0.097	220	1.325	0.27	331	0.35	0.76
45	0.7071	152.7	1.37	0.213	203	1.385	0.177	305	0.65	0.785
50	0.6428	139	1.322	0.3465	175	1.41	0.0415	278	0.925	0.74
55	0.5736	124	1.25	0.503	166	1.4	0.128	248	1.17	0.594
60	0.5	108	1.145	0.677	144	1.342	0.359	216	1.34	0.359
65	0.4226	91.3	1.01	0.85	122	1.235	0.593	182.6	1.41	0.02586
70	0.342	74	0.85	1.025	98.5	1.07	0.84	148	1.355	0.355
75	0.2588	56	0.66	1.186	74.5	0.85	1.06	112	1.17	0.75
80	0.1736	37.6	0.45	1.31	50	0.598	1.26	75.2	0.86	1.1
85	0.0872	18.8	0.22	1.395	25.1	0.305	1.382	37.6	0.45	1.338
90	0.0000	0.0	0.000	1.4142	1.0	0.000	1.4142	0.0	0.000	1.4142

$h = 0.75\lambda$ yields $\delta = 540° \cos\theta$			$h = \lambda$ yields $\delta = 720° \cos\theta$			For vertical $\frac{\lambda}{2}$ radiator	$h = 0.1\lambda$ yields $\delta = 72° \cos\theta$			$h = 0.05\lambda$ yields $\delta = 36° \cos\theta$	
δ, deg	$\sqrt{1 - \cos\delta}$	$D_\theta\sqrt{1 + \cos\delta}$	δ, deg	$\sqrt{1 - \cos\delta}$	$D_\theta\sqrt{1 + \cos\delta}$	D_θ (from Table 25)	δ, deg	$\sqrt{1 - \cos\delta}$	$D_\theta\sqrt{1 + \cos\delta}$	δ, deg	$\sqrt{1 - \cos\delta}$
540	1.414	0.0000	720	0.0000	0.0000	0.0000	72	0.83	*Cannot* be realized, since $h = 0.1\lambda$ and with a vertical $\lambda/2$ radiator h *cannot* be smaller than 0.25λ	36	0.431
538	1.412	0.0018	718	0.02	0.1128	0.08	71.8	0.828		35.9	0.43
531	1.405	0.0156	710	0.12	0.2	0.142	71.0	0.82		35.5	0.425
521	1.395	0.049	695	0.305	0.29	0.21	69.5	0.805		34.75	0.419
508	1.352	0.109	675	0.535	0.37	0.28	67.5	0.785		33.75	0.408
490	1.28	0.21	652	0.79	0.41	0.35	65.2	0.76		32.6	0.39
467.5	1.14	0.349	623	1.06	0.3875	0.417	62.3	0.73		31.15	0.375
441	0.915	0.525	590	1.28	0.294	0.49	59	0.696		29.5	0.36
414	0.64	0.7	551	1.405	0.072	0.556	55.1	0.65		27.55	0.33
381	0.26	0.87	509	1.356	0.239	0.628	50.9	0.609		25.45	0.31
348	0.14	0.975	464	1.115	0.602	0.693	46.4	0.55		23.2	0.28
311	0.585	0.97	415	0.65	0.94	0.752	41.5	0.5		20.75	0.25
270	1.000	0.816	360	0.000	1.15	0.816	36	0.43		18	0.218
228	1.29	0.53	305	0.65	1.08	0.862	30.5	0.37		15.25	0.18
185	1.41	0.057	246	1.185	0.7	0.912	24.6	0.3		12.3	0.15
140	1.325	0.459	186	1.408	0.0665	0.95	18.6	0.223		9.3	0.11
94	1.035	0.94	125.7	1.256	0.638	0.98	12.57	0.15		6.285	0.08
47.1	0.55	1.293	63	0.735	1.205	0.999	6.3	0.08		3.15	0.039
0.0	0.000	1.4142	0.0	0.000	1.4142	1.000	0.0	0.000		0.000	0.000

Remarks: $\sqrt{1 - \cos\delta}$ determines shape of the vertical P_θ pattern for a horizontal radiator; $D_\theta\sqrt{1 + \cos\delta}$ determines shape of a vertical P_θ pattern for a vertical radiator.

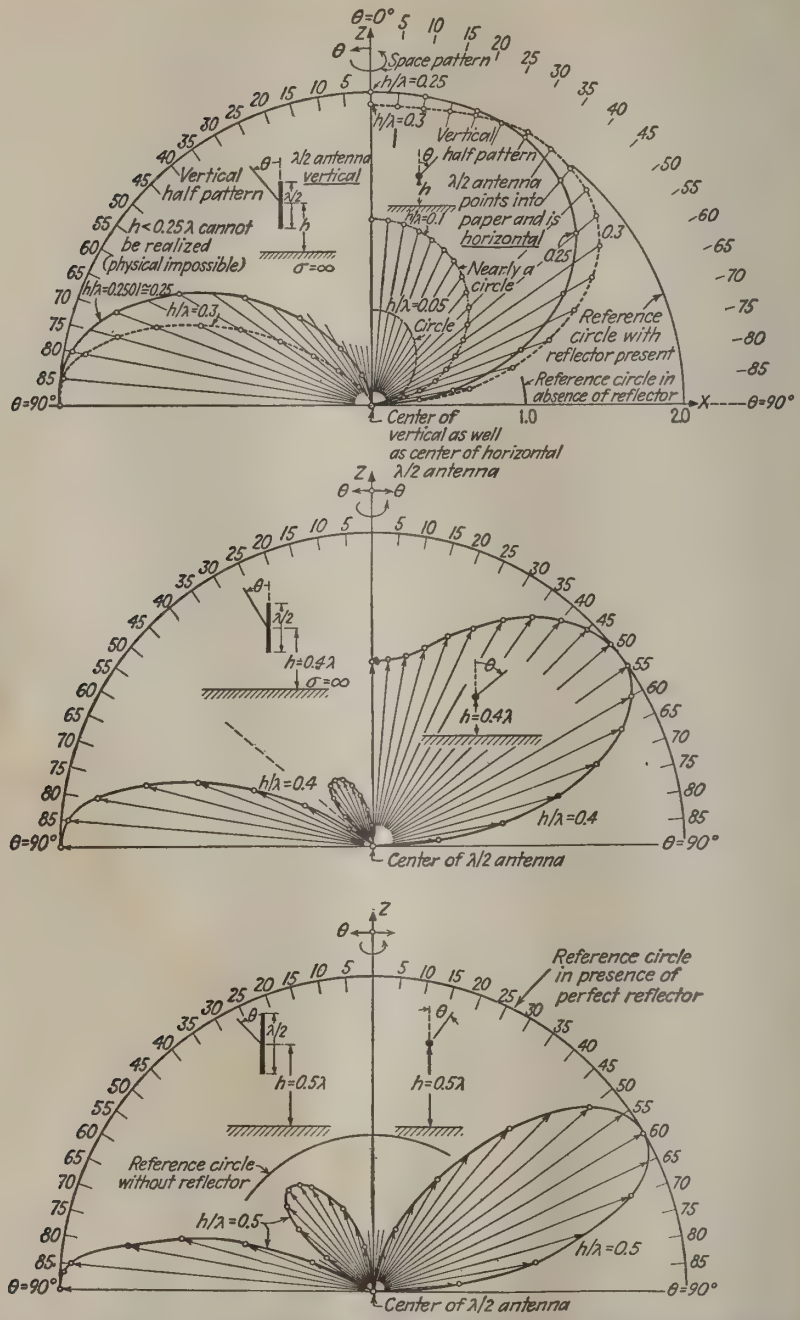

FIG. 255. Directivity of half-wave antennas perpendicular and parallel to a metal plane (which acts like a quasi-perfect reflector) with their centers at different distances from the metal plane.

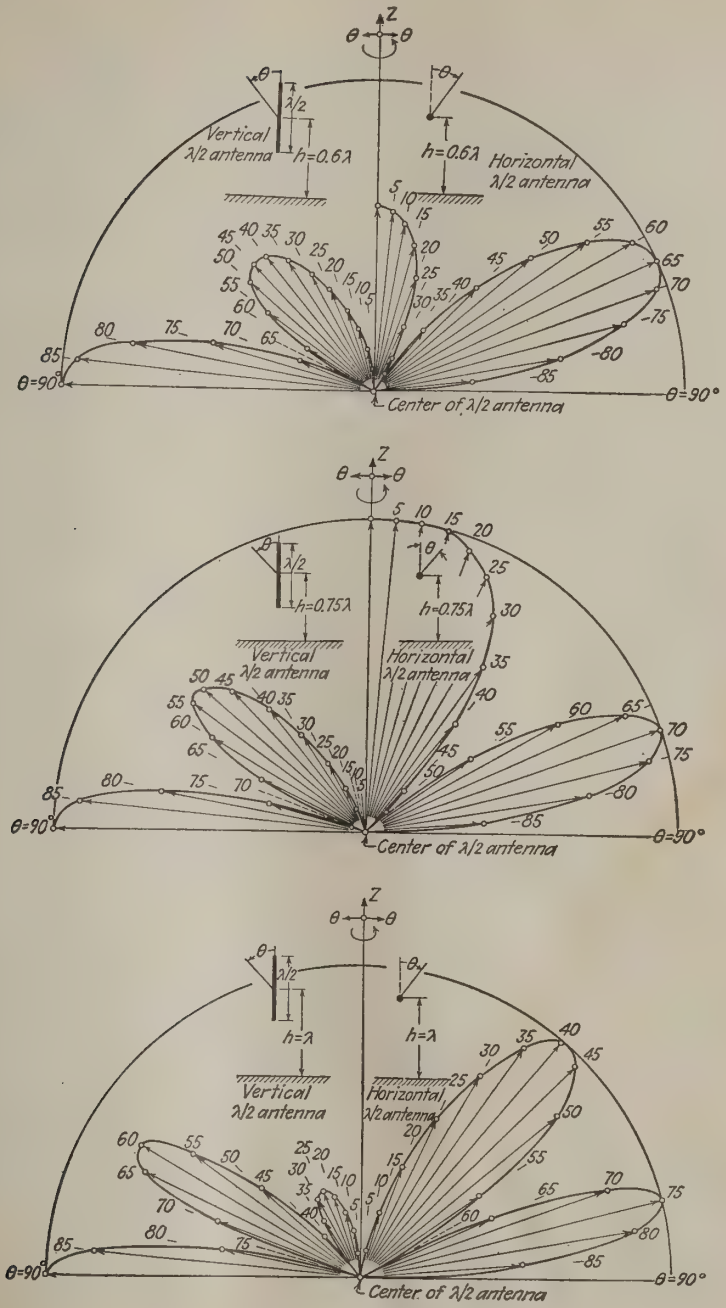

FIG. 255. (*Continued*).

upper left representation shows that for a vertical half-wave radiator, the directivity is decidedly along the horizon with weak high-angle effects. This is especially the case for $h = 0.3\lambda$. For horizontal half-wave radiators, we have again the corresponding patterns, as is discussed in connection with Fig. 254. We note that the $h/\lambda = 0.25$ and $h/\lambda = 0.3$ patterns are both favorable for high-angle direction effects, up to straight upward directivity ($\theta = 0$ deg), but not so for vertical half-wave radiators (left upper representation of Fig. 255). The P_θ effect along the Z axis is twice as much for $0.25\lambda = h$ with a metal reflector as without the reflector. This is expected, since a quasi-perfect reflector must double the effect along the Z direction, because the metal is a quasi-perfect mirror. For elevations that are $h < 0.25\lambda$, the delay angle $\delta = 720° \times (h/\lambda) \cos\theta$ degrees has, at its upper limit, a value that is smaller than $\delta = 180° \cos\theta$, since this angle holds for the limiting case $h/\lambda = 0.25$. Since $P_\theta = \sqrt{2}\sqrt{1 - \cos\delta}$ for horizontal half-wave radiators, for $\theta = 0$ deg, we have $\cos\delta < -1$, and $\sqrt{1 - \cos\delta}$ must be smaller than $\sqrt{2}$ and $P_\theta < 2$. The length of the P_θ maximum can never reach the reference circle of radius 2. This is evident if we compare the P_θ pattern for $h/\lambda = 0.1$ and $h/\lambda = 0.05$ in the upper left representation of Fig. 255. Therefore when the horizontal half-wave radiator almost touches the metal reflector to which it is parallel, the P_θ pattern must essentially vanish. For such a case, the actual half-wave radiator and its image are so close to each other that owing to the antiphase condition, the total field practically vanishes. What is of interest in the upper left representation is that for a horizontal half-wave dipole, as well as for a vertical half-wave dipole, the space pattern is a surface of revolution about the Z axis. The middle representation to the left of Fig. 255 gives the comparisons for $h = 0.4\lambda$, showing that for the vertical half-wave radiator, a small high-angle lobe also exists. For $h = 0.5\lambda$, this additional side lobe becomes more pronounced.

166. Effect of Radiator and Receiver Antenna Location with Respect to the Actual Ground on the Received Electromagnetic Field. The days have passed when we dealt only with ground-to-ground communication. Therefore, we need to meet conditions where, for instance, a transmitter for television is located on a mountain and we wish to receive in a valley, at higher mountains, or, in some cases, in an aircraft at still higher altitudes. This places the elevation h_1 of a transmitter antenna high above sea level and the elevation of the receiver antenna at an entirely different h_2 level. The resultant field in the radiation region where a receiving antenna is located may then be at a space region where we have a very strong resultant field. It may also be a region where a satisfactory recep-

tion is almost impossible, because we are in a destructive interference zone, which is a zone of no field. Such zones occur for short waves oftener in a certain space than for waves that are longer unless we use two carrier frequencies with one and the same modulation so that the strong fields for one wave fill out the weak field gaps of the other wave. We could also use a supersonic carrier-frequency "wobble," which likewise fills out the entire space with modulated fields, and have the receiver tuned to two or three carrier frequencies that, owing to the diversity effect, will always pick up a signal. The latter expedient requires a wider frequency channel because of the carrier-frequency swing. The subject of this section is to show what will happen if we have a carrier of a fixed frequency dependent on the locations h_1 and h_2 of the radiation and reception centers.

Let us take first the case of flat ground with vertical as well as horizontal polarizations. Assume that we deal with a radiator and pickup antenna over wet soil with a relative dielectric constant $\kappa_r = 30$ and a conductivity of $\sigma = 10^{-2}$ mho/m. We then find $n = \sqrt{30 - jq}$ for the relative index of refraction in ground with respect to air, with $q = 1.8 \times 10^4[10^{-2}/f^{(\text{Mc})}]$. Therefore, even for as low a value as 40 Mc/sec, we have $q = 4.5$, which, for the other limit of $\sigma = 10^{-3}$, gives $q = 0.45$. Therefore, for frequencies above 100 Mc/sec, we have essentially a quasi dielectric with $n \cong \sqrt{30}$, and the reflection curves of Fig. 259 can be used. For the radiation center of the transmitting antenna at T_1 as in Fig. 256, we have this center at an altitude h_1 meters with respect to flat ground. By means of the image location T_1', just as far below the ground, we can construct the ray diagram for a certain angle θ_1 of wave incidence. We find then the indirect ray $T_1G_1 + G_1R_1$ by producing $T_1'G_1$ toward R_1, which is a possible receiver location in the radiation region. By means of the normal T_1A_1 on $T_1'R_1$ and the parallel T_1R_1 for a distant field point, we find the direct path $T_1R_1 = r$ meters, and the indirect path $T_1G_1 + G_1R_1 = T_1'G_1 + G_1R_1 = T_1'A_1 + A_1R_1 = d_1 + r = 2h_1 \cos \theta_1 + r$. If it were not for the difference d_1 and the time phase of the ground reflection at G_1, the direct and the indirect waves would arrive at the distant receiver location R_1 in phase. The amplitude of the direct wave at R_1 is $\mathcal{E}_0/r$ and of the indirect wave $\rho_v\mathcal{E}_0\epsilon^{j\varphi_v}/(r + d_1)$. We then have to use a phase factor $\epsilon^{j(\omega t-\beta r)}$ for the direct wave and $\epsilon^{j[\omega t+\varphi_v-\beta(r+d_1)]}$ for the indirect wave. According to the previous sections on the same subject, the resultant field at R_1 has a phase factor $\epsilon^{j(\omega t+\delta+\varphi_v)}$ for $\delta = (-720°n_0fh_1 \cos \theta_1)/(3 \times 10^8)$ degrees and $f = \omega/6.28$ cycles per second. We can often take the atmospheric index n_0 of refraction equal to 1 and find

$$\mathcal{E}_R^{(\text{volts/m})} = \frac{D_{\theta'}\mathcal{E}_0}{r}\,\epsilon^{j(\omega t-\beta r)} + \frac{\rho_v D_\theta \mathcal{E}_0}{r}\,\epsilon^{j[\omega t+\varphi_v-\beta(d_1+r)]} \qquad \text{for vertical polarization}$$

$$\mathcal{E}_R^{(\text{volts/m})} = \underbrace{\frac{\mathcal{E}_0}{r}\,\epsilon^{j(\omega t-\beta r)}}_{\text{direct field}} + \underbrace{\frac{\rho_h \mathcal{E}_0}{r}\,\epsilon^{j[\omega t+\varphi_h-\beta(d_1+r)]}}_{\text{indirect field}} \qquad \text{for horizontal polarization}$$

Respective meridian directivities D'_θ and D_θ appear for vertically polarized waves, since the direction of the direct ray with respect to the vertical radiator is generally θ' and the direction of the indirect ray toward ground is θ with respect to the radiator as well as the normal to ground. For horizontally polarized waves, the reference field intensity $\mathcal{E}_0$ at 1 m distance from the radiator in its equatorial plane is the same all around the radiation center, since the radiator is perpendicular to the paper in Fig. 256. We also found that

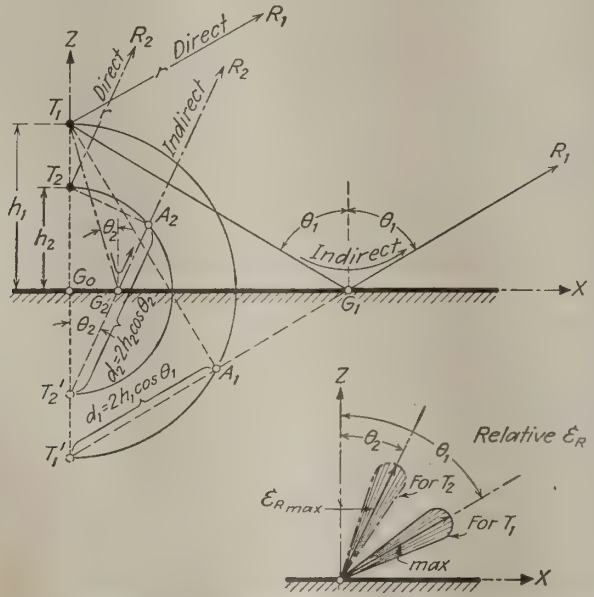

FIG. 256. Graphical solution for the maximum field intensity for longer ranges. For flat earth surface, T_1 and T_2 are the symmetry (mid-) points of actual transmitter antennas (T_1' and T_2' are their images).

Direct path r to R_1 and R_2; indirect path $r + d$ to R_1 and R_2. $\Delta = \varphi - 2.4fh \cos\theta°$ for f in Mc/sec. d_1, d_2, h_1, h_2, and r are in meters.

$$\Delta = \varphi - 2.4fh_1 \cos\theta_1 \qquad \text{deg} \tag{883}$$

where f is now in megacycles per second and h_1 in meters. The polarity of φ depends then on the electromagnetic property of the reflecting medium. Thus, if the earth's crust acts for certain frequencies as a

fairly good conductor in effect, we have for vertical polarization $\rho = \rho_v$ positive and a negative value $\rho = \rho_h$ for horizontal polarization. Since, in the short-wave range, wet and dry ground act essentially as quasi dielectrics, we find from Fig. 259 for wet soil that for angles of incidence θ up to almost 80 deg (exactly 79.7 deg), we have $\varphi_v = 0$ deg, at the Brewster angle for no reflection $\varphi_v = 90$ deg; and above this angle ($\theta = >79.7$ to 90 deg), we have $\varphi_v = 180$ deg. This means that ρ_v has negative values. For the entire range $\theta = 0$ to 90 deg, we have negative values for ρ_h. Therefore, for *all angles of incidence for horizontal polarization* and angle θ from about 80 to 90 deg, *i.e.*, 10-deg elevation to grazing incidence, *for vertical polarization*, reflection occurs with a loss of one-half wavelength (one-half cycle jump), because this corresponds to $\varphi = 180$ time degrees. When, therefore, the path difference d_1 is such that a half wavelength also is developed along it, *i.e.*, $d_1 = \lambda/2 = 0.5 \times 3 \times 10^8/(10^6 f) = 150/f$ meters, where f is in megacycles per second, the direct and indirect waves arrive in phase at the receiver location. Therefore, for $\Delta = 0, 2 \times 180, 4 \times 180, \cdots$ deg, we have receiving points of maximum field intensity. For $\Delta = 180, 3 \times 180, 5 \times 180, \cdots$ deg, we have field points of minimum field intensity. Suppose now that for a radiation center T_1 in Fig. 256, the path difference d_1 is equal to $\lambda/2$, *i.e.*, equal to $150/f$ meters, and assume the case for which the reflection coefficient causes an equivalent $\lambda/2$ "jump" at reflection point G_1; then at the reception center R_1, we have a maximum resultant field condition for the angle θ_1 of incidence. Suppose we lower the radiation center to a point T_2 corresponding to an elevation h_2 over ground. The requirement that field point R_2 is also a location of maximum resultant field condition necessitates the path difference $d_2 = 150/f$ meters, *i.e.*, $d_1 = d_2$. It is, therefore, necessary only to draw a semicircle about the ground point G_0 with a radius h_2 and make $T_2'A_2 = d_1$. The line $T_2'A_2$ then points toward the desired location R_2, and the angle $T_2T_2'A_2$ gives the angle θ_2 of incidence that causes maximum resultant field condition at the reception center R_2. We note, therefore, that the angle θ of incidence for which the path difference $d = \lambda/2$ occurs is all the smaller the lower the radiation center for a fixed frequency f. The smaller the angle θ the higher will be the altitude of the corresponding reception center R with respect to ground. Inasmuch as an inphase condition at R exists for every *even* multiple of 180 deg, *i.e.*, for $\Delta = 0, 2 \times 180, 4 \times 180, 6 \times 180, \cdots$ deg, several angles of wave incidence may exist for which maximum resultant values of $\mathcal{E}_R$ occur for one and the same frequency. A closer inspection of (883) reveals that for a given ground and fixed elevation h_1 of the radiation center, resultant field maxima can be obtained by varying either the exciter frequency f or the angle of

incidence or both, where the angle φ depends on θ. It also shows that the product fh_1 generally gives a measure of what happens for different angles of wave incidence θ, since (883) can be put into the form

$$\Delta = \varphi - 2.4p \cos \theta; \qquad p = h_t f \tag{883a}$$

where p denotes the phase coefficient due to the radiation center, h_t is the altitude in meters, and the operating frequency f is in megacycles per second. Since (883a) gives the same relative phase difference between direct and indirect fields at the receiving center as long as the product fh_t remains fixed, we can satisfy a desired vertical elevation as, for instance, $90° - \theta_1$ for a maximum resultant field $\mathcal{E}_R$, either by changing f for a fixed height h_t of the transmitting antenna center or by choosing h_t for a given fixed frequency f. When both h_t and f can be readily varied, as for an airplane radiator, we have a very flexible expedient for causing maximum radiation effects at a desired reception center in the radiation field. We then choose for a known value of φ (taken from curves for the reflection coefficient and its phase) the value of $p = h_t f$ such that $2.4p \cos \theta$ together with φ yields 360 deg or any other integer multiple of 360 deg. Quite often, minimum values of $\mathcal{E}_R$ are of concern, since they may account for regions of reception centers of essential zero field intensity. All that is then necessary is to choose for p in (883a) such a magnitude that Δ comes out -180 deg or any odd-integer multiple of -180 deg.

167. Numerical Data of the Effect of the Transmitter Antenna Location on the Resultant Space Field for Comparatively Short Ranges. In Sec. 166, it is assumed that the range r to the receiving center in space above ground is large compared with the location of the radiation center above ground. Direct and indirect rays are then essentially parallel, and the foot point A_1 on $T_1'R_1$ in Fig. 256 is then given by the normal T_1A_1 on $T_1'R_1$, which is also normal to T_1R_1. For short waves, we may have conditions for which the radiation center T as well as the reception center R are as in Fig. 257. The altitudes h_t and h_r are then *no longer negligible in comparison with the range* r, and r and r_2 are no longer parallel. We deal then with a direct ray $TR = r$ and an image ray $T'R = r + d$, which are *not parallel* but make an angle $TRT' = \theta' - \theta$, where θ is the angle of incidence of ray $TG = r_1$ with respect to the normal to ground and θ' is the angle of the direct path $IR = r$ with respect to the normal to ground. The geometry and the associated formulas in Fig. 257 show that in order to satisfy the normal T_1A_1 of Fig. 256 on both the direct and the image rays, we must describe in Fig. 257 an arc TA about R, so that direct and image rays become perpendicular to this curved projection at T and at A. The foot point A then again divides the image path

$T'R$ into the path difference $T'A = d$ and a length AR, which is equal to the direct range r. Since the heights h_t and h_r are known[1] as well as the separation D, which for flat ground (short-distance communication) is horizontal, for curved earth (long-distance communication) D can be

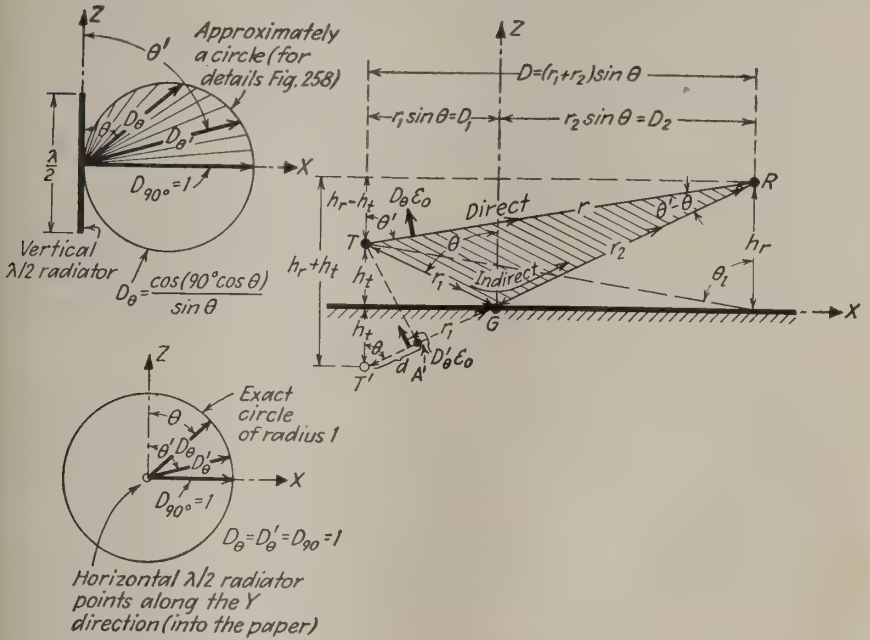

Direct Path $r = \sqrt{D^2 + (h_r - h_t)^2}$ $\qquad \theta' = \tan^{-1}\left(\frac{D}{h_r - h_t}\right) = \sin^{-1}\left(\frac{D}{r}\right)$

Indirect Path $r_1 + r_2 = \sqrt{D^2 + (h_r + h_t)^2}$ $\qquad \theta = \tan^{-1}\left(\frac{D}{h_r + h_t}\right) = \sin^{-1}\left(\frac{D}{r_1 + r_2}\right)$

Path Difference $d = r_1 + r_2 - r$; $\qquad = \sin^{-1}\left(\frac{D}{r + d}\right)$

FIG. 257. For relative short ranges at VHF's and UHF's, we must distinguish between θ' and θ, since TR and GR are no longer parallel (we have also a limiting angle θ_l). Phase delay of indirect field relative to direct field at R is $\Delta = \varphi° - 1.2fd°$. φ is phase jump at reflection point G. Straight-line propagation case ($n_0 = 1$). T and R are transmitting and reception centers; all dimensions are in meters and f is in Mc/sec.

taken parallel with the tangential plane through the reflection point G, where respective heights h_t and h_r are taken radial, or D can be taken as in the case for flat earth just as the directions of h_t and h_r, except that h_t and h_r are produced as far as to the tangential plane as is explained.[2]

[1] For irregular earth surface h_t and h_r are the distances to the tangential plane through the reflection point G. This point is so chosen that the angle of incidence is equal to the angle of reflection. For details consult A. HUND, "Frequency Modulation," p. 143 and Fig. 38, McGraw-Hill Book Company, Inc., New York, 1942.

[2] *Ibid.*

In each case, the geometry will lead to suitable expressions. According to Fig. 257, the path difference can be computed from

$$d = \sqrt{D^2 + (h_r + h_t)^2} - \sqrt{D^2 + (h_r - h_t)^2} \qquad \text{m} \quad (883b)$$

which for $D^2 \gg (h_r + h_t)^2$ and $(h_r - h_t)^2$ yields the approximation $d \cong 2h_t h_r/D$. This approximation however, does *not always apply* for the condition of Fig. 257 dealt with in this section. For any angle of incidence θ, we can compute the path length r_1 of the ground incident beam and the length r_2 of the reflected beam, since the distances D_1 and D_2 are known for given radiation center T and reception center R locations. Since $1.2f$, for f in megacycles per second, denotes the portion of the wave distribution along a linear path in air in degrees for each meter of the path, we find, for a phase "jump" φ degrees at the reflection point G, a phase delay

$$\Delta = \varphi^\circ - 1.2fd \qquad \text{deg}$$

which yields maximum resultant field intensities for $\Delta = 2 \times 180$, 4×180, 6×180, $\cdots$ deg, while field minima occur for $\Delta = 180$, 3×180, 5×180, $\cdots$ deg. We have different angles θ' and θ for the direct beam TR and the image beam $T'R$ and at the receiving center R a resultant field

$$\left.\begin{aligned}
&\mathcal{E}_R^{(\text{volts/m})} = \frac{D_{\theta'}\mathcal{E}_0}{r}\,\epsilon^{j(\omega t - \beta r)} + \frac{\rho_v D_\theta \mathcal{E}_0}{r+d}\,\epsilon^{j[\omega t + \varphi_v - \beta(r+d)]} \\
&\qquad\qquad \text{for vertical polarization} \\
&\mathcal{E}_R^{(\text{volts/m})} = \frac{\mathcal{E}_0}{r}\,\epsilon^{j(\omega t - \beta r)} + \frac{\rho_h \mathcal{E}_0}{r+d}\,\epsilon^{j[\omega t + \varphi_h - \beta(r+d)]} \\
&\qquad\qquad \text{for horizontal polarization} \\
&D_{\theta'} = \frac{\cos(90^\circ \cos\theta')}{\sin\theta'}; \qquad D_\theta = \frac{\cos(90^\circ \cos\theta)}{\sin\theta} \\
&\qquad\qquad \text{for a } \frac{\lambda}{2} \text{ radiator} \\
&\theta = \tan^{-1}\left(\frac{D}{h_r + h_t}\right) = \sin^{-1}\left(\frac{D}{r+d}\right); \\
&\theta' = \tan^{-1}\left(\frac{D}{h_r - h_t}\right) = \sin^{-1}\left(\frac{D}{r}\right)
\end{aligned}\right\} \quad (883c)$$

The application of (883c) is relatively simple. For the case of horizontal polarization over wet soil, we can use the reflection curves of Fig. 259 and note that for all angles of incidence, $\varphi_h = -180$ deg. Suppose we have a horizontal half-wave dipole 100 m above such soil (then $h_t = 100$ m) and we are interested in what happens at different altitudes at a horizontal separation of 2,000 m. Then $D = 2{,}000$ m. Since $\varphi_h = -180$ deg, we obtain field maxima for $1.2fd = 180$, 3×180, 5×180, $\cdots$ deg.

For a 100-Mc excitation, this may happen for a path difference $d = {}^{180}\!/_{120} = 1.5$ m, $3 \times 1.5 = 4.5$ m, $5 \times 1.5 = 7.5$ m, $7 \times 1.5 = 10.5$ m, 13.5 m, 16.5 m, 19.5 m, ... Minimum field effects occur for $1.2fd = 2 \times 180, 4 \times 180, 6 \times 180, \cdots$ deg. For a 100-Mc excitation, we find $d = {}^{360}\!/_{120} = 3$ m, 6 m, 9 m, $\cdots$ path difference. From a knowledge of $D = 2{,}000$ m and $h_t = 100$ m, we can compute the corresponding altitude h_r for the receiving center by means of formula (883*b*). This is by no means an *easy* numerical evaluation unless we can apply the approximation $d \cong 2h_th_r/D$. It should be noted that for the above numerical values of D and h_t, *not all* angles θ of incidence from 0 to 90 deg *are possible*, since according to Fig. 257, for angles $\theta = \theta_l$ and larger, *i.e.*, from this limiting angle on, a *reflected beam is no longer possible* for a horizontal separation D. This limiting angle is found from $\tan (90° - \theta_l) = h_t/D = 100/2{,}000 = 0.05$, yielding $90° - \theta_l \cong 2.9$ deg or $\theta_l = 87.1$ deg. For different possible angles of incidence, we then obtain the computations of Table 55. After finding the path difference d for 100 Mc/sec, we have $120d$ degrees time lag due to d. It is only the fractional portion of 360 deg that is of interest, since for every 360 deg we have the same phase condition again. For this reason, we consider only a corresponding length d_1 smaller than a full wavelength for each d value found in Table 55. If, therefore, we take the case for $\theta = 60$ deg incidence, we find first the ratio $d/\lambda = {}^{95}\!/_{3} = 31.667$. This means that the path difference d accounts for 31.667 wavelengths, or $31\lambda + 0.667\lambda$. Calling k the number of *complete* wavelengths in d, we have, in this case, $k = 31$; and calling k' the number of *fractional* wavelengths, we have $k' = 0.667$. We have the general relations

$$d = k\lambda + k'\lambda = k\lambda + d_1 \quad \text{m}; \qquad d_1 = d - k\lambda \quad \text{m} \qquad (883d)$$

Applying (883*d*) to the above example, we have $d_1 = 95 - k\lambda = 95 - 31 \times 3 = 2$ m, since $d_1 = k'\lambda = 0.667\lambda = 0.667 \times 3 = 2$ m. We use then only the portion d_1 and have

$$\Delta = \varphi - 1.2fd = \varphi - 1.2fd_1 \text{ deg} = -180 - 120 \times 2 = -420 \text{ deg}$$

It is only the excess over 360 deg or integer multiples of 360 deg that counts, and the phase delay is -60 deg or $\Delta = -60$ deg, since $-420 = -360 - 60$. For all values in Table 55 for which $d = k\lambda$ and $k = 1, 2, 3, 4, \ldots$, we have $\Delta = -180$ deg and a minimum resultant field $\mathcal{E}_R$. For $\theta = 10$ deg, we have antiphase conditions and find, for horizontal polarization, the maximum values

$$\mathcal{E}_{10°} = \frac{\mathcal{E}_0}{r} - \frac{\rho_h \mathcal{E}_0}{r + d} = \frac{\mathcal{E}_0}{r} - \rho_h \frac{r}{r + d}\frac{\mathcal{E}_0}{r} = \frac{\mathcal{E}_0}{r}\left(1 - \rho_h \frac{r}{r + d}\right)$$

$$= \frac{\mathcal{E}_0}{11{,}380}(1 - 0.695 \times 0.99) = 2.71 \times 10^{-5}\mathcal{E}_0 \qquad \text{volts/m}$$

The angle $\theta = 10$ deg in Table 55 corresponds to a reception center R, which is $h_r = 11.29$ km above ground. We used (883*c*) for this evaluation, with the reflection coefficient ρ. The coefficients for vertical as well as horizontal polarization are based on plane wave fronts. Therefore, not too much faith can be put in evaluations close to ground that

TABLE 55. TRANSMISSION OVER WET SOIL AND HORIZONTAL POLARIZATION*

θ, deg	$\sin\theta = \frac{D}{r+d}$	$\tan\theta = \frac{D}{h_r+h_t}$	$h_t+h_r = \frac{D}{\tan\theta}$ m	$h_r = \frac{D}{\tan\theta} - 100$ m	$r+d = \frac{D}{\sin\theta}$ m	$h_r-h_t = h_r - 100$ m	$\frac{D}{h_r-h_t} = a$ numeric	$\theta' = \tan^{-1}(a)°$	$\frac{D}{r} = \sin\theta$ numeric	$r = \frac{D}{\sin\theta'}$ m
10	0.1736	0.1763	11,390	11,290	11,500	11,190	0.179	10.15	0.176	11,380
20	0.342	0.364	5,510	5,410	5,840	5,310	0.376	20.6	0.3518	5,690
30	0.5	0.5774	3,475	3,375	4,000	3,275	0.610	31.4	0.512	3,905
40	0.6428	0.8391	2,385	2,285	3,100	2,185	0.916	42.5	0.6756	2,965
50	0.766	1.1918	1,680	1,580	2,610	1,480	1.35	53.5	0.8039	2,490
60	0.866	1.7321	1,158	1,058	2,310	958	2.09	64.45	0.9022	2,215
70	0.9397	2.7475	728	628	2,135	528	3.8	75.25	0.967	2,075
80	0.9848	5.6713	354	254	2,030	154	13	85.6	0.9971	2,010
85	0.9962	11.43	175	75	2,008	−25	−80	90.7	0.9999	2,000

θ, deg	Path difference $d = (r+d) - r$ m	$\frac{d}{\lambda} = \frac{d}{3}$ numeric	$d = \lambda(k+k')$ m	$d_1 = d - 3k = 3k'$ m	Time lag $\Delta = \varphi_h - 1.2fd_1 = -180 - 120d_1$ deg	From Fig. 259 ρ_h	$\frac{\mathcal{E}_0/(r+d)}{\mathcal{E}_0/r} = \frac{r}{r+d}$ numeric
10	120	40	$\lambda(40+0)$	0	−180	0.695	0.99
20	150	50	$\lambda(50+0)$	0	−180	0.705	0.97
30	95	31.667	$\lambda(31+0.667)$	2	$-(180+240) = -420$	0.725	0.979
40	135	45	$\lambda(45+0)$	0	−180	0.75	0.957
50	120	40	$\lambda(40+0)$	0	−180	0.785	0.952
60	95	31.667	$\lambda(31+0.667)$	2	−60	0.83	0.913
70	60	20	$\lambda(20+0)$	0	−180	0.88	0.975
80	20	6.667	$\lambda(6+0.667)$	2	−60	0.94	0.99
85	8	2.667	$\lambda(2+0.667)$	2	−60	0.97	1.000

* $D = 2{,}000$ m, $h = 100$ m, $f = 100$ Mc/sec, $\lambda = 3$ m (see Fig. 257).
Remarks: $-420° = -360° - 60°$ or $-60°$, in effect; $\lambda = {}^{30}\!/_{100} = 3$ m.

owing to its surface departure from plane ground, give, to begin with, a wave front of the reflected wave that is no longer plane. For $\theta = 20$ deg corresponding, according to Table 55, to a location $h_r = 5.41$ km of the receiving center above ground and $\theta = 40$ deg with $h_r = 2.285$ km altitude, we find in the same way

$$\left.\begin{aligned} \mathcal{E}_{20°} &= \frac{\mathcal{E}_0}{r}\left(1 - \rho_h \frac{r}{r+d}\right) = \frac{\mathcal{E}_0}{5{,}690}(1 - 0.705 \times 0.97) \\ &= 5.62 \times 10^{-5}\mathcal{E}_0 \\ \mathcal{E}_{40°} &= \frac{\mathcal{E}_0}{2{,}965}(1 - 0.75 \times 0.957) = 9.48 \times 10^{-5}\mathcal{E}_0 \end{aligned}\right\} \text{volts/m}$$

For $\theta = 70$ deg, corresponding to a reception center of altitude $h_r = 628$ m, we find

$$\mathcal{E}_{70°} = \frac{\mathcal{E}_0}{2{,}075}(1 - 0.88 \times 0.975) = 6.24 \times 10^{-5}\mathcal{E}_0 \quad \text{volts/m}$$

Taking the case for an incidence $\theta = 30$ deg corresponding to a reception altitude of $h_r = 3.375$ km, we must deal with a time delay of 60 deg, *i.e.*, a phase factor $\epsilon^{-j60°} = \cos 60° - j \sin 60° = 0.5 - j0.866$. We can then assume the field $\mathcal{E}_0/r$ of the direct wave at R along the real axis and the image field $\rho_h[r/(r+d)](\mathcal{E}_0/r)$ lagging 60 time degrees behind. Hence, we may add both fields as though in phase but must multiply the image field by $\cos \Delta = \cos 60° = 0.5$. This leads then to the formula for horizontal polarization, for any time delay,

$$\mathcal{E}_R^{(\text{volts/m})} = \frac{\mathcal{E}_0}{r}\left(1 + \rho_h \frac{r}{r+d} \cos \Delta\right) \tag{883e}$$

and the applications

$$\mathcal{E}_{30°} = \frac{\mathcal{E}_0}{3{,}905}(1 + 0.725 \times 0.979 \times 0.5) = 34.5 \times 10^{-5}\mathcal{E}_0 \quad \text{volts/m}$$

$$\mathcal{E}_{60°} = \frac{\mathcal{E}_0}{2{,}215}(1 + 0.83 \times 0.913 \times 0.5) = 62.2 \times 10^{-5}\mathcal{E}_0 \quad \text{volts/m}$$

$$\mathcal{E}_{80°} = \frac{\mathcal{E}_0}{2{,}010}(1 + 0.94 \times 0.99 \times 0.5) = 72.8 \times 10^{-5}\mathcal{E}_0 \quad \text{volts/m}$$

$$\mathcal{E}_{85°} = \frac{\mathcal{E}_0}{2{,}000}(1 + 0.97 \times 1 \times 0.5) = 74.25 \times 10^{-5}\mathcal{E}_0 \quad \text{volts/m}$$

$$\mathcal{E}_{50°} = \frac{\mathcal{E}_0}{2{,}490}(1 - 0.785 \times 0.952) = 10.1 \times 10^{-5}\mathcal{E}_0 \quad \text{volts/m}$$

showing well the minimum conditions in comparison with values corresponding to 60 deg time lag for the arriving image field. The maximum values for which inphase addition occurs, *i.e.*, for which $\cos \Delta = 1$, are completely missed for the angles θ of incidence used in Table 55.

It is now of interest to get numerical data for vertical polarization and to compare the results with those for horizontal polarization. From formula (883*c*), we note two essential differences, one with respect to the reflection coefficients ρ_v and ρ_h, for respective polarizations, and the other with respect to the two directions factors $D_{\theta'}$ and D_θ. We note from the curves in Fig. 259 that the magnitude of ρ_v varies over the total possible range, *i.e.*, 100 per cent. With respect to $D_{\theta'}$ and D_θ, both follow the same law for a given radiator length in terms of the wavelength distribution along it. But for the conditions of Fig. 257, the incidence θ is generally not at all equal to θ', since we deal with relatively short ranges r. By range is always meant the shortest distance from the radiation center T to the receiving center R in the case of rectilinear propagation. In the presence of atmospheric refraction, the actual direct path is curved and r is, in effect, the length of the curved path. If still longer ranges are obtained owing to diffraction, the ray theory

no longer applies. Figure 258 shows what happens for vertical polarization in comparison with a point-source radiator. Again calling $\mathcal{E}_0$ the hypothetical maximum reference field intensity at 1 m distance from the radiation center due to radiation *only* and based on the inverse distance law, the vertical radiation pattern is a circle in the ZX plane. The circle has a radius of $\mathcal{E}_0$ volts per meter, if T is the point source as well as the center of the circle (if taken for the conditon of 1 m distance). The space pattern is, therefore, a sphere. A point source is hypothetical

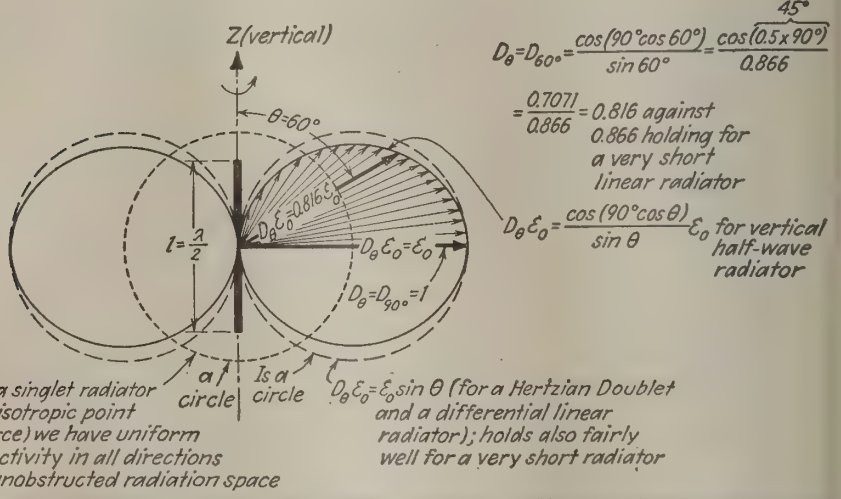
Z(vertical)
θ=60°
$D_\theta=D_{60°}=\frac{\cos(90°\cos 60°)}{\sin 60°}=\frac{\cos(0.5\times 90°)}{0.866}$
45°
$=\frac{0.7071}{0.866}=0.816$ against 0.866 holding for a very short linear radiator
$D_\theta\mathcal{E}_0=\frac{\cos(90°\cos\theta)}{\sin\theta}\mathcal{E}_0$ for vertical half-wave radiator
$D_\theta\mathcal{E}_0=0.816\mathcal{E}_0$
$D_\theta\mathcal{E}_0=\mathcal{E}_0$
$D_\theta=D_{90°}=1$
$l=\frac{\lambda}{2}$
For a singlet radiator (an isotropic point source) we have uniform Directivity in all directions in unobstructed radiation space
a circle
Is a circle
$D_\theta\mathcal{E}_0=\mathcal{E}_0\sin\theta$ (for a Hertzian Doublet and a differential linear radiator); holds also fairly well for a very short radiator

FIG. 258. Radiation patterns in any meridian plane for a half-wave radiator, a very short linear radiator, and a point source.

but a ready means of comparison with actual radiator actions. If we use a two-point source connected through a thin conductor of infinitesimal length, we have a Hertzian doublet radiator. We deal then with a fixed current distribution along the infinitesimal length. The doublet is, in effect, the same as an infinitesimal current element radiator. In either case, we find the meridian pattern made up of two circles each of radius $\mathcal{E}_0$ in the ZX meridian plane. Since these directivities apply to any meridian plane with the infinitesimal radiator element as the polar axis, we have again a space pattern that is the figure-8 pattern rotated about the Z axis. The 8 is lying down in this pattern. For an angle θ with the linear radiator, we have the relative field $D_\theta\mathcal{E}_0$, since the factor 2 in $2\mathcal{E}_0$ is fixed. The directivity of the infinitesimal linear radiator is then $D_\theta = \sin\theta$, and $D_\theta\mathcal{E}_0$ is the corresponding field effect $\mathcal{E}_0 \sin\theta$ in any θ direction. For a half-wave dipole or any half-wave radiator, we have in any meridian plane of the half-wave radiator $D_\theta\mathcal{E}_0 = [\mathcal{E}_0 \cos(90° \cos\theta)]/\sin\theta$. We can now proceed with Table 56 for vertical polarization. Some of the

TABLE 56. A VERTICAL HALF-WAVE RADIATOR AT AN ALTITUDE h_t METERS ABOVE WET SOIL FOR A HORIZONTAL SEPARATION $D = 2$ KM AND $f = 100$ MC/SEC, YIELDING $\lambda = {}^{300}/_{100} = 3$ METERS (FIG. 257)

θ, deg	$\sin\theta = \frac{D}{r+d}$	$\cos\theta$	$90° \cos\theta$	$\cos(90° \cos\theta)$ numeric	$D_\theta = \frac{\cos(90° \cos\theta)}{\sin\theta}$	Taken from Table 55					
						h_r, m	Path difference d, m	θ', deg	r, m	$r+d$, m	d_1, m
10	0.1736	0.9848	88.7	0.0227	0.1305	11,290	120	10.15	11,380	11,500	0
20	0.342	0.9387	84.3	0.0993	0.29	5,410	150	20.6	5,690	5,840	0
30	0.5	0.866	78	0.2079	0.416	3,375	95	31.4	3,905	4,000	2
40	0.6428	0.766	69	0.3584	0.556	2,285	135	42.5	2,965	3,100	0
50	0.766	0.6428	58	0.5299	0.69	1,580	120	53.5	2,490	2,610	0
60	0.866	0.5	45	0.7071	0.816	1,058	95	64.45	2,215	2,310	2
70	0.9387	0.342	30.8	0.859	0.912	628	60	75.25	2,075	2,135	0
$\theta_B = 79.7$	0.9839	0.1788	16.1	0.9608	0.975	262	21	85.5	2,011	2,032	0
80	0.9848	0.1736	15.7	0.9627	0.98	254	20	85.6	2,010	2,030	2
85	0.9962	0.0872	7.8	0.9907	0.999	75	8	90.7	2,000	2,008	2

θ, deg	Reflection coefficient Fig. 259		Time lag $\Delta = \varphi_v - 120d_1$, deg	$\frac{\varepsilon_0/(r+d)}{\varepsilon_0/r} = \frac{r}{r+d}$	$\cos\theta'$	$90° \cos\theta'$ deg	$\cos(90° \cos\theta')$	From Table 55 $\sin\theta'$	$D_{\theta'} = \frac{\cos(90° \cos\theta')}{\sin\theta'}$
	ρ_v	$\varphi_v°$							
10	0.691	0.0	0.0	0.99	0.9843	88.5	0.0262	0.176	0.149
20	0.69	0.0	0.0	0.97	0.9361	84	0.1045	0.3518	0.297
30	0.675	0.0	−240	0.979	0.8536	77	0.2250	0.512	0.439
40	0.62	0.0	0.0	0.957	0.7373	66.2	0.4035	0.6756	0.597
50	0.562	0.0	0.0	0.952	0.5948	53.5	0.5948	0.8039	0.74
60	0.47	0.0	−240	0.913	0.4312	38.9	0.7782	0.9022	0.861
70	0.311	0.0	0.0	0.975	0.2546	23	0.9205	0.967	0.952
$\theta_B = 79.7$	0.000	−90	−90	0.98	0.0785	7.06	0.9923	0.9969	0.995
80	0.018	−180	−(180 + 240)	0.99	0.0767	6.9	0.9928	0.9971	0.996
85	0.76	−180	−60	1.000	−0.999	−89.9	0.0017	0.9999	0.0017

Remarks: For the incidence of $\theta = 80$ deg, we find the time lag $\Delta = -(180 + 240)° = -420° = -360° - 60°$ = minus a complete cycle minus 60 deg. Therefore, $\Delta = -60$ deg, θ_B is the Brewster angle of incidence.

values of Table 55 can be used directly in Table 56 for vertical polarization. From the phase-delay values of Δ degrees in Table 56, we note that for the angles θ chosen, we have straight inphase additions for the direct and image field arrivals at the centers R in Fig. 257, which are 11.29, 5.41, 2.285, 1.58, and 0.628 km above ground if the horizontal separation D of radiation center T and reception center R is 2 km, since these altitudes correspond to $\Delta = 0$ deg delay. At the Brewster inci-

dence $\theta_B = 79.7$ deg, the down-coming wave energy goes completely into the wet soil; and at the reception center R, only the direct field can be effective.

For any possible angle θ of ground incidence, formula (883c), expressed in amplitude[1] values, yields then for vertical polarization

$$\mathcal{E}_R = \frac{D_{\theta'}\mathcal{E}_0}{r} + \frac{\rho_v D_\theta \mathcal{E}_0}{r+d}\,\epsilon^{j\Delta} \qquad \text{volts/m}$$

In the factor $\epsilon^{j\Delta} = \cos\Delta + j\sin\Delta$, it is the *real* part that counts, and realizing that

$$\frac{\mathcal{E}_0}{r+d} = \frac{r}{r+d}\,\frac{\mathcal{E}_0}{r}$$

leads to the formula for vertical polarization

$$\mathcal{E}_R = \frac{\mathcal{E}_0}{r}\left(D_{\theta'} + \rho_v \frac{r}{r+d} D_\theta \cos\Delta\right) \qquad \text{volts/m} \qquad (883f)$$

Applying this result for a height $h_r = 11.29$ km, we note from Table 56 that such a location of the receiving center R corresponds to a phase delay $\Delta = 0$ deg, yielding $\cos\Delta = 1$ and $\theta = 10$ deg. We have then $r = 11.38$ km, $r + d = 11.5$ km, $D_\theta = 0.1305$, $D_{\theta'} = 0.149$, and $\rho_v = 0.691$. This gives the solution

$$\mathcal{E}_{10} = \frac{\mathcal{E}_0}{11{,}380}\left(0.149 + \frac{0.691 \times 11.38 \times 0.1305}{11.5}\right) = 2.08 \times 10^{-5}\mathcal{E}_0$$

volts/m

At an altitude $h_r = 262$ m for the receiving center R in Fig. 257, we have $\rho_v = 0$, since $\theta = \theta_B = 79.7$ deg is the polarization angle and only the direct field can arrive at R. We have then

$$\mathcal{E}_{79.7^\circ} = \frac{\mathcal{E}_0}{r} D_{\theta'} = \frac{\mathcal{E}_0}{2{,}011}\,0.995 = 49.5 \times 10^{-5}\mathcal{E}_0 \qquad \text{volts/m}$$

Computing the resultant receiving field $\mathcal{E}_R$ for all other significant angles of incidence (for obtaining a curve), we find by means of (883f) the comparisons given in Table 57. It will be noted that formula (883f) also holds for horizontal polarization if we replace ρ_v by ρ_h and φ_v by φ_h. We then have also the directivities $D_{\theta'}$ and D_θ equal to unity. If we compare the time delay Δ in Tables 55 and 56, we note that for wet soil (for short waves) and generally for all ground, the soil behaves like a quasi-dielectric mirror. The direct and indirect fields act against each other for certain angles of incidence ($\theta = 10$, 20, 40, 50, 70 deg) in the

[1] The effective field at R is $\mathcal{E}_R/1.4142$ volts per meter.

case of horizontal polarization. For vertical polarization, we have algebraic additions of the fields. Such addition means maximum field gain due to the full image field, while antiphase conditions ($\Delta = -180$ deg) means a loss of field intensity due to destructive interference of the reflected wave at R with the direct wave. Therefore, if we use a 45-deg radiator with respect to ground (a 45-deg electric polarization breaks up into a horizontal and a vertical $\mathcal{E}$ field), we obtain the benefits inherent

Table 57. Resultant Space Field Intensity for Vertical and Horizontal Polarizations and Wet Ground, *i.e.*, Wet Soil

Altitude h_r of receiving center R, m	θ, deg	Vertical polarization						Horizontal polarization $\mathcal{E}_R \times 10^{-5}\mathcal{E}_0$, volts/m
		$\frac{r}{r+d}$	$\cos\Delta$	$D_{\theta'}$	r	$\rho_v \frac{r}{r+d} D_\theta \times \cos\Delta$	$\mathcal{E}_R \times 10^{-5}\mathcal{E}_0$, volts/m	
11,290	10	0.99	1	0.149	11,380	0.089	2.08	2.71
5,410	20	0.97	1	0.297	5,690	0.194	8.65	5.62
3,375	30	0.979	0.5	0.439	3,905	0.1375	7.7	34.5
2,285	40	0.957	1	0.597	2,965	0.329	31.25	9.48
1,580	50	0.952	1	0.74	2,490	0.37	44.7	10.1
1,058	60	0.913	0.5	0.861	2,215	0.176	30.8	62.2
628	70	0.975	1	0.952	2,075	0.277	59.2	6.24
262	79.7	0.98	0	0.995	2,011	0.000	49.5	*
254	80	0.99	0.5	0.996	2,010	0.087	53.6	72.8
75	85	1.000	0.5	0.0017	2,000	0.19	9.58	74.25

* Brewster angle of 79.7 deg has no reference to horizontal polarization.

Remarks: For a horizontal separation D = 2,000 m, a fixed radiation center altitude h_t = 100 m, a variable receiving center altitude h_r, f = 100 Mc/sec.

with either type of polarization. The field pattern over ground will then not show pronounced minima and maxima effects. Figure 259 is a plot for the resultant field intensity $\mathcal{E}_R$ at the reception center R for either type of polarized radiation, together with the reflection curves (which are effective at 100 Mc/sec and higher over wet soil). The angle θ of wave incidence is also marked with the corresponding altitude h_r of the reception center R for a 2,000-m horizontal spacing between radiation and reception centers. It is understood that the straight connection lines between $\mathcal{E}_R$ points of same polarization are *only field values, where marked*, since extreme values and between values of $\mathcal{E}_R$ are missed by using only 10-deg intervals for the θ values of Tables 55 to 57. The $\mathcal{E}_R$ fluctuations with altitude h_r and a fixed transmitter altitude h_t are more pronounced for vertical polarization, since we have "hit" some direct algebraic additions of direct and image fields of arrival, but we

have completely missed altitudes of algebraic subtraction (minimum effects). In Table 56, we have found only time delays $\Delta = 0$ deg, -60 deg, and -240 deg. Since $\epsilon^{j\Delta} = \epsilon^{-j60°} = \cos 60° - j \sin 60°$, we have to multiply the arriving image field by 0.5. For the phase factor

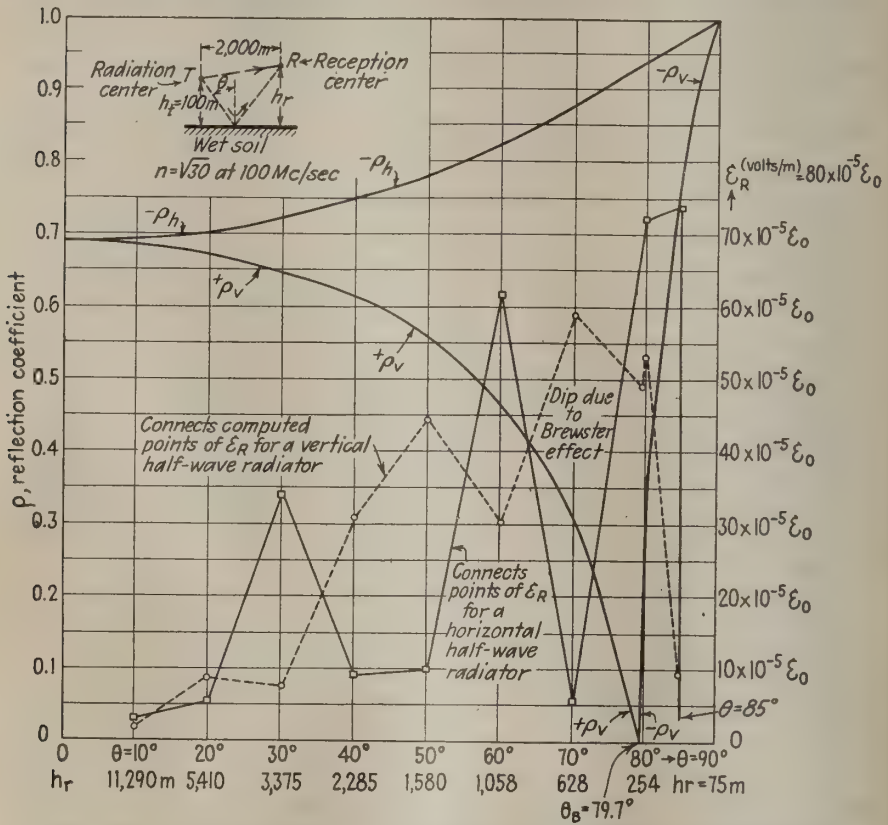

FIG. 259. Resultant space field for a 100-megacycle wave propagation over wet ground for a horizontal and a vertical half-wave radiator. Only ○ and □ points have a meaning.

$\epsilon^{j\Delta} = \epsilon^{-j240°} = \cos 240° - j \sin 240°$, we have to multiply the arriving image field by (-0.5). For horizontal polarization, we have completely missed the maximum conditions (algebraic additions), but have hit several minimum conditions (corresponding to $\Delta = -180$ deg, antiphase conditions). We also note that $\theta = 10$ deg gives a minimum and $\theta = 20$ deg gives another minimum condition for horizontal polarization. Hence, $\theta = 15$ deg looks like a reasonable angle for expecting either another minimum resultant effect $\Delta = -180$ deg or a maximum effect, for which $\Delta = -360$ deg or any integer multiple of it. We then find, just as in Table 55, $\theta = 15$ deg, $\sin 15° = 0.2588 = D(r + d)$,

tan 15° = 0.2679 = $D/(h_r + h_t)$, $h_t + h_r$ = 2,000/0.2588 = 7,480 m, yielding h_r = 7,380 m, $r + d = D/\sin\theta$ = 2,000/0.2588 = 7,750 m, $D/(h_r - h_t)$ = 2,000/7,280 = 0.275 = tan θ', θ' = 15.4 deg, sin θ' = 0.2656 = D/r, r = 2,000/0.2656 = 7,510, which renders $(r + d) - r = d$ = 7,750 − 7,510 = 240 m, $d/\lambda = 240/3 = 80$ full wavelengths, giving *another* $\Delta = -180$-deg condition, since $d_1 = 0$. From Fig. 259, we find for θ = 15 deg, the coefficient $\rho_h = -0.7$, the *minus* sign expressing *antiphase* condition, *i.e.*, $\Delta = -180$ deg. We have then for the resultant field at R, which is 7,380 m above the ground,

$$\mathcal{E}_{15^\circ} = \frac{\mathcal{E}_0}{7{,}510}\left(1 - 0.7\,\frac{7{,}510}{7{,}750}\right) = 4.25 \times 10^{-5}\mathcal{E}_0 \qquad \text{volts/m}$$

From the values θ and θ' in Table 55, we note that the difference $\theta' - \theta$, even for this short distance D = 2,000 m, is relatively small, being a maximum for θ = 85 deg. We have then $\theta' - \theta$ = 90.7 − 85 = 4.7 deg, which is $47/85$ = 5.52 per cent only of the angle of incidence. For the other extreme, which is θ = 10 deg, we have $\theta' - \theta$ = 0.15 and $15/10$ = 1.5 per cent only of the angle of wave incidence. Therefore, for larger horizontal separations, say D = 10 km and more, little error is made by assuming $\theta' - \theta \cong 0$ deg. This means that the direct and the reflected rays are parallel, and we can use formula (883). The error for θ = 85 deg is then found, according to the formulas and the geometry of Fig. 257, as

$$h_t + h_r = \frac{D}{\tan\theta} = \frac{10{,}000}{11.43} = 875 \text{ m}$$

yielding h_r = 775 m and $h_r - h_t$ = 675 m; hence

$$\theta' = \tan^{-1}\left(\frac{D}{h_r - h_t}\right) = \tan^{-1}\left(\frac{10{,}000}{675}\right) = \tan^{-1}(14.8) = 86.15^\circ$$

and the error is $115/85$ = 1.35 per cent only. A horizontal separation of 10 km corresponds to a distance of only 6.214 statute miles. For a horizontal separation of 10 miles and more and a transmitter location as in this example, the parallelism of direct and reflected ray is then a justified assumption.

168. Numerical Examples of the Resultant Space Field for Large Angles of Wave Incidence. This condition corresponds to the geometry of Fig. 257, where the incident TG and the reflected GR rays make comparatively small angles with the tangential plane through the reflection point G if curved earth is taken. The tangential plane is then the XY plane of Fig. 257, the Y axis being normal to the paper. Suppose we assume a horizontal distance D = 20 km and take the location of the

radiation center T such that $h_t = 100$ m. The limiting angle θ_l, from which reflections are *no longer possible*, is then $\theta_l = \tan^{-1}(D/h_t) = \tan^{-1}(200) = 89.7$ deg. This angle requires that $h_r = 0$. If we work with a vertical half-wave dipole, in the case of 100-Mc waves, the lower end of the $\frac{1}{2}\lambda$ antenna must at least clear the ground.

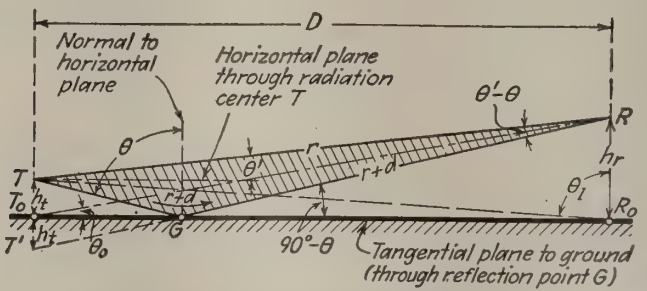

FIG. 260. The shaded path triangle is shown exaggerated, since $\theta' - \theta$ is vanishing in our application. $TR = r$; $TG + GR = r + d = T'R$; d is path difference; θ_l limiting angle $90° - \theta_l = \tan^{-1}(h_t/D)$; $\theta_l = 89.7°$; $D = 20{,}000$ m; $h_t = 100$ m.

Inasmuch as we are interested only in rays for which θ is large (close to 89.7 deg), we find that for $(h_r + h_t)^2$ as well as for $(h_r - h_t)^2 \ll D^2$, the indirect path in Fig. 257 as well as the direct path is

$$\left.\begin{aligned} r_1 + r_2 = \sqrt{D^2 + (h_r + h_t)^2} &= D\sqrt{1 + \frac{(h_r + h_t)^2}{D^2}} \\ &\cong D\left[1 + \frac{1}{2}\frac{(h_r + h_t)^2}{D^2}\right] \\ r = \sqrt{D^2 + (h_r - h_t)^2} &\cong D\left[1 + \frac{1}{2}\frac{(h_r - h_t)^2}{D^2}\right] \end{aligned}\right\} \qquad (883g)$$

with a path difference

$$d = r_1 + r_2 - r; \qquad d \cong \frac{2h_t h_r}{D} \quad \text{m}$$

This formula is easy to evaluate numerically, compared with the rigorous formula (883*b*). We find then for the above values of $D = 20{,}000$ m and $h_t = 100$ m, the expression $d = 10^{-2}h_r$ meters. For a reflector that is good enough as a conductor compared with its dielectric effect, we have $\varphi_h = -180$ deg for horizontal polarization and $\varphi_v = 0$ for vertical polarization. Relation (883*g*) is then a ready means of finding at which altitudes of the receiving center we have inphase and antiphase additions of the direct and indirect fields, since

$$\left.\begin{aligned}
\Delta^\circ &= -2.4\frac{fh_th_r}{D} && \text{for } \textit{vertical} \text{ polarization (for } \textit{good} \text{ conducting medium)}\\
\Delta^\circ &= -180^\circ - 2.4\frac{fh_th_r}{D} && \text{for } \textit{horizontal} \text{ polarization (for } \textit{good} \text{ conducting medium)}\\
\Delta^\circ &= \varphi_v - \frac{2.4fh_th_r}{D} && \text{for } \textit{vertical} \text{ polarization (for any ground and general medium)}\\
\Delta^\circ &= \varphi_h - \frac{2.4fh_th_r}{D} && \text{for } \textit{horizontal} \text{ polarization (for any ground and general medium)}
\end{aligned}\right\} \quad (883h)$$

The time phase angles φ_v and φ_h are taken from curves or computed as is shown at different places of this text. For a fixed radiation center height h_t, we can also express (883h) in terms of the angle θ of wave incidence and find, according to (883),

$$\left.\begin{aligned}
\Delta^\circ &= \varphi_v - 2.4fh_t\cos\theta && \text{for } \textit{vertical} \text{ polarization}\\
\Delta^\circ &= \varphi_h - 2.4fh_t\cos\theta && \text{for } \textit{horizontal} \text{ polarization}
\end{aligned}\right\} \quad (883i)$$

since in Fig. 260, for large angles θ of wave incidence and $(h_r + h_t)^2 \ll D$, we have $\theta' - \theta \cong 0$ and GR practically parallel with TR. Hence, any line, such as T_0R, within this vanishing angular spread $\theta' - \theta$ must also be parallel with GR. Therefore, $\theta_0 = 90^\circ - \theta$, and the ratio h_r/D in (883h) gives

$$\frac{h_r}{D} = \tan\theta_0 = \tan(90^\circ - \theta) = \frac{\pi}{2} - \theta \qquad \text{radians (numeric)}$$

This is the case because $90^\circ - \theta$ is very small, since θ is close to 89.7 deg or 89.7/57.3 = 1.56 radians. But $\pi/2 - \theta = 1.57 - 1.56 = 0.01$ radian. An inspection of trigonometric tables discloses that even 4 deg or 4/57.3 = 0.0699 radian checks exactly the value tan 4 deg = 0.0699. Therefore, the approximation $h_r/D \cong 0.5\pi - \theta$ radians holds at least for angles of θ_0 up to 4 deg, as a matter of fact somewhat higher. We have then $\tan\theta_0 \cong \sin\theta_0 \cong \theta_0$ radians and, therefore, $h_r/D = \sin\theta_0 = \sin(90^\circ - \theta) = \cos\theta$, proving that (883$i$) is actually also the outcome of (883h) because $\cos\theta = h_r/D$ for wave incidences that make small angles with the tangential plane through G of the ground.

Formulas (883i) have the advantage that for any ground, we can find the time delay of the image field arrival with respect to the direct field arrival at a possible space point of reception if we know the location of the radiation center T and the angle θ of incidence. Formula (883h) requires, however, the knowledge of h_t, h_r, and D. The case of $\theta_0 =$ 4 deg corresponds to $\theta = 86$ deg, giving a distance $T_0G = h_t/\tan\theta_0 =$ 100/0.0699 = 1,435 m and $GR_0 = 20{,}000 - 1{,}435 = 18{,}565$ m. Since

tan 4 deg is also equal to $h_r/18{,}565$, we find $h_r = 18{,}565 \times 0.0699 \cong 1{,}300$ m. This yields $h_t + h_r \cong 1{,}400$ m and $(h_t + h_r)^2 = 196 \times 10^4$ as against $D^2 = 4 \times 10^8$, making D^2 about $(4 \times 10^8)/(196 \times 10^4) = 204$ times larger than $(h_r + h_t)^2$ and still larger than $(h_r - h_t)^2$. Therefore, for angles of incidence between 86 and 89.7 deg, formulas (883*h*) and (883*i*) can be used. Inasmuch as in a general medium with a relative index of refraction $n = \sqrt{\kappa_r - jq}$ with $q = 1.8 \times 10^4(\sigma/f)$ and f in megacycles per second, we can distinguish between the extremes $n \cong \sqrt{\kappa_r}$ and $n \cong \sqrt{-jq}$, we have at VHF's and UHF's quite a frequency range, where the condition $n \cong \sqrt{-jq}$ applies as for ocean water and $n \cong \sqrt{\kappa_r}$ holds surely above 100 Mc/sec and even somewhat below. Therefore, when the conduction term q outweighs the effect of the κ_r value, which acts in quadrature, we have the conditions

$$\left.\begin{aligned} &\frac{2.4fh_th_r}{D} = 2.4fh_t \cos\theta = 180k \\ &\text{for } k = 1, 3, 5, 7, \cdots \begin{cases} \textit{in}\text{phase conditions } (\mathcal{E}_R \text{ maxima}) \\ \text{for } \textit{horizontal} \text{ polarization} \\ \textit{anti}\text{phase conditions } (\mathcal{E}_R \text{ minima}) \\ \text{for } \textit{vertical} \text{ polarization} \end{cases} \\ &\text{for } k = 0, 2, 4, 6, \cdots \begin{cases} \textit{anti}\text{phase conditions } (\mathcal{E}_R \text{ minima}) \\ \text{for } \textit{horizontal} \text{ polarization} \\ \textit{in}\text{phase conditions } (\mathcal{E}_R \text{ maxima}) \\ \text{for } \textit{vertical} \text{ polarization} \end{cases} \end{aligned}\right\} \quad (883j)$$

But if we deal with ground effects that are caused by *dielectric* mirror reflections, as, for instance, in Fig. 259, for short waves and wet soil as well as dry soil, when the κ_r value for such soil is used, we have a half-wavelength jump, at the reflection point for all angles of wave incidence θ in the case of horizontal polarization. According to Fig. 259, we also have a half-wavelength loss (which is a half-cycle loss) for vertical polarization, for wave incidence θ beyond the Brewster angle $\theta_B = 79.7$ deg, *i.e.*, for $\theta = >79.7$ deg up to 86 deg. We have resultant field $\mathcal{E}_R$ maxima for either polarization for $k = 1, 3, 5, 7, \cdots$ and $\mathcal{E}_R$ minima for $k = 0, 2, 4, 6, \cdots$. For *dry* ground, the actual relative dielectric constant κ_r has values from about 5 to 8, and the Brewster angle has an average value $\theta_B = \tan^{-1}\sqrt{6.5} = \tan^{-1} 2.55 = 68.6$ deg. At all UHF's and a good range of the VHF's, dry ground then acts as a quasi-dielectric mirror; and for possible angles between 68.6 to 90 deg of wave incidence we have, as for horizontal polarization, a -180-deg phase jump upon reflection. If the UHF is very high, we have, for ocean, $n \cong \sqrt{80}$ with a quasi Brewster angle of $\theta_B = \tan^{-1} 8.944 = 89.45$ deg. This means that for most angles of wave incidence for which the ocean surface

acts as a dielectric mirror, we have no phase change at the reflection point in the case of *vertical* polarization. Only in the range >89.45 to 90 deg (a 0.55 deg range), which is essentially tangential incidence ,we have a 180-deg phase jump or a phase reversal. Taking $\sigma = 4$ mhos/m as the average conductivity for ocean, we find an equivalent relative dielectric constant $\kappa'_e = 80 - j7.2[10^4/f^{(\text{Mc})}]$, which, for $f = 90{,}000$ Mc/sec, yields $\kappa'_e = 80 - j0.8$. If we call the quadrature effect of 0.8 negligible in comparison with the real value of 80, the ocean behaves for this and higher frequencies as a quasi-dielectric mirror as far as wave reflections are concerned. Since, in (833j), the magnitude $2.4fh_th_r/D$ determines the maximum and minimum resultant field intensity $\mathcal{E}_R$ locations, we find that for numerical dimensions $D = 20{,}000$ m and $h_t = 100$ m, we have $fh_r = 15{,}000k$ or

$$h_r = \frac{1.5 \times 10^4 k}{f^{(\text{Mc/sec})}} \quad \text{m} \tag{883k}$$

Therefore, for the reflector in effect essentially only conductive ($n \cong \sqrt{-jq}$), we find from (883j) the first maximum field conditions for $k = 1$. We find this to be the case at 50 Mc/sec, since, for ocean, $\kappa'_e = 80 - j7.2(10^4/50) = 80 - j1{,}444$, where the quadrature effect of 1,444 is dominant in comparison with the effect of 80, since we have $10\sqrt{64 + 20{,}881} \cong 10\sqrt{20{,}881} = 1{,}444$. According to (883$k$), we find then that the first maximum field condition occurs at a receiving center altitude $h_r = 1.5(10^4/50) = 300$ m. The second maximum field condition occurs at $h_r = 3 \times 300 = 900$ m; the next at $5 \times 300 = 1{,}500$ m; etc. Minimum resultant filed effects occur for $k = 0, 2, 4, \cdots$, and we find the first minimum for $k = 0$ or $h_r = 0$. The second minimum occurs for $k = 0$, corresponding to an altitude of the receiving center of $h_r = 1.5 \times 10^4 \times \frac{2}{50} = 600$ m; the third at 1,200 m; the fourth at 1,800 m; etc. All minimum field values are halfway between the altitudes holding for maximum field effects. These heights correspond to definite angles θ of incidence, since, according to (883j), we have for $h_t = 100$ m in place of (883k), the expression

$$\cos\theta = \frac{0.75k}{f^{(\text{Mc})}} \tag{883l}$$

For 50-Mc waves, we find then the first maximum for an angle of incidence $\theta = \cos^{-1}(0.75/50) = \cos^{-1}(0.015) \cong 89.1$ deg, which is an incident ground ray almost parallel with the tangential ground or ocean plane. This angle could also have been found by means of the corresponding value $h_r = 300$ m for the first field maximum, since, in Fig. 260 for $\theta' - \theta = 0$ on which condition relations (883j), (883k), and (883l) are

based, $\tan \theta_0 = \tan (90° - \theta) = h_r/D = 300/20{,}000 = 0.015$, giving $90° - \theta \cong 0.9$ deg or $\theta = 90° - 0.9 = 89.1$ deg, as found above.

We note that for $f = 50$ Mc/sec, we deal with very small angles with respect to the horizon. For the second maximum, (883l) yields $\theta = \cos^{-1} (3 \times 0.015) \cong 87.4$ deg. For the third maximum, we find $\theta = \cos^{-1} (5 \times 0.015) = 85.7$ deg. The fourth maximum yields $\theta = \cos^{-1} (7 \times 0.015) \cong 84$ deg. As far as the incidence $90° - \theta$ with respect to the horizon is concerned, we have the successive maximum resultant space field conditions $90° - \theta = 0.9$, 2.6, 4.3, 6, · · · degrees, with a difference of 1.7 deg, which are, *indeed, very small angular steps.* The first minimum value happens for $k = 0$, and (883l) yields $\cos \theta = 0$ or $\theta = 90$ deg, *i.e.*, tangential wave incidence with the surface of the ocean. The second minimum field condition occurs for $k = 2$, and (883l) yields $\cos \theta = 0.75 \times \frac{2}{50}$ or $\theta = \cos^{-1} (0.03) = 88.3$ deg. This value is to be expected because 1.7 deg $= 90° - \theta$ is halfway between the first and the second maximum condition. The third minimum occurs for $\theta = \cos^{-1} (0.75 \times 4/50) = \cos^{-1} (0.06) \cong 86.5$ deg. Formula (883l) shows that respective angles θ for maximum and minimum resultant field conditions move all the *closer* toward more grazing incidence the *higher the frequency* f is chosen, as long as the frequency still exercises a q value that is dominant in comparison with the κ_r value of the reflecting medium. Owing to the limiting angle θ_l of wave incidence (largest angle of incidence in Fig. 260, for a given horizontal separation D), the reflections may cover only angles that are more or less away from incidences close to the grazing incidence. This limiting angle is $\theta_l = 89.7$ deg in the above numerical example. We can, therefore, also realize the first field maximum and all other maxima, since we found that the values $\theta = 89.1$, 87.4, 85.7, 84, · · · deg. Therefore, all receiving centers R with altitudes 300, 900, 1,500, · · · m exist above the reflector. It must be realized that our reflection formulas are based on plane electromagnetic waves. The distance TG in Fig. 260 must be large enough so that a plane wave front exists at least over an area equal to the square of a wave-

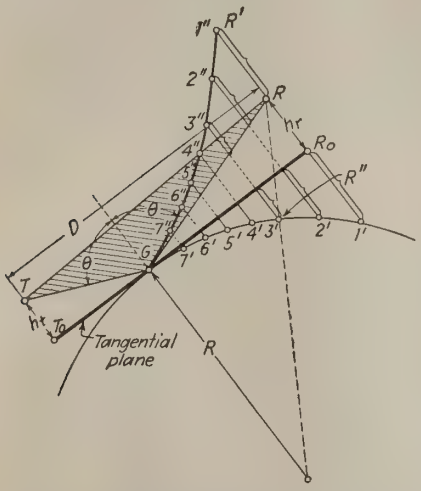

FIG. 261. Reflected beam GR is curved up just as much as the spherical earth surface is below the tangential plane, and G7''6''5'' . . . R' is the equivalent beam.

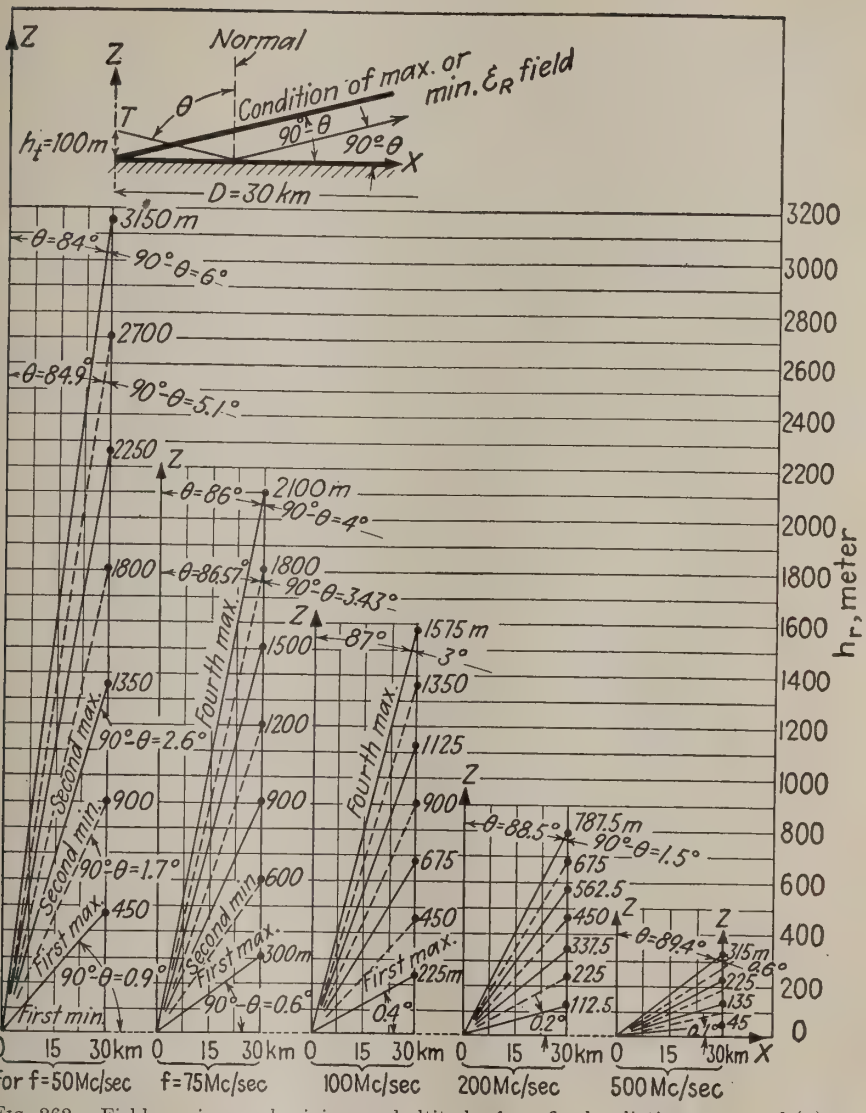

FIG. 262. Field maxima and minima and altitudes for a fixed radiation center. $h_r^{(m)} = 75kD/h_tf = 22{,}500k/f$; $\theta° = \cos^{-1}(0.75k/f)$. D, h_t, and h_r are in meters; f is in Mc/sec. Formulas hold for $(h_t + h_r)^2 \ll D^2$.

length, with no dimension of this area less than a wavelength. To increase the horizontal distance changes nothing in the above formulas, since the plane T_0GR_0 in Fig. 260 is the tangential plane to spherical ground, and we have then the conditions shown in Fig. 261. The reflected beam GR is then taken "curved-up" just as much *over* the tan-

TABLE 58. FIELD MAXIMA AND MINIMA AND ALTITUDES OF RECEPTION CENTER R FOR A FIXED RADIATION CENTER ALTITUDE

Frequency, f, Mc/sec	First maximum $k = 1$		Second Maximum $k = 3$		Third maximum $k = 5$		Fourth maximum $k = 7$		First minimum	Second Minimum $k = 2$		Third minimum $k = 4$		Fourth minimum $k = 6$	
	θ, deg	h_r, m	θ, deg	h_r, m	θ, deg	h_r, m	θ, deg	h_r, m		θ, deg	h_r, m	θ, deg	h_r, m	θ, deg	h_r, m
50	89.1	450	87.4	1,350	85.7	2,250	84	3,150	$k = 0$; $h_r = 0$	88.3	900	86.57	1,800	84.9	2,700
75	89.4	300	88.3	900	87.1	1,500	86	2,100	$\cos\theta = 0$	88.85	600	87.7	1,200	86.57	1,800
100	89.56	225	88.71	675	87.15	1,125	87	1,575	$\theta = 90°$	89.11	450	88.28	900	86.43	1,350
200	89.8	112.5	89.4	337.5	89	562.5	88.5	787.5		89.6	225	89.1	450	88.7	675
500	89.9	45	89.75	135	89.6	225	89.4	315		89.8	90	89.65	180	895	270

Remarks: This table is based on (883j), which reads

$$\frac{2.4fh_th_r}{D} = 180k; \qquad \frac{h_r}{D} = \cos\theta$$

where f is in Mc/sec and $h_t = 100$ m.

$$D = 30{,}000 \text{ m}; \qquad h_r = \frac{22{,}500k}{f} \text{ m}; \qquad \theta = \cos^{-1}\left(\frac{0.75k}{f}\right)$$

Maxima for $k = 1, 3, 5, \cdots$; minima for $k = 0, 2, 4, \cdots$.

The lower frequency values hold for ocean as a reflector, while the upper frequency values give only rough approximations, since the q value becomes smaller as f increases and $\kappa_r = 80$.

gential plane GR_0 as the spherical surface $G7'6'5'4'3'2'1'$ is *below* this plane. We may also take the reception center location height as RR'', which is perpendicular to the spherical earth surface.

In Table 58, the respective reception altitudes h_r and the correspond-

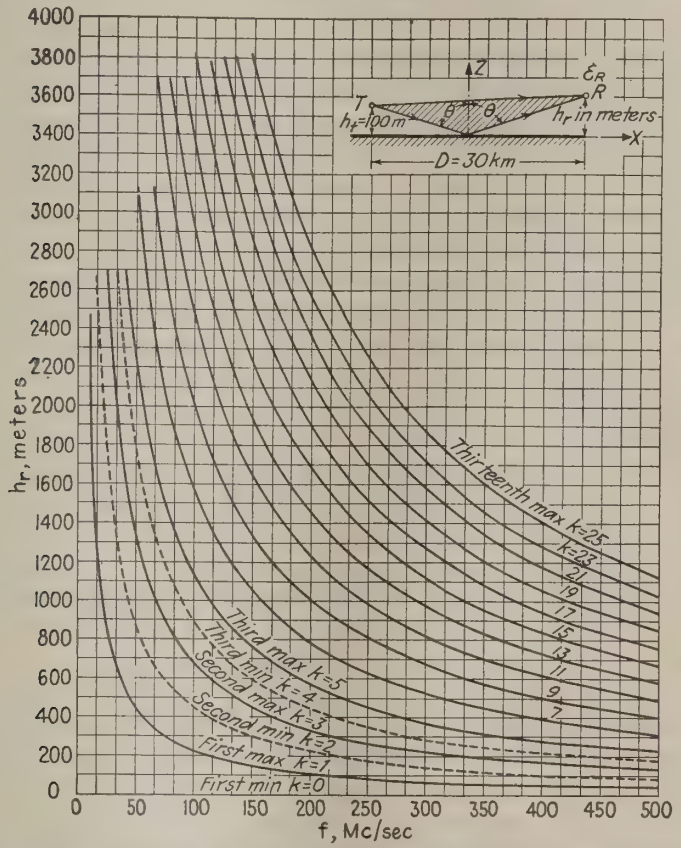

FIG. 263. Height of receiving center for maximum and minimum resultant field intensity dependent on frequency. $h_r^{(m)} = 75kD/h_tf = 22{,}500k/f$ for h_t and D in meters and f in Mc/sec assumes one half-wavelength loss upon reflection (holds for wet soil for horizontal polarization). Maxima for $k = 1, 3, 5, 7, 9, \ldots$; minima for $k = 0, 2, 4, 6, 8, \ldots$. *Note:* curves hold also for vertical polarizations, since θ is larger than Brewster angle θ_B for $(h_t + h_r)^2 \ll D^2$.

ing angles θ are given for a radiation center altitude $h_t = 100$ m and $D = 30$ km, for *horizontal* polarization and *different frequencies*. Figure 262 gives the results of this table. The abscissa unit in this figure is *greatly reduced* compared with the ordinate unit, because the angles $90° - \theta$ with respect to the tangential ground plane are small and require exaggeration in order to bring out details. From the directions in the

vertical ZX plane for maximum and minimum resultant field values, we note that at 50 Mc/sec, the angle of the reflected ray with the horizon is only 0.9 deg and only 5.1 deg for the fourth $\mathcal{E}_R$ maximum condition; while at 500 Mc/sec, the corresponding angles are 0.1 and 1.5, respectively. Hence, for a fixed radiation center location, the vertical radiation lobes are *more* crowded toward the horizon the *higher the frequency.* The maxima and minima conditions hold for horizontal polarization. As mentioned in Table 58, the frequency range is taken to quite a high value, so that the upper portion of the range is somewhat affected by the dielectric effect of the reflecting medium. The error made is, however, not great, and we have a comparison that shows the effect of the frequency on the space distribution of extreme field values. Figure 263 gives a plot for 13 maxima with minima values halfway between consecutive maxima. This corresponds to 13 lobes in the vertical ZX plane. These curves give directly the height h_r of the receiving center R, for a radiation center altitude $h_t = 100$ m and a horizontal separation $D = 30$ km. The height at any other distance can be found, as in Fig. 262, by scaling off along the abscissa axis the horizontal separation $D = 30{,}000$ m from the origin and making the ordinate equal to h_r meters for the abscissa D for a certain frequency taken from Fig. 263. The hypotenuse from the origin to the point found in this way then gives the locus for the various heights h_r for different separations D if atmospheric refraction is negligible, *i.e.*, rectilinear propagation prevails.

169. Numerical Data on Vertical Radiation Patterns over Actual Ground. If we take wet ground with $\kappa_r = 30$ and $\sigma = 10^{-3}$ mho/m, the relative equivalent dielectric constant becomes $\kappa_e' = 30 - j1.8 \times 10^4(10^{-3}/100) = 30 - j0.18 \cong 30$ for 100 Mc/sec and higher. The reflection curves of Fig. 259 then apply. From Table 58 and Fig. 262, we note that the first field maximum occurs for horizontal polarization for an angle $\theta = 89.56$ deg and the first minimum exists for $\theta = 0$ deg. We have, for such conditions, the arriving image field in phase and in antiphase, respectively, with the arriving direct field at the reception center R. If we desire the radiation pattern for three vertical lobes, we must cover, according to Table 58, the angle up to the fourth minimum. This is an angular range from $\theta = 90$ to $\theta = 87.4$ deg. We compute the time delay from (883), which reads

$$\Delta = -(180 + 2.4 \times 10^4 \cos \theta) \qquad \text{deg}$$

since $\varphi_h = -180$ deg and $h_t = 100$ m. Since, for horizontal polarization, we have $D_{\theta'} = 1 = D_\theta$ and for $D^2 \gg (h_t + h_r)^2$ and $r \cong r + d$, the resultant field becomes

$$\mathcal{E}_R = \frac{\mathcal{E}_0}{r}(1 + \rho_h \cos \Delta) = \frac{\mathcal{E}_0}{r} P_\theta \qquad \text{volts/m}$$

if $\mathcal{E}_0$ denotes again the reference field in volts per meter at a distance of 1 m from the radiator in its equatorial plane and P_θ is the resultant directivity, giving the polar pattern in the vertical ZX plane. We find then the evaluations of Table 59. In the θ column, for values larger than 180 deg, we must always subtract 180, 2×180, 3×180, $\cdots$ deg, since the reflection coefficient has a 180-deg phase. Every time $\Delta = -180° - 180°$ is reached, we have again an inphase condition, and the relative delay starts all over again from zero value (from inphase toward lagging phase). We note from the table that for horizontal polarization, only for ideal reflection (ground acting in effect with 100 per cent reflection in antiphase) can we expect absolute zero for the minimum resultant field effect. For wet soil, we deal strictly with field minima only. Nevertheless, the first lobe (corresponding to the first maximum) closest to ground gives essentially the same polar P_θ pattern as for perfect ground. But as we go to successive lobes of the P_θ pattern, the effect of the coefficient of reflection (with a value smaller than unity) becomes more apparent. The ground effect for horizontal polarization is, however, not very different from that for perfect ground. If we take the case of vertical polarization and also for wet soil, as in Table 60, a pronounced ground effect exists, because the magnitude of ρ_v changes from -1 to -0.018 as θ changes from 90 to 80 deg. Since, according to Fig. 259, for wet soil at 100 Mc/sec and higher, the phase φ_v of the reflection coefficient ρ_v is, for vertical reflection, also -180 deg, and this between 90 deg to the Brewster angle $\theta_B = 79.7°$. We have

$$\Delta = -(180° - 2.4 \times 10^4 \cos \theta)$$

and the phase-delay values of Table 59 can be used. But for vertical polarization, we have to take the directivities $D_{\theta'}$ and D_θ into account. Since, for $(h_t + h_r)^2 \ll D^2$, the difference $\theta' - \theta \cong 0$, we have $D_{\theta'} = D_\theta$; and besides, $r/(r + d) \cong 1$ as far as the inverse distance effect on the field amplitude is concerned. For a vertical half-wave radiator $D_\theta = [\cos (90° \cos \theta)]/\sin \theta \cong \sin \theta$, since we deal only with wave incidences close to $\theta = 90$ deg. The resultant field is, therefore, found from the simplified expression

$$\mathcal{E}_R = \frac{\mathcal{E}_0}{r} (1 + \rho_v \cos \Delta) \sin \theta = \frac{\mathcal{E}_0}{r} P_\theta \qquad \text{volts/m for vertical polarization}$$

The polar pattern in the vertical ZX plane is

$P_\theta = (1 + \rho_\theta \cos \Delta) \sin \theta$ for vertical polarization ($\theta \geqq 82°$ to $90°$)
$P_\theta = 1 + \rho_h \cos \Delta$ for horizontal polarization (any angle θ)

TABLE 59. HORIZONTAL POLARIZATION OVER WET SOIL AT 100 MC/SEC

θ, deg	cos θ	$2.4 \times 10^4 \cos\theta$, deg (only values not exceeding 180° are of interest)	Relative time delay $\Delta = -180 - 2.4 \times 10^4 \cos\theta$, deg (only values between 0 and 360° are of interest)	cos Δ	Polar directivity $P_\theta = 1 + \cos\Delta$ for perfect reflector) $\sigma = \infty$)	Polar directivity over wet soil at 100 Mc/sec		
						ρ_h from Fig. 259	$\rho_h \cos\Delta$	$P_\theta = 1 + \rho_h \cos\Delta$
90	0.0000	0.0	−180	−1.0000	0.0000	1.0000	−1.0000	0.0000
89.9	0.0017	40.8	−220.8 = −(180 + 40.8)	−0.757	0.243	0.9992	−0.757	0.243
89.8	0.0035	84	−264 = −(180 + 84)	−0.1045	0.8955	0.9987	−0.1043	0.8957
89.7	0.0052	125	−305 = −(270 + 35)	0.5736	1.5736	0.998	0.571	1.571
89.6	0.007	168	−348 = −(270 + 78)	0.9781	1.9781	0.9975	0.97	1.97
89.58					Max			
89.5	0.0087	209 = 180 + 29	−389 = −(360 + 29)	0.8746	1.8746	0.997	0.87	1.87
89.4	0.0105	252.5 = 180 + 72.5	−432.5 = −(360 + 72.5)	0.3007	1.3007	0.9962	0.299	1.299
89.3	0.0122	292.5 = 180 + 112.5	−472.5 = −(360 + 90 + 22.5)	−0.3827	0.6173	0.9957	−0.38	0.62
89.2	0.014	336 = 180 + 156	−516 = −(360 + 90 + 66)	−0.9135	0.0865	0.995	−0.908	0.092
89.11					Min			
89.1	0.0157	366 = 2 × 180 + 6	−546 = −(360 + 180 + 6)	−0.9945	0.0055	0.9943	−0.99	0.01
89.0	0.0175	420 = 2 × 180 + 60	−(3 × 180 + 60)	−0.5	0.5	0.9939	−0.496	0.504
88.9	0.0192	461 = 2 × 180 + 101	−641 = −(7 × 90 + 11)	0.1908	1.1908	0.9932	0.189	1.189
88.8	0.0209	503 = 2 × 180 + 143	−(7 × 90 + 53)	0.7986	1.7986	0.9927	0.79	1.79
88.71					Max			
88.7	0.0227	544 = 3 × 180 + 4	−(2 × 360 + 4)	0.9976	1.9976	0.992	0.99	1.00
88.6	0.0244	585 = 3 × 180 + 45	−(2 × 360 + 45)	0.7071	1.7071	0.9913	0.7	0.3
88.5	0.0262	630 = 3 × 180 + 90	−(9 × 90 + 0)	0.0000	1.0000	0.9908	0.0	1.0
88.4	0.0279	670 = 3 × 180 + 130	−(9 × 90 + 40)	−0.6428	0.3572	0.9902	−0.635	0.365
88.3	0.0297	713 = 3 × 180 + 173	−(9 × 90 + 83)	−0.9925	0.0075	0.9897	−0.98	0.02
88.28					Min			
88.2	0.0314	753 = 4 × 180 + 33	−(5 × 180 + 33)	−0.8387	0.1613	0.989	−0.826	0.174
88.1	0.0322	798 = 4 × 180 + 78	−(5 × 180 + 78)	−0.2079	0.7921	0.9884	−0.205	0.795
88.0	0.0349	838 = 4 × 180 + 118	−(11 × 90 + 18)	0.309	1.3090	0.9878	0.304	1.304
87.9	0.0366	880 = 4 × 180 + 160	−(11 × 90 + 70)	0.9397	1.9397	0.9872	0.924	1.924
87.85					Max			
87.8	0.0384	920 = 5 × 180 + 20	−(3 × 360 + 20)	0.9387	1.9387	0.9868	0.922	1.922
87.7	0.0401	963 = 5 × 180 + 63	−(3 × 360 + 63)	0.454	1.454	0.986	0.446	1.446
87.6	0.0419	1006 = 5 × 180 + 106	−(13 × 90 + 16)	−0.2756	0.7244	0.9855	−0.271	0.729
87.5	0.0436	1050 = 5 × 180 + 150	−(13 × 90 + 60)	−0.866	0.134	0.985	−0.85	0.15
87.4	0.0454	1090 = 6 × 180 + 10	−(7 × 180 + 10)	−0.9848	0.0152	0.984	−0.97	0.03

Remarks: cos (−Δ) = cos (Δ); cos (180° + x) = −cos (x); cos (270° + x) = sin (x). Computations for h_t = 100 m and f = 100 Mc/sec for horizontal polarization over perfect ground and over wet soil. Note that P_θ oscillates between 0 and 2. A perfect reflector has $\rho_h = -1$ (100 per cent antiphase reflection).

TABLE 60. VERTICAL POLARIZATION OVER WET SOIL AT 100 MC/SEC

θ, deg	From Table 59		$D_\theta = \sin\theta$	Polar directivity for perfect reflector $P_{\theta'} = D_\theta(1 + \cos\Delta)$	ρ_v from Fig. 259	$\rho_v \cos\Delta$	Over wet soil $P_\theta \sin\theta \times (1 + \rho_v \cos\Delta)$	$P_{\theta'}$ over perfect soil ($\sigma = \infty$)	
	$\cos\Delta$	$1 + \cos\Delta$						$\cos\Delta'$, $\Delta' = -2.4 \times 10^4 \times \cos\theta$	$P_{\theta'} \cong 1 + \cos\Delta'$
90	−1.0000	0.0000	1.0000	$\Delta' = \varphi_v - 2.4 \times 10^4 \cos\theta$	1.000	−1.000	0.0000	1.0000	2.0000
89.9	−0.757	0.243	1.0000	$= 0 - 2.4 \times 10^4 \cos\theta$ is	0.999	−0.75	0.25	0.757	1.757
89.8	−0.1045	0.8955	1.0000	used in the last col-	0.98	−0.102	0.898	0.1045	1.1045
89.7	0.5736	1.5736	1.0000	umn. The values of θ	0.97	0.558	1.558	−0.5736	0.4264
89.6	0.9781	1.9781	1.0000	in this table (corre-	0.96	0.938	1.938	−0.9781	0.0219
89.58		Max		sponding to three max-					Min = 0
89.5	0.8746	1.8746	1.0000	ima or three lobes); D_θ	0.95	0.83	1.83	−0.8746	0.1254
89.4	0.3007	1.3007	0.9999	$\cong \sin\theta = 1$, and the	0.94	0.281	1.281	−0.3007	0.6993
89.3	−0.3827	0.6173	0.9999	column for $1 + \cos\Delta$	0.93	−0.356	0.644	0.3827	1.3827
89.2	−0.9135	0.0865	0.9999	gives practically the ver-	0.92	−0.84	0.16	0.9135	1.9135
89.11		Min		tical polar pattern P_θ					Max = 2
89.1	−0.9945	0.0055	0.9999	for perfect ground ($\sigma =$	0.91	−0.905	0.095	0.9945	1.9945
89.0	−0.5	0.5	0.9998	∞), if Δ' as mentioned.	0.9	−0.45	0.55	0.5	1.5
88.9	0.1908	1.1908	0.9998	$D_\theta \cong \sin\theta$ does *not* hold	0.89	0.17	1.17	−0.1908	0.8092
88.8	0.7986	1.7986	0.9998	for θ values much smal-	0.88	0.701	1.701	−0.7986	0.2014
88.71		Max		ler than 85°					Min = 0
88.7	0.9976	1.9976	0.9997		0.871	0.868	1.868	−0.9976	0.0024
88.6	0.7071	1.7071	0.9997		0.862	0.608	1.608	−0.7071	0.2929
88.5	0.0000	1.0000	0.9997		0.85	0.000	1.000	0.0000	1.0000
88.4	−0.6428	0.3572	0.9996		0.841	−0.542	0.4548	0.6428	1.6428
88.3	−0.9925	0.0075	0.9996		0.832	−0.825	0.175	0.9925	1.9925
88.28		Min							Max = 2
88.2	−0.8387	0.1613	0.9995		0.823	−0.689	0.311	0.8387	1.8387
88.1	−0.2079	0.7921	0.9995		0.812	−0.168	0.832	0.2079	1.2079
88.0	0.309	1.309	0.9994		0.802	0.247	1.247	−0.309	0.691
87.9	0.9397	1.9397	0.9993		0.793	0.742	1.742	−0.9397	0.0603
87.85		Max							Min = 0
87.8	0.9387	1.9387	0.9993		0.784	0.735	1.735	−0.9387	0.0613
87.7	0.454	1.454	0.9992		0.772	0.35	1.35	−0.454	0.546
87.6	−0.2756	0.7244	0.9991		0.763	−0.211	0.789	0.2756	1.2756
87.5	−0.866	0.134	0.999		0.752	−0.65	0.35	0.866	1.866
87.4	−0.9848	Min 0.0152	0.999		0.745	−0.733	0.267	0.9848	Max = 2 1.9848

Remarks: h = 100 m above the reflector, where wet soil is one case and ideal soil ($\rho = \infty$) is the other case at f = 100 Mc/sec. Ideal soil is equivalent to a perfectly conducting metal plate.

The results of Tables 59 and 60 are plotted in Fig. 264, showing that for perfectly reflecting ground of the polar pattern P_θ, we can expect reception *next to ground* for *vertical* polarization, but *not* for horizontal polarization. For *actual* ground, which in our example is wet soil, we find at

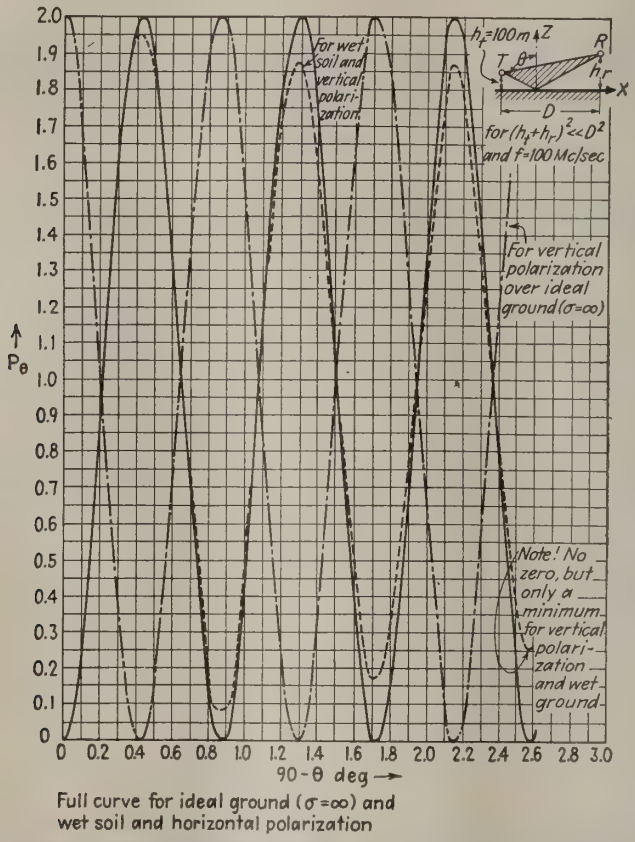

FIG. 264. Vertical directivity pattern for vertical and horizontal polarization over wet soil and perfect ground at f = 100 Mc/sec.

100 Mc/sec and a radiation center[1] h_t = 100 m above the tangential ground plane that for both the vertical as well as the horizontal polarization, no reception is possible close to the surface of the ground. We have then, in effect, a horizon that, so to speak, *curves up* as much from the true line of sight as the lower boundary of the first radiation lobe curves up with respect to the tangential plane (Figs. 265 and 261).

[1] Attention is called again to the fact that $h_t f$ accounts for the pattern for a particular ground; and if we change the ground effects by changing either h_t or f or both, the pattern must change accordingly.

Figures 264 and 265 are self-explanatory. That vertical polarization gives, in this case, a *virtual* horizon, which is curved up above the line of sight and should *not* be taken as a generality. Inspecting, for instance, the various reflection curves of Fig. 236 for complex ground, we note that there is no abrupt phase jump at the Brewster angle θ_B corresponding to a time phase $\varphi_v = -90$ deg for the vertical reflection coefficient. We

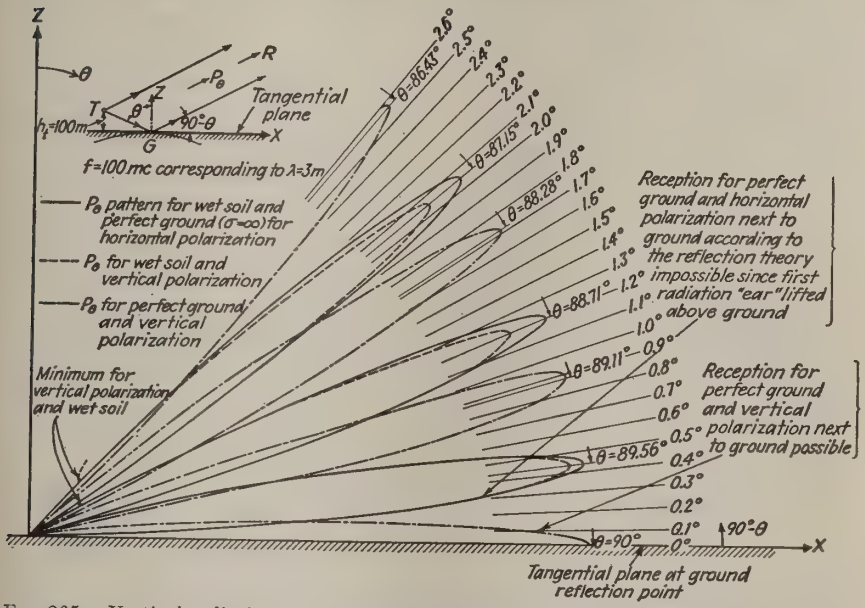
Z
R
θ
P_θ
T
Z
θ
90°-θ
Tangential plane
h_t=100m
G
X
f=100mc corresponding to λ=3m
P_θ pattern for wet soil and perfect ground (σ=∞) for horizontal polarization
P_θ for wet soil and vertical polarization
P_θ for perfect ground and vertical polarization
Minimum for vertical polarization and wet soil
θ=86.45°
θ=87.15°
θ=88.28°
θ=88.71°
θ=89.11°
θ=89.56°
θ=90°
2.6° 2.5° 2.4° 2.3° 2.2° 2.1° 2.0° 1.9° 1.8° 1.7° 1.6° 1.5° 1.4° 1.3° 1.2° 1.1° 1.0° 0.9° 0.8° 0.7° 0.6° 0.5° 0.4° 0.3° 0.2° 0.1° 0°
Reception for perfect ground and horizontal polarization next to ground according to the reflection theory impossible since first radiation "ear" lifted above ground
Reception for perfect ground and vertical polarization next to ground possible
90°-θ
X
Tangential plane at ground reflection point

Fig. 265. Vertical radiation pattern of resultant space field for ideal and wet soil for vertical and horizontal polarization. *Note:* For both horizontal and vertical polarization over wet soil the first radiation "ear" is lifted away from ground, while for perfect ground and vertical polarization reception next to ground is possible. A metallic reflector acts as a quasi-perfect ground (reflector).

find, however, a gradual change of the phase φ_v, just as we have a gradual change of the phase φ_h for horizontally polarized waves. The change in φ_v is more rapid, however, for angles close to grazing incidence. It is the ratio q/κ_r that counts for $q = 1.8 \times 10^4(\sigma/f)$ and f in megacycles per second. If the conduction term q becomes large compared with the relative dielectric constant κ_r of ground, matters are different from those found in Fig. 265. The computation is then the same as in Tables 59 and 60, except that φ_v and φ_h change with the angle of wave incidence just as ρ_v and ρ_h change for either type of polarization, and we deal with a Brewster dip. This discussion brings out the difference between a dielectric and a conductive electromagnetic mirror. In Fig. 265, we deal, in effect, with a quasi-dielectric mirror as far as wave reflections

are concerned for wet soil at 100 Mc/sec. This is the reason why the first radiation lobe is lifted away from the horizon. For a perfect ground, we have a conductive reflector and a corresponding mirror effect. Therefore, for grazing ground incidence and vertical polarization over perfect ground, the reflection factor must be $\rho_v = +1$, since the image current and its phase are the same as the actual antenna current and its phase. The electric lines of force then enter the conductive mirror perpendicularly, which satisfies $\rho_v = +1$ and $\varphi_v = 0$ deg. For horizontal polarization right next to ground (tangential to perfect ground), there can be no tangential $\mathfrak{E}$ field (along the metallic mirror). Therefore, at any place along the ground (right next to it), we must have on either side of the ground surface tangential equal $\mathfrak{E}$ fields that are in phase opposition. This means that $\rho_h = -1$ or $|\rho_h| = +1 \cdot \epsilon^{j180^\circ} = \cos 180^\circ - j \sin 180^\circ = -1$, so that $\varphi_h = 180$ deg, which is phase opposition. But as soon as the ground becomes electromagnetically a quasi-dielectric mirror, we find the conditions shown in Fig. 265.

170. Possibility of Stratum Waves in the Lower Atmosphere and Separation of Stratum, or "Close-to-ground," Waves from Space Waves. Experience shows that electromagnetic waves may glide along the earth's surface. This led J. Zenneck, as early as 1906, to the idea of surface waves and A. Sommerfeld, as early as 1909, to the distinction between surface and space waves. This was later followed up by Weyl, Van der Pol, and Bremmer and finally revised by K. Norton, so as to be useful for computing the field intensity of ground waves in the standard broadcast range[1] of carrier frequencies. There is quite a difference between the presentation of Weyl and the "revised" presentation of Sommerfeld, when the displacement current in the earth crust approaches the value of the conduction current. This means that the term κ_r approaches the numerical value of the term $q = 1.8 \times 10^4(\sigma/f)$ for σ in mhos per meter and f in megacycles per second.

As is shown in Sec. 164, guided surface-wave conditions can also take place for short waves, and apparent forward tilts of the electric vector $\mathfrak{E}$ up to 22 deg with respect to the surface of the earth may occur. The surface-wave condition can, however, also be explained by a waveguide action between two boundaries, one being the XY plane in Fig. 266 and the other the surface of the ground. A layer a few hundred meters thick above ground may act as a medium κ_2, μ_2, σ_2 while the atmosphere above it behaves as κ_1, μ_1, and the ground itself behaves as κ_3, μ_3,

[1] Some theoretical writers do not agree with the A. Sommerfeld theory; but from a present-day radio-engineering point of view, it must be admitted that the outcome of Sommerfeld's theory and numerical distance gives a useful means of predicting standard broadcast coverage.

σ_3. We then mostly meet conditions such that $\mu_1 = \mu_0 = \mu_2 = \mu_3$ and $\sigma_2 = 0$. An incident beam *ab* will then be reflected back into the upper atmosphere and be partially refracted as a beam *bd* into medium 2, partially refracted into ground, and partially reflected as a beam *de*. The latter beam causes a refracted beam into the upper atmosphere and, in turn, reflected beams *eg*, *gk*, etc. We must then consider three typical field points, namely, the free-space points P_1; the stratum, or layer, points P_2, and ground points P_3. The last points are of no practical

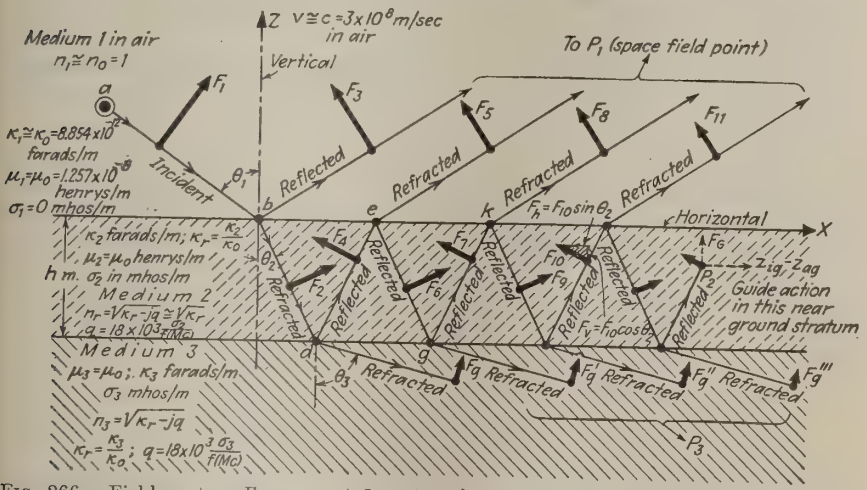

FIG. 266. Field vectors F represent $\mathcal{E}$ vectors for vertical and H vectors for horizontal polarization. h is thickness of stratum which may give rise to guide action. n are relative indexes of refraction referred to vacuum.

concern, since for short waves any power penetrating ground is lost and does not go very far before being dissipated. This is also essentially the case for the lower HF range. It is points P_1 and P_2 that concern us, since they account for space and guided ground waves. Points P_2 also account, in some cases, for diffracted radiation beyond and below the line of sight. Such radiation may, under certain conditions, cover far more distance than expected from the free-space inverse distance law and follow a law that may even be as favorable as an inverse law of the square root of the distance. This would account for large transmission ranges, sometimes several times the line-of-sight distance. These distances exceed considerably the distance due to the ray theory, even for a downward-curved path, because of atmospheric refraction. As far as space waves are concerned (affecting points P_1), it is necessary only to add geometrically the effects of the reflected field F_3 and refracted fields

F_5, F_8, F_{11}, . . . and to use the proper reflection and refraction coefficients. We have then, for plane waves, the various field vectors

$$\left.\begin{aligned} F_1 &= F_0 \epsilon^{j[\omega t - \beta(x \sin\theta_1 - z\cos\theta_1)]} && \text{for incident beam } ab \\ F_2 &= R_{12} F_0 \epsilon^{j[\omega t - \beta n_2(x \sin\theta_2 - z\cos\theta_2)]} && \text{for refracted beam } bd \\ F_3 &= \rho_{12} F_0 \epsilon^{j[\omega t - \beta(x\sin\theta_1 + z\cos\theta_1)]} && \text{for reflected beam } bP_1 \end{aligned}\right\} \quad (884)$$

where the refraction coefficient R_{12} and reflection coefficient ρ_{12} are interrelated.[1] These coefficients are

$$\left.\begin{aligned} \rho_{12} &= \frac{n_2^2 \cos\theta_1 - p}{n_2^2 \cos\theta_1 + p} && \text{for } \textit{vertical} \text{ polarization} \\ \rho_{12} &= \frac{\cos\theta_1 - p}{\cos\theta_1 + p} && \text{for } \textit{horizontal} \text{ polarization} \\ p &= \sqrt{n_2^2 + \cos^2\theta_1 - 1} \end{aligned}\right\} \quad (884a)$$

[1] For details, consult the derivations in Table 44 steps 15, 16, 17, 18, etc. It is shown that at perpendicular incidence ($\theta_1 = 0$), we have, for respective reflection coefficients $\rho_v = -\rho_h$, where the vertical coefficient ρ_v of reflection is a particular case of $\rho_\parallel$, i.e., $\mathcal{E}$ is parallel with plane of incidence, and the general case for ρ_h is $\rho_\perp$, *i.e.*, $\mathcal{E}$ is normal to the plane of wave incidence. For any mediums we have the corresponding refraction coefficients

$$R_\parallel = \frac{2\mu_1\Gamma_2}{\mu_1\Gamma_2 + \mu_2\Gamma_1} \quad \text{and} \quad R_\perp = \frac{2\mu_2\Gamma_1}{\mu_2\Gamma_1 + \mu_1\Gamma_2}$$

$$\Gamma = j\omega\sqrt{\mu\kappa_e}; \qquad \kappa_e = \kappa - j\frac{\sigma}{\omega} \quad \text{farads/m}$$

For $\mu_1 = \mu_2 = \mu_0$, we obtain

$$R_\parallel = \frac{2\Gamma_2}{\Gamma_1 + \Gamma_2}; \qquad R_\perp = \frac{2\Gamma_1}{\Gamma_1 + \Gamma_2}$$

$n_{12} = \Gamma_2/\Gamma_1$ relative index of refraction of medium 2 with respect to medium 1. For $\kappa_1 \cong \kappa_0$, $\mu_1 = \mu_0$, $\sigma_2 = 0$, κ_2 slightly different from κ_1, $\mu_2 = \mu_0$, we obtain

$$\Gamma_1 \cong j\omega\sqrt{\mu_0\kappa_0}; \qquad \Gamma_2 = j\omega\sqrt{\mu_0\kappa_2}; \qquad n_{12} = \frac{\Gamma_2}{\Gamma_1} = \sqrt{\frac{\kappa_2}{\kappa_0}} = \sqrt{\kappa_r} = n_2$$

yielding

$$R_{12} = \frac{2\Gamma_2}{\Gamma_1 + \Gamma_2} = \frac{2\sqrt{\kappa_2}}{\sqrt{\kappa_0} + \sqrt{\kappa_2}} = \frac{2\sqrt{\kappa_r}}{1 + \sqrt{\kappa_r}} \quad \text{for } \textit{vertical} \text{ polarization}$$

$$R_{12} = \frac{2\Gamma_1}{\Gamma_1 + \Gamma_2} = \frac{2\sqrt{\kappa_0}}{\sqrt{\kappa_0} + \sqrt{\kappa_2}} = \frac{2}{1 + \sqrt{\kappa_r}} \quad \text{for horizontal polarization}$$

These coefficients stand for the ratio F_2/F_1 at refraction point b in Fig. 266, while the reflection coefficient ρ_{12} denotes the ratio F_3/F_1 at b. The reflection coefficient ρ_{21} is the ratio F_6/F_4 at reflection point e; the ratio F_9/F_7 at reflection point k, etc. The reflection coefficient ρ_{23} is the ratio F_4/F_2 at reflection point d; it is also the ratio F_7/F_6 at reflection point g; etc. The coefficient ρ_{23} is complex, because $n_{23} = n_3/n_2$ is complex (since n_3 is complex).

Depending upon the thickness h of the stratum, we find the field vectors

$$F_2 = F_0 \frac{(\rho_{12}^2 - 1)\epsilon^{j\,\delta h}(\cos\theta_1 + p)}{\rho_{12}^2 - p\epsilon^{j2\,\delta h}}; \qquad F_3 = F_0 \frac{\rho_{12}^2(1 - p\epsilon^{j2\,\delta h})}{\rho_{12}^2 - p\epsilon^{j2\,\delta h}} \tag{884b}$$

When, therefore, $\theta_1 = 0$ deg, *i.e.*, perpendicular wave incidence, the refracted field intensity F_2 will be a maximum when $h/\lambda = K/(2\sqrt{\kappa_r})$ for $K = 1, 2, 3, \cdots$ and a minimum for $h/\lambda = (2K + 1)/(2\sqrt{\kappa_r})$, since the delay $\delta = -(4\pi h \cos\theta_1)/\lambda$ and $\lambda = 300/f$, where f is in megacycles per second and λ in meters. In Fig. 266, the various F fields denote $\mathcal{E}$ field intensities in volts per meter for vertical polarization. For horizontal polarization, the $\mathcal{E}$ vectors are normal to the paper and F denotes the magnetic field vectors in amperes per meter. For a guided F_G wave in the stratum, only the vectors $F_2, F_4, F_6, F_7, \ldots$ are of concern; while for the space wave, only the vectors $F_3, F_5, F_8, \ldots$ play a part, and the resultant field at P is $\mathcal{E}_3 + \mathcal{E}_5 + \mathcal{E}_8 + \cdots$. For the other indicated field vectors, we find

$$\left.\begin{aligned} F_4 &= R_{12} \cdot \rho_{23} \cdot F_0\epsilon^{j\{\omega t - \beta n_2[x\sin\theta_2 + (2h+z)\cos\theta_2]\}} \\ F_5 &= R_{12} \cdot \rho_{23} \cdot R_{21} \cdot F_0\epsilon^{j[\omega t - \beta n_2(2h\cos\theta_2) - \beta(x\sin\theta_1 + z\cos\theta_1)]} \cdots \end{aligned}\right\} \tag{884c}$$

The phase difference ψ between F_5 and F_3, as well as between F_8 and F_5, is

$$\psi = -2\beta n_2 h\cos\theta_2$$

since, for the difference of F_5 and F_3, we find

$$\beta[(-2n_2h\cos\theta_2 - x\sin\theta_1 - z\cos\theta_1) - (-x\sin\theta_1 - z\cos\theta_1)] = -2\beta n_2 h\cos\theta_2$$

When expressing $\omega/6.28$ per radian or $\omega/360$ per degree in megacycles per second, we find

$$\beta = 360^\circ \times \frac{10^6 f}{3 \times 10^8} = 1.2f = \frac{\omega}{3 \times 10^8} \quad \text{Mc/m}$$

with a formula

$$\psi = -2.4 f n_2 h\cos\theta_2 \text{ deg} = -12.56 n_2 \frac{h}{\lambda}\cos\theta_2 \quad \text{radians} \tag{884d}$$

where the wavelength λ in meters is $300/f^{(\text{Mc})}$. The quantity ψ may be complex if the refractive index n_2 is complex. This, however, hardly ever happens, since the atmosphere up to a few hundred meters above the ground is nonconductive, except next to spraying ocean surface. We have also $\rho_{12} = -\rho_{21}$ and $R_{12} \cdot R_{21} - \rho_{12} \cdot \rho_{21} = 1$, according to Table 44. For the abbreviations

$$A = \epsilon^{j[\omega t - \beta(x\sin\theta_1 + z\cos\theta_1)]}; \qquad a = -j2\beta n_2 h$$

we can derive an expression for the intensity of the space wave that is caused by wave reflections. At a space point P_1, we find

$$\mathcal{E}_P = \underbrace{\rho_{12}\mathcal{E}_0 A}_{=\mathcal{E}_3} + \underbrace{R_{12}\rho_{23}R_{21}\mathcal{E}_0 A\epsilon^{a\cos\theta_2}}_{=\mathcal{E}_5} + \underbrace{\mathcal{E}_5\rho_{21}\cdot\rho_{23}\epsilon^{a\cos\theta_1}}_{=\mathcal{E}_8} + \underbrace{\mathcal{E}_5(\rho_{21}\cdot\rho_{23})^2\epsilon^{2a\cos\theta_2}}_{=\mathcal{E}_{11}} + \cdots \quad \text{volts/m} \quad (884e)$$

since reflections above the top surface of the stratum occur with a reflection coefficient ρ_{12}. The reflections below the top surface of the stratum back into the stratum occur with a coefficient ρ_{21}. The reflections from the ground surface back into the stratum occur with a coefficient ρ_{23}. Therefore, ρ_{12} depends on the relative index of refraction $n_{12} = n_2/n_1 = \sin\theta_1/\sin\theta_2$, since it is the relative index of refraction of the stratum medium with respect to the medium above the stratum. But n_1 holds for the atmosphere above the stratum and is practically equal to n_0 holding for vacuum; therefore, $n_1 = 1$. Hence, $n_2/n_1 = n_2/1 = n_2 = \sqrt{\kappa_r - jq} \cong \sqrt{\kappa_r} = \sqrt{\kappa_2/\kappa_0}$, because, for the stratum next to the ground, $\sigma_2 = 0$ and a real index $n_2 = \sqrt{\kappa_r}$ is obtained. This is also evident from the fact that for the upper atmosphere, κ_1 is essentially κ_0; while for the lower atmosphere in the stratum, it is slightly different from the magnitude of κ_1 and equal to κ_2. The relative index of refraction n_{12} of the stratum with respect to the atmosphere above it is $n_{12} = \sin\theta_1/\sin\theta_2 = v_1/v_2 = \sqrt{\mu_2\kappa_2}/\sqrt{\mu_1\kappa_1} = \sqrt{\kappa_2/\kappa_0} = \sqrt{\kappa_r}$, since we have a real medium. It is this index $n_2 = n_{12} = \sqrt{\kappa_r}$ which is to be used in (884a) in order to find the corresponding reflection coefficient ρ_{12}. In (884e), it can be seen that the trigonometric cosine function of angles θ_2, θ_1 appears alternately in the consecutive $\mathcal{E}_5$, $\mathcal{E}_8$, $\mathcal{E}_{11}$, $\mathcal{E}_{14}$, . . . terms; and for $\nu = \rho_{21}\cdot\rho_{23}$, we find, from (884$e$),

$$\mathcal{E}_{P_1} = A\mathcal{E}_0[\rho_{12} + R_{12}\rho_{23}R_{21}\epsilon^{a\cos\theta_2}(1 + \nu\epsilon^{a\cos\theta_1} + \nu^2\epsilon^{2a\cos\theta_2} + \cdots)] \quad (884f)$$

Expressing the angle of incidence θ_1 in terms of the angle θ_2 by means of the refraction law $\sin\theta_1 = n_2\sin\theta_2$ and $\cos\theta_1 = \sqrt{1 - n_2\sin^2\theta_2}$, we can bring the above expression into the form

$$\mathcal{E}_{P_1}^{(\text{volts/m})} = \mathcal{E}_0\frac{\rho_{12}\epsilon^{-a\cos\theta_2} + \rho_{23}(R_{12} + R_{21} - \rho_{12}\cdot\rho_{21})}{\epsilon^{-a\cos\theta_2} - \rho_{21}\cdot\rho_{23}} = \mathcal{E}_0\frac{\rho_{12}\epsilon^{-a\cos\theta_2} + \rho_{23}}{\epsilon^{-a\cos\theta_2} + \rho_{12}\cdot\rho_{23}} \quad (884g)$$

The simplification is due to $\rho_{12} = -\rho_{21}$ and $R_{12}R_{21} - \rho_{12}\rho_{21} = 1$. Ex-

pressing (884g) in terms of θ_1 by putting $\cos\theta_2 = \sqrt{1-\sin^2\theta_2} = \sqrt{1-(\sin^2\theta_1/n_2^2)}$ and using the abbreviation for a in the forms

$$\left.\begin{aligned} a &= -j\frac{4\pi fhn_2}{3\times 10^8} = -j12.56\frac{h}{\lambda}n_2 \quad \text{radians (for } f \text{ in cycles/sec)} \\ a &= -j\frac{720^\circ\times 10^6 fhn_2}{3\times 10^8} = -j2.4fhn_2 \quad \text{deg (for } f \text{ in Mc/sec)} \end{aligned}\right\} \tag{884h}$$

for the stratum height h and the operating wavelength λ are in meters and n_2 as the numeric relative value of refraction of the stratum, we have then

$$\mathcal{E}_{P_1}^{(\text{volts/m})} = \mathcal{E}_0\frac{\rho_{12}\epsilon^{j2.4fh\sqrt{n_2^2-\sin^2\theta_1}}+\rho_{23}}{\epsilon^{j2.4fh\sqrt{n_2^2-\sin^2\theta_1}}+\rho_{12}\cdot\rho_{23}} \tag{884i}$$

for the amplitude $\mathcal{E}_0$ of the reference field, h in meters and f in megacycles per second. The coefficients of refraction are now eliminated, and we have ρ_{12} as in (884a), and

$$\left.\begin{aligned} \rho_{23} &= \frac{pn_3^2-p_1n_2^2}{pn_3^2+p_1n_2^2} \quad \text{for vertical polarization} \\ \rho_{23} &= \frac{p-p_1}{p+p_1} \quad \text{for horizontal polarization} \\ p &= \sqrt{n_2^2-\sin^2\theta_1} = \sqrt{n_2^2+\cos^2\theta_1-1} \\ p_1 &= \sqrt{n_3^2-\sin^2\theta_1} = \sqrt{n_3^2+\cos^2\theta_1-1} \end{aligned}\right\} \tag{884j}$$

for the relative indices of refraction n_2 and n_3 of the stratum and the ground as given in Fig. 266. The second forms of p and p_1 have the advantage that for ρ_{12} in (884a) and ρ_{23} in (884j), we have only to look up the $\cos\theta_1$ value and use its square. The index n_3 of the ground is generally complex for short waves for ocean, since even at 900 Mc/sec, the quantity q is numerically equal to the κ_r value (equal to about 80). For dry land, the ground acts as a quasi dielectric just as wet soil behaves above 100 Mc/sec. As far as a field point P_2 in the stratum is concerned, we can resolve any of the various field vectors such as F_{10}, for instance, along the vertical as $F_v = F_{10}\cos\theta_2$ and along the horizontal as $F_h = F_{10}\sin\theta_2$. For vertical polarization, F_v would be the value due to F_{10} if a vertical receiving antenna were used. For horizontal polarization, the receiving antenna must be normal to the paper in Fig. 266. This should not be confused with the horizontal F_h field factor of F_{10}, since F_h is longitudinal along the X direction instead of transverse to it. It is then not necessary to multiply the F_{10} value by the trigono-

metric function. If the field point is moved to vector F_{10}, we have the zigzag field $\mathcal{E}_G = \mathcal{E}_{10} \cos \theta_2$ for vertical polarization. As far as the phase delay between consecutive field vectors F_4 and F_2 or F_6 and F_4 is concerned, it must be the same, since for

$$\mathcal{E}_2 = R_{12}\mathcal{E}_0\epsilon^{j[\omega t-\beta n_2(x \sin \theta_2 - z \cos \theta_2)]}$$
$$\mathcal{E}_4 = R_{12} \cdot \rho_{23} \cdot R_{21} \cdot \mathcal{E}_0\epsilon^{j[\omega t-\beta n_2[x \sin \theta_2+(2h+z) \cos \theta_2]]}$$

we find a phase delay

$$\beta n_2(-x \sin \theta_2 - 2h \cos \theta_2 - z \cos \theta_2 + x \sin \theta_2 - z \cos \theta_2) = -2\beta n_2(h + z)$$

and we have a guided action with a zigzag that is symmetrical with respect to the direction of the resultant energy transfer. This will be discussed in Sec. 171.

It should be realized that under certain conditions, an electromagnetic wave may be guided in a pure dielectric layer without energy dissipation. This requires that the boundaries are likewise surfaces of a pure dielectric medium. We can then have a zigzag plane wave moving against the normal of each boundary under an angle θ and cause a wave motion along the layer with a phase velocity $c' = v/\sin \theta$ and a group velocity $c'' = v \sin \theta$, where v denotes the velocity $1/\sqrt{\mu\kappa}$ of the zigzag wave. This assumes, however, that the layer is electromagnetically *denser* than the pure dielectric boundaries, so that *total* reflection can take place. The angle θ of wave incidence then has to be equal to or greater than the critical angle $\theta_c = \sin^{-1}\sqrt{\mu_1\kappa_1/\mu\kappa}$, where μ_1 and κ_1 are the electromagnetic constants on either side of the layer. We have then a minimum frequency for a certain thickness of the layer, above which some electromagnetic field energy, upon reflection at the dielectric boundaries, will partially leak into the boundary regions.

171. Wave-guide Action in the Dielectric Space between Boundary Planes. Let us find out what happens in the stratum of Fig. 266 and consider first the case where we make the surface of the ground coincide with the XY plane as in Fig. 267*a*, for vertical polarization and horizontal polarization, respectively. We have the general case of vertical polarization, which is known as "parallel" polarization, since the incident $\mathcal{E}_i$ vector can generally be decomposed into a component along the X and a component along the Z axis. For the electric vector $\mathcal{E}_i$ normal to the plane of wave incidence, we have two H_i components. Figure 267*b* shows the conditions for incidence against a perfectly conducting plane, with the expressions for the transverse field associations $\mathcal{E}_i \cos \theta$ volts per meter and H_i amperes per meter for parallel polarization and $-H_i \times \cos \theta$ amperes per meter and $\mathcal{E}_i$ volts per meter for perpendicular polariza-

XZ plane is plane of wave incidence; XY plane is a perfect reflector.

$$d = \underbrace{AD}_{z\cos\theta} + \underbrace{DB}_{x\sin\theta}$$

Therefore, a motion d along the incident direction is equivalent to $x \sin\theta + z\cos\theta$, so that incident field $\mathcal{E}_i = \mathcal{E}_0\epsilon^{j(\omega t-\beta d)} = \mathcal{E}_0\epsilon^{j[\omega t-\beta(x\sin\theta+z\cos\theta)]}$

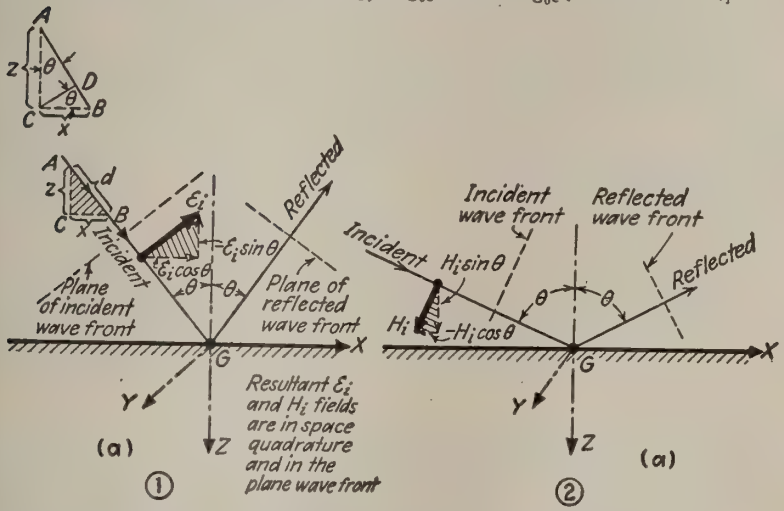

Parallel polarization ($\mathcal{E}$ vectors in plane of wave incidence). Only H_i intensity is perpendicular to XZ plane.

Perpendicular polarization (H vectors in plane of wave incidence). Only $\mathcal{E}_i$ vector perpendicular to XZ plane.

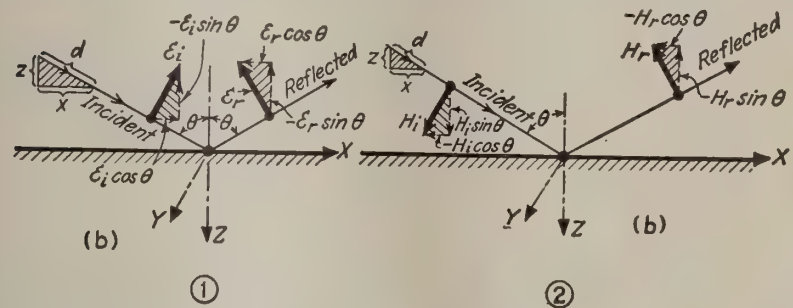

Parallel polarization:

$$\mathcal{E}_i = \mathcal{E}_0\epsilon^{j(\omega t-\beta d)} = \mathcal{E}_0\epsilon^{j[\omega t-\beta(x\sin\theta+z\cos\theta)]}$$
$$= \underbrace{\mathcal{E}_0\epsilon^{j[\omega t-\beta(x\sin\theta+z\cos\theta)]}\cos\theta}_{\mathcal{E}_i\cos\theta \text{ is transverse component}} - \underbrace{\mathcal{E}_0\epsilon^{j[\omega t-\beta(x\sin\theta+z\cos\theta)]}\sin\theta}_{-\mathcal{E}_i\sin\theta \text{ is longitudinal component traveling along } Z \text{ axis}}$$

$$\frac{\mathcal{E}_i\cos\theta}{H_i} = \frac{\mathcal{E}_0\epsilon^{j[\omega t-\beta(x\sin\theta+z\cos\theta)]}\cos\theta}{H_0\epsilon^{j[\omega t-(\beta x\sin\theta+z\cos\theta)]}}$$

$$= \frac{\mathcal{E}_0}{H_0}\cos\theta = \sqrt{\frac{\mu}{\kappa}}\cos\theta \text{ ohms}$$

for a nondissipative reflector

Perpendicular polarization:

$$H_i = H_0\epsilon^{j(\omega t-\beta d)}$$
$$= \underbrace{-H_0\epsilon^{j(\omega t-\beta d)}\cos\theta}_{-H_i\cos\theta \text{ is transverse to motion along } Z \text{ axis}} + \underbrace{H_0\epsilon^{j(\omega t-\beta d)}\sin\theta}_{+H_i\sin\theta \text{ is longitudinal to motion along } Z \text{ axis}}$$

$$\frac{\mathcal{E}_i}{H_i\cos\theta} = \frac{\mathcal{E}_0}{H_0\cos\theta} = \frac{\sqrt{\mu\kappa}}{\cos\theta}$$

FIG. 267. Analysis of parallel and perpendicular polarization over a perfect reflector.

tion. What is of interest is what happens when the direct and reflected fields combine at the surface of reflection. All reflections occur in the XY plane, for which $z = 0$. Since we deal with a perfect reflector surface, we can have no electric fields along the XY plane and the respective field components $\mathcal{E}_i \cos \theta$ and $\mathcal{E}_r \cos \theta$, which are opposing, must cancel at $z = 0$, satisfying that the coefficient $\rho_v = 1$ (for perfect reflectors), *i.e.*, $\mathcal{E}_r/\mathcal{E}_i = 1$ in the case of parallel polarization. For perpendicular polarization, we must satisfy for such reflectors the requirement $\mathcal{E}_r/\mathcal{E}_i = -1$. We then find resultant fields above the reflector, if taken normal to the reflecting plane, as

$$\left.\begin{aligned} \mathcal{E}_x &= -j2\sqrt{\frac{\mu}{\kappa}}\, H_0 \epsilon^{j(\omega t - \beta x \sin\theta)} \cos\theta \sin(\beta z \cos\theta) \quad \text{volts/m} \\ \mathcal{E}_z &= -j2\sqrt{\frac{\mu}{\kappa}}\, H_0 \epsilon^{j(\omega t - \beta x \sin\theta)} \sin\theta \cos(\beta z \cos\theta) \quad \text{volts/m} \\ H &= H_y = 2H_0 \epsilon^{j(\omega t - \beta x \sin\theta)} \cos(\beta z \cos\theta) \quad \text{amps/m} \end{aligned}\right\} \text{for } \textit{parallel} \text{ polarization (includes vertical polarization)} \tag{885}$$

and

$$\left.\begin{aligned} H_x &= 2\sqrt{\frac{\kappa}{\mu}}\, \mathcal{E}_0 \epsilon^{j(\omega t - \beta x \sin\theta)} \cos\theta \cos(\beta z \cos\theta) \\ H_z &= -j2\sqrt{\frac{\kappa}{\mu}}\, \mathcal{E}_0 \epsilon^{j(\omega t - \beta x \sin\theta)} \sin\theta \sin(\beta z \cos\theta) \quad \text{amp/m} \\ \mathcal{E} &= \mathcal{E}_y = -j2\mathcal{E}_0 \epsilon^{j(\omega t - \beta x \sin\theta)} \sin(\beta z \cos\theta) \quad \text{volts/m} \end{aligned}\right\} \text{for } \textit{perpendicular} \text{ polarization (such as horizontal polarization)} \tag{885a}$$

Either result shows that we deal with stationary space waves in the region above the perfect reflector. We have then maxima effects and minima effects, depending on the argument $\beta z \cos \theta$ of the respective sine and cosine functions. The fields with the cos $(\beta z \cos \theta)$ factor become a maximum whenever $\beta z \cos \theta = 0, 180, 2 \times 180°$ and generally $k180$ deg for $k = 0, 1, 2, 3, \cdots$. They become zero for $\beta z \cos \theta = 90$ deg and generally for $k_1 90$ deg for $k_1 = 1, 3, 5, \cdots$. For the fields with the sin $(\beta z \cos \theta)$ factor, we have maxima effects whenever $\beta z \cos \theta = k_1 90°$ and have zero whenever $\beta z \cos \theta = k180°$. This can also be expressed by means of $k = 1, 2, 3, \cdots, \lambda^{(m)} = 1/f\sqrt{\mu\kappa}$, where f is in cycles per second, μ in henrys per meter, and κ in farads per meter. We have then

$$\left.\begin{array}{l}\left.\begin{array}{l}\text{Maximum values of } \mathcal{E}_z \text{ and } H_y \text{ and zero values of } \mathcal{E}_x \\ \text{Maximum values of } \mathcal{E}_x \text{ and zero values of } \mathcal{E}_z \text{ and } H_y\end{array}\right\} \text{at locations } z = -\dfrac{k\lambda}{2\cos\theta} \text{ and } -\dfrac{(2k+1)\lambda}{4\cos\theta} \text{ for } \textit{vertical} \text{ polarization} \\ \left.\begin{array}{l}\text{Maximum values of } H_x \text{ and zero values of } \mathcal{E}_y \text{ and } H_z \\ \text{Maximum values of } \mathcal{E}_y \text{ and } H_z \text{ and zero values of } H_x\end{array}\right\} \text{at locations } z = -\dfrac{k\lambda}{2\cos\theta} \text{ and } -\dfrac{(2k+1)\lambda}{4\cos\theta} \text{ for } \textit{horizontal} \text{ polarization}\end{array}\right\} \quad (885b)$$

Let us apply this result to horizontal polarization, for instance. We have then, in Fig. 268*a*, the electric $\mathcal{E}$ vector parallel to either conducting plane and conditions as given by the above-mentioned relations. At each perfectly conducting boundary, the wave is so reflected that the *total* $\mathcal{E}$ field along the boundary vanishes. The electric fields of the incident and reflected waves must be equal and opposite. We note that for $z = 0$, this is the case. For the other boundary $z = h$, the tangential electric field $\mathcal{E}_y$ vanishes whenever $\beta z \cos\theta = \beta h \cos\theta = 0$, 180 deg, 2×180 deg, 3×180 deg, $k180$ deg for $k = 0, 1, 2, 3, \cdots$ or $h = k\lambda/(2\cos\theta)$ meters, where, for air as the wave medium, $\lambda^{(m)} = \dfrac{300}{f^{(Mc/sec)}}$.

The zigzag uniform plane wave of Fig. 268*a* is then nothing but the well-known $TE_{m,0}$ guided wave, which is a complementary wave and known as the TE wave, since only a longitudinal magnetic vector exists and the electric field is purely transverse with respect to the direction of motion. In exactly the same way, we find that for parallel polarizations, we can regard the zigzag wave motion between the parallel conducting planes as a TM wave (transverse magnetic wave). This is evident from the results of Fig. 267*b*, since the conducting parallel planes for an angle of wave incidence θ must be such that the separation is $k\lambda/(2\cos\theta)$, in order to render the tangential electric field equal to zero. Figure 268*b* shows how the steepness of wave incidence affects the parallel metal planes. The ray 1–2 is incident to the lower plane; 2–3 is the reflected beam; 3–4 is the reflected beam of the beam 2–3; etc. If the medium between the conductive planes is air, the zigzag beam will travel essen-

tially with the velocity of 3×10^8 m/sec. The motion along the X direction occurs with a velocity depending on the angle θ with no propagation whatsoever for $\theta = 0$ deg, which is perpendicular wave incidence. It is, therefore, evident that for pure dielectric boundaries as well as at surfaces of the general medium, a zigzag wave propagation in a stratum produces, in effect, a sort of wave-guide action. As a matter of fact in a rectangular wave guide, we have a symmetrical zigzag of elementary waves A and B as in Fig. 269*a*, since we may have a sinusoidal $\mathcal{E}_y$ distribution so as to make the tangential electric field $\mathcal{E}_y$ along the Y and Y' sides vanish. The magnetic lines have, however, a transverse H_z as well as a longitudinal H_x component. We then have to use two plane waves within the guide (in counterzigzag). If we had only the A zigzag plane wave, it would be reflected from the top plane in the same direction as the B wave. If we had only the B zigzag wave, it would be reflected from the bottom plane in the same direction as the A wave. Superimposing the A and the B waves must give the general action between two reflecting planes. The requirement is then that the A and the B plane waves have the same amplitude and add up to zero value along definite surfaces, so that no tangential fields can exist along the top and bottom metal surfaces. We have then essentially *only one wave, since each wave is the reflection of the other wave.* Figure 269 shows the difference between the wavelength of such an elementary wave and the wavelength of the guide. The slanting lines *ab* and *cd* are then the wave fronts of wave A with a positive maximum field value, while $a'b'$ and $c'd'$ hold for the B wave and positive maximum field value. Thus $b'c'$ is the location for the negative peak value of wave A, and bc the location for the negative peak value of wave B.

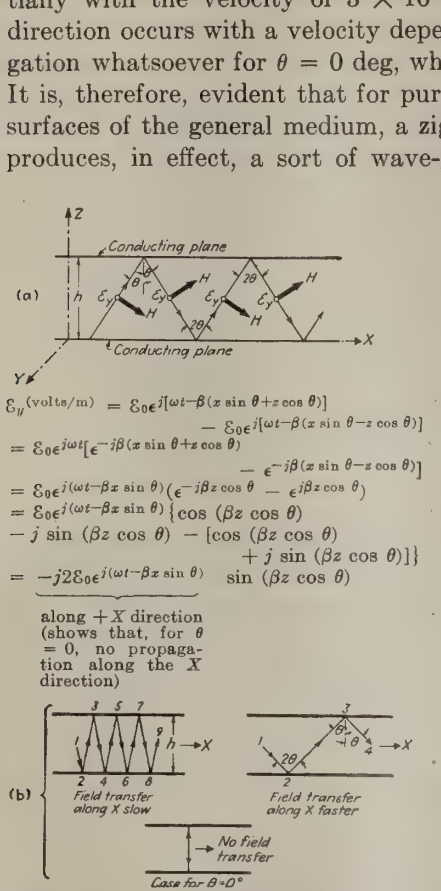
Z
Conducting plane
(a)
h
θ
2θ
H
X
Conducting plane
Y
$\mathcal{E}_{y'}$(volts/m) $= \mathcal{E}_0 \epsilon^{j[\omega t - \beta(x \sin\theta + z\cos\theta)]}$
$- \mathcal{E}_0 \epsilon^{j[\omega t - \beta(x \sin\theta - z\cos\theta)]}$
$= \mathcal{E}_0 \epsilon^{j\omega t}[\epsilon^{-j\beta(x\sin\theta + z\cos\theta)}$
$- \epsilon^{-j\beta(x\sin\theta - z\cos\theta)}]$
$= \mathcal{E}_0 \epsilon^{j(\omega t - \beta x \sin\theta)}(\epsilon^{-j\beta z\cos\theta} - \epsilon^{j\beta z\cos\theta})$
$= \mathcal{E}_0 \epsilon^{j(\omega t - \beta x\sin\theta)}\{\cos(\beta z\cos\theta)$
$- j\sin(\beta z\cos\theta) - [\cos(\beta z\cos\theta)$
$+ j\sin(\beta z\cos\theta)]\}$
$= -j2\mathcal{E}_0 \epsilon^{j(\omega t - \beta x\sin\theta)} \sin(\beta z\cos\theta)$
along +X direction (shows that, for θ = 0, no propagation along the X direction)
(b)
3 5 7
1 9
h
X
2 4 6 8
Field transfer along X slow
Field transfer along X faster
No field transfer
Case for θ=0°

FIG. 268. Effect of the angle of incidence on the energy transfer in the space between two reflectors. Only field $\mathcal{E} = \mathcal{E}_y$ is parallel to the metal planes of large extensions.

172. The Dielectric Constant of the Troposphere. The troposphere is the part of the atmosphere below about 10 km altitude where the temperature varies appreciably with the altitude. On account of nonuniformities in this portion of the atmosphere, such as rapid temperature and humidity changes (below about 1 km = 0.6214 statute mile = 0.5396 nautical mile) as well as temperature inversions, which may occur fairly close to ground, the path of electromagnetic propagation for short waves may become *curved*. Nonrectilinear wave propagation is caused by the gradient $d\Gamma/dh$ of the propagation constant Γ in a desired direction with respect to the altitude h above ground. It is essentially only the first few hundred feet and at most a thickness of a few thousand feet above ground that can cause anomalous wave paths.[1]

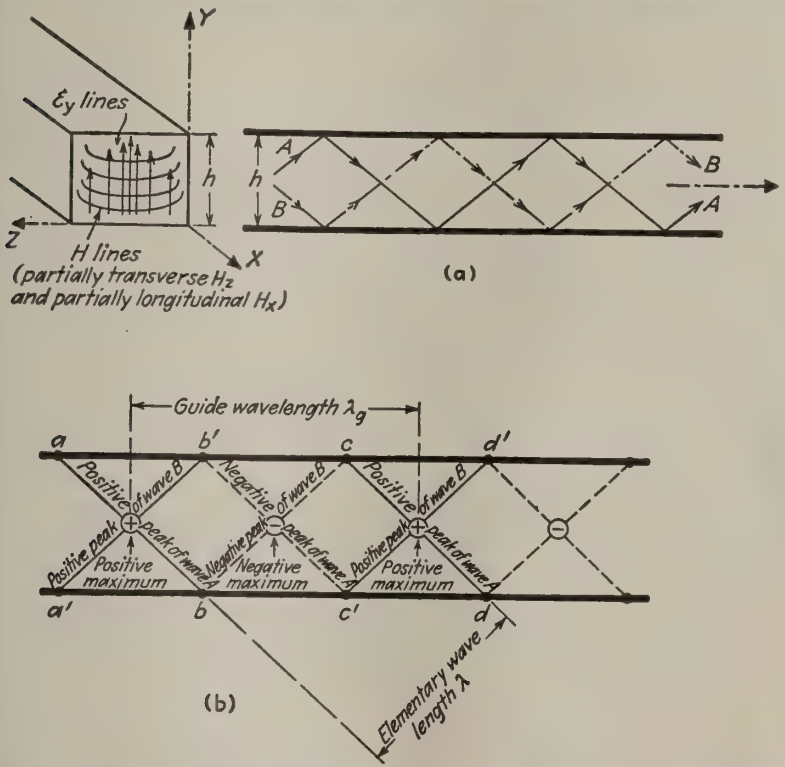

FIG. 269. Elementary and guide wavelengths. For air as the dielectric $\lambda^{(m)} = 300/f^{(Mc/sec)}$.

[1] It cannot be emphasized enough that anamolous wave propagation for short waves is by no means an infrequent occurrence, and we can expect very long ranges for hours and sometimes for seasons in certain portions of the earth's atmosphere. Other details on refraction and superrefraction are given in the Appendix.

For this reason, the lower atmosphere plays the part for short waves that the ionosphere does for longer radio waves, such, for instance, as used in the standard broadcast range of carrier frequencies. Unlike the ionosphere, we do not deal essentially with an ionized medium in the lower atmosphere. We have practically a nondissipative medium. Therefore, the relative index n of refraction at a certain space point in the lower atmosphere is the ratio of $c = 3 \times 10^8$ m/sec, for the speed of propagation in empty space, to the speed $v = 1/\sqrt{\mu\kappa}$ meters per second in the troposphere. Therefore, $n = c/v = \sqrt{\mu\kappa}/\sqrt{\mu_0\kappa_0} = \sqrt{\kappa/\kappa_0} = \sqrt{\kappa_r}$, since the permeability μ in the lower atmosphere is equal to $\mu_0 = 1.257 \times 10^{-6}$ henry/m and $\kappa/\kappa_0 = \kappa/(8.854 \times 10^{-12})$ denotes the numeric relative dielectric constant κ_r. The rate of change $dn/dh = d(\sqrt{\kappa_r})/dh$ then gives a means of accounting for any deviation from a rectilinear direction of electromagnetic wave propagation. Inasmuch as κ_0 in $\kappa_r = \kappa/\kappa_0$ is fixed, it is actually the change $d\sqrt{\kappa}/dh$ that accounts for the curved path of wave propagation.

From this introduction, we note that the knowledge of the dielectric constant κ and, more conveniently, of its relative value κ_r with respect to vacuum is important. The dielectric constant of any gas or a mixture of gases containing, in addition, water vapor, as in the case of the lower atmosphere, depends upon the temperature and the humidity. The change in κ with the temperature and the air pressure is slight, so that for air at 0°C at 1 atm pressure, we have the experimental Boltzmann value $\kappa_r = 1.00059$ instead of unity value holding for vacuum. At room temperature (about 19°C) and a pressure of $p = 20$ atm, the experimental value (due to Tangl) is $\kappa_r = 1.0108$, increasing to 1.0218 for twice this pressure. With a fair degree of approximation, the κ_r and, therefore, also the $\kappa = 8.854 \times 10^{-12}\kappa_r$ value in farads per meter can be computed from the density D_a of a nonpolar gas from

$$\kappa = 8.854 \times 10^{-12}(1 - KD_a) \quad \text{farads/m} \qquad (886)$$

where K is a constant. This is the outcome of the classic Clausius-Mossoti relation

$$\frac{\kappa_r - 1}{D_a(\kappa_r + 2)} = \text{constant} \qquad (886a)$$

since $(\kappa_r - 1)/(\kappa_r + 2) \cong (\kappa_r - 1)/3$ and "3 × constant = K." Experience and computations show that the effect of the humidity in the atmosphere causes *essentially* about the change in the value of κ_r in the troposhere.

Generally, short waves propagate in the lower troposphere along curved paths owing to electromagnetic refraction. It is caused by gradients of the dielectric con-

stants of the lower atmosphere, which are due principally to the distribution of moisture content and of temperature. For so-called "standard" atmosphere, we have a well-mixed air condition between transmitting and receiving stations. The dielectric constant κ then decreases slightly with the height above ground level, causing a relative gradient of about -2.4×10^{-6} per 100 ft. For such a standard lower atmosphere, electromagnetic waves then have a radius of curvature equal to about four times the radius of the earth. This means that the electromagnetic field will arrive at the receiver location with an angle of elevation slightly above the true elevation angle at the transmitter location. As is shown on page 988, if the dielectric constant decreases faster than the standard rate with the height more pronounced, downward bending occurs. Upward bending due to refraction occurs if the dielectric constant increases with height above ground.

173. The Foundations of the Classic Clausius-Mossoti Relation and of the Lorentz-Lorenz Law for Molar Refraction. This section is included in order to show what assumptions are made in the derivations leading to (886). If dl is the length of an infinitesimal current filament, expressed in meters with a uniform current distribution of I amperes along dl, then $I\,dl$ is known as the "electric current moment" of the current element. If $d\tau$ represents a cylindrical space element of a pure dielectric with a diameter of the circular cross section small compared with dl (axial length), then $I\,d\tau$ is the electric moment and I may be called the electric moment per unit volume of dielectric polarization. The electric field $\mathcal{E}$ along the axis is then the force acting on a unit charge of the cylindrical cavity. If, however, the end faces of the cylindrical cavity are brought close to each other, so that only a narrow space exists between said faces, we have to take into account also the Maxwellian electric displacement $D = \kappa\mathcal{E}$ coulombs per square meter per unit charge, where D is larger than $\mathcal{E}$ by an amount $4\pi I$, and we arrive at the well-known relation

$$D = \kappa_0\mathcal{E} + 4\pi I = \kappa\mathcal{E} = \kappa_0\kappa_r\mathcal{E} \tag{886b}$$

The field force F acting on a molecule with an electric moment M, when taken over a certain time interval, yields the mean value

$$M = PF \tag{886c}$$

for the moment, where P denotes the polarizability. This relation holds below the dielectric saturation. We have now the three quantities $\mathcal{E}$, D, and F, which characterize the pure dielectric. For a space like the troposphere, we deal with many molecules and generally particles having dimensions that may be large compared with customary space dimensions. Suppose we pick out such a particle that is positively charged and between parallel conducting planes, which are large in extension compared with their relative separation. We have then the force $F = F_1 + F_2 + F_3$ acting on such a particle. Suppose the left plate has a surface charge density $+q$ and the right-hand plate a surface charge density $-q$. We have then the force $F_1 = 2\pi q$. The force F_2 accounts for the action on the particle due to the dielectric between the surface of the particle and the metal plates. The force F_3 acts on the

particle owing to the conditions within the particle. If the particle is a sphere of radius r with a surface element dS, we have F_2 caused by two forces, one force F' due to layers of induced charges on the dielectric facing the conducting plates. It is $F' = -4\pi I$. The other force F'' is due to charges on the surface of the sphere. For the angle φ of I, we have the normal component $I \cos \varphi$. According to Coulomb's law, the force on the interior of the particle is, per surface element, $(I \cos \varphi \, dS)/r^2$, and

$$F'' = \int \frac{I \cos \varphi \, dS}{r^2} \cos \varphi = 2 \int_0^{\pi/2} \frac{I \cos \varphi}{r^2} 2\pi r^2 \sin \varphi \, d\varphi = \frac{4\pi I}{3}$$

Hence, $F_2 = -4\pi I + (4\pi I/3)$. The component force F_3 is generally an involved function depending on several parameters, such as the temperature, for instance. In the Clausius-Mossoti relation, it is *assumed* that $F_3 = 0$ and, therefore,

$$F = \underbrace{4\pi q}_{D} - 4\pi I + \frac{4\pi I}{3} = \kappa_0 \mathcal{E} + \frac{4\pi I}{3}$$

since $D = \kappa_0 \mathcal{E} + 4\pi I$, according to (886*b*). The force F acts on one molecule and, according to (886*c*), with an average electric moment $M = PF$. Hence, for N molecules per cubic meter dielectric and the polarization I per unit volume, we find

$$I = NM = NPF = NP\left(\kappa_0 \mathcal{E} + \frac{4\pi I}{3}\right) \tag{886d}$$

From (886*b*), we find

$$\kappa_0 \mathcal{E} + 4\pi I = \kappa_0 \kappa_r \mathcal{E}$$

or the polarization per cubic meter as

$$I = \frac{\kappa_0 \mathcal{E}(\kappa_r - 1)}{4\pi} \tag{886e}$$

which, inserted in (886*d*), eliminates I and yields

$$\frac{\kappa_0 \mathcal{E}(\kappa_r - 1)}{4\pi} = NP\left[\kappa_0 \mathcal{E} + \frac{\kappa_0 \mathcal{E}(\kappa_r - 1)}{3}\right] = \frac{NP\kappa_0 \mathcal{E}}{3} \underbrace{[3 + (\kappa_r - 1)]}_{\kappa_r + 2}$$

or

$$\frac{\kappa_r - 1}{\kappa_r + 2} = \frac{4\pi P}{3} N \tag{886f}$$

For a constant polarizability P, the ratio $(\kappa_r - 1)/(\kappa_r + 2)$ is proportional to the number of molecules, *i.e.*, proportional to the density D_a, referred to 1 cu m. Hence, the outcome of (886*f*) confirms the Clausius-Mossoti relation (886*a*) for a fixed value of P. Inasmuch as κ_r is almost unity for the troposphere, we have $(\kappa_r - 1)/(\kappa_r + 2) \cong (\kappa_r - 1)/3$, and $(\kappa_r - 1)$ is practically proportional to the density of the air. This is the reason why the *difference* $(\kappa_r - 1)$ enters the atmospheric refraction relations. From now on, we can change over from the Giorgi mks system to the customary classic cgs system, since κ_r is numeric and has the same value for 1 cu cm as it has for a cubic meter in Giorgi units. Multiplying, therefore, each side of (886*f*) by the

molecular weight W in grams and dividing each side by the density D_a in grams per cubic centimeter, we find

$$\frac{\kappa_r - 1}{\kappa_r + 2}\frac{W}{D_a} = \frac{4\pi P}{3}A \tag{886g}$$

since $A = NW/D_a$ is the Avogadro constant 6.064×10^{23} mole^{-1}, because of the number of moles for 1 g molecular weight. The molar polarization then becomes

$$P_m = \frac{\kappa_r - 1}{\kappa_r + 2}\frac{W}{D_a} = 2.538 \times 10^{24}P \tag{886h}$$

For an ideal gas, the molar volume $W/D_a = 22.4 \times 10^3$ cu cm at 0°C and 1 atm. Therefore,

$$\frac{\kappa_r - 1}{\kappa_r + 2}22.4 \times 10^3 = P_m = 2.54 \times 10^{24}P$$

The polarizability becomes then

$$P = 8.87 \times 10^{21}\frac{\kappa_r - 1}{\kappa_r + 2} \tag{886i}$$

For κ_r essentially unity, we find

$$P \cong \frac{8.87 \times 10^{21}(\kappa_r - 1)}{3} = 2.95 \times 10^{21}(\kappa_r - 1) \tag{886j}$$

The molar polarization P_m is, according to (886h) and (886m),

$$P_m = 2.538 \times 10^{24}\left(P_0 + \frac{M_0^2}{3kT}\right) = A + \frac{B}{T}$$

The final form holds for the case where the molecule is polar. The intercept A and the slope B of this line give a way of finding M_0 from the constant B if the P_m line is plotted for two experimental values of different absolute temperatures $T = 273° + C°$. If P does not vary with T, we have a horizontal line and $M_0 = 0$. This is the case for *nonpolar* molecules. Inasmuch as in electromagnetic refraction the index of refraction n accounts for the degree of ray bending and for the troposphere $n = \sqrt{\kappa_r}$, we have for the molar refraction

$$P_m = \frac{n^2 - 1}{n^2 + 2}\frac{W}{D_0} = 2.54 \times 10^{24}P \tag{886k}$$

174. Physical Properties of the Atmospheric Index of Refraction. The atmosphere is a mixture of gases, and Eq. (886f) leads to the general expansion

$$\frac{\kappa_r - 1}{\kappa_r + 2} = \frac{4\pi}{3}(P_1N_1 + P_2N_2 + P_3N_3 + \cdots) \tag{886l}$$

where the numeric relative dielectric constant κ_r of the mixture is the square of the atmospheric index of refraction n, the quantity N_1 denotes

the number of molecules per unit volume of gas 1 with a polarizability P_1, the quantity N_2 is the number of molecules of gas 2 of polarizability P_2, etc. The respective polarizabilities P are given by the expression

$$P = P_0 + \frac{M_0^2}{3kT} \tag{886m}$$

where P_0 is the polarizability that is fixed (is constant) in the HF field, M_0 is the permanent moment, $k = 1.3708 \times 10^{-16}$ erg · deg^{-1} is the well-known Boltzmann constant,[1] and T is the absolute temperature 273°+C°. The permanent moment M_0 vanishes for *non*polar molecules. Since for the lower atmosphere we have $\kappa_r \cong 1$, we have again

$$\frac{(\kappa_r - 1)}{(\kappa_r + 2)} \cong \frac{(\kappa_r - 1)}{3},$$

and Eq. (886*l*) reads

$$\kappa_r - 1 = 12.56(P_1N_1 + P_2N_2 + P_3N_3 + \cdots) \tag{886n}$$

This relation is useful, since

$$\kappa_r = 1 + 12.56\Sigma PN \tag{886o}$$

gives us the relative dielectric constant of a gas mixture with respect to $\kappa_0 = 8.854 \times 10^{-12}$ farad/m, holding for empty space. The number N of molecules per unit space of a gas is found from the knowledge that 1 mole with 6.064×10^{23} at 76 cm Hg atmospheric pressure at 0°C occupies 22.4×10^3 cu cm volume (Avogadro law), and $NW/D_0 = 6.064 \times 10^{23}$ mole^{-1}, where W is the molecular weight in grams and D_0 the density in grams per cubic centimeter. It is then more convenient to express the dielectric constant or its version in terms of the index n of atmospheric refraction by $n^2 - 1 = 12.56\Sigma PN$, instead of $n^2 = 1 + 12.56\Sigma PN$, since $n = \sqrt{\kappa_r}$ can differ only by very little from unity for atmosphere, because $\kappa_r \cong 1$. *However, the difference* $\kappa_r - 1$, say, for air next to ground and $\kappa_r - 1$ for an altitude of 500 ft above the ground may be noticeable and of different magnitude.

Experience and numerical speculations show that the *humidity* in the lower atmosphere is *mostly responsible* for the gradient dn/dh of the index of refraction. It may cause downward bending of the electromagnetic ray and, in some cases, even an upward curvature of the ray.

A *humid atmosphere* is a mixture of dry air and water vapor. For normal atmospheric conditions (76 cm Hg and 0°C), we have $D_a = D_0 = 0.001293$ g/cm^3 = 1.293 kg/m^3, corresponding to $\kappa_r - 1 = 0.00059$,

[1] The quantity k is the gas constant per mole ($= 8.313 \times 10^7$ erg · deg^{-1} · mole^{-1} divided by the Avogadro constant $A = 6.064 \times 10^{23}$ mole^{-1}.

showing that the relative dielectric constant is $\kappa_r = 1.00059$ instead of unity and the actual dielectric constant is $\kappa = 1.00059 \times 8.854 \times 10^{-12}$ farad/m. The density D_a for dry air is then, for any pressure and temperature,

$$D_a = \underbrace{0.001293 \frac{T_0 \cdot p}{T \cdot p_0}}_{=D_0} = \frac{0.001293H}{(1 + 0.00367°\text{C})76} \qquad (886p)$$

where 0.001293 g/cm³ is the density D_0 at the absolute temperature $T_0 = 273° + 0°$ and pressure p_0 and D_a is the density for the temperature $T = 273° + \text{C}°$ and pressure p. In the second expression for the value of the density D_a, the quantity H stands for the height of the mercury column in centimeters for the pressure p. We find, therefore, at 10°C and $H = 73$ cm

$$D_a = \frac{0.001293 \times 73}{(1 + 0.00367 \times 10)76} = 0.001198 \text{ g/cm}^3$$

while at room temperature (20°C) and $H = 72$ cm Hg column, we find $D_a = 0.001141$ g/cm³ for dry air. For the density of moist air, we find for the barometric pressure H in centimeters of mercury, a water vapor pressure e of the moisture in air in centimeters and the absolute temperature $T = 273° + \text{C}°$

$$D_a = 0.001293 \frac{273.13(H - 0.3783e)}{76T} = \frac{0.00463(H - 0.3783e)}{T} \text{ g/cm}^3 \qquad (886q)$$

where $H - 0.3783e$ is the corrected pressure in the mercury column due to water vapor. The quantity $0.3783e$ can be directly obtained from dew-point tables, where e is usually taken as the vapor pressure in air in millimeters. This can be readily changed to centimeters. When wet- and dry-bulb thermometer readings are made, the value of e can be found in the Table on Reduction of Psychrometric Observation and the Hygrometric and Barometric Tables.[1] Referring to such tables, the value of $1.293 \times 273.13/T$ and $(H - 0.3783e)76$, a multiplication will give the density in grams per cubic centimeter. If we desire, for instance, the density of humid atmosphere for a barometric pressure $H = 75$ cm, a dew point at 10°C and an air temperature of 20°C, we find in such tables for $0.3783e$ the value 0.348 cm, yielding the pressure as $75 - 0.348 = 74.652$ cm $= H - 0.3783e$ in (886q). The final expressions for (886q) leads to the evaluation

[1] Such tables are in the "Handbook of Chemistry and Physics," 27th ed. This reference also gives tables for $B - 0.3783e$, where B is the barometric pressure in millimeters ($= 0.1H$) and e in millimeters column of mercury. There are also tables in the Smithsonian Physical Tables.

$$D_a = \frac{0.00463 \times 74.652}{273 + 20} = 0.001183 \text{ g/cm}^3$$

This result corresponds to a density of 1.183 kg/m³ instead of 1.293 kg/m³ (in the case of dry air for standard reference condition, 0°C and $H = 76$ cm Hg column). Table 61 gives possible values of the atmospheric density D_a for different altitudes h above the surface of the earth.

TABLE 61. POSSIBLE ATMOSPHERIC DENSITY AT DIFFERENT ALTITUDES ABOVE GROUND

Altitude h above ground, km	Atmospheric density D_a, kg/m³	h, km	D_a, kg/m³	h, km	D_a, kg/m³	h, km	D_a, kg/m³
1.0	1.13	4.0	0.812	7.0	0.585	10.0	0.41
1.5	1.05	4.5	0.77	7.5	0.555	10.5	0.385
2.0	1.00	5.0	0.728	8.0	0.528	11.0	0.35
2.5	0.948	5.5	0.69	8.5	0.496	11.5	0.326
3.0	0.900	6.0	0.652	9.0	0.465	12.0	0.300
3.5	0.852	6.5	0.619	9.5	0.435	12.5	0.28

Remarks: 1 km = 1,000 m = 0.6214 statute mile = 0.5396 nautical mile = 3,281 ft; 1 kg = 1,000 g = 2.20462 standard pounds; 1 kg/m³ = 16.02 lb/ft³; 1 lb/ft³ = 6.243×10^{-2} kg/m³.

A plot of these values shows that the density D_a is not a linear function of h. This would be expected, since the atmospheric pressure is cumulative as h decreases toward the surface of the earth. Figure 270 gives curves for the relation $(\kappa_r - 1)$ for humidity present and without it. The value of 0.00059 holds at the surface of the earth for dry air in the case of 1 atm and 0°C (1 at = 14.71 lb/in.² = 1,013 kilodynes/cm² at sea level for 76 cm $\cong$ 30 in. Hg column at 0°C = 273°K). For all other densities, we can compute $(\kappa_r - 1)$, since the number of N_1 molecules is proportional to D_a.

Since the index n of refraction is not very different from unity, we find, from $n = \sqrt{\kappa_r} = \sqrt{1 - (\kappa_r - 1)} \cong 1 + \frac{1}{2}(\kappa_r - 1)$ and for the gradient of the atmospheric refraction,

$$\frac{dn}{dh} \cong 0.5 \frac{d(\kappa_r - 1)}{dh}; \qquad n - 1 \cong 0.5(\kappa_r - 1) \tag{886r}$$

It is this *gradient* which accounts for the curvature of the radio beam due to electromagnetic atmospheric refraction and *not* the value of n *itself*. A fixed value of n with respect to a definite altitude change would mean only a phase velocity c', which is somewhat different from $c = 3 \times 10^8$ m/sec *but* which is still *constant*. Therefore, in the case of $\kappa_r \neq 1$, we have a different fixed phase velocity

$$c' = \frac{1}{\sqrt{\mu_0 \kappa}} = \frac{1}{\sqrt{\mu_0 \kappa_r \kappa_0}} = \frac{c}{\sqrt{\kappa_r}} = \frac{c}{n} \tag{886s}$$

from $c = 1/\sqrt{\mu_0 \kappa_0} = 3 \times 10^8$ m/sec. This is then also a fixed index $n = c/c'$ and corresponds to a rectilinear wave propagation. According to (886*r*), it is the *change* in the $(\kappa_r - 1)$ value *that counts*, and curves as given in Fig. 270 can be used for finding the curvature of the electromagnetic ray.

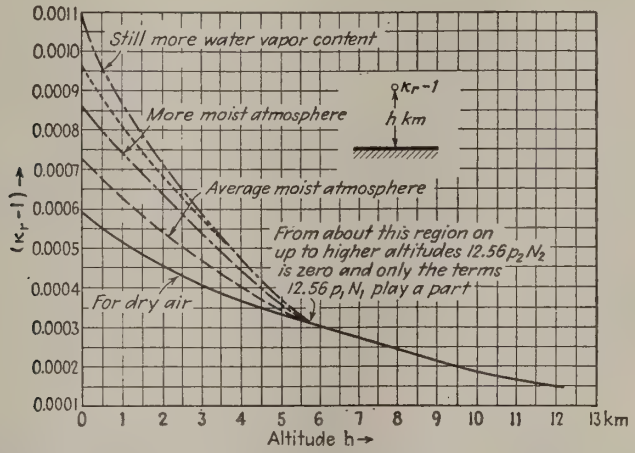

$\kappa_r = (\kappa/8.854)10^{12}$; κ is the dielectric constant in farads/m at an altitude of h km; n is the corresponding electromagnetic index of refraction.

$$(\kappa_r - 1) = \underbrace{12.56 p_1 N_1}_{\text{due to dry air}} + \underbrace{12.56 p_2 N_2}_{\text{due to water vapor}} = 2(n-1)$$

Fig. 270. Variation of the relative dielectric constant κ_r in the troposphere.

175. Remarks on the Dielectric Constant and the Index of Refraction of the Ionosphere. The value of the relative dielectric constant κ_r of the lower atmosphere is, according to Eq. (886*n*), given by $\kappa_r = 1 + 12.56 \Sigma NP$, where we usually consider only two terms, $N_1 P_1 + N_2 P_2$, in order to account for the effect of dry air and the effect due to water vapor in the atmosphere.

Suppose we have a plane electromagnetic wave passing through a medium along the X axis and polarized along the Z axis, and suppose the medium is ionized.[1] Then $\mathcal{E}_z$ volts per meter and H_y amperes per meter are the electric and magnetic constituents. The wave motion can then be expressed by

$$\mathcal{E}_z = \mathcal{E}_0 \epsilon^{j\omega\left(t - \frac{x}{c'}\right)} \quad \text{volts/m} \tag{887}$$

[1] Hund, A., "Phenomena in High-frequency Systems," pp. 367–405, McGraw-Hill Book Company, Inc., New York, 1936.

where the distance x is in meters and the phase velocity c' in meters per second. Across a square-meter plane normal to the Z direction, we have an instantaneous current density of

$$J_t = J + \kappa \frac{\partial \mathcal{E}_z}{\partial t} \qquad \text{amp/m}^2 \tag{887a}$$

where J is the conduction current density and $\kappa(\partial \mathcal{E}_z/\partial t) = j\omega\kappa\mathcal{E}_z$ the displacement current density. This is exactly what happens in an imperfect dielectric of a two-plate condenser. The electric field is then

$$\mathcal{E}_z = \mathcal{E}_0 \epsilon^{-j\omega(x/c')}(\cos \omega t + j \sin \omega t) \qquad \text{volts/m}$$

where the propagation term $\exp[-j\omega(x/c')]$ is of no concern if we are interested only in the dielectric constant of the field medium. Suppose first we have only one ion of charge q. Then $\mathcal{E}_z$ will exert a force $q\mathcal{E}_z$ on the ion, while the associated H_y field normally has only a negligible effect. If m is the mass of the ion, then $m(d^2z/dt^2) = q\mathcal{E}_z$ is the well-known equation of motion of the ion, since $m(d^2z/dt^2)$ is mass times acceleration and $q\mathcal{E}_z$ is a force. We have then, for the displacement z of the ion,

$$z = -\frac{q}{m\omega^2}\mathcal{E}_z \qquad \text{meters} \tag{887b}$$

against the direction of $\mathcal{E}_z$. If ω is large as for short waves, the ionic displacement can be only very small, because z is inversely proportional to the square of $6.28f$. Hence, if we have electrons instead of ions, the electrons can be moved rapidly, on account of their much smaller mass, and without much energy dissipation, provided the electron density N (numbers of electrons per cubic meter) is not too large. The conduction current density, in amperes across each square meter, is for N ions of charge q and mass m given by $J = Nqv$, where v is the ionic velocity in meters per second. This happens because J is the number of charges crossing each square meter per second. But the velocity $v = dz/dt$, and we find from $J = Nqv$ and (887b)

$$J = Nq\frac{dz}{dt} = -j\frac{Nq^2}{m\omega}\mathcal{E}_z = \sigma\mathcal{E}_z \qquad \text{amp/m}^2 \tag{887c}$$

But $J/\mathcal{E}_z$ represents a conductivity

$$\sigma = -j\frac{Nq^2}{m\omega} \tag{887d}$$

We have, therefore, ions mixed with the dielectric, which without ions would have practically a dielectric constant of κ_0 farads per meter. In

the presence of ions, we must then expect in the ionized medium a value $\kappa_e = \kappa_r\kappa_0$ farads per meter. This dielectric property of the ionized medium can be found from (887*a*), since we have

$$\left.\begin{aligned} J_t^{(\text{amp/m}^2)} = J + \kappa_0 \frac{\partial \mathcal{E}_z}{\partial t} &= \sigma\mathcal{E}_z + j\omega\kappa_0\mathcal{E}_z = j\left(\omega\kappa_0 - \frac{Nq^2}{m\omega}\right)\mathcal{E}_z \\ &= \left(\kappa_0 - \frac{Nq^2}{m\omega^2}\right)\frac{\partial \mathcal{E}_z}{\partial t} = \kappa_e \frac{\partial \mathcal{E}_z}{\partial t} \\ \kappa_e = \kappa_0 - \frac{Nq^2}{m\omega^2} &= \kappa_0\left(1 - \frac{f_c^2}{f^2}\right) \qquad \text{farads/m} \end{aligned}\right\} \tag{887e}$$

The quantity κ_e is then the equivalent dielectric constant in the presence of N ions. The quantity f is the operating frequency, and f_c represents the critical frequency for which κ_e becomes zero. This happens for $\kappa_0 = Nq^2/m\omega^2$, and

$$f_c = 5.37 \times 10^{-2}\, q\sqrt{\frac{N}{m}} \qquad \text{Mc/sec} \tag{887f}$$

Zero equivalent dielectric constant κ_e means a phase velocity $c' = 1/\sqrt{\mu_0 0} = \infty$ and a group velocity $c'' = \dfrac{9 \times 10^{16}}{c'} = 0$ in the ionosphere. Therefore, for the critical frequency f_c, the ionized medium will no longer permit an electromagnetic energy transfer. This is then the frequency for *selective absorption.*

That such a frequency must exist can also be seen from (887*e*), since

$$J_t = \sigma\mathcal{E}_z + j\omega\kappa_0\mathcal{E}_z = -j\frac{Nq^2}{m\omega}\mathcal{E}_z + j\omega\kappa_0\mathcal{E}_z$$

where $(-jNq^2/m\omega)\mathcal{E}_z$ is a displacement current density, $j\omega\kappa_0\mathcal{E}_z$ is an inductive current density, and respective j terms can balance themselves and cause complete cancellation. Such a condition may be called "ionic medium resonance," where the ionic excursions become so pronounced as to use up all the field energy due to collisions.

According to (887*e*) for the relative dielectric constant of the ionized medium with N ions, each ion of charge q coulombs and mass m in kilograms, we have

$$\kappa_e' = \frac{\kappa_e}{\kappa_0} = 1 - \frac{Nq^2}{\kappa_0 m\omega^2} = 1 - 2.87 \times 10^9 \frac{Nq^2}{mf^2} \tag{887g}$$

where f is in cycles per second. Since the index of refraction is $n = c/c'$, we find

$$n = \frac{\sqrt{\mu_0\kappa_e}}{\sqrt{\mu_0\kappa_0}} = \sqrt{\frac{\mu_0\kappa_0\kappa_e'}{\mu_0\kappa_0}} = \sqrt{1 - 2.87 \times 10^{-3}\frac{Nq^2}{mf^2}} \tag{887h}$$

where f is in megacycles per second. In terms of the operating frequency f and the critical frequency f_c, we have

$$n = \sqrt{1 - \left(\frac{f_c}{f}\right)^2} \tag{887i}$$

From (887*e*), we note that κ_e is smaller than the dielectric constant of empty space. From (887*b*), we note that the displacement z against the electric field $\mathcal{E}_z$ is all the smaller the higher the frequency. At the top level of the troposphere (about 10 km above ground), we shall hardly encounter an ionized region. Therefore, any reflections coming down from the troposphere are, rather, due to abrupt changes of κ_r values. The energy of such returned rays cannot amount to much, since the reflection coefficient would be of the order of 0.01 or even less.

From experimental experience, as well as theoretical speculations, the ionized region of the upper atmosphere can hardly play an important part for radiators and receiving antennas that are located *below* the ionosphere at frequencies above about 100 Mc/sec, since wave return for such frequencies does not occur often and is anomalous. Matters are, however, different when a certain moving object with a short-wave radiator passes within or even above the ionized region of the upper atmosphere. Such radiation can cause field effects below the ionosphere and be used to locate from ground stations the moving object mentioned.

176. General Remarks on the Effect of the Refractive Index Variations in the Troposphere on Radiation Beams. So far, we have found that the relative index n of refraction is larger than unity in the lower atmosphere, because the relative dielectric constant κ_r in the lower atmosphere is somewhat larger than unity value. We have for it the value $\kappa_r = 1 + 12.56\Sigma NP$. In the ionized medium, κ_r is, however, smaller than unity value. Moreover, for two electromagnetic mediums with no conductivity effects as for the atmosphere, for respective indexes n_1 and n_2, we have the Snell law $n_1 \sin \theta_1 = n_2 \sin \theta_2$, *i.e.*, $n \sin \theta =$ constant, and

$$\frac{\sin \theta_1}{\sin \theta_2} = \frac{n_2}{n_1} = \frac{\sqrt{\mu_2 \kappa_2}}{\sqrt{\mu_1 \kappa_1}} = \frac{c_1}{c_2} = n \tag{888}$$

Since the troposphere is not magnetic, we have $\mu_1 = \mu_2 = \mu_0$ henrys per meter and $n = \sqrt{\kappa_2/\kappa_1}$, where κ_1 is in farads per meter for medium 1 and $c_1 = 1/\sqrt{\mu_0 \kappa_1}$ meters per second is the corresponding velocity of wave propagation. For medium 2, we have the dielectric constant κ_2 and velocity c_2. The quantity θ_1 is the angle of incidence on the surface of separation between medium 1 and medium 2, where incidence θ_1 occurs in medium 1 against the normal to the surface of medium separation.

The quantity θ_2 is the angle of refraction for wave transmission into medium 2, likewise with respect to the normal to the surface of medium separation. We can then imagine the lower atmosphere as being made up of *many* layers, each of a somewhat different refractive index n corresponding to relative dielectric constants κ_1/κ_0, κ_2/κ_0, κ_3/κ_0, κ_4/κ_0, ... Such a concept will lead to successive refractions as in Fig. 271. For the condition that air is *denser* at lower levels than at higher levels, the incident ray AB making an angle θ_1 with the normal to the h_1 level will be refracted *away* from the normal by an angle θ_2, causing a transmitted beam BC, etc., until at D horizontal gliding would take place (just before $\theta = 90$ deg). However, just before this happens, the reflection law breaks down and, according to Gans, total reflection takes place. Thereafter, the ray again goes through consecutive refractions. Assuming that the heights $h_1, h_2, h_3, \ldots$ are such that $n_1, n_2, n_3, \ldots$ are fixed average values for thicknesses h_1, $h_2 - h_1$, $h_3 - h_2$, $\cdots$, then a ray AB starting out with an angle $90° - \theta$, with respect to the horizon, will cause angles θ_2, θ_3, . . . , according to Snell's refraction law $(\sin \theta_1)/(\sin \theta_2) = n_2/n_1$, $(\sin \theta_2)/(\sin \theta_3) = n_3/n_2$, $\cdots$, where for quite a wave progress the equality $n_2/n_1 = n_3/n_2$, $\cdots$ may prevail. For such a condition, we should have the same ray curvature along the electromagnetic path. For a gradual change dn/dh of n, as is normally the case, we have $n \sin \theta$ fixed and the conditions of Fig. 272. If then, at a certain altitude h, the index of refraction is $n = \sqrt{\kappa_r}$, then, at the altitude $h + dh$, it must be

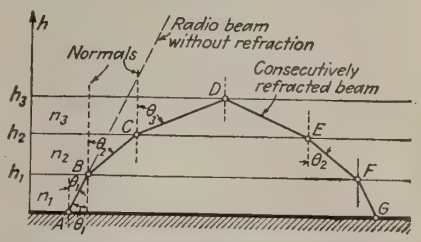

FIG. 271. How a radio beam becomes a curved beam by means of consecutive refraction.

$$n + \frac{\partial n}{\partial h}\,dh = \sqrt{\kappa_r + \frac{\partial \kappa_r}{\partial h}\,dh}$$

At the altitude h, we have the dielectric constant $\kappa = \kappa_0\kappa_r$ farads per meter; and at the altitude $h + dh$, we find

$$\kappa + \frac{\partial \kappa}{\partial h}\,dh = \kappa_0\left(\kappa_r + \frac{\partial \kappa_r}{\partial h}\,dh\right) \qquad \text{farads/m}$$

If, as is often the case, we have dry atmosphere, $\kappa > \kappa + (\partial\kappa/\partial h)\,dh$, with a phase velocity c' at D along the arc DG that is less than the phase velocity $c' + \Delta c'$ at E along arc EF, because

$$c' = \frac{1}{\sqrt{\mu_0 \kappa}} \quad \text{and} \quad c' + \Delta c' = c' + \frac{\partial c'}{\partial h}\, dh = \frac{1}{\sqrt{\mu_0 \left(\kappa + \frac{\partial \kappa}{\partial h}\, dh\right)}} \text{ m/sec} \qquad (888a)$$

At point E of the wave-front element ED, we have a larger phase velocity $c' + \Delta c'$ acting than at point D, where it is only c' meters per second. If the angle $d\theta$ is taken sufficiently small, as well as the width dh of the wave front, AEF and BDG will be concentric circles of radii $\rho + dh$ and ρ of practically the same curvature $1/\rho$. The original wave front $dh = AB$ facing somewhat upward, due to the larger phase velocity $c' + \Delta c'$ along the A circle than the phase velocity c' along the B circle, will gradually turn vertical as ED and afterward face somewhat downward as FG. The wave front BA, by traveling with B on point G, is, therefore, no longer with point A on point A' (as would be the case for equal-phase velocities) but has turned by an angle $d\theta$ into position GF. Since $d\theta$ is exceedingly small, we find tan $(d\theta) = d\theta$ radians and $GF = dh$. Hence,

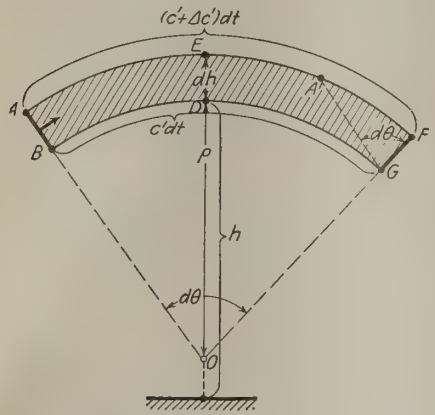

FIG. 272. Condition for the same curvature along the electromagnetic path. AB elementary upward-tilted wave front at the beginning of the wave motion; ED wave front at height h; GF downward-tilted wave front; arc AF m $= (c' + \Delta c')dt^{(\text{sec})}$; arc $BG = c'dt$ m; c' and $c' + \Delta c'$ are phase velocities in m/sec. Curvature due to $n \sin \theta =$ constant for a sector angle $d\theta$; n is index of refraction of the wave medium.

$$d\theta = \frac{(c' + \Delta c')\, dt - c'\, dt}{dh} = \frac{\Delta c' \cdot dt}{dh}$$

proving that the electromagnetic beam follows a curved path owing to the variable phase velocity. The radius ρ of the curvature is found from $\rho\, d\theta = c'\, dt$, where $d\theta$ is in radians and the curvature

$$\frac{1}{\rho} = \frac{d\theta}{c'\, dt} = \frac{\Delta c'(dt/dh)}{c'\, dt} = \frac{\Delta c'/dh}{c'}$$

But $\Delta c' = (\partial c'/\partial h)\, dh$, and

$$\frac{1}{\rho} = \frac{\partial c'/\partial h}{c'} = \frac{d[\log_\epsilon (c')]}{dh} \qquad (888b)$$

is the relation for the curvature. The expression $dc'/dh = c'/\rho$ then fixes the radius ρ of the curved beam. Since $c' = c/n$ and $c = 3 \times 10^8$ m/sec is a constant, we have, for the *equation of ray bending*,

$$\frac{1}{\rho} = n\frac{d(n^{-1})}{dh} = n\left(-\frac{1}{n^2}\right)\frac{dn}{dh} = -\frac{1}{n}\frac{dn}{dh} \tag{888c}$$

This expression gives the path relation in terms of the radius ρ of curvature if the index n of refraction, is, as in our case, known everywhere.

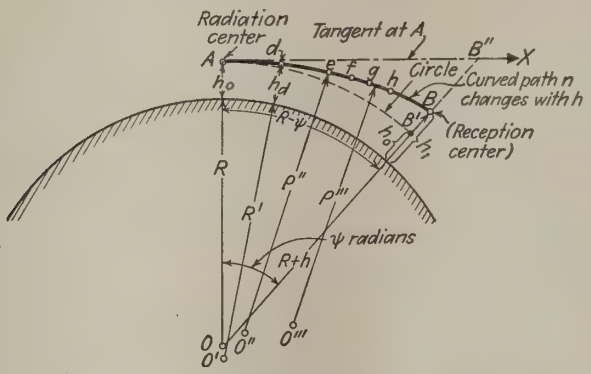

$R' + h_d = \rho$ for arc AD

Curved path AB requires the least time to move electromagnetic wave energy from A through angle ψ to line OB''

$$\int_0^{\psi} \frac{\sqrt{(R+h)^2 + [d(R+h)/d\psi]^2}}{n(R+h)}\,d\psi = \text{minimum}$$

Index n of refraction depends only on variable radius $R + h$, and h varies from h_0 to h_1.

FIG. 273. Actual ray path $AdefghB$ from radiation center A to reception center B due to atmospheric electromagnetic refraction (according to Fermat's law this is the path of fastest wave propagation).

Inasmuch as we know $\kappa_r - 1$ and for atmosphere, according to (886r),

$$n \cong 0.5(\kappa_r - 1) + 1; \qquad \frac{dn}{dh} = \frac{d[0.5(\kappa_r - 1)]}{dh}$$

we find

$$\frac{1}{\rho} = -\frac{0.5}{1 + 0.5(\kappa_r - 1)}\frac{d(\kappa_r - 1)}{dh} = -\frac{[d(\kappa_r - 1)]/dh}{2 + (\kappa_r - 1)} \tag{888d}$$

where for the troposphere $2 + (\kappa_r - 1)$ is very nearly equal to 2, as will be seen from examples that will follow.

177. Remarks on the Path of an Electromagnetic Wave in the Lower Atmosphere. In Fig. 273, the location A denotes the radiation center and $AdefghB$ represents the curved path due to atmospheric electromagnetic refraction, since the index n varies with the height h above ground. The curvature AB is given by formula (888c) as well as by formula

(888*d*) in terms of the relative dielectric constant κ_r of the atmosphere. According to *Fermat's law*, the curvature AB is the path for the fastest propagation, while path AB'' would result if the index n of refraction were constant for all heights h. The path AB' would hold if the curvature $1/\rho$ remained fixed while the wave front turned through an angle ψ.

According to (888*d*), the curves for $\kappa_r - 1$ are as in Fig. 270. These

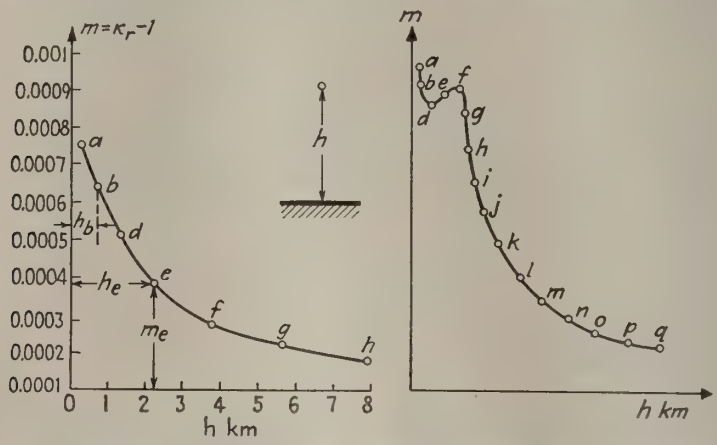

FIG. 274. Characteristic ($\kappa_r - 1$) curves. General equation of the curves is $m = A + Bh + Dh^2 + Eh^3 + Fh^4 + \cdots$, where A, B, D, F, etc., are constants.

curves are then of the form as shown in Fig. 274, and the process of finding the curvatures of path AB in Fig. 273 is as follows.

Any curve can be approximated by a function

$$m = A + Bh + Dh^2 + Eh^3 + Fh^4 + \cdots$$

if A, B, D, E, F, . . . are constants and m is a function of h. The curves in Fig. 270 and the curve to the left of Fig. 274 are single-valued and without inversions. We can then neglect terms higher than h^2 and have parabolas, yielding

$$\kappa_r - 1 = A + Bh + Dh^2 \tag{888e}$$

This is an easy form to differentiate and yields, in combination with (888*d*), the ray curvature

$$\frac{1}{\rho} = -\frac{B + 2Dh}{2 + (A + Bh + Dh^2)} \tag{888f}$$

and a ready means for computing the path AB of Fig. 273. In order to find out to which portion of the $\kappa_r - 1$ curve of Fig. 274 the approximation (888*e*) applies, we choose, for instance, points a, e, and g in Fig. 274 with the corresponding coordinates m and h, which, for point e, are m_e and h_e, respectively. We have then the three equations

$$\underbrace{m_a = A + Bh_a + Dh_a^2;}_{\text{for point } a} \qquad \underbrace{m_e = A + Bh_e + Dh_e^2;}_{\text{for point } e} \qquad \underbrace{m_g = A + Bh_g + Dh_g^2}_{\text{for point } g} \tag{888g}$$

from which the three constants A, B, and D can be found, since the numerical values of h_a, h_e, h_g, m_a, m_e, and m_g are found from the $\kappa_r - 1$ curve of Fig. 274. Inserting the numerical values thus found for A, B, and D in (888e), we find the approximation function for the *abdefhg* curve. If points b, f, and h with their respective coordinates also satisfy (888e) with the numerical constants A, B, and D, found from (888g), the entire curve *abdefg* in Fig. 274 is given by (888e). If this is not practically the case, we know that points a, e, and g, yielding (888g), were chosen too far apart. It is then necessary only to use points closer together, such as a, b, and d, and determine the numerical values of A, B, and D from

$$\underbrace{m_a = A + Bh_a + Dh_a^2;}_{\text{for point } a} \qquad \underbrace{m_b = A + Bh_b + Dh_b^2;}_{\text{for point } b} \qquad \underbrace{m_d = A + Bh_d + Dh_d^2}_{\text{for point } d} \tag{888h}$$

This outcome will then hold to a fair degree of approximation for curve *abd* of Fig. 274.

Equations (888h) are conveniently solved by determinants,[1] in order to find the constants A, B, and D. For the divisor, we have the determinant

$$\Delta = \begin{vmatrix} 1 & h_a & h_a^2 \\ 1 & h_b & h_b^2 \\ 1 & h_d & h_d^2 \end{vmatrix} = 1\begin{vmatrix} h_b & h_b^2 \\ h_d & h_d^2 \end{vmatrix} + 1\begin{vmatrix} h_a & h_a^2 \\ h_d & h_d^2 \end{vmatrix} + 1\begin{vmatrix} h_a & h_a^2 \\ h_b & h_b^2 \end{vmatrix}$$

$$= h_b h_d^2 - h_d h_b^2 + h_a h_d^2 - h_d h_a^2 + h_a h_b^2 - h_b h_a^2$$

A rearrangement of these terms, by using the common factors, is of no value when dealing, as in practice, with numerical values for h_a, h_b, and h_d. The application is just as easy in the form in which the above relations are written. For the sum determinants, we find in the same way

$$\Delta_A = \begin{vmatrix} m_a & h_a & h_a^2 \\ m_b & h_b & h_b^2 \\ m_d & h_d & h_d^2 \end{vmatrix} = m_a\begin{vmatrix} h_b & h_b^2 \\ h_d & h_d^2 \end{vmatrix} + m_b\begin{vmatrix} h_a & h_a^2 \\ h_d & h_d^2 \end{vmatrix} + m_d\begin{vmatrix} h_a & h_a^2 \\ h_b & h_b^2 \end{vmatrix}$$

$$= m_a(h_b h_d^2 - h_d h_b^2) + m_b(h_a h_d^2 - h_d h_a^2) + m_d(h_a h_b^2 - h_b h_a^2)$$

For the numerical values of m_a, m_b, m_d, h_a, h_b, and h_d, we have

$$\Delta_B = \begin{vmatrix} 1 & m_a & h_a^2 \\ 1 & m_b & h_b^2 \\ 1 & m_d & h_d^2 \end{vmatrix} = 1\begin{vmatrix} m_b & h_b^2 \\ m_d & h_d^2 \end{vmatrix} + 1\begin{vmatrix} m_a & h_a^2 \\ m_d & h_d^2 \end{vmatrix} + 1\begin{vmatrix} m_a & h_a^2 \\ m_b & h_b^2 \end{vmatrix}$$

$$= m_b h_d^2 - m_d h_b^2 + m_a h_d^2 - m_d h_a^2 + m_a h_b^2 - m_b h_a^2$$

$$\Delta_D = \begin{vmatrix} 1 & h_a & m_a \\ 1 & h_b & m_b \\ 1 & h_d & m_d \end{vmatrix} = 1\begin{vmatrix} h_b & m_b \\ h_d & m_d \end{vmatrix} + 1\begin{vmatrix} h_a & m_a \\ h_d & m_d \end{vmatrix} + 1\begin{vmatrix} h_a & m_a \\ h_b & m_b \end{vmatrix}$$

$$= h_b m_d - h_d m_b + h_a m_d - h_d m_a + h_a m_b - h_b m_a$$

We have

$$A = \frac{\Delta_A}{\Delta}; \qquad B = \frac{\Delta_B}{\Delta}; \qquad D = \frac{\Delta_D}{\Delta}; \qquad m = A + Bh + Dh^2$$

for portion *abd* of the $\kappa_r - 1$ curve of Fig. 274.

[1] HUND, A., "High-frequency Measurements," p. 438, McGraw-Hill Book Company, Inc., New York, 1933.

Inserting the numerical values A, B, and D in (888f), we need use only one point of the abd portion if satisfactorily approximated by (888e), say mid-point b. We find then from the numerical value h_b, which happens to be about unity, since $h_b \cong 1$ km in Fig. 274, and

$$\frac{1}{\rho} = -\frac{B + 2Dh_b}{2 + A + Bh_b + Dh_b^2} \cong 0.5B + Dh_b \qquad (888i)$$

where ρ denotes the radius of curvature for the altitude range h_a to h_d. Suppose h_0 in Fig. 273 is equal to h_a and h_d is the altitude of path point d. The center O' of curvature Ad is found by locating the intersection of circles with radius ρ about A and d as centers. The arc Ad with O' as center and ρ as radius gives the path Ad. In the same way, all other consecutive portions de, ef, fg, gh, . . . of path AB are found. This procedure gives directly the correct curved path AB with respect to curved earth. It is understood that the readings for the $\kappa_r - 1$ curves must be taken at different altitudes at different locations along the desired direction of wave propagation, since the curved path AB of Fig. 273 may be 40 to 100 miles long and the atmospheric conditions for one and the same height, at $\psi = 0$, may be very different at other angles. This means that the gradient dn/dh_g is not necessarily the same as dn/dh_d. The difference will be especially pronounced the last few hundred feet toward ground.

178. Possible Gradients and Interpretations of Curved Paths and Concept of the Equivalent Earth Radius. Figure 275 shows a curved ray $abdeghk$, whose length is drawn exaggerated with respect to the earth radius R in order to separate respective centers O_1, O_2, O_3 of curvatures ad, dg, and gk. For curvature ad, we have sector O_1adO_1; for sector O_2dgO_2, we have the curvature dg; and curvature gk belongs to sector O_3gkO_3. The curved ray is shown twice in Fig. 278 in order to bring out more clearly the difference between the actual heights h of the actual ray. These heights, such as $h = h_a$ for path point a and $h = h_d$ for point d, must be normal to the circle of earth radius R and *not* to the circle of curvature radii ρ_1, ρ_2, . . . , since these radii are not known to begin with but computed from the $\kappa_r - 1$ curve. The representation to the left of Fig. 275 brings out why $\kappa_r - 1$ curves for different locations along the desired propagation directions are needed in ray diagrams. This is the case, since the same height at point a surely cannot have the same $\kappa_r - 1$ value as at a far-off point at the same altitude, just as we should not always expect the same temperature and the same humidity at locations, say, 40 miles apart, even though at the same level. There is especially a great difference if we deal with locations of gradient inversions and generally with locations close to ground and separated over larger distances. The left illustration of Fig. 275 also shows that a ray may start out with a variable curvature $abde$ and actually pass through a region *above* the tangential plane on a sphere of radius $R + h$ through the radiation center a until the curved ray (refracted ray) cuts through

the plane and curves, according to dn/dh, which is the index of refraction variation along the remainder of the path, such as ghk. Between h and k, the ray actually cuts through the geometric optic line-of-sight plane. This means that reception is possible at certain places in the so-called "electro-optical" shadow region and up to point k. Therefore, *refracted* electromagnetic wave energy can readily pass in the geometrical shadow region. We shall also find that even longer ranges and considerable space below the line-of-sight plane can be filled

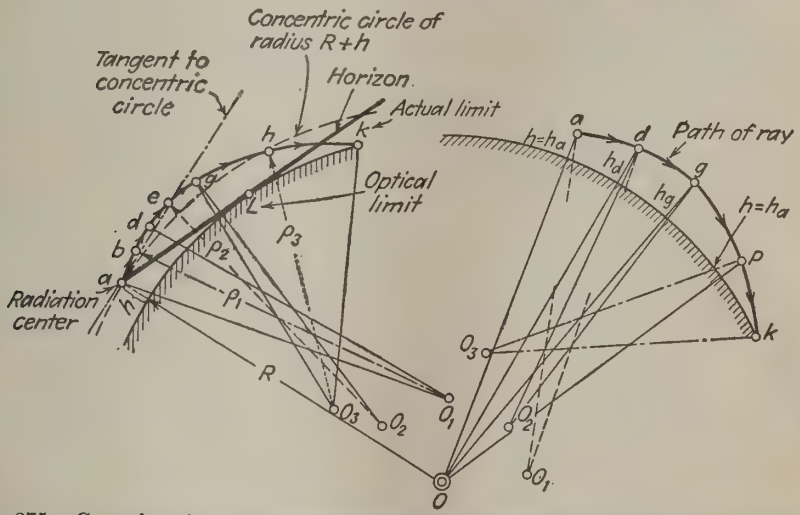

FIG. 275. Curved path of an electromagnetic wave (showing that wave propagation is possible beyond the optical limit L on account of atmospheric refraction). Altitudes h shown exaggerated with respect to radius R of earth. $abdeghk$ is curved ray path. R is radius of earth with center O; ρ_1 is radius of curvature abd and center O_1; ρ_2 of curve deg and center O_2; ρ_3 of curve hk and center O_3.

with electromagnetic fields owing to *diffraction* effects. We then deal with Fresnel diffraction patterns also.

When plotting ray diagrams, we can do this with respect to a circular abscissa axis and extensions of radii for the corresponding height ordinates, as in Fig. 274. This can be done more conveniently by means of rectangular coordinates, for which the distance or range is along the X axis and the height along the Z axis. Such perpendicular reference axes will require a *modification* of the path curvature, as can be readily seen from the representations of Fig. 276. Since the gradient dn/dh, *i.e.*, the variation in the atmospheric index of refraction n with respect to altitude h, accounts for the shape of the path, the polarity of dn/dh as well as the value of d^2n/dh^2 play a part also. The polarity may be *positive as well as negative; i.e.*, $+dn/dh$ or $-dn/dh$ gradients may occur. This

means simply that we have either an increase or a decrease, respectively, for the value of n as h is changed. We can, therefore, have rays that are curved *downward* (convex) and portions of rays that are curved *upward* (concave). For standard atmosphere, we have then a *negative* refraction

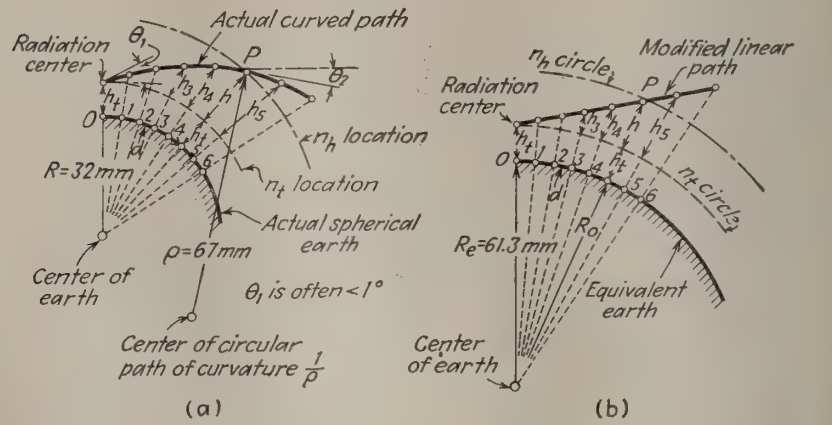

Requirement: $n \sin \theta = \text{constant}$

$$\frac{1}{R_e} = \frac{1}{R} - \frac{1}{\rho}$$

applies *only* when dn/dh is constant. n is index of atmospheric refraction, and h is height above the radiation center.

FIG. 276. Construction of modified path from actual curved path due to atmospheric refraction.

gradient, since the dielectric constant κ_r decreases with the height h, and we have $dn/dh = d(\sqrt{\kappa_r})/dh$ as a negative gradient. It is

$$\frac{dn}{dh} = -(3.5 \times 10^{-8} \text{ to } 3.95 \times 10^{-8}) \text{ per m}$$
$$= -(1.065 \times 10^{-8} \text{ to } 1.2 \times 10^{-8}) \text{ per ft altitude change}$$

For dry air, we find from Fig. 270, for instance, between heights 4 and 5 km, essentially a linear progress; *i.e.*, the tangent on the $h = 4.5$ km point gives about the same slope as the curve portion connecting $h = 4$ and $h = 5$ km points. We can, therefore, use these two points to find the negative dn/dh gradient. We find, for $h = 4$ km, the value $\kappa_r - 1 = 3.70 \times 10^{-4}$ and, for $h = 5$ km, the value $\kappa_r - 1 = 3.41 \times 10^{-4}$. Hence, the gradient

$$\frac{d(\kappa_r - 1)}{dh} = \frac{(3.7 - 3.41)10^{-4}}{4 - 5} = -0.29 \times 10^{-4} \text{ per km}$$

This gradient is the same as the gradient $d(\kappa_r)/dh$, since the constant 1

in $(\kappa_r - 1)$ *cannot* affect the value of the derivative. But $n = \sqrt{\kappa_r} = \sqrt{1 + (\kappa_r - 1)} \cong 1 + 0.5(\kappa_r - 1)$ or

$$n - 1 \cong \tfrac{1}{2}(\kappa_r - 1) \tag{888j}$$

The refractive gradient then becomes

$$\frac{dn}{dh} = \frac{d(n-1)}{dh} = \frac{1}{2}\frac{d(\kappa_r - 1)}{dh} = -0.145 \times 10^{-4} \text{ per km altitude change}$$

For the $h = 0$ to $h = 1$ km region for dry atmosphere, *i.e.*, the first kilometer region above ground, from Fig. 270, we find for $h = 0$ km or at the ground surface, the value $(\kappa_r - 1) = 0.00059$. For an altitude $h = 1$ km, we find $(\kappa_r - 1) = 0.00052$, yielding

$$\frac{dn}{dh} = \frac{[0.5(5.9 - 5.2)10^{-4}]}{0 - 1} = -0.35 \times 10^{-4}$$

per kilometer altitude change right above ground (for the first kilometer region above ground). The values per kilometer show that we have about an average gradient of -25×10^{-6} per kilometer in this region.

Equations (886*p*) and (888*j*) can be brought into the form

$$n - 1 = \frac{1}{2}(\kappa_r - 1) = \frac{79.5 \times 10^{-6}}{T}\left(p_1 + \frac{4{,}800 p_2}{T}\right) \tag{888k}$$

where T denotes the absolute temperature 273+°C, the quantity p_1 is the pressure in millibars for *dry air*, and p_2 is the pressure in millibars for *water vapor*. One millibar is a bar divided by thousand. The definition of a bar, *i.e.*, the cgs unit the "barye," is the pressure of 1 dyne/cm^2. The megabar is 10^6 dynes/cm^2, and the millibar is 10^{-3} dyne/cm^2. We have the relations

$$1 \text{ bar} = 1 \text{ barye} = \text{dynes/cm}^2 = 98.07 \text{ kg/m}^2 = 478.8 \text{ lb/ft}^2 = 6.895 \times 10^4 \text{ lb/in.}^2$$

Figure 276*a* shows a curved path that leaves the radiation center under an angle θ_1 with respect to the horizontal. The radiation center is at a height h_t with respect to ground, while the point P of the curved path makes another angle θ_2 with respect to the horizontal. The $R + h_t$ circle is the location for the reference value n_t, which can be taken *fixed only* for altitudes *higher than* 3 *km* above ground, since, for the lower atmosphere, n_t may vary considerably along the $(R + h_t)$ circle if arcs, say, 20 to 100 miles in length are of concern. The same holds true for the $(R + h_t + h)$ circle if $h_t + h$ is not out of the humidity region of the atmosphere. The simplest curvature condition happens

when the gradient dn/dh is everywhere constant. For such a constancy, we have the same curvature $1/\rho$ or degree of ray bending, which for *standard atmosphere*, according to (888*d*), would be

$$\frac{1}{\rho} = -\frac{\dfrac{d(\kappa_r - 1)}{dh}}{2 + (\kappa_r - 1)} = -\frac{\dfrac{(5.9 - 5.2)10^{-4}}{0 - 1}}{2 + 0.5(5.9 + 5.2)10^{-4}}$$
$$= +\frac{0.7 \times 10^{-4}}{2 + 0.000275} \cong 0.35 \times 10^{-4} \text{ per km}$$

This holds approximately for standard atmosphere (dry air) of the $(\kappa_r - 1)$ curve of Fig. 270 for the first kilometer atmospheric concentric shell. In the denominator for $(\kappa_r - 1)$, the average value for $h = 0$ and $h = 1$ km is taken. It corresponds to $h = 500$ m above ground. Since the radius of the earth taken at the equator is about $R = 6{,}378.4$ km, the curvature of the earth is $1/R = 1.64 \times 10^{-4}$ per kilometer. The path of the electromagnetic wave is, therefore, flatter (less curved) than the surface of spherical earth crust. We have $1.64/0.35 = 4.69$ times more earth curvature. This difference can be expressed by a *modification* of the earth curvature as well as by a *modification* of the actual ray curvature. In one case, we simply take the difference $1/R - 1/\rho = 1/R_e$; and in the other case, we take the difference $(1/\rho) - (1/R)$ and apply it to the ray curvature. Taking up the first case, we find for the equivalent earth curvature $1/R_e$ corresponding to the equivalent radius R_e of the earth

$$\frac{1}{R_e} = \frac{1}{R} - \frac{1}{\rho} \tag{888l}$$

Applying such a concept to the above numerical case, we find

$$\frac{1}{R_e} = (164 - 35)10^{-6} = 129 \times 10^{-6} \text{ per km}$$

We have then an equivalent earth radius $R_e = 10^6/129 = 7{,}750$ km, which yields a ratio $R_e/R = 7{,}750/6{,}378 = 1.22$, or an equivalent earth radius that is 22 per cent larger than the actual earth radius.

For the numerical evaluation for the ray curvature, we note that $1/\rho = -0.5d(\kappa_r - 1)\,dh$ holds essentially, since, even for the severe condition next to the ground, the denominator in Eq. (888*d*), namely, $2 + (\kappa_r - 1) \cong 2$, yields the 0.5 factor in the numerator. Therefore, the curvature of the ray is essentially equal to the refractive gradient or

$$\frac{1}{\rho} = -\frac{dn}{dh} \tag{888m}$$

for most tropospheric rays. This is a simple outcome indeed. We have a *downward* curvature for *negative* and an *upward* curvature for *positive* gradients because $1/\rho$ comes out positive if dn/dh is negative and vice versa.

The above computation is made for R_e, in the case of dry atmosphere, and taken from Fig. 270 for an air layer 1 km thick and next to ground. If we take the average gradient for the entire $(\kappa_r - 1)$ curve for standard (dry) atmosphere, we have, as already computed, $dn/dh = -25 \times 10^{-6}$ per kilometer $= -1/\rho$, and

$$\frac{1}{R_e} = \frac{1}{R} - \frac{1}{\rho} = (164 - 25)10^{-6} = 139 \times 10^{-6} \text{ per km}$$

The equivalent earth radius then becomes $R_e = 10^6/139 = 7{,}194$ km with a ratio $R_e/R = 7{,}194/6{,}378 = 1.13$, *i.e.*, only 13 per cent more radius. In some work, a factor $R_e/R = 1.33$ is employed. This makes $R_e = 1.33 \times 6{,}378 \cong 8{,}500$ km and $1/R_e = 117.8 \times 10^{-6}$ per kilometer. Hence, $1/\rho = 1/R - 1/R_e = (164 - 117.8)10^{-6} = 46.2 \times 10^{-6}$ per kilometer. This refers to a refractive gradient of -0.46×10^{-4} per kilometer or -4.6×10^{-8} per meter. This is the same as -1.4×10^{-8} per foot altitude change. The ratio R_e/R can be computed directly from the formula

$$\frac{R_e}{R} = \frac{1}{1 + R(dn/dh)} \qquad (888n)$$

since

$$\frac{1}{R_e} = \frac{1}{R} - \frac{1}{\rho} = \frac{1}{R} - \frac{dn}{dh} = \frac{1}{R} + \frac{dn/dh}{1} = \frac{1 + R(dn/dh)}{R}$$

It should be realized that the concept of the equivalent radius R_e of the earth has *significance only when dn/dh is constant.* This holds approximately for dry atmosphere, *but not at all* for anomalous atmosphere and conditions with inversions and humidity effects.

In Fig. 276*a*, the actual path, with point P on it, is on an arc with a radius of 67 units, for instance, $\rho = 67$ mm, while the earth is drawn with a radius $R = 32$ mm. Hence,

$$\frac{1}{R_e} = \frac{1}{R} - \frac{1}{\rho} = (3.12 - 1.49)10^{-2} = 1.63 \times 10^{-2} \text{ per millimeter}$$

yielding an effective earth radius $R_e = 100/1.63 = 61.3$ mm. Figure 276*b* gives the equivalent condition with a straight or *modified* path. The representations of Fig. 277 give similar curved-into-linear-equivalent path modifications, for several rays and direct and indirect rays, if the

refractive gradient is fixed (holding only for standard propagation conditions). The construction is exactly the same for each curved ray, as is given in Fig. 276*a* and *b*. It is based on the dn/dh = constant assumption, and the index n_h at altitude $h + h_t$ is fixed along the n_h circle, as is the index of refraction n_t at altitude h_t, corresponding to a circle

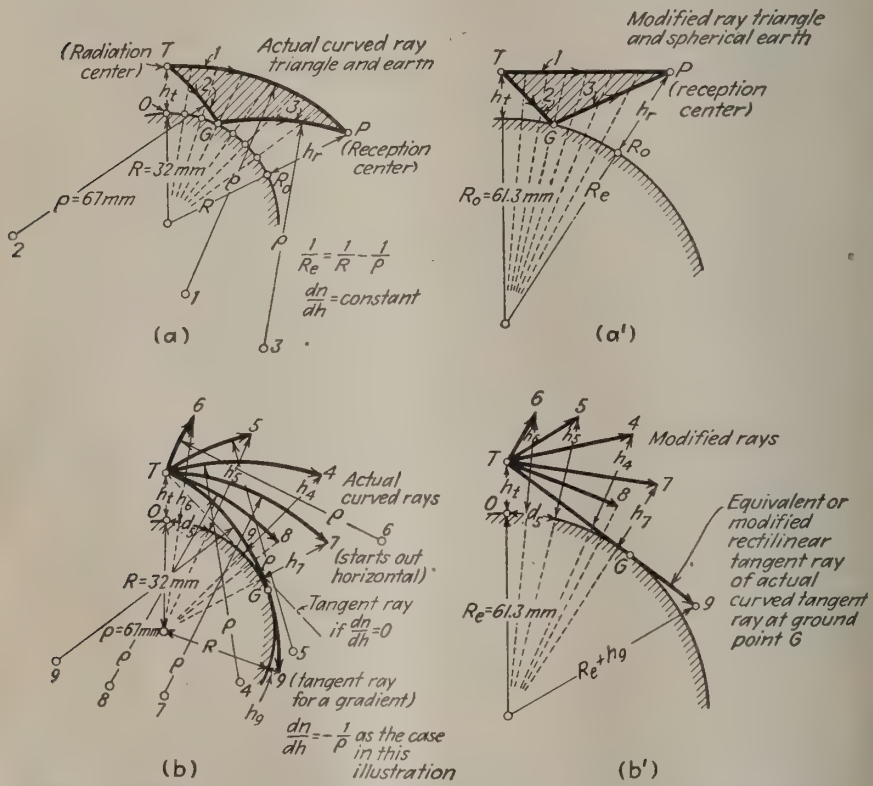

FIG. 277. Modification of curved ray traces. 1, 2, 3, 4, 5, 6, 7, 8, and 9 are centers of circular paths marked with like numbers. *T* is radiation center.

through the radiation center. The distances 0–1, 0–2, 0–3, 0–4, 0–5, 0–6 along the actual spherical earth surface of Fig. 276*a* are the same as the distance 0–1, 0–2, 0–3, . . . along the equivalent spherical earth surface of Fig. 276*b*. In Fig. 277, the height scale is likewise greatly exaggerated. We note that $R_e/R = 61.3/32 = 1.92$ is also a larger ratio now, since it corresponds to an equivalent earth radius of $1.92 \times 6378 = 12{,}246$ km. Such a large ratio as well as the equivalent radius may happen, since, according to (888*l*), for $1/R = 1/\rho$, *i.e.*, equal earth and ray curvature, we have $1/R_e = 0$ or $R_e = \infty$. A ratio R_e/R of infinity is, therefore, a possibility. In Fig. 277*a'*, we have a modified ray pattern

of pattern Fig. 277*a*. The pattern of Fig. 277*b*′ is a modification of the representation of Fig. 277*b*. Inasmuch as linear rays occur in the modified or equivalent ray diagrams, it is not necessary to construct the equivalent linear ray pattern by many points as in Fig. 276. It is necessary only to find the corresponding end point of each ray. Therefore, the modified ray 5 of Fig. 277*b*′ is found by scaling off the distance d_5 from earth point O and increasing the radius R_e by a length equal to h_5. This yields then point 5. The line from T to 5 is then the desired modified ray. In exactly the same way, the direct ray of Fig. 277*a*′ is found by scaling off the same distance OR_0 of Fig. 277*a* (along the actual spherical earth) along the equivalent earth of Fig. 277*a*′ and increasing the radius R_e by h_r. This yields the space point P in Fig. 277*a*′. The direct ray is then the straight connection from T to P in Fig. 277*a*′. By scaling off the distance OG taken from Fig. 277*a* along the R_e circle in Fig. 277*a*′ and connecting G with P, the remainder of the ray triangle is found in Fig. 277*a*′. On account of the exaggerated h scale, the angles appear many times larger (angles of incidence and reflection). The curved tangent ray $TG9$ in Fig. 277*b* shows in comparison with the dash-dot-dash line-of-sight straight ray that much wave energy may be refracted into the optical shadow region and over a considerable distance *beyond and below the optical horizon*. Moreover, since $R = 32$ mm in this figure corresponds actually to $R = 6{,}378$ km, we have 1 mm equivalent to $6{,}378/32 = 199.3$ km. Therefore, in Fig. 277, we have $\rho = 67$ mm actually as $67 \times 199.3 = 13{,}330$ km. According to (880*m*), the fixed refractive index gradient becomes $dn/dh = -1/13{,}330 = -75 \times 10^{-6}$ per kilometer altitude change. But

$$\frac{dn}{dh} = 0.5\,\frac{d(\kappa_r - 1)}{dh} = 0.5\,\frac{d\kappa_r}{dh} = -75 \times 10^{-6} \text{ per km}$$

Calling κ_1 the relative value of a certain concentric layer of the atmosphere at the altitude h_1 and κ_2 the relative dielectric constant of a concentric layer of height h_2 above the earth surface, where h_2 is 1 km below h_1, we find

$$\frac{d\kappa_r}{dh} = \frac{\kappa_1 - \kappa_2}{h_1 - h_2} = -15 \times 10^{-5} \text{ per km}$$

Assuming that at h_1 we have a relative value $\kappa_1 = 1.0$, and since -15×10^{-5} is the negative gradient per kilometer, we have $h_1 - h_2$ equal to unity, and

$$\frac{\kappa_1 - \kappa_2}{h_1 - h_2} = 1 - \kappa_2 = -15 \times 10^{-5}; \qquad \kappa_2 = 1.00015$$

This yields an average value $\kappa_r = 1.000075$ for the concentric atmospheric

shell of thickness $h_1 - h_2 = 1$ km. The concentric shell is then bounded by spheres of radii $R + h_1$ and $R + h_2$, where $R = 6{,}370$ km. This corresponds to an average dielectric constant of $1.000075 \times 8.854 \times 10^{-12}$ farad/m, which is essentially the value holding for empty space. The reason for this is that we assumed respective altitudes close to the location where the value for empty space prevails, since κ_1 was taken as 1.0 for h_1 and h_2 is only 1 km shorter than h_1. If we were to go to a layer of altitude h_3, which is another 1 km closer to ground, we should have, at altitude h_3, a relative dielectric constant $\kappa_3 = \kappa_2 + 15 \times 10^{-5} = 1.0003$. For the next altitude h_4 another 1 km closer to ground, we find $\kappa_4 = 1.00045$, since Fig. 277 is based on a constant value of dn/dh.

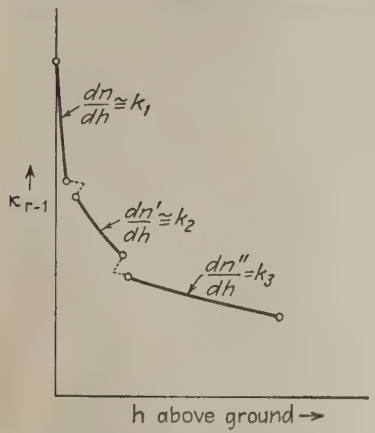

FIG. 278. Conditions in the lower atmosphere that may occur.

The assumption of a constant refractive gradient is rather an ideal case. It may be realized in practice, however, in the case of dry atmosphere over quite a range if next to ground. It may also happen for humid air for certain altitude ranges. We may then have a range with a constant value dn/dh, from ground up to about 0.5 km; then an erratic variation, which may be partially caused by a positive gradient (due to a temperature inversion) for an atmospheric thickness of about 200 m (above the 0.5 km altitude); then another linear decrease dn'/dh of different steepness for another 1 km, for instance; then again an erratic variation; then again another linear decrease, but of steepness dn''/dh; etc. Such conditions, which may happen, are indicated in Fig. 278.

We must distinguish between wave propagation for standard tropospheric conditions and tropospheric conditions of the lower atmosphere, for which this is not the case. For standard atmosphere, the index n of refraction varies steadily with the altitude h above ground level. The ray bending is then often taken care of by using an effective earth radius R_e, which is equal to $\frac{4}{3}$ times the true earth radius R at the earth surface. Owing to changes in climatic conditions in the lower atmosphere, such as temperature inversions when warm dry air blows over a cool body like ocean and sometimes over certain earth surfaces, we deal with anomalous atmosphere and a corresponding anomalous short-wave propagation. It is then customary to employ a modified index M of refraction defined by

$$M = 10^{+6}\left(n - 1 + \frac{h}{R}\right)$$

where n denotes the actual index of tropospheric refraction at height h above ground level and R is again the radius of the earth at said ground level. We have then the following tropospheric graphs if we plot h against the modified index M. For standard tropospheric conditions, the graph represents a *forward*-tilted line in the h against M plot, and the customary ray theory can be used (we need a uniform slope). However, when the slope does not remain uniform, we deal with a slope variation of the h-against-M curve. This will cause a bending of the resultant field intensity pattern. If the plot starts out at ground level ($h = 0$) with a *backward*-tilted straight line until it reaches a height of h_1 above ground level and then continues with a straight-line *forward* tilt toward higher altitude h values, the wave-duct theory must be used, and we can normally expect a wave duct for the atmospheric layer with a thickness h_1. This is known as simple "surface trapping." The value of h_1 may be any value from a few hundred to a few thousand feet, depending upon the operating frequency and the atmospheric conditions. The trapped wave energy may then be guided in the duct for very long distances, and a receiving aerial *within* the *duct* will make possible anomalous long-distance reception. The layer forming the duct is seldom as ideal as mentioned, and complete wave trapping can hardly be expected. If we have a plot for which a linear *forward* tilt occurs for a layer above ground up to a height h_1 and then a continuation that is a smaller *forward* tilt, we have a condition known as "substandard." Normally, the h-against-M plot[1] is not so simple but starts out with a forward "knee" and continues with a smaller linear forward tilt, for instance. We have then essentially a linear forward tilt from $h = 0$ to $h = h_1$, corresponding to $M = M_0$ and $M = M_1$, respectively. The plot then continues with a linear forward tilt of the same slope until the altitude $h = h_2$ is reached, corresponding to $M = M_2$. The plot then continues with a linear backward tilt up to about an altitude $h = h_3$, corresponding to $M = M_3$. The plot then continues rather abruptly to a linear forward tilt for larger values than h_3, but with less forward slope than the forward slope for the plot between $h = 0$ and $h = h_2$. Near altitudes h_2 and h_3, the transitions in the plot are curved. For such a condition, we can cause an *elevated* wave duct between h_1 and h_3. The plot assumes that $M_0 < M_1$, $M_2 > M_1 > M_3$, and $M_1 = M_3$.

[1] For details consult a declassified report by I. Katz of the MIT Radiation Laboratory. See also M. Katzin, R. W. Bauchman, and W. Binnan, *Proc. IRE*, **35**, 891–905, September, 1947.

Generally, it may be said that for a troposphere for which the index n of refraction decreases with height h, electromagnetic rays of sufficiently small initial elevation with the ground level will be refracted downward with a curvature proportional to the rate of decrease of n with h. If the radius of the curvature then becomes smaller than the radius R of the earth, the electromagnetic ray reaches a maximum height h_{max} above ground level and becomes "trapped" between h_{max} and $h = 0$. Trapping of electromagnetic field energy within a wave duct requires that the M plot must have a region of *negative* slope. The quantity M represents the excess over unity in parts per million. Experimental results carried out under the auspices of the Naval Research Laboratory, Washington, D.C., by Katzin, Bauchman, and Binnan[1] in the Atlantic trade-wind area off the east coast of Antigua, British West Indies, showed that *low*-level wave ducts of a strength of 5 to 10 M units existed all the time when the measurements were made. This infers that the height and strength of the wave duct appear to depend on the wind speed, for which low winds cause low ducts of moderate strength while higher winds cause higher ducts of weaker strength. The measurements refer to microwaves of about 3- and 9-cm wavelength (10,000 and 3,333.3 Mc/sec) between ship and shore stations. The ducts were as low as $h = 20$ and 60 ft over the ocean surface, providing a trade wind prevailed. The height of the duct as well as its strength changes with the wind speed. For wind speeds of 8 to 15 knots, a low and moderately strong duct is caused; while for speeds from 20 to 30 knots, a higher but weaker duct is caused, *i.e.*, a smaller M deficit duct. Passing squalls and rain showers do not decrease the received signal strength. The measurements also show that the rates of attenuation yield higher values on 3-cm waves than predicted by the duct theory and that there may be an optimum range of frequencies for the utilization of such low ducts. For 9-cm waves, there seems to be a decided decrease in the attenuation rate for distances beyond about 80 miles. On 3-cm waves, antenna locations at $h = 6$ to 15 ft give stronger reception effects and greater reception ranges; while on 9-cm waves, stronger fields exist at heights h up to at least 100 ft.

With respect to propagation of waves in the lower troposphere, reference is also made to a paper by J. B. Smyth and L. G. Trolese[2] of the U.S. Navy Electronics Laboratory at San Diego, Calif. It is shown that there is a possibility of wave propagation over longer ranges in the

[1] *Loc. cit.*

[2] *Proc. IRE*, **35**, 1198–1202, November, 1947. PEKERIS, C. L., Perturbation Theory of Normal Modes for an Exponential M-curve in Nonstandard Propagation of Microwaves, *Jour. Appl. Phys.*, **17**, 678–684, August, 1946.

lower atmosphere and over distances many times the optical line of sight on the higher frequencies, while longer waves are diffracted around the earth's surface and a small frequency range of intermediate frequencies may come down from the ionosphere. Typical index n of refraction curves are also given in this paper, with several useful references on the same subject matter. This paper is based on experimental work and refers particularly to an elevated refracting stratum, which is taken as a plane reflecting layer and agrees with the experimental frequency dependency. For layers greater than the critical height, height-gain calculations in the optical region, together with reflection coefficients, yield the electromagnetic fields to be expected beyond the optical horizon. If we had a well-mixed troposphere, the refractive index n would decrease essentially linearly with increasing altitude h above ground level. For this reason, refraction may be substituted by diffraction of electromagnetic waves around a spherical earth of equivalent radius $R_e = 4R/3$ where R denotes the actual radius at the ground level. For the R_e sphere, we deal with an equivalent homogeneous surrounding air of index $n = B$. Reflection from elevated layers of horizontally stratified atmosphere yields a field amplitude reflection coefficient

$$\rho = \frac{\sinh [\pi(\alpha - \beta)]}{\sinh [\pi(\alpha + \beta)]}$$

for $\alpha = pB_1 \cos \theta_1$ and $\beta = pB_3 \cos \theta_3$, where θ_1 is the angle at which the electromagnetic wave is incident upon the transition stratum and θ_3 denotes the refracted angle into the stratum layer. The index of refraction variation through the transition region between two air masses, according to P. S. Epstein and C. Eckart,[1] is approximately given by $[B_z]^2 = \frac{1}{2}(B_3^2 + B_1^2) + \frac{1}{2}(B_3^2 - B_1^2) \tanh (\frac{1}{2}u)$ where B_1 and B_3 are the values of the index of refraction in medium 1 and 3, respectively, and $u = (2\pi/\lambda)(z/p)$. The factor p determines the thickness of the transition region, and z is the altitude h. An index n of refraction variation occurs, for instance, through the interface between two different air masses, one mass, having considerable water-vapor content.

179. Modified Electromagnetic Wave Paths for an Equivalent Flat Earth and for Oblique Coordinates. By subtracting the curvature $1/\rho$ of the ray from the curvature $1/R$ of the actual spherical earth, we have succeeded (in Figs. 276 and 277) in obtaining rectilinear propagation paths by the concept of an equivalent earth curvature $1/R_e$, which is equal to the difference $(1/R) - (1/\rho)$. There is no difficulty, however,

[1] Epstein, P. R., Reflection of Waves in an Inhomogeneous Absorbing Medium, *Natl. Acad. Sci.* **16**, 627–637, October, 1930. Eckart, C., The Penetration of a Potential Barrier by Electrons, *Phys. Rev.*, **35**, 1303–1309, June, 1930.

in working directly with curved paths as in Fig. 277*a* and *b*, where we deal with the actual radius R of the earth. The reason for this is that the path difference between the indirect ray *TGP* and the direct ray *TP* can be *found rapidly by* means of *a map measure.* However, in some work, it may be of advantage to work with angular or oblique coordinates. The range d along the earth surface is then plotted as abscissa and the altitude along certain oblique coordinates. To do this, we have to

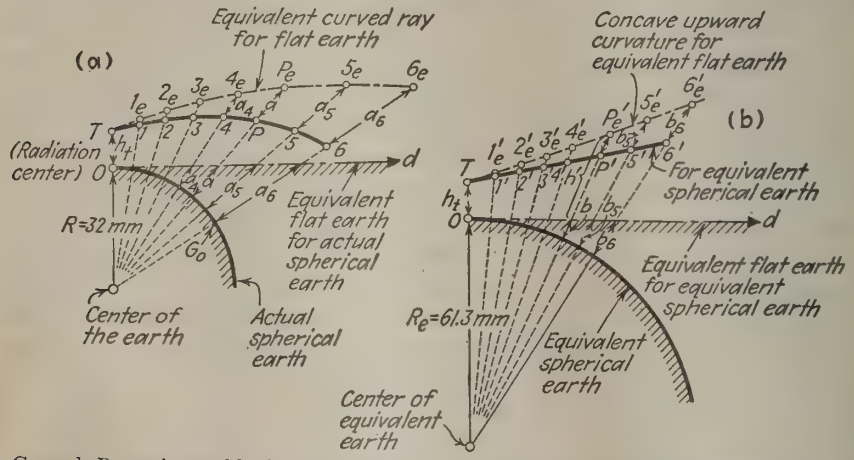

Curved P_e path would also hold when curvature of actual path T, 1, 2, 3, 4, P, 5, 6 varies or dn/dh varies

Concave upward doubly modified TP_e path (holds only for dn/dh = constant). Singly modified path TP' is obtained from relation $\frac{1}{R_e} = \frac{1}{R} - \frac{1}{\rho}$

FIG. 279. Modified path with oblique ordinates and changed *Od* scale.

modify the equivalent rectilinear ray diagrams of Fig. 277*a'* and *b'* to paths with respect to equivalent flat earth. The method used is shown in Fig. 279. It is seen that we may deal with two kinds of equivalent flat earth. For one kind (Fig. 279*a*), the actual spherical earth is basic; and for the other kind (Fig. 279*b*), a larger equivalent spherical earth is basic. The first kind (Fig. 279*a*) has the advantage that the construction of the T, 1_e, 2_e, 3_e, 4_e, P_e, 5_e, 6_e curved path holds even if the gradient dn/dh is not the same everywhere. The gradient may, therefore, vary. It applies then also when the absolute humidity gradient with respect to altitude is mostly responsible for the ray curvature. The construction of *Fig.* 279*b holds only for actual circular paths* T, 1, 2, 3, 4, P, 5, 6, *i.e., for a constant gradient* dn/dh. We have then always upward curvatures. The constructions are as follows:

For either kind, we draw a tangent (a tangent plane) at the foot point of the radiation center on respective spheres. These are the dash-dot-dash lines *Od* in

Fig. 279*a* and *b*. Since, in each case, the respective spherical earth is below this tangent plane, the corresponding modified rays T, 1_e, 2_e, 3_e, 4_e, P_e, 5_e, 6_e and T, $1'_e$, $2'_e$, $3'_e$, $4'_e$, P'_e, $5'_e$, $6'_e$ must be above the actual path T, 1, 2, 3, 4, P, 5, 6 and linear path $TP'G'$, respectively. We then find in Fig. 279*a* the point 6_e of the modified path by producing the radius vector of point 6 of the actual path and adding length a_6. This brings point G_0 on the actual earth to the corresponding point on the equivalent earth. In the same way, all the other points 5_e, P_e, 4_e, 3_e, 2_e, 1_e are found in Fig. 279*a*. We have, therefore, oblique ordinates. In Fig. 279*b*, we have always upward

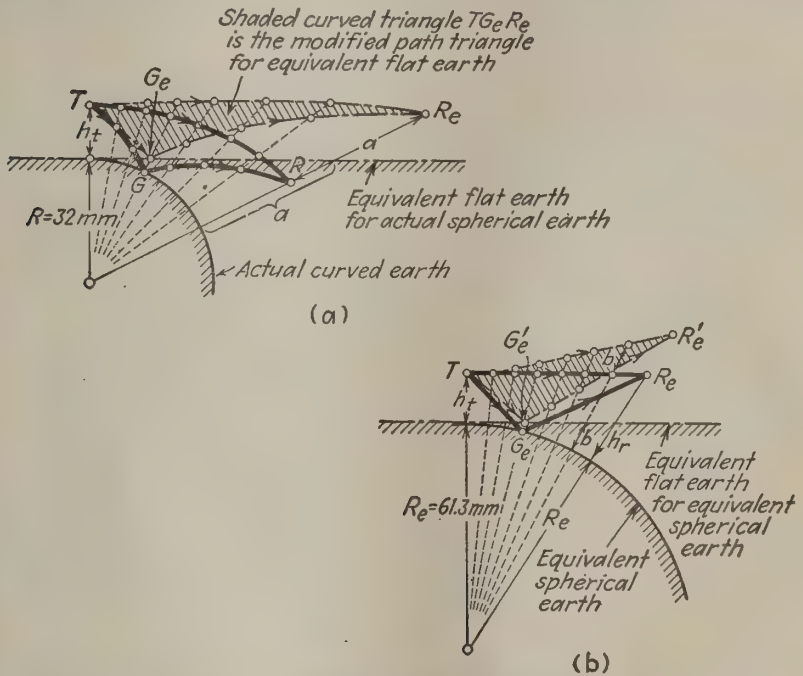

FIG. 280. Ray triangle for actual spherical earth modified to flat earth, and for equivalent spherical earth modified to flat earth. Full-line curved path triangle TGR for actual spherical earth. T is radiation center; R_e and R_e' are reception centers. (*a*) Can be applied to cases for which dn/dh is variable or constant and when d(absolute humidity)/dh causes essentially the gradient. (*b*) Holds only for dn/dh = constant.

curvature in the modified TP'_e path, because the various distances b_1, b_5, b, b_4, b_3, b_2, and b_1 change the equivalent spherical earth circle into the tangent line Od, and the straight line T, 1′, 2′, 3′, 4′, P', 5′, 6′ changes consequently into the upward path T, $1'_e$, $2'_e$, $3'_e$, $4'_e$, P'_e, $5'_e$, $6'_e$. In these modified path diagrams of Fig. 279, it should be realized that even though the distance d along the surface can be called an abscissa, it is only one height, namely, height h_t, that is an orthodox ordinate. All other heights such as h' for point P'_e in Fig. 279*b* are always along the corresponding radius of the spherical earth.

Figure 280 shows other ray diagrams for equivalent flat earth, using the construction procedure of Fig. 279. We note that for equivalent spherical earth (Fig. 280*b*), the triangle TG_eR_e modified to plane earth becomes a concave curved triangle $TG'_eR'_e$ while for Fig. 280*a* the rays are convex and form the triangle TG_eR_e.

180. Modified Wave Paths for Equivalent Flat Earth with Rectangular Coordinates. We have now orthodox rectangular coordinates with the heights plotted perpendicular with respect to the horizontal range. The method is based on

$$\left.\begin{aligned} &\frac{1}{R}-\frac{1}{\rho}=\frac{1}{R_e} && \text{determines equivalent earth radius } R_e \\ &\frac{1}{\rho}-\frac{1}{R}=\frac{1}{\rho_e} && \text{determines equivalent curvature } \frac{1}{\rho_e} \text{ for equivalent flat earth} \end{aligned}\right\} \quad (888o)$$

In Fig. 281, the construction of the equivalent ray curvature $1/\rho_e$ is given. The actual as well as the equivalent spherical earth, respectively,

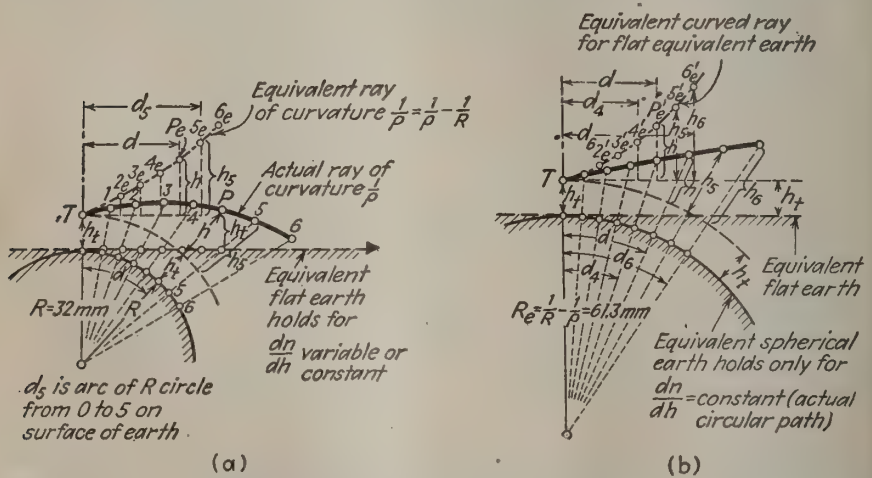
Equivalent ray of curvature $\frac{1}{\rho}=\frac{1}{\rho}-\frac{1}{R}$
Actual ray of curvature $\frac{1}{\rho}$
Equivalent flat earth holds for $\frac{dn}{dh}$ variable or constant
d_5 is arc of R circle from 0 to 5 on surface of earth
R=32mm
(a)
Equivalent curved ray for flat equivalent earth
Equivalent flat earth
Equivalent spherical earth holds only for $\frac{dn}{dh}$=constant (actual circular path)
$R_e=\frac{1}{R}-\frac{1}{\rho}$=61.3mm
(b)

FIG. 281. More convenient modifications by means of equivalent earth radius R_e and equivalent ray curvature $1/\rho_e$, respectively.

is bent over, as it were, into flat earth surface. This also requires that the actual curved ray in Fig. 281*a* and the equivalent straight ray in Fig. 281*b* be likewise correspondingly deformed into respective rays T, 1_e, 2_e, 3_e, 4_e, P_e, 5_e, 6_e in Fig. 281*a* and T, $1'_e$, $2'_e$, $3'_e$, $4'_e$, P'_e, $5'_e$, $6'_e$ in Fig. 281*b*. The procedure consists in scaling off, for instance, along the dash-dot-dash tangential abscissa, for point P, the distance d along the actual spherical earth of radius R and choosing as the corresponding perpendicular ordinate a length $h_t + h$, yielding point P_e in Fig. 281*a*. We find in exactly the same way the point P'_e in Fig. 281*b*, except that we have a larger equivalent spherical earth of radius R_e. Inasmuch as Fig. 281*b* is a "double" modification, namely, from actual spherical earth to equivalent spherical earth and then from equivalent spherical earth into

equivalent flat earth, nothing seems to be gained by going through two modifications, since the equivalent flat earth is most likely to be used. For this reason, Figs. 282 and 283 deal only with equivalent flat earth with respect to actual earth curvature. For both equivalent ray diagrams, the distances d along the tangential plane direction are then actual distances along the actual spherical earth, corresponding to an earth radius of about 6,378 km. The corresponding ordinates are the actual heights above ground. It should be realized that this *procedure*

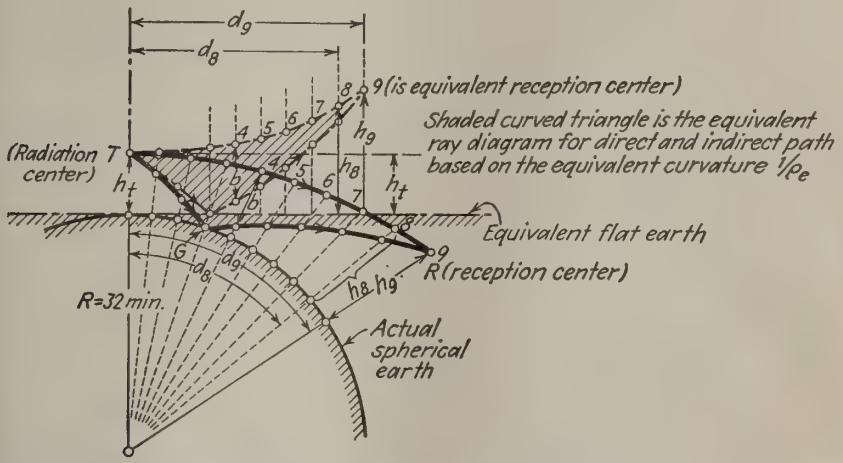

FIG. 282. Modification based on equivalent ray curvature $1/\rho_e = (1/\rho) - (1/R)$ (seems preferred modification). Full-line curved triangle is actual ray traces. TGR is the actual curved path diagram. h scale is greatly exaggerated. *Note:* This construction does *not* assume that dn/dh = constant and holds for any direct path TR curvature change as well as for any indirect ($TG + GR$) curvature change.

applies to any dn/dh variation, since it is based on the subtraction of the earth curvature $1/R$ from the actual ray curvature $1/\rho$, in order to yield the equivalent ray curvature $1/\rho_e$. The result is again a curved-ray triangle. The curvature is no hindrance, since, for the evaluation of the path difference between the indirect and direct rays, we use *a map measure.* There is no difficulty in following a curved trace with a map measure. Figure 283 shows how the procedure can be applied for ray traces based on height-distance coordinates that are rectangular. We have in this figure, for the actual rays A, B, C and D above actual spherical earth, the corresponding equivalent rays A_e, B_e, C_e and D_e in the case of equivalent flat earth. The construction for the equivalent rays is indicated in this figure. The D ray is one for which the curvature changes, while rays A, B, and C have fixed curvature, *i.e.*, a fixed dn/dh condition.

181. Concluding Remarks on Ray Traces. The procedure just described in connection with Figs. 281*a*, 282, and 283 seems to be about the most useful method of plotting rays, since it *holds for any refractive gradient dn/dh irrespective of gradient changes.* The D path can then be translated into an equivalent D_e path for equivalent flat earth and rectangular coordinates. In connection with such work, it must be realized, however, that the over-all shape of the ray depends on two parameters.

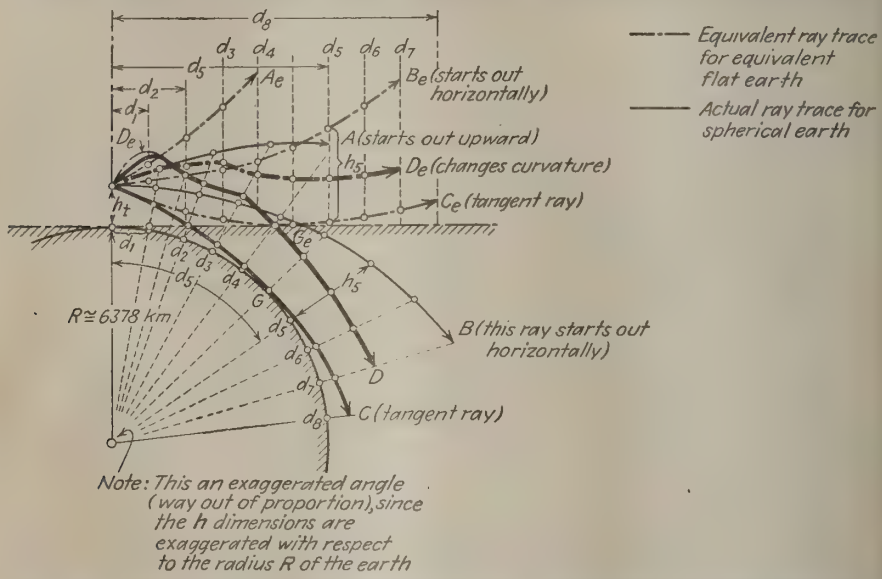
Equivalent ray trace for equivalent flat earth
Actual ray trace for spherical earth
Be (starts out horizontally)
A (starts out upward)
De (changes curvature)
Ce (tangent ray)
B (this ray starts out horizontally)
D
C (tangent ray)
R ≅ 6378 km
Note: This an exaggerated angle (way out of proportion), since the h dimensions are exaggerated with respect to the radius R of the earth

FIG. 283. Construction of the equivalent ray traces for an equivalent flat earth (for a constant and a variable index of refraction gradient dn/dh). A, B, C, and D are actual rays, and A_e, B_e, C_e, and D_e are equivalent rays. Actual rays A, B, and C have constant curvature $1/\rho$, since dn/dh = constant. Actual ray D varies the $1/\rho$ value because dn/dh varies.

One parameter is the gradient dn/dh, which may be referred to the radiation center location and the relative index of refraction of the atmosphere with respect to vacuum. Calling the relative index of refraction at the radiation center n_t at h_t, the ratio of the relative index n_h at another altitude h to the value at altitude h_t, or n_h/n_t, can only partially characterize the ray shape, since this ratio may and will normally be different along the direction of wave propagation for a large field coverage. In Figs. 250, 251, and 252, we have shown space patterns. If the atmospheric refraction is ignored, the space patterns will look like the solid patterns in Fig. 284; while for atmospheric refraction, the patterns are as indicated roughly by the dash-dot-dash contours. If the concept of equivalent earth curvature $1/R_e$ is taken into account, the ratio R_e/R of equivalent to actual earth radius changes with warm and moist atmosphere. Better

coverage (longer ranges) occur for larger R_e/R values. Warm winds seem to increase this ratio. Ratios from 1.2 to 2.0 and higher occur often, and ranges up to 100 miles against 20 miles (normal coverage) may occur. For altitudes larger than about 1 km, the ratio R_e/R falls off and, at 7.5 km altitude, falls to values of 1.05 and may even be less.

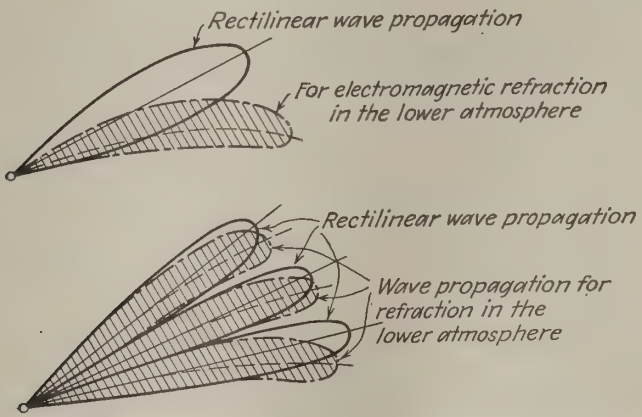
Rectilinear wave propagation
For electromagnetic refraction in the lower atmosphere
Rectilinear wave propagation
Wave propagation for refraction in the lower atmosphere

FIG. 284. Polar field intensity pattern in planes normal to the tangential ground plane through the radiation center and its foot point.

Even though atmospheric water vapor causes only small changes in the dielectric constant, we may have coverages due to such causes that are up to 10 fold and more.

182. Effect of a Perfectly Conducting Plane Reflector on the Gain in a Preferred Direction of a Radiator That Is in Front of the Reflector. Numerical speculations in some of the previous sections show that a copper plate acts with practically 100 per cent reflection to short waves. It is also a comparatively easy matter to employ such reflectors for short waves, since the dimensions of the reflector extensions are not prohibitive. For a copper sheet as in Fig. 285, a distance d meters from a distant field point P, we have for a half-wave dipole AB a distance of x meters in front of the reflector, for the sheet extending strictly to infinity, an inverted image dipole $A'B'$ just as far behind the reflector. The electric field intensity at the distant field point is then due to the effects of the actual and the image dipoles, given by

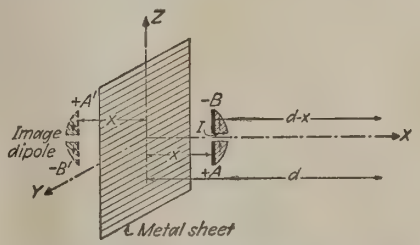

FIG. 285. Half-wave linear dipole in front of a quasi-perfect reflector. I is in amp; d, x, λ in meters. $\beta = 2\pi/\lambda$; $1/(d + x) \cong 1/d \cong 1/(d - x)$.

$$\mathcal{E} = \underbrace{j\frac{60I}{d-x}\epsilon^{-j\beta(d-x)}}_{\text{due to } AB} - \underbrace{j\frac{60I}{d+x}\epsilon^{-j\beta(d+x)}}_{\text{due to } A'B'}$$

$$\cong j\frac{60I}{d}\epsilon^{-j\beta d}(\epsilon^{j\beta x} - \epsilon^{-j\beta x}) = j\frac{120I}{d}\epsilon^{-j\beta d}\sin(\beta x) \quad \text{volts/m} \qquad (889)$$

If we take I as the effective value in amperes for the dipole entrance current, then $\mathcal{E}_r$ represents the effective electric field intensity at field point P in the presence of the reflector, since $\epsilon^{-j\beta d}$ is the space phase factor. We have then

$$\mathcal{E}_r = \frac{120I}{d}\sin(\beta x) \quad \text{volts/m} \qquad (889a)$$

The actual antenna requires an input voltage

$$E = IZ_s - I_{\text{image}}Z_m = I(Z_s - Z_m) \quad \text{volts}$$

for the self-impedance $Z_s = R_s + jX_s$ of the actual half-wave dipole, in absence of the metal sheet, and the mutual impedance $Z_m = R_m + jX_m$ due to the image antenna caused by the presence of the reflecting sheet. The power delivered to the actual radiator then becomes

$$P = (R_s - R_m)I^2 = \frac{\mathcal{E}_r^2 d^2(R_s - R_m)}{120^2\sin^2(\beta x)} \quad \text{watts}$$

When the reflector is removed, we have $Z_s = 73.4 + j42.9$ ohms, according to pages 650, 651, 654–655, 661, 667, 670, 697, 716, if the current filament theory with a sinusoidal current distribution is employed. We have then $\mathcal{E}_s = 60I_s/d$ volts per meter at the field point P, and

$$P = I_s^2 R_s = \frac{\mathcal{E}_s^2 d^2 R_s}{60^2} \quad \text{watts}$$

yielding the comparisons

$$\left.\begin{aligned} \mathcal{E}_s^{(\text{volts/m})} &= \frac{60}{d}\sqrt{\frac{P}{R_s}} \quad \text{for } \frac{\lambda}{2} \text{ radiator without reflector} \\ \mathcal{E}_r^{(\text{volts/m})} &= \frac{120\sin(\beta x)}{d}\sqrt{\frac{P}{R_s - R_m}} \quad \text{for } \frac{\lambda}{2} \text{ radiator } \textit{with} \text{ reflector} \\ R_s &= 73.4 \text{ ohms} \end{aligned}\right\} \qquad (889b)$$

This yields a field gain G at point P of

$$G = 20\log_{10}\left(\frac{\mathcal{E}_r}{\mathcal{E}_s}\right) = 20\log_{10}\left(\frac{2\sin(\beta x)}{\sqrt{1 - (R_m/R_s)}}\right) \quad \text{db} \qquad (889c)$$

An application of this outcome is then as follows:

Suppose a half-wave radiator is a distance $x = \lambda/4$ in front of a conducting plane. The image antenna, which is in antiphase excitation, is a distance $2x = 0.5\lambda$ meters from the actual antenna. Table 30 shows that for such a distance, we have a mutual radiation resistance $R_m = -12.48$ ohms owing to the image effect. Therefore, $R_m/R_s = -12.48/73.4 = -0.17$; $\sqrt{1 - (R_m/R_s)} = \sqrt{1.17} = 1.08$; $\beta x = 2\pi\lambda/4\lambda =$

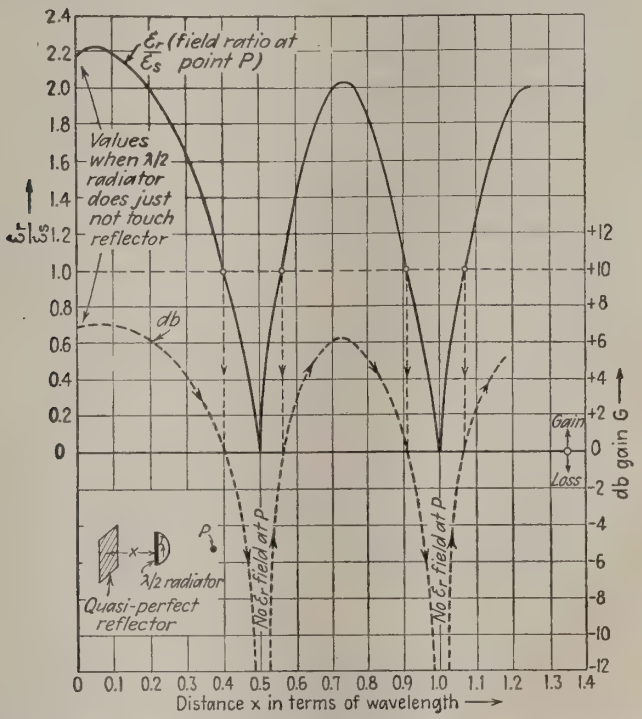

FIG. 286. Ratio of the electric field $\mathcal{E}_r$ with a *quasi-perfect* reflector to electric field $\mathcal{E}_s$ without a perfect reflector.

$\pi/2$, or 90 electrical degrees; $2 \sin(\beta x) = 2$; and $G = 20 \log_{10}(2/1.08) = 5.36$ db gain, for field points P straight ahead along the $+X$ axis of Fig. 285. Formula (889*c*) shows that for a distance $x = \frac{1}{2}\lambda, 1\lambda, 1.5\lambda, 2\lambda, 2.5\lambda, \ldots$, the ratio $\mathcal{E}_r/\mathcal{E}_s$ vanishes, since $\sin(\beta x) = 0$. It is the field intensity $\mathcal{E}_r$ in presence of a perfect reflector that becomes zero for such integer half-wavelength spacings, according to (889*a*). Table 62 gives the application for several spacings, and the curves of Fig. 286 give the ratio for $\mathcal{E}_r/\mathcal{E}_s$ as well as the field gain in the presence of a perfect reflector.

It is seen that for a plane reflector, unlike a tuned radiator, a quarter wavelength behind the actual radiator, we have only a field ratio 1.85, corresponding to 5.36 db gain, instead of a ratio 2, yielding a 6.02-db gain. But for other spacings there are maxima that exceed the latter gain. An optimum maximum, corresponding to the ratio $\mathcal{E}_r/\mathcal{E}_s = 2.24$,

TABLE 62. HALF-WAVE RADIATOR IN FRONT OF A METAL SHEET

Distance x to reflector	$q = \frac{\mathcal{E}_r}{\mathcal{E}_s}$	$\log_{10}(q)$	Field gain $G = 20 \times \log_{10}(q)$, db	Distance x to reflector	q	$\log_{10}(q)$	Gain G, db
Almost 0λ	2.2	0.3424	6.848	0.5λ	0.00		
0.05λ	2.23	0.3483	6.966	0.52λ	0.28	−0.5528	−11.05 loss
0.06λ	2.24	0.3502	7.004	0.53λ	0.4	−0.3979	−7.958 loss
0.1λ	2.2	0.3424	6.848	0.56λ	1.0	0.0000	0 gain
0.2λ	2.0	0.301	6.02	0.58λ	1.2	0.0792	1.584 gain
0.25λ	1.85	0.2672	5.344	0.62λ	1.6	0.2041	4.082 gain
0.3λ	1.64	0.2148	4.296	0.7λ	2.0	0.301	6.02 gain
0.4λ	1.0	0.0000	0.000	0.73λ	2.04	0.3096	6.192 gain
0.45λ	0.6	−0.2218	−4.456 (loss)	1λ	0.00		

Remarks: Negative gain values are field loss on the free-space field without a reflector and the same power input. Negative decibel example: $q = 0.6 = \frac{6}{10}$, $\log q = \log 6 - \log 10 = 0.7781 - 1 = -0.2218$.

occurs for a spacing $x \cong 0.06\lambda$, giving a field gain of about 7 db. By the spacing $x \cong 0$ is meant that the radiator just does not touch the reflector.

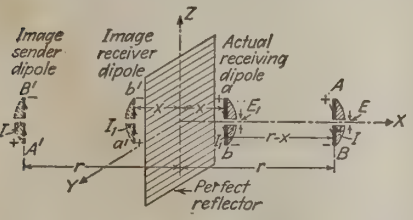

FIG. 287. Distant transmitter dipole and close receiving dipole in front of a perfect reflector. $\beta = 2\pi/\lambda$; I and I_1 represent effective antinode currents in amp; x, r, λ are in meters. E is impressed and E_1 induced effective voltage in volts. Actual transmitting dipole. $1/(r - x) \cong 1/r \cong 1/(r + x)$, since r is relatively large.

183. Effect of a Perfectly Conducting Plane Reflector on a Parallel Receiving Half-wave Dipole. We have for such a condition a mutual dipole alignment as in Fig. 287. The actual receiving dipole ab has an inverted image $a'b'$, and the transmitting dipole AB has an inverted image $A'B'$. The ZY plane is then in the distant radiation region with respect to the radiation center of the actual radiator AB. The total field intensity at the location of the actual receiving half-wave dipole, in the presence of a perfect reflector, is then

$$\mathcal{E}_r = \underbrace{j\frac{60I}{r-x}\epsilon^{-j\beta(r-x)}}_{\text{due to } AB} - \underbrace{j\frac{60I}{r+x}\epsilon^{-j\beta(r+x)}}_{\text{due to } A'B'}$$

$$\cong j\frac{60I\epsilon^{-j\beta r}}{r}\underbrace{(\epsilon^{j\beta x} - \epsilon^{-j\beta x})}_{=2\sin(\beta x)} = j\frac{120I\epsilon^{-j\beta r}}{r}\sin(\beta x)$$

causing an induced voltage

$$E_1 = E_r = j\frac{120I\epsilon^{-j\beta r}}{\beta r}\sin(\beta x) \quad \text{volts} \tag{889d}$$

On account of the image receiver antenna $a'b'$, we also have a mutual impedance $Z_m = Z_{2x} = R_{2x} + jX_{2x}$, in addition to the self-impedance $Z_s = R_s + jX_s = 73.4 + j42.9$ ohms. In these relations, the subscript $2x$ refers to the distance between the image-receiving dipole $a'b'$ and the actual receiving half-wave dipole ab. Since the actual received current I_1 effective amperes at the dipole gap and the equal image current are in *anti*phase, we have

$$E_1^{(\text{volts})} = I_1(Z_s - Z_{2x}) = I_1[R_s - R_{2x} + \underbrace{j(X_s - X_{2s})}_{\substack{\text{can be canceled by} \\ \text{tuning or matching} \\ \text{stub}}}]$$

$$= I_1(R_s - R_{2x}) = j\frac{120I\epsilon^{-j\beta r}}{\beta r}\sin(\beta x) \quad \text{for canceled reactance}$$

Therefore, the received effective gap current in dipole ab, in the presence of the metal reflector, becomes

$$I_r = I_1 = j\frac{120I\epsilon^{-j\beta r}\sin\beta x}{\beta r(R_s - R_{2x})} \quad \text{amp} \tag{889e}$$

where $\epsilon^{-j\beta r}$ accounts for the phase lag of I_1 with respect to the antinode current I of the half-wave radiator. If we have no reflecting metal sheet, there can be no images; and at the ab location, we have an effective electric field

$$\mathcal{E}_s^{(\text{volts/m})} = j\frac{60I}{r - x}\epsilon^{-j\beta(r-x)} \cong j\frac{60I}{r}\epsilon^{-j\beta(r-x)}$$

This causes in ab an induced effective voltage

$$E_s = E_1 = j\frac{60I}{\beta r}\epsilon^{-j\beta(r-x)} \quad \text{volts} \tag{889f}$$

which has now only to overcome the self-impedance $Z_s = R_s + jX_s$ ohms, because we have no image dipole and no mutual impedance effect. The received effective gap current I_s then becomes

$$I_s = \frac{E_s}{R_s + jX_s}$$

jX_s balanced out by matching stub yields

$$I_s = \frac{E_s}{R_s} = j\frac{60I\epsilon^{-j\beta(r-x)}}{\beta r R_s} \quad \text{amp}$$

TABLE 63. HALF-WAVE RECEIVING DIPOLE IN FRONT OF A METAL SHEET

x, m	$q = \frac{I_r}{I_s}$	$G = \log_{10}(q)$, db	x	q	G, db
0.05λ	8.1	18.2	0.4λ	0.85	−1.41
0.1λ	4.3	12.7	0.45λ	0.52	−5.68
0.15λ	2.7	8.63	0.5λ	0.00	$-\infty$
0.2λ	2.05	6.24	0.56λ	1.00	0.00
0.25λ	1.71	4.66	0.6λ	1.51	3.58
0.3λ	1.4	2.92	0.65λ	1.9	5.58
0.35λ	1.2	1.58	0.7λ	2.05	6.24
0.38λ	1.0	0.00	1.0λ	0.00	$+\infty$

Remarks: $R_s = 73.4$ ohms and $R_{2x} = R_m$ ohms computed as is shown in Sec. 135.

The current advantage I_r/I_s, due to the presence of the reflector, then is

$$\left.\begin{aligned} \frac{I_r}{I_s} &= \frac{2R_s \sin(\beta x)}{R_s - R_{2x}}\epsilon^{-j\beta x} = \frac{2\sin(\beta x)}{1 - (R_{2x}/R_s)}\epsilon^{-j\beta x} \\ \epsilon^{-j\beta x} &= \cos(\beta x) - j\sin(\beta x) \end{aligned}\right\} \quad (889g)$$

In the presence of the reflector, we find, for the I_r/I_s advantage, a gain

$$G = 20\log_{10}\left[\frac{2\sin(\beta x)}{1 - (R_{2x}/R_s)}\right] \quad \text{db} \quad (889h)$$

When, therefore, the receiving half-wave dipole ab is a distance $x = \frac{1}{4}\lambda$ in front of a perfectly conducting plate, we find $\beta x = \pi/2$ or 90 electrical degrees, $R_{2x} = -12.48$ ohms, since the image dipole $a'b'$ is a distance $2x = \frac{1}{2}\lambda$ from the actual half-wave receiving antenna ab. Table 30 gives the mutual resistance value of -12.48 ohms for such a separation. Since $R_s = 73.4$ ohms, we find $1 - (R_{2x}/R_s) = 1 + 12.48/73.4 = 1.17$ and $G = 20\log_{10}(2/1.17) = 20\log_{10}(1.71) = 4.66$-db receiver gain. For different spacings x between the metal reflector and the half-wave receiving dipole, we find the computations of Table 63 and the results of Fig. 288. The received current in the presence of a metal reflector must vanish for distances x, which render the function

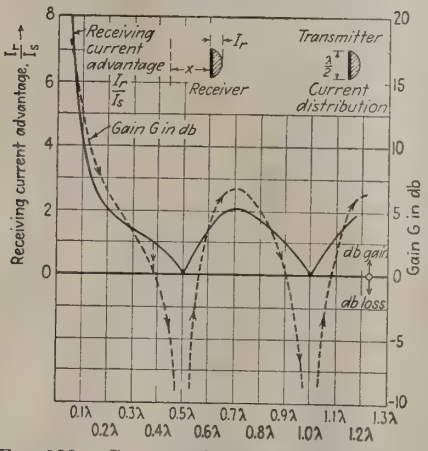

FIG. 288. Current advantage in a receiver half-wave antenna along its equatorial X direction due to a perfect reflector. Distance x is expressed in wavelengths.

$\sin(\beta x) = 0$. This means that for distances $x = 0.5\lambda, \lambda, 1.5\lambda, 2\lambda, \ldots$. From the gain curve as well as the I_r/I_s curve of Fig. 288, it is noted that the antenna pickup increases rapidly as the receiving half-wave dipole approaches the perfect reflector. In actual practice, this is *not* the case, since very close to the reflector where this happens we have to deal also with the proximity effect and, besides, we have no perfect reflectors with infinite conductivity. The decibel as well as the current advantage curves, therefore, cannot have asymptotic approaches but will, in reality,

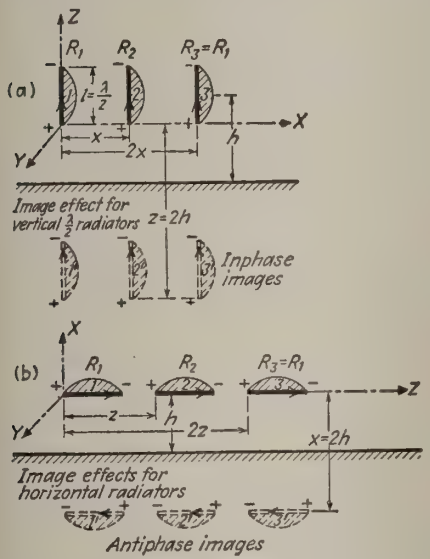

$$R_1 = R_3 = 73.4 + R_x + R_{xz} + R_z + R_{x,z} + R_{2z,z}$$
$$R_2 = 73.4 + 2R_x + R_z + 2R_{x,z}$$
$$R_r = 2R_1 + R_2 \text{ ohms}$$

$$R_1 = R_3 = 73.4 + R_z + R_{2z} - R_x - R_{x,z} - R_{x,2z}$$
$$R_2 = 73.4 + 2R_z - R_x - 2R_{x,z}$$
$$R_r = 2R_1 + R_2$$

Use the table of Fig. 149 for the mutual values R_x, R_{2x}, R_z, R_{2z}, $R_{x,z}$, $R_{2x,z}$, $R_{x,2z}$

FIG. 289. Radiation resistance of half-wave radiators in front of a reflector (metal sheet) for horizontal and vertical polarizations.

bend around, causing again a decreasing characteristic as x approaches a zero value. Also here it seems that the quarter-wave distance does not yield an optimum value, since there are other x values for which a better pickup is possible. In regions in the neighborhood of $x = 0.5\lambda$, λ, 1.5λ, 2λ, . . . , we have minimum effects. The experiment alone can show what the reflector effect actually is and where the optimum pickup occurs. It is in the range of $x = 0.1\lambda$ to 0.22λ.

184. Radiation Resistance of Antenna Arrays over a Perfect Reflector. As mentioned on several occasions, a thin metal sheet of copper will approximately serve as such a reflector. We must then take the image effects into account, since they interfere with the radiation pattern of the actual radiators. Figure 289 shows the conditions for three half-wave radiators that are either normal to a metal plane or parallel with it. In Fig. 289*a*, we then have equal inphase image currents and, in

Fig. 289*b*, equal opposing currents in the image antennas. The procedure on pages 667–675 then applies, and the radiation resistance of actual radiator 1 in Fig. 289*a* becomes

$$R_1 = R_s + \underbrace{R_x + R_{2x}}_{=A} + \underbrace{R_z + R_{x,z} + R_{2x,z}}_{=B} = R_3$$

ohms (due to symmetry = R_1)

where R_s is the self-radiation resistance 73.4 ohms; A is the mutual effect of radiators 2 and 3 on 1; B is the mutual effect of image radiators 1′, 2′, and 3′ on actual radiator 1; $R_2 = R_s + 2R_x + R_z + 2R_{x,z}$ ohms; $2R_x$ is due to adjacent radiators 1 and 3; R_z is due to image radiator 2′; and $2R_{x,z}$ is due to image radiators 1′ and 3′. The total radiation resistance R_r of the array can come only from the *actual* radiator 1, 2, and 3, and we have

$$R_r = R_1 + R_2 + R_3 = 2R_1 + R_2 = 3R_s + 4R_x + 2R_{2x} + 3R_z + 4R_{x,z} + 2R_{2x,z} \quad \text{ohms}$$

For n radiators arranged as in Fig. 289*a*, we have the general formula for the total radiation resistance R_r of the array

$$\left.\begin{aligned} R_r &= nR_0 + 2(n-1)R_1 + 2(n-2)R_2 + 2(n-3)R_3 \\ &\quad + 2(n-4)R_4 + \cdots + 2R_{n-1} \quad \text{ohms} \\ R_k &= R_{kx,0} + R_{kx,z} \qquad \text{for } k = 0, 1, 2, 3, 4, \cdots \end{aligned}\right\} \quad (890)$$

Applying this expression to the array of Fig. 289*a*, we have $n = 3$. and

$$\left.\begin{aligned} R_0 &= R_{0,0} + R_{0,z} = R_s + R_z \qquad \text{ohms, since } k = 0 \\ R_1 &= R_{x,0} + R_{x,z} = R_x + R_{x,z} \qquad \text{ohms, since } k = 1 \\ R_2 &= R_{2x} + R_{2x,z} \qquad \text{ohms, since } k = 2 \end{aligned}\right\} \quad (890a)$$

The term $R_{0,0}$ means, that we deal only with one radiator, because the orientation 0,0 makes the particular two radiators slip into each other, and $R_{0,0}$ must be the self-radiation resistance of 73.4 ohms. Inserting the values of (890*a*) into general formula (890) for $n = 3$, we find

$$R_r = 3(R_s + R_z) + \underbrace{2(3-1)}_{=4}(R_x + R_{x,z}) + \underbrace{2(3-2)}_{=2}(R_{2x} + R_{2x,z}) \quad \text{ohms}$$

This checks the result found before. The application is then not difficult. Suppose we have in Fig. 289*a* the actual vertical half-wave radiators a distance $h = 0.5\lambda$ above the metal plane and $z = \lambda$. For a spacing $x = 0.5\lambda$ between the radiators, we find from the table on page 672, for the mutual resistances, $R_x = -12.48\,\Omega$, $R_{2x} = 4.1\,\Omega$, $R_z = -4.064\,\Omega$, $R_{x,z} = -0.78\,\Omega$, $R_{2x,z} = 3.56\,\Omega$, and $R_1 = R_s + R_x + R_{2x} +$

$$R_z + R_{x,z} + R_{2x,z} = 73.4 - 12.48 + 4.1 - 4.064 - 0.78 + 3.56 = 63.74\,\Omega$$

$$R_3 = R_1 = 63.74\,\Omega$$

$$R_2 = R_s + 2R_x + R_z + 2R_{x,z} = 73.4 + (-12.48) + (-4.064) + 2(-0.78) = 42.82\,\Omega$$

$$R_r = 2R_1 + R_2 = 170.296\,\Omega$$

We have, therefore, a total radiation resistance of 170.296 ohms in comparison with $3 \times 73.4 = 220.2$ ohms if no mutual effects are present and as against 178.48 ohms if no reflectors are present.

For the half-wave radiator array of Fig. 289*b*, the mutual effects due to antiphase image antennas 1′, 2′, and 3′ are negative, and

$$\left.\begin{aligned} &R_1 = R_s + R_z + R_{2z} - R_x - R_{x,z} - R_{x,2z} = R_3 \quad \text{ohms} \\ &R_2 = R_s + 2R_z - R_x - 2R_{x,z} \quad \text{ohms} \\ &\text{Total array radiation resistance } R_r = 2R_1 + R_2 \\ &\quad = 3R_s + 4R_z + 2R_{2z} - 3R_x - 4R_{x,z} - 2R_{x,2z} \quad \text{ohms} \\ &\text{For } n \text{ radiators } R_r = nR_0 + 2(n-1)R_1 + 2(n-2)R_2 \\ &\quad + 2(n-3)R_3 + 2(n-4)R_4 + \cdots + 2R_{n-1} \quad \text{ohms} \end{aligned}\right\} \qquad (890b)$$

where R_s is the self-effect of 1, R_z is due to 2, R_{2z} is due to 3, $-R_x$ is due to image 1′, $-R_{x,z}$ is due to 2′, $-R_{x,2z}$ is due to 3′, and for $k = 0, 1, 2, 3, 4, \cdots$, $R_k = R_{kz,0} - R_{kz,x}$. For $n = 3$, as in Fig. 289*b*,

$$\begin{aligned} R_0 &= R_{0,0} + R_{0,x} = R_s - R_x \quad \text{ohms, since } k = 0 \\ R_1 &= R_{z,0} - R_{z,x} = R_z - R_{z,x} \quad \text{ohms, since } k = 1 \\ R_2 &= R_{2z} - R_{2z,x} \quad \text{ohms, since } k = 2 \end{aligned}$$

The quantity $R_{0,0}$ represents a single radiator effect, *i.e.*, $R_s = 73.4$ ohms; and for $n = 3$ we have

$$R_r = 3(R_s - R_x) + 4(R_z - R_{z,x}) + 2(R_{2z} - R_{2z,x}) \quad \text{ohms}$$

Also if x and z are integer multiples of $\frac{1}{2}\lambda$, we can use here the values of the table on page 672 for the mutual resistances. For all other cases, we have to employ the method described in Sec. 135. The single half-wave radiator case over perfect ground is then found for $n = 1$, since we have then, in Fig. 289, only one actual radiator, namely, 1, and its image 1′. Therefore, $R_r = R_s + R_z$ ohms for Fig. 289*a*, and $R_r = R_s - R_x$ ohms for Fig. 289*b*, where $R_s = 73.4$ ohms in either case. For different elevations h, we have then the values of Table 64. The radiation resistance oscillates about the free-space value of 73.4 ohms for different values of h. However, for a few wavelengths above the metal reflector, we have $R_r \cong 73.4$ ohms. This is also brought out in Fig.

290. If we have seven half-wave radiators lined up as in Fig. 291, we find, owing to the image effect of a perfect reflector, the respective input resistances $R_1 = R_7$, $R_2 = R_6$, $R_3 = R_5$, and R_4, as given in this figure for different elevations h above the reflector. This would be the value of the characteristic impedance of the respective dipole feeders if the reactance of each actual radiator is stubbed out (neutralized). The case of $h = \frac{1}{4}\lambda$ means that the lower ends of respective dipoles *just do*

TABLE 64. HALF-WAVE RADIATOR IN THE NEIGHBORHOOD OF A METAL REFLECTOR AND RADIATION RESISTANCE IN TERMS OF THE SPACING FROM THE REFLECTOR

Vertical radiator (Fig. 289*a*, $n = 1$)				Horizontal radiator (Fig. 289*b*, $n = 1$)		
h, m	z, m	Due to image R_z ohms	$R_r = 73.4 + R_z$ ohms	x, m	Due to image R_x ohms	$R_r = 73.4 - R_x$ ohms
0.00λ	Condition impossible			0.0λ*	73.4	0.00
0.25λ†	0.5λ	26.4	99.8	0.5λ	−12.48	85.88
0.5λ	1λ	−4.06	69.34	λ	4.1	69.3
0.75λ	1.5λ	1.78	75.18	1.5λ	−1.77	75.17
1λ	2λ	−0.96	72.44	2λ	1.18	72.22
1.25λ	2.5λ	0.58	73.98	2.5λ	−0.75	74.15
1.5λ	3λ	−0.43	72.97	3λ	0.42	72.98
$\infty\lambda$	$\infty\lambda$	0.00	73.4	$\infty\lambda$	0.00	73.4

* Horizontal $\lambda/2$ dipole just not touching reflector.
† Lower end of vertical radiator just not touching reflector.
Remarks: R_r is the value for which the feeder has to be designed, if the reactance X_r is stubbed out.

not touch the reflector. For all other consecutive heights, the elevation h is successively increased by $\lambda/8$. The case $h = \infty$ means that the reflector does not exist in effect. It is seen from the table in this figure that for an elevation $h = 3\lambda/4$, the effect of the metal reflector is very small, because nearly the same radiation resistance values are obtained as for $h = \infty$. The total radiation resistance R_r of the alignment oscillates about the unobstructed space radiation resistance of 395.6 ohms.

185. Notes on the Form Factor of Linear Radiators over a Perfect Reflector. This has reference to the arrangements of Fig. 292*a* for any fractional wavelength distribution, the quarter-wavelength distribution along the actual radiator of Fig. 292*b* as well as the half-wave distribution of Fig. 292*c*. The indicated current distribution is drawn with respect to the effective current value of I_z amperes. For the general case of Fig. 292*a*, the current I_1 represents the effective input current, and I denotes the current value at the current antinode. The values r_1 and

r_2, for a distant field point P, can be put equal to r as far as the inverse distance effect is concerned. But we have to retain the values r_1 and

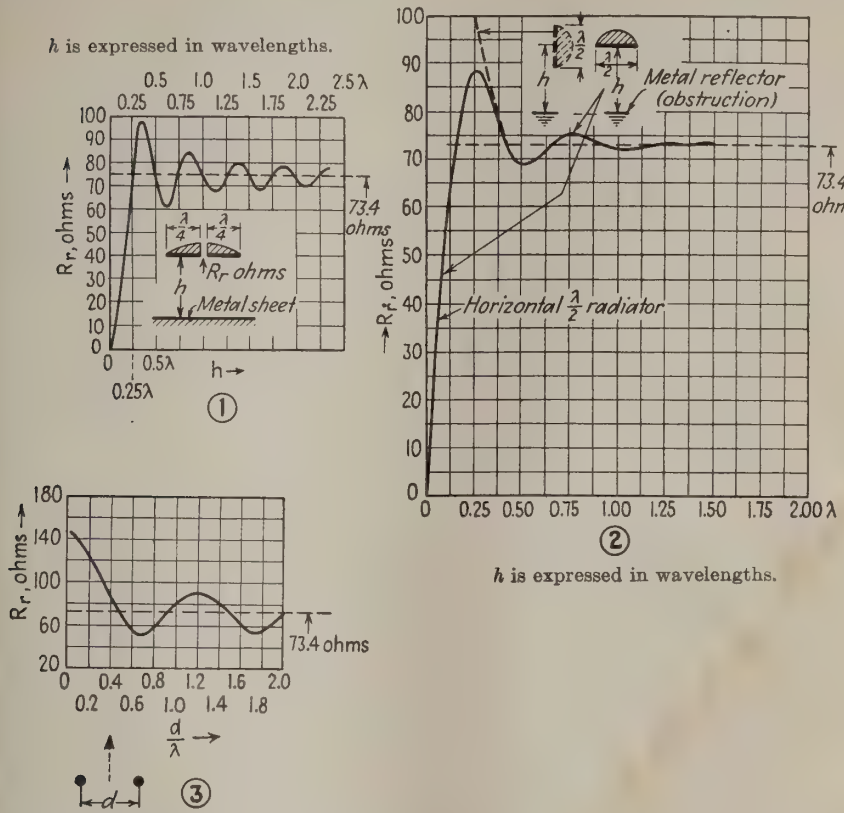

Radiation resistance R_r ohms of two inphase $\lambda/2$ radiators (parallel) spaced a distance d for unobstructed radiation space.

FIG. 290. Radiation resistance of half-wave radiators without a reflector and in the presence of a perfect reflector.

r_2 in the phase factors $\epsilon^{-j\beta r_1}$ and $\epsilon^{-j\beta r_2}$ and find the symmetrical field contributions

$$d\mathcal{E}_{\theta_1} = j30\beta \frac{I_z}{r} \epsilon^{-j\beta r_1} dz \sin\theta \qquad \text{volts/m}$$

$$d\mathcal{E}_{\theta_2} = j30\beta \frac{I_z}{r} \epsilon^{-j\beta r_2} dz \sin\theta \qquad \text{volts/m}$$

since $z \cos\theta$ in $r_1 = r - z\cos\theta$ and $r_2 = r + z\cos\theta$ accounts for the phase advance and phase delay of the self- and mutual field contributions at P, due to the dz element, with respect to the field coming from the

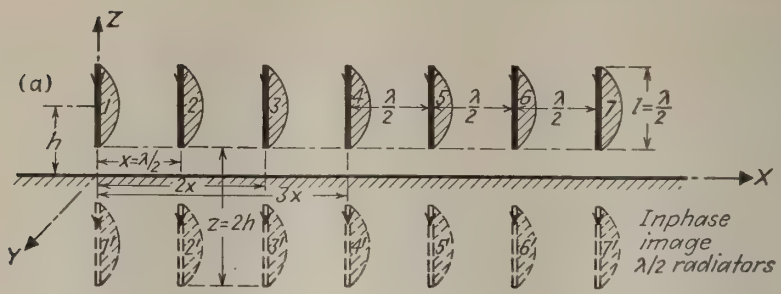

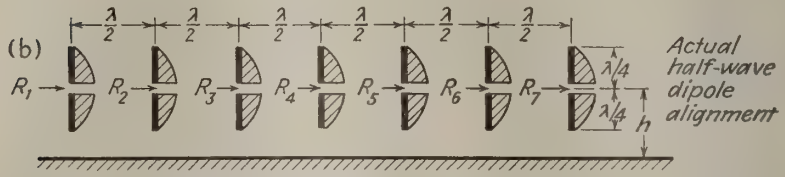

$h = \frac{z}{2}$	Resistance in ohms					Remarks (assumes thin linear radiators)
	$R_1 = R_7$	$R_2 = R_6$	$R_3 = R_5$	R_4	R_r	
$\frac{\lambda}{4}$	84.7	58.2	74.7	62	497.3	Total radiation resistance of above alignment is $R_r = R_1 + R_2 + R_3 + R_4 + R_5 + R_6 + R_7 =$ $2(R_1 + R_2 + R_3) + R_4$ ohms. The table shows how, with increasing elevation above the metal reflector, the radiation resistance of unobstructed space is approached
$\frac{3}{8}\lambda$	65	41.8	59.8	43.7	376.8	
$\frac{\lambda}{2}$	62.8	44.7	58.8	42.2	374.8	
$\frac{5}{8}\lambda$	65.8	50.5	59	51.2	401.8	
$\frac{3}{4}\lambda$	66.4	51.2	55.5	54.4	400.6	
$h = \infty$	66	51.2	56.1	53.2	395.6	

FIG. 291. Individual and total radiation resistance of half-wave radiators in the neighborhood of a metal reflector.

origin (in the case of a perfect reflection at the equatorial XY plane). Since $\epsilon^{-j\alpha} = \cos\alpha - j\sin\alpha$ and $\epsilon^{j\alpha} = \cos\alpha + j\sin\alpha$ correspond to a phase lag or a phase lead of $2\pi r/\lambda$ degrees, for $\alpha = \beta r$, we find for

$$\epsilon^{-j\beta r_1} = \epsilon^{-j\beta(r - z\cos\theta)} = \epsilon^{-j\beta r}\epsilon^{j\beta z\cos\theta}$$

$$\epsilon^{-j\beta r_2} = \epsilon^{-j\beta(r + z\cos\theta)} = \epsilon^{-j\beta r}\epsilon^{-j\beta z\cos\theta}$$

$$\epsilon^{-j\beta r_1} + \epsilon^{-j\beta r_2} = \epsilon^{-j\beta r}(\epsilon^{j\beta z\cos\theta} + \epsilon^{-j\beta z\cos\theta}) = A$$

$$A = \epsilon^{-j\beta r}[\cos(\beta z\cos\theta) + j\sin(\beta z\cos\theta) + \cos(\beta z\cos\theta) - j\sin(\beta z\cos\theta)]$$

$$= 2\epsilon^{-j\beta r}\cos(\beta z\cos\theta)$$

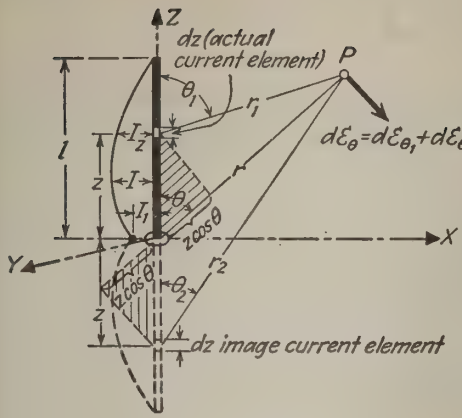

(a)

$d\mathcal{E}_{\theta_2}$ is mutual effect of image element dz on $d\mathcal{E}_{\theta_1}$ (self-effect) of actual element dz.

$$I_z = I \sin(\beta l - \beta z) = \frac{I_1 \sin(\beta l - \beta z)}{\sin(\beta l)}$$

since $I_1 = I \sin \beta l$.

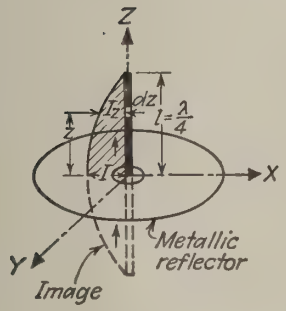

(b)

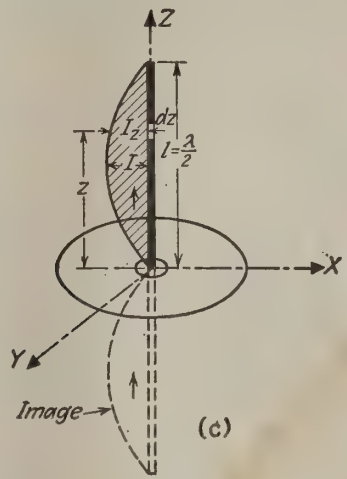

(c)

$$I_z = I \sin(\beta l - \beta z) = I \cos(\beta z)$$

$$\beta l = \frac{\pi}{2}$$

$$\beta l = \pi$$

$$I_z = I \sin(\beta l - \beta z)$$

Image antenna effect in phase with actual antenna effect.

FIG. 292. Linear radiators projecting through a metal reflector. In distant radiation region $\theta_1 \cong \theta \cong \theta_2$ and $1/r_1 \cong 1/r \cong 1/r_2$; r_1, r_2, r_3, dz, λ are in meters; I_z is in amp, and $d\mathcal{E}_\theta$ in volts/m. XY plane is reflector $\beta = 2\pi/\lambda$; electrical length βl.

For the field contribution of the actual antenna element dz in presence of a metal reflector a distance z below it, at a distant field point P, we have

$$d\mathcal{E}_\theta = j \frac{60\beta\epsilon^{-j\beta r} \sin\theta}{r} \int_{z=0}^{z=l} I_z \cos(\beta z \cos\theta)\, dz \qquad \text{volts/m}$$

The solution of this integral is given on page 531. The total field $\mathcal{E}_\theta$ due to the entire actual radiator length l above the reflecting XY plane is then

$$\mathcal{E}_\theta = j\frac{60I_1\epsilon^{-j\beta r}}{r}FD_\theta \tag{891}$$

where D_θ is the unobstructed directivity of the linear radiator, in any meridian plane of the radiator with the length l as the polar axis, and F represents the form factor. We have then

$$F = \beta \sin\theta \int_{z=0}^{z=l} \frac{I_z}{I_1}\cos(\beta z\cos\theta)\,dz \tag{891a}$$

$$D_\theta = \frac{\beta\sin\theta\int_{z=0}^{z=l}(I_z/I_1)\cos(\beta z\cos\theta)\,dz}{F} \tag{891b}$$

where I_1 is the effective current value in the XY plane (where the linear

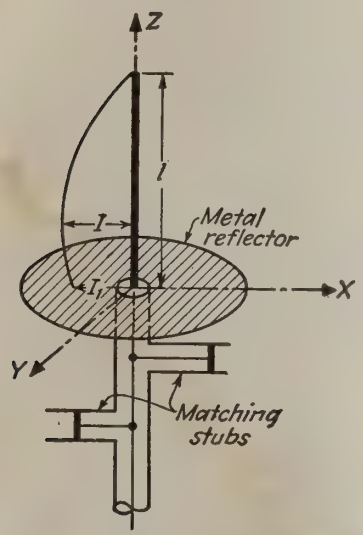

Radiation resistance with respect to loop current I

$$R_r = 30\{-\tfrac{1}{2}\cos(2\alpha)[0.5772 + \log_\epsilon(4\alpha) - \mathrm{Ci}(4\alpha)] + [1 + \cos(2\alpha)][0.5772 + \log_\epsilon(2\alpha) - \mathrm{Ci}(2\alpha)] + \sin(2\alpha)[(\tfrac{1}{2}\,\mathrm{Si}(4\alpha) - \mathrm{Si}(2\alpha)]\}\ \text{ohms}$$

$$\alpha = \beta l = \frac{2\pi}{\lambda}l$$

With respect to input current I_1 we must divide R_r by $\sin^2\alpha$

FIG. 293. Radiation resistance R_r of a thin linear radiator of length l with a metal reflector.

radiator emerges through a small hole in the copper plane, forming the XY plane). A useful system is shown in Fig. 293. In the reflector plane, we have $\theta = 90$ deg, and

$$F = \beta\int_{z=0}^{z=l}\frac{I_z}{I_1}\,dz = \beta\int_{z=0}^{z=l}\frac{\sin(\beta l - \beta z)}{\sin(\beta l)}\,dz$$

since in Fig. 292*a*, we have $I_z = [I_1\sin(\beta l - \beta z)]/\sin(\beta l)$. As for the radiation resistance, we have to refer the form factor F to a particular current value along the linear radiator. The feeder current I_1, at the input end, is a logical reference value, and we have for this effective value

$$F = \frac{1 - \cos(\beta l)}{\sin(\beta l)}; \qquad D_\theta = \frac{\cos(\beta l \cos\theta) - \cos(\beta l)}{\sin\theta[1 - \cos(\beta l)]} \tag{891c}$$

yielding $D_\theta = D_{90} = 1$, which directivity would be expected in the XY plane. With respect to the effective current I at the current antinode of Fig. 292*a*, we have

$$F_{\text{current antinode}} = 1 - \cos(\beta l) \tag{891d}$$

For a half-wave linear radiator, we have $l = \frac{1}{2}\lambda$ and $F = 1 - \cos\pi = 1 - \cos 180° = 1 - (-1) = 2$. If we have n equal-phased half-wave distributions along the radiator length l, the form factor becomes $F = 2n$. The above derivations assume that the phase velocity along the linear radiator is $c = 3 \times 10^8$ m/sec. Experience shows this is not exactly true. If c' denotes the actual phase velocity in meters per second. relation (891*d*) changes to

$$F_{\text{current antinode}} = \frac{c'}{c}[1 - \cos(\beta l)]; \qquad \beta l = \frac{2\pi l/\lambda}{c'/c} \tag{891e}$$

CHAPTER VIII

ELECTROMAGNETIC DIFFRACTION

Although it is often thought that short electromagnetic waves travel according to geometric optics (nothing below the line of sight) but somewhat below this line if atmospheric refraction exists, experiments show that waves may reach much farther into the geometric shadow region than refraction can account for. Wave reflections do *not* occur only at one point but, according to Huygens' wavelet principle, from the entire surface of the earth that is electromagnetically illuminated. Wavelets reradiate then in all directions from the multitude of elementary radiation centers of the earth surface, receiving incident electromagnetic wave energy. We also find that waves bend slightly around edges of a wave obstacle. We have the same case as in monochromatic light passing through a slit, which will cause a bright band somewhat wider than the slit. This band will be followed up at the edges by a few narrower bands, which are alternately blind zones (dark for monochromatic light) and zones of strong intensities. For wave reflections from smooth earth surface in a particular direction, only a small elliptical reflection area is essentially operative (with the reflection point somewhere near the symmetry point of this area). The operative reflection area has then a definite relation to the first Fresnel zone, well known in optics. In the electromagnetic case, however, we must satisfy the boundary conditions with respect to the electric as well as with respect to the magnetic field associations. The boundary is then the surface of a particular wave obstacle that receives primary electromagnetic waves. Generally, it may be said that for multifrequency waves we can separate such waves into spectral components either by diffraction or by refraction, respectively, since *diffraction* as well as *refraction depends on* the operating *wavelength.* The longer the wavelength, the more pronounced are the diffraction effects, *but* the longer the wavelength, the *less* significant are the refraction effects.

186. Basic Concepts of Diffraction. Diffraction is a phenomenon accompanying all forms of wave motion, its effect being more marked as the *wavelength* relative to the obstacle dimensions *increases.* Diffraction effects *differ* from refraction effects inasmuch as ray bending due to refraction may occur in unobstructed space. But we deal with variations

from a straight-line course when partially cut off by an obstacle, such as when an electromagnetic wave passes near edges of an opening (wedge-shaped mountains) or a hole that may cause wave interference. Wave propagation behind the horizon (in the geometric shadow region of the earth) may be partially due to diffraction.

In the case of optics, it is known from experiments, as well as confirmed by theory, that a screen with a narrow aperture (slit) will pass, for instance, monochromatic light to another screen behind the first one in such a way that instead of a sharp image of the opening, either a blurred wider image or several bright and dark images of the slit appear. Similar patterns are observed when two or more narrow apertures are used with a common light source. However, this is *not* true for different light sources acting simultaneously. The reason for this is that such effects can be explained by Huygens' wavelet concept, modified by Fresnel by means of interference between component waves. According to Fresnel, we deal with a *pure* wave phenomenon, which is surely the case in electromagnetic waves.

For light, we have a dual theory, *i.e.*, not a pure wave phenomenon. Photoelectric effects are explained by means of properties of corpuscles, for which each train of waves is taken as a distinct entity known as a quantum of an energy W, which is related to its frequency f by the relation $W = hf$, where h is Planck's constant. The momentum of the quantum is then hf divided by the velocity of light. Maxwell's equations can be made to account for the correct average result if we deal with many quanta taken collectively. With such a concept in mind, it can be understood why we do *not* obtain, in the case of *light* waves, the interference diffraction patterns with two or more light sources. For several sources, we have a multitude of separate wave trains, or quanta. A condition of this kind may be assumed to be equivalent to sudden phase "jumps," which in the case of two or more light sources do *not* coincide and change the phase in the same fashion. Real wave addition and wave subtraction then will *not* occur as in the case of a single light source. As far as radio waves are concerned, we have no limitation as to the number of radiating sources.

187. Huygens' Principle, Fresnel Wave Interference, and Imaginary Radiation Surfaces. According to Christian Huygens, the wave front of a wave consists of *many* point sources (Fig. 294), each one sending out its own wave or *wavelet*. If this is assumed, any such source emits a spherical electromagnetic wave toward unobstructed space. The wave front of an electromagnetic wave can then be taken as a mosaic of point source radiators. This is the reason why, in this text, we read at times of "wave-front radiators."

It seems worth while to review the fundamentals of the diffraction theory in order to learn to what extent it can be applied to electromagnetic waves. We must satisfy the boundary conditions if a wave meets another medium, such as at the surface of obstacles. We also have *two* functions,

namely, that of the electric field $\mathfrak{E}$ and that of the magnetic field H, and *not a single* wave function. Owing to the boundary conditions, the wave

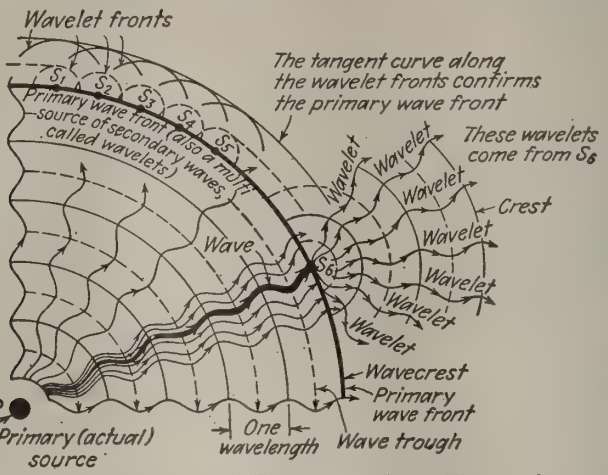

FIG. 294. Primary wave expansion and Huygens wavelets. The wavelet concept is of significance only when dealing with wave obstructions. A wave front is a surface of equal phase.

front passing through an opening of an obstacle must become *perturbed* because of what happens at the boundary. This means that at the inner surface of an opaque screen[1] with an aperture, we generally have wave reflections as well as absorptions unless special provisions are met. For the sake of presenting well-known fundamentals, we deal, to begin with, with a single wave function w and assume that $w = 0$ at the inner surface of the screen and the normal derivative $\partial w/\partial n = 0$, so that for the surface of an aperture, the wave condition is identical with the incident unperturbed wave. Doing this in Fig. 295, with T as the radiation center of primary source of spherical waves about this center and the full-line circles as wave crests and the dash circles as the troughs, we may consider the full-line outer circle as a wave

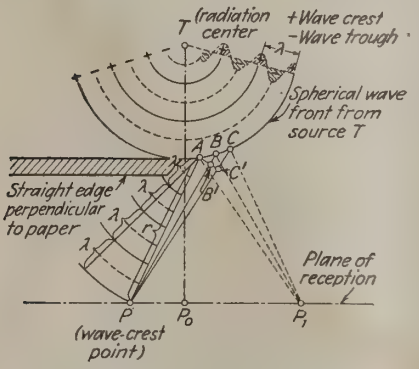

FIG. 295. How a primary wave front ABC originating from the primary source T (transmitter) acts as a multitude of secondary wavelet centers such as A, B, and C (Huygens transmitting centers). T is *primary* radiation center; points A, B, and C are secondary radiation centers (Huygens wavelet sources in the primary wave front).

[1] For diffraction of slots, rectangular and circular apertures, it is understood that the obstructing screen on the rear which faces the primary radiation absorbs incident primary radiation, and forward energy passes *only* through the aperture.

front containing Huygens wavelet sources such as A, B, C. These *secondary* radiation centers are all on a surface of *equal phase*. Each one of these wavelet centers starts out spherical waves about A, B, and C, so that wave energy also reaches to portions like point P of the geometrical shadow region. Space point P is then a reception center of three arriving wave trains. The paths of rays AP, BP, and CP are r, $r + BB'$, and $r + CC'$ if arc $AB'C'$ is a circle with radius r about P as the center. In Fig. 295, the length r is chosen such that it is exactly 4 wavelengths long ($=4\lambda$). This means that the wavelet originating at the Huygens center A must cause a wave crest at reception point P. Expressing the path differences BB' and CC' by d and d', the corresponding phase delays are $\delta = \beta d$ and $\delta = \beta d'$ for $\beta = 2\pi/\lambda$. If δ were exactly equal to a half wavelength, the crest of train AP would meet a trough of the BP wave train at P. For the distance r containing many wavelengths, instead of only 4, we have the inverse distance effect $1/r \cong 1/(r + d)$. Therefore, at reception center P, the arriving A wavelet effect will cancel the arriving B wavelet effect. The field AP can then be due only to the C wavelet, which for a wave function w yields, for the initial value W of w,

$$w = \frac{W}{d} \epsilon^{j[\omega t - \beta(r+d)]}$$

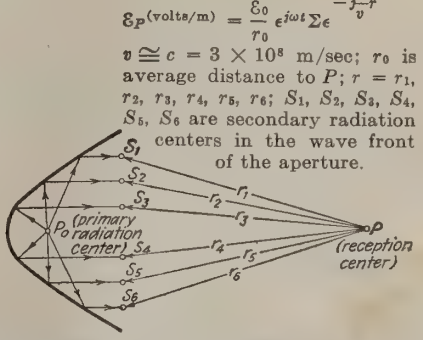
$\mathcal{E}_P$(volts/m) $= \frac{\mathcal{E}_0}{r_0} \epsilon^{j\omega t} \Sigma\epsilon^{-j\frac{\omega}{v}r}$
$v \cong c = 3 \times 10^8$ m/sec; r_0 is average distance to P; $r = r_1$, r_2, r_3, r_4, r_5, r_6; S_1, S_2, S_3, S_4, S_5, S_6 are secondary radiation centers in the wave front of the aperture.
S_1
S_2
S_3
S_4
S_5
S_6
r_1
r_2
r_3
r_4
r_5
r_6
P_0 (primary radiation center)
P (reception center)

FIG. 296. Parabolic reflector causes Huygens wavelet centers in its opening if the primary source is located at P_0.

Generally, such ideal conditions do not occur, and the three wavelets arriving at P with their effects also cause wave interference all along the imaginary plane of reception. We have very many Huygens wavelet centers; and at the imaginary reception plane, we have places of maximum reception effects as well as of minimum reception effects. It is then necessary to sum up all the effects at the various points of this imaginary reception plane.

Therefore, as far as the reception effect is concerned, the basis of the Huygens-Fresnel wavelet effect is that we deal *not directly* with the original source (primary radiation center T) but with a multitude of secondary radiation centers located in the wave front of the primary wave. Even though diffraction is less pronounced around edges as the waves become shorter, the diffraction effect, in many cases, cannot be ignored. For instance, in the radiation system of Fig. 296, where P_0 denotes the pri-

mary radiation center of a half-wave dipole along the focal line of a paraboloid, which acts as a reflector, we have an infinite number of secondary radiation centers S_1, S_2, S_3, S_4, S_5, . . . in the aperture plane (secondary wavelet window) of the paraboloid. We can then take these radiation centers as the sources and integrate the effect of the sources in the aperture plane at a distant field point P. The reason for doing this is that due to the geometry of such a reflector, all reflected rays from P_0 to S_1, S_2, S_3, . . . are equally long and the aperture of the paraboloid with the wavelet centers is a locality of equal phases. We have then, in effect, a plane wave front of the wave caused only a short distance away (from P_0), and the plane wave front can be regarded as a plane with many radiators, which are all excited in phase.

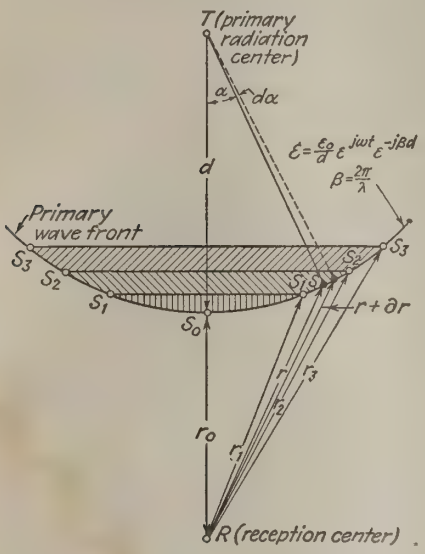

FIG. 297. Fresnel zones on an advancing primary wave front. $\mathcal{E}_0$ is the reference value of unity distance from the primary source. Shaded surfaces are the Fresnel zones. S_0, S_1, S_2, S_3 are secondary wavelet (radiation) centers in the primary wave front. Fresnel zones are such that $r_1 = r_0 + (\lambda/2)$; $r_2 = r_1 + (\lambda/2) = r_0 + \lambda$; $r_3 = r_2 + (\lambda/2) = r_0 + 1.5\lambda$; $r_4 = r_0 + 2\lambda$; etc. $r = r_0 + b(\lambda/2)$, and b is the value between 1 and 2.

188. Remarks[1] on Fresnel Zones (Applied to Electromagnetic Waves). In Fig. 297, T denotes a radiation center where the primary source is located, and the spherical wave front contains Huygens radiation centers, such as S_0, S_1, S_2, S_3, S_4, ... From these secondary centers, wavelets start out, all with inphase excitations, and R denotes a particular reception center. According to Fresnel, we divide the spherical wave front into indicated circular zones. The lowest, or central, zone reaches from secondary radiation centers S_0 to secondary radiation centers S_1 in such a way that RS_1 is longer by $\lambda/2$ than the distance RS_0. In the same way, r_2 exceeds r_1 by a half wavelength as also r_3 exceeds the distance r_2. The radiation effect on field point R must be the geometrical sum of all the radiation centers of the spherical wave front. One such center S is located somewhere in the second Fresnel zone a distance r from the reception center R, while another wavelet center next to S in the same zone is a distance $r + \partial r$ from the field point R. These two points form an elementary zone in the second Fresnel

[1] This assumes that the boundary conditions for $\mathcal{E}$ and H fields are satisfied.

zone, as well as in the entire spherical wave front with a surface area

$$\partial A = 2\pi d^2 \sin \alpha \, \partial\alpha$$

which includes many secondary radiation centers. For the triangle TSR, we have the sides $TR = d + r_0$, $RS = r$, and $TS = d$ and find

$$\left.\begin{aligned} r^2 &= d^2 + (r_0 + d)^2 - 2d(r_0 + d) \cos \alpha \\ 2r \, \partial r &= 2d(r_0 + d) \sin \alpha \, \partial\alpha \end{aligned}\right\} \quad \text{hence,} \quad \left\{ \partial A = \frac{2\pi d}{r_0 + d} r \, \partial r \right. \tag{892}$$

The received field at the reception center is proportional to the elementary surface ∂A. Calling K the proportionality constant, we have, for the field intensity contribution $\partial \mathcal{E}$ at R due to the elementary spherical zone ∂A,

$$\partial \mathcal{E} = \frac{K\mathcal{E}\epsilon^{-j\beta r}}{r} \partial A = \frac{K\mathcal{E}_0 \epsilon^{j[\omega t - \beta(d+r)]}}{rd} \partial A$$

$$= \frac{6.28K\mathcal{E}_0}{r_0 + d} \epsilon^{j[\omega t - \beta(d+r)]} \partial r \quad \text{volts/m} \tag{892a}$$

where r_0, r, d, λ are in meters, $\omega/6.28$ is in cycles per second, and $\beta = 6.28/\lambda$ in circular radians per meter. The proportionality constant K depends only upon the inclination between the elementary zone ∂A and the corresponding distance r. If d is large compared with r_0, as is the case when the spherical wave front is essentially plane, and located in the distant radiation region of the transmitter T, then $K = K_n$ for the nth Fresnel zone is constant. The field contribution $\mathcal{E}_n$ at R, due to any zone, such as the central zone between S_0 and S_1 or, for instance, the third zone between S_2 and S_3 corresponding to the distance range from r_2 to r_3 from the wave front, is

$$\mathcal{E}_n = \int \partial \mathcal{E} = \frac{2\pi K_n \mathcal{E}_0 \epsilon^{j\omega t}}{r_0 + d} \int_{r_{n-1}}^{r_n} \epsilon^{-j\beta(d+r)} \partial r = \frac{2\pi K_n}{\beta(r_0 + d)} \mathcal{E}_0 \epsilon^{j\omega t} \left| \epsilon^{-j\beta(d+r)} \right|_{r_{n-1}}^{r_n}$$

$$= \frac{K_n \lambda \mathcal{E}_0}{r_0 + d} \left\{ \cos\left[2\pi \left(ft - \frac{d + r_{n-1}}{\lambda} \right) \right] - \cos\left[2\pi \left(ft - \frac{d + r_n}{\lambda} \right) \right] \right\} \quad \text{volts/m} \tag{892b}$$

since in

$$\epsilon^{j\omega t} \epsilon^{-j\beta(d+r)} = \cos\left[2\pi \left(ft - \frac{d + r}{\lambda} \right) \right] + j \sin\left[2\pi \left(ft - \frac{d + r}{\lambda} \right) \right]$$

only the real cosine term plays a part in the instantaneous value of $\mathcal{E}_n$. For Fresnel zones, consecutive radii are *always* $\frac{1}{2}\lambda$ longer than the pre-

vious one, or $r_n - r_{n-1} = \frac{1}{2}\lambda$. Therefore,

$$r_{n-1} = r_0 + (n-1)\frac{\lambda}{2}; \qquad r_n = r_0 + n\frac{\lambda}{2}$$

yielding together with (892*b*), for any Fresnel zone, the field at R as

$$\mathcal{E}_n = (-1)^{n+1}\frac{2K_n\lambda\mathcal{E}_0}{r_0 + d}\cos\left[2\pi\left(ft - \frac{r_0 + d}{\lambda}\right)\right] \quad \text{volts/m} \quad (892c)$$

The factor $(-1)^{n+1}$ indicates the polarity of field contributions $\mathcal{E}_n$ due to successive Fresnel zone changes from plus to minus to plus to minus, etc., and the total received field $\mathcal{E}_R$ at field point R becomes

$$\mathcal{E}_R^{(\text{volts/m})} = \mathcal{E}_1 - \mathcal{E}_2 + \mathcal{E}_3 - \mathcal{E}_4 + \mathcal{E}_5 - \cdots + (-1)^{n+1}\mathcal{E}_n \quad (892d)$$

where $\mathcal{E}_1$ is the field contribution due to the lower or central zone (lower cap $S_1S_0S_1$ in Fig. 297), $\mathcal{E}_2$ is the antiphase contribution of the second Fresnel zone $S_1S_2S_2S_1$, $\mathcal{E}_3$ is the inphase contribution with $\mathcal{E}_1$ due to the third zone $S_2S_3S_3S_2S_2$, etc. Since K_n and, therefore, also $\mathcal{E}_n$ decrease continuously as n increases (because the inclination of the zonal area ∂A increases with respect to the distance r), we have then alternate plus and minus polarities, and the total effect on $\mathcal{E}_R$ must be smaller than $\mathcal{E}_1$. It is $\mathcal{E}_R = \Sigma\mathcal{E}_n = 0.5\mathcal{E}_1$, *i.e.*, equal to half the amplitude or a quarter of the field energy, *due to the first or central Fresnel zone.*

It is of interest to note that the radii of the Fresnel zones are to each other as the square-root values of natural numbers, making the width of the zones as $(\sqrt{1} - \sqrt{0})$ to $(\sqrt{2} - \sqrt{1})$ to $(\sqrt{3} - \sqrt{2})$ to $\cdots$. This will be followed up in connection with Cornu's spiral.

189. Exact and Approximate Magnitudes of Zonal Areas and Other Zonal Parameters. Formula (892) is the expression for the elementary area ∂A in any zone of a spherical wave front indicated in Fig. 297. The surface of any Fresnel zone, therefore, becomes

$$A_n = \frac{2\pi d}{r_0 + d}\int_{r_{n-1}}^{r_n} r\,\partial r = \frac{\pi d}{r_0 + d}(r_n^2 - r_{n-1}^2)$$

$$r_n^2 - r_{n-1}^2 = (r_n + r_{n-1})(r_n - r_{n-1}) = (2r_{\text{avg}})\frac{\lambda}{2} \qquad \text{since } r_n - r_{n-1} = \frac{\lambda}{2}$$

$$r_{\text{avg}} = \frac{r_n + r_{n-1}}{2}$$

The value r_{avg} denotes the average value between the largest and the smallest distances r from the wave-front zone to the reception point R. We have then

$$A_n = \frac{\pi d\,\lambda r_{\text{avg}}}{r_0 + d} \qquad \text{sq m} \qquad (892e)$$

where all dimensions are in meters. The Fresnel zones are proportional to the wavelength. This is expected, because consecutive distances r_{n-1} and r_n from one extreme to the other extreme of a zone of a wave front with respect to a field point P are chosen in steps proportional to the wavelength. In optics, we deal with exceedingly small zonal areas. Since the factor r_{avg} is also involved, it may seem, at first, as if successive zones become larger. However, it is not the increase of the zonal areas A_{n-1} and A_n alone that counts as far as the field contributions $\mathcal{E}_{n-1}$ and $\mathcal{E}_n$ of consecutive zones are concerned. According to (892*a*), the contribution $\partial\mathcal{E}$ is inversely proportional to any r value and directly proportional to ∂A and, as such, cancels the same effect in the value of A_n in (892*e*). The respective field contributions $\mathcal{E}_1$, $\mathcal{E}_2$, $\mathcal{E}_3$, . . . , $\mathcal{E}_{n-1}$, and $\mathcal{E}_n$ of consecutive zones would be equal if it were not for the factor K_n in (892*c*). This factor deals with the angle that a particular zone makes with the corresponding average direction r_{avg} toward the reception center R. The difference between consecutive zonal areas is

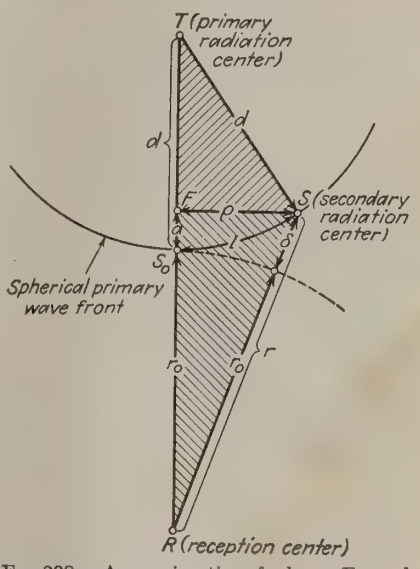

FIG. 298. Approximations for lower Fresnel zonal areas A_n. Assumes arc l small compared with d and r_0 (holds for lower Fresnel zones). Radius of circle is formed by intersection of plane perpendicular to TR through S. $\rho \cong l$; a^2 is negligible, since a is very small; δ is very small; $r = r_0 + \delta$, and $r + r_0 = 2r_0 + \delta \cong 2r_0$.

$$A_n - A_{n-1} = (\bar{r}_n - \bar{r}_{n-1}) \frac{\pi\lambda d}{r_0 + d} = 1.57 \frac{\lambda^2 d}{r_0 + d} \qquad (892f)$$

where $\bar{r}_n$ and $\bar{r}_{n-1}$ represent the average values for any consecutive zones. The difference of these average values is equal to the $\lambda/2$ Fresnel zone step. We have then a fixed increase.

Formulas (892*e*) and (892*f*) are rigorous. In many cases, approximations are useful. For Fresnel zones of low numbers, such as $n = 1$, the lower spherical cap $S_0S_1S_1S_0$ of Fig. 297, and $n = 2$ for the zone $S_1S_2S_2S_1$, . . . , we find, in the corresponding Fig. 298, the given approximations, and we have

$$a \cong \frac{0.5\rho^2}{d} \qquad (892g)$$

since, for triangle TFS,

$$d^2 = (d - a)^2 + \rho^2 = d^2 - 2ad + a^2 + \rho^2 \cong d^2 - 2ad + \rho^2$$

For triangle FSR, we have

$$r^2 = (r_0 + a)^2 + \rho^2 = r_0^2 + 2ar_0 + a^2 + \rho^2 \cong r_0^2 + 2ar_0 + \rho^2$$

Substituting the value for a from (892g), we find

$$r^2 = r_0^2 + \frac{\rho^2 r_0}{d} + \rho^2 = r_0^2 + \rho^2 \frac{r_0 + d}{d}$$

Hence,

$$\frac{r_0 + d}{d}\rho^2 = r^2 - r_0^2 = (r + r_0)(r - r_0) = (2r_0)(\delta)$$

Therefore, the circular wave front of length l and radius ρ yields a common expression

$$\rho = \sqrt{\frac{2\delta r_0 d}{d + r_0}} = l \tag{892h}$$

If, therefore, the secondary wavelet or radiation center lies at the outer contour of the nth Fresnel zone, the excess δ over the r_0 value is n times $\frac{1}{2}\lambda$ or $\delta = 0.5n\lambda$ as long as n is not so large that $l \cong \rho$ no longer holds. For such a zone, we have the approximation formula

$$\rho_n = l_n = \sqrt{\frac{n\lambda r_0 d}{d + r_0}} \tag{892i}$$

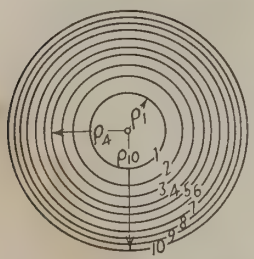

FIG. 299. Zonal rings up to $n = 10$ based upon the formula $\rho_n = k\sqrt{n}$; k is a constant. Examples: $\rho_4 = k\sqrt{4} = 2k$; $\rho_9 = k\sqrt{9} = 3k$.

This result shows that for $n = 1$, we have zone $S_1S_0S_1$ in Fig. 297; for $n = 2$, we have the zone $S_2S_1S_1S_2$; for $n = 3$, 4, . . . , the radii ρ_1, ρ_2, ρ_3, ρ_4, vary proportionally with $\sqrt{1}$, $\sqrt{2}$, $\sqrt{3}$, $\sqrt{4}$, . . . , as in Fig. 299. The radius ρ_1 is, therefore, $k\sqrt{1} = k$, where the constant $k = \sqrt{r_0\lambda d/(d + r_0)}$. This is the radius of the outer boundary of the first zone ($S_1S_0S_1$ spherical cap and radius of S_1S_1 circle of Fig. 297). This is also the radius ρ_1 in Fig. 299. We find also $\rho_2 = k\sqrt{2} = 1.4142k$, $\rho_3 = k\sqrt{3} = 1.73k$, $\rho_4 = 2k$, $\rho_5 = k\sqrt{5}$, ... The quantity ρ_2 is the radius of the outer boundary, and ρ_1 is the radius of the boundary next to the first zone, both radii holding for the second zone. If we deal with a wave front for which $d = 5{,}000$ m, the free-space wavelength $\lambda = 1$ m, and $r_0 = 2{,}000$ m, we find

$$k = \sqrt{\frac{5 \times 10^3 \times 2 \times 10^3}{7 \times 10^3}} = 37.8 \text{ m}$$

The radius ρ_1 of the outer boundary of the first zone is then $\rho_1 = 37.8$ m; while for the fourth zone, we have $\rho_4 = 37.8\sqrt{4} = 75.6$ m. If a wavelength $\lambda = 0.01$ m or 1 cm were used, the first zone would have a radius of only $\rho = 3.78$ m. The area of the nth zone becomes

$$A_n \cong \pi(\rho_n^2 - \rho_{n-1}^2) = \pi\left[\frac{n\lambda r_0 d}{d + r_0} - \frac{(n-1)\lambda r_0 d}{d + r_0}\right] = \frac{3.14\lambda r_0 d}{d + r_0} \quad \text{sq m} \tag{892j}$$

According to this result, all lower zonal areas are equal, which result, in some cases, may not be a good enough approximation, so that formula (892*e*) should be used for greater accuracy. Since (892*h*) is also the expression for the arc length l in meters, the circular wave front (circular in the plane of the paper, but spherical in space) of the nth zone and the arc length l_{n-1} of the $(n-1)$th zone, according to (892*i*), yield

$$l_n - l_{n-1} = \sqrt{\frac{r_0\lambda d}{d + r_0}}\,(\sqrt{n} - \sqrt{n-1}) \qquad \text{m} \tag{892k}$$

For the second zone, we have $\sqrt{n} - \sqrt{n-1} = \sqrt{2} - \sqrt{1} = 0.4142$, and $l_n - l_{n-1} = 0.4142\sqrt{r_0\lambda d/(d + r_0)}$ meters; while for the fourth zone, it would be only $\sqrt{4} - \sqrt{3} = 0.27$ times the square-root value. Unlike in optics, we deal with short waves with appreciable dimensions, and there may be some use for such results.

190. Magnitudes of Zonal Areas and Dimensions for Plane Wave Fronts. For plane wave fronts, we have, in Fig. 298, the quantities $d = \infty$ and $a = 0$. This means that arc $l = SS_0$ must coincide with SF. We have then, in triangle SFR,

$$\rho^2 + r_0^2 = r^2 = (r_0 + \delta)^2 = r_0^2 + 2\delta r_0 + \delta^2 \cong r_0^2 + 2\delta r_0$$

Since, in many cases, the quantity δ is also very small compared with r_0 and δ^2 is negligible compared with r_0^2, we have also $\rho = \sqrt{2\delta r_0}$. But $\delta = 0.5n\lambda$, for $n = 1, 2, 3, \cdots$, and for the outer border of the nth zone, we find a radius

$$\rho_n = \sqrt{nr_0\lambda} \qquad \text{m} \tag{892l}$$

and the area A_n of the nth zone as

$$A_n = \pi(\rho_n^2 - \rho_{n-1}^2) = r_0\lambda[n - (n-1)] = \pi r_0\lambda \quad \text{sq m} \tag{892m}$$

Applying this to the above example, where $\lambda = 1$ m, $r_0 = 2{,}000$ m, we find for the outer radius of the first zone a value $\rho_1 = \sqrt{1 \times 2{,}000 \times 1} = 44.7$ m in comparison with 37.8 m obtained by taking the actual curvature of 1/5,000 per meter into account. If we had assumed a wave front of radius $d = 20$ km, Eq. (892*i*) would have yielded $\rho_1 = \sqrt{20{,}000 \times 2{,}000/22{,}000} = 42.7$ m, giving a better check on the value $\rho_1 = 44.7$ m found for a plane wave front [Eq. (892*l*)]. It is, therefore, not necessary to approach the value $d = \infty$ very closely. This is due to the fact that the relative value of r_0 with respect to the curvature $1/d$ of the wave front also plays a part. If, for instance, a smaller portion of the $1/d$ curvature is used, as in the case of an obstructing screen with an aperture, only a short arc of the effective primary wave front can be effective, and we deal essentially with a plane wave front. For instance,

if we choose $r_0 = 500$ m and leave the original value of $d = 5{,}000$ m. Eq. (892i) yields $\rho_1 = \sqrt{\frac{5{,}000 \times 500}{5{,}500}} = 21.3$ m, while Eq. (892l) yields $\rho_1 = \sqrt{500} = 22.36$ m, which is more in agreement. The decrease of r_0 can be driven only to a certain limit, since it impairs the number of lower zones that can be used, because δ^2 is to be negligible in comparison with r_0^2 in (892l). Inasmuch as for a plane wave front ρ_n also represents the so-called "stretched-out" arc l of Fig. 298, the difference $\rho_n - \rho_{n-1}$ must also represent the length of the plane wave front of the nth zone.

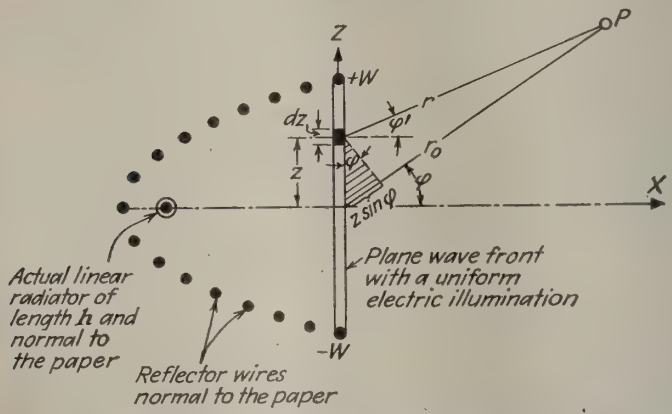

FIG. 300. Parabolic cage reflector with a linear radiator along the focal line. $\varphi' \cong \varphi$ and $r_0 - r \cong z \sin \varphi$ for P in the distant radiation region. XZ is the equatorial plane of the parabolic radiating system.

From this discussion, it can be seen that a portion of a wave front arriving at an edge of an obstacle or at a suitable opening of a wave obstruction may cause a deviation of the wave propagation from a straight course. The degree of the deviation depends upon the dimensions of the wave front as well as on the reception center orientation and on the frequency.

191. Application of the Wavelet Concept to a Parabolic Electromagnetic Projector. Inasmuch as the Huygens-Fresnel wavelet effect applies to any wave front, we can consider such a front as a surface with an infinite number of secondary radiators, all radiating with the same inphase amplitude. Since, in reality, the field intensity at a reception center is due to a variable current flow in the actual radiator that causes the primary wave front, we can also consider the wave front as a current surface for which all imaginary secondary currents are equal and in phase. By integrating the current effects at a reception point with

respect to the entire wave front, the resultant field at the reception point is obtained. In Fig. 300, we have a single linear radiator of length h along the focal length of a parabolic reflector, the top view being given in Fig. 300. Instead of linear reflector wires, a metallic copper reflector sheet bent into a parabolic shape can also be used. Since all *reflected* rays coming from the actual linear radiator have the same length from the source to the plane front surface of the reflector aperture, the elementary fields of all points of the aperture are in phase and of same intensity. This assumes that any direct rays from the radiator are screened off. We can then take the window of the reflector as a current sheet $2w$ meters wide and h meters high with a uniform current density $i = i_{max} \sin \omega t$ amperes per square meter. For such an action, it does not matter whether we divide the current sheet into current strips along the Y direction (parallel with the actual current flow) or parallel with the Z axis. The former is used here, since we are interested in the beaming effect of the paraboloid, and this can occur only in the XZ plane. This effect is, as we shall see, controllable either by the width $2w$ or by the wavelength or by both. It is then of interest to find an expression that gives the directivity D_φ in terms of the ratio $2w/\lambda$, *i.e.*, the opening or width, expressed by the operating wavelength. For a plane-wave-front element of width dz, we have a current content $dI = \int_{-w}^{+w} i\, dz = 2wi$, for a current strip dz wide and $2w$ long. Comparing this content with the actual antenna current I_A, we find a reflector effect I/I_A. Each front face strip $2w$ meters long and dz meters wide is, therefore, a fixed current and fixed phase radiator of current $2wi_{max} \sin \omega t$ if we are interested only in the field right next to this current strip. But for a field point a distance r meters away, this current is delayed in phase, since its effect must travel with the finite velocity of 3×10^8 m/sec $= c$. Each secondary strip radiator acts for such field points with a retarded effect $2wi_{max} \times \sin [\omega(t - r/c)]$. Inasmuch as the uniform current sheet is just as high as the actual antenna of length h meters, the size of the current sheet is $2wh$ square meters. For a width dz and a height h, we have for such a strip the moment M for the current distribution

$$M = \int_0^h i\, dz\, dh = hi\, dz = h\, dzi_{max} \sin \omega t$$

which has a retarded value

$$M' = h\, dzi_{max} \sin \omega t'; \qquad t' = t - \frac{r}{c}; \qquad c = 3 \times 10^8 \text{ m/sec} \quad (893)$$

As shown elsewhere in this text, it is the time derivative of M' that plays

a part[1] in the distant radiation region where field point P is located. We find then for the distant radiation region

$$\frac{dM'}{dt} = \omega h\, dz i_{\max} \cos \omega t' \tag{893a}$$

Since P is located in the equatorial plane of the radiating system, the field contribution at P, due to the current strip of area $h\, dz$ is,

$$d\mathcal{E} = -\frac{\omega h i_{\max} \cos(\omega t')}{r}\, dz \qquad \text{volts/m} \tag{893b}$$

This is exactly the expression which would be obtained from the $d\mathcal{E}_t$ relation given in the footnote on this page, since in the equatorial plane $\sin\theta = \sin 90° = 1$. Using the abbreviations $A = hi_{\max}/r$ and $\beta = \omega/c$ and introducing the path difference $r_0 - r = z \sin\varphi$, for $\omega t' = \omega t - \beta r_0$, we have, for any field point P in the equatorial XZ plane,

$$\begin{aligned} d\mathcal{E} &= -\omega A \cos(\omega t - \beta r_0 + \beta z \sin\varphi)\, dz \\ &= -\omega A[\cos\omega t' \cos(\beta z \sin\varphi) - \sin\omega t' \sin(\beta z \sin\varphi)]\, dz \end{aligned}$$

The total field contribution from the entire current sheet, *i.e.*, secondary radiation centers with wavelets, in the plane aperture of the paraboloid yields

[1] It is the component $\mathcal{E}_t$ that is significant, where $\mathcal{E}_t$ is normal to the direction of propagation, *i.e.*, tangent to the wave front at P. For $\beta = \omega/c$, very short length dh, and θ the angle that r makes with the current element dh, we find

$$d\mathcal{E}_t^{(\text{volts/m})} = \frac{cI\, dh \sin\theta}{\beta} \frac{}{r^3} \underbrace{(\cos\omega t' - \beta r \sin\omega t' - \beta^2 r^2 \cos\omega t')}_{\substack{\text{negligible together with} \\ 1/r^3}}$$

$$\cong -\frac{cI\beta\, dh \sin\theta}{r} \cos(\omega t - \beta r) = -\frac{18.84 \times 10^8 I\, dh \sin\theta}{\lambda r} \cos\left(\omega t - 6.28\frac{r}{\lambda}\right)$$

$$d\mathcal{E}_t = -\frac{\omega I\, dh \sin\theta}{r} \cos\left[\omega\left(t - \frac{r}{c}\right)\right] \qquad \text{volts/m}$$

The perpendicular associated H field is $dH = d\mathcal{E}_t/376.7$ amperes per meter, since

$$dH = \frac{I\, dh \sin\theta}{r^2}(\sin\omega t' - \beta r \cos\omega t') \cong -\frac{\beta I\, dh \sin\theta}{r} \cos(\omega t - \beta r)$$

The radial field (along the direction of propagation) is

$$d\mathcal{E}_r = -\frac{2cI\, dh \cos\theta}{\beta r^3}(\cos\omega t' - \beta r \sin\omega t') \cong 0 \text{ volts/m in the radiation region}$$

$$\mathcal{E} = \int_{-w}^{+w} d\mathcal{E} = -\omega A \left[\cos(\omega t') \int_{-w}^{+w} \cos(\beta z \sin\varphi)\, dz - \sin(\omega t') \int_{-w}^{+w} \sin(\beta z \sin\varphi)\, dz \right] = -\omega A \cos(\omega t') \frac{2}{\beta \sin\varphi} \sin(\beta w \sin\varphi)$$

Hence,

$$\mathcal{E} = -cA \cos(\omega t') \frac{2 \sin\left(\frac{2\pi}{\lambda} w \sin\varphi\right)}{\sin\varphi} = 2cA \cos(\omega t') D_\varphi \quad \text{volts/m} \tag{893c}$$

We have then a directivity in the equatorial XZ plane

$$D_\varphi = \frac{\sin\left(360° \frac{w}{\lambda} \sin\varphi\right)}{\sin\varphi} \tag{893d}$$

Assuming the half width $w = \frac{1}{2}\lambda$, $= \lambda$, and equal to 1.5λ gives the

TABLE 65. BEAMING EFFECT OF THE PARABOLIC PROJECTOR FOR DIFFERENT OPENINGS

For $k = \frac{w}{\lambda} = 1$. Since for $\varphi = 0°$ we have $D_\varphi = \frac{0}{0}$ (undeterminate) $\varphi = 1°$ is used					For $k = \frac{w}{\lambda} = 0.5$			For $\frac{w}{\lambda} = 1.5 = k$, we have two side lobes		
φ, deg	$\sin\varphi$	$\psi = 360 \frac{w}{\lambda} \sin\varphi$, deg	$\sin\psi$	$D_\varphi = \frac{\sin\psi}{\sin\varphi}$	$\psi' = 360 \frac{w}{\lambda} \sin\varphi$, deg	$\sin\psi'$	$D'_\varphi = \frac{\sin\psi'}{\sin\varphi}$	$\psi'' = 540 \sin\varphi$, deg	$\sin\psi''$	$D''_\varphi = \frac{\sin\psi''}{\sin\varphi}$
1	0.0175	6.3	0.1097	6.29	3.15	0.0549	3.125	9.45	0.1641	9.38
10	0.1736	62.7	0.8886	5.1	31.35	0.519	2.97	94	0.9976	5.73
20	0.342	123	0.8387	2.45	61.5	0.8788	2.56	185	−0.0875	−0.0255
30	0.5	180	0.0000	0.00	90	1.0000	2.000	270	−1.0000	−2.0000
40	0.643	232	−0.788	−1.22	116	0.8988	1.39	347	−0.225	−0.35
50	0.766	276	−0.9945	−1.3	138	0.6691	0.872	414	0.809	1.058
60	0.866	311	−0.7547	−0.875	155.5	0.4147	0.48	468	0.9511	1.1
70	0.9397	339	−0.3584	−0.38	169.5	0.1822	0.194	508	0.5299	0.564
80	0.985	355	−0.0872	−0.089	177.5	0.0436	0.0443	532	0.1392	0.141
90	1.0000	360	0.0000	0.000	180	0.0000	0.0000	540	0.0000	0.000

computation procedure of Table 65 and the directivity patterns of Fig. 301. The most important direction is the $\varphi = 0$ deg direction, which

gives an undeterminate solution, since $D_\varphi = 0/0$. This is the reason why in Table 65 a small angle such as $\varphi = 1$ deg is also used. The value for this small angle then gives a means of finding the value for $\varphi = 0$ deg by the method of graphical interpolation. When the opening $2w$ of the paraboloid becomes larger than 1 wavelength, side lobes appear owing to wave interference. This corresponds then to wave-front excitations for which $w > \frac{1}{2}\lambda$. Figure 301*a* shows the limiting case corresponding

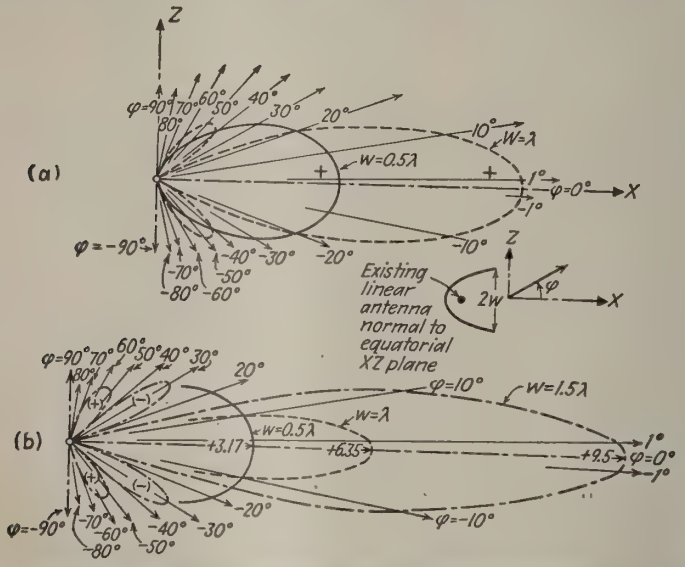

FIG. 301. Diffraction pattern of parabolic electromagnetic projector in the equatorial plane [ignoring the forward factor 1 + cos (angle)].

to $w = 0.5\lambda$, with only one lobe in comparison with an opening of $w = \lambda$, for which we have the upper limit from which on side lobes are also caused. The side lobes are of negative polarity with respect to the polarity of the main lobe. Figure 301*b* gives the comparisons of the main lobes for $w = 0.5\lambda$, λ, and 1.5λ. The four side lobes for $w = 1.5\lambda$ are then of negative and positive polarities if the main lobe is taken as positive. We shall find six side lobes for $w > 1.5\lambda$ up to and including to $2\lambda = w$. We note that the main beaming is decidedly more for $w = 1.5\lambda$ than for the other openings of the paraboloid. The ratios in the preferred direction are 9.5:6.35:3.17 as far as the field intensities $\mathcal{E}$ and H are concerned. The beaming with respect to the field energy is then in the ratios $9.5^2:6.35^2:3.17^2$. The polarity of respective lobes does not matter, since it means only that respective electric and magnetic field vectors are subjected to it. It is, however, the field energy that counts, and the polarity of energy is always positive. Besides, each

side lobe belongs to a particular angular region, regardless of its polarity. The sharpness of the main lobe can be increased by increasing the plane-wave-front width. Therefore, if k is larger in $w = k\lambda$, we have sharper main beaming but also more "side brush" due to more side lobes. In some cases, these side lobes may be screened off. For $k = 10$, we have $\psi = 3{,}600° \sin \varphi$; and for $\varphi = 1$ deg, we find $\psi = 3{,}600 \times 0.0175 = 63$ deg, $\sin \psi = 0.891$, and $D_\varphi = \sin \psi / \sin \varphi = 0.891/0.0175 = 51$. This is a much larger value than any of the corresponding values in Table 65. The angle $\varphi = 1$ deg, for $k = 10$, is not a good enough approach for the $\varphi = 0$ deg condition, even though it is an approximation for $k = 1$, since then ψ is $360 \times 0.0175 = 6.3$ deg in comparison with 63 deg for $k = 10$. We must then take $\varphi = 0.1$ deg for $k = 10$ and find $\sin 0.1° = 0.0017$, $\psi = 3{,}600 \times 0.0017 = 6.1$ deg, and $D_\varphi = \sin 6.1°/\sin 0.1° = 0.1063/0.0017 = 62.5$. This is then about the value for $\varphi = 0$ deg.

In formula (893*d*) and the discussion of Sec. 192, the right side of formula (893*d*) must (strictly taken) also be multiplied by the *forward factor* $(1 + \cos \varphi)$. Doing this, still *more emphasizes* the main beaming and *deemphasizes* any *side-lobe effects*. The main lobe is desired radiation, and any side lobes are undesired radiation. The forward factor was purposely ignored in Table 65 and the corresponding polar diagrams, in order to show how sharp the main beaming can be made, even without the Huygens forward factor. We work quite often with a very sharp main beam which occupies only a very sharp angle for which the forward factor has essentially the value 2, since $(1 + \cos \varphi) \cong 2$ for φ small.

192. Notes on the Beam Width of a Plane Wave Front with Wavelets. It is the width of the main beam that is of importance. Minima values occur in (893*d*) whenever $\sin [360°(w/\lambda) \sin \varphi] = 0$, *i.e.*, for $(w/\lambda)360° \times \sin \varphi = 0$; 180; 360 deg or equal to $q180$ deg for $q = 0, 1, 2, 3, 4, 5, \cdots$. The condition $q = 0$ does not apply, since we know that maximum effect must occur along the main axis (X axis of Fig. 301) corresponding to $\varphi = 0$ and $\psi = 0$. Since $\psi = 0$ will not apply, it is $\psi = 180$ deg that determines the sharpness of the main beam. From Table 65 as well as Fig. 301, we note that for $w/\lambda = 0.5$, the only beam is broad, because $\psi = 180$ deg occurs when we have $\varphi_b = 90$ deg. For $k = 1$ instead of 0.5, the main beam is much narrower, since it occupies an angular spread of only 2×30, or 60 deg. For $k = 1.5$, we have $\psi = 540 \sin \varphi_b = 180$ deg and $\sin \varphi_b = {}^{180}\!/_{540} = {}^{1}\!/_{3} = 0.3333$, yielding $\varphi_b = 19.5$ deg with a beam spread of $2 \times 19.5 = 39$ deg. We have, therefore, the main beam spread $B = 2\varphi_b$ or

$$B = 2 \sin^{-1}\left(0.5 \frac{\lambda}{w}\right) \quad \text{deg} \qquad (893e)$$

or $B = 2 \sin^{-1} (0.5/k)$ degrees. Table 66 gives the evaluations for this angle, and Fig. 302 shows how the opening of a paraboloid affects the main beam width. It is seen that very sharp main beaming is possible, since B degrees is the total main beam width. For instance, for $k = 30$, the total spread is only $B = 1.9$ deg. Since $k = 30 = w/\lambda$ expresses, for 3-cm waves, a full aperture width, $b = 2w = 2k\lambda = 2 \times 30 \times 3 = 180$ cm or only 5 ft 10.8 in. The beam width angle of B degrees refers here to the spread between the first two zero positions of the radiation pattern with the main beam in the spread. In some work, the beam width is not taken to absolute zero values as here, but either to 70.7 per

TABLE 66. MAIN BEAM WIDTH FOR FORWARD FACTOR IGNORED

$k = \frac{w}{\lambda}$	$\frac{1}{2k} = \sin \varphi_b$	φ_b, deg	$B = 2\varphi_b$, deg	k	$\frac{1}{2k}$	φ_b, deg	B, deg	k	$\frac{1}{2k}$	φ_b, deg	B, deg
0.5	1.0000	90	180	1.5	0.333	19.5	39	8	0.065	3.6	7.2
0.6	0.832	56.3	112.6	2	0.25	14.5	29	10	0.05	2.9	5.8
0.7	0.712	45.4	90.8	3	0.1665	9.6	19.2	12	0.0417	2.4	4.8
0.75	0.667	41.8	83.6	4	0.125	7.2	14.4	15	0.0333	1.9	3.8
1.0	0.5	30	60	5	0.1	5.8	11.6	20	0.025	1.4	2.8
1.25	0.4	23.6	47.2	6	0.0832	4.8	9.6	30	0.0166	0.95	1.9

cent of the maximum value (to half-power points) or sometimes to 50 per cent of the maximum value. Formula (893*e*) will give impossible solutions if $k = w/\lambda$ becomes smaller than $\frac{1}{2}$, since for smaller values $\sin \varphi_b = 0.5/k$ becomes larger than unity. As far as the Huygens forward factor is concerned, it has effect essentially in the main-beaming forward direction.

The main feature of the parabolic projector is that we can produce plane electromagnetic waves over very short distances from the primary radiator, since at the aperture of the paraboloid we have plane waves. Such waves can then be used to measure reflection coefficients of objects close to the source, since the Fresnel reflection theory assumes a plane wave front.

193. Wave Propagation through Apertures. We shall see in the following sections that even the modified simple theory due to W. Voigt[1] and the more rigorous general wave solution by G. Kirchhoff[2] with his

[1] VOIGT, W., "Kompendium der theoretischen Physik," Vol. II, p. 776, Leipzig, 1916.

[2] KIRCHHOFF, G., *Wied. Ann.*, **18**, 663 (1883). DRUDE, P., "Theory of Optics," translation by C. R. Mann and R. A. Millikan, pp. 174–181, Longmans, Green & Co., Inc., New York, 1939. H. POINCARÉ, "Théorie mathématique de la lumière," Vol. II.

wave function $w \equiv F[x, y, z, t - (r/c)]$ avert some of the shortcomings of the original Huygens principle and that of the Fresnel modification. The experimental verification in optics seems essentially due to the fact that the ratio of the wavelength of light to the largest dimension of an opening in a screen is exceedingly small. Hence, the arriving wave at the screen is practically *forced* through the opening along the direction

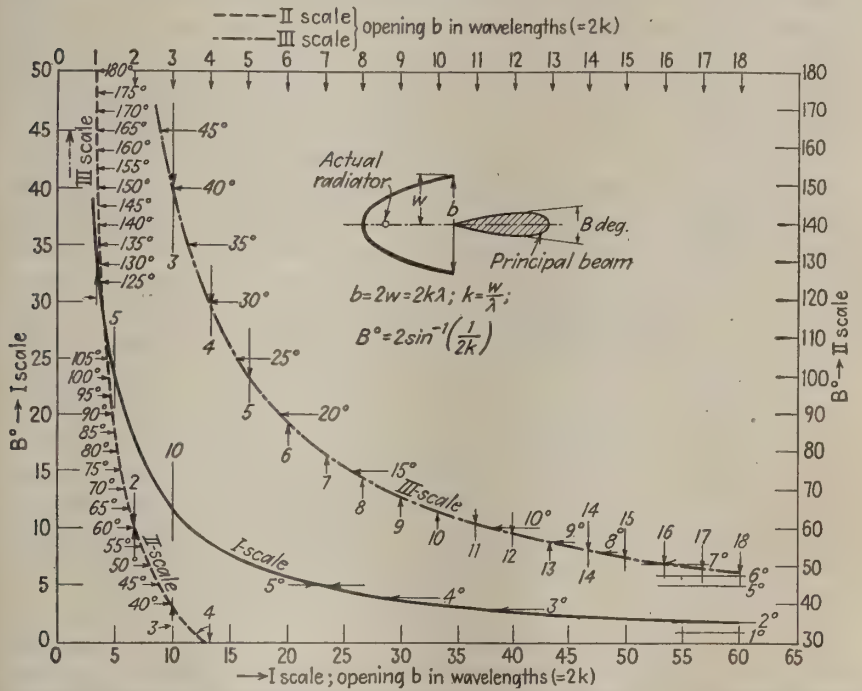

FIG. 302. Width B deg of principle beam of paraboloid in dependence of the aperture width b in wavelengths.

of incidence, so that on the inside of the screen (its shadow side) the intensity essentially vanishes. *With radio waves,* such as used in wave guides, in electromagnetic horns, the wavelength is close to the order of the dimensions of the opening and the *polarization must play a part.* As in many short-wave cases, a compromise must be made in order to satisfy observed experimental facts. Experimental facts are what count.

Nevertheless, we can apply many of the optical aperture observations to radio problems if the dimensions are changed accordingly. For instance, we know that a half-wave linear conductor is an efficient radiator and that a metal plate behind such a radiator diverts electromagnetic field energy efficiently into the forward direction, owing to the mirror effect. We also know that a half-wave reflector wire, say one-quarter

of a wavelength, behind a half-wave radiator also diverts the electromagnetic field energy efficiently forward. It therefore seems reasonable to expect that a half-wave slot in an obstruction to electromagnetic waves should let some wave energy pass into the medium behind the screening obstacle. As a matter of fact, this should also happen to a certain degree when the slot differs in length from a half wavelength. If we have several slots, according to the Huygens-Fresnel principle, we should then expect that wavelets originating in the openings or slots would cause wave penetration behind the screen and partially into the geometric shadow region. We can then speak of slot radiators that transmit waves. We may have then a resonant slot that is a half wavelength long and narrow in a metal sheet, where the wave polarization is such that a horizontal slot causes vertically polarized waves as would a vertical half-wave metal radiator and a vertical slot causes horizontally polarized waves as would a horizontal linear metal radiator. We have then two types of slots that can be used as linear wave-front radiators. The slots are then placed in positions where they can intercept currents in the walls of wave guides, for instance. Slots that interrupt longitudinal currents down the broad faces of wave guides are then series coupled. We can then apply shunt-displaced slots in the broad face or shunt-inclined slots in the narrow face for directivity devices.[1] For such wave-front radiators, the Babinet principle in optics can be used. Similar diffraction patterns are then caused by two complementary screens, where the opaque portion of one corresponds to the transparent portion of the other. The slot then behaves similarly to that of a complementary dipole with the metal removed from the metal sheet.

As mentioned in Sec. 187, we must take care of the change of the field conditions in an aperture due to the boundary conditions, which must be satisfied for electromagnetic waves. However, in order to bring out the diffraction principles, we shall assume to begin with that the wave front in an aperture is unperturbed. Doing this in Fig. 303*a*, we can imagine a slot 1-0-2 in a metal screen having behind it a medium that can absorb any arriving incident wave energy, so that we can assume the wave

[1] A Report on the Convention on the London Radio-location, *Radio*, **30,** (5), May, 1946, released by O. P. Ferrell, and reports by H. G. Booker, D. W. Fry, E. C. Jordan, and W. E. Miller, Slotted Cylinder Antenna, *Electronics*, February, 1947. A thin slot is in effect equivalent to an array of magnetic dipoles (*small* current loops). Axial slots in vertical cylinders give horizontal radiation patterns (consult Fig. 30). It is possible with such slot radiators to obtain horizontally polarized pattern effects which are almost circular. When radiation occurs from an aperture of a U-shape surface, the size of the surface has only a secondary effect on the omnidirectional transverse radiation pattern, if the spacing between the sides is smaller than $\lambda/8$. For a slot aperture in a metallic plane screen, the directivity pattern in a plane transverse to the slot depends on the dimensions of the screen. In longitudinal planes the directivity pattern depends essentially on the length of the slot.

front in the opening unperturbed. Let us also assume that the orientation of the slot is such that waves can pass through it. We can take then all points of the 1-0-2 slot as Huygens wavelet centers and have conditions as in Fig. 303*b*, with the symmetry line TOP_0. Suppose that we have only radiation centers 1 and 2. Then a wavelet starts out at 1, and a wavelet at secondary radiation center 2. Since, at the aperture, the wave front is a trough condition, the first solid wavelet circles must correspond to wave-crest conditions. Therefore, at R_1 we must have a *double-crest effect*, since the 1 and 2 wavelets arrive in phase and with their crests. Similarly at R_2, we have a *double-trough effect*. Each position is then a seat of a maximum field

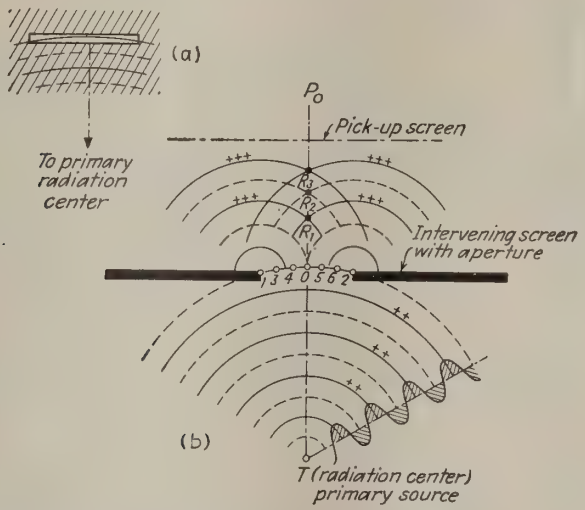

1 and 2 are secondary radiation centers (Huygens wavelet sources); full circles denote wave crests and dashed circles denote wave troughs.

FIG. 303. Wave penetration through an aperture of a screen by means of the Huygens wavelet concept.

condition. Hencé, for only two radiation centers, such as 1 and 2, along OP_0, we have localities of reinforced crests and localities of reinforced troughs. Therefore, halfway between such locations, we have conditions of zero field effects. We have to take into consideration all the possible wavelet centers of the aperture in Fig. 303, since secondary radiation centers 3, 4, 5, . . . are also effective. We then find that all along the line TP_0, we have a field condition, *i.e.*, an electromagnetic illumination. This would correspond to the central bright illumination on a pickup screen. But in optics, we also find experimentally that the illumination due to the slot opening is not sharp on the pickup screen. The illumination blurs over the edges. As a matter of fact, if we use a monochromatic light source, in the case of a narrow slit, we have a central bright illumination corresponding to the symmetry location TP_0 (a picture of the width of the opening) and, on each side of it, ribbons that are alternately dark and bright. These are then alternate cancellations and reinforcements. Taking all possible wavelets into account, we find the conditions of Fig. 304. Suppose a plane wave front arrives at the aperture 1-0-2. Suppose points P_1 are so located that (as in Fig. 304*b*) the distance from 1 to P_1 is equal to d_1 and the distance from 2 to P_1 is a full wavelength longer, or $d_1 + \lambda$. The distance OP_1 is then $d_1 + \frac{1}{2}\lambda$.

Therefore wavelets traveling along $1P_1$ and OP_1 must essentially cancel if $d_1 \gg \lambda$ and the slot is narrow. If this condition is not fulfilled, only a minimum resultant effect will ensue at P_1. Now we have other pairs of wavelets. We have also the path difference $3'P_1 - 3P_1 = \frac{1}{2}\lambda$. This will likewise give rise to destructive wave interference at P_1. Therefore, all portions of the wave-front halves 1 to 0 and 0 to 2 cause destructive interference at field point P_1. In exactly the same way, a point P_2, with a distance from 2 to P_2 equal to d_2 and from 1 to P_2 equal to $d_2 + \frac{1}{2}\lambda$, will

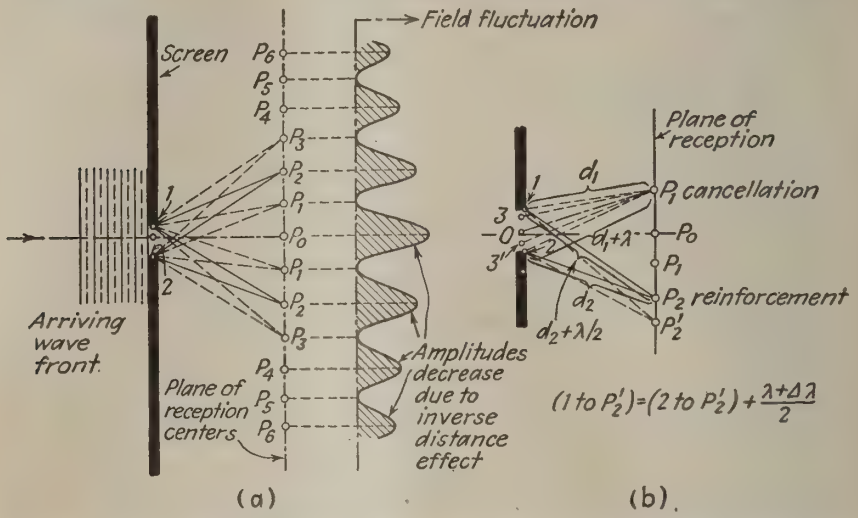

FIG. 304. Field energy fluctuations due to reinforcements and destructive wave interference.

cause maximum field effects at P_2, when all possible wavelet contributions are taken into account at the reception center P_2. Therefore, for any point P, for which

$$(1 \text{ to } P) - (2 \text{ to } P) = 0.5q\lambda \tag{894}$$

we find *maximum* resultant field effects for $q = 0, 1, 3, 5, 7, \cdots$, corresponding to reception centers $P_0, P_2, P_4, P_6, \ldots$, and *minimum* resultant field effects for $q = 2, 4, 6, 8, \cdots$, corresponding to reception centers $P_1, P_3, P_5, \cdots$. This is the case because wavelet pairs, being 0.5λ out of step, cause destructive effects and wavelet pairs, being $1.5\lambda, 2.5\lambda, 3.5\lambda, \ldots$ out of phase, have components in phase opposition. The higher the order (9.5λ is a higher order than 8.5λ) the smaller will be the minimization effect, since the inverse distance effect of the component fields must also be considered.

Inasmuch as in Fig. 304*b* the diffraction OP_2 for maximum field effect at P_2 is less for an operating wavelength λ than for the OP_2' effect with a wavelength $\lambda + \Delta\lambda$, we realize *why diffraction becomes more marked for longer wavelengths.*

194. Diffraction from a Sharp Edge (Optical Straight-edge Approximation). Figure 305 shows what may happen when a plane wave arrives at a sharp edge at E normal to the ZX plane. We have then the exaggerated diffraction pattern, which, according to Sommerfeld, is a diffrac-

tion pattern in the geometrical shadow region FG as well as in the unobstructed region FH. This explains the experimental optical observation that an edge E along the Y axis behaves like a linear light source, emitting cylindrical waves in the $\pm Z$, $\pm Y$, and $+X$ directions. The cylindrical waves proceed below and behind the edge E, with a $1/\sqrt{\text{distance}}$ law, *i.e.*, a *small wave spread amplitude decrease;* while in the unobstructed space

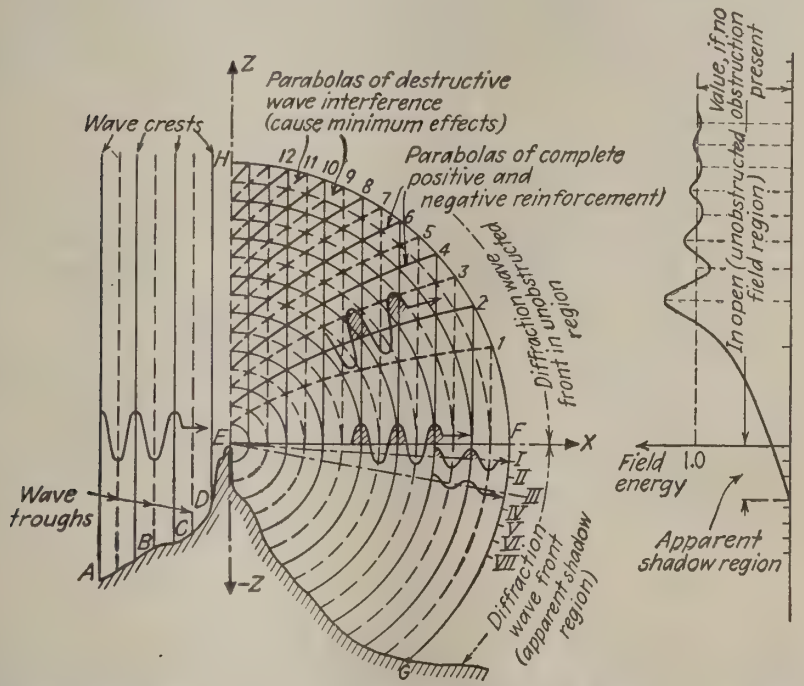

FIG. 305. Electromagnetic diffraction behind a sharp mountain wedge in the geometrical shadow zone as well as in the unobstructed zone behind the wedge. Y axis is normal to paper.

above and behind the edge E, we have *wave interference* between arriving plane waves and the secondary spherical waves. In order to bring out details, the scales in this figure are greatly exaggerated. We have then diffraction *below and above the edge E*. The wave spread into the region below the E edge refers to a portion of the geometric shadow zone. The interference pattern between cylindrical and plane waves yields parabolas. We then have maxima effects for the full-drawn parabolas and minima for the dash-dash parabolas. The waves radiated by the edge E decrease with $1/\sqrt{\text{distance}}$, while there can be no space attenuation for the arriving plane waves, since there is no spread. The inverse-square-root law holds along a path of fixed diffraction, but the amplitude does not

change when the interference pattern moves along the parabolic path, because the decrease of the angle of diffraction *just offsets* the amplitude decay and causes an amplitude increase. The energy pattern as well as the corresponding amplitude pattern on either side of the edge can be explained by means of the Cornu spiral, as well as by Fresnel zones. We have then, for partial zones, conditions as in Fig. 306. Above the Y axis, as in Fig. 306*b*, on the positive side of Z of the edge, there is no obstruction for the arriving plane wave or any curved wave front originating at a primary source. But for the $-Z$ side, we are in the geometric

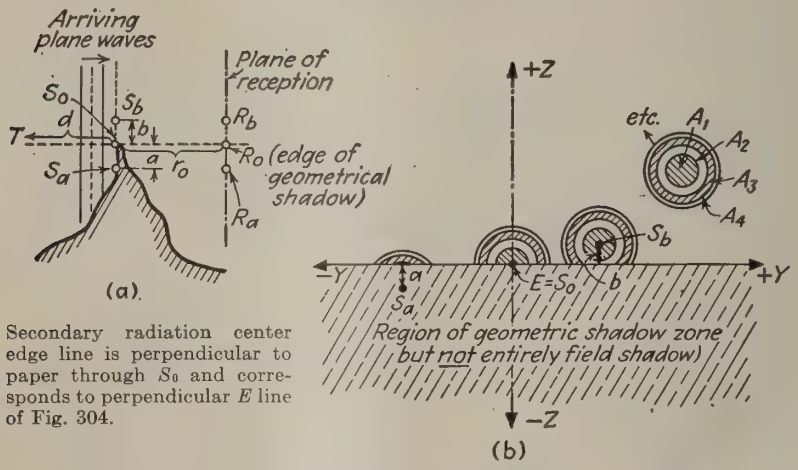

FIG. 306. Application of zonal rings to a sharp-wedge diffraction.

shadow zone if we first take point S_0 at the very edge of the obstruction. This corresponds to points E in Fig. 305 and point E in Fig. 306*b*. The points E of the arriving plane wave front are then wavelet centers, and S_0 as such a point emits a wavelet, which is represented by the circular wave front. If the entire edge length along the Y axis is taken into account, these circles must be cross sections of the corresponding secondary cylindrical wave propagation. The radiation effect of the S_0 wavelet can be expressed by Fresnel zones of areas A_1, A_2, A_3, A_4, . . . , of which only four consecutives zones are shown in Fig. 306*b*. This can be done, since the field contribution at the corresponding reception center becomes smaller and smaller for consecutive zones. This can be understood from (892*d*), since the resultant field $\mathcal{E}_R = \mathcal{E}_1 - \mathcal{E}_2 + \mathcal{E}_3 - \mathcal{E}_4 + \cdots = 0.5\mathcal{E}_1$, *i.e.*, equals half the field contribution of the central zone A_1 (Fig. 296). At the very edge E (Fig. 306), the Fresnel zones are only half-circular ring segments, as shown in Fig. 306*b*, since the lower half of the arriving wave front at E is obstructed below the

YX plane (it is assumed that the wave front above this plane is the same as when the edge is absent). The resultant field due to the S_0 radiation is, therefore, only $0.5\mathcal{E}_R$ or $0.25\mathcal{E}_1$. This means that the field at the reception center R_0 is only half and the corresponding field energy only one-quarter of the field if the total Fresnel zones were operative, *i.e.*, not half obstructed by the edge. Now S_a represents a wavelet center a distance *a below* the Y edge. This means that still fewer of the zonal areas are effective. The resultant field at the corresponding reception center R_a must be smaller than at R_0 and much smaller when no obstruction is present. Hence, as the distance a is increased, the corresponding resultant field at R_a will rapidly fall toward zero value, as is roughly indicated in the energy diagram of Fig. 305. But for a wave-front location S_b in Fig. 306, which is a distance b above the Y axis, more and more complete Fresnel zones are unobstructed, and the field at the corresponding reception center R_b may become larger than for the condition with the obstructing edge absent. The reason for this is that the effects of the consecutive Fresnel zones are *alternately additive and subtractive;* and according to the zones not operating (partially obstructed), the received field intensity is stronger or weaker. For instance, for an even number of complete zones operative (two for S_b), a minimum field condition results and $\mathcal{E}_b = 0.5\mathcal{E}_R + \mathcal{E}_1 - \mathcal{E}_2$; while if only the first A_1 zone were unobstructed, $\mathcal{E}_b = 0.5\mathcal{E}_R + \mathcal{E}_1 = (0.5\mathcal{E}_1/2) + \mathcal{E}_1 = 1.25\mathcal{E}_1$. This is a maximum effect. Hence, as b increases, we move through maxima and minima, which gradually approach the normal level of unity. This is roughly indicated in Fig. 305.

Inasmuch as an increase in b uncovers more and more Fresnel zones, the consecutive maxima and minima cannot be equally spaced but are according to the radii of the Fresnel zones. The distances b from the obstructing edge must, therefore, be proportional to $\sqrt{1}$, $\sqrt{2}$, $\sqrt{3}$, $\sqrt{4}$, ... We can, therefore, apply the Cornu spiral procedure for a more accurate interpretation of diffraction into unobstructed regions, as shown in Fig. 305.

195. The Cornu Spiral Procedure for Interpreting Fresnel Integrals. There are two Fresnel integrals that play an important part in radiation problems. These integrals have the form

$$x = \int_0^s \cos\left(\frac{\pi s^2}{2}\right) ds; \qquad y = \int_0^s \sin\left(\frac{\pi s^2}{2}\right) ds \tag{895}$$

If the quantity s denotes the upper limit of the respective x and y integrals, we obtain the well-known values for x and y of Table 67. The corresponding graphical integration is shown in Fig. 307, where the upper limit s gives the s units along the spiral as well as along X and Y

TABLE 67. TABLE FOR FRESNEL INTEGRALS, EQ. (895) AND THE GRAPHICAL CORNU SPIRAL SOLUTION OF FIG. 307

s	x	y	s	x	y	s	x	y
0.0	0.0000	0.0000	3.1	0.5616	0.5818	6.2	0.4676	0.5398
0.1	0.099	0.0005	3.2	0.4663	0.5933	6.3	0.4760	0.4555
0.2	0.1999	0.0042	3.3	0.4057	0.5193	6.4	0.5496	0.4965
0.3	0.2994	0.0141	3.4	0.4385	0.4297	6.5	0.4816	0.5454
0.4	0.3975	0.0334	3.5	0.5326	0.4153	6.6	0.469	0.4631
0.5	0.4923	0.0647	3.6	0.5880	0.4923	6.7	0.5467	0.4915
0.6	0.5811	0.1105	3.7	0.5419	0.5750	6.8	0.4831	0.5436
0.7	0.6597	0.1721	3.8	0.4481	0.5656	6.9	0.4732	0.4624
0.8	0.723	0.2493	3.9	0.4223	0.4752	7.0	0.5455	0.4997
0.9	0.7648	0.3398	4.0	0.4984	0.4205	7.1	0.4733	0.5360
1.0	0.7799	0.4383	4.1	0.5737	0.4758	7.2	0.4887	0.4572
1.1	0.7648	0.5365	4.2	0.5417	0.5632	7.3	0.5393	0.5199
1.2	0.7154	0.6234	4.3	0.4494	0.5540	7.4	0.4601	0.5161
1.3	0.6386	0.6863	4.4	0.4383	0.4623	7.5	0.5160	0.4607
1.4	0.5431	0.7135	4.5	0.5258	0.4342	7.6	0.5156	0.5389
1.5	0.4453	0.6975	4.6	0.5672	0.5162	7.7	0.4628	0.4820
1.6	0.3655	0.6389	4.7	0.4914	0.5669	7.8	0.5395	0.4896
1.7	0.3238	0.5492	4.8	0.4338	0.4968	7.9	0.4760	0.5323
1.8	0.3337	0.4509	4.9	0.5002	0.4351	8.0	0.4998	0.4602
1.9	0.3945	0.3734	5.0	0.5636	0.4992	8.1	0.5228	0.5320
2.0	0.4883	0.3434	5.1	0.4987	0.5624	8.2	0.4638	0.4859
2.1	0.5814	0.3743	5.2	0.4389	0.4969	8.3	0.5378	0.4932
2.2	0.6362	0.4556	5.3	0.5078	0.4404	8.4	0.4709	0.5243
2.3	0.6268	0.5531	5.4	0.5573	0.5140	8.5	0.5142	0.4653
2.4	0.5550	0.6197	5.5	0.4784	0.5537	∞	0.5000	0.5000
2.5	0.4574	0.6192	5.6	0.4517	0.4700			
2.6	0.3889	0.5500	5.7	0.5385	0.4595			
2.7	0.3926	0.4529	5.8	0.5298	0.5461			
2.8	0.4675	0.3915	5.9	0.4484	0.5163			
2.9	0.5624	0.4102	6.0	0.4995	0.4469			
3.0	0.6057	0.4163	6.1	0.5495	0.5165			

Remarks: For the Fresnel integrals $x = \int_0^s p\,ds$, $y = \int_0^s q\,ds$, $p = \cos(0.5\pi s^2)$, $q = \sin(0.5\pi s^2)$, s is the length along the Cornu spiral.

directions, and $\cos(0.5\pi s^2)$ and $\sin(0.5\pi s^2)$ of the x and y integrals are the coordinates. Hence, the areas under the curves to any value s must be the respective Fresnel integrals, *i.e.*, the values x and y in Table 67 or in Eq. (895). This table as well as the corresponding p and q curves in Fig. 308 show that the values of the integrals oscillate about a zero value, and the p and the q curves show that no fixed repetition exists, since, with increasing upper limit of the integral, the areas of the respective oscillations become smaller and smaller. As the limit approaches

infinity, *i.e.*, $s \to \infty$, we find

$$x = \int_0^{\pm\infty} p\, ds = y = \int_0^{\pm\infty} q\, ds = \pm 0.5$$

These values become even more significant when examining the Cornu spiral of Fig. 307, which represents the equation

$$\psi = 0.5\pi s^2 \tag{895a}$$

where s is the distance measured from the origin of the XY system along the scale of the Cornu spiral to a certain point P of the spiral. The

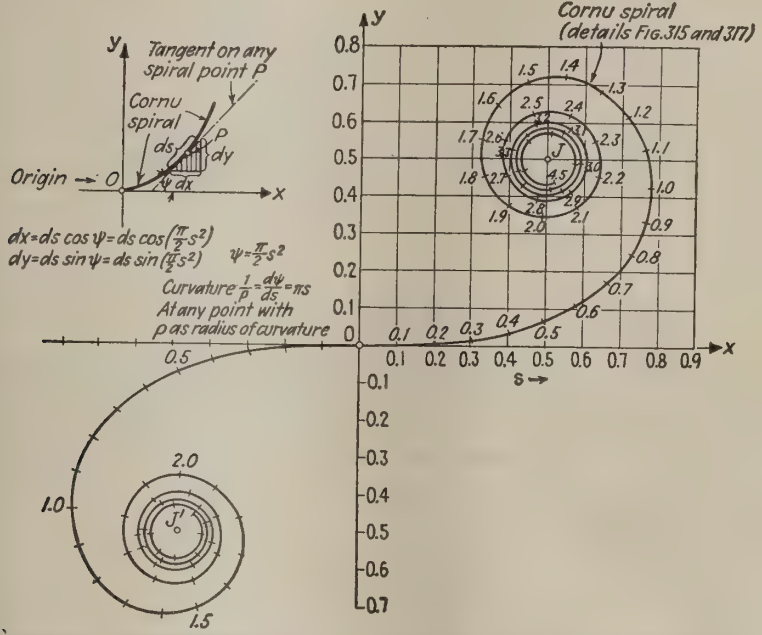

FIG. 307. Cornu spiral (graphical interpretation of the Fresnel integrals).

quantity ψ denotes the angle of the tangent at this point P with the X axis. The constant $0.5\pi = 1.57$ determines the scale along the spiral, since ψ is in radians. The same scale applies also for the X and Y axes.

For practical applications, the quantity s need not be infinite in order to yield the 0.5 value for the x or the y integral, and a value of s of a few thousand yields essentially $x = 0.5 = y$. Since the upper limit may be $\pm\infty$, the x and y values of ± 0.5 will be coordinates of respective asymptotic points J and J' reached for such limits. From Fig. 307, it is seen that for $s = 0$, the curve must be tangent to the X axis at the origin, since then $\psi = 0$ radians. The origin is also an inflec-

tion point, since s in the $+X$, $+Y$ quadrant is positive and in the $-X$, $-Y$ quadrant is negative. The outstanding feature of the Cornu spiral is that for $\psi = \pi/2$ radians, we have $\psi = 0.5\pi s^2 = \pi/2$ or $s = \pm 1$, because $s = \sqrt{1}$. For $\psi = \pi$, we have then $s = \sqrt{2} = 1.4142$. For $\psi = 1.5\pi$, 2π, 2.5π, $\cdots$, we find $s = \sqrt{3}$, $\sqrt{4}$, $\sqrt{5}$, $\cdots$, or $s = \pm 1.73$, ± 2, ± 2.236, $\cdots$. The curve can, therefore, be plotted roughly from such characteristic points. Another feature of this spiral is based on the above numerical outcome. The lengths for successive 90-deg or $\pi/2$ turns of the spiral are $\sqrt{1}$, $\sqrt{2} - \sqrt{1}$, $\sqrt{3} - \sqrt{2}$, $\sqrt{4} - \sqrt{3}$, $\sqrt{5} - \sqrt{4}$, $\cdots$, *i.e.*, 1, 0.4142, 0.32, 0.27, 0.236, $\cdots$.

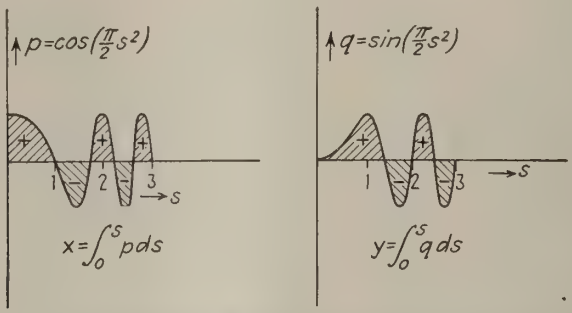

FIG. 308. Areas under respective curves are the solutions for the Fresnel integrals x and y.

Equations (895), representing the respective Fresnel integrals, can be readily found from the differential dy, dx, ds triangle of Fig. 307, since

$$dx = \cos \psi \, ds = \cos (0.5\pi s^2) \, ds; \qquad dy = \sin \psi \, ds = \sin (0.5\pi s^2) \, ds$$

Generally, any distance s along a spiral between the origin and a point corresponding to x is given by

$$s = \int_0^x \sqrt{(dx)^2 + (dy)^2} = \int_0^x ds = x \tag{895b}$$

because any short curve element ds of the spiral has, according to (895), the respective projections $dx = ds \cos (0.5\pi s^2)$ and $dy = ds \sin (0.5\pi s^2)$, rendering $ds = \sqrt{dx^2 + dy^2}$. The radius ρ of the curvature at any point P is $\rho = ds/d\psi$, where $\tan \psi = dy/dx = \tan (0.5\pi s^2)$ and $\psi = 0.5\pi s^2$ denotes the angle between the tangent at any point P and the X axis. Therefore,

$$\rho = \frac{ds}{d\psi} = \frac{1}{\pi s} \qquad \text{is radius of curvature for any portion of the Cornu spiral} \tag{895c}$$

Since J and J' represent the asymptotic points for $s = \pm \infty$, we have the corresponding coordinates for J and J' as $x = \int_0^{\pm \infty} \cos (0.5\pi s^2) \, ds$ and $y = \int_0^{\pm \infty} \sin (0.5\pi s^2) \, ds$. By means of (895c), we can also construct the Cornu spiral, using different consecutive radii (ever-shortening radii ρ). The procedure is as follows: Plot $x = 0.1$ along the

X axis, being an interval small enough to give practically the corresponding fixed curvature $1/\rho$. Since at the origin the spiral is tangent to the X axis, we scale off from the origin along the Y axis a distance $\rho = 1/\pi s = 10/\pi = 3.185$ and draw an arc with this radius, which is 0.1 long and passes through the origin. At the end point, we add another arc with the radius $\rho = 1/\pi s = 1/0.2\pi = 1.5925$, which makes an angle $\psi = 0.5\pi s^2 = 0.5\pi \times 0.04 = 0.02\pi$ radians with the axis X. Since π radians are 180 deg, we have $\psi = 0.02 \times 180$ deg $= 3.6$ deg.

The two Fresnel integrals of (895) and the corresponding Cornu spiral of Fig. 307 are useful for computing radiation patterns of electromagnetic horns, paraboloids, gains of such radiators, etc., since we can apply Huygens' wavelet concept together with the improvement due to

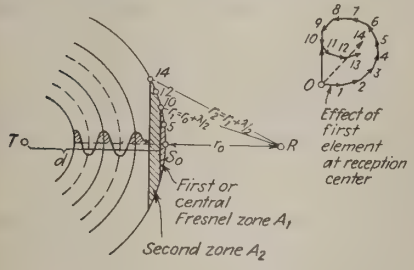
Effect of first element at reception center
0–10 resultant field due to first half zone; 0–14 resultant field due to first half and second half zones.
First or central Fresnel zone A_1
Second zone A_2
R
r_0
S_0
d

FIG. 309. Resultant effects due to different Fresnel zones.

Fresnel, who introduced the interference principle of waves traveling through different paths and arriving at a certain common field point.

196. Application of Cornu's Spiral and Tables for Fresnel Integrals. The many fictitious secondary radiation centers of an arriving exposed wave front, due to a primary radiator, are the poles of the wavelets emitted from such centers. In Fig. 309, the successive zones of the wave-front surface are so subdivided that the distance from the reception center R to the secondary wavelet center 10 is 0.5λ longer than the shortest distance r_0, etc. Each portion of such Fresnel zones contributes field energy at a chosen reception center R. We can divide the first or central zone into 10 portions such that each portion causes one unit field at R. The geometrical addition of all 10 such fields, designated 1, 2, 3, 4, 5, 6, 7, 8, 9, and 10, yields a resultant 0 to 10 with a phase change of 180 deg, because the secondary radiation center S_{10} is $\lambda/2$ farther from R than the secondary center S_0. The resultant 0 to 10 must then be the total field at R due to $A_1/2$, *i.e.*, half of the first Fresnel zonal area. By dividing the second zone, for instance, into four sections, we find the geometrical additions of vectors 11, 12, 13, and 14. The length 10 to 14 is then the field contribution of the second half Fresnel zone due to the area $A_2/2$, and the vector length 0 to 14 must be the total field due to the zonal area $\frac{1}{2}(A_1 + A_2)$. The consecutive vectors form a half

Cornu spiral, where O denotes the origin. The secondary radiation centers S_0, S_1, S_2, . . . of Fig. 310 can now be any distance $r_0 + \Delta r$ from the reception center R and within any particular Fresnel zone, since a straight edge (an obstruction) may partially cover such zones (Fig. 306*b*). A harmonic field effect of sin ωt variation at the secondary radiation center S_0 of Fig. 310, for a wave-front element dl at the edge where S_0 is located, causes at R an effect that is proportional to sin $(\omega t - \beta r_0)\, dl$. The secondary center S_1 adds an effect proportional to sin $[\omega t - \beta(r_0 + \Delta r)]\, dl$. In each case, we also have to multiply by a factor that expresses the inverse distance law $1/r_0$ and $1/(r_0 + \Delta r)$, for which $r_0 \gg l$.

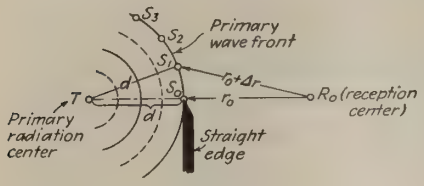

FIG. 310. Advancing primary wave front against a sharp-edged obstruction. dl is an infinitesimal length of the wave front.

The total field effect due to the entire operating wave front (wave front above the obstruction in Fig. 310) is proportional to $\int_0^l \sin\,[\omega t - \beta(r_0 + \Delta r)\, dl$. The field energy is proportional to the square of the respective amplitudes of the components along rectangular coordinates, that is, $k\left\{\left[\int_0^l \cos\,(\beta\Delta r)\, dl\right]^2 + \left[\int_0^l \sin\,(\beta\Delta r)\, dl\right]^2\right\}$. If the length l along the wave front refers to arc S_0S_1 and $l \ll d$ as well as $\ll r_0$, we have l essentially linear and $\Delta r \cong l^2(d + r_0)/(2r_0d)$.

We then find the common argument $\beta\,\Delta r$ of the variable functions under the integrals as

$$\beta\,\Delta r = \frac{2\pi}{\lambda}\,\frac{(d + r_0)l^2}{2r_0d} = \pi\,\frac{(d + r_0)l^2}{r_0\lambda d} = \frac{\pi}{2}\,s^2 \tag{895d}$$

for

$$s = l\sqrt{\frac{2(d + r_0)}{r_0\lambda d}} \tag{895e}$$

Hence,

$$l = s\sqrt{\frac{r_0\lambda d}{2(d + r_0)}}; \qquad dl = \sqrt{\frac{r_0\lambda d}{2(d + r_0)}}\,ds \tag{895f}$$

and

$$\text{Field power} = k\,\frac{r_0\lambda d}{2(d + r_0)}\left\{\left[\int_0^s \cos\left(\frac{1}{2}\,\pi s^2\right) ds\right]^2 + \left[\int_0^s \sin\left(\frac{1}{2}\,\pi s^2\right) ds\right]^2\right\}$$
$$= k\,\frac{r_0\lambda d}{2(d + r_0)}\,(x^2 + y^2) \tag{895g}$$

where x and y are the Fresnel integrals defined by (895) with values as given in Table 67. It is, therefore, possible to use the Cornu spiral for interpreting the case illus-

trated in Fig. 305. This figure applies, for instance, if radio waves pass across wedge-shaped mountain ridges. Relation (895*g*) then gives the expression for the field energy at the reception point R_0 of Fig. 310. We have ignored the actual boundary conditions at the straight-edge obstacle, since we assume that the obstacle does not perturb the arriving wave front owing to reflections. We then find the Cornu spiral application of Fig. 311 for two wave obstacles, for which only the primary wave front corresponding to $l_1 + l_2$ is exposed at an aperture. Formulas (895*f*) then give the corresponding s values, where s is the distance along the spiral, while x and y of

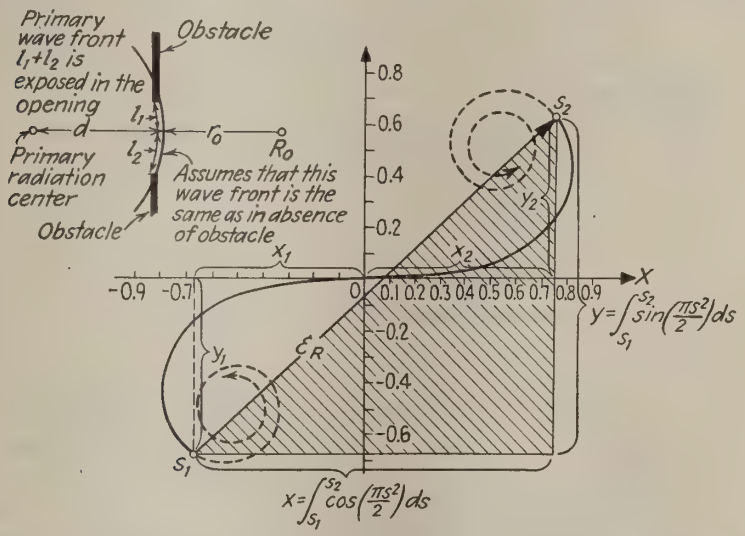

FIG. 311. Cornu spiral method applied to an exposed undisturbed wave front. Field power $= k(x^2 + y^2)$, since $\sqrt{x^2 + y^2}$ is a measure for the field amplitude. s_1 is the distance along the lower spiral, and s_2 along the upper spiral. s_1 and s_2 represent the corresponding l_1 and l_2 values.

Table 67 give the corresponding coordinates. Since the square of ε_R is proportional to the field energy, the hypotenuse ε_R must represent the corresponding amplitude.

197. The Cornu Spiral Procedure for Sharp-wedge Diffraction. For an arriving spherical wave front $S_aS_0S_b$, we have results as given in Fig. 312*a*. For the reception center R_0, only the upper semicircular Fresnel zones can be operative, since, below S_0, the arriving primary wave front cannot penetrate the space behind the wedge. If the wedge obstruction were not present, the straight length AB in Fig. 312*b* of the Cornu spiral would be equal to the resultant field amplitude. Hence, the lower half of the spiral cannot play a part, and OB must denote the resultant field amplitude ε_0 at R_0. For all the other wave-front poles, such as S_a and S_b, we have the corresponding reception centers R_a and R_b. Calling l the length of the arc S_0S_b and z the distance R_0R_b, we find $l = zd/(d + r_0)$, because both z and l are small compared with d and r_0. From $s =$

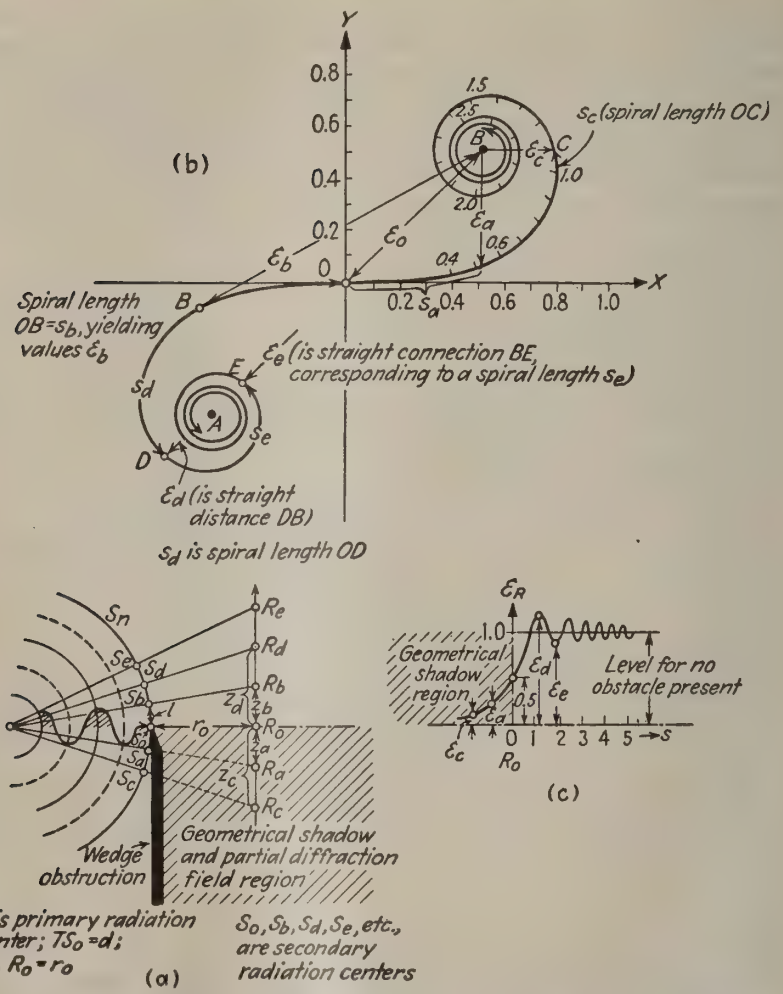

FIG. 312. Construction of the field fluctuations due to diffraction in the unobstructed field region and the field decay in the geometrical shadow region behind the wedge.

$l\sqrt{2(d + r_0)/(r_0\lambda d)}$, as given in (895$e$), we find

$$s = z\sqrt{\frac{2d}{(r_0 + d)r_0\lambda}} \tag{895h}$$

which relation defines the relative position of reception center R_b with respect to the R_0 position for a corresponding pole S_b on the primary wave front. Therefore, we have located the point on the spiral by means of (895h), where s is the distance along the spiral from the origin O.

The quantity l represents the length along the wave front from the edge point S_0 to pole S_b, and z is the location of the reception center R_b with respect to R_0. For the reception center R_a, corresponding to pole S_a on the primary arriving wave front, we deal with a pole that is covered by the obstruction, and *not* all Fresnel zones can be effective and, if so, only partially. Only the wave-front portion $S_0S_bS_n$ can be operative. But for the field point R_a, the corresponding pole S_a represents the origin O of the Cornu spiral. The portion s_a of the spiral, which is ineffective, is computed from (895h) by means of the z_a value, which is the distance by which R_a is below R_0. The closing vector $\mathfrak{E}_a$ is then the resultant field at reception point R_a. For S_c, we have a corresponding reception center R_c, which is still farther in the geometrical shadow region. We find then by means of z_c in (895h) the distance s_c along the spiral. The decay of $\mathfrak{E}$ for still larger values of z in the geometrical shadow region is much more rapid than indicated (for the sake of clearness in Fig. 312) and *without* any oscillations, since the spiral shrinks with respect to point B, to which the vectorial closing radii refer. This explains, therefore, the field diffracted into the geometrical shadow region of Fig. 312c. Now let us take a wavelet center S_b, which is the mid-surface point of the first spherical Fresnel zone, located in the *unobstructed* field region. This gives a value for s for the z value, indicated in Fig. 312a, by using formula (895h). This distance must be added now from O on the other portion of the spiral (beyond the inflection point O). This yields the closing vector $\mathfrak{E}_b$, which is longer than any of the values discussed so far. For a wavelet center S_d in the unobstructed zone, we have located a corresponding reception center R_d, for which the z_d value yields in (895h) an s_d value. The closing vector from B gives the optimum maximum value $\mathfrak{E}_d = BD$. For the spiral addition s_e, corresponding to receiving center R_e, we find the value $\mathfrak{E}_e$, which is the next minimum. We have, therefore, in the unobstructed radiation space, a diffraction pattern with maxima and minima. This means that we have values which are larger and smaller than would hold for the field in the absence of the wedge obstruction. This is readily seen in Fig. 312c and explains in detail the case illustrated in Fig. 305.

198. Electromagnetic Diffraction Due to Wedge-shaped Mountains for Short Waves. The optical diffraction case due to a straight-edge obstacle, as applied to electromagnetic wave propagation and illustrated in Fig. 305, has been partially borne out by experiment. We have then the resultant intensity curves on the far side of the wedge a distance r_0 away, as given in Fig. 313. This curve is the outcome of the Fresnel integrals and evaluated by means of the Cornu spiral. We must distinguish between *two diffraction regions,* since the wave energy not only

diffracts into the geometrical shadow region behind the obstructing wedge but *diffracts also into* the *unobstructed* region above the XY plane. In the last section, we found that *below* the XY plane, the diffracted field falls off, according to the radius vector along a spiral, while *above* the

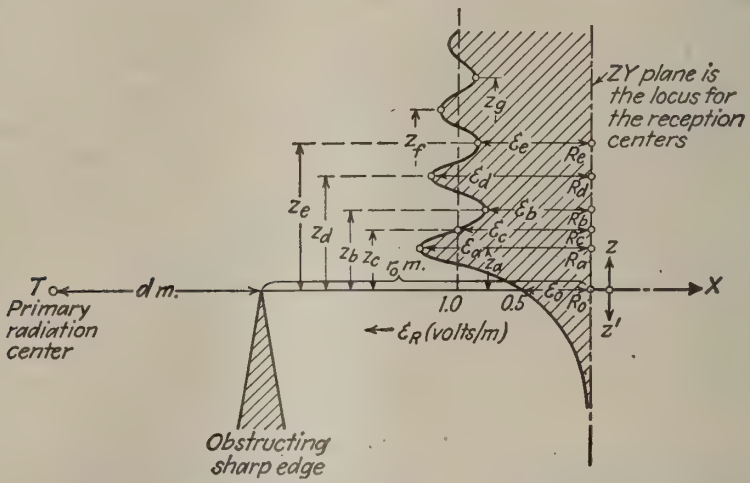

z_a, z_d, z_f are consecutive maximum field locations. z_b, z_e, z_g are consecutive minimum field locations. Y dimension is along sharp edge normal to paper. Complex field fluctuations (damped oscillating decay) due to diffraction in the unobstructed region above the XY plane. Exponential field decay in the geometric shadow region (below the XY plane) due to diffraction. $\mathcal{E}_R = 1$ volt/m is assumed at reception center R_0, a distance $(d + r_0)$ m from the primary radiation center T in absence of the obstruction; $\mathcal{E}_0 = 0.5$ volt/m is the value in presence of the edge obstruction.

$$\left.\begin{aligned} z_{\max} &= \sqrt{\frac{(2p-1)\lambda r_0(d+r_0)}{d}} \\ z_{\min} &= \sqrt{\frac{2p\lambda r_0(d+r_0)}{d}} \end{aligned}\right\} \text{ for } p = 1, 2, 3, 4, \ldots$$

Applications:

$$z_a = \sqrt{\frac{r_0(d+r_0)}{d}}\,\lambda = \sqrt{1}\,z_a = z_a;\ z_b = \sqrt{\frac{2r_0(d+r_0)}{d}}\,\lambda = 1.41 Z_a = \sqrt{2}\,Z_a$$

$$z_d = \sqrt{3}\,Z_a;\ z_e = \sqrt{4}\,z_a;\ z_f = \sqrt{5}\,z_a;\ z_g = \sqrt{6}\,z_a;\ \ldots$$

FIG. 313. Formulas and field display for the sharp-edge diffraction.

XY plane in the ZY reception plane, we have, at first, a rapid field increase until the first maximum value $\mathcal{E}_a$ is obtained. Hereafter, with increasing elevation z, the resultant field decreases until at a certain elevation z_c above the wedge, a distance r_0 away, a value $\mathcal{E}_c = 1$ volt/m is reached, which would be the same in the absence of the obstruction. For still higher elevation z, the field decreases, until for a value z_b, with respect to the geometrical line-of-sight level, where reception center R_0 is located, a minimum value $\mathcal{E}_b$ occurs, etc. The resultant field at reception centers R_0, R_a, R_c, R_b, . . . , oscillates about the free-field intensity

existing in the absence of the obstructing wedge. After the value of the first maximum is reached, we have a complex field intensity display, resembling a damped wave train; *i.e.*, we have an exponential space amplitude decay combined with an angular or phase shift variation. This is the reason why we lay out z' values along the $-Z$ axis and z values along the $+Z$ axis. Both values employ the same scale. The formulas given in Fig. 313 apply only to the z values. By means of these formulas, the oscillating field distribution can be found by graphical interpolation if maximum and minimum points are located. According to the Cornu spiral, the value at the reception center R_0 in the line of sight is not 1 volt/m, but only 0.5 volt/m. This can be explained, since some of the wave energy is diverted through diffraction into the shadow as well as into the unobstructed region.

According to experiments, horizontally polarized waves are diffracted more than vertically polarized waves if the edge of the wedge is also horizontal. This seems obvious, since "the rolling around the wedge" diffraction effect requires such a relative orientation. Experiments bear out that diffraction decreases with an increase of the frequency. This is also compatible with the theory.

It is now of interest to find the height z with respect to the line-of-sight level R_0, for maxima and minima, when λ is fixed and the horizontal spacing $d + r_0$ changes and vice versa. We have the equation $\lambda = 300/f$ meters, for f in megacycles per second, and find the evaluations of Table 68 for $d_0 = r_0 = 10{,}000$ m, since, for $p = 1, 2, 3, \cdots$,

$$\left.\begin{aligned} z &= 141.42\sqrt{(2p-1)\lambda} \quad \text{m for maxima} \\ z &= 200\sqrt{p\lambda} \quad \text{m for minima} \end{aligned}\right\} \tag{895i}$$

For the first maxima and minima values, we have in Table 68, the values $\sqrt{1}\,z_a = z_a$ and $\sqrt{2}\,z_a = z_b$ for $p = 1$ in (895i). For the second extreme values, we have $z_d = \sqrt{3}\,z_a$ and $z_e = \sqrt{4}\,z_a$. For the third maxima and minima values, we have $p = 3$ and $2p - 1 = 5$. Hence, $z_f = 141.42\sqrt{5}\sqrt{\lambda} = \sqrt{5}\,z_a$ and $z_g = 200\sqrt{3\lambda} = 141.42\sqrt{6\lambda} = \sqrt{6}\,z_a$. The factors $\sqrt{1}$, $\sqrt{2}$, $\sqrt{3}$, $\sqrt{4}$, $\sqrt{5}$, $\sqrt{6}$, . . . are characteristic of the Cornu spiral as well as the Fresnel zones. The results of Table 68 are plotted in Fig. 314. Three groups of z curves are plotted. One group refers to the A and B scales, for the frequency range from 1 to 150 Mc/sec. The second group brings out details in the 100 to 1,500-Mc/sec range, using C and D scales. The third group belongs to the range of 1,000 to 10,000 Mc/sec, with E and F scales. In each group, the solid curves refer to maximum values and the dash curves to minimum values. All curves show that for *longer* waves (lower frequencies), *diffraction* becomes *more pronounced*. For instance, at 1 Mc/sec, the first maximum distance is at a distance $z_a = 2{,}440$ m above the geometrical shadow level; while at 10 Mc/sec, z_a is only 770 m; and at 30,000 Mc/sec, we have z_a only 14.1 m above the line-of-sight level. It can also be seen that the distance between consecutive maxima as well as between consecutive minima is not fixed. For instance, at 1,000 Mc/sec, we have $z_d - z_a = 133 - 77 = 56$ m and $z_f - z_d = 172.5 - 133 = 39.5$ m. We have

$z_f - z_d = 2.24z_a - 1.73z_a = (\sqrt{5} - \sqrt{3})z_a$ and $z_d - z_a = (\sqrt{3} - \sqrt{1})z_a$. Formulas (895*i*) were obtained by putting $d = r_0 = 10{,}000$ m in the expressions of Fig. 313. These expressions likewise show that diffraction increases as the operating wavelength λ is increased, because then the z values for maxima and minima move such reception centers more above the geometrical shadow region. Since, in the formulas of Fig. 313, the ratio $r_0(d + r_0)/d$ under the square root also determines

TABLE 68. DIFFRACTION MAXIMA AND MINIMA

$\sqrt{\lambda}$	f, Mc/sec	λ, m	First maximum and minimum $p = 1$		Second maximum and minimum $p = 2$		Third maximum and minimum $p = 3$	
			$z_a = 141.42\sqrt{\lambda}$, m	$z_b = 1.4142z_a$, m	$z_d = 1.73z_a$, m	$z_e = 2z_a$, m	$z_f = 2.24z_a$, m	$z_g = 2.45z_a$, m
17.32	1	300	2,440	3,464	4,225	4,880	5,480	6,000
5.48	10	30	770	1,085	1,330	1,540	1,725	1,884
3.46	25	12	490	690	847	980	1,100	1,200
2.45	50	6	345	485	597	690	773	845
2.00	75	4	282	397	488	564	631	690
1.73	100	3	244	345	423	488	547	600
1.225	200	1.5	183	258	316	366	410	449
1.000	300	1.0	141	200	245	282	316	346
0.866	400	0.75	122	172	211	244	273	299
0.774	500	0.6	109.5	154	189	219	245	268
0.707	600	0.5	99.9	141	173	200	224	245
0.632	750	0.4	89.1	126	154	178.2	200	219
0.548	1,000	0.3	77	108.5	133	154	172.5	188.4
0.447	1,500	0.2	63	89	108.8	126	141	154
0.316	3,000	0.1	44.6	63	77	89.2	100	109.8
0.245	5,000	0.06	34.5	48.5	59.7	69	77.3	84.5
0.173	10,000	0.03	24.4	34.5	42.3	48.8	54.7	60
0.100	30,000	0.01	14.1	20	24.5	28.2	31.6	34.6

Remarks: For $d = r_0 = 10$ km and diffractions into the unobstructed space above the geometric line-of-sight plane XY of Fig. 313. $z^{(m)} = 141.42\sqrt{(2p-1)\lambda}$; $z^{(m)} = 200\sqrt{p\lambda}$; $\sqrt{(2p-1)\lambda}$ for maxima, $\sqrt{p\lambda}$ for minima $p = 1, 2, 3, \cdots$.

partially the value of z, we note that for a fixed $d + r_0$ value, the z value increases as the ratio r_0/d increases.

199. Notes on the Numerical Evaluation of the Resultant Field Diffracted into the Geometrical Shadow as Well as into the Unobstructed Region behind Wedge-shaped Mountains. It is now of interest to find the resultant field anywhere behind the wedge of Figs. 313 and 314 and for reception centers above as well as below the geometrical line-of-sight plane. Figure 315 gives the Cornu spiral, where s is the distance along the spiral from the origin and the same unit is used for the x and y scales.

As we know, the quantities x and y define any point on the spiral and $\sqrt{x^2 + y^2}$ denotes the amplitude. Equation (895h) connects the value of the level of a reception center with respect to the level of the geometrical line-of-sight plane TS_0R_0, where T is the primary radiation center (actual radiation center), S_0 the corresponding wavelet center just touching the

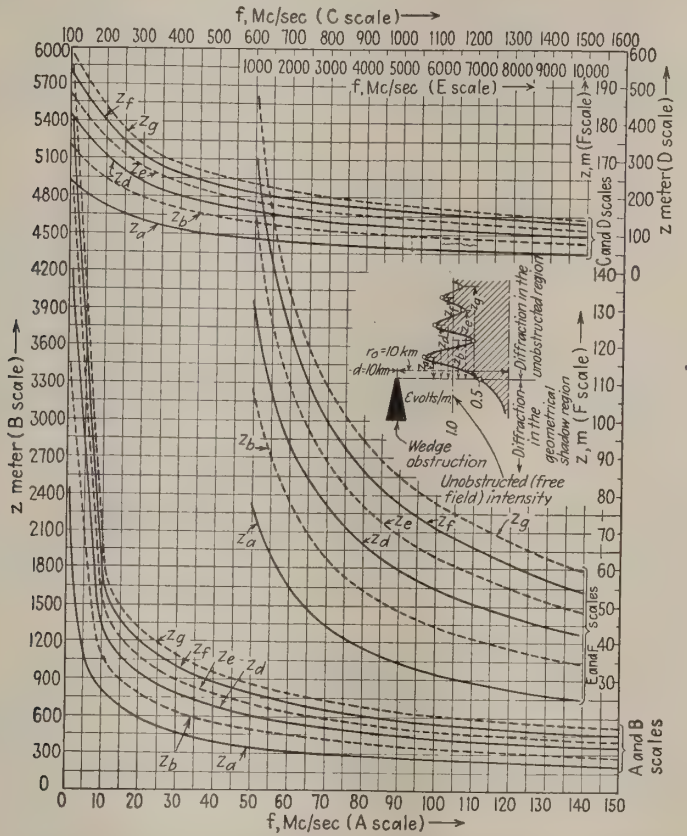

FIG. 314. Curves for significant values for diffraction effects due to a sharp-wedge obstruction.

edge of the obstructing wedge, and R_0 the reference reception center a distance r_0 along the line of sight. In Eq. (895h) and Fig. 315, the quantity l is the *curved* length along the primary wave front, while z is the corresponding relative altitude in the vertical plane of reception centers. The two quantities become numerically equal if plane waves arrive at the wedge, since then d is very large (theoretically infinite) and $d + r_0 \cong d$, so that $2(d + r_0)/(dr_0\lambda) \cong 2d/(dr_0\lambda) = 2/(r_0\lambda)$ and $l = z$. Without restricting ourselves to plane waves, we have

$$s = z\sqrt{\frac{2d}{[(r_0 + d)r_0\lambda]}}$$

which, for our numerical case $d = r_0 = 10{,}000$ m, yields

$$s = \frac{0.02l}{\sqrt{\lambda}}\text{ m} = \frac{0.01z}{\sqrt{\lambda}}\text{ m} \qquad (895j)$$

For an exciter frequency $f = 300$ Mc/sec, we have $\lambda = {}^{300}/_{300} = 1$ m and $s = 0.02l = 0.01z$ meters. The quantity z is used in the Cornu

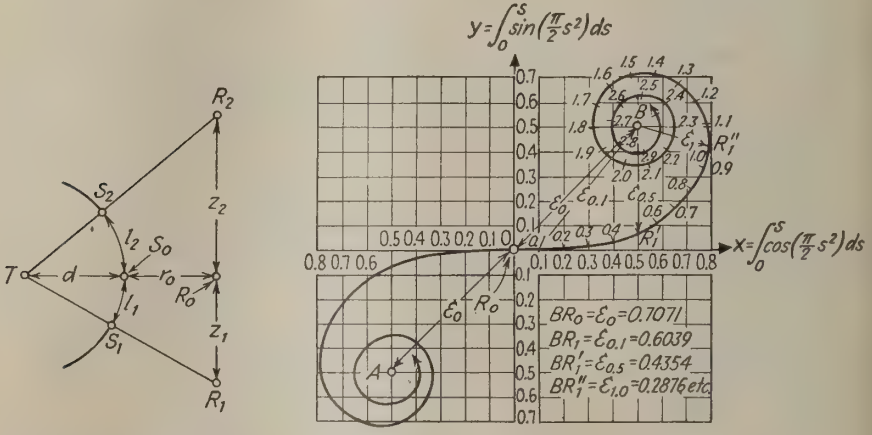

l_1 and l_2 are exposed portions of the primary wave front.

$$s = l\sqrt{\frac{2(d + r_0)}{r_0\lambda d}} = z\sqrt{\frac{2d}{(r_0 + d)r_0\lambda}} \qquad \text{Eq. (895}h\text{)}$$

s, l, z, d, r_0, and λ in meters. $\mathcal{E}_0$ is free-field amplitude in volts/m when no obstructing wedge is present. $OB = \mathcal{E}_0 = \sqrt{x^2 + y^2} = \sqrt{0.5^2 + 0.5^2} = 0.7071$ corresponding to 50% of the free-field intensity in absence of a wedge.

FIG. 315. Procedure of using the Cornu spiral for determining the effect of exposed primary wave fronts.

spiral procedure as well as in Table 67. Inasmuch as the s scale as well as the x and y scales use the *same units* in Fig. 315, it is only necessary to multiply the same arbitrary unit by the factor $0.01z/\sqrt{\lambda}$ or by $0.02l/\lambda$ in order to meet the actual dimensions. We multiply then by $z/100$ for waves that are 1 m long. The resultant field at R_0 corresponds to a distance $s = 0$, since $z = 0$. Since half of the arriving primary wave front is below the wedge, it cannot contribute wavelets. Hence, OB in Fig. 315 represents the amplitude of the resultant field at R_0, because O is the operating point for $s = 0$ and B is the theoretical limit of the spiral. The total amplitude is, therefore, $\sqrt{x^2 + y^2}$ or equal to the hypotenuse

OB, with projections $x = 0.5 = y$. This makes the resultant proportional to $\sqrt{0.5^2 + 0.5^2} = 0.7071$. If the wedge were absent, we should also have to add the field OA, yielding a total field that is proportional to $2 \times 0.7071 = 1.4142$. In Fig. 316, if we make the ordinate 0.5 equal to OB, *i.e.*, $0.7071s$ units, we have the field at the reception center R_0. For points in the geometrical shadow region (below the line-of-sight plane TS_0R_0), we proceed as follows: We have then z_2 as the various levels,

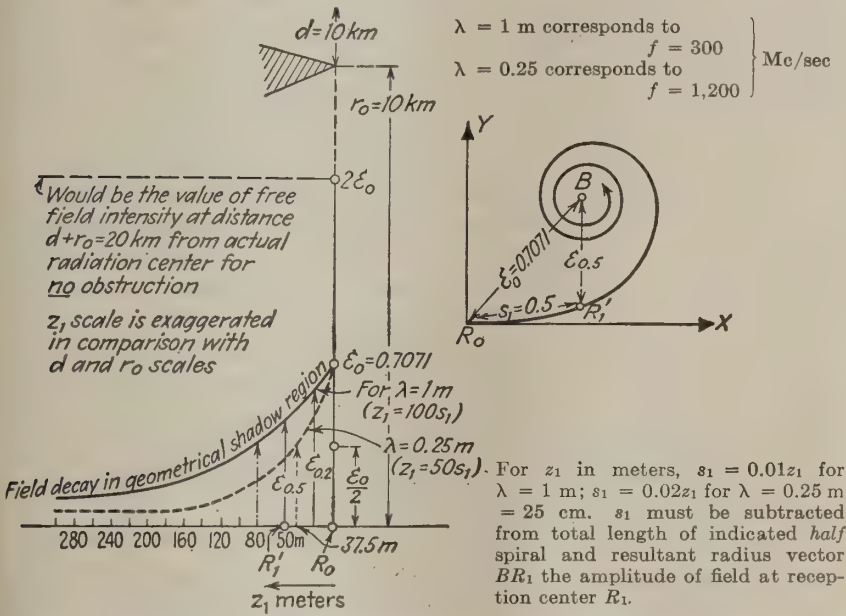

For z_1 in meters, $s_1 = 0.01z_1$ for $\lambda = 1$ m; $s_1 = 0.02z_1$ for $\lambda = 0.25$ m $= 25$ cm. s_1 must be subtracted from total length of indicated *half* spiral and resultant radius vector BR_1 the amplitude of field at reception center R_1.

FIG. 316. Conditions for the diffraction effects into the geometrical shadow region in the case of a wedge-shaped obstruction.

because it is below the TR_0 plane. For $z_1 = 10$ m, according to (895j), and $\lambda = 1$ m, we find $s_1 = 0.01z_1 = 0.1$ m. Subtracting $s = 0.1$ m from the upper right spiral length, we find the spiral point R_1 and the total field contribution at R_1 as $R_1B = \mathcal{E}_{0.1} = \sqrt{x^2 + y^2}$. Table 67 gives, for $s_1 = 0.1$ corresponding to reception center R_1, the values $x_1 = 0.1$ and $y_1 = 0.0005$, while B has the coordinates $x_B = 0.5$ and $y_B = 0.5$. The total x and y coordinates are, therefore, $x = x_B - x_1 = 0.5 - 0.1 = 0.4$ and $y = y_B - y_1 = 0.5 - 0.0005 = 0.4995$. We have then $\mathcal{E}_{0.1} = \sqrt{0.4^2 + 0.4995^2} = \sqrt{0.4095} = 0.6039$ in comparison with 0.7071 as for reception center R_0. For $z_1 = 20, 30, 40, 50, \cdots$ m, we find from (895j) and Table 67, for $\lambda = 1$ m, the values $s = 0.2, 0.3, 0.4, 0.5, \cdots$ m. For $s = s_1 = 0.5$ m, Table 67 yields $x_1 = 0.4923$, $y_1 = 0.0647$, $x = x_B - x_1 = 0.5 - 0.4923 = 0.0077$, $y = y_B - y_1 = 0.5 - 0.0647 = 0.4353$, and

$\mathcal{E}_{0.5} = \sqrt{0.0077^2 + 0.4353^2} = 0.4354$. This is the length of the radius vector BR_1' in Fig. 315. For $z_1 = 100$ m, we find $s = s_1 = 0.01 \times 100 = 1$ m with coordinates $x_1 = 0.7799$ and $y_1 = 0.4383$ and $x = 0.5 - 0.7799 = -0.2799$ and $y = 0.5 - 0.4343 = 0.0657$, yielding $\mathcal{E}_{100} = \sqrt{(-0.2799)^2 + 0.0657^2} = 0.2876$.

200. Numerical Application of the Cornu Spiral Method to Diffraction into the Geometrical Shadow Zone. From Sec. 199, we note that the numerical application of this procedure is exactly the same for all z_1 levels below the line-of-sight plane TR_0 (Figs. 315 and 316). The method, based on ascertaining the Fresnel coordinates x and y, can be avoided when we scale off directly the various vectors, such as OR_1, OR_1', OR_1'', . . . , where R_1, R_1', R_1'', . . . are obtained by means of formula (895j). For the particular application for which $f = 300$ Mc/sec, we have $\lambda = {}^{300}\!/_{300} = 1$ m and $s_1 = 0.01z_1$. The various reception centers then correspond to levels of z_1 meters *below* the line-of-sight reception point R_0. Figure 316 gives the curve for the relative resultant fields for a distance $r_0 = 10$ km from the obstructing wedge. The decrease in the resultant field is rapid, since the z_1 scale is in meters while the r_0 distance is in kilometers. To obtain a feeling of the diffraction, let us find the value of the amplitude $\mathcal{E}$, when it is only 50 per cent of the optimum value $\mathcal{E}_0$ at R_0. This happens for $\lambda = 1$ m for a level $z_1 \cong 80$ m below the line-of-sight plane. This corresponds, therefore, to a drop of 80×10^{-3} km at a horizontal range of $r_0 = 10$ km or an angle $\theta = \tan^{-1}(0.08/10)$ deg, which is somewhat smaller than 0.5 deg. At this angle of diffraction, the field energy would have dropped to 25 per cent. Let us now see what the effect of the frequency is for the same field energy decrease of 75 per cent with respect to the value at R_0. For $f = 1{,}200$ Mc/sec, or 4×300 Mc/sec, we have a free-space wavelength only one-fourth as long and (895j) gives, for the geometrical shadow region, $s_1 = 0.01z_1/\sqrt{0.25} = 0.01z_1\sqrt{4} = 0.02z_1$. From this result, we note that a much more rapid decay takes place. The dash curve of Fig. 316 shows that the half-amplitude reception (quarter-power reception) occurs now at about $z_1 = 37.5$ m below the line-of-sight plane, corresponding to a diffraction angle $\theta = \tan^{-1}(37.5 \times 10^{-3}/10) = \tan^{-1}(0.0037)$, which is somewhat less than 0.2 deg. This shows again that as the operating *frequency is increased,* the *diffraction becomes less* significant.

201. Numerical Application of the Cornu Spiral Method to Diffraction into the Unobstructed Region above the Geometrical Shadow Zone. Taking up this case for a 300-Mc excitation corresponding to $\lambda = 1$ m, we find $s = s_2 = 0.01z_2$ in Fig. 315, because we deal with conditions above the TS_0R_0 line. Only the reception center R_0 corresponds to

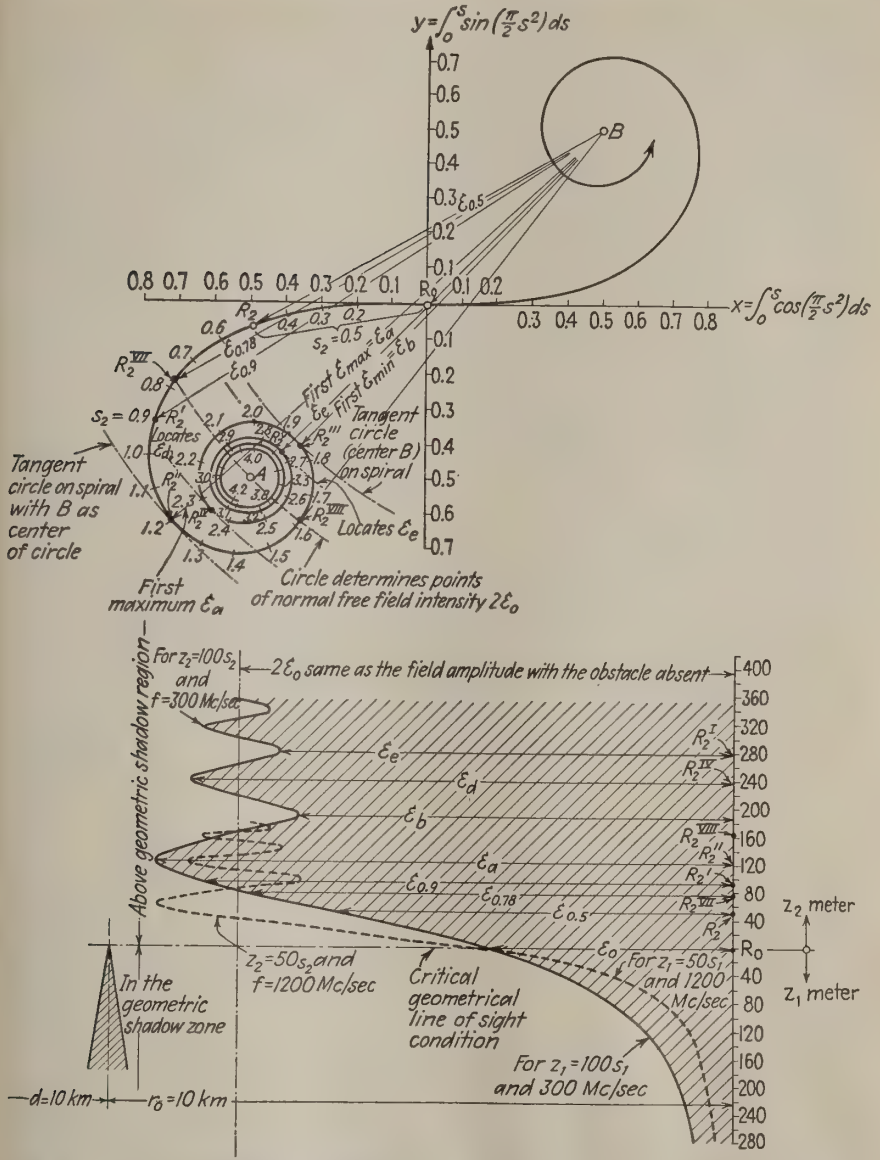

Fig. 317. Diffraction display details beyond a wedge obstruction applied to 300- and 1,200-Mc waves. As point R_2 moves along the lower spiral, the corresponding radius vector BR_2, expressing the magnitude of the field, grows at first to a maximum value $\mathcal{E}_a$, decreases again to a minimum value $\mathcal{E}_b$, increases again to a smaller maximum value $\mathcal{E}_d$, etc. S_2 is added from origin R_0 along the left lower spiral half and closing radius vector BR_2. $S_2 = 0.01z_2$ for z_2 in meters, and $\lambda = 1$ m ($f = 300$ Mc/sec); $d = r_0 = 10$ km. A and B are ultimate terminations of respective spirals occurring for $x = y = 0.5$. For such extreme spiral points the amplitude of the total field illumination becomes $2\mathcal{E}_0$, *i.e.*, equal to the unobstructed field intensity (obstruction absent).

half of the primary wave front. The length R_0B, closing the half spiral, then represents the field amplitude at R_0. But for points such as R_2 in Fig. 315, the inscribed formula, giving s in terms of z_2, yields $s = s_2 = 0.01z_2$, for $d = r_0 = 10$ km and $\lambda = 1$ m. The value $s_2 = 0.01z_2$ is then to be added to the right half spiral along the left spiral. The construction is then as shown in Fig. 317, since the secondary radiation center S_2 on the primary wave front will now give several complete Fresnel zones, except for the very outer zones. Inasmuch as the vector BR_2 for the spiral point R_2, moving along the lower spiral, oscillates in length, we obtain the indicated field distribution with maxima and minima. The construction of the pattern is then as follows: For the reception center R_0, we have, as in Fig. 316, the value $\mathcal{E}_0$, since the pole of the Fresnel zones coincides with the secondary radiation center S_0 and only half of the wave front can contribute to the field at R_0. At the reception center R_2, we have the field amplitude $BR_2 = \mathcal{E}_{0.5}$, since the curve $R_0R_2 = s_2 = 0.5$ must be added in order to account for the additional field contribution at the reception center R_2, which is 50 m above the line-of-sight plane. This is obvious if we realize that for $\lambda = 1$ m or $f = 300$ Mc/sec, we have $s_2 = 0.01z_2$ and $z_2 = 100s_2 = 100 \times 0.5 = 50$ m. Any other point on the Cornu spiral, such as R_2', gives a spiral length $s_2 = 0.9$ from the origin R_0 and corresponds to a reception center R_2' a distance $z_2 = 100s_2 = 100 \times 0.9 = 90$ m above the reception point R_0 and 10 km behind the wedge that causes the diffraction. The vector BR_2' on the Cornu spiral then yields the corresponding field amplitude $\mathcal{E}_{0.9}$. This amplitude is scaled off as ordinate at the $z_2 = 90$ m distance from R_0. Hence, any point on the spiral, such as 1.5, represents a level $1.5 \times 100 = 150$ m above the line-of-sight altitude. Maximum field values occur whenever BR_2 becomes a maximum. This happens when circles about B as a center just touch the outer contours of consecutive convolutions, giving the extreme field values $\mathcal{E}_c$, $\mathcal{E}_d$, . . . , corresponding to reception centers R_2'', R_2^{IV}, ... For the circles just touching the consecutive inner convolutions, we find the minimum field amplitudes $\mathcal{E}_b$, $\mathcal{E}_e$, . . . , corresponding to reception centers R_2''', R_2^{V}, ... Free field values $2\mathcal{E}_0$ occur whenever the circle with $2\mathcal{E}_0$ about B, *i.e.*, the circle with a radius BA about center B, intersects spiral points. The point R_2^{VII} is such a point, corresponding to an added spiral length $s_2 = 0.78$, which is a relative altitude $z_2 = 78$ m above the line-of-sight plane. The entire construction of Fig. 317 is then self-evident. The dash field curves hold for $f = 1{,}200$ Mc/sec, showing less diffraction into the unobstructed as well as into the geometrical shadow regions.

202. Notes on Experimental Confirmation of Fresnel Diffraction Effects of Mountain Ridges. Knife-edge diffraction is based strictly

on optical evidence. For short-wave radio propagation, it is not exactly an easy matter to separate atmospheric refraction, reflection from ground, and other obstructions and diffractions, as discussed in this chapter. However, H. Selvidge[1] has described diffraction measurements based on field runs along a path B obstructed by a mountain ridge and an unobstructed path A, as is indicated in Fig. 318. The obstructed path was formed by a long ridge of blunt knife-edge shape, which is 437 ft high for a length of about ¼ mile. Figure 318 gives the geographical layout of

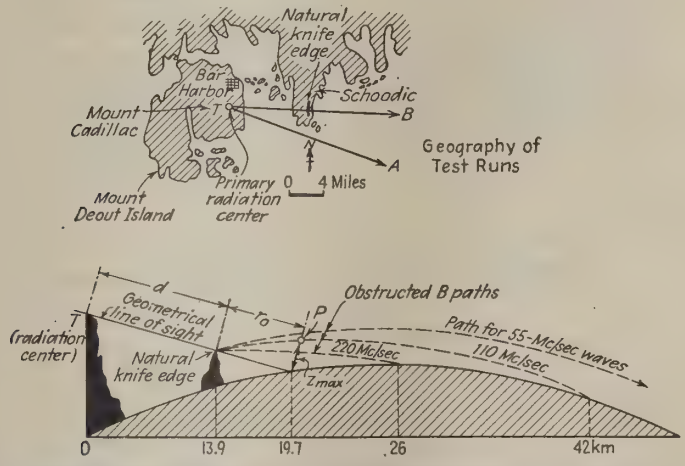

Fig. 318. Conditions and geographical layout of experiments by H. Selvidge with a natural knife-edge mountain ridge near Bar Harbor, Maine.

the experiments, in comparison with the profile of the computed field pattern for the first diffraction maxima and frequencies of 55, 110, and 220 Mc/sec. The line-of-sight path is about 19.7 km from the primary radiation center. The first maximum pattern for a particular frequency f in megacycles per second is found by first computing $\lambda = 300/f$ meters, then z_a, *i.e.*, z_{max}, for $p = 1$ in the maximum relation of Fig. 313, for different r_0 values, with d and λ fixed. Figure 319 gives the experimental curves indicating a fair confirmation of the optical diffraction pattern, except that in the deep shadow region, decided humps occur. These humps *cannot* be explained by the Cornu spiral method. (It must be realized that we assume in our theory that the wave front is *not* perturbed, owing to the electromagnetic effects of the mountain ridge.) Inasmuch as the indicated diffraction patterns are, for the path B, picked up on a small surface vessel, we have at least some experimental evidence for reception over sea water. It is seen that in the deep shadow region, the

[1] *Proc. IRE*, **29**, 10, January, 1941.

horizontal polarized signal happens to be stronger. More experimental data on such diffractions seem, therefore, worth-while contributions.

203. Notes on the Kirchhoff Diffraction Theory. This theory *tacitly assumes* that at a diffraction screen, the arriving wave is stopped while, at the apertures, the field penetrates through the openings in the same way *as though the screen were not present.* This is indeed a very broad assump-

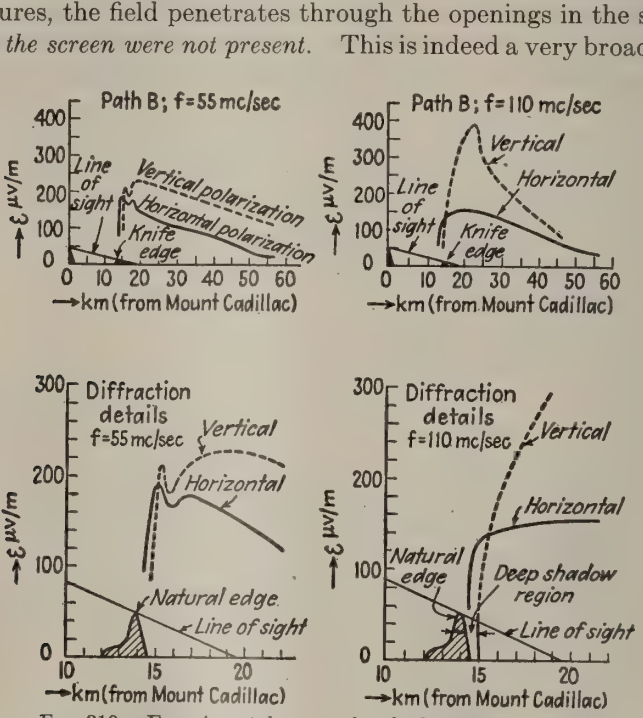

FIG. 319. Experimental curves for the layout of Fig. 317.

tion in the case of radio waves, where we have to meet the boundary conditions of two fields, the electric $\mathcal{E}$ and magnetic H fields. The theory, therefore, assumes that at the inner surface of the screen, the wave function $w = 0$ and $\partial w/\partial n = 0$. This means that we have a discontinuity over the contour of the aperture. This *conflicts* with Green's theorem, which applies only to continuous functions. The Huygens wavelet principle is expressed by the universal differential equation

$$\frac{\partial^2 w}{\partial t^2} = v^2\left(\frac{\partial^2 w}{\partial x^2} + \frac{\partial^2 w}{\partial y^2} + \frac{\partial^2 w}{\partial z^2}\right) \qquad \text{for Cartesian coordinates}$$

where v denotes the velocity of propagation, w is the wave disturbance at any instant t of a space point P of coordinates x, y, and z. The treatment is surely not electromagnetic since it is irrespective of such field associations as $\mathcal{E}$ and H. We need a solution that is more rigorous.

The Kirchhoff solution is then based on the condition of Fig. 320, where T denotes the primary radiation center of the wave disturbance, which is at any instant

$$w = \frac{w}{r_1} \cos\left[\omega\left(t - \frac{r_1}{v}\right)\right]$$

where W is the amplitude at unit distance from T. If P_0 is a field point within an arbitrary closed surface S, which *excludes* the source T, we have, for the differentiations $\partial/\partial r$ and $\partial/\partial n$ along r and the normal n, by means of Green's theorem, at field point P_0,

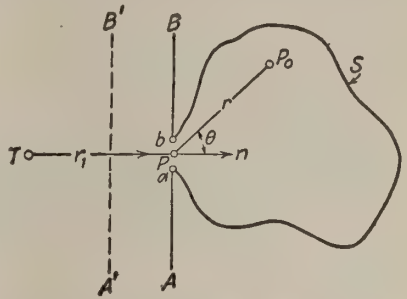

FIG. 320. The diffracted beam PP_0 due to an incident primary beam TP.

$$\left.\begin{aligned} w_0 &= \frac{1}{4\pi}\int\int \left\{ \frac{\partial\left[\dfrac{w\left(t - \dfrac{r}{v}\right)}{r}\right]}{\partial r} \cos(nr) - \frac{1}{r}\frac{\partial\left[w\left(t - \dfrac{r}{v}\right)\right]}{\partial n} \right\} dS \\ &= \frac{W}{2\lambda}\int\int \frac{1}{rr_1} \sin\left[\omega\left(t - \frac{r + r_1}{v}\right)\right] [\cos(nr) - \cos(nr_1)]\, dS \\ w_0 &= W\int\int \frac{K}{rr_1} \cos\left[\omega\left(t - \frac{r + r_1}{v}\right)\right]; \qquad \lambda = \frac{v}{f} \\ K &= \frac{1}{2\lambda}[\cos(nr) - \cos(nr_1)] \end{aligned}\right\} \quad (896)$$

The quantity K denotes the *inclination* factor. If a diffracting screen $A'B'$ is located as in Fig. 320, the wave disturbance at any point of the closed surface S will no longer be known. But if a screen AB forms part of the closed surface, with an opening ab, we need only to integrate over that portion of S which coincides with the aperture ab, because for the rest of the surface, the integral becomes zero. Assuming the dimensions of the aperture ab small compared with r and r_1, the cosines of (896) are essentially constant over the opening ab, and we have

$$w_0 = \frac{W}{2\lambda r r_1}[\cos(nr) - \cos(nr_1)] \int\int_S \sin\left[\omega\left(t - \frac{r + r_1}{v}\right)\right] dS \quad (896a)$$

To find dw_0, due to a wave-front element, we use an element dS normal

to rr_1 and have $\cos(nr_1) = 1$. Since $\cos(rn) = \cos\theta$, we find

$$dw_0 = \underbrace{A(1 + \cos\theta)}_{\text{forward factor}} \sin\left[\omega\left(t - \frac{r + r_1}{v}\right)\right] dS; \qquad A = \frac{W}{2\lambda r r_1} \tag{896b}$$

Therefore, each small portion of the primary wave front acts as a secondary source emitting a Huygens wavelet with amplitude A, which is proportional to $(1 + \cos\theta)$. The maximum amplitude is then $A_m = 2A$ for $\theta = 0$. Along the direction of the primary wave and for any angle θ, we have

$$\rho = \frac{A}{A_m} = 0.5(1 + \cos\theta) = \cos^2\left(\frac{\theta}{2}\right) \tag{896c}$$

proving that *no straight backward radiation is possible* (Fig. 321). Later on, we shall find that *electromagnetically*, the radiation intensity of a Huygens source is $k(1 + \cos\theta)^2$, if $k = z_0/8\lambda^2$ and $z_0 = \sqrt{\mu/\kappa} \cong 376.7$ ohms for air as a wave medium. Such a source is then due to an association of an *electric* current element of moment 1 m · amp and of a *magnetic* current element of moment 1 m · volt. These moments act at right angles to each other. The result of (896c) is then an improvement over the original Huygens principle, since the Huygens wavelet concept fails to explain why radiation does *not* proceed straight backward through an aperture. The Kirchhoff theory gives, therefore, a means of computing the inclination factor K of (896) when a diffracting screen is used between the primary source and the pickup center. The neglect of electromagnetic effects due to the material of the obstructing medium is, no doubt, a great objection to the Kirchhoff theory and Voigt's simplified Kirchhoff theory. In optics, such assumptions as w and $\partial w/\partial n$ both zero, at all points of the screen that faces the primary source, seem to be justified, since the wavelengths of light with respect to the largest dimension of the aperture in a screen are always exceedingly small and essentially the entire wave energy arriving at an aperture passes through the aperture unperturbed. This is not the case even for the shortest commercial electromagnetic waves, besides the fact that we have to consider the type of polarization.

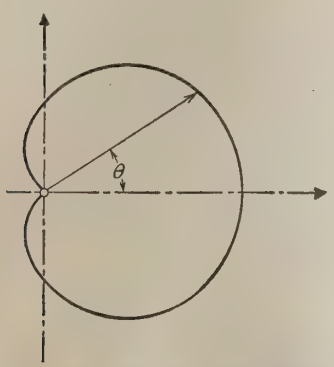

FIG. 321. The Huygens-Kirchhoff forward effect. *Only* in the straight backward direction is there zero effect.

204. Notes on the Sommerfeld Diffraction Theory. A. Sommerfeld[1] has rigorously solved the case of diffraction of waves by a straight edge, using a contour integral representation. P. M. Morse and P. Rubenstein applied a similar solution for diffraction through a slit or by a ribbon by separating the wave equation into elliptic cylinder coordinates. The values of the resulting Mathieu function solutions are then computed as originally suggested by Sieger. The original theory by Sommerfeld also applies to the case where the angle of diffraction is *large, i.e.,* when the reception center lies in the deep geometrical shadow region. In the Sommerfeld theory, Maxwell's equations are taken into account. The diffracting screen is assumed infinitely conducting, having either an ideal wedge form of a given angle or a perfect metal reflector that is infinitely thin. We then deal with ideal cases of a single straight edge, with the radiation source at infinity, for the case when the electric vector is either parallel or perpendicular to the diffracting edge. The case of the single-slit opening is treated by K. Schwarzschild. In the Sommerfeld theory, we have

$$\frac{1}{v^2}\frac{\partial^2 w}{\partial t^2} = \left(\frac{\partial^2 w}{\partial x^2} + \frac{\partial^2 w}{\partial y^2} + \frac{\partial^2 w}{\partial z^2}\right) \qquad \text{the universal wave equation}$$

which must satisfy certain boundary conditions of the diffracting screen. For simplicity's sake, let us assume that the wave disturbance w *cannot* depend on the Z coordinate, so that the above expression simplifies to

$$\frac{\partial^2 w}{\partial t^2} = v^2\left(\frac{\partial^2 w}{\partial x^2} + \frac{\partial^2 w}{\partial y^2}\right) \tag{897}$$

This happens to be the case when the radiating source is infinitely long and parallel with the Z axis, which axis also forms the sharp edge of the ideally reflecting screen (perfect conductors). The X axis is then the positive side of the screen and in the plane of the screen. The boundary condition for such a screen is then $w = 0$ if the arriving electromagnetic wave is polarized in a plane perpendicular to the edge of the screen. We then have $\mathcal{E}$ in place of w oscillating parallel with the edge of the screen. The boundary condition can also be such that $\partial w/\partial y = 0$. This means that the arriving primary wave front is polarized parallel to the edge of the screen. In this case, the magnetic H vector oscillates

[1] SOMMERFELD, A., *Math. Ann.*, **47,** 317 (1896). RIEMANN-WEBER, *Diff. Gl. Phys.*, **2,** 433 (1927) (by Sommerfeld). GEIGER and SCHEEL, *Handb. Phys.*, **20,** 266. Consult also SOMMERFELD, *Zeit. fur Math. Phys.*, **46,** 11 (1911). SCHWARZSCHILD, *Math. Ann.*, **55,** 177 (1902). MORSE, P. M., and PEARL J. RUBENSTEIN, *Phys. Rev.*, **54,** 895 (1938). SIEGER, *Ann. Physik*, **27,** 626 (1908). SCHWARZSCHILD, K., *Math. Ann.*, **55,** 177 (1902).

parallel with the edge. Both field associations $\mathcal{E}$ and H are now taken into account, and the boundary conditions must satisfy the surface of the screen. This means that at points $x > 0$ and $y = 0$.

For polar coordinates $x = r \cos \varphi$ and $y = r \sin \varphi$, we then find the corresponding differential equation

$$\frac{\partial^2 w}{\partial t^2} = v^2 \left(\frac{\partial^2 w}{\partial r^2} + \frac{1}{r} \frac{\partial w}{\partial r} + \frac{1}{r^2} \frac{\partial^2 w}{\partial \varphi^2} \right) . \qquad (897a)$$

where, according to whether $w = 0$ or $\partial w/\partial y = 0$ boundary conditions, we deal with either $\mathcal{E}$ or H values, instead of w. If the radiator is at infinity and the incident beam makes an angle ψ with the X axis, we find for

$$a = \beta r \cos (\varphi - \psi); \qquad b = \beta r \cos (\varphi + \psi); \qquad \beta = \frac{2\pi}{\lambda}$$

$$d = \sqrt{\frac{8r}{\lambda}} \sin \left[\frac{1}{2} (\varphi - \psi) \right]; \qquad e = - \sqrt{\frac{8r}{\lambda}} \sin \left[\frac{1}{2} (\varphi + \psi) \right]$$

the wave function w as

$$\left.\begin{aligned} w &= \tfrac{1}{2}(1 + j) W_1 \epsilon^{j\omega t} \left(\epsilon^{-ja} \int_{-\infty}^{d} \epsilon^{-j\frac{\pi s^2}{2}} ds - \epsilon^{-jb} \int_{-\infty}^{e} \epsilon^{-j\frac{\pi s^2}{2}} ds \right) \\ &\qquad\qquad \text{for } w = 0 \\ w &= \tfrac{1}{2}(1 + j) W_1 \epsilon^{j\omega t} \left(\epsilon^{-ja} \int_{-\infty}^{d} \epsilon^{-j\frac{\pi s^2}{2}} ds + \epsilon^{-jb} \int_{-\infty}^{e} \epsilon^{-j\frac{\pi s^2}{2}} ds \right) \\ &\qquad\qquad \text{for } \frac{\partial w}{\partial y} = 0 \end{aligned}\right\} \qquad (897b)$$

Inasmuch as w is complex, we can write

$$w = \overbrace{(W_1 + jW_2)\epsilon^{j\omega t}}^{\text{real part}} = (W_1 + jW_2) \cos \omega t + j(W_1 + jW_2) \sin \omega t$$

$$= W_1 \cos \omega t - W_2 \sin \omega t + j(W_2 \cos \omega t + W_1 \sin \omega t)$$

It is *only* the *real part* that *counts*, giving a resultant amplitude $\sqrt{W_1^2 + W_2^2}$ and a corresponding power coefficient $W_1^2 + W_2^2$. This is obvious from (897*b*), since

$$\int \epsilon^{j0.5\pi s^2} ds = \int \cos (0.5\pi s^2)\, ds + j \int \sin (0.5\pi s^2)\, ds$$
$$= \text{one Fresnel integral} + j(\text{other Fresnel integral}) \qquad (898)$$

The Cornu spiral method can, therefore, be applied to find the amplitude factor $\sqrt{x^2 + y^2}$ and the factor $x^2 + y^2$ to which the power is proportional.

205. Proof That Eq. (897a) Satisfies Maxwell's Theory. The derivations of (897*a*) and (897*b*) as well as of the simplified expression (897) are based on the orientation of Fig. 322. The perfectly conducting screen is in the ZX plane of Fig. 322*a*, and the boundary condition requires that $\mathcal{E}_x = 0 = \mathcal{E}_z$ at $y = 0$ and $x > 0$, since the tangential electric field along a perfect conductor (screen) must vanish. When the arriving wave is polarized with its $\mathcal{E}$ vector parallel with the edge (parallel with

the Z axis), we have no $\mathcal{E}_x$ and $\mathcal{E}_y$ components of the electric field. For plane electromagnetic waves, we have $H_z = 0$, since the associated magnetic vector must be normal to the Z edge. However, when the arriving plane wave is polarized perpendicular to the Z straight edge, we have $\mathcal{E}_z = H_x = H_y = 0$. For either case, we then have conditions as brought out in Table 69. The final result of this table shows that Maxwell's equations with the correct boundary conditions for respective selected $\mathcal{E}$ polarizations, relative to the Z edge of the perfectly conducting screen, satisfy the general wave equation (897a). In Eq. (VII) of this table, we must satisfy the respective boundary conditions $w = 0$ or $\partial w/\partial\varphi = 0$ at the surface of the screen. This *caused Sommerfeld to assume a mathematical space* containing a virtual image source. The trace of the actual radiator in the XY plane is then a point T for which the linear radiator is at first assumed in finite location and a symmetrical parallel image radiator with respect to the X axis. The *diffracting edge is* then *assumed as a line in a Riemann space.* If we limit ourselves to the XY plane only, we deal with a double-leaf Riemann surface, with branch points zero and infinity, using the positive X axis as a separation line. This gives, for the actual radiator at infinity, the solution (VII) of Table 69 as $w(r, \varphi, \psi) = \exp[j\beta r \cos(\varphi - \psi)]$. This is the procedure employed in the classic Sommerfeldian theory, leading to the result expressed in (897b).

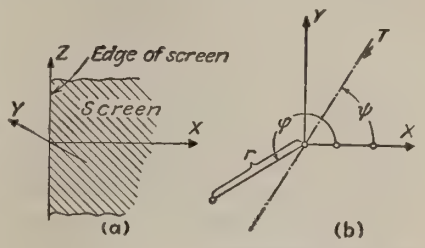

ψ is the polar angle of wave normal of range $\pi > \psi > 0$ if the incident wave arrives in the upper half plane.

FIG. 322. For the proof that the general wave equation can be made to satisfy Maxwell's equations.

206. Cornu Spiral for the Case of Diffraction of Electromagnetic Waves around the Earth Surface. As early as 1918, G. N. Watson[1]

[1] WATSON, G. N., The Diffraction of Electric Waves by the Earth, *Proc. Roy. Soc.* (*London*), *A*, **95,** 83–89, October, 1918; 546–563, July, 1919. LOVE, A. E. H., *Phil. Trans. Roy. Soc.*, **225,** *A*, 105–131 (1915). EPSTEIN, P. S., *Nat. Acad. Sci., U.S.* **21,** 62 (1930). VAN DER POL, B., and H. BREMMER, The Diffraction of Electromagnetic Waves from an Electric Point Source round a Finitely Conducting Sphere, with Applications to Radiotelegraphy and the Theory of the Rainbow, *Phil. Mag.*, Ser. **7,** **24,** 141–175, July, 1937; 825–864, November supplement, 1937; **27,** 261–275, March, 1939. WWEDENSKY, B., The Diffraction Propagation of Radio Waves, *Tech. Phys.* (*USSR*), **2,** (6) 624–639 (1935); **3** (11) 915–925 (1936); **4** (8) 579–591 (1937). ECKERSLEY, T. L., and G. MILLINGTON, Application of the Phase Integral Method to the Analysis of the Diffraction and Refraction of Wireless Waves round the Earth, *Phil. Trans. Roy. Soc* (*London*), **237,** 273–209, June, 1938. ECKERSLEY, T. L., Ultra-short-

started the present diffraction theory around spherical earth. Watson's original paper assumed an infinite conductivity. Van der Pol and Bremmer, who gave about the most rigorous solution, treat the cases of perfectly conducting spherical earth and strongly absorbing (dielectric) earth. For the first case, $\sigma = \infty$ mhos per meter; and for the second case, the relative equivalent dielectric constant $\kappa_e' = \kappa_r - j1.8 \times 10^4(\sigma/f)$ of the earth crust, with f in megacycles per second, is taken into account. The value is taken large, which happens for long radio waves over ocean surface. C. R. Burrows and M. C. Gray give curves for any values of κ_e' for which the expression

$$\mathcal{E} = 2\mathcal{E}_0 A_1 F_s G_1 G_2 \qquad \text{volts/m} \tag{899}$$

is employed. The quantity $\mathcal{E}_0$ denotes the free-space field in volts per meter, *i.e.*, $2\mathcal{E}_0$ field for vertical polarization over perfect ground, $\sigma = \infty$; A_1 is the plane earth attenuation factor; F_s the shadow factor; and G_1 and G_2 are height factors. If both antennas are on ground, we have $G_1 = 1 = G_2$.

The rigorous solution for a given frequency is based on Maxwell's equations satisfying the boundary conditions at the surface of the earth. The solution leads to an *infinite* series of spherical harmonics with coefficients, containing 12 Bessel functions. For microscopic and submicroscopic spheres (particles), the series converges rapidly, so that a few terms yield a good approximation.

It is the dimension of the obstacle to wave propagation *with respect to* the *wavelength* that counts in electromagnetic diffraction. For a radius R of the sphere, the ratio $6.28R/\lambda$ *determines* the *number of terms.* For electromagnetic waves, we have then ratios anywhere from 10^3 to 10^8, with a corresponding *slow* convergence of the series. As far back as 1915, A. E. H. Love found a solution of the series for a ratio $6.28R/\lambda = 8{,}000$, while the Watson solution transforms the series at first by contour integration into a more rapidly converging series. T. L. Eckersley used the phase integral method while P. S. Epstein applied Huygens' principle in order to simplify the solution. It is the work of Van der Pol and Bremmer that extended the Watson treatment *beyond the optical horizon, i.e.*, into the geometrical shadow region, leading to the shadow factor.

---

wave Refraction and Diffraction, *Jour. IEE (London)*, **80,** 286–304, March, 1937. MILLINGTON, G., The Diffraction of Wireless Waves round the Earth, *Phil. Mag.*, Ser. 7, **27,** 517–542, May, 1939. GRAY, M. C., The Diffraction and Refraction of a Horizontally Polarized Electromagnetic Wave over Spherical Earth, *Phil. Mag.*, Ser. 7, **27,** 421–436, April, 1939. BURROWS, C. R., and M. C. GRAY, The Effect of the Earth's Curvature on Ground Wave Propagation, *Proc. IRE*, **29,** 16–24, January, 1941.

TABLE 69. PROOF THAT (897a) SATISFIES THE BOUNDARY CONDITIONS

General electromagnetic field relations	Electric vector of arriving wave vibrates parallel with Z edge of a perfectly conducting screen ($\mathcal{E}_x = \mathcal{E}_y = H_z = 0$)	Electric vector is normal to Z edge $\mathcal{E}_z = H_x = H_y = 0$
$\frac{\partial \mathcal{E}_z}{\partial y} - \frac{\partial \mathcal{E}_y}{\partial z} = -j\omega\mu H_x$	$\frac{\partial \mathcal{E}_z}{\partial y} = -j\omega\mu H_x$ (I)	$-\frac{\partial \mathcal{E}_y}{\partial z} = 0$
$\frac{\partial \mathcal{E}_x}{\partial z} - \frac{\partial \mathcal{E}_z}{\partial x} = -j\omega\mu H_y$	$\frac{\partial \mathcal{E}_z}{\partial x} = j\omega\mu H_y$ (II)	$\frac{\partial \mathcal{E}_x}{\partial z} = 0$
$\frac{d\mathcal{E}_y}{\partial x} - \frac{\partial \mathcal{E}_x}{\partial y} = -j\omega\mu H_z$	$0 = 0$	$\frac{\partial \mathcal{E}_y}{\partial x} - \frac{\partial \mathcal{E}_x}{\partial y} = -j\omega\mu H_z$ (III)
$\frac{\partial H_z}{\partial y} - \frac{\partial H_y}{\partial z} = (\sigma + j\omega\kappa)\mathcal{E}_x$	$-\frac{\partial H_y}{\partial z} = 0$	$\frac{\partial H_z}{\partial y} = (\sigma + j\omega\kappa)\mathcal{E}_x$ (IV)
$\frac{\partial H_x}{\partial z} - \frac{\partial H_z}{\partial x} = (\sigma + j\omega\kappa)\mathcal{E}_y$	$\frac{\partial H_x}{\partial z} = 0$	$-\frac{\partial H_z}{\partial x} = (\sigma + j\omega\kappa)\mathcal{E}_y$ (V)
$\frac{\partial H_y}{\partial x} - \frac{\partial H_x}{\partial y} = (\sigma + j\omega\kappa)\mathcal{E}_z$	$\frac{\partial H_y}{\partial x} - \frac{\partial H_x}{\partial y} = (\sigma + j\omega\kappa)\mathcal{E}_z$ (VI)	$0 = 0$
For $\sigma = 0$, $\mu = \mu_0$, and $\kappa = \kappa_0$	From (I), we find $H_x = -\frac{1}{j\omega\mu_0}\frac{\partial \mathcal{E}_z}{\partial y}$ and $\frac{\partial H_x}{\partial y} = -\frac{1}{j\omega\mu_0}\frac{\partial^2 \mathcal{E}_z}{\partial y^2}$ (Ia) From (II), we find $H_y = \frac{1}{j\omega\mu_0}\frac{\partial \mathcal{E}_z}{\partial x}$ and $\frac{\partial H_y}{\partial x} = \frac{1}{j\omega\mu_0}\frac{\partial^2 \mathcal{E}_z}{\partial x^2}$ (IIb) Substituting the values $\partial H_x/\partial y$ and $\partial H_y/\partial x$ of (Ia) and (IIb) in (VI) yields, after multiplying by $j\omega\mu_0$, $\frac{\partial^2 \mathcal{E}_z}{\partial x^2} + \frac{\partial^2 \mathcal{E}_z}{\partial y^2} = -\omega\mu_0\kappa_0\mathcal{E}_z$ or $\frac{\partial^2 \mathcal{E}_z}{\partial x^2} + \frac{\partial^2 \mathcal{E}_z}{\partial y^2} + \beta^2\mathcal{E}_z = 0$ (VIa)	From (IV), we find $\mathcal{E}_x = \frac{1}{j\omega\kappa_0}\frac{\partial H_z}{\partial y}$ and $\frac{\partial \mathcal{E}_x}{\partial y} = \frac{1}{j\omega\kappa_0}\frac{\partial^2 H_z}{\partial y^2}$ (IVc) From (V), we find $\mathcal{E}_y = -\frac{1}{j\omega\kappa_0}\frac{\partial H_z}{\partial x}$ and $\frac{\partial \mathcal{E}_y}{\partial x} = \frac{1}{j\omega\kappa_0}\frac{\partial^2 H_z}{\partial x^2}$ (Vb) Substituting the values $\partial \mathcal{E}_x/\partial y$ and $\partial \mathcal{E}_y/\partial x$ of (IVa) and (V_b) in (III) yields, after multiplying by $-j\omega\kappa_0$, $\frac{\partial^2 H_z}{\partial x^2} + \frac{\partial^2 H_z}{\partial y^2} = -\omega^2\mu_0\kappa_0 H_z$ or $\frac{\partial^2 H_z}{\partial x^2} + \frac{\partial^2 H_z}{\partial y^2} + \beta^2 H_z = 0$ (IIIa)

TABLE 69. PROOF THAT (897*a*) SATISFIES THE BOUNDARY CONDITIONS.—(*Continued*)

General electromagnetic field relations	Electric vector of arriving wave vibrates parallel with Z edge of a perfectly conducting screen ($\mathcal{E}_x = \mathcal{E}_y = H_z = 0$)	Electric vector is normal to Z edge $\mathcal{E}_z = H_x = H_y = 0$
	The boundary condition $\mathcal{E}_z = 0$ at the surface of the screen together with (VI*a*) gives $\mathcal{E}_z$, and H_x and H_y can be found from (I) and (II)	The boundary condition $\mathcal{E}_x = 0$ gives $\partial H_z/\partial y = 0$ for $y = 0$ and $x > 0$. It is necessary only to integrate (III*a*) with the boundary condition $\partial H_z/\partial y = 0$ and $\mathcal{E}_x$ and $\mathcal{E}_y$ can be found from (IV) and (V) for $\sigma = 0$ and $\kappa = \kappa_0$

Using the polar coordinates $x = r \cos \varphi$ and $y = r \sin \varphi$ in the XY plane of Fig. 322, either $\mathcal{E}$ polarization relative to the straight edge Z yields the same differential equation

$$\frac{\partial^2 w}{\partial r^2} + \frac{1}{r}\frac{\partial w}{\partial r} + \frac{1}{r^2}\frac{\partial^2 w}{\partial \varphi^2} + \beta^2 w = 0 \qquad \text{(VII)}$$

which corresponds to (897*a*), since $\partial w/\partial t = j\omega w$ and $\partial^2 w/\partial t^2 = -\omega^2 w$

The solution of (VII) is for the respective boundary conditions for $\varphi = 0$ and $\varphi = 2\pi$	Boundary condition $w = 0$	Boundary condition $\frac{\partial w}{\partial \varphi} = 0$

Remarks: For medium constants μ henrys/m, κ farads/m, σ mhos/m.

For air $\sigma = 0$, $\kappa \cong \kappa_0 = 8.854 \times 10^{-12}$ farad/m, $\mu = \mu_0 = 1.257 \times 10^{-6}$ henry/m, $v = 1/\sqrt{\mu\kappa} = 1/\sqrt{\mu_0\kappa_0} = 2.998 \times 10^8$ m/sec $= c \cong 3 \times 10^8$ m/sec, $\mathcal{E}$ is in volts/m, H in amp/m. $\beta = 2\pi/\lambda = \omega/c = \omega\sqrt{\mu_0\kappa_0}$. Orientation as in Fig. 322.

They also find that at about 43 Mc/sec, the attenuation of electromagnetic waves due to the finite conductivity considerably outweighs the attenuation due to round-the-earth diffraction.

With respect to the most complete solutions, due to Van der Pol and Bremmer, we obtain transmission conditions over actual spherical earth, as is shown in Fig. 323, where $\prod$ denotes the *total Hertz vector* $\prod = \prod_p + \prod_s$, if $\prod_p$ is the Hertz vector in the absence of the diffracting earth and due only to the actual primary radiation from a radiation center T, which is 100 m above ground, with the receiving pickup center next to the ground. The vector $\prod_s$ is due to secondary radiation, which comes from the spherical earth surface. The theory of this is dealt with on

page 336. The ratio $\prod/\prod_p$ is, therefore, a measure for the effect of the earth's presence, since it expresses whether the spherical reradiator causes reinforcement or partial field cancellation. In Fig. 323, the range from the primary radiation center T to a reception center P is always with P next to the ground, and TG represents the geometrical line of sight or the horizon. The curves are for a frequency range from about 43 to about 43,000 Mc/sec. The curves show that diffractions

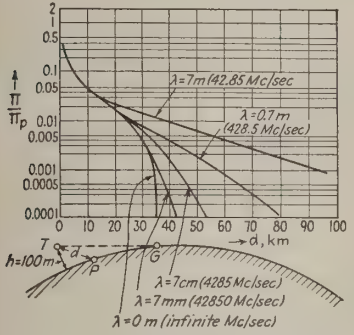

Fig. 323. Transmission conditions over spherical earth crust based on diffraction. Electromagnetic ground properties are $\sigma_2 = 10^{-2}$ mho/m; $\kappa_2 = 3.542 \times 10^{-11}$ farad/m; $\mu_2 = 1.57 \times 10^{-6}$ henry/m. $h_T = 100$ m; $h_R = 0$ m. T is radiation center; R is receiving center such as point P. Π is total Hertz vector $= \Pi_p + \Pi_s$. The vector Π_p is Hertz vector in absence of the diffracting earth surface. Π_s Hertz vector due to secondary radiation from the spherical surface of the earth.

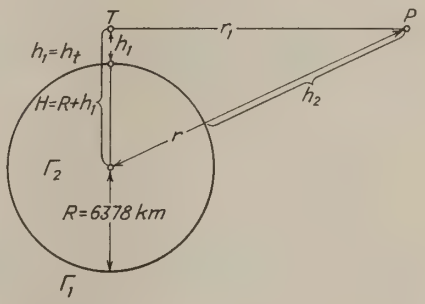

Fig. 324. Space point P at any desired height h_2 above ground. Γ_1 and Γ_2 are the propagation constants in the atmosphere outside the spherical earth surface and below the spherical earth surface, respectively. (Note the respective heights h_1 for the radiation center T and h_2 for the reception center P are shown far out of proportion with respect to the earth radius R.)

greatly favor the lower region of carrier frequencies. Theoretically, there can be no diffraction at an infinite frequency, for which reason the corresponding fictitious propagation curve defines the location of the horizon, *i.e.*, the start of the geometric shadow region. The general theory with Hertzian vector contributions due to primary and secondary radiation is given on pages 258, 273, 338, so we can restrict ourselves here to essential Van der Pol relations, which have a bearing on their theoretical curves. Figure 324 gives the space point P for the reception center at any desired height h_2 above the ground, and h_1 is the altitude of the actual radiation center T with respect to ground level. The distance from radiation center T to the center of the earth is H.

We have then σ_2, κ_2, and μ_2 for the electromagnetic properties, in mhos per meter, farads per meter, and henrys per meter, of the earth crust. For the atmosphere

above the earth surface, we have essentially $\kappa_1 \cong \kappa_0 = 8.854 \times 10^{-12}$ farad/m and $\mu_1 = \mu_0 = 1.257 \times 10^{-6}$ henry/m with $\sigma_1 = 0$ mhos/m. We can also take for average earth $\mu_1 = \mu_0$, since we generally do not deal with ferromagnetic earth crust. The atmosphere *excludes* the ionosphere here, which can hardly play a part at UHF's. The total Hertz vector $\prod$ in space leads to the series

$$\left.\begin{aligned}
\prod = \prod_p + \prod_s &= \frac{\epsilon^{jr_1\Gamma_1}}{jr_1\Gamma_1} \sum_{q=0}^{q=\infty} (2q+1) R_q \frac{\psi_q(R\Gamma_1)}{\zeta_q^{(1)}(R\Gamma_1)} \\
&\qquad \times \zeta_q^{(1)}(H\Gamma_1)\zeta_q^{(1)}(r\Gamma_1) P_q(\cos\theta) \qquad \text{for } r > R \\
\prod = \prod_p + \prod_s &= \frac{\Gamma_1^2}{\Gamma_2^2} \sum_{q=0}^{q=\infty} (2q+1)(1+R_q) \frac{\psi_q(R\Gamma_1)}{\psi_q(R\Gamma_2)} \\
&\qquad \times \zeta^{(1)}(H\Gamma_1)\psi_q(r\Gamma_2) P_q(\cos\theta) \qquad \text{for } r < R \\
\Gamma = j\omega\sqrt{\mu\kappa_e}; \qquad \kappa_e &= \kappa - \frac{\sigma}{\omega} \qquad \text{farads/m}
\end{aligned}\right\} \tag{899a}$$

where $\omega/6.28$ is in cycles per second. If x stands for the respective arguments, such as $R\Gamma_1$, $r\Gamma_1$, $R\Gamma_2$, . . . , and J and H for the Bessel and Hankel symbols, respectively, we find

$$\left.\begin{aligned}
\zeta_q^{(1)}(x) &= \sqrt{\frac{0.5\pi}{x}}\, H^{(1)}_{q+\frac{1}{2}}(x) = x^q \left(-\frac{1}{x}\frac{d}{dx}\right)^q \left(\frac{\epsilon^{jx}}{jx}\right) \\
\zeta_q^{(2)}(x) &= \sqrt{\frac{0.5\pi}{x}}\, H^{(2)}_{q+\frac{1}{2}}(x) = x^q \left(-\frac{1}{x}\frac{d}{dx}\right)^q \left(j\frac{\epsilon^{-jx}}{x}\right) \\
\log &= \log_\epsilon \\
\psi_q(x) &= \frac{1}{2}[\zeta_q^{(1)}(x) - \zeta_q^{(2)}(x)] = \sqrt{\frac{0.5\pi}{x}}\, J_{q+\frac{1}{2}}(x) = x^q \left(-\frac{1}{x}\frac{d}{dx}\right)^q \left(\frac{\sin x}{x}\right) \\
R_q &= \frac{-\frac{1}{x}\left\{\frac{d}{dx}\log[x\psi_q(x)]\right\}_{x=R\Gamma_1} + \left\{\frac{1}{x}\frac{d}{dx}\log[x\psi_q(x)]\right\}_{x=R\Gamma_2}}{\left\{\frac{1}{x}\frac{d}{dx}\log[x\zeta_q^{(1)}(x)]\right\}_{x=R\Gamma_1} - \left\{\frac{1}{x}\frac{d}{dx}\log[x\psi_q(x)]\right\}_{x=R\Gamma_2}}
\end{aligned}\right\} \tag{899b}$$

At the radiation center, we have a singularity of form $(\epsilon^{jr_1\Gamma_1})/(jr_1\Gamma_1)$, and the primary field becomes

$$\left.\begin{aligned}
\frac{\epsilon^{jr_1\Gamma_1}}{jr_1\Gamma_1} &= \sum_{q=0}^{q=\infty} (2q+1)\zeta_q^{(1)}(r\Gamma_1)\psi_q(H\Gamma_1)P_q(\cos\theta) \qquad \text{for } r > H \\
\frac{\epsilon^{jr_1\Gamma_1}}{jr_1\Gamma_1} &= \sum_{0}^{\infty} (2q+1)\zeta_q^{(1)}(H\Gamma_1)\psi_q(r\Gamma_1)P_q(\cos\theta) \qquad \text{for } r < H
\end{aligned}\right\} \tag{899c}$$

If the first of Eqs. (899*a*) is written completely as a harmonic series, by substituting

the second of Eqs. (899c) in the upper expression of (889a) and using the Wronksian

$$\psi_q(x)\zeta_q^{(1)}(x) - \zeta_q^{(1)}(x)\psi_q^{(1)}(x) = \frac{j}{x^2}$$

We find the total Hertz vector

$$\prod = \frac{j}{(R\Gamma_1)^3} \sum_{q=0}^{q=\infty} (2q+1) \frac{\zeta_q^{(1)}(H\Gamma_1)}{\zeta_q^{(1)}(R\Gamma_1)} \frac{1}{N_q} P_q(\cos\theta) \tag{899d}$$

For the Neumann symbol N, we have

$$N_q(x, y) = \left\{ \frac{1}{x}\frac{d}{dx} \log [x\, \zeta_q^{(1)}(x)] \right\}_{x=R\Gamma_1} - \left\{ \frac{1}{y}\frac{d}{dy} \log [y\psi_q(y)] \right\}_{y=R\Gamma_2} \tag{899e}$$

Watson transforms (899d) into a continuous integral, leading to

$$\prod = \frac{1}{(R\Gamma_1)^3} \int_L \frac{q\, dq}{\cos(\pi q)} \frac{\zeta^{(1)}{}_{q-\frac{1}{2}}(H\Gamma_1)}{\zeta^{(1)}{}_{q-\frac{1}{2}}(R\Gamma_1)} \frac{1}{N_{q-\frac{1}{2}}} P_{q-\frac{1}{2}}[\cos(\pi-\theta)]$$
$$+ \frac{1}{(R\Gamma_1)^3} \int_0^{j\infty} \frac{q\, dq}{\cos(\pi q)} \frac{\zeta^{(1)}{}_{q-\frac{1}{2}}(H\Gamma_1)}{\zeta^{(1)}{}_{q-\frac{1}{2}}(R\Gamma_1)} \left(\frac{1}{N_{-\frac{1}{2}}} - \frac{1}{N_{-q-\frac{1}{2}}} \right) P_{q-\frac{1}{2}}[\cos(\pi-\theta)] \tag{899f}$$

For the absolute ratio $0.5\prod/\prod_p$, we find the radiated power P in kilowatts, and

$$\mathcal{E} = \frac{3\times 10^5 \sqrt{P}}{d} \left| \frac{\prod}{2\prod_p} \right| \quad \mu\text{v/m} \tag{899g}$$

If the height functions $f_s(h_1)$ and $f_s(h_2)$ for the transmitter and receiver are introduced, we find

$$\prod = \frac{4\pi j}{(R\Gamma_1)^3} \sum_{s=0}^{\infty} \frac{q_s \epsilon^{j\pi q_s}}{\left(\frac{\partial M_q - 0.5}{\partial q} \right)_{q=q_s}} f_s(h_1) f_s(h_2) P_{q_s-0.5}[\cos(\pi-\theta)] \tag{899h}$$

for

$$M_q = \left\{ \frac{1}{x}\frac{d}{dx} \log [x\zeta_q^{(1)}(x)] \right\}_{x=R\Gamma_1} - \left\{ \frac{1}{x}\frac{d}{dx} \log [x\zeta_q^{(2)}(x)] \right\}_{x=R\Gamma_2} = 0 \tag{899i}$$

The height factors are

$$f_s(h_1) = \frac{\zeta^{(1)}_{q_s-0.5}(H\Gamma_1)}{\zeta^{(1)}_{q_s-0.5}(R\Gamma_1)}; \qquad f_s(h_2) = \frac{\zeta^{(1)}_{q_s-0.5}(r\Gamma_1)}{\zeta^{(1)}_{q_s-0.5}(R\Gamma_1)} \tag{899j}$$

For $h_1 = h_2 = 0$ (both radiation and pickup centers next to ground), we have

$$\prod \cong 2 \frac{\epsilon^{j\theta R\Gamma_1}}{j\theta R\Gamma_1} \sqrt{2\pi j\chi} \sum_{s=0}^{\infty} f_s(h_1) f_s(h_2) \frac{\epsilon^{j\tau_s\chi}}{2\tau_s - \frac{1}{\delta^2}} \tag{899k}$$

where the details are given in Secs. 58, 59. The quantity δ is

$$\delta = \frac{j(\Gamma_2/\Gamma_1)^2}{\sqrt[3]{R\Gamma_1}\sqrt{(\Gamma_2/\Gamma_1)^2 - 1}} \tag{899l}$$

with a final solution

$$\prod \cong \underbrace{\frac{\epsilon^{jd\Gamma_1}}{jd\Gamma_1}}_{\text{incident}} + \underbrace{D\,\rho\,\frac{\epsilon^{j(R_1+R_2)\Gamma_2}}{j(R_1+R_2)\Gamma_1}}_{\text{reflected}} \tag{899m}$$

where d is the distance or range as shown in Fig. 323 and $R_1 + R_2$ is the indirect path. The quantity D is the divergence factor due to spherical earth, and ρ denotes the *spherical* reflection coefficient. Relation

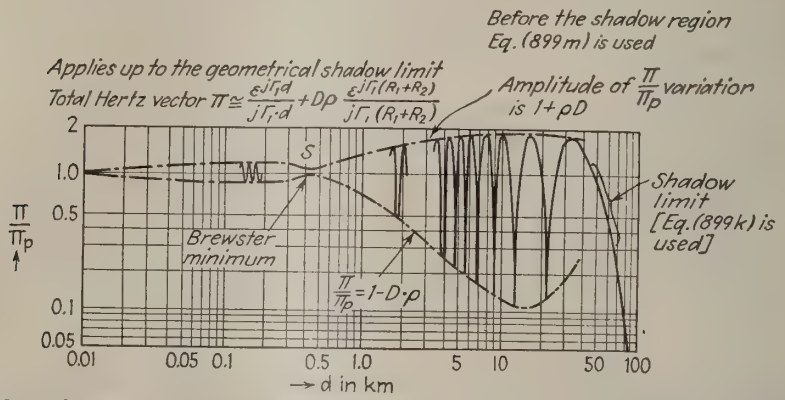

FIG. 325. Value of the ratio Π/Π_p for above given conditions. D is divergence factor; ρ is spherical reflection coefficient. Close to the radiator $\Pi/\Pi_p \cong 1$. Radiation and reception centers are 100 m above the spherical earth; $f = 428.5$ Mc/sec; $\sigma_2 = 10^{-2}$ mho/m; $\kappa_2 = 3.542 \times 10^{-11}$ farad/m; $\mu_2 = 1.257 \times 10^{-6}$ henry/m.

(899m) applies to distances d before the geometric shadow limit is reached. Figure 325 shows what takes place when the ratio $\prod/\prod_p$ is plotted for various ranges d in kilometers, for the condition that both the radiation center and the pickup center are 100 m above the ground ($h_1 = h_2 =$ 100 m) and the frequency is 428.5 Mc/sec (corresponding to a 70-cm free-space wavelength). For distances close to the radiation center, the ratio $\prod/\prod_p$ is almost unity, since $\prod_p$ outweighs any secondary radiation effects. Up to the geometrical shadow limit, we have alternate maxima and minima effects. A position S is also in the line-of-sight region, for which the amplitude curve shrinks to a minimum. This condition is due to the *Brewster dip*, since at this location, the incident ground wave would be perfectly matched with the electromagnetic medium of the ground, a perfect dielectric ($\sigma_2 = 0$), and all the arriving wave energy

would pass into the ground and stay there. Figure 326 gives the different field fluctuations in the line-of-sight region (also for the case $h_1 = h_2 =$ 100 m) and for 42.85-, 428.5-, 4,285-, and 42,850-Mc/sec excitations. Figure 326*a* shows again that diffraction into the geometric shadow region is all the more pronounced for lower ultrahigh frequency. Figure 326*b* gives the corresponding Cornu spiral for the 42.85-Mc excitation. If

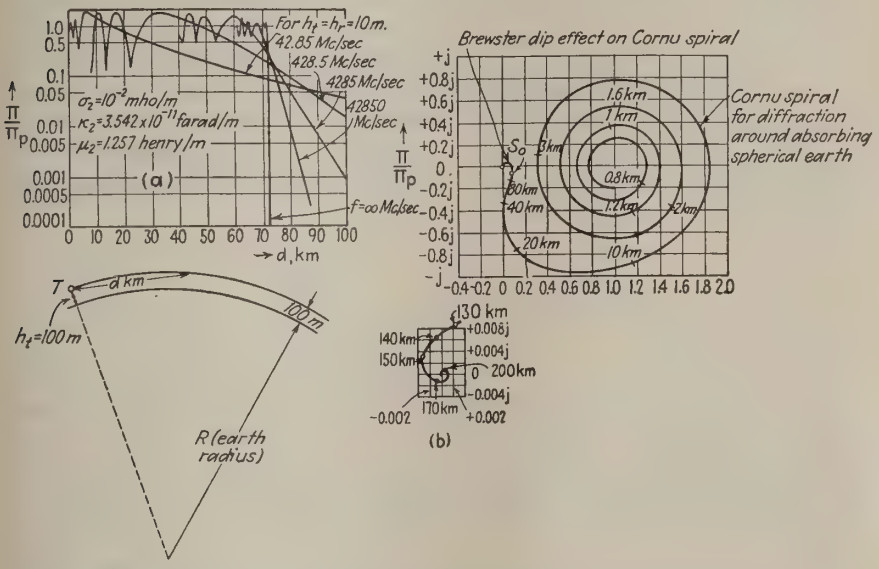

FIG. 326. Cornu spiral and Π/Π_p curves for diffraction of actual spherical earth condition. 2, 3, 10 km are the distances between the radiation center and the receiving center. Vector from origin O to any point of the spiral gives the amplitude as well as the phase (ratio of actual Hertz vector Π to vector Π_p in absence of the diffracting earth surface).

we follow the spiral from the center $1 + jO$, corresponding to a pickup reception center near the transmitter, it first spirals out and shrinks again to a minimum, owing to the Brewster dip. There is an inflection at S_0, where the geometrical shadow limit is reached. Then the spiral bends around with inverse rotation to approach the origin O along a spiral path. The linear connection of any point of the spiral to the origin O (the cross point of the real and the imaginary axes) gives the field amplitude corresponding to the indicated ranges d in kilometers. Before the horizon, the curve approaches asymptotically the limiting value $f \to \infty$, and the ground conduction current is negligible compared with the displacement current, so that $\Gamma_2 \to -\omega^2\mu\kappa$, and

$$\frac{\Pi}{\Pi_p} = \frac{2\kappa_r \cos\theta_1}{\kappa_r \cos\theta_1 + \sqrt{\kappa_r - \sin^2\theta_1}}$$

where θ_1 is the angle of wave incidence of the primary direct wave with respect to the normal to the ground.

207. The Burrows-Gray Diffraction Formula and Curves. The previous section shows that the ratio $6.28R/\lambda$ expresses to what extent we can expect diffraction around spherical earth. The quantity R is then the radius of the earth. Figure 327 shows the radiation center T and the pickup center P drawn for the equivalent earth radius $R_e = kR$. If the relative altitudes of T and P, with respect to the earth surface, are large compared with the deviations of the earth surface from a plane, we have the resultant field at P

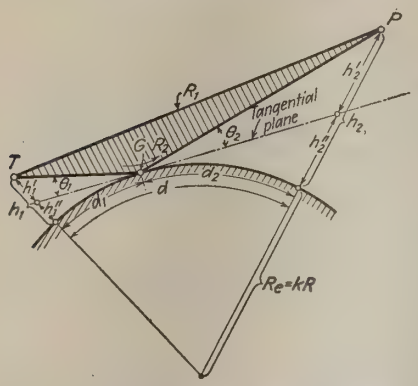

FIG. 327. Path triangle due to direct path R_1 and indirect path R_2. R is actual radius of the earth. Heights h_1 and h_2 are greatly exaggerated with respect to radius R_e. All dimensions are in meters. For $k = \frac{4}{3}$, we have $R_e = 8{,}500 \times 10^3$ m; $h_1'' = d_1^2/2R_e$; $h_2'' = d_2^2/2R_e$; $h_1'/d_1 = \tan\theta_1 = h_2'/d_2 = \tan\theta_2$.

$$\mathcal{E}_P = \mathcal{E}_0\left(\frac{\epsilon^{-j\beta R_1}}{R_1} + D\rho\epsilon^{j\varphi}\frac{\epsilon^{-j\beta R_2}}{R_2}\right) \quad \text{volts/m} \qquad (900)$$

where $\mathcal{E}_0$ is the reference free-space field intensity in the equatorial plane of the radiator at 1 m distance. The length of the direct path R_1 and indirect path R_2 is in meters, and ρ and φ denote the magnitude and the phase of the plane earth reflection coefficient, depending on the polarization. The quantity D accounts for the increasing divergence of the wave upon reflection, due to earth curvature. It is

$$D = \frac{1}{\sqrt{1+p}}; \qquad p = \frac{4h_1''d_2}{h_1'd} = \frac{4h_2''d_1}{h_2'd} \qquad (900a)$$

The quantity β is the phase factor $6.28/\lambda$, where λ is the free-space wavelength in meters found from $300/f^{(\text{Mc})}$. For low antennas, we have

$$\mathcal{E} = 2\mathcal{E}_0 A F_s G_1 G_2 \qquad \text{volts/m} \qquad (900b)$$

where A is the plane earth attenuation factor for antennas on ground, F_s is the universal shadow factor (ratio of field over spherical earth to field over plane earth for same ground constants), and G_1 and G_2 are the height-gain factors (independent of earth curvature and range). The factor F_s does not depend upon the antenna height. For the radiation and pickup antennas next to ground, we have $G_1 = 1 = G_2$. At great dis-

tances, we have

$$\mathcal{E} = \frac{4\pi h_1 h_2}{\lambda d}\,\mathcal{E}_0 F_s g_1 g_2; \qquad g_{1,2} = \frac{G_{1,2}}{\chi_{v,h}} \tag{900c}$$

where for moderate heights $g_1 = 1 = g_2$. For the universal shadow factor F_s, the ratio a/b, for $a = 6.28d/\lambda$ and $b = (6.28R_e/\lambda)^{2/3}$, plays a part. The factor A in (900b) depends on the electromagnetic properties of the earth crust, the operating frequency, and the type of polarization employed. In the height-gain factors G_1 and G_2, the terms $6.28h/\lambda$ and $6.28R_e/\lambda$ and the relative equivalent dielectric constant $\kappa_e' = \kappa_r - j1.8 \times 10^4(\sigma/f)$ play a part. The quantity κ_r denotes the actual relative numeric dielectric constant of the earth crust, f is in megacycles per second, and σ in mhos per meter. In connection with the curves, we use the relations

$$\left.\begin{aligned} K_v &= \frac{(\kappa_e')^2}{\kappa_e' - 1} \\ K_h &= \kappa_e' - 1 \\ \kappa_e' &= \kappa_r - j1.8 \times 10^4 \frac{\sigma^{(\text{mhos/m})}}{f^{(\text{Mc/sec})}} = \kappa_r - j60\sigma\lambda \\ \lambda^{(\text{m})} &= \frac{300}{f^{(\text{Mc/sec})}} \end{aligned}\right\} \tag{900d}$$

where κ_e' is the relative equivalent numeric dielectric constant of ground. The distance parameter ζ depends on the polarization, and we have

$$\zeta_v = \frac{\beta d}{K_v \lambda} \text{ for vertical polarization}; \quad \zeta_h = \frac{\beta d}{K_h \lambda} \text{ for horizontal polarization} \tag{900e}$$

leading to the distance parameter formulas

$$\left.\begin{aligned} \zeta = \zeta_v &= \frac{6.28(d/\lambda)\sqrt{(\kappa_r - 1)^2 + 3{,}600(\lambda\sigma)^2}}{\kappa_r^2 + 3{,}600(\lambda\sigma)^2} \\ &= \frac{2.09 \times 10^{-2} fd\sqrt{(\kappa_r - 1)^2 + 3.24 \times 10^8\,(\sigma/f)^2}}{\kappa_r^2 + 3.24 \times 10^8\,(\sigma/f)^2} \\ \zeta = \zeta_h &= \frac{6.28(d/\lambda)}{\sqrt{(\kappa_r - 1)^2 + 3{,}600(\lambda\sigma)^2}} \\ &= \frac{2.09 \times 10^{-2} fd}{\sqrt{(\kappa_r - 1)^2 + 3.24 \times 10^8(\sigma/f)^2}} \end{aligned}\right\} \tag{900f}$$

The application of these expressions is as follows: Suppose we deal with ocean surface, for which we have a relative dielectric constant κ_r of about 80 and a conductivity $\sigma \cong 5$ mhos/m. For a 100-Mc wave excitation, we find at a distance of 18.6 nautical miles the value $d = 539.6 \times 18.6 = 10^4$ m, since 1 nautical mile is 0.5396 km. We have $\kappa_r - 1 = 79$ and $(\kappa_r - 1)^2 = 6{,}241$, $(\sigma/f)^2 = (5/100)^2 = 25 \times 10^{-4}$ and fd

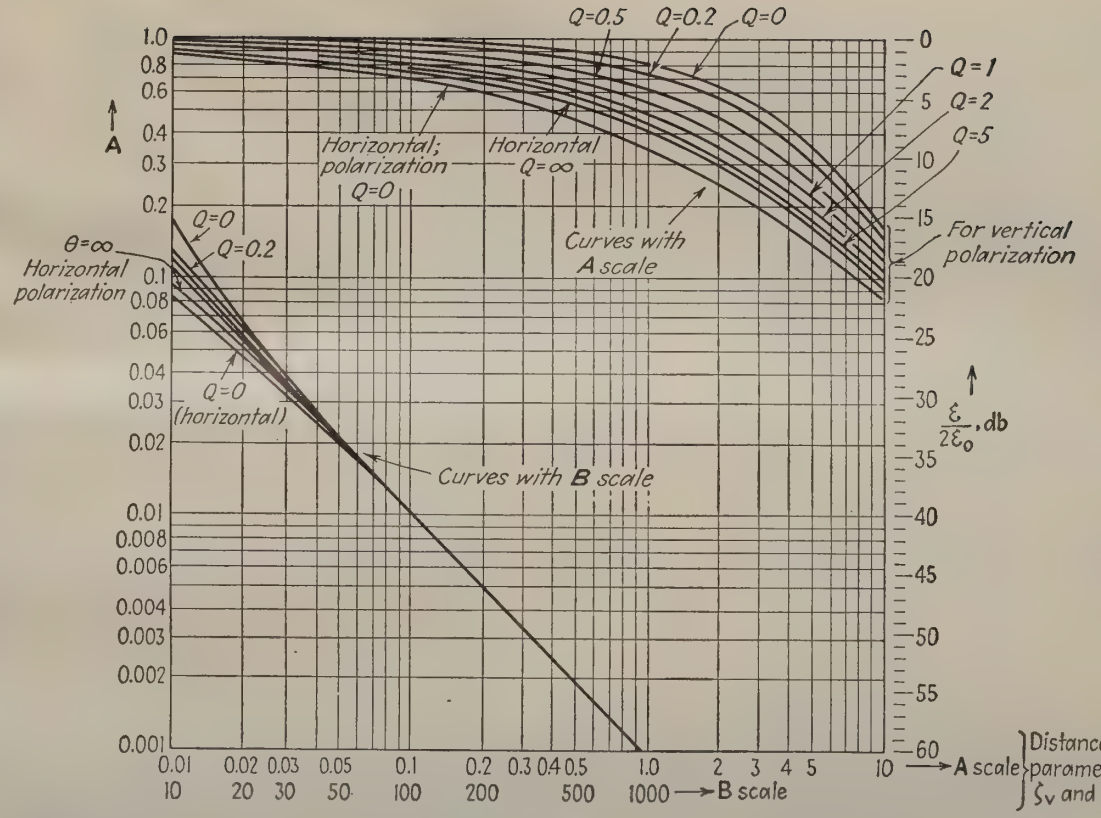

FIG. 328. The Burrows-Gray plane earth attenuation factor as a function of the distance parameters ζ_v and ζ_h for vertical and horizontal polarization for actual earth crust exhibiting different Q values. Quality of medium is $Q = \kappa_r f/(18 \times 10^3\sigma)$; f in Mc/sec, σ in mhos/m, κ_r dielectric constant of ground relative to vacuum.

$= 100 \times 10^4 = 10^6$. Hence, for horizontally polarized waves, we find the distance parameter

$$\zeta_h = \frac{2.09 \times 10^{-2} \times 10^6}{\sqrt{6{,}241 + 3.24 \times 10^8 \times 25 \times 10^{-4}}} = \frac{20{,}900}{\sqrt{6{,}241 + 810{,}000}} = 23.1$$

where 6,241 is the displacement effect, 810,000 is the conduction effect, and the square-root terms show that for a frequency of 100 Mc/sec, the ocean conduction currents

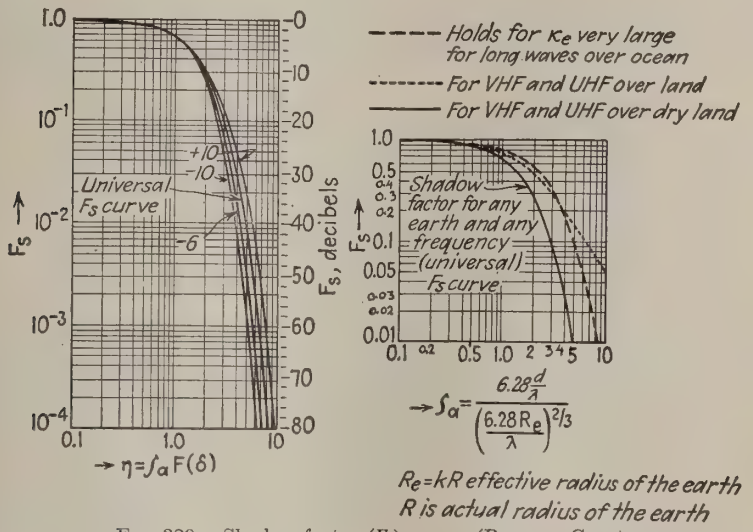
Holds for κ_e very large for long waves over ocean
For VHF and UHF over land
For VHF and UHF over dry land
Universal F_s curve
+10
-10
-6
F_s
F_s, decibels
Shadow factor for any earth and any frequency (universal) F_s curve
$\rightarrow \eta = \zeta_a F(\delta)$
$\rightarrow \zeta_a = \frac{6.28 \frac{d}{\lambda}}{\left(\frac{6.28 R_e}{\lambda}\right)^{2/3}}$
$R_e = kR$ effective radius of the earth
R is actual radius of the earth

FIG. 329. Shadow factor (F_s) curves (Burrows-Gray).

are essentially responsible (ocean displacement currents comparatively small). The distance parameter for vertical polarization is

$$\zeta_v = \frac{20{,}900 \times 903.4}{816{,}241} = 23.1$$

and *happens* to be the same value as for horizontal polarization. Figure 328 shows how the plane earth attenuation factor A of Eq. (900*b*) varies with the distance parameter ζ for different Q values of the ocean. In the above example, we have a quality $Q = (80 \times 100)/(1.8 \times 10^4 \times 5) = \frac{8}{90} = 0.0889$, which is quite small. The curves yield for vertical polarization, for $\zeta_v = 23.1$, a value of about $A_v = A \cong 0.05$. This corresponds to about 26 db for $\varepsilon/2\varepsilon_0$. For horizontal polarization, the distance parameter $\zeta_h = 23.1$ yields a value $A_h = A \cong 0.04$, which corresponds to 28 db. The curves of Fig. 328 show that for large values of the numerical distance ζ, the *same* attenuation factor A results for any Q value and irrespective of the polarization. On account of the earth curvature, the free-space field ε_0 in addition to factor A must be multiplied also by the shadow factor F_s, since this factor is the ratio of the actual field received to the field over plane earth with the same electromagnetic properties. Figure 329 gives the curves for the shadow factor F_s. The solid F_s curve with ζ_a as abscissa gives the shadow factor for horizontal polarization. It is

the universal F_s curve, which is also drawn for the η scale. The distance parameter η then becomes

$$\left.\begin{aligned} \eta = \eta_h &= \frac{6.28(d/\lambda)}{[6.28(R_e/\lambda)]^{2/3}} = \zeta_a \qquad \text{for } \textit{horizontal} \text{ polarization} \\ \eta = \eta_v &= \zeta_a F(\delta) = \zeta_a \left(\frac{6.28R_e}{\lambda}\right)^{2/3} \frac{1}{K_v} \qquad \text{for } \textit{vertical} \text{ polarization} \end{aligned}\right\} \quad (900g)$$

The curves in Fig. 330 give the proportionality factor $F(\delta)$ in terms of the earth constant $\delta = (6.28R_e/\lambda)^{2/3}/K_v$. Since, according to (900d), the quantity K_v in $K_v = (\kappa_e')^2/(\kappa_e' - 1)$ is complex, the quantity δ with the absolute amount $|\delta|$ generally has a

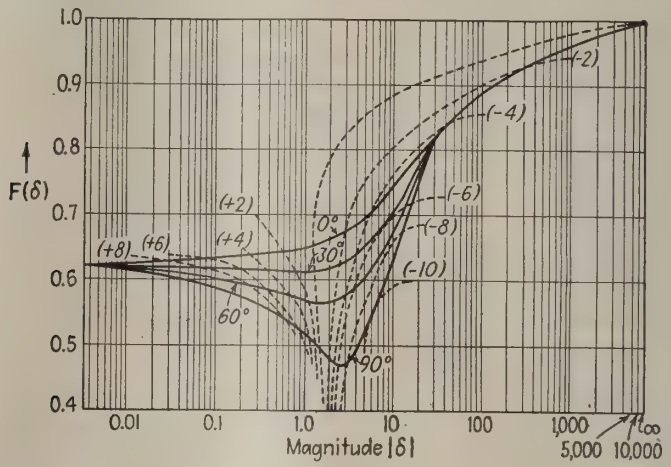

$$\delta = \frac{(2.09 \times 10^{-2} R_e f)^{2/3}}{(\kappa_e')^2} (\kappa_e - 1)$$

$$\kappa_e' = \kappa_r - 18 \times 10^3 \frac{\sigma}{f}$$

κ_r numeric; σ in mhos/m
$R_e = kR$ in meters; f in Mc/sec

FIG. 330. Curves for the $F(\delta)$ function used in Fig. 332 as a function for the ground constants. Solid curves for short distances. Numbers on broken curves correspond to numbers on shadow factor curve of Fig. 329 holding for all distances.

phase angle also (since δ is complex with a magnitude as well as a direction). The numbers on the curves give the argument of δ in degrees. The ordinates of the solid curves give the $F(\delta)$ value to be used in Fig. 329 with the η abscissa scale in the case of short distances. The broken curves hold for longer distances. For low antenna heights, the respective antenna gain factors G_1 and G_2 are computed from

$$\left.\begin{aligned} G = 1 + jx; \qquad x = x_v &= \frac{6.28h/\lambda}{\sqrt{K_v}} \qquad \text{for vertical polarization} \\ x = x_h &= 6.28 \frac{h}{\lambda} \sqrt{K_h} \qquad \text{for horizontal polarization} \end{aligned}\right\} \quad (900h)$$

when h is the altitude of respective antenna centers with respect to ground. At

short distances, $(900h)$ is limited to heights for which $6.28h_1h_2/(\lambda d)$ is somewhat less than unity and, at long distances, to values less than 0.5, for

$$\chi = \frac{\chi_v}{\sqrt{\delta}} = \frac{6.28h/\lambda}{\sqrt[3]{6.28(R_e/\lambda)}}$$

In Fig. 331, we have the relative height factors χ

$$\left.\begin{aligned}
\chi = \chi_v &= \frac{6.28h/\lambda}{\sqrt[4]{\kappa_r^2 + 3{,}600(\sigma\lambda)^2}} \sqrt[4]{\frac{(\kappa_r - 1)^2 + 3{,}600(\sigma\lambda)^2}{\kappa_r^2 + 3{,}600(\sigma\lambda)^2}} \\
&= \frac{2.09 \times 10^{-2} fh}{\sqrt[4]{\kappa_r^2 + 3.24 \times 10^8(\sigma/f)^2}} \sqrt[4]{\frac{(\kappa_r - 1)^2 + 3.24 \times 10^8(\sigma/f)^2}{\kappa_r^2 + 3.24 \times 10^8(\sigma/f)^2}} \\
\chi = \chi_h &= 6.28 \frac{h}{\lambda} \sqrt[4]{(\kappa_r - 1)^2 + 3{,}600(\sigma\lambda)^2} \\
&= 2.09 \times 10^{-2} fh \sqrt[4]{(\kappa_r - 1)^2 + 3.24 \times 10^8 \left(\frac{\sigma}{f}\right)^2}
\end{aligned}\right\} \quad (900i)$$

for h and λ in meters, f in megacycles per second, and σ in mhos per meter. The relative dielectric constant κ_r for the earth crust is anywhere between 4 and 80, the upper limit holding for ocean and lakes and rivers and the range from 4 to about 30 holding for dry rock to wet soil. There is a gap between 30 and 80 if we think of customary values given in standards tables. The height-gain factors G_1 and G_2 in Fig. 331 depend on the polarization (either χ_v or χ_h must be used). For large values such as $\chi \geqq 20$, we have essentially a common characteristic for the G curve. This means that the electromagnetic ground properties μ, κ, and σ no longer play a part. Therefore, the received field must be independent of the electromagnetic merit Q of the earth crust and the polarization. This applies to quite a range of short wavelengths and can be experimentally verified. For great heights, such as $\chi_a \geqq 0.5$, we find

$$\mathcal{E}^{(\text{volts/m})} = 12.56 \frac{h_1h_2}{\lambda d} \mathcal{E}_0 F_s g_1 g_2 = 4.19 \times 10^{-2} \frac{h_1h_2 f^{(\text{Mc})}}{d} \mathcal{E}_0 F_s g_1 g_2 \qquad (900j)$$

where for sufficiently great ranges, the respective height factors g_1 and g_2 do not depend on the range but on the relative height factor parameter

$$\left.\begin{aligned}
&\chi_\delta = \chi_v g(\delta) \qquad \text{for vertical polarization} \\
&\chi_\delta = \chi_a = \frac{6.28h/\lambda}{\sqrt[3]{6.28(R_e/\lambda)}} = \frac{2.09 \times 10^{-2} hf}{\sqrt[3]{2.09 \times 10^{-2} R_e f}} \qquad \text{for horizontal polarization}
\end{aligned}\right\} \quad (900k)$$

where f is in megacycles per second and $\delta = (6.28R_e/\lambda)^{2/3}/K_v$. For an atmospheric refraction such that the effective earth radius R_e in meters is $\frac{4}{3}$ times the actual radius R, we find $\chi_a = 0.0167h\lambda^{2/3}$, where h and λ are in meters. Figure 332 gives curves for the respective factors g_1 and g_2 of formula $(900j)$. We have also for vertical polarization

$$\chi_\delta = \chi_a g(\delta); \qquad g_v = g_h g_\delta \qquad (900l)$$

Figure 333 gives the curves for the $g(\delta)$ and g_δ values depending on the absolute value $|\delta|$ of δ.

208. Remarks on the Application of the Classic Theory of Apertures in Optics to Diffraction of Electromagnetic Waves. We know that the classic Kirchhoff solution is based on a scalar wave function w, while

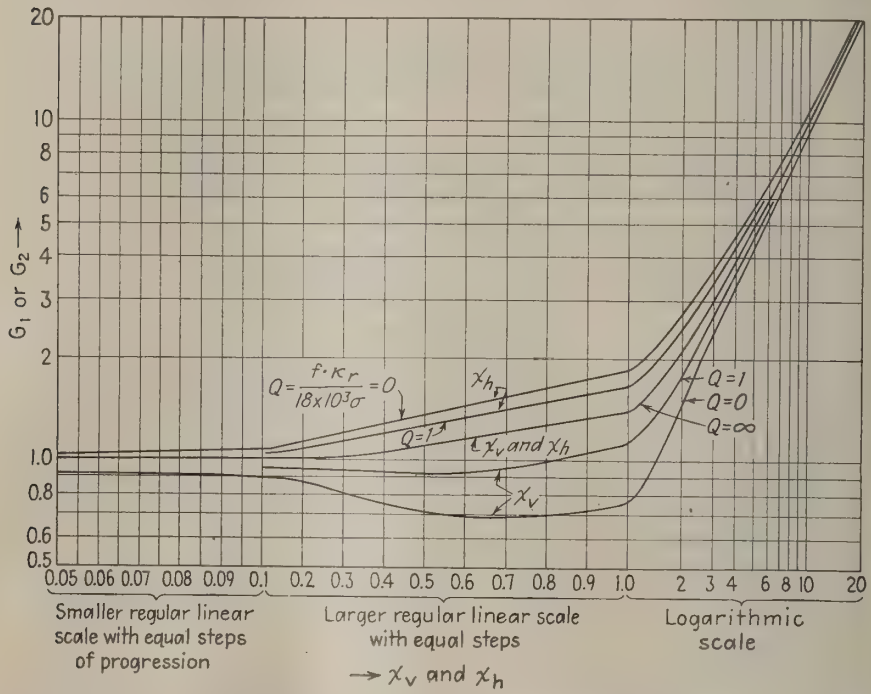

For values of $\chi > 20$ we have $G \cong \chi_v$ for vertical polarization. For values of $\chi > 20$ we have $G \cong \chi_h$ for horizontal polarization and A approaches $1/\zeta_v$ and $1/\zeta_h$ making $\mathcal{E}^{(\text{volts/m})} = 2\mathcal{E}_0 F_s \chi^2/\zeta = 12.56(h_1 h_2/\lambda d)\mathcal{E}_0 F_s$. h_1 and h_2 are the heights of the radiating and pickup centers above ground in meters.

FIG. 331. Height-gain factor G as a function of χ parameter.

for electromagnetic waves, we have to deal with $\mathcal{E}$ and H functions due to such fields and have to meet boundary conditions. According to Huygens' principle, the wave front can be taken as a multitude of secondary wavelet sources. Such sources are also compatible with the electromagnetic induction theorem. For this theorem, any of the secondary sources is an association of electric and magnetic current elements whose respective moments are proportional to the electric and magnetic field intensities, which are *tangent* to the wave front of the primary wave. For instance, for a large aperture in a perfectly absorbing screen, the electromagnetic field in the aperture must be essentially the same as

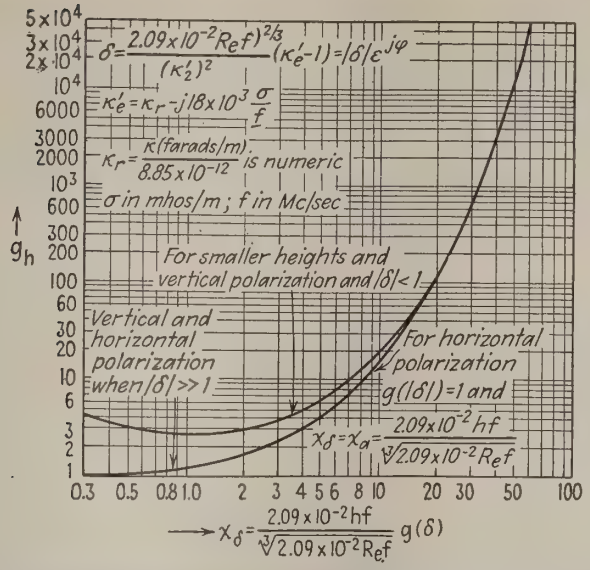

FIG. 332. Height-gain factors g_1 and g_2 from pages 1075, 1078–1080. g_h are the values for g_1 and g_2 for horizontal polarization. For vertical polarization $g_h g_\delta$ gives the values for g_1 and g_2, depending on whether $h = h_1$ or $h = h_2$ is used. h_1 and h_2 are radiation and pickup center altitudes in meters above ground.

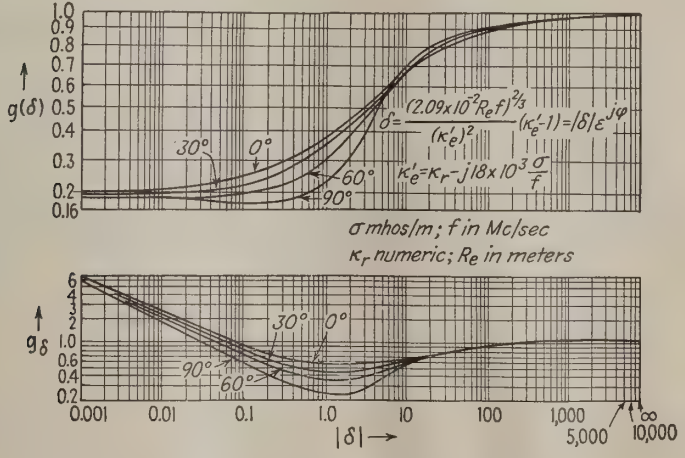

FIG. 333. The parameters $g(\delta)$ and g_δ for Fig. 335.

though the screen were not present. There can be no back reflection and, therefore, also no interference with the primary wave front, which arrives at the aperture. A circular opening in a screen of a diameter 1 wavelength is, for instance, 90 per cent efficient as far as the radiation through the circular aperture is concerned. This statement is based on the power radiated by electric and magnetic current sheets at the aperture. We have entirely different conditions from these for light waves,

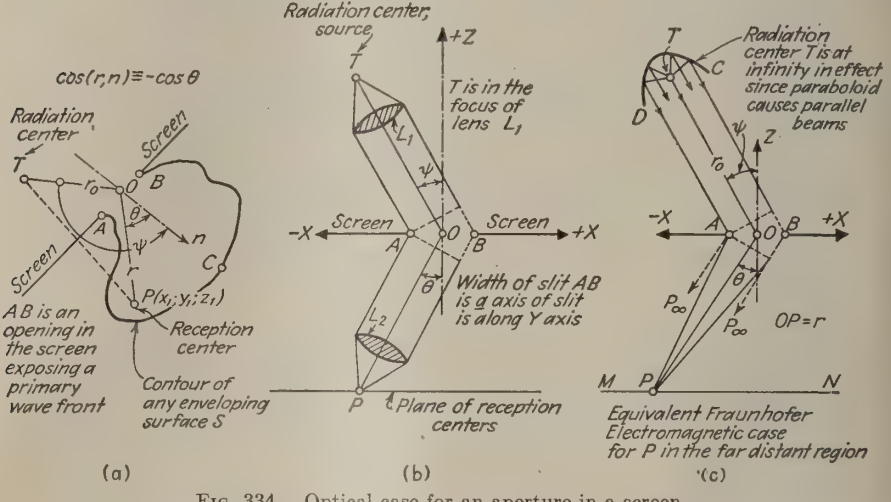

FIG. 334. Optical case for an aperture in a screen.

where the diameter of the aperture or the width of a slit are small but *always very* large compared with the wavelength.

In optics, we deal in the case of apertures in a screen as is indicated in Fig. 334*a* and *b*. In Fig. 334*a*, the location T represents the primary radiation center, which is a distance r_0 away from the reference point O in the opening AB of the screen. The surface S encloses any suitable space behind the screen. According to Sec. 203, we have, at the reception center P, the elementary wave disturbance $dw = k \sin \{\beta[vt - (r + r_0)]\}$ for $\beta = \omega/v = 2\pi/\lambda$ and the velocity v of propagation. The Kirchhoff formula has the form

$$w = \frac{W}{2\lambda} \int\int_S \frac{1}{rr_0} (\cos \theta - \cos \psi) \sin \{\beta[vt - (r + r_0)]\}\, dS$$

$$r_0 \gg \lambda$$

Since the integrand over the envelope ACB *behind* the screen vanishes, we have only to integrate over the surface AB, which forms the aperture. We found that for small dimensions of the aperture compared with r_0 and r, the quantities r_0, r, $\cos \psi$, and $\cos \theta$ are constants and

$$w = \frac{W(\cos \theta - \cos \psi)}{2rr_0\lambda} \int\int_S \sin \{\beta[vt - (r + r_0)]\}\, dS$$

Inasmuch as we are interested in this relation in the wavelets coming from the primary wave front occupying the aperture, we choose an elementary surface dS for each elementary effect dw at field point P, in such a way that $\cos \psi = \cos 180° = -1$. This means that dS is normal to r_0 and

$$\left.\begin{aligned} dw &= \frac{W(1 + \cos\theta)}{2rr_0\lambda} \sin\left[\omega\underbrace{\left(t - \frac{r + r_0}{v}\right)}_{=t'}\right] = K(1 + \cos\theta)\sin\omega t' \\ K &= \frac{W}{2rr_0\lambda} \end{aligned}\right\} \quad (901)$$

This relation shows that each primary wave-front element in the aperture AB acts as an elementary secondary radiator, emitting a wavelet with an amplitude that is proportional to $(1 + \cos\theta)$. The directivity pattern D_θ of each secondary radiator is then $1 + \cos\theta$, which is a *cardioid* and has *no* straight backward directivity, since $\cos\theta = \cos 180° = -1$ and $D_{180} = 1 - 1 = 0$. The field power of the wavelet is then proportional to $(1 + \cos\theta)^2$. We have an action similar to that for two linear parallel radiators that are a quarter wavelength apart. A similar action also exists when radiation occurs from plane electric and magnetic current sheets with respective current densities J_θ and $J_{m\varphi}$ in amperes per square meter and volts per square meter, respectively. We have then polar coordinates r, θ, and φ with a power flow per unit solid angle in the θ, φ direction, which is likewise proportional to $(1 + \cos\theta)^2$ and inversely proportional to λ^2. Figure 334*b* illustrates the classic optical case where T denotes the light source that, by means of a lens L_1, causes parallel rays and diffracts these rays through a slit of width a toward a focal point P, owing to the action of a focusing lens L_2. The equivalent electromagnetic case is illustrated in Fig. 334*c*, where a plane electromagnetic wave is caused by means of a parabolic reflector with the actual or primary linear radiator along the focal line of a paraboloid. In the electromagnetic case of Fig. 334*c*, as well as in the optical case of Fig. 334*b*, the primary radiation center T acts as though at infinity as far as the plane wave front is concerned at the aperture. By choosing the reception center P in Fig. 334*c* a very large distance from the primary wave front in the slit of width AB, the rays AP and BP must become essentially parallel, and P acts as though at infinity. Hence, the lens L_2 is avoided in the electromagnetic case. We could, however, place the points P along the focal line of a receiving paraboloid and produce the same effect. In either case, we have then at points P the conditions for an *electromagnetic Fraunhofer diffraction pattern*. If such a provision is not made in Fig. 334*c*, we should have at points P an *electromagnetic Fresnel diffraction pattern*. For the latter, we have to sum up all effects at a field point P with respect to amplitude as well as to time phase.

Inasmuch as the slit is in the XY plane, the surface element of the aperture is $dx\,dy$. For small ranges of angle ψ of incidence and angle θ of diffraction, we can put $K(1 + \cos\theta)$ equal to a constant as far as the integration of (901) is concerned, where the integration extends only over the area of the slit or aperture. Since r_0 and r also do not depend on y, we can take all independent terms in front of the integral and call it a factor K_1, requiring only the solution of $w = K_1 \int \sin\{\beta[vt - (r +$

$r_0)]\}\ dx$ between the limits $x = -\frac{1}{2}a$ and $x = +\frac{1}{2}a$, where a is the width of the slit in the X direction. Using O, a point halfway between AB in Fig. 334*c*, as a reference point and calling the distance $r + r_0 = k_0\lambda$, we have, for any other point along the width AB, a path length

$$r + r_0 = k_0\lambda + x(\cos\psi - \cos\theta) \qquad \textit{actual} \text{ length}$$

$$\beta(r + r_0) = 2\pi\left[k_0 + \frac{x(\cos\psi - \cos\theta)}{\lambda}\right] = 2\pi(k_0 + x\delta) \quad \textit{electrical} \text{ length}$$

$$\delta = \frac{\cos\psi - \cos\theta}{\lambda}$$

We have then

$$w = K_1\int_{x=-a/2}^{x=+a/2} \sin\beta[vt - (r + r_0)]\,dx = K_1\int_{-a/2}^{a/2} \sin\,[2\pi(ft - k_0 - x\delta)]\,dx$$

$$\sin\,[2\pi(\underbrace{ft - k_0}_{k_1} - x\delta)] = \sin\,[2\pi(k_1 - x\delta)]$$

$$= \sin\,(2\pi k_1)\cos\,(2\pi x\delta) - \cos\,(2\pi k_1)\sin\,(2\pi x\delta)$$

and

$$w = K_1\left[\sin\underbrace{(2\pi k_1)}_{\alpha}\int_{-a/2}^{a/2}\cos\,(2\pi x\delta)\,dx - \cos\alpha\int_{-a/2}^{a/2}\sin\,(2\pi x\delta)\,dx\right]$$

$$= K_1\left[\sin\alpha\left|-\frac{\sin\,(2\pi x\delta)}{2\pi\delta}\right|_{-a/2}^{a/2} - \cos\alpha\left|\frac{\cos\,(2\pi x\delta)}{2\pi\delta}\right|_{-a/2}^{a/2}\right]$$

For $\gamma = \pi a\delta$, we find

$$w = -K_1\left[\sin\alpha\,\frac{\sin\gamma - \sin\,(-\gamma)}{2\pi\delta} - \cos\alpha\,\frac{\cos\gamma - \cos\,(-\gamma)}{2\pi\delta}\right]$$

$$= -K_1\left[\sin\alpha\,\frac{\sin\gamma}{\gamma/a} - (\cos\alpha)\times 0\right] = -aK_1\,\frac{\sin\alpha\sin\gamma}{\gamma}$$

We find at any point P along the line MN in Fig. 334*c*, provided the range of angle θ of diffraction is small,

$$w = -aK_1\,\frac{\sin\gamma}{\gamma}\sin\alpha = -K_2\,\frac{\sin\,(\pi a\delta)}{\pi a\delta}\sin\,[2\pi(ft - k_0)]$$

$$= -K_2D_\delta\sin\,[2\pi(ft - k_0)] \quad (901a)$$

because the width a is fixed for a certain aperture and $aK_1 = K_2$ is a new constant. For $p = \pi a\delta$, the diffractivity D_δ is

$$D_\delta = \frac{\sin p}{p}; \qquad p = 3.14a\,\frac{\cos\psi - \cos\theta}{\lambda} \qquad (901b)$$

The function $(\sin p)/p$ is the distribution variation of the amplitude $(K_2\sin p)/p$ in the XZ plane of Fig. 334*c*, provided the ranges ψ and θ

TABLE 70. FIELD AMPLITUDE AND RADIATION INTENSITY DISTRIBUTION

p		tan p	sin p	Amplitude at P is proportional to $\frac{\sin p}{p}$	Radiated power at P is proportional to $\frac{\sin^2 p}{p^2}$	p		tan p	sin p	$\frac{\sin p}{p}$	$\frac{\sin^2 p}{p^2}$	p		tan p	sin p	$\frac{\sin p}{p}$	$\frac{\sin^2 p}{p^2}$
Deg	Radians					Deg	Radians					Deg	Radians				
0	0.0000	0.0000	0.0000	1.000	1.000	100	1.745	−5.67	0.9848	0.563	0.317	300	5.23	−1.73	−0.866	−0.165	0.021
5	0.0873	0.0875	0.0872	0.999	0.998	110	1.92	−2.75	0.9387	0.49	0.24	310	5.41	−1.192	−0.766	−0.141	0.02
10	0.1745	0.1763	0.1736	0.995	0.99	120	2.09	−1.73	0.866	0.415	0.172	320	5.58	−0.839	−0.643	−0.116	0.013
15	0.262	0.2679	0.2588	0.987	0.974	130	2.27	−1.192	0.766	0.337	0.114	330	5.76	−0.577	−0.5	−0 087	0.0076
20	0.3491	0.364	0.342	0.98	0.96	140	2.44	−0.839	0.6428	0.265	0.0702	340	5.93	−0.364	−0.342	−0.058	0.0034
25	0.436	0.4663	0.4226	0.967	0.935	150	2.62	−0.577	0.5	0.193	0.037	350	6.11	−0.176	−0.1736	−0.0284	0 0008
30	0.524	0.5774	0.5	0.952	0.906	160	2.79	−0.364	0.342	0.123	0.015	360	6.28	0.000	0.0000	0.0000	0.000
35	0.611	0.7002	0.5736	0.94	0.884	170	2.97	−0.176	0.174	0.0588	0.00346	380	6.63	0.364	0.342	0 0515	0.0026
40	0.698	0.8391	0.6428	0.925	0.856	180	3.14	0.000	0.000	0.0000	0.00000	400	6.98	0.839	0.643	0.0925	0.0086
45	0.785	1.0000	0.7071	0.9	0.81	190	3.16	0.176	−0.174	−0.055	0.00302	420	7.33	1.73	0.866	0.118	0.014
50	0.873	1.192	0.766	0.875	0.766	200	3.49	0.364	−0.342	−0.098	0.0096	440	7.68	5.67	0.985	0.129	0.017
55	0.96	1.4281	0.8192	0.852	0.726	210	3.66	0.577	−0.5	−0.136	0.0185	460	8.03	−5.67	0.985	0.123	0.015
60	1.05	1.7321	0.866	0.825	0.681	220	3.84	0.839	−0.643	−0.168	0.028	480	8.38	−1.73	0.866	0.104	0.011
65	1.134	2.1445	0.9063	0.802	0.643	230	4.01	1.192	−0.766	−0.1905	0.036	500	8.71	−0.839	0.643	0.074	0.00055
70	1.22	2.7475	0.9397	0.77	0.593	240	4.19	1.73	−0.866	−0.206	0.042	520	9.18	−0.364	0.342	0.037	0.00014
75	1.31	3.7321	0.9659	0.736	0.542	250	4.36	2.75	−0.94	−0.215	0.046	540	9.41	0.000	0.000	0.000	0.00000
80	1.41	5.671	0.9848	0.705	0.497	260	4.54	5.67	−0.985	−0.217	0.0471	560	9.76	0.364	−0.342	−0.035	0.00012
85	1.48	11.43	0.9962	0.672	0.452	270	4.71	∞	−1.0	−0.212	0.045	580	10.15	0.839	−0.643	−0.0635	0.0004
90	1.571	∞	1.0000	0.637	0.406	280	4.89	−5.67	−0.985	−0.201	0.04	600	10.47	1.73	−0.866	−0.082	0.00067
						290	5.06	−2.75	−0.94	−0.186	0.034						

Remarks: Since sin p is numeric, we must use the numeric radian value of p for the ratios $(\sin p)/p$ and $(\sin^2 p)/p^2$. Maximum amplitude and radiation intensity (energy) effects occur for $p = 0$, $p = 1.43\pi$, which is less than $3\pi/2$, $p = 2.459\pi$, which is less than $5\pi/2$, etc. Since $p = 1.43\pi = 4.493$ or $4.493 \times 57.295 = 257$ deg, yielding $\sin 257° = -0.9744$ with a relative field amplitude, $(\sin p)/p = -0.9744/4.493 = -0.217$ yields point A_2 in Fig. 335.

are not too large. The radiation intensity, *i.e.*, the radiated power, varies as $(\sin^2 p)/p^2$. Maximum amplitude as well as energy values occur for

$$\left.\begin{aligned} \frac{d[(\sin p)/p]}{dp} = 0 \quad \text{or} \quad \frac{\sin p - p\cos p}{\sin^2 p} = 0 \\ \text{i.e., } \sin p - p\cos p = 0 \end{aligned}\right\} \quad (901c)$$

or

$$\tan p = p$$

Hence, we need only draw the slanting $y_1 = p$ line and intersect it with

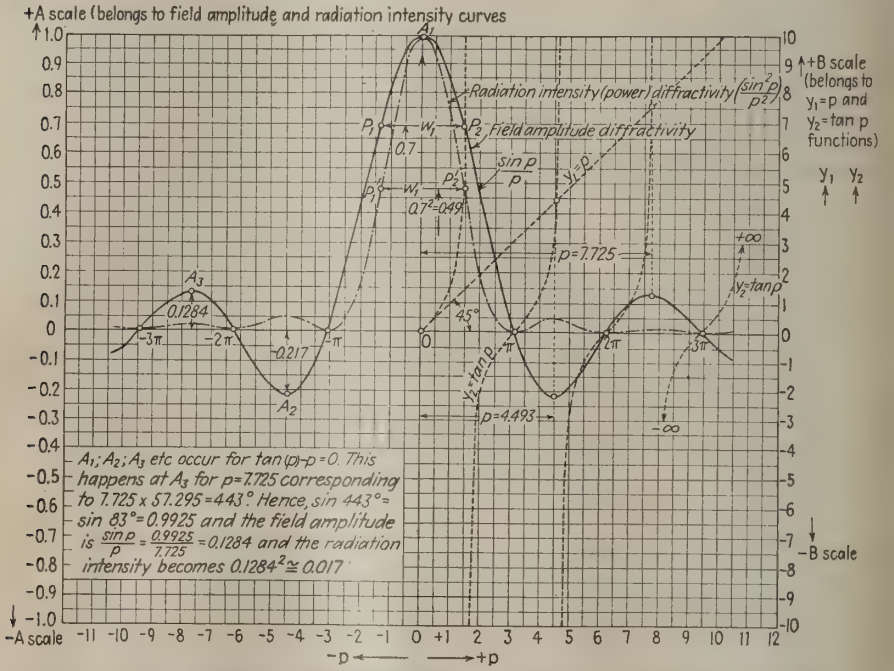
+A scale (belongs to field amplitude and radiation intensity curves
+B scale (belongs to y1=p and y2=tan p functions)
Radiation intensity (power) diffractivity (sin²p/p²)
Field amplitude diffractivity
sin p/p
y1=p
y2=tan p
p=7.725
p=4.493
45°
A1; A2; A3 etc occur for tan(p)−p=0. This happens at A3 for p=7.725 corresponding to 7.725 x 57.295=443.° Hence, sin 443.°= sin 83°=0.9925 and the field amplitude is sin p/p = 0.9925/7.725 = 0.1284 and the radiation intensity becomes 0.1284²≅0.017
−B scale
−A scale
−p
+p

FIG. 335. Field amplitude and radiation intensity patterns. *Note:* First lobe with A_1 peak is twice as wide (2π) as side lobes A_2, A_3, etc., of width π.

the various consecutive finite branches of the $y_2 = \tan p$ curve of Fig. 335. This occurs for $p = 0$, $= 1.43\pi = 4.493$, $= 2.459\pi = 7.725$, $= 3.47\pi = 10.9$, $= 4.479\pi = 14.07$, $\cdots$, since for these values $\tan p = p$. Table 70 gives evaluations for diffractivity D_δ given by formula (901*b*), in terms of the argument p as well as the tan functions. The square of the diffractivity must be a measure for the radiation intensity, since this intensity refers to energy distribution. The radiation intensity curves can also be found directly from the D_δ curve in Fig. 335 by the method of equal-lobe widths w_1 for the D_δ and D_δ^2 curves. We then choose the

ordinates for certain fixed widths, such as 0.7, 0.8, 0.9, 0.6, 0.5, 0.4, ... We have then the corresponding squares 0.49, 0.64, 0.81, 0.36, 0.25, 0.16, ... It is then only necessary to transpose the lobe width w_1 (in Fig. 335) from the 0.7 ordinate, for instance, to the $0.7^2 = 0.49$ ordinate in order to find the two extreme points P_1' and P_2' of the radiation intensity curve from the P_1 and P_2 points of the field amplitude curve. The latter curve is, in reality, only the diffractivity D_δ in this figure. Hence, when the ordinate value is n for the diffractivity curve D_δ corresponding to a width w_n, we have only to shift the w_n width to an ordinate value n^2.

It is now of importance to apply the diffraction pattern of Fig. 335 to the case of electromagnetic waves, where the wave function of the Kirchhoff expressions must satisfy the respective field associations $\mathcal{E}$ volts per meter and H amperes per meter, as well as the boundary conditions. This means that we must relate the factor p as well as the factor K_2 of (901*a*) to such field vectors and their requirements.

According to the classic theory, we deal with a single wave function w and have the relation $\Delta^2 w + \Gamma^2 w = 0$, where Γ denotes the propagation constant and $w(x,y,z)$ is the solution for any isotropic homogeneous medium. According to Green's theorem, for any point x_1,y_1,z_1 within any closed surface S, we have

$$w(x_1,y_1,z_1) = \frac{1}{4\pi} \int \int_S \left(\frac{\partial w}{\partial n} q - w \frac{\partial q}{\partial n} \right) dS; \qquad q = \frac{\epsilon^{-r\Gamma}}{r} \tag{901d}$$

if any point x,y,z on the enclosing surface S is a distance

$$r = \sqrt{(x_1 - x)^2 + (y_1 - y)^2 + (z_1 - z)^2}$$

from an interior enclosed point x_1,y_1,z_1. The derivatives are *normal* to all surface elements (expressed by operator ∂n). This is the case if any aperture point along the opening AB in Fig. 334 is a location x,y,z. We have then

$$w = -\frac{\Gamma}{4\pi} \int \int_S \frac{\epsilon^{-(r+r_0)\Gamma}}{r r_0} (\cos \theta - \cos \psi)\, dS \tag{901e}$$

where the wave disturbance w is due to a source whose wave front forms a portion of surface S and is a distance r_0 meters from the source, while r meters is the distance from point x,y,z located in the primary wave front, acting as an aperture in said surface to a point x_1,y_1,z_1. The degree of diffraction is practically such that the straight connection TP in Fig. 334*a* passes close to the edge of the aperture. For nondissipative mediums, such as atmosphere, the propagation constant $\Gamma = \alpha + j\beta$ simplifies to $j\beta$. The factor $\epsilon^{-j\beta(r+r_0)}$ represents a *rapidly* oscillating function of the field point location, while $\cos \theta - \cos \psi = 2 \cos \delta_0$ varies relatively *slowly*. If we now choose the difference of $\cos \theta$ and $\cos \psi$ equal to $2 \cos \delta_0$, the quantity δ_0 will represent the angle between the straight connection PT and the normal to the aperture. Such a substitution leads to the *restricted* Kirchhoff relation

$$w = -j \frac{\beta \cos \delta_0}{2\pi r r_0} \int \int_S \epsilon^{-j\beta(r+r_0)}\, dS \tag{901f}$$

It is now convenient to fix the coordinate system as in Fig. 336. Since the aperture of the screen is part of the surface S, only this surface portion requires integration. The quantity $dS = dx\,dy$ is a surface ele-

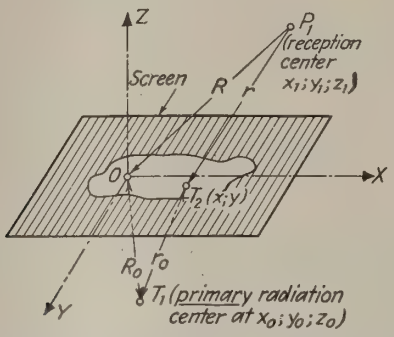

FIG. 336. Conditions for any aperture in a screen with respect to significant distances to primary radiation center and reception center from Huygens wavelet centers.

$$r_0 = \sqrt{(x_0 - x)^2 + (y_0 - y)^2 + z_0^2}; \qquad r = \sqrt{(x_1 - x)^2 + (y_1 - y)^2 + z_1^2};$$
$$R_0 = \sqrt{x_0^2 + y_0^2 + z_0^2}; \qquad R = \sqrt{x_1^2 + y_1^2 + z_1^2}.$$

Any point x, y in the aperture of the screen is one of the many secondary Huygens radiation centers (T_2 is such a point).

ment with an elementary wavelet center. Inasmuch as x/R_0, y/R_0, x/R, and y/R are small numbers, we can write

$$r_0 = R_0 - \frac{x_0x + y_0y}{R_0} + \frac{x^2 + y^2}{2R_0} - \frac{(x_0x + y_0y)^2}{2R_0^3} + \cdots$$
$$r = R - \frac{x_1x + y_1y}{R} + \frac{x^2 + y^2}{2R} - \frac{(x_1x - y_1y)^2}{2R^3} + \cdots$$

which, inserted in (901f), yields

$$w = -j\frac{\beta\epsilon^{-j\beta(R+R_0)}\cos\delta_0}{2\pi RR_0}\int\int_{\text{aperture}}\epsilon^{-j\beta F(x,y)}\,dx\,dy$$
$$= K_0\int\int\epsilon^{-j\beta F(x,y)}\,dx\,dy \qquad (901g)$$

where the integration is taken only over the aperture surface, because the remainder of the closing surface S is a screen and *cannot* contribute anything at the reception center P. We have the function

$$F(x, y) = -\frac{x_0x + y_0y}{R_0} + \frac{x^2 + y^2}{2R_0} - \frac{(x_0x + y_0y)^2}{2R_0^2} + \cdots$$
$$-\frac{x_1x + y_1y}{R} + \frac{x^2 + y^2}{2R} - \frac{(x_1x + y_1y)^2}{2R^3} + \cdots \qquad (901h)$$

The constant K_0 multiplied by the double integral is then the *Fraunhofer amplitude in the presence of diffraction.* It can be applied to electromagnetic waves if suitable precautions are taken to satisfy the boundary conditions at the surface of the screen and the tangential electromagnetic field forces at the aperture are known.

209. Electromagnetic Huygens Wavelet[1] Radiators in the Primary Wave Front. In the distant radiation region, we deal essentially with plane electromagnetic waves. The plane wave front then represents

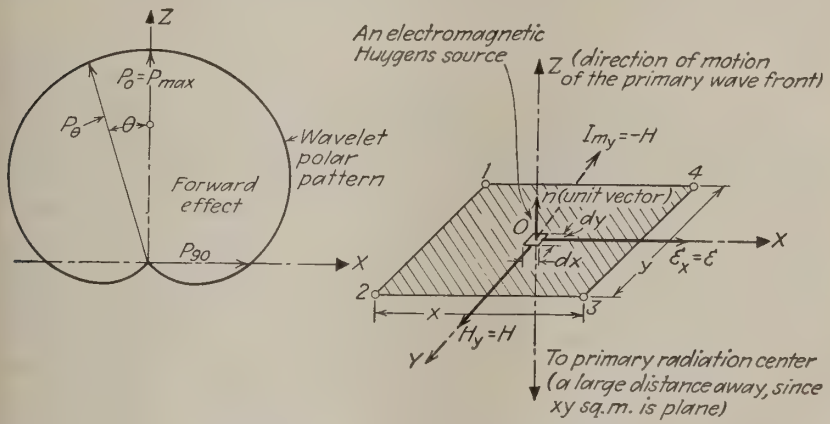

Note: $(P_{90°})^2$ is 6 db below $(P_{0°})^2 = (P_{max})^2$ for a secondary radiation center but only 3 db below for a well-known end-fire line-up of linear radiators.

$dx\,dy = dS$ is a Huygens wavelet source in the primary wave front.

$S = xy$ sq m

$Z_0 = \sqrt{\frac{\mu}{\kappa}} \cong 376.7$ ohms

$J_x = -\mathcal{E} = -Z_0 H$ volts/m

FIG. 337. Conditions for an electromagnetic wavelet source.

the unperturbed primary wave front due to a primary electromagnetic radiator, and it is an easy matter to apply the Huygens wavelet concept *rigorously.* The primary wave front of Fig. 337 is the plane area 1-2-3-4-1 at the instant; it just passes the XY plane while traveling in parallel planes with a velocity of $v = 1/\sqrt{\mu\kappa} = 3 \times 10^8$ m/sec in a direction normal to this plane, since such a front is a place of constant phase. The $\mathcal{E} = \mathcal{E}_x$ and the $H = H_y$ polarizations are, therefore, tangential to the area 1-2-3-4-1. The plane wave front can then, according to Secs. 61 to 64, be replaced, in effect, by electric and magnetic current sheets, which are in this plane. Formulas (515) and (516) show then how the electric current density J_x amperes per meter and the magnetic current J_{m_y} volts per

[1] Electromagnetic Huygens sources were treated by S. A. Schelkunoff in his paper on A General Radiation Formula, *IRE*, **27**, 664, October, 1939. It is also used later in his "Electromagnetic Waves," D. Van Nostrand Co., Inc., 1943, on pp. 354–355.

meter of the equivalent electric and magnetic current sheets may be numerically related to the magnetic field intensity H_y amperes per meter and electric field intensity $\mathcal{E}_x$ volts per meter. The infinitely small area $dS = dx\,dy$ with the sides parallel to $\mathcal{E}_x$ and H_y represents a Huygens wavelet radiator, *i.e.*, a secondary radiation center. Since $J_x\,dS$ is the electric moment and $J_{m_y}\,dS$ the magnetic moment of a wavelet radiator and we have $J_x = -H_y = -H$ amperes per meter and $J_{m_y} = -\mathcal{E}_x = -\mathcal{E} = -Z_0 H$ volts per meter, we find the radiation vector

$$dN_x = -H\,dS = -\frac{\mathcal{E}_x\,dS}{Z_0} \quad \text{m} \cdot \text{amp}; \qquad dL_y = -\mathcal{E}\,dS = -\mathcal{E}_x\,dS \quad \text{m} \cdot \text{volts} \tag{902}$$

which is the radiation vector of an electromagnetic Huygens source, according to Sec. 124 and formulas (831). In order to obtain the electric radiation vector N_x, we have to compute the integral $\int\int_S dN_x$ for the area xy square meters. For the magnetic radiation vector of area 1-2-3-4-1, we have, similarly, $L_y = \int\int_S dL_y$. In this section, we are interested mainly in the effect of a *Huygens* radiator, for which we have formulas (902) if expressed in Cartesian coordinates. For spherical components, we find

$$\left.\begin{aligned} dN_\theta &= -H\,dS\cos\theta\cos\varphi \\ dN_\varphi &= H\,dS\sin\theta \end{aligned}\right\}\ \text{m} \cdot \text{amps}$$

$$\left.\begin{aligned} dL_\theta &= -\mathcal{E}\,dS\cos\theta\sin\varphi = -Z_0 H\,dS\cos\theta\sin\varphi \\ dL_\varphi &= -\mathcal{E}\,dS\cos\varphi = -Z_0 H\,dS\cos\varphi \end{aligned}\right\}\ \text{m} \cdot \text{volts}$$

$$Z_0 = \sqrt{\frac{\mu}{\kappa}} \cong 376.7 \text{ ohms} \tag{902a}$$

According to Secs. 125 and 126, the elementary power directivity dD_p, which is the same as the radiation intensity, can be found from formula (838*b*) as

$$dD_p = 1.39 \times 10^{-6} f^2 \left[376.7(|dN_\theta|^2 + |dN_\varphi|^2) + \frac{1}{376.7}(|dL_\theta|^2 + |dL_\varphi|^2) + 2(|dN_\theta\,dL_\varphi| - |dN_\varphi\,dL_\theta|) \right] = \frac{0.125}{\lambda^2}[\ ] \quad \text{watts}$$

for f in megacycles per second and λ in meters. We then find

$$dD_p = \frac{(\mathcal{E}\,dS)^2}{8Z_0\lambda^2}[(-\cos\theta\cos\varphi - \cos\varphi)^2 + (\sin\varphi + \sin\varphi\cos\theta)^2] \quad \text{watts}$$

or

$$dD_p = \frac{(\mathcal{E}\, dS)^2}{8Z_0\lambda^2}(1 + \cos\theta)^2 = \frac{Z_0(H\, dS)^2}{8\lambda^2}(1 + \cos\theta)^2$$
$$= 1.39 \times 10^{-6} f^2 Z_0 (H\, dS)^2 (1 + \cos\theta)^2$$
$$= 1.39 \times 10^{-6} f^2 \frac{(\mathcal{E}\, dS)^2}{Z_0}(1 + \cos\theta)^2 \quad \text{watts} \quad (902b)$$

In air, we have, for $Z_0 \cong 376.7$ ohms,

$$dD_p = 5.25 \times 10^{-4}(fH\, dS)^2(1 + \cos\theta)^2$$
$$= 3.69 \times 10^{-9}(f\mathcal{E}\, dS)^2(1 + \cos\theta)^2 \quad \text{watts} \quad (902c)$$

which is the equivalent electromagnetic Huygens radiation intensity. This result shows that the field amplitude is a function of $(1 + \cos\theta)$ as in optics, if compared with Eq. (896*c*). We have then a directivity $(1 + \cos\theta) = 2\cos^2(\theta/2)$ as in Fig. 337 in the XY plane, for the field amplitude of an electromagnetic Huygens wavelet radiator.

210. Radiation Effect of a Slot Radiator (Wave-front Radiator of Finite Rectangular Area). In such a case, it is of advantage to orient the plane of the slot in the XY plane. Depending on the conditions of the electromagnetic field at the primary wave front occupying the slot area S in Fig. 338, we must now make certain *assumptions*, just as is done in optics, where we assume that the wave front at an aperture is the unperturbed wave front that would exist at the same plane area $S = ab$ square meters if the screen were not present. In optics, such an assumption is justified, since the wavelength of all light waves is exceedingly small compared with the dimensions of even a small aperture. We can then do the following for short electromagnetic waves: (1) We assume the primary radiation center far away and choose the screen in which the rectangular opening S of Fig. 338 represents the useful primary wave front of very large extensions in its plane. If the aperture is not too small, we can, as an approximation, neglect the edge effect and assume that the area S represents approximately an unperturbed plane primary wave front with an infinitesimal number of Huygens wavelet centers P_1, each causing a power directivity as found in Sec. 213. (2) We can also assume that the area S is large enough and in a screen that has, at least on the side facing the arriving primary wave, wave-absorbing properties so that any back reflections can be ignored. (3) We can imagine the area S as the aperture of a paraboloid with a linear radiator at the focal line of the parabolic reflector with a front opening $S = ab$ square meters. Also in this case, we have, in effect, a plane wave front, even though the distance to the primary radiator is small. (4) We can assume that the mouth of an electromagnetic horn, which is a pyramidal horn,

has in the plane of the mouth only tangential $\mathfrak{E}$ and H fields operative. This applies then also to the mouth of a rectangular wave guide in approximation, since we have to realize that in any guide, we have also, in addition, either a longitudinal $\mathfrak{E}$ or a longitudinal H field, respectively, arriving at the opening. However, as far as the distant radiation effect of the secondary mouth radiators are concerned, only the tangential

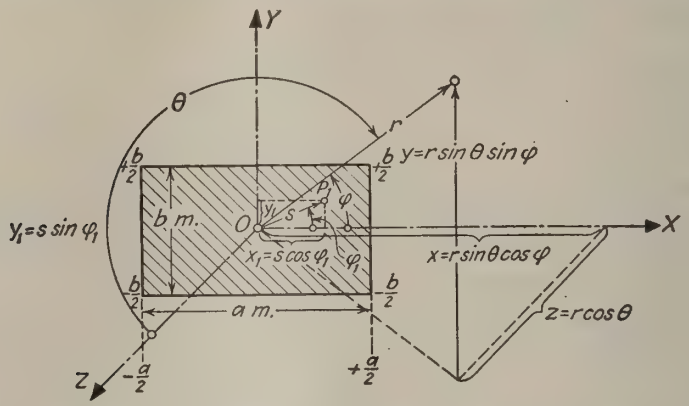

FIG. 338. Phase factor for the multitude of Huygens sources in the primary wave front of ab sq m.

$$s\cos(\varphi-\varphi_1) = \overbrace{s\cos\varphi_1}^{x_1}\cos\varphi + \overbrace{s\sin\varphi_1}^{y_1}\sin\varphi\,.$$

$S = ab$ sq m is a wave-front radiator with $dS = dx_1\,dy_1$ as a typical Huygens wavelet radiator element at P_1. φ is the angle that the projection of r makes on the XY plane with the $+X$ axis. Primary wave front in XY plane. According to Fig. 135, we have ψ as the angle between the φ, θ and φ_1, θ_1 directions based on the relation $\cos\psi_1 = \cos\theta\cos\theta_1 + \sin\theta\sin\theta_1\cos(\varphi-\varphi_1)$. Since all wavelet centers P_1 are at $x_1, y_1, z_1 = 0$, we have $\theta_1 = 90°$ (since the entire wave front is in XY plane). Hence, $\cos\psi_1 = \cos\theta\cos 90° + \sin\theta\sin 90° \times\cos(\varphi-\varphi_1) = \sin\theta\cos(\varphi-\varphi_1)$. *Note:* The angle ψ_1 has nothing in common with the angle ψ of primary wave incidence. $\epsilon^{j\beta s\sin\theta\cos(\varphi-\varphi_1)}$ is the phase factor of the various dS Huygens wavelet radiators at points P_1 all over the total radiation area $S = ab$ sq m.

fields can play a part. We can then, in effect, assume that we have fictitious electric and magnetic current sheets in the S plane of Fig. 338. We can also proceed with a solution as given in Sec. 246 of the Appendix. We have then the *ideal* case of a curtain radiator, as is discussed in Secs. 117, 118, 119. The field amplitude pattern is then based on formula (822), if applied to a curtain S with Huygens wavelet radiators like a mosaic making up the S surface. This means that we have only to multiply the dD_p elementary directivity given by (902c) by the group characteristic D_g^2 in order to obtain the power directivity of a slot radiator. The square-root value of this result must then be the amplitude directivity of wave-front radiator S. The general formula (822), for which $D_xD_yD_z$ denotes the *amplitude* group characteristic, reduces,

according to Sec. 119, to $D_g = D_x D_y$, and we can account for individual radiators, even if not excited in time phase. However, since we deal with wave-front radiators that are plane, we also have this simplification, and all Huygens wavelets start out with a common time phase. Therefore, when the plane wave front in the S opening is such that the tangential fields are $\mathcal{E}_x$ volts per meter and H_y amperes per meter, we have $\mathcal{E}_x/H_y = \sqrt{\mu/\kappa} = Z_0 \cong 376.7$ ohms. This means, in effect, that we have the [current densities $J_x = -H_y$ and $J_{m_y} = -\mathcal{E}_x$ in the coinciding electric and magnetic fictitious current sheets of the slot plane S. We find then, from (902c) and the reduced (882c) formula, where

$$\left.\begin{aligned} D_p = [dD_p]D_g^2 &= \left[0.125\,\frac{\mathcal{E}_x^2(1+\cos\theta)^2}{Z_0\lambda^2}\,S^2\right]D_g^2 \\ &= \left[0.125\,\frac{H_y^2(1+\cos\theta)^2}{\lambda^2}\,Z_0S^2\right]D_g^2 \\ D_p = [dD_p]D_g^2 &= [5.25\times 10^{-4} f^2S^2H_y^2(1+\cos\theta)^2]\,D_g^2 \\ &= [3.69\times 10^{-9} f^2S^2\mathcal{E}_x^2(1+\cos\theta)^2]\,D_g^2 \\ D_g = \frac{\sin\left(\frac{\pi a}{\lambda}\sin\theta\cos\varphi\right)}{\frac{\pi a}{\lambda}\sin\theta\cos\varphi}&\,\frac{\sin\left(\frac{\pi b}{\lambda}\sin\theta\sin\varphi\right)}{\frac{\pi b}{\lambda}\sin\theta\sin\varphi}; \qquad \lambda^{(\mathrm{m})} = \frac{300}{f^{(\mathrm{Mc})}} \end{aligned}\right\} \quad (902d)$$

a, b are in meters and (dD_p) is for all Huygens radiators taken over the total area $S = ab$ square meters.

This result can be readily proved by means of the geometry of Fig. 338. We need only to multiply the differential power directivity dD_p (power radiated by a Huygens radiator in a given direction per unit solid angle) by the phase factor $\exp[\beta s \sin\theta \times \cos(\varphi - \varphi_1)]$ and carry out the integration over the area S. We then find the total power directivity (also called "radiation intensity") as

$$\begin{aligned} D_p &= \int\int_S \epsilon^{j\beta s\sin\theta\cos(\varphi-\varphi_1)}\,dD_p \\ &= 0.125\,\frac{\mathcal{E}_x^2(1+\cos\theta)^2}{Z_0\lambda^2}\left|\int\int_{S=ab}\epsilon^{j\beta s\sin\theta\cos(\varphi-\varphi_1)}\,dS\right|^2 \\ &= 0.125\,\frac{\mathcal{E}_x^2(1+\cos\theta)^2}{Z_0\lambda^2}\left|\int_{x_1=-a/2}^{x_1=a/2}\int_{y_1=-b/2}^{y_1=b/2}\epsilon^{j\beta(x_1\cos\varphi+y_1\sin\varphi)}\,dx_1\,dy_1\right|^2 \\ &= 0.125\,\frac{\mathcal{E}_x^2a^2b^2(1+\cos\theta)^2}{Z_0\lambda^2}\,D_g^2; \qquad a^2b^2 = S^2 \text{ and } D_g \end{aligned}$$

as in (902d).

The variable portion of this result depends on the angle θ and yields the electromagnetic *Fraunhofer* pattern, which must be distinguished from the electromagnetic *Fresnel* pattern. For the Fraunhofer diffrac-

tion, all Huygens wavelets coming from the primary wave-front radiator arrive in phase at field points P on the normal to the wave front. This means that we deal with distances that are so large *in effect* (by means of a focusing lens or a focusing paraboloid) that there is no phase difference between arriving wavelets. The rays from the various Huygens dS radiators at points P_1 of area S in Fig. 338 to the distant field point P are then parallel in effect. For *Fresnel* diffraction, we also deal with distances r large compared with the dimensions of the primary wave front as well as with respect to the operating wavelength, but the distances are not of such an order of magnitude that the time phase differences between wavelets can be ignored. We even have phase differences if the primary wave arrives perpendicularly to the aperture, which acts as a mosaic of elementary Huygens radiators. The function $D_g^2(1 + \cos\theta)^2$ of (902*d*) is then the Fraunhofer pattern for electromagnetic *field energy* distribution in the distant radiation region, and $D_g(1 + \cos\theta)$ is the pattern of the *field amplitude*. Inasmuch as the rectangular wave-front radiator of Fig. 338 forces electromagnetic field flux in all directions above the plane of the paper, we should expect maximum field effect along the $+Z$ direction. For such a direction, we have $\theta = 0$, $(1 + \cos\theta) = 2$, $(1 + \cos\theta)^2 = 4$, and $D_g = 1$, since

$$D_g = \frac{\sin\left(\frac{\pi a}{\lambda}\sin\theta\cos\varphi\right)}{\underbrace{\frac{\pi a}{\lambda}\sin\theta\cos\varphi}_{=0}}\frac{\sin(0°)}{0} = \frac{0}{0} \qquad \text{undeterminate}$$

but sin (0 deg) is the sine of an angle *almost* 0 deg, or

$$\sin\left(\frac{\pi a}{\lambda}\sin\theta\cos\varphi\right) \cong \frac{\pi a}{\lambda}\sin\theta\cos\varphi$$

and

$$D_g \cong \frac{\frac{\pi a}{\lambda}\sin\theta\cos\varphi\,\frac{\pi b}{\lambda}\sin\theta\sin\varphi}{\frac{\pi a}{\lambda}\sin\theta\cos\varphi\,\frac{\pi b}{\lambda}\sin\theta\sin\varphi} = 1 \qquad \text{for } \theta \text{ very small or } \theta \to 0°$$

The power directivity yields then a maximum value

$$\left.\begin{aligned}
(D_p)_{\max} &= \frac{0.5Z_0H_y^2S^2}{\lambda^2} = \frac{0.5a^2b^2\mathcal{E}_x^2}{Z_0\lambda^2} \qquad \text{watts}\\
(D_p)_{\max} &= 2 \times 10^{-3}f^2a^2b^2H_y^2 = 1.475 \times 10^{-8}f^2a^2b^2\mathcal{E}_x^2 \qquad \text{watts}\\
a,b,\lambda &= \frac{300}{f} \qquad \text{m}
\end{aligned}\right\} \qquad (902e)$$

for f in megacycles per second, $\mathcal{E}_x$ in effective volts per meter and H_y in effective amperes per meter. We have then

$$\left.\begin{aligned} D_p &= 0.125\,\frac{\mathcal{E}_x^2(1+\cos\theta)^2}{Z_0^2\lambda^2}\,a^2b^2\,\frac{\sin^2\left(\frac{\pi a}{\lambda}\sin\theta\right)}{\frac{\pi^2a^2}{\lambda^2}\sin^2\theta} \\ &\qquad \text{watts in the } XZ \text{ plane (since } \varphi = 0°) \\ D_p &= 0.125\,\frac{\mathcal{E}_x^2(1+\cos\theta)^2}{Z_0^2\lambda^2}\,a^2b^2\,\frac{\sin^2\left(\frac{\pi b}{\lambda}\sin\theta\right)}{\frac{\pi^2b^2}{\lambda^2}\sin^2\theta} \\ &\qquad \text{watts in the } YZ \text{ plane (since } \varphi = 90°) \end{aligned}\right\} \quad (902f)$$

In these two characteristic planes, the *amplitude* directivity pattern has the form

$$\left.\begin{aligned} &k(1+\cos\theta)\,\frac{\sin p}{p}; \qquad p = \frac{\pi a}{\lambda}\sin\theta \qquad \text{in the } XZ \text{ plane} \\ &p = \frac{\pi b}{\lambda}\sin\theta \qquad \text{in the } YZ \text{ plane} \end{aligned}\right\} \quad (902g)$$

where we have expressions that are well known in optical diffraction theory, and we can make use of the computations of Table 70 and the corresponding distribution curves, since the parameter p is known from (902h).

With respect to directivity patterns of a slotted cylinder surface, reference is made to Figs. 393 and 394, and the description given in connection with these figures on page 1036 and in Sec. 250 of the Appendix. We can use a single axial slot aperture or several axial slots around the periphery of the cylindric conduction surface, in order to obtain (approach) a circular pattern in the XY plane if the slot as well as the cylinder axis is along the Z direction. For an almost circular XY pattern the respective slots must be driven by equal inphase voltages and the slots are equispaced around the cylinder. As far as the XY pattern in the radiation region is concerned, it is essentially independent of the axial field distribution along the axial slot if the slot width is chosen small compared with the operating wavelength. According to E. C. Jordan and W. E. Miller,[1] the vertical directivity pattern of a vertically slotted cylinder is about the same as for a slot aperture in a perfectly conducting sheet of very large extensions.

211. Diffractivity Tables and Curves. In Sec. 210, we found that in the XZ plane, we have an amplitude field pattern $[F_\theta \sin (p)]/p$ if

[1] *Electronics*, **20**, 90, February, 1947.

$F_\theta = (1 + \cos\theta)$ and $p = (\pi a \sin\theta)/\lambda$. In the YZ plane, we have the ratio b/λ instead of a/λ in the p relation. Table 71 gives the evaluations in terms of the a dimension but can also be applied to the b dimension in place of a. For a slot width $a = 1$, 2, 5, 10, and 20 cm, we have the patterns for the field amplitude of Fig. 339. It applies then to $\mathcal{E}_x$ and H_y polarizations and formulas (902*d*), (902*e*), (902*f*), and (902*g*). For a 3,000-Mc excitation of the primary wave, we deal then with a free-space wavelength of $\lambda = 300/3{,}000 = 0.1$ m with the corresponding ratios $a/\lambda = 0.1$, 0.2, 0.5, 1, and 2, respectively. We find the diffraction patterns in the vertical XZ plane, as in Fig. 339. If there is no backing-up screen, as at the mouth of a rectangular wave guide, we also have diffractivity below the XY plane, but no effect along the $-Z$ direction, due to the Huygens factor $(1 + \cos\theta) = (1 + \cos 180°) = 0$. We must realize, however, that at the very end of an open wave guide we have a plane with some reflections, since we have also at least one longitudinal field component in addition to the tangential $\mathcal{E}$ and H fields at the mouth. It is the tangential fields that can be substituted by fictitious electric and magnetic current sheets. We therefore have such patterns only in approximation. Besides, it is difficult to realize that the outside of the open-ended wave guide, under such conditions, is free from currents that creep around the open edge and are partially caused by such diffraction fields. However, the patterns above the XY plane of Fig. 339 should give a better approximation. Since the amplitude directivity of such a wave-front radiator, as in Fig. 339, with sufficient opening area (in order to render the edge effects small) is

$$\left.\begin{aligned} D_{\theta,\varphi} &= (1 + \cos\theta)\,\frac{\sin p}{p}\,\frac{\sin p'}{p'} \\ p &= (\sin\theta\cos\varphi)\,\frac{\pi a}{\lambda}; \qquad p' = (\sin\theta\sin\varphi)\,\frac{\pi b}{\lambda} \end{aligned}\right\} \tag{902h}$$

in the plane of the rectangular wave-front radiator ($\theta = 90$ deg), we have

$$p = \frac{\pi a}{\lambda}\cos\varphi \qquad \text{and} \qquad p' = \frac{\pi b}{\lambda}\sin\varphi \tag{902i}$$

Figure 339 shows that for $a = 2\lambda$, there can be *no* field along the $\pm X$ directions in the XY plane, which is the plane of the wave-front radiator. It is understood that the application of Table 71 and the associated Fig. 339 is much broader, since they apply for the given ratios a/λ generally and are not limited to the centimeter dimensions for a, which has *meaning only if expressed in terms of* the 0.1-m *wavelength* corresponding to a 3,000-Mc/sec excitation. This is generally true in all radiation problems, since it is *not* the absolute value of a dimension but the value of a par-

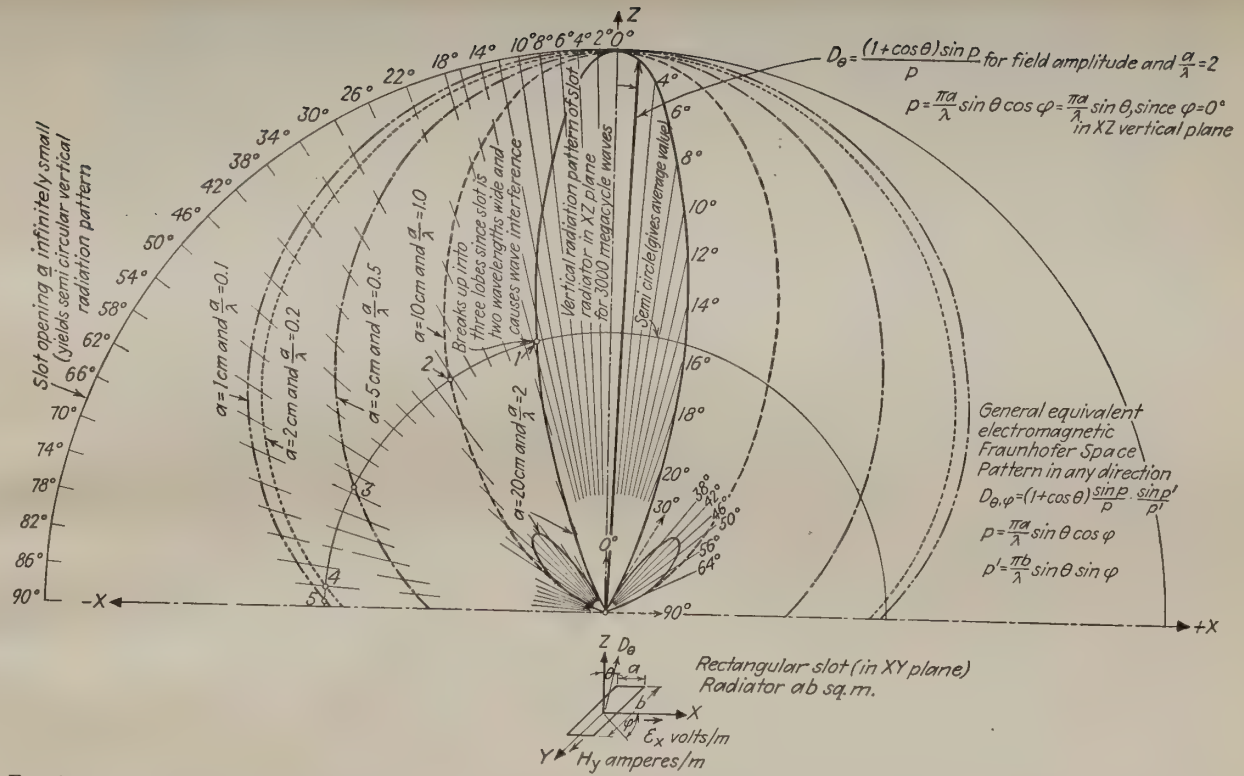
Z
0° 2° 4° 6° 8° 10° 14° 18° 22° 26° 30° 34° 38° 42° 46° 50° 54° 58° 62° 66° 70° 74° 78° 82° 86° 90°
$D_\theta = \frac{(1+\cos\theta)\sin p}{p}$ for field amplitude and $\frac{a}{\lambda}=2$
$p = \frac{\pi a}{\lambda}\sin\theta\cos\varphi = \frac{\pi a}{\lambda}\sin\theta$, since $\varphi=0°$ in XZ vertical plane
Slot opening a infinitely small (yields semi circular vertical radiation pattern
$a=1$cm and $\frac{a}{\lambda}=0.1$
$a=2$cm and $\frac{a}{\lambda}=0.2$
$a=5$cm and $\frac{a}{\lambda}=0.5$
$a=10$cm and $\frac{a}{\lambda}=1.0$
Breaks up into three lobes since slot is two wavelengths wide and causes wave interference
$a=20$cm and $\frac{a}{\lambda}=2$
Vertical radiation pattern of slot radiator in XZ plane for 3000 megacycle waves
Semi circle gives average value
General equivalent electromagnetic Fraunhofer Space Pattern in any direction
$D_{\theta,\varphi}=(1+\cos\theta)\frac{\sin p}{p}\cdot\frac{\sin p'}{p'}$
$p=\frac{\pi a}{\lambda}\sin\theta\cos\varphi$
$p'=\frac{\pi b}{\lambda}\sin\theta\sin\varphi$
-X
+X
90°
Rectangular slot (in XY plane) Radiator ab sq. m.
Z D_θ
a
b
X
Y
$\mathcal{E}_x$ volts/m
Hy amperes/m

FIG. 339. Fraunhofer diffraction field amplitude pattern for an electromagnetic slot radiator. Points 1, 2, 3, 4, and 5 show vertical direction vector extremities giving average possible radiation effect.

TABLE 71. DIFFRACTION PATTERN IN THE XZ PLANE FOR $\mathcal{E}_x$ AND H_y POLARIZATIONS (FIG. 339)*

θ, deg	Wave forward factor $F_\theta = 1 + \cos\theta$	Slot width $a = 1$ cm makes $\frac{a}{\lambda} = 0.1$ and $p = 0.314 \sin\theta = p_1$; $\frac{\sin p}{p}$ is taken from Table 70 or from Fig. 335				Slot width $a = 2$ cm; $\frac{a}{\lambda} = 0.2$; $p = 0.618 \sin\theta = 2p_1$			Slot width $a =$ 5 cm; $\frac{a}{\lambda} = 0.5$; $p = 5p_1$			Slot width $a =$ 10 cm; $\frac{a}{\lambda} = 1$; $p =$ $3.14 \sin\theta = 10p_1$			Slot width $a = 20$ cm; $\frac{a}{\lambda} = 2$; $p = 20p_1$		
		$\sin\theta$	$p = p_1$	$\frac{\sin p}{p}$	$F_\theta \times \frac{\sin p}{p}$	$p = 2p_1$	$\frac{\sin p}{p}$	$F_\theta \times \frac{\sin p}{p}$	$p = 5p_1$	$\frac{\sin p}{p}$	$F_\theta \times \frac{\sin p}{p}$	$p = 10p_1$	$\frac{\sin p}{p}$	$F_\theta \times \frac{\sin p}{p}$	$p = 20p_1$	$\frac{\sin p}{p}$	$F_\theta \frac{\sin p}{p}$
0	2.000	0.0000	0.000	1.0000	2.000	0.000	1.0000	2.000	0.000	1.0000	2.000	0.000	1.0000	2.000	0.000	1.0000	2.000
2	1.999	0.035	0.011	1.0000	1.999	0.022	0.9999	1.999	0.055	0.9996	1.999	0.11	0.998	1.998	0.22	0.992	1.98
4	1.998	0.07	0.022	0.9999	1.998	0.044	0.9997	1.993	0.11	0.998	1.99	0.22	0.992	1.984	0.44	0.968	1.92
6	1.994	0.104	0.0325	0.9998	1.994	0.065	0.9993	1.993	0.162	0.9954	1.982	0.325	0.9825	1.96	0.65	0.9311	1.86
8	1.99	0.139	0.0436	0.9997	1.99	0.0872	0.9988	1.985	0.218	0.992	1.978	0.436	0.9688	1.925	0.872	0.8775	1.74
10	1.985	0.174	0.0545	0.9996	1.985	0.109	0.998	1.98	0.272	0.9879	1.96	0.545	0.9512	1.9	1.09	0.8134	1.62
12	1.9781	0.208	0.0654	0.9994	1.98	0.1308	0.9972	1.97	0.327	0.9819	1.94	0.654	0.9303	1.84	1.308	0.7375	1.46
14	1.9703	0.242	0.076	0.9989	1.968	0.152	0.9962	1.96	0.38	0.9761	1.92	0.76	0.9065	1.78	1.52	0.657	1.295
16	1.9613	0.276	0.087	0.9987	1.958	0.174	0.9949	1.95	0.435	0.9687	1.9	0.87	0.8785	1.72	1.74	0.5665	1.11
18	1.9511	0.309	0.097	0.9983	1.945	0.194	0.9938	1.94	0.485	0.9612	1.87	0.97	0.8504	1.66	1.94	0.4807	0.937
20	1.939	0.342	0.107	0.998	1.934	0.214	0.9924	1.923	0.535	0.953	1.847	1.07	0.8198	1.59	2.14	0.3936	0.765
22	1.927	0.375	0.118	0.9976	1.925	0.236	0.9907	1.91	0.59	0.943	1.82	1.18	0.7836	1.52	2.36	0.2985	0.575
24	1.913	0.407	0.128	0.9972	1.9	0.256	0.9891	1.88	0.64	0.9331	1.78	1.28	0.7484	1.426	2.56	0.2146	0.411
26	1.899	0.438	0.138	0.9967	1.89	0.276	0.9883	1.87	0.69	0.9225	1.75	1.38	0.7115	1.35	2.76	0.13493	0.255
28	1.883	0.47	0.148	0.9963	1.87	0.296	0.9854	1.85	0.74	0.9112	1.72	1.48	0.6729	1.265	2.96	0.06101	0.1145
30	1.866	0.5	0.157	0.9957	1.86	0.314	0.9836	1.84	0.785	0.9004	1.68	1.57	0.6369	1.185	3.14	0.00000	0.0000
32	1.848	0.53	0.166	0.9952	1.84	0.332	0.9812	1.82	0.83	0.8891	1.64	1.66	0.6	1.11	3.32	−0.065	−0.12
34	1.829	0.56	0.176	0.9946	1.82	0.352	0.9793	1.79	0.88	0.8758	1.6	1.76	0.558	1.02	3.52	−0.1	−0.183
36	1.809	0.59	0.186	0.994	1.8	0.372	0.977	1.76	0.93	0.862	1.56	1.86	0.5153	0.932	3.72	−0.14	−0.254
38	1.788	0.616	0.194	0.9937	1.78	0.388	0.9752	1.74	0.97	0.8504	1.52	1.94	0.4807	0.86	3.88	−0.163	−0.291
40	1.766	0.643	0.202	0.9933	1.76	0.404	0.9728	1.72	1.01	0.8384	1.48	2.02	0.4459	0.79	4.04	−0.192	−0.34
42	1.743	0.67	0.21	0.9927	1.73	0.42	0.9709	1.7	1.05	0.8261	1.44	2.1	0.4111	0.715	4.2	−0.21	−0.365

	44	1.719	0.695	0.218	0.992	1.705	0.436	0.9686	1.66	1.09	0.8134	1.4	2.18	0.3762	0.65	4.36	−0.215	−0.37
	46	1.695	0.72	0.225	0.9916	1.68	0.450	0.9666	1.63	1.125	0.8019	1.36	2.25	0.3458	0.585	4.5	−0.216	−0.366
	48	1.669	0.74	0.232	0.9911	1.66	0.464	0.9643	1.61	1.16	0.7903	1.32	2.32	0.3156	0.503	4.64	−0.21	−0.35
	50	1.643	0.766	0.24	0.9904	1.62	0.48	0.962	1.58	1.2	0.7767	1.275	2.4	0.2814	0.46	4.8	−0.206	−0.339
	52	1.6157	0.788	0.246	0.99	1.6	0.492	0.96	1.55	1.23	0.7663	1.24	2.46	0.2561	0.414	4.92	−0.2	−0.323
	54	1.5878	0.809	0.253	0.989	1.57	0.506	0.958	1.52	1.265	0.7533	1.2	2.53	0.2269	0.36	5.06	−0.185	−0.294
	56	1.5592	0.829	0.259	0.9887	1.545	0.518	0.9552	1.49	1.295	0.7430	1.16	2.59	0.2023	0.311	5.18	−0.172	−0.268
	58	1.5299	0.848	0.265	0.9884	1.51	0.53	0.9538	1.46	1.325	0 7320	1.12	2.65	0.1781	0.265	5.3	−0.157	−0.244
	60	1.5	0.866	0.271	0.9879	1.48	0.542	0.9515	1.43	1.355	0.7209	1.08	2.71	0.1544	0.231	5.42	−0.14	−0.21
	62	1.4695	0.8829	0.276	0.9874	1.445	0.552	0.9496	1.4	1.38	0.7115	1.05	2.76	0.1388	0.204	5.52	−0.12	−0.176
	64	1.4384	0.8988	0.281	0.987	1.42	0.562	0.9480	1.36	1.405	0.7020	1.01	2.81	0.1158	0.167	5.62	−0.098	−0.141
	66	1.4067	0.9135	0.286	0.9864	1.39	0.572	0.9463	1.334	1.43	0.6924	0.975	2.86	0.0972	0.137	5.72	−0.08	−0.113
	68	1.3746	0.9272	0.29	0.986	1.345	0.58	0.9449	1.295	1.45	0.6846	0.94	2.9	0.0825	0.113	5.8	−0.06	−0.082
	70	1 342	0.9397	0.294	0.9855	1.32	0.588	0.943	1.26	1.47	0.6768	0.905	2.94	0.0668	0.09	5.88	−0.046	−0.0615
	72	1.309	0.9511	0.299	0.9852	1.29	0.598	0.9415	1.235	1.495	0.6670	0.87	2.99	0.0505	0.066	5.98	−0.02	−0.0262
	74	1.2756	0.9613	0.302	0.9849	1.25	0.604	0.9404	1.195	1.51	0.661	0.84	3.02	0.0402	0.051	6.04	−0.01	−0.0127
	76	1.2419	0.9703	0.304	0.9846	1.22	0.608	0.9398	1.16	1.52	0.657	0.81	3.04	0.0334	0.0414	6.08	−0.005	−0.0062
	78	1.2079	0.9781	0.306	0.9844	1.19	0.612	0.9388	1.135	1.53	0.6531	0.79	3.06	0.0266	0.0322	6.12	−0.003	−0.0036
	80	1.1736	0.9848	0.308	0.9842	1.15	0.616	0.9379	1.1	1.54	0.649	0.76	3.08	0.0199	0.0234	6.16	−0.002	−0.0023
	82	1.1392	0.9903	0.31	0.9841	1.12	0.62	0.9372	1.065	1.55	0.645	0.73	3.1	0.0134	0.0152	6.2	−0.001	−0.0011
	84	1.1045	0.9945	0.312	0.9840	1.085	0.624	0.9362	1.03	1.56	0.641	0.71	3.12	0.0069	0.0076	6.24	−0.0006	−0.0006
	86	1.0698	0.9976	0.313	0.9838	1.055	0.626	0.9358	1.00	1.565	0.6389	0.68	3.13	0.0037	0.00395	6.26	−0.0004	−0.0004
	88	1.0349	0.9994	0.3135	0.9837	1.015	0.627	0.9357	0.96	1.567	0.638	0.655	3.135	0.0018	0.00186	6.27	−0.0002	−0.0002
	90	1.0000	1.0000	0.314	0.9835	0.9835	0.628	0.9356	0.936	1.57	0.6369	0.637	3.14	0.0000	0.0000	6.28	0.0000	0.0000
	95	0.9128	0.9962	0.312	0.984	0.9	0.624	0.9362	0.853	1.56	0.649	0.59	3.12	0.0069	0.0063	6.24	−0.0006	−0.00054
	100	0.8264	0.9848	0.309	0.9841	0.813	0.618	0.9375	0.77	1.545	0.647	0.533	3.09	0.0167	0.0138	6.18	−0.001	−0.00082
	105	0.7412	0.9659	0.303	0.9847	0.73	0.606	0.94	0.696	1.515	0.6590	0.487	3.03	0.0367	0.0271	6.06	−0.007	−0.0052
	110	0 658	0.9387	0.294	0.9855	0 645	0.588	0.943	0.62	1.47	0.6768	0.444	2.94	0.0668	0.0438	5.88	−0.046	−0.035
	115	0.5774	0.9063	0.284	0.9867	0.568	0.568	0.947	0.543	1.42	0.6962	0.4	2.84	0.1046	0.063	5.68	−0.08	−0.046
This range applies	120	0.5	0.866	0.271	0.9879	0.4939	0.542	0.9515	0.4757	1.355	0.7209	0.3604	2.71	0.1544	0.0772	5.42	−0.14	−0.07
only when no	125	0.4264	0.8192	0.256	0.9892	0.42	0.512	0.9571	0.407	1.28	0.7484	0.318	2.56	0.2146	0.0915	5.12	−0.178	−0.076
backing-up	130	0.3572	0.766	0.24	0.9904	0.354	0.48	0.962	0.344	1.2	0.7767	0.276	2.4	0.2814	0.1	4.8	−0.206	−0.0735
screen exists	135	0.2929	0.7071	0.221	0.992	0.29	0.442	0.9675	0.282	1.105	0.8085	0.236	2.21	0.3632	0.106	4.42	−0.215	−0.063
	140	0.234	0.6428	0.202	0.9933	0.233	0.404	0.9728	0.227	1.01	0.8384	0.196	2.02	0.4459	0.104	4.04	−0.192	−0.0449
	150	0.134	0.5	0.157	0.9957	0.133	0.314	0.9836	0.132	0.785	0.9004	0.1205	1.57	0.6369	0.085	3.14	0.000	0.0000
	160	0.0603	0.342	0.107	0.998	0.06	0.214	0.9924	0.059	0.535	0.9529	0.0573	1.07	0.8198	0.0494	2.14	0.3936	0.0236
	170	0.0152	0.1736	0.055	0.9996	0.0152	0.11	0.998	0.01518	0.275	0.9875	0.015	0.55	0.9503	0.0144	1.1	0.8134	0.0123
	180	0.0000	0.0000	0.000	1.0000	0.0000	0.000	1.0000	0.000	0.000	1.0000	0.0000	0.00	1.0000	0.0000	0.00	1.0000	0.0000

* See *Remarks* on p. 1100.

Remarks (with the patterns of Fig. 339): $F_\theta(\sin p)/p$ is the diffraction field pattern in the XZ plane of Fig. 338 for which $\varphi = 0$ deg and $p = \pi(a/\lambda) \sin \theta$, according to formula (902*h*). If we replace a by the b dimension, we have the pattern in the YZ plane. We have $F_\theta = 1 + \cos \theta$; the angle θ is the angle that the direction r, from the center of the wave front $S = ab$ sq m to the distant field point P, makes with the normal to the wave front. Generally, the field amplitude space directivity is

$$D_{\theta,\varphi} = (1 + \cos \theta) \frac{\sin p}{p} \frac{\sin p'}{p'}$$

for

$$p = \frac{\pi a}{\lambda} \sin \theta \cos \varphi$$

$$p' = \frac{\pi b}{\lambda} \sin \theta \sin \varphi$$

where a m is along the X axis and b m along the Y axis. $x = r \sin \theta \cos \varphi$, $y = r \sin \theta \sin \varphi$ and $z = r \cos \theta$ are the coordinates of the distant field point P with respect to the central point of the aperture in the screen (mid-point of the primary wave front). Note that the evaluations for $\theta = 90$ to 180 deg *cannot* be instrumental if we deal with a slot radiator or a wave-front window in a large screen, but it plays a part in a parabolic projector and in open-ended rectangular wave guides.

For $f = 3{,}000$ Mc/sec,

$$\lambda = \frac{300}{3{,}000} = 0.1 \text{ m}$$

ticular *dimension in terms of the operating wavelength. In optics, we are fortunate,* since the wavelengths of all light waves are exceedingly short. Thus the green spectrum line from a mercury-vapor source is only $\lambda = 0.00005461$ cm, and it takes 2.54 cm to make an inch. This is the reason why we use angstrom units in optics, where *one* angstrom unit (AU) $= 10^{-8}$ cm. For this reason, even the smallest obstacle in optics throws a shadow (gives a dark zone behind it). For the very shortest *commercial* radio waves, we are still in the centimeter, perhaps also in the millimeter, range for the wavelength, and we can avoid the no-field zone due to a small obstacle, since the wavelength of the electromagnetic wave may be large enough to *diffract around the obstacle.* Let us see what happens to the field amplitude in the general case of a vertical plane (a plane normal to the wave-front radiator of Fig. 339, making an angle of $\varphi = 45$ deg with the XZ plane, and a square-shaped wave-front radiator, with sides that are either a half wavelength long or 2λ long, respectively. Table 72 gives the evaluations and Fig. 340 gives the corresponding diffraction patterns for the field amplitude. In Table 75 and Fig. 339, we found for $\theta = 30$ deg a dead spot if the vertical pattern is in the XZ plane ($\varphi = 0$ deg) and $a = 2\lambda$. This also holds for $a = b = 2\lambda$. But in Table 72 and Fig. 340, we find that for the vertical plane ($\varphi = 45$ deg), the dead spot moves about equal to $\theta = 45$ deg, since in Table 76, for $\theta = 44$ deg, we have $p = 3.07$ and, for $\theta = 46$ deg, we have $p = 3.17$, where $p = 3.14$ makes $(\sin p)/p = 0$. Therefore, somewhere between 44 and 46 deg, we must have a zero field region. Table 73 gives the computations for the horizontal patterns of square-shaped wave-front radiators for the respective side lengths 0.1λ, 0.5λ, λ, and 2λ meters. The corresponding patterns of Fig. 341 show that for a wave-front area of $0.25\lambda^2$ square meters, we have a circular pattern of relative amplitude 0.637 as against unity value, which is the largest magnitude possible in the XY plane, while the value 2 is the optimum value of the amplitude normal to the slot, on account of the wavelet factor $(1 + \cos\theta) = (1 + \cos 0 \text{ deg}) = 2$. All other patterns given in Figs. 341 and 342, in the plane of the rectangular wave-front radiators, show that the pattern in the plane of the wave-front radiator may break up into lobes, leaving regions with no electromagnetic field energy. In Table 73, we note that the magnitudes of the D_φ values, for $a = b = 0.1\lambda$, λ, and 2λ, are relatively small compared with the magnitudes of the D_φ values for $a = b = \lambda/2$. For this reason, the patterns in Fig. 341 use a tenfold D_φ scale for the 0.1λ, 1λ, and 2λ sides of the square wave-front radiator in order to show the diffractivities in comparison with the 0.5λ sides of a square wave-front radiator. Table 74 and Fig. 342 show what happens in the plane of a rectangular wave front ($a \neq b$). The computations are based

Table 72. Evaluation of the Vertical Diffraction Pattern, for Which $\varphi = 45°$ Is the Angle against the XZ Plane

θ, deg	$D_{\theta,\varphi} = (1 + \cos\theta)\left(\frac{\sin p}{p}\right)^2$ for $\varphi = 45°$ and $a = b = \frac{\lambda}{2}$					$D_{\theta,\varphi}$ for $\varphi = 45°$ and $a = b = 2\lambda$			
	p	$\frac{\sin p}{p}$	$\left(\frac{\sin p}{p}\right)^2$	$1 + \cos\theta = F_\theta$	$D_{\theta,\varphi}$	p	$\frac{\sin p}{p}$	$\left(\frac{\sin p}{p}\right)^2$	$D_{\theta,\varphi}$
0	0.000	1.0000	1.000	2.0000	2.000	0.00	1.0000	1.0000	2.0000
4	0.078	0.999	0.998	1.998	1.99	0.31	0.9841	0.968	1.93
8	0.154	0.995	0.99	1.99	1.97	0.615	0.938	0.88	1.75
12	0.231	0.991	0.982	1.9781	1.94	0.923	0.864	0.746	1.48
16	0.306	0.984	0.968	1.9613	1.9	1.23	0.7663	0.586	1.15
20	0.378	0.976	0.952	1.939	1.84	1.51	0.661	0.436	0.845
24	0.451	0.967	0.935	1.913	1.78	1.81	0.537	0.288	0.55
28	0.522	0.954	0.91	1.883	1.71	2.09	0.415	0.172	0.325
30				1.866		2.21	0.363	0.132	0.246
32	0.59	0.943	0.889	1.848	1.64	2.34	0.307	0.094	0.174
36	0.66	0.929	0.863	1.809	1.56	2.62	0.1902	0.036	0.065
40	0.715	0.917	0.841	1.766	1.48	2.85	0.10087	0.0102	0.018
44	0.77	0.904	0.817	1.719	1.4	3.07	0.0233	0.0005	0.00086
46				1.695		3.17	−0.02	0.0004	0.00068
48	0.82	0.892	0.794	1.669	1.33	3.26	−0.05	0.0025	0.00416
52	0.87	0.878	0.771	1.6157	1.24	3.46	−0.09	0.0081	0.0131
56	0.91	0.868	0.753	1.5592	1.18	3.65	−0.13	0.0169	0.0264
60	0.955	0.854	0.729	1.5	1.09	3.84	−0.16	0.0256	0.0385
64	0.99	0.844	0.712	1.4384	1.02	3.96	−0.18	0.0324	0.0465
68	1.02	0.835	0.697	1.3746	0.955	4.1	−0.2	0.04	0.0548
72	1.06	0.823	0.677	1.309	0.885	4.21	−0.21	0.0441	0.0578
76	1.07	0.8198	0.672	1.2419	0.835	4.28	−0.213	0.0454	0.0563
80	1.09	0.8134	0.661	1.1736	0.775	4.35	−0.215	0.0462	0.054
84	1.1	0.8102	0.656	1.1045	0.72	4.4	−0.217	0.0471	0.052
88	1.11	0.8069	0.651	1.0349	0.69	4.41	−0.216	0.0467	0.048
90	1.11	0.8069	0.651	1.0000	0.65	4.41	−0.214	0.0467	0.0467

Remarks (patterns in Fig. 340): Since $a = b = 0.5\lambda$, and $\varphi = 45$ deg, for which $\sin\varphi = 0.7071$, we have in the general diffraction formula of Fig. 340 the arguments $p = p'$ and

$$D_{\theta,\varphi} = (1 + \cos\theta)\frac{\sin^2 p}{p^2}$$

where

$$p = 0.5\pi \cdot 0.7071 \sin\theta = 5p_1 \cdot 0.7071.$$

The value of $5p_1$ is taken from the $p = 5p_1$ column of Table 71. For $a = b = 2\lambda$, we use the $p = 20p_1$ column of Table 71 and multiply by 0.7071.

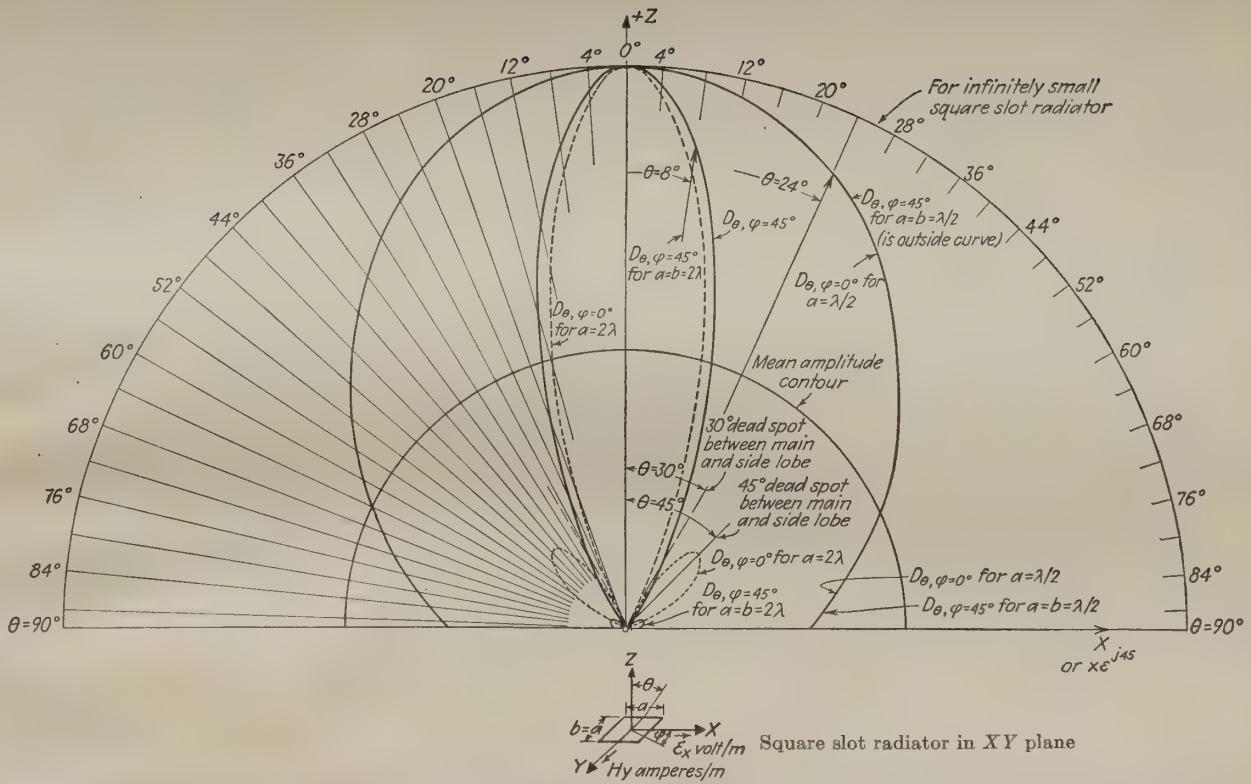

FIG. 340. Fraunhofer diffraction field amplitude pattern for a square-shaped electromagnetic slot radiator. *Note:* Dead spot shifts from 30 to 45° as vertical plane is turned by 45° from the ZX orientation about the Z axis.

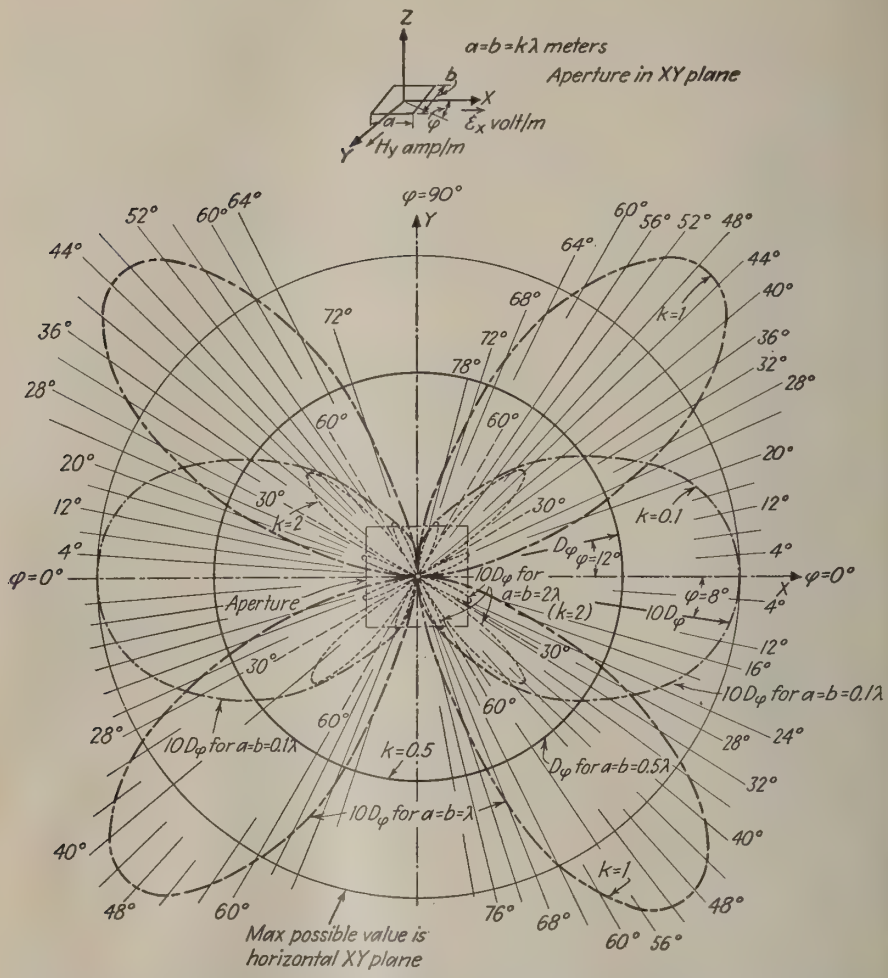

FIG. 341. Fraunhofer equivalent radiation patterns for electromagnetic aperture radiators in the plane of the aperture about the Z axis. Note that the 0.1λ, λ, and 2λ patterns for the side of the square primary wave front on which the many wavelet radiation centers are located require a tenfold large radius vector in order to show up the D_φ pattern.

on choosing appropriate dimensions, so that the evaluations of Table 73 can be applied. For instance, if we have a slot radiator of dimensions $a = 0.1\lambda$ long and $b = 0.5\lambda$ meters wide, where a is along the X and b along the Y axis, with $\mathcal{E}_x$ and H_y polarizations, we find

$$p = 0.1\pi \sin\theta \cos\varphi = 0.314 \cos\varphi; \qquad p' = 0.5\pi \sin\theta \sin\varphi = 1.57 \sin\varphi$$

in the plane of the slot. It is then only necessary to use the column of $(\sin p)/p$ values, for $a = b = 0.1\lambda$ computations of Table 73, and to

TABLE 73. HORIZONTAL ELECTROMAGNETIC FRAUNHOFER FIELD AMPLITUDE PATTERNS FOR SQUARE-SHAPED WAVE-FRONT RADIATORS

φ, deg	$a = b = \frac{\lambda}{2}$ renders $p = 0.5\pi \cos\varphi$, $p' = 0.5\pi \sin\varphi$ $= 5p_1$, where p_1 is taken from Table 75 by substituting φ for θ						$a = b = \lambda$ renders $p = \pi \cos\varphi$ and $p' = \pi \sin\varphi = 10p_1$, where $10p_1$ and $(\sin p')/p'$ are taken from Table 75				$a = b = 2\lambda$ renders $p = 6.28 \cos\varphi$ and $p' = 6.28 \sin\varphi = 20p_1$, where $20p_1$ and $(\sin p')/p'$ are taken from Table 75				$a = b = 0.1\lambda$ renders $p = 0.314 \times \cos\varphi$ and $p' = 0.314 \sin\varphi = p_1$, where p_1 and $(\sin p')/p'$ are taken from Table 75			
	$\cos\varphi$	$1.57 \times \cos\varphi = p$	$\frac{\sin p}{p}$	$\frac{\sin p'}{p'}$	$D\varphi = \frac{\sin p}{p}\frac{\sin p'}{p'}$		$p = 3.14 \times \cos\varphi$	$\frac{\sin p}{p}$	$\frac{\sin p'}{p'}$	$D\varphi$	$p = 6.28 \times \cos\varphi$	$\frac{\sin p}{p}$	$\frac{\sin p'}{p'}$	$D\varphi$	$p = 0.314 \times \cos\varphi$	$\frac{\sin p}{p}$	$\frac{\sin p'}{p'}$	$D\varphi$
0	1.0000	1.57	0.6369	1.0000	0.6369		3.14	0.0000	1.0000	0.0000	6.28	0.000	1.0000	0.0000	0.314	0.1000	1.0000	0.10000
4	0.9976	1.565	0.639	0.998	0.6385		3.13	0.004	0.992	0.00396	6.26	−0.001	0.968	−0.00097	0.313	0.1	0.9999	0.09999
8	0.9903	1.555	0.643	0.992	0.6395		3.1	0.0134	0.9688	0.013	6.2	−0.004	0.8775	−0.0035	0.31	0.099	0.9997	0.0989
12	0.9781	1.54	0.649	0.9819	0.64		3.06	0.027	0.9303	0.0251	6.12	−0.008	0.7375	−0.0059	0.306	0.096	0.9994	0.0959
16	0.9613	1.51	0.661	0.9687	0.64		3.02	0.0402	0.8785	0.0351	6.04	−0.012	0.5665	−0.0068	0.302	0.094	0.9987	0.0937
20	0.9387	1.47	0.6768	0.953	0.645	Approximate	2.94	0.068	0.8198	0.0558	5.88	−0.035	0.3936	−0.0138	0.294	0.089	0.998	0.0887
24	0.9135	1.44	0.6885	0.933	0.648	slide-rule re-	2.86	0.0972	0.7484	0.0727	5.72	−0.08	0.2146	−0.0172	0.286	0.084	0.9972	0.0837
28	0.8829	1.38	0.7115	0.911	0.65	sults, but in	2.77	0.1311	0.6729	0.088	5.54	−0.11	0.061	−0.0067	0.277	0.077	0.9963	0.0766
30	0.866					reality a cir-					5.42	−0.128	0.0000	0.0000				
32	0.848	1.33	0.7302	0.8891	0.65	cular pattern	2.65	0.1781	0.6	0.107	5.3	−0.155	−0.065	0.01	0.265	0.071	0.9952	0.0707
36	0.809	1.27	0.752	0.862	0.65	(Fig. 341) of	2.53	0.227	0.5153	0.117	5.06	−0.187	−0.14	0.0261	0.253	0.065	0.994	0.0647
40	0.766	1.2	0.7767	0.8384	0.65	radius $2/\pi$ =	2.41	0.2772	0.4459	0.124	4.82	−0.205	−0.192	0.0394	0.241	0.058	0.9933	0.0577
44	0.7193	1.13	0.8004	0.8134	0.65	0.6337	2.25	0.3458	0.3762	0.131	4.5	−0.217	−0.215	0.0466	0.225	0.051	0.992	0.0507
48	0.6691	1.05	0.8261	0.7903	0.65		2.09	0.4154	0.3156	0.1315	4.18	−0.208	−0.21	0.04	0.209	0.045	0.9911	0.0445
52	0.6157	0.965	0.851	0.7663	0.65		1.93	0.4851	0.2561	0.124	3.86	−0.16	−0.2	0.032	0.193	0.038	0.99	0.0376
56	0.5592	0.88	0.8758	0.743	0.65		1.75	0.5623	0.2023	0.114	3.5	−0.1	−0.172	0.0172	0.175	0.03	0.9887	0.0295
60	0.5	0.785	0.905	0.721	0.65		1.57	0.6369	0.1544	0.098	3.14	0.0000	−0.14	0.0000	0.157	0.024	0.9869	0.0237
64	0.4384	0.685	0.9235	0.702	0.65		1.37	0.7153	0.1158	0.083	2.74	0.14267	−0.098	−0.014	0.137	0.018	0.987	0.0178
68	0.3746	0.59	0.943	0.685	0.649		1.18	0.7836	0.0825	0.0747	2.36	0.2985	−0.06	−0.0179	0.118	0.014	0.986	0.0138
72	0.309	0.485	0.9612	0.667	0.642		0.97	0.8504	0.0505	0.043	1.94	0.481	−0.02	−0.00962	0.097	0.01	0.9852	0.009852
76	0.2419	0.38	0.9761	0.657	0.64		0.76	0.9065	0.0334	0.0302	1.52	0.657	−0.005	−0.00334	0.076	0.006	0.9846	0.0059
80	0.1736	0.272	0.9877	0.649	0.64		0.546	0.949	0.0199	0.0188	1.092	0.813	−0.002	−0.00162	0.0546	0.0025	0.9842	0.00246
84	0.1045	0.164	0.9982	0.641	0.64		0.326	0.9825	0.0069	0.0068	0.652	0.9308	−0.0006	−0.00056	0.0326	0.0009	0.984	0.000885
88	0.0349	0.055	0.9996	0.638	0.638		0.109	0.998	0.0018	0.0018	0.218	0.049	−0.0002	−0.00001	0.0109	0.0001	0.9837	0.0000984
90	0.0000	0.000	1.0000	0.6369	0.6369		0.000	1.0000	0.0000	0.0000	0.000	0.0000	0.0000	0.00000	0.0000	0.0000	0.9835	0.0000000

Remarks: Since the diffractivity $D_{\theta,\varphi}$ in any space direction θ, φ is

$$D_{\theta,\varphi} = (1 + \cos\theta)\frac{\sin p}{p}\frac{\sin p'}{p'}$$

we have in the XY plane $\theta = 90$ deg,

$$(1 + \cos\theta) = 1 \qquad p = \frac{\pi a}{\lambda}\sin\theta\cos\varphi = \frac{\pi a}{\lambda}\cos\varphi \qquad p' = \frac{\pi b}{\lambda}\sin\theta\sin\varphi = \frac{\pi b}{\lambda}\sin\varphi$$

We have for square-shaped wave-front radiators $a = b$, and the $(\sin p')/p'$ factor in this table must be exactly the same for φ values of this table as is the corresponding $(\sin p)/p$ factor for θ values in Table 71. Table 73 gives the evaluations for square wave-front radiators of areas equal to $0.01\lambda^2$, $0.25\lambda^2$, λ^2, and $4\lambda^2$ sq m. The $4\lambda^2$ sq m pattern gives a maximum directivity along 45-deg directions with respect to the X and Y axes, while no radiation occurs along the $\pm X$ and $\pm Y$ directions of the plane of the wave front.

TABLE 74. ELECTROMAGNETIC FRAUNHOFER DIFFRACTIVITY IN THE PLANE OF A RECTANGULAR WAVE-FRONT RADIATOR

φ, deg	Wave-front radiator $a = 0.1\lambda$ and $b = 0.5\lambda$			$a = 0.5\lambda$; $b = 0.1\lambda$			$a = \lambda$; $b = 0.1\lambda$			$a = 0.5\lambda$; $b = \lambda$			$a = \lambda$; $b = 0.5\lambda$		
	$A = \frac{\sin p}{p}$	$B = \frac{\sin p'}{p'}$	$D_\varphi = AB$	$A = \frac{\sin p}{p}$	$B = \frac{\sin p'}{p'}$	$D_\varphi = AB$	$A = \frac{\sin p}{p}$	$B = \frac{\sin p'}{p'}$	$D_\varphi = AB$	$A = \frac{\sin p}{p}$	$B = \frac{\sin p'}{p'}$	$D_\varphi = AB$	$A = \frac{\sin p}{p}$	$B = \frac{\sin p'}{p'}$	$D_\varphi = AB$
0	0.1000	1.0000	0.1000	0.6369	1.0000	0.637	0.0000	1.0000	0.0000	0.6369	1.0000	0.6369	0.0000	1.0000	0.0000
4	0.1	0.998	0.0998	0.639	0.9999	0.639	0.004	0.9999	0.004	0.639	0.992	0.633	0.004	0.998	0.00398
8	0.099	0.992	0.0983	0.643	0.9997	0.643	0.0134	0.9997	0.0134	0.643	0.9688	0.621	0.0134	0.992	0.0133
12	0.096	0.9819	0.0945	0.649	0.9994	0.649	0.027	0.9994	0.027	0.649	0.9303	0.605	0.027	0.9819	0.0265
16	0.094	0.9687	0.091	0.661	0.9987	0.661	0.0402	0.9987	0.0401	0.661	0.8785	0.58	0.0402	0.9687	0.0388
20	0.089	0.953	0.085	0.6768	0.998	0.672	0.068	0.998	0.0678	0.6768	0.8198	0.553	0.068	0.953	0.0649
24	0.084	0.933	0.0785	0.6885	0.9972	0.685	0.0972	0.9972	0.0968	0.6885	0.7484	0.514	0.0972	0.933	0.0908
28	0.077	0.911	0.0703	0.7115	0.9963	0.707	0.1311	0.9963	0.1305	0.7115	0.6729	0.48	0.1311	0.911	0.119
32	0.071	0.8891	0.063	0.7302	0.9952	0.727	0.1781	0.9952	0.177	0.7302	0.6	0.44	0.17812	0.8891	0.158
36	0.065	0.862	0.056	0.752	0.994	0.748	0.227	0.994	0.226	0.752	0.5153	0.388	0.227	0.862	0.196
40	0.058	0.8384	0.0485	0.7767	0.9933	0.77	0.2772	0.9933	0.275	0.7767	0.4459	0.346	0.2772	0.8384	0.232
44	0.051	0.8134	0.0415	0.8004	0.992	0.795	0.3458	0.992	0.344	0.8004	0.3762	0.302	0.3458	0.8134	0.281
48	0.045	0.7903	0.0355	0.8261	0.9911	0.82	0.4154	0.9911	0.41	0.8261	0.3156	0.262	0.4154	0.7903	0.328
52	0.038	0.7663	0.029	0.851	0.99	0.841	0.4851	0.99	0.48	0.851	0.2561	0.218	0.4851	0.7663	0.371
56	0.03	0.743	0.0224	0.8758	0.9887	0.865	0.5623	0.9887	0.555	0.8758	0.2023	0.177	0.5623	0.743	0.419
60	0.024	0.721	0.0174	0.905	0.9879	0.89	0.6369	0.9879	0.627	0.905	0.1544	0.139	0.6369	0.721	0.46
64	0.018	0.702	0.0126	0.9235	0.987	0.91	0.7153	0.987	0.705	0.9235	0.1158	0.107	0.7153	0.702	0.502
68	0.014	0.685	0.0096	0.943	0.986	0.93	0.7836	0.986	0.773	0.943	0.0825	0.078	0.7836	0.685	0.538
72	0.01	0.667	0.0067	0.9612	0.9852	0.947	0.8504	0.9852	0.837	0.9612	0.0505	0.0485	0.8504	0.667	0.57
76	0.006	0.657	0.00394	0.9761	0.9846	0.96	0.9065	0.9846	0.89	0.9761	0.0334	0.0325	0.9065	0.657	0.593
80	0.0025	0.649	0.00162	0.9877	0.9842	0.975	0.949	0.9842	0.935	0.9877	0.0199	0.0197	0.949	0.649	0.615
84	0.0009	0.641	0.00058	0.9982	0.984	0.983	0.9825	0.984	0.965	0.9982	0.0069	0.00689	0.9825	0.641	0.63
88	0.0001	0.638	0.00006	0.9996	0.9837	0.9833	0.998	0.9837	0.982	0.9996	0.0018	0.0018	0.998	0.638	0.635
90	0.0000	0.6369	0.0000	1.0000	0.9835	0.9835	1.0000	0.9835	0.9835	1.0000	0.0000	0.0000	1.0000	0.6369	0.6369

Remarks: Figure 342 gives the patterns, and A and B are the values taken from Table 73. We have $\mathcal{E}_x$ and H_y polarizations and $D_{\theta=0°,\varphi} = D\varphi$, where $D\varphi = (\sin p/p)(\sin p'/p')$, since $(1 + \cos\theta) = 1$. We also have $p = (\pi a/\lambda)\cos\varphi$, $p' = (\pi b/\lambda)\sin\varphi$. For the above dimensions in terms of the wavelength, we can use the computations of Table 73.

copy the column values of $(\sin p')/p'$ for $a = b = 0.5\lambda$ of Table 73. We then multiply the corresponding values of these ratios in order to find the D_φ value of Table 74. In the same way, all the other values of Table 74 are found. The corresponding diffractivity patterns in Fig. 342

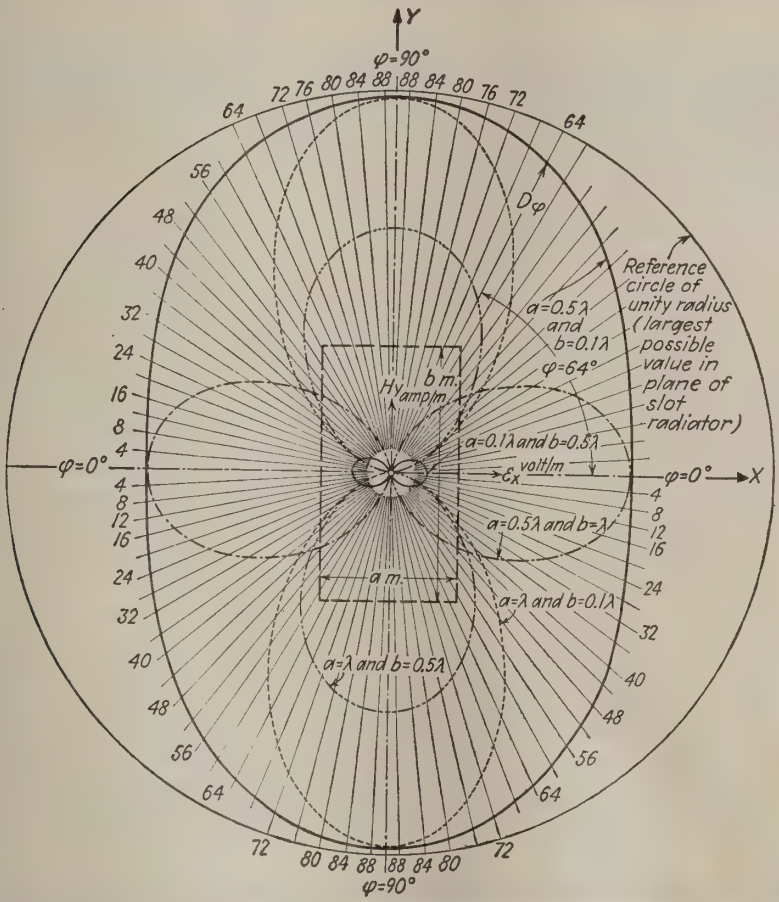

FIG. 342. Electromagnetic Fraunhofer field amplitude pattern in the plane of an electromagnetic slot radiator of rectangular shape ab, with $\mathcal{E}_x$ and H_y wave-front polarizations.

show a great difference for the $a = 0.1\lambda$ and $b = 0.5\lambda$ slot radiator if compared with the $a = 0.5\lambda$ and $b = 0.1\lambda$ slot radiator. In one case, $\mathcal{E}_x$ is along the narrow slot dimension; and in the other case, it is along the longer slot dimension. For $\mathcal{E}_x$ along the longer slot dimension, we have more pronounced radiation in the plane of the slot (larger pattern area) and D_φ in all directions, from $\varphi = 0$ to 360 deg. For $\mathcal{E}_x$ along the shorter slot dimension, we have, for the above ratios, a very small

amplitude pattern, with no radiation whatsoever along the $\pm Y$ directions and emphasis along the $\pm X$ directions.

For any space direction, it is now an easy matter to find the $D_{\theta,\varphi}$ values from the relation

$$D_{\theta,\varphi} = (1 + \cos\theta)\frac{\sin p}{p}\frac{\sin p'}{p'}$$

by means of the tables and the corresponding diffractivity patterns given in this section. For instance, for $a = 0.5\lambda$ and $b = \lambda$, for $\theta = 60$ deg and $\varphi = 40$ deg, where θ is the angle with the Z axis and φ the angle with respect to the $+X$ axis, we find

$$p = \frac{\pi a}{\lambda}\sin\theta\cos\varphi = 1.57\sin 60^\circ\cos 40^\circ = 1.57 \times 0.866 \times 0.766 = 1.09$$

$$p' = \frac{\pi b}{\lambda}\sin\theta\sin\varphi = 3.14\sin 60^\circ\sin 40^\circ = 3.14 \times 0.866 \times 0.6428 = 1.78$$

$$(1 + \cos\theta) = (1 + \cos 60^\circ) = 1.5$$

From Table 70 or from the corresponding curve in Fig. 335, we find then

$$\frac{\sin p}{p} = \frac{\sin (1.09 \text{ radians})}{1.09} = 0.8134$$

$$\frac{\sin p'}{p'} = \frac{\sin (1.78 \text{ radians})}{1.78} = 0.55$$

$$D_{\theta=60^\circ,\,\varphi=40^\circ} = 1.5 \times 0.8134 \times 0.55 = 0.67$$

Only *experiment* can tell to what extent such patterns may be of value, since, for slot openings that are too narrow, the wave front can be unperturbed only when the side of the screen (in which we have the slot) *facing* the primary arriving wave front, is a perfect wave absorber. In the derivations of the formulas, we tacitly assumed that the edge effect of the slot is also negligible. This, no doubt, requires a comparatively large opening. Moreover, according to the classic Hertzian experiments, a narrow slot should let radiation pass beyond the aperture only when the electric $\mathcal{E}$ vector is normal to the long slot dimension and in the plane of the slot. The patterns of Fig. 342 show, however, that for an 0.1λ times 0.5λ opening, wave propagation with $\mathcal{E}$ polarizations parallel and normal to the narrow side is possible. When taking the vertical pattern in the XZ plane of Fig. 339 also into consideration, we note that with such screen openings and ratios of a/b, in terms of the wavelengths mentioned above, at least a diffraction "spill" pattern seems possible. It must be borne in mind that with the grating used by Hertz for proving that the waves are transverse, the wires were fairly close together compared with the wavelength and a coherer was used as the agency for

detecting waves. Weak diffraction fields ("spills") then may have not been sufficient to cause a response in the coherer. The small figure-eight pattern along the $\pm X$ directions for $a = 0.1\lambda$ and $b = 0.5\lambda$ of Fig. 342 can be taken as a diffraction spill pattern in the plane of the slot radiator, while we can think of the large $a = 0.5\lambda$ and $b = 0.1\lambda$ pattern as a pronounced pattern.

212. Remarks on the $D_{\theta,\varphi}$ Formula for Computing Diffraction Patterns of Rectangular Slot Radiators. The diffractivity expression $D_{\theta,\varphi}$ used in Sec. 211 is based on two factors of a sine of an angle divided by the argument of the angle; while in formulas (901*b*), the diffractivity $D_\delta = (\sin p)/p$ contains only one such factor. We also found for the general wave function w in (901*g*) a relation of the form

$$w = K_0 \int\int \epsilon^{j\beta F(x,y)}\, dx\, dy \qquad \text{the result of (901}g\text{)}$$

where $\beta = 2\pi/\lambda$ and the function $F(x, y)$, which defines locations in the primary wave-front area of the slot, can be written as a series. Equation (901*g*) has reference to Fig. 336, where T_1 denotes the primary radiation center located at x_0, y_0, z_0, which is a distance $R_0 = \sqrt{x_0^2 + y_0^2 + z_0^2}$ from the origin. The XY plane of an XYZ coordinate system is the plane of the screen containing points T_2, located at x, y in an *aperture* of the screen. This means that T_2 is a Huygens wavelet center. On the other side of the screen, we have, at locations x_1, y_1, z_1, reception centers P_1, being a distance $R = \sqrt{x_1^2 + y_1^2 + z_1^2}$ away from the origin of the XYZ system. We have then

$$P_1T_2 = r = \sqrt{(x_1 - x)^2 + (y_1 - y)^2 + z_1^2}$$
$$T_2T_1 = r_0 = \sqrt{(x_0 - x)^2 + (y_0 + y)^2 + z_0^2}$$
$$\frac{r_0}{R_0} = \sqrt{1 + \frac{x^2 + y^2 - 2(xx_0 + yy_0)}{R_0^2}}$$

Since the dimension of the aperture is small compared with R_0 and R in Fig. 336, we have x/R_0, y/R_0, x/R, and y/R also very small. But for $n \ll 1$ in $\sqrt{1 + n}$, we find the series $\sqrt{1 + n} = 1 + 0.5n - 0.125n^2 + \cdots$. Hence,

$$n = \frac{x^2 + y^2 - 2(xx_0 + yy_0)}{R_0^2}$$

$$\frac{r_0}{R_0} = 1 + \frac{x^2 + y^2 - 2(xx_0 + yy_0)}{2R_0^2} - \frac{[x^2 + y^2 - 2(xx_0 + yy_0)]^2}{8R_0^2} + \cdots$$

$$r_0 = R_0 + \frac{x^2 + y^2}{2R_0} - \frac{xx_0 + yy_0}{R_0} - \frac{(xx_0 + yy_0)^2}{2R_0^3} + \cdots$$

In the same way, r/R can be put in a series. Using such results in the wave function

$$w = -\frac{j\beta}{2\pi}\frac{\cos\,\delta_0}{rr_0}\int\int \epsilon^{j\beta(r+r_0)}\, dx\, dy$$

yields, for the (901g) relation, the function

$$F(x, y) = \frac{x^2 + y^2}{2R_0} - \frac{x_0x + y_0y}{R_0} - \frac{(x_0x + y_0y)^2}{2R_0^3} + \cdots$$
$$- \frac{x_1x + y_1y}{R} + \frac{x^2 + y^2}{2R} - \frac{x_1x + y_1y}{2R^3} + \cdots$$
$$= (\alpha_0 - \alpha)x + (\beta_0 - \beta')y + \frac{1}{2}\left[\left(\frac{1}{R_0} + \frac{1}{R}\right)(x^2 + y^2)\right.$$
$$\left. - \frac{(\alpha_0x + \beta_0y)^2}{R_0} - \frac{(\alpha x + \beta' y)^2}{R}\right] + \cdots \qquad (903)$$

for the direction cosines of R_0 and R with respect to the XY plane, defined by $\alpha_0 = -\frac{x_0}{R_0}$, $\beta_0 = \frac{y_0}{R_0}$, $\alpha = \frac{x_1}{R}$, and $\beta' = \frac{y_1}{R}$. We limit ourselves to only a few terms of such a series. Retaining only the linear terms of x and y yields the function

$$\epsilon^{j\beta F(x,y)} = \epsilon^{j\beta[(\alpha_0-\alpha)x+(\beta_0-\beta')y]} = \underbrace{\epsilon^{j\beta(\alpha_0x-\beta_0y)}}_{\text{plane wave}} \cdot \underbrace{\epsilon^{-j\beta(\alpha x+\beta' y)}}_{\text{plane wave}} \qquad (903a)$$

The integration must be made over the result of (903a) in Eq. (901g), since we are interested only in that portion of the primary wave front which occupies the aperture of the screen. Equation (903a) represents a multiplication of two plane waves. One plane wave depends on the direction cosines α_0, β_0 (primary radiation center to aperture), and the other plane wave depends on the direction cosines α, β' (aperture to distant reception center P_1), where T_2 may be any secondary radiation center emitting a Huygens wavelet. Since we have plane waves, both R_0 and R are infinitely (theoretically) far from the screen. This is what is known as *Fraunhofer* diffraction. If we use in the series for $F(x, y)$ the next best approximation, *i.e.*, only terms up to the square of x and y, we can account for the curvature of the wave front in the aperture (at least for the square terms), and we deal with what is known as the *Fresnel* diffraction. Then since wave-front curvature is considered, R_0 and R are no longer theoretically infinitely large, and we deal with primary radiation and reception centers that are no longer very remote from the aperture but still far enough to make the largest dimension of the aperture negligible with respect to R_0 and R. We must then consider the time phases. According to (901g), we have the factor

$$K_0 = j\frac{\beta \cos \delta_0 \epsilon^{j\beta(R+R_0)}}{2\pi R R_0}$$

It depends only on the location of the primary radiation center and the location of the reception center, expressing that K_0 is a mere factor.

For a rectangular primary wave front (aperture) with the dimension a along the X direction and the dimension b along the Y direction, we have, for the classic wave disturbance w at the reception center,

$$w = K_0 \int\int \epsilon^{-j\beta(Ax+By)}\, dx\, dy \tag{903b}$$

where A and B denote the relative coordinates of any reception center with respect to the geometric image point O of source T_1. Hence A and B have no dimensions, since we deal with the ratio of R (Fig. 336) to the distance through which O moves if the radiation center T_1 moves through unity distance.

Equation (903b) is a double integral, since both dx and dy of the elementary area $dS = dx\, dy$ of the rectangular aperture must be taken into account for the primary wave energy arriving at the rectangular opening and the field energy leaving the opening in the form of wavelet energy. On page 1084, we carried out the integration only with respect to the x dimension, *i.e.*, over the limits $-a/2$ to $+a/2$, and found the result of $(\sin p)/p$, which is shown in Fig. 335. But Eq. (903b) requires double integration, for which we have

$$w = K_0 \left(\int_{-a/2}^{+a/2} \epsilon^{-j\beta Ax}\, dx \int_{-b/2}^{+b/2} \epsilon^{-j\beta By}\, dy \right)$$

$$\int_{-a/2}^{a/2} \epsilon^{-j\beta Ax}\, dx = \left| \frac{\epsilon^{-j\beta Ax}}{j\beta A} \right|_{-a/2}^{a/2} = \left| \frac{\cos(\beta Ax) - j \sin(\beta Ax)}{j\beta A} \right|_{-a/2}^{+a/2}$$

$$= \frac{\cos(\beta aA/2) - j \sin(\beta aA/2) - [\cos(-\beta aA/2) - j \sin(-\beta aA/2)]}{j\beta A}$$

but $\cos(-x) = \cos(x)$, $\sin(-x) = -\sin(x)$, and

$$\int_{-a/2}^{+a/2} \epsilon^{-j\beta Ax}\, dx = -\frac{\sin(\beta aA/2)}{\beta A/2}; \qquad \int_{-b/2}^{+b/2} \epsilon^{-j\beta By}\, dy = -\frac{\sin(\beta bB/2)}{\beta B/2}$$

which, inserted in the above relation for w, yields

$$w = K_0 \frac{\sin(0.5\beta aA)}{0.5\beta A} \frac{\sin(0.5\beta bB)}{0.5\beta B}$$

But $K_0 = ab/\lambda$; and if θ and θ_1 are the angles measured from the normal to the aperture at its center, in planes through the normal parallel to a and b, we find

$$\left.\begin{aligned} p = \frac{1}{2}\beta a \sin\theta = \frac{\pi a}{\lambda}\sin\theta; \qquad p' = \frac{1}{2}\beta b \sin\theta_1 = \frac{\pi b}{\lambda}\sin\theta_1 \\ w = \frac{ab}{\lambda}\frac{\sin p}{p}\frac{\sin p'}{p'} \end{aligned}\right\} \tag{903c}$$

confirming the formulas for $D_{\theta,\varphi}$ used for the $\mathcal{E}_x$ and H_y polarizations in Sec. 211.

213. Relations for Several Parallel-slot Radiators. Suppose we have two rectangular plane-wave-front radiators as in Fig. 343. The total wave-front area, with Huygens wavelet centers, is then $2ab$ square meters and requires integration in the expression (903*b*). We have then only to add up the effect of each wave-front radiator at a certain distant field

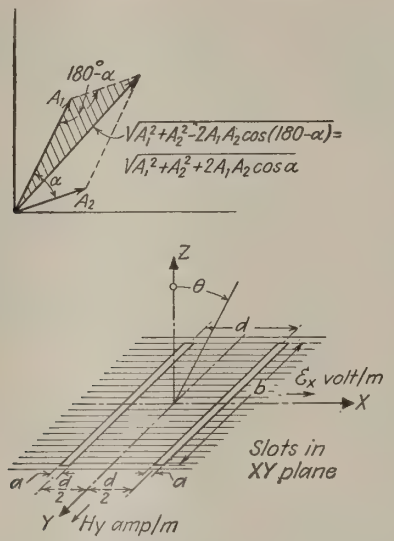

FIG. 343. Case of two rectangular apertures exposing primary wave fronts.

point with respect to the proper phase, just as is done for several linear radiators.

As far as the pattern in the XZ plane is concerned, we find, for the amplitude directivity D_θ, that we need consider only the integral $\int \epsilon^{-j\beta Ax}\,dx$ and have for $j\beta A = q$

$$\int \epsilon^{qx}\,dx = \int_{(-d-a)/2}^{(-d+a)/2} \epsilon^{qx}\,dx + \int_{(d-a)/2}^{(d+a)/2} \epsilon^{qx}\,dx = \left|\frac{\epsilon^{qx}}{q}\right|_{(-d-a)/2}^{(-d+a)/2} + \left|\frac{\epsilon^{qx}}{q}\right|_{(d-a)/2}^{(d+a)/2}$$

$$= \frac{1}{q}\left[\epsilon^{q(-d+a)/2} - \epsilon^{q(-d-a)/2} + \epsilon^{q(d+a)/2} - \epsilon^{q(d-a)/2}\right] =$$

$$\frac{\epsilon^{-0.5q(d-a)} - \epsilon^{-0.5q(d+a)} + \epsilon^{0.5q(d+a)} - \epsilon^{0.5q(d-a)}}{q}$$

but

$$0.5q(d+a) = j0.5\beta A(d+a) = j\nu; \qquad 0.5q(d-a) = j0.5\beta A(d-a) = j\nu'$$

$$\epsilon^{jx} - \epsilon^{-jx} = 2j \sin x$$

hence

$$\int \epsilon^{qx}\,dx = \frac{\epsilon^{0.5q(d+a)} - \epsilon^{-0.5q(d+a)} - \left[\epsilon^{0.5q(d-a)} - \epsilon^{-0.5q(d-a)}\right]}{q}$$

$$= \frac{\epsilon^{j\nu} - \epsilon^{-j\nu} - (\epsilon^{j\nu'} - \epsilon^{-j\nu'})}{q} = j\frac{2}{q}(\sin \nu - \sin \nu')$$

But

$$j\frac{2}{q} = j\frac{2}{j\beta A} = \frac{2}{\beta A}$$

$$\sin \nu - \sin \nu' = 2 \sin \left(\frac{\nu - \nu'}{2}\right) \cos \left(\frac{\nu + \nu'}{2}\right)$$

$$\sin \nu - \sin \nu' = 2 \sin \frac{\beta A(d + a) - \beta A(d - a)}{2} \cos \frac{\beta A(d + a) + \beta A(d - a)}{2}$$

$$\sin \nu - \sin \nu' = 2 \sin [0.5 \times 0.5(2\beta A a)] \cos [0.5 \times 0.5(2\beta A d)]$$

$$= 2 \sin \left(\frac{\beta A a}{2}\right) \cos \left(\frac{\beta A d}{2}\right)$$

Therefore,

$$\int \epsilon^{qx}\, dx = \frac{4}{\beta A} \sin \left(\frac{\beta A a}{2}\right) \cos \left(\frac{\beta A d}{2}\right) = \frac{2}{0.5\beta A} \sin \left(\frac{\beta A a}{2}\right) \cos \frac{\beta A d}{2}$$

$$= 2 \frac{\sin p}{p} \cos \left(\frac{\beta A d}{2}\right) = \frac{2\lambda}{\pi A} \sin \left(\frac{\pi A a}{\lambda}\right) \cos \left(\frac{\pi A d}{\lambda}\right)$$

If θ is the angle in the XZ plane with the Z axis (normal to the central symmetry point of the slot radiator array), we have, in any θ direction in this plane, $p = (\pi a \sin \theta)/\lambda$. In front of the integral, we also have the Huygens wavelet forward-movement factor $(1 + \cos \theta)$.

The diffractivity D_θ in the XZ plane, with the two parallel-slot radiators in the XY plane and the origin of the XYZ system as symmetry point of the slot array, then becomes

$$D_\theta = (1 + \cos \theta) \frac{\sin [(\pi a/\lambda) \sin \theta]}{(\pi a/\lambda) \sin \theta} \cos \left(\frac{\pi d}{\lambda} \sin \theta\right) \qquad (903d)$$

The outcome of the integral $\int \epsilon^{qx}\, dx$ can be readily checked by the fact that the effect at any reception center due to two equal slots laid out as in Fig. 343 is nothing but the resultant of the effects due to each slot radiator if added vectorially. We have found that the amplitude A_1 of a single-slot radiator a meters wide is, in the XZ plane for $F_\theta = 1 + \cos \theta$ and $p = (\pi a/\lambda) \sin \theta$, equal to $(kF_\theta \sin p)/p$, where k is a proportionality constant. But when two vectors A_1 and A_2 with a relative phase angle α are geometrically added, according to Fig. 343, the resultant vector becomes $\sqrt{A_1^2 + A_2^2 + 2A_1A_2 \cos \alpha}$. But the amplitudes of respective slot radiation fields are equal, and the phase angle α is due to the path difference $d \sin \theta$, so that

$$\alpha = \frac{2\pi}{\lambda} d \sin \theta = \beta d \sin \theta$$

since all wavelets start out in the plane wave front of either slot with the same phase.

The resultant amplitude A_r, therefore, becomes

$$A_r = \sqrt{2A_1^2 + 2A_1^2 \cos \alpha} = \sqrt{2}\, A_1 \sqrt{1 + \cos \alpha} = \sqrt{2}\, A_1 \sqrt{\frac{2(1 + \cos \alpha)}{2}}$$

$$= 2A_1 \sqrt{\frac{1 + \cos \alpha}{2}} = 2A_1 \cos \frac{\alpha}{2} = 2k \frac{\sin p}{p} F_\theta \cos \frac{\alpha}{2}$$

$$= \underbrace{2k(1 + \cos \theta) \frac{\sin [(\pi a/\lambda) \sin \theta]}{(\pi a/\lambda) \sin \theta} \cos \left(\frac{\pi d}{\lambda} \sin \theta \right)}_{= D_\theta}$$

which confirms the above formula.

From the expressions of identical inphase linear radiators, we know that the main beam can be made sharper by using several linear radiators. This should then also be the case for N equal parallel-wave-front radiators as in Fig. 343, where N is equal only to 2. The field amplitude of a single-slot radiator at a very large distance is again A_1 for reception centers in the XZ plane of Fig. 343. The field contribution due to the adjacent radiating slot is $A_1 \epsilon^{-j\alpha}$, where α again denotes the phase delay $\beta d \sin \theta$. The resultant field amplitude at the reception center due to N parallel-slot radiators then becomes

$$A_r = A_1[1 + \epsilon^{-j\alpha} + \epsilon^{-j2\alpha} + \epsilon^{-j3\alpha} + \cdots + \epsilon^{-j(N-1)\alpha}]$$

$$= \sum_{n=0}^{n=N-1} \epsilon^{-jn\alpha} = A_1 \frac{1 - \epsilon^{-jN\alpha}}{1 - \epsilon^{-j\alpha}} = A_1 \frac{1 - \cos (N\alpha) + j \sin (N\alpha)}{1 - \cos \alpha + j \sin \alpha}$$

The received power is proportional to the square of the field amplitude, and

$$A_r^2 = A_1^2 \frac{(1 - \epsilon^{-jN\alpha})(1 - \epsilon^{jN\alpha})}{(1 - \epsilon^{-j\alpha})(1 - \epsilon^{j\alpha})}$$

$$= A_1^2 \frac{[1 - \cos (N\alpha) + j \sin (N\alpha)][1 - \cos (N\alpha) - j \sin (N\alpha)]}{(1 - \cos \alpha + j \sin \alpha)(1 - \cos \alpha - j \sin \alpha)}$$

$$= \frac{1 - \cos (N\alpha)}{1 - \cos \alpha} A_1^2$$

The received field amplitude then becomes

$$A_r = A_1 \sqrt{\frac{1 - \cos (N\alpha)}{1 - \cos \alpha}} = A_1 \frac{\sin (N\alpha/2)}{\sin (\alpha/2)}$$

Inasmuch as the relation for the single-slot radiator is the elementary characteristic and the relation just derived the group characteristic, we need only to multiply these characteristics in order to find the total field amplitude pattern, and

$$D_{\text{total}} = k(1 + \cos \theta) \frac{\sin [(\pi a/\lambda) \sin \theta]}{(\pi a/\lambda) \sin \theta} \cdot \frac{\sin [(\pi N d/\lambda) \sin \theta]}{\sin [(\pi d/\lambda) \sin \theta]} \quad (903e)$$

where D_{total}/k is the diffractivity D_θ in the XZ plane for N parallel-wave-front radiators in the XY plane (as in Fig. 343 with the origin of the XYZ system as the symmetry center for the N parallel rectangular wave-front radiators). For $N = 2$, we find the wave-front separation factor

$$F_s = \frac{\sin [(\pi N/\lambda) \sin \theta]}{\sin [(\pi d/\lambda) \sin \theta]} = \frac{\sin [(2\pi d/\lambda) \sin \theta]}{\sin [(\pi d/\lambda) \sin \theta]}$$

For $\frac{\pi d}{\lambda} \sin \theta = m$, we have

$$F_s = \frac{\sin (2m)}{\sin (m)} = \frac{2 \sin (m) \cos (m)}{\sin (m)} = 2 \cos (m) = 2 \cos \left(\frac{\pi d}{\lambda} \sin \theta\right)$$

which checks the result found before.

214. Comparisons of Radiation Effects of Electromagnetic Huygens Wavelet Center Radiators with Normal and Inclined Primary Rectangular Wave-front Incidence. So far, we have discussed the cases for which an aperture is in the plane of the arriving plane primary wave front. This is what is meant here by normal wave incidence from the actual or primary electromagnetic radiator. The angle ψ of incidence is then the angle between the normal to the plane of the rectangular aperture in a screen and the wave normal. By wave normal is meant the normal to the arriving plane wave front. The angle of diffraction θ is the angle that the path from the symmetry center of the aperture to the distant field point makes with the normal to the aperture. For normal wave incidence, we have then $\psi = 0$ deg, if taken with respect to the normal of the aperture pointing toward the arriving plane wave front. It is an angle equal to 180 deg, if taken as in Fig. 334 with the normal of the aperture pointing toward the distant field region, toward which actual wave progression takes place. If the rectangular aperture is again in the XY plane as in Fig. 338, we have, for the power directivity D_p, the comparisons

$$\left.\begin{aligned}
&D_p = 0.125 \frac{\mathcal{E}_x^2 a^2 b^2 (1 + \cos \theta)^2}{Z_0 \lambda^2} D_g \quad \text{watts} \\
&D_g = \frac{\sin \left(\frac{\pi a}{\lambda} \sin \theta \cos \varphi\right)}{\frac{\pi a}{\lambda} \sin \theta \cos \varphi} \cdot \frac{\sin \left(\frac{\pi b}{\lambda} \sin \theta \sin \varphi\right)}{\frac{\pi b}{\lambda} \sin \theta \sin \varphi} \\
&\qquad \text{for } \textit{normal} \text{ primary-wave-front incidence } (\psi = 0°) \\
&D_g = \frac{\sin \left\{\frac{\pi a}{\lambda} [\sin (\theta) \cos (\varphi) - \psi]\right\}}{\frac{\pi a}{\lambda} [\sin (\theta) \cos (\varphi) - \psi]} \frac{\sin \left(\frac{\pi b}{\lambda} \sin \theta \sin \varphi\right)}{\frac{\pi b}{\lambda} \sin \theta \sin \varphi} \\
&\qquad \text{for } \textit{inclined} \text{ plane-wave-front incidence } (\psi \text{ is } \textit{small})
\end{aligned}\right\} \quad (904)$$

where θ and φ are in degrees, ψ in radians, a and b in meters, $\mathcal{E}_x$ in volts per meter, H_y in amperes per meter, $\lambda^{(m)} = 300/f^{(Mc/sec)}$, and $Z_0 = \sqrt{\mu/\kappa} \cong 376.7$ ohms. In either case, it is assumed that the wave normal is parallel to the XZ plane (as in Fig. 338), and we have, in either case, essentially indicated $\mathcal{E}_x$ and H_y fields.

Owing to the increasing phase lag for inclined wave incidence, we must account, along the X direction, for a $\beta x_1 \psi$ delay for the wavelets and have the comparisons

$$\int\int_{S=ab} = \int_{x_1=-a/2}^{x_1=a/2} \int_{y_1=-b/2}^{y_1=b/2} \epsilon^{j\beta x_1 \sin\theta^\circ \cos\varphi^\circ} \epsilon^{j\beta y_1 \sin\theta^\circ \sin\varphi^\circ}\, dx_1\, dy_1$$

for normal wave incidence

$$\int\int = \int_{-a/2}^{a/2} \int_{-b/2}^{b/2} \epsilon^{j\beta x_1(\sin\theta^\circ \cos\varphi^\circ - \psi)} \epsilon^{j\beta y_1(\sin\theta^\circ \cos\varphi^\circ)}\, dx_1\, dy_1$$

for inclined wave incidence

for the double integral, for summing up all the Huygens wavelet effects. The evaluation of these respective double integrals is, according to the details of (902d), to be multiplied by the square of the Kirchhoff factor $(1 + \cos\theta)^2$ and $\mathcal{E}_x^2 a^2 b^2/(8Z_0\lambda^2)$, since the double integral yields only the square of the Huygens amplitude group characteristic D_g, where $D_g(1 + \cos\theta)$ is the amplitude space characteristic of the wave-front radiator. We note that in the plane of wave incidence, (904) simplifies greatly, since $\varphi = 0$.

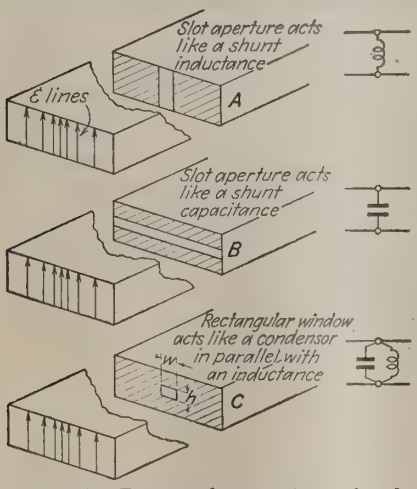

FIG. 344. Rectangular apertures in the cross section of a rectangular wave guide.

215. Possible Applications of Parallel-slot Radiators and Field Patterns. This discussion refers to several rectangular wave-front radiators. We know from a parallel-wire transmission line that a shunted inductance across the line will cause storage of magnetic field energy, just as a condenser across the line will cause a storage of electric field energy. Therefore, when an inductance and a capacitance are connected across the same points of a double line, the stored field effects will be partially electric and partially magnetic; and for a certain frequency, we shall have parallel resonance, which for a high Q value of the combination places in effect a very high impedance across the double line, so that hardly any reflections take place where these reactances are connected. This means that the capacitance and the inductance act as though not present. Now if we have (Fig. 344) a rectangular wave guide that is

excited, for instance, with a $TE_{1,0}$ wave, the shorter side is customarily parallel with the direction of the electric $\mathcal{E}$ polarization and vertical. If we insert into the guide a metal screen A with a slot that is parallel with the transverse $\mathcal{E}$ field, a current can readily pass from the top to the bottom faces with an essential magnetic local field. This is equivalent to saying that the metal screen with the vertical slot acts, in effect, as an inductance. Placing the screen so that we have the slot normal to the transverse $\mathcal{E}$ lines as in Fig. 344B, no conduction current can flow from the top to the bottom, but charges will be stored on the upper and lower portions of the metal screen. This means that the local field must be essentially electric, and we have in effect a condenser action. If we use a window aperture in the metal screen as in Fig. 344C, we have either a resultant inductance or resultant capacitance action, depending on the relative values of the aperture dimensions. In all three cases, we have wave reflections at the plane of the screen, since during one half of the cycle field energy is accumulated and during the other half of the cycle it is returned. This means that at the plane of the screen with the aperture, we have a wave motion in either direction. We have quite a range of pass frequencies between the lower cutoff frequency and the next higher mode cutoff frequency. Therefore, when the metal screen is placed at the end of the guide and the ratio h/w in the metal screen is properly chosen or the frequency of the $TE_{1,0}$ wave is properly adjusted or both adjustments are made properly so that the capacitance effect just cancels the inductance effect, then the end face of the guide acts as a very high impedance and the end face acts as though it were not present. We have then created a rectangular Huygens slot radiator of area hw square meters if we ignore the effect of the longitudinal H component, which also arrives at the opening. This component, however, will not be responsible for the radiation action in the distant field region. We can therefore cut several equal windows in the end metal screen and cause equally separated wavelet slots. We can also arrange slot radiators as in Fig. 345, which may be cut in the aperture of a paraboloid if the aperture is closed with a metal screen having such slot openings in it. This assumes that the rear of the screen must absorb the arriving wave energy and that only reflected waves from the parabolic mirror are responsible for the field in the slots. Therefore, the forward radiation

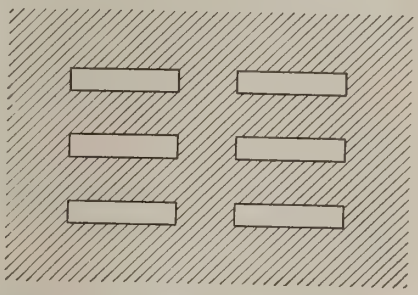

Fig. 345. A curtain of wave-front radiators.

from the actual linear radiator in the focal line must be prevented. Such requirements are by no means an easy task from a practical point of view. The rectangular openings could also be the open ends of six rectangular wave-guide branches, which cause inphase fields at all slots. Table 75 gives the computations for multislot electromagnetic radiators. The computations are for the XZ diffraction pattern for $a = 0.1\lambda$, $d = 0.3\lambda$, for $N = 2$ and $N = 5$ slot radiators, respectively. For $a = 0.1\lambda$, we find $p = 0.314 \sin \theta$, since $p = (\pi a \sin \theta)/\lambda$. For $d = 0.3\lambda$, we find $q = (\pi d \sin \theta)/\lambda = 0.942 \sin \theta$. For $N = 2$ rectangular wave-front radiators, as in Fig. 343, with the a dimension along the X axis, the slot in the XY plane, and the separation d between centers of adjacent slots, formula (903e) holds, and we find for the XZ plane

$$D_\theta = 2(1 + \cos \theta) \frac{\sin p}{p} \cos q$$

For five slots ($N = 5$), formula (903e) gives, for $r = (\pi N d \sin \theta)/\lambda = 0.942 \times 5 \sin \theta = 4.71 \sin \theta$ and $q = (\pi d \sin \theta)/\lambda = 0.942 \sin \theta$, the amplitude pattern

$$D_\theta = (1 + \cos \theta) \frac{\sin p}{p} \frac{\sin r}{\sin q} = (1 + \cos \theta) \frac{\sin p}{p} \frac{\sin (5q)}{\sin (q)}$$

In connection with such computations, we must realize that the separation factor $(\sin Nq)/(\sin q)$ approaches the value of N for $\theta = 0$ deg, as is brought out under Remarks in Table 75. This is evident also from the fact that $\theta = 0$ deg is equivalent to the approach $\theta \to 0$. But such an approach means that $\sin (Nq) \cong Nq$ radians, $\sin (q) \cong q$ radians, and

$$\frac{\sin (Nq)}{\sin (q)} \cong \frac{Nq}{q} = N = 5 \qquad \text{for } \theta \to 0$$

Radiation along a $\theta = 0$ deg direction means radiation along the Z axis or along the direction normal of the common plane of the slot radiators. It is normal to the common plane of all slot planes, through the symmetry center of these planes. But for $\theta = 0$ deg, we also have the forward Kirchhoff wavelet factor $1 + \cos \theta = 2$, which is another maximum condition, meaning that for $N = 2$ and $\theta = 0$ deg, we have the amplitude directivity $D_\theta = 2N = 4$ and the energy directivity $D_\theta^2 = 16$ in either case, in comparison with the unity value, if only one slot radiator is present. This is, therefore, an *improved* field advantage in comparison with linear radiator arrays, since even with one wave-front radiator, we have an optimum gain *because of the forward factor* $(1 + \cos \theta)$. For $N = 3$, *i.e.*, three equal rectangular wave-front radiators, we have, normal

TABLE 75. PATTERN EVALUATION FOR SEVERAL SLOT RADIATORS (FIG. 346)

			Two-slot radiators ($N = 2$); $D_\theta = 2ABC$						Five-slot radiators ($N = 5$); $D_\theta = ABD$					
θ, deg	$1 + \cos\theta = A$	$\sin\theta$	$p = 3.14 \sin\theta$, radians	$\frac{\sin p}{p} = B$	$q = 0.942 \times \sin\theta$, radians	q, deg	$\cos q = C$	$0.5D_\theta$	$r = 4.71 \times \sin\theta$, radians	r, deg	$\sin r$	$\sin q$	$D = \frac{\sin r}{\sin q}$	D_θ
0.0	2.0000	0.0000	0.0000	1.0000	0.0000	0.0	1.0000	2.000	0.000	0.0	0.0000	0.0000	5.0000	10.000
3	1.9986	0.0523	0.0162	0.9999	0.0494	2.83	0.9988	1.99	0.246	14.1	0.2436	0.0488	5.00	9.999
6	1.9945	0.1045	0.0328	0.9998	0.098	5.67	0.995	1.98	0.494	28.3	0.4741	0.0993	4.76	9.5
9	1.9877	0.1564	0.0492	0.9996	0.148	8.5	0.989	1.97	0.736	42.2	0.6717	0.1478	4.55	8.95
12	1.9781	0.208	0.0655	0.9995	0.196	11.25	0.9808	1.94	0.98	56	0.829	0.1925	4.3	8.5
15	1.9659	0.259	0.081	0.9989	0.244	14	0.9703	1.905	1.22	70	0.9397	0.2419	3.9	7.7
18	1.9511	0.309	0.097	0.9984	0.29	16.6	0.9583	1.865	1.45	83	0.9925	0.2857	3.48	6.8
21	1.9336	0.358	0.112	0.998	0.337	19.3	0.9438	1.82	1.69	97	0.9925	0.3305	3.0	5.8
24	1.9135	0.407	0.128	0.9973	0.385	22.1	0.9265	1.76	1.92	110.5	0.9367	0.3762	2.48	4.75
27	1.891	0.454	0.142	0.9966	0.426	24.5	0.91	1.71	2.14	123	0.8387	0.4147	2.02	3.8
30	1.866	0.5	0.157	0.9959	0.471	27.1	0.8902	1.66	2.35	135	0.7071	0.4555	1.55	2.9
33	1.8387	0.545	0.171	0.9952	0.515	29.5	0.8704	1.6	2.57	147.5	0.5373	0.4924	1.09	2.05
36	1.809	0.588	0.184	0.9944	0.552	31.6	0.8517	1.53	2.76	158	0.3746	0.524	0.716	1.29
39	1.7771	0.629	0.197	0.9935	0.59	33.9	0.83	1.47	2.95	169.8	0.1771	0.5577	0.318	0.562
42	1.7431	0.669	0.209	0.9928	0.63	36.2	0.807	1.4	3.15	181	−0.0175	0.591	−0.0295	−0.051
45	1.7071	0.7071	0.221	0.9919	0.668	38.4	0.7837	1.33	3.32	190.5	−0.1822	0.6211	−0.291	−0.495
48	1.6691	0.743	0.234	0.9908	0.7	40.2	0.7638	1.27	3.5	201	−0.3584	0.6455	−0.553	−0.92
51	1.6293	0.777	0.244	0.99	0.73	41.9	0.7443	1.2	3.65	210	−0.5	0.6678	−0.75	−1.215
54	1.5878	0.809	0.254	0.9892	0.76	43.6	0.7242	1.14	3.81	219	−0.6293	0.6896	−0.915	−1.44
57	1.5446	0.8387	0.263	0.9885	0.79	45.4	0.7022	1.07	3.95	227	−0.7314	0.712	−1.03	−1.56
60	1.5	0.866	0.271	0.9878	0.817	46.7	0.6858	1.01	4.07	234	−0.809	0.7278	−1.11	−1.64
63	1.454	0.891	0.28	0.987	0.841	48.4	0.6639	0.95	4.2	241	−0.8746	0.7478	−1.175	−1.68
66	1.407	0.9135	0.286	0.9864	0.862	49.5	0.6494	0.9	4.3	246	−0.9135	0.7604	−1.2	−1.66
69	1.3584	0.934	0.294	0.9856	0.88	50.7	0.6334	0.85	4.4	252	−0.9511	0.7738	−1.225	−1.64
72	1.309	0.951	0.3	0.9851	0.9	51.7	0.6198	0.8	4.48	256	−0.9703	0.7848	−1.23	−1.585
75	1.259	0.966	0.304	0.9849	0.91	52.2	0.6129	0.76	4.55	261	−0.9877	0.7902	−1.245	−1.545
78	1.208	0.978	0.306	0.9846	0.92	52.8	0.6046	0.72	4.6	264	−0.9945	0.7965	−1.25	−1.49
81	1.1564	0.988	0.309	0.9843	0.93	53.3	0.598	0.682	4.65	267	−0.9986	0.802	−1.24	−1.42
84	1.045	0.994	0.312	0.984	0.94	54.0	0.5878	0.605	4.7	270	−1.0000	0.809	−1.238	−1.28
87	1.0323	0.999	0.313	0.9839	0.941	54.1	0.5864	0.594	4.71	271	−0.9998	0.81	−1.235	−1.25
90	1.0000	1.000	0.314	0.9837	0.942	54.2	0.585	0.575	4.71	271	−0.9998	0.8111	−1.23	−1.21

Remarks: The computations are based on formula (903e) for N slot radiators with a and d as in Fig. 343 with the separation factor $[\sin(Nq)]/[\sin(q)]$, where $q = (\pi d/\lambda)\sin\theta$ and q radians = 57.3 deg, shows that for $N = 2$ radiators, we have $[\sin(2q)]/[\sin(q)] = (2\sin q\cos q)/(\sin q) = 2\cos q$; for $\cos\theta = 0$, we find $2\cos q = 2$; for $r = 5q$ and $\theta = 0$, we have $[\sin(5q)]/[\sin(q)] = 0/0$ undeterminate. We choose then a very small angle, such as $\theta = 0.01$ radians, and find $\sin(5q) \cong 5q = 0.01$ radians; then $\sin q = 0.01/5$ radians, and $[\sin(5q)]/[\sin(q)] = 5$, where 5 is the limiting value for $\theta = 0$. Evaluations for $a = 0.1\lambda$ and $d = 0.3\lambda$. B is found from Table 70 for p.

to their plane and through the symmetry center, an amplitude directivity of $3N = 9$ and an energy directivity that is 81 fold compared with the value for only one wave-front radiator. It must be realized, however, that this is true only for the Fraunhofer diffraction patterns, but such patterns should apply in some cases. Only experiment can actually tell if such field gains can be realized in practice. Figure 346 gives the field amplitude (D_θ) patterns in Cartesian as well as polar coordinates. The

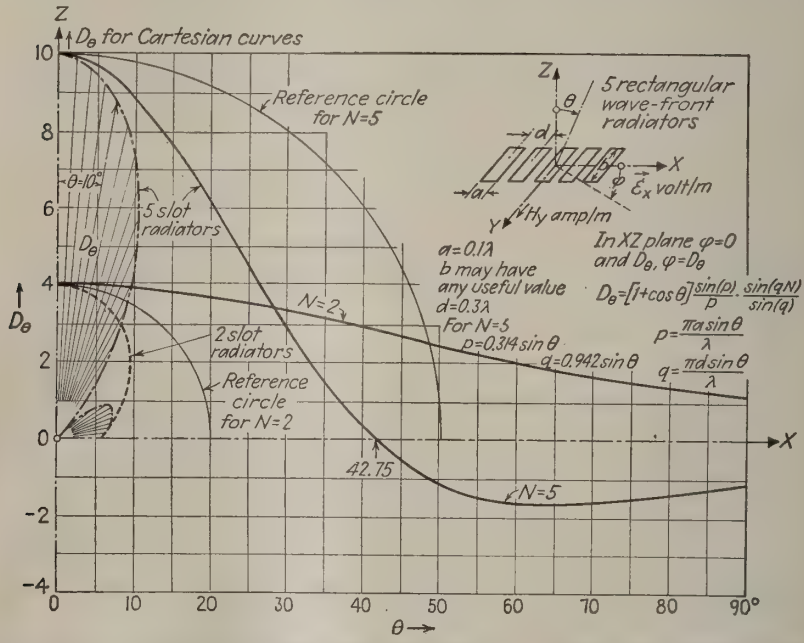

FIG. 346. Principal vertical Fraunhofer field amplitude patterns for two- and five-slot radiators.

plot in Cartesian coordinates is much better if readings are taken from the plot, *i.e.*, for graphical interpolation. We computed only for every 3 deg for the angle θ; and for a high order of patterns, it is likely that zero field regions and maximum field regions are missed by such angular steps. For the plot in polar coordinates, it is then difficult to read off accurately near zero field values, but it is an easy matter to do this for a plot in Cartesian coordinates. However, this feature is completely offset if we desire a mental picture (a feel) of what happens in actual space. It is the polar plot that will tell what takes place. We see, for instance, that the area of the side lobe in the XZ plane and for polar coordinates is not so serious in comparison with the main lobe; while for the plot in Cartesian coordinates, the side lobe becomes altogether

too prominent. It is seen from Fig. 346 that for two slot radiators, the field is over the entire quadrant (in reality, all over the left quadrant, which is not shown). We then have no regions of zero electromagnetic field intensity. For five equal wave-front radiators, the radiation is decidedly diverted toward the Z direction. This is evident, since we found that along the normal symmetry axis, we have a twofold N value for D_θ, *i.e.*, $2 \times 5 = 10$ relative amplitude directivity. Therefore, for

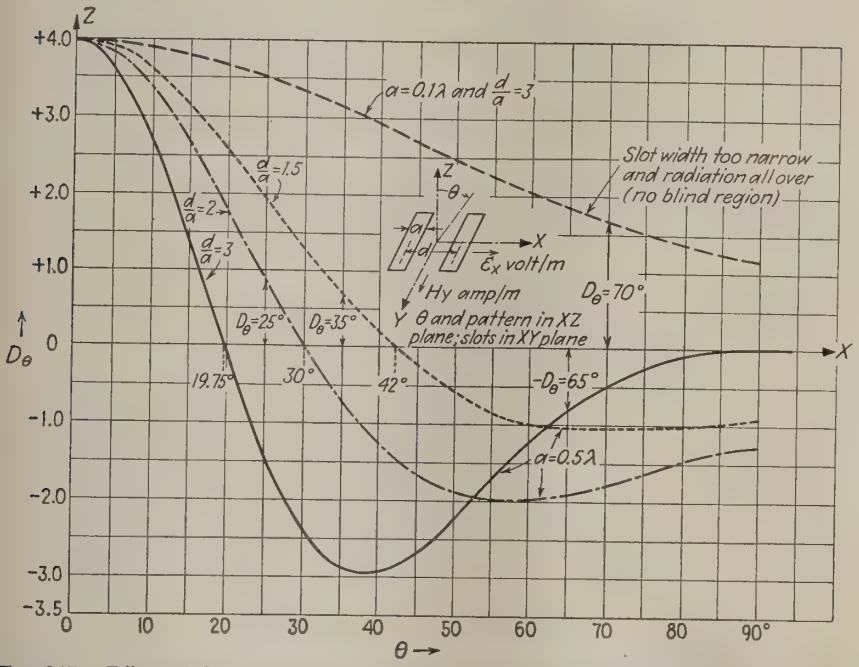

Fig. 347. Effect of slot separation for a two-slot radiator. *Note:* A larger ratio d/a, *i.e.*, more slot separation, favors better main beaming but also emphasizes the intensity of the side lobe, which has opposite polarity.

angles of θ toward $\theta = 0$ deg, we cannot expect small D_θ values, and we have *decided forward main beaming.* According to Fig. 339, a width $a/\lambda = 0.5$, instead of $a/\lambda = 0.1$, gives a larger directivity area for a single-slot radiator polarized as in Fig. 346. This is done in the evaluations of Table 76 and in the amplitude directivity patterns of Figs. 347 and 348. In Fig. 347, we note that the base width of the main beam in the XZ plane is 2×19.75 deg for $a = 0.5\lambda$ and $d/a = 3$ but is as much as 2×42 deg for a ratio $d/a = 1.5$ for the same slot width $a = 0.5\lambda$.

It is important to realize that with *more* than one rectangular wave-front radiator, we no longer have conditions that can be termed a "pure" diffraction pattern but we have what may be called an "intermodulated" diffraction pattern, owing to mutual

TABLE 76. AMPLITUDE PATTERN EVALUATION FOR DIFFERENT d/a RATIOS AND $N = 2$ SLOT RADIATORS

θ, deg	Forward factor $A = 1 + \cos\theta$	$\sin\theta$	Two-slot radiators, $a = 0.5\lambda$, $\frac{d}{a} = 3$, $D_\theta = 2ABC$						Two-slot radiators, $a = 0.5\lambda$, $\frac{d}{a} = 2$, $D_\theta = 2ABC'$				Two-slot radiators, $a = 0.5\lambda$, $\frac{d}{a} = 1.5$, $D_\theta = 2ABC''$			
			$p = 1.57 \times \sin\theta$	$B = \frac{\sin p}{p}$	$q = 471 \sin\theta$, radians	q, deg	$C = \cos q$	D_θ	$q = 3.14 \sin\theta$, radians	q, deg	$C' = \cos q$	D_θ	$q = 2.355 \times \sin\theta$, radians	q, deg	$C'' = \cos q$	D_θ
0.0	2.0000	0.0000	0.0000	1.0000	0.000	0.000	1.0000	4.000	0.000	0.000	1.0000	4.0000	0.000	0.0000	1.0000	4.0000
3	1.9986	0.0523	0.081	0.9989	0.248	14.1	0.9699	3.85	0.162	9.3	0.9869	3.9	0.124	7.05	0.9924	3.95
6	1.9945	0.1045	0.164	0.9955	0.494	28.3	0.8805	3.49	0.328	18.8	0.9466	3.75	0.247	14.15	0.9696	3.84
9	1.9877	0.1564	0.246	0.9899	0.736	42.2	0.7408	2.92	0.492	28.2	0.8813	3.48	0.368	21.1	0.933	3.66
12	1.9781	0.208	0.3275	0.9824	0.98	56	0.5592	2.17	0.655	37.6	0.7923	3.08	0.49	28	0.8829	3.44
15	1.9659	0.259	0.405	0.9728	1.22	70	0.342	1.31	0.81	46.5	0.6884	2.63	0.66	35	0.8192	3.14
18	1.9511	0.309	0.485	0.9611	1.45	83	0.1219	0.458	0.97	55.8	0.5621	2.1	0.725	41.5	0.749	2.8
21	1.9336	0.358	0.56	0.9485	1.69	97	−0.1219	−0.445	1.12	64.1	0.4368	1.6	0.845	48.5	0.6626	2.43
24	1.9135	0.407	0.64	0.9331	1.92	110.5	−0.3502	−1.25	1.28	73.7	0.2807	1.0	0.96	55.25	0.57	2.04
27	1.891	0.454	0.71	0.9181	2.14	123	−0.5446	−1.891	1.42	81.5	0.1478	0.51	1.07	61.5	0.4772	1.65
30	1.866	0.5	0.785	0.9004	2.35	135	−0.7071	−2.37	1.57	90	0.0000	0.0000	1.175	67.5	0.3827	1.28
33	1.8387	0.545	0.855	0.8824	2.57	147.5	−0.8434	−2.75	1.71	98	−0.1392	−0.452	1.285	73.75	0.2798	0.908
36	1.809	0.588	0.92	0.8648	2.76	158	−0.9272	−2.9	1.84	106	−0.2756	−0.865	1.38	79	0.1908	0.599
39	1.7771	0.629	0.985	0.846	2.95	169.8	−0.9842	−2.96	1.97	113.5	−0.3987	−1.2	1.475	84.9	0.0889	0.268
42	1.7431	0.669	1.045	0.8277	3.15	181	−1.0000	−2.87	2.09	120	−0.5	−1.44	1.575	90.5	−0.009	−0.0259
45	1.7071	0.7071	1.105	0.8085	3.32	190.5	−0.9833	−2.71	2.21	127	−0.6018	−1.67	1.66	95.25	−0.0915	−0.251
48	1.6691	0.743	1.17	0.787	3.5	201	−0.9336	−2.45	2.34	134	−0.6947	−1.82	1.75	100.5	−0.1822	−0.476
51	1.6293	0.777	1.22	0.7698	3.65	210	−0.866	−2.16	2.44	140	−0.766	−1.91	1.825	105	−0.2588	−0.65
54	1.5878	0.809	1.27	0.752	3.81	219	−0.7771	−1.86	2.54	146	−0.829	−1.98	1.905	109.5	−0.3338	−0.8
57	1.5446	0.8387	1.315	0.7357	3.95	227	−0.682	−1.543	2.63	151	−0.8746	−1.98	1.975	113.5	−0.3987	−0.905
60	1.5	0.866	1.355	0.7209	4.07	234	−0.5878	−1.26	2.71	156	−0.9135	−1.98	2.035	117	−0.454	−0.98
63	1.454	0.891	1.4	0.7039	4.2	241	−0.4848	−0.99	2.8	161	−0.9455	−1.93	2.1	120.5	−0.5075	−1.04
66	1.407	0.9135	1.43	0.6924	4.3	246	−0.4067	−0.8	2.86	165	−0.9659	−1.88	2.15	123	−0.5446	−1.07
69	1.3584	0.934	1.47	0.6768	4.4	252	−0.309	−0.567	2.94	169	−0.9816	−1.8	2.2	126	−0.5878	−1.08
72	1.309	0.951	1.5	0.665	4.48	256	−0.2419	−0.42	3.0	172	−0.9903	−1.73	2.24	128	−0.6157	−1.072
75	1.259	0.966	1.52	0.657	4.55	261	−0.1564	−0.258	3.04	174	−0.9945	−1.64	2.275	130.5	−0.6494	−1.07
78	1.208	0.978	1.53	0.6531	4.6	264	−0.1045	−0.166	3.06	176	−0.9976	−1.58	2.3	132	−0.6691	−1.055
81	1.1564	0.988	1.545	0.647	4.65	267	−0.0523	−0.0785	3.09	177	−0.9986	−1.5	2.325	133.5	−0.6884	−1.03
84	1.045	0.994	1.56	0.641	4.7	270	0.0000	0.000	3.12	179	−0.9998	−1.34	2.35	135	−0.7071	−0.94
87	1.0323	0.999	1.565	0.6389	4.71	271	0.0000	0.000	3.13	179.5	−1.0000	−1.31	2.355	135.5	−0.7133	−0.94
90	1.0000	1.000	1.57	0.637	4.71	271	0.0000	0.000	3.14	180	−1.0000	−1.27	2.355	135.5	−0.7133	−0.91

Remarks: D_θ amplitude diffraction pattern holds for the vertical XZ plane with the slot radiators parallel to the Y axis and in the XY plane. The a dimension is parallel to the X axis, and we have $\mathcal{E}_x$ and H_y resultant fields. We also have $p = (\pi a/\lambda) \sin\theta = 1.57 \sin\theta$; for $d/a = 3$ and $d = 1.5\lambda$, we have $q = (\pi d/\lambda) \sin\theta = 4.71 \sin\theta$; for $d/a = 1.5$, we have $q = 2.355 \sin\theta$; a and d dimensions are as in Fig. 343; $2\pi = 6.28$ radians $= 360$ deg; q radians $= 57.295q$ deg. $2\pi = 6.28$ radians $= 360$ deg; q radians $= 57.295q$ deg.

slot pattern interference. The reason for this is that a pure diffraction is the result only at a particular distant field point, because wavelet interference arrives at the point from *all* the secondary radiation centers of *one and the same* rectangular wave-front radiator. For two or more slot radiators, even though in time phase, each particular primary rectangular wave-front radiator causes a pure diffraction field at the distant space point, and it is the three diffraction fields, in the case of three slots, that

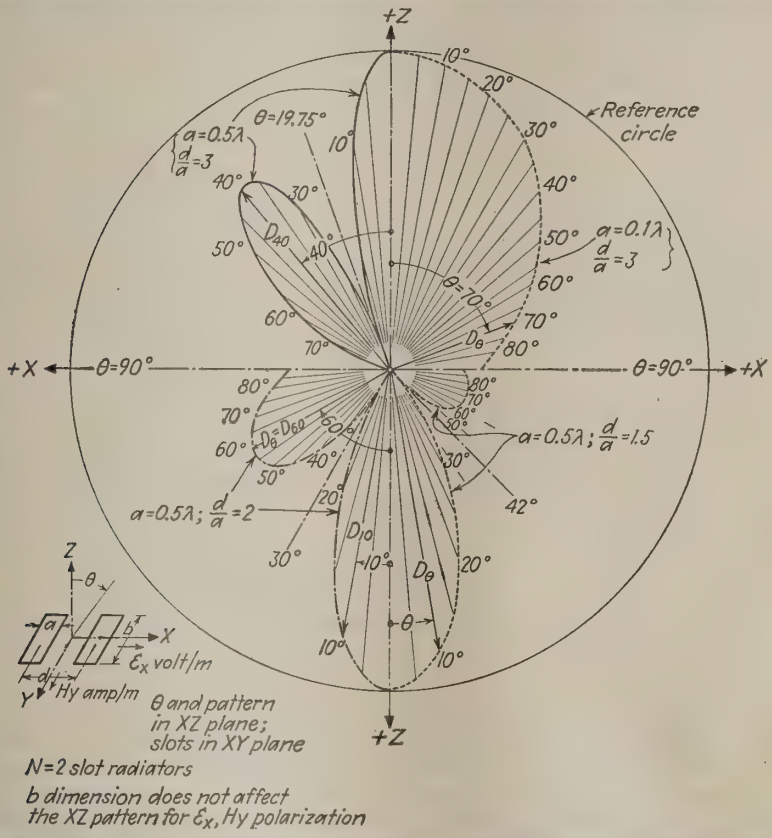

FIG. 348. Polar Fraunhofer field amplitude pattern (semipattern) for different slot width to slot separation ratios.

interfere with each other at the field point and cause the resultant field. The forward factor $(1 + \cos \theta)$ exists in the diffraction expression whether we deal with one or several slot radiators. But for more than one radiator, we must multiply the $(\sin p)/p$ function by the separation function $[\sin (qN)]/(\sin q)$, as is seen in Fig. 346. This is also mathematically a more complicated mechanism than in the case of a single wave-front radiator. It has about the same relation to the single wave-front radiation condition as an AM current has to an unmodulated carrier current. This is brought out in Fig. 349. The AM current envelope has then the characteristic of the current that modulates the carrier level. The envelope of the resultant amplitude diffractivity pattern has the characteristic shape of the single-slot pattern, which is

the $(\sin p)/p$ pattern. Therefore, only the a dimension for the ZX pattern is instrumental in the envelope characteristic of the resultant diffraction pattern for several slots. However, by means of the $[\sin (qN)]/[\sin (q)]$ function (where $q = (\pi d/\lambda) \sin \theta$), the separation dimension d plays a part as far as the number of field oscillations under the envelope are concerned, just as the carrier frequency of a modulated current determines how densely a modulation envelope is filled out with carrier-frequency current. The acuteness of the main or principal beam has much to do with the ratio d/a. It is the ratio a/λ that fixes the acuteness of the principal beam of one slot radiator by itself, since $(\sin p)/p$, for $p = (\pi a/\lambda) \sin \theta$, fixes the base width of the principal beam of the envelope by the values $(a/\lambda) \sin \theta = \pm 1$. This is the case because the envelope curve cuts the first time symmetrically through the abscissa

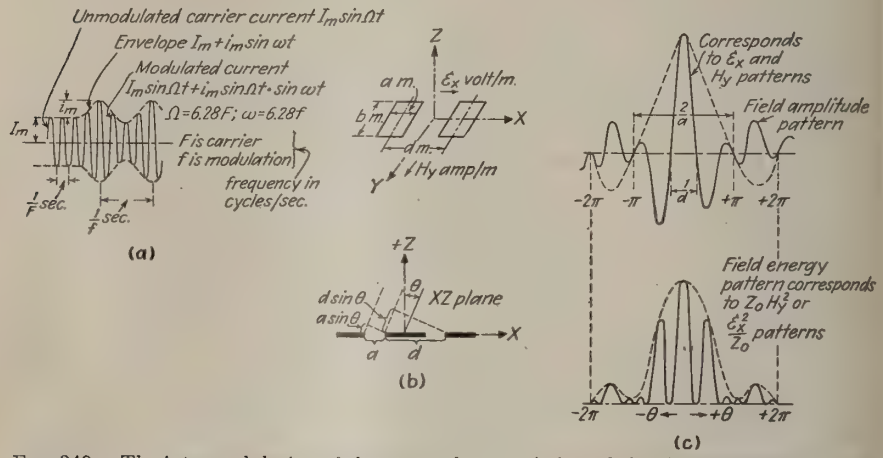

FIG. 349. The intermodulation of the group characteristic and the characteristic of a one-slot radiator.

axis whenever $p = \pm\pi$. Hence, when we can fill out the single slot or envelope characteristic only with the main beam (due to a suitable separation distance d), *we can expect a sharper main beam with only small side lobes.* This is the case, because the envelope amplitudes fall off rapidly beyond $p > \pm\pi$. This is brought out in Fig. 350. We note that the number N of equally spaced and phased slot radiators (where a and d are fixed) affects the number of field oscillations. We have then several principal beams, such as A, B, C, D, E, etc. For an infinite number of slots, the consecutive main lobes change, as it were, into spectrum lines. If the slot separation d is properly chosen, we may find essentially only one principal beam. This is indicated in the lower representation of Fig. 350. It then seems advantageous to choose the slot width a comparable to the slot separation d.

216. The Diffraction Pattern of the Electromagnetic Wave Escaping from a Rectangular Wave Guide. Inasmuch as we have no return conductor in a wave guide, we need either an additional longitudinal H component for a TE wave or an additional *longitudinal* $\mathcal{E}$ component for a TM wave. We shall discuss in this section radiation effects due to a

TE wave, which is written as $TE_{m,n}$. We have then a twofold infinite number of possible waves, corresponding to combinations of integers m and n, where we have m half sine variations along the X direction and n half sine variations along the Y direction. The $TE_{1,0}$ is the dominant wave and is independent of one dimension of the rectangular cross section (the b dimension along the Y direction). By making this dimension small enough in comparison with the a dimension along the X direction,

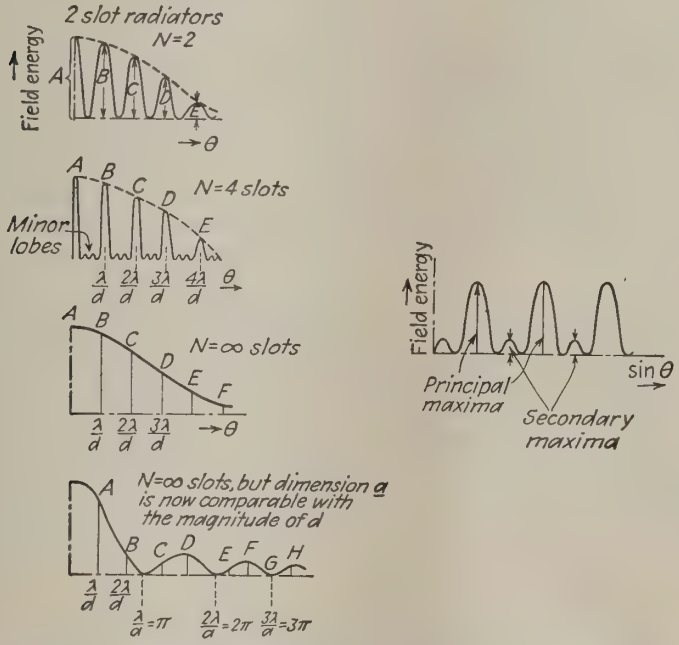

Fig. 350. Field energy distributions. a and d are fixed.

we have the feature that the $TE_{1,0}$ wave will pass only along the guide with a lower cutoff frequency

$$f_c = \frac{10^{-6}}{2a\sqrt{\mu\kappa}} \cong \frac{300}{2a} \quad \text{Mc/sec;} \quad a \text{ in meters and } \frac{1}{\sqrt{\mu\kappa}} \cong 3 \times 10^8 \text{ m/sec for air} \quad (905)$$

since for this mode, the longest wave that ever can pass through the guide must be shorter than $\lambda_c = 2a$ meters. This mode has also the *inherent* advantage that the attenuation due to the finite conductivity of the metal around the air dielectric is comparatively small. Figure 351 shows that within the guide the *transverse* field associations $\mathcal{E}_y$ volts

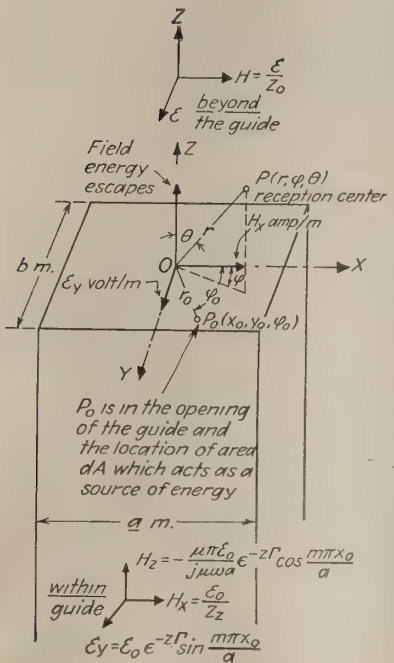

$$\left.\begin{aligned} \mathcal{E}_y &= \mathcal{E}_0 \sin \frac{\pi x_0}{a} \\ H_x &= -\frac{\rho}{Z_0}\,\mathcal{E}_y \end{aligned}\right\} \text{ for the } \mathrm{TE}_{1,0} \text{ wave}$$

Wave impedance in the Z direction

$$Z_z = \frac{j\omega\mu}{\Gamma} = \frac{Z_0}{\rho} \text{ ohms}$$

$$Z_0 = 377 \text{ ohms}; \quad \rho = \sqrt{1 - \left(\frac{f_c}{f}\right)^2}$$

Propagation constant within guide along the Z axis

$$\Gamma = \sqrt{\frac{m^2\pi^2}{a^2} - \frac{4\pi^2}{\lambda^2}} \text{ for } \mathrm{TE}_{m,0} \text{ waves and } m = 1, 2, 3, \ldots$$

$$f_c = \frac{3 \times 10^8}{\lambda_c} = \frac{3 \times 10^8 m}{2a} = \frac{m}{2a\sqrt{\mu\kappa}}$$

$$\frac{1}{\sqrt{\mu\kappa}} \cong \frac{1}{\sqrt{\mu_0\kappa_0}} = 3 \times 10^8 \text{ meters/sec}$$

(for air within the guide)

For unattenuated propagation Γ is imaginary and $\lambda < \lambda_c$, and

$$\Gamma = j\sqrt{\frac{4\pi^2}{\lambda^2} - \frac{m^2\pi^2}{a^2}} = j\sqrt{\frac{4\pi^2}{\lambda^2} - \frac{4\pi^2 m^2}{m^2\lambda_c^2}}$$

$$= j\frac{2\pi}{\lambda}\sqrt{1 - \left(\frac{\lambda}{\lambda_c}\right)^2} = j\beta\sqrt{1 - \left(\frac{f_c}{f}\right)^2}$$

$$= j\beta\rho = j\beta_z; \quad \rho = \sqrt{1 - \left(\frac{f_c}{f}\right)^2};$$

$$Z_z = \frac{j\omega\mu}{\Gamma} = \frac{\omega}{\beta}\frac{\mu}{\rho} = 3 \times 10^8 \frac{\mu}{\rho}$$

$$= \frac{1}{\sqrt{\mu\kappa}}\frac{\mu}{\rho} = \frac{\sqrt{\mu/\kappa}}{\rho} = \frac{Z_0}{\rho};$$

$$\lambda_z = \frac{2\pi}{\beta_z} = \frac{2\pi}{\beta\rho} = \frac{\lambda}{\rho} \text{ meters};$$

$$v_z = \frac{\omega}{\beta_z} = \frac{\omega}{\beta\rho} = \frac{3 \times 10^8}{\rho} \text{ meters/sec}$$

FIG. 351. Conditions for $\mathrm{TE}_{m,0}$ waves in a rectangular wave guide. For $\mathrm{TE}_{1,0}$ wave $m = 1$, $n = 0$, $\lambda_c = 2a$ meters. λ_z is a guide wavelength and is always greater than the unbounded wavelength λ in the same medium ($\lambda_{air} = 300/f^{(\mathrm{Mc/sec})}$).

per meter and H_x amperes per meter are such that

$$\left.\begin{aligned} \frac{\mathcal{E}_y}{H_x} = Z_z = \frac{Z_0}{\rho} \quad \text{ohms}; \qquad Z_0 = \sqrt{\frac{\mu}{\kappa}} \cong 376.7 \text{ ohms for air} \\ \rho = \sqrt{1 - \left(\frac{f_c}{f}\right)^2} \end{aligned}\right\} \tag{905a}$$

where f denotes the operating frequency and f_c is the frequency of the $\mathrm{TE}_{1,0}$ wave from which on and below which no wave propagation through

the guide is possible. Beyond the open end of the guide, we have, in the radiation region, the field associations $\mathcal{E}$ and H, and $\mathcal{E}/H = 376.7$ ohms. We have also a longitudinal H_z field, as in Fig. 351, within the guide. Hence, a transition must take place at the mouth of the rectangular wave guide and close to it in order to bring about the required impedance transformation. For customary radiation from a current-carrying conductor, this done by the induction field interlinked with the conductor and inseparable from it. This field acts, as it were, as an electromagnetic catalyzer, which is no longer present in the true radiation region but is part of the electromagnetic field structure in the near region of the radiator. We also know that close to a radiating linear conductor we have a longitudinal electric field component. We must make assumptions so that we can consider the mouth of the guide as being made up of an electric and a magnetic current sheet. We assume, therefore, that the discontinuity at the mouth does not change the transverse fields $\mathcal{E}_y$ and H_x. We also assume that no current creeps around the guide at the open end; *i.e.*, we consider the outside of the guide free from charges.

Strictly, the transverse $\mathcal{E}_y$ field arriving at the opening is Z_z times the value of the transverse H_x field [according to (905*a*)]. The impedance Z_z can be equal to the characteristic impedance Z_0 for unbounded (unguided) space only if $\rho = \sqrt{1 - (f_c/f)^2} = 1$. This means that $(f_c/f)^2$ must be negligible compared with unity. The operating frequency f must then be high compared with the cutoff frequency. From the $\mathcal{E}_y$ field distributions for the consecutive $TE_{m,0}$ modes in Fig. 352, we note that we have half sinusoidal, full sinusoidal, and one and a half sinusoidal distributions along the a dimension of the guide. Therefore, the consecutive cutoff frequencies are given by

$$f_c = \frac{300m}{2a}; \qquad m = 1, 2, 3, \cdots \tag{905b}$$

where a is in meters. This means that for an operating frequency f equal to about twice the cutoff frequency of the $TE_{1,0}$ wave and larger, $TE_{2,0}$ also can pass. For a frequency f equal to about three times the cutoff frequency of the $TE_{1,0}$ wave and larger, both the $TE_{2,0}$ and $TE_{3,0}$ waves also can pass in the guide. Hence, $(f_c/f)^2 = 0.25$ is the smallest value for which only $TE_{1,0}$ waves can exist at the opening of the guide. We have, for the phase velocity c' along the guide and the corresponding wavelength λ_g,

$$\left.\begin{aligned} c' = v_z &= \frac{c}{\rho} = \frac{3 \times 10^8}{\sqrt{1 - (f_c/f)^2}} \quad \text{m/sec} \\ \lambda_g = \lambda_z &= \frac{\lambda}{\sqrt{1 - (f_c/f)^2}} = \frac{300}{f\rho} = \frac{300}{\sqrt{f^2 - f_c^2}} \quad \text{m} \end{aligned}\right\} \tag{905c}$$

where f is in megacycles per second.

If we are not operating too close to a possible cutoff frequency f_c or beyond it, with only $TE_{1,0}$ waves, we can assume that we have no serious

wave-front distortion. Suppose we deal with a distant reception center P, located at r, φ, θ. At any point P_0, with coordinates $x_0, y_0, z_0 = 0 = z$, we have an electromagnetic Huygens wavelet radiator $dS = dx_0\, dy_0$.

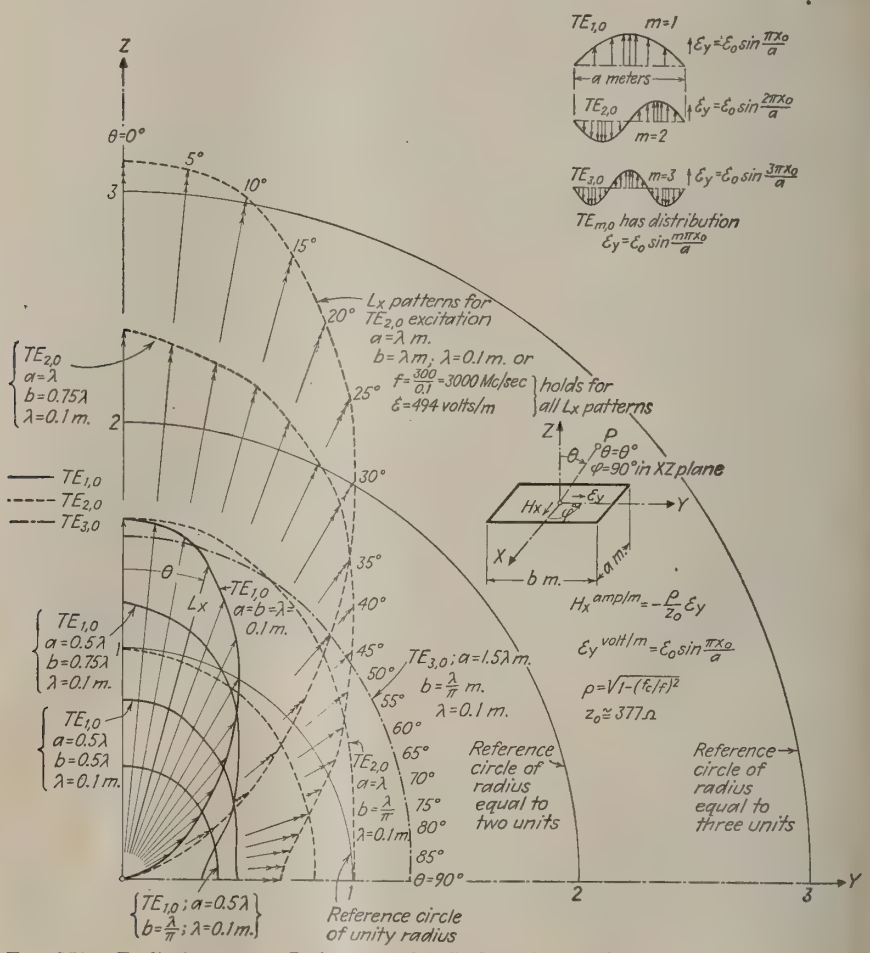

FIG. 352. Radiation vector L_x in vertical YZ plane ($\varphi = 90°$ everywhere, but $\theta = \theta°$).

Over the entire area $S = ab$ square meters, we have the tangential field associations

$$\left.\begin{aligned} &\mathcal{E}_y = \mathcal{E}_0 \sin\left(\frac{\pi x_0}{a}\right) \text{ volts/m}; \qquad H_x = -\frac{\rho}{Z_0}\,\mathcal{E}_y \text{ amp/m} \\ &Z_0 = \sqrt{\frac{\mu}{\kappa}} \cong 376.7 \text{ ohms}; \qquad \rho = \sqrt{1 - \left(\frac{f_c}{f}\right)^2} \end{aligned}\right\} \tag{905d}$$

for the guide excited in the $TE_{1,0}$ mode. The sinusoidal $\pi x_0/a$ function satisfies the zero electric field requirements on the metal surfaces $x_0 = \pm\frac{1}{2}a$ of the guide. If $d(m_e)$ represents the moment of an element of electric current at P_0, the corresponding[1] differential magnetic radiation vector is $dN = \epsilon^{-j\beta\sqrt{x_0^2+y_0^2}\cos\psi} d(m_e)$ meter · amperes. In the same way, an element of a magnetic current sheet in the opening plane of the guide, by virtue of its magnetic current moment $d(m_m)$, causes a corresponding differential magnetic radiation vector $dL = \epsilon^{-j\beta\sqrt{x_0^2+y_0^2}\cos\psi} d(m_m)$ meter · volts. The total radiation vector effects, at reception center P, are then

$$\begin{aligned} N &= \iint \epsilon^{-j\beta\sqrt{x_0^2+y_0^2}\cos\psi} d(m_e) \qquad \text{m} \cdot \text{amp} \\ L &= \iint \epsilon^{-j\beta\sqrt{x_0^2+y_0^2}\cos\psi} d(m_m) \qquad \text{m} \cdot \text{volts} \\ \cos\psi &= \cos\theta + \sin\theta\cos\varphi(\varphi - \varphi_0) \end{aligned}$$

In these expressions, $\sqrt{x_0^2 + y_0^2}$ is the distance OP_0 from the symmetry center O of the opening (this is also taken as the origin of the XYZ system) to the surface element $dS = dx_0\, dy_0$ at P_0, which is a Huygens radiator. The direction OP with the direction OP_0 makes the angle ψ. Since the general location of P_0 is x_0, y_0, φ_0 and if P is r, φ, θ, the above $\cos\psi$ relation holds. Inasmuch as we have, in the guide opening, the tangential field associations $\mathcal{E}_y = \mathcal{E}_0 \sin(\pi x_0/a)$ and $H_x = -\rho\mathcal{E}_y/Z_0$, we have the elementary moments

$$d(m_{e_y}) = -H_x\, dS; \qquad d(m_{m_x}) = -\mathcal{E}_y\, dS$$

The respective radiation vectors then become

$$\left.\begin{aligned} L_x &= \mathcal{E}_0 \int_{x_0=-a/2}^{x_0=a/2} \int_{y_0=-b/2}^{y_0=b/2} \sin\left(\frac{\pi x_0}{a}\right) \epsilon^{j\beta(x_0\cos\varphi + y_0\sin\varphi)\sin\theta}\, dx_0\, dy_0 \text{ m} \cdot \text{volts} \\ N_y &= -\frac{\rho}{Z_0} L_x \text{ m} \cdot \text{amp}; \quad Z_0 = \sqrt{\frac{\mu}{\kappa}} \cong 376.7 \text{ ohms}; \quad \rho = \sqrt{1 - \left(\frac{f_c}{f}\right)^2} \end{aligned}\right\} \tag{905e}$$

The double integral can also be taken for the limits O to a and O to b, and

$$\int_0^a \int_0^b = \left[\int_0^{x_0=a} \sin\left(\frac{\pi x_0}{a}\right) \epsilon^{j\beta x_0\cos\varphi\sin\theta}\, dx_0\right]\left(\int_0^{y_0=b} \epsilon^{j\beta y_0\sin\varphi\sin\theta}\, dy_0\right) \tag{905f}$$

Putting $\beta\cos\varphi\sin\theta = m$ and $\beta\sin\varphi\sin\theta = n$, we find

$$\left.\begin{aligned} \int\int &= \left[\int_0^a \sin\left(\frac{\pi x_0}{a}\right) \epsilon^{jmx_0}\, dx_0\right]\left(\int_0^b \epsilon^{jny_0}\, dy_0\right) \\ \int_0^b \epsilon^{jny_0}\, dy_0 &= \left|\frac{\epsilon^{jny_0}}{jn}\right|_0^b = -j\,\frac{\epsilon^{jnb} - 1}{n} \end{aligned}\right\} \tag{905g}$$

[1] For details consult Sec. 124.

For $\pi/a = q$, we have

$$\int_0^a \epsilon^{jmx_0} \sin\left(\frac{\pi x_0}{a}\right) dx_0 = \int_0^a \sin(qx_0)[\cos(mx_0) + j\sin(mx_0)\,dx_0]$$

$$= \int_0^a \sin(qx_0)\cos(mx_0)\,dx_0 + j\int_0^a \sin(qx_0)\sin(mx_0)\,dx_0$$

$$= \left| -\frac{\cos(q-m)x_0}{2(q-m)} - \frac{\cos(q+m)x_0}{2(q+m)} + j\left[\frac{\sin(q-m)x_0}{2(q-m)} - \frac{\sin(q+m)x_0}{2(q+m)}\right]_0^a \right.$$

$$= \left| \frac{\epsilon^{jmx_0}[jm\sin(qx_0) - q\cos(qx_0)]}{q^2 - m^2} \right|_0^a$$

$$= \frac{\epsilon^{jma}[jm\sin(qa) - q\cos(qa)] + r}{q^2 - m^2} = \frac{\epsilon^{jma}[jm\sin(\pi) - q\cos(\pi)] + r}{q^2 - m^2}$$

or

$$\int_0^a \epsilon^{jmx_0} \sin\left(\frac{\pi x_0}{a}\right) dx_0 = \frac{(\epsilon^{jma} + 1)q}{q^2 - m^2} \tag{905h}$$

Using the results of (905*f*), (905*g*), and (905*h*), we have

$$\int_0^a \int_0^b = j\frac{(1 - \epsilon^{jnb})(1 + \epsilon^{jma})q}{n(q^2 - m^2)} \tag{905i}$$

But

$$\left.\begin{aligned} q^2 - m^2 &= \frac{\pi^2 - \beta^2 a^2 \sin^2\theta\cos^2\varphi}{a^2} \\ n(q^2 - m^2) &= \frac{\beta\sin\theta\sin\varphi(\pi^2 - \beta^2 a^2\sin^2\theta\cos^2\varphi)}{a^2} \\ \frac{q}{n(q^2 - m^2)} &= \frac{\pi/a}{n(q^2 - m^2)} = \frac{\pi a}{\beta\sin\theta\sin\varphi(\pi^2 - \beta^2 a^2\sin^2\theta\cos^2\varphi)} \end{aligned}\right\} \tag{905j}$$

Putting $ma = A$ and $nb = B$, we find the *absolute* value

$$|(1 - \epsilon^{jnb})(1 + \epsilon^{jma})| = \sqrt{(1 - \epsilon^{jB})(1 - \epsilon^{-jB})}\sqrt{(1 + \epsilon^{jA})(1 + \epsilon^{-jA})}$$

$$= \sqrt{2 - (\epsilon^{jB} + \epsilon^{-jB})}\sqrt{2 + (\epsilon^{jA} + \epsilon^{-jA})} = \sqrt{2 - 2\cos B}\sqrt{2 + 2\cos A}$$

$$= 4\sqrt{\frac{1 - \cos B}{2}}\sqrt{\frac{1 + \cos B}{2}} = 4\sin\left(\frac{B}{2}\right)\cos\left(\frac{A}{2}\right) \tag{905k}$$

Using (905*i*), (905*j*), and (905*k*) in (905*e*), we find, since $4\pi/\beta = 2\lambda$,

$$\left.\begin{aligned} L_x &= j\frac{2a\lambda\mathcal{E}_0\sin(B/2)\cos(A/2)}{\sin\theta\sin\varphi(\pi^2 - \beta^2 a^2\sin^2\theta\cos^2\varphi)} \quad \text{m}\cdot\text{volts} \\ N_y &= -\frac{\rho}{Z_0}L_x \quad \text{m}\cdot\text{amp}; \qquad \frac{A}{2} = \frac{\pi a}{\lambda}\cos\varphi\sin\theta \\ \frac{B}{2} &= \frac{\pi b}{\lambda}\sin\varphi\sin\theta \\ \beta &= \frac{2\pi}{\lambda}; \qquad \lambda = \frac{300}{f^{(\text{Mc/sec})}} \quad \text{meters}; \qquad \rho = \sqrt{1 - \left(\frac{f_c}{f}\right)^2} \\ Z_0 &= \sqrt{\frac{\mu}{\kappa}} \cong 376.7 \text{ ohms} \end{aligned}\right\} \tag{905l}$$

Since, for a fixed operating frequency f, the quantity N_y is proportional to L_x and negative, for a constant of proportionality ρ/Z_0, it is necessary to inspect only the D_x radiation vector in order to see what happens for either radiation vector. For the reception points P in the XZ plane, we have $\varphi = 0$ with the simplifications

$$\frac{A}{2} = \frac{\pi a}{\lambda} \sin\theta; \qquad \frac{B}{2} = 0; \qquad \sin\left(\frac{B}{2}\right) = 0; \qquad L_x = 0 = N_y$$

For reception centers in the YZ plane, we have $\varphi = 90$ deg, and

$$\left.\begin{aligned} &\frac{A}{2} = 0; \qquad \cos\left(\frac{A}{2}\right) = 1; \qquad \frac{B}{2} = \frac{\pi b}{\lambda} \sin\theta \\ &L_x = j \frac{0.203 a\lambda \mathcal{E}_0 \sin\left[\left(\frac{\pi b}{\lambda}\right) \sin\theta\right]}{\sin\theta} \qquad \text{m} \cdot \text{volts} \end{aligned}\right\} \qquad (905m)$$

In the XY plane (plane of the guide opening), we have

$$\left.\begin{aligned} &\theta = 90°; \qquad \sin\theta = 1; \qquad \frac{A}{2} = \frac{\pi a}{\lambda} \cos\varphi; \qquad \frac{B}{2} = \frac{\pi b}{\lambda} \sin\varphi \\ &L_x = j \frac{2a\lambda \mathcal{E}_0 \sin\left[(\pi b/\lambda) \sin\varphi\right] \cos\left[(\pi a/\lambda) \cos\varphi\right]}{\sin\varphi[\pi^2 - (4\pi^2 a^2/\lambda^2) \cos^2\varphi]} \qquad \text{m} \cdot \text{volts} \end{aligned}\right\} \qquad (905n)$$

Table 77 gives the computations for the L_x pattern in the YZ plane for an $\mathcal{E}_0$ value of 494 volts/m, so that 0.203×494 becomes 100. Choosing $b = \lambda/\pi$ meters, we have $\pi b/\lambda = 1$; and for the three successive $TE_{m,0}$ modes, $a\lambda = 0.5\lambda^2$, λ^2, and $1.5\lambda^2$. Table 77 shows that a broad L_x pattern is obtained in the YZ plane and that the order $m = 1, 2, 3, \cdots$ causes only a multiplying factor w. The ratio $(\sin\alpha)/(\sin\theta)$ affects the pattern mostly. If we had taken the y dimension $b = 0.5\lambda$, 0.75λ, and λ, respectively, we should have found the evaluations of Table 78. Figure 352 gives the L_x patterns and shows that by means of the b dimension, it is possible to sharpen the pattern. For $b = \lambda/\pi$, the L_x pattern is quite broad; while for $b = \lambda$, there is a beaming along the Z axis. If we had chosen b still larger, side lobes would have appeared.

217. Notes on the Actual Field Amplitude and Energy Pattern Escaping from an Open-ended Rectangular Wave Guide for $TE_{m,0}$ Waves. The power directivity D_p (or radiation intensity) at the distant field point P of Fig. 351 represents the amount of electromagnetic field power flowing per unit solid angle in the φ, θ direction. It is found from the elementary solid angle $\sin\theta\, d\theta\, d\varphi$. Each of the secondary radiation centers (electromagnetic Huygens wavelet centers) in the opening plane

of the rectangular wave guide acts, in effect, as coinciding electric and magnetic current sheets of elementary area $dS = dx_0\,dy_0$, expressed in square-meter units, even though vanishingly small. According to Secs. 61 to 64, such current sheets $\int\int J_y\,dS$ and $\int\int J_{m_x}\,dS$, of electric current

TABLE 77. PATTERN OF L_x RADIATION VECTOR IN THE YZ PLANE

θ, deg	sin θ numeric	$\alpha = 57.3 \sin\theta$, deg	sin α numeric	$v = \frac{\sin\alpha}{\sin\theta}$	L_x value $= jwv$		
					$TE_{1,0}$ vw_1	$TE_{2,0}$ vw_2	$TE_{3,0}$ vw_3
0.0	0.0000	0.00	0.0000	1.000	0.5000	1.000	1.5000
5	0.0872	5.0	0.0872	1.0	0.5	1.0	1.5
10	0.1736	9.9	0.1719	0.989	0.4945	0.989	1.4835
15	0.2588	14.8	0.2554	0.985	0.4925	0.985	1.4775
20	0.342	19.6	0.3355	0.98	0.49	0.98	1.47
25	0.4226	24.2	0.4099	0.97	0.485	0.97	1.455
30	0.5	28.7	0.4802	0.96	0.48	0.96	1.44
35	0.5736	33	0.5446	0.95	0.475	0.95	1.425
40	0.6428	37	0.6018	0.932	0.466	0.932	1.398
45	0.7071	40.5	0.6494	0.918	0.459	0.918	1.377
50	0.766	44	0.6947	0.908	0.454	0.908	1.362
55	0.8192	47	0.7314	0.895	0.4475	0.895	1.3425
60	0.866	49.7	0.7627	0.882	0.441	0.882	1.325
65	0.9063	52	0.788	0.87	0.435	0.87	1.305
70	0.9397	54	0.809	0.862	0.431	0.862	1.293
75	0.9659	55.2	0.8211	0.85	0.425	0.85	1.275
80	0.9848	56.5	0.8339	0.848	0.424	0.848	1.272
85	0.9962	57	0.8387	0.843	0.4215	0.843	1.2645
90	1.0	57.3	0.8415	0.841	0.4205	0.841	1.2615

Remarks: $\mathcal{E}_0 = 494$ volts/m; $b = \lambda/\pi$ m; $\sin[(\pi b/\lambda)\sin\theta] = \sin(57.3\sin\theta) = \sin\alpha°$. For $\lambda = 10$ cm $= 0.1$ m, we have $\lambda^2 = 0.01$ sq m, and

$$L_x = j\,\frac{0.203a\lambda\mathcal{E}_0 \sin\left(\frac{\pi b}{\lambda}\sin\theta\right)}{\sin\theta} \quad \text{m} \cdot \text{volts}$$

$$0.203a\lambda\mathcal{E}_0 = w; \qquad \frac{\sin\left(\frac{\pi b}{a}\sin\theta\right)}{\sin\theta} = v; \qquad v = \frac{\sin\alpha}{\sin\theta}$$

For $TE_{1,0}$ excitation $a = \lambda/2$, $a\lambda = 0.5\lambda^2 = 0.5 \times 10^{-2}$, $w = w_1 = 0.203 \times 0.5 \times 10^{-2} \times 494 = 0.5$. For $TE_{2,0}$ excitation $w = w_2 = 1$. For $TE_{3,0}$ excitation, $a\lambda = 1.5\lambda^2$, and $w = w_3 = 1.5$.

density J_y amperes per meter and magnetic current density J_{m_x} volts per meter, account for discontinuities in $\mathcal{E}_y$ and H_x at the opening of the wave guide. We have also seen that for the distance r_0 (Fig. 351) from symmetry point O of the opening to a Huygens radiator dS at P_0 and the angle P_0OP (angle ψ), we have

$$r_0 \cos\psi = (x_0 \cos\varphi + y_0 \sin\varphi)\sin\theta$$

TABLE 78. PATTERNS OF L_x RADIATION VECTOR FOR $TE_{1,0}$ AND $TE_{2,0}$ GUIDE EXCITATIONS AND DIFFERENT b VALUES

		For $b = 0.5\lambda$				For $b = 0.75\lambda$				For $b = \lambda$			
θ, deg	$\sin\theta$	$\alpha = 90 \sin\theta$, deg	$\sin\alpha$	$TE_{2,0}$ $v = \frac{\sin\alpha}{\sin\theta}$	$TE_{1,0}$ $wv = \frac{v}{2} = \frac{L_x}{j}$	$\alpha = 135 \sin\theta$, deg	$\sin\alpha$	$TE_{2,0}$ $v = \frac{\sin\alpha}{\sin\theta}$	$TE_{1,0}$ $wv = \frac{v}{2} = \frac{L_x}{j}$	$\alpha = 180 \sin\theta$, deg	$\sin\alpha$	$TE_{2,0}$ $\frac{\sin\alpha}{\sin\theta} = v$	$TE_{1,0}$ $wv = \frac{v}{2} = \frac{L_x}{j}$
0.0	0.0000	0.00	0.0000	1.56	0.78	0.00	0.0000	2.4	1.2	0.0	0.0000	3.12	1.56
5	0.0872	7.85	0.1365	1.56	0.78	11.8	0.2045	2.34	1.17	15.7	0.2706	3.11	1.555
10	0.1736	15.7	0.2706	1.56	0.78	23.5	0.3987	2.28	1.14	31.4	0.521	3.0	1.5
15	0.2588	23.3	0.3955	1.53	0.765	35	0.5736	2.22	1.11	46.5	0.7254	2.8	1.4
20	0.342	30.7	0.5105	1.49	0.745	46	0.7193	2.1	1.05	61.5	0.8788	2.56	1.28
25	0.4226	38	0.6157	1.46	0.73	57	0.8387	1.98	0.99	76	0.9703	2.3	1.15
30	0.5	45	0.7071	1.4142	0.7071	67.5	0.9239	1.89	0.945	90	1.0000	2.00	1.00
35	0.5736	51.8	0.7859	1.37	0.685	77.5	0.9763	1.7	0.85	103	0.9744	1.7	0.85
40	0.6428	58	0.848	1.32	0.66	86.5	0.9981	1.55	0.785	116	0.8988	1.39	0.695
45	0.7071	63.5	0.8949	1.27	0.635	95	0.9962	1.41	0.705	127	0.7986	1.13	0.565
50	0.766	69	0.9336	1.22	0.61	103	0.9744	1.28	0.64	138	0.6691	0.875	0.4375
55	0.8192	73.5	0.9588	1.17	0.585	110	0.9387	1.15	0.575	147	0.5446	0.67	0.335
60	0.866	78	0.9781	1.13	0.565	117	0.891	1.03	0.565	156	0.4067	0.47	0.235
65	0.9063	81.5	0.989	1.09	0.545	122	0.848	0.935	0.4675	163	0.2924	0.323	0.1615
70	0.9397	84.5	0.9954	1.06	0.53	126	0.809	0.86	0.43	169	0.1908	0.204	0.102
75	0.9659	87	0.9986	1.03	0.515	130	0.766	0.795	0.3975	174	0.1045	0.1085	0.05425
80	0.9848	88.5	0.9997	1.01	0.505	133	0.7314	0.745	0.3725	177	0.0523	0.0535	0.02675
85	0.9962	89.5	1.0000	1.005	0.5002	134	0.7193	0.72	0.36	179	0.0175	0.0176	0.0088
90	1.0000	90	1.0000	1.000	0.5	135	0.7071	0.7071	0.3535	180	0.0000	0.0000	0.0000
1	0.0175	1.58	0.0276	1.56		2.36	0.0412	2.34		3.15	0.0549	3.12 } for 0/0	
0.1	0.0017	0.153	0.00265	1.56		0.23	0.0041	2.11		0.306	0.0053	3.12 } determination	

Remarks: $\mathcal{E}_0 = 494$ volts/m so that $0.203 \times 494 = 100$. For $b = \lambda/2$, we have $\pi b/\lambda = 1.57$ radians, $\sin[(\pi b/\lambda)\sin\theta] = \sin(1.57 \times 57.3 \sin\theta) = \sin\alpha°$, $\alpha° = 90° \sin\theta$. For $b = 0.75\lambda$, we find $\pi b/\lambda = 0.75\pi = 2.35$ radians and $\sin\alpha° = \sin(2.35 \times 57.3 \sin\theta) = \sin(135° \sin\theta)$. For $b = \lambda$, $\sin\alpha° = \sin(180° \sin\theta)$. For $\lambda = 0.1$ m, $w = w_1 = 0.5$ as in Table 77, for $TE_{1,0}$ wave excitation; and for $v = (\sin\alpha)/(\sin\theta)$, we find $L_x = jwv$, if $w = 0.203a\lambda\mathcal{E}_0$. The $\theta = 1$ deg and $\theta = 0.1$ deg evaluations are for angles $\theta \to 0$ deg, since $(\sin\alpha)/(\sin\theta) = 0/0$ (undeterminate for $\theta = 0$ deg).

and the radiation vectors

$$\left.\begin{aligned} N_y &= \int\int_S J_y(x_0, y_0)\epsilon^{j\beta r_0 \cos\psi}\, dS \qquad \text{m} \cdot \text{amp} \\ L_x &= \int\int_S J_{mx}(x_0, y_0)\epsilon^{j\beta r_0 \cos\psi}\, dS \qquad \text{m} \cdot \text{volts} \end{aligned}\right\} \tag{905o}$$

since N and L generally refer to volume integrals

$$N = \int\int\int_\tau J(x_0, y_0, z_0)\epsilon^{j\beta r_0 \cos\psi}\, d\tau; \qquad L = \int\int\int_\tau J_m(x_0, y_0, z_0)\epsilon^{j\beta r_0 \cos\psi}\, d\tau$$
$$d\tau = dx_0\, dy_0\, dz_0$$

where J is in amperes per square meter; J_m in volts per square meter, and formulas (831) are basic. We have also respective moments $d(m_e)$ and $d(m_m)$ of the electric current element $J_y\, dS$ and the magnetic current element $J_{m_x}\, dS$ proportional to the tangential $\mathcal{E}_y$ and H_x field associations at the opening of the guide. As we know, the Poynting vector p yields the actual power density in watts per square meter at a field point P. We can, however, use the power directivity D_p (the power radiated from the end of the guide in a given direction φ, θ per unit solid angle), which refers to the average value of p on a sphere of 1 m radius. This can be understood from Eqs. (829), (829a), (834), (834a), and (835), since $P_r = \int_0^\pi \int_0^{2\pi} D_p \sin\theta\, d\theta\, d\varphi$ watts. We have also the general Laplace transformations of (835a), if N_x, N_y, N_z denote, for $N = \sqrt{N_x^2 + N_y^2 + N_z^2}$, the Cartesian components and N_θ and N_φ the components along the θ and φ spherical coordinates. We have similar relations for the L radiation vector, and

$$\left.\begin{aligned} D_p &= \frac{Z_0}{8\lambda^2}\left(\left|N_\theta + \frac{L_\varphi}{Z_0}\right|^2 + \left|N_\varphi - \frac{L_\theta}{Z_0}\right|^2\right) \\ Z_0 &= \sqrt{\frac{\mu}{\kappa}} \cong 376.7 \text{ ohms for air}; \qquad \lambda = \frac{300}{f^{(\text{Mc/sec})}} \qquad \text{m} \end{aligned}\right\} \tag{905p}$$

since, according to (834), (834a), (835), (838), (838a), (838b), and (838c). the *magnitudes* | | *must* be used. We have, according to (905l), the ratio

$$\frac{L_x}{N_y} = -\frac{Z_0}{\rho} = -\frac{\sqrt{\mu/\kappa}}{\sqrt{1 - \left(\frac{f_c}{f}\right)^2}} = Z_z \qquad \text{ohms}$$

The field amplitude is proportional to the square root of the power directivity D_p, or equal to $k\sqrt{D_p}$, with the result

$$\mathcal{E}_P = k\sqrt{\underbrace{\left[(\rho + \cos\theta)^2 + \left(\frac{f_c}{f}\right)^2 \sin^2\theta \sin^2\varphi\right]}_{=F(f,\,\varphi,\,\theta)}} \frac{L_x N_y}{8\lambda^2}$$

$$= \frac{ka\mathcal{E}_0 \sin(B/2)\cos(A/2)}{\sin\theta \sin\varphi(\pi^2 - \beta^2 a^2 \sin^2\theta\cos^2\varphi)} \sqrt{\frac{F(f,\varphi,\theta)}{2Z_0}} \quad \text{volts/m} \quad (905q)$$

We have now a *generalized* Huygens-Kirchhoff factor

$$\sqrt{F(f,\varphi,\theta)} = \sqrt{(\rho + \cos\theta)^2 + \left(\frac{f_c}{f}\right)^2 \sin^2\theta \sin^2\varphi}$$

$$= \sqrt{\left[\sqrt{1 - \left(\frac{f_c}{f}\right)^2} + \cos\theta\right]^2 + \left(\frac{f_c}{f}\right)^2 \sin^2\theta \sin^2\varphi}$$

in the place of the classic forward factor $1 + \cos\theta$. Comparing (905*a*) with (905*l*), we note that we have only to multiply the L_x patterns of Fig. 352 by the factor $\sqrt{F(f,\varphi,\theta)}$ in order to give the actual field amplitude pattern, since k is a constant of proportionality and $2Z_0 = 2 \times 376.7$ ohms is likewise a constant for a certain guide medium (air in this particular case). For the power directivity pattern

$$D_p = 0.5 \frac{a^2\mathcal{E}_0^2 F(f,\varphi,\theta) \sin^2(B/2)\cos^2(A/2)}{Z_0 \sin^2\theta \sin^2\varphi(\pi^2 - \beta^2 a^2 \sin^2\theta\cos^2\varphi)} \quad (905r)$$

we have only to multiply the squared length of the various L_x radius vectors of Fig. 352 by the function $F(f,\varphi,\theta)$. The generalized Huygens-Kirchhoff factor $\sqrt{F(f,\varphi,\theta)}$ shows that besides the θ function, we also have to take into account the φ function as well as the operating frequency. This means that we do *not always* have a true forward wavelet effect. But the forward effect becomes satisfied when the operating frequency f is sufficiently high in comparison with the cutoff frequency f_c. The second term $(f_c/f)^2 \sin^2\varphi \sin^2\theta$ is then negligible, and the remaining part of the first term of $\sqrt{F(f,\varphi,\theta)}$ is essentially $1 + \cos\theta$. For the cutoff frequency, we have $\rho = 0$, and

$$\sqrt{F(f,\varphi,\theta)} = \sqrt{(0 + \cos\theta)^2 + \sin^2\theta \sin^2\varphi} = \sqrt{\cos^2\theta + \sin^2\theta \sin^2\varphi}$$

$$\sqrt{F(f,\varphi,\theta)} = \pm\cos\theta \qquad \text{along the } Z \text{ axis, since } \varphi = 0°$$

Such a condition, however, has no value, since the $TE_{m,0}$ wave *no longer* passes with useful energy transfer through the guide. For f values that are guided, we find

$$\sqrt{F(f,\varphi,\theta)} = \sqrt{\left[\sqrt{1 - \left(\frac{f_c}{f}\right)^2} + \cos\theta\right]^2} = \sqrt{1 - \left(\frac{f_c}{f}\right)^2} + \cos\theta$$

for $\varphi = 0°$ (along the Z axis)

The forward radiation is then proportional to the condition for which $\theta = 0$ deg, *i.e.*, proportional to $(\rho + 1)$; while for the backward radiation ($\theta = 180$ deg), the radiation is proportional to $\rho - 1 = \sqrt{1 - (f_c/f)^2} - 1$. In the YZ plane, we have $\varphi = 90$ deg, and

$$\mathcal{E}_P = \frac{ka\mathcal{E}_0 \sin [(\pi b/\lambda) \sin \theta]}{\pi^2 \sin \theta} \sqrt{\frac{F(f,\theta,\varphi = 90°)}{2Z_0}} \quad \text{volts/m}$$

$$Z_0 = \sqrt{\frac{\mu}{\kappa}} \cong 376.7 \text{ ohms for air}$$

$$F(f,\theta,\varphi = 90°) = (\rho + \cos \theta)^2 + \left(\frac{f_c}{f}\right)^2 \sin^2 \theta$$

218. Classic and Electromagnetic Radiation from a Circular Plane Primary Wave Front. Instead of having the aperture in the XY plane of Fig. 336 rectangular and of ab square meters area, we can also treat the case for which we have a circular primary wave front of radius a meters and $S = 3.14a^2$ square meters area. We then can again use the general wave equation for the wave disturbance w at a reception center located at any point x_1, y_1, z_1 as in Fig. 353. The reception center is then a distance $\sqrt{x_1^2 + y_1^2 + z_1^2}$ from the origin of the XYZ system. This leads to the comparison relations

$$\left.\begin{aligned} w &= K_0 \int\int \epsilon^{j\beta F(x,y)}\, dx\, dy \cong K_0 \int\int \epsilon^{-j\beta(Ax+By)}\, dx\, dy \\ &\qquad\qquad \text{for Fig. 336 and Eq. (901}g\text{)} \\ w &= K_0 \int_0^a \int_0^{2\pi} \rho \epsilon^{-j\beta\rho' \rho \cos(\varphi - \varphi')}\, d\rho\, d\varphi \qquad \text{for Fig. 353 and} \\ A &= \rho' \cos \varphi'; \qquad B = \rho' \sin \varphi' \end{aligned}\right\} \quad (906)$$

We have $\rho' \cos \varphi'$ and $\rho' \sin \varphi'$ as the polar coordinates of the distant field point P in a plane parallel to the XY plane through P with respect to the origin O. Any of the wavelet centers T_2 depend on the transformations $x = \rho \cos \varphi$ and $y = \rho \sin \varphi$ in Fig. 353. We no longer deal with rectangular conditions and, when dealing with space functions, must meet cylindrical forms. For this reason, the second of Eqs. (906) can be satisfied by a Bessel function, which reads for the nth order

$$J_n(z) = \frac{j^{-n}}{2\pi} \int_0^{2\pi} \epsilon^{jz \cos \varphi} \epsilon^{jn\varphi}\, d\varphi$$

We have then the differential equation

$$z \frac{dJ_n}{dz} + nJ_n = zJ_{n-1}$$

The first-order Bessel function ($n = 1$) is of interest here. It leads to

$$z \frac{dJ_1}{dz} + J_1 = zJ_0 \quad (906a)$$

For the zeroth order, we have the form

$$\frac{d^2y}{dz^2} + \frac{1}{z}\frac{dy}{dz} + a^2y = 0; \quad y = J_0(az) = 1 - \frac{(az)^2}{2^2} + \frac{(az)^4}{(2 \times 4)^2} - \frac{(az)^6}{(2 \times 4 \times 6)^2} + \cdots$$

which for $a = 1$ yields

$$y = 1 - \frac{z^2}{2^2} + \frac{z^4}{(2 \times 4)^2} - \frac{z^6}{(2 \times 4 \times 6)^2} + \cdots = J_0(z)$$

the gradient yields

$$\frac{dy}{dz} = \frac{d[J_0(z)]}{dz} = -\frac{z}{2} + \frac{z^3}{2^2 \times 4} - \frac{z^5}{2^2 \times 4^2 \times 6} + \cdots$$

$$= -z\left(\frac{1}{2} - \frac{z^2}{2^2 \times 4} + \frac{z^4}{2^2 \times 4^2 \times 6} - \cdots\right) = -J_1(z)$$

The first derivative of the zeroth-order solution is then the negative value of the

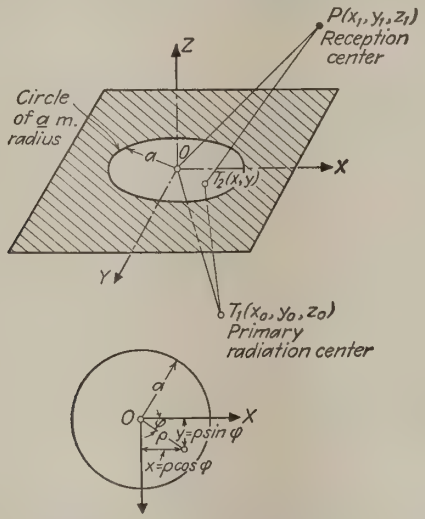

FIG. 353. Significant space geometry for diffraction due to a circular opening in a screen. T_2 is any wavelet center (secondary radiation center). For Fraunhofer diffraction T_1 and P are, in effect, an infinite distance from the screen with the circular aperture.

solution of the first-order Bessel equation. We can then find one equation by differentiating the other and find the other if we integrate. The latter is now applied by integrating (906*a*), with the result

$$J_1(z) = \frac{1}{z}\int_0^z J_0(q)q\,dq \tag{906b}$$

Since, for the *Fraunhofer* diffraction, the function $F(x, y)$ includes only *linear* terms and $J_0(z)$ is linear, we can express (906) (holding for Fig. 353) by means of

$$w = \beta \int_0^a J_0(\beta\rho\rho')\rho\,d\rho \tag{906c}$$

Putting the argument $\beta\rho\rho'$ equal to q and writing (906b) as

$$w = \frac{1}{\beta(\rho')^2}\int_0^{\beta\rho' a} J_0(q)q\,dq = \frac{a}{\rho'}J_1(\beta\rho' a) = \frac{a}{\rho'}J_1(p) \qquad (906c')$$

for $p = \beta\rho' a$. According to the abbreviations $A = \rho'\cos\varphi'$ and $B = \rho'\sin\varphi'$, the quantity ρ' denotes the radius of the circle through the reception center x_1, y_1, z_1 parallel with the XY plane. It corresponds to the circle of radius ρ in Fig. 353, covering the wavelet centers T_2 of the primary wave front in the circular aperture. The radiation intensity (wavelet energy) is proportional to the area πa^2, and we have $\int\int|w^2|\,dA\,dB = \pi a^2$; and according to the left relation of (906),

$$w = K_0\psi(A, B) = K_0\int\int\psi_1(x, y)\epsilon^{-j\beta(Ax+By)}\,dx\,dy$$

for the function $\psi(A, B)$ and function $\psi_1(x, y)$. According to Fourier,

$$\psi_1(x, y) = \frac{1}{\lambda^2}\int\int\psi(A, B)\epsilon^{j\beta(Ax+By)}\,dA\,dB$$

resulting in

$$\int\int|\psi_1(x, y)|^2\,dx\,dy = \frac{1}{K_0\lambda^2}\int\int|w|^2\,dA\,dB$$

We obtain from (906c') for the field amplitude

$$A = K\frac{J_1(p)}{p} \qquad (906d)$$

for the factor K, which for large diffraction ranges ($\theta > 4$ deg) contains the Huygens-Kirchhoff factor $(1 + \cos\theta)$ as well as $\pi a^2/\lambda$, since the energy is proportional to

$$\left(\frac{\pi a^2}{\lambda}\right)^2\left(\frac{2J_1(p)}{p}\right)^2 \quad \text{and} \quad (1 + \cos\theta) \cong 2 \quad \text{for } \theta \leqq 4°$$

From the above results, we have the comparisons for the field amplitude

$$\left.\begin{aligned}\text{Field amplitude} &= k_1\frac{\sin(p)}{p} && \text{for } \textit{rectangular} \text{ wave-front radiators}\\ \text{Field amplitude} &= k_2\frac{J_1(p)}{p} && \text{for } \textit{circular} \text{ wave-front radiators}\end{aligned}\right\} \qquad (906e)$$

Table 79 gives the evaluations for the characteristic ratio $J_1(p)/p$, since the proportionality constant k_1, depending on the electromagnetic polarization and the Kirchhoff-Huygens forward factor, is not taken into account. The function $J_1(p)/p$ vanishes for all values for which p has a magnitude, and the Bessel function $J_1(p)$ vanishes. This happens

TABLE 79. EVALUATIONS OF THE $[J_1(p)]/p$ PATTERN FOR CIRCULAR APERTURES

p	$J_1(p)$	$\frac{J_1(p)}{p}$	p	$J_1(p)$	$\frac{J_1(p)}{p}$	p	$J_1(p)$	$\frac{J_1(p)}{p}$	p	$J_1(p)$	$\frac{J_1(p)}{p}$	p	$J_1(p)$	$\frac{J_1(p)}{p}$
0.0	0.0000	0.5000	2.3	0.5399	0.2335	4.6	−0.2566	−0.056	6.9	−0.0349	−0.0050	9.2	0.2174	0.0237
0.1	0.0499	0.499	2.4	0.5202	0.216	4.7	−0.2791	−0.0595	7.0	−0.0047	−0.0007	9.3	0.2004	0.0215
0.2	0.0995	0.4975	2.5	0.4971	0.199	4.8	−0.2985	−0.062	7.1	0.0252	0.00355	9.4	0.1816	0.0194
0.3	0.1483	0.4943	2.6	0.4708	0.1815	4.9	−0.3147	−0.0642	7.2	0.0543	0.00755	9.5	0.1613	0.01695
0.4	0.196	0.49	2.7	0.4416	0.164	5.0	−0.3276	−0.06552	7.3	0.0826	0.0113	9.6	0.1395	0.0145
0.5	0.2423	0.4846	2.8	0.4097	0.146	5.1	−0.3371	−0.0662	7.4	0.1096	0.01485	9.7	0.1166	0.01205
0.6	0.2867	0.4777	2.9	0.3754	0.13	5.2	−0.3432	−0.066	7.5	0.1352	0.01785	9.8	0.0928	0.00945
0.7	0.329	0.47	3.0	0.3391	0.1130	5.3	−0.346	−0.0655	7.6	0.1592	0.0209	9.9	0.0684	0.00691
0.8	0.3688	0.461	3.1	0.3009	0.0967	5.4	−0.3953	−0.0638	7.7	0.1813	0.0235	10.0	0.0435	0.00435
0.9	0.4059	0.451	3.2	0.2613	0.0815	5.5	−0.3414	−0.0621	7.8	0.2014	0.0258	10.1	0.0184	0.00182
1.0	0.4401	0.4401	3.3	0.2207	0.0671	5.6	−0.3343	−0.0597	7.9	0.2192	0.0276	10.2	−0.0066	−0.000645
1.1	0.4709	0.429	3.4	0.1792	0.0525	5.7	−0.3241	−0.0568	8.0	0.2346	0.0293	10.3	−0.0313	−0.00304
1.2	0.4983	0.415	3.5	0.1374	0.0392	5.8	−0.311	−0.0535	8.1	0.2476	0.0306	10.4	−0.0555	−0.00532
1.3	0.522	0.4015	3.6	0.0955	0.0265	5.9	−0.2951	−0.05	8.2	0.258	0.0315	10.5	−0.0789	−0.0075
1.4	0.5419	0.3875	3.7	0.0538	0.0145	6.0	−0.2767	−0.0462	8.3	0.2657	0.0321	10.6	−0.1012	−0.00955
1.5	0.5579	0.371	3.8	0.0128	0.0034	6.1	−0.2559	−0.042	8.4	0.2708	0.0323	10.7	−0.1224	−0.0114
1.6	0.5699	0.355	3.9	−0.0272	−0.0069	6.2	−0.2329	−0.0376	8.5	0.2731	0.032	10.8	−0.1422	−0.0131
1.7	0.5778	0.339	4.0	−0.066	−0.0165	6.3	−0.2081	−0.033	8.6	0.2728	0.0317	10.9	−0.1603	−0.0147
1.8	0.5815	0.323	4.1	−0.1033	−0.0251	6.4	−0.1816	−0.0284	8.7	0.2697	0.0309	11.0	−0.1768	−0.0161
1.9	0.5812	0.306	4.2	−0.1386	−0.0332	6.5	−0.1538	−0.0237	8.8	0.2641	0.0299	11.1	−0.1913	−0.0172
2.0	0.5767	0.2883	4.3	−0.1719	−0.04	6.6	−0.125	−0.01895	8.9	0.2559	0.0288	11.2	−0.2039	−0.0182
2.1	0.5683	0.27	4.4	−0.2028	−0.0462	6.7	−0.0953	−0.01425	9.0	0.2453	0.0272	11.3	−0.2143	−0.0189
2.2	0.56	0.254	4.5	−0.2311	−0.0515	6.8	−0.0652	−0.00959	9.1	0.2324	0.0256	11.4	−0.2225	−0.0193

Remarks: $[J_1(p)]/p = 0$ for $p = 3.83, 7.02, 10.17, 13.32, \cdots$. $[J_1(0)]/0 = 0/0$, which may be any value, but the trend in this table indicates that $[J_1(0)]/0 = 0.5$, which is half the value of $[\sin(0°)]/0^{(\text{radians})}$. Figure 354 gives the comparisons of the $[J_1(p)]/p$ function for circular wave-front radiators in comparison with the $[\sin(p)]/p$ function for rectangular radiators.

for $p = 1.22\pi = 3.83$, $2.233\pi = 7.02$, $3.238\pi = 10.17$, $4.25\pi = 13.32$, ... Figure 354 gives the plot for this function in comparison with the $(\sin p)/p$ function holding for a rectangular wave-front radiator. If the $J_1(p)/p$ curve is changed to an ordinate scale, which gives unity

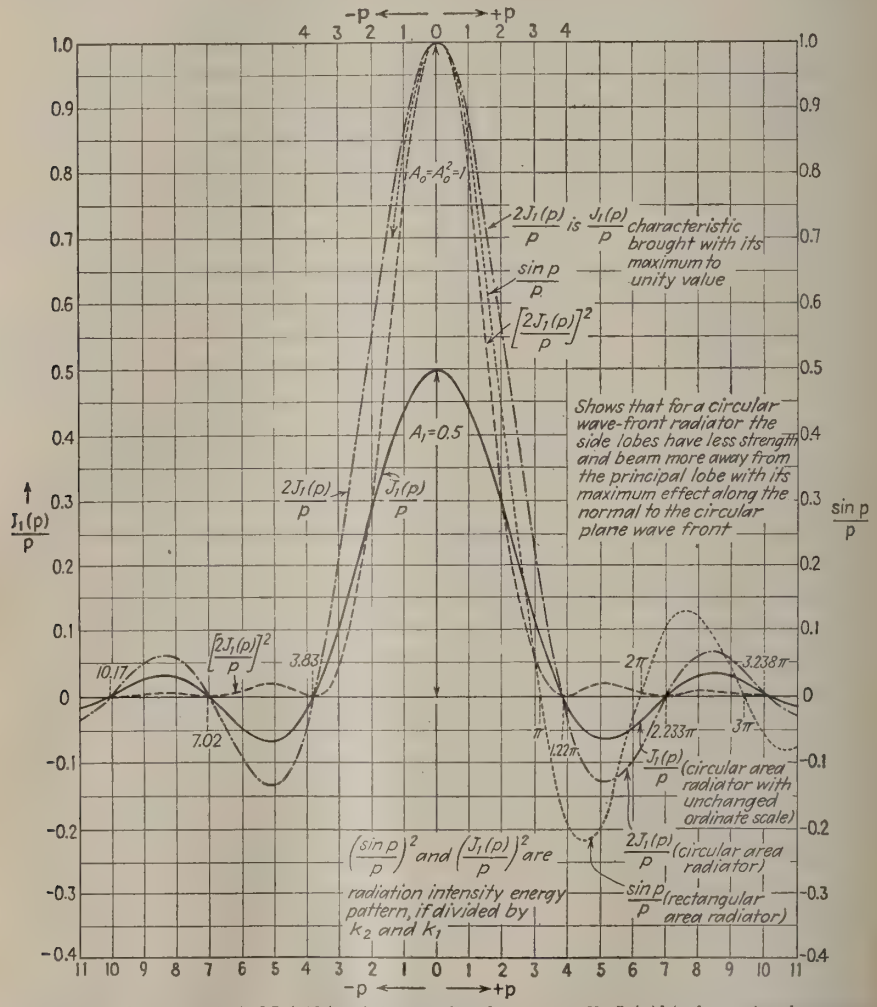

FIG. 354. Characteristic $[J_1(p)]/p$ of the amplitude pattern $[k_1 J_1(p)]/p$ for a circular wave-front radiator compared with the characteristic $[k_2 \sin (p)]/p$ of a rectangular wave-front radiator.

value for the pattern perpendicular to the circular wave front, and compared with rectangular wave-front radiators, we find essentially the same main beam diffractivity. The side lobes are *decidedly less pronounced* for circular wave-front radiators and angled off the main beam somewhat

more than for rectangular radiators. The circular diffractivity $J_1(p)/p$ must now be brought in agreement with Maxwell's equations. We found that for plane electric and magnetic current sheets, we have a power directivity

$$D_p = 0.125Z_0 \frac{(1 + \cos\theta)^2|N|^2}{\lambda^2} = 0.125Z_0 f^2 \frac{(1 + \cos\theta)^2|N|^2}{300^2} \quad \text{watts}$$

where λ is in meters and f in megacycles per second.

$$Z_0 \cong 376.7 \text{ ohms for air}; \qquad Z_0 J(x, y) = J_m(x, y)$$

leading to the comparisons

$$\left.\begin{aligned} D_p^{(\text{watts})} &= \frac{Z_0\pi^2 H^2}{2\lambda^2}(1 + \cos\theta)^2 \left| \int_0^a J_0(\beta\rho \sin\theta)\rho\, d\rho \right|^2 \\ &= \frac{Z_0\pi^2 a^4 H^2}{2\lambda^2}\left[\frac{J_1(\beta a \sin\theta)}{\beta a \sin\theta}\right]^2 (1 + \cos\theta)^2 \qquad \text{for a } \textit{circular} \text{ aperture } S = \pi a^2 \text{ sq m} \\ D_p^{(\text{watts})} &= \frac{Z_0 H^2 a^2 b^2}{8\lambda^2} \frac{\sin^2\left(\frac{\pi a}{\lambda}\sin\theta\cos\varphi\right)}{\frac{\pi^2 a^2}{\lambda^2}\sin^2\theta\cos^2\varphi} \\ &\times \frac{\sin^2\left(\frac{\pi b}{\lambda}\sin\theta\sin\varphi\right)}{\frac{\pi^2 b^2}{\lambda^2}\sin^2\theta\sin^2\varphi}(1 + \cos\theta)^2 \qquad \text{for a rectangular aperture } S = ab \text{ sq m and } H_y \text{ and } \mathcal{E}_x \text{ polarizations; } H \text{ in amp/m} \end{aligned}\right\} \quad (906f)$$

We have, therefore,

$$\begin{aligned} D_p &= \frac{1.858 \times 10^3 a^4 H^2 (1 + \cos\theta)^2}{\lambda^2}\left[\frac{J_1(\beta a \sin\theta)}{\beta a \sin\theta}\right]^2 \\ &= 2.064 \times 10^{-2} a^4 (1 + \cos\theta)^2 f^2 \left[\frac{J_1(\beta a \sin\theta)}{\beta a \sin\theta}\right]^2 \quad \text{watts} \end{aligned} \quad (906g)$$

where H is in amperes per meter, a and λ are in meters, and f is in megacycles per second. The corresponding field amplitude is proportional to $\sqrt{D_p}$, yielding an amplitude directivity at P

$$D_{\theta,\varphi} = D_\theta = (1 + \cos\theta)\frac{J_1[6.28(a/\lambda)\sin\theta]}{6.28(a/\lambda)\sin\theta} \quad (906h)$$

Table 80 gives the computations for the amplitude diffraction pattern in planes normal to the circular wave-front radiator. Figure 355 gives the field amplitude diffraction pattern for $a = 0.1\lambda$, 0.25λ, 0.5λ, and $a = \lambda$, while Fig. 356 gives complete and semipatterns for the field ampli-

TABLE 80. EVALUATION OF THE DIFFRACTIVITY FOR THE FIELD AMPLITUDE OF A CIRCULAR PLANE-WAVE-FRONT RADIATOR

θ, deg	$A = 1 + \cos\theta$	Radius $a = 0.1\lambda$; $p = 6.28 \times 0.1 \times \sin\theta = 0.628 \sin\theta = p_1$; $D_\theta = AB$					$\frac{a}{\lambda} = 0.25$; $p_2 = 1.57 \sin\theta$; $D_\theta = AB'$				$\frac{a}{\lambda} = 0.5$; $p = 3.14 \sin\theta = 2p_2$; $D_\theta = AB''$				$\frac{a}{\lambda} = 1$; $p = 6.28 \sin\theta = 10p_1$; $D_\theta = AB'''$				$\frac{a}{\lambda} = 2$; $p = 12.56 \sin\theta = 20p_1$; $D_\theta = AB^{IV}$			
		$\sin\theta$	$p_1 = 0.628 \times \sin\theta$	$J_1(p)$	$\frac{J_1(p)}{p_1} = B$	$D_\theta = A'$	p_2	$J_1(p_2)$	$\frac{J_1(p_2)}{p_2} = B'$	$D_\theta = A'$	$p = 2p_2$	$J_1(p)$	$\frac{J_1(p)}{p} = B''$	$D_\theta = A'$	$p = 10p_1$	$J_1(p)$	$\frac{J_1(p)}{p} = B'''$	$D_\theta = A'$	$p = 20p_1$	$J_1(p)$	$\frac{J_1(p)}{p} = B^{IV}$	$D_\theta = A'$
0.0	2.0000	0.0000	0.0000	0.0000	0.5000	1.000	0.0000	0.0000	0.5000	1.000	0.0000	0.0000	0.5000	1.0000	0.000	0.0000	0.5000	1.0000	0.0000	0.0000	0.5000	1.0000
3	1.9986	0.0523	0.0329	0.0167	0.508	0.999	0.0821	0.041	0.499	0.995	0.1642	0.0817	0.498	0.994	0.329	0.1612	0.49	0.98	0.658	0.3115	0.475	0.95
6	1.9945	0.1045	0.0658	0.033	0.502	0.998	0.164	0.0817	0.4975	0.99	0.328	0.1612	0.49	0.98	0.658	0.3115	0.474	0.945	1.316	0.5256	0.399	0.795
9	1.9877	0.1564	0.0983	0.0489	0.496	0.995	0.246	0.122	0.495	0.98	0.492	0.2386	0.485	0.965	0.983	0.4344	0.441	0.878	1.966	0.5788	0.293	0.58
12	1.9781	0.2079	0.1305	0.0649	0.495	0.985	0.326	0.1609	0.493	0.975	0.652	0.3089	0.472	0.93	1.305	0.522	0.4	0.79	2.61	0.468	0.179	0.354
15	1.9659	0.2588	0.612	0.0807	0.497	0.98	0.406	0.1988	0.49	0.965	0.812	0.3735	0.4575	0.9	1.62	0.5718	0.353	0.692	3.24	0.2452	0.076	0.15
18	1.9511	0.309	0.194	0.0966	0.4975	0.97	0.485	0.2354	0.485	0.945	0.97	0.4302	0.443	0.86	1.94	0.5799	0.298	0.58	3.88	−0.0193	−0.00496	−0.0097
21	1.9336	0.3584	0.225	0.1118	0.4975	0.96	0.561	0.2696	0.479	0.924	1.122	0.4772	0.426	0.823	2.25	0.5484	0.243	0.47	4.5	−0.2311	−0.0515	−0.099
24	1.9135	0.4067	0.255	0.1265	0.4975	0.95	0.639	0.3030	0.476	0.91	1.278	0.5176	0.404	0.77	2.55	0.4843	0.19	0.364	5.1	−0.3371	−0.066	−0.126
27	1.891	0.454	0.284	0.1406	0.4975	0.94	0.71	0.3331	0.47	0.888	1.42	0.5455	0.383	0.722	2.84	0.3963	0.14	0.265	5.68	−0.3264	−0.0578	−0.109
30	1.866	0.5	0.314	0.1549	0.495	0.925	0.785	0.3631	0.463	0.866	1.57	0.5667	0.36	0.67	3.14	0.2852	0.091	0.17	6.28	−0.02132	−0.034	−0.063
33	1.8387	0.5446	0.341	0.1681	0.493	0.908	0.856	0.3901	0.456	0.84	1.712	0.5783	0.337	0.62	3.41	0.1751	0.0512	0.0945	6.82	−0.0592	−0.0087	−0.016
36	1.809	0.5878	0.368	0.1809	0.4925	0.89	0.92	0.413	0.448	0.81	1.84	0.5819	0.317	0.575	3.68	0.0621	0.0169	0.0306	7.36	0.0099	0.00134	0.00244
39	1.777	0.6293	0.394	0.1932	0.491	0.875	0.985	0.4351	0.442	0.786	1.97	0.579	0.293	0.52	3.94	−0.0429	−0.01085	−0.0192	7.88	0.2158	0.0275	0.049
42	1.7431	0.6691	0.419	0.2051	0.491	0.855	1.046	0.4547	0.433	0.75	2.092	0.5693	0.271	0.472	4.19	−0.1352	−0.0323	−0.056	8.38	0.27	0.0323	0.056
45	1.7071	0.7071	0.444	0.2166	0.491	0.84	1.108	0.4738	0.4265	0.73	2.216	0.553	0.25	0.428	4.44	−0.2144	−0.0484	−0.0826	8.88	0.2577	0.0291	0.0495
48	1.6691	0.7431	0.466	0.2268	0.487	0.812	1.166	0.49	0.42	0.7	2.332	0.534	0.23	0.385	4.66	−0.2704	−0.058	−0.097	9.32	0.1968	0.0211	0.0352
51	1.6293	0.7771	0.486	0.2360	0.486	0.79	1.22	0.5033	0.411	0.67	2.44	0.5113	0.21	0.342	4.86	−0.3086	−0.0632	−0.103	9.72	0.1119	0.0115	0.0188
54	1.5878	0.809	0.508	0.2458	0.485	0.77	1.27	0.5153	0.405	0.643	2.54	0.487	0.192	0.305	5.08	−0.3355	−0.066	−0.105	10.16	0.0034	0.000326	0.00052
57	1.5446	0.8387	0.525	0.2535	0.482	0.74	1.32	0.5263	0.398	0.613	2.64	0.4595	0.171	0.263	5.25	−0.345	−0.0657	−0.101	10.5	−0.0789	−0.0075	−0.0116
60	1.5	0.866	0.542	0.2612	0.482	0.72	1.36	0.5344	0.394	0.59	2.72	0.4354	0.16	0.24	5.42	−0.3448	−0.0635	−0.095	10.84	−0.1496	−0.0137	−0.0205
63	1.454	0.891	0.56	0.2692	0.48	0.693	1.4	0.5419	0.389	0.565	2.8	0.4097	0.146	0.212	5.6	−0.3343	−0.0596	−0.086	11.2	−0.2039	−0.0182	−0.0264
66	1.4067	0.9135	0.572	0.2745	0.477	0.675	1.435	0.548	0.382	0.54	2.87	0.3859	0.1345	0.189	5.72	−0.3218	−0.0561	−0.0791	11.44	−0.2251	−0.0197	−0.0278
69	1.3584	0.9336	0.587	0.2815	0.481	0.655	1.465	0.5529	0.379	0.515	2.93	0.3647	0.1245	0.169	5.87	−0.3002	−0.0511	−0.0695	11.74	−0.2332	−0.0199	−0.0271
72	1.309	0.9511	0.599	0.2863	0.481	0.63	1.495	0.5577	0.374	0.49	2.99	0.3428	0.1145	0.15	5.99	−0.2786	−0.0466	−0.061	11.98	−0.2247	−0.0189	−0.0247
75	1.2588	0.9659	0.606	0.2892	0.477	0.6	1.52	0.5607	0.37	0.465	3.04	0.324	0.1065	0.134	6.06	−0.2645	−0.0436	−0.055	12.12	−0.214	−0.0177	−0.0223
78	1.2079	0.9781	0.612	0.2918	0.477	0.579	1.54	0.5632	0.366	0.443	3.08	0.3087	0.1005	0.121	6.12	−0.2514	−0.041	−0.0497	12.24	−0.2015	−0.0165	−0.02
81	1.1564	0.9877	0.619	0.2947	0.477	0.553	1.55	0.5644	0.365	0.42	3.1	0.3009	0.0967	0.112	6.19	−0.2353	−0.038	−0.044	12.38	−0.1836	−0.0149	−0.0179
84	1.1045	0.9945	0.623	0.2966	0.477	0.523	1.56	0.5656	0.3635	0.4	3.12	0.2931	0.0938	0.103	6.23	−0.2257	−0.0363	−0.04	12.46	−0.1718	−0.0138	−0.0152
87	1.0523	0.9986	0.626	0.2978	0.477	0.5	1.565	0.5661	0.361	0.38	3.13	0.2892	0.0922	0.097	6.26	−0.2182	−0.035	−0.0368	12.52	−0.1623	−0.013	−0.0136
90	1.0000	1.0000	0.628	0.2991	0.477	0.477	1.57	0.5667	0.36	0.36	3.14	0.2852	0.091	0.091	6.28	−0.2132	−0.034	−0.034	12.56	−0.1556	−0.0124	−0.0124

Remarks: For the $a/\lambda = 2$ computation, the first maximum $J_1(p) = 0.5819$ corresponds to $p = 1.84$, corresponding to $\sin\theta = 1.84/12.56 = 0.146$ or $\theta = 8.3$ deg. The $J_1(p)$ curve has zero values for $p = 3.83$, 7.02, 10.17, 13.32, ... Hence, $3.83/12.56 = 0.304 = \sin\theta$ or $\theta = 17.7$ deg, $7.02/12.56 = 0.557 = \sin\theta$ or $\theta = 33.8$ deg, $10.17/12.56 = 0.806 = \sin\theta$ or $\theta = 53.8$ deg, $13.32/12.56$ is larger than unity and is, therefore, *no possible value*. First minimum for $J_1(p) = -0.3461$ and $p = 5.33$, yielding $5.33/12.56 = 0.425$ and $\theta = 25.1$ deg. Second maximum for $J_1(p) = 0.2733$, yielding $p = 8.53$ and $8.53/12.56 = 0.675$; hence, $\theta = 42.5$ deg. The second minimum occurs for $J_1(p) = -0.2333$ for $p = 11.71$, yielding $11.71/12.56 = 0.93$, $\theta = 68.4$ deg.

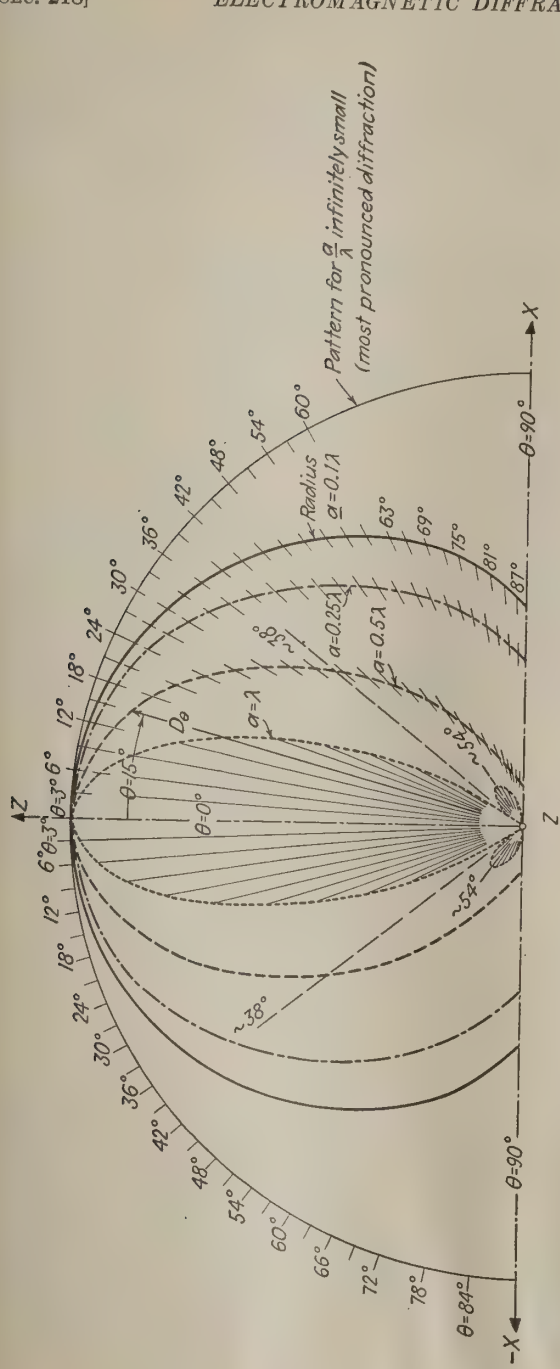

FIG. 355. Vertical field amplitude (Fraunhofer) pattern for circular plane wave-front radiators.

tude in comparison with rectangular wave-front radiators. It can be seen that for $a = 0.1\lambda$, the diffractivity for both wave-front shapes is essentially the same while for larger values, such as $a = 0.5\lambda$ and λ, the circular wave-front radiator gives a decidedly sharper main beam.

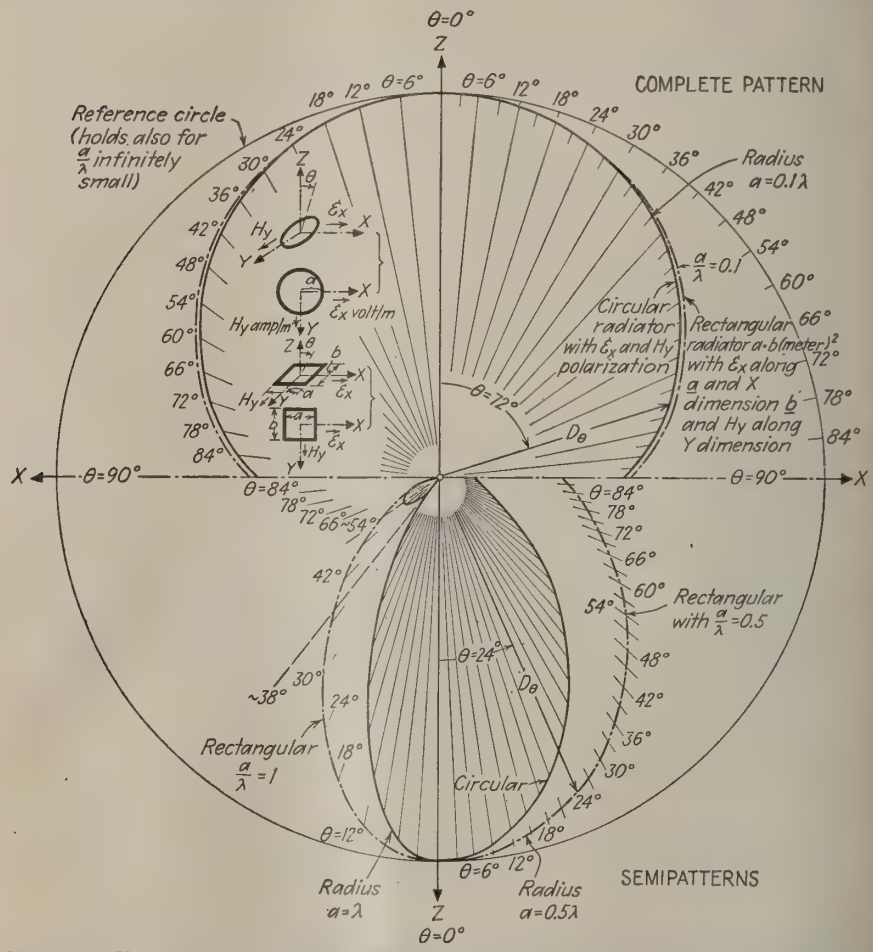

FIG. 356. Vertical *XZ* Fraunhofer diffraction pattern for circular and rectangular plane wave-front radiators. *Note:* Circular radiator produces a small side lobe for $a = \lambda$, while rectangular radiator has only one lobe or beam, which is relatively broad.

This is especially evident when the patterns of Fig. 357 are inspected. Besides, the circular wave-front radiator has less intense side lobes. The sharpness of the main beam and the minuteness of the side lobes are still more pronounced the larger the radius a is chosen in terms of λ. This can be seen from Table 81 and Fig. 358.

Circular and circular-ring diffraction radiators have been investigated by M. S. Neumann and A. A. Pistolkors.[1] They are dealt with in Sec. 249 of the Appendix and in Figs. 391 and 392. As with slits in metal cylinders and such apertures in conical surfaces, a high-frequency

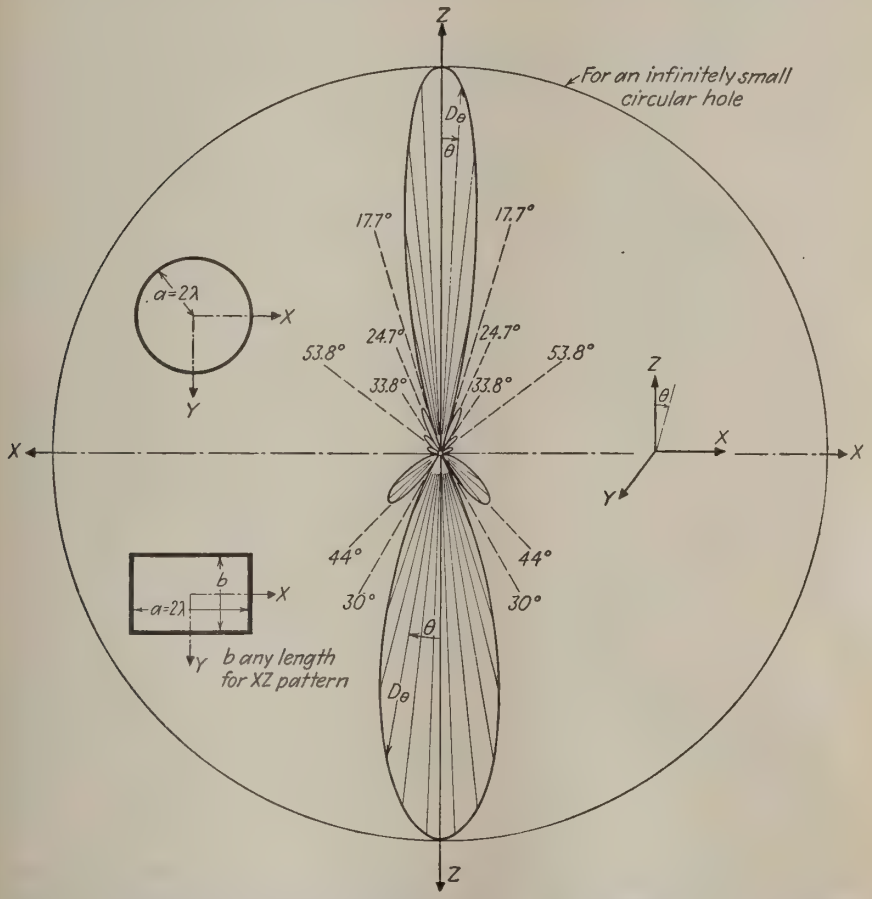

Fig. 357. Vertical XZ Fraunhofer pattern for circular and rectangular plane wave-front radiators with significant dimension equal to 2λ.

voltage is applied across the slit. For a circular slit, either in a large conducting plane or the end surface of a wave guide, or one metal surface of a cavity, we must take the mode of the wave behind the conducting screen into consideration. The current distribution in the conducting screen can then be used for computing the entrance admittance of the slit

[1] *Proc. IRE*, **36**, 56, January, 1948.

gap. The reciprocal of the real portion of the admittance is the radiation resistance. The surface current density appears as the sum of an infinite number of wave modes. The radiation conductance increases in steps with increasing radius of the slit, like an oscillating sphere excited at the equator.[1]

TABLE 81. COMPUTATIONS OF DIFFRACTIVITY FOR THE FIELD AMPLITUDE OF A CIRCULAR PLANE-WAVE-FRONT RADIATOR OF A RADIUS EQUAL TO 3 AND 5 WAVELENGTHS, RESPECTIVELY

θ, deg	$A = 1 + \cos\theta$	Radius $a = 3\lambda$ yields $p = 6.28 \times 3 \sin\theta = 18.84 \sin\theta$					Radius $a = 5\lambda$ yields $p = 5 \times 6.28 \sin\theta = 31.4 \sin\theta$			
		$\sin\theta$	p	$J_1(p)$	$\frac{J_1(p)}{p} = B$	$D\theta = AB$	p	$J_1(p)$	$\frac{J_1(p)}{p} = B'$	$D\theta = AB'$
0	2.0000	0.0000	0.000	0.0000	0.5000	1.0000	0.00	0.0000	0.5000	1.0000
1	1.9998	0.0175	0.329	0.1623	0.494	0.988	0.55	0.2647	0.481	0.962
2	1.9994	0.0349	0.658	0.3116	0.475	0.95	1.09	0.468	0.43	0.86
3	1.9986	0.0523	0.987	0.4358	0.443	0.886	1.642	0.5735	0.348	0.696
4	1.9976	0.0698	1.38	0.5383	0.388	0.77	2.18	0.5587	0.255	0.51
5	1.9962	0.0872	1.64	0.5735	0.35	0.698	2.74	0.4291	0.157	0.314
6	1.9945	0.1045	1.96	0.579	0.294	0.585	3.28	0.2289	0.07	0.14
7	1.9925	0.1219	2.29	0.5416	0.236	0.47	3.81	0.0088	0.0023	0.00457
8	1.9903	0.1392	2.61	0.468	0.179	0.356	4.35	−0.1876	−0.0433	−0.086
9	1.9877	0.1564	2.94	0.3611	0.123	0.244	4.92	−0.3175	−0.0645	−0.129
10	1.9848	0.1736	3.27	0.233	0.0715	0.142	5.43	−0.3445	−0.063	−0.126
11	1.9806	0.1908	3.6	0.0955	0.0265	0.0527	5.99	−0.2786	−0.0467	−0.0925
12	1.9781	0.2079	3.91	−0.0312	−0.008	−0.0158	6.52	−0.1481	−0.0228	−0.0454
13	1.9744	0.225	4.24	−0.1522	−0.036	−0.071	7.02	0.0	0.0	0.0
14	1.9703	0.2419	4.55	−0.2442	−0.0538	−0.106	7.6	0.1592	0.0209	0.0414
15	1.9659	0.2588	4.86	−0.3086	−0.0635	−0.125	8.12	0.2499	0.0306	0.0601

Remarks: First maximum is $J_1(p) = 0.5819$ for $p = 1.84$. For $a = 3\lambda$, we have $\sin\theta = 1.84/188.84 = 0.978$ and $\theta = 78$ deg. First zero $J_1(p) = 0$ is for $p = 3.83$ and $3.83/18.84 = 0.203 = \sin\theta$ with $\theta = 11.7$ deg. This table shows that essentially only a narrow main beam exists. For $a = 5\lambda$, the argument $p = 3.83$ yields $3.83/31.4 = 0.122 = \sin\theta$, and $\theta \cong 7$ deg half beam width.

219. Remarks on Plane-wave-front Radiators of Any Contour. In Fig. 336, an arbitrarily shaped aperture in a screen is shown. If x and y are again the coordinates of any secondary radiation center T_2, in the plane primary wave front occupying the aperture, we have the general wave function

$$w = K_0 \iint \epsilon^{-j\beta(Ax+By)}\, dx\, dy = \rho K_0 \iint \epsilon^{-j\beta(A'x'+B'y')}\, dx'\, dy'$$
$$= \rho w_0(A', B') = \rho w_0(\rho A, B)$$

This relation is based on the following reasoning: If we distort an aperture

[1] STRATTON, J. A., and L. J. CHU, Steady-state Solutions of Electromagnetic Field Problems, *Jour. Appl. Physics*, **12**, 236, March, 1941.

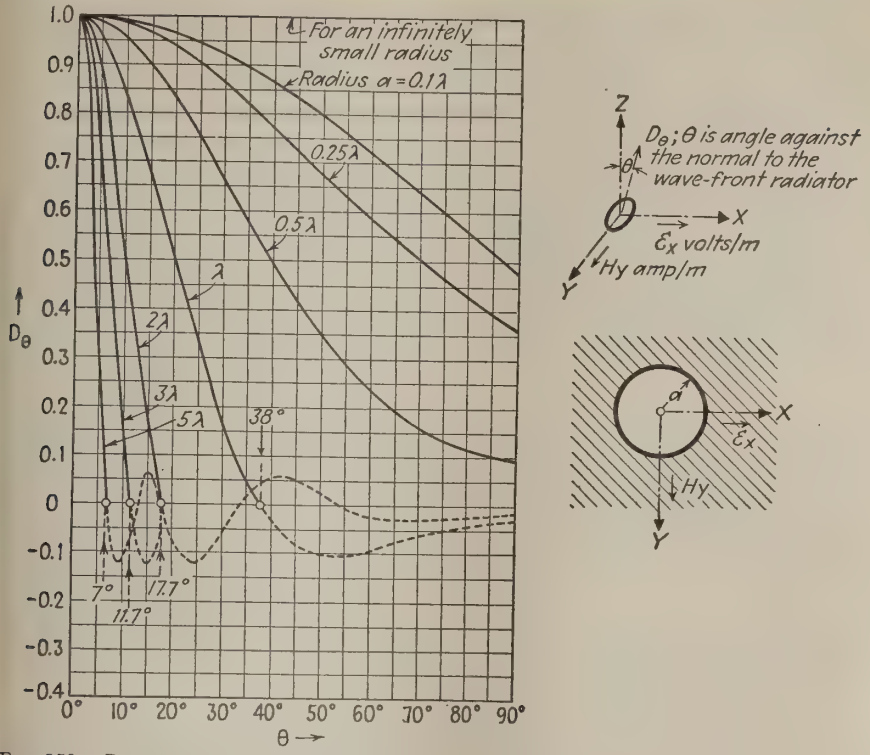

FIG. 358. Beaming effect of circular wave-front radiators. Broken curves refer to side lobes; continuous curves refer to the principal beam or lobe.

uniformly in one direction only, such as in Fig. 359, then we simply have new coordinates x' and y' instead of the original undistorted coordinates x and y, where $x/x' = \rho$ and $y/y' = 1$. We then integrate over the same region of the $X'Y'$ plane as before in the XY plane. The function $w_0(A, B)$ then gives the diffraction pattern of the new wave-front radiator deformed by ρ. Instead of A and B, we have the new variable $A' = \rho a$ and $B' = B$, where A' and B' are again the coordinates of an arbitrary reception center relative to the origin of the XYZ system in the plane of possible reception centers parallel to the screen. The above relations show that the corresponding diffraction pattern is likewise linearly deformed, but in a crosswise fashion, because an elongation of the primary wave front causes a corresponding contraction in the

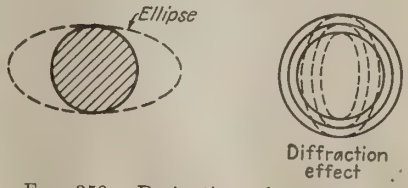

FIG. 359. Derivation of an elliptical area from a circular area.

diffraction characteristic. If we have no uniform deformation, we can treat the case by means of curvilinear coordinates, for which the contour of the arbitrarily shaped wave front is a coordinate line.

220. Arrays of Circular Wave-front Radiators. Such arrays are conveniently made up of like individual wave-front radiators, which are uniformly distributed in space, in an area, or along a central line, as for instance, in Fig. 360. The case for several rectangular radiators is treated in Sec. 217. In the same way, we can derive expressions for the effect of several circular wave-front radiators, which are all in phase (for instance, part of the *same* primary plane wave front). The diffraction pattern of the individual circular wave-front radiator defines the envelope contour of the pattern that encloses the resultant field pattern holding for the array. Each individual radiator is then referred to an origin (a zero reference point). Hence, for q-like (may be any shape) wave-front radiators, the coordinates would be $x_1, y_1; x_2, y_2; x_3, y_3; \ldots; x_q, y_q$. The total effect at the reception center is then

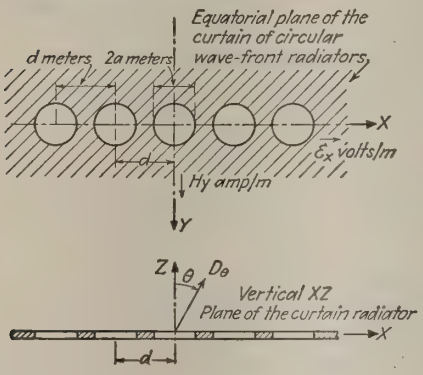

FIG. 360. A curtain of circular wave-front radiators.

$$w = K_0 \sum_q \int\int \epsilon^{-j\beta[(x_q+x)A+(y_q+y)B]}\, dx\, dy$$

$$= \overbrace{\sum_q \epsilon^{-j\beta(x_qA+y_qB)}}^{=r} \; \overbrace{K_0 \int\int \epsilon^{-j\beta(Ax+By)}\, dx\, dy}^{=s}$$

where r accounts for the relative radiator distribution and s is due to the individual wave-front radiator. This expression resembles a modulation product. It also behaves similarly, as is brought out on page 1124. Therefore, for an alignment as in Fig. 360, the factor containing the double integral accounts for the individual Fraunhofer diffraction w_0, while the factor under the $\sum_q$ symbol is the disposition or distribution factor of the aligned circular wave-front radiators. The value w represents the group value for which all radiators affect a particular reception center simultaneously. If I_0 denotes the radiation intensity of one wave-front radiator, the received intensity I_r due to all radiators is

$$I_r = I_0 \left[\sum_q \epsilon^{-j\beta(Ax_q+By_q)}\right]^2 = I_0 \sum_q \sum_r \epsilon^{-j\beta[A(x_q-x_r)+B(y_q-y_r)]} \qquad (907)$$

For two like radiators, we have for q and r only values 1 and 2, and

$$\left.\begin{aligned}
\sum_q \sum_r &= 2 + \epsilon^{j\beta[A(x_1-x_2)+B(y_1-y_2)]} + \epsilon^{j\beta[A(x_2-x_1)+B(y_2-y_1)]} \\
\epsilon^{jz} &= \cos z + j \sin z \\
\sum_q \sum_r &= 2 + 2\cos\left\{\beta[A(x_1 - x_2) + B(y_1 - y_2)]\right\} \\
&= 4\cos^2\left\{\frac{\beta}{2}[A(x_1 - x_2) + B(y_1 - y_2)]\right\} \\
I_r &= 4I_0 \cos^2 \Omega \\
\Omega &= \tfrac{1}{2}[A(x_1 - x_2) + B(y_1 - y_2)]
\end{aligned}\right\} \quad (907a)$$

Now let us see how (907) applies to a line-up of circular plane-wave-front radiators as in Fig. 360. For N circular radiators, each of radius a meters and spaced d meters between centers, we have $x_q = qd$ and $y_q = 0$, since the alignment is along the X axis, where $q = 0, 1, 2, 3, \cdots, (N-1)$ are the point distributions. If the primary beam meets the circular planes in the XY plane under an angle ψ with respect to the normal (or the Z_e axis direction) and θ denotes the angle with respect to the Z axis of the diffracted beam, we have $A = \sin\theta - \sin\psi$, and

$$w = w_0 \sum_{q=0}^{q=N-1} \epsilon^{-j\beta Aqd} = w_0 \frac{1 - \epsilon^{-j\beta ANd}}{1 - \epsilon^{-j\beta Ad}} \quad (907b)$$

For perpendicular primary wave incidence, we have $A = \sin\theta$, which, in practical cases, is likely to happen (since most efficient wave incidence occurs), and

$$w = w_0 \frac{1 - \epsilon^{-j\beta Nd\sin\theta}}{1 - \epsilon^{-j\beta d\sin\theta}} \quad (907c)$$

where w_0 is the wave disturbance of one circular wave-front radiator. For $D = \beta d \sin\theta$, the received radiation intensity I_r is proportional to w^2, or $I_r = kw^2$, and

$$I_r = kw^2 = kw_0^2\left[\sqrt{\frac{(1 - \epsilon^{jND})(1 - \epsilon^{-jND})}{(1 - \epsilon^{jD})(1 - \epsilon^{-jD})}}\right]^2 = kw_0^2 \frac{1 - \cos(ND)}{1 - \cos(D)} \quad (907d)$$

But

$$\sin\left(\frac{x}{2}\right) = \sqrt{\frac{1 - \cos x}{2}}$$

$$\frac{1 - \cos(ND)}{1 - \cos(D)} = \frac{\sin^2(ND/2)}{\sin^2(D/2)} = \frac{\sin^2(0.5\beta Nd\sin\theta)}{\sin^2(0.5\beta d\sin\theta)}$$

The corresponding field amplitude A_θ is proportional to $\sqrt{I_r}$, and w_0 is then the amplitude A_0 at the reception center if only one circular wave-front radiator is present.

For N such radiators, we have the Fraunhofer diffractivity

$$A_\theta = A_0 \frac{\sin\left(d\frac{\pi N}{\lambda}\sin\theta\right)}{\sin\left(\frac{\pi d}{\lambda}\sin\theta\right)}; \qquad A_0 = K\frac{J_1(\beta a\sin\theta)}{\beta a\sin\theta}(1+\cos\theta) \tag{907e}$$

From (907e), we note that the amplitude directivity is given by

$$D_\theta = \frac{J_1\left(6.28\frac{a}{\lambda}\sin\theta\right)}{6.28\frac{a}{\lambda}\sin\theta}\frac{\sin\left(3.14\frac{Nd}{\lambda}\sin\theta\right)}{\sin\left(3.14\frac{d}{\lambda}\sin\theta\right)}(1+\cos\theta) \tag{907f}$$

where $(1+\cos\theta)$ is the forward factor, which, for two circular wave-front radiators, yields

$$N = 2; \qquad \sin(2x) = 2\sin(x)\cos(x)$$

$$D_\theta = (1+\cos\theta)\frac{J_1\left(6.28\frac{a}{\lambda}\sin\theta\right)}{3.14\frac{a}{\lambda}\sin\theta}\cos\left(3.14\frac{d}{\lambda}\sin\theta\right) \tag{907g}$$

Table 82 gives the evaluations for an alignment as in Fig: 361 for $N = 1$, 2, 3, and 4 circular wave-front radiators in the XY plane for $a = \frac{1}{2}\lambda$ and $d/a = 3$. The corresponding semipolar amplitude diffraction patterns are given in Fig. 362. For $N = 4$, we have

$$\left.\begin{aligned}\frac{\sin(4q)}{\sin(q)} &= \frac{2\sin(2q)\cos(2q)}{\sin(q)} = \frac{4\sin(q)\cos(q)\cos(2q)}{\sin(q)} \\ &= 4\cos(q)\cos(2q) \\ D_\theta &= (1+\cos\theta)\frac{J_1(p)}{0.25p}\cos(q)\cos(2q)\end{aligned}\right\} \tag{907h}$$

221. The Fresnel Diffraction Patterns. For the Fraunhofer diffraction (Fig. 334) in optics we use two lenses. The first lens "bundles" all rays coming from a primary point source into parallel rays at an aperture. This places the primary radiation center, in equivalence, infinitely far from the aperture in an obstructing screen. The second lens converges all rays beyond the aperture into a common reception point (the focus of the second lens). This also puts the reception center, in effect, infinitely far away from the aperture. Electromagnetically, we can do this for a linear primary radiator along the focal line of a paraboloid and the reception center along the focal line of a receiving paraboloid.

Table 82. Evaluations for an Alignment of Circular Wave-front Radiators

For $a = 0.5\lambda$, use formulas (907f) and (907g). General formula is $D_\theta = (1 + \cos\theta)\frac{J_1(p)}{p}\frac{\sin(Nq)}{\sin(q)}$ for $p = 6.28\frac{a}{\lambda}\sin\theta$ and $q = 3.14\frac{d}{\lambda}\sin\theta$

θ, deg	A'	sin θ	$q = 3.14\frac{d}{\lambda}\sin\theta$		$N = 2$; $D_\theta = 2A'\cos q$		$N = 3$; $D_\theta = A'B$					$N = 4$; $D_\theta = A'B'$			
			Radians	Deg	cos q	$0.5D_\theta$	sin q	Nq, deg	sin (Nq)	$B = \frac{\sin(Nq)}{\sin(q)}$	D_θ	Nq, deg	sin (Nq)	$B' = \frac{\sin(Nq)}{\sin(q)}$	D_θ
0.0	1.000	0.0000	0.000	0.000	1.0000	1.0000	0.0000	0.0	0.0000	3.0000	3.000	0.000	0.0000	4.0000	4.0000
3	0.994	0.0523	0.218	12.5	0.97	0.96	0.2164	37.5	0.6088	2.8	2.79	50	0.766	3.54	3.52
6	0.98	0.1045	0.492	28.2	0.8813	0.865	0.4726	74.6	0.9641	2.04	2.0	112.8	0.9219	1.96	1.92
9	0.965	0.1564	0.735	42.1	0.742	0.718	0.6704	126.3	0.8059	1.2	1.16	168.4	0.2011	0.3	0.29
12	0.93	0.2079	0.98	56	0.5592	0.519	0.829	168	0.2079	0.251	0.234	224	−0.6947	−0.838	−0.777
15	0.9	0.2588	1.22	70	0.342	0.308	0.9397	210	−0.5	−0.531	−0.48	280	−0.9848	−1.05	−0.945
18	0.86	0.309	1.46	84	0.1045	0.089	0.9945	252	−0.9511	−0.96	−0.825	336	−0.4067	−0.41	−0.354
21	0.823	0.3584	1.69	97	−0.1219	−0.099	0.9925	291	−0.9336	−0.94	−0.77	388	0.4695	0.474	0.39
24	0.77	0.4067	1.92	110	−0.342	−0.264	0.9387	330	−0.5	−0.531	−0.41	440	0.9848	1.05	0.81
27	0.722	0.454	2.14	123	−0.5446	−0.395	0.8387	369	0.1564	0.186	0.134	492	0.7431	0.885	0.617
30	0.67	0.5	2.36	136	−0.7193	−0.48	0.6947	408	0.7431	1.07	0.71	544	−0.0698	−0.01	−0.0067
33	0.62	0.5446	2.56	147	−0.8387	−0.52	0.5446	441	0.9877	1.81	1.12	588	−0.7431	−1.36	−0.841
36	0.575	0.5878	2.76	158	−0.9272	−0.532	0.3746	474	0.9135	2.43	1.4	632	−0.9994	−2.65	−1.52
39	0.52	0.6293	2.95	169	−0.9816	−0.51	0.1908	507	0.5446	2.86	1.49	676	−0.6947	−3.65	−1.89
42	0.472	0.6691	3.15	180	−1.0000	−0.472	0.0000	540	0.0000	3.0	1.42	720	0.0000	−4.00	−1.89
45	0.428	0.7071	3.32	190	−0.9848	−0.421	−0.1736	570	−0.5	2.87	1.23	760	0.6428	−3.7	−1.58
48	0.385	0.7431	3.5	201	−0.9336	−0.36	−0.3584	603	−0.891	2.495	0.96	804	0.9945	−2.77	−1.07
51	0.342	0.7771	3.66	210	−0.866	−0.296	−0.5	630	−1.0000	2.000	0.684	840	0.866	−1.73	−0.59
54	0.305	0.809	3.8	218	−0.788	−0.24	−0.6157	654	−0.9135	1.48	0.452	872	0.4695	−0.76	−0.231
57	0.263	0.8387	3.95	226	−0.6947	−0.182	−0.7193	678	−0.6691	0.93	0.245	904	−0.0698	0.097	0.0255
60	0.24	0.866	4.08	234	−0.5878	−0.141	−0.809	702	−0.309	0.382	0.092	936	−0.5878	0.725	0.174
63	0.212	0.891	4.21	241	−0.4848	−0.1025	−0.8746	723	0.0523	−0.0595	−0.0126	964	−0.8988	1.02	0.215
66	0.189	0.9135	4.3	246	−0.4067	−0.077	−0.9135	738	0.309	−0.338	−0.064	984	−0.9945	1.09	0.206
69	0.169	0.9336	4.4	253	−0.2924	−0.0495	−0.9563	759	0.6293	−0.657	−0.111	1.012	−0.9272	0.97	0.164
72	0.15	0.9511	4.5	258	−0.2079	−0.0312	−0.9781	774	0.809	−0.822	−0.124	1.032	−0.7431	0.763	0.115
75	0.134	0.9659	4.55	261	−0.1564	−0.0209	−0.9877	783	0.891	−0.9	−0.121	1.044	−0.5878	0.595	0.0795
78	0.121	0.9781	4.6	264	−0.1045	−0.0126	−0.9945	792	0.9511	−0.955	−0.115	1.056	−0.4067	0.41	0.0496
81	0.112	0.9877	4.65	267	−0.0523	−0.00585	−0.9986	801	0.9877	−0.988	−0.111	1.068	−0.2079	0.208	0.0233
84	0.103	0.9945	4.7	270	0.0	0.0	−1.0000	810	1.000	−1.000	−0.103	1.080	0.0000	0.000	0.0000
87	0.097	0.9986	4.705	270.5	0.0	0.0	−1.0000	811.5	0.9997	−1.000	−0.097	1.082	0.0349	−0.0349	−0.36
90	0.091	1.0000	4.71	271	0.0175	0.00159	−0.999	813	0.9986	−1.000	−0.091	1.084	0.0698	−0.0699	−0.765

Remarks: For $d/a = 3$, we have $d/0.5\lambda = 3$ or $d/\lambda = 1.5$, $q = 3.14(d/\lambda)\sin\theta = 4.71\sin\theta^{(\text{radians})} = 57.3 \times 4.71\sin\theta°$. For two circular wave-front radiators, we find $N = 2$ and $D_\theta = 2A\cos(q)$. For $N = 3$, the first zero occurs for $N_q = 3.19$, or $3 \times 4.71\sin\theta = 6.28 = 0.2225$ or $\theta \cong 12.9$ deg. The next zero occurs for $\sin\theta = 6.28/14.13 = 0.445$ or $\theta = 26.4$ deg, etc. For $N = 4$ (four wave-front radiators), the first zero occurs for $\sin\theta = 3.14/4 \times 4.71 = 0.167$ or $\theta \cong 9.6$ deg; the second zero occurs for $\sin\theta = 0.334$ or $\theta = 19.5$ deg; $A' = (1 + \cos\theta)J_1(p)/p$ is taken from Table 80.

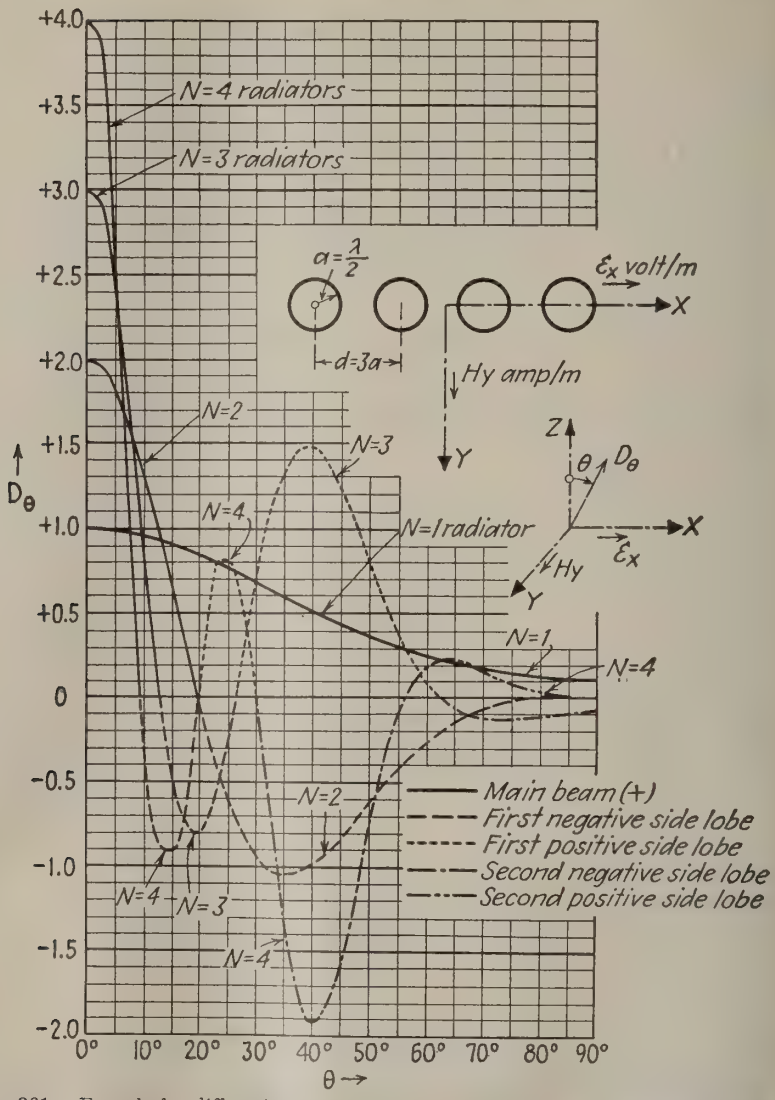

FIG. 361. Fraunhofer diffraction semipattern for circular plane wave-front radiators.

The Fresnel diffraction does away with such restrictions, since both the primary radiation center as well as any of the reception centers may be at a finite distance from the primary wave-front section, which acts in effect, as a mosaic of Huygens wavelet centers. It is then no longer permissible to assume that all field contributions act in phase at a reception center. In Fig. 336, in connection with the Fraunhofer diffraction,

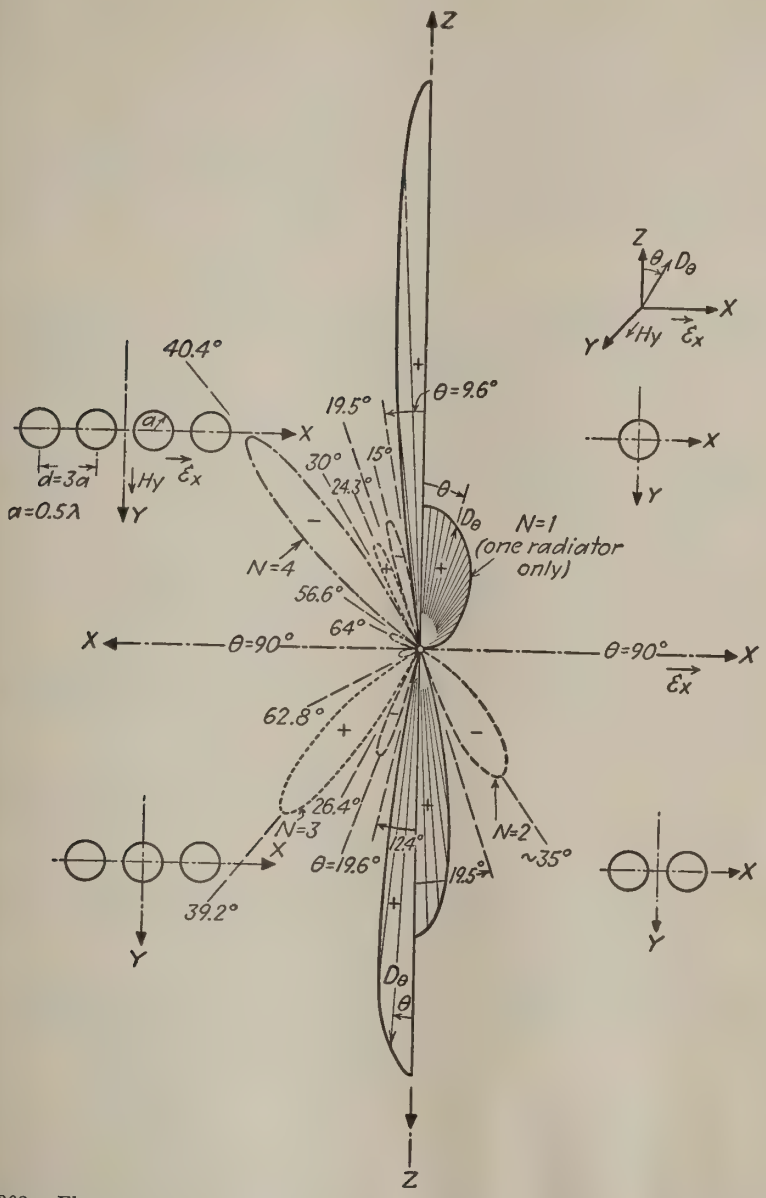

FIG. 362. Electromagnetic Fraunhofer patterns (semi-) for a multicircular plane wavefront radiator alignment.

we found, for the angle $\delta_0 = 0.5(\cos\theta - \cos\psi)$ (see Fig. 363), the wave disturbance w at the reception center P as

$$w = K_0 \int\int_{\text{area of aperture}} \epsilon^{j\beta F(x,y)}\, dx\, dy; \qquad K_0 = -j\frac{\beta\epsilon^{j\beta(R+R_0)}\cos\delta_0}{2\pi R R_0}$$

For the direction cosines of R_0 against the XY plane, defined by $\alpha_0 = -x_0/R_0$ and $\beta_0 = -y_0/R_0$, and the direction cosines of R against the

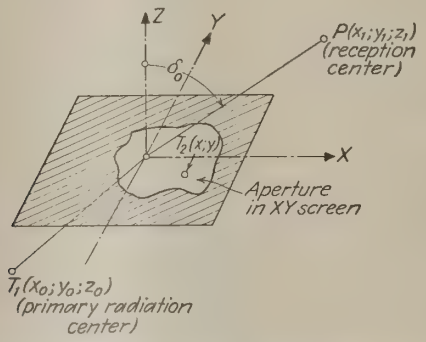

FIG. 363. General diffraction conditions for any plane aperture exposing a primary wave front. T_2 is any secondary radiation center.

same plane, defined by $\alpha_1 = x_1/R$ and $\beta_1 = y_1/R$, we have the function

$$F(x, y) = x(\alpha_0 - \alpha_1) + y(\beta_0 - \beta_1) + \frac{1}{2}\left[\left(\frac{1}{R_0} + \frac{1}{R}\right)(x^2 + y^2) - \frac{(\alpha_0 x + \beta_0 y)^2}{R_0} - \frac{(\alpha_1 x + \beta_1 y)^2}{R}\right] \quad (908)$$

where we *must retain at least* terms including *squared terms of x and y* in order to *account for a curved wave front.* We have then the condition as in Fig. 363. In the w expression, we then find

$$\left.\begin{aligned} \int\int \epsilon^{j\beta F(x,y)}\, dx\, dy &= \int\int \cos[\beta F(x, y)]\, dx\, dy \\ &\quad + j\int\int \sin[\beta F(x, y)]\, dx\, dy = C + jS \\ w = K_0(C + jS); \qquad I_r &= kw^2 = K_0 k^2(C^2 + S^2) \end{aligned}\right\} \quad (908a)$$

since the classic radiation intensity I_r is proportional to the square of the wave disturbance arriving at reception center P and w denotes the absolute amount for the wave disturbance. In order to evaluate the double integrals expressed by C and S, we simplify Figs. 336 to 363 by placing the origin O in the intersection of the straight line connecting

the primary radiation center with a particular reception center. This requires a variable coordinate system for a *fixed* T_1 location but a *variable* location P. However, we gain the advantage in the $F(x, y)$ expression that $\alpha_0 = \alpha_1$ and $\beta_0 = \beta_1$, leaving only the square terms, so that

$$F(x, y) = \frac{1}{2}\left[\left(\frac{1}{R_0} + \frac{1}{R}\right)(x^2 + y^2) - \frac{(\alpha_0 x + \beta_0 y)^2}{R_0} - \frac{(\alpha_1 x + \beta_1 y)^2}{R}\right] \tag{908b}$$

It is now the incident beam T_1O with the direction cosines, defined by $\alpha_0 = \sin \delta_0$, $\beta_0 = 0$, and $\gamma_0 = \cos \delta_0$, and the continued beam OP with the direction cosines $\alpha_1 = \sin \delta_0$, $\beta_1 = 0$, and $\gamma_1 = \cos \delta_0$. Relation (908*b*) then changes to

$$\begin{aligned} F(x, y) &= \frac{1}{2}\left[\left(\frac{1}{R_0} + \frac{1}{R}\right)(x^2 + y^2) - \left(\frac{x^2 \sin^2 \delta_0}{R_0} + \frac{x^2 \sin^2 \delta_0}{R}\right)\right] \\ &= \frac{1}{2}\left[\left(\frac{1}{R_0} + \frac{1}{R}\right) x^2(1 - \sin^2 \delta_0) + \left(\frac{1}{R_0} + \frac{1}{R}\right) y^2\right] \\ &= \frac{1}{2}\left(\frac{1}{R_0} + \frac{1}{R}\right)(x^2 \cos^2 \delta_0 + y^2) \end{aligned}$$

The C and S functions for the double integrals then become

$$\begin{aligned} C &= \int\int \cos\left[\frac{2\pi}{\lambda} F(x, y)\right] dx\, dy \\ &= \int\int \cos\left[\frac{\pi}{\lambda}\left(\frac{1}{R_0} + \frac{1}{R}\right)(x^2 \cos^2 \delta_0 + y^2)\right] dx\, dy \\ S &= \int\int \sin\left[\frac{\pi}{\lambda}\left(\frac{1}{R_0} + \frac{1}{R}\right)(x^2 \cos^2 \delta_0 + y^2)\right] dx\, dy \end{aligned}$$

The common argument of the cosine and sine functions can be expressed by new variables ξ and η if we write for the argument

$$\frac{\pi}{\lambda}\left(\frac{1}{R_0} + \frac{1}{R}\right)(x^2 \cos^2 \delta_0 + y^2) = \frac{\pi}{\lambda}\left(\frac{1}{R_0} + \frac{1}{R}\right) x^2 \cos^2 \delta_0 + \frac{\pi}{\lambda}\left(\frac{1}{R_0} + \frac{1}{R}\right) y^2$$

where

$$\frac{\pi}{\lambda}\left(\frac{1}{R_0} + \frac{1}{R}\right) x^2 \cos^2 \delta_0 \equiv \frac{1}{2}\pi\xi^2; \qquad \frac{\pi}{\lambda}\left(\frac{1}{R_0} + \frac{1}{R}\right) y^2 \equiv \frac{1}{2}\eta^2$$

The substitution renders

$$\left.\begin{aligned} dx\,dy &= \frac{\lambda}{2}\frac{d\xi\,d\eta}{\left(\frac{1}{R_0}+\frac{1}{R}\right)\cos\delta_0};\\ C &= K_1\int\int \cos\left[\frac{\pi}{2}(\xi^2+\eta^2)\right]d\xi\,d\eta\\ S &= K_1\int\int \sin\left[\frac{\pi}{2}(\xi^2+\eta^2)\right]d\xi\,d\eta\\ K_1 &= \frac{\frac{1}{2}\lambda}{\left(\frac{1}{R_0}+\frac{1}{R}\right)\cos\delta_0} \end{aligned}\right\} \quad (908c)$$

We must then integrate in a corresponding ξ, η plane for an aperture corresponding to the opening shown in Fig. 363. When the integration in the ξ, η plane is to be taken over a rectangular area, with the sides parallel to the reference axes, we find

$$\left.\begin{aligned} C &= K_1\left[\int\int \cos\left(\frac{\pi}{2}\xi^2\right)\cos\left(\frac{\pi}{2}\eta^2\right)d\xi\,d\eta - \int\int \sin\left(\frac{\pi}{2}\xi^2\right)\sin\left(\frac{\pi}{2}\eta^2\right)d\xi\,d\eta\right]\\ S &= K_1\left[\int\int \sin\left(\frac{\pi}{2}\xi^2\right)\cos\left(\frac{\pi}{2}\eta^2\right)d\xi\,d\eta + \int\int \cos\left(\frac{\pi}{2}\xi^2\right)\sin\left(\frac{\pi}{2}\eta^2\right)d\xi\,d\eta\right] \end{aligned}\right\} \quad (908d)$$

where

$$x = \int_0^s \cos\left(\frac{\pi}{2}s^2\right)ds \qquad \text{and} \qquad y = \int_0^s \sin\left(\frac{\pi}{2}s^2\right)ds$$

are the Fresnel values of Table 67 and can also be found from the Cornu spiral. It is now of interest to apply these results to possible electromagnetic cases.

222. Distant Radiation Region Effect Due to a Wave-front Radiator of Any Contour. In Fig. 364, the elementary area dA, generally at x_0, y_0 of the XY plane, denotes a wavelet radiator.[1] This area is part of an essentially plane wave front

$$\mathcal{E}_x = \mathcal{E}_0\epsilon^{-j\beta z} \text{ volts/m}; \qquad H_y = H_0\epsilon^{-j\beta z} = \frac{\mathcal{E}_0}{376.7}\epsilon^{-j\beta z} \text{ amp/m}$$

[1] The area is now expressed by A in order to distinguish it from the function S as given in (908d).

which travels with a velocity $v = \omega/\beta$ meters per second along the $+Z$ direction. The equivalent electric and magnetic current sheets, in place

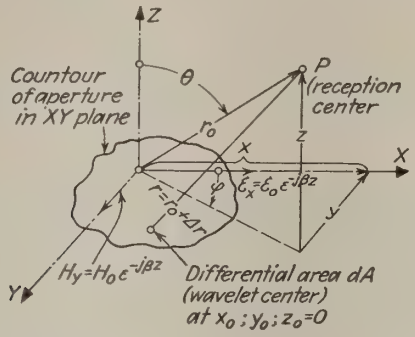

For planes parallel to the screen with the aperture $r = \sqrt{(x - x_0)^2 + (y - y_0)^2 + z^2}$
$r \cong z + \dfrac{(x - x_0)^2 + (y - y_0)^2}{2z}$ for z large compared with any dimension of the aperture A

FIG. 364. Useful expressions for reception centers in planes parallel with a plane primary wave front. Area of plane aperture is A sq ms. P is far enough away so that $1/r \cong 1/r_0$, but $\epsilon^{-j\beta r}$ is the phase factor.

of dA of the wavelet radiator dA, cause the electric and magnetic moments

$$d(m_x) = -H_0\, dA \quad \text{m} \cdot \text{amp}; \qquad d(m_{my}) = -\mathcal{E}_0\, dA \quad \text{m} \cdot \text{volts}$$

According to Secs. 124 and 213 and the transformation

$$N_\theta = N_x \cos\theta \cos\varphi + N_y \cos\theta \sin\varphi - N_z \sin\theta;$$
$$N_\phi = N_y \cos\varphi - N_x \sin\varphi$$

into polar coordinates, we find the elementary field contributions at P as

$$d\mathcal{E}_\theta = j\frac{\mathcal{E}_0\, dA}{2r\lambda}\epsilon^{-j\beta r}(1 + \cos\theta)\cos\varphi \qquad \text{volts/m}$$

$$d\mathcal{E}_\phi = -j\frac{\mathcal{E}_0\, dA}{2r\lambda}\epsilon^{-j\beta r}(1 + \cos\theta)\sin\varphi; \qquad d\mathcal{E}_x = j\frac{\mathcal{E}_0\, dA}{2r\lambda}(1 + \cos\theta)$$

$$d\mathcal{E}_y = 0 \text{ volts/m}$$

We must now integrate *all* the *wavelet effects* and find by omitting the $\epsilon^{j\omega t}$ factor

$$\left.\begin{aligned} &\mathcal{E}_x = j\frac{1 + \cos\theta}{2\lambda}\int\int_A \mathcal{E}_0\frac{\epsilon^{-j\beta r}}{r}\,dA \qquad \text{volts/m} \\ &r = \sqrt{(x - x_0)^2 + (y - y_0)^2 + z^2}; \\ &r \cong z + \frac{(x - x_0)^2 + (y - y_0)^2}{2z} \qquad \text{for } z \text{ large compared with any of the aperture dimensions} \end{aligned}\right\} \quad (909)$$

For angles of diffraction $\theta \leqq 4$ deg, we find the forward factor $(1 + \cos\theta) \cong 2$. We also have

$$r = [(x - x_0)^2 + (y - y_0)^2 + z^2]^{1/2} = z\left[\frac{(x - x_0)^2 + (y - y_0)^2}{z^2} + 1\right]^{1/2}$$
$$\cong z\left[1 + \frac{1}{2}\frac{(x - x_0)^2 + (y - y_0)^2}{z^2}\right] = z + \frac{(x - x_0)^2 + (y - y_0)^2}{2z}$$

since $[(x - x_0)^2 + (y - y_0)^2]/z^2$ is small, compared with unity. This value of r can be used in the Fresnel phase factor $\epsilon^{-j\beta r}$. We have also, for z very large compared with the largest dimension of the area A and the operating wavelength λ, the approximation $z \cong r$ meters in the factor $1/r$. Hence, for angles of diffractions θ *not exceeding about* 4 *deg*, with the normal to the area A of the aperture, we find at the reception center P

$$\left.\begin{aligned} \mathcal{E}_x &\cong \frac{j}{z\lambda}\int\int_A \mathcal{E}_0\epsilon^{-j\beta\left[z + \frac{(x-x_0)^2+(y-y_0)^2}{2z}\right]}\,dA \\ &= j\frac{\epsilon^{-j\beta z}}{z\lambda}\int\int_A \mathcal{E}_0\epsilon^{-j\beta\frac{(x-x_0)^2+(y-y_0)^2}{2z}}\,dA \end{aligned}\right\}$$ for *inclined* primary-wave-front incidence on area A in XY plane (volts/m)

and

$$\left.\begin{aligned} \mathcal{E}_x &\cong \frac{j}{z\lambda}\int\int_A \mathcal{E}_0\epsilon^{-j\beta\left[z + \frac{(x-x_0)^2+(y-y_0)^2}{2z}\right]}\,dA \\ &= j\frac{\mathcal{E}_0\epsilon^{-j\beta z}}{z\lambda}\int\int \epsilon^{-j\beta\frac{(x-x_0)^2+(y-y_0)^2}{2z}}\,dA \end{aligned}\right\}$$ for *perpendicular* primary-wave incidence ($\mathcal{E}_0$ = constant) (909*a*)

For normal primary-wave incidence, the double integral leads to

$$\int\int = \underbrace{\int\int_A \cos\left[\pi\frac{(x - x_0)^2 + (y - y_0)^2}{z\lambda}\right]dA}_{D}$$
$$\underbrace{- j\int\int_A \sin\left[\pi\frac{(x - x_0)^2 + (y - y_0)^2}{z\lambda}\right]dA}_{E}$$

$$\beta = \frac{2\pi}{\lambda}; \qquad dA = dx_0\,dy_0$$

Putting

$$\pi\frac{(x - x_0)^2}{z\lambda} = \alpha_0; \qquad \pi\frac{(y - y_0)^2}{z\lambda} = \beta_0$$

we find

$$\sin(\alpha_0 + \beta_0) = \sin\alpha_0\cos\beta_0 + \cos\alpha_0\sin\beta_0$$
$$\cos(\alpha_0 + \beta_0) = \cos\alpha_0\cos\beta_0 - \sin\alpha_0\sin\beta_0$$

and for

$$\frac{\pi(x - x_0)^2}{z\lambda} = p; \qquad \frac{\pi(y - y_0)^2}{z\lambda} = q$$

we find

$$\left.\begin{aligned}\int\int &= \underbrace{\int\int_A \cos p \cos q \, dx_0 \, dy_0 - \int\int_A \sin p \sin q \, dx_0 \, dy_0}_{D} \\ &+ j\Big(\underbrace{\int\int_A \sin p \cos q \, dx_0 \, dy_0 + \int\int_A \cos p \sin q \, dx_0 \, dy_0}_{E}\Big); \int\int = D + jE\end{aligned}\right\} \tag{909b}$$

so that

$$\mathcal{E}_x = j \frac{\mathcal{E}_0 \epsilon^{-j\beta z}}{z\lambda} \sqrt{D^2 + E^2} \Big/ \tan^{-1}\left(\frac{E}{D}\right) \quad \text{volts/m} \tag{909c}$$

Such a result would be expected, since we deal now with Fresnel wavelet summations and must add the effects with respect to amplitude *as well as phase*. The double integration is then carried out by changing the functions to Fresnel integrals, which have the form

$$x = \int \cos\left(\frac{\pi}{2} s^2\right) ds; \qquad y = \int \sin\left(\frac{\pi}{2} s^2\right) ds$$

where x and y are the abscissa and ordinate projections of the length s along a Cornu spiral. Putting

$$0.5\pi s^2 = \pi \frac{(x - x_0)^2}{z\lambda} \qquad \text{and} \qquad 0.5\pi s_1^2 = \pi \frac{(y - y_0)^2}{z\lambda}$$

we find

$$s = (x - x_0)\sqrt{\frac{2}{z\lambda}}; \qquad ds = -dx_0 \sqrt{\frac{2}{z\lambda}}$$

$$s_1 = (y - y_0)\sqrt{\frac{2}{z\lambda}}; \qquad ds_1 = -dy_0 \sqrt{\frac{2}{z\lambda}}$$

because the distant field point P of coordinates x, y, and z in Fig. 364 is fixed. The minus signs before dx_0 and dy_0 are of no concern, since we could also have written $\sqrt{(x_0 - x)^2 + (y_0 + y)^2 - z^2}$ for the distance of the particular field point P from the particular wavelet center x_0, y_0, $z_0 = 0$ in the aperture A of the XY plane. Therefore,

$$\left.\begin{aligned} s &= (x_0 - x)\sqrt{\frac{2}{z\lambda}}; \qquad ds = dx_0 \sqrt{\frac{2}{z\lambda}} \\ s_1 &= (y_0 - y)\sqrt{\frac{2}{z\lambda}}; \qquad ds_1 = dy_0 \sqrt{\frac{2}{z\lambda}} \\ \int \cos\left[\frac{\pi(x_0 - x)^2}{z\lambda}\right] dx_0 &\equiv \sqrt{\frac{z\lambda}{2}} \int \cos\left(\frac{\pi}{2} s^2\right) ds = x_1 \\ \int \cos\left[\frac{\pi(y_0 - y)^2}{z\lambda}\right] dy_0 &\equiv \sqrt{\frac{z\lambda}{2}} \int \cos\left(\frac{\pi}{2} s_1^2\right) ds_1 = x \\ \int \sin\left[\frac{\pi(x_0 - x)^2}{z\lambda}\right] dx_0 &\equiv \sqrt{\frac{z\lambda}{2}} \int \sin\left(\frac{\pi}{2} s^2\right) ds = y_1 \\ \int \sin\left[\frac{\pi(y_0 - y)^2}{z\lambda}\right] dy_0 &\equiv \sqrt{\frac{z\lambda}{2}} \int \sin\left(\frac{\pi}{2} s_1^2\right) ds_1 = y_2 \end{aligned}\right\} \tag{909d}$$

where x_1, x_2 are the projections on the abscissa axis and y_1, y_2 are the projections on the ordinate axis of respective lengths s and s_1 along a Cornu spiral. We have then in (909*b*), for $x_0 - x$ and $y_0 - y$ instead of $x - x_0$ and $y - y_0$, respectively, the relations

$$\left.\begin{aligned} D &= \frac{z\lambda}{2}\left[\int \cos\left(\frac{\pi}{2}s^2\right)ds \int \cos\left(\frac{\pi}{2}s_1^2\right)ds_1 \right. \\ &\qquad \left. - \int \sin\left(\frac{\pi}{2}s^2\right)ds \int \sin\left(\frac{\pi}{2}s_1^2\right)ds_1\right] = \frac{z\lambda}{2}(x_1x_2 - y_1y_2) \\ E &= \frac{z\lambda}{2}\left[\int \sin\left(\frac{\pi}{2}s^2\right)ds \int \cos\left(\frac{\pi}{2}s_1^2\right)ds_1 \right. \\ &\qquad \left. + \int \cos\left(\frac{\pi}{2}s^2\right)ds \int \sin\left(\frac{\pi}{2}s_1^2\right)ds_1\right] = \frac{z\lambda}{2}(x_1y_2 - x_2y_1) \end{aligned}\right\} \quad (909e)$$

The total field at P, due to the entire primary wave-front radiator, becomes

$$\left.\begin{aligned} \mathcal{E}^{(\text{volts/m})} &= j\frac{\mathcal{E}_0}{2}\epsilon^{-j\beta z}\sqrt{(x_1x_2 - y_1y_2)^2 + (x_1y_2 + x_2y_1)^2}\,\underline{/\psi} \\ &= j\frac{\mathcal{E}_0}{2}\epsilon^{-j\beta z}\sqrt{(x_1^2 + y_1^2)(x_2^2 + y_2^2)}\,\Big/\underline{\psi = \tan^{-1}\left(\frac{x_1y_2 - x_2y_1}{x_1x_2 - y_1y_2}\right)} \end{aligned}\right\} \quad (909f)$$

We can use the Cornu spiral procedure and find the values x_1, x_2, y_1, and y_2 of (909*d*) by means of s and s_1 values if the appropriate integration limits are used. These limits depend, according to (909*d*), on the limits of the area A.

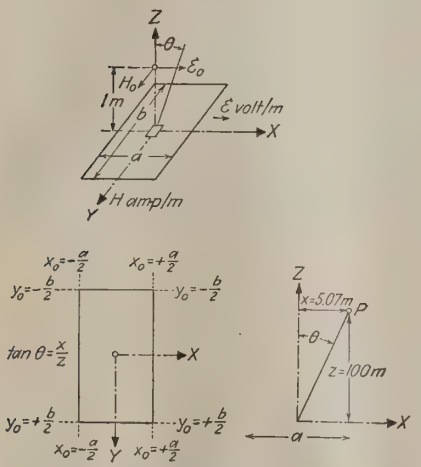

FIG. 365. Rectangular wave-front radiator. $\mathcal{E}_0$ and H_0 are the reference field associations at 1-m distance from the elementary radiator dA; $A = ab$ sq m. $\mathcal{E}$ and H are the polarizations of the primary wave front. a and b are in meters. $a = 0.5\lambda$; $\lambda = 0.1$ m.

223. Application to Fresnel Diffraction of an Electromagnetic Rectangular Primary Wave-front Radiator. Figure 365 shows such a wave-front radiator of area $A = ab$ square meters, and $\mathcal{E}_0$ volts per meter and H_0 amperes per meter are the reference fields at unit distance (1 m distance) normal to a primary wave-front element $dA = dx_0\,dy_0$, which is in the XY plane. Inasmuch as the integrations of (909*b*) and of the corresponding integrals of (909*d*) must be taken over the limits $x_0 = \mp a/2$ and $y_0 = \mp b/2$, according to the s and s_1 formulas of (909*d*), we have the spiral lengths

$$s = \mp \frac{a}{2} - x\sqrt{\frac{2}{z\lambda}} = \frac{\mp a - 2x}{\sqrt{2z\lambda}} = -\frac{a \pm 2x}{\sqrt{2z\lambda}}$$

$$s_1 = \mp \frac{b}{2} - y\sqrt{\frac{2}{z\lambda}} = \frac{\mp b - 2y}{\sqrt{2z\lambda}} = -\frac{b \pm 2y}{\sqrt{2z\lambda}}$$

These expressions hold, since the positive limit value must be subtracted from the negative limit value after finding the expression for the integral.

The Fresnel integrals of form $x = \int \cos(0.5\pi s^2)\,ds$ and $y = \int \sin(0.5\pi s^2)\,ds$, on account of the cosine or C type and of the sine or S type, are often written in classic optics as

$$\int \cos(0.5\pi s^2)\,ds = C(s); \qquad \int \sin(0.5\pi s^2)\,ds = S(s)$$

where $C(s)$ and $S(s)$ are the values for the particular numerical component magnitudes of s. They are found from the projections on the abscissa and the ordinate axis, respectively, for a particular spiral length s of a Cornu spiral. We have the identities for (909d)

$$q\int \cos\left(\frac{\pi}{2}s^2\right)ds \equiv \int_{x_0=-a/2}^{x_0=a/2} \cos p\,dx_0; \qquad p = \frac{\pi(x_0 - x)^2}{z\lambda}$$

$$q\int \cos\left(\frac{\pi}{2}s_1^2\right)ds_1 \equiv \int_{y_0=-b/2}^{y_0=b/2} \cos r\,dy_0; \qquad r = \frac{\pi(y_0 - y)^2}{z\lambda}$$

$$q\int \sin\left(\frac{\pi}{2}s^2\right)ds \equiv \int_{-a/2}^{a/2} \sin p\,dx_0; \qquad q\int \sin\left(\frac{\pi}{2}s_1^2\right)ds_1 \equiv \int_{-b/2}^{b/2} \sin r\,dy_0$$

for $q = \sqrt{z\lambda/2}$. For the total field $\mathcal{E}_x$, due to the wave-front radiator of $A = ab$ square meters,

$$\left.\begin{aligned}
\mathcal{E}_x^{(\text{volts/m})} &= j\frac{\mathcal{E}_0}{2}\epsilon^{-j\beta z}(D_1 - jE_1)(D_2 - jE_2)\\
D_1 &= C\left(\frac{a + 2x}{\sqrt{2z\lambda}}\right) + C\left(\frac{a - 2x}{\sqrt{2z\lambda}}\right);\\
D_2 &= C\left(\frac{b + 2y}{\sqrt{2z\lambda}}\right) + C\left(\frac{b - 2y}{\sqrt{2z\lambda}}\right)\\
E_1 &= S\left(\frac{a + 2x}{\sqrt{2z\lambda}}\right) + S\left(\frac{a - 2x}{\sqrt{2z\lambda}}\right);\\
E_2 &= S\left(\frac{b + 2y}{\sqrt{2z\lambda}}\right) + S\left(\frac{b - 2y}{\sqrt{2z\lambda}}\right)
\end{aligned}\right\} \qquad (909g)$$

where a, b, x, y, z, and λ are in meters and $\theta \leqq 4$ deg. Since $(D_1 - jE_1)(D_2 - jE_2) = D_1D_2 - E_1E_2 - j(D_1E_2 + D_2E_1)$, we find

$$\left.\begin{aligned}
&\mathcal{E}_\theta = j0.25(1 + \cos\theta)\cos\varphi\mathcal{E}_0\epsilon^{-j\beta z}M/\psi \quad \text{volts/m}\\
&M = \sqrt{(D_1D_2 - E_1E_2)^2 + (D_1E_2 + D_2E_1)^2};\ \psi = \tan^{-1}\left(\frac{D_1E_2 + D_2E_1}{D_1D_2 - E_1E_2}\right)\\
&\mathcal{E}_\varphi = -j0.25(1 + \cos\theta)\sin\varphi M\mathcal{E}_0\epsilon^{-j\beta z}/\psi
\end{aligned}\right\} \qquad (909h)$$

Formula (909h) applies for any angle θ of diffraction (*no* limitation, such as $\theta \leqq 4$ deg), for normal primary-wave incidence on the aperture A. When we are interested only in $\mathcal{E}_x$ fields along a direction parallel with the X axis at a distance z meters from the XY plane, we find the Fresnel directivity

$$D_x = (1 + \cos\theta) \times \sqrt{\left[C\left(\frac{2x+a}{\sqrt{2z\lambda}}\right) - C\left(\frac{2x-a}{\sqrt{2z\lambda}}\right)\right]^2 + \left[S\left(\frac{2x+a}{\sqrt{2z\lambda}}\right) - S\left(\frac{2x-a}{\sqrt{2z\lambda}}\right)\right]^2} \quad (909i)$$

since the terms involving b are of no concern in the XZ plane. Since all the terms under the square root contain $+2x$ and x denotes the horizontal distance of the reception center P parallel with the X axis, we need only to draw half of the Cornu spiral (as in Fig. 366) in order to illustrate the application of (909i). This spiral has been shown to be a plot of $S(s)$ against $C(s)$, so that any point of the spiral, such as A, with coordinates $C[(2x - a)/\sqrt{2z\lambda}] = C(s)$ as abscissa and $S(s)$ as ordinate is so located that the distance from the origin O along the spiral to A is equal to s. The value $s_1 = (2x + a)/\sqrt{2z\lambda}$ gives the coordinates $C(s_1)$ and $S(s_1)$ of the spiral point B, and the arc OB is now equal to s_1. Since, in (909i), we have the differences $C(s_1) - C(s)$ and $S(s_1) - S(s)$, the arc, *i.e.*, the curve length, AFB must be equal to $s_1 - s$. However, the chord AB must be equal to the square-root value, because $AB = \sqrt{[C(s_1) - C(s)]^2 + [S(s_1) - S(s)]^2}$. Since the halfway point F along the spiral AFB is such that

$$\text{Arc } OAF = 0.5(s + s_1) = \frac{2x}{2z\lambda}$$

we note that the *location* of the spiral length AFB depends upon the x coordinate of the reception center P *but the length* of the spiral AFB depends upon the *width* a of the wave-front radiator, since the spiral

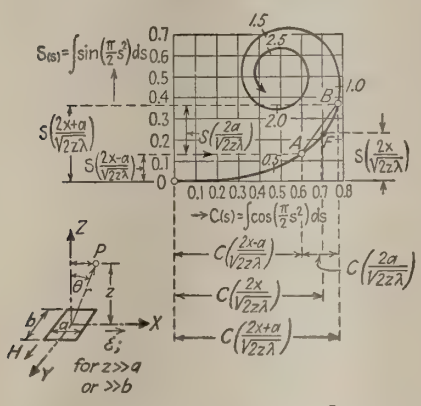
Operating spiral length $AFB = \frac{2a}{\sqrt{2z\lambda}}$ m
$s = \frac{2x-a}{\sqrt{2z\lambda}}$; $s_1 = \frac{2x+a}{\sqrt{2z\lambda}}$;
$D_x = (1 + \cos\theta) \times \sqrt{[C(s_1) - C(s)]^2 + [S(s_1) - S(s)]^2}$
$= (1 + \cos\theta)AB$
for $z \gg a$ or $\gg b$

FIG. 366. Application of the Cornu spiral method to Fresnel diffraction (only half of the spiral, positive half, is needed).

length AB is equal to $s_1 - s = 2a/\sqrt{2z\lambda}$. Therefore, the x coordinate of the reception center P determines, for a fixed wave-front width a, the magnitude of chord AB. The length of this chord, multiplied by $(1 + \cos\theta)$, gives the directivity in the XZ plane for the z coordinate fixed. For the reception center P along the $+Z$ axis, we have $x = 0$. Scaling off from the origin O the distance $a/\sqrt{2z\lambda}$ along the spiral, the chord from O to this spiral point must be equal to half the square-root value, since the other half is found by scaling off the same length from the inflection point O of the symmetrical spiral to the left. The square-root value thus obtained is a principal maximum, since the spiral is straightest and almost equal with the chord if $2a/\sqrt{2z\lambda}$ is not too large. The value of $(1 + \cos\theta)$ is likewise near its maximum value of 2. Therefore, maximum field intensity must be expected along the Z axis if measured along a fixed distance r. As the reception center P, for a *fixed* ordinate z, moves to the right in the XZ plane, the value x increases and the spiral length AB, which is equal to $s_1 - s = 2a/\sqrt{2z\lambda}$, slides farther out along the spiral, since its mid-point F moves out. The corresponding chord length AB decreases toward smaller values, until a minimum value is reached. For still larger x values, the chord length *increases* again (the spiral winds around) and comes to a second maximum (somewhat smaller than the first maximum), decreases again toward a second somewhat smaller minimum value, etc. Hence, we have successive weakening field fluctuations, which, in addition, owing to the factor $(1 + \cos\theta)$, are still more reduced, since this factor varies from a value of 2 toward unity value for $x = \infty$. Keeping the wave-front dimensions as well as x fixed but changing the z coordinate of reception center P can only decrease the s and s_1 values, according to a $1/\sqrt{z}$ law. As such, it produces a corresponding decrease in the spiral length $ABC = s_1 - s$, as well as in the chord length AB. If we keep the location x,y,z of the reception center x,y,z fixed and increase the dimension a, we increase AB or the square-root value of $(909i)$, since A and B move farther away from the fixed mid-point F. Hence, we also obtain corresponding field fluctuations at P. Table 83 gives the evaluations when the reception center P in Fig. 365 as well as Fig. 366 moves from a location $z = 50$ m above the mid-point of a rectangular wave-front radiator, parallel with the XY plane, to a distance of $x = 10.25$ m (in the XZ plane). In this table, values of the Fresnel integral Table 67 are used, instead of the Cornu spiral procedure described in connection with Fig. 366. If the Cornu spiral method is used, we have only to compute and look up the $C(s)$, $C(s_1)$, $S(s)$, and $S(s_1)$ values. Since, for such a small $AFB = s_1 - s$ value as found from $2a/\sqrt{2z\lambda} = 0.1$, the value of $\sqrt{p + q}$ changes only toward a somewhat smaller value without any

TABLE 83. FRESNEL PATTERN FOR $a = 0.5\lambda$, $= \lambda$ METERS, AND $z = 50$ METERS

$D_x = (1 + \cos\theta)\sqrt{[C(s_1) - C(s)]^2 + [S(s_1) - S(s)]^2} = (1 + \cos\theta)\sqrt{p + q}$; $p = [C(s_1) - C(s)]^2$; $q = [S(s_1) - S(s)]^2$

x, m	$2x$, m	$2x - a$ meters	$s = \frac{2x - a}{10}$	$2x + a$ meters	$s_1 = \frac{2x + a}{10}$	From Fresnel Table 67				Computations								
						$C(s_1)$	$C(s)$	$S(s_1)$	$S(s)$	$C(s_1) - C(s)$	$p = [C(s_1) - C(s)]^2 10^{-8}$	$S(s_1) - S(s)$	$q = [S(s_1) - S(s)]^2 10^{-8}$	$\sqrt{p+q}$	$\frac{q}{50}$	$\theta^\circ = \tan^{-1}(x/50)$	$1 + \cos\theta$	D_x
0.0000	0.00	−0.5	−0.05	0.5	0.05	0.0499	−0.0499	0.00025	−0.00025	0.0999	998,001	0.0005	25	0.0999	0.000	0.0000	2.0000	0.2000
0.75	1.5	1.0	0.1	2.0	0.2	0.1999	0.0999	0.0042	0.0005	0.0995	990,025	0.0037	1,369	0.09955	0.015	0.86	1.9999	0.2
1.25	2.5	2.0	0.2	3.0	0.3	0.2994	0.1999	0.0141	0.0042	0.0995	990,025	0.0099	9,801	0.1	0.025	1.45	1.9997	0.2
1.75	3.5	3.0	0.3	4.0	0.4	0.3975	0.2994	0.0334	0.0141	0.0981	962,361	0.0193	37,249	0.09985	0.035	2.0	1.9994	0.1999
2.25	4.5	4.0	0.4	5	0.5	0.4923	0.3975	0.0647	0.0334	0.0948	898,704	0.0313	97,969	0.09985	0.045	2.6	1.999	0.1995
2.75	5.5	5	0.5	6	0.6	0.5811	0.4923	0.1105	0.0647	0.0888	788,544	0.0458	209,764	0.0999	0.055	3.2	1.9984	0.199
3.25	6.5	6	0.6	7	0.7	0.6597	0.5811	0.1721	0.1105	0.0786	617,796	0.0616	379,456	0.09985	0.065	3.7	1.9979	0.1985
3.75	7.5	7	0.7	8	0.8	0.723	0.6597	0.2493	0.1724	0.0633	400,689	0.0772	595,984	0.09985	0.075	4.3	1.9972	0.1983
4.25	8.5	8	0.8	9	0.9	0.7648	0.723	0.3398	0.2493	0.0418	174,724	0.0905	819,025	0.0997	0.085	4.85	1.9964	0.1982
4.75	9.5	9	0.9	10	1.0	0.7799	0.7648	0.4383	0.3398	0.0151	22,801	0.0985	970,225	0.09965	0.095	5.4	1.9956	0.1981
5.25	10.5	10	1.0	11	1.1	0.7648	0.7799	0.5365	0.4383	−0.0151	22,801	0.0982	964,324	0.09935	0.105	6	1.9945	0.1979
5.75	11.5	11	1.1	12	1.2	0.7154	0.7648	0.6234	0.5365	−0.0494	24,036	0.0869	755,161	0.0999	0.115	6.6	1.9934	0.1977
6.25	12.5	12	1.2	13	1.3	0.6386	0.7154	0.6863	0.6234	−0.0768	589,824	0.0631	398,161	0.0994	0.125	7.1	1.9923	0.1975
6.75	13.5	13	1.3	14	1.4	0.5431	0.6386	0.7135	0.6863	−0.0955	912,025	0.0272	73,984	0.0993	0.135	7.7	1.991	0.1973
7.25	14.5	14	1.4	15	1.5	0.4453	0.5431	0.6975	0.7135	−0.0978	956,484	−0.016	25,600	0.0991	0.145	8.3	1.9895	0.197
7.75	15.5	15	1.5	16	1.6	0.3655	0.4453	0.6389	0.6975	−0.0798	636,804	−0.0586	343,396	0.099	0.155	8.8	1.9882	0.1965
8.25	16.5	16	1.6	17	1.7	0.3238	0.3655	0.5492	0.6389	−0.0417	173,889	−0.0897	804,609	0.0989	0.165	9.4	1.9866	0.1962
8.75	17.5	17	1.7	18	1.8	0.3337	0.3238	0.4509	0.5492	0.0099	9,801	−0.0983	966,289	0.0988	0.175	9.9	1.9851	0.196
9.25	18.5	18	1.8	19	1.9	0.3945	0.3337	0.3734	0.4509	0.0608	369,664	−0.0775	600,625	0.0985	0.185	10.5	1.9833	0.195
9.75	19.5	19	1.9	20	2.0	0.4883	0.3945	0.3434	0.3734	0.0938	879,844	−0.03	90,000	0.09848	0.195	11	1.9816	0.1942
10.25	20.5	20	2.0	21	2.1	0.5814	0.4883	0.3743	0.3434	0.0931	866,761	+0.0109	95,481	0.0981	0.205	11.6	1.9796	0.1941
10.75	21.5	21	2.1	22	2.2	0.6362	0.5814	0.4536	0.3743	0.0548	300,304	0.0813	660,969	0.09805	0.215	12.1	1.9778	0.194
11.25	22.5	22	2.2	23	2.3	0.6268	0.6362	0.5531	0.4556	−0.0094	8,836	0.0975	950,625	0.09795	0.225	12.7	1.9755	0.193

11.75	23.5	23	2.3	24	2.4	0.555	0.6268	0.6197	0.5531	−0.0718	515,524	0.0666	443,556	0.09795	0.235	13.2	1.9736	0.1922
12.25	24.5	24	2.4	25	2.5	0.4574	0.555	0.6192	0.6197	−0.0976	952,576	−0.0005	25	0 0976	0.245	13.8	1.9711	0.192
12.75	25.5	25	2.5	26	2.6	0.3889	0.4574	0.55	0.6192	−0.0685	469,225	−0.0692	478,864	0.0974	0.255	14.3	1.969	0.1915
13.25	26.5	26	2.6	27	2.7	0.3926	0.3889	0.4529	0.55	0.0100	10,000	−0.0971	942,841	0.0976	0.265	14.9	1.9664	0.191
13.75	27.5	27	2.7	28	2.8	0.4675	0.3926	0.3915	0.4529	0.0749	561,001	−0.0614	376,996	0.0969	0.275	15.4	1.9641	0.19
14.25	28.5	28	2.8	29	2.9	0.5624	0.4675	0.4102	0.3915	0.0949	900,601	0.0187	34,969	0.0967	0.285	15.9	1.9617	0.189
14.75	29.5	29	2.9	30	3.0	0.6057	0.5624	0.4963	0.4102	0.0433	187,489	0.0861	741,321	0.0964	0.295	16.4	1.9593	0.1885
15.25	30.5	30	3.0	31	3.1	0.5616	0.6057	0.5818	0.4963	−0.0441	194,481	0.0855	731,025	0.0962	0.305	17	1.9563	0.188
15.75	31.5	31	3.1	32	3.2	0.4663	0.5616	0.5933	0.5818	−0.0953	908,209	0.0115	13,225	0.0962	0.315	17.5	1.9537	0.187
16.25	32.5	32	3.2	33	3.3	0.4057	0.4663	0.5193	0.5923	−0.0606	367,236	−0.0740	547,600	0.09565	0.325	18	1.9511	0.186
16.75	33.5	33	3.3	34	3.4	0.4385	0.4057	0.4217	0.5193	0.0328	107,584	−0.0896	802,816	0 0954	0.335	18.5	1.9483	0.1858
17.25	34.5	34	3.4	35	3.5	0.5326	0.4385	0.4153	0.4297	0.0941	885,481	−0.0144	20,736	0.0952	0.345	19	1.9455	0.185
17.75	35.5	35	3.5	36	3.6	0.5880	0.5326	0.4923	0.4153	0.0554	306,916	0.0776	602,176	0.09535	0.355	19.5	1.9426	0.182
18.25	36.5	36	3.6	37	3.7	0.5419	0.5880	0.5750	0.4923	−0.0461	212,521	0.0827	683,929	0.0947	0.365	20.05	1.9387	0.1817
18.75	37.5	37	3.7	38	3.8	0.4481	0.5419	0.5656	0.5750	−0.0938	879,844	−0.0094	8,836	0.0943	0.375	20.55	1.9367	0.1814
19.25	38.5	38	3.8	39	3.9	0.4223	0.4481	0.4752	0.5656	−0.0258	66,564	−0.0904	817,216	0.094	0.385	21.05	1.9336	0.181
19.75	39.5	39	3.9	40	4.0	0.4984	0.4223	0.4205	0.4752	0.0761	579,121	−0.0547	299,209	0.0937	0.395	21.55	1.9304	0.1805
20.25	40.5	40	4.0	41	4.1	0.5737	0.4984	0.4758	0.4205	0.0753	567,009	0.0553	305,809	0.09345	0.405	22.05	1.9272	0.18
20.75	41.5	41	4.1	42	4.2	0.5417	0.5737	0.5632	0.4758	−0.0320	102,400	0.0874	763,876	0.0931	0.415	22.55	1.9239	0.1766
21.25	42.5	42	4.2	43	4.3	0.4494	0.5417	0.5540	0.5632	−0.0923	851,929	−0.0092	8,464	0.09275	0.425	23	1.9205	0.1761
21.75	43.5	43	4.3	44	4.4	0.4383	0.4494	0.4623	0.5540	−0.0111	12,321	−0.0917	840,889	0.0924	0.435	23.5	1.9171	0.1756
22.25	44.5	44	4.4	45	4.5	0.5258	0.4383	0.4342	0.4623	0.0875	765,625	−0.0281	78,961	0.0919	0.445	24	1.9135	0.175
22.75	45.5	45	4.5	46	4.6	0.5672	0.5258	0.5162	0.4342	0.0414	171,396	0.0820	672,400	0.09185	0.455	24.5	1.91	0.1745
23.25	46.5	46	4.6	47	4.7	0.4914	0.5672	0.5669	0.5162	−0.0758	574,564	0.0507	257,049	0.0912	0.465	24.95	1.907	0.174
23.75	47.5	47	4.7	48	4.8	0.4338	0.4914	0.4968	0.5669	−0.0576	331,776	−0.0701	491,401	0.09075	0.475	25.4	1.9033	0.172
24.25	48.5	48	4.8	49	4.9	0.5002	0.4338	0.4351	0.4968	0.0664	440,896	−0.0617	380,689	0.09065	0.485	25.9	1.8996	0.171
27.25	54.5	54	5.4	55	5.5	0.4784	0.5573	0.5537	0.5140	−0.0789	622,521	0.0397	157,609	0.08835	0.545	28.6	1.878	0.166
29.75	59.5	59	5.9	60	6.0	0.4995	0.4484	0.4469	0.5163	0.0511	261,121	−0.0694	481,636	0.0862	0.595	30.8	1.859	0.1605
32.25	64.5	64	6.4	65	6.5	0.4816	0.5496	0.5454	0.4965	−0.068	462,400	0.0489	239,121	0.08375	0.645	32.8	1.8406	0.154
34.75	69.5	69	6.9	70	7.0	0.5455	0.4732	0.4997	0.4624	0.0723	522,729	0.0373	139,129	0.0814	0.695	34.8	1.8211	0.148
37.25	74.5	74	7.4	75	7.5	0.5160	0.4601	0.4607	0.5161	0.0559	312,481	−0.0554	306,916	0.0787	0.745	36.7	1.8018	0.142
39.75	79.5	79	7.9	80	8.0	0.4998	0.4760	0.4602	0.5323	0.0238	56,644	−0.0721	519,841	0.0759	0.795	38.5	1.7826	0.135
42.25	84.5	84	8.4	85	8.5	0.5142	0.4709	0.4653	0.5243	0.0433	187,489	−0.059	348,100	0.0732	0.845	40.2	1.7651	0.129

Remarks: Spiral lengths $s = (2x - a)/\sqrt{2z\lambda}$ and $s_1 = (2x + a)/\sqrt{2z\lambda}$, $\sqrt{2z\lambda} = \sqrt{2 \times 50 \times 1} = 10$ m, $a = 0.5\lambda = 0.5$ m. From Fig. 365, we find $\theta = \tan^{-1}(x/z) = \tan^{-1}(x/50)$. For such relative dimensions, we find the operating spiral length AFB of Fig. 366 rather small and equal to only $2a/\sqrt{2z\lambda} = 2 \times 0.5/10 = 0.1$. This explains why the D_x value shows only a rather slow decrease, because such a short length must be carried much farther into the small spiral end.

fluctuations, we note that we have quite a broad diffraction pattern, as has already been found for the corresponding Fraunhofer diffraction pattern, for $a = 0.5\lambda$. If we make the wave-front radiator $a = \lambda$ meters wide, with all the other dimensions as in Table 83, we find the computations of Table 84. In order to facilitate the computations, the Fresnel integrals $C(s)$ and $S(s)$ are plotted as curves in Fig. 367, so that the differences $C(s_1) - C(s)$ and $S(s_1) - S(s)$ can be read directly from these curves with an accuracy good enough for such evaluations. This

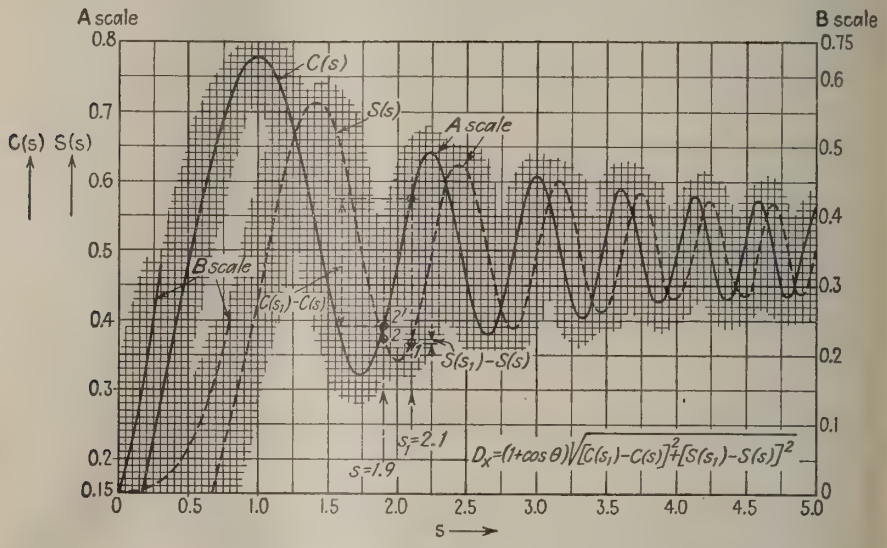

FIG. 367. Fresnel curves $C(s) = \int \cos\left(\frac{\pi}{2}s^2\right) ds$ and $S(s) = \int \sin\left(\frac{\pi}{2}s^2\right) ds$.

figure also gives an example for the case applying to Table 84, if the horizontal distance $x = 10$ m, for a fixed altitude $z = 50$ m and a wave-front width $a = \lambda = 1$ m. This yields the *numerical* distances $s_1 = 2.1$ and $s = 1.9$. The width between s and s_1 ordinates, *i.e.*, $s_1 - s$, is $2a/\sqrt{2z\lambda}$ can be marked on a transparent sheet with an ordinate scale slider calibrated in an (ordinate scale)^2-scale. This permits the differences $[C(s_1) - C(s)]^2$ and $[S(s_1) - S(s)]^2$ to be read off directly if the slider is set with its zero value on the lowest intersection with the s or s_1 ordinate, depending upon which ordinate causes the lowest intersection with respect to the $C(s)$ and $S(s)$ curves. Figure 368 gives the plots of Tables 87 and 84, together with the θ variation. To apply the formulas to much smaller altitudes z would give rise to errors, since it is assumed, in formula (909*i*), that the largest dimension of the wave-front radiator is small compared with the value of z.

It seems of interest to gain an idea as to what extent the assumption

$$r = \sqrt{(x - x_0)^2 + (y - y_0)^2 + z^2} \cong z + \frac{(x - x_0)^2 + (y - y_0)^2}{2z}$$

holds, where x,y,z is the location of the reception center P and $x_0,y_0,z_0 = 0$ the location of any Huygens wavelet center in the primary wave front. Suppose we take the reception center P along the Z axis, for which $x = 0 = y$, and again choose as in Tables 83 and 84 $z = 50$ m and $\lambda = 1$ m, corresponding to $^{300}/_{1} = 300$ Mc/sec.

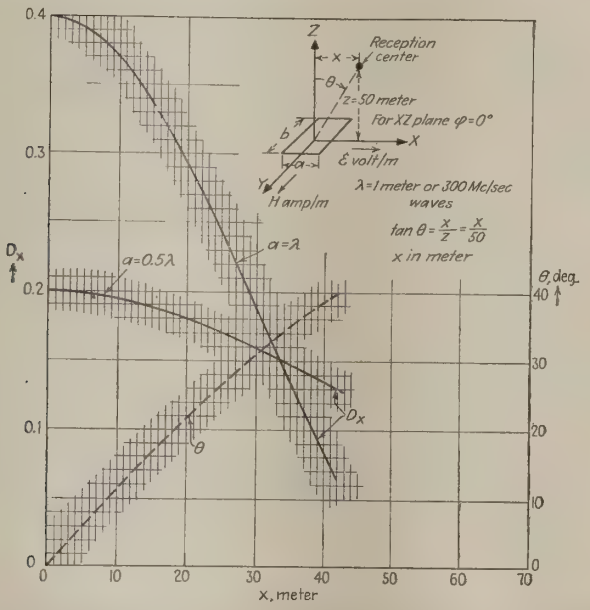

FIG. 368. Fresnel diffraction pattern for half-wavelength and full-wavelength width and same altitude ($z = 50$ m).

The most severe conditions occur at the boundary of the wave-front radiator. Assume that we have $a = b = 2\lambda$; then $x_0 = y_0 = 1$ m, and

$$r = \sqrt{(0 - 1)^2 + (0 - 1)^2 + 50^2} = \sqrt{2,502};$$

$$r \cong 50 + \frac{(0 - 1)^2 + (0 - 1)^2}{2 \times 50} = 50.02$$

The logarithm of 2,502 is 3.39829 and $\sqrt{2,502} = \frac{1}{2} \times 3.39829 = \bar{1}.699145$, with a numeric $r = 50.02$ (checks approximation). For $x = 41$ m, we have, for P in the XZ plane,

$$r = \sqrt{(41 - 1)^2 + (0 - 1)^2 + 50^2} = \sqrt{1,600 + 1 + 2,500} = \sqrt{4,101}$$

$$r \cong 50 + \frac{(41 - 1)^2 + (0 - 1)^2}{2 \times 50} = 50 + \frac{1,601}{100} = 66.01$$

TABLE 84. FRESNEL DIFFRACTION EVALUATIONS IN THE XZ PLANE, ALONG THE X DIRECTION AT A DISTANCE $z = 50$ METERS FOR $a = \lambda = 1$ METER

x, m	$2x$, m	$2x - a$, m	$s = \frac{2x - a}{10}$	$2x + a$, m	$s_1 = \frac{2x + a}{10}$	From Fig. 367 $C(s_1) - C(s)$	$p = [C(s_1) - C(s)]^2$	From Fig. 367 $S(s_1) - S(s)$	$q = [S(s_1) - S(s)]^2$	$\sqrt{p + q}$	$\frac{x}{50}$	$\theta^\circ = \tan^{-1}(x/50)$	$1 + \cos\theta$	D_x
0.0	0.0	−1.0	−0.1	1.0	0.1	0.1998	0.039601	0.001	0.000001	0.1998	0.00	0.00	2.0000	0.4000
1	2.0	1.0	0.1	3.0	0.3	0.1995	0.0398	0.0136	0.000185	0.1996	0.02	1.15	1.9998	0.4
2	4	3	0.3	5	0.5	0.1929	0.037249	0.0506	0.00256	0.1994	0.04	2.3	1.9992	0.398
3	6	5	0.5	7	0.7	0.1674	0.027889	0.1074	0.011449	0.1985	0.06	3.4	1.9982	0.396
4	8	7	0.7	9	0.9	0.1051	0.011025	0.1677	0.028224	0.198	0.08	4.6	1.9968	0.395
5	10	9	0.9	11	1.1	0.0000	0.000000	0.1967	0.03881	0.1967	0.1	5.7	1.9951	0.392
6	12	11	1.1	13	1.3	0.1262	0.015876	0.1498	0.0225	0.196	0.12	6.8	1.993	0.39
7	14	13	1.3	15	1.5	0.1933	0.037249	0.0112	0.000125	0.1933	0.14	8	1.9903	0.384
8	16	15	1.5	17	1.7	0.1215	0.014641	0.1483	0.0219	0.191	0.16	9.1	1.9874	0.379
9	18	17	1.7	19	1.9	0.0707	0.004998	0.1758	0.03098	0.1896	0.18	10.2	1.9842	0.376
10	20	19	1.9	21	2.1	0.1869	0.034969	0.009	0.000081	0.187	0.2	11.3	1.9806	0.37
11	22	21	2.1	23	2.3	0.0454	0.002061	0.1788	0.032041	0.1848	0.22	12.4	1.9767	0.366
12	24	23	2.3	25	2.5	0.1694	0.028561	0.0661	0.00436	0.181	0.24	13.5	1.9724	0.356
13	26	25	2.5	27	2.7	0.0648	0.004199	0.1663	0.027556	0.178	0.26	14.6	1.9677	0.35
14	28	27	2.7	29	2.9	0.1698	0.0289	0.0427	0.00182	0.175	0.28	15.6	1.9632	0.343
15	30	29	2.9	31	3.1	0.0008	64×10^{-8}	0.1716	0.029584	0.172	0.3	16.7	1.9578	0.337
16	32	31	3.1	33	3.3	0.1559	0.024649	0.0625	0.00391	0.169	0.32	17.7	1.9527	0.33
17	34	33	3.3	35	3.5	0.1269	0.016129	0.1040	0.01082	0.164	0.34	18.8	1.9466	0.32
18	36	35	3.5	37	3.7	0.0093	0.000086	0.1597	0.0256	0.1602	0.36	19.8	1.9409	0.31

19	38	37	3.7	39	3.9	0.1196	0.0144	0.0958	0.00918	0.1536	0.38	20.8	1.9348	0.297
20	40	39	3.9	41	4.1	0.1514	0.022801	0.0006	36×10^{-8}	0.1514	0.4	21.8	1.9285	0.291
21	42	41	4.1	43	4.3	0.1243	0.015376	0.0782	0.006115	0.1466	0.42	22.8	1.9219	0.282
22	44	43	4.3	45	4.5	0.0764	0.00584	0.1198	0.0144	0.142	0.44	23.75	1.9153	0.271
23	46	45	4.5	47	4.7	0.0344	0.00118	0.1327	0.017689	0.1374	0.46	24.7	1.9085	0.262
24	48	47	4.7	49	4.9	0.0088	0.000077	0.1318	0.017424	0.1318	0.48	25.65	1.9014	0.25
25	50	49	4.9	51	5.1	0.0015	225×10^{-8}	0.1273	0.01613	0.1273	0.5	26.6	1.8942	0.24
26	52	51	5.1	53	5.3	0.0091	8.28×10^{-5}	0.122	0.01488	0.122	0.52	27.5	1.887	0.23
27	54	53	5.3	55	5.5	0.0294	0.00086	0.1133	0.0128	0.117	0.54	28.4	1.8796	0.22
28	56	55	5.5	57	5.7	0.0601	0.00361	0.0942	0.00887	0.1115	0.56	29.25	1.8725	0.207
29	58	57	5.7	59	5.9	0.0901	0.00812	0.0568	0.00323	0.1065	0.58	30.1	1.8652	0.198
30	60	59	5.9	61	6.1	0.1011	0.0102	0.0002	4×10^{-8}	0.1011	0.6	31	1.8572	0.188
31	62	61	6.1	63	6.3	0.0735	0.0054	0.0610	0.00372	0.0955	0.62	31.8	1.8499	0.176
32	64	63	6.3	65	6.5	0.0056	0.0000314	0.0899	0.00808	0.09	0.64	32.6	1.8425	0.166
33	66	65	6.5	67	6.7	0.0651	0.00424	0.0539	0.0029	0.0845	0.66	33.4	1.8348	0.154
34	68	67	6.7	69	6.9	0.0735	0.0054	0.0291	0.00085	0.079	0.68	34.2	1.8271	0.145
35	70	69	6.9	71	7.1	0.0001	1×10^{-8}	0.0736	0.00541	0.0736	0.7	35	1.8192	0.134
36	72	71	7.1	73	7.3	0.066	0.00436	0.0161	0.00026	0.068	0.72	35.75	1.8116	0.123
37	74	73	7.3	75	7.5	0.0233	0.000543	0.0592	0.0035	0.064	0.74	36.5	1.8039	0.115
38	76	75	7.5	77	7.7	0.0532	0.00283	0.0213	0.000454	0.057	0.76	37.25	1.796	0.1025
39	78	77	7.7	79	7.9	0.0132	0.00017	0.0503	0.00253	0.052	0.78	38	1.788	0.093
40	80	79	7.9	81	8.1	0.0468	0.00219	0.0003	9×10^{-8}	0.0468	0.8	38.7	1.7804	0.0833
41	82	81	8.1	83	8.3	0.015	0.00022	0.0388	0.0015	0.0415	0.82	39.35	1.7732	0.0735
42	84	83	8.3	85	8.5	0.0236	0.00056	0.0279	0.00078	0.0365	0.84	40	1.765	0.064

Remarks: $D_x = (1 + \cos\theta)\sqrt{p + q}$; $p = [C(s_1) - C(s)]^2$; $q = [S(s_1) - S(s)]^2$; $s = (2x - a)/\sqrt{2z\lambda}$; $s_1 = \dfrac{2x + a}{\sqrt{2z\lambda}}$; $\sqrt{2z\lambda} = \sqrt{2 \times 50 \times 1} = 10$ m; $a = 1\lambda = 1$ m. According to Fig. 365, we have $\theta = \tan^{-1}(x/z)$ deg. Figure 367 shows how $C(s_1) - C(s)$ may be found for $x = 10$ m by means of $s_1 = 2.1$ and $s = 1.9$. The polarity of $C(s_1) - C(s)$ and $S(s_1) - S(s)$ is ignored in this table.

The evaluation of $\sqrt{4{,}101}$ is $\frac{1}{2} \times 3.16289 = 1.581445$, and $r = 64.04$ as against the approximation 66.01. It is, therefore, better not to use $a = 2\lambda$ for $z = 50$ m if values of x of the order of 41 m are used.

Formula (909g) shows that for a reception center P along the Z axis, we have $x = 0 = y$ and $z = z_1$. In comparison with a circular wave-front radiator of radius a meters, we find

$$\left.\begin{aligned} &\mathcal{E}_x^{(\text{volts/m})} = A\epsilon^{-j\beta z}[C(s_0) - jS(s_0)][C(s_1) - jS(s_1)] \\ &\qquad\qquad \text{for a rectangular wave-front radiator} \\ &\text{and} \\ &\mathcal{E}_x^{(\text{volts/m})} = A\epsilon^{-j\beta z_1} \sin\left(\frac{\pi a^2}{2z\lambda}\right) \qquad \text{for a circular wave-front radiator} \\ &s_0 = \frac{a}{\sqrt{2z\lambda}}; \qquad s_1 = \frac{b}{\sqrt{2z\lambda}}; \qquad z_1 = z + \frac{a^2}{4z}; \qquad A = j2\mathcal{E}_0 \\ &\qquad\qquad \lambda^{(\text{m})} = \frac{300}{f^{(\text{Mc/sec})}} \end{aligned}\right\} \quad (909j)$$

Since the radius $a = \sqrt{qz\lambda}$ meters, we note that *zero field* occurs whenever $q = 2, 4, 6, \cdots$, *i.e.*, for a vertical distance z from the circular wave-front radiator of $z = a^2/2\lambda, a^2/4\lambda, a^2/6\lambda, \cdots$. But *maximum field* effects of $z = a^2/\lambda, a^2/3\lambda, a^2/5\lambda, \cdots$ occur for $q = 1, 3, 5, \cdots$. Formulas (909j) also show that for a rectangular wave-front radiator, the function $\sqrt{[C^2(s_0) + S^2(s_0)][C^2(s_1) + S^2(s_1)]}$ gives the Fresnel diffraction pattern when the perpendicular $\mathcal{E}$ and H field associations are along the X and Y directions, respectively. For a square wave-front radiator, we have $a = b$ meters and $s_0 = s_1$, so that $D_{z_z} = C^2(s) + S^2(s)$ for a general orientation of the perpendicular $\mathcal{E}$ and H field vectors. We have then the relation

$$\mathcal{E}_x = j2\mathcal{E}_0 \sqrt{\cos^2\left(2\pi\frac{z}{\lambda}\right) + \sin^2\left(2\pi\frac{z}{\lambda}\right)}\left[C^2\left(\frac{a}{2z\lambda}\right) + S^2\left(\frac{a}{2z\lambda}\right)\right] \quad \text{volts/m}$$

the square-root factor being due to the *fixed* phase factor $\epsilon^{-j\beta z}$.

224. Significance of Fresnel Zones When Applied to Circular Electromagnetic Wave-front Radiators. The expression (909j) for the circular wave-front radiator is based on Fresnel zones (Secs. 188 to 190). It was shown that a spherical wave front in a circular aperture can be divided into Fresnel zones corresponding to 0.5λ steps. Adjacent zones then cause antiphase effects along the principal, or Z, direction (Fig. 369). The distance from any point on the circular boundary of a particular zone to a reception center P along the Z axis differs by 0.5λ from a point on a circular boundary of the next Fresnel zone. Taking, as in Fig. 369, the center of a circular wave-front radiator in the XY plane, at the

origin of a compromise XYZ system, the distance to P on the $+Z$ axis is the z coordinate of P, since $x = 0 = y$. The boundary of the first zone then requires such a radius a that any point on the circumference $2\pi a$ meters is a distance $z + 0.5\lambda$ from the reception center P. This distance is a hypotenuse, with two perpendicular sides a and z, respectively, so that $\sqrt{a^2 + z^2}$ is equal to $z + 0.5\lambda$. Therefore, $\sqrt{a^2 + z^2} -$

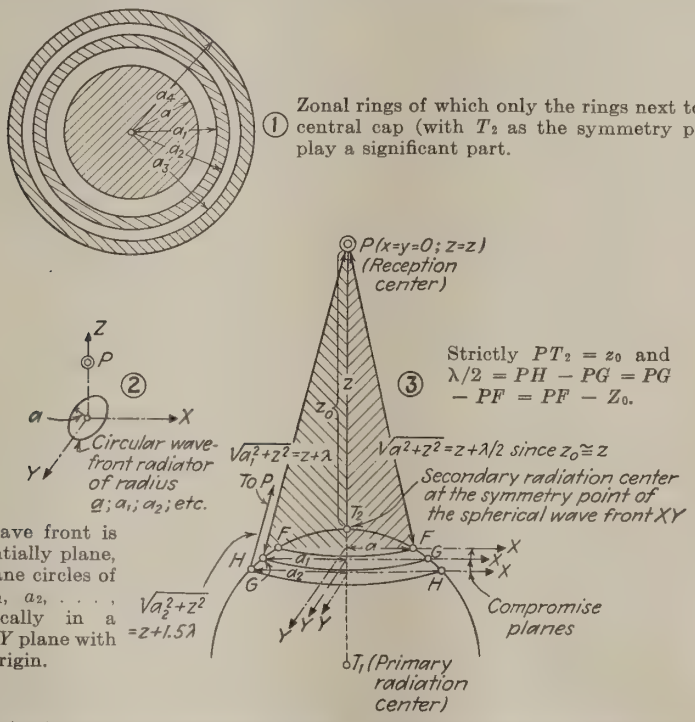

FIG. 369. Application of consecutive Fresnel zones which cause alternately antiphase effects.

$z = 0.5\lambda$ and is also equal to $z\lambda/(2z)$. This is the same as $a^2/(2z)$ for $q = 1$ in our relation $a = \sqrt{qz\lambda}$, for a maximum amplitude effect. The same relation also holds for the *outer* boundary of the *second* Fresnel zone, with a radius a_1 such that any point on the circumference $2\pi a_1$ meters from P is $\sqrt{a_1^2 + z^2} = z + 2 \times 0.5\lambda = z + \lambda$, because we must advance another antiphase condition, *i.e.*, another half wavelength. This, with respect to the reception center P on the Z axis, gives another full wavelength. Therefore, $\sqrt{a_1^2 + z^2} - z = \lambda$. We also have

$$\sqrt{a_2^2 + z^2} - z = 1.5\lambda$$

etc., for $z \cong z_0$. Hence, for PT_2 and T_1T_2 sufficiently large so that the

primary wave-front radiator coincides essentially with the actual XY plane passing through T_2 of the true primary wave front, we can assume that the wave-front radiator is plane and divided into concentric Fresnel rings as in Fig. 299. We found that for such a wave-front radiator, we have *practically only the first Fresnel zone* (in reality, the first spherical Fresnel cap). This means that the field at the reception center P along the Z axis is twice as large as the field for no such limitation of the primary wave front. This is the case because no out-of-phase radiation proceeds along the $+Z$ axis, *i.e.*, for all the wavelets, originating on the primary wave front of area πa^2 square meters. If, however, we use a quasi-plane-wave-front radiator whose radius is larger than the radius a, fixed by the first Fresnel zone boundary, we also have antiphase field contributions at P, *i.e.*, wavelet interference effects. By avoiding radiation from antiphase Fresnel zones, *i.e.*, from zones between radii $r = a$ to $r = a_1$, $r = a_2$ to $r = a_3$, etc., the shaded wavelet center rings of Fig. 369 should cause still *more beaming* effect toward the field point P. The successive field additions, however, become smaller and smaller, since the first, or central, Fresnel zone already causes the greatest gain effect at P. Therefore, by a *suitable radius* of the circular wave-front radiator and shielding off interfering wavelet contributions, a field gain is expected along the $+Z$ axis. A circular wave-front radiator may then be said to have a field concentration effect at suitable reception center locations along the $+Z$ axis for a radius a large compared with λ. Such locations are $z = a^2/\lambda$, even though the interference Fresnel zones with antiphase effects are not prevented from emitting wavelets. This happens because then $\sqrt{z^2 + a^2} - z = a^2/(2z)$ yields 0.5λ. Such an effect all along the $+Z$ axis was already found for the various Fraunhofer diffraction patterns, because the principal beam increases its magnitude along the $+Z$ axis for a radius a becoming larger in terms of the operating wavelength λ. This seems an *inherent feature of the circular wave-front radiator.* K. A. Norton and A. C. Omberg[1] have recently given expressions for the characteristics of *elliptical* ground-reflection Fresnel zones of plane earth surface.

225. Notes on Complementary Wave-front Radiators. If the shaded portions of Fig. 370*a* represent wave-front radiators, the shaded portions of Fig. 370*b* can be called the "complementary" wave-front radiators. The field amplitude $\mathcal{E}_1$ is then proportional to $\sqrt{C^2(s_1) + S^2(s_1)}$, where $C(s_1)$ and $S(s_1)$ denote the Fresnel integrals taken over the primary-wave-front area A_1 of Fig. 370*a*. For the primary-wave-front area A_2 of Fig. 370*b*, the field amplitude $\mathcal{E}_2$ is proportional to $\sqrt{C^2(s_2) + S^2(s_2)}$ if $C(s_2)$ and $S(s_2)$ hold for A_2. Therefore, if we have a single wave-front

[1] *Proc. IRE*, **35**, 24, January, 1947.

radiator of size *cdef* occupied by the boundary of respective rectangular slot arrays of Fig. 370, the Fraunhofer diffraction field amplitude $\mathcal{E}$ is proportional to $\sqrt{C^2(s_1) + S^2(s_1)} + \sqrt{C^2(s_2) + S^2(s_2)}$. When no diffraction screen is interposed between two lenses, this condition corresponds to the optical case where the first lens causes a plane wave front and the second lens focuses the light into a point, yielding a minute image of the source. This can be the case only when $C(s_1) = -C(s_2)$ and $S(s_1) = -S(s_2)$, which expresses the well-known *Babinet theorem* that the Fraunhofer diffraction patterns of complementary primary-wave-front radiators are not complementary but identical *except for a minute central region.* This region corresponds to a diffraction angle θ,

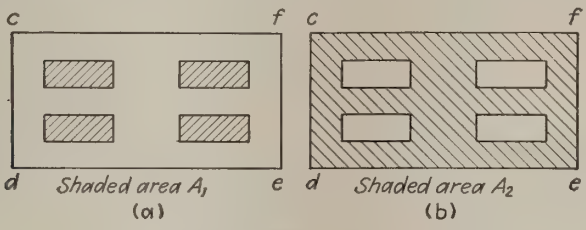

Fig. 370. Complementary wave-front radiators.

which is zero. For the *Fresnel* pattern, primary radiation and reception centers are no longer in effect at infinity from the wave front. The *central region* is then relatively large and *contains most* of the important *reception center locations.* The Fresnel diffraction pattern is then *different for complementary wave-front radiators.* This can be realized if we recall that we must add up the field effects according to their relative phase. Therefore, if, in Fig. 370*a*, we have a resultant vector $\mathfrak{E}_1$ and, in Fig. 370*b*, a resultant field vector $\mathfrak{E}_2$ at a certain reception center, then a wave front of size *cdef* will cause a field vector $\mathfrak{E} = \mathfrak{E}_1 + \mathfrak{E}_2$, which vector triangle can have any shape even if the closing vector $\mathfrak{E}$ has the same magnitude. Vector $\mathfrak{E}_1$ can then have many values and may even vanish, and similarly for vector $\mathfrak{E}_2$. If the wave-front array of Fig. 370*a* causes, at a certain reception center, $\mathfrak{E}_1 = 0$ while the wave-front frame *cdef* causes a value $\mathfrak{E}$, the complementary radiator of Fig. 370*b* must have a value $\mathfrak{E}_2 = \mathfrak{E} - \mathfrak{E}_1 = \mathfrak{E}$. But for the Fraunhofer pattern, we have the algebraic addition $\mathcal{E} = \mathcal{E}_1 + \mathcal{E}_2$ instead of the vector sum.

226. Rectangular and Circular Gate Radiators. The opening *cd* in the *XY* plane of Fig. 371 is assumed large enough to prevent wave-front distortion of a primary electromagnetic wave arriving from the radiation center T_1. In addition to this, the lower side of the *XY* plane must be a good absorber. The gate opening may be circular or rectangular. Figure 371*a* gives the approximations for $r = \sqrt{x_0^2 + y_0^2 + z^2}$ and

$r_0' = \sqrt{x_0^2 + y_0^2 + r_0^2}$, since the coordinates x_0, y_0 of a wavelet center T_2 are taken negligibly small compared with either r_0 or r and also $\lambda \ll$ than either r_0 or r. The area of the gate, which radiates in terms of secondary radiation centers T_2 as Huygens wavelets, is $A = ab$ square meters for a gate of a meters width along the X axis and b meters along the Y axis. For a circular gate of radius a meters, we have $A = \pi a^2$ square meters. Calling dA an elementary area at wavelet center T_2, each such area gives rise to an electric current moment $d(m) = -H_0\, dA$ meter · amperes,

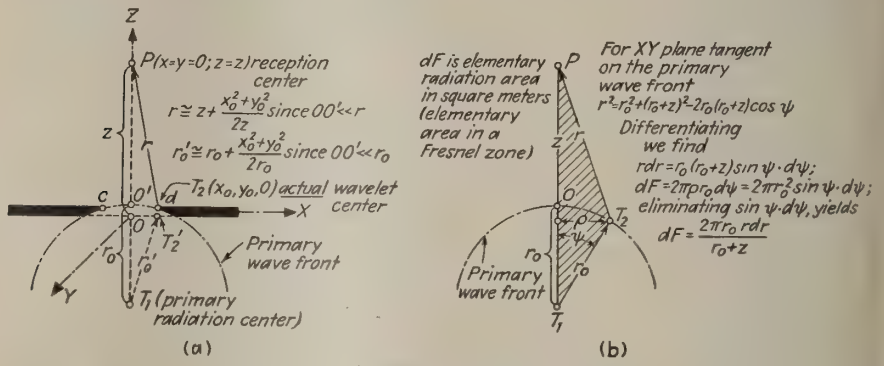

FIG. 371. Conditions for gate radiators.

and an associated magnetic moment $d(m_m) = -\mathcal{E}_0\, dA$ meter · volts. These moments are perpendicular to each other, as are the corresponding fields H_0 amperes per meter and $\mathcal{E}_0$ volts per meter. The field associations of a wavelet at any distance r are

$$d\mathcal{E} = \mathcal{E}_0 \epsilon^{-j\beta r} \cos\delta \quad \text{volts/m}; \qquad dH = H_0 \epsilon^{-j\beta r} \cos\delta \quad \text{amp/m}$$

where δ is the angle that the direction of r makes with the normal to the wavelet radiator dA. Hence, for a gate as in Fig. 371a, for which the spherical cap of the primary wave front with its pole O' slips, as it were, into the cd plane, we have, along the Z directions, the field associations $d\mathcal{E} = \mathcal{E}_0 \epsilon^{-j\beta z}$ and $dH = H_0 \epsilon^{-j\beta z}$. Suppose we have a linear current-carrying radiator with its mid-point at T_1. The radiator is parallel to the XY plane (parallel to the gate). At the gate, for the effective length l_e meters of the radiator and its moment $l_e I$ meter · amperes, we find

$$\left.\begin{aligned} \mathcal{E}_0^{(\text{volts/m})} &= -j\,\frac{0.5 Z_0 I l_e \epsilon^{-j\beta r_0}}{r_0 \lambda}\, \epsilon^{-j\beta(x_0^2+y_0^2)/(2r_0)} \\ Z_0 &= \sqrt{\frac{\mu}{\kappa}} \cong 376.7 \text{ ohms} \end{aligned}\right\} \qquad (910)$$

This relation is the outcome of

$$\epsilon^{-j\beta r_0'} = \epsilon^{-j\beta\sqrt{x_0^2+y_0^2+r_0^2}} \cong \epsilon^{-j\beta[r_0+(x_0^2+y_0^2)/(2r_0)]} = \epsilon^{-j\beta r_0}\epsilon^{-j\beta(x_0^2+y_0^2)/(2r_0)}$$

since, at the secondary radiation center T_2 of differential area dA, we have

$$\mathcal{E}_0 = -j\frac{0.5Z_0 I l_e \epsilon^{-j\beta r_0'}}{r_0\lambda} \qquad \text{volts/m}$$

where I is the loop current in amperes at T_1. We see that as far as the phase is concerned, we must use the actual distance $T_1T_2 = r_0'$ in terms of the wavelength; *i.e.*, we must use the phase factor exp $(-j\beta r_0')$. But as far as the inverse distance law of the field amplitude plays a part, we can use the average distance $T_1O' = r_0 = T_1O$, because $r_0 \gg cd$. The corresponding magnetic field is

$$H_0^{(\text{amp/m})} = -j\frac{0.5Il_e\epsilon^{-j\beta r_0}}{r_0\lambda}\epsilon^{-j\beta(x_0^2+y_0^2)/(2r_0)} \tag{910a}$$

According to Secs. 187, 188, 221 and Fig. 371*b*, we have, for the amplitude of a wave disturbance of a wavelet leaving the surface element dF of a Fresnel zone, a value $[(K\epsilon^{-j\beta r})/r]\,dF$, if the wavelet is a distance r from dF and K denotes a direction function, including other factors that are constant. If the amplitude of the primary excitation (due to the primary radiation) in the Fresnel zone element dF is $\epsilon^{-j\beta r_0}/r_0$, for each Fresnel zone element dF, we have, at the reception center, a wave disturbance contribution

$$dw = \frac{K\epsilon^{-j\beta r_0}}{r_0}\frac{\epsilon^{-j\beta r}}{r}\,dF$$

and a total effect due to an entire Fresnel zone of

$$w = \frac{\epsilon^{-j\beta r_0}}{r_0}\int\int K\frac{\epsilon^{-j\beta r}}{r}\,dF$$

According to the derivation for dF in Fig. 371*b*, we find, for the pth Fresnel zone,

$$w = \frac{2\pi K_p\epsilon^{-j\beta r_0}}{r_0+z}\int_{r=z+(p-1)\lambda/2}^{r=z+(p\lambda/2)}\epsilon^{-j\beta r}\,dr$$

$$= -j\frac{2\pi K_p\epsilon^{-j\beta(r_0+z)}\epsilon^{-j\beta(p\lambda/2)}}{\beta(r_0+z)}[1-\epsilon^{-j\beta(p\lambda/2)}]$$

where K_p now refers to the direction function of the pth zone. But

$$\epsilon^{-j\beta(p\lambda/2)}[1-\epsilon^{-j\beta(p\lambda/2)}] = \epsilon^{-j\beta(2\pi/\lambda)(p/2)\lambda}(1-\epsilon^{-j\pi p}) = 2(-1)^p$$

For the first Fresnel zone, we have $p = 1$, and

$$\epsilon^{-j\pi p} - \epsilon^{-j2\pi p} = \cos(\pi p) - j\sin(\pi p) - \cos(2\pi p) + j\sin(2\pi p)$$

$$= \cos\pi - j\sin\pi - \cos 2\pi + j\sin 2\pi = -2$$

For the second Fresnel zone, $p = 2$ gives

$$\cos(2\pi) - j\sin(2\pi) - \cos(4\pi) + j\sin(4\pi) = +1 + 0 + 1 + 0 = 2 = 2(-1)^2$$

In the electromagnetic case, we are not primarily interested in particular Fresnel zones for which $p = 1, 2, 3, \cdots$. But we are interested in the *total* area A of the gate surface. This surface is the seat of a mosaic of Huygens wavelet radiators. We have then the comparisons of Table 85. We obtain the resultant field at reception centers P along the $+Z$ axis for distances z very large compared with the largest dimension of the gate area A as

$$\mathcal{E}_p = j\int\int \frac{\mathcal{E}_0\epsilon^{-j\beta r}}{r\lambda}\,dA = \frac{0.5Z_0 l_e I\epsilon^{-j\beta r_0}}{r_0 z\lambda^2}\int\int \epsilon^{-j\beta(x_0^2+y_0^2)/(2r_0)}\epsilon^{-j\beta r}\,dA$$

since

$$r \cong z + \frac{x_0^2 + y_0^2}{2z}; \qquad \epsilon^{-j\beta r} = \epsilon^{-j\beta z}\epsilon^{-j\beta(x_0^2+y_0^2)/(2z)}$$

TABLE 85. GENERAL WAVE FUNCTION w COMPARED WITH THE WAVE FUNCTIONS FOR ELECTROMAGNETIC WAVES

General wave function w	→	Electromagnetic case
dF		dA
Areas of all significant Fresnel zones $(F_1 + F_2 + F_3 + F_4 + F_5 + \cdots)$		Total area $A = ab$ (rectangular) and πa^2 (circular gate), which may contain zonal areas
$\dfrac{K'\epsilon^{-j\beta r_0}}{r_0\lambda}$		$\mathcal{E}_0$ value of Eq. (910)
$\dfrac{\epsilon^{-j\beta r}}{r}\,dF$	corresponds to	$\dfrac{\epsilon^{-j\beta r}}{r}\,dA$
$\displaystyle\sum_{p=p_1}^{p=q} \frac{\epsilon^{-j\beta r_0}}{r_0\lambda}\int\int K'\frac{\epsilon^{-j\beta r}}{r}\,dF$ for q significant zones		$\displaystyle j\int\int \frac{\mathcal{E}_0\epsilon^{-j\beta r}}{r\lambda}\,dA$

For Fresnel zones, the field contribution w_p, due to the pth zone of area F_p, is w_p = constant $\times$ $(F_p/r_p)(1 + \cos\theta)$, if r_p is the mean distance $r_p = z + (p - \frac{1}{2})\lambda/2$ from this zone to the reception center P and θ is the angle with the Z axis under which the beam leaves the zone. Since the field amplitude contributions $w_1, w_2, w_3, w_4, \ldots$ at P have alternate polarity, *i.e.*, add as $w_1 - w_2 + w_3 - w_4 + \cdots$, there *cannot* be too many such terms that are numerically significant. For p zones, the resultant amplitude at P is $0.5(w_1 \pm w_p)$; the minus sign is for even p zones. Hence, for $p = \infty$, we have $w_p = 0$ and $0.5w_1$ as the result

where the factor $\exp(-j\beta z)$ can be taken before the double integral, since, for a particular reception center location P, the distance z is fixed. For a rectangular gate of a meters along the X axis and b meters along the Y axis, we have the integration limits $x_0 = \pm a/2$ and $y_0 = \pm b/2$. Since $dA = dx_0\, dy_0$, we find

$$\left.\begin{aligned}
K &= \frac{0.5 Z_0 l_e I \epsilon^{-j\beta(z+r_0)}}{r_0 z \lambda^2} \\
\mathcal{E}_P &= K \int\int \epsilon^{-j\beta(x_0^2+y_0^2)/(2r_0)} \epsilon^{-j\beta(x_0^2+y_0^2)/(2z)}\, dx_0\, dy_0 \\
&= K \int_{x_0=-a/2}^{x_0=a/2} \epsilon^{-j\beta\left(\frac{1}{2r_0}+\frac{1}{2z}\right)x_0^2} dx_0 \int_{y_0=-b/2}^{y_0=b/2} \epsilon^{-j\beta\left(\frac{1}{2r_0}+\frac{1}{2z}\right)y_0^2} dy_0 \\
\beta\left(\frac{1}{2r_0}+\frac{1}{2z}\right) &= \frac{\pi}{\lambda}\left(\frac{1}{r_0}+\frac{1}{z}\right) \\
\mathcal{E}_P^{(\text{volts/m})} &= K\left(\left\{\int_{-a/2}^{a/2} \cos\left[\frac{\pi}{\lambda}\left(\frac{1}{r_0}+\frac{1}{z}\right)x_0^2\right] dx_0 \right.\right. \\
&\quad - j\int_{-a/2}^{a/2} \sin\left[\frac{\pi}{\lambda}\left(\frac{1}{r_0}+\frac{1}{z}\right)x_0^2\right] dx_0 \Big\} \Big\{ \int_{-b/2}^{b/2} \cos\left[\frac{\pi}{\lambda}\left(\frac{1}{r_0}+\frac{1}{z}\right)y_0^2\right] dy_0 \\
&\quad \left. - j\int_{-b/2}^{b/2} \sin\left[\frac{\pi}{\lambda}\left(\frac{1}{r_0}+\frac{1}{z}\right)y_0^2\right] dy_0 \Big\}\right)
\end{aligned}\right\} \quad (910b)$$

Bringing these integrals into the Fresnel forms $\int \cos(0.5\pi s^2)\, ds$ and $\int \sin(0.5\pi s^2)\, ds$, with the trigonometric argument $0.5\pi s^2$, we have the identities

$$0.5\pi s_1^2 \equiv \frac{\pi}{\lambda}\left(\frac{1}{r_0}+\frac{1}{z}\right)x_0^2; \qquad 0.5\pi s_2^2 \equiv \frac{\pi}{\lambda}\left(\frac{1}{r_0}+\frac{1}{z}\right)x_0^2$$

giving, for $p = (1/r_0) + (1/z)$,

$$x_0 = s_1\sqrt{\frac{\lambda}{2p}}; \qquad dx_0 = ds_1\sqrt{\frac{\lambda}{2p}}; \qquad y_0 = s_2\sqrt{\frac{\lambda}{2p}}; \qquad dy_0 = ds_2\sqrt{\frac{\lambda}{2p}} \quad (910c)$$

We also have the relations

$$\left.\begin{aligned}
\int \cos\left(\frac{\pi}{\lambda} p x_0^2\right) dx_0 &= \int \cos\left(\frac{\pi}{\lambda} p s_1^2 \frac{\lambda}{2p}\right) ds_1 \sqrt{\frac{\lambda}{2p}} \\
&= \sqrt{\frac{\lambda}{2p}} \int \cos\left(\frac{\pi}{2} s_1^2\right) ds_1 = \sqrt{\frac{\lambda}{2p}}\, C(s_1) \\
\int \sin\left(\frac{\pi}{\lambda} p x_0^2\right) dx_0 &= \sqrt{\frac{\lambda}{2p}} \int \sin\left(\frac{\pi}{2} s_1^2\right) ds_1 = \sqrt{\frac{\lambda}{2p}}\, S(s_1) \\
\int \cos\left(\frac{\pi}{\lambda} p y_0^2\right) dy_0 &= \sqrt{\frac{\lambda}{2p}} \int \cos\left(\frac{\pi}{2} s_2^2\right) ds_2 = \sqrt{\frac{\lambda}{2p}}\, C(s_2) \\
\int \sin\left(\frac{\pi}{\lambda} p y_0^2\right) dy_0 &= \sqrt{\frac{\lambda}{2p}} \int \sin\left(\frac{\pi}{2} s_2^2\right) ds_2 = \sqrt{\frac{\lambda}{2p}}\, S(s_2)
\end{aligned}\right\} \quad (910d)$$

The integrations must be taken over the respective limits $x_0 = \pm \frac{1}{2}a$ and $y_0 = \pm \frac{1}{2}b$. From (910*c*), we find these limits, in terms of s_1 and s_2, as

$$s_1 = \pm \frac{a}{2}\sqrt{\frac{2p}{\lambda}} = \pm a\sqrt{\frac{p}{2\lambda}}; \qquad s_2 = \pm b\sqrt{\frac{p}{2\lambda}} \qquad \text{Fresnel limits} \qquad (910e)$$

The arguments s_1 and s_2 appear in sine as well as cosine Fresnel integrals. Hence, it does not matter whether we solve the $\int \sin(\frac{1}{2}\pi s^2)\,ds$ or the $\int \cos(\frac{1}{2}\pi s^2)\,ds$ integrals in order to find the value of s. Doing this for the cosine integral, we have, for the expressions of (910*d*) and (910*e*),

$$\int_{s=-a\sqrt{p/2\lambda}}^{s=+a\sqrt{p/2\lambda}} \cos(0.5\pi s^2)\,ds = 2\int_{s_1=0}^{s_1=a\sqrt{p/2\lambda}} \cos(0.5\pi s_1^2)\,ds_1$$

$$\int_{s=-b\sqrt{p/2\lambda}}^{s=+b\sqrt{p/2\lambda}} \cos(0.5\pi s^2)\,ds = 2\int_{s_2=0}^{s_2=b\sqrt{p/2\lambda}} \cos(0.5\pi s_2^2)\,ds_2$$

Since the $\cos(0.5\pi s^2)$ function is symmetrical, the integration can be taken from $s = 0$ to either limit if the integral is multiplied by 2. The Fresnel arguments lead to

$$s_1 = a\sqrt{\frac{p}{2\lambda}} = a\sqrt{\frac{1}{2\lambda}\left(\frac{1}{r_0}+\frac{1}{z}\right)}; \qquad s_2 = b\sqrt{\frac{1}{2\lambda}\left(\frac{1}{r_0}+\frac{1}{z}\right)} \qquad (910f)$$

The resultant field at reception center O along the $+Z$ axis, for a and b very small compared with the distance z, then becomes, according to (910*b*), (910*d*), (910*f*),

$$\mathcal{E}_P = 4K\frac{\lambda}{2p}[C(s_1) - jS(s_1)][C(s_2) - jS(s_2)] \quad \text{volts/m}$$

$$K\frac{\lambda}{2p} = \frac{\dfrac{Z_0}{2}l_e \pm \epsilon^{-j\beta(z+r_0)}}{r_0 z\lambda^2}\,\frac{\lambda}{2(z+r_0)/(r_0 z)} = \frac{(Z_0/4)l_e I\epsilon^{-j\beta(z+r_0)}}{\lambda(r_0+z)}$$

with a scalar value (magnitude) of

$$\left|4K\frac{\lambda}{2p}\right| = \frac{Z_0 l_e I}{\lambda(r_0+z)}$$

where I stands for the effective current in amperes and $Z_0 \cong 376.7$ ohms. The magnitude of the field at P is then

$$\left.\begin{aligned} &\mathcal{E}_P = \frac{Z_0 l_e I}{\lambda(r_0+z)}\sqrt{[C^2(s_1)+S^2(s_1)][C^2(s_2)+S^2(s_2)]} \quad \text{volts/m} \\ &s_1 = a\sqrt{\frac{1}{2\lambda}\left(\frac{1}{r_0}+\frac{1}{z}\right)}; \qquad s_2 = b\sqrt{\frac{1}{2\lambda}\left(\frac{1}{r_0}+\frac{1}{z}\right)} \end{aligned}\right\} \qquad (910g)$$

If the linear primary radiator at T_1 of the effective length l_e (Fig. 371) is parallel with the X axis at reception center P, we find

$$\mathcal{E}_x = \frac{Z_0 l_e I}{\lambda(r_0+z)}\sqrt{C^2\left[a\sqrt{\frac{1}{2\lambda}\left(\frac{1}{r_0}+\frac{1}{z}\right)}\right] + S^2\left[a\sqrt{\frac{1}{2\lambda}\left(\frac{1}{r_0}+\frac{1}{z}\right)}\right]} \quad \text{volts/m} \qquad (910h)$$

For a circular gate, the integration must be made over an opening determined according to Fig. 371*a* by a circle of radius a meters in the XY plane. The most general case occurs when the actual spherical wave front $cO'd$ is taken into account with the actual seat of wavelet centers rather than the plane surface cOd given by the area πa^2 in the XY plane. This will be considered now.

227. Circular Gate Radiator with a Spherical Wave Front. If, in Fig. 371*a*, the radius a in the XY plane is very small in comparison with either r_0 or z, then $O'O$ is essentially negligible. We can also use the approximations for r and r_0' and deal with the actual wave-front point T_2. At the circular gate, we then have again formulas (910) and (910*a*) for the $\mathcal{E}_0$ volts per meter and H_0 amperes per meter fields. Each elementary area dA of the actual spherical primary wave-front cap $cO'd$, with the chord $cd = 2a$ meters, causes, at any field point r, φ, θ (for θ against the Z axis), the field contribution

$$d\mathcal{E}_\theta = j\frac{\mathcal{E}_0\, dA}{2r\lambda}\,\epsilon^{-j\beta r}(1 + \cos\theta)\cos\varphi \qquad \text{volts/m} \tag{911}$$

with a similar field relation $d\mathcal{E}_\varphi$, except that $\sin\varphi$ appears in place of $\cos\varphi$ and the expression has a negative polarity. For reception centers P along the Z axis, we have $1 + \cos\theta = 2$. In the XZ plane, we have $\cos\varphi = 1$ and

$$d\mathcal{E}_x = j\frac{\mathcal{E}_0\, dA}{r\lambda}\,\epsilon^{-j\beta r} \qquad \text{volts/m}$$

The total field due to the entire spherical-wave-front area $cO'd$ then is

$$\mathcal{E}_x = \frac{j}{\lambda}\int\int_{cO'd}\frac{\mathcal{E}_0\epsilon^{-j\beta r}}{r}\,dA \qquad \text{volts/m} \tag{911a}$$

The elementary area is now conveniently taken as an infinitesimal narrow zonal ring around the primary spherical wave front, passing through the wavelet radiation center T_2 of Fig. 371*b*, which is in the XZ plane. We have a semichord of length ρ, which changes from $\rho = 0$ to $\rho = a$ meters in order to account for the entire exposed primary wave front with Huygens wavelet centers such as T_2. The integration is also to be extended for r values, since $PT_2 = r$ varies over the extreme values PO' to $PT_2 \cong \sqrt{z^2 + a^2}$, because $\rho = a$ is the maximum value that we can ever attain. The derivation of the elementary Fresnel area dF is given in Fig. 371 and is for the case of Fig. 371*a*. The location T_2 is given by $r = z + (p\lambda/2)$ for $p = 1, 2, 3, 4, \cdots$ and T_2 boundary points between adjacent zones. However, we are not concerned with Fresnel zones but with the actual area A of the *entire effective spherical primary*

wave cap cO'd. But as far as the elementary area dF in a particular Fresnel zone, say F_1, is concerned, it is exactly the same elementary area as dA, and we have

$$dA = \frac{2\pi r_0 r\, dr}{r_0 + z} \qquad \text{sq m}$$

If we are interested in only the actual wave-front area A, we find

$$A = \frac{2\pi r_0}{r_0 + z} \int_{r=z}^{r=\sqrt{z^2+a^2}} r\, dr = \frac{\pi r_0}{r_0 + z} [(z^2 + a^2) - z^2] = \frac{\pi r_0 a^2}{r_0 + z} \qquad \text{sq m}$$

Inserting in (911a) the value for $\mathcal{E}_0$ from (910) and using also the substitution $x_0^2 + y_0^2 = \rho^2$ for any wavelet center T_2, we find, for the inverse distance effect $1/r \cong 1/z$ taken as fixed,

$$\mathcal{E}_x = \frac{0.5 Z_0 I l_e \epsilon^{-j\beta r_0}}{\lambda r_0 z} \int\int \epsilon^{-j\beta\rho^2/(2r_0)} \epsilon^{-j\beta r}\, dA \qquad \text{volts/m}$$

$$k = \frac{0.5 Z_0 I l_e \epsilon^{-j\beta r_0}}{\lambda r_0 z} \qquad \text{since } \epsilon^{-j\beta r} = \epsilon^{-j\beta\left(z + \frac{\rho^2}{2z}\right)} = \underbrace{\epsilon^{-j\beta z}}_{\text{fixed}} \epsilon^{-j\beta\frac{\rho^2}{2z}}$$

$$dA = \frac{2\pi r_0 r\, dr}{r_0 + z}$$

$$r \cong \sqrt{z^2 + \rho^2} = z\sqrt{1 + \frac{\rho^2}{z^2}} \cong z\left(1 + \frac{1}{2}\frac{\rho^2}{z^2}\right) = z + \frac{\rho^2}{2z}$$

$$dr = \frac{\rho}{z}\, d\rho; \qquad dr = \frac{\rho}{z}\, d\rho$$

$$dA = \frac{2\pi r_0}{r_0 + z} \frac{(2z^2 + \rho^2)\rho}{2z^2}\, d\rho = \underbrace{\frac{\pi r_0}{(r_0 + z)z^2}}_{\text{fixed}} (2z^2 + \rho^2)\rho\, d\rho$$

Since z is very large compared with any value that ρ may assume, we have $2z^2 + \rho^2 \cong 2z^2$ and

$$\left.\begin{aligned} dA &\cong \frac{\pi r_0 2z^2}{(r_0 + z)z^2}\rho = \underbrace{\frac{2\pi r_0}{r_0 + z}}_{\text{fixed}} \rho\, d\rho \\ \mathcal{E}_x &= k \frac{2\pi r_0}{r_0 + z} \epsilon^{-j\beta z} \int \rho \epsilon^{-j\beta\rho^2/(2r_0)} \epsilon^{-j\beta\rho^2/(2z)}\, d\rho \\ &= \underbrace{\frac{\pi Z_0 I l_e \epsilon^{-j\beta(r_0+z)}}{z(r_0 + z)\lambda}}_{K} \int_{\rho=0}^{\rho=a} \rho \epsilon^{-j\beta\left(\frac{1}{2r_0} + \frac{1}{2z}\right)\rho^2}\, d\rho \qquad \text{volts/m} \end{aligned}\right\} \qquad (911b)$$

For

$$\beta\left(\frac{1}{2r_0} + \frac{1}{2z}\right) = \frac{\pi}{\lambda}\left(\frac{1}{r_0} + \frac{1}{z}\right) \equiv p \qquad (911c)$$

we find, for the field amplitude,

$$\mathcal{E}_x = K \int_{\rho=0}^{\rho=a} \rho \epsilon^{-jp\rho^2}\, d\rho \qquad \text{volts/m} \tag{911d}$$

This requires an integration by parts of the forms

$$\int_0^a u\, dv = \left|uv\right|_0^a - \int_0^a v\, du \qquad \text{or} \qquad \int_0^a u\, dv = \left|uv\right|_0^a - \int_0^a v \frac{du}{dv}\, dv \tag{911e}$$

Applying this to (911*d*) and realizing that

$$\epsilon^{-jp\rho^2} = \cos\,(p\rho^2) - j \sin\,(p\rho^2)$$

we find, in comparison with the argument $0.5\pi s^2$ of the Fresnel integrals,

$$p\rho^2 = 0.5\pi s^2; \qquad \rho = s\sqrt{\frac{0.5\pi}{p}}; \qquad d\rho = ds\sqrt{\frac{0.5\pi}{p}};$$

$$\int \cos\,(p\rho^2)\, d\rho = \int \cos\left(ps^2 \frac{0.5\pi}{p}\right) ds \sqrt{\frac{0.5\pi}{p}}$$

$$= \sqrt{\frac{0.5\pi}{p}} \int \cos\left(\frac{\pi}{2} s^2\right) ds = \sqrt{\frac{0.5\pi}{p}}\, C(s)$$

and

$$\int \epsilon^{-jp\rho^2}\, d\rho = \sqrt{\frac{0.5\pi}{p}}\, [C(s) - jS(s)] \tag{911f}$$

We find for $u = \rho$ and $du = d\rho$

$$\int \underbrace{\rho}_{u} \underbrace{\epsilon^{-jp\rho^2}\, d\rho}_{dv} = \int u\, dv; \qquad v = \sqrt{\frac{0.5\pi}{p}}\, [C(s) - jS(s)] = q$$

Applying these substitutions in Eq. (911*e*), we have

$$\int_0^a \rho \epsilon^{-jp\rho^2}\, d\rho = \left|q\rho\right|_0^a - \int_0^a q\, d\rho = qa - \int q\, d\rho$$

$$= \sqrt{\frac{0.5\pi}{p}} \left\{ C(s) - jS(s) - \int_0^a \left[\int \cos\left(\frac{\pi}{2} s^2\right) ds - j \int \sin\left(\frac{\pi}{2} s^2\right) ds \right] d\rho \right\} \tag{911g}$$

This outcome still leaves the Fresnel integrals under an integral, which could be evaluated by drawing the corresponding functions (graphical evaluation). Since, according to (911*c*), the quantity p is a *positive real* constant, we can integrate (911*d*) by putting $x = -jp\rho^2 = +p\rho^2/j$ so that $dx/d\rho = 2p\rho/j$, and

$$\mathcal{E}_x^{(\text{volts/m})} = j \frac{K}{2p} \int_0^{-jpa^2} \epsilon^x\, dx = \frac{jK}{2p} (\epsilon^{-jpa^2} - 1)$$

$$= j \frac{K}{2p} [\cos\,(pa^2) - 1 - j \sin\,(pa^2)] = \frac{K}{2p} [\sin\,(pa^2) - j(1 - \cos\,(pa^2)]$$

$$= \frac{K}{p} \sin\left(\frac{pa^2}{2}\right) \left[\cos\left(\frac{pa^2}{2}\right) - j \sin\left(\frac{pa^2}{2}\right) \right] = 0.5 \frac{K}{p} \epsilon^{-j(pa^2/2)} \sin\left(\frac{pa^2}{2}\right) \tag{911h}$$

for

$$p = \frac{\pi}{\lambda}\left(\frac{1}{r_0} + \frac{1}{z}\right); \qquad K = \frac{\pi Z_0 I l_e \epsilon^{-j\beta(r_0+z)}}{z(r_0+z)\lambda}; \qquad Z_0 \cong 376.7 \text{ ohms} \qquad (911i)$$

This result shows that we have patterns which are similar to the Fraunhofer patterns.

With respect to the theory of radiation of electromagnetic field energy through round and rectangular apertures as well as through a circular split in a conducting plane (acts as electromagnetic screen), reference is made to papers by J. A. Stratton and L. J. Chu, M. S. Neumann, and A. A. Pistolkors.[1] For a circular slot aperture in a large metal screen of inner radius ρ_1 and outer radius ρ_2, a voltage is impressed across the gap opening $\rho_2 - \rho_1$, so that the corresponding $\mathcal{E}$ lines of electric force which are along the radii exist only in the plane of the aperture. Due to the very high conductivity of the metal screen of large dimensions, any tangential $\mathcal{E}$ components can be only vanishingly small, while the magnetic H lines form concentric circles with the circular ring aperture. The theory can then be based on the classic Fresnel-Kirchhoff diffraction concept. We can then derive relations for the distant electromagnetic field and find the directivity patterns.

S. Seely[2] has recently also applied the diffraction theory to the case of a parabolic cylindrical antenna in order to obtain formulas for the calculation of the vertical directivity pattern and the gain. The results of the formulas are compared also with experimental results.

With respect to the slotted cylinder antenna, reference is made to the work of E. C. Jordan and W. E. Miller.[3]

J. C. Slater has treated in his book[4] arrays of dipoles and image dipoles in rectangular wave guides and discussed the *diffraction* field of a lattice of this kind. Electromagnetic horns[5] were discussed by several

[1] STRATTON, J. A., and L. J. CHU, Steady-state Solutions of the Electromagnetic Field Problems and Forced Oscillations of a Conducting Sphere, *Jour. Appl. Phys.*, **12,** 236–240, March, 1941. NEUMANN, M. S., Radiation of Electromagnetic Energy through Apertures, *Izvestija Elektropromyshlennosti Slabogo Toka*, **6,** 11 (1940). PISTOLKORS, A. A., Theory of the Circular Diffraction Antenna, *Proc. IRE*, **36,** 56–60 January, 1948. (Consult also Sec. 249 of "Short-wave Radiation Phenomena.")

[2] *Proc. IRE*, **35,** 1092–1095, October, 1947.

[3] *Electronics*, February, 1947.

[4] "Microwave Transmission," pp. 280–288, McGraw-Hill Book Company, Inc., 1942.

[5] SCHELKUNOFF, S. A., Some Equivalence Theorems of Electromagnetics and Their Application to Radiation Problems, *BSTJ*, **15,** 92–112 (January, 1936); On Diffraction and Radiation of Electromagnetic Waves, *Phys. Rev.*, **56,** 308–316 (Aug. 15, 1939); "Electromagnetic Waves," pp. 360–365, D. Van Nostrand Co., Inc., 1940; BARROW, W. L., and F. D. LEWIS, The Sectorial Electromagnetic Horn, *Proc. IRE*, **27,** 41–50 (1939); BARROW, W. L., and L. J. CHU, Theory of the Electromagnetic

authors. Such diffraction radiators have inherent features, since they are *independent* of resonance effects and operate, therefore, over a wide frequency range. Horns are used for causing an electromagnetic field energy stream to concentrate into sharp directivity patterns beyond the aperture of the horn. Rectangular and circular apertures are used. Conical horns seem to give the most simple diffraction radiators, and in the range of moderate antenna gains (in the neighborhood of 20 db) are quite compact in size. Inasmuch as the length of a conical horn increases *directly* with the power gain, the length of the horn may come out objectionably long for high field power gains. The directivities are similar to those obtained for rectangular and pyramidal horns. Generally, a conical horn forms a section of a right circular cone and is energized by a cylindrical wave guide, where the guide joins the horn. However, a rectangular wave guide which is gradually flared into a circular wave guide or into a horn can be used. For the dominant $TE_{1,0}$ excitation in a rectangular guide or the $TE_{1,1}$ excitation in a circular guide about the same directivity patterns are obtained. If a rectangular guide feeds a flared-out horn with a $TE_{0,1}$ wave, we have a rectangular aperture of $A = ab$ square meters for the mouth of the radiator in the XY plane with b meters in the Y direction and a meters in the X direction if the radiator points along the Z axis of the XYZ system. The flare angle holds then for planes parallel with the XZ plane where for mentioned excitation the dimension b is smaller than the dimension a. The shape of the rectangular aperture then fixes the radiation pattern; the elementary dipoles act over the aperture and are parallel with the vertical Y axis. The radiated field is then proportional to the forward factor $(1 + \cos\theta)$, as well as to $\mathcal{E}$ volts/m at the aperture, where the dipole is instrumental. The angle θ is the angle that the direction toward a particular field point makes with the Z axis. The Z axis is normal to the aperture and passes through the symmetry point of the ab area. If the horn points toward the Z direction (maximum effect), and is used as a field pickup, the ratio of the electromagnetic field energy picked up by the

---

Horn, *Proc. IRE*, **27**, 51–64 (1939); Barrow, W. L., and C. Shulman, Multiunit Electromagnetic Horns, *Proc. IRE*, **28**, 130–136 (1940); Southworth, G. C., and A. P. King, Metal Horns as Directive Receivers of Short Waves, *Proc. IRE*, **27**, 95 (1939); Bennett, H. S., Transmission-line Characteristics of the Sectoral Horn, *Proc. IRE*, **37**, 738 (July, 1949); Horton, C. W., On the Theory of the Radiation Patterns of Electromagnetic Horns of Moderate Flare Angles, *Proc. IRE*, **37**, 744, (July, 1949); King, A. P., The Radiation Characteristics of Conical Horn Antennas, *Proc. IRE*, **38**, 249, March 1950; "Ultra-high Frequency Techniques," edited by J. G. Brainerd, p. 481, D. Van Nostrand Co., Inc., 1942; Terman, F. E., "Radio Engineers' Handbook," pp. 824–837, McGraw-Hill Book Company, Inc., 1943.

rectangular aperture $A = ab$ square meters to the picked-up field energy of an elementary electric dipole is $8.4A/\lambda^2$, where A/λ^2 is the area in square wavelengths. This relationship becomes inaccurate when the smaller b dimension becomes comparable with $\lambda/4$ or shorter than $\lambda/4$, respectively. Schelkunoff has shown that for TE waves in guides and electromagnetic horns of moderate flare angles, we may assume a suitable distribution of surface *electric* currents J and of surface *magnetic* currents J_m which act in the aperture that radiates. Previously[1] we found $J = n \times H$ and $J_m = -n \times \mathcal{E}$, where n is normal to the aperture and H and $\mathcal{E}$ are the values of magnetic and electric fields at the aperture. We deal then with magnetic and electric current sheets in the aperture, and can find the electric as well as the magnetic field at a distant space point P from a magnetic vector potential Λ_m and an electric vector potential Λ_e, as is shown in the Appendix in Sec. 246. C. W. Horton[2] has given patterns in the $\mathcal{E}$ plane caused by the $TE_{0,1}$ excitation and in the H plane by the same excitation in a bisectoral horn. For a cylindric guide of diameter d, feeding a conical horn of diameter D at the aperture, we have an aperture diameter D/λ in terms of the operating wavelength. The horn starts then with a diameter d and flares to a diameter D. Extending the cone to its apex (this does not exist in reality), we find the axial length L with the mentioned extension. With the same extension l denotes the radial length. A. P. King[3] has shown that for optimum horns, we have the relations

$$\frac{l}{\lambda} - \frac{L}{\lambda} = 0.3 \qquad \text{and} \qquad \frac{L}{\lambda} \cong 0.3\left(\frac{D}{\lambda}\right)^2$$

A. P. King has also given a plot for D/λ against the absolute gain in decibels for different values of L. Gains up to about 30 db are then possible. With respect to the effective area A_e of conical horns, it is defined by $g\lambda^2/(4\pi)$ where g is the absolute power gain and λ denotes the free-space wavelength. If we deal with a radiator whose intensity distribution as well as polarization and phase is uniform over the aperture, we would have $A_e = A = \pi D^2/4$, which is the actual area in square meters if D is in meters. But this is not the case in many applications, and we use A_e/A as the relative numerical value. We have then

$$\frac{A_e}{A} = \frac{g}{\pi^2(D/\lambda)^2}$$

Values of A_e/A from 20 to about 85 per cent are then possibilities.

[1] Pages 143, 348–360, 367, 1030, 1092.
[2] *Op. cit.* on p. 1183.
[3] *Proc. IRE*, **38**, 249, March, 1950.

CHAPTER IX

WAVE GUIDES AND CAVITIES

Wave guides differ from customary transmission lines, such as a parallel-wire feeder and a concentric line feeder, respectively, since we have normally only *one* conductor within which we have a dielectric, usually of rectangular or of circular cross section. The energy is transferred either by TE waves or by means of TM waves in the dielectric, within metal tubes. Inasmuch as the dielectric is the medium in which field energy is being transferred, it is also possible that under certain conditions a wave may be guided in a dielectric tube that has *no* metal boundaries. Cavity resonators are sections of metal wave guides that are closed by metal at both ends. They form metal wave boxes, so that no field energy can escape into the space outside the box. As in the case of customary transmission lines, which are short-circuited at either end, cavity resonators exhibit an infinite number of resonance frequencies; and for each mode of transmission, there are resonance modes that correspond to an integral number of guide half wavelengths. Inasmuch as in a wave guide we have no return conductor, we have *at least one longitudinal field component along the guide* direction (Fig. 19). Thus for the TM waves, we have in addition to the transverse electric field also a longitudinal electric field, besides the completely transverse magnetic field. For TE waves, we have in addition to the transverse magnetic field also a longitudinal magnetic field along the guide direction, besides the completely transverse electric field. For this reason, the TM waves are often also called "longitudinal E" waves and the TE waves are often also called "longitudinal H" waves. So far in the text, we have already dealt with TE and TM waves, and it is, therefore, possible to treat the subject of wave guides briefly and with respect to essential features.

228. Possible Waves in Guides Due to Boundary Conditions. When dealing with metal guides, it is convenient first to assume metal walls of infinite conductivity. Even for finite conductivities, such as for copper walls, any small electric field components along the conducting inside surfaces of the guide will supply only the attenuation losses due to the finite conductivity. Therefore, even with actual guide materials such as copper walls, only electric field components entering or leaving the metal walls perpendicularly, can play a part in the field energy transfer along the guide. Table 10 compares the theories of TE and TM

waves in guides along the Z direction. Formulas are given in this table for guides with a rectangular cross section (a meters along the X direction and b meters along the Y direction) as well as for a guide with a circular cross section with a radius of a meters. For the circular cross section, we have a cylindric guide and, therefore, must use cylinder coordinates r, φ, z, as shown in steps 20 to 25 of Table 10. We deal then with *Bessel*

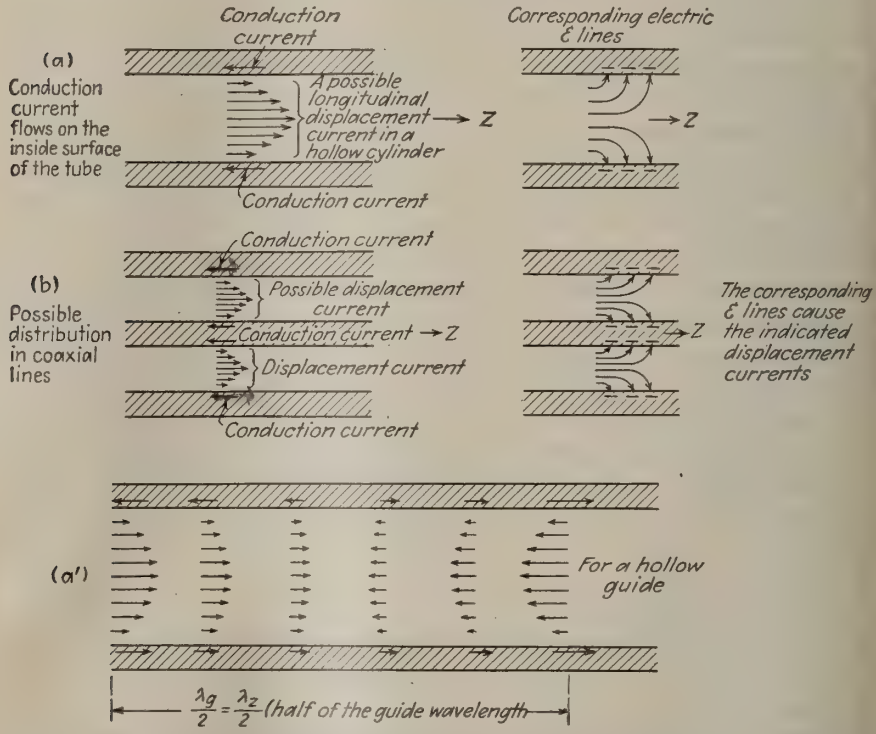
Conduction current
Corresponding electric E lines
(a)
Conduction current flows on the inside surface of the tube
A possible longitudinal displacement current in a hollow cylinder
Z
Conduction current
(b)
Possible distribution in coaxial lines
Possible displacement current
Displacement current
The corresponding E lines cause the indicated displacement currents
(a')
For a hollow guide
λg/2 = λz/2 (half of the guide wavelength)

FIG. 372. Possible displacement currents and corresponding electric $\mathcal{E}$ lines for a TM wave in a hollow guide and in a coaxial line.

distributions instead of *sinusoidal* distributions in order to meet the boundary conditions. Formulas (405) and (406) give the expressions for the wavelength along the guide ($\lambda_z = \lambda_g$) in terms of the unobstructed space wavelength λ of the dielectric medium within the guide. For air as the medium, we have $\lambda = 300/f$ meters, where f is in megacycles per second. Table 10 also gives expressions for the respective cutoff wavelengths λ_c in meters, above which, *i.e.*, $\lambda \geqq \lambda_c$ meters, the guide acts as an attenuator and no useful guide action is possible. For a frequency $f \leqq f_c$, where f_c is the corresponding cutoff frequency, we likewise no longer have wave-guide action. It is now of interest to find out what is meant by the different modes of TE and TM waves in guides with such cross sections. Figure 372 indicates possible longitudinal displacement

current distributions for a hollow metal cylinder and in the space between coaxial cylinders. We note that the longitudinal displacement current value must fall off toward zero value as it approaches a metal surface, since the tangential $\mathcal{E}$ component along such a surface must

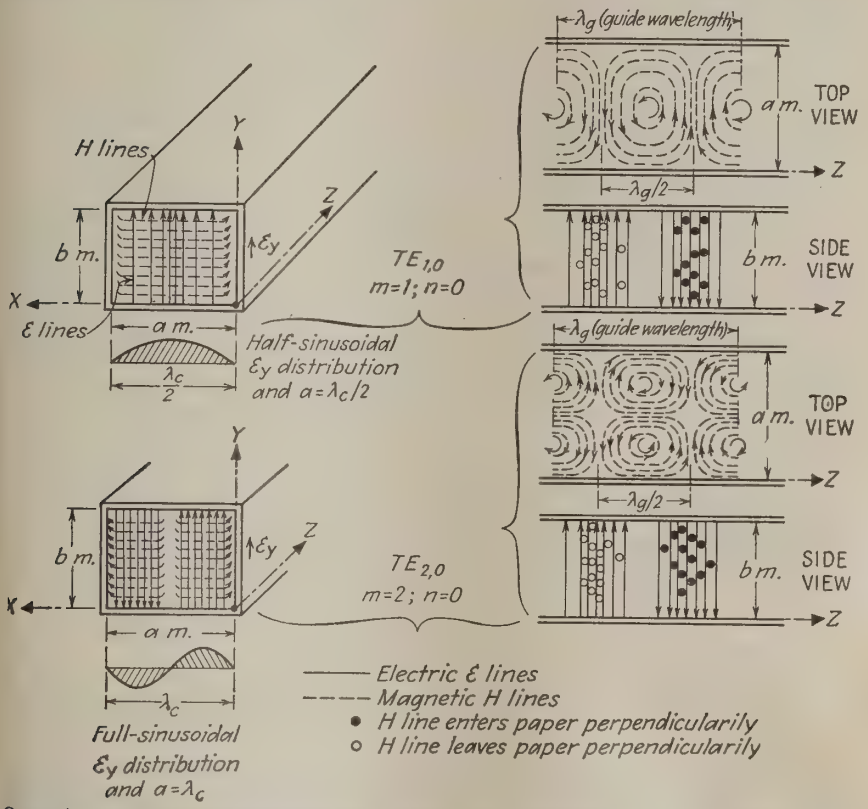

Operating wavelength must be shorter than the cutoff wavelength λ_c; $\mathcal{E} = \mathcal{E}_y$ entirely along Y direction and transverse to wave motion (hence TE wave); H is partially transverse (along X direction) and partially longitudinal (along Z direction) within the guide. $\lambda_c f_c = 1/\sqrt{\mu\kappa}$ m/sec where μ henrys/m and κ farads/m are the constants of the wave medium within the guide. For air $\lambda_c f_c = 300$ if f_c is in Mc/sec and λ_c in meters.

FIG. 373. Field configurations of fundamental $TE_{m,n}$ waves in a rectangular wave guide.

vanish for $\sigma = \infty$ mhos per meter. The corresponding electric $\mathcal{E}$ lines then show a longitudinal as well as a transverse component if they are not too close to the metal boundaries. At the metal boundaries, we can have only an $\mathcal{E}$ field normal to the boundary for an infinite metal conductivity. The displacement current distribution acts, in effect, as the *return* for TM wave excitations. Figure 373 shows two possible field configurations within rectangular guides for $TE_{m,n}$ excitations. The subscript m is the number of *half*-period variations of the field along the

X direction, which represents here (as usually) the larger dimension of a meters, and the subscript n is the number of half-period field variations along the Y direction. Since only the $\mathcal{E}$ field in Fig. 373 is entirely along the Y direction, *i.e.*, along the shortest dimension of b meters, we have $\mathcal{E} = \mathcal{E}_y$ volts per meter. For a rectangular cross section of ab square meters, we deal with Cartesian coordinates. The boundary conditions then require an electric field $\mathcal{E}_y$ distribution along the a dimension, which may be perpendicular to the top and bottom surfaces of the rectangular guide, but can have *no* tangential field along the perfectly conducting side faces of the guide. The simplest harmonic $\mathcal{E}_y$ distribution is then the half sinusoid, known as the $TE_{1,0}$ mode, because $n = 0$ for $\mathcal{E}_x = 0$. For this distribution, we have *no* tangential $\mathcal{E}$ field along any of the guide metal faces and deal with the dominant wave excitation of the guide. The next higher mode of $TE_{m,0}$ waves is the $TE_{2,0}$ wave for which we have a *full*-period $\mathcal{E}_y$ variation along the a dimension. We found in Table 10, that the cutoff wavelength λ_c in meters and the cutoff frequency $f_c = 300/\lambda_c$ in megacycles per second, if air is used within the guide ($v' = 1/\sqrt{\mu\kappa} \cong 1/\sqrt{\mu_0\kappa_0} = c = 3 \times 10^8$ m/sec), are found from

$$\left.\begin{aligned}
&\lambda_c = \frac{2}{\sqrt{(m/a)^2 + (n/b)^2}} \quad \text{and} \quad f_c = \frac{300}{\lambda_c} \text{ Mc/sec} \quad \text{for } TE_{m,n} \text{ waves} \\
&\text{where } m = 1, 2, 3, \cdots; \; n = 1, 2, 3, \cdots; \text{ and } a \text{ and } b \text{ are in meters.} \\
&\lambda_c = \frac{2a}{m} \text{ and } f_c = \frac{300}{\lambda_c} = \frac{150m}{a} \text{ Mc/sec} \quad \text{for } TE_{m,0} \text{ waves } (\mathcal{E} = \mathcal{E}_y,\ H_x,\ H_z) \\
&\lambda_c = \frac{2b}{n} \quad \text{and} \quad f_c = \frac{150n}{b} \text{ Mc/sec} \quad \text{for } TE_{0,n} \text{ waves } (\mathcal{E} = \mathcal{E}_x,\ H_y,\ H_z) \\
&\lambda_c = \frac{2a}{m} = \frac{2a}{1} = 2a \text{ and } f_c = \frac{150}{a} \text{ Mc/sec} \quad \text{for } TE_{1,0} \text{ waves (half-period variation along } X \text{ direction)} \\
&\lambda_c = \frac{2a}{2} = a \text{ and } f_c = \frac{150 \times 2}{a} = \frac{300}{a} \text{ Mc/sec} \quad \text{for } TE_{2,0} \text{ waves (full-period variation along } X \text{ direction)} \\
&\lambda_c = \frac{2a}{3} = \frac{a}{1.5} \text{ and } f_c = \frac{150 \times 3}{a} = \frac{450}{a} \text{ Mc/sec} \quad \text{for } TE_{3,0} \text{ waves (one and one and one-half period variation along } X \text{ direction)} \\
&\lambda_c = \frac{2b}{1} = 2b \text{ and } f_c = \frac{150}{b} \text{ Mc/sec} \quad \text{for } TE_{0,1} \text{ waves (half-period variation along } Y \text{ direction for } \mathcal{E}_x) \\
&\lambda_c = \frac{2b}{2} = b \text{ and } f_c = \frac{300}{b} \text{ Mc/sec} \quad \text{for } TE_{0,2} \text{ waves (full-period variation along } Y \text{ direction)} \\
&\lambda_c = \frac{2b}{3} = \frac{b}{1.5} \text{ and } f_c = \frac{450}{b} \text{ Mc/sec} \quad \text{for } TE_{0,3} \text{ waves (one and one-half period } \mathcal{E}_x \text{ variation along } Y \text{ direction)}
\end{aligned}\right\} \quad (912)$$

From these results, we note that for frequencies higher than $150/a$ megacycles per second, we have, for the rectangular guide of Fig. 373, a possibility of guide action for all $TE_{m,0}$ waves, *i.e.*, for $TE_{1,0}$, $TE_{2,0}$, $TE_{3,0}$, . . . waves, if only $\mathcal{E}_y$ electric polarizations prevail within the guide. Figure 374 shows how we can, for instance, excite $TE_{1,0}$, $TE_{2,0}$, $TE_{3,0}$, and $TE_{4,0}$ waves with $\mathcal{E} = \mathcal{E}_y$ fields and H_x and H_z fields. Figure 375 gives the comparisons between the field configurations for $TE_{1,0}$

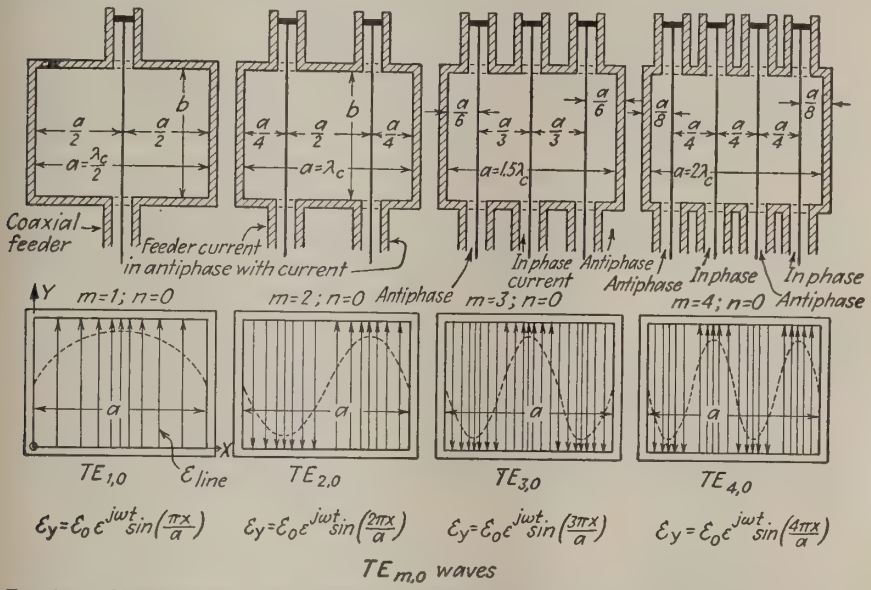

FIG. 374. Excitations of $TE_{m,0}$ waves by means of coaxial feeders with their central wires exposed within the guide along maximum $\mathcal{E}$ lines.

and $TE_{1,1}$ excitations in rectangular guides and the $TE_{1,1}$ excitation in a cylindrical guide. For the $TE_{1,1}$ excitation of the rectangular wave guide, we have transverse H_x and H_y magnetic field components in addition to the longitudinal H_z magnetic field component. We have also the transverse $\mathcal{E}_x$ and $\mathcal{E}_y$ components. This would be expected, since the TE wave is of the general $TE_{m,n}$ form, with a cutoff wavelength λ_c and the corresponding frequency f_c, which depend upon the a as well as the b dimension of the guide.

Figure 376 gives the electric $\mathcal{E}$ lines in the rectangular and circular wave-guide cross sections for some of the TE modes as well as the H lines for some of the lower TM modes. Figure 377 gives the electric as well as the magnetic field configurations in the cross section as well as along the guide for circular cross sections of a meters radius. Table 10 shows how to compute the cutoff frequency f_c, below which no useful guide

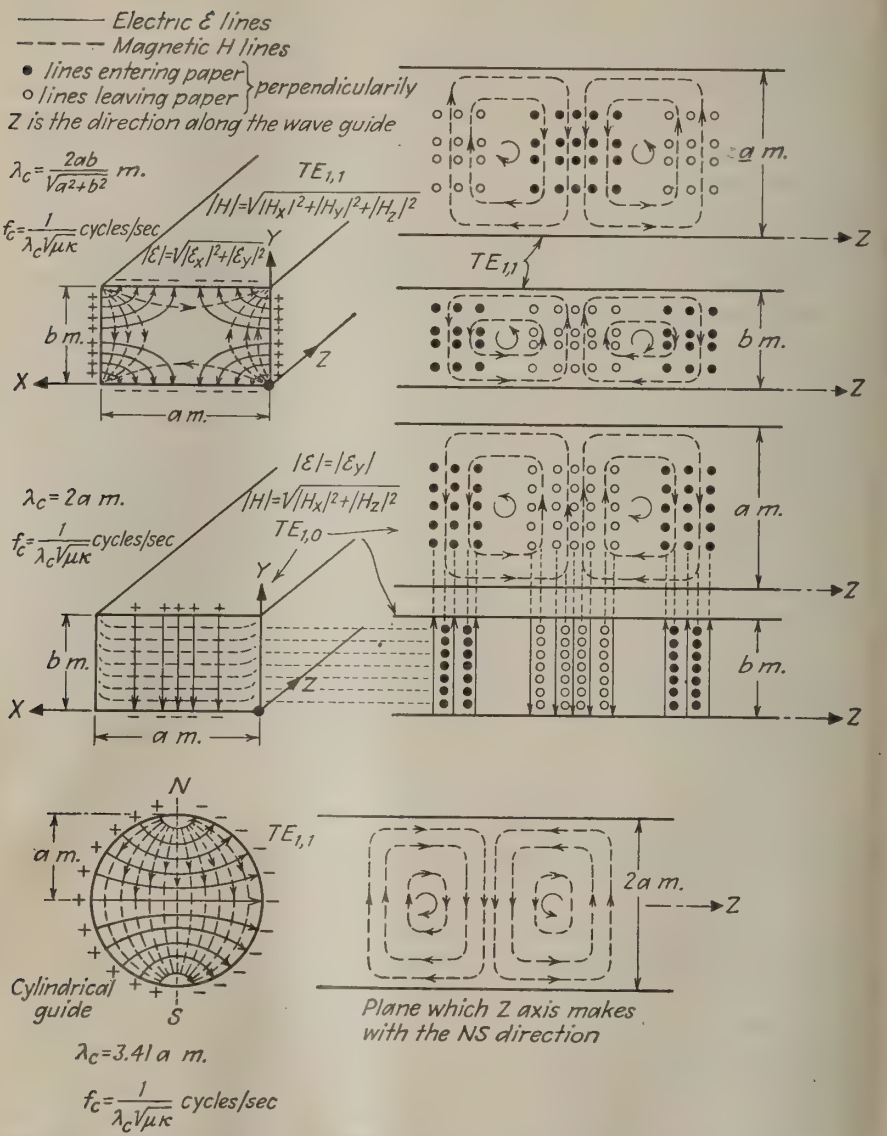

FIG. 375. Electric ℰ and magnetic H lines of typical rectangular and circular guides. μ henrys/m and κ farads/m are the constants of the medium within the guide ($\sigma = 0$).

action is possible. We may have then, for instance, $TE_{n,m}$ waves in a circular guide as well as $TM_{n,m}$ waves. If $n = 0$ in the $TE_{n,m}$ mode, we have the $TE_{0,m}$ *circular* wave, where m is the number of cylinders (including the metal boundary $r = a$ meters of the guide) from which the ℰ field vanishes. Therefore, the $TE_{0,1}$ mode must have the lowest cutoff

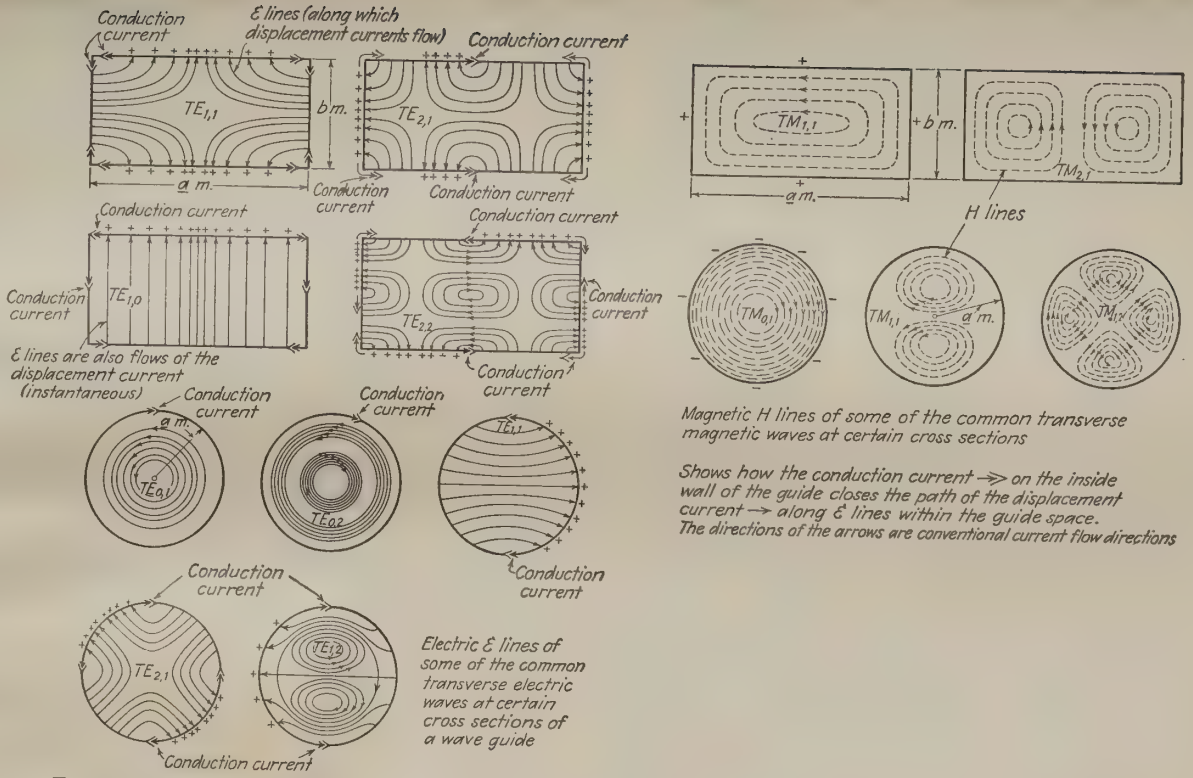

FIG. 376. E lines and *H* lines for some customary TE and TM modes in rectangular and circular wave guides.

frequency. For the guide along the Z direction (as in Tables 10 and 86), we have the cylinder coordinates r, φ, and z, where r is any radial distance from $r = 0$ to $r = a$ meters, where a is the inside radius of the circular guide. In the $TE_{n,m}$ waves, we deal with *non*circular waves if $n \neq 0$; and according to the definitions of the IRE on guided waves, n is the

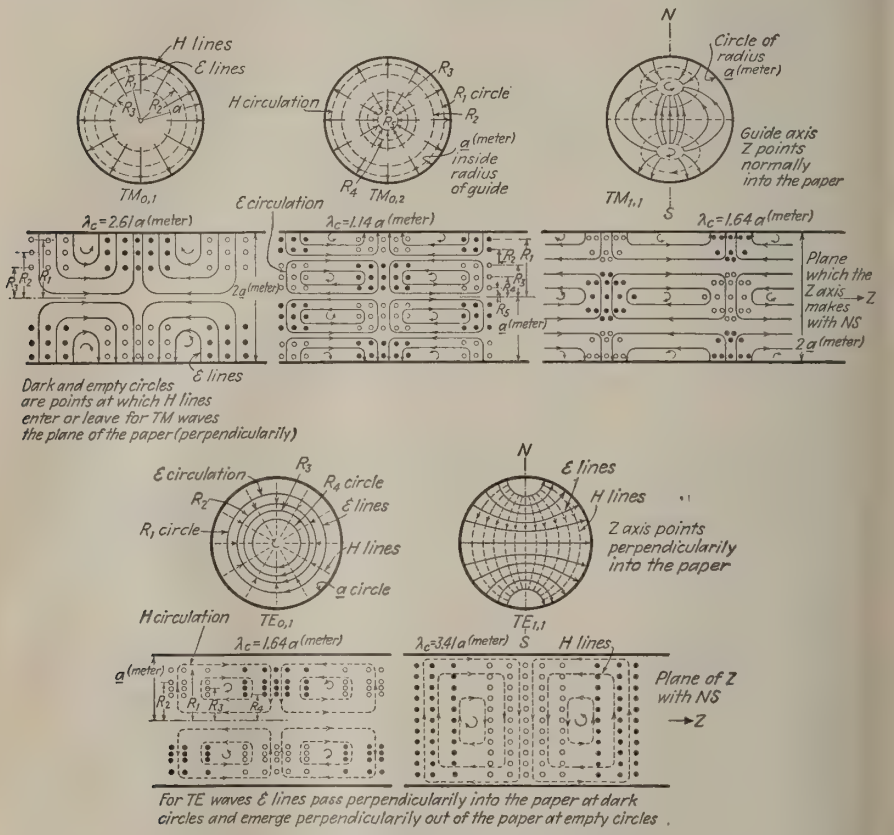

FIG. 377. Typical $\mathcal{E}$ and H circulations in cylindrical wave guides.

number of axial planes and m is the number of cylinders (including the metal boundary of radius $r = a$ meters) to which the $\mathcal{E}$ vector is normal. The $TE_{1,1}$ mode is then the dominating wave, with the $\mathcal{E}$ lines approximately parallel with the diameter. The $TM_{o,m}$ is likewise a circular wave, but a circular magnetic wave, where m is the number of cylinders (including the guide metal cylindrical inside surface) to which the electric vector is normal. The $TM_{0,1}$ circular magnetic wave has the lowest cutoff frequency. For $n \neq 0$, we have *non*circular magnetic waves, with n as the number of axial planes to which the $\mathcal{E}$ vector is normal, and m

is the number of cylinders (including the metal boundary) to which the $\mathcal{E}$ vector is normal. Since for a rectangular guide the cutoff wavelength $\lambda_c = 2a$ meters, the $TE_{1,0}$ mode requires that $a > \lambda_c/2$ meters, where, for air as the guide dielectric, $\lambda_c = 300/f_c^{(Mc)}$. For the $TE_{0,1}$ mode, we have the requirement that $b > \lambda_c/2$ or the operating wavelength $\lambda < 2b$ meters. We have similar relations for all the other modes, since wave

TABLE 86. CUTOFF CHARACTERISTICS AND FIELDS IN CIRCULAR GUIDES FOR TM AND TE WAVES

Wave type	Fields	$k_{n,m}$	$K_{n,m}$	Cutoff wavelength, m $\lambda_c = \frac{6.28}{K_{n,m}}$	Cutoff frequency, Mc/sec $f_c = \frac{300}{\lambda_c}$
$TM_{0,1}$	$\mathcal{E}_z$, $\mathcal{E}_r$, H_φ	2.405	$\frac{2.405}{a}$	$2.61a$	$\frac{115}{a}$
$TM_{0,2}$	$\mathcal{E}_z$, $\mathcal{E}_r$, H_φ	5.52	$\frac{5.52}{a}$	$1.135a$	$\frac{264}{a}$
$TM_{0,3}$	$\mathcal{E}_z$, $\mathcal{E}_r$, H_φ	8.65	$\frac{8.65}{a}$	$0.725a$	$\frac{414}{a}$
$TM_{1,1}$	$\mathcal{E}_z$, $\mathcal{E}_r$, $\mathcal{E}_\varphi$, H_r, H_φ	3.832	$\frac{3.832}{a}$	$1.64a$	$\frac{183}{a}$
$TE_{0,1}$	H_z, H_r, $\mathcal{E}_\varphi$	3.832	$\frac{3.832}{a}$	$1.64a$	$\frac{183}{a}$
$TE_{1,1}$	H_z, H_r, H_φ, $\mathcal{E}_r$, $\mathcal{E}_\varphi$	1.84	$\frac{1.84}{a}$	$3.41a$	$\frac{88}{a}$

Remarks (for air as dielectric): Radius a is in meters. The $k_{n,m}$ values are taken from step 25 of Table 10. In Table 86 no distinction is made between $k_{n,m}$ and $k_{n,m}'$, since the results of step 25 are used. $f_c = \frac{c'}{\lambda_c} = \frac{1}{\sqrt{\mu\kappa}\,\lambda_c} \cong \frac{3 \times 10^8}{\lambda_c}$ cycles/sec for air.

guides are *high-pass* feeders, and for frequencies below the cutoff value f_c, the guide acts as an *attenuator*.

229. Notes on Surface Conduction Currents and Displacement Current of Guides. When electric $\mathcal{E}$ lines of force terminate on the inner metal surfaces enclosing the guide space, as in Fig. 375, they cause surface charges of opposite polarity as at the surface element from which they emerge. We have then displacement currents along the lines of electric force. There must also be surface currents, which bring about an equalization of the above-mentioned surface charges. Figure 378 gives the details of displacement currents J_d and conduction currents J, both in amperes per meter, if taken in thin layers of the inside dielectric of the

guide and along the inside metal surfaces, respectively. The rectangular guide is excited in the dominant $TE_{1,0}$ mode. These current density dimensions are based on the fact that at UHF's, the currents in a volume

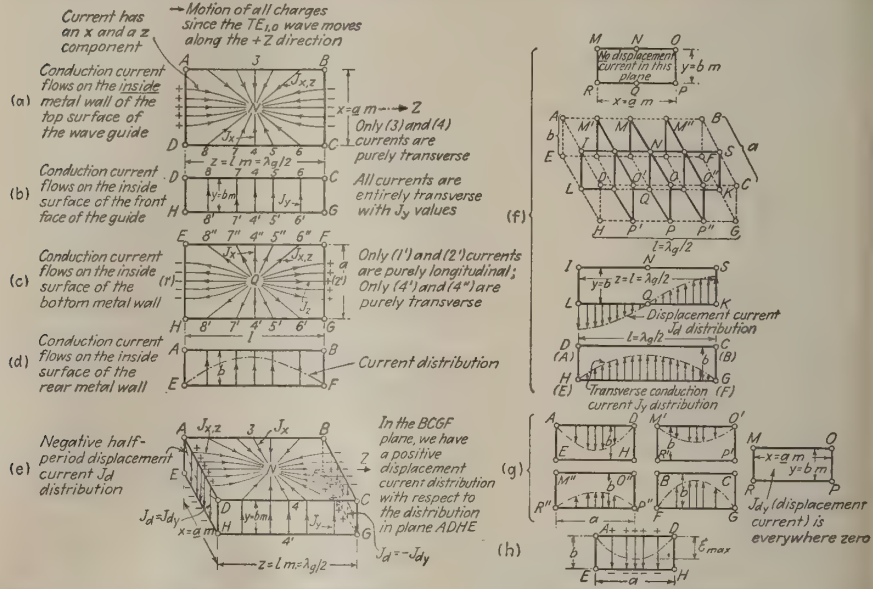
Current has an x and a z component
Motion of all charges since the TE1,0 wave moves along the +Z direction
(a) Conduction current flows on the inside metal wall of the top surface of the wave guide
Only (3) and (4) currents are purely transverse
(b) Conduction current flows on the inside surface of the front face of the guide
All currents are entirely transverse with Jy values
(c) Conduction current flows on the inside surface of the bottom metal wall
Only (1') and (2') currents are purely longitudinal; Only (4') and (4") are purely transverse
(d) Conduction current flows on the inside surface of the rear metal wall
Current distribution
(e) Negative half-period displacement current Jd distribution
In the BCGF plane, we have a positive displacement current distribution with respect to the distribution in plane ADHE
(f)
No displacement current in this plane
Displacement current Jd distribution
Transverse conduction current Jy distribution
(g)
Jdy (displacement current) is everywhere zero
(h)

FIG. 378. Conduction and displacement current flows for a $TE_{1,0}$ excitation in a rectangular wave guide.

of metal flow only in a very thin surface layer on surfaces of the metal *next to the field* that causes the currents.

We must realize that in wave guides, we normally do not apply an HF voltage (though this could be done) between suitable points on the inside of the guide. We apply a field inside a guide by means of a linear radiator or a small current loop which projects properly into the guide space in order to excite a particular mode (for instance, as in Fig. 374, where the inside conductor of a concentric line acts as a linear radiator, which fits in with the electric field distribution, while for a small single loop the orientation of the loop fits in with the desired magnetic field orientation of a particular mode). Therefore, with the customary excitation of guide waves, we start with field sources within the guide, and any surface conduction currents can be only on the *inner* metal skin of the guide (except at the open end of a guide, where, if proper precautions are not taken, a surface current may *creep around* toward a thin outside surface layer). For customary parallel-wire lines, we impress a voltage across the input terminals of the double line, and *start* with a current that, by virtue of its effects, causes fields within the wires and around the wires. For short waves and good conductors, such as copper wires, the inside field exists essentially only next to the conductor surface, and we have a current flow only along a thin outside *surface* skin of the wires. If we apply a voltage to a concentric line, the external field, which is associated with the current flow, is then essentially only between

the outside surface skin of the inner conductor and the inside surface skin of the outer conductor at VHF's and UHF's. However, if we deal with LF currents, the thickness of the outside conductor may not be great enough to accommodate the inside surface skin along which a current flows, and the concentric line may be "hot" outside, *i.e.*, cause alternating fields outside the concentric line, even if the line is infinitely long or closed at either end. This outcome that the current flows only at VHF's and UHF's along *very* thin surface skins of a conductor, *next* to the fields that cause the currents, can also be explained by the expressions and evaluations of pages 3, 10, 43, 45–52, 1197, where it is shown that electromagnetic fields arriving at the surface of conductors are partially reflected from it and partially transmitted to a very small depth because, on account of the high conductivity of good conductors at high frequencies and especially at UHF's, the attenuation of the penetrating waves is exceedingly high.

Figure 378*e* shows a section of a rectangular wave guide for which the dominant $TE_{1,0}$ wave travels along the $+Z$ direction. For such a mode, we have the electric field entirely transverse to the direction of wave propagation, as well as entirely along the Y directions. This means that the excitation in the rectangular cross section is as in Fig. 378*h*, with a half-period $\mathcal{E}_y$ distribution along the a dimension. This causes then, for the chosen direction of transverse $\mathcal{E}_y$ lines, positive charges along the inside line AD, falling off according to a sinusoidal law toward A and B, since we cannot have a tangential $\mathcal{E}_y$ field along AE or along DH. In Fig. 378*a*, *b*, *c*, *d*, and *e*, we deal with a guide length $z = l$ meters, which is chosen equal to half of the wavelength λ_g along the Z direction. This means that if the left $ADHEA$ plane (cross section) in Fig. 378*e* has an $\mathcal{E}_y$ distribution, as in Fig. 378*h*, the right cross section $BCGFB$ must have an *equal antiphase* $\mathcal{E}_y$ distribution. It also means that somewhere between these end planes, namely, in cross section $MNOPQRM$ (Fig. 378*f*), we must have *no* $\mathcal{E}_y$ fields *at all*. On account of the antiphase $\mathcal{E}_y$ distributions at respective end cross sections, we have positive charges along AD in Fig. 378*e* but negative charges along EH on the inside metal surface, with no such charges at A, D, E, and H, due to the sinusoidal half-period distribution. We know that along electric $\mathcal{E}$ lines in dielectrics, we have displacement currents with a density in amperes per square meter. Therefore, when the $\mathcal{E}$ lines of equal intensity arrive normally to a metal surface of 1 sq m, they will cause a charge of $\kappa_0\mathcal{E}$ coulombs per square meter at the metal surface (for details read page 65). In wave guides, we do not have $\mathcal{E}$ lines with a uniform distribution but have, as in Fig. 378*h*, a half-sinusoidal $\mathcal{E}_y$ distribution of a maximum strength $\mathcal{E}_{max}$. Therefore, in Fig. 378*e*, we have, in the same $ADHEA$ cross-sectional plane, corresponding linear displacement currents J_{d_y}, which are likewise distributed along a half sinusoid. The corresponding *positive* charges along the AD edge and

negative charges along the *EH* metal edge are then strongest at the midpoint of edges *AD* and *EH* and fall off cosinoidally toward *A* and *D* and *E* and *H*, toward zero value. In the same way, we have, in Fig. 378 at the end cross section *BCGFB*, charge distributions along the metal edges *BC* and *FG*, but with opposite polarities. These charges then cause the indicated quasi-surface conduction currents $J_{x,z}$ in amperes per meter along the upper and lower metal *inside* surfaces *ADCB* and *EHGF* of Fig. 378. Only a few of these surface currents are shown and marked with subscript *x*, *z*, since they are generally in such a direction that there is a longitudinal J_z and a transverse J_x component of $J_{x,z}$. There are also completely transverse J_y conduction surface currents on the *inside* guide metal *front* and *rear* faces. This can be readily understood by examining representations *a*, *b*, *c*, and *d* in Fig. 378. It is understood as the $TE_{1,0}$ moves along the $+Z$ guide direction with the phase velocity

$$c' = \frac{\omega}{\beta_z} = \frac{3 \times 10^8}{\sqrt{1 - (\lambda/2a)^2}} \quad \text{m/sec}; \qquad \lambda^{(m)} = \frac{300}{f^{(Mc/sec)}} \tag{912a}$$

where *a* is in meters for air as inside dielectric, causing the wavelength $\lambda_g = \lambda_z$ meters along the guide as

$$\lambda_g{}^{(m)} = \frac{\lambda}{\sqrt{1 - (0.5\lambda/a)^2}} \qquad \text{for } \lambda < \lambda_c < 2a \text{ m} \tag{912b}$$

Therefore, all indicated conditions in Fig. 378 move to the right with the above-mentioned phase velocity. We note that at *N* in Fig. 378*a* and *e* and at *Q* in Fig. 378*c*, we have a "bucking" conduction current interference. From Fig. 378*f* and *g*, we learn that we have a longitudinal half sinusoid for the transverse conduction current J_y in the *front* and *rear* face planes and a distribution as indicated for the transverse displacement current J_{d_y} in the central *ISKLI* plane. Figure 378*g* shows the different displacement current distributions J_{d_y}. In exactly the same way, surface currents and displacement currents can be shown for other modes as well as for different modes in circular wave guides.

230. Internal Impedance of a Plane Conductor. There is no conductor with a *perfect* conductivity, even though annealed copper has a value in the neighborhood of $\sigma = 5.8 \times 10^7$ mhos/m. We then always have a small electric tangential $\mathcal{E}$ component along the metal surface, which accounts for the wave energy entering a thin skin of the copper surface. This energy is dissipated in the thin skin as joulean heat. At the boundary (the copper surface), we have a discontinuity, since the magnetic field *H* amperes per meter is tangential to the boundary just

outside the metal surface (in air) and is zero on the other side of the thin copper skin. The discontinuity must then be equal to the surface current flowing on the surface of a plane conductor. A *surface* current is the limiting case of a volume current, just as a linear current is the limiting case of a surface current. The thickness of the surface current skin is all the smaller the higher the conductivity and also decreases with the operating frequency. If we have a block of copper with its XY surface *next* to an electromagnetic field and a thickness along the Z direction, a tangential H_y field, in amperes per meter, must measure the surface current in amperes per meter. Therefore, if the copper surface is 1 m wide, the surface current is H amperes. The internal or surface impedance of a conductor is the total voltage at the surface divided by the total current in the conductor, no matter how deeply the current penetrates below the surface of the conductor. For a perfectly conducting metal block, there can be no tangential $\mathcal{E}$ field at the surface of the conductor and therefore no field energy flow into the conducting block. This means that the ratio of tangential field components $\mathcal{E}_x = 0$ and H_y yields a zero impedance $\mathcal{E}_x/H_y = 0$ ohms. If we could *find* a medium that would approximate $\mathcal{E}_x/H_y = \infty$ (infinite impedance), we should have the tangential field $H_y \cong 0$. Good conductors, such as copper, cause very low impedance values, and we have, for the tangential fields along the surface of a copper block, the small value of

$$\left.\begin{aligned} Z_0 = \frac{\mathcal{E}_x}{H_y} = \sqrt{\frac{\mu\omega}{2\sigma}}\,(1+j) = R_0 + jX_0 \quad \text{ohms;} \\ f = \frac{\omega}{6.28} \quad \text{cycles/sec} \\ \mu = \mu_0 = 1.257 \times 10^{-6} \text{ henry/m;} \qquad \sigma = 5.8 \times 10^7 \text{ mhos/m} \end{aligned}\right\} \tag{913}$$

The derivations on pages 43, 829, 855, 858–859, 863–867, 914 show that the characteristic impedance is independent of the angle of wave incidence. We find for $f = 100$ Mc/sec

$$Z_0 = \sqrt{\frac{1.257 \times 10^{-6} \times 6.28 \times 100 \times 10^6}{2 \times 5.8 \times 10^7}} = 0.002608 \text{ ohms}$$

Formula (913) and the propagation constant Γ in a good conductor

$$\Gamma = \sqrt{0.5\sigma\mu\omega}\,(1+j) = \alpha + j\beta \tag{913a}$$

were found from the differential equation

$$\left.\begin{aligned} \frac{d^2J_x}{dz^2} = j\omega\mu\sigma J_x; \qquad \text{solution } J_x = J_0\epsilon^{-(1+j)z/\delta}; \qquad \delta = \frac{1}{\sqrt{\pi\mu\sigma f}} \\ f = \frac{\omega}{6.28} \quad \text{cycles/sec} \end{aligned}\right\} \tag{913b}$$

where μ is in henrys per meter, σ in mhos per meter, z in meters; δ is the penetration along the Z direction (normal to surface of metal and *into the metal*) at which the current density J_x is only $0.369J_0$ ($= J_0/\epsilon$), and J_0 denotes the current density at the surface of the metal (at $z = 0$ m). But the current density at the surface is $J_0 = \sigma\mathcal{E}_x$, where $\mathcal{E}_x$ is the small tangential electric field component along the metal surface due to an electromagnetic wave arriving from the air dielectric. The total current I_x per meter width is then the summation of all the $J_x\,dz$ effects taken over the limits $z = 0$ to $z = \infty$. Hence,

$$\left.\begin{aligned} I_x &= \int_{z=0}^{z=\infty} J_x\,dz = \int_0^{\infty} \sigma\mathcal{E}_x\epsilon^{-(1+j)z/\delta}\,dz = \frac{\delta\sigma\mathcal{E}_x}{1+j} \quad \text{amp/m} \\ \mathcal{E}_x &= (1+j)\frac{I_x}{\sigma\delta} \quad \text{volts/m} \end{aligned}\right\} \tag{913c}$$

The surface impedance (internal impedance of the conductor) becomes, per square meter surface (1 m wide and 1 m long),

$$\left.\begin{aligned} Z_s = \frac{\mathcal{E}_x}{I_x} = \frac{1+j}{\sigma\delta} = (1+j)\sqrt{\frac{\mu f\pi}{\sigma}} &= \underbrace{\sqrt{\frac{3.14\mu f}{\sigma}}}_{R_s} + j\underbrace{\sqrt{\frac{3.14\mu f}{\sigma}}}_{\omega L_i} \\ &\quad \text{ohms } \angle 45° \\ \frac{\omega}{6.28} = f &\quad \text{cycles/sec} \end{aligned}\right\} \tag{913d}$$

where μ is in henrys per meter and the internal inductance L_i is in henrys. For silver, copper, and brass, we have $\mu = \mu_0 = 1.257 \times 10^{-6}$ henry/m and find

$$\left.\begin{aligned} R_s &= 2.52 \times 10^{-4}\sqrt{f} \quad \text{ohms for silver} \\ R_s &= 2.61 \times 10^{-4}\sqrt{f} \quad \text{ohms for annealed copper} \\ R_s &= 5.01 \times 10^{-4}\sqrt{f} \quad \text{ohms for brass} \end{aligned}\right\} \tag{913e}$$

where f is in megacycles per second. We have very thin current skins at the surface of the metal, since

$$\left.\begin{aligned} \delta^{(m)} &= \frac{6.42 \times 10^{-5}}{\sqrt{f}} \quad \text{for silver} \\ \delta^{(m)} &= \frac{6.6 \times 10^{-5}}{\sqrt{f}} \quad \text{for annealed copper} \\ \delta^{(m)} &= \frac{1.27 \times 10^{-4}}{\sqrt{f}} \quad \text{for brass} \end{aligned}\right\} \tag{913f}$$

where f is in megacycles per second and $\delta = z$ meters is the thickness of the skin for which the current density J_x has fallen to 36.9 per cent of the value at the surface. We then can readily coat the inside metal

guide with a thin layer of silver in order to improve the efficiency of the guide, since even for 100 Mc/sec only, we find $\delta = 6.42 \times 10^{-6}$m $= 6.42 \times 10^{-3}$ mm, where 1 mm is about the thickness of a pencil line. Such a coating would then give a surface resistance R_s, at 100 Mc/sec, of only 2.52×10^{-3} ohm, while an annealed copper guide has 2.61×10^{-3} ohm at this frequency.

231. Remarks on the Power Flow along a Wave Guide. For perfect guide conductivity, a power transfer is possible only for operating frequencies higher than the cutoff frequency f_c. Table 10 shows how to compute the limiting frequency f_c. Formulas (912) give details on the evaluations for rectangular guides, and in Table 86 are details for circular guides. From Table 10, we also note that for *all shapes* of guides, it is convenient to define the characteristic wave impedances Z_{TM} and Z_{TE} in terms of the three-dimensional wave impedance $Z_0 = \sqrt{\mu/\kappa}$ ohms holding for the *unbounded* (unguided) wave medium and in terms of the cutoff frequency f_c as well as of the operating frequency f. We have then

$$\left.\begin{aligned} Z^{(\text{ohms})} &= Z_{TM} = \rho Z_0 \qquad \text{for TM waves;} \\ Z &= Z_{TE} = \frac{Z_0}{\rho} \qquad \text{for TE waves} \\ Z_0 &= \sqrt{\frac{\mu}{\kappa}} \cong 376.7 \text{ ohms for air as inside dielectric} \\ \rho &= \sqrt{1 - \nu^2}; \qquad \nu = \frac{f_c}{f} \end{aligned}\right\} \tag{914}$$

These wave impedances are based on the ratio of the *transverse* electric and magnetic fields with respect to the guide direction. Along the guide, we have the phase velocity $c' = v_z$, which determines the guide wavelength $\lambda_z = \lambda_g$. We have

$$\left.\begin{aligned} v_z &= \frac{1}{\rho\sqrt{\mu\kappa}} \quad \text{m/sec}; \qquad \lambda_g = \frac{v_z}{f_{\text{cycles/sec}}} \quad \text{m} \\ \frac{1}{\sqrt{\mu\kappa}} &\cong 3 \times 10^8 \text{ m/sec for air within the guide} \end{aligned}\right\} \tag{914a}$$

The flow of field energy in a hollow guide can be found from the *inphase transverse* electric and magnetic fields by means of the Poynting vector $p = \mathcal{E} \times H$. According to (12), for the power density flowing through the guide along guide axis Z, we have

$$\left.\begin{aligned} p_z &= \mathcal{E}_x H_y - \mathcal{E}_y H_x \qquad \text{for } \textit{rectangular} \text{ guides} \\ p_z &= \mathcal{E}_\varphi H_r - \mathcal{E}_r H_\varphi \qquad \text{watts/m}^2 \text{ for } \textit{cylindrical} \text{ guides} \end{aligned}\right\} \tag{914b}$$

since all these field components are *tangential* with the cross section of either a rectangular guide or a circular guide, respectively, and the power flow p_z per unit cross-sectional area must be along the Z axis of the guide. Now for a rectangular guide, according to Table 10, for a *TM wave*, for instance, we have to solve the differential equation $\nabla^2_{x,y}\mathcal{E}_z = -K^2\mathcal{E}_z$ yielding the two-dimensional Laplace equation

$$\frac{\partial^2\mathcal{E}_z}{\partial x^2} + \frac{\partial^2\mathcal{E}_z}{\partial y^2} = -K^2\mathcal{E}_z; \qquad K = \sqrt{\left(\frac{m\pi}{a}\right)^2 + \left(\frac{n\pi}{b}\right)^2} \tag{914c}$$

just as for *TE waves* we have

$$\nabla^2_{x,y}H_z = -K^2H_z; \qquad \frac{\partial^2 H_z}{\partial x^2} + \frac{\partial^2 H_z}{\partial y^2} = -K^2H_z \tag{914d}$$

where a meters is the cross-section dimension along the X direction and b meters along the Y axis. We have then the following details:

For

$$A = \frac{m\pi}{a}; \qquad B = \frac{n\pi}{b}; \qquad Z_0 = \sqrt{\frac{\mu}{\kappa}}; \qquad \beta_z = \rho\omega\sqrt{\mu\kappa}$$

$$\rho = \sqrt{1-\nu^2}; \quad \nu = \frac{f_c}{f}; \quad f_c = \frac{K}{6.28\sqrt{\mu\kappa}} \text{ cycles/sec}; \quad K = \sqrt{A^2+B^2}$$

$$\tau = \exp\,[j(\omega t - \beta_z z)]$$

with a and b in meters, we find

all relations for TM waves

$$\begin{aligned}
\mathcal{E}_z &= \mathcal{E}_0\tau \sin(xA)\sin(yB) \quad \text{volts/m};\\
H_x &= j\tau\frac{\nu B}{KZ_0}\mathcal{E}_0 \sin(xA)\cos(yB) \quad \text{amp/m}\\
H_y &= -j\tau\frac{\nu A}{KZ_0}\mathcal{E}_0 \cos(xA)\sin(yB) \quad \text{amp/m}\\
\mathcal{E}_x &= \rho Z_0 H_y \quad \text{volts/m}\\
\mathcal{E}_y &= -\rho Z_0 H_x \quad \text{volts/m}
\end{aligned} \tag{914e}$$

all relations for TE waves

$$\begin{aligned}
H_z &= H_0\tau\cos(xA)\cos(yB) \quad \text{amp/m}\\
\mathcal{E}_x &= j\tau\frac{\nu B Z_0}{K}H_0\cos(xA)\sin(yB) \quad \text{volts/m}\\
\mathcal{E}_y &= -j\tau\frac{\nu A Z_0}{K}H_0\sin(xA)\cos(yB) \quad \text{volts/m}\\
H_x &= -\rho\frac{\mathcal{E}_y}{Z_0} \quad \text{amp/m}\\
H_y &= \rho\frac{\mathcal{E}_x}{Z_0} \quad \text{amp/m}
\end{aligned}$$

Applying the left relation of (914*b*) to a rectangular guide of ab square meters cross section, we find, for the general $TE_{m,n}$ mode, the Poynting energy flow

$$p_z = \underbrace{\frac{\kappa\omega\pi^2\beta_z}{K^2}\mathcal{E}_0^2\left\{\frac{m^2}{a^2}\left[\sin^2\left(\frac{m\pi x}{a}\right)\cos^2\left(\frac{n\pi y}{b}\right)\right]\right.}_{\rightarrow}$$

$$\underbrace{\left.+\frac{n^2}{b^2}\left[\cos^2\left(\frac{m\pi x}{a}\right)\sin^2\left(\frac{n\pi y}{b}\right)\right]\right\}}_{=p_0}\sin^2(\omega t - \beta_z z) \quad \text{watts/m}^2$$

It is the *average* power of P_z watts across the *entire* cross section of ab square meters that gives the *total* power flow along the guide. The average value of the time function $\sin^2(\omega t - \beta_z z)$ is equal to $\frac{1}{2}$; and by integrating over the cross-sectional area of the rectangular guide, we find

$$P_z = \frac{1}{2}\int_{x=0}^{x=a}\int_{x=0}^{x=b} p_0\,dx\,dy = \frac{\kappa\omega\beta_z}{8}ab\mathcal{E}_0^2 \quad \text{watts for } m = 1 = n \qquad (914f)$$

where $\omega/6.28$ is in cycles per second, κ in farads per meter, $\mathcal{E}_0$ in volts per meter, a and b in meters, and β_z is as in (914*e*).

The guided field power is then proportional to the square of the maximum *longitudinal* $\mathcal{E}_0$ value of the $\mathcal{E}_z$ field occurring at the center of the guide. That the *longitudinal* instead of the customary transverse unbounded (unguided) space maximum value plays a part is evident, since the longitudinal field is, in equivalence, the return instead of the second metal conductor. We then find the following results in the same way:

$$\left.\begin{aligned}
P_z^{(\text{watts})} &= 7.85\times10^5\kappa\beta_z f ab\mathcal{E}_0^2 && \text{for a rectangular guide and } TM_{1,1}\\
P_z &= 7.85\times10^5\kappa\beta_z f(a\mathcal{E}_0)^2 && \text{for a square guide } (a=b) \text{ and } TM_{1,1}\\
P_z &= 7.85\times10^5\mu\frac{\beta_z f(3.14n)^2}{bK^4}aH_0^2 && \text{for a rectangular guide and TE mode}\\
P_z &= 3.19\times10^5\mu\beta_z f ab^3H_0^2 && \text{for a rectangular guide and } TE_{0,1}\\
K &= \sqrt{\left(\frac{m\pi}{a}\right)^2+\left(\frac{n\pi}{b}\right)^2}
\end{aligned}\right\} \qquad (914g)$$

where β_z is as in (914*e*), f is in megacycles per second, a and b are in meters, μ is in henrys per meter, κ is in farads per meter, $\mathcal{E}_0$ is the maximum value of *axial* $\mathcal{E}_z$ field in volts per meter, and H_0 is the maximum value of *axial* H_z field in amperes per meter. For *all* cross sections (such as

circular, rectangular, square), we have, for the *power* guided along the Z direction, the formulas

$$\left.\begin{aligned} P_z^{(\text{watts})} &= \frac{q}{2Z_0^2}\int\int_S \mathcal{E}_z^2\, dS \qquad \text{for TM waves} \\ P_z^{(\text{watts})} &= \frac{qZ_0^2}{2}\int\int_S H_z^2\, dS \qquad \text{for TE waves} \end{aligned}\right\} \tag{914h}$$

where $q = \dfrac{\sqrt{1-\nu^2}}{\nu^2}$; $\nu = \dfrac{f_c}{f}$; $Z_0 = \sqrt{\dfrac{\mu}{\kappa}} \cong 376.7$ ohms for guides containing air; $S = ab$ sq m for rectangular guides; $S = \pi a^2$ sq m for circular guides. Double integration must be extended over Cartesian x, y, z coordinates for rectangular guides and over cylinder coordinates r, φ, z for circular guides. These relations are the outcome of the Poynting vector method used above, where we find the time average for the power component as

$p_z = \frac{1}{2}$ Re $(\mathcal{E} \times H^*)$ watts/m^2; total power flow $P_z = \frac{1}{2}$ Re $\int\int_S (\mathcal{E} \times H^*)_n\, dS$ watts

$$p_z = \frac{\mathcal{E}\cdot H^*}{2} = \frac{1}{2}\rho Z_0 H\cdot H^* = \frac{1}{2}\rho Z_0(H_x\cdot H_x^* + H_y\cdot H_y^*) \qquad \text{for TM waves}$$

$$p_z = \frac{1}{2}\mathcal{E}\cdot H^* = \frac{1}{2}\frac{\mathcal{E}\cdot\mathcal{E}^*}{Z_0/\rho} = \frac{1}{2}\frac{\rho}{Z_0}(\mathcal{E}_x\cdot\mathcal{E}_x^* + \mathcal{E}_y\cdot\mathcal{E}_y^*) \qquad \text{for TE waves}$$

since

$$\rho Z_0 = Z_{\text{TM}}; \qquad \frac{Z_0}{\rho} = Z_{\text{TE}}; \qquad \rho = \sqrt{1-\left(\frac{f_c}{f}\right)^2}; \qquad Z_0 = \sqrt{\frac{\mu}{\kappa}}$$

We have also for TM waves

$$H_x = j\frac{\omega\kappa}{K^2}\frac{\partial\mathcal{E}_z}{\partial y}; \qquad H_y = -j\frac{\omega\kappa}{K^2}\frac{\partial\mathcal{E}_z}{\partial x}$$

with the phase factor $\epsilon^{j(\omega t-\beta_z z)}$, and find

$$H_x\cdot H_x^* = \left(j\frac{\omega\kappa}{K^2}\frac{\partial\mathcal{E}_z}{\partial y}\right)\left(-j\frac{\omega\kappa}{K^2}\frac{\partial\mathcal{E}_z}{\partial y}\right) = \frac{\omega^2\kappa^2}{K^4}\left(\frac{\partial\mathcal{E}_z}{\partial y}\right)^2$$

$$H_y\cdot H_y^* = \left(-j\frac{\omega\kappa}{K^2}\frac{\partial\mathcal{E}_z}{\partial x}\right)\left(+j\frac{\omega\kappa}{K^2}\frac{\partial\mathcal{E}_z}{\partial x}\right) = \frac{\omega^2\kappa^2}{K^4}\left(\frac{\partial\mathcal{E}_z}{\partial x}\right)^2$$

where $K = 2\pi f_c\sqrt{\mu\kappa}$. Hence, for TM waves

$$p_z = \frac{1}{2}\rho Z_0\frac{\omega^2\kappa^2}{K^4}\left[\left(\frac{\partial\mathcal{E}_z}{\partial x}\right)^2 + \left(\frac{\partial\mathcal{E}_z}{\partial y}\right)^2\right]$$

where $[\ ] = (\nabla\mathcal{E}_z)^2$ and $\nabla\mathcal{E}_z$ is a gradient *along the X and Y* directions.

$$P_z = \frac{1}{2}\rho Z_0 \frac{\omega^2\kappa^2}{K^4}\int\int_S (\nabla\mathcal{E}_z)^2\,dS = \frac{1}{2}\rho Z_0\frac{\omega^2\kappa^2}{K^2}\int\int_S \mathcal{E}_z\,dS \qquad \text{watts}$$

$$\frac{0.5\rho Z_0\omega^2\kappa^2}{K^2} = \frac{0.5\sqrt{1-\nu^2}\,Z_0\omega^2\kappa^2}{\omega_c^2\mu\kappa} = \frac{1}{2}Z_0\sqrt{1-\nu^2}\left(\frac{\omega}{\omega_c}\right)^2\frac{\kappa}{\mu} = \frac{Z_0}{2}\sqrt{1-\nu^2}\,\frac{1}{\nu^2}\frac{1}{Z_0^2}$$

and

$$\frac{0.5\rho Z_0\omega^2\kappa^2}{K^2} = \frac{0.5q}{Z_0}$$

$$P_z = \frac{q}{2Z_0}\int\int_S \mathcal{E}_z^2\,dS \qquad \text{watts}$$

In exactly the same way, the second relation for TE waves in (914*h*) is confirmed. The procedure of conjugate vector multiplication, such as $H \cdot H^*$, is described on page 117.

232. Power Dissipation and Attenuation in Wave Guides Due to the Finite Conductivity of the Metal Walls. Inasmuch as we must expect some attenuation for a finite conductivity of the metal wall, the power flow along the guide must gradually decrease. Since both the electric field as well as the magnetic field are, for an attenuation constant α, dependent on a decay factor $\epsilon^{-\alpha z}$, the *energy* flow along the guide must decay according to an $\epsilon^{-2\alpha z}$ law while traveling along the Z direction. If P_z denotes the energy flow, the above exponential decay expresses that $d(P_z)/dz = -2\alpha P_z$. In Sec. 231, we found that P_z is the integral of the Poynting vector p_z over the cross section of ab square meters for rectangular guides and over πa^2 for circular guides. Therefore, $-d(P_z)/dz$ must represent the energy *dissipated* in the guide walls for 1 m distance, *i.e.*, the watt loss in the metal surface of the guide for a guide 1 m long. We have then the relation

$$\alpha^{(\text{nepers/m})} = \frac{\frac{1}{2}\int\int_{S_1}\text{Re}\,(\mathcal{E}\times H^*)_n\,dS_1}{2\left[\frac{1}{2}\int\int_S \text{Re}\,(\mathcal{E}\times H^*)_n\,dS\right]}$$

$$= \frac{\text{rate of field energy flow into the metal wall}}{2P_z}$$

$$\cong \frac{\text{power dissipated in the guide walls of 1 m length}}{\text{twice the power transfer along the guide}} \qquad (915)$$

Since, in each case, the double integral represents the summation of the Poynting field energy flow *normal* to respective surface elements dS_1 and dS, where dS_1 is a surface element of the inside metal wall of the guide and dS is a surface element of the cross section of the guide, we can use the P_z value of (914*h*) if the appropriate values for q are employed for a particular mode of wave excitation. For finite metal conductivities, we can use the surface resistance R_s as given in (913*e*) together with all

the current densities occurring on the *inner* surface skins of the guide wall. The power loss in the walls of the wave guide is then

$$\mathcal{L} = \tfrac{1}{2} R_s \oint_{l_0} \sum J \cdot J^* \, dl_0 \qquad \text{watts/m guide length} \qquad (915a)$$

where the integration is to be taken around the inside contour of the metal wall. For TE waves, we have two summation terms under the Σ sign, since owing to the longitudinal H_z field when tangential to the inner guide surface, we have a *transverse* circulating current and, owing to the transverse resultant H field, a *longitudinal* current. For TM waves we have only a resultant transverse magnetic field and, therefore, only one current density (which is longitudinal) under the Σ sign. We then find the expressions

$$\left.\begin{aligned} \mathcal{L} = \mathcal{L}_{TM} &= \frac{1}{2} \frac{R_s}{(\nu K Z_0)^2} \oint \left(\frac{\partial \mathcal{E}_z}{\partial n}\right)^2 dl_0 \qquad \text{for TM waves} \\ \mathcal{L} = \mathcal{L}_{TE} &= \frac{R_s}{2} \oint \left[H_z^2 + \frac{1 - \nu^2}{(\nu K)^2} \left(\frac{\partial H_z}{\partial l_0}\right)^2 \right] dl_0 \qquad \text{for TE waves} \\ Z_0 &= \sqrt{\frac{\mu}{\kappa}} \qquad \text{ohms; } \mathcal{L} \text{ watts/m;} \qquad \nu = \frac{f_c}{f}; \\ K &= 6.28 \times 10^6 f_c \sqrt{\mu\kappa} \end{aligned}\right\} \qquad (915b)$$

where f and f_c are in megacycles per second, μ is in henrys per meter, and κ is in farads per meter. These relations *tacitly assume* that the currents in good conductors are essentially of the same magnitude as for ideal conductors ($\sigma = \infty$ mhos/m). This assumption is somewhat justified, since we found, from formula (913), a very low wave impedance at VHF's and UHF's as well as very low surface resistance values from (913*e*). For instance, J. C. Slater[1] has shown that the field energy dissipated per cycle in a good conductor equals the magnetic field energy contained in a thin sheet of the metal surface, which is only 3.14δ meters thick, for which the energy concentration is the same as immediately outside this metal skin. Equations (913*f*) show that the quantity δ is very small indeed, so 3.14δ must likewise be very small at VHF's and UHF's and especially at S and X band frequencies. The energy lost per cycle must, therefore, be a very small fraction of the total field energy. We can therefore assume, in our current density summation of (915*a*), that we have only a normal derivative $\partial\mathcal{E}/\partial n$ at the surface of a good conductor but no such derivative of any electric field vector $\mathcal{E}$ along the conductor surface. This will give the condition for an ideal conductor as far as the current is concerned. For the same reason, we

[1] "Microwave Transmission," p. 141, McGraw-Hill Book Company, New York, 1942.

can have no normal derivative $\partial H/\partial n$ of a magnetic vector at the surface of a good conductor but essentially only a tangential derivative $\partial H/\partial l_0$. This is the reason why, in (915*b*), the longitudinal $\mathcal{E}_z$ field for TM waves appears with the normal derivative *only* and the longitudinal H_z field for TE waves in guides appears as the tangential derivative $\partial H_z/\partial l_0$.

Since, for TM waves, the resultant magnetic field is entirely in the plane of the cross section of a guide, there can be only one longitudinal current density J_z in amperes per meter along the inside walls of the guide, and the absolute value $\sqrt{|H_x^2 + H_y^2|}$ of the tangential magnetic field must numerically equal the absolute value $|J_z|$. But for TE waves, we have *also a longitudinal H_z field*, which causes (when tangential) a transverse current density J_t on the inside metal wall, and we have the comparisons in (915*a*) as

$$\left.\begin{aligned} &\tfrac{1}{2}\Sigma J \cdot J^* = \tfrac{1}{2}J_z \cdot J_z^* = \tfrac{1}{2}(H_x \cdot H_x^* + H_y \cdot H_y^*) \qquad \text{for TM waves} \\ &\frac{1}{2}\sum J \cdot J^* = \frac{1}{2}(J_z \cdot J_z^* + J_t \cdot J_t^*) = \frac{H_x \cdot H_x^* + H_y \cdot H_y^* + H_z \cdot H_z^*}{2} \\ &\qquad\qquad\qquad\qquad\qquad\qquad \text{for TE waves} \end{aligned}\right\} \quad (915c)$$

But for respective TM and TE waves, we have

$$H_x^{(\text{amp/m})} = j\frac{\omega\kappa}{K^2}\frac{\partial \mathcal{E}_z}{\partial y} \qquad \text{for TM waves}$$

$$H_x^{(\text{amp/m})} = -j\frac{\beta_z}{K^2}\frac{\partial H_z}{\partial x} \qquad \text{for TE waves}$$

$$H_y^{(\text{amp/m})} = -j\frac{\omega\kappa}{K^2}\frac{\partial \mathcal{E}_z}{\partial x} \qquad \text{for TM waves}$$

$$H_y^{(\text{amp/m})} = -j\frac{\beta_z}{K^2}\frac{\partial H_z}{\partial y} \qquad \text{for TE waves}$$

$$\beta_z = \rho\omega\sqrt{\mu\kappa}; \qquad \rho = \sqrt{1-\nu^2}; \qquad \nu = \frac{f_c}{f}; \qquad K = 2\pi f_c\sqrt{\mu\kappa};$$

$$\omega_c = 2\pi f_c; \qquad Z_0 = \sqrt{\frac{\mu}{\kappa}}$$

$$H_x \cdot H_x^* + H_y \cdot H_y^* = \left(j\frac{\omega\kappa}{K^2}\frac{\partial \mathcal{E}_z}{\partial y}\right)\left(-j\frac{\omega\kappa}{K^2}\frac{\partial \mathcal{E}_z}{\partial y}\right)$$
$$+\left(-j\frac{\omega\kappa}{K^2}\frac{\partial \mathcal{E}_z}{\partial x}\right)\left(+j\frac{\omega\kappa}{K^2}\frac{\partial \mathcal{E}_z}{\partial x}\right) = \frac{\omega^2\kappa^2}{K^4}\left[\left(\frac{\partial \mathcal{E}_z}{\partial x}\right)^2 + \left(\frac{\partial \mathcal{E}_z}{\partial y}\right)^2\right] \qquad \text{for TM waves}$$

and

$$[\ \ ] = (\nabla \mathcal{E}_z)^2 \cong \left(\frac{\partial \mathcal{E}_z}{\partial n}\right)^2$$

$$H_x \cdot H_x^* + H_y \cdot H_y^* = \left(-j\frac{\beta_z}{K^2}\frac{\partial H_z}{\partial x}\right)\left(+j\frac{\beta_z}{K^2}\frac{\partial H_z}{\partial x}\right)$$
$$+\left(-j\frac{\beta_z}{K^2}\frac{\partial H_z}{\partial y}\right)\left(+j\frac{\beta_z}{K^2}\frac{\partial H_z}{\partial y}\right) = \frac{\beta_z^2}{K^4}\left[\left(\frac{\partial H_z}{\partial x}\right)^2 + \left(\frac{\partial H_z}{\partial y}\right)^2\right] \qquad \text{for TE waves}$$

and

$$[\ \ ] = (\nabla H_z)^2 \cong \left(\frac{\partial H_z}{\partial l_0}\right)^2$$

$$\sum J \cdot J^* = (H_x \cdot H_x^* + H_y \cdot H_y^*) = \frac{\omega^2\kappa^2}{K^4}\left(\frac{\partial \mathcal{E}_z}{\partial n}\right)^2 = \frac{\omega^2\kappa^2\left(\frac{\partial \mathcal{E}_z}{\partial n}\right)^2}{K^2\omega_c^2\mu\kappa} = \frac{\left(\frac{\partial \mathcal{E}_z}{\partial n}\right)^2}{K^2 Z_0^2 \nu^2}$$

for TM waves

$$\sum J \cdot J^* = (H_x \cdot H_x^* + H_y \cdot H_y^* + H_z \cdot H_z^*) = \frac{\beta_z^2}{K^4}\left(\frac{\partial H_z}{\partial l_0}\right)^2 + H_z^2$$

$$= \frac{\rho^2\omega^2\mu\kappa}{K^2\omega_c^2\mu\kappa}\left(\frac{\partial H_z}{\partial l_0}\right)^2 + H_z^2 = \frac{\sqrt{1-\nu^2}}{K^2\nu^2}\left(\frac{\partial H_z}{\partial l_0}\right)^2 + H_z^2 \qquad \text{for TE waves}$$

which results used in (915*a*) confirm the expressions of (915*b*).

Using the results of (915*b*) for the joulean heat loss per meter length of a guide together with the power flow across the cross section of the guide, as given in (914*h*), we find, by means of (915), the attenuation

$$\left.\begin{aligned} \alpha^{(\text{nepers/m length of guide})} &= \frac{\mathfrak{L}_{TM}}{2(P_z)_{TM}} \qquad \text{for TM waves} \\ \alpha &= \frac{\mathfrak{L}_{TE}}{2(P_z)_{TE}} \qquad \text{for TE waves} \end{aligned}\right\} \qquad (915d)$$

The application of (915) is not difficult. Suppose we take the dominant $TE_{1,0}$ mode of a rectangular guide, such as shown in Figs. 373, 375, and 378. We have then $m = 1$ and $n = 0$ and only one transverse $\mathcal{E} = \mathcal{E}_y$ electric field distribution parallel with the b dimension, but such that no tangential $\mathcal{E}_y$ value exists along the b surfaces of the guide. We have then the well-known half-period (half-sinusoidal) $\mathcal{E}_y$ distribution along the a dimension of the guide. The magnetic H circulations around the displacement currents (along the $\mathcal{E}$ lines) are then in planes parallel to the XZ plane of Fig. 379, with the guide length along the Z direction. We have, therefore, *closed* magnetic lines, which generally have H_x as well as H_z components. Therefore, whenever the H loops become tangent to the side faces of the metal guide we have, owing to the tangential H_z field in Fig. 379, a corresponding J_y current density of magnitude $|H_z|$ amperes per meter. But when the H loops become tangent to the inside guide walls of the top or the bottom face of the guide, we generally have H_x and H_z components, which cause the current density J_z amperes per meter of magnitude $|H_x|$ and the current density J_x of magnitude $|H_z|$ amperes per meter. The metal loss in watts per 1 m

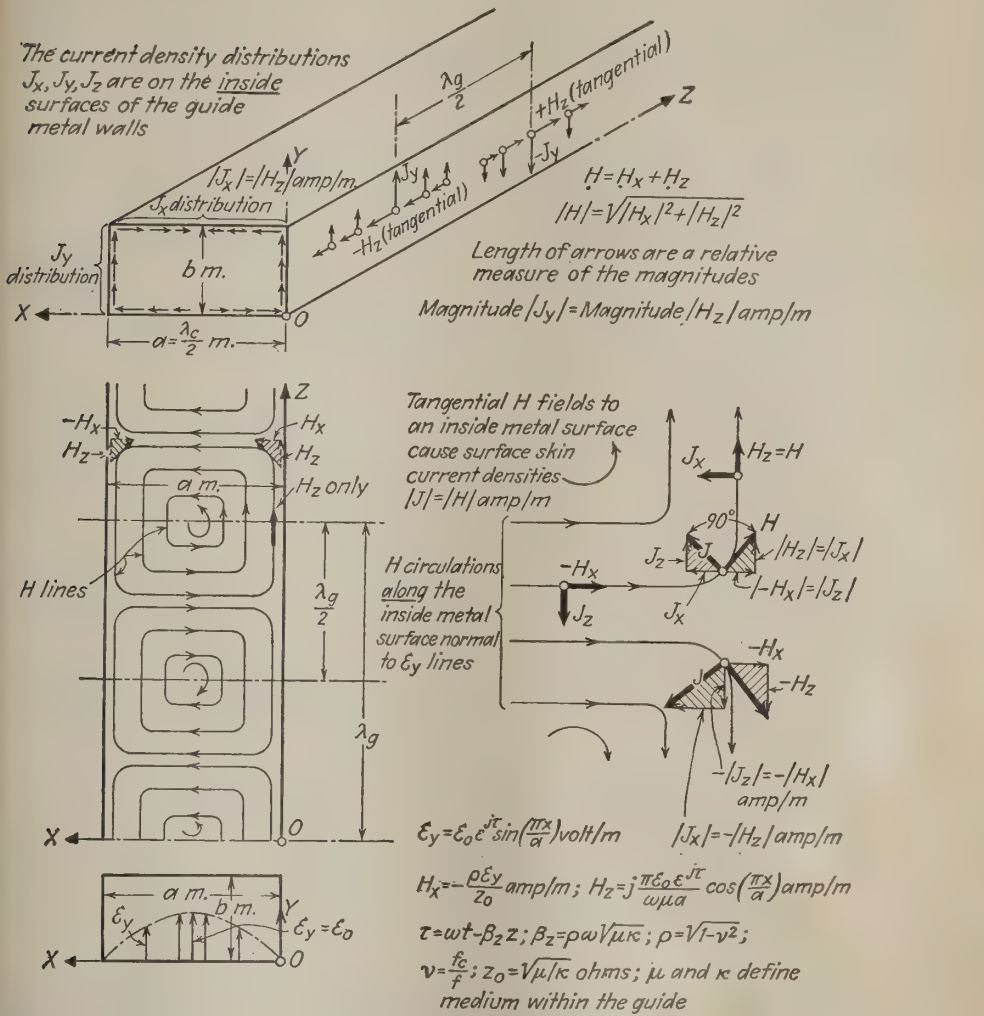

FIG. 379. Surface conduction current densities on the inside metal surfaces due to tangential magnetic fields for a $TE_{1,0}$ wave in a rectangular guide.

guide length then becomes

$$\mathfrak{L} = \underbrace{\tfrac{1}{2}R_s \int_{y=0}^{y=b} H_z \cdot H_z^* \, dy}_{\text{watts lost on left inside wall}} + \underbrace{\tfrac{1}{2}R_s \int_0^b H_z \cdot H_z^* \, dy}_{\text{watts lost on right inside wall}}$$

$$+ \underbrace{\tfrac{1}{2}R_s \int_{x=0}^{x=a} (H_x \cdot H_x^* + H_z \cdot H^*) \, dx}_{\text{watts lost on bottom inside wall}}$$

$$+ \underbrace{\tfrac{1}{2}R_s \int_0^a (H_x \cdot H_x^* + H_z \cdot H_z^*) \, dx}_{\text{watts lost on top inside wall}} \quad \text{watts/m} \qquad (915e)$$

For the power transferred along the guide, we need only integrate the Poynting vector p_z over the cross section of ab square meters. We find then

$$\left.\begin{aligned} P_z &= \frac{1}{2}\int_{x=0}^{x=a}\int_{y=0}^{y=b} \mathcal{E}_y \cdot H_x^*\, dx\, dy = \frac{1}{2}\int_0^a\int_0^b \frac{\mathcal{E}_y \cdot \mathcal{E}_y^*}{Z_0/\rho} \\ &\qquad\qquad \text{total watts perpendicular to } ab \text{ sq m} \\ Z_0 &= \sqrt{\frac{\mu}{\kappa}}; \qquad \rho = \sqrt{1 - \left(\frac{f_c}{f}\right)^2} \end{aligned}\right\} \tag{915f}$$

According to Fig. 379, we have for an $\mathcal{E}_y$ excitation, *i.e.*, a $TE_{1,0}$ mode,

$$\mathcal{E}_y = \mathcal{E}_0 \epsilon^{j\tau} \sin\left(\frac{\pi x}{a}\right) \text{ volts/m}; \qquad H_x = -\frac{\rho \mathcal{E}_y}{Z_0} \text{ amp/m}$$

$$H_z = j\frac{\pi \mathcal{E}_0 \epsilon^{j\tau}}{\omega\mu a}\cos\left(\frac{\pi x}{a}\right) \text{ amp/m}; \qquad \epsilon^{j\tau} = \epsilon^{j(\omega t - \beta_z z)}; \qquad \beta_z = \rho\omega\sqrt{\mu\kappa}$$

$$\rho = \sqrt{1 - \nu^2}; \qquad \nu = \frac{f_c}{f}; \qquad \mathcal{E}_y \cdot \mathcal{E}_y^* = \mathcal{E}_0^2 \sin^2\left(\frac{\pi x}{a}\right)$$

since

$$\epsilon^{j\tau} \cdot \epsilon^{-j\tau} = 1; \qquad P_z = \frac{\rho \mathcal{E}_0^2}{2Z_0}\int_0^a\int_0^b \sin^2\left(\frac{\pi x}{a}\right) dx\, dy$$

$$= \frac{\rho \mathcal{E}_0^2}{2Z_0}\left[\int_{y=0}^{y=b} dy\right]\left[\int_{x=0}^{x=a} \sin^2\left(\frac{\pi x}{a}\right) dx\right]$$

or

$$\left.\begin{aligned} \underline{P_z} &= \frac{\rho b \mathcal{E}_0^2}{2Z_0}\int_0^a \sin^2\left(\frac{\pi x}{a}\right) dx = \frac{\rho b \mathcal{E}_0^2}{2Z_0}\left|\frac{x}{2} - \frac{a}{4\pi}\sin\left(\frac{2\pi x}{a}\right)\right|_0^a \\ &= \frac{\rho b \mathcal{E}_0^2}{2Z_0}\left[\frac{a}{2} - \underbrace{\frac{a}{4\pi}\sin\left(\frac{2\pi a}{a}\right)}_{=0} - 0\right] = \underline{\frac{\rho a b}{4Z_0}\,\mathcal{E}_0^2} \quad \text{watts} \end{aligned}\right\} \tag{915g}$$

In (915*e*), we can combine the integrals for the inside guide faces, which are parallel with the $\mathcal{E}_y$ excitation and which are normal to the $\mathcal{E}_y$ excitation, respectively, and find, for the heat loss per meter guide length,

$$\mathcal{L}^{(\text{watts/m})} = \underbrace{R_s\int_0^b H_z \cdot H_z^*\, dy}_{\substack{\text{loss in metal skins,}\\ \text{parallel with } \mathcal{E}_y\\ \text{(causes } J_y \text{ currents)}}} + \underbrace{R_s\int_0^a H_x \cdot H_x^*\, dx + R_s\int_0^a H_z \cdot H_z^*\, dx}_{\substack{\text{loss in metal skins, normal to } \mathcal{E}_y \text{ excita-}\\ \text{tions (causes } J_y \text{ and } J_z \text{ currents in Fig.}\\ 379)}} \tag{915h}$$

$$\left.\begin{aligned} H_x &= -\frac{\rho}{Z_0}\mathcal{E}_y = -\frac{\rho\epsilon^{j\tau}}{Z_0}\mathcal{E}_0 \sin\left(\frac{\pi x}{a}\right); \qquad H_x \cdot H_x^* = H_x^2 = \frac{\rho^2}{Z_0^2}\mathcal{E}_0^2 \sin^2\left(\frac{\pi x}{a}\right) \\ R_s\int_0^a H_x \cdot H_x^*\, dx &= \frac{\rho^2}{Z_0^2}\mathcal{E}_0^2 R_s\int_0^a \sin^2\left(\frac{\pi x}{a}\right) dx = \frac{\rho^2 a}{2Z_0^2} R_s \mathcal{E}_0^2 \quad \text{watts/m} \end{aligned}\right\} \tag{915i}$$

Moreover

$$\left.\begin{aligned} H_z &= j\frac{\pi\mathcal{E}_0\epsilon^{j\tau}}{\omega\mu a}\cos\left(\frac{\pi x}{a}\right) \\ H_z\cdot H_z^* &= \left[j\frac{\pi\mathcal{E}_0\epsilon^{j\tau}}{\omega\mu a}\cos\left(\frac{\pi x}{a}\right)\right]\left[-j\frac{\pi\mathcal{E}_0\epsilon^{-j\tau}}{\omega\mu a}\cos\left(\frac{\pi x}{a}\right)\right] \\ &= \frac{\pi^2\mathcal{E}_0^2}{\omega^2\mu^2a^2}\cos^2\left(\frac{\pi x}{a}\right) \\ R_s\int_0^b H_z\cdot H_z^*\,dy &= R_s\frac{\pi^2\mathcal{E}_0^2}{\omega^2\mu^2a^2}\underbrace{\cos^2\left(\frac{\pi x}{a}\right)}_{\substack{=1 \text{ since } x=\\ 0 \text{ for } y=0\\ \text{to } y=b}}\int_0^b dy = \frac{\pi^2 b}{\omega^2\mu^2a^2}R_s\mathcal{E}_0^2 \quad \text{watts/m} \end{aligned}\right\} \quad (915j)$$

$$R_s\int_0^a H_z\cdot H_z^*\,dx = R_s\frac{\pi^2\mathcal{E}_0^2}{\omega^2\mu^2a^2}\int_{x=0}^{x=a}\cos^2\left(\frac{\pi x}{a}\right)dx$$

$$= R_s\frac{\pi^2\mathcal{E}_0^2}{\omega^2\mu^2a^2}\overbrace{\left|\frac{a}{4\pi}\sin\left(\frac{2\pi x}{a}\right)+\frac{x}{2}\right|_0^a}^{=a/2} = \frac{\pi^2\mathcal{E}_0^2}{2\omega^2\mu^2a}R_s\mathcal{E}_0^2 \quad \text{watts/m} \quad (915k)$$

Combining the results of (915*i*), (915*j*), and (915*k*) yields, in (915*h*), the total watt loss per 1 m guide length for a perfect dielectric (such as dry air)

$$\left.\begin{aligned} \mathfrak{L} &= \underbrace{\frac{\pi^2 b}{\omega^2\mu^2a^2}R_s\mathcal{E}_0^2}_{\substack{\text{loss on inside}\\ \text{metal skins,}\\ \text{parallel with}\\ \mathcal{E}_y \text{ polarization}}} + \underbrace{\left(\frac{a\rho^2}{2Z_0^2}+\frac{\pi^2}{2a\mu^2\omega^2}\right)R_s\mathcal{E}_0^2}_{\substack{\text{loss on inside metal}\\ \text{skins, normal to } \mathcal{E}_y\\ \text{lines}}} = \frac{R_s\mathcal{E}_0^2}{2}(A+B+C) \\ A &= \frac{2\pi^2 b}{\omega^2\mu^2a^2}; \qquad B = \frac{a\rho^2}{Z_0^2}; \qquad C = \frac{\pi^2}{a\mu^2\omega^2}; \qquad Z_0 = \sqrt{\frac{\mu}{\kappa}} \quad \text{ohms} \end{aligned}\right\} \quad (915l)$$

where R_s is the skin surface resistance of (913*e*). According to Table 10, we have for $TE_{1,0}$ waves, $m = 1$ and $n = 0$ and $K = \sqrt{(m\pi/a)^2 + (n\pi/b)^2} = \pi/a = \omega_c\sqrt{\mu\kappa}$, which can also be seen from formulas (914*e*). We have then the transformations

$$A = \frac{\pi^2}{a^2}\frac{2b}{\omega^2\mu^2} = \frac{\pi^2}{a^2}\frac{2b\kappa}{\omega^2\mu\mu\kappa} = \frac{\pi^2}{a^2}\frac{2b}{\omega^2\mu\kappa(\mu/\kappa)}$$

$$= \left(\frac{\pi^2}{a^2}\right)\frac{2b}{\omega^2\mu\kappa Z_0^2} = (\omega_c^2\mu\kappa)\frac{2b}{\omega^2\mu\kappa Z_0^2} = \left(\frac{\omega_c}{\omega}\right)^2\frac{2b}{Z_0^2} = \nu^2\frac{2b}{Z_0^2}$$

since

$$\frac{\omega_c}{\omega} = \frac{f_c}{f} = \nu; \qquad B = \frac{a\rho^2}{Z_0^2} = \frac{a(1-\nu^2)}{Z_0^2}$$

$$C = \frac{\pi^2}{a\mu^2\omega^2} = \frac{\pi^2}{a^2}\frac{a}{\mu^2\omega^2} = \frac{\pi^2}{a^2}\frac{a\kappa}{\omega^2\mu\kappa\mu} = \left(\frac{\pi^2}{a^2}\right)\frac{a}{\omega^2\mu\kappa Z_0^2} = (\omega_c^2\mu\kappa)\frac{a}{\omega^2\mu\kappa Z_0^2} = \nu^2\frac{a}{Z_0^2}$$

$$A+B+C = \frac{a}{Z_0^2}\left(\frac{2b}{a}\nu^2+1-\nu^2+\nu^2\right) = \frac{a}{Z_0^2}\left(1+\frac{2b}{a}\nu^2\right)$$

inserted in (915*l*), yields

$$\mathfrak{L} = \mathfrak{L}_m = \frac{0.5aR_s\mathcal{E}_0^2}{Z_0^2}\left(1 + \frac{2b}{a}\nu^2\right) \quad \text{watts/m guide length} \qquad (915m)$$

for $Z_0 = \sqrt{\mu/\kappa}$ ohms and R_s the skin resistance as in (913*e*).

In order to analyze the effect of the relative dimension b/a and the effect of the operating frequency f, it is convenient to distinguish in (915*m*) between the metal faces of the inside skin that are *parallel* with the $\mathcal{E}_y$ excitation of the $TE_{1,0}$ mode and *normal* to the $\mathcal{E}_y$ lines, respectively (Fig. 379). We find for the joulean heat loss in the inner metal walls

$$\mathfrak{L}_m = \frac{1}{2}R_s\mathcal{E}_0^2A + \frac{1}{2}R_s\mathcal{E}_0^2(B + C) = b\frac{R_s\mathcal{E}_0^2}{Z_0}\nu^2 + a\frac{R_s\mathcal{E}_0^2}{2Z_0^2}$$

$$= \underbrace{2.5 \times 10^{-13}\frac{b}{a^2}\frac{R_s\mathcal{E}_0^2}{\mu^2f^2}}_{=D} + \underbrace{a\frac{R_s\mathcal{E}_0^2}{2Z_0^2}}_{=E} \quad \text{watts/m guide length} \qquad (915n)$$

where D is the watt loss of metal skins parallel with $\mathcal{E}_y$ lines in Fig. 379, E is the loss in metal skins perpendicular to the $\mathcal{E}_y$ lines, f is in megacycles per second, a and b are in meters, and R_s is as in (913*e*), since

$$\nu = \frac{f_c}{f} = \frac{\lambda}{\lambda_c} = \frac{\lambda}{2a} = \frac{v/f}{2a} = \frac{1}{2af\sqrt{\mu\kappa}} \quad \text{for } f \text{ in cycles/sec}$$

$$\nu^2 = \frac{1}{4a^2f^2\mu\kappa}; \qquad \frac{\nu^2}{Z_0^2} = \frac{\kappa\nu^2}{\mu} = \frac{1}{4\mu^2a^2f^2}$$

Since R_s/f^2, in the first term, is proportional to $\sqrt{f}/f^2$, the metal loss in the side inside metal skins is proportional to $f^{-1.5}$ as well as to the ratio b/a^2. Since, in the second term of (915*n*), the frequency f appears only in the R_s factor, the metal loss in the inside metal skins of the top and bottom faces is proportional to $f^{0.5}$ as well as to the width a of the rectangular guide cross section. The values of $Z_0 = \sqrt{\mu/\kappa}$ and μ in the respective terms of (915*n*) are fixed for a certain guide dielectric within the guide. For air as the dielectric, we have $Z_0 \cong 376.7$ ohms and $\mu = \mu_0 = 1.257 \times 10^{-6}$ henry/m. The *loss in* the *side walls decreases*, therefore, *as the frequency is increased*. That this happens for an $\mathcal{E}_y$ polarization is obvious, since the top and bottom inside skins act like the plates of a condenser while the metal side walls are in shunt with these condenser plates. At certain times, the top and bottom inside metal skins then collect or receive both displacement currents due to the $\mathcal{E}_y$ lines (depending upon the polarity) as well as conduction currents coming or going, respectively, from or to the side walls. The *higher* the operating frequency is chosen the *less* conduction current we shall have in comparison with the displacement current passing across the

top and bottom inside metal skins. Only if the dielectric within the guide is perfect can we then gain as the frequency is increased as far as the loss in the side faces is concerned. According to (915), (915*g*), and (915*m*), we find the attenuation due to the metal of the guide

$$\alpha_m^{(\text{nepers/m guide length})} = \frac{\mathcal{L}_m}{2P_z} = \frac{\dfrac{1 + 2b(\nu^2/a)}{2Z_0^2}\, aR_s\mathcal{E}_0^2}{2ab\rho\mathcal{E}_0^2/(4Z_0)}$$

$$= \frac{1 + 2b(\nu^2/a)}{\rho b Z_0} R_s = \frac{1 + 2(b/a)\nu^2}{bZ_0\sqrt{1 - \nu^2}} R_s; \qquad \nu = \frac{f_c}{f} \tag{915o}$$

$$f_c = \frac{10^{-6}}{2a\sqrt{\mu\kappa}} \quad \text{Mc/sec}$$

where a and b are in meters, $Z_0 = \sqrt{\mu/\kappa}$ is in ohms, μ is in henrys/m, κ is in farads/m, R_s is as in (913*e*), for air $Z_0 = 376.7$ ohms, and $f_c = 150/a$ megacycles per second. The quantity α_m refers to the operating frequency $f > f_c$, which passes the $TE_{1,0}$ wave.

The above solution is in terms of the Poynting energy flux normal to the rectangular cross section of the guide, which upon integration, when expressed by the real value as in (915*f*) and (915*g*), gives the total average watts P_z across a guide cross section of ab square meters. The loss $\mathcal{L}_m$, according to (915*e*), is the *real* part of the Poynting energy flux entering normal to the inside metal guide faces. It is tacitly assumed that the respective current distributions are about of the same order of magnitude as for infinite conductivity. This is essentially the case, since the surface impedance of good conductors is small and given by $Z_s = R_s + jX_s = R_s + jR_s$, where $R_s = \sqrt{\mu\omega/2\sigma}$ ohms for $\omega/6.28$ in cycles per second, μ in henrys per meter, and σ in mhos per meter for the metal wall. This can be readily seen from the discussions in Sec. 230 and particularly from Eqs. (913), (913*d*), and (913*e*). The power entering *normal* to a 1-sq-m metal plane is then $p_n = \frac{1}{2}R_s|H_t|^2 = \frac{1}{2}R_sH_t \cdot H_t^*$ watts, where H_t is the *tangential* magnetic field along the inside metal skin of the guide walls. We could also have used formula (915*d*), if applied to the $TE_{1,0}$ wave, for which formulas (914*h*) and (915*b*) are basic for the denominator and numerator of (915*d*). As far as the $\mathcal{L}$ expression in (915*b*) is concerned, the integral is to be taken around the inside guide surface. This was done also in the above example, since, in (915*e*), we integrate first from $y = 0$ to $y = b$ of the rectangular cross section. Then we integrate again over a length b in order to account for the opposite inside surface, which is parallel with the $\mathcal{E}_y$ vector and 1 m long along the axial direction Z of the guide. Hereafter, we integrate over the top width of a meters and the bottom width of a meters. This means that we cover the integral $\int dl_0$ over the *total* inside circumference $l_0 = 2a + 2b$ meters and for an area of $2(a + b)$ square meters, since the length along the Z direction is 1 m. Therefore, we did, in effect, what the second expression $\mathcal{L}_{TE_{1,0}}$ of (915*b*) gives more quickly. As far as the denominator of (915*d*) is concerned, we deal with twice the value given by (914*h*), which is the surface integral of the second of Eqs. (914*h*) applied to $TE_{1,0}$ waves. It is just as easy to apply (915*d*) to circular guides, since, according to Table 10, we use only the $F_1(r, \varphi)$ function for the cross section of the guide instead of the function $F_1(x,y)$ holding for a rectangular guide. We have then the transformations $x = r\cos\varphi$ and $y = r\sin\varphi$. The field distribution function is then

$$F_1(r,\varphi) = J_n(rK)\cos(n\varphi)$$
$$F_1(r,\varphi) = J_n(rK)\sin(n\varphi)$$

The comparisons for the guide wavelength λ_g, in the case of rectangular and circular guide cross sections, are given in Eqs. (405) and (406), where K is given by $K = \omega_c\sqrt{\mu\kappa}$ for any cross section and the phase constant along the guide by

$$\beta_z = \sqrt{\omega^2\mu\kappa - K^2}$$

for $f > f_c$ (for which case we are in the pass region of the guide), so that for a perfect dielectric within the guide, we have the attenuation $\alpha_z = 0$, since the propagation constant $\Gamma_z = j\beta_z$ for frequencies above the cutoff frequency (a guide is a high-pass feeder). According to step 24 of Table 10, we have also

Longitudinal field along the guide axis $= H_z = H_0 J_n'(rK)\cos(n\varphi)\epsilon^{-z\Gamma_z}$ for TE waves
Longitudinal field along the guide axis $= \mathcal{E}_z = \mathcal{E}_0 J_n(rK)\cos(n\varphi)\epsilon^{-z\Gamma_z}$ for TM waves
} leading to the formulas for circular guides

$$\left.\begin{aligned}
&\mathcal{E}_z = \mathcal{E}_0 J_n(rK)\epsilon^{j\tau}\cos(n\varphi);\\
&\mathcal{E}_z = \mathcal{E}_0 J_n(rK)\epsilon^{j\tau}\sin(n\varphi)\\
&H_r = -j\frac{n\mathcal{E}_0\epsilon^{j\tau}}{r\nu Z_0 K}J_n(rK)\sin(n\varphi);\\
&H_r = -j\frac{n\mathcal{E}_0\epsilon^{j\tau}}{r\nu Z_0 K}J_n(rK)\cos(n\varphi)\\
&H_\varphi = -j\frac{\mathcal{E}_0\epsilon^{j\tau}}{\nu Z_0}J_n'(rK)\cos(n\varphi);\\
&H_\varphi = -j\frac{\mathcal{E}_0\epsilon^{j\tau}}{\nu Z_0}J_n'(rK)\sin(n\varphi)\\
&\mathcal{E}_\varphi = Z_0\sqrt{1-\nu^2}\,H_r;\\
&\mathcal{E}_r = Z_0\sqrt{1-\nu^2}\,H_\varphi
\end{aligned}\right\}\text{ All relations for TM waves}$$

$$\left.\begin{aligned}
&H_z = H_0\epsilon^{j\tau}J_n(rK)\cos(n\varphi);\\
&H_z = H_0\epsilon^{j\tau}J_n(rK)\sin(n\varphi)\\
&\mathcal{E}_r = j\frac{nZ_0H_0\epsilon^{j\tau}}{r\nu K}J_n(rK)\sin(n\varphi);\\
&\mathcal{E}_r = j\frac{nZ_0H_0\epsilon^{j\tau}}{r\nu K}J_n(rK)\cos(n\varphi)\\
&\mathcal{E}_\varphi = j\frac{Z_0}{\nu}H_0\epsilon^{j\tau}J_n'(rK)\cos(n\varphi);\\
&\mathcal{E}_\varphi = j\frac{Z_0}{\nu}H_0\epsilon^{j\tau}J_n'(rK)\sin(n\varphi)\\
&H_\varphi = \frac{\sqrt{1-\nu^2}}{Z_0}\mathcal{E}_r;\\
&H_r = -\frac{\sqrt{1-\nu^2}}{Z_0}\mathcal{E}_\varphi
\end{aligned}\right\}\text{ All relations for TE waves}$$

(916)

$$K = 2\pi f_c \sqrt{\mu\kappa} \text{ for } f_c \text{ in cycles/sec}; \qquad J'_n(rK) = \frac{d[J_n(rK)]}{d(rK)}$$

The radius of the circular guide cross section is a meters. We have

$$K = \frac{k_{n,m}}{a} = K_{n,m} \qquad \text{for TM waves}$$

$$K = \frac{k'_{n,m}}{a} = K'_{n,m} \qquad \text{for TE waves}$$

$$\lambda_c = \frac{2\pi}{K} = \frac{2\pi a}{k'_{n,m}} \qquad \text{for TE waves}$$

$$\lambda_c = \frac{2\pi a}{k_{n,m}} \qquad \text{for TM waves} \tag{916}$$

For details consult Table 10, step 25, which gives numerical values for $k_{n,m}$ and $k'_{n,m}$; $\tau = \omega t - \beta_z z$;

$$\beta_z = \sqrt{\omega^2\mu\kappa - K^2}; \qquad \nu = \frac{f_c}{f}; \qquad f_c = \frac{K}{2\pi\sqrt{\mu\kappa}} \text{ cycles/sec}$$

$$f_c = 3 \times 10^8 \frac{K}{6.28} \text{ for air as guide dielectric with } Z_0 = \sqrt{\frac{\mu}{\kappa}} \cong 376.7 \text{ ohms}$$

The application of (915d) then includes the use of (914h) and (915b), which for circular guides and $TM_{n,m}$ waves, for

$$A = \frac{q}{2Z_0} = \frac{\sqrt{1-\nu^2}}{2Z_0\nu^2},$$

yield

$$\begin{aligned} P_z &= A \int\int_{S=\pi a^2} \mathcal{E}_z^2 \, dS \\ &= A \int_{\varphi=0}^{\varphi=2\pi} \int_{r=0}^{r=a} \mathcal{E}_0^2 J_n^2(rK) \epsilon^{j\tau} \cos^2(n\varphi) \underbrace{r d\varphi \, dr}_{dS} \\ &= A\mathcal{E}_0^2 \left[\int_{\varphi=0}^{\varphi=2\pi} \cos^2(n\varphi) \, d\varphi \right] \left[\int_{r=0}^{r=a} r J_n^2(rK) \, dr \right] \qquad \text{watts} \end{aligned}$$

But

$$\int_0^{2\pi} \cos^2(n\varphi) \, d\varphi = \left| \frac{1}{4n} - \sin(2n\varphi) + \frac{\varphi}{2} \right|_0^{2\pi}$$

$$= \frac{1}{4n} \overbrace{\sin(4\pi n)}^{\substack{=0 \text{ since} \\ n \text{ an integer}}} + \frac{2\pi}{2} - \overbrace{\left[\frac{1}{4n} \sin(0) + 0 \right]}^{=0} = \pi$$

$$\int_{r=0}^{r=a} r J_n^2(rK) \, dr = \frac{a^2}{2} \left\{ [J'_n(aK)]^2 + \left(1 + \frac{n^2}{r^2K^2} \right) J_n^2(aK) \right\}$$

but $J_n^2(aK) = 0$ for TM waves (step 20 of Table 10) and

$$\int_{r=0}^{r=a} r J_n^2(rK) \, dr = \tfrac{1}{2}a^2[J'_n(aK)]^2$$

Hence,

$$\left.\begin{aligned} P_z &= \frac{\pi}{2}\, a^2[J_n'(aK)]^2 A\mathcal{E}_0^2 = \frac{\pi\sqrt{1-\nu^2}}{4Z_0\nu^2}\, a^2\mathcal{E}_0^2[J_n'(aK)]^2 \quad \text{watts} \\ \nu &= \frac{f_c}{f}; \qquad Z_0 = \sqrt{\frac{\mu}{\kappa}} \end{aligned}\right\} \tag{916a}$$

For the abbreviation $B = \frac{1}{2}[R_s/(\nu K Z_0)^2]$, we find, from (915*b*) and (916), the metal loss in watts per 1 m length of the circular guide

$$\mathfrak{L}_m^{(\text{watts/m})} = B\oint\left(\frac{\partial\mathcal{E}_z}{\partial n}\right)^2 dl = B\oint_{\varphi=0}^{\varphi=2\pi} K^2\mathcal{E}_0^2[J_n'(aK)]^2\cos^2(n\varphi)\underbrace{a\,d\varphi}_{dl}$$

since we have to take the *normal* derivative of $\mathcal{E}_z$ *at* the *inner* metal surface of the guide cylinder of a meter radius, yielding

$$\frac{\partial\mathcal{E}_z}{\partial n} = [K\mathcal{E}_0 J_n'(rK)\cos(n\varphi)]_{r=a}$$

Since the integration must be made around the inside cylinder surface, 1 m in axial length, the line element dl_0 is $a\,d\varphi$, and only the cosine^2 function remains under the integral. We have then

$$\mathfrak{L}_m = aBK^2\mathcal{E}_0^2[J'(aK)]^2\underbrace{\oint_{\varphi=0}^{\varphi=2\pi}\cos^2(n\varphi)\,d\varphi}_{=\pi\text{ as above}} = \pi aBK^2\mathcal{E}_0^2[J'(aK)]^2 \quad \text{watts/m} \tag{916b}$$

For the TM wave in a circular guide, we have the attenuation

$$\left.\begin{aligned} \alpha_m^{(\text{nepers/m})} &= \frac{\mathfrak{L}_m}{2P_z} = \frac{\pi aBK^2\mathcal{E}_0^2[J_n'(aK)]^2}{2\dfrac{\pi\sqrt{1-\nu^2}}{4Z_0\nu^2}\, a^2\mathcal{E}_0^2[J_n'(aK)]^2} = \frac{2Z_0K^2\nu^2}{a\sqrt{1-\nu^2}}B \\ &= \frac{2Z_0K^2\nu^2}{a\sqrt{1-\nu^2}}\frac{R_s}{2K^2Z_0^2\nu^2} = \frac{R_s}{aZ_0\sqrt{1-\nu^2}} \quad \text{nepers/m} \\ Z_0 &= \sqrt{\frac{\mu}{\kappa}} \quad \text{ohms } (=376.7 \text{ ohms for air}); \qquad \nu = \frac{f_c}{f} \\ f_c &= \frac{10^{-6}K}{6.28\sqrt{\mu\kappa}} \text{ Mc/sec}; \quad f_c = 47.8K \text{ Mc/sec for air inside guide} \end{aligned}\right\} \tag{916c}$$

where K is as in (916) and Table 10.

233. Dielectric Energy Dissipation and Attenuation in Wave Guides Due to an Imperfect Dielectric within the Guide. The propagation constant Γ_z, together with the timing ωt at the wave origin, causes the factor $\epsilon^{j\omega t - z\Gamma_z}$ when a wave moves along the Z direction. According to the flow function ψ of Sec. 57, we have $\psi = F_1(x, y)F(z)$ and find the expression of Eq. (404). This is applied to TE and TM waves in step 10 of Table

10, where the cross-section factor is $F_1(x, y)$ for rectangular guides and $F_1(r, \varphi)$ for cylindric wave guides. We have then the propagation constant along the guide (along the Z direction), for a perfect conductivity of the walls,

$$\left.\begin{aligned} \Gamma_z &= \sqrt{K^2 - \omega^2\mu\kappa} && \text{for a perfect dielectric} \\ \Gamma_z &= \sqrt{K^2 - \omega^2\mu\kappa_e} && \text{for a dissipative dielectric wave-guide medium} \end{aligned}\right\} \quad (917)$$

where

$$\left.\begin{aligned} K &= \sqrt{\left(\frac{m\pi}{a}\right)^2 + \left(\frac{n\pi}{b}\right)^2} && \text{for a rectangular guide (step 19 of Table 10)} \\ K &= \frac{R'}{a} && \text{for TE waves} \\ K &= \frac{R}{a} && \text{for TM waves} \end{aligned}\right\} \quad \text{for circular guides (step 25 of Table 10)} \quad (917a)$$

where a and b in meters are the guide dimensions along X and Y directions of rectangular guides, a is the meter radius for a circular guide, $\omega/6.28$ is in cycles per second, μ is in henrys per meter, κ is in farads per meter, $\kappa_e = \kappa - j(\sigma/\omega)$ in farads per meter, and σ is in mhos per meter for a dissipative guide medium. Since K^2 and $\omega^2\mu\kappa$ are always real values, the value of Γ_z for a perfect guide dielectric becomes

$$\left.\begin{aligned} \Gamma_z &= j\beta_z = j\sqrt{\omega^2\mu\kappa - K^2} && \text{for } K < \omega\sqrt{\mu\kappa} \text{ or } f > f_c \\ \Gamma_z &= \alpha_z = \sqrt{K^2 - \omega^2\mu\kappa} && \text{for } K > \omega\sqrt{\mu\kappa} \text{ or } f < f_c \\ f_c &= \frac{10^{-6}K}{6.28\sqrt{\mu\kappa}} && \text{Mc/sec} \end{aligned}\right\} \quad (917b)$$

where the cutoff frequency is found from the condition for which the value under the square root vanishes ($K^2 = \omega_c^2\mu\kappa$). We have then, as with high-pass filters, a region for which TE and TM waves pass without inherent attenuation ($f > f_c$) and a region for which $\Gamma_z = \alpha_z$ nepers per meter ($f < f_c$); the hollow tube behaves like a pure attenuator. The attenuation α_z has *nothing* to do with the α_m value discussed in Sec. 232, since the α_m attenuation is due to metal losses and belongs to the $f > f_c$ range of operating frequencies.

When we have a *dissipative* dielectric within the guide (σ mhos per meter in addition to μ henrys per meter and κ farads per meter), we must have medium dissipation at *all* possible frequencies, owing to dielectric losses. This means that we can *no longer* have a *sharp cutoff*, as for

perfect wave mediums. This can be seen from the second of Eqs. (917), which can be written as

$$\Gamma_z = \sqrt{K^2 - \omega^2\mu\kappa_e} = \sqrt{K^2 - \omega^2\mu\left(\kappa - j\frac{\sigma}{\omega}\right)} = \sqrt{K^2 - \omega^2\mu\kappa + j\omega\mu\sigma} = \alpha_z + j\beta_z \quad (917c)$$

since $K^2 - \omega^2\mu\kappa + j\omega\mu\sigma$ can never completely vanish. Since the value under the square-root sign holding for any operating frequency f is complex, it can, at best, yield only a *minimum* value. The condition for this minimum may be referred to a *pseudo* cutoff frequency. A low-quality wave medium is not likely to be used in a wave guide, and we can then assume a Q value, which is $Q = \omega\kappa/\sigma$ and large, for the wave medium within the guide. The pseudo cutoff frequency is then found from the condition for which the real part under the square root in (917*c*) vanishes. We then find $K^2 = \omega_c^2\mu\kappa$, as for a perfect wave medium. Writing (917*c*) for frequencies *f higher* than the cutoff frequency, we find

$$\begin{aligned}\Gamma_z &= j\sqrt{\omega^2\mu\kappa_e - K^2} = j\sqrt{\omega^2\mu\kappa - j\omega\mu\sigma - \omega_c^2\mu\kappa} \\ &= j\omega\sqrt{\mu\kappa}\sqrt{1 - j\frac{\omega\mu\sigma}{\omega^2\mu\kappa} - \frac{\omega_c^2\mu\kappa}{\omega^2\mu\kappa}} = j\omega\sqrt{\mu\kappa}\sqrt{1 - j\frac{\sigma}{\omega\kappa} - \left(\frac{f_c}{f}\right)^2} \\ &= j\omega\sqrt{\mu\kappa}\sqrt{(1 - \nu^2) - j\frac{\sigma}{\omega\kappa}} = \alpha_z + j\beta_z\end{aligned}$$

If we are not using an operating frequency f too close to the pseudo cutoff frequency f_c and realize that $j(\sigma/\omega\kappa) = j/Q$ is a very *small* absolute quantity compared with unity, we find, for the abbreviations $x = 1 - \nu^2$ and $y = -j/Q$,

$$\begin{aligned}\sqrt{(1 - \nu^2) - j\frac{\sigma}{\omega\kappa}} &= \sqrt{(1 - \nu^2) - \frac{j}{Q}} = \sqrt{x + y} = (x + y)^{1/2} \\ &= x^{1/2} + \frac{1}{2}x^{-1/2}y + \frac{\frac{1}{2}(\frac{1}{2} - 1)}{2}x^{-3/2}y^2 + \cdots \\ &= (1 - \nu^2)^{1/2} + \frac{1}{2}(1 - \nu^2)^{-1/2}\left(-\frac{j}{Q}\right) + \left(-\frac{1}{8}\right)(1 - \nu^2)^{-3/2}\frac{1}{Q^2} + \cdots \\ &= \sqrt{1 - \nu^2} - j\frac{1}{2\sqrt{1 - \nu^2}\,Q} - \underbrace{\frac{1}{8\sqrt{(1 - \nu^2)^3}\,Q^2} \cdots}_{\text{negligible}} \\ &\cong \sqrt{1 - \nu^2} - j\frac{\sigma}{2\omega\kappa\sqrt{1 - \nu^2}}\end{aligned}$$

Therefore,

$$\left.\begin{aligned}
\Gamma_z &= j\omega\sqrt{\mu\kappa}\sqrt{(1-\nu^2)-j\frac{\sigma}{\omega\kappa}} \\
&\cong j\omega\sqrt{\mu\kappa}\left(\sqrt{1-\nu^2}-j\frac{\sigma}{2\omega\kappa\sqrt{1-\nu^2}}\right) \\
&= j\omega\sqrt{\mu\kappa}\sqrt{1-\nu^2}+\frac{\omega\sqrt{\mu\kappa}\,\sigma}{2\omega\kappa\sqrt{1-\nu^2}} \\
\Gamma_z &= \underbrace{\frac{\sigma Z_0}{2\sqrt{1-\nu^2}}}_{\alpha_d}+\underbrace{j\omega\sqrt{\mu\kappa}\sqrt{1-\nu^2}}_{j\beta_z}=\alpha_z+j\beta_z \\
Z_0 &= \sqrt{\frac{\mu}{\kappa}}\ \text{ohms}; \qquad \nu=\frac{f_c}{f}; \qquad f_c=\frac{10^{-6}K}{6.28\sqrt{\mu\kappa}}\ \text{Mc/sec} \\
&\qquad\qquad\qquad\qquad\qquad\qquad\qquad\qquad \alpha_z=\alpha_d
\end{aligned}\right\} \quad (917d)$$

In the pass region ($f > f_c$) with the operating frequency f not too close to the cutoff frequency f_c, for a dissipative guide medium with a high Q value (which is easy to meet practically), we have an attenuation due to dielectric losses of

$$\alpha_d = \frac{\sigma Z_0}{2\sqrt{1-(f_c/f)^2}} \ \text{nepers/m guide length}; \quad Z_0=\sqrt{\frac{\mu}{\kappa}}\ \text{ohms} \quad (917e)$$

where μ is in henrys per meter, κ in farads per meter, σ in mhos per meter. We have then a total attenuation of $\alpha_m + \alpha_d$ nepers per meter, for a finite conductivity of the guide wall and some dissipation in the inside dielectric. The attenuation α_d due to dielectric wave-medium losses is *independent* of the *shape* of the cross section and depends only on the volume of the wave medium per meter length of the guide. This volume is not directly seen in (917*e*) but is indicated by the ratio f_c/f, since f_c depends on the mode of excitation and its *magnitude* is *affected by the dimensions* of a rectangular guide or the radius of a circular guide, respectively.[1]

234. Significant Properties of Waves in Guides, Characteristic Curves, and Formulas for Attenuation. For alternating-current phenomena, we are under the impression that *magnetic H* lines of force are *always closed* while the *electric* $\mathcal{E}$ lines of force terminate on opposite charges, *i.e.*, at surfaces of conductors. So far, experiments show that magnetic *H lines are always closed*, regardless of the frequency range and modes of waves. Magnetic H lines loop around conduction currents as well as displacement currents. For complementary waves, such as TE

[1] With respect to attenuation below the cutoff frequency and near this frequency, reference is made to E. G. Linder, *Proc. IRE*, **30**, 554, December, 1942.

and TM waves, we found that electric $\mathfrak{E}$ lines *may also be closed*, though not always, since a longitudinal $\mathfrak{E}_z$ field for a TM wave is due to *open* $\mathfrak{E}$ lines starting somewhere on inside metal points and terminating somewhere farther down on the inside metal wall of a guide. Closed $\mathfrak{E}$ lines require a variable H field. Equations (1) in this text verify that we may have closed $\mathfrak{E}$ lines as well as H lines, since these equations refer to a curl $\mathfrak{E}$ and a curl H. A "curl" means a "whirling around." In a wave medium, we cannot have one curl without the other curl. These curls belong together. It is, as it were, the electromagnetic Castor and Pollux, the constellation of Gemini. The reason we often overlook complementary modes of waves in customary alternating-current networks is that the transverse dimensions of supply lines, for instance, are so small in comparison with the wavelength λ that the corresponding cutoff wavelength λ_c is altogether too short. The higher modes can then, at best, display themselves only as *end effects* ($f < f_c$). We then realize that we have slight field distortions at the terminations. In wave guides, we always have at least one field that is also longitudinal with respect to the wave propagation. The *longitudinal field*, so to speak, *substitutes* the *missing return conductor*. That this must be the case we note, for instance, in the field configuration of a TM guide wave. For a circular guide, we have circular H lines around the guide axis, which extend to the very inner surface of the cylindrical metal wall. Since the H lines can, at best, be only tangent, no current on the metal wall could cause them, since the H loops do not cut the conductor. *But* the longitudinal electric field causes a longitudinal displacement current, around which we have such circular H lines. In exactly the same way, we have, for TE waves in circular guides, circular $\mathfrak{E}$ lines around the longitudinal H field, since this field causes a corresponding magnetic displacement current, which is also longitudinal.

For a rectangular guide excited in the $TE_{1,0}$, we have a constant transverse wave configuration, for which the electric field excitation is usually along the smaller side of the cross section. The charge densities are then always along the inner wider sides of the guide. This mode depends only on the longer a dimension (Fig. 379) of the cross section. Since this mode is *independent of the smaller b dimension*, other complementary waves can be avoided without seriously increasing the attenuation α_m due to metal losses if compared with other modes and guides of about the same cross section. *However*, the b dimension should *not* be chosen *too small*, since otherwise the α_m value will increase too much. The voltage gradient between the upper and lower surfaces will then also become larger and may give rise to a voltage breakdown. The $TE_{1,1}$ dominant mode of a circular guide is likewise a much *preferred* type of

wave excitation. Generally, it is important to prevent other complementary waves from passing through the guide. The $TM_{0,1}$ mode in circular guides is circularly symmetrical, and it makes no difference if the field rotates (spirals) as it progresses along the guide. For a contour length of 3π inches, for a circular cross section of a guide, we have

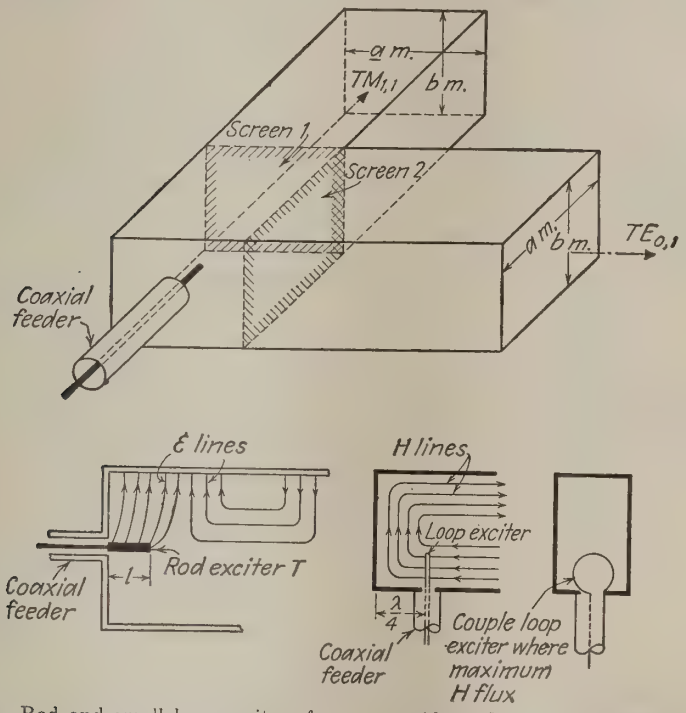

FIG. 380. Rod and small loop exciters for wave guides. T is a short linear rod wave exciter. With metal screen 1 in place but screen 2 removed, we excite $TE_{0,1}$ waves; with metal screen 2 in place but screen 1 removed, we excite $TM_{1,1}$ waves, since a longitudinal $\mathcal{E}$ field causes transverse H circulations around T. The length l is different for different sizes of guide and exciter frequency.

$f_c = 2{,}310$ Mc/sec for $TE_{1,1}$ waves in a circular guide and $f_c = 3{,}020$ Mc/sec for a $TM_{0,1}$ wave in the same guide. But for a $TE_{0,1}$ wave with a square cross section, we find $f_c = 3{,}070$ Mc/sec. The $TM_{0,1}$ mode requires then a size more than sufficient for the $TE_{1,1}$ mode. Therefore, both modes may accidentally pass along the guide, even though only the $TM_{0,1}$ mode is desired. Nevertheless, since the $TM_{0,1}$ mode is circularly symmetrical, it has the *inherent advantage* that it can be placed anywhere on the circumference of the guide for transmitting or receiving purposes. We note that there is not much difference between the cutoff value for the square guide with the $TE_{0,1}$ excitation and the circular

guide with the $TM_{0,1}$ mode. However, the square-type guide has a cutoff frequency dependent only on *one* dimension, the side length normal to the $\mathcal{E}$ field. It may then pass the given mode in two positions with transverse $\mathcal{E}$ lines in space quadrature if not exactly normal. This is not a feature when used for receiving, since the detector adaptor to the square incoming guide is fixed and can utilize only one polarization. This is the reason why the $TE_{1,0}$ excitation is *preferred* and the a dimension normal to the $\mathcal{E}$ lines is made slightly larger than the critical value required for the cutoff frequency. The b dimension (parallel with the $\mathcal{E}$ lines) is made slightly smaller. A ratio $a/b \cong 1.18$ is then a good value. Besides making changes in the relative dimensions with respect to causing only one mode to pass and preventing a mode that is in space quadrature with respect to the desired polarization, we also have to take into account the value of α_m. There exist minimum α_m values, which are different for various sizes of guides and various modes. Thus the $TE_{1,1}$ mode has a smaller α_m value than the $TM_{0,1}$ mode. If the length of the guide is relatively short, the effect of α_m can be overlooked if mode discrimination can be obtained by a change of the dimension. With respect to excitations of certain modes, reference is made to Figs. 374, 380, and 381. In Fig. 382, we have an electromagnetic horn with a rectangular mouth and driven with the fixed polarization of the $TE_{1,0}$ mode. It is not practical to use a rectangular guide all the way up to the point where the horn is located, and especially when picking up stations or spotting particular receiver locations. For such operations, the vertical guide must be rotated about its axis. We then use a cylindrical guide for the guide section, which can be rotated and in the $TM_{0,1}$ excitation; while on either side of this guide, we convert to rectangular guides with the $TE_{1,0}$ excitation. Figure 382 also shows a polarization shifter, bends and twists in rectangular guides, as well as a matching section between rectangular guides of different sizes. As in the case of linear radiators, the

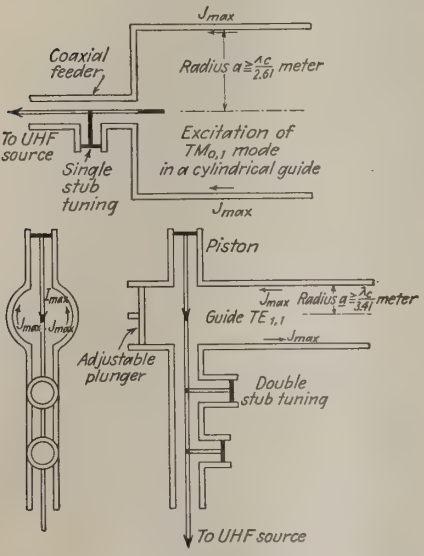

FIG. 381. Excitation of cylindrical guides by means of a coaxial feeder and an exposed inside wire section of the feeder. For air within the guide $f_c = 300/\lambda_c$ Mc/sec.

length of an electromagnetic horn, in terms of the operating wavelength, has much to do with the input impedance. We know that a linear radiator about 10 wavelengths long and driven at one end behaves as a very long electric line with an input impedance practically equal to the characteristical impedance of the radiator. This is also about the case for

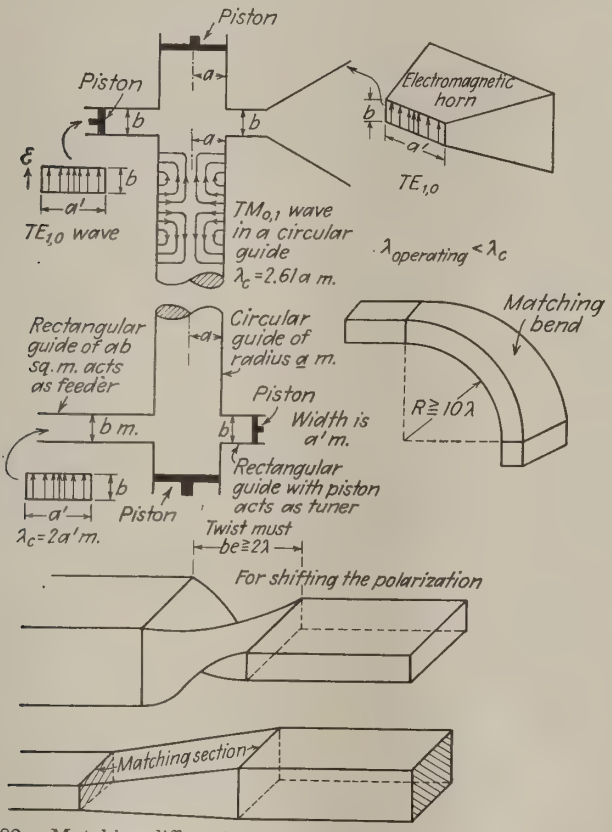

Fig. 382. Matching different cross sections and different modes of guides.

a horn of such a length in terms of the wavelength, and the guide becomes terminated in its characteristic impedance, so that we no longer have standing-wave patterns in the guide. Each half-wave portion radiates a certain amount of power and passes it on to the next half-wave section, etc., until at the end practically no energy is left. Table 87 gives the properties of some of the rectangular and circular wave guides. It shows how to compute the attenuation α_m due to metal losses. In this table, we can find the cutoff frequency for rectangular and circular guides, where for circular guides the numerical values of Step 25 of Table 10 are

TABLE 87. CHARACTERISTIC EXPRESSIONS FOR SOME GUIDES

Mode	Cross section	Fields	K	$\lambda_c = \frac{2\pi}{K}$ meters	$f_c = \frac{10^{-6}}{\lambda_c \sqrt{\mu\kappa}}$, Mc/sec	α_m, nepers/meter	Cutoff frequency $f_c = \frac{300}{\lambda_c}$ Mc/sec for air in the guide
$TE_{1,0}$ $m = 1; n = 0$	Rectangular	H_z, H_x, $\mathcal{E}_y$	$\frac{\pi}{a}$	$2a$	$\frac{10^{-6}}{2a\sqrt{\mu\kappa}}$	$\frac{1 + 2(b/a)\nu^2}{bZ_0\sqrt{1-\nu^2}} R_s$	$\frac{150}{a}$
$TE_{1,1}$ $m = 1; n = 1$	Rectangular	H_z, H_x, H_y $\mathcal{E}_x$, $\mathcal{E}_y$	$\frac{\pi\sqrt{a^2+b^2}}{ab}$	$\frac{2ab}{\sqrt{a^2+b^2}}$	$\frac{10^{-6}\sqrt{a^2+b^2}}{2ab\sqrt{\mu\kappa}}$	$\frac{2R_s}{bZ_0\rho}(A + \rho^2 B)$; $\rho = \sqrt{1-\nu^2}$; $A = \left(1 + \frac{b}{a}\right)\nu^2$; $B = \frac{\frac{b}{a}\left(\frac{b}{a}m^2 + n^2\right)}{\frac{b^2m^2}{a^2} + n^2}$; $TE_{1,1} = TE_{m,n}$ and use $m = 1$ and $n = 1$	$\frac{150\sqrt{a^2+b^2}}{ab}$
$TE_{2,1}$ $m = 2; n = 1$	Rectangular	H_z, H_x, H_y $\mathcal{E}_x$, $\mathcal{E}_y$	$\frac{\pi\sqrt{a^2+4b^2}}{ab}$	$\frac{2ab}{\sqrt{a^2+4b^2}}$	$\frac{10^{-6}\sqrt{a^2+4b^2}}{2ab\sqrt{\mu\kappa}}$	Use α_m expression for $TE_{1,1}$ for $m = 2$ and $n = 1$	$\frac{150\sqrt{a^2+4b^2}}{ab}$
$TE_{1,2}$ $m = 1; n = 2$	Rectangular	H_z, H_x, H_y $\mathcal{E}_x$, $\mathcal{E}_y$	$\frac{\pi\sqrt{4a^2+b^2}}{ab}$	$\frac{2ab}{\sqrt{4a^2+b^2}}$	$\frac{10^{-6}\sqrt{4a^2+b^2}}{2ab\sqrt{\mu\kappa}}$	Use α_m expression for $TE_{1,1}$ for $m = 1$ and $n = 2$	$\frac{150\sqrt{4a^2+b^2}}{ab}$

$TE_{2,2}$ $m = 2; n = 2$	Rectangular	H_z, H_x, H_y $\mathcal{E}_x$, $\mathcal{E}_y$	$\dfrac{2\pi\sqrt{a^2+b^2}}{ab}$	$\dfrac{ab}{\sqrt{a^2+b^2}}$	$\dfrac{10^{-6}\sqrt{a^2+b^2}}{ab\sqrt{\mu\kappa}}$	Use α_m expression for $TE_{1,1}$ for $m = 2$ and $n = 2$	$\dfrac{300\sqrt{a^2+b^2}}{ab}$
$TM_{1,1}$ $m = 1; n = 1$	Rectangular	$\mathcal{E}_z$, $\mathcal{E}_x$, $\mathcal{E}_y$ H_x, H_y	$\dfrac{\pi\sqrt{a^2+b^2}}{ab}$	$\dfrac{2ab}{\sqrt{a^2+b^2}}$	$\dfrac{10^{-6}\sqrt{a^2+b^2}}{2ab\sqrt{\mu\kappa}}$	$\dfrac{2R_s}{bZ_0\rho}\left[\dfrac{m^2\left(\dfrac{b}{a}\right)^3+n^2}{m^2\left(\dfrac{b}{a}\right)^2+n^2}\right]$ where $m = 1 = n$ and $\rho = \sqrt{1-\nu^2}$; $\nu = \dfrac{f_c}{f}$	$\dfrac{150\sqrt{a^2+b^2}}{ab}$
$TM_{2,1}$ $m = 2; n = 1$	Rectangular	$\mathcal{E}_z$, $\mathcal{E}_x$, $\mathcal{E}_y$ H_x, H_y	$\dfrac{\pi\sqrt{a^2+4b^2}}{ab}$	$\dfrac{2ab}{\sqrt{a^2+4b^2}}$	$\dfrac{10^{-6}\sqrt{a^2+4b^2}}{2ab\sqrt{\mu\kappa}}$	Above $TM_{1,1}$ general expression yields for $m = 2$ and $n = 1$ $\dfrac{2R_s\left[4\left(\dfrac{b}{a}\right)^3+1\right]}{bZ_0\rho\left[4\left(\dfrac{b}{a}\right)^2+1\right]}$	$\dfrac{150\sqrt{a^2+4b^2}}{ab}$
$TM_{2,2}$ $m = 2; n = 2$	Rectangular	$\mathcal{E}_z$, $\mathcal{E}_x$, $\mathcal{E}_y$ H_x, H_y	$\dfrac{2\pi\sqrt{a^2+b^2}}{ab}$	$\dfrac{ab}{\sqrt{a^2+b^2}}$	$\dfrac{10^{-6}\sqrt{a^2+b^2}}{ab\sqrt{\mu\kappa}}$	$\dfrac{8R_s[(b/a)^3+1]}{bZ_0\rho[(b/a)^2+1]}$ found from the general expression for $m = 2 = n$	$\dfrac{300\sqrt{a^2+b^2}}{ab}$

TABLE 87. CHARACTERISTIC EXPRESSIONS FOR SOME GUIDES.—(*Continued*)

Mode	Cross section	Fields	K	$\lambda_c = \frac{2\pi}{K}$ meters	$f_c = \frac{10^{-6}}{\lambda_c \sqrt{\mu\kappa}}$, Mc/sec	α_m, nepers/meter	Cutoff frequency $f_c = \frac{300}{\lambda_c}$ Mc/sec for air in the guide
$TE_{0,1}$ $n = 0; m = 1$	Circular	H_z, H_r, $\mathcal{E}_\varphi$	$\frac{3.83}{a}$ (from step 25 of Table 10)	$1.64a$	$\frac{0.609}{a\sqrt{\mu\kappa}} 10^{-6}$	$\frac{\nu^2 R_s}{aZ_0\sqrt{1-\nu^2}}$	$\frac{183}{a}$
$TE_{1,1}$ $n = 1; m = 1$	Circular	H_z, H_r, H_φ $\mathcal{E}_r$, $\mathcal{E}_\varphi$	$\frac{1.84}{a}$ (from step 25 of Table 10)	$3.41a$	$\frac{0.293}{a\sqrt{\mu\kappa}} 10^{-6}$	$\frac{R_s(\nu^2 + 0.42)}{aZ_0\sqrt{1-\nu^2}}$	$\frac{88}{a}$
$TM_{0,1}$ $n = 0; m = 1$	Circular	$\mathcal{E}_z$, $\mathcal{E}_r$, H_φ	$\frac{2.405}{a}$ (from step 25 of Table 10)	$2.61a$	$\frac{0.383}{a\sqrt{\mu\kappa}} 10^{-6}$	$\frac{R_s}{aZ_0\sqrt{1-\nu^2}}$	$\frac{115}{a}$
$TM_{0,2}$ $n = 0; m = 2$	Circular	$\mathcal{E}_z$, $\mathcal{E}_r$, H_φ	$\frac{5.52}{a}$ (from step 25 of Table 10)	$1.14a$	$\frac{0.877}{a\sqrt{\mu\kappa}} 10^{-6}$	$\frac{R_s}{aZ_0\sqrt{1-\nu^2}}$	$\frac{263}{a}$

$TM_{0,3}$ $n = 0; m = 3$	Circular	$\mathcal{E}_z$, $\mathcal{E}_r$, H_φ	$\frac{8.654}{a}$ (from step 25 of Table 10)	$0.724a$	$\frac{1.38}{a\sqrt{\mu\kappa}} 10^{-6}$	$\frac{R_s}{aZ_0\sqrt{1-\nu^2}}$	$\frac{415}{a}$
$TM_{1,1}$ $n = 1; m = 1$	Circular	$\mathcal{E}_z$, $\mathcal{E}_r$, $\mathcal{E}_\varphi$ H_r, H_φ	$\frac{3.832}{a}$ (from step 25 of Table 10)	$1.64a$	$\frac{0.609}{a\sqrt{\mu\kappa}} 10^{-6}$	$\frac{R_s}{aZ_0\sqrt{1-\nu^2}}$	$\frac{183}{a}$
$TM_{2,3}$ $n = 2; m = 3$	Circular	$\mathcal{E}_z$, $\mathcal{E}_r$, $\mathcal{E}_\varphi$ H_r, H_φ	$\frac{11.62}{a}$ (from step 25 of Table 10)	$0.54a$	$\frac{1.851}{a\sqrt{\mu\kappa}} 10^{-6}$	$\frac{R_s}{aZ_0\sqrt{1-\nu^2}}$	$\frac{556}{a}$

Remarks: For a slightly dissipative medium, f_c denotes the pseudo cutoff frequency and we have $8.686(\alpha_m + \alpha_d)$ db/meter.

For a rectangular guide, we have a m along the X direction and b m along the Y direction. For a circular cross section, a m is the radius of the metal cylinder (*inner* radius). The dielectric within the guide is taken perfect with the properties of κ farads/m and μ henrys/m, where $\mu = 1.257 \times 10^{-6}$ henry/m. $Z_0 = \sqrt{\mu/\kappa}$ ohms $\cong$ 376.7 ohms for air as the dielectric; $1/\sqrt{\mu\kappa}$ m/sec is the velocity of propagation in the "unguided" dielectric (*no* metal boundaries); $\nu = f_c/f = \lambda/\lambda_c$. The phase velocity $c' = v_z$ along the Z direction (direction of the guide) is $c' = 1/(\rho\sqrt{\mu\kappa})$ m/sec, where $\rho = \sqrt{1-\nu^2}$. The group velocity c'' is $c'' = 9 \times 10^{16}/c'$ m/sec. The guide wavelength λ_g m is as in formulas (405) and (406); R_s ohms is the surface resistance as in formula (913*e*). The attenuation α_m, due to metal losses, is given by formula (915*d*). Inherent attenuation α_z below the cutoff frequency ($f < f_c$) is

$$\alpha_z = K\sqrt{1-\left(\frac{1}{\nu^2}\right)} \text{ nepers/m} = 8.686K\sqrt{1-\left(\frac{1}{\nu^2}\right)} \text{ db/m};$$

K is as in Eqs. (917*a*) and step 25 of Table 10 for circular guides. Examples: A rectangular guide that is $a = 0.1$ m wide and $b = 0.08$ m high has then for a $TE_{1,0}$ excitation a cutoff frequency $f_c = 150/a = 150/0.1 = 1{,}500$ Mc/sec. For the $TE_{0,1}$ excitation, we have an $\mathcal{E}_z$ excitation, in place of the $\mathcal{E}_y$ excitation, and H_y and H_z fields, since $TE_{0,1} = TE_{m,n}$ and $m = 0$ and $n = 1$. The cutoff frequency is then $f_c = 150/b = 150/0.08 = 1{,}875$ Mc/sec. For the $TM_{1,1}$ mode we have

$$f_c = \frac{150\sqrt{0.1^2 + 0.08^2}}{0.1 \times 0.08} = \frac{150 \times 12.806 \times 10^{-2}}{8 \times 10^{-2}} = 2{,}402 \text{ Mc/sec}$$

utilized. It is the cutoff frequency that is of importance in the design of wave guides; and if the guide is not short, the attenuation α_m also must be taken into account, since there is quite a range in pass frequencies for a particular mode, and by a suitable selection of the excitation and guide dimension, for a particular operating frequency, the Q value of the guide can be kept high. We found that if the dielectric within the guide space also exhibits a certain conductivity σ mhos per meter, but such that $\omega\kappa/\sigma$ is large (a high figure of merit for the general complex wave medium), and we do not operate too close to the cutoff frequency f_c and not below it, we have also an additional attenuation α_d due to dielectric losses. The total guide attenuation loss in the pass region is then

$$\alpha = \alpha_m + \alpha_d \text{ nepers/m} = 8.686(\alpha_m + \alpha_d) \text{ db/m} \qquad (918)$$

where α_m is as in Eqs. (917*e*) and (915*d*) and Table 87. Inspecting Table 87, we note that the *cutoff frequency depends upon* the *mode* of operation *as well as the shape of the cross-sectional area of the guide.* For the modes and shapes specified in this table, the $TE_{1,1}$ mode, in a circular guide of radius a meters, gives the *lowest cutoff frequency*, which is $88/a$ megacycles per second. This means that the operating frequency f must be greater than 88 Mc/sec for a guide radius $a = 1$ m $= 39.37$ in. This is, *indeed, a very large circular opening* to justify a wave guide. The frequency must be larger than 183 Mc/sec for both the $TE_{0,1}$ and the $TM_{1,1}$ modes in a circular guide of the above-mentioned opening. Hence, if we choose the operating frequency $f = 150$ Mc/sec, for a desired $TE_{1,1}$ mode, this would *exclude* any $TE_{0,1}$ wave but gives the possibility of a $TM_{0,1}$ mode passing through the guide, since, for a 1-m radius, the frequency must be only above 115 Mc/sec. This requires, of course, that the $TM_{0,1}$ mode also be excited. For rectangular modes, we note that the $TE_{1,0}$ mode gives a cutoff frequency of $150/a$ megacycles per second, just as the $TE_{0,1}$ mode would give a cutoff frequency of $150/b$ megacycles per second. Therefore, by making the b dimension in meters (along the Y direction) somewhat smaller than the a dimension (along the X direction) and exciting the $TE_{1,0}$ mode with a rod tip along the Y direction and a frequency larger than $150/a$ megacycles per second, any slight $\mathcal{E}_x$ component of the desired $\mathcal{E}_y$ excitation can *never* give rise to a $TE_{0,1}$ mode along the guide, which is in the pass region of the guide. We have then *mode excitation discrimination* by choosing unequal sides and polarizing parallel with the shorter side b of the rectangular cross section. For the propagation constant Γ_z, phase velocity $c' = v_z$, and wavelength $\lambda_z = \lambda_g$ along the guide, for a pure dielectric within the guide ($\sigma = 0$ for wave medium), we have

$$\Gamma_z = j\beta_z = j\sqrt{\omega^2\mu\kappa - K^2} \qquad \text{for } f > f_c;$$

$$\omega_c^2\mu\kappa = K^2; \ [K \text{ as in } (917a)]$$

$$v_z = \frac{\omega}{\beta_z} = \frac{\omega}{\sqrt{\omega^2\mu\kappa - \omega_c^2\mu\kappa}} = \frac{1}{\sqrt{\mu\kappa}\sqrt{1-\nu^2}} \quad \text{m/sec}$$

$$\nu = \frac{f_c}{f} = \frac{\lambda}{\lambda_c}; \qquad \lambda_g = \frac{v_z}{f} = \frac{1}{f\sqrt{\mu\kappa}\sqrt{1-\nu^2}} \ \text{m}; \qquad \lambda_g f = v_z$$

$$\lambda f = \frac{1}{\sqrt{\mu\kappa}} \ \text{m/sec}; \qquad \lambda_g = \frac{\lambda}{\sqrt{1-\nu^2}}$$

$$\frac{\lambda}{\lambda_g} = \sqrt{1-\nu^2} = \sqrt{1-\left(\frac{f_c}{f}\right)^2} = \sqrt{1-\left(\frac{\lambda}{\lambda_c}\right)^2}$$

for all TE and TM complementary waves and shapes of all guides (918a)

Figure 383*a*, gives the relation for the ratio of the operating wavelength in the unbounded wave medium to the guided wavelength λ_g, as a function of ν. It can be seen that this relation is given by means of a circle in the quadrant formed by the positive ν and λ/λ_g axes. This relation holds for any guide and TE as well as TM waves provided we are in the

TABLE 88. COMPUTATIONS OF CUTOFF FREQUENCIES

a or b, m	*Rectangular* cross section		*Circular* cross section						
	$TE_{1,0}$	$TE_{0,1}$	$TE_{0,1}$	$TM_{1,1}$	$TE_{1,1}$	$TM_{0,1}$	$TM_{0,2}$	$TM_{0,3}$	$TM_{2,3}$
f_c, Mc/sec	$\frac{150}{a}$	$\frac{150}{b}$	$\frac{183}{a}$		$\frac{88}{a}$	$\frac{115}{a}$	$\frac{263}{a}$	$\frac{415}{a}$	$\frac{556}{a}$
0.01	15,000		18,300		8,800	11,500	26,300	41,500	55,600
0.02	7,500		9,150		4,400	5,750	13,150	20,750	27,800
0.03	5,000		6,100		2,933.33	3,833.3	8,766.7	13,833.3	18,533.3
0.04	3,750		4,575		2,200	2,875	6,575	10,375	13,900
0.05	3,000		3,660		1,760	2,300	5,260	8,300	11,120
0.06	2,500		3,050		1,466.7	1,916.7	4,383.3	6,916.7	9,266.7
0.07	2,143		2,614.3		1,257.7	1,642.8	3,757.1	5,928.5	7,942.8
0.0762 = 3 in.	1,970		2,400		1,155	1,510	3,450	5,440	7,310
0.09	1,667		2,033.3		977.8	1,277.8	2,922.2	4,611.1	6,177.8
0.10	1,500		1,830		880	1,150	2,630	4,150	5,560
0.12	1,250		1,525		733.3	958.3	2,191.6	3,458.3	4,633.3
0.14	1,071		1,307.1		628.6	821.4	1,878.5	2,964.3	3,971.4
0.16	937.5		1,143.7		550	718.75	1,643.3	2,593.7	3,475
0.18	833.3		1,016.7		488.9	638.9	1,461.1	2,305.5	3,088.9
0.20	750		915		440	575	1,315	2,075	2,780

Remarks: We have the conversions a m = 39.37a in. and a in. = $2.54 \times 10^{-2}a$ m. The relations $f = k/a$ are hyperbolas, and k stands for the various numerical factors, which are taken from Table 87.

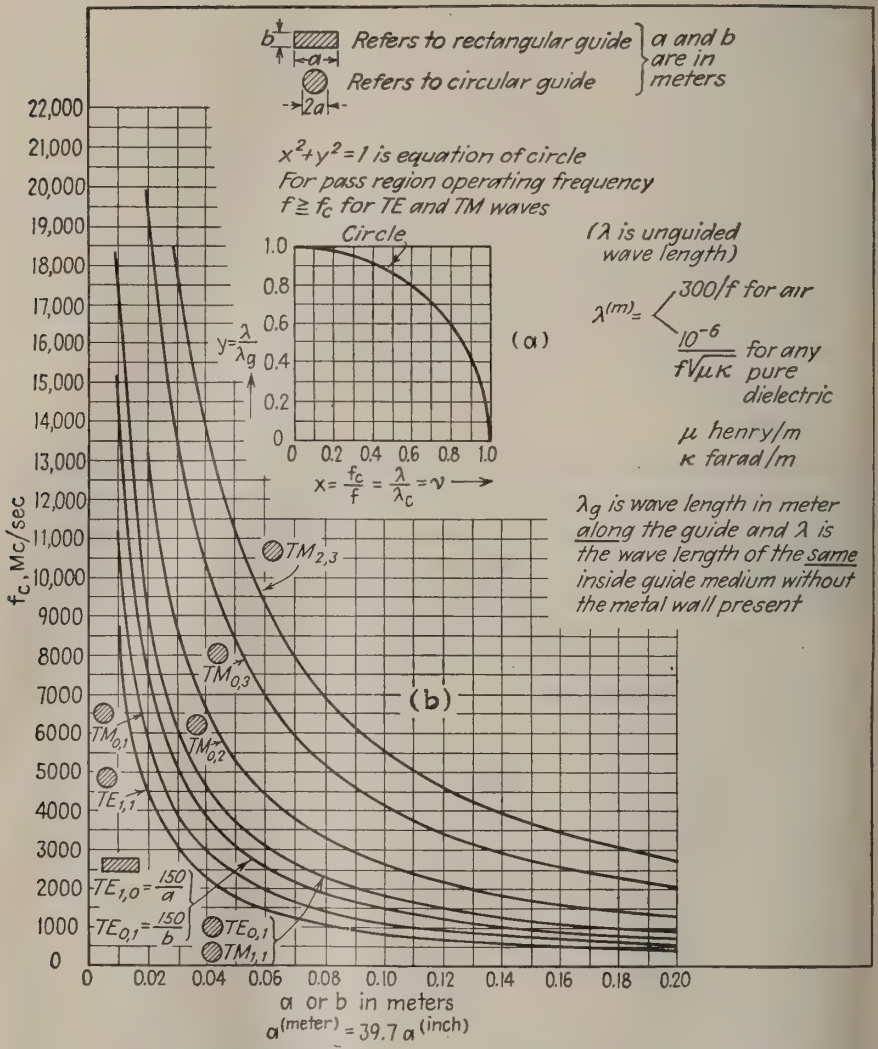

FIG. 383. Relations and curves for the cutoff frequency f_c. $x^2 + y^2 = 1$ is equation of a circle. For pass region operating frequency $f \geqq f_c$ for TE and TM waves. λ is unguided wavelength. $\lambda^{(m)} = 300/f$ for *air*, $\lambda^{(m)} = 10^{-6}/f\sqrt{\mu\kappa}$ *for any pure dielectric* of μ henrys/m and κ farads/m. λ_g is the wavelength in meters *along* the guide, and λ is the wavelength of the same guide medium without the metal walls present.

pass region ($f > f_c$). Figure 383*b* gives the cutoff frequency for typical rectangular and circular wave guides with respect to the dimension that determines this frequency. For more details, reference is made to Table 88. Figure 384*a* gives the relation between the surface resistance R_s of different guide materials based on formula (913*e*). Figure 384*b*

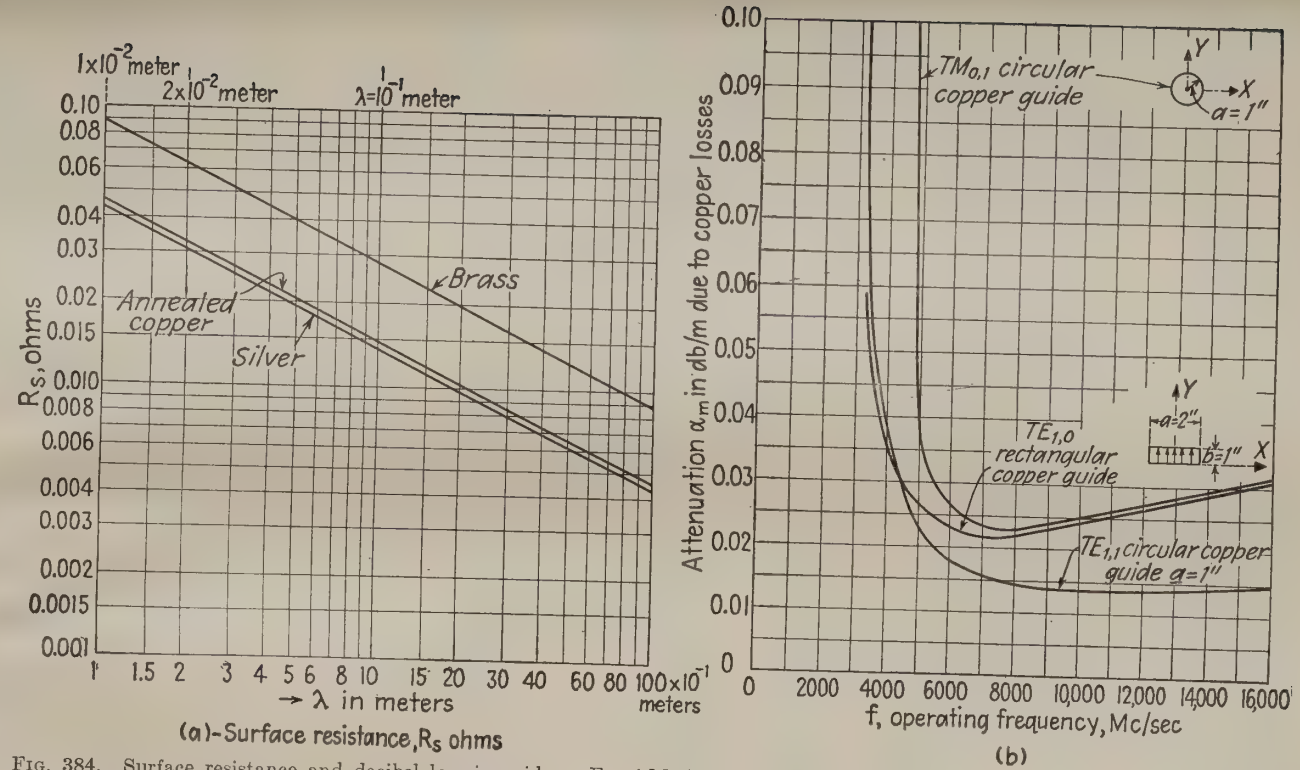

FIG. 384. Surface resistance and decibel loss in guides. For f Mc/sec as the operating frequency of the guide with medium of μ henrys/m and κ farads/m, $\lambda^{(m)} = 10^{-6}/(f\sqrt{\mu\kappa})$, $\lambda^{(m)} = 300/f$ for air within the guide.

shows the trend of the attenuation loss in decibels per meter guide length if annealed copper walls are used.

235. Notes on Wave Transmission in Coaxial Lines. As for hollow cylinders, we can have, in the space between the inner and the outer

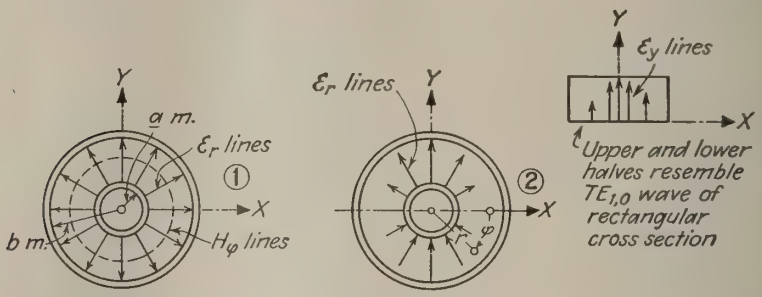

Principal TEM wave

$\lambda_c = \infty\,; f_c = 0$

All frequencies can pass

$TE_{1,1}$ wave

$\lambda_c = (a + b)\pi \cong$ mean circumference in meters

$$f_c = \frac{10^{-6}}{\lambda_c \sqrt{\mu\kappa}} \text{ Mc/sec}$$

μ henrys/m and κ farads/m medium within guide.

Since *circular* symmetry exists, all variations with respect to φ must *vanish*. For a pure dielectric medium ($\mu = \mu_0$, $\kappa = \kappa$ and $\sigma = 0$) the curl equations (138) read

$$\frac{\partial \mathcal{E}_z}{\partial \varphi} - r\frac{\partial \mathcal{E}_\varphi}{\partial z} = -j\omega\mu r H_r; \quad \frac{\partial H_z}{\partial \varphi} - r\frac{\partial H_\varphi}{\partial z} = j\omega r\kappa \mathcal{E}_r$$

$$\frac{\partial \mathcal{E}_r}{\partial z} - \frac{\partial \mathcal{E}_z}{\partial r} = -j\omega\mu H_\varphi; \quad \frac{\partial H_r}{\partial z} - \frac{\partial H_z}{\partial r} = j\omega\kappa \mathcal{E}_\varphi$$

$$\frac{\partial (r\mathcal{E}_\varphi)}{\partial r} - \frac{\partial \mathcal{E}_r}{\partial \varphi} = -j\omega\mu r H_z; \quad \frac{\partial (rH_\varphi)}{\partial r} - \frac{\partial H_r}{\partial \varphi} = j\omega r\kappa \mathcal{E}_z$$

The $\mathcal{E}$ field has only a radial transverse $\mathcal{E}_r$ component and $\mathcal{E}_\theta = 0$ if the concentric line is excited by a radial $\mathcal{E}_r$ field or by applying a voltage across the cylinders at one end, and we find

$$-\frac{\partial H_\varphi}{\partial z} = j\omega\kappa \mathcal{E}_r \text{ (I)}$$

$$\frac{1}{r}\left[\frac{\partial (rH_\varphi)}{\partial r}\right] = j\omega\kappa \mathcal{E}_z \text{ (II)}$$

$$\frac{\partial \mathcal{E}_r}{\partial z} - \frac{\partial \mathcal{E}_z}{\partial r} = -j\omega\mu H_\varphi \text{ (III)}$$

basic for transverse $\mathcal{E}$ waves. It leads to

$$\frac{\partial^2 \mathcal{E}_z}{\partial r^2} + \frac{1}{r}\frac{\partial \mathcal{E}_z}{\partial r} + K^2 \mathcal{E}_z = 0$$

$$K = \Gamma_z^2 + \mu\kappa\omega^2$$

$$\mathcal{E}_z = A_n J_n(rK) - B_n N_n(rK)$$

FIG. 385. Conditions for waves in a concentric line.

cylinders of a concentric line, TM as well as TE waves if the operating frequency f is above the respective cutoff frequency. Normally, such lines are used for the propagation of TEM waves, since we have a go and a return conductor. Even though TEM waves have no restrictions as to operating frequency, at very high UHF's, the transverse dimension of a coaxial opening may be large enough for complementary waves to be excited also and to pass along the inner dielectric space. For instance, a customary 1⅝-in. coaxial line would give rise to complementary guide excitations in the 3,000-Mc/sec band, while a ½-in. concentric line would

do the same thing in the 10,000-Mc/sec band. It is, therefore, not advisable to expect a pure transverse electromagnetic excitation for such coaxial lines in the above-mentioned frequency ranges. As with hollow cylinders, we may have complementary waves with radial variations and waves with circumferential variations in addition to the possible TEM, or principal, waves. A transmission mode in any double line, such as a coaxial line, may then be any of the TEM, TE, and TM types, for which a wave of *fixed* operating frequency is propagated without a change in form along the dielectric space bounded by respective metal cylinders. For the circumferential $TE_{n,m}$ mode, for which $n = 1$ and $m = 1$, the cutoff wavelength λ_c is about equal to the mean circumference $\pi(a + b)$ meters (Fig. 385), while for any nth order, where $n = 1, 2, 3, 4, 5, \cdots$, $\lambda_c \cong [\pi(a + b)]/n$ meters. The dominant TM wave has a cutoff wavelength $\lambda_c \cong 2(b - a)$ meters. It is equal to $b - a$ meters for the next higher order; $[2(b - a)]/3$ for the third order; etc.

Suppose we proceed with the relations (I), (II), and (III) of Fig. 385. The phase factor along the common axis (Z axis) is then $\epsilon^{j\omega t - z\Gamma_z}$, changing the relations to

$$\Gamma_z H_\varphi = j\omega\kappa \mathcal{E}_r \quad \text{(Ia)}; \qquad r\frac{\partial H_\varphi}{\partial r} + H_\varphi = j\omega\kappa r \mathcal{E}_z \quad \text{(IIa)}; \qquad \Gamma_z \mathcal{E}_r + \frac{\partial \mathcal{E}_z}{\partial r} = j\omega\mu H_\varphi \quad \text{(IIIa)}$$

Inasmuch as for guide action the $\mathcal{E}_z$ component acts, in effect, as a return for a complementary wave, we express it in terms of any radial distance r within the space between the conducting cylindrical surfaces. We find then

$$\mathcal{E}_r = \frac{\Gamma_z H_\varphi}{j\omega\kappa} \quad \text{(Ib)}; \qquad \frac{\Gamma_z^2 H_\varphi}{j\omega\kappa} + \frac{\partial \mathcal{E}_z}{\partial r} = j\omega\mu H_\varphi \qquad \text{(IIIb)}$$

or

$$H_\varphi\left(j\omega\mu - \frac{\Gamma_z^2}{j\omega\kappa}\right) = \frac{\partial \mathcal{E}_z}{\partial r} \qquad \text{or} \qquad H_\varphi = -j\frac{\omega\kappa(\partial \mathcal{E}_z/\partial r)}{\omega^2\mu\kappa + \Gamma_z^2}$$

$$\frac{\partial H_\varphi}{\partial r} = -j\underbrace{\frac{\omega\kappa}{\omega^2\mu\kappa + \Gamma_z^2}}_{=K^2}\frac{\partial^2 \mathcal{E}_z}{\partial r^2} \qquad \text{(IIIc)}$$

Using the H_φ and $\partial H_\varphi/\partial r$ terms in (IIa) yields

$$-j\frac{\omega\kappa r}{K^2}\frac{\partial^2 \mathcal{E}_z}{\partial r^2} - j\frac{\omega\kappa}{K^2}\frac{\partial \mathcal{E}_z}{\partial r} = j\omega\kappa r \mathcal{E}_z$$

or

$$\left.\begin{aligned} &\frac{\partial^2 \mathcal{E}_z}{\partial r^2} + \frac{1}{r}\frac{\partial \mathcal{E}_z}{\partial r} + K^2 \mathcal{E}_z = 0 \qquad \text{Bessel equation} \\ &\underbrace{\mathcal{E}_z = A_n J_n(rK) + B_n N_n(rK)}_{\text{Bessel solution}} \end{aligned}\right\} \qquad (919)$$

where $J_n(rK)$ is the Bessel function of the nth order with the argument rK and $N_n(rK)$ is the corresponding Neumann function.

Inasmuch as the differential equation (919) as well as the differential equations (I), (II), and (III) in Fig. 385 are the basic relations, we have TM waves, since we also have a longitudinal component $\mathcal{E}_z$. For such waves, according to Table 10, the boundary conditions require that *along* perfect metal skins, at $r = a$ and $r = b$ meters, the tangential $\mathcal{E}_z$ field *must vanish*. Hence,

$$\left.\begin{aligned} \mathcal{E}_{z_a} &= A_n J_n(aK) + B_n N_n(aK) = 0 \\ \mathcal{E}_{z_b} &= A_n J_n(bK) + B_n N_n(bK) = 0 \\ \frac{J_n(aK)}{N_n(aK)} &= \frac{J_n(bK)}{N_n(bK)} \end{aligned}\right\} \qquad (919a)$$

For TE waves, a longitudinal H_z component and $\partial H_z/\partial n$ *normal* to the metal skins *must vanish*. This leads to

$$\left.\begin{aligned} A'_n J'_n(aK) + B'_n N'_n(aK) &= 0; \qquad A'_n J'_n(bK) + B'_n N'_n(bK) = 0 \\ \frac{J'_n(aK)}{N'_n(aK)} &= \frac{J'_n(bK)}{N'_n(bK)} \\ J'_n(x) &= \frac{\partial[J_n(x)]}{\partial x}; \qquad N'_n(x) = \frac{\partial[N_n(x)]}{\partial x} \end{aligned}\right\} \qquad (919b)$$

Equations (919*a*) and (919*b*) are transcendental and yield, in terms of respective radii a and b, the K value, from which we find

$$\lambda_c = \frac{2\pi}{K} \text{ m}; \qquad f_c = \frac{K}{2\pi\sqrt{\mu\kappa}} 10^6 \text{ Mc/sec} \qquad (919c)$$

For TM waves, we find, from the $\mathcal{E}_{z_a}$ and $\mathcal{E}_{z_b}$ relations of (919*a*),

$$\left.\begin{aligned} &\frac{A_n}{B_n} = -\frac{N_n(bK)}{J_n(bK)} = \frac{N_n(aK)}{J_n(aK)} \\ &\text{For } n = 0 \text{ and large arguments } x = aK \text{ and } x = bK, \text{ respectively, we have the approximations} \\ &J_0(x) \cong \pm\sqrt{\frac{2}{\pi x}}\cos\left(x - \frac{\pi}{4}\right) \qquad \text{for } x \geqq 10 \qquad \text{and} \\ &\qquad\qquad N_0(x) \cong \pm\sqrt{\frac{2}{\pi x}}\sin\left(x - \frac{\pi}{4}\right) \\ &\frac{A}{B} = -\frac{\sin\left(aK - \frac{\pi}{4}\right)}{\cos\left(aK - \frac{\pi}{4}\right)} = \frac{\sin\left(bK - \frac{\pi}{4}\right)}{\cos\left(bK - \frac{\pi}{4}\right)} \qquad \text{or} \\ &\qquad\qquad n\pi + aK - \frac{\pi}{4} = bK - \frac{\pi}{4} \\ &K(b - a) = n\pi; \qquad K = \frac{n\pi}{b - a}; \qquad \Gamma_z = \sqrt{\left(\frac{n\pi}{b - a}\right)^2 - a^2\mu\kappa} \end{aligned}\right\} \qquad (919d)$$

236. Essentials on Cavity Resonators. A resonant cavity is a closed metallic space tank in which electric and magnetic fields are excited and emphasized by virtue of a natural excitation. Also here we may have a hollow circular and a hollow rectangular cavity space. We have, in

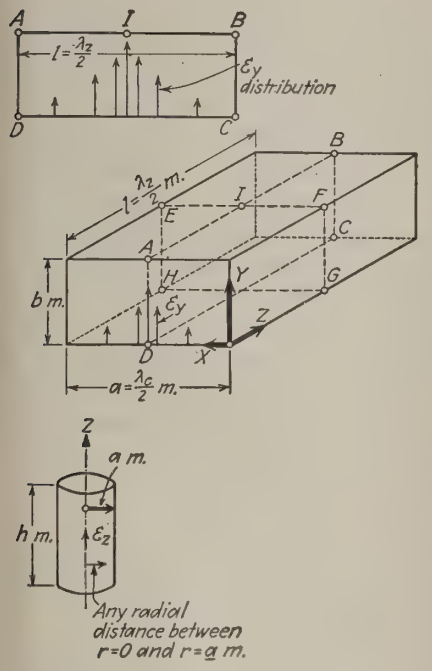

λ_z is the wavelength along the guide (along Z axis). $\beta_z = 2\pi/\lambda_z = \sqrt{\omega^2\mu\kappa - K^2}$; $K^2 = \omega_c\mu\kappa$; μ henrys/m and κ farads/m characterize the pure dielectric medium within the guide

$$\lambda_z = \frac{2\pi}{\beta_z} = \frac{2\pi}{\sqrt{\omega^2\mu\kappa - \omega_c{}^2\mu\kappa}}$$

$\omega/(2\pi)$ is the operating frequency f in cycles/sec. For a $TE_{1,0}$ excitation causing $TE_{1,0,1}$ cavity resonance: from above

$$\lambda_z = \frac{2\pi}{\omega\sqrt{\mu\kappa}\sqrt{1-(f_c/f)^2}} = \frac{1}{f\sqrt{\mu\kappa}\sqrt{1-(\lambda/\lambda_c)^2}} = \frac{1}{f\sqrt{\mu\kappa}\sqrt{1-(\lambda/2a)^2}} = 2l \text{ m}$$

$$\underbrace{f\sqrt{\mu\kappa}}_{=\frac{1}{\lambda}}$$

$$\text{yields } \lambda = \frac{2al}{\sqrt{a^2+l^2}} \text{ m}$$

$$\text{and } f = \frac{v}{\lambda} = \frac{1}{\lambda\sqrt{\mu\kappa}} \text{ cycles/sec}$$

$TM_{0,1}$ at cutoff:

$$\mathcal{E}_z = \mathcal{E}_0 J_0(rK); \quad H_\varphi = j\frac{\mathcal{E}_0}{\sqrt{\mu/\kappa}} J_1(rK)$$

According to Step 25 of Table 10, we have $K = K_{0,1} = 2.4048/a$, and $\lambda = 2\pi/K = 2\pi a/2.405 = 2.61a$ m. $f = 300/2.61a = 115/a$ Mc/sec for air inside the resonance cavity.

FIG. 386. Formulas for resonant cavities.

effect, a wave guide that is closed at either end. For $TE_{m,n}$ and $TM_{m,n}$ waves in a hollow rectangular cavity, we have the cutoff wavelength

$$\lambda_c = \frac{2}{\sqrt{(m/a)^2 + (n/b)^2}} \quad \text{m} \tag{920}$$

for the width a meters along the X direction and the dimension b meters along the Y direction. Resonance occurs, regardless of the shape of the cross section, when the length l along the Z direction is $q(\lambda_z/2)$, for $q = 1, 2, 3, \cdots$, and λ_z denotes the wavelength within the cavity along the Z direction. It differs from the wavelength $\lambda = 1/(f\sqrt{\mu\kappa})$ meters for the operating frequency f in cycles per second, which holds for the same medium without any boundaries. Figure 386 shows a parallelepiped

of unequal sides of a, b, and l meters along the X, Y, and Z directions, respectively. For possible resonance frequencies, we must have a *stationary*-wave pattern within the enclosed space in the cavity. Suppose we have first a rectangular wave guide that is excited with an $\mathcal{E}_y$ electric polarization. For the gravest mode of the $TE_{m,0}$ type, we have a half-period $\mathcal{E}_y$ distribution along the a dimension and $a = 2\lambda_c$ meters, where λ_c denotes the cutoff wavelength. Such an $\mathcal{E}_y$ distribution satisfies zero tangential $\mathcal{E}_y$ values. If now the rectangular guide is closed at either end, the indicated $\mathcal{E}_y$ distribution in the front rectangular ab plane must vanish, but we may have such distributions in ab planes, which are not tangent with metal surfaces. In the vertical $EFGH$ plane, for instance, we have such a distribution. For the gravest cavity resonance, we have also the indicated $\mathcal{E}_y$ distribution in the vertical $ABCD$ plane, which satisfies the boundary conditions for metal surfaces, along which we *cannot* have an electric field component. We then deal again with a half-period variation *but* corresponding to a wavelength $\lambda_z = 2l$ meters, for which we have the phase constant β_z. We then have the solutions of Fig. 386 and an unbounded operating wavelength $\lambda = 2al/\sqrt{a^2 + l^2}$ for the gravest resonance condition. Since this wavelength holds for the free-space wavelength, in a dielectric of $\mu = \mu_0$ henrys per meter and κ farads per meter the resonance frequency becomes

$$\left.\begin{aligned} f &= \frac{10^{-6}}{\lambda\sqrt{\mu\kappa}} = \frac{10^{-6}\sqrt{a^2 + l^2}}{2al\sqrt{\mu\kappa}} \qquad \text{for a pure dielectric} \\ f &= \frac{150\sqrt{a^2 + l^2}}{al} \qquad \text{for air, within the cavity} \end{aligned}\right\} \text{Mc/sec} \quad (920a)$$

For $l = a$ meters, we have then $\lambda = 1.4142a$ meters with a corresponding resonance frequency of $f = 300/(a\sqrt{2}) = 212/a$ megacycles per second. Both cases then refer to half-period variations in planes parallel with the XY plane and half-period variations in planes parallel with the YZ plane. The resonance frequencies are then

$$\left.\begin{aligned} f &= \frac{10^{-6}}{2\sqrt{\mu\kappa}}\sqrt{\frac{m^2}{a^2} + \frac{n^2}{b^2} + \frac{q^2}{l^2}} \qquad \text{for a pure dielectric } \mu, \kappa, \sigma = 0 \\ f &= 150\sqrt{\frac{m^2}{a^2} + \frac{n^2}{b^2} + \frac{q^2}{l^2}} \qquad \text{for air within the cavity} \end{aligned}\right\} \text{Mc/sec} \quad (920b)$$

only *one* of the three integers m, n, and q may vanish. The resonance frequency is then generally $f = f_{m,n,q}$. In the first example, we have $m = 1$, $n = 0$, and $q = 1$, since we have *only* $\mathcal{E}_y$ variations along the X

and Z directions.

For $\mathcal{E}_y$, we find

$$f = f_{m,n,q} = f_{1,0,1} = 150\sqrt{\frac{1}{a^2} + \frac{1}{l^2}}$$

$$= 150\frac{\sqrt{a^2 + l^2}}{al} \quad \text{Mc/sec, for } TE_{1,0,1} \text{ cavity resonance}$$

For $\mathcal{E}_x$, we find

$$f = f_{0,1,1} = 150\sqrt{\frac{1}{b^2} + \frac{1}{l^2}}$$

$$= 150\frac{\sqrt{b^2 + l^2}}{bl} \quad \text{Mc/sec, for } TE_{0,1,1} \text{ resonance}$$

For $\mathcal{E}_y$, we have

$$f = f_{2,0,1} = 150\sqrt{\frac{m^2}{a^2} + 0 + \frac{q^2}{l^2}} = 150\sqrt{\frac{4}{a^2} + \frac{1}{l^2}}$$

$$= 150\frac{\sqrt{4l^2 + a^2}}{al} \quad \text{Mc/sec, for } TE_{2,0,1} \text{ resonance}$$

For $\mathcal{E}_y$, we find

$$f = f_{3,0,2} = 150\sqrt{\frac{9}{a^2} + \frac{4}{l^2}}$$

$$= 150\frac{\sqrt{9l^2 + 4a^2}}{al} \quad \text{Mc/sec, for } TE_{3,0,2} \text{ cavity resonance}$$

where $\mathcal{E}_y$ expresses that the *entire* $\mathcal{E}$ polarization acts parallel only with the Y direction. For the $\mathcal{E}_x$ case, we have only $\mathcal{E}$ polarizations parallel with the X axis. For the $TE_{3,0,2}$ cavity resonance frequency, there are three half-period variations along the a dimension and two half-period variations along the l dimension. The resonance wavelengths of cylindrical cavities are

$$\left.\begin{aligned} \lambda &= \frac{1}{\sqrt{(1/\lambda_c)^2 + (q/2l)^2}} \quad \text{m} \\ f &= \frac{10^{-6}}{\lambda\sqrt{\mu\kappa}} \quad \text{Mc/sec for a pure dielectric } \mu, \kappa, \sigma = 0 \\ f &= \frac{300}{\lambda} \quad \text{Mc/sec for air within the cavity; } q = 1, 2, 3, \cdots \end{aligned}\right\} \quad (920c)$$

where l is the length of the cylinder in meters, q is the number of half-period variations of the field along the cylinder axis, and λ_c denotes the cutoff wavelength for the particular mode along the cylinder axis. We can then use the λ_c values of Table 87 and write, for the wavelength λ of (920c),

$$\left.\begin{aligned} \lambda &= \frac{2l}{q\sqrt{1 + (2l/q\lambda_c)^2}} \quad \text{m} \\ f &= \frac{10^{-6}}{\lambda\sqrt{\mu\kappa}} \quad \text{for a pure dielectric } \mu \text{ and } \kappa \\ f &= \frac{300}{\lambda} \quad \text{for air} \end{aligned}\right\} \text{Mc/sec} \qquad (920d)$$

Suppose we deal with a TE wave in a cylindrical resonator, of length l meters and radius a meters. If we have *one* half-period field variation along the axis of the cylinder, we have $q = 1$. If the number of φ variations is zero, then we have in $TE_{n,m,q}$, the subscript $n = 0$; and if the number of r variations is one, we have $m = 1$. This results in the $TE_{0,1,1}$ cylindrical cavity resonator. The n,m variations *belong* to the *cross* section of the cylindrical resonator, and we find, from Table 87 for the $TE_{n,m} = TE_{0,1}$ mode, a cutoff wavelength $\lambda_c = 1.64a$ meters. The resonance wavelength in unbounded space and the corresponding resonance frequency are then

$$\left.\begin{aligned} \lambda &= \frac{2l}{\sqrt{1 + (2l/1.64a)^2}} \quad \text{m} \\ f &= \frac{300}{\lambda} \quad \text{Mc/sec for air in a } TE_{0,1,1} \text{ resonator} \\ \lambda &= \frac{l}{\sqrt{1 + (l/1.64a)^2}} \quad \text{m in a } TE_{0,1,2} \text{ resonator} \\ \lambda &= \frac{0.667l}{\sqrt{1 + (0.667l/1.64a)^2}} \quad \text{m in a } TE_{0,1,3} \text{ cavity resonator} \end{aligned}\right\} \qquad (920e)$$

where f is the resonance frequency. In exactly the same way, we find the dielectric space resonance wavelengths for the modes of Fig. 387. Figure 386 shows a resonance excitation at cutoff, with zero variation along the axis. We have only an $\mathcal{E}$ field along the cylinder axis, independent of the φ coordinate. The resonance frequency then becomes $115/a$ megacycles per second.

237. Basic Propagation Theory of Low-level Atmospheric Waveguide Action (Low-level Wave Ducts). Low-level-stratum wave-duct actions occur in the lower centimeter range of wavelengths, corresponding to a frequency range of 3,000 to 10,000 Mc/sec, as described by C. L. Pekeris[1] and experimentally confirmed by the United States Naval Research Laboratory expedition. The experiments confirm, for instance, that waves of 10,000 Mc/sec can be propagated in low-level over-ocean

[1] *Proc. IRE*, **35**, 453, May, 1947.

ducts by means of first and second modes with small db losses. Theoretical losses of 0 and 0.5 db per nautical mile may be anticipated for first- and second-mode propagations. Microwaves in the frequency range of 3,000 to 10,000 Mc/sec may be received over distances as far

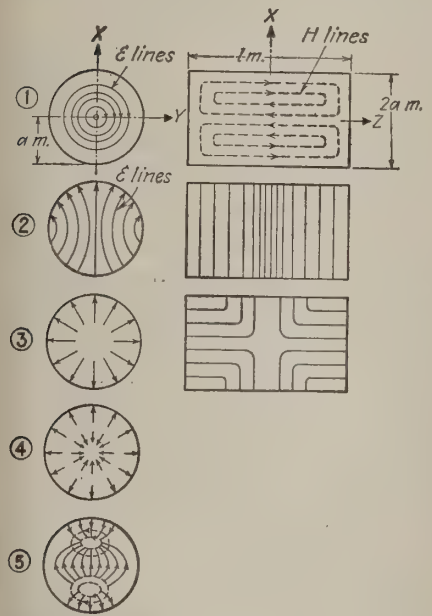

$$\mathrm{TE}_{0,1,1} \qquad \lambda = \frac{2l}{\sqrt{1 + (2l/1.649)^2}} \text{ m}$$

$$\mathrm{TE}_{1,1,1} \qquad \lambda = \frac{2l}{\sqrt{1 + (2l/3.41a)^2}} \text{ m}$$

$$\mathrm{TM}_{0,1,1} \qquad = \frac{2l}{\sqrt{1 + (2l/2.61a)^2}} \text{ m}$$

$$\mathrm{TM}_{0,2,1} \qquad \lambda = \frac{2l}{\sqrt{1 + (2l/1.4a)^2}} \text{ m}$$

$$\mathrm{TM}_{1,1,1} \qquad \lambda = \frac{2l}{\sqrt{1 + (2l/1.64a)^2}} \text{ m}$$

Moreover, $\mathrm{TM}_{0,3,1}$ has $\lambda = \dfrac{2l}{\sqrt{1 + (2l/0.724a)^2}}$ m

$\mathrm{TM}_{2,2,1}$ has $\lambda = \dfrac{2l}{\sqrt{1 + (2l/0.54a)^2}}$ m

Fig. 387. Formulas for different modes of cylindrical cavity resonators. *Note:* For all modes the circular cross section shows at places, where a field is possible, the same field configuration as a guide for which the field moves along the guide. For any pure dielectric the resonance frequency is found from $f = 10^{-6}/(\lambda \sqrt{\mu\kappa})$ Mc/sec. For air within the cavity the corresponding operating frequency is found from $f = 300/\lambda$ Mc/sec.

as about 200 nautical miles (N nautical miles = 0.8684 N statute miles). Such duct actions were originally theoretically treated by H. G. Booker and experimented with by his group in England. It was also followed up by J. B. Smyth and L. G. Trolese and their groups during World War II at the United States Navy Radio and Sound Laboratory, San Diego, Calif.[1] The theoretical foundations are due to H. G. Booker, C. R. Burrows, J. E. Freehafer, W. H. Furry, D. R. Hartree, T. Pearcy, M. H. L. Pryce, C. L. Pekeris, and others. For microwaves the frac-

[1] Cf. footnote 2 on p. 996.

tional change of the index n of refraction with respect to altitude is small and we can use the Hertzian potential $\prod$ for finding the electromagnetic field. We can then apply solution (358) on page 273, since the electric Hertzian potential satisfies the wave equation. We deal with a non-dissipative wave-duct medium and can then express (358) as

$$\nabla^2 \prod + \beta^2 n^2 \prod = 0; \qquad \beta = \frac{2\pi}{\lambda} \tag{921}$$

since in (358), $\mu\kappa = 1/v^2$ and the refractive index n of the wave duct is introduced. This relation includes, of course, the time factor $\epsilon^{j\omega t}$ and applies to vertical polarization, for which $\prod$ is the vertical component of the Hertz vector, as it is usually called. For horizontal polarization we use in (921) the Fitzgerald vector $\prod_m$ in place of the Hertz vector $\prod$, since the magnetization potential is in order, and $\prod_m$ denotes the vertical component of the Fitzgerald vector. The following conditions are to be satisfied by (921). At great distances r from the radiator, $\prod$ as well as $\prod_m$ are outward-moving functions, and for small distances of r, we have the form $(\epsilon^{j\omega t - j\beta r})/r$. Besides these requirements $\prod$ and $\prod_m$, respectively, must vanish at the earth crust.[1]

A wave duct in which extended microwave propagation takes place has such a tropospheric condition, close to the earth surface, that super-refraction occurs.[2] It is a state of the troposphere for a suitable variation of the refractive index n of atmospheric refraction to radio waves. Thus, if n decreases with the height h above the earth surface for some distance above the surface of the earth, the electromagnetic rays which start at the radiation center with a slight upward inclination toward the horizontal will curve downward. The rays must then experience reflection at the earth's surface, from where they are continued with additional reflections. For normal atmospheric conditions the field would, however, escape into space; but for mentioned refraction, the field energy propagates as a guided wave close to the earth surface and over much longer distances in a wave duct. Such conditions are enhanced and cause a wave duct when humidity decreases or temperature increases with elevation h, or both occur simultaneously.

The use of n_m, the modified index of refraction,[1] in place n in (921) changes the space so that the surface of the earth plane and the rays

[1] SCHELLENG, J. C., C. R. BURROWS, and E. B. FERRELL, *Proc. IRE*, **21**, 427, March, 1933 (on modified index n_m of refraction simplification).

[2] Cf. pp. 986–997.

become curved. We have then

$$n_m = \frac{R' \times n(R')}{R_1 \times n(R_1)}$$

where R' is the distance from the center of the earth and R_1 is the radius at some reference level. For R_1 equal to the radius of the earth R, we find

$$\frac{R'}{R} = 1 + \frac{h}{R}; \qquad \frac{n(R')}{n(R)} = 1 + h\frac{dn}{dh} + n'(h);$$

$$n_m \cong 1 + h\left(\frac{dn}{dh} + \frac{1}{R}\right) + n'(h)$$

where dn/dh is the orthodox vertical gradient of n, if h is the altitude above ground level and $n'(h)$ is the refraction anomaly, *i.e.*, the deviation of n from standard conditions. The term $h(dn/dh)$ modifies the radius of the earth R to a radius R_e (equivalent value), since

$$\frac{1}{R_e} = \frac{1}{R} + \frac{dn}{dh} \tag{922}$$

where often R_e/R is assumed equal to $\frac{4}{3}$, as is shown at other places in this text. It is customary to use the quantity M (modified index), given by

$$M - M_0 = 10^6(n_m - 1)$$

yielding

$$M = \frac{79p}{T} + \frac{3.8 \times 10^5 e}{T^2} + 0.048h \tag{923}$$

for absolute temperature T, atmospheric pressure p, vapor pressure e of water in millibars, and h in feet. The term $0.048h$ is $10^6(h/R)$. For standard conditions the sum of the first two terms of (923) changes with h as $-0.012h$, yielding

$$M_{\text{standard}} = M_0 + 0.036h \tag{924}$$

For normal modes we have then

$$\left.\frac{\Pi}{\Pi_m}\right| = -j\pi \sum_1^\infty H_0^{(2)}(\beta_m d) U_m(h_1) U_m(h_2) \tag{925}$$

for the horizontal distance d along the great circle and heights h_1 and h_2 of the radiation and reception centers above ground, where β_m is complex

with a negative imaginary part. The height-gain functions satisfy

$$\left.\begin{aligned} &\frac{d^2U_m}{dh^2} + (\beta^2 n_m^2 - \beta_m^2)U_m = 0; \qquad \beta = \frac{2\pi}{\lambda}; \qquad \text{normalized to} \\ &\lim_{I(k)\to 0} \int_0^\infty U_m^2(h)\, dh = 1 \end{aligned}\right\} \tag{926}$$

For other details reference is made to the paper of C. L. Pekeris[1] and further references given in it. Formula (925) represents the solution for the normal mode for the wave equation (921) as given by H. Lamb.[2] The requirement that either $\prod$ or $\prod_m$, respectively, in the wave equation (921) stand for an outgoing function at great distances from the radiation center means that at large heights h the base of $U_m(h)$ must decrease with larger values of h. The requirement that the electric polarization vector $\prod$ or the magnetization vector $\prod_m$ vanish at the earth surface is $U_m(0) = 0$. For an outgoing wave function at large distances the Hankel function of the second kind applies, and

$$H_0^{(2)}(\beta_m d) \to \sqrt{\frac{2}{\pi\beta_m d}}\, \epsilon^{-j\beta_m d + j(1/4)} \tag{927}$$

There exists a case similar to diffraction spectra, since we have in ducts incident and ground-reflected waves and, therefore, wave interference. This similarity comes much closer in the case of "wave trapping" in a duct. Such trapping occurs when the modified index yields a minimum value at some h value, for which channeling occurs through such a level. In most applications the duct actions are not ideal and a leakage field escape must be expected above the upper duct boundary.

238. Remarks on Electromagnetic Reflectors and Lenses Based on Wave-guide Action. It is often desired to design an aerial system for a certain forward field pattern. A special reflector and an electromagnetic lens can be used. The reflector is located behind the actual aerial, in a position similar to that of an optical reflector. The electromagnetic lens adapted to form a desired field pattern is located between the actual aerial and the distant field region. For the reflector and the lens system we must choose: the *front face* of the reflector, which faces the actual aerial; and the *entire shape* of the lens, to satisfy the desired electromagnetic field pattern, either transmitted or received. Reflector designs, like

[1] *Proc. IRE*, **35**, 453, May, 1947.

[2] *Phil. Trans. Roy. Soc.* A,**203,** 1–42, January, 1904, gives an exact solution for the radiation from a point source in an isotropic elastic half space. Lamb treats only the normal mode (the Rayleigh wave), while H. Jeffreys applied the Lamb procedure to a medium with layers, yielding an infinite number of modes, called *love waves* (*Beitr. Geophysik*, **30,** 336–350, June, 1931).

paraboloids, radar dishes, etc., are well known in the art, but electromagnetic lenses are of more recent date.[1]

Electromagnetic lenses are based on the optical-ray concept. The lens dimensions must, therefore, be large with respect to the free-space wavelength, corresponding to the operating radio frequency, in order to avoid any appreciable diffraction effects. At the present time we have

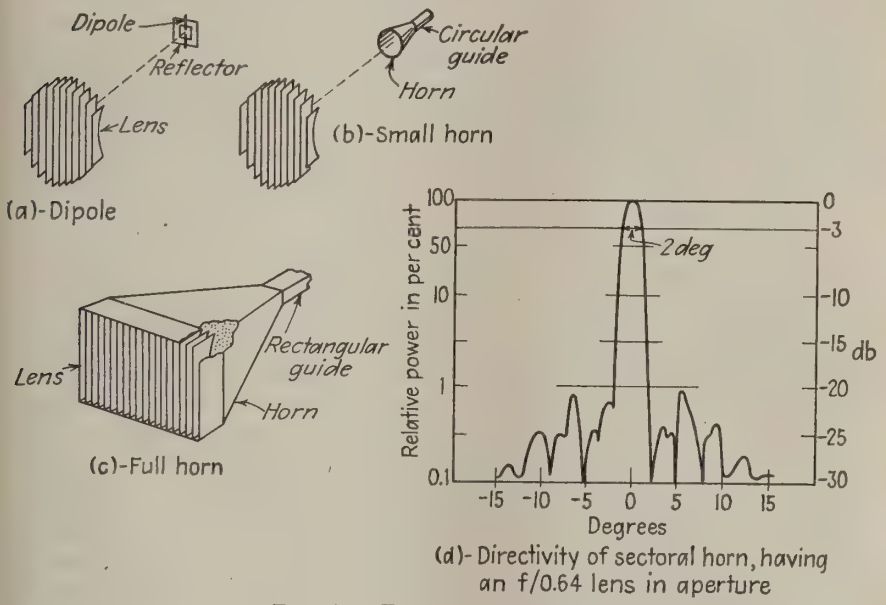

Fig. 388. Electromagnetic lenses.

electromagnetic lenses which are like customary optical lenses, and based on Snell's refraction law (consult pages 790–793). If the lens is applied, as here, to electromagnetic rays, we can use one for which the relative index n of refraction is based on a phase velocity c' within the refracting lens that is *smaller* than for the surrounding air of the lens. The index of refraction n is then $n = c/c' = \sqrt{\mu\kappa}/\sqrt{\mu_0\kappa_0} > 1$, since in the refracting lens $c' = 1/\sqrt{\mu_0\kappa}$ m/sec and for the surrounding air the velocity is about $c = 1/\sqrt{\mu_0\kappa_0}$ m/sec. The quantity κ is the dielectric constant of the lens in farad/m, and μ_0 henry/m holds for the space surrounding the

[1] Kock, W. E., Metal-lens Antennas, *Proc. IRE*, **34**, 828–836, November, 1946, Path-length Microwave Lenses, *Proc. IRE*, **37**, 852–855, August, 1949, Metallic Delay Lenses, *BSTJ*, **27**, 58–82, January, 1948; Devore, H. B., and H. Iams, Microwave Optics between Parallel Conducting Sheets, *RCA Rev.*, **9**, 721, December, 1948; Friis, H. T., and W. D. Lewis, "With Respect to Scanning Aberrations," in their paper on Radar Antennas, *BSTJ*, **26**, 219–247, April, 1947; Ruze, John, Wide-angle Metal-plate Optics, *Proc. IRE*, **38**, 53–59, January, 1950.

lens and the space occupied by the lens. There is also an electromagnetic lens, due to W. E. Kock (*loc. cit.*), which is based on phase velocities c' for the lens which are greater than the velocity c holding for empty space. We have then an index of refraction $n = c/c' < 1$. Such a lens uses, as in Fig. 388*a*, *b*, *c*, and *d*, TE waves by means of a number of conducting plates of suitable shape spaced a distance s meters apart. To cause TE waves through the length of the lens, the spacing s between consecutive metal faces must be greater than one-half of the free-space wavelength $\lambda_0 = 300/f$ meters, if f is in Mc/sec. It is assumed that the extensions of the metal faces between which TE waves pass are sufficient. For parallel faces (metal) which are also parallel to the electric field vector, we have a phase velocity c' of the lens and an index of refraction n.

$$c' = c/\sqrt{1 - p^2}; \qquad n = c/c' = \sqrt{1 - p^2}; \qquad p = \frac{\lambda_0}{2s} \tag{928}$$

provided nonferromagnetic conducting metal plates are used and the wave medium about the lens is air, so that $c \cong 1/\sqrt{\mu_0 \kappa_0}$ meters/sec.

The method of designing a reflector surface, as well as an electromagnetic lens, is to find first the space-directivity pattern of the particular aerial without a reflecting surface or a lens. After having found such a pattern for unobstructed space, it is compared with the desired pattern and by space geometry as well as Snell's refraction law (in the case of a lens), the required shape is determined. For lenses, the thickness of certain lens portions as well as the dielectric constant of the lens and its shape is used for producing the desired pattern. It must be noted that for electromagnetic lenses, using a lens similarly as in optics, the entrance of the ray and its emergence on the other side of the lens is given by Snell's refraction law. For a lens depending on a wave-guide action, we deal also with a conversion from TEM into TE and back to TEM waves. It has been shown that by a superposition of electric and magnetic current sheets such changes can be accounted for.

APPENDIX

With respect to the symbols employed in this text, unless otherwise specified, we have the nomenclature of Table 89. Table 90 gives the conversions from the rationalized mks units into electrostatic cgs units as well as into electromagnetic cgs units. The Giorgi mks system is based on the mass in kilograms, length in meters, time in seconds, and charge in coulombs. Since the coulomb is used as an *independent* unit, we find for vacuum $\mu_0 = 4\pi 10^{-7} = 1.257 \times 10^{-6}$ henry/m, $c = 2.9979 \times 10^8$ m/sec, and $\kappa_0 = 8.854 \times 10^{-12}$ farad/m. On pages 595 and 596 of "Phenomena in High-frequency Systems" it is shown that by means of the Heaviside system of units, as used by H. Hertz as well as by H. A. Lorentz, the factor 4π can be eliminated. In the classic Gauss system of units, we have the velocity c as is specified above, and $\mu_0 = 1 = \kappa_0$ and $c = 1/\sqrt{\mu_0\kappa_0}$. Any relation given in mks units can be transformed readily to Gaussian units by replacing κ_0 and μ_0 each by $1/c$, the current density J by J/c, and the specific conductivity σ by $c \cdot \sigma$. In each system of units, we satisfy the conditions that in the electromagnetic field relations the product $\mu_0\kappa_0$ and the ratio μ_0/κ_0 are of consequence, but neither μ_0 nor κ_0 by itself. As in any theory, units are based on *experimental* facts, generally observed by motion of a body due to a force. Thus a force F, appearing in the well-known Coulomb law, is equal to $Kq_1q_2/(\kappa r)^2$, where the dielectric constant κ defines an electric property of the medium in which electric charges q_1 and q_2 are located and experience a mutual force F when separated a distance r in such a medium. A similar experimental law $F = Km_1m_2/(\mu r^2)$ exists in a magnetic system for respective magnetic masses m_1 and m_2 and μ defining the magnetic property of the medium in which m_1 and m_2 are located. Using M, L, and T for the customary symbols for mass, length, and time, we can readily arrive at the well-known classic systems of units. The constant K in either system is a mere number, depending upon the units employed. For instance, in the es-cgs system, we have $K = 1$, while in Heaviside-Lorentz units $K = 1/(4\pi)$ is basic. Hence, in es-cgs units $F = q_1q_2/(\kappa r^2)$, where neither q nor κ can be expressed. But for equal and opposite charges of value q, the ratio q^2/κ is equal to force times r^2. But force F is also mass times acceleration, or ML/T^2 in units and when multiplied by r^2, *i.e.*, by L^2, yields the dimensions for q^2/κ equal to $|ML^3T^{-2}|$, and for q we have the dimensions $|\sqrt{ML^3T^{-2}\kappa}| = |M^{1/2}L^{3/2}T^{-1}\kappa^{1/2}|$ if M stands for the mass unit in grams, L is in centimeters, and T in seconds. Taking as in the es-cgs system, $\kappa = 1 = \kappa_0$ for vacuum, then q may be taken unity when F is the force of 1 dyne. All the other units are found by the same reasoning and similarly for the em-cgs system.

From Table 90 we note that many of the classic electromagnetic relations are unrational, so that conversion factors must be used. For instance, the ampere turn per meter in the rationalized mks system for the magnetic field intensity must be multiplied by the factor $4\pi 10^{-3}$ in order to bring about the conversion to the H value in oersteds, as used in the unrationalized em-cgs system. Thus

$$\text{curl}\, H = 4\pi c\sigma \mathcal{E} + \frac{\kappa}{c}\frac{\partial \mathcal{E}}{\partial t}$$

TABLE 89. LIST OF CUSTOMARY SYMBOLS UNLESS SPECIFIED OTHERWISE†

Symbol	Stands for	Remarks or dimension
A, A_1, A_2, . . .	A factor, an abbreviation for several terms, an area	If an area, in m^2
a, a_1, a_2, . . .	A factor, an abbreviation for terms, a dimension such as a radius	If a linear dimension, in m
α, α_1, α_2, . . .	An angle, attenuation constant	If an angle, in degrees or in radians; if attenuation constant, in nepers/m
B, B_1, B	Magnetic flux density, B fundamental magnetic vector of magnitude B, dot below is often omitted for simplicity's sake	Magnitude of B is in webers/m^2 or volt · sec/m^2; B is also known as magnetic induction
b, b_1, b_2, . . .	A constant, an abbreviation, a distance	If a distance, in m
β, β_1, β_2, . . .	An angle, phase constant	If an angle, in deg or in radians; if phase constant, in circular radians/m
C, C_1, C_2, . . .	A factor, capacitance	If capacitance, in farads
c, c', c''	A factor, an abbreviation, the velocity of ideal propagation in vacuum and along ideal lines; c' is phase velocity; c'' is group velocity (consult pp. 7, 366, 368–373, 376–388)	If velocity, in m/sec
γ, γ_1, γ_2, . . .	Angle	In deg or in radians
Γ, Γ_1, . . .	Gamma function, propagation constant $\Gamma_1 = j\omega\sqrt{\mu_0\left(\kappa_1 - j\frac{\sigma_1}{\omega}\right)} = \alpha_1 + j\beta_1$, for $\omega/6.28$ in cycles/sec; $\mu_1 = \mu_0$	If propagation constant, in generalized hyperbolic radians/m, since equal to $\alpha + j\beta$, where α is in *hyperbolic* radians/m (*i.e.*, nepers/m) and β in *circular* radians/m) (consult pp. 30, 44, 45, 46, 48, 53, 58, 59, 70, 127, 801)
D, D_1, D_2, . . .	A factor, electric flux density, also known as electric displacement, a diameter	If electric flux density, in coulombs/m^2; if a diameter, in m
d, d_1, d_2, . . .	A constant, an abbreviation for several terms, a distance such as a diameter; a differential operator	If a distance, in m

TABLE 89. LIST OF CUSTOMARY SYMBOLS UNLESS SPECIFIED OTHERWISE.† (*Continued*)

Symbol	Stands for	Remarks or dimension
δ	An angle, a small thickness, a decrement	If an angle, in circular radians or deg; if a thickness, in m
Δ, Δl, ΔV, $\Delta \mathcal{E}$, ΔH	An operator of a small total quantity like Δl which is a very short length; Δ expresses also a determinant	Δl is expressed in m; ΔV is expressed in volts; $\Delta \mathcal{E}$ in volts/m; ΔH in amp/m; Δ is also Murphy's operator; $\Delta \equiv \nabla^2$
∇, $\nabla \cdot F$, $\nabla \times F$	∇ is the del operator in vector analysis; $\nabla \cdot F$ is a "dot" product, and is also known as the divergence of vector F or div F; $\nabla \times F$ is a "cross" product, and known as the curl of vector F or curl F or rot F	The vector F stands, for instance, for the field vector H or the field vector $\mathcal{E}$, respectively, curl $F \equiv \nabla \times F \equiv$ rot F; div $F \equiv \nabla \cdot F$
E, E_1, E_2, . . . E_s, E_{11}, E_{22}, E_m, E_{12}, . . .	Voltage, E_s self-voltage, E_{11} self-voltage of conductor 1, E_{22} self-voltage of conductor 2, E_m mutual voltage due to another conductor or radiator, E_{12} mutual voltage of radiator 2 on radiator 1	All voltages in volts (for other details consult pp. 650–654, 656–665)
e, e_1, . . .	Instantaneous voltages	In volts
ϵ	Base of natural logarithm	$\epsilon = 2.7182818$; we have also $\log_\epsilon N = 2.302585 \log_{10} N$
$\mathcal{E}$, $\mathcal{E}_s$, $\mathcal{E}_m$	Electric field vector, self-value, mutual value	In volts/m; $\mathcal{E}^*$ is conjugate vector of $\mathcal{E}$ (consult pp. 118–124, 210–214)
F F, F', F'' . . .	General field vector, may be $\mathcal{E}$ or H, function symbol, first derivative of function, second derivative, etc.	$\mathcal{E}$ in volts/m, H in amp/m, $F(x)$ is a function of x; F^* is conjugate vector (pp. 118–124, 210, 610)
f	Frequency	In cycles/sec, in kc/sec or 10^3 cycles/sec, in Mc/sec or 10^6 cycles/sec
G	Leakance conductance per unit length of a transmission line (parallel-wire line, concentric line)	In mhos/m
H, H^*	Magnetic field intensity, magnetic field vector; H^* is conjugate vector (pp. 118–124, 210–214)	In amp/m

TABLE 89. LIST OF CUSTOMARY SYMBOLS UNLESS SPECIFIED OTHERWISE.† (*Continued*)

Symbol	Stands for	Remarks or dimension
$H_n^{(1)}(x)$, $H_n^{(2)}(x)$	Hankel functions, also known as Bessel functions of the *third* kind of order n and argument x	For details consult pp. 295, 323, 333, 339, 343, 479, 1232
h, h_1, h_2, h_e	Height of a vertical linear radiator, height of a radiation center above ground level, height of a reception center above ground level, any altitude above ground level	Measured in m (h_e is effective height)
I, I_0, I_m, I_1, I_2, . . . I^*	Currents; I^* is conjugate vector of vector I (consult pp. 210–214)	In amp
i, i_1, i_2, . . .	Instantaneous currents; i is also used as a unit vector (pp. 197, 1268–1271)	In amp
J, $J_n(x)$, J_m	J is electric current density; $J_n(x)$ is a Bessel function of the first kind of order n and argument x; J_m is magnetic current density	J is in amp/m^2 J_m is in volts/m^2
j	The imaginary unit equal to $\sqrt{-1}$	j is also used as a unit vector in vector analysis (consult pp. 197, 1268–1271)
K, K_1	A factor, expressing several terms	For wave guides K is as in formula (916)
k, k_1, $k_{n,m}$	A factor, expressing several terms; an integer such as 1, 2, 3, 4, . . . ; k is also a unit vector (pp. 197, 1268–1271)	$k_{n,m}$ and $k'_{n,m}$ are given in Eq. (916) and Table 10
κ, κ_0, κ_e, κ'_e, κ_r	κ *actual* dielectric constant of any medium; κ_0 dielectric constant of a vacuum; $\kappa_e = \kappa - j\sigma/\omega$ *equivalent* dielectric constant of general medium; $\kappa_r = \kappa/\kappa_0$ *relative* dielectric constant of a perfect dielectric medium; $\kappa'_e = \kappa_e/\kappa_0 = \kappa_r - j18{,}000\sigma/f$ for f in Mc/sec for medium with heat losses ($\sigma \neq 0$ mhos/m)	κ_0, κ, κ_e in farads/m; $\kappa_0 = 8.854 \times 10^{-12}$ farad/m for a vacuum; κ_r, κ'_e are the *relative numeric* values of the actual dielectric and equivalent dielectric constants with respect to value κ_0 of a vacuum; $\omega/62.8$ is in cycles/sec; σ is mhos/m
L, L_{12}, L_{21}	Self-inductance, mutual inductance of circuit 1 on circuit 2 and vice versa	In henrys

TABLE 89. LIST OF CUSTOMARY SYMBOLS UNLESS SPECIFIED OTHERWISE.† (*Continued*)

Symbol	Stands for	Remarks or dimension
l, l_e	Actual length, equivalent electrical length	In meters (consult pp. 7, 166, 195, 243, 517, 1243, 1252)
λ, λ_0, λ_g	Wavelength, wavelength in vacuum (essentially so for air), wavelength *along* a wave guide	In meters
	The symbol λ is also used in the Sommerfeld integral $\frac{\epsilon^{jk\rho}}{\rho} = \int_0^\infty J_0(\lambda\rho) f(h)\lambda\, d\lambda$; $f(h) = \int_0^\infty J_0(\lambda\cdot\rho)\epsilon^{jk\rho}\, d\rho = \frac{\lambda\, d\lambda}{\sqrt{\lambda^2 - k^2}}$; $k > 0$, leading to the Sommerfeld relation $(1/r)\epsilon^{jkr} = \int_0^\infty \epsilon^{\pm z\sqrt{\lambda^2-k^2}} J_0(\lambda\cdot\rho)\frac{\lambda\, d\lambda}{\sqrt{\lambda^2 - k^2}}$ where the upper and lower signs are taken according to $z \lessgtr 0$ (for other details see p. 593)	
Λ, Λ_m, Λ_e	Λ_m usually written as Λ, is the retarded *magnetic* vector potential at a distant field point; Λ_e is the retarded electric vector potential	Λ_m in volt · sec/m; Λ_e in amp · sec/m (details on pp. 87, 92, 214, 218, 229, 249, 258, 290, 1277–1278)
M	Vector volume density of magnetization; mass, mutual inductance; M is also modified index of refraction	Mass in kg, mutual inductance in henrys
m, m_0, m_e, m_m, m_1, m_2	m_1 and m_2 stand for magnetic matters that act on each other; m is the electric charge moment $q\, dl$ of a Hertz doublet; m_e is the instantaneous current moment $dlI\epsilon^{j\omega t}$ of an infinitesimal dl radiator; $m_0 = \sigma_m\, dS$ is magnetic matter for an elementary magnetic dipole, causing a magnetic moment $m_m = m_0\, dl$ for a magnetic surface density σ_m	$m = q\, dl$ m · coulombs; $m_e = i\, dl$ m · amp
μ, μ_0, μ_r	Permeability (magnetic) of a wave medium; μ_0 for a vacuum (and practically so for air and nonmagnetic matter); $\mu_r = \mu/\mu_0$ is *numeric relative* magnetic permeability with respect to vacuum	In henrys/m; $\mu_0 = 1.257 \times 10^{-6}$ henry/m; $1/\mu$ m/henry is absolute magnetic reluctivity

TABLE 89. LIST OF CUSTOMARY SYMBOLS UNLESS SPECIFIED OTHERWISE.† (*Continued*)

Symbol	Stands for	Remarks or dimension
$N, N_1, N_2, \ldots$	Certain numbers, in some cases these numbers stand for integers such as 1, 2, 3, 5, . . . , for instance	$N_n(x)$ is Neumann function second independent solution of Bessel equation (pp. 295, 304, 322)
$n, n_1, n_2, n_{1,2}$	n is relative index of refraction of general medium with respect to vacuum (numeric); n_1 is relative index for air as medium 1 (where $\mu_1 = \mu_0$, $\kappa_1 \cong \kappa_0$ and $\sigma_1 = 0$); n_2 is relative index of medium 2 (where $\kappa_2 \neq \kappa_0$, $\mu_2 = \mu_0$, and $\sigma_2 \neq 0$); $n_{1,2} = n_2/n_1$ is relative value for wave passage from medium 1 into medium 2; $n_{1,2} = (\sin \theta_1/\sin \theta_2) = n_2/n_1$	θ_1 is angle of wave incidence, and θ_2 is angle of refraction into medium 2 with the *normal* to the plane of medium separation. [For details consult Sec. 13 and formulas (33), (34), in that section] $n_{1,2} = \dfrac{\sin \theta_1}{\sin \theta_2} = \dfrac{\Gamma_2}{\Gamma_1}$
ν	$\nu = f_c/f = \lambda/\lambda_c$ in wave guides	f_c is frequency below which no power transfer without attenuation is possible; f is operating frequency
$P, P_{\varphi,\theta}$; $P_n(\cos \theta)$	P is power in watts; P is usually a distant field point; $P_{\varphi,\theta}$ is such a point at location $r, \varphi, P_n(\cos \theta)$ surface zonal harmonics or Legendre polynomials (p. 328)	r is distance in m to field point; θ is angle that r makes with $+Z$ axis, and φ is angle that the projection of r into the XY plane makes with $+X$ axis
p	A parameter, used for an abbreviation, used as a factor, Poynting vector	Poynting vector, real part, is in watts/m^2
π	$\pi = 3.1415927$ occurs in ω as $2\pi f$	f in cycles/sec
$\prod$	Hertz vector; or used as the *Gauss* function such as $\prod(x) = \Gamma(x+1)$ in relation to the *Gamma* function $\Gamma(x+1)$; $\prod_m$ magnetization vector (pp. 222, 312, 1275–1277 and Secs. 245, 246)	If $\prod$ is Hertz vector, then dimension is in m · volts. For Gauss function $\prod(x)$ consult Appendix under Gauss and Gamma functions (Sec. 241)
$\varphi, \varphi_1, \varphi'$	If applied to spherical and cylindrical coordinates, φ, denotes the angle that the projection of the distance r to the field point P (Figs. 3, 17, 18, 26) into the XY plane makes with $+X$; φ may be any other angle in deg or radians; φ may be the argument of the power factor cos φ	

TABLE 89. LIST OF CUSTOMARY SYMBOLS UNLESS SPECIFIED OTHERWISE.† (*Continued*)

Symbol	Stands for	Remarks or dimension
$\Phi, \Phi_1, \Phi_2, \Phi_3$	Φ may be the total magnetic flux in webers; Φ_1, Φ_2, Φ_3 may be function signs as in $\Phi(x)$; Φ may be a potential in volts	$\Phi = BA = \mu HA$ for B in webers per m, area A normal to which flux acts in m^2, H in ampere turns/m, μ in henrys/m
$\psi, \psi_1, \ldots$	May be any phase angle	In deg or radians
Ψ	A current or flow function	In amp
$Q, Q_n (\cos\theta)$	Q denotes the quality (or figure of merit) of a wave medium (Sec. 13); second solution of Legendre's equation (p. 322) is given by $Q_n (\cos\theta)$	$Q = \omega\kappa/\sigma$
$q, q_1, q_2, \ldots$	Charges in coulombs; sometimes q is used as an abbreviation	Charge in amp · sec
$R, R_{00}, R_{11}, R_{22}, R_s, R_m, R_r, R_1, R_2, \ldots R_v, R_h$	Resistances; R_s self-resistance; R_m mutual resistance contributions; $R_{12}, R_{13}, R_{23}, \ldots$ mutual resistances (for details pp. 517–521, 609, 652–696, 1007–1014); R_r radiation resistance; R_1 input and R_2 output resistance	In ohms; R_v and R_h are the coefficients of refraction (numeric) for vertical and horizontal polarization (Table 44)
$r, r_1, r_2, \ldots$	Resistances; r may also be a radius or any distance to a field point	In ohms if resistance; in m if distance
ρ	Magnitude of reflection coefficient (pp. 794, 798–824, 827, 829); for wave guides, we have $\rho = \sqrt{1 - (f_c/f)^2}$ as in Eq. (915f); ρ may also be the charge concentration in space; ρ may also be a distance such as to a field point or a radius	For ρ as a reflection factor ρ is *numeric;* for ρ as a distance ρ is in m; ρ as the space charge density is in coulombs/m^3
$S, S_1, dS, \ldots$	Surfaces	Area of surfaces in m^2
$\sigma, \sigma_1, \sigma_2, \sigma_m$	Specific space conductivity of a medium; σ_m is magnetic surface density	In mhos/m (is number of mhos between two parallel square-meter planes of medium spaced 1 m apart

TABLE 89. LIST OF CUSTOMARY SYMBOLS UNLESS SPECIFIED OTHERWISE† (*Continued*)

Symbol	Stands for	Remarks or dimension
$\sum_r$	Summation sign with r parts	$\sum_{r=1}^{r=3} P_r = P_1 + P_2 + P_3$
T, TEM, TE, TM	T is period $1/f$ of excitation; TEM is transverse electromagnetic wave; TE is transverse electric wave; TM is transverse magnetic wave	T in sec and f in cycles/sec; TE and TM waves exist only within a guide and next to a radiator
t, t_1, . . .	Time	In sec
τ, $d\tau$	τ any volume; $d\tau$ elementary volume	In m^3
U, dU	Resultant and elementary magnetic potential at a field point	In amp
u	An argument as in the sine integral Si and cosine integral Ci functions, as in $\text{Si } x = \int_0^x \frac{\sin u}{u}\, du; \qquad \text{Ci } x = -\int_x^\infty \frac{\cos u}{u}\, du$	
V, V_1, V_2	V scalar potential, and potential differences V_1 and V_2	In volts
v	Used generally as the velocity of propagation. Since $v = \omega/\beta$, we deal with what is known as the phase velocity	In m/sec
w	Width, also used for wave function	If width, then in m
X, X_1, X_2, X_s, X_{11}, X_m, X_{12}	Reactances; X_s, X_{11} self-reactance of circuit 1; X_m mutual reactance contribution; X_{12} mutual reactance of circuit 1 due to circuit 2	In ohms (may be positive or negative) (consult pp. 409, 417–421, 519, 609, 650–671, 690–697, 712–717)
x	Cartesian coordinate along X axis	In m
Y	Admittance	In mhos; if for a double line we have mhos/m

TABLE 89. LIST OF CUSTOMARY SYMBOLS UNLESS SPECIFIED OTHERWISE† (*Continued*)

Symbol	Stands for	Remarks or dimension
y	Cartesian coordinate along Y direction	In meters
Z, Z_1, Z_2, Z_s, Z_{11}, Z_m, Z_{12}	Impedances; Z_s, Z_{11} self-impedance of circuit 1; Z_m mutual impedance contribution; Z_{12} mutual impedance in circuit 1 due to circuit 2	In complex ohms (for details consult pp. 409, 417–421, 519, 609, 650–671, 690–697, 712–717)
z	Cartesian coordinate along Z direction	In m
ξ, η, ζ	Cartesian coordinates (consult Fig. 27)	In m
θ, θ_1, θ_2, θ'	An angle or the θ coordinate along a meridian in a spherical coordinate system (Fig. 27)	In deg or radians
ω	$2\pi f$ angular velocity, f in cycles/sec	In radians/sec
Ω	Expresses ohms or is used as an abbreviation (pp. 408, 710)	

† The necessary dimensions are always given with significant formulas, and special symbols are always explained where they appear. The symbol κ was used for the dielectric constant in order not to confuse this constant with the symbol ϵ, which stands for the base of the natural logarithm. The symbol ϵ appears often in the same expression as κ.

for $\mathcal{E}$ and κ in the es-cgs and H and μ in the em-cgs system, respectively, is the well-known curl equation[1] linking magnetic H and electric $\mathcal{E}$ vectors by means of the velocity of light $c = 3 \times 10^{10}$ cm/sec for a medium of dielectric constant κ, permeability μ, and conductivity σ. But

$$\text{curl } H = 4\pi\sigma\mathcal{E} + \frac{\kappa}{c^2}\frac{\partial \mathcal{E}}{\partial t}$$

is the converted expression when all quantities are expressed in em-cgs units.[2]

A derivation for a plane electromagnetic wave traveling along the X axis of an

[1] HUND, A., "Phenomena in High-frequency Systems," p. 595, McGraw-Hill Book Company, Inc., New York.

[2] *Ibid.*, p. 329.

TABLE 90. QUANTITIES THAT OCCUR OFTEN IN ELECTROMAGNETIC RELATIONS, COMPARED IN CLASSIC CGS AND MKS SYSTEMS OF UNITS; $c = 3 \times 10^8$ m/sec*

Quantity	Mks	Electromagnetic cgs	Electrostatic cgs
Voltage	p volts	$p10^8$ abvolts	$\frac{p10^8}{c}$ statvolts
Current	p amp	$p10^{-1}$ abamp	$pc10^{-1}$ statamp
Resistance	p ohms	$p10^9$ abohms	$\frac{p10^9}{c^2}$ statohms
Power	p watts	p joules/sec	$p10^7$ ergs/sec
Charge	p coulombs	$p10^{-1}$ abcoulomb	$pc10^{-1}$ statcoulomb
Capacitance	p farads	$p10^{-9}$ abfarad	pc^210^{-9} statfarad
Inductance	p henrys	$p10^9$ abhenrys	$\frac{p10^9}{c^2}$ stathenrys
Magnetic flux density	B webers/m^2	10^4B gauss/cm^2	$\frac{10^{-6}B}{3}$
Magnetic flux	Φ webers	$10^8\Phi$ maxwells	$\frac{10\Phi}{3}$
Specific conductivity	σ mhos/m	$10^{-11}\sigma$	$9 \times 10^9\sigma$
Magnetomotive force	p amp turns	$4\pi10^{-1}p$ gilbert	$12\pi10^9p$
Magnetic field intensity	H amp turns/m	$4\pi10^{-3}H$ oersted	$12\pi10^7H$
Dielectric displacement	D coulombs/m^2	$4\pi10^{-5}D$	$12\pi10^5D$
Electric field intensity	$\mathcal{E}$ volts/m	$10^6\mathcal{E}$ abvolts/cm	$\frac{10^6\mathcal{E}}{c}$ statvolts/cm
Permeability	μ henrys/m	$10^7\mu$ abhenrys/cm	$\frac{10^7\mu}{c^2}$ stathenrys/cm
Dielectric constant	κ farads/m	$10^{-11}\kappa$ abfarad/cm	$10^{-11}c\kappa$ statfarad/cm

* If we compare the mks, Gaussian, es-cgs, and em-cgs systems, we must satisfy the relation $u/\sqrt{\mu_0\kappa_0} = c = 3 \times 10^8$ m/sec, which is a length dimension divided by a time dimension. For the mks system, we have the unit vector $u = 1$, $\mu_0 = 1.257 \times 10^{-6}$ henry/m, and $\kappa_0 = 8.854 \times 10^{-12}$ farad/m. For the Gaussian system $u = c$, $\mu_0 = 1 = \kappa_0$. For the es-cgs units, $u = 1$, $\mu_0 = 10^{-20}/9$ sec/cm^2 and $\kappa_0 = 1$. For the em-cgs units $u = 1$; $\mu_0 = 1$ and $\kappa_0 = 10^{-20}/9$ (sec/cm)^2. Hence, when the charge q_e is measured in es-cgs units and q_m is the value, measured in em-cgs units, we have $q_e = cq_m$.

XYZ coordinate system in perfect dielectrics leads to the simplified expressions

$$\frac{d^2H_y}{dt^2} = \frac{1}{\mu\kappa}\frac{d^2H_y}{dx^2}; \qquad \frac{d^2\mathcal{E}_z}{dt^2} = \frac{1}{\mu\kappa}\frac{d^2\mathcal{E}_z}{dx^2}$$

both expressions may be thought of in the same units

$$H_y = f_1(x - vt) + f_2(x + vt)$$
$$\mathcal{E}_z = f_1(x - vt) + f_2(x + vt)$$

general solution of which only one term applies to a motion along $+X$ axis

showing that magnetic and electric field vectors are perpendicular to each other (along the Y and Z axes) and move, as it were, with plane YZ along the X axis with a velocity $v = 1/\sqrt{\mu\kappa}$, which for empty space is the velocity of light $c = 3 \times 10^{10}$ cm/sec. For any wave (not necessarily plane) if we express the field components $\mathcal{E}_x$, $\mathcal{E}_y$, and $\mathcal{E}_z$ along the XYZ directions in es-cgs units, the conversion to em-cgs units is accomplished by just writing $\mathcal{E}_x/c$, $\mathcal{E}_y/c$, $\mathcal{E}_z/c$, and $1(\mu c^2)$ for $\mathcal{E}_x$, $\mathcal{E}_y$, $\mathcal{E}_z$, and κ.

In the classic publications, we find then (1) the electrostatic centimeter-gram-second system (es-cgs), (2) the electromagnetic centimeter-gram-second system (em-cgs), (3) the Gaussian system for which the electrical quantities have the same dimensions as in the es-cgs system and the magnetic quantities have the same dimensions as in the em-cgs system. The Heaviside system avoids most of the factors such as 4π and $\sqrt{4\pi}$ and gives, for instance, the symmetrical forms

$$\text{curl } H = \frac{1}{c}\frac{\partial \mathcal{E}}{\partial t} \qquad \text{and} \qquad \text{curl } \mathcal{E} = -\frac{1}{c}\frac{\partial H}{\partial t}$$

instead of the unsymmetrical forms

$$\text{curl } H = \frac{\kappa}{c^2}\frac{\partial \mathcal{E}}{\partial t} \qquad \text{and} \qquad \text{curl } \mathcal{E} = -\mu\frac{\partial H}{\partial t}$$

for a nondissipative wave medium. However, in the rationalized mks system of units, we have the simple expressions

$$\text{curl } H = \kappa\frac{\partial \mathcal{E}}{\partial t} \qquad \text{and} \qquad \text{curl } \mathcal{E} = -\mu\frac{\partial H}{\partial t}$$

for a pure dielectric wave medium. Such comparisons, as well as the expressions given in Table 94, show the great simplification of the mks system and the reason why it is used exclusively in this text. The intercomparisons give, besides, a means of translating relations given in classic theory into more up-to-date expressions.

239. Notes on the Relation of the Modified Index M of Atmospheric Refraction to Electromagnetic Wave Propagation. Some writers prefer such an index M of refraction instead of the customary index n. For the case of flat earth, we have

$$M = \frac{k_1 p}{T} - \frac{k_2 p_v}{T} + \frac{k_3 p_v}{T^2} + k_4 h \tag{929}$$

which is based on the expression

$$M = \left[(n - 1) + \frac{h}{R}\right] 10^6 \tag{930}$$

and the outcome of the Debye theory. Such relations were used by Englund, Crawford, and Mumford and others, but in more recent years we have secured many

experimental data for determining the coefficients k_1, k_2, k_3, and k_4. We have for M values from about 300 to 550 and the modified gradient dM/dh may be found for height intervals dh equal to about 15 to 25 m. Englund, Crawford, and Mumford used coefficients of the order of magnitude $k_1 = 79.1$, $k_2 = 10.9$ and $k_3 = 3.81 \times 10^5$, the coefficient k_4 being the ratio $10^6/R$ with R being the radius of the earth in meters and h being the height in meters above sea level.

The moisture of the lower atmosphere is expressed in terms of the *relative* humidity (or vapor pressure). The relative humidity is the ratio of amount of water vapor present to the amount of water vapor for saturation. The absolute humidity would be the mass of water present in unit volume of the atmosphere, usually measured as grams per cubic meter. It may also be expressed in terms of the actual pressure of the water vapor present. This is based on the fact that customary atmosphere is a mixture of dry air and water vapor. According to Dalton's law the total atmospheric pressure is then the sum of the pressure due to dry air and the pressure due to water vapor. In the same way relative humidity can also be expressed in terms of pressure, since the pressure due to the vapor is approximately proportional to the amount of vapor present. Hence, the relative humidity is the ratio of the pressure of the water vapor actually present in the atmosphere divided by the pressure that would be exerted by the water vapor if the atmosphere were saturated at the existing temperature. If we multiply this ratio by 100, we have the relative humidity in per cent.

It is understood that the coefficients k_1, k_2, and k_3 have to do with atmospheric conditions and are determined from soundings (temperature and pressure readings) and k_4 is about 0.157. In above formulas p denotes the barometric pressure in millibars (1-mm column of H_g corresponds to 1.333 millibars), p_v is the water vapor pressure in millibars and about 1 per cent of p, T denotes the absolute temperature 273+°C. Wet- and dry-bulb thermometers are mostly used for finding the relative humidity of the lower atmosphere.

240. Notes on Lommel's Expressions for Fresnel Integral Evaluations. In Fresnel integrals

$$C(s) = \int_0^s \cos\,(0.5\pi s^2)\,ds \qquad \text{and} \qquad S(s) = \int_0^s \sin\,(0.5\pi s^2)\,ds \tag{931}$$

when used with diffraction problems we may employ either the Cornu spiral or the corresponding values $x = C(s)$ and $y = S(s)$ as given in Table 67. This table is carried up to arguments as high as 8.5.

According to Lommel, we can evaluate the above integrals for any argument to any desired accuracy by means of

$$\left.\begin{aligned} C(s) &= \tfrac{1}{2}\int_0^z J_{-\frac{1}{2}}(z)\,dz = \sqrt{2}\,[P(z)\cos\,(\tfrac{1}{2}z) + Q(z)\sin\,(\tfrac{1}{2}z)] \\ S(s) &= \tfrac{1}{2}\int_0^z J_{+\frac{1}{2}}(z)\,dz = \sqrt{2}\,[P(z)\sin\,(\tfrac{1}{2}z) - Q(z)\cos\,(\tfrac{1}{2}z)] \end{aligned}\right\} \tag{932}$$

where $P(z)$ and $Q(z)$ are given by the Bessel terms

$$\left.\begin{aligned} P(z) &= J_{\frac{1}{2}}(\tfrac{1}{2}z) - J_{\frac{5}{2}}(\tfrac{1}{2}z) + J_{\frac{9}{2}}(\tfrac{1}{2}z) - \cdots \\ Q(z) &= J_{\frac{3}{2}}(\tfrac{1}{2}z) - J_{\frac{7}{2}}(\tfrac{1}{2}z) - J_{1\frac{1}{2}}(\tfrac{1}{2}z) - \cdots \end{aligned}\right\} \tag{933}$$

since these series converge and we have only to add up from Bessel tables of order $(2n + 1)/2$ and to use successive alternate functions for a desired argument. Then,

also, for the field amplitude A in our diffraction solutions

$$A = \sqrt{C^2(s) + S^2(s)} = \tfrac{1}{2}\sqrt{\left[\int_0^z J_{-\frac{1}{2}}(z)\,dz\right]^2 + \left[\int_0^z J_{\frac{1}{2}}(z)\,dz\right]^2} \tag{934}$$

where A is the length of the chord from the symmetry point (origin) of the Cornu spiral to a point along the spiral that is equal to the value of s.

These formulas for the numerical evaluation of the Fresnel integrals are based on the identity or substitution

$$\frac{\pi}{2}s^2 \equiv z$$

yielding

$$s = \sqrt{\frac{2z}{\pi}} = \sqrt{\frac{2}{\pi}}\,z^{\frac{1}{2}}; \qquad ds = \frac{1}{2}\sqrt{\frac{2}{\pi}}\,z^{-\frac{1}{2}}\,dz = \frac{1}{2}\sqrt{\frac{2}{\pi z}}\,dz$$

and

$$\left.\begin{aligned} C(s) &= \int_0^s \cos\,(0.5\pi s^2)\,ds = \int_0^z \cos\left(\frac{\pi}{2}\frac{2z}{\pi}\right)\frac{1}{2}\sqrt{\frac{2}{\pi z}}\,dz \\ &= \frac{1}{2}\int_0^z \sqrt{\frac{2}{\pi z}}\cos z\,dz = \frac{1}{2}\int_0^z J_{-\frac{1}{2}}(z)\,dz \\ S(s) &= \int_0^s \sin\,(0.5\pi s^2)\,ds = \frac{1}{2}\int_0^z \sqrt{\frac{2}{\pi z}}\sin z\,dz = \frac{1}{2}\int_0^z J_{\frac{1}{2}}(z)\,dz \end{aligned}\right\} \tag{935}$$

Inasmuch as

$$J'_n(z) = \tfrac{1}{2}[J_{n-1}(z) - J_{n+1}(z)]$$

we may write

$$J_{-\frac{1}{2}}(z) = 2J'_{\frac{1}{2}}(z) + J_{\frac{3}{2}}(z) = 2J'_{\frac{1}{2}}(z) + 2J'_{\frac{5}{2}}(z) + \cdots + 2J'_{(4n+1)/2}(z) + J_{(4n+3)/2}(z)$$

Hence

$$\tfrac{1}{2}\int_0^z J_{-\frac{1}{2}}(z)\,dz = J_{\frac{1}{2}}(z) + J_{\frac{5}{2}}(z) + \cdots + J_{(4n+1)/2}(z) + \tfrac{1}{2}\int_0^z J_{(4n+3)/2}(z)\,dz$$

When the value of $(4n + 3)/2$ is chosen large enough, we can make the value of $\int_0^z J(z)\,dz$ of the order $(4n + 3)/2$ sufficiently small and arrive at the formulas

$$\left.\begin{aligned} C(s) &= \tfrac{1}{2}\int_0^z J_{-\frac{1}{2}}(z)\,dz = J_{\frac{1}{2}}(z) + J_{\frac{5}{2}}(z) + J_{\frac{9}{2}}(z) + \cdots \\ S(s) &= \tfrac{1}{2}\int_0^z J_{\frac{1}{2}}(z)\,dz = J_{\frac{3}{2}}(z) + J_{\frac{7}{2}}(z) + J_{1\frac{1}{2}}(z) + \cdots \end{aligned}\right\} \tag{936}$$

or series expressions that are convergent.

241. Gauss and Gamma Functions. These functions occur with Bessel functions $J_n(\rho)$ of the first kind if the order n is not a positive integer. We have then

$$\left.\begin{aligned} J_n(\rho) &= \sum_{m=0}^{m=\infty} \frac{(-1)^m (0.5\rho)^{n+2m}}{\prod(m)\prod(n+m)} \\ &= \frac{\rho^n}{2^n \prod(n)}\left[1 - \frac{\rho^2}{2(2n+2)} + \frac{\rho^4}{2\times 4(2n+2)(2n+4)} - \cdots\right] \\ J_n(\rho) &= \sum_{m=0}^{m=\infty} \frac{(-1)^m (0.5\rho)^{n+2m}}{m!\Gamma(n+m+1)} \\ &= \frac{(0.5\rho)^n}{\Gamma(n+1)} - \frac{(0.5\rho)^{n+2}}{\Gamma(n+2)} + \frac{(0.5\rho)^{n+4}}{2\Gamma(n+3)} - \frac{(0.5\rho)^{n+6}}{6\Gamma(n+4)} + \cdots \end{aligned}\right\} \quad (937)$$

where, for instance, $\prod(n+m)$ is known as the *Gauss* function and $\Gamma(n+m+1)$ is the *corresponding Gamma* function. Putting $n+m=x$, Table 91 can be used for numerical computations. We have also

$$\Gamma(x) = \lim_{n\to\infty} \frac{n!n^x}{x(x+1)\cdots(x+n)}; \qquad \frac{1}{\Gamma(x)} = \epsilon^{\gamma x} x \prod_1^\infty \left[\left(1+\frac{x}{n}\right)\epsilon^{-\frac{x}{n}}\right] \quad (938)$$

for the Euler constant $\gamma = 0.577216$, and

$$\Gamma(x+1) = x\Gamma(x); \qquad \prod(x) = \Gamma(x+1); \qquad \prod(x) = x\prod(x-1) \quad (939)$$

The Gamma function is defined by

$$\Gamma(\rho) \equiv \int_0^\infty \epsilon^{-z} z^{\rho-1}\, dz \quad (940)$$

which can be used to compute all *positive* integral values of argument ρ, as is shown in solutions (945) and (946). We have also $\Gamma(0) = \infty$ and

$$\Gamma(\rho) = \frac{\Gamma(\rho+1)}{\rho} \quad (941)$$

which gives a means for computing $\Gamma(\rho)$ when $\Gamma(\rho-1)$ is known.

Generally, if we put a Gauss function $\prod(k, \rho)$ equal to

$$\frac{1\times 2\times 3\cdots k}{(\rho+1)(\rho+2)(\rho+3)\cdots(\rho+k)}$$

we have

$$\prod(k,\rho) = \frac{1\times 2\times 3\cdots k}{(\rho+1)(\rho+2)(\rho+3)\cdots(\rho+k)}\, k^\rho$$

$$= \frac{1\times 2\times 3\cdots \rho}{\left(1+\frac{1}{k}\right)\left(1+\frac{2}{k}\right)\left(1+\frac{3}{k}\right)\cdots\left(1+\frac{\rho}{k}\right)}$$

if ρ is an integer. We also have

$$\prod(k, \rho+1) = \prod(k,\rho)\frac{1+\rho}{1+(1+\rho)/k} \quad (942)$$

TABLE 91. FOR $\prod(x) = \Gamma(x+1) = \Gamma(\rho)$, $x = \rho - 1$, FOR GAMMA AND GAUSS FUNCTIONS

$x = \rho - 1$		0	1	2	3	4	5	6	7	8	9	$\rho = x + 1$
0.0	0.9	999	943	888	835	784	735	687	642	597	555	1.0
0.1	.....	514	474	436	399	364	330	298	267	237	209	1.1
0.2	.....	182	156	131	108	085	064	044	025	007	*990	1.2
0.3	0.8	975	960	946	934	922	912	902	893	885	879	1.3
0.4	.....	873	868	864	860	858	857	856	856	857	859	1.4
0.5	.....	862	866	870	876	882	889	896	905	914	924	1.5
0.6	.....	935	947	959	972	986	*001	*017	*033	*050	*068	1.6
0.7	0.9	086	106	126	147	168	191	214	238	262	288	1.7
0.8	.....	314	341	368	397	426	456	487	518	551	584	1.8
0.9	.....	618	652	688	724	761	799	837	877	917	958	1.9
1.0	1.0	000	043	086	131	176	222	269	316	365	415	2.0
1.1	.....	465	516	568	621	675	730	786	842	900	959	2.1
1.2	1.1	018	078	140	202	266	330	395	462	529	598	2.2
1.3	.....	667	738	809	882	956	*031	*107	*184	*262	*341	2.3
1.4	1.2	422	503	586	670	756	842	930	*019	*109	*201	2.4
1.5	1.3	293	388	483	580	678	777	878	981	*084	*190	2.5
1.6	1.4	296	404	514	625	738	852	968	*085	*204	*325	2.6
1.7	1.5	447	571	696	824	953	*084	*216	*351	*487	*625	2.7
1.8	1.6	765	907	*051	*196	*344	*494	*646	*799	*955	**113	2.8
1.9	1.8	274	436	600	767	936	*108	*281	*457	*636	*816	2.9
2.0	2	000	019	037	057	078	095	115	136	156	177	3.0
2.1	.....	198	219	240	262	284	307	330	353	376	400	3.1
2.2	.....	424	448	473	498	524	549	575	602	629	656	3.2
2.3	.....	683	711	740	768	798	827	857	888	918	950	3.3
2.4	.....	981	*013	*046	*079	*112	*146	*181	*216	*251	*287	3.4
2.5	3	323	360	398	436	474	513	553	593	634	675	3.5
2.6	.....	717	760	803	846	891	936	981	*028	*075	*122	3.6
2.7	4	171	220	269	320	371	423	476	529	583	638	3.7
2.8	.....	694	751	808	867	926	986	*047	*108	*171	*235	3.8
2.9	5	299	365	431	499	567	637	707	779	851	925	3.9
3.0	6	000	076	153	231	311	391	473	556	640	726	4.0
3.1	.....	813	901	990	*081	*173	*267	*362	*458	*556	*656	4.1
3.2	7	757	859	963	*069	*176	*285	*396	*508	*622	*738	4.2
3.3	8	855	975	*096	*219	*344	*471	*600	*731	*864	*999	4.3
3.4	10	136	275	417	561	707	855	*005	*158	*314	*471	4.4
3.5	11	632	795	960	*128	*299	*472	*648	*827	**009	**194	4.5
3.6	13	381	572	766	962	*162	*366	*572	*782	*995	**211	4.6
3.7	15	431	655	882	*113	*348	*586	*829	**075	**325	**579	4.7
3.8	10 × 1	784	810	837	864	891	920	948	977	*006	*036	4.8
3.9	10 × 2	067	098	129	161	194	227	260	294	329	364	4.9

The equations show that for a given value of ρ the function $\prod(k, \rho)$ approaches a limiting value as k approaches infinity with a finite limiting value. Inasmuch as $\prod(\infty, \rho)$ is dependent only on ρ, we may call it $\prod(\rho)$ and Eq. (942) shows that

$$\prod_{(\rho+1)} = (\rho + 1)\prod(\rho)$$

and if ρ is an integer, $\prod(\rho)$ is the faculty of ρ.

We have then

$$\left.\begin{aligned} \prod(\rho) &= \rho! \qquad \text{for } \rho \text{ an integer} \\ \prod(\rho) &= \underbrace{\Gamma(\rho + 1)}_{\substack{\text{is Gamma} \\ \text{function of} \\ \text{Euler}}} \qquad \text{for any case} \end{aligned}\right\} \tag{943}$$

Formula (941) can be used for proving that

$$\Gamma(\rho + 1) = \rho\Gamma(\rho) = \rho! \tag{944}$$

We have according to (940) for $\rho = 1$

$$\Gamma(1) \equiv \int_0^\infty \epsilon^{-z} z^{\rho-1}\, dz = \int_0^\infty \epsilon^{-z}\, dz = 1 \tag{945}$$

Using (941) we find for $\Gamma(\rho + 1) = \Gamma(2), \Gamma(3), \Gamma(4), \ldots,$

$$\left.\begin{aligned} &\Gamma(2) = \underbrace{\Gamma(\rho + 1) = \rho\Gamma(\rho)}_{\text{formula (941)}} = 1\Gamma(1) = 1! \\ &\Gamma(3) = \Gamma(\rho + 1) = 2\Gamma(2) = 1 \times 2 = 2! \\ &\Gamma(4) = \Gamma(\rho + 1) = 3\Gamma(3) = 1 \times 2 \times 3 = 3! \\ &\Gamma(5) = \Gamma(\rho + 1) = 4\Gamma(4) = 1 \times 2 \times 3 \times 4 = 4! \\ &\ldots\ldots\ldots\ldots\ldots\ldots\ldots\ldots, \\ &\ldots\ldots\ldots\ldots\ldots\ldots\ldots\ldots \\ &\Gamma(\rho) = (\rho - 1)\Gamma(\rho - 1) = (\rho - 1)! \\ &\Gamma(\rho + 1) = \rho\Gamma(\rho) = \rho! \end{aligned}\right\} \textit{Note: } \Gamma(2) = \Gamma(1) = 1 \tag{946}$$

proving (944) and showing how to compute $\Gamma(\rho)$ for all positive integer values of ρ such as $\rho = 1, 2, 3, 4, 5, \ldots$. For *negative* values of ρ in $\Gamma(\rho)$ we use recursion formula (941) together with $\Gamma(0) = \infty$. Hence, for $\rho = -1$ and $\rho = -2$, etc., we obtain

$$\Gamma(-1) = \Gamma(\rho) = \frac{\Gamma(\rho + 1)}{\rho} = \frac{\Gamma(-1 + 1)}{-1} = \frac{\Gamma(0)}{-1} = -\infty;$$

$$\Gamma(-2) = \Gamma(\rho) = \frac{\Gamma(-2 + 1)}{-2} = \frac{\Gamma(-1)}{-2} = +\infty$$

$$\Gamma(-3) = \Gamma(\rho) = \frac{\Gamma(-3 + 1)}{-3} = \frac{\Gamma(-2)}{-3} = -\infty, \qquad \ldots,$$

$$\Gamma(-\rho) = \Gamma(\rho) = \frac{\Gamma(-\rho + 1)}{-\rho} = \infty$$

for ρ an integer. In the same way, we can compute values that are *not integers* and

like $\rho = -0.5, -0.7, -0.9, \cdots$, since

$$\Gamma(-0.5) = \Gamma(\rho) = \frac{\Gamma(\rho+1)}{\rho} = \frac{\Gamma(-0.5+1)}{-0.5} = \frac{\Gamma(0.5)}{-0.5};$$

$$\Gamma(-0.7) = \Gamma(\rho) = \frac{\Gamma(-0.7+1)}{-0.7} = \frac{\Gamma(0.3)}{-0.7};$$

$$\Gamma(-0.9) = \Gamma(\rho) = \frac{\Gamma(-0.9+1)}{-0.9} = \frac{\Gamma(0.1)}{-0.9}$$

and we can reduce such computations between $\rho = 0$ and $\rho = -1$ to values that are *positive integers*. For such fractional values of ρ, we find from (944), for instance, for $\rho = 0.5$

$$\rho! = \Gamma(\rho+1) = \Gamma(1.5) = +0.5!; \qquad \Gamma(\rho+1) = \Gamma(0.5) = -0.5!$$

We then use (940) and find, for instance, for $\rho = 1.5$

$$\Gamma(1.5) = \int_0^\infty \epsilon^{-z} z^{1.5-1}\, dz = \int_0^\infty \epsilon^{-z} z^{0.5}\, dz = \int_0^\infty \epsilon^{-x^2} x^2\, dx$$

for $x^2 = z$. This expression can be changed to a double integral and by means of a transformation into polar coordinates into another double integral, which can be evaluated and yields $\Gamma(1.5) = \sqrt{3.14}/2 \cong 0.89$, the exact value being $\Gamma(1.5) = 0.8862$ of Table 91 where we must look under argument $x = 1.5 - 1.0 = 0.5$, since this table is arranged for $\Gamma(x+1)$. Then the above procedure also gives us $\Gamma(0.5)$ as $\sqrt{3.14} = 1.772$, which result according to $\rho! = \Gamma(\rho+1)$ would also be equal to $(-0.5)!$

When using Table 91 we need not carry on the double-integration transformation into polar coordinates to find, for instance, the above result $\Gamma(0.5) = 1.772$. We then have

$$\Gamma(0.5) = \Gamma(x+1) = \Gamma(-0.5+1)$$

Inasmuch as Table 91 is not extended to $-x$ values so that we can read for arguments (-0.5) the $\Gamma(x+1) = \Gamma(-0.5+1)$ value, we first use (944) for $\rho = +0.5$ and find

$$\Gamma(0.5) = \Gamma(\rho) = \frac{\Gamma(\rho+1)}{\rho} = \frac{\Gamma(+0.5+1)}{+0.5} = 2\Gamma(1.5)$$

and

$$2\Gamma(1.5) = 2\Gamma(x+1) = 2\Gamma(0.5+1)$$

We arrive, therefore, at a positive value for x, namely, $x = 0.5$, which in Table 91 yields $2\Gamma(x+1) = 2 \times 0.8862 = 1.7724 = \Gamma(0.5)$. This checks the result obtained by the double-integral evaluation.

From this computation we note that for values of ρ between 0 and 1 we have to compute $\Gamma(\rho)$ from

$$\Gamma(\rho) = \frac{\Gamma(1+\rho)}{\rho}$$

and then find the values in Table 92. Figure 389 gives the corresponding Gamma curves confirming the results of (935) and (936) that $\Gamma(1) = 1$ as well as $\Gamma(2) = 1$. Hence, at some point between $\rho = 1$ and $\rho = 2$, say at about 1.5, the lowest value for $\Gamma(\rho)$ must occur. We note that for $\Gamma(0)$ an infinite value occurs.

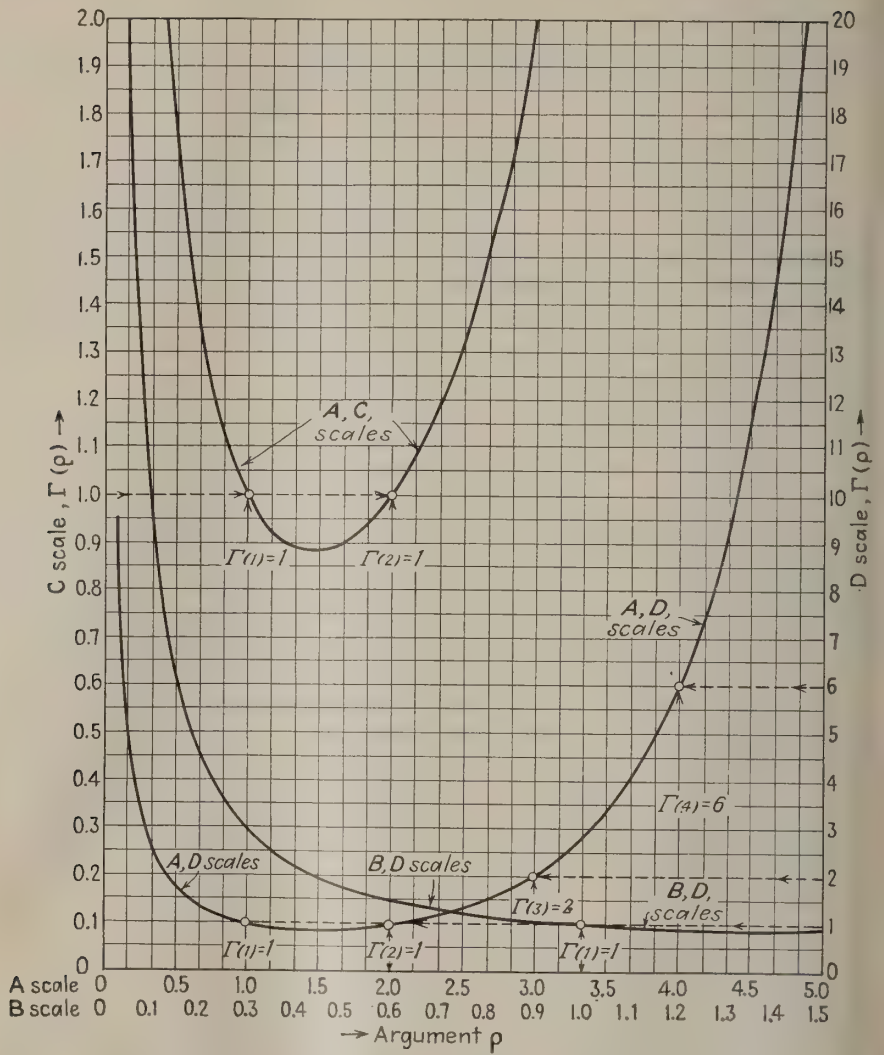

FIG. 389. Gamma curves $\Gamma(\rho)$ for $\rho = 0$ to $\rho = 4.9$. *Note:* By means of $\Gamma(\rho + 1) = \rho\Gamma(\rho) = \rho(\rho - 1)(\rho - 2) \cdots (\rho - r)\Gamma(\rho - r)$, we find the reduction of Γ (4.65) = $3.65\Gamma(3.65) = 3.65 \times 2.65\Gamma(2.65) = 3.65 \times 2.65 \times 1.65\Gamma(1.65)$. But $\Gamma(1.65) = 0.9001$, and $\Gamma(4.65) = 3.65 \times 2.65 \times 1.65 \times 0.9001 = 14.3665$. It is also $\Gamma(4.65) = 3.65 \times 2.65 \times 1.65 \times 0.65\Gamma(0.65) = 3.65 \times 2.65 \times 1.65 \times 0.65 \times 1.385 = 14.366$.

The values of the second Euler integral given by (940) and known as the Gamma function are sometimes given by the $\log \Gamma(\rho) + 10$, and as far as positive values are concerned, only values between $\rho = 1$ and $\rho = 2$ are needed, since formula (941) gives a means for reducing a large argument to a smaller argument. This is done by

$$\Gamma(\rho + 1) = \rho\Gamma(\rho) = \rho(\rho - 1) \cdots (\rho - r)\Gamma(\rho - r)$$

TABLE 92*

ρ	$1+\rho$	$\Gamma(1+\rho)$	$\Gamma(\rho)=\frac{\Gamma(1+\rho)}{\rho}$	ρ	$1+\rho$	$\Gamma(1+\rho)$	$\Gamma(\rho)=\frac{\Gamma(1+\rho)}{\rho}$
0.00	1.00	1.0000	∞	0.50	1.50	0.8862	1.7724
0.02	1.02	0.9888	49.5	0.52	1.52	0.887	1.702
0.04	1.04	0.9784	24.4	0.54	1.54	0.8882	1.64
0.06	1.06	0.9687	16.2	0.56	1.56	0.8896	1.59
0.08	1.08	0.9597	12.0	0.58	1.58	0.8914	1.538
0.10	1.10	0.9514	9.51	0.60	1.60	0.8935	1.49
0.12	1.12	0.9436	7.87	0.62	1.62	0.8959	1.445
0.14	1.14	0.9364	6.68	0.64	1.64	0.8986	1.405
0.16	1.16	0.9298	5.8	0.66	1.66	0.9017	1.365
0.18	1.18	0.9237	5.12	0.68	1.68	0.905	1.33
0.20	1.20	0.9182	4.575	0.70	1.70	0.9086	1.295
0.22	1.22	0.9131	4.15	0.72	1.72	0.9126	1.265
0.24	1.24	0.9085	3.79	0.74	1.74	0.9168	1.24
0.26	1.26	0.9044	3.475	0.76	1.76	0.9214	1.21
0.28	1.28	0.9007	3.2	0.78	1.78	0.9262	1.19
0.30	1.30	0.8975	2.99	0.80	1.80	0.9314	1.16
0.32	1.32	0.8946	2.79	0.82	1.82	0.9368	1.14
0.34	1.34	0.8922	2.61	0.84	1.84	0.9426	1.123
0.36	1.36	0.8902	2.465	0.86	1.86	0.9487	1.1
0.38	1.38	0.8885	2.33	0.88	1.88	0.9551	1.085
0.40	1.40	0.8873	2.21	0.90	1.90	0.9618	1.07
0.42	1.42	0.8864	2.105	0.92	1.92	0.9688	1.05
0.44	1.44	0.8858	2.01	0.94	1.94	0.9761	1.035
0.46	1.46	0.8856	1.92	0.96	1.96	0.9837	1.025
0.48	1.48	0.8857	1.84	0.98	1.98	0.9917	1.01

*Computed from Table 95.

Remarks: Formula (941)

$$\Gamma(\rho) = \frac{\Gamma(1+\rho)}{\rho} = \Gamma(x+1) = \Pi(x)$$

$\Gamma(\rho)$ is the Gamma function, $\Gamma(x+1)$ is the Euler Gamma function, and $\Pi(x)$ is the Gauss function. $1+\rho$ is the ρ value of Table 92. Hence, for $(1+\rho) = 1.5$ in this table we find under 1.5 in Table 92 the Gamma value 0.8862 which is the same as the $\Gamma(1+\rho)$ value of this table.

The Gamma function can also be used for evaluating an integral of the form

$$\int_0^{\frac{1}{2}\pi} \cos^n x\, dx = \frac{\sqrt{\pi}}{2} \frac{\Gamma\left(\frac{n+1}{2}\right)}{\Gamma\left(\frac{n+2}{2}\right)} \tag{947}$$

In some computations, for instance, generally almost any fractional argument x for Bessel coefficients of positive and negative nonintegers n in $J_n(x)$ functions of the first kind may occur. This requires the use of Gamma functions that have not only

a positive argument ρ in $\Gamma(\rho)$ but also a negative argument. Table 93 then gives the computations for such arguments. The method employed uses again formula (941), which, for consecutive reductions of the argument, reads when applied to numerical

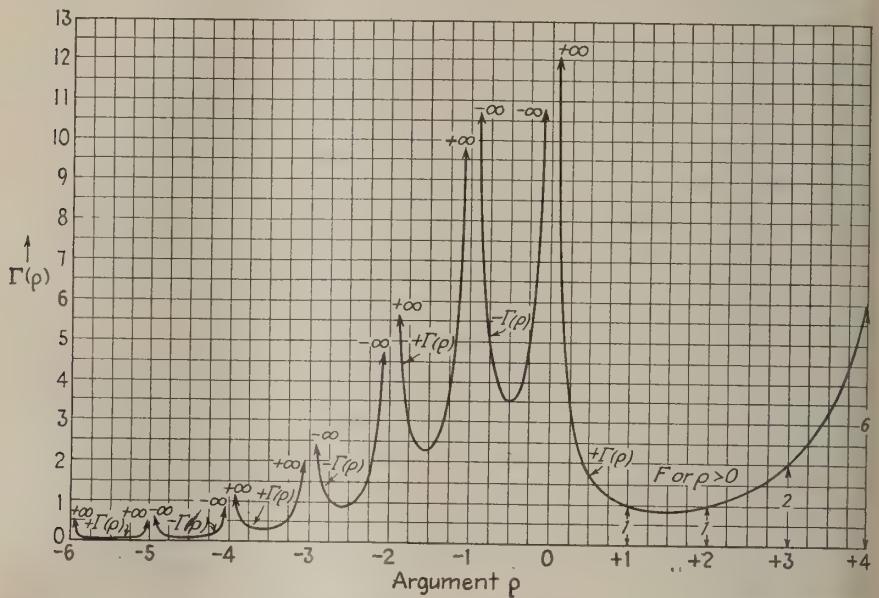

FIG. 390. Γ (Gamma) curve. *Several* $\Gamma(\rho)$ curve branches for $\rho < 0$. [*Note:* for *negative* integer arguments ρ we have $\Gamma(-1) = \mp\infty$, $\Gamma(-2) = \pm\infty$, $\Gamma(-3) = \mp\infty$, $\Gamma(-4) = \pm\infty$, $\Gamma(-5) = \mp\infty$, . . .] *Single* $\Gamma(\rho)$ curve branch for $\rho > 0$ *starts* with $\Gamma(0) = +\infty$, *decreases* rapidly over $\Gamma(1) = 1$ to a *minimum* value $\Gamma(1.5) = 0.8862$, *ascends* over $\Gamma(2) = 1$ to $\Gamma(3) = 2 = 1 \times 2 \times 2!$, to $\Gamma(4) = 3! = 1 \times 2 \times 3 = 6$, to $\Gamma(5) = 4! = 1 \times 2 \times 3 \times 4 = 24$; to $\Gamma(6) = 5!$ . . . $\Gamma(n) = (n-1)!$

cases such as $\rho = (-0.6), (-1.6), (-2.6), (-3.6), (-4.6)$

$$\Gamma(-0.6) = \Gamma(\rho) = \frac{\Gamma(\rho+1)}{\rho} = \frac{\Gamma(-0.6+1)}{-0.6} = \frac{\Gamma(0.4)}{-0.6} = \frac{2.2!}{-0.6} = -3.7$$

$$\Gamma(-1.6) = \frac{\Gamma(-1.6+1)}{-1.6} = \frac{\Gamma(-0.6)}{-1.6} = \frac{-3.7}{-1.6} = +2.31$$

$$\Gamma(-2.6) = \frac{\Gamma(-2.6+1)}{-2.6} = \frac{\Gamma(-1.6)}{-2.6} = \frac{+2.31}{-2.6} = -0.89$$

$$\Gamma(-3.6) = \frac{\Gamma(-3.6+1)}{-3.6} = \frac{\Gamma(-2.6)}{-3.6} = \frac{-0.89}{-3.6} = +0.2475$$

$$\Gamma(-4.6) = \frac{+0.2475}{-4.6} = -0.054; \qquad \Gamma(-5.6) = \frac{-0.054}{-5.6} = +0.0096; \cdots$$

We note that, for negative arguments ρ of $\Gamma(\rho)$, the $\Gamma(-\rho)$ curve *breaks up* into alternate negative and positive curve branches as in Fig. 390 which proceed toward minus and positive infinity values for both branches, since $\Gamma(-1) = [\Gamma(0)]/(-1) = \infty/(-1) = -\infty$, $\Gamma(-2) = [\Gamma(-1)]/(-2) = +\infty$, $\Gamma(-3) = -\infty$, etc. Table 93 can, therefore, be readily computed if taken from $-0.n$ to $-1.n$, $-2.n$, $3.n$, . . . values, where

TABLE 93. NEGATIVE ARGUMENTS OF THE GAMMA FUNCTION*

$\rho = 0.n$	-0.1	-0.2	-0.3	-0.4	-0.5	-0.6	-0.7	-0.8	-0.9
$\Gamma(\rho+1)$	$\Gamma(0.9) = 1.07$	$\Gamma(0.8) = 1.16$	$\Gamma(0.7) = 1.295$	$\Gamma(0.6) = 1.49$	$\Gamma(0.5) = 1.772$	$\Gamma(0.4) = 2.21$	$\Gamma(0.3) = 2.99$	$\Gamma(0.2) = 4.575$	$\Gamma(0.1) = 9.51$
$\Gamma(\rho) = \dfrac{\Gamma(\rho+1)}{\rho}$	$\dfrac{+1.07}{-0.1} = -10.7$	$\dfrac{1.16}{-0.2} = -5.8$	$\dfrac{1.295}{-0.3} = -4.3$	$\dfrac{1.49}{-0.4} = -3.72$	$\dfrac{1.772}{-0.5} = -3.54$	$\dfrac{2.21}{-0.6} = -3.7$	$\dfrac{2.99}{-0.7} = -4.26$	$\dfrac{4.575}{-0.8} = -5.71$	$\dfrac{9.51}{-0.9} = -10.6$
$\rho = 1.n$	-1.1	-1.2	-1.3	-1.4	-1.5	-1.6	-1.7	-1.8	-1.9
$\Gamma(0.n)$	-10.7	-5.8	-4.3	-3.725	-3.544	-3.7	-4.26	-5.71	-10.6
$\Gamma(\rho) = \Gamma(1.n) = \dfrac{\Gamma(0.n)}{1.n}$	$+9.75$	$+4.82$	$+3.31$	$+2.65$	$+2.36$	$\dfrac{-3.7}{-1.6} = +2.31$	$+2.51$	$+3.18$	$+5.59$
$\rho = 2.n$	-2.1	-2.2	-2.3	-2.4	-2.5	-2.6	-2.7	-2.8	-2.9
$\Gamma(1.n)$	$+9.75$	$+4.82$	$+3.31$	$+2.65$	$+2.36$	$+2.31$	$+2.51$	$+3.18$	$+5.59$
$\Gamma(\rho) = \dfrac{\Gamma(1.n)}{2.n}$	-4.65	-2.19	-1.44	-1.105	-0.942	$\dfrac{+2.31}{-2.6} = -0.89$	-0.93	-1.135	-1.92
$\rho = 3.n$	-3.1	-3.2	-3.3	-3.4	-3.5	-3.6	-3.7	-3.8	-3.9
$\Gamma(\rho) = \Gamma(3.n) = \dfrac{\Gamma(2.n)}{3.n}$	$+1.5$	$+0.685$	$+0.436$	$+0.325$	$+0.268$	$\dfrac{-0.89}{-3.6} = +0.2475$	$+0.251$	$+0.297$	$+0.493$
$\rho = 4.n$	-4.1	-4.2	-4.3	-4.4	-4.5	-4.6	-4.7	-4.8	-4.9
$\Gamma(\rho) = \Gamma(4.n) = \dfrac{\Gamma(3.n)}{4.n}$	-0.366	-0.163	-0.101	-0.074	-0.0595	$\dfrac{+0.2475}{-4.6} = -0.0096$	-0.0533	-0.0618	-0.1005
$\rho = 5.n$	-5.1	-5.2	-5.3	-5.4	-5.5	-5.6	-5.7	-5.8	-5.9
$\Gamma(\rho) = \dfrac{\Gamma(4.n)}{5.n}$	$+0.0718$	$+0.0314$	$+0.0191$	$+0.0137$	$+0.0108$	$\dfrac{-0.0096}{-5.6} = 0.00171$	$+0.00935$	$+0.0107$	$+0.0171$

* For $n = 1, 2, 3, \cdots, 9$ and $1.n = 1.1, 1.2, \cdots, 1.9$; $3.n = 3.1, 3.2, \cdots, 3.9$, etc.

$\Gamma(-1) = \Gamma(-3) = \Gamma(-5) = \Gamma(-7) \cdots = \mp\infty$; $\quad \Gamma(-2) = \Gamma(-4) = \Gamma(-6) \cdots = \pm\infty$

n is the decimal figure like 6 in -0.6; -1.6; -2.6; -3.6, etc. A slide-rule setting for the answer $\Gamma(-0.n)$ can be used for computing the $\Gamma(1.n)$ value by just dividing this setting, namely, $\Gamma(0.n)$, by $1.n$. This is self-evident by merely inspecting Table 93. Figure 390 gives not only the results of this table but also the outcome of Tables 91 and 92. We note that the $\Gamma(\rho)$ branches taper down to smaller and smaller minimum values for negative argument ranges $\rho = -0.1$ to -0.9, -1.1 to -1.9, -2.1 to -2.9, -3.1 to -3.9, -4.1 to -4.9, -5.1 to -5.9, etc. For the last of such ranges shown in Fig. 390, namely, range $\rho = -5.1$ to -5.9, the Gamma minimum is already very small, while toward $\rho = -5$ and $\rho = -6$ values it climbs very rapidly toward infinite values. This characteristic of the function $\Gamma(\rho)$ should be borne in mind when such functions are used in practical applications. The rapid increase toward infinite values can only be indicated on a curve sheet, but by means of the procedure brought out in detail in Table 93 we can always quickly compute the exact magnitude of such large values as, for instance, occur near negative integers.

Inasmuch as the Gamma function is defined by

$$\int_0^\infty \epsilon^{-x} x^{n-1}\, dx = \Gamma(n)$$

we have by parts

$$\int \epsilon^{-x} x^n\, dx = -\epsilon^{-x} x^n + n \int \epsilon^{-x} x^{n-1}\, dx$$

Putting these between the limits, it is easy to prove that $-\epsilon^{-x} x^n$ vanishes when $x = 0$ and $x = \infty$, and we find

$$\int_0^\infty \epsilon^{-x} x^n\, dx = n \int_0^\infty \epsilon^{-x} x^{n-1}\, dx$$

or

$$\Gamma(n+1) = n\Gamma(n) = 1 \cdot 2 \cdot 3 \cdot 4 \cdot \cdots \cdot n = n!$$

where $n!$ has a meaning only when n is an integer, while $\Gamma(n)$ is a function of *any value* of n. Many useful definite integrals can be solved by means of the Gamma function, as, for instance,

$$\int_0^{\frac{1}{2}\pi} \sin^n \theta\, d\theta = \int_0^{\frac{1}{2}\pi} \cos^n \theta\, d\theta = \frac{1}{2}\sqrt{\pi}\,\Gamma\left(\frac{n+1}{2}\right) \div \Gamma\left(\frac{1}{2}n + 1\right)$$

$$\int_0^1 x^{m-1}(1-x)^{n-1}\, dx = \int_0^\infty \frac{x^{m+1}\, dx}{(1+x)^{m+1}} = \frac{\Gamma(m)\Gamma(n)}{\Gamma(m+n)};$$

$$\int_0^\infty \epsilon^{-a^2x^2}\, dx = \frac{1}{2a}\,\Gamma\left(\frac{1}{2}\right) = \frac{1}{2a}\sqrt{\pi}$$

$$\int_0^\infty x^n \epsilon^{-ax}\, dx = a^{-(n+1)}\Gamma(n+1); \qquad \int_0^1 x^m \log_\epsilon\left(\frac{1}{x}\right)^n dx = \frac{\Gamma(n+1)}{(m+1)^{n+1}};$$

$$\int_0^\infty \frac{\epsilon^{-z}\, dz}{2a\sqrt{z}} = \frac{1}{2a}\,\Gamma\left(\frac{1}{2}\right)$$

$$\frac{1}{2}\int_0^1 z^{(\frac{1}{2})l-1}(1-z)^{m-1}\, dz = \Gamma\left(\frac{1}{2}l\right)\Gamma(m) \div 2\Gamma\left(\frac{1}{2}l + m\right);$$

$$\int_0^{\frac{1}{2}\pi} \sin^p \theta \cos^q \theta\, d\theta = \frac{\Gamma\left(\frac{p+1}{2}\right)\Gamma\left(\frac{q+1}{2}\right)}{2\Gamma\left(\frac{p+q}{2}+1\right)}$$

242. Notes on Si x and Ci x Functions. These are sine and cosine integral functions defined by

$$\text{Si } x = \int_0^x \frac{\sin u}{u}\,du \qquad \text{and} \qquad \text{Ci } x = \int_\infty^x \frac{\cos u}{u}\,du$$

They are given by means of curves and tables in Fig. 147 as well as in another publication.[1] The most extended table for arguments $x = 10$ to 100 is in Table of Sine and Cosine Integrals of the Federal Works Agency Work Projects Administration under the sponsorship of the National Bureau of Standards. The curves of Fig. 147 show that for increasing values of x, the Si x curve oscillates about the $\frac{1}{2}\pi$ value into such a value, while for the Ci x curve the zero value is approached with increasing argument x and Ci x starts with $-\infty$. The consecutive zero values occur for Ci x for $x \cong 0.62$, 3.4, 6.4, 9.4, 12.64, 15.77. Maximum positive and negative fluctuations about the Ci $x = 0$ value occur for $x = 0.5\pi = 1.57$ with Ci $1.57 = +0.472$, $x = 1.5\pi$ with Ci $1.5\pi = -0.19841$ with other consecutive arguments $x = 2.5\pi$, 3.5π, 4.5π, 5.5π, . . . , and values Ci $2.5\pi = +0.12377$, Ci $3.5\pi = -0.089564$, Ci $4.5\pi = +0.070065$, Ci $5.5\pi = -0.057501$, Ci $6.5\pi = +0.048742$, Ci $7.5\pi = -0.042292$, Ci $8.5\pi = +0.037345$, ... For the Si x function, the fluctuation is about the 0.5π value, and for $x = \pi$; 2π, 3π, 4π, 5π, 6π, 7π, . . . , with $+0.28114$, -0.15264, $+0.10396$, -0.078635, $+0.063168$, -0.052762, $+0.045289$, . . . , swings about the value Si 1.57.

243. Notes on Bessel Functions.[2] We have, for the arguments $x \sin\theta$ in sine and cosine functions, the relations

$$\left.\begin{aligned} \cos(x\sin\theta) &= J_0(x) + 2[J_2(x)\cos(2\theta) + J_4(x)\cos(4\theta) + \cdots] \\ \sin(x\sin\theta) &= 2[J_1(x)\sin\theta + J_3(x)\sin(3\theta) + J_5(x)\sin(5\theta) + \cdots] \end{aligned}\right\} \quad (948)$$

For the Bessel coefficient t^n of argument x and order n, we have

$$\sum_{n=-\infty}^{n=\infty} t^n J_n(x) = \epsilon^{0.5x(t-1/t)} = \sum_{r=0}^{r=\infty} \frac{(0.5x)^r t^r}{r!} \sum_{m=0}^{m=\infty} \frac{(-0.5x)^m t^{-m}}{m!} \quad (949)$$

where the right side is the generating function of the Bessel coefficients. To obtain Bessel coefficients of negative order, we have

$$J_{-n}(x) = (-1)^n J_n(x); \qquad \epsilon^{0.5x[t-(1/t)]} = J_0(x) + \sum_{n=1}^{n=\infty} [t^n + (-1)^n] J_n(x) \quad (950)$$

For $r = n + m$ and n a positive integer or zero, we find

$$J_n(x) = \sum_{m=0}^{m=\infty} \frac{(-1)^m (0.5x)^{n+2m}}{m!(n+m)!} = \frac{x^n}{2^n n!}\left[1 - \frac{x^2}{2^2 \cdot 1(n+1)} + \frac{x^4}{2^4 \cdot 1 \cdot 2(n+1)(n+2)} - \cdots\right] \quad (951)$$

$$J_0(x) = 1 - \frac{x^2}{2^2} + \frac{x^4}{2^2 \cdot 4^2} - \frac{x^6}{2^2 \cdot 4^2 \cdot 6^2} + \cdots \quad (952)$$

[1] HUND, A., "Frequency Modulation," McGraw-Hill Book Company, Inc., New York, 1942; see also Jahnke and Emde in following footnote.

[2] Extended tables and curves are given in E. Jahnke and F. Emde "Tables of Functions," Dover Publications, Inc., New York, 1945. N. W. McLachlan, "Bessel Functions for Engineers," Oxford University Press, New York, 1934; A. Hund, *op. cit.*

For x real or complex, we find

$$|J_n(x)| \leqq |0.5x|^n \sum_{m=0}^{m=\infty} \frac{|0.5x|^{2m}}{m!(n+m)!} \leqq \frac{|0.5x|^n}{n!} \sum_{m=0}^{m=\infty} \frac{|0.5x|^{2m}}{m!(n+1)^m} \tag{953}$$

$$J_{n-1}(x) + J_{n+1}(x) = \frac{2n}{x} J_n(x); \qquad J_{n-1}(x) - J_{n+1}(x) = 2J'_n(x);$$

$$0.5x[J_{n-1}(x) + J_{n+1}(x)] = nJ_n(x) \tag{954}$$

$$J'_0(x) = -J_1(x) \qquad \text{where} \qquad \frac{d[J_0(x)]}{dx} = J'_0(x) \tag{955}$$

$$2^r \frac{d^r[J_n(x)]}{dx^r} = \sum_{m=0}^{r} (-1)^m {}_rC_m J_{n-r+2m}(x) \qquad \text{where } {}_rC_m \text{ is a binomial coefficient} \tag{956}$$

$$J_n(x) = \frac{1}{2\pi} \int_0^{2\pi} \cos(n\varphi - x \sin\varphi)\, d\varphi = \frac{1}{2\pi} \int_0^{\pi} [\epsilon^{j(n\varphi - x\sin\varphi)} + \epsilon^{-j(n\varphi - x\sin\varphi)}]\, d\varphi$$

$$= \frac{1}{\pi} \int_0^{\pi} \cos(n\varphi) \cos(x \sin\varphi)\, d\varphi + \frac{1}{\pi} \int_0^{\pi} \sin(n\varphi) \sin(x \sin\varphi)\, d\varphi \tag{957}$$

$$J_0(\sqrt{x^2 - y^2}) = \frac{1}{\pi} \int_0^{\pi} \epsilon^{y\cos\varphi} \cos(x \sin\varphi)\, d\varphi;$$

$$J_0(2j\sqrt{x}) = \frac{1}{\pi} \int_0^{\pi} \epsilon^{(1+x)\cos\varphi} \cos[(1-x)\sin\varphi]\, d\varphi \tag{958}$$

$$\epsilon^{\pm jx\sin\varphi} = J_0(x) + \sum_{n=1}^{n=\infty} (\pm 1)^n [\epsilon^{jn\varphi} + (-1)^n \epsilon^{-jn\varphi}] J_n(x)$$

$$= J_0(x) + 2 \sum_{n=1}^{n=\infty} J_{2n}(x) \cos(2n\varphi) \pm j2 \sum_{n=0}^{n=\infty} J_{2n+1}(x) \sin[(2n+1)\varphi] \tag{959}$$

$$J_n(x+y) = \sum_{m=-\infty}^{m=\infty} J_m(x) J_{n-m}(y) \tag{960}$$

when n is also unrestricted like x, *i.e.*, n has no longer to be an integer, we find

$$J_n(x) = \frac{(\frac{1}{2}x)^n}{\Gamma(x + \frac{1}{2})\Gamma(\frac{1}{2})} \int_0^{\pi} \cos(x\cos\varphi) \sin(2n\varphi)\, d\varphi = \sum_{m=0}^{m=\infty} \frac{(-1)^m (\frac{1}{2}x)^{n+2m}}{m!\Gamma(n+m+1)} \tag{961}$$

We have also the relations

$$\underbrace{\int_0^{\pi} \cos(n\varphi) \cos(x\sin\varphi)\, d\varphi}_{p} = \pi J_n(x) \qquad \text{for } n \textit{ even} \text{ or zero; } = 0 \qquad \text{for } n \textit{ odd} \tag{962}$$

$$\int_0^{\pi} p = \tfrac{1}{2}\pi(1 + j^n) J_n(x) \qquad \text{is single formula for } \textit{odd and even} \text{ values of } n \tag{963}$$

$$\int_0^{\pi} q = \tfrac{1}{2}\pi(1 - j^n) J_n(x) \qquad \text{for odd and even values} \qquad \text{and}$$

$$q = \sin(n\varphi) \sin(x\sin\varphi)\, d\varphi \tag{964}$$

Adding (963) and (964) yields, for n zero or any positive integer,

$$\int_0^\pi \cos\,(n\varphi - x\sin\varphi)\,d\varphi = \pi J_n(x) \tag{965}$$

Moreover,

$$\begin{aligned}\cos x &= J_0(x) - 2J_2(x) + 2J_4(x) - \cdots\\ \sin x &= 2J_1(x) - 2J_3(x) + 2J_5(x) - \cdots\end{aligned} \tag{966}$$

The *modified* Bessel function of the first kind is

$$I_n(x) = j^{-n}J_n(jx)$$

and we have the formulas

$$\left.\begin{aligned}\cosh x &= I_0(x) + 2I_2(x) + 2I_4(x) + \cdots\\ \sinh x &= 2I_1(x) + 2I_3(x) + 2I_5(x) + \cdots\\ x\cos x &= 2[J_1(x) - 3^2J_3(x) + 5^2J_5(x) - \cdots]\\ \cosh(x\sin\varphi) &= I_0(x) - 2I_2(x)\cos(2\varphi) + 2I_4(x)\cos(4\varphi) - \cdots\\ \sinh(x\sin\varphi) &= 2I_1(x)\sin\varphi - 2I_3(x)\sin(3\varphi) + 2I_5(x)\sin(5\varphi) - \cdots\\ \cosh(x\cos\varphi) &= I_0(x) + 2I_2(x)\cos(2\varphi) + 2I_4(x)\cos(4\varphi) + \cdots\\ \sinh(x\cos\varphi) &= 2I_1(x)\cos\varphi + 2I_3(x)\cos(3\varphi) + 2I_5(x)\cos(5\varphi) + \cdots\\ \cosh(x\cosh\varphi) &= J_0(x) - 2J_2(x)\cosh(2\varphi) + 2J_4(x)\cosh(4\varphi) - \cdots\\ \sinh(x\cosh\varphi) &= 2I_1(x)\cosh\varphi\\ &\quad + 2I_3(x)\cosh(3\varphi) + 2I_5(x)\cosh(5\varphi) + \cdots\end{aligned}\right\} \tag{967}$$

We have also

$$\left.\begin{aligned}&\frac{1}{\pi}\int_0^\pi \cos\,[r\cos(\varphi+\theta)]\,d\varphi = J_0(r)\\ &\frac{1}{\pi}\int_0^\pi \epsilon^{jx\cos\varphi}\cos(y\sin\varphi)\,d\varphi = J_0(\sqrt{x^2+y^2})\\ &J_n(x) = \frac{(-j)^n}{\pi}\int_0^\pi \epsilon^{jx\cos\varphi}\cos(n\varphi)\,d\varphi\\ &\epsilon^{\pm pq\sin\varphi} = I_0(pq) + 2\sum_{n=1}^{\infty}(-1)^nI_{2n}(pq)\cos(2n\varphi)\\ &\qquad\qquad \pm 2\sum_{n=0}^{\infty}(-1)^nI_{2n+1}(pq)\sin(2n+1)\varphi\\ &\epsilon^{\pm pq\cos\varphi} = I_0(pq) + 2\sum_{n=1}^{\infty}I_n(\pm pq)\cos(n\varphi)\\ &\epsilon^{jp\cos\varphi} = J_0(p) + 2\sum_{n=1}^{\infty}j^nJ_n(p)\cos(n\varphi)\end{aligned}\right\} \tag{968}$$

244. Notes on Scalar and Vector Relations in Cartesian, Cylindrical, and Spherical Coordinates. In *Cartesian* coordinates x, y, z meters, a space point P is a distance

$r = \sqrt{x^2 + y^2 + z^2}$ meters from the origin of the XYZ system and an elementary length is $dl = \sqrt{dx^2 + dy^2 + dz^2}$. A volume element at P is $d\tau = dx\,dy\,dz$ with elementary surfaces $dy\,dz$, $dz\,dx$, and $dx\,dy$. In *cylindrical* coordinates r, φ, z, we have $r = \sqrt{x^2 + y^2}$; $x = r\cos\varphi$, $y = r\sin\varphi$ meters. Hence, φ is the angle, in circular radians, that r makes with the $+X$ direction when in planes parallel with the XY plane. We have the elementary length $dl = \sqrt{(dr)^2 + (r\,d\varphi)^2 + (dz)^2}$. At P we have the volume element $d\tau = r\,dr\,d\varphi\,dz$, since dr, $r\,d\varphi$, and dz are the components along the characteristic r, φ, and z directions. Normal to the r coordinate, we have the elementary area $r\,d\varphi\,dz$; normal to the φ direction, we have the area $dr\,dz$; and normal to z, we have $r\,dr\,d\varphi$, all areas being expressed in square meters, even though infinitesimal. In *spherical* r, φ, θ coordinates, we have $r = \sqrt{x^2 + y^2 + z^2}$ meters as the distance of P from the origin in *any* space direction, for the Laplace transformations $x = r\sin\theta\cos\varphi$, $y = r\sin\theta\sin\varphi$, and $z = r\cos\theta$, since θ is the angle that r makes with the $+Z$ axis and φ is the angle that the projection of the resultant r into the XY plane makes with the $+X$ axis. The resultant line element is given by $dl = \sqrt{(dr)^2 + (r\,d\theta)^2 + (r\sin\theta\,d\varphi)^2}$, since the components are now along the r, φ, and θ directions and are dr, $r\,d\theta$, and $r\sin\theta\,d\varphi$, respectively. The elementary volume at any space point P is $d\tau = r^2\,dr\,d\varphi\sin\theta\,d\theta$. At any point $P(r, \varphi, \theta)$, we have normal to the r coordinate the elementary area $r^2\sin\theta\,d\varphi\,d\theta$, normal to the φ coordinate an area $r\,dr\,d\theta$, and normal to the θ coordinate the elementary area $r\sin\theta\,dr\,d\varphi$.

There are several ways of expressing scalar functions and vectors. Thus J. A. Stratton expresses scalar functions by Greek letters and uses Roman letters for vectors. The nomenclature used in this text, with a dot below the letter, is employed for convenience, so that we can omit the dot below as long as it is understood that we deal with a quantity which has magnitude as well as direction. The magnitude of a quantity refers then to the maximum value. Throughout the text H and $\mathcal{E}$ are used for the sake of simplicity and the solution always shows whether we deal with any instantaneous value, a vector, or a maximum value, for H and $\mathcal{E}$.

For two vectors $\underset{\cdot}{A}$ and $\underset{\cdot}{B}$ (electrical and magnetic field vectors are examples) of magnitudes A and B, which make an angle ψ with each other, we have

$$\left.\begin{aligned} \underset{\cdot}{A} \cdot \underset{\cdot}{B} &= AB\cos\psi \qquad \textit{scalar} \text{ or } \textit{dot} \text{ product } (\cdot \text{ product}) \\ \underset{\cdot}{A} \times \underset{\cdot}{B} &= \underset{\cdot}{\nu} AB\sin\psi \qquad \textit{vector} \text{ or } \textit{cross} \text{ product } (\times \text{ product}),\ \underset{\cdot}{\nu} \text{ unit vector} \end{aligned}\right\} \tag{969}$$

The dot *below* is usually omitted for the sake of simplification in this book. The first product with the vector $\underset{\cdot}{B}$ turned into the $\underset{\cdot}{A}$ direction is a scalar, since $B\cos\psi$ is the projection of $\underset{\cdot}{B}$ on $\underset{\cdot}{A}$ or of $\underset{\cdot}{A}$ on $\underset{\cdot}{B}$. Therefore, we have inphase condition. If $\underset{\cdot}{A}$ were a voltage $\underset{\cdot}{E}$ and $\underset{\cdot}{B}$ a current $\underset{\cdot}{I}$, the scalar $EI\cos\psi$ would be the power in watts, just as for $A = \mathcal{E}$ volts per meter and $B = H$ amperes per meter we have $\underset{\cdot}{\mathcal{E}} \cdot \underset{\cdot}{H} = \mathcal{E}H\cos\psi$ watts per square meter for a wave propagation normal to the plane that $\underset{\cdot}{\mathcal{E}}$ makes with $\underset{\cdot}{H}$. Since $A = \sqrt{A_x^2 + A_y^2 + A_z^2}$ and $B = \sqrt{B_x^2 + B_y^2 + B_z^2}$, for unity vectors i, j, and k along the Cartesian X, Y, and Z directions, we have the relations $\underset{\cdot}{A} = iA_x + jA_y + kA_z$ and $\underset{\cdot}{B} = iB_x + jB_y + kB_z$. Since $ik = |ik|\cos 90° = 0$ if $|ik|$ denotes the absolute amount of the product, we have

$$iA_x jA_y = jA_y kA_z = kA_z iA_x = 0$$

and the same way for $\underset{\cdot}{B}$ in place of $\underset{\cdot}{A}$ or any other vector, since any two unit vectors

are perpendicular to each other. Hence,

$$\underset{\cdot}{A} \cdot \underset{\cdot}{B} = A_xB_x + A_yB_y + A_zB_z = AB \cos \theta = \underset{\cdot}{B} \cdot$$

It is an operation as in algebra, since we can multiply $\underset{\cdot}{A}$ by $\underset{\cdot}{B}$ or $\underset{\cdot}{B}$ by $\underset{\cdot}{A}$ with the same *scalar* result. *However, for* the *cross product* we have $\underset{\cdot}{A} \times \underset{\cdot}{B} = -\underset{\cdot}{B} \times \underset{\cdot}{A}$ and in each case a *new vector* as the result. This vector (or cross product) is then a vector in either the positive or the negative direction normal to the plane in which $\underset{\cdot}{A}$ and $\underset{\cdot}{B}$ are located. For this reason the vector product with an absolute value of $AB \sin \theta$ is also to be multiplied by a unit vector $\underset{\cdot}{v}$. Due to the vector property and the perpendicular direction, we now have

$$i \times j = k = -j \times i; \qquad j \times k = i = -k \times j; \qquad k \times i = j = -i \times k \quad (970)$$

since the remaining unit vector, which does not enter the cross product, is always normal to the vectors that are multiplied and in the direction that a right-hand screw would move. The polarity of the resultant vector is found by using the alphabetical order x, y, z and i, j, k, making then, for instance, $iA_x \times jB_y = kA_xB_y$ a positive quantity, since the alphabetical order applies. But for the cross product $jA_y \times iB_x$, both y and x and j and i are in the *reverse* alphabetical order, and we find the new vector, which represents the cross product equal to $-kA_yB_x$. We have, therefore,

$$\left.\begin{array}{l} \left\{\begin{array}{l} iA_x \times jB_y = +kA_xB_y \\ jA_y \times iB_x = -kA_yB_x \end{array}\right\}; \qquad \left\{\begin{array}{l} jA_y \times kB_z = +iA_yB_z \\ kA_z \times jB_y = -iA_zB_y \end{array}\right\} \\ \qquad\qquad \left\{\begin{array}{l} kA_z \times iB_x = +jA_zB_x \\ iA_x \times kB_z = -jA_xB_z \end{array}\right\} \end{array}\right\} \quad (971)$$

Hence,

$$\left.\begin{array}{l} \underbrace{iA_x \times jB_y + jA_y - iB_x}_{(\underset{\cdot}{A} \times \underset{\cdot}{B})_z} = k(A_xB_y - A_yB_x) \\ \underbrace{jA_y \times kB_z + kA_z \times jB_y}_{(\underset{\cdot}{A} \times \underset{\cdot}{B})_x} = i(A_yB_z - A_zB_y) \\ \underbrace{kA_z \times iB_x + iA_x \times kB_z}_{(\underset{\cdot}{A} \times \underset{\cdot}{B})_y} = j(A_zB_x - A_xB_z) \\ \underset{\cdot}{A} \times \underset{\cdot}{B} = (\underset{\cdot}{A} \times \underset{\cdot}{B})_x + (\underset{\cdot}{A} \times \underset{\cdot}{B})_y + (\underset{\cdot}{A} \times \underset{\cdot}{B})_z \\ \qquad = i(A_yB_z - A_zB_y) + j(A_zB_x - A_xB_z) + k(A_xB_y - A_yB_x) \end{array}\right\} \quad (972)$$

A *gradient* is the partial derivative of a space function Φ along a desired direction, and a *maximum* gradient occurs when taken *normal* to level surfaces. For the point function Φ in space, even though a scalar quantity, the gradient along a certain direction is a vector, and the resultant gradient is grad $\Phi = (\partial\Phi/\partial n)\underset{\cdot}{v}_n$, where n means the normal direction to the level surface and $\underset{\cdot}{v}_n$ is a unit vector along this direction. We have then

$$\frac{\partial \Phi}{\partial n} = \sqrt{\left(\frac{\partial \Phi}{\partial x}\right)^2 + \left(\frac{\partial \Phi}{\partial y}\right)^2 + \left(\frac{\partial \Phi}{\partial z}\right)^2} = \frac{\partial \Phi}{\partial x} \cos \alpha + \frac{\partial \Phi}{\partial y} \cos \beta + \frac{\partial \Phi}{\partial z} \cos \gamma \quad (973)$$

where α, β, and γ are the angles that the normal direction n makes with the X, Y, and Z directions.

A line integral of a vector $\underset{\cdot}{A}$ is defined by $\int_l \underset{\cdot}{A}\, dl$ if l denotes the length in meters

over the curve it is to be taken. This length may be a closed path, and the line integral is then written as $\oint_l A\,dl$ and known as a circulation, which, when referred to a vanishingly small closed contour and taken per unit area, is the rotation of vector $\mathfrak{A}$ or curl $\mathfrak{A}$. It is then a vector normal to the plane of the closed path l. Integrals of this type where we use, for instance, $\mathfrak{A} = \mathfrak{H}$ or $\mathfrak{A} = \mathfrak{E}$, respectively, express the magnetomotive force $\oint \mathfrak{H}\,dl$ amperes or the electromotive force $\oint \mathfrak{E}\,dl$ volts, respectively. Both the gradient of a space location function Φ and the curl of a vector $\mathfrak{A}$ have components, because in either case we deal with vectors, even though Φ may be a scalar quantity. We find then

$$\left.\begin{aligned}
&\operatorname{grad}_x \Phi = \frac{\partial \Phi}{\partial x}; \quad \operatorname{grad}_y \Phi = \frac{\partial \Phi}{\partial y}; \quad \operatorname{grad}_z \Phi = \frac{\partial \Phi}{\partial z} \\
&\left.\begin{aligned}
\operatorname{curl}_x \mathfrak{A} &= \frac{\partial A_z}{\partial y} - \frac{\partial A_y}{\partial z} \\
\operatorname{curl}_y \mathfrak{A} &= \frac{\partial A_x}{\partial z} - \frac{\partial A_z}{\partial x} \\
\operatorname{curl}_z \mathfrak{A} &= \frac{\partial A_y}{\partial x} - \frac{\partial A_x}{\partial y}
\end{aligned}\right\} \text{since} \\
&\operatorname{curl} \mathfrak{A} \equiv \nabla \times \mathfrak{A} \equiv \begin{vmatrix} i & j & k \\ \dfrac{\partial}{\partial x} & \dfrac{\partial}{\partial y} & \dfrac{\partial}{\partial z} \\ A_x & A_y & A_z \end{vmatrix} \equiv \operatorname{curl}_x \mathfrak{A} + \operatorname{curl}_y \mathfrak{A} + \operatorname{curl}_z \mathfrak{A}
\end{aligned}\right\} \text{in Cartesian } XYZ \text{ system} \tag{974}$$

Generally $\operatorname{curl}_s \mathfrak{A}$ of curl $\mathfrak{A}$ in the s direction is equal to the work done by a force $\mathfrak{A}$ in the s surface per square meter for a vanishingly small surface. In cylindrical coordinates r, φ, and z, we have

$$\left.\begin{aligned}
&\operatorname{grad}_r \Phi = \frac{\partial \Phi}{\partial r}; \quad \operatorname{grad}_\varphi \Phi = \frac{\partial \Phi}{r\,\partial \varphi}; \quad \operatorname{grad}_z \Phi = \frac{\partial \Phi}{\partial z}; \quad \operatorname{curl}_r \mathfrak{A} = \frac{1}{r}\frac{\partial A_z}{\partial \varphi} - \frac{\partial A_\varphi}{\partial z} \\
&\operatorname{curl}_\varphi \mathfrak{A} = \frac{\partial A_r}{\partial z} - \frac{\partial A_z}{\partial r}; \quad \operatorname{curl}_z \mathfrak{A} = \frac{1}{r}\frac{\partial (rA_\varphi)}{\partial r} - \frac{1}{r}\frac{\partial A_r}{\partial \varphi}
\end{aligned}\right\} \tag{975}$$

In spherical r, φ, θ, we have

$$\left.\begin{aligned}
&\operatorname{grad}_r \Phi = \frac{\partial \Phi}{\partial r}; \quad \operatorname{grad}_\varphi \Phi = \frac{1}{r \sin \theta}\frac{\partial \Phi}{\partial \varphi}; \quad \operatorname{grad}_\theta \Phi = \frac{1}{r}\frac{\partial \Phi}{\partial \theta}; \\
&\operatorname{curl}_r \mathfrak{A} = \frac{\dfrac{\partial (\sin \theta A_\varphi)}{\partial \theta} - \dfrac{\partial A_\theta}{\partial \varphi}}{r \sin \theta}; \quad \operatorname{curl}_\varphi \mathfrak{A} = \frac{\dfrac{\partial (rA_\theta)}{\partial r} - \dfrac{\partial A_r}{\partial \theta}}{r} \\
&\operatorname{curl}_\theta \mathfrak{A} = \frac{\dfrac{\partial A_r}{\partial \varphi} - \sin \theta \dfrac{\partial (rA_\varphi)}{\partial r}}{r \sin \theta}
\end{aligned}\right\} \tag{976}$$

where, for instance, $\operatorname{curl}_r \mathfrak{A} \equiv \operatorname{rot}_r \mathfrak{A}$ is the work done around an elementary area located at a space point $P(r, \varphi, \theta)$ and normal to the r direction divided by the infinitesimal area. The orthogonal sides are $r\,d\theta$, $r\,d\varphi \sin \theta$. The portion $[\partial(\sin \theta A_\varphi)]/\partial\theta$ is the rate of change in the θ direction of the absolute amount A, and the portion $\partial A/\partial \varphi$ is the rate of change along the φ coordinate. In a similar way, the partial

differentiations of argument rA_θ with respect to r and A_r with respect to θ are the respective rates of change in the r and θ directions for the elementary area normal to the φ direction. The elementary area is then made up of pairs of orthogonal sides dr and $r\,d\theta$, causing an area of $r\,dr\,d\theta$, expressed in square meters. For the $\text{curl}_\theta \underset{\sim}{A}$, the sides are dr and $r \sin\theta\, d\varphi$ with $r \sin\theta\, dr\, d\theta$ for the elementary area.

The divergence of a vector is a *scalar* and written as

$$\left.\begin{aligned}
\text{div } \underset{\sim}{A} \equiv \nabla \cdot \underset{\sim}{A} &= \frac{\partial A_x}{\partial x} + \frac{\partial A_y}{\partial y} + \frac{\partial A_z}{\partial z} && \text{Cartesian} \\
\text{div } \underset{\sim}{A} \equiv \nabla \cdot \underset{\sim}{A} &= \frac{1}{r}\frac{\partial (rA_r)}{\partial r} + \frac{1}{r}\frac{\partial A_\varphi}{\partial \varphi} + \frac{\partial A_z}{\partial z} && \text{cylindrical} \\
\text{div } \underset{\sim}{A} \equiv \nabla \cdot \underset{\sim}{A} &= \frac{1}{r^2}\frac{\partial (r^2 A_r)}{\partial r} + \frac{1}{r \sin\theta}\left[\frac{\partial (A_\theta \sin\theta)}{\partial \theta} + \frac{\partial A_\varphi}{\partial \varphi}\right] && \text{spherical}
\end{aligned}\right\} \tag{977}$$

We also have

$$\text{curl } \underset{\sim}{A} \equiv \nabla \times \underset{\sim}{A}; \qquad \text{div } \underset{\sim}{A} \equiv \nabla \cdot \underset{\sim}{A} \tag{978}$$

and the relation

$$\nabla \times (\nabla \times \underset{\sim}{A}) = \nabla(\nabla \cdot \underset{\sim}{A}) - \nabla^2 \underset{\sim}{A} \tag{979}$$

for any vector. The operator ∇ is usually given as

$$\nabla \equiv i\frac{\partial}{\partial x} + j\frac{\partial}{\partial y} + k\frac{\partial}{\partial z}$$

denoting a directional derivative. When ∇ operates on a *scalar* point function $\Phi(x, y, z)$, it produces

$$\nabla\Phi \equiv i\frac{\partial \Phi}{\partial x} + j\frac{\partial \Phi}{\partial y} + k\frac{\partial \Phi}{\partial z}$$

which is a *vector* point function. It has at every point the direction of *greatest* rate of increase of the scalar function with a magnitude that is a measure of the rate of increase. The directional derivative of a scalar is then $\underset{\sim}{n} \nabla\Phi \equiv \partial\Phi/\partial n$ where $\underset{\sim}{n}$ is the external normal unit. This vector operator can also be written as

$$\nabla \equiv \lim_{\tau \to 0}\left(\frac{1}{\tau}\int\int_S \underset{\sim}{n}\, dS\right)$$

giving for the gradient of a scalar Φ

$$\nabla\Phi \equiv \text{grad } \Phi \equiv \lim_{\tau \to 0}\left(\frac{1}{\tau}\int\int_S \underset{\sim}{n}\Phi\, dS\right)$$

Since ∇ operates[1] also on vectors, we find for a vector $\underset{\sim}{A}$

[1] With respect to the Hamiltonian nabla ∇, the ∇^2, and the del operator Δ, we have for any function $\Phi(x,y,z,)$ the expression for nabla phi

$$\nabla\Phi \equiv i\frac{\partial \Phi}{\partial x} + j\frac{\partial \Phi}{\partial y} + k\frac{\partial \Phi}{\partial z}$$

$$\nabla \cdot \underset{\cdot}{A} \equiv \lim_{\tau \to 0} \left(\frac{1}{\tau} \int \int_S \underset{\cdot}{n} \underset{\cdot}{A} \, dS \right) \equiv \text{div } \underset{\cdot}{A} \qquad \text{expresses a strength of a source}$$

and for the cross product

$$\nabla \times \underset{\cdot}{A} \equiv \lim_{\tau \to 0} \left(\frac{1}{\tau} \int \int_S \underset{\cdot}{n} \times \underset{\cdot}{A} \, dS \right) \equiv \text{curl } \underset{\cdot}{A} \qquad \text{expresses a kinematic rotary action} \tag{980}$$

The operator ∇^2 refers then to another differentiation, for instance,

$$\nabla^2 = i \frac{\partial^2}{\partial x^2} + j \frac{\partial^2}{\partial y^2} + k \frac{\partial^2}{\partial z^2}$$

as occurs in the well-known Poisson equation $\nabla^2 V = -\rho/\kappa_0$ for the scalar potential V in volts, the volume density ρ in coulombs per cubic meter, and the dielectric constant of air $\kappa \cong \kappa_0 = 8.854 \times 10^{-12}$ farad/m. When no charges are present, we have the Laplace equation $\nabla^2 V = 0$. The corresponding relations with the magnetic vector potential Λ are $\nabla^2 \Lambda = -\mu_0 J$ for the Poisson and $\nabla^2 \Lambda = 0$ for the Laplace relation, with $\mu_0 = 1.257 \times 10^{-6}$ henry/m and J the current density in amperes per square meter, associated with a unit volume. The curl of a vector $\underset{\cdot}{A}$ is, according to the above,

$$\text{curl } \underset{\cdot}{A} \equiv \nabla \times \underset{\cdot}{A} = \lim_{\tau \to 0} \frac{\int \int_S \nabla \times \underset{\cdot}{A} \, dS}{\tau} \tag{981}$$

for τ cubic meters enclosed by the surface of S square meters. An application to the

---

since the directional derivative $\partial\Phi/\partial l$ in any direction of l has components $\partial\Phi/\partial x$, $\partial\Phi/\partial y$, $\partial\Phi/\partial z$ expressed by

$$\frac{d\Phi}{dl} = \frac{\partial\Phi}{\partial x}\frac{dx}{dl} + \frac{\partial\Phi}{\partial y}\frac{dy}{dl} + \frac{\partial\Phi}{\partial z}\frac{dz}{dl}$$
$$= \frac{\partial\Phi}{\partial x}\cos(l,x) + \frac{\partial\Phi}{\partial y}\cos(l,y) + \frac{\partial\Phi}{\partial z}\cos(l,z)$$

If ∇ is operating on a scalar point function, it must cause a vector point function at all points with a direction of greatest rate of increase of the scalar function. In orthogonal curvilinear coordinates (Fig. 27), we have

$$\nabla^2\Phi = \frac{1}{k_1 k_2 k_3}\left(\frac{\partial}{\partial a}\frac{k_2 k_3}{k_1}\frac{\partial\Phi}{\partial a} + \frac{\partial}{\partial b}\frac{k_1 k_3}{k_2}\frac{\partial\Phi}{\partial b} + \frac{\partial}{\partial c}\frac{k_1 k_2}{k_3}\frac{\partial\Phi}{\partial c} \right)$$

For the Murphy operator Δ, we have

$$\Delta\Phi \equiv \nabla^2\Phi \equiv \text{div grad } \Phi$$
$$\Delta\underset{\cdot}{\Lambda} \equiv \nabla^2\underset{\cdot}{\Lambda} \equiv \text{grad div } \underset{\cdot}{\Lambda} = -\text{curl curl } \underset{\cdot}{\Lambda}$$
$$\nabla^2\Phi + \text{div}\frac{\partial \underset{\cdot}{\Lambda}_m}{\partial t} = -\frac{\bar{\rho}}{\kappa_0}$$
$$\nabla^2\underset{\cdot}{\Lambda}_m - \text{grad div } \underset{\cdot}{\Lambda}_m = \mu_0\left(-\overline{\rho_m v} + \kappa_0 \text{ grad } \Phi + \kappa_0 \frac{\partial^2 \underset{\cdot}{\Lambda}_m}{\partial t^2} \right)$$

general medium, with all three properties μ, κ, and σ effective, yields

$$\text{curl } \mathcal{E} = -\frac{\partial B}{\partial t} = -\frac{\partial(\mu H)}{\partial t}; \qquad \text{curl } H = \frac{\partial D}{\partial t} + J = \frac{\partial(\kappa \mathcal{E})}{\partial t} + \sigma \mathcal{E} \tag{982}$$

For a perfect dielectric wave medium ($\sigma = 0$), we have

$$\left.\begin{aligned} \nabla \times (\nabla \times \mathcal{E}) &= -\mu \frac{\partial(\text{curl } H)}{\partial t} = \mu\kappa \frac{\partial^2 \mathcal{E}}{\partial t^2}; \\ \nabla \times (\nabla \times H) &= \kappa \frac{\partial(\text{curl } \mathcal{E})}{\partial t} = -\mu\kappa \frac{\partial^2 H}{\partial t^2} \end{aligned}\right\} \tag{983}$$

For solenoidal conditions, *i.e.*, div $\mathcal{E} \equiv \nabla \cdot \mathcal{E} = 0$ and div $H \equiv \nabla \cdot H = 0$, we have

$$\nabla^2 \mathcal{E} = \frac{\partial^2 \mathcal{E}}{\partial x^2} + \frac{\partial^2 \mathcal{E}}{\partial y^2} + \frac{\partial^2 \mathcal{E}}{\partial z^2} = \mu\kappa \frac{\partial^2 \mathcal{E}}{\partial t^2}; \qquad \nabla^2 H = \frac{\partial^2 H}{\partial x^2} + \frac{\partial^2 H}{\partial y^2} + \frac{\partial^2 H}{\partial z^2} = \mu\kappa \frac{\partial^2 H}{\partial t^2} \tag{984}$$

For a scalar point function Φ, we have the vector $\underset{\sim}{A} = \text{grad } \Phi$, and

$$\text{div } \underset{\sim}{A} = \text{div (grad } \Phi) \equiv \nabla \cdot \text{grad } \Phi = \nabla^2 \Phi = \frac{\partial^2 \Phi}{\partial x^2} + \frac{\partial^2 \Phi}{\partial y^2} + \frac{\partial^2 \Phi}{\partial z^2} \tag{985}$$

For two vectors $\underset{\sim}{A}$ and $\underset{\sim}{B}$, we have the *important* identity

$$\text{div } (\underset{\sim}{A} \times \underset{\sim}{B}) \equiv \underset{\sim}{B} \cdot \text{curl } \underset{\sim}{A} - \underset{\sim}{A} \cdot \text{curl } \underset{\sim}{B} \tag{986}$$

Applying this to the electric $\mathcal{E}$ and magnetic H vectors of an electromagnetic wave, we find

$$\begin{aligned} \text{div } (\mathcal{E} \times H) &= H \cdot \text{curl } \mathcal{E} - \mathcal{E} \cdot \text{curl } H = -H \frac{\partial B}{\partial t} - \mathcal{E} \frac{\partial D}{\partial t} \\ &= -\left[H \frac{\partial(\mu H)}{\partial t} + \mathcal{E} \frac{\partial(\kappa \mathcal{E})}{\partial t} \right] = \frac{1}{2} \frac{\partial(\mu H^2 + \kappa \mathcal{E}^2)}{\partial t} \end{aligned}$$

a relation that is much used in this text. We have also

$$\text{curl (curl } \underset{\sim}{A}) \equiv \text{grad (div } \underset{\sim}{A}) - \nabla^2 \underset{\sim}{A} \tag{987}$$

which can also be written as

$$\nabla \times \nabla \times \underset{\sim}{A} = \nabla\nabla \cdot \underset{\sim}{A} - \nabla^2 \underset{\sim}{A}$$

since div $\underset{\sim}{A}$ is identical with $\nabla \cdot \underset{\sim}{A}$ and the gradient of $\nabla \cdot \underset{\sim}{A}$ is $\nabla\nabla \cdot \underset{\sim}{A}$. Applying this to electromagnetic fields yields

$$\text{grad div } \mathcal{E} - \nabla^2 \mathcal{E} + \frac{\partial[\text{curl } (\mu H)]}{\partial t} = 0 \tag{988}$$

for a scalar potential of V volts and a magnetic vector potential of Λ volt · sec/m, we find

$$\mathcal{E}^{(\text{volts/m})} = -\text{grad } V - \frac{\partial \Lambda}{\partial t}; \qquad H^{(\text{amp/m})} = \text{curl } \Lambda \tag{989}$$

This relation is likewise very important and applied in this text. This relation must likewise be used when *transit time* effect in a vacuum tube plays a part. For an isotropic wave medium of σ mhos per meter, μ henrys per meter, and κ farads per meter, for which div $\Lambda + \sigma\mu V + \mu\kappa\, \partial V/\partial t$ is fixed, we find

$$\nabla^2\Lambda - \sigma\mu\frac{\partial\Lambda}{\partial t} - \mu\kappa\frac{\partial^2\Lambda}{\partial t^2} = 0; \qquad \nabla^2 V - \sigma\mu\frac{\partial V}{\partial t} - \mu\kappa\frac{\partial^2 V}{\partial t^2} = 0 \tag{990}$$

which compared with

$$\nabla^2\mathcal{E} - \sigma\mu\frac{\partial\mathcal{E}}{\partial t} - \mu\kappa\frac{\partial^2\mathcal{E}}{\partial t^2} = 0; \qquad \nabla^2 H - \sigma\mu\frac{\partial H}{\partial t} - \mu\kappa\frac{\partial^2 H}{\partial t^2} = 0 \tag{991}$$

shows that the wave equation

$$\nabla^2 - \sigma\mu\frac{\partial}{\partial t} - \mu\kappa\frac{\partial^2}{\partial t^2} = 0 \tag{992}$$

is applicable. The wave equation plays a great part in diffraction problems, such as utilized in connection with wave-front radiators. Moreover, we have the identities

$$\text{div}\,(\Phi\underline{A}) \equiv \Phi\cdot\text{div}\,\underline{A} + \underline{A}\cdot\text{grad}\,\Phi; \qquad \text{curl}\,(\Phi\underline{A}) \equiv \Phi\cdot\text{curl}\,\underline{A} - \underline{A}\times\text{grad}\,\Phi \tag{993}$$

For the *second* differential Laplace operator ∇^2, we have $\nabla^2\Phi = \text{div}\,(\nabla\Phi)$, while curl $(\nabla\Phi) = 0$, and

$$\left.\begin{aligned}
\nabla^2\Phi &= \frac{\partial^2\Phi}{\partial x^2} + \frac{\partial^2\Phi}{\partial y^2} + \frac{\partial^2\Phi}{\partial z^2} && \text{in Cartesian } x,\ y,\ z \text{ coordinates}\\
\nabla^2\Phi &= \frac{1}{r}\left[\frac{\partial\left(r\dfrac{\partial\Phi}{\partial r}\right)}{\partial r} + \frac{1}{r}\left(\frac{\partial^2\Phi}{\partial\varphi^2}\right) + r\left(\frac{\partial^2\Phi}{\partial z^2}\right)\right] && \text{in cylindrical } r,\ \varphi,\ z \text{ coordinates}\\
\nabla^2\Phi &= \frac{1}{r^2\sin\theta}\left[\sin\theta\frac{\partial\left(r^2\dfrac{\partial\Phi}{\partial r}\right)}{\partial r} + \frac{1}{\sin\theta}\frac{\partial^2\Phi}{\partial\varphi^2} + \frac{\partial\left(\sin\theta\dfrac{\partial\Phi}{\partial\theta}\right)}{\partial\theta}\right] && \text{in spherical } r,\ \varphi,\ \theta \text{ coordinates}
\end{aligned}\right\} \tag{994}$$

Summarizing all important solutions, we find for vectors $\underline{A}$, $\underline{B}$, $\underline{C}$ and scalar Φ

$$\left.\begin{aligned}
&\nabla\times\nabla\times\underline{A} = \nabla\nabla\cdot\underline{A} - \nabla\cdot\nabla\underline{A}; \qquad \text{div}\,(\text{curl}\,\underline{A}) = 0; \qquad \text{curl grad}\,\Phi = 0\\
&\text{curl}\,(\text{curl}\,\underline{A}) \equiv \text{grad}\,(\text{div}\,\underline{A}) - \nabla^2\underline{A}; \qquad \text{div}\,(\Phi\underline{A}) = \Phi\,\text{div}\,\underline{A} + \underline{A}\,\text{grad}\,\Phi\\
&\text{curl}\,(\Phi\underline{A}) = \Phi\,\text{curl}\,\underline{A} + \underline{A}\times\text{grad}\,\Phi\\
&\text{div}\,(\underline{A}\times\underline{B}) = \underline{B}\,\text{curl}\,\underline{A} - \underline{A}\,\text{curl}\,\underline{B}\\
&\text{curl}\,(\underline{A}\times\underline{B}) = \underline{A}\,\text{div}\,\underline{B} - \underline{B}\,\text{div}\,\underline{A} + (\underline{B}\nabla)\underline{A} - (\underline{A}\nabla)\underline{B}
\end{aligned}\right\} \tag{995}$$

Fundamental rules are

$$\left.\begin{aligned}
&\underline{A}\cdot(\underline{B}\times\underline{C}) = \underline{B}\cdot(\underline{A}\times\underline{C}) = \underline{C}\cdot(\underline{A}\times\underline{B})\\
&\underline{A}\times(\underline{B}\times\underline{C}) = \underline{B}\cdot(\underline{A}\cdot\underline{C}) - \underline{C}\cdot(\underline{A}\cdot\underline{B})\\
&\nabla\cdot\underline{A} = \nabla\underline{A} \equiv \text{div}\,\underline{A} && \text{gives absolute intensity of force}\\
&\nabla\times\underline{A} \equiv \text{curl}\,\underline{A} && \text{refers to a kinetic rotation}
\end{aligned}\right\} \tag{996}$$

We have also the rules

$$\left.\begin{aligned}
&\text{curl}\,(\nabla\Phi) = 0; \qquad \text{div}\,(\nabla\Phi) = \nabla^2\Phi; \qquad \text{div}\,(\Phi\underline{A}) = \Phi\,\text{div}\,\underline{A} + \underline{A}\cdot\nabla\Phi\\
&\text{curl}\,(\Phi\underline{A}) = \Phi\,\text{curl}\,\underline{A} + \nabla\Phi\times\underline{A}\\
&\nabla(\underline{A}\cdot\underline{B}) = (\underline{A}\nabla)\underline{B} + (\underline{B}\nabla)\underline{A} + \underline{A}\times\text{curl}\,\underline{B} + \underline{B}\times\text{curl}\,\underline{A}\\
&\text{grad}\,\Phi \equiv \nabla\Phi; \qquad \text{div}\,\underline{A} \equiv \nabla\cdot\underline{A}; \qquad \text{curl}\,\underline{A} \equiv \nabla\times\underline{A}
\end{aligned}\right\} \tag{997}$$

Note. Curl of any gradient and divergence of any curl is zero; *i.e.*,

$$\text{curl } (\nabla\Phi) \equiv 0 \qquad \text{and} \qquad \text{div (curl } \underline{A}) \equiv 0 \tag{998}$$

Because

$$\text{div } (\mathcal{E} \times H) \equiv \nabla \cdot (\mathcal{E} \times H) \equiv H \cdot \nabla \times \mathcal{E} - \mathcal{E} \cdot \nabla \times H$$

we find for the complex Poynting vector p^*, if $\mathcal{E}^*$ is the *conjugate* of vector $\mathcal{E}$ and H^* is the conjugate of vector H,

$$\left.\begin{aligned} p^* = \tfrac{1}{2}\mathcal{E} \times H^* = \tfrac{1}{2}\mathcal{E}^* \times H; \qquad \nabla \times \mathcal{E} = -j\omega\mu H^* \\ \nabla \times H^* = (\sigma - j\omega\kappa)\mathcal{E}^* \\ \text{div } p^* \equiv \nabla \cdot p^* = \tfrac{1}{2}[H \cdot j\omega\mu H^* - \mathcal{E}(\sigma - j\omega\kappa)\mathcal{E}^*] \\ = -\tfrac{1}{2}\sigma\mathcal{E} \cdot \mathcal{E}^* + j\omega\tfrac{1}{2}(\mu H \cdot H^* - \kappa\mathcal{E} \cdot \mathcal{E}^*) \\ \text{since } \nabla \times \mathcal{E} = +j\omega\mu H \qquad \text{and} \qquad \nabla \times H = (\sigma + j\omega\kappa)\mathcal{E} \end{aligned}\right\} \tag{999}$$

Inasmuch as for any distance $r = \sqrt{x^2 + y^2 + z^2}$ meters from the origin of an XYZ system to a field point $P(x, y, z)$ we have vectorially $\underline{r} = ix + jy + kz$, we find $\nabla \cdot \underline{r} = 3$ and $\nabla \times \underline{r} = 0$. For any area of S square meters fixed by a closed contour of l meters and a unity vector $\underline{n}$ normal to the surface element dS, we find

$$\int\int_S \nabla \times \underline{A} \cdot \underline{n}\, dS = \oint_l \underline{A}\, dl; \qquad \int\int_S \underline{n} \times \nabla\Phi\, dS = \oint_l \Phi\, dl \tag{1000}$$

If the surface of S square meters encloses the volume of τ cubic meters, we find for $\underline{n}$ *normal to* dS *and outward*

$$\left.\begin{aligned} \int\int\int_\tau \nabla\Phi\, d\tau = \int\int_S \Phi\underline{n}\, dS; \qquad \int\int\int_\tau \nabla \cdot \underline{A}\, d\tau = \int\int_S \underline{A} \cdot \underline{n}\, dS \\ \int\int\int_\tau \nabla \times \underline{A}\, d\tau = \int\int_S \underline{n} \times \underline{A}\, dS \end{aligned}\right\} \tag{1001}$$

We have the fundamental electromagnetic applications

$$\left.\begin{aligned} \nabla \times \mathcal{E} = -\frac{\partial(\mu H)}{\partial t}; \quad \nabla \times H = J + \frac{\partial(\kappa\mathcal{E})}{\partial t}; \quad \nabla \cdot (\kappa\mathcal{E}) = \rho; \quad \nabla \cdot (\mu H) = 0 \\ \nabla \cdot J + \frac{\partial(\nabla \cdot \kappa\mathcal{E})}{\partial t} = 0; \quad \nabla^2 V = -\frac{\rho}{\kappa}; \qquad \nabla^2 \Lambda = -\mu J \end{aligned}\right\} \tag{1002}$$

where ρ is the charge density in coulombs per cubic meter, J the current density in amperes per square meter, and V the scalar potential in volts.

245. Hertzian Doublet Oscillator as a Special Case of the General Wave Equation. Equation (358) of Sec. 51 shows that the Hertz vector satisfies the wave equation. The electric $\mathcal{E}$ and magnetic H vectors depend only upon a complex quantity $U = \prod_m \mp j\prod$ according to the associated $\mathcal{E}$ and H fields. The $\mathcal{E}$ field is governed by the vector $\prod$, and the magnetic field by the vector $\prod_m$. We have, therefore, a means of solving a condition for which the H vector normal to a medium vanishes. This enables us to deal with obstacles in the electromagnetic wave path. The Hertzian oscillator is, in effect, an oscillating *electric* doublet; hence $\prod_m$ must vanish, and the complex quantity U degenerates to $U = \mp j\prod$, leaving only the Hertzian vector $\prod$. The classic Hertz vector $\prod$ depends on the *electric* current density J, where both $\prod$

and J are *complex* vectors. We have the fundamental relations

$$\left.\begin{aligned} \text{curl } H &= J + \kappa \frac{\partial \mathcal{E}}{\partial t} \\ \text{curl } \mathcal{E} &= -\mu \frac{\partial H}{\partial t} \\ \kappa \text{ div } \mathcal{E} &= \rho; \qquad \mu \text{ div } H = 0 \end{aligned}\right\} \text{ where } H \text{ can be represented by the curl of some vector field } \partial \prod / \partial t$$

We have then $\mu H = \mu\kappa \text{ curl } \partial \prod / \partial t$, $-\mu \partial H / \partial t = -\mu\kappa \text{ curl } \partial^2 \prod / \partial t^2$, and curl $\mathcal{E} = -\mu\kappa \text{ curl } \partial^2 \prod / \partial t^2$. But the curl appears on each side of the relation, and we may express $\mathcal{E}$ as $\mathcal{E} = -\mu\kappa(\partial^2 \prod / \partial t^2) + \text{grad } \Phi$, where Φ is an arbitrary *scalar*. We have then also

$$\text{curl curl } \frac{\partial \prod}{\partial t} = \frac{\partial \mathcal{E}}{\partial t} + \frac{J}{\kappa}; \qquad \text{curl curl } \prod = \mathcal{E} + \frac{\int J \, dt}{\kappa}$$

If we *postulate* similarly a *magnetic* current density J_m, which is now in volts per square meter instead of amperes per square meter, and a magnetic space charge ρ_m concentration per cubic meter, we can write down the corresponding relations

$$\left.\begin{aligned} \text{curl } H &= \kappa \frac{\partial \mathcal{E}}{\partial t} \\ \text{curl } \mathcal{E} &= -\mu \frac{\partial H}{\partial t} - J_m \\ \kappa \text{ div } \mathcal{E} &= 0; \qquad \mu \text{ div } H = \rho_m \end{aligned}\right\} \text{ where } \mathcal{E} \text{ can be represented by the curl of some vector field } \partial \prod_m / \partial t$$

We have then similarly

$$\text{curl curl } \prod_m = -\text{ grad (div } \prod_m) + \mu\kappa \frac{\partial^2 \prod_m}{\partial t^2} = \frac{\int J_m \, dt}{\mu}$$

$$H = -\mu\kappa \frac{\partial^2 \prod_m}{\partial t^2} \text{ grad (div } \prod_m); \qquad \mathcal{E} = -\mu \text{ curl } \frac{\partial \prod_m}{\partial t}$$

$$\prod_m(x, y, z) = \frac{1}{4\pi\mu j\omega} \int\int\int_\tau \frac{J_m(x_0, y_0, z_0)\epsilon^{-j\omega r\sqrt{\mu\kappa}}}{r} \, d\tau \tag{1003}$$

if compared with

$$\prod(x, y, z) = \frac{1}{4\pi\kappa j\omega} \int\int\int_\tau \frac{J(x_0, y_0, z_0)\epsilon^{-j\omega r\sqrt{\mu\kappa}}}{r} \, d\tau \tag{1004}$$

where $\prod_m$ is in meter · amperes and $\prod$ in meter · volts in a μ, κ wave medium.

246. Notes on the Usefulness of the Equivalence Principle. This principle is advocated in several of the publications by S. A. Schelkunoff. It plays a useful part especially when dealing with wave-front radiators. It is the electromagnetic wave case of the Huygens-Kirchhoff wavelet explanations. We deal in the electromagnetic case with an electromagnetic *known* field distribution over a closed surface, with a primary source within the enclosed space. This principle seems to be valid even for apertures in such a surface, with main dimensions that compare with the operating

wavelength. We use then the *tangential* fields in the aperture and compute from the respective $\mathcal{E}$ and H fields the corresponding electromagnetic field vectors in the radiation region. It can therefore also be applied to the open mouth of a wave guide by ignoring the normal field component. It is true that certain assumptions have to be made and we deal with an approximation procedure. We must admit, however, that we meet also in some of the classic theories on electromagnetism a paradox; this means a condition which physically *cannot* exist. This is brought out at places of the text where it belongs. What happens in the equivalence-principle case is that we account for discontinuities across an aperture by means of electric and magnetic *current sheets*. According to Maxwell a tangential H field discontinuity at a certain boundary is equal to the surface electric current density $\dot{J}$ and we may write $\dot{J} = -n \times \dot{H}$, where n is a unit vector along the outward direction normal to the boundary. In our case this is normal to the aperture. We must, however, work with a magnetic current density also and postulate the relation $\dot{J}_m = n \times \dot{\mathcal{E}}$, where $\dot{\mathcal{E}}$ refers also to a *tangential* $\mathcal{E}$ field. This J_m concept we just must imagine in this procedure, since physically as well as according to the boundary conditions this concept is a violation. If we assume electric and magnetic current sheets in the primary tangential $\mathcal{E}$ and H field plane of the above-mentioned aperture, behind which is a primary radiator, respective current densities must be $\dot{J} = n \times \dot{H}$ and $\dot{J}_m = -n \times \dot{\mathcal{E}}$ in order to account for the radiated field beyond the aperture of the enclosure. We arrive now at conditions for which we have electric current densities in amperes per meter and magnetic current densities in volts per meter, since the infinitesimal thickness of the boundary changes the customary area from square meters to a linear dimension of meters. Just as in the preceding section for the general case $\prod$ and $\prod_m$, we shall now deal with a magnetic vector potential Λ_m and electric vector potential Λ_e, since in a nondissipative medium

$$\text{curl } \dot{\mathcal{E}} \equiv \nabla \times \dot{\mathcal{E}} = -\dot{J}_m - \mu \frac{\partial \dot{H}}{\partial t}; \qquad \text{curl } \dot{H} \equiv \nabla \times \dot{H} = \dot{J} + \kappa \frac{\partial \dot{\mathcal{E}}}{\partial t}$$

Since for nondissipative wave mediums $\Gamma = \alpha + j\beta = j\beta$, we may write the respective operating vector potentials Λ_m and Λ_e as

$$\Lambda_m = \frac{\mu}{12.56} \int\int_S \frac{\dot{J} \epsilon^{-j\beta r}}{r} dS \quad \text{volt} \cdot \text{sec/m}; \qquad \Lambda_e = \frac{\kappa}{12.56} \int\int_S \frac{\dot{J}_m \epsilon^{-j\beta r}}{r} dS \quad \text{amp} \cdot \text{sec/m} \quad (1005)$$

where r meters is the distance from the symmetry point of the aperture to any field point in the distant true radiation region *beyond* the aperture. Suppose we deal with a rectangular opening in the screen or in the mouth plane of a guide. We choose then conveniently the origin of an XYZ system, such that the long side of the opening is along the Y axis and short side along the X axis. The origin of the coordinate system then coincides with the above-mentioned symmetry point (intersection of the respective diagonals of the aperture). Any radiation field point has then the coordinates x, y, z, while any point in the opening can have only x_0, y_0 coordinates, since z_0 must be zero. In the above expressions we have $r = \sqrt{x^2 + y^2 + z^2}$. Assuming in the opening of such dimensions that we deal with a plane tangential wave front and $\mathcal{E}$ along the X axis so that H is along the Y axis and the normal to the outward direction along $+Z$, we find the distance from any wavelet point $P_0\,(x_0, y_0)$ in the aperture to an outside field point $P(x, y, z)$ as $r_1 = r - (xx_0 - yy_0)/r$ meters. For this particular

arrangement, we have then $J_{x_0} = -H_{y_0}$ amperes per meter and $J_{m_{y_0}} = -\mathcal{E}_{x_0}$ volts per meter, where $Z_0 = \mathcal{E}_{x_0}/H_{y_0} = \Lambda_{m_x}/\Lambda_{e_y}$ ohms, because the fields that correspond to the current densities are in the plane of the aperture, *but* the vector potentials act at the radiation field point $P(x, y, z)$. We find then the only operating components of the retarded vector potentials

$$\Lambda_{m_x} = -\frac{\mu H_{y_0}}{12.56}\int\int_S \frac{\epsilon^{-j\beta r_1}}{r_1}\,dS; \qquad \Lambda_{e_y} = -\frac{\kappa \mathcal{E}_{x_0}}{12.56}\int\int_S \frac{\epsilon^{-j\beta r_1}}{r_1}\,dS \tag{1006}$$

where the double integration extends only over the area of the rectangular aperture and respective magnetic and electric fields can be taken before the integral, since we deal with *uniform* current density distributions in the plane of the aperture. We also assume that we deal with the *distant* radiation region so that r and r_1 are *very large* compared with the operating wavelength and the dimensions of the aperture. We can then in the relations (taken from the text) for the respective field vectors

$$\left.\begin{aligned} \dot{\mathcal{E}} &= -j\omega\dot{\Lambda}_m - \frac{1}{\kappa}\nabla \times \dot{\Lambda}_e - j\frac{\nabla(\nabla \cdot \dot{\Lambda}_m)}{\omega\mu\kappa} \\ \dot{H} &= -j\omega\dot{\Lambda}_e + \frac{1}{\mu}\nabla \times \dot{\Lambda}_m - j\frac{\nabla(\nabla \cdot \Lambda_e)}{\omega\mu\kappa} \end{aligned}\right\}; \qquad v = \frac{1}{\sqrt{\mu\kappa}} \quad \text{m/sec} \tag{1007}$$

neglect the last term in the $\mathcal{E}$ relation, because it is inversely proportional to $1/r^2$. We can then operate with the relation

$$\dot{\mathcal{E}} \cong -j\omega\dot{\Lambda}_m - \frac{1}{\kappa}\nabla \times \dot{\Lambda}_e$$

But in this relation

$$\nabla \times \dot{\Lambda}_e \equiv \text{curl } \dot{\Lambda}_e = \frac{\partial(\Lambda_{e_y})}{\partial x}k - \frac{\partial(\Lambda_{e_y})}{\partial z}i$$

where k and i are unit vectors. The first component refers in effect to an $\mathcal{E}_z$ component at $P(x, y, z)$, which can hardly play a part for our field orientation in the aperture. Therefore

$$\dot{\mathcal{E}} = -j\omega\dot{\Lambda}_m - \frac{-\partial(\dot{\Lambda}_{e_y})}{\kappa\partial z}i \qquad \text{and} \qquad \mathcal{E}_x = -j\omega\Lambda_{m_x} + \frac{1}{\kappa}\frac{\partial(\Lambda_{e_y})}{\partial z} \tag{1008}$$

But

$$\Lambda_{m_x} = Z_0\Lambda_{e_y} \qquad \text{and} \qquad \mathcal{E}_x = \frac{1}{\kappa}\frac{\partial(\Lambda_{e_y})}{\partial z} - j\omega Z_0\Lambda_{e_y} \tag{1009}$$

We have now a simple differential equation for which Λ_{e_y} can be evaluated from (1006) by using the expression for r_1, given before. We arrive then at solution for $\mathcal{E}_x$ in volts per meter, as given in the text.

247. Additional Expressions Used in Electromagnetic Wave Problems. In the text it is shown that the wave equation of wave function w yields

$$\frac{\partial^2 w}{\partial r^2} + \frac{2}{r}\frac{\partial w}{\partial r} + \frac{1}{r^2 \sin\theta}\frac{\partial[(\partial w/\partial\theta)\sin\theta]}{\partial\theta} + \frac{1}{r^2\sin\theta}\frac{\partial^2 w}{\partial\varphi^2} + \beta^2 w = 0$$

which can be satisfied by the factor solution

$$w = \Phi_1(r) \cdot \Phi_2(\varphi) \cdot \Phi_3(\theta)$$

For electromagnetic fields in air (rigorously in a $\mu_0\kappa_0$ wave medium), where n in the partial solutions is zero[1] the interpretations of elementary wave functions for plane waves is

$$\left.\begin{matrix}(1/r)\epsilon^{i\omega t}\epsilon^{-i\beta r}\\(1/r)\epsilon^{i\omega t}\epsilon^{+i\beta r}\end{matrix}\right\}\ progressive\ \left\{\begin{matrix}\text{divergent waves } (1/r)\cos\beta(\omega t-r)\\\text{convergent waves } (1/r)\cos\beta(\omega t+r)\end{matrix}\right\} \tag{1009a}$$

and

$$\left.\begin{matrix}(1/r)\cos(\beta r)\\(1/r)\sin(\beta r)\end{matrix}\right\}\ standing\ \left\{\begin{matrix}\textit{forced} \text{ waves (source at origin) } (1/r)\cos\beta r\\ \qquad\qquad\qquad\qquad\qquad\qquad \times\cos\beta ct\\\textit{free} \text{ waves } (1/r)\cos\beta r\cdot\cos\beta ct\end{matrix}\right\} \tag{1009b}$$

For cylindrical waves we deal then with $H^{(1)}(\beta r)$, $H^{(2)}(\beta r)$, $J_n(\beta r)$, and $N_n(\beta r)$ functions.

If a volume integral is extended throughout the volume τ within a closed surface S we have

$$\int\int\int_\tau\left(\frac{\partial A_x}{\partial x}+\frac{\partial A_y}{\partial y}+\frac{\partial A_z}{\partial z}\right)d\tau=\int\int_S[A_x\cos(nx)+A_y\cos(ny)+A_z\cos(nz)]dS$$

which is generally written as

$$\int\int\int_\tau \operatorname{div} A=\int\int_S A_n\,dS \tag{1009c}$$

If we substitute for A the vector $u,\nabla v$ we find the *Green theorem*

$$\int\int\int_\tau u\nabla^2 v\,d\tau=\int\int_S u\frac{\partial v}{\partial n}\,dS-\int\int\int_\tau\left(\frac{\partial u}{\partial x}\frac{\partial v}{\partial x}+\frac{\partial u}{\partial y}\frac{\partial v}{\partial y}+\frac{\partial u}{\partial z}\frac{\partial v}{\partial z}\right)d\tau \tag{1009d}$$

which for $\mu=v$ gives

$$\int\int\int_\tau u\nabla^2 u\,d\tau=\int\int\int_S u\frac{\partial u}{\partial n}\,dS-\int\int\int_\tau\left[\left(\frac{\partial u}{\partial x}\right)^2+\left(\frac{\partial u}{\partial y}\right)^2+\left(\frac{\partial u}{\partial z}\right)^2\right]d\tau \tag{1009e}$$

There exists also a *symmetrical* form of the Green theorem. It is found by interchanging u and v in (1009d) and subtracting respective equations. The symmetrical form reads

$$\int\int\int_\tau(u\nabla^2 v-v\nabla^2 u)\,d\tau=\int\int_S\left(u\frac{\partial v}{\partial n}-v\frac{\partial u}{\partial n}\right)dS \tag{1009f}$$

where $v=(1/r)\epsilon^{\pm i\beta r}\cdot\epsilon^{i\omega t}$ is a spherical wave function and u is equal to one of the complex rectangular coordinates of the electromagnetic field given by the Hertz vector. An application to a diffraction radiator is given in Sec. 249.

248. Booker's Application of the Babinet Principle to Slot Radiators and Complementary Wire Radiators.[2] The well-known Babinet principle of complementary

[1] SOMMERFELD, A., *Jahresbericht des deutsch. math. Vereins*, **21**, 1913.

[2] BOOKER, H. G., *J. IEE (London)*, Part IIIA, **93**, No. 4, 620–626, 1946.

optical screens is applied to resonant slot apertures cut in a thin plane of a conducting screen. A half-wavelength slot with an input impedance of about 485 ohms gives a directivity pattern similar to a customary half-wave electric dipole, but with the directions of vibration of electric $\mathcal{E}$ and magnetic H fields interchanged. As shown in this text, resonant slots can then be used like customary half-wave dipoles to give linear and broadside arrays.

249. Green Function, Green Theorem, and Their Relation to Electromagnetic Diffraction. Unlike the geometric-ray theory, applied to electromagnetic waves, problems of electromagnetic diffraction require wave optics. The concentric ring diffraction radiator of Fig. 391*a* is an example.[1] A ring-shaped opening of respective radii

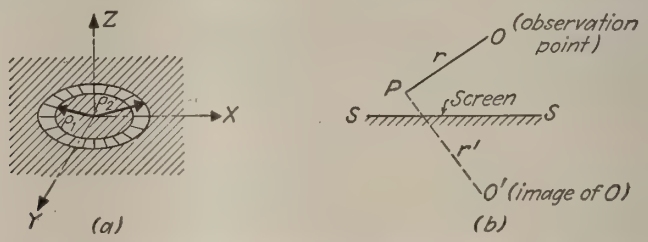

FIG. 391. Ring-shaped slit aperture acts as a diffraction radiator. (*a*) Conducting screen surface in XY plane. ρ_1 and ρ_2 are radii of slit in XY plane. s is area of slit. High-frequency voltage is applied across the slit gap. (*b*) Green function active in space above S-S plane. $\mathcal{E}$ are field values. P has coordinates (variables of integration). $\beta = 2\pi/\lambda$.

ρ_1 and ρ_2 respectively denotes the diffraction radiator. The shaded area in the XY plane is a metallic screen, which for wave-front radiators must be absorptive on the lower face of the XY plane. The conducting shaded surface can also be the front face of a suitable cavity resonator, as well as the opening of a suitable guide. M. S. Neumann has, for instance, investigated "endo-vibrators." In Fig. 391*a* a radio-frequency voltage E is impressed across the ring-shaped aperture. The instantaneous electric field in the aperture is then as shown, while the associated H lines are concentric circles (not shown). It is understood that for a completely enclosed space *below* the XY plane the reference field $\mathcal{E}_0$, basic in our formulas, depends on the design of the aperture as well as on the cavity below the XY plane and on the mode of excitation. Such a diffraction radiator has terms which are inversely proportional to the distance r and directly proportional to $1/r^2$, where, of course, only the $1/r$ term can act in the distant radiation region. For a very large conducting metallic screen as well as for a limited screen with an enclosed cavity below it, inasmuch as only the aperture can produce radiation above the XY plane, we need only to integrate over the area of the aperture. In the expressions given, it is assumed that the gap is sufficiently narrow.

The Green function is given by

$$G = \left.\frac{\epsilon^{-j\beta r}}{r} - \frac{\epsilon^{-j\beta r'}}{r'}\right\} \text{ in the space over the conducting screen } S\text{-}S \text{ of Fig. 391}b$$

The conducting screen is in effect assumed of infinite conductivity. We have, therefore, on either side of S-S no tangential electric field in effect. If an electric dipole is

[1] PISTOLKORS, A. A., Theory of the Circular Diffraction Antenna, *Proc. IRE*, **36**, 56, January, 1948; NEUMANN, M. S., Radiation of Electromagnetic Energy through Apertures (in Russian), *Izvestija Electropromyshlennosti Slabogo Toka*, **6**, 11, (1940).

parallel with the X axis, then the Hertz vector is $\prod = \prod_x$. If such a dipole is normal to the XY plane, we have $\prod = \prod_z$. The first case applies then to a condition for which the dipole axis is parallel with the screen S-S, while the second case holds for the dipole axis perpendicular to S-S. We have, therefore, the respective relations

$$\left.\begin{aligned} \mathcal{E}_x &= \beta^2 \prod_x + \frac{\partial[(\partial \prod_x)/(\partial x)]}{\partial x}; \qquad \mathcal{E}_y = \frac{\partial[(\partial \prod_x)/(\partial x)]}{\partial y} \\ \text{and} \\ \mathcal{E}_x &= \frac{\partial[(\partial \prod_z)/(\partial z)]}{\partial x}; \qquad \mathcal{E}_y = \frac{\partial[(\partial \prod_z)/(\partial x)]}{\partial y} \end{aligned}\right\} \text{for the tangential components of } \mathcal{E}$$

For a plane wave the exciting electric dipole is normal to the plane of wave incidence, which corresponds to the first case, while for the second case the electric dipole is in the plane of wave incidence. It seems then more convenient to use the concept of a magnetic dipole. Moreover, at the surface of the conducting screen S-S the tangential electric field must vanish and we have $\prod_x = 0$ for the first case, but $(\partial \prod_z)/\partial_z = 0$ for the second case.

The Green function must vanish on the plane, where $r = r'$. For w_0 the value of the function on the plane and w the value of the function at point O, it can be shown[1] that

$$4\pi w = \int\int_s w_0 \frac{\partial g}{\partial n}\, ds$$

where the partial derivative is with respect to the external normal. The surface s to be integrated is that of the aperture, since this is the *only* surface in the XY plane where an electric field can exist. Now according to Huygens' principle we find for the normal partial derivative of the Green function, according to Fig. 391*b*, for $(1/r)\epsilon^{-j\beta r} = a$ and $(1/r')\epsilon^{-j\beta r'} = b$,

$$\frac{\partial G}{\partial n} = \frac{\partial a}{\partial r} \cos\,(n, r) - \frac{\partial b}{\partial r} \cos\,(n,r')$$

Integrating point P in the symmetry plane of O and O', and $r = r'$ and $\cos\,(n,r) = -\cos\,(n,r)$, yields

$$\frac{\partial G}{\partial n} = 2\frac{\partial a}{\partial r} \cos\,(n, r)$$

Therefore,

$$4\pi w = -2\int\int_s w_0 \frac{\partial a}{\partial r} \cos\,(n, r)\, ds = -2\int\int_s w_0 \frac{\partial a}{\partial n}\, ds$$

$$\frac{\partial a}{\partial r} = -(j\beta/r)\epsilon^{-j\beta r}[1 - 1/(j\beta r)] = -j\frac{\beta\epsilon^{-j\beta r}}{r} + \underbrace{\frac{\epsilon^{-j\beta r}}{r^2}}_{\substack{\text{vanishes in} \\ \text{distant} \\ \text{radiation} \\ \text{region}}}$$

[1] Frank, P., and R. Mises, "Differential und Integral Gleichungen der Mechanik und Physik," Vol. II, 1936.

Now in Fig. 391*a* the conducting screen (shaded) is in the XY plane and the w function can be either the $\mathcal{E}_x$ or the $\mathcal{E}_y$ component of the electrical field $\mathcal{E}$ to be found. We can find the radial component by computing $\mathcal{E}_x$ for $y = 0$ or $\mathcal{E}_y$ for $x = 0$. If, therefore, $\mathcal{E}_{x_0}$ denotes the electric field value in the XY plane, we find the radial field component as

$$\mathcal{E}_r = \frac{1}{2\pi} \int\int_s \mathcal{E}_{x_0} \frac{\partial a}{\partial z}\, ds; \qquad a = \frac{\epsilon^{-j\beta r}}{r}$$

The magnetic field H is found from curl $H = j\omega\kappa\mathcal{E}$. This gives in cylindric coordinates r'', φ, z'' of the observation point O

$$j\omega\kappa\mathcal{E}_r = -\frac{\partial H_\varphi}{\partial z''}$$

The integration yields

$$H_\varphi = -j\omega\kappa \int \mathcal{E}_r\, dz'' = -j\frac{\omega\kappa}{2\pi} \int\int\int_s \mathcal{E}_{x_0} \frac{\partial a}{\partial z}\, ds\, dz'' = jf\kappa \int\int_s a\mathcal{E}_{x_0}\, ds$$

since $\omega\kappa/(2\pi) = 2\pi f\kappa/(2\pi) = f\kappa$. The radial field component is then given by

$$\mathcal{E}_r = -\frac{j}{\lambda} \int\int_s a\mathcal{E}_{x_0} \cos(z, r)\, ds; \qquad a = \frac{\epsilon^{-j\beta r}}{r}$$

for the distant radiation region, since $-j\beta/(2\pi) = -j/\lambda$. Since at very great distances the distances r from all points of the ring aperture are parallel, we may take the inverse distance $1/r$ before the integral as well as the factor $\cos(z, r)$ and have for the very distant radiation region the expression

$$\mathcal{E}_r = -j\frac{\cos(z, r)}{r\lambda} \int\int_{\text{aperture}} \mathcal{E}_{x_0}\epsilon^{-j\beta r}\, ds$$

where s is the area of the ring-shaped aperture in Fig. 391*a*. Figure 392*a* shows the parallel reaches r and r_0 for the very great distant-radiation region, and we have then

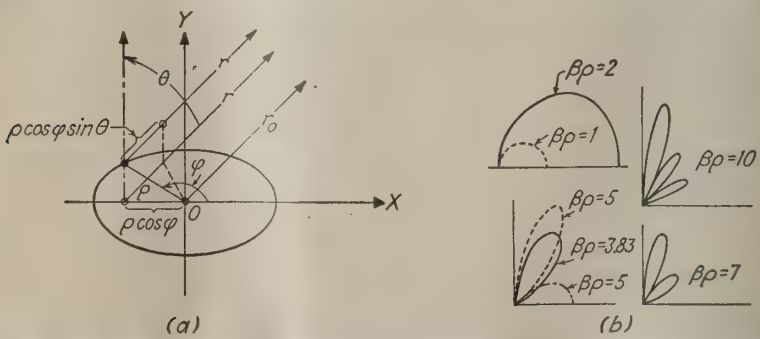

FIG. 392. Ring-shaped diffraction slit radiator patterns. (*a*) Parallel ranges r and r_0 into distant radiation region. (*b*) Directivities in vertical plane for different radii.

$r = r_0 - \rho\cos\varphi\sin\theta$ and $\mathcal{E}_{x_0} = \mathcal{E}_0\cos\varphi$, where $\mathcal{E}_0$ is the radial component of the electric field in the gap, *i.e.*, in the aperture. For the potential difference E_0 between

the edges of the gap aperture we have $\int \mathcal{E}_0 r\, dr = \rho E_0$, since we integrate only over the gap aperture for which we have the elementary area $ds = r\, dr\, d\varphi$. This leads to the final expression for $\mathcal{E}_r$, which for $\cos\theta = \cos(z, r)$ is

$$\mathcal{E}_r = -[j\beta\rho(E_0\epsilon^{-j\beta r_0}\cos\theta)/(2\pi r_0)] \int_{-\pi}^{+\pi} \epsilon^{j\beta\rho\cos\varphi\sin\theta}\, d\varphi$$

Since

$$J_1(x) = \frac{j}{\pi}\int_0^{\pi} \epsilon^{jx\cos\omega}\cos\omega\, d\omega$$

the radial component has a solution

$$\mathcal{E}_r = \frac{\beta\rho E_0}{r_0} J_1(\beta\rho\sin\theta)\epsilon^{-j\beta r}\cos\theta$$

Inasmuch as in the far-distant field region the electric field vector $\mathcal{E}$ of a spherical wave is normal to the range direction r_0 (Fig. 392*a*) and makes an angle $\pi - \theta$ with $\mathcal{E}_x$, we have

$$\mathcal{E}_x = -\mathcal{E}\cos\varphi; \qquad \mathcal{E} = \frac{\beta\rho E_0}{r_0} J_1(\beta\rho\sin\theta)$$

where $\mathcal{E}$ and E_0 are effective values and $\epsilon^{-j(\beta r_0 - \pi)}$ is the phase. Figure 392*b* then shows the directivities in the vertical planes. In Fig. 48 the roots of the Bessel function $J_1(x)$ are inscribed. They are the consecutive intersections of the dash $J_1(k_1, m)$ curve in the upper representation with the $k_{n,m}$ reference axis. We have then the root values 3.83, 7.02, 10.17, 13.32, 16.47, 19.62, 22.76, 25.90, 29,05, 32.19, etc. The corresponding radii ρ/λ in terms of the wavelength λ are then 0.61, 1.12, 1.62, 2.12, 2.62, 3.12, 3.62, 4.12, 4.62, 5.12, etc., for circular diffraction antennas. For radius ρ small with respect to λ we have the approximation

$$J_1(\beta\rho\sin\theta) \cong 0.5\beta\rho\sin\theta$$

and

$$\mathcal{E} = \frac{\beta^2\rho^2 E_0}{2r_0}\sin\theta$$

rendering the small circular diffraction radiator in effect equal to the grounded Hertzian electric doublet for which we have the current moment of the Il and

$$\mathcal{E} = \frac{60\beta lI}{r_0} \text{ volt/m}$$

if $\mathcal{E}$ and I are the effective values and $Il = \beta\rho^2 E_0/120$.

250. Notes on Radiation Directivities of Slots in Metal Cylinders. This subject has been dealt with by several investigators.[1] Such aperture radiators give considerable control over the directivities by using arrays of slot apertures. If the formula for the radiated field from a single slot is used, we can compute the horizontal pattern with

[1] JORDAN, E. C., and W. E. MILLER, Slotted Cylinder Antennas, *Electronics*, **20**, 90, February, 1947; ALFORD, A., Long Slot Antennas, *Proc. Nat. Electronics Conf.*, Chicago, Ill., 143, 1946; SINCLAIR, G., The Patterns of Slotted-cylinder Antennas, *Proc. IRE*, **36**, 1487, December, 1948; RIBLET, H. J., Microwave Omnidirectional Antennas, *Proc. IRE*, **35**, 474, May, 1947.

a good degree of accuracy. The slots are axial to the surface of the conducting cylinder. In Fig. 393 the slot aperture is parallel with the Z axis along the cylinder

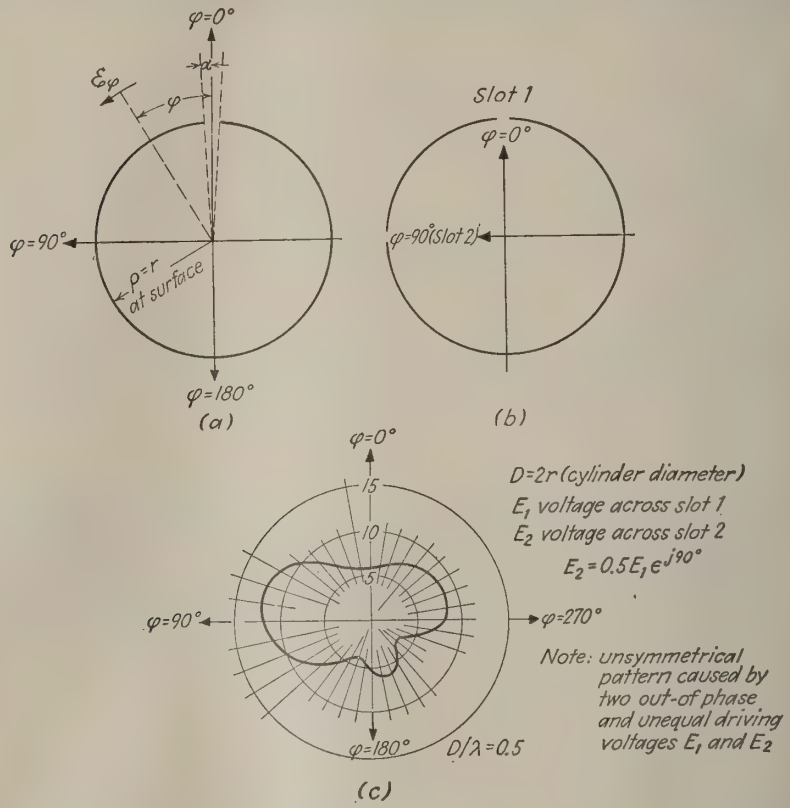

FIG. 393. Slot aperture antenna on cylinder. (*a*) XY plane where ρ = any radius, and $\rho = r$ at surface of cylinder. 2α angular slot width in radians. Slot width small compared with wavelength λ. (*b*) Two axial slot apertures 1 and 2. (*c*) Slots at $\varphi = 0°$ and $\varphi = 90°$ as in (*b*).

surface ($D = 2r$), at $\varphi = 0°$. The field along the slot is taken uniform so that only an $\mathcal{E}_\varphi$ component is effective, which means that at the cylinder surface

$$\mathcal{E}_\varphi = \mathcal{E}_0 \epsilon^{j\omega t} \qquad \text{for } -\alpha < \varphi < \alpha$$

while for all other places (all other φ values) we have $\mathcal{E}_\varphi = 0$. We have then

$$\left.\begin{aligned} \mathcal{E}_\varphi &\cong (K/2\pi)[A_0 + \sum_{n=1}^{\infty} A_n \cos(n\varphi)] \\ A_0 &= \frac{1}{2H_0^{(2)\prime}(\beta r)}; \qquad A_n = \frac{j^n}{H_n^{(2)\prime}(\beta r)}; \qquad \beta = \frac{2\pi}{\lambda} \end{aligned}\right\}$$

The patterns of Fig. 394*a* and *b* hold for a single slot in the cylindric surface with the axial slot direction at $\varphi = 0°$. The patterns of Fig. 394*c* and *d* hold for D large com-

pared with the operating wavelength. The slot is likewise located at $\varphi = 0°$. The patterns of Fig. 394*e* and *f* are for two slots in the cylindric surface for $D = 0.5\lambda$. For Fig. 394*e* we have diametrically opposed slots fed equally and in phase, while for Fig.

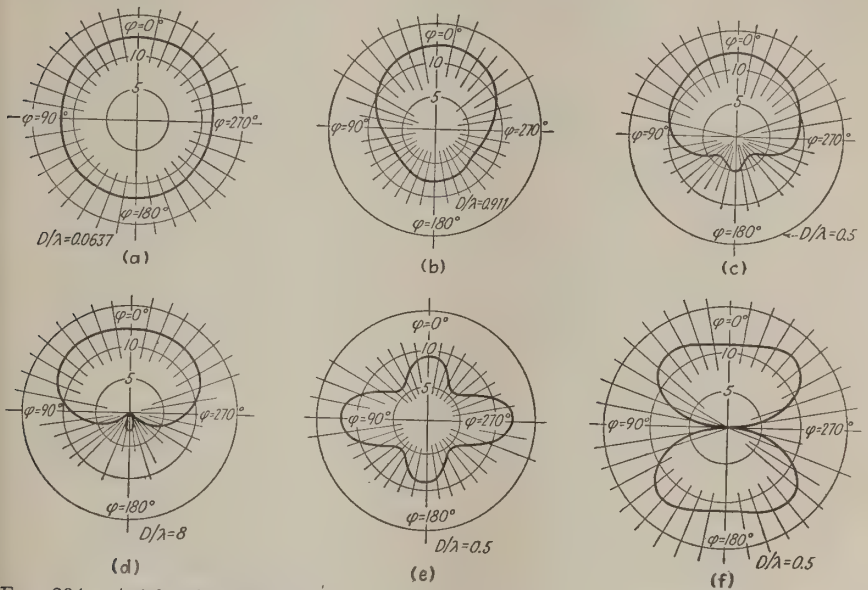

FIG. 394. Axial cylinder aperture directivities. (*a*) and (*b*) Patterns for one slot at $\varphi = 0°$. (*c*) and (*d*) Patterns for one slot at $\varphi = 0°$; cylinder has diameter large compared with wavelength λ. (*e*) Pattern with two slots at extremities of diameter $D = \lambda/2$ excited in phase and with same current. (*f*) Two slots but excited with antiphase equal currents.

394*f* the diametrically opposed slots are fed equally in antiphase. All experimental patterns are due to G. Sinclair (*loc. cit.*).

251. Half-wave Dipole and Folded Dipole Values. A half-wave dipole has a radiation resistance of about 75 ohms, while such a folded dipole (Fig. 144) has about 300 ohms with some broad-band features. As far as present-day FM and TV carrier-frequency assignments are concerned, we have for the FM band 88 to 108 Mc/sec and could use a folded half-wave dipole of over-all half-wave extension of $l \cong 57$ in. for a mid-band compromise, while an over-all extension of $l = 54$ in. is better for the high-end assignments and $l \cong 60$ in. favors the lower channels. Of course, a compromise for TV assignments is by far more difficult, since we have a lower frequency band of channels as well as a higher frequency band of channels, besides the fact that there is quite a frequency space between the lower and higher bands. This makes also the compromise of the reflector spacing toward the actual pickup antenna quite difficult. For a single-frequency operation, a spacing of one-quarter of the free-space wavelength λ_0 would be correct with a reflector length somewhat longer than the customary half wavelength. As has been brought out in this text, the half wavelength along a conductor is somewhat shorter than the free-space value. If we assume 5 per cent less actual radiator length, we have for a free-space wavelength $\lambda_0^{(\text{meters})} = 300/f^{(\text{Mc/sec})}$ and for a *half-wave* dipole an actual length of $l^{(\text{meters})} \cong \lambda/2 = 0.95\lambda_0/2 = 0.95 \times 150/f^{(\text{Mc/sec})}$. We have then the formulas as given in Table 94 for the actual length of

a half wave as well as of the folded half-wave dipole, since l meters = 3.281 l ft = 39.37 l in.

Table 94. Actual Half-wave and Folded Dipole Lengths l in Meters and Inches

f, Mc/sec	l, meters	l, inches	f, Mc/sec	l, meters	l, inches
30	4.85	187	210	0.679	26.7
40	3.57	140.5	220	0.648	25.55
50	2.85	112.3	230	0.62	24.4
60	2.37	93.5	240	0.594	23.4
70	2.04	80.3	250	0.57	22.45
80	1.785	70.1	260	0.549	21.6
90	1.585	62.3	270	0.528	20.8
100	1.422	56.1	280	0.509	20.1
110	1.295	51.05	290	0.491	19.35
120	1.189	46.8	300	0.485	18.7
130	1.095	43.1	320	0.445	17.55
140	1.02	40.1	340	0.419	16.5
150	0.951	37.4	360	0.396	15.6
160	0.892	35.1	380	0.376	14.78
170	0.839	33.0	400	0.357	14.05
180	0.792	31.2	420	0.339	13.4
190	0.75	29.5	440	0.324	12.75
200	0.713	28.1	460	0.31	12.2

Remarks: l is the half wavelength along the conductor, based on the formulas

$$l^{(\text{meters})} = 0.95 \times 150/f = \frac{142.25}{f^{(\text{Mc/sec})}}$$

$$l^{(\text{inches})} = 142.25 \times 39.37/f = \frac{5{,}610}{f^{(\text{Mc/sec})}}$$

It is by far easier to use the decimal meter scales, since we can read off on such scales one-hundredth of 1 meter, namely the centimeter, and one-thousandth of 1 meter, the millimeter (the thickness of a pencil line. Usually ⅜- or ½-in. aluminum-alloy tubing is used for low TV band and ¼-in. for high TV band.

In the following tables the lengths l are given in meters since we can read off accurately within 1 millimeter. For TV assignments we have in the lower frequency band the channels 2, 3, 4, 5, and 6, and in the higher frequency band, the channels 7, 8, 9, 10, 11, 12, and 13, with a small frequency space between channels 4 and 5 and a large frequency space between channels 6 and 7. We must compromise over the entire frequency space of all channels as far as gap matching is concerned. In many cases the folded dipole is cut to the center frequency (mid-channel in each band).

TABLE 95. FOLDED DIPOLE

Channel	f, Mc/sec	λ, feet and inches	λ, meters	$\lambda/2$, meters	$\lambda/4$, inches	$\lambda/4$, meters
2	54–60	16′ 5″	5.0	2.5	49¼	1.25
3	60–66	14′ 10″	4.525	2.2625	44½	1.131
4	66–72	13′ 6″	4.12	2.06	40	1.03
5	76–82	11′ 9″	3.58	1.79	35¼	0.895
6	82–86	11′ 0″	3.35	1.675	33	0.8375
7	174–180	5′ 4″	1.628	0.814	16	0.407
8	180–186	5′ 1″	1.55	0.775	15¼	0.3875
9	186–192	4′ 11″	1.5	0.75	14¾	0.375
10	192–198	4′ 9″	1.45	0.725	14¼	0.3625
11	198–204	4′ 7½″	1.41	0.705	13⅞	0.3525
12	204–210	4′ 6″	1.371	0.6855	13½	0.34275
13	210–216	4′ 5″	1.348	0.674	13¼	0.337

Remarks: Wavelength λ is measured along antenna conductor.

TABLE 96. LENGTH l BETWEEN ROUNDED ENDS OF FOLDED DIPOLE FOR GREATEST GAIN

Channel	l		Channel	l	
	Inches	Meters		Inches	Meters
2	102.1	2.6	8	30.5	0.775
3	92.0	2.34	9	29.5	0.75
4	83.6	2.125	10	28.5	0.725
5	72.6	1.842	11	27.6	0.702
6	67.1	1.705	12	26.8	0.682
7	31.5	0.801	13	26.0	0.661

Remarks: For a 300-ohm termination at the folded dipole gap.

TABLE 97. SPACING s OF DIPOLE REFLECTOR BEHIND THE DIPOLE FOR OPTIMUM GAIN

Channel	Spacing s		Reflector length		Channel	Spacing s		Reflector length	
	Inches	Meters	Inches	Meters		Inches	Meters	Inches	Meters
2	40	1.035	108	2.745	8	12¼	0.312	34	0.864
3	36	0.915	98	2.49	9	11¾	0.291	32½	0.825
4	33	0.839	88	2.24	10	11½	0.292	30½	0.775
5	29	0.736	78	1.98	11	11¼	0.286	30	0.764
6	26	0.661	72	1.83	12	11	0.280	29½	0.750
7	13	0.330	36	0.915	13	10¾	0.273	29	0.736

Remarks: The reflector linear length is somewhat longer.

LIST OF REFERENCES

"Short-wave Radiation Phenomena" contains information on theoretical as well as on experimental contributions to electromagnetic radiation from the days of J. C. Maxwell and H. Hertz to the present, and publications applying directly or indirectly to this text are given below; pertinent references appear in footnotes and in the text.

Books

J. A. Stratton, "Electromagnetic Theory," McGraw-Hill Book Company, Inc., New York. S. Schelkunoff, "Electromagnetic Waves," D. Van Nostrand Company, Inc., New York. J. C. Slater, "Microwave Transmission," McGraw-Hill Book Company, Inc., New York. H. H. Skilling, "Fundamentals of Electric Waves," John Wiley & Sons, Inc., New York. R. W. P. King, "Electromagnetic Engineering," Vol. I, McGraw-Hill Book Company, Inc., New York. R. W. P. King, H. R. Mimno, and A. H. Wing, "Transmission Lines, Antennas and Wave Guides," McGraw-Hill Book Company, Inc., New York. J. G. Brainerd, G. Koehler, H. J. Reich, and L. F. Woodruff, "Ultra-high-frequency Techniques," D. Van Nostrand Company, Inc., New York. R. I. Sarbacher and W. A. Edson, "Hyper and Ultra-high Frequency Engineering," John Wiley & Sons, Inc., New York. G. P. Harnwell, "Principles of Electricity and Electromagnetism" (contains a very clear chapter on radiation), McGraw-Hill Book Company, Inc., New York. K. Kupfmueller, "Einfuehrung in die theoretische Electrotechnik" (Introduction to Theoretical Electrical Engineering), Verlag Julius Springer, Berlin. F. Ollendorff, "Potential Felder der Elektrotechnik" (Potential Fields of Electrical Engineering), Verlag Julius Springer, Berlin. S. Ramo and J. R. Whinnery, "Fields and Waves in Modern Radio," John Wiley & Sons, Inc., New York. W. E. Weber, "Electromagnetic Fields, Theory and Application," Vol. I, John Wiley & Sons, Inc., New York.

For classical books, employing classical systems of units, reference is made to the following: J. C. Maxwell, "Electricity and Magnetism," Vol. II, Oxford University Press, New York. H. Hertz, "Electric Waves" (authorized English translation by D. E. Jones), Macmillan & Co., Ltd., London. M. Abraham, "Elektromagnetische Wellen" (Electromagnetic Waves), Art. V., 18, Enzyklopaedie der mathematischen Wissenschaft, B. G. Teubner, Leipzig. Abraham-Becker, "The Classical Theory of Electricity and Magnetism," Blackie & Son, Ltd., Glasgow. Abraham-Foeppl, "Theorie der Elektrizitaet" (Theory of Electricity), Vol. I, B. G. Teubner, Leipzig. M. Planck, "Einfuehrung in die Theorie der Elektrizitaet und des Magnetismus" (Introduction to the Theory of Electricity and Magnetism), S. Hirzel, Leipzig. R. Becker, "Theorie der Elektrizitaet" (Theory of Electricity), Vol. II, B. G. Teubner, Leipzig. J. H. Jeans, "The Mathematical Theory of Electricity and Magnetism," Cambridge University Press, London. M. Mason and W. Weaver, "The Electromagnetic Field," University of Chicago Press, Chicago. Wien-Harms, "Handbuch der Experimentalphysik," consult volume by G. Mie on Electrodynamic, Akademische Verlagsgesellschaft m.b., H. Leipzig. W. R. Smythe, "Static and Dynamic Electricity," McGraw-Hill Book Company, Inc., New York. L. Page and N. I. Adams, "Principles of Electricity," also "Electrodynamics," D. Van Nostrand Company, Inc., New York. R. B. Lindsay and H. Margenau, "Foundations of Physics," Chap. VI, John Wiley & Sons, Inc., New York. G. W. Pierce, "Electric Oscillations

and Electric Waves," McGraw-Hill Book Company, Inc., New York. M. Brillouin, "Propagation de l'électricité" (Propagation of Electricity), Hermann & Cie, Paris. E. Bennett and H. M. Crothers, "Introductory Electrodynamics for Engineers," McGraw-Hill Book Company, Inc., New York.

Periodicals

Electronics April 1942 issue gives a status on UHF's at that time, namely: A. G. Kandoian, I, Radiation Systems and Wave Propagation; I. E. Mouromtseff, R. C. Retherford, and J. H. Findley, II, Ultrahigh Frequency Generators; B. Dudley, III, U-H-F Reception and Receivers; B. L. Jaffe, IV, Wide Band Amplifiers and Frequency Multiplication; R. F. Lewis, V, Measurements in the U-H-F Spectrum.

The American Institute of Electrical Engineers gives in the March–September 1943 issues (Special Reprint 6) a compilation on ultrashort electromagnetic waves, namely, E. Weber, Electromagnetic Theory; J. R. Ragazzini, Transmission Lines at Ultrahigh Frequencies; I. E. Mouromtseff, Generation; S. A. Schelkunoff, Guided Propagation; A. Alford, Radiation; B. Trevor, Reception. All papers contain many useful references.

Inasmuch as the *Proceedings of the IRE* are available in most libraries, reference is made, first, to papers in this periodical in chronological order. These references are significant for short and microwaves and are as follows: M. I. Pupin, A Discussion on Experimental Tests of the Radiation Law for Radio Oscillators, together with A. N. Goldsmith, L. Espenschied, R. H. Marriot, and J. Martin, **1,** 3, 10, 12, January, 1913. A. H. Taylor and A. S. Blatterman, Variations in Nocturnal Transmission, **4,** 131, 149, April, 1916. C. A. Culver, Notes on Radiation from Horizontal Antennas, **4,** 449, October, 1916. E. W. Marchant, The Heaviside Layer, **4,** 511, 521, December, 1916. E. Bennett, Feasibility of Low Antenna in Radio Telegraphy, **5,** 237, 266, October, 1918. W. H. Eccles, On Measurement of Signal Strength, **7,** 267, 279, June, 1919. J. M. Miller, Electrical Oscillations in Antennas and Inductance coils, **7,** 299, June, 1919; 652 (John H. Morecroft), December, 1919; (A. Hund), 424, October, 1920. G. W. Pickard, Static Elimination by Directional Reception, **8,** 358, 395, 416, 421, October, 1920. L. W. Austin, The Reduction of Atmospheric Disturbances in Radio Reception, **9,** 41, February, 1921. F. Cutting, A Simple Method of Calculating Radiation Resistance, **10,** April, 1922. L. W. Austin, Receiving Measurements and Atmospheric Disturbances at the Naval Research Laboratory, Bureau of Standards, **10,** 239, August, 1922. R. Bown, C. R. Englund, and H. T. Friis, Radio Transmission Measurements, **11,** 115, April, 1923. F. W. Dunmore, Continuous Wave Transmission on a Wave Length of 100 Meters, Using a Special Type of Antenna, **11,** 243, June, 1923. F. W. Dunmore and F. H. Engel, A Method of Measuring Very Short Radio Wave Lengths and Their Use in Frequency Standardization, **11,** 467, October, 1923; 647, October, 1925. F. Conrad, Short Wave Radio Broadcasting, **12,** 723, 739, December, 1924. S. Ballantine, On the Radiation Resistance of a Simple Vertical Antenna at Wave Lengths below the Fundamental, **12,** 823, December, 1924. S. Ballantine, On the Optimum Transmitting Wave Length for a Vertical Antenna over Perfect Earth, **12,** 833, December, 1924. M. Baeumler, Recent Investigations on the Propagation of Electromagnetic Waves, **13,** 5, February, 1925. G. W. Pickard, The Polarization of Radio Waves, **14,** 205, April, 1926; 391 (E. W. Alexanderson), June, 1926. A. H. Taylor, Relation between the Height of the Kennelly-Heaviside Layer and High Frequency Radio Transmission Phenomena, **14,** 521, August, 1926. A. Heising, J. C. Schelleng, and G. C. Southworth, Some Measurements of Short Wave Transmission, **14,** 613, October, 1926. S. A. Levin and C. J. Young, Field Distribu-

tion and Radiation Resistance of a Straight Vertical Unloaded Antenna Radiating at One of Its Harmonics, **14,** 675, October, 1926; 8, January, 1927; 245, March, 1927; 439, May, 1927. E. Quaeck, Propagation of Short Waves around the Earth, **15,** 341, April, 1927; 1065, December, 1927; also discussion by G. W. O. Howe, 1069, December, 1927. S. Uda, High Angle Radiation of Short Electric Waves, **15,** 377, May, 1927. H. E. Hallborg, L. A. Briggs, and C. W. Hansell, Short-wave Commercial Long-distance Communication, **15,** 467, June, 1927. E. J. Alway, Propagation of Short Waves during A Solar Eclipse, **15,** 998, December, 1927. R. A. Heising, Experiments and Observations Concerning the Ionized Regions of the Atmosphere, **16,** 75, January, 1928. E. O. Hulburt, Ionization in the Upper Atmosphere, **16,** 174, February, 1928. P. O. Pedersen, The Propagation of Radio Waves along the Surface of the Earth (a book review by J. C. F. Rybner), **16,** 219, February, 1928. E. O. Hulburt, On Round-the-world Signals, **16,** 287, March, 1928. O. Dahl and L. A. Gebhardt, Measurements of the Effective Heights of the Conducting Layer and the Disturbances of August, 1927, **16,** 290, March, 1928. A. H. Taylor and L. C. Young, Studies of High Frequency Radio Wave Propagation, **16,** 561, May, 1928. H. T. Friis, Oscillographic Observations on the Direction of Propagation and Fading of Short Waves, **16,** 658, May, 1928. L. Espenschied, Technical Considerations Involved in the Allocation of Short Waves, Frequencies between 1.5 and 30 Megacycles, **16,** 773, June, 1928. G. Breit, M. A. Tuve, and O. Dahl, Effective Heights of the Kennelly-Heaviside Layer in December, 1927, and January, 1928, **16,** 1236, September, 1928. S. Ballantine, The Chireix-Mesny Directive Antenna for Short Waves (a review of current literature), **16,** 1261, September, 1928. A. Meissner and H. Rothe, On the Determination of the Optimum Radiation Angle for Horizontal Antennas, **17,** 35, January, 1929. J. K. Clapp, Some Experiments in Short-distance Short-wave Radio Transmission, **17,** 479, March, 1929. H. B. Maris and E. O. Hulburt, Wireless Telegraphy and Magnetic Storms, **17,** 494, March, 1929. A. A. Pistolkors, The Radiation Resistance of Beam Antennas, **17,** 562, March, 1929. G. W. Kenrick and C. K. Jen, Measurements of the Height of the Kennelly-Heaviside Layer, **17,** 711, April, 1929. E. H. Lange, Note on Earth Reflection of Ultra-short Radio Waves, **17,** 745, April, 1929. E. Quaeck and H. Moegel, Double and Multiple Signals with Short Waves, 17, 791, May, 1929; Short Range Echoes with Short Waves, 824, May, 1929. C. B. Mirick and E. R. Hentschel, A New Method of Determining the Height of the Kennelly-Heaviside Layer, **17,** 1034, June, 1929. A. H. Taylor and L. C. Young, Studies of Echo Signals, **17,** 1491, September, 1929. G. Breit, Group Velocity and Long Retardations of Radio Echoes, **17,** 1508, September, 1929. L. R. Hafstad and M. A. Tuve, Further Studies of the Kennelly-Heaviside Layer, **17,** 1513, September, 1929. E. O. Hulbert, Ionization in the Atmosphere of Mars, **17,** 1523, September, 1929. C. N. Anderson, Notes on the Effect of Solar Disturbances on Transatlantic Radio Transmission, **17,** 1528, September, 1929. L. R. Hafstad and M. A. Tuve, An Echo Interference Method for the Study of Radio Wave Paths, **17,** 1786, October, 1929. P. O. Pedersen, Wireless Echoes of Long Delay, **17,** 1750, October, 1929. G. Breit, The Significance of Observations of the Phase of Radio Echoes, **17,** 1815, October, 1929. A. S. Eve, D. A. Keyes, and F. W. Lee, The Penetration of Rock by Electromagnetic Waves and Audio Frequencies, **17,** 2072, November, 1929. F. H. Drake and R. M. Wilmotte, On the Daylight Transmission of Horizontally and Vertically Polarized Waves from Airplanes, **17,** 2242, December, 1929. B. Rolf, Graphs to Prof. Sommerfeld's Attenuation Formula for Radio Waves, **18,** 391, March, 1930. A. Esau and W. M. Hahnemann, Report on Experiments with Electric Waves of about 3 Meters, Their Propagation and Use, **18,** 471,

March, 1930. G. W. Kenrick and G. W. Pickard, Summary of Progress in the Study of Radio Wave Propagation Phenomena, **18,** 649, April, 1930. R. K. Potter, Transmission Characteristics of a Short-wave Telephone Circuit, **18,** 581, April, 1930. J. H. Dellinger, H. Diamond, and F. W. Dunmore, Development of the Visual-type Airway Radio-beacon System, **18,** 796, May, 1930. J. C. Schelleng, Some Problems of Short-wave Telephone Transmission, **18,** 913, June, 1930. S. Uda, Radiotelegraphy and Radiotelephony on Half-meter Waves, **18,** 1047, June, 1930. J. A. Stratton, The Effect of Rain and Fog on the Propagation of Very Short Radio Waves, **18,** 1064, June, 1930. W. J. Brown, Ultra-short Waves for Limited Range Communication, **18,** 1129, July, 1930. E. O. Hulburt, Wireless Telegraphy and the Ionization in the Upper Atmosphere, **18,** 1231, July, 1930. G. C. Southworth, Certain Factors Affecting the Gain of Directive Antennas, **18,** 1502, September, 1930. Lee De Forest, An Early Note on Wave Propagation, **18,** 1600, September, 1930. M. L. Presscott, The Diurnal and Seasonal Performance of High Frequency Radio Transmission over Various Long Distance Circuits, **18,** 1797, November, 1930. N. H. Edes, Some Experiences with Short-wave Wireless Telegraphy, **18,** 2011, December, 1930. E. L. Hall, Accurate Method of Measuring Transmitted Wave Frequencies at 5000 and 20,000 Kilocycles per Second, **19,** 35, January, 1931. A. H. Taylor, Note on Skip Distance Effects on Superfrequencies, **19,** 103, January, 1931. T. R. Gilliland, Kennelly-Heaviside Layer Height Observations, for 4045 and 8650 Kc, **19,** 114, January, 1931. H. Moegel, Monitoring the Operation of Short-wave Transmitters, **19,** 214, February, 1931. G. W. Kenrick, A. H. Taylor, and L. C. Young, Note on High Frequency Transmission during Summer of 1930, **19,** 252, February, 1931. G. W. Pickard, Note on the Fifteen-month Period in Solar Activity, Terrestrial Magnetism, and Radio Reception, **19,** 353, March, 1931. R. Bechmann, Calculation of Electric and Magnetic Field Strengths of Any Oscillating Straight Conductors, **19,** 461, March, 1931; 682, April, 1931. H. H. Beverage and H. O. Peterson, Diversity Receiving System of RCA Communications, Inc., **19,** 531, April, 1931. H. Diamond and F. W. Dunmore, A Radio Beacon and Receiving System for Blind Landing of Aircraft, **19,** 585, April, 1931. M. Baeumler, K. Krueger, H. Plendl, and W. Pfitzer, Radiation Measurements of a Short-wave Directive Antenna at the Nauen High Power Radio Station, **19,** 812, May, 1931. G. J. Elias, Reflection of Electromagnetic Waves at Ionized Media with Variable Conductivity and Dielectric Constant, **19,** 891, May, 1931. V. I. Bashenoff and N. A. Mjasoedoff, The Effective Height of Closed Aerials, **19,** 984, June, 1931. N. H. Edes, The Multiple Refraction and Reflection of Short Waves, **19,** 1024, June, 1931. G. W. Pickard, A Note on the Relation of Meteor Showers and Radio Reception, **19,** 1166, July, 1931. E. J. Sterba, Theoretical and Practical Aspects of Directional Transmitting Systems, **19,** 1184, July, 1931. H. H. Beverage, H. O. Peterson, and C. W. Hansell, Application of Frequencies above 30,000 Kilocycles to Communication Problems, **19,** 1313, August, 1931. A. H. Taylor and H. F. Hastings, The Determination of Power in the Antenna at High Frequencies, **19,** 1370, August, 1931. E. Bruce, Developments in Short-wave Directive Antennas, **19,** 1406, August, 1931. J. P. Schafer and W. M. Goodall, Radio Transmission Studies of the Upper Atmosphere, **19,** 1434, August, 1931. R. Bechmann, On the Calculation of Radiation Resistance of Antennas and Antenna Combinations, **19,** 1471, August, 1931. P. A. de Mars, G. W. Kenrick, and G. W. Pickard, Use of Automatic Recording Equipment in Radio Transmission Research, **19,** 1618, September, 1931. C. R. Burrows, The Propagation of Radio Short Waves over the North Atlantic, **19,** 1634, September, 1931. N. H. Edes, The Relation Connecting Skip Distance, Wave Length, and the Constants of the Ionized Layers, **19,** 1663,

September, 1931. R. K. Potter, High Frequency Atmospheric Noise, **19,** 1731, October, 1931. S. Namba, E. Iso, and S. Ueno, Polarization of High Frequency Waves and Their Direction Finding, **19,** 2000, November, 1931. T. R. Gilliland and G. W. Kenrick, Preliminary Note on an Automatic Recorder Giving a Continuous Height Record of the Kennelly-Heaviside Layer, **20,** 540, March, 1932. M. v. Ardenne, The Transmission and Reception of Ultra-short Waves That Are Modulated by Several Modulated High Frequencies, **20,** 933, June, 1932. P. S. Carter, Circuit Relations in Radiating Systems and Applications to Antenna Problems, **20,** 1004, June, 1932. J. P. Schafer and W. M. Goodall, Kennelly-Heaviside Layer Studies Employing a Rapid Method of Virtual Height Determination, **20,** 1131, July, 1932. E. J. Sterba and C. B. Feldman, Transmission Lines for Short-wave Radio Systems, **20,** 1163, July, 1932. R. K. Potter, An Estimate of the Frequency Distribution of Atmospheric Noise, **20,** 1512, September, 1932. T. L. Eckersley, Direct-ray Broadcast Transmission, **20,** 1555, October, 1932. N. Carrara, The Detection of Microwaves, **20,** 1615, October, 1932. H. R. Lubcke, Television Image Reception in an Airplane, **20,** 1732, November, 1932. J. A. Stratton and H. A. Chinn, The Radiation Characteristics of a Vertical Half-wave Antenna, **20,** 1892, December, 1932. A. M. Skellett, The Ionizing Effect of Meteors in Relation to Radio Propagation, **20,** 1933, December, 1932. J. P. Schafer and W. M. Goodall, Observations of the Kennelly-Heaviside Layer Heights during the Leonid Shower of November, 1931, **20,** 1941, December, 1932. R. M. Morris and W. A. R. Brown, Transoceanic Reception of High-frequency Telephone Signals, **21,** 63, January, 1933. C. R. Burrows and E. J. Howard, Short-wave Transmission to South America, **21,** 102, January, 1933. S. Namba, General Theory on the Propagation of Radio Waves in the Ionized Layer of the Upper Atmosphere, **21,** 238, February, 1933. L. F. Jones, A Study of the Propagation of Wavelengths between Three and Eight Meters, **21,** 349, March, 1933. B. Trevor and P. S. Carter, Notes on the Propagation of Waves below Ten Meters in Length, **21,** 387, March, 1933. J. C. Schelleng, C. R. Burrows, and E. B. Ferrell, Ultra-short-wave Propagation, **21,** 427, March, 1933. C. R. Englund, A. B. Crawford, and W. W. Mumford, Some Results of a Study of Ultra-short Wave Transmission Phenomena, **21,** 464, March, 1933. C. B. Feldman, The Optical Behavior of the Ground for Short Waves, **21,** 764, June, 1933. H. Musykens and J. D. Kraus, Some Characteristics of Ultra-high Frequency Transmission, **21,** 1302, September, 1933. R. Whitmer, Radiation Resistance of Concentric Conductor Transmission Lines, **21,** 1343, September, 1933. Report of Committee on Radio Propagation Data, **21,** 1419, October, 1933. E. Kramer, A New Field of Application for Ultra-short Waves, **21,** 1519, November, 1933. R. R. Ramsey, Radiation and Induction, **21,** 1586, November, 1933. H. T. Friis, C. B. Feldman, and W. M. Sharpless, The Determination of the Direction of Arrival of Short Radio Waves, **22,** 47, January, 1934. L. S. Palmer and D. Taylor, Rectangular Short-wave Frame Aerials, for Reception, **22,** 93, January, 1934. T. R. Gilliland, Note on a Multi-frequency Automatic Recorder of Ionosphere Heights, **22,** 236, February, 1934. G. H. Brown and R. King, High-frequency Models in Antenna Investigations, **22,** 457, April, 1934. S. S. Kirby, L. V. Berkner, and D. M. Stuart, Studies of the Ionosphere and Their Application to Radio Transmission, **22,** 481, April, 1934. F. G. Kear, Maintaining the Directivity of Antenna Arrays, **22,** 847, July, 1934; 1313 November, 1934. N. Janco, Echoes of Radio Waves, **22,** 923, July, 1934; 1405, November, 1935. L. V. Berkner and H. W. Wells, Report of Ionosphere Investigations at the Huancayo Magnetic Observatry (Peru) during 1933, **22,** 1102, September, 1934. M. A. Bontch-Bruewitch, Measurements of Electric State of Upper Strato-

sphere in Polar Regions (Kennelly-Heaviside Layer), **22,** 1124, September, 1934. W. L. Barrow, On the Impedance of a Vertical Half-wave Antenna above an Earth of Finite Conductivity, **23,** 150, February, 1935. G. H. Brown, The Phase and Magnitude of Earth Currents near Radio Transmitting Antennas, **23,** 168, February, 1935. H. Pratt, A Review of Radio Communication in the Fixed Services for the Year 1934, **23,** 415, May, 1935. B. Trevor and R. W. George, Notes on Propagation at a Wavelength of Seventy-three Centimeters, **23,** 461, May, 1935. C. R. Burrows, Radio Propagation over Spherical Earth, **23,** 470, May, 1935. E. V. Appleton and S. Chapman, Report on Ionization Changes during a Solar Eclipse, **23,** 658, May, 1935. J. P. Schafer and W. M. Goodall, Diurnal and Seasonal Variations, in the Ionosphere during the Years 1933 and 1934, **23,** 670, May, 1935. J. W. Labus, A Broadcast Antenna for "Low Angle" Radiation, **23,** 935, August, 1935. E. Kramer, The Present State in the Art of Blind Landing of Airplanes Using Ultra-short Waves in Europe, **23,** 1171, October, 1935. E. O. Hulburt, The Ionosphere, Skip Distances of Radio Waves, and the Propagation of Microwaves, **23,** 1492, December, 1935. C. R. Burrows, A. Decino, and L. E. Hunt, Ultra-short-wave Propagation over Land, **23,** 1507, December, 1935. G. H. Brown, A Critical Study of the Characteristics of Broadcast Antennas as Affected by Antenna Current Distribution, **24,** 48, January, 1936. H. E. Hallborg, Terrestrial Magnetism and Its Relation to World-wide Short-wave Communications, **24,** 455, March, 1936. F. R. Stansel, A Study of the Electromagnetic Field in the Vicinity of a Radiator, **24,** 802, May, 1936. H. K. Morgan, Rain Static, **24,** 959, July, 1936. S. S. Kirby, T. R. Gilliland, and E. B. Judson, Ionosphere Studies during Partial Solar Eclipse of Feb. 3, 1935, **24,** 1027, July, 1936. P. S. Carter and G. S. Wickizer, Ultra-high Frequency Transmission between the RCA Building and the Empire State Building in New York City, **24,** 1082, August, 1936. H. A. Wheeler and V. E. Whitman, The Design of Doublet Antenna Systems, **24,** 1257, October, 1936. K. A. Norton, The Propagation of Radio Waves over the Surface of the Earth and in the Upper Atmosphere, **24,** 1367, October, 1936; 1203, September, 1937; 1366, November, 1937, gives a correction. S. A. Schelkunoff, Modified Sommerfeld's Integral and Its Application, **24,** 1388, October, 1936. R. C. Colwell and A. W. Friend, Ultra-high Frequency Wave Propagation over Plane Earth and Fresh Water, **25,** 32, January, 1937. E. B. Judson, Comparison Data on the Ionosphere, Sunspots, and Terrestrial Magnetism, **25,** 38, January, 1937. G. H. Brown, Directional Antennas, **25,** 78, January, 1937. C. R. Burrows The Surface Wave in Wave Propagation over Plane Earth, **25,** 219, January, 1937. P. v. Handel and W. Pfister, Ultra-short-wave Propagation along the Curved Earth's Surface, **25,** 346, March, 1937; 240, February, 1938. G. H. Brown and J. G. Leitch, The Fading Characteristics of the Top-loaded WCAU Antenna, **25,** 583, May, 1937; 115, January, 1938. H. T. Friis and C. B. Feldman, A Multiple Unit Steerable Antenna for Short-wave Reception, **25,** 841, July, 1937. J. H. Dellinger, Sudden Disturbances of the Ionosphere, **25,** 1253, October, 1937. H. O. Peterson and D. R. Goddard, Field Strength Observations of Transatlantic Signals, 40 to 45 Megacycles, **25,** 1291, October, 1937. T. Nakai, Some Notes on Rain Static in Japan, **25,** 1381, November, 1937. W. M. Goodall, On the Ionization of the F_2 Region, **25,** 1414, November, 1937. C. R. Mingins, Electromagnetic Wave Fields near the Earth's Surface, **25,** 1419, November, 1937. S. A. Schelkunoff, Transmission Theory of Plane Electromagnetic Waves, **25,** 1457, November, 1937. H. Diamond and F. W. Dunmore, Experiments with Underground Ultra-high-frequency Antenna for Aircraft Landing Beam, **25,** 1542, December, 1937. E. Kramer and W. Hahnemann, The Ultra-short-wave Guide-ray Beacon and Its Application, **26,** 17, January, 1938;

276, March, 1938. H. G. Smith, Precise Measurements of Electromagnetic Fields, **26,** 45, January, 1938. W. W. Hansen and J. R. Woodyard, A New Principle in Directional Antenna Design, **26,** 333, March, 1938. C. R. Burrows, A. Decino, and L. E. Hunt, Stability of Two-meter Waves, **26,** 516, May, 1938. G. W. Kenrick, A. M. Braaten, and J. General, The Relation between Radio-transmission Path and Magnetic-storm Effects, **26,** 831, July, 1938. J. A. Pierce, Abnormal Ionization in the E Region of the Ionosphere, **26,** 892, July, 1938. H. Diamond, W. S. Hinman, Jr., and F. W. Dunmore, A Method for the Investigation of the Upper Air Phenomena and Its Application to Radio Meteorography, **26,** 1235, October, 1938. T. R. Gilliland, S. S. Kirby, N. Smith, and S. E. Reymer, Maximum Usable Frequencies for Radio Sky-wave Transmission 1933–1937, **26,** 1347, November, 1938. W. L. Barrow and F. M. Greene, Rectangular Hollow-pipe Radiators, **26,** 1498, November, 1938. L. J. Chu and W. L. Barrow, Electromagnetic Waves in Hollow Metal Tubes of Rectangular Cross Section, **26,** 1520, December, 1938. D. R. Goddard, Observations on Sky-wave Transmission on Frequencies above 40 Megacycles, **27,** 12, January, 1939. E. H. Conklin, 56-megacycle Reception via Sporadic-E-layer Reflections, **27,** 36, January, 1939. W. L. Barrow and F. D. Lewis, The Sectoral Electromagnetic Horn, **27,** 41, January, 1939. W. L. Barrow and L. J. Chu, Theory of the Electromagnetic Horn, **27,** 51, January, 1939. G. C. Southworth and A. P. King, Metal Horns as Directive Receivers of Ultra-short Waves, **27,** 95, February, 1939. J. P. Schafer and W. M. Goodall, Peak Field Strength of Atmospherics Due to Local Thunderstorms at 150 Megacycles, **27,** 202, March, 1939. N. Smith, The Relation of Radio Sky-wave Transmission to Ionosphere Measurements, **27,** 332, May, 1939. K. G. MacLean and G. S. Wickizer, Notes on the Random Fading of 50-megacycle Signals over Nonoptical Paths, **27,** 501, August, 1939. A. W. Friend and R. C. Colwell, The Heights of Reflecting Regions in the Troposphere, **27,** 626, October, 1939. C. B. Feldman, Deviations of Short Radio Waves from the London-New York Great Circle Path, **27,** 635, October, 1939. J. H. Dellinger, Report of Commission II, Radio Wave Propagation, International Scientific Radio Union, **27,** 645, October, 1939. D. R. Goddard, Transatlantic Reception of London Television Signals, **27,** 692, November, 1939. W. M. Goodall, The Solar Cycle and the F_2 Region of the Ionosphere, **27,** 701, November, 1939. J. H. Piddington, The Scattering of Radio Waves in the Lower and Middle Atmosphere, **27,** 753, December, 1939. W. E. Jackson, The Impetus Which Aviation Has Given to the Application of Ultra-high Frequencies, **28,** 49, February, 1940. J. D. Kraus, Antenna Arrays with Closely Spaced Elements, **28,** 76, February, 1940. W. L. Barrow and C. Shulman, Multiunit Electromagnetic Horns, 28, 130, March, 1940. F. Hamburger, C. V. Larrick, and M. Jones, High-frequency Propagation Characteristics, **28,** 175, April, 1940. A. W. Melloh, Damped Electromagnetic Waves in Hollow Metal Pipes, **28,** 179, April, 1940. W. L. Barrow and W. W. Mieher, Natural Oscillations in Electrical Cavity Resonators, **28,** 184, April, 1940. G. S. Wickizer, Field Strength Survey, 52.75 Megacycles from Empire State Building, **28,** 291, July, 1940. R. C. Colwell, The Troposphere and Radio Waves, **28,** 299, July, 1940. C. R. Englund, A. B. Crawford, and W. W. Mumford, Ultra-short-wave Transmission over a 39 Mile "Optical" Path, **28,** 360, August, 1940. J. H. Dellinger and A. T. Cosentino, A Radio Transmission Anomaly between the United States and Argentina, **28,** 431, October, 1940. A. H. Waynick, Experiments on the Propagation of Ultra-short Radio Waves, **28,** 468, October, 1940. J. D. Kraus, The Corner-reflector Antenna, **28,** 513, November, 1940. H. Selvidge, Diffraction Measurements at Ultra-high Frequencies, **29,** 10, January, 1941. C. R. Burrows and M. C. Gray, The Effect

of the Earth's Curvature on Ground-wave Propagation, **29,** 16, January, 1941; 105, February, 1942 (a correction). E. C. Jordan and W. L. Everitt, Acoustic Models of Radio Antennas, **29,** 186, April, 1941. C. F. Edwards and K. G. Jansky, Measurements of the Delay and the Direction of Arrival of Echoes from Near-by Short-wave Transmitters, **29,** 322, June, 1941. E. A. Laport and J. B. Knox, Radiating System for 75-megacycle Cone-of-silence Marker, **30,** 26, January, 1942. A. J. Ebel, A Note on the Sources of Spurious Radiations in the Field of Two Strong Signals, **30,** 81, February, 1942. C. W. Harrison, Jr., The Inclined Rhombic Antenna, **30,** 241, May, 1942. G. L. Haller, Aircraft Antennas, **30,** 357, August, 1942. S. A. Schelkunoff and C. B. Feldman, On Radiation from Antennas, **30,** 511, November, 1942. E. G. Linder, Attenuation of Electromagnetic Fields in Pipes Smaller Than the Critical Size, **30,** 554, December, 1942. G. F. Levy, Loop Antennas for Aircraft, **31,** 56, Feb., 1943. C. W. Harrison, Jr., A Note on the Characteristics of the Two-antenna System, **31,** 75, Feb., 1943. G. C. Southworth, Beyond the Ultra-short Waves, **31,** 319, July, 1943. C. W. Harrison, Jr., Radiation from Vee Antennas, **31,** 362, July, 1943. G. F. Levy, Corrections to "Loop Antennas for Aircraft," **31,** 384, July, 1943. E. W. Herold and L. Malter, Some Aspects of Radio Reception at Ultra-high Frequency, **31,** 423, August, 1943. E. W. Herold, The Antenna and the Receiver Input Circuits, **31,** 423, August, 1943. W. H. Pickering, The Radio Sonde, **31,** 479, September, 1943. R. W. King, Coupled Antennas and Transmission Lines, **31,** 626, November, 1943. M. S. Neiman, The Principle of Reciprocity in Antenna Theory, **31,** 666, December, 1943. A. Bronwell, Transmission Line Analogies for Plane Electromagnetic Wave Reflections, **32,** 233, April, 1944. F. S. Howes and F. M. Wood, Note on the Bearing Error and Sensitivity of a Loop Antenna in an Abnormally Polarized Field, **32,** 231, April, 1944. J. R. Whinnery and S. Ramo, A New Approach to the Solution of High Frequency Field Problems, **32,** 284, May, 1944. G. Kron. Equivalent Circuit of the Field Equations of Maxwell, **32,** 289, May, 1944. J. R, Whinnery, Jr., Network Analyzer Studies of Electromagnetic Cavity Resonators, **32,** 360, June, 1944. J. C. Hromada, The Development of a New Station Location or Z-marker, **32,** 454, August, 1944. J. B. Sherman, Circular Loop Antennas at Ultra-high Frequencies, **32,** 534, September, 1944. D. Foster, Loop Antennas with Uniform Current, **32,** 603, October, 1944. H. W. Kohler, Antenna Design for Field-strength Gain, **32,** 611, October, 1944. J. H. DeWitt, Jr., and A. D. Ring, Significant Radiation from Directional Antennas of Broadcast Stations for Determining Sky-wave Interference at Short Distances, **32,** 668, November, 1944. J. G. Rountree, A Calculator for Two-element Directive Arrays, **32,** 760, December, 1944. M. W. Scheldorf, A New Studio-to-transmitter Antenna, **33,** 106, February, 1945. F. E. Terman and J. M. Pettit, The Compensated Loop Direction Finder, **33,** 307, May, 1945. A. W. Friend, A Summary and Interpretation of Ultra-short-wave Propagation Collected by the Late Ross A. Hull, **33,** 358, June, 1945. G. Glinski, Note on Impedance Matching of Shunt-fed Half-wave Dipole, **33,** June, 1945. B. E. Montgomery, A Very-high-frequency Aircraft Antenna for Reception of 109-megacycle Localizer Signals, **33,** 767, November, 1945. C. Stewart, Jr., A Proposed Standard Dummy Antenna for Testing Aircraft Radio Transmitters, **33,** 772, November, 1945; S. S. Mackeown and J. W. Miles, The Plane-wave Resolution of Guided Waves, **33,** 805 (1945). A. G. Kandoian, Three New Antenna Types and Their Applications, Waves and Electrons **1,** 70W, February, 1946. R. A. Kirkman and M. Kline, The Transverse Electric Modes in Coaxial Cavities, **34,** 14P, January, 1946. S. D. Robertson and A. P. King, The Effect of Rain upon the Propagation of Waves in the 1- and 3-centimeter Regions, **34,** 178P, April, 1946. G. E. Mueller, Propagation of

6-millimeter Waves, **34,** 181P. H. T. Friis, A Note on a Simple Transmission Formula, **34,** 254, May, 1946. C. L. Dolph, A Current Distribution for Broadside Arrays Which Optimizes the Relationship between Beam Width and Side-lobe Level, **34,** 335, June, 1946. W. Kelvin, The Radiation Field of an Unbalanced Dipole, **34,** 440, July, 1946. K. J. Affanasiev, Simplifications in the Consideration of Mutual Effects between Half-wave Dipoles in Collinear and Parallel Orientations, **34,** 635, September, 1946. R. Bateman, Elimination of Interference-type Fading at Microwave Frequencies with Spaced Antennas, **34,** 662, September, 1946. J. W. Miles, The Equivalent Circuit for a Plane Discontinuity in a Cylindrical Wave Guide, **34,** 728, October, 1946. W. E. Kock, Metal-lens Antennas, **34,** 828, November, 1946. W. M. Sharpless, Measurement of the Angle of Arrival of Microwaves, **34,** 837, November, 1946. A. B. Crawford and W. M. Sharpless, Further Observations of the Angle of Arrival of Microwaves, **34,** 845, November, 1946. Luke Chia-Liu Yuan, Ultra-high-frequency Radiosonde Direction Finding, **34,** 852, November, 1946. G. H. Brown and W. C. Morrison, The RCA Antenna Analyzer—An Instrument Useful in the Design of Directional Antenna Systems, **34,** 992, December, 1946. R. Baum, Design of Directive Broad-band Antennas, **34,** 956, December, 1946. E. F. George, Electronic Collisional Frequency in the Upper Atmosphere, **35,** 249, March, 1947. F. E. Terman and J. M. Pettit, Correction to the "Compensated-loop Direction Finder," **35,** 269, March, 1947. S. Hershfield and R. King, Discussion on "Concerning Hallén's Integral Equation for Cylindrical Antennas" by S. A. Schelkunoff, **35,** 282, March, 1947. K. A. Norton, A New Source of Systematic Error in Radio Navigation Systems Requiring the Measurement of the Relative Phases of Propagated Waves, **35,** 284, March, 1947. L. J. Anderson, J. P. Day, C. H. Freres, and A. P. D. Stokes, Attenuation of 1.25-centimeter Radiation through Rain, **35,** 351, April, 1947. C. L. Pekeris, Wave Theoretical Interpretation of Propagation of 10-centimeter and 3-centimeter Waves in Low-level Ocean Ducts, **35,** 453, May, 1947. H. J. Riblet, Microwave Omnidirectional Antennas, **35,** 474, May, 1947. H. J. Riblet and C. L. Dolph, Discussion on "A Current Distribution for Broadside Arrays Which Optimizes the Relationship between Beam Width and Side-lobe Level" by G. L. Dolph, **35,** 489, March, 1947. H. E. Newell, Jr., Abstract of "A Method for Calculating Electric Field Strength in the Interference Region," **35,** 777, August, 1947. S. B. Cohn, Properties of Ridge Wave Guide, **35,** 783, August, 1947. K. A. Norton, A. C. Omberg, and J. Freedman, Discussion on the Maximum Range of a Radar Set, **35,** 927, September, 1947. M. Kline, R. A. Kirkman, and W. H. Huggins, **35,** Discussion on the TE Modes in Coaxial Cavities, **35,** 931, September, 1947. L. A. Manning, The Determination of Ionospheric Electron Distribution, **35,** 1203, November, 1947. C. C. Cutler, Parabolic Antenna Design for Microwaves, **35,** 1284, November, 1947. W. A. Tyrrell, Hybrid Circuits for Microwaves, **35,** 1294, November, 1947. A. H. Waynick, Ultra-short-wave Propagation Studies beyond the Horizon, **35,** 1334, November, 1947. P. I. Richards, Scalar and Vector Potential Treatment, **35,** 1334, November, 1947. M. Katzin, Quantitative Radar Measurements, **35,** 1333, November, 1947. G. Sinclair, E. C. Jordan, and E. W. Vaughan, Measurement of Aircraft Antenna Patterns Using Models, **35,** 1451, December, 1947. G. W. Pickard and H. T. Stetson, A Study of Tropospheric Reception at 42.8 Mc and Meteorological Conditions, **35,** 1445, December, 1947. C. C. Cutler, A. P. King, and W. E. Lindenblad, Microwave Antenna Measurements, **35,** 1462, December, 1947. N. E. Lindenblad, Slot Antennas, **35,** 1472, December, 1947. H. A. Wheeler, Fundamental Limitations of Small Antennas, **35,** 1479, December, 1947. H. A. Wheeler, A. Helical Antenna for Circular Polarization, **35,** 1184, December, 1947.

A. A. Pistolkors, Theory of the Circular Diffraction Antenna, **36,** 56, January, 1948. A. L. Durkee, Results of Microwave Propagation Tests on a 40-mile Overland Path, **36,** 197, February, 1948. G. Wilkes, Wavelength Lenses, **36,** 206, February, 1948.

Important and associated papers in the *Bell System Technical Journal* are the following: W. H. Wise, Asymptotic Dipole Radiation Formulas, **8,** 662, October, 1929. G. C. Southworth, Certain Factors Affecting the Gain of Directive Antennas, **10,** 63, January, 1931 (has a very complete bibliography of about 150 papers in several languages). E. J. Sterba and C. B. Feldman, Transmission Lines for Short-wave Radio Systems, **11,** 411, July, 1932. J. C. Schelleng, C. R. Burrows, and E. B. Ferrell, Ultra-short Wave Propagation, **12,** 125, April, 1933. C. R. Englund, A. B. Crawford, and W. W. Mumford, Some Results of a Study of Ultra-short Wave Transmission Phenomena, **12,** 197, April, 1933. S. A. Schelkunoff, The Electromagnetic Theory of Coaxial Transmission Lines and Cylindrical Shields, **13,** 532, October, 1934 (has a list of about 35 references). C. R. Burrows, L. E. Hunt, and A. Decino, Ultra-short Wave Propagation: Mobile Urban Transmission Characteristics, **14,** 253, April, 1935. C. R. Englund, A. B. Crawford, and W. W. Mumford, Further Results of a Study of Ultra-short Wave Transmission Phenomena, **14,** 369, July, 1935. C. R. Burrows, Radio Propagation over Spherical Earth, **14,** 632, October, 1935. G. C. Southworth, Hyper-frequency Wave Guides—General Considerations and Experimental Results, **15,** 310, April, 1936 [consult also Lord Rayleigh, On the Passage of Electric Waves through Tubes or the Vibrations of Dielectric Cylinders, *Phil. Mag.*, **43,** 125 (1897)]. J. R. Carson, A. P. Mead, and S. A. Schelkunoff, Hyper-frequency Wave Guides—Mathematical Theory, **15,** 310, April, 1936. C. R. Burrows, Radio Propagation over Plane Earth, **16,** 45, January, 1937. S. A. Schelkunoff, The Impedance Concept, **17,** 17, January, 1938.

With respect to wave guides, consult also the IRE references and L. Brillouin, Propagation of Electromagnetic Waves in Tubes, *Rev. gén. élec.*, **40,** 227 (1936). A. G. Clavier and V. Altovsky, Experimental Researches on the Propagation of Electromagnetic Waves in Dielectric (cylindrical) Guides, *Elec. Commun.*, **18,** 81 (1939). A. G. Clavier, Theoretical Relationships of Dielectric Guides (cylindrical) and Coaxial Cables, *Elec. Commun.*, **17,** 276 (1939). L. Brillouin, Hyperfrequency Waves and Their Practical Use, *Elec. Commun.*, **20,** 118 (1941). L. Page and N. I. Adams, Electromagnetic Waves in Conducting Tubes, *Phys. Rev.*, **52,** 647 (1937). J. Kemp, Electromagnetic Waves in Metal Tubes of Rectangular Cross Section, *J. IEE*, **20,** 73, September, 1941 (has 14 references). D. Hondros and P. Debye, Electromagnetic Waves in Dielectric Wires, *Ann. Physik*, **32,** 465, June, 1910. H. Zahn, Uber den Nachweis elektromagnetischer Wellen an dielektrischen Draehten (Detection of Electromagnetic Waves in Dielectric Wires), *Ann. Physik.*, **49,** 907, May, 1916. O. Schriever, Elektromagnetische Wellen an dielektrischen Draehten (Electromagnetic Waves in Dielectric Conductors), *Ann. Physik*, **63,** 645, December, 1920. L. Bergman and L. Kruegel, Messungen im Strahlungsfeld einer im Innern eines metallischen Hohlzylinders erregten Linear Antennen (Measurement in the Radiation Field of a Linear Antenna Excited inside a Hollow Metal Cylinder), *Ann. Physik*, **21,** 113, October, 1934. G. W. O. Howe, Electromagnetic Waves in Rectangular Metal Tubes, *Wireless Engr.*, **19,** 93, March, 1942. W. W. Hansen, A Type of Electrical Resonator, *J. Applied Phys.*, **9,** 654, October, 1938. E. U. Condon, Forced Oscillations in Cavity Resonators, *J. Applied Phys.*, **12,** 129, February, 1941. A. Clavier and E. Rostas, Some Problems of Hyperfrequency Technique, *Elec. Commun.*, **16,** 269, January, 1938. F. Borgnis, The Electrical Fundamental Oscillations of Cylindrical Cavities, *Z. Hochfreq.*, **54,** 121 (1939). H. Buchholtz, Ultra-short Waves

in Coaxial Cables and Cavity Resonators, Shaped as Sections of such Cables, *Z. Hochfreq.*, **54,** 161 (1939). F. Luedi, Characteristic Frequencies of E-type in a Capacity-loaded Cylindrical Cavity Resonator, *Helv. Phys. Acta*, **14,** 328 (1941).

Additional reference papers include the following: F. Babin, Efficiency and Radiation of Antenna Systems, *Onde élec.*, **18,** 335, 375 (1939). W. Bach, Investigations in the Field near Parabolic Mirrors of Rotation, *Z. Hochfreq.*, **53,** 115 (1939). L. Bergmann, Radiation Measurements of Straight Wire Antennas Excited at Fundamental and Harmonic Waves, *Ann. Physik*, **82,** 504 (1927). G. H. Brown, A Turnstile Antenna for Use at UHF's, *Electronics*, April, 1936. E. C. Jordan and W. E. Miller, Slotted Cylinder Antenna, *Electronics*, February, 1947. K. Bruene, On the Propagation of Electromagnetic Waves in Water, *Z. Hochfreq.*, **50,** 73 (1937). F. M. Colebrook, The Electric and Magnetic Fields of a Linear Radiator Carrying a Progressive Wave, *J. IEE*, **86,** 169 (1940). W. Daellenbach and W. Kleinsteuber, Reflection and Absorption of Decimeter Waves at Plane Dielectric Layers, *Z. Hochfreq.* **51,** 152 (1938), **52,** 147 (1938). G. Eckart and H. Plendl, The Propagation of Ultrashort Waves, *Ergeb. exakt. Natur Wiss.*, **17,** 325 (1938). E. Fendler, The Variations of Propagation Conditions of a Border Wave (10 m) in the Years 1935–37, *Z. Hochfreq.*, **52,** 14, 147 (1938). K. Fraenz, Gain and Absorption Area of Large Directional Antennas, *Z. Hochfreq.*, **54,** 198 (1939). K. Fraenz, The Absorption of Extremely Short Waves by Clouds and Fog, *Z. Hochfreq.*, **55,** 141 (1940). K. Fraenz, observations on the Absorption Area of Directional Antennas, *Z. Hochfreq.*, **61,** 51 (1943). H. Gutton and J. Ortusi, Measurement of the Field inside a Wave Guide, *Compt. rend. acad. sci.*, **27,** 18 (1943). G. Hara, Radiation and Current Distribution of a Linear Antenna, *Z. Hochfreq.*, **44,** 185 (1934). J. S. Hey, Solar Radiations in the 4–6 Meter Radio Wavelength Band, *Nature*, **157,** 47 (1946). N. Jachnow, Theoretical Investigations of the Radiation Pattern and Radiation Resistance for Progressive Waves of Different Phase Velocities, *Elekt. Nachr., Tech.* **19,** 147 (1942). H. Koenig, The Similarity Laws of the Electromagnetic Field and Their Application to Cavity Resonators, *Z. Hochfreq.*, **58,** 171 (1941). N. v. Korshenewsky, On Oscillations of an Antenna in a Radiation Field, *Z. Tech. Physik*, **10,** 604 (1929). E. Loeb, The Dielectric Coefficient and Loss Angle of Dry and Moist Sand for Decimeter Waves, *Z. Hochfreq.*, **61,** 35 (1943). J. S. McPetrie, L. H. Ford, and J. A. Saxton, Polar Diagrams of Half-wave Receiving Aerials, *Wireless Engr.*, **22,** 263 (1945). J. S. McPetrie and J. A. Saxton, The Electrical Properties of Soil at Wave Lengths of 5 Meters and 2 Meters, *J. IEE*, **92,** 247 (1945). H. O. Peterson, Ultra-high-frequency Propagation Formulas, *RCA Rev.*, **4,** 162 (1939). A. Riedinger, Measurements of Attenuation and Propagation Velocity of Electromagnetic Waves in Metal Tubes, *Z. Hochfreq.*, **58,** 21 (1941). O. H. Roth, On the Mode of Action of Single and Multiple Wire Reflectors, *Z. Hochfreq.*, **48,** 45 (1936). R. L. Smith-Rose, The Solar Eclipse of 1945 and Radio Propagation, *Nature*, 157, 40 (1946). G. C. Southworth, Microwave Radiation from the Sun, *J. Franklin Inst.*, **239,** 285 (1945); **241,** March 1946. M. J. O. Strutt, Radiation of Antennas in Dependence of the Properties of Soil, *Ann. Physik*, **1,** 721 (1929); **4,** 1 (1929); **9,** 67 (1931). M. J. O. Strutt, Reflection Measurements Using Very Short Electromagnetic as Well as Acoustic Waves, *ENT*, **7,** 387 (1930). M. J. O. Strutt, Measurements of Electrical Properties of Soil between 20 Cps and 20 Mc. Sec, *ENT*, **7,** No. 10 (1930).

Many important papers and very good editorial comments appear also in the British magazine *Wireless Engineer.*

With respect to wave duct propagation reference is made to the following: J. C. Schelleng, C. R. Burrows, and E. B. Ferrell, Ultra-short Wave Propagation, *Proc.*

IRE, **21,** 427, March, 1933. J. E. Freehafer, The Effect of Atmospheric Refraction on Short Radio Waves, *MIT Radiation Lab. Rept.* 447 (1943). C. L. Pekeris, Accuracy of the Earth-flattening Approximation in the Theory of Microwave Propagation, *Phys. Rev.*, **70,** 518, October, 1946. C. L. Pekeris, Theory of Propagation of Sound in a Half-space of Variable Sound Velocity under Conditions of Formation of a Shadow Zone, *J. Acoust. Soc. Am.*, **18,** 295, October, 1946. C. L. Pekeris, Wave Theoretical Interpretation of Propagation of 10-centimeter and 3-centimeter Waves in Low-level Ocean Ducts, *Proc. IRE*, **35,** 453, May, 1947. W. H. Furry, Theory of Characteristic Functions in Problems of Anomalous Propagation, *MIT Radiation Lab. Rept.* 680, Feb., 1945 (with other references). H. Lamb, On the Propagation of Tremors over the Surface of an Elastic Solid, *Phil. Trans. Roy. Soc.*, A, **203,** 1, January, 1904. H. Jeffreys, The Formation of Love Waves, *Beitr. angew. Geophys.*, **30,** 336, June, 1931.

Additional references are G. W. O. Howe, The Radiation Resistance of a Half-wave Dipole Aerial, *Wireless Engr.*, **22,** 153, April, 1945; D. I. Lawson, Multipath Interference in Television Transmission, *J. IEE (London)*, **92,** Part III, 125, September 1945; C. Mihul, Reflection of Electromagnetic Waves by Media Whose Optical Constants Vary in a Continuous Fashion, *Jassy Univ., Physik. Berichte*, **24,** 1323, 1943; B. Polic, The Investigation of Propagation of Electromagnetic Waves in Mountain and River Valleys, Fiords, etc., by Means of Models, *Telegraphen-Fernsprech und Funk-Technik*, **33,** 63, April, 1944; E. M. Studenkov, Propagation of Electromagnetic Waves in Branched Hollow Pipe Lines, *J. Phys. (USSR)*, **7,** 308, 1943; N. Maloff, On the Calculation of the Radiation Field of a Wave Guide, *Zhur. Eksptl' i Teoret. Fiz.*, **14,** No. 6, 224, 1944; M. Jouguet, On the Propagation of Electromagnetic Waves in Curved Pipes, *Compt. rend.*, **222,** 440, Feb. 18, 1946; R. E. Burgess, Iron-cored Loop Receiving Aerial, *Wireless Engr.*, **23,** 172, June, 1946; D. A. Bell, Anomalous Attenuation in Wave Guides, *Wireless Engr.*, **23,** 287, October, 1946; E. S. Akeley, A Theory of Narrow Resonant Slit in a Wave Guide Partition, *Phys. Rev.*, **69,** 697, June, 1946; P. Feuer and E. S. Akeley, The Scattering of Electromagnetic Radiation by a Thin Circular Ring in a Circular Wave Guide, *Phys. Rev.*, **69,** 697, June, 1946; L. Page, The Magnetic Antenna, *Phys. Rev.*, **69,** 645, June, 1946; J. Mueller-Strobel, and J. Patry, The Calculation of Auxiliary Functions for Straight Receiving Aerials of Any Height, *Helv. Phys. Acta*, **17,** No. 6, 445, 1944; E. B. Moullin, Radiation from Large Circular Loops, *J. IEE (London)*, **93,** 345, September, 1946; T. Kahan, Reflection of an Electromagnetic Wave by a Disk Located in a Wave Guide, *Compt. rend.*, **222,** 998, April, 1946; F. Duerden, The Wide-band Dipole, *Elec. World*, **18,** 382, December, 1946; K. Fraenz, Aerials, *ETZ*, **65,** 229, June, 1944; H. G. Booker, Slot Aerials and Their Relation to Complementary Wire Aerials (Babinet's Principle), *J. IEE (London)* **93,** 620, 1946; C. E. G. Bailey, Slot Feeders and Slot Aerials, *J. IEE (London)*, **93,** No. 4, 615, 1946; R. Tabard, Line-of-sight Aerials, *Télév. Franc.*, 9 and 11, 22 and 19, January and March, 1946; D. G. Reid, The Gain of an Idealized Yagi Array, *J. IEE (London)*, **93,** 564, 1946; W. Walkinshaw, Theoretical Treatment of Short Yagi Aerials, *J. IEE (London)*, **93,** 598, 1946; S. Tetelbaum, On Some Problems of the Theory of Highly Directive Antenna Arrays, *J. Phys. (USSR)*, **10,** 285, 1946; A. L. Cullen and F. K. Goward, The Design of a Waveguide Fed-array of Slots to give a Specified Radiation Pattern, *J. IEE (London)*, **93,** 683, 1946; L. H. Dawson and N. M. Rust, A Wide-band Linear Array Aerial, *J. IEE (London)*, **93,** 693, 1946; D. Taylor and C. H. Westcott, Divided Broadside Aerials with Applications to 200 Mc/sec Ground Radiolocation Systems, *J. IEE (London)*, **93,** 588, 1946; G. E. Bacon, Variable-elevation Beam-aerial Systems for 1½ Meters, *J. IEE (London)*, **93,** 539, 1946; E. G. Brewitt-Taylor, A Detailed Experimental Study of the Factors Influencing the Polar Diagram of a

Dipole in a Parabolic Mirror, *J. IEE* (*London*), **93,** 679, 1946; F. G. Friedlander, A Dielectric Lens Aerial for Wide-angle Beam-scanning, *J. IEE* (*London*), **93,** 725, 1946; W. H. Watson, Resonant Slots, *J. IEE* (*London*), **93,** 747, 1946; E. Roubine, Recent Theories of the Aerial, *Onde élect.*, **27,** 32–37 and 57–64, January and February, 1947; D. C. Cleckner, Fundamental Beam Patterns, *QST*, **31,** 23, 1947; A. G. Clavier, Attenuation and Q Factors in Wave-guides, *Elec. Commun.*, **23,** 436, December, 1946; C. Micheletta, Propagation Characteristics of a Uniform Line, *Alta Frequenza*, **16,** 47, 1947; E. M. Wells, Radiation Resistance of Horizontal and Vertical Aerials Carrying a Progressive Wave, *Marconi Rev.* **9,** 129, October and December, 1946; B. K. Banerjea, On the Propagation of Electromagnetic Waves through the Atmosphere, *Proc. Roy. Soc.* (*London*), **A, 190,** 67, June, 1947; L. Infeld, The Influence of the Width of the Gap upon the Theory of Antennas, *Quart. Appl. Math*, **5,** 113, 1947; G. E. Mueller and W. A. Tyrrell, Polyrod Antennas, *BSTJ*, **26,** 837, 1947; J. Benoit, Omnidirectional Centimeter-wave Aerial Using a Slotted Waveguide and $E_{0,1}$ Waves, *Compt. rend.*, **225,** 1296, December, 1947; L. de Broglie, On Wave Propagation in Waveguides, *Radio Tech. Dig.* (*Franc.*), **2,** 20, February, 1948; L. J. Chu and W. W. Hansen, The Theory of Disk-loaded Waveguides, *J. Appl. Phys.*, **18,** 996, November, 1947; D. A. Bell, Slot Aerials, *Wireless World*, **54,** 57, February, 1948; M. L. Levin, On the Theory of Slot Aerials, *Compt. rend. acad. sci.* (*USSR*), **58,** 1039, November, 1947 (in Russian); A. A. Pistolkors, Radiation from Transverse Slots on the Surface of a Circular Cylinder, *Zhur. Tekh. Fiz.*, **17,** No. 3, 377, 1947 (in Russian); J. Patry, On the Radiation Impedance of an Electromagnetic Dipole, *Helv. Phys. Acta*, **20,** 455, December, 1947 (in French); Z. Szepesi, Systems of Slots in the Wall of a Circular Waveguide Giving a Spindle-shaped Radiation Diagram, *Compt. rend.*, **226,** 883, March, 1948; Y. N. Feld, Radiating Slits in Circular Wave Guides, *Radiotekhnika* (*Moscow*), **2,** 42, May and June, 1947 (in Russian); W. L. Price, Radio Shadow Effects in the Atmosphere by (Temperature) Inversions, *Proc. Phys. Soc.* (*London*), **61,** 59, July, 1948; H. G. Booker, The Elements of Wave Propagation Using the Impedance Concept, *J. IEE* (*London*), Part III, **95,** 203, May, 1948; H. R. L. Lamont and J. A. Saxton, Intensity-Distance Law of Radiation, *Wireless Engr.*, **25,** 269, August, 1948; R. L. Smith-Rose, Radio Wave Propagation Research in the Department of Scientific and Industrial Research during the Years 1937–46, *J. IEE* (*London*), Part IIIA, **94,** No. 16, 879–891, 1947; P. Lejay, The Forecasting of Maximum Usable Frequencies for Radio Links, *Onde élect.*, **28,** 268–274 and 328–336, July, August, and September, 1948; J. A. Ratcliffe, Diffraction from the Ionosphere and the Fading of Radio Waves, *Nature*, **162,** 9, July 3, 1948; L. S. Schwartz, Transmission Frequencies for Line-of-sight Systems, *Proc. NEC*, **3,** 350–370, 1947; J. Voge, Guided Propagation in Metal Tubes and in Atmosphere, *Onde élec.*, **28,** 29–38, January, 1948; H. Bremmer, On the Propagation of Radio Waves around the Earth, *Physica*, **14,** 301–318, June, 1948; J. S. Prichard and A. H. Mankin, Measurement of Aircraft Antenna Patterns in Flight, *Proc. NEC*, **3,** 349, 1947; H. Page, Ring Aerial Systems, *Wireless Engr.*, **25,** 308, October, 1948; J. D. Kraus, Helical Beam Antennas for Wide-band Applications, *Proc. IRE*, **36,** 1236, October, 1948; F. Kiebitz, On the Illustration of Dipole Radiation, *Arch. Elektrotech.*, **2,** 49–57, February and March, 1948; Y. N. Feld, Multi-slot Aerials, *Zhur. Tekh. Fiz.*, **18,** 1265–1272, October, 1948 (in Russian); R. Becker, Aerial Absorption Surfaces and Their Measurement for Decimeter and Centimeter Waves, *Arch. Elektrotech.*, **2,** 120–123, April and May, 1948; C. J. Bouwkamp, Hallén's Theory for a Straight, Perfectly Conducting Wire, Used as a Transmitting and Receiving Aerial, *Physica*, 's Grav., **9,** 609–631, July, 1942; M. W. Scheldorf and J. F. Bridges, New Principle of Broad Band Antennas, *Tele-Tech*, **8,** 43, June, 1949; R. Franz, Propaga-

tion Characteristics of Tenth-millimeter Waves, *Radio Tech. (Vienna)*, **25,** 461 and 581, August and October, 1949. C. E. Shannon, Communication in Presence of Noise, *Proc. IRE*, **37,** 10, January, 1949; W. E. Gordon, A Theory on Radar Reflections from the Lower Atmosphere, *Proc. IRE*, **37,** 41, January, 1949; A. H. Benner, Predicting Maximum Usable Frequency from Long Distance Scatter, *Proc. IRE* **37,** 44, January, 1949; A. W. Friend, Theory and Practice of Tropospheric Sounding by Radar, *Proc. IRE*, **37,** 116, February, 1949; Yung-Ching Yeh, The Received Power of a Receiving Antenna and the Criteria for its Design, *Proc. IRE*, **37,** 155, February, 1949; J. H. DeWitt, Jr., and E. K. Stodola, Detection of Radio Signals Reflected from the Moon, *Proc. IRE*, **37,** 229, March, 1949; J. S. McPetrie, B. Starnecki, H. Jarkowski, and L. Sicinski, Oversea Propagation on Wave Lengths of 3 and 9 Centimeters, *Proc. IRE*, **37,** 243, March, 1949; J. D. Kraus, The Helical Antenna, *Proc. IRE*, **37,** 263, March, 1949; D. W. R. McKinley and P. M. Millman, A Phenomenological Theory of Radar Echoes from Meteors, *Proc. IRE*, **37,** 364, April, 1945; E. Istvánffy, Antenna Impedance Measurement by Reflection Method, *Proc. IRE*, **37,** 604, June, 1949; J. T. Bolljahn, Some Properties of Radiation from Rectangular Waveguides, *Proc. IRE*, **37,** 617, June, 1949; C. W. Horton, On the Theory of the Radiation Patterns of Electromagnetic Horns of Moderate Flare Angles, *Proc. IRE*, **37,** 744, July, 1949; K. Spangenberg, G. Walters, and F. Schott, Electrical Analyzers for the Solution of Electromagnetic Field Problems, *Proc. IRE*, **37,** 866, August, 1949; R. L. Smith-Rose, Speed of Radio Waves and Its Importance in Some Applications, *Proc. IRE*, **38,** 16, January, 1950; K. Bullington, Radio Propagation Variations at VHF and UHF, *Proc. IRE*, **38,** 27, January, 1950; A. W. Straiton, A. H. Grone, H. W. Smith, Comparison of Measured and Calculated Micro-wave Signal Strength, Phase and Index of Refraction, *Proc. IRE*, **38,** 45, January, 1950; J. Ruze, Wide Angle Metal Plate Optics, *Proc. IRE*, **37,** 53, January, 1950; A. G. Clavier, Reciprocity between General Mutual Impedance in Closed and Open Circuits, *Proc. IRE*, **38,** 69, January, 1950; J. W. Green, On the Deduction of Refractive Index Profile of a Stratified Atmosphere from Radio Field Measurements, *Proc. IRE*, **38,** 80, January, 1950; J. P. Day and L. G. Trolese, Propagation of Short Waves over Desert Terrain, *Proc. IRE*, **38,** 165, February, 1950; H. G. Booker and W. E. Gordon, A. Theory of Radio Scattering in the Troposphere, *Proc. IRE*, **38,** 401, April, 1950; W. B. Wholey, A New Type of Slotted Line Section, *Proc. IRE*, **38,** 244, March, 1950; A. P. King, The Radiation Characteristics of Conical Horn Antennas, *Proc. Ire*, **38,** 249, March, 1950.

NAME INDEX

(References to pages in Volume I are in **boldface** type.)

A

Abraham, M., **493, 552, 705, 706, 711, 727,** 1288
Abraham, M., and R. Becker, 1288
Abraham, M., and A. Foeppl, 1288
Adams, N. I., **705, 727,** 1288, 1297
Affanasiev, K. J., 1296
Akeley, E. S., 1299
Alford, A., 1289
Altovsky, V., 1279
Alway, E. J., 1290
Ampère, A. M., **11, 13, 28, 52, 103, 196**
Anderson, C. N., 1290
Anderson, L. J., 1296
Appleton, E. V., 1293
Ardenne, M. v., 1292
Austin, L. W., 1289

B

Babin, F., 1298
Babinet, J., 1036, 1173, 1279
Bach, W., 1298
Baeumler, M., 1289, 1291
Bailey, C. E. G., 1299
Ballantine, S., 1289, 1290
Banerjea, B. K., 1300
Barrow, W. L., **76, 259,** 1182, 1183, 1293, 1294
Bashenoff, V. I., 1291
Bateman, H., **221**
Bateman, R., 1296
Bauchmann, R. W., 995, 996
Bechmann, R., **235, 641, 648, 727,** 1291
Beck, E. A. C., **458**
Becker, R., 1300
Bell, D. A., 1299, 1300
Benner, A. H., 1301
Bennett, E., and H. M. Crothers, 1289
Bennett, H. S., 1183
Benoit, J., 1300
Bergman, L., 1297, 1298
Berkner, L. V., 1292
Bessel, F. W., **294–295, 304, 307, 309–310, 322–323, 326, 329–333, 338–339, 343, 378–379, 496–498,** 749–750, **756–765, 769–774,** 1136–1146, 1150–1151, 1212–1214, 1230–1232, 1246, 1254–1255, 1265–1267, 1283
Beverage, H. H., **458,** 1291
Binnen, W., 995, 996
Biot, J. P., and F. Savart, **217**
Blake, F. G., **705, 706, 711, 713, 715, 727**
Blatterman, A. S., 1289
Bolljahn, J. T., 1301
Boltzmann, L., 974
Bontsch-Bruenwitsch, M. A., **557,** 1292
Booker, H. G., 1036, 1237, 1279, 1299, 1300, 1301
Borgnis, F., 1297
Bouwkamp, C. J., **705,** 1300
Bown, R., 1289
Braaten, A. M., 1294
Brainerd, J. G., 1183, 1288
Breit, G., 1290
Bremmer, H., **346,** 1065, 1300
Brewitt-Taylor, E. G., 1299
Brewster, D., 931
Bridges, J. F., 1300
Briggs, L. A., 1290
Brillouin, L., **235, 648, 705, 706, 709,** 1289, 1297
Brown, G. H., **648, 727,** 1292, 1293, 1296, 1298
Brown, R., 1289
Brown, W. A. R., 1292
Brown, W. J., 1291
Brownell, A., 1295
Bruce, E., **458,** 1291
Bruene, K., 1298
Bucholtz, H., 1297
Bureau of Standards, **331,** 1265
Burgess, R. E., **787,** 1299
Burrows, C. R., **346,** 1066, 1074, 1077, 1237, 1238, 1291, 1292, 1293, 1294, 1297, 1298

C

Carrara, N., 1292
Carson, J. R., **492, 493, 496, 497, 498,** 1297
Carter, P. S., **648, 704, 727,** 1292, 1293
Chapman, S., 1293
Chinn, H. A., 1292
Chireix, H., and R. Mesny, 1290
Chu, E. Z., 1300
Chu, L. J., **76, 705, 743,** 1146, 1182, 1294
Clapp, J. K., 1290
Clavier, A. G., 1297, 1300, 1301
Cleckner, D. C., 1300
Cohen, S. B., 1296
Colebrook, F. M., 1298

Colwell, R. C., 1293, 1294
Condon, E. U., 1297
Conklin, E. H., 1294
Conrad, F., 1289
Cosentino, A. T., 1294
Coulomb, C. A., **215**
Crawford, A. B., 1254, 1292, 1294, 1296, 1297
Crothers, H. M., and E. Bennett, 1289
Cullen, E. L., 1299
Culver, A., 1289
Cutler, C. C., 1296
Cutting, F., 1289

D

Daellenback, W., 1298
Dahl, O., 1290
Dawson, L. H., 1299
Day, J. P., 1296, 1301
de Broglie, L., 1300
Debye, P., **311,** 971, 1253, 1297
Decino, A., 1293, 1294, 1297
DeForest, L., 1291
Dellinger, J. H., 1291, 1293, 1294
de Mars, P. A., 1291
Devore, H. B., 1241
DeWitt, J. H., Jr., 1295, 1301
Diamond, H., 1291, 1293, 1294
Dolph, C. L., 1296
Drake, F. H., 1290
Drude, P., 1034
Dudley, B., 1289
Duerden, F., 1299
Dunmore, F., 1289, 1291, 1293, 1294
Durkee, A. L., 1297

E

Ebel, J., 1295
Eccles, W. H., 1289
Eckart, C., 997, 1298
Eckersley, T. L., 1065, 1292
Edes, N. H., 1291
Edson, W. A., 1288
Edwards, G. F., 1295
Eisenstein, J., **442**
Elias, G. J., 1291
Emde, F., and E. Jahnke, **331, 643**
Engel, F. H., 1289
Englund, C. R., 1254, 1289, 1292, 1294, 1297
Epstein, P. S., 997, 1065
Esau, A., 1290
Espenschied, L., 1289, 1290
Euler, L., **465, 512, 717**
Eve, A. S., 1290
Everitt, W. L., 1295

F

Faraday, M., **11, 26, 103, 196, 219**
Feld, Y. N., 1300
Feldman, C. B., **493,** 1292, 1293, 1294, 1295, 1297
Fendler, E., 1298
Ferrell, E. B., 1036, 1238, 1292, 1297, 1298
Feuer, P., 1299
Field, L. M., **417**
Findley, J. H., 1289
Fitzgerald, F., **153, 219, 222,** 1238, 1277
Ford, L. H., 1298
Foster, D., 1295
Foster, R. M., **594**
Fraenz, K., 1298, 1299
Frank, P., 1281
Franz, R., 1300
Fraunhofer, J., 1082, 1093
Freedman, J., 1296
Freehafer, J. E., 1237, 1299
Freres, C. H., 1296
Fresnel, A. J., 1083, 1093
Friedlander, F. G., 1300
Friend, A. W., 1293, 1294, 1295, 1301
Friss, H. T., 1241, 1289, 1290, 1292, 1293, 1296
Fry, D. W., 1036
Furry, W. H., 1237, 1299

G

Gauss, K. F., **7, 24, 108–109, 120–122, 196–197, 331,** 1243, 1248, 1252, 1255, 1257–1258
Gebhardt, L. A., 1290
General, J., 1294
George, E. F., 1296
George, R. W., 1293
Gilliland, T. R., 1291, 1292, 1293, 1294
Giorgi, G., **7,** 195, 1243, 1252
Glinski, G., **704,** 1295
Goddard, D. R., 1293, 1294
Goldsmith, A. N., 1289
Goodall, W. M., 1291, 1292, 1293, 1294
Gordon, W. E., 1301
Goward, F. K., 1299
Gray, M. C., **346, 705, 721,** 1066, 1074, 1077, 1294
Green, G., **311,** 1061, 1087, 1279, 1280–1283
Green, J. W., 1301
Greene, F. M., **259,** 1294
Grone, A. H., 1301
Gutton, H., 1298

H

Hafstadt, L. A., 1290
Hahnemann, W. M., 1290, 1293
Hall, E. L., 1291
Hallborg, H. E., 1290, 1293
Hallén, E., **705, 706, 709, 711, 713, 715, 717, 718, 719, 721, 727, 728, 743**
Haller, G. L., 1295
Hamburger, F., 1294
Hamilton, R., **22, 198,** 1271
"Handbook of Chemistry and Physics," 975
Handel, P. v., 1293

Hankel, H., **295, 323, 333, 339, 343**
Hansell, C. W., 1290, 1291
Hansen, W. W., 1294, 1297, 1300
Hara, G., 1298
Harnwell, G. P., 1288
Harrison, C. W., Jr., **705–706, 711, 715, 719, 722, 727–728, 787,** 1295
Hartree, D. R., 1237
Hastings, H. F., 1291
Heaviside, O., **221, 311,** 1243
Heising, R. A., 1289, 1290
Hentschel, E. R., 1290
Herold, E. W., 1295
Hershfield, S., 1296
Hertz, H., **31, 89–90, 153, 157–165, 168–187, 194, 218–222, 235, 241–283, 311–314, 336–346, 492–493,** 1243, 1248, 1275, 1277, 1288
Hey, J. S., 1298
Hinmann, W. S., Jr., 1294
Hollmann, H. E., **557**
Hondros, D., 1297
Horton, C. W., 1183, 1301
Howard, E. J., 1292
Howe, G. W. O., 1290, 1299
Howes, F. S., 1295
Hromada, J. G., 1295
Huggins, W. H., 1296
Hulbert, E. O. 1290, 1291, 1293
Hull, Ross, 1295
Hunt, L. E., 1293, 1294, 1297
Huygens, C., **260,** 1019–1020, 1036, 1089, 1092

I

Iams, H., 1241
Infeld, L., 1300
Iso, E., 1292
Istvanffy, E., 1301

J

Jachnow, N., 1298
Jackson, W. E., 1294
Jaffe, B. L., 1289
Jahnke, E., and F. Emde, **331, 643,** 1265
Janco, N., 1292
Jansen, J., **76**
Jansky, K. G., 1295
Jarkowski, H., 1301
Jeans, J. H., 1288
Jeffreys, H., 1240, 1299
Jen, C. K., 1290
Jones, D. E., 1288
Jones, L. F., 1292
Jones, M., 1294
Jordan, E. C., 1036, 1095, 1182, 1295, 1296, 1298
Jouquet, M., 1299
Judson, E. B., 1293

K

Kahan, T., 1299
Kandoian, A. G., **728,** 1289, 1295
Katz, I., 995
Katzin, M., 995, 996, 1296
Kaufmann, H., **704**
Kear, F. G., 1292
Kelvin, W., 1296
Kemp, J., 1297
Kennelly, A., and O. Heaviside, 977–980
Kenrick, G. W., 1290, 1291, 1292, 1294
Keyes, D. A., 1290
Kiebitz, F., 1300
King, A. P., 1183, 1294, 1295, 1296, 1301
King, R., 1292
King, R. W., 1295
King, R. W. P., **153, 222, 705, 706, 709, 711, 713, 715, 717, 719, 727, 728, 743, 787,** 1288
Kirby, S. S., 1292, 1293, 1294
Kirchhoff, G. R., **68, 97, 258, 262, 267, 311,** 1034, 1060, 1080, 1087
Kirkmann, R. A., 1295, 1296
Kleinsteuber, W., 1298
Kliatzkin, **648**
Kline, M., **648,** 1295, 1296
Knox, J. B., 1295
Kock, W. E., 1241, 1242, 1296
Koehler, G., 1288
Koenig, H., 1298
Kohler, H. W., 1295
Korshenewsky, N. v., 1298
Kramer, E., 1292, 1293
Kraus, J. D., 1292, 1294, 1300, 1301
Kron, G., 1295
Kruegel, L., 1297
Krueger, K., 1291
Kupfmueller, K., 1288

L

Labus, J. W., **648, 704,** 1293
Lamb, H., 1240, 1299
Lamont, H. R. L., 1300
Lamor, J., **311**
Lange, E. H., 1290
Laplace, P. S., **145, 220,** 1272
Laport, E. A., 1295
Larrick, G. V., 1294
Lawson, D. I., 1299
Lee, F. W., 1290
Leitsch, J. G., 1293
Lejay, P., 1300
Levin, M. L., 1300
Levin, S. A., 1289
Levy, G. F., 1295
Lewis, F. D., 1182, 1294
Lewis, R. F., 1289
Lewis, W. D., 1241
Lindenblad, W. E., 1296
Linder, E. G., 1217, 1295
Lindsay, R. B., and H. Margenau, 1288

Loeb, E., 1298
Lommel, E. V., 1254
Lorentz, H. A., **218,** 1293
Love, A. E. H., **356,** 1065
Lowry, L. R., **458**
Lubcke, H. R., 1292
Luedi, F., 1298
Luke Chia-Liu Yuan, 1296

M

MacDonald, H. M., **356**
Mackeown, S. S., 1295
McKinley, D. W. R., 1301
McLachlan, N. W., **331,** 1265
MacLean, K. G., 1294
McPetrie, J. S., 1298, 1301
Maloff, N., 1299
Malter, L., 1295
Mankin, A. H., 1300
Mann, C. R., 1034
Mannebeck, C., **493**
Manning, L. A., 1296
Marchant, E. W., 1289
Margenau, H., and R. B. Lindsay, 1288
Maris, H. B., 1290
Marriott, R., 1289
Martin, J., 1289
Mason, M., and W. Weaver, **153,** 1288
Mathieu, E., **311**
Maxwell, J. C., **11, 13, 17, 28,** 31, **52, 68, 97, 103, 147–151, 196, 200–201, 204, 218, 259,** 1288
Mead, A. P., 1497
Meissner, A., 1290
Melloh, A. W., 1294
Micheletta, C., 1300
Mie, G., **493, 705,** 1288
Mieher, W. W., 1294
Mihul, C., 1299
Miles, J. W., 1295, 1296
Millazo, S., **787,** 795
Miller, J. M., 1289
Miller, W. E., 1036, 1095, 1182
Millikan, R. A., 1034
Millman, P. M., 1301
Mimno, H. R., 1288
Mingins, C. R., 1293
Mirrick, C. B., 1290
Mises, R., 1281
Mjasoedoff, N. A. M., 1291
Moegel, H., 1290
Montgomery, B. E., 1295
Morecroft, J. H., 1289
Morgan, H. K., 1293
Morris, R. M., 1292
Morrison, W. C., 1296
Morse, P. M., 1063
Moullin, E. B., 1299
Mouromtseff, I. E., 1289
Mueller, G. E., 1295, 1300
Mueller-Strobel, J., 1299
Mumford, W. W., 1254, 1292, 1294, 1297
Musykens, H., 1292

N

Nakai, T., 1293
Namba, S., 1292
Neumann, C., **295, 304, 309, 329–330, 332**
Neumann, M. S., 1145, 1182, 1280, 1295
Newell, H. L., 1296
Nielsen, N., **311**
Norton, K. A., **346,** 958, 1172, 1293, 1296

O

Oersted, H. C., 1252
Ohm, G. S., **4**
Ohmberg, A. C., 1172, 1296
Ollendorf, F., 1288
Ortusi, J., 1298
Oseen, C. W., **705, 709**

P

Page, H., 1300
Page, L., **705, 727,** 1288, 1297, 1299
Palmer, L. S., 1292
Patry, J., 1299, 1300
Pearcy, T., 1237
Pederson, P. O., 1290
Pekeris, C. L., 996, 1236–1237, 1240, 1296, 1299
Peterson, H. O., 1291, 1293, 1298
Pettit, J. M., 1295, 1296
Pfitzer, W., 1291, 1293
Planck, M., 1288
Plendl, H., 1291, 1298
Pickard, G. W., 1289, 1291, 1296
Pickering, W. H., 1295
Piddington, J. H., 1294
Pierce, G. W., 1288
Pierce, J. A., 1294
Pierce, J. R., **417**
Pistolkors, A. A., **235, 648, 727,** 1145, 1182, 1280, 1290, 1297, 1300
Poincaré, H., 1034
Poisson, S. D., **151, 299–300, 301,** 1272
Polic, P., 1299
Potter, R. K., 1291, 1292
Poynting, J. H., **19, 35, 37, 65, 71, 73, 115, 124, 127–128, 132, 136, 138, 201–204, 206–212, 249**
Pratt, H., 1293
Prescott, M. L., 1291
Price, W. L., 1300
Prichard, J. S., 1300
Pryce, M. H. L., 1237
Pupin, M. I., 1289

Q

Quaeck, E., 1290

R

Raggazini, J. R., 1289
Ramo, S., and J. R. Whinnery, 1288, 1295
Ramsay, R. R., 1292
Ratcliffe, J. J., 1300
Rayleigh, L., **332,** 1240, 1297
Reich, H. J., 1288
Reid, D. G., 1299
Retherford, R. C., 1289
Reymer, S. E., 1294
Riblet, H. J., 1296
Richards, P. I., 1296
Riedmyer, A., 1298
Ring, A. D., 1295
Robertson, S. D., 1295
Rolf, B., 1290
Rostas, E., 1297
Roth, O. H., 1298
Rothe, H., 1290
Roubine, E., 1300
Rountree, J. G., 1295
Rubenstein, P., 1063
Rust, N. M., 1299
Ruze, J., 1241, 1301
Rybner, J. C. F., 1290

S

Sarbacher, R. I., and W. A. Edson, 1288
Saxton, J. A., 1298, 1300
Schafer, J. P., 1291, 1292, 1293, 1294
Scheldorf, M. W., 1295, 1300
Schelkunoff, S. A., **76, 85, 356, 361, 609, 648, 705–706, 709, 718, 721, 728, 734, 745,** 1089, 1182, 1276, 1288, 1289, 1293, 1295, 1296, 1297
Schelleng, J. C., 1238, 1289, 1291, 1292, 1297, 1298
Schott, F., 1301
Schriever, O., 1297
Schwartz, L. S., 1300
Schwarzschild, K., 1063
Seely, S., 1182
Selvidge, H., 1059–1060, 1294
Shannon, C. E., 1301
Sharpless, W. M., 1292, 1296
Sherman, J. B., **747,** 1295
Shulman, C., 1183, 1294
Sichak, W., **787,** 795
Sicinski, L., 1301
Siegel, E., **704**
Silberstein, L., **220–221, 311**
Sinclair, G., **787,** 1296
Skellett, A. M., 1292
Skilling, H. H., 1288
Slater, J. C., **153,** 1182, 1204, 1288
Smith, H. G., 1294
Smith, H. W., 1301
Smith, N., 1294
Smith-Rose, R. L., 1298, 1300, 1301
Smyth, J. B., 996, 1237
Smythe, W. R., 1288
Snow, C., **327**
Sommerfeld, A., **311, 370, 493, 496, 497–498,** 958, 1063, 1247, 1279
Southworth, G. C., **594,** 1183, 1289, 1291, 1294, 1295, 1297, 1298
Spangenberg, K., 1301
Stansel, F. R., 1293
Starnecki, B., 1301
Sterba, E. J., **493,** 1291, 1292, 1297
Stetson, H. T., 1296
Stewart, C., 1295
Stodala, E. K., 1301
Stokes, A. P. D., **15, 25, 311, 332,** 1296
Stratton, J. A., **153, 221, 222, 235, 370, 389, 641, 705, 743,** 1146, 1182, 1288, 1291, 1292
Strutt, M. J. O., 1298
Stuart, D. M., 1292
Studenkov, E. M., 1299
Szepesi, Z., 1300

T

Tabard, R., 1299
Taylor, A. H., 1289, 1290, 1291
Taylor, D., 1292, 1299
Terman, F. E., 1183, 1295, 1296
Tetelbaum, S., 1299
Thoma, A., **557**
Trevor, B., 1289, 1293
Trolese, L. G., 996, 1237, 1301
Tuve, M. A., 1290
Tyrrell, W. A., 1296, 1300

U

Uda, S., 1290, 1291
Ueno, S., 1292

V

Van der Pol, B., **346,** 958, 1065, 1069
Vaughn, E. W., 1296
Voge, S., 1300
Voigt, W., 1034

W

Walkinshaw, W., 1299
Walters, G., 1301
Watson, G. N., 1065
Watson, W. H., 1300
Waynick, A. H., 1294, 1296
Weaver, M., **153,** 1288
Weber, W. E., 1288, 1289
Wells, E. M., 1300
Wells, H. W., 1292
Westcott, C. H., 1299
Weyl, 958
Wheeler, H. A., 1293, 1296
Whinnery, J. R., 1288, 1295
Whitmann, V. E., 1293
Whitmer, R., 1292
Whittaker, E. T., **311**

Wholey, W. B., 1301
Wickizer, G. S., 1293, 1294
Wilkes, G., 1297
Wilmotte, R. M., 1290
Wing, A. H., **442,** 1288
Wise, W. H., 1297
Wood, F. M., 1295
Woodruff, L. F., 1288
Woodyard, J. R., 1294
Wwedensky, B., 1065

Y

Young, C. J., 1289
Young, L. C., 1290, 1291
Yung-Ching Yeh, 1301

Z

Zahn, H., 1297
Zenneck, J., 958

SUBJECT INDEX

(References to pages in Volume I are in **boldface** type.)

A

Aberration, scanning, 1241
Abraham, M., linear radiator concepts, **552**
Abrupt phase jump, Brewster wave incidence, 854
Absolute directivity, definition of, **624**
Absolute gain, electromagnetic horn, 1184
Absolute value of obstacle dimensions in wavelength, affecting diffraction, 1096
Absorbing wave medium, inhomogeneous, 997
Absorption, by earth crust, **3, 9, 12, 16, 29, 30, 35, 38, 43, 45, 46, 52, 54**
  by metal plates, **6, 16, 45**
  by ocean, **47–50, 54**
  total, upon reflection, **49**
    upon refraction, **42, 45, 56–63**
Accelerated electrons, **3**
Accelerated field, energy of, **3**
Acoustical radiation reference standard, **623**
Actual current sheet, **350**
Actual and ideal earth crust effects, comparison of, 918
Actual and image antennas, currents, vector addition of, 848
  locations of, 830, 849, 864, 868, 877, 887, 918, 921, 930, 933, 944, 1003, 1006, 1009, 1015
Actual length and equivalent length, comparison of, **518**
Actual power directivity compared with equivalent directivity, **630**
Addition of vectors, **93, 115, 184, 197, 201, 207, 208**
Admittance, input, relation for single-stub matching, **433**
  line measurements, **438**
  open-ended and short-circuited stubs, **442**
  numerical, of load and its conjugate, **443**
  of load on double line, **442**
  per unit length, crosswise, of double line, **407**
Advance, phase, injected, **446**
Advancing and reflected waves, **115, 337, 357, 364, 410, 412, 413,** 417–**420, 422, 426, 456, 735,** 791, 793, 796, 797, 830, 831, 843, 845, 848–852, 855, 860, 868, 870, 877, 881, 884, 887, 895, 908
  computation of, **115**
Advancing wave front, **8, 17, 367,** 1020–1022, 1025, 1034, 1037–1039, 1045, 1046, 1048, 1054, 1089, 1092
  and current sheets, **367,** 1030, 1089
  magnitude and vector relations of, **354, 355**
  primary, and Fresnel zones, 1022
Advantage, current, half-wave dipole pick-up, 1008
  radiation, definition of, **623**
    half-wave radiator, **629–630**
    any integer half-wavelength distribution along linear radiator, **629**
Aerial, alignment, biconical, **76–86**
  conical, **73–76**
  electric dipole, **86–92, 144, 151–153, 158–187, 243**
  electric doublet, **8, 31, 86–92, 144, 151–153, 158–187, 243**
  half-wave dipole, **32, 91, 166**
  hollow cylinder, **766–772**
  image effects, 830
  linear, **9, 89–91, 153, 191**
    radiation of, **529**
  loop, **572**
  magnetic dipole, **144, 151–153, 158–187**
  model theory, **297–299**
  receiving, arbitrary linear polarization of, **787**
  rhombic (diamond), **458**
Air, density of, dry, 975
  dielectric constant of, **4–7**
  masses of different water-vapor content, 970–971, 973–977, 983, 987–997
    and temperature, 973–975, 989
  pressure and humidity effect, wave propagation, **6,** 987–997
  wave medium, Poynting vector, **41**
    propagation constant of, **59, 70**
    velocity of propagation of, **29, 59**
    wave impedance, **4, 8, 41, 70**
Airplane-to-airplane or airplane-to-ground-station condition, 870
$AJ_1(x) + BK_n(x)$, Bessel equation, n an integer (1, 2, 3, . . .), **330**
$AJ_n(x) - BJ_n(x)$ for n not an integer, **330**
  standard comparison Bessel equation, **330**
Algebraic division applied to wave impedance, **247**

Alignment, collinear antennas, **587**
eight linear parallel radiators, inphase and alternate antiphase, **581**
formula applied to several half-wave radiators, directivity and electric field formulas, **585–586**
four linear parallel radiators, **581**
n linear radiators, **579**
and phasing, half-wave radiators, front and reflector conditions, **602**
six linear parallel radiators, **581**
Alternate and antiphase exciter currents, antenna array, formulas, **605**
Alternate equal-phase and antiphase exciter currents, bilateral beaming along alignment, **581**
Alternate solutions, particular wave equation, application of, **497**
Altitude, effect of, on half-wave radiator, 939
gradients of refraction, **143**
AM and FM, phase and group velocity, **371**
AM wave and phase and group velocity, **369, 371**
Ambiguous sign, coefficient of, **335**
Amperian current whirl, **154**
Amplitude contour velocity, AM wave, **368**
Amplitude decay, formula for line, **371**
with real negative exponent, 806
divergent wave, **332**
wave-medium loss, **138**
wave propagation, **35, 43–46, 52–56, 129, 136, 138, 164**
due to wave spread, 871, 885–886
Amplitude decrease, inverse distance effect, diffraction, 1038
general, **86**
Amplitude directivity, circular wave-front radiator, 1141
in equatorial plane, two inphase equal-current radiators, **580**
half-wave radiator, **633**
linear radiator, odd and even current distributions, **623**
N circular aperture radiators, 1150
patterns, coaxial radiator, **774**
electromagnetic diffraction, 1083, 1097, 1103, 1104, 1107, 1119–1123, 1137, 1139, 1141–1148
and power directivity, table, half-wave radiator, **535**
Amplitude distribution, function, **306–310**
TE and TM waves, **306**
Amplitude and phase distortion, in lines, **371**
for wave propagation, conditions, 394
Amplitude reduction, field in metallic wave medium, **45, 477**
Angle, Brewster (*see* Brewster angle)
critical, applied, 964
of equivalent delay, relative phase condition for, 872
imaginary, interpreted, **61**
Angle, limiting, 933, 944
of polarization, 940
pseudo Brewster, formula, 828
of refraction, 804
solid, **641**
elementary, **626**
in terms of complementary value, application to refraction and reflection, 838
of wave incidence, effect on power transfer between two reflectors, 968
of reflection and refraction, at plane of medium separation, 793
Anomalous dispersion, **370**
Anomalous short-wave propagation, modified refractive index, 994–995
Anomalous wave propagation, **784,** 969
Antenna, antinode, **166**
beam, **56–63**
biconical, **76–86, 735, 737**
conical, **33, 73, 76, 735, 737**
cylindric cage, **772–774**
differential, **86–90, 144, 161, 163**
discone, **728**
feeding, **191**
gain and directivity, **620**
height factor, **348**
height and length (actual), **163, 166, 193**
and image currents, 830
actual and image antenna, vertical and horizontal polarization compared, 845–853
image effects, 830
due to wave obstruction, 929, 930, 933, 944
linear (*see* Linear antenna)
model theory, **297–299**
pattern, height-frequency product, 956
pickup center (receiving), altitudes for different frequencies for maximum and minimum field effects, curves for, 951
radiation resistance of, **72, 76, 159–161, 187–193, 194**
over reflector, 917
rhombic (diamond), **458**
transmitting locations, space field value, 932
vertical, 917, 1102
Antenna arrays, **573–609**
directivity, unequal spacing between radiators, **605–609**
effective, associated field values, in terms of power directivity, **622**
gain formulas numerically applied, **621**
power and field advantages in db, **621**
receiving resultant current, formulas, **445**
Antenna constants, lumped and distributed, **451–455**
Antinode, on line, **166**
Antinode currents, driven half-wave and parasitic half-wave radiators, **652**

Antiphase current excitation, of radiator, **10**
of two parallel half-wave radiators, radiation resistance, **667**
Antiphase field conditions, space fields, 946
Antiphase and inphase excitations, computations, linear radiators, **578**
field contributions of zonal areas, 1024
half-wave radiations, radiation resistance formulas, **672**
Antiphase parallel elementary radiators, electric field compared with field of one elementary radiator, **569**
Aperiodic feeder, J antenna, **702**
quarter-wave and half-wave sections, **699**
single and double line, radiation of, **456**
turnstile bay, **700**
Aperiodic single-line radiation, **466–468**
Aperture, circular, **18,** 1136, 1140, 1143–1148, 1151–1153
space geometry, 1137
in cylinder, 1036, 1095, 1182, 1284
diffraction effects, 1061, 1082
in diffraction screen, 1061, 1065, 1082, 1088, 1089, 1092, 1097, 1103, 1104, 1107, 1112, 1116, 1117, 1120–1124, 1126, 1128, 1137, 1140, 1143–1145, 1147, 1148
general, **17,** 1154, 1157
in guide, 1116, 1117
and equivalent current sheets, **350, 352, 353**
as location of electric and magnetic current sheets, **359**
narrow slit, diffraction, 1019, 1036, 1095, 1182, 1280, 1284
parabolic projector, beaming effect, 1031
electric and magnetic current element, moment, 1062
moment of current distribution, 1029
paraboloid, 1022, 1035
radiator, 1184
rectangular, double integral solution, 1111
rectangular and circular, 1020
in screen, 1061, 1082, 1280
primary radiation center, Huygens wavelet centers, 1088
in wave obstructions, **784**
wave penetration through, 1037
wave propagation, 1034
Aperture slot, **17, 18,** 1091, 1112, 1116, 1117, 1120, 1121, 1123
inclined, 1036
several, derivation of, 1112
Approximation $(1 + a)^m = 1 + ma$, applied to wave propagation, 874
Arbitrary elliptical polarization, numeric parameter l_n concept, 787–788
and reception of plane waves, **787**
vector $\bar{l}$ concept, **787–788**
Arbitrary linear polarization and receiving aerial, **787**
Arbitrary orientation, two linear radiators, **607**
Arbitrary polarization, **786**
of electromagnetic field, **787**
Arbitrary radiator shape, Schelkunoff theory, **705**
Arbitrary wave directions, **787**
Area, effective, aperture, **184**
nth Fresnel zone, 1026
Arguments, imaginary, integral logarithm, **643**
significant, for vanishing Bessel factors, **704**
Array, antenna (*see* Antenna arrays)
circular wave-front radiators, 1148
linear, end-on, **446**
radiators, half-wave, different beam width, vertical and horizontal planes, **604**
irregular arrangement and phasing, formula, **683**
radiation gain referred to single half-wave radiator, **620**
Asymptotic points, Cornu spiral, 1044
Asymptotic series, $h_q^1(x)$ function, **332**
Atmosphere, humid, 974
lower, refractive index of, 970
path of electromagnetic wave in, 983
standard, definition of, 994
warm and moist, concept of equivalent earth curvature, 1002
Atmospheric density, at different elevations, 976
Atmospheric guide action, **6,** 959, 994–997, 1236–1240
Atmospheric index of refraction (*see* Index of refraction)
Atmospheric refraction, general wave equation, **319**
Atmospheric wave ducts, **6, 319,** 959, 994–997, 1236–1240
Atmospheric wave trapping, **6,** 959, 994–997, 1236–1240
Atom, **152**
electric and magnetic dipole effects, **152**
electric and magnetic polarization, **152, 153**
external and internal forces, **152**
magnetization, **153**
polarization, **152, 153**
Atomic dipole moment, **153**
Atomic dipoles, **152**
Attenuation, coaxial line, **483**
concentric line, computed from field energy transfer, **481**
conducting wave medium, **45**
dissipative wave medium, **123–128**
near earth crust, 909
in field, penetrating earth crust, **30, 136, 138, 164**
penetrating good conductor, **16, 44–45, 48, 477**
geometrical, 886

Attenuation, per meter, of wave travel, **123–125, 136**
space field, **30, 138**
wave guide (*see* Wave guide, attenuation)
Attenuation constant, **364–365**
Attenuation factor, plane earth, 1076
Attenuation formulas, **30, 136, 138, 164**
guide, curves, 1229
for line, **371**
for wave guide TE and TM waves, 1206
Attenuation ratio, **365**
Auxiliary potentials, electric polarization and magnetic polarization potentials, **219, 222, 313,** 1238–1240, 1275–1276
Hertz and Fitzgerald vectors, **219, 222, 313,** 1238–1240, 1275–1276
Average charge density, **240**
Average cosine value applied, **36, 37, 133, 250**
Average divergence, **39, 109, 197, 202**
Average field power density, **210**
Average flow, **64**
per unit area, **65**
Average power, **36, 65, 75, 117, 210, 211, 213, 214**
directivity, linear radiator, **626**
independent of radius of expanding spherical wave front, for pure dielectric, **250**
Average Poynting vector, **629**
expression applied to double-line solution, **474**
Average surface power density, radiation field, **629**
Average time, **118, 189**
Average value, of $\cos^2$ time function, **75, 113, 536**
of difference of electric and magnetic volume energy field content, **120**
of directivity, graphical method, **632**
of power directivity, half-wave radiator, **630**
of square of directivity, unobstructed space, applied, **509**
of time functions, **189**
Avogadro constant, 973
Avogadro law, 974
Axial cylinder slot radiator, 1036, 1095, 1182, 1284–1285
patterns, 1284–1285
Axial electric field, circular radiator, different circle length, **755**
value, circular wire radiator, **754**
Axial field vectors, **93, 95, 163**
Axial slot apertures, 1036, 1095, 1182, 1284
Axial slots in vertical metal cylinder, radiation pattern of, 1036
Axis of magnetization, **154**

B

B, definition and analysis of, **196**
B vector, at interface boundary, **65**
$b_q(x)$ function, **333**
Babinet principle, of optics, applied to electromagnetic waves, 1036, 1173, 1279
slot and wire radiator, applied, comparison, 1173
Backup and front alignment, half-wave radiators, **602**
Backup reflector, 912
metal, and linear radiator, 864
Backward and forward radiation, **638–639,** 1062
Backward-traveling wave, **76, 333, 337, 735,** 887, 895
Balanced output, concentric, **527**
by means of a third quarter-wavelength line, **528**
Balanced parallel line converted to unbalanced coaxial line, **526**
Balanced shielded Lecher line, formulas for, **403**
Balanced shielded parallel-wire feeder, characteristic impedance of, **403**
Bar-to-dyne and barye conversion, 989
Barye unit, 989
Bay, turnstile (*see* Turnstile bay)
Bazooka, coaxial sleeve, **526**
Beacon beam, **61**
Beads, standoff effect on characteristic impedance of feeder, **405**
Beam, electromagnetic, horizontal and vertical polarization compared, 796–826
ray, refracted, **143**
equivalent radio, 948
incident, reflected and refracted, boundary conditions, 791
formulas, 960
modifications, 998
radio (*see* Radio beam)
refracted, relations, dissipative wave medium, 822
traces of, **57, 59, 62**
Beam curvature, formula, 982
Beam width, collinear half-wave radiators, due to spacing in wavelength, **604**
plane wave front, with wavelets, 1033
vertical and horizontal planes, **604**
Beaming, broadside and bilateral, **581**
formula, **584**
broadside and end-firing, **637, 639**
diffraction, 1172
discussion of radiator systems, **627–641**
effect, circular wave-front radiator, 1147
parabolic projector, different openings, 1031
end-firing, formulas, **584**
field, for lines with partial radiation suppression, **564**
forward, slot separation effect, 1121
thrust factor, **603**
main, emphasized, side-lobe beaming deemphasized, 1033

Beaming, main, and forward factor, 1034
parabolic projector, 1029
unilateral, **638**
and end-firing, formula, **584**
suitable phasing, **596**
Bearing error, radiation beam, **60**
radio navigation, **56–63**
Bechmann, R., linear antenna, solutions, **641**
theory, **648**
Bechmann coefficient, line radiators, **657**
Beck, E. A. C., rhombic Bruce antenna, **458**
Bending, of rays, **6**, 973, 974, 983
degree of, 973
downward, 974
equation of curvature, 983
upward, 974
of wave guide, 1221
Bernoulli solution of wave equation with elementary functions, **321**
Bessel coefficient t^n of argument x and order n, 1265–1267
Bessel curve, derivative, **309**
applied to cylindric guide, 1213
Bessel differential equation, general form, **339**
Bessel equation, **304, 330, 331, 334, 338**
general integral, **339**
modified, **330, 338**, 1267
solution form, $y = \sqrt{x}\, Z_n(\beta x)$, **338**
solution of wave equation, separation constants, **324–335**
standard form, **325**
comparison form, **330**
with solution $y = \sqrt{x}\, Z_n(\beta x)$, **338**
two independent solutions, **322**
Bessel factors, vanishing, significant arguments, **704**
Bessel function, **309, 310, 339**, 1265–1267
applied, **497**
circular wave-front radiator, 1137
circular wire radiator, **756–759**
coaxial radiators, **773–774**
cylindric cage aerial, **772–774**
cylindric metal surface radiator, **767–772**
disk radiator, **760–765**
argument and order, **325, 330**
cylindric coordinates, argument of, **325**
differentiation, **307, 309, 310**, 1212, 1232
expansion, **331, 339**
first kind modified, 1267
fractional order, **295, 322, 323, 332, 756**
half-integral order, **339**
$I_n(x)$ type, 967, 1267
$J_n(x)$ type, **304, 309, 749, 750, 756, 757, 758, 759, 760, 761**, 762, **767, 769, 770, 771, 772, 773, 774**, 1254–1255, 1265–1267
no integer parameter, $q + \frac{1}{2}$, **295, 322, 323**
Bessel function, mth root for guide, **307**
roots, wave guide, **310**
(satisfying) boundary conditions, cylindrical wave guide, **309, 379**
third kind, Hankel functions, **322, 339, 497**
useful formulas, 1254–1255, 1265–1267
Bessel and Neumann circular guide, 1231
Bessel and Neumann functions, compared, **295, 304**
curves, **301, 704**
first order, **330**
general, **304**
order $q + \frac{1}{2}$, **295, 322**
wave-guide solutions, **304**
Bessel roots, **304, 310, 378, 704**
derivatives, **310**
significant, **704, 769**
TM wave-guide modes, **379**
Bessel solution, exponential factor $\epsilon^{jp\cos\delta}$, **749**
Bessel values, $J_0(k)$ function, **704**
Between-field region, **168**
Beverage wave antenna, directivity, **457–461**
Bicones, electric and magnetic fields, transverse voltages and longitudinal currents, TEM wave, principal wave, **735**
Biconical antenna, complementary and principal voltage and current distributions, **738**
Biconical dipole, entrance impedance, curves, related functions, **741**
double line, **76**
Biconical line, complementary waves, **736–738**
first-order TM wave, **737**
regions I and II, extremes of bicones on I and II boundary, **736**
TEM waves, voltages and currents, **736–738**
theory (Schelkunoff), **734–742**
relations, **735**
transmission, characteristic impedance, **84**
voltages and currents, principal and complementary wave contributions, **738**
Bilateral beaming, along alignment, alternate inphase and antiphase exciter currents, **581**
normal to alignment, equal inphase exciter currents, **581**
Binomial expansion, applied, general wave medium, **395**
Binomial theorem, applied, expansion of wave impedance, **246**
Biot-Savart law, **164, 217**
Bisectoral horn, 1184
Blurred image effect, 822, 850
Boltzmann constant, applied, 974
Boltzmann value, experimental, 970
Bontsch-Bruenwitsch, M. A., concentric open-line section radiation, **557**

Booker, H. G., Babinet principle applied, 1036, 1173, 1279
Booker wave ducts, 1036, 1237
Bound electron and charge, **152**
Bound field, next to radiator, **3**
Boundary conditions, **78, 307, 309, 319, 350–353, 379,** 790, 802, 1022, 1067, 1232
applied, 802
incident, reflected, refracted waves, 791
between radiation space and wave obstacle, 790
cavity resonator, 1232
circular guide, **307, 309, 379,** 1232
cylindric guide, from J_0 Bessel intersections, details, **378, 379**
$\mathcal{E}$ vector, certain wave propagation, **319**
electric and magnetic current sheets, **351–355**
electric and magnetic fields, diffraction, 1022
electromagnetic waves, wave equation, 1067
general, **65–66**
guide, **307, 309,** 1205, 1213, 1214, 1232
interface of two mediums, **351**
magnetic flux density and magnetic field intensity, **65**
rectangular guide, **308**
spherical S surface of bicones, satisfied by complementary waves, **78**
surface of medium separation, 896
TE waves, **307–309**
TM waves, **307–309**
wave guide, **308–309,** 1205, 1213–1214, 1232
Boundary requirement, 802
Bounded and guided wave transmission, **364**
Brewster angle, 931, 946
applied, 939, 951, 953
and dip, actual earth crust, 860
formula, 829, 857
magnitude, perfect dielectric medium, 821
pseudo, wave incidence, significance of, 853–860
total refraction, vertically polarized wave, 814–815
wave incidence, feature of vertical polarization, 815
numerical application, 861–863
values, 829–839
Brewster dip, 849, 851, 852, 942
on Cornu spiral, earth crust diffraction, 1073
minimum reflection coefficient, vertical polarization, time phase and magnitude of reflection coefficient, 871
ocean surface, 852
values, 849, 851, 852, 855, 858, 860
Brewster reflection minimum (or dip) at 90 time deg, 854
Brewster wave incidence, dielectric medium, for separating vertical from horizontal polarization, 815, 817
Brillouin, L., radiation resistance, **648**
explaining confusing distance function, linear aerial, **707**
Brillouin, M., wave propagation, **370**
Broadness, vertical pattern, linear antenna array, factor determining, **603**
Broadside beaming, **581, 584, 637**
and end-fire beaming, **639**
unilateral conditions, **599**
width of beam, **639**
Broadside bilateral beaming, formula, **584**
Broadside energy concentration, **679**
Brown, G. H., linear antenna radiation, **648**
Bruce, E., rhombic (diamond) antenna, **458**
Burgess, R. E., aerial characteristics and polarization, **787**
Burrows, C. R., wave duct, 1237
Burrows-Gray diffraction, 1066
curves and formulas, **347,** 1074
Burrows-Gray field formulas, **347,** 1074

C

C and S functions, Fresnel diffraction, 1156
$c'c'' = c^2$, relation, in ionosphere, **368**
$c'c'' = v^2$, relation for $H_{m,n}$ and other modes, **382**
Cage aerial, **722–774**
Bessel functions applied to formulas, **772–774**
relative amplitude directivity patterns, **772**
Cage (parabolic) reflector, applied to electromagnetic diffraction, 1028
Capacitance and inductance, formulas, lines based on Maxwell's field relations, **402**
parallel-wire line and coaxial line compared, **484**
Carson, J. R., extension of original Sommerfeld solution, **497**
Carson line solution, general wave equation, **493**
Carter, P. S., linear antenna radiation, **648**
Cartesian coordinates, **18, 27, 105, 109, 145**
Cartesian gradient, **22**
Catacaustics and diacaustics, **319**
Cavity resonator, 1185, 1233–1236
boundary conditions, 1234
cutoff wavelength formula, 1233
cylindric, 1233
formulas, 1233–1236
frequency, 1234
rectangular, 1233
Cell surface, bounded, by finite current circulation, **156**
by finite magnetic field circulation, **139**
Center-fed dipole, actual and equivalent network, **680**
Center of radiation, **608**
and reception of antennas, **20**
Central Fresnel zone, field energy, 1024
Cgs and Gaussian units, **7,** 1243, 1252

Changed self-radiation resistance and self-reactance, linear radiator, due to another radiator, **653–656**
Characteristic impedance, average value, formula, **743**
biconical double line, **77, 78, 79, 84, 735**
C and L, bicones, **78**
coaxial and Lecher line, compared, **484**
coaxial line and shielded Lecher wires with spacers, **405**
conductive wave medium, **43, 45**
dielectric wave medium, **41**
dipoles, various shapes, **743**
double cone, Schelkunoff line, **77**
double-cone radiator compared with parallel ribbon line, **79**
double line, different for principal TEM and complementary waves, **97**
propagation constant, **69**
double ribbon line, **79**
electromagnetic waves, **4, 8, 31, 36, 40–45, 50, 53, 55, 64, 126, 136**
expansion, **246–249**
formulas, **4, 36, 40–45, 50, 53, 55, 70, 73, 78, 79, 84, 158, 160, 163, 164, 213, 241, 245–248, 281, 291, 317, 375, 402, 403, 405, 407, 408, 414, 425, 482, 484,** 1197, 1199
general wave medium, **17, 36, 40, 42, 45, 46**
and generalized electrical length Ω of double line, formulas, **410**
good feeder, **452**
ground (earth crust), **17, 36, 40, 45**
line, assumptions often used, **408**
guided TEM wave, **67–73**
open-ended and short-circuited measurements, **410**
phase angle, **407**
resistive and reactive components, **407**
nominal, cylindric dipole, **747**
ocean medium, **41, 43**
quarter-wave section inserted, **436**
space waves, **4, 7, 17, 36, 41, 42, 43**
three-dimensional field, **40–45, 50, 53–55**
and wave impedance, compared, **40–41**
Characteristic velocity, **4, 8, 29, 45, 51, 54**
Characteristic wave impedance, general (dissipative) wave medium, **70, 127**
in terms of Q, R, and X, **52–56**
medium, three-dimensional space, **316**
resistive and reactive components, **53, 54, 55**
wave guide, 1199
Characteristic wavelength, **10, 19, 49, 51, 54**
Characteristics of propagation, **362–401**
Charge, bound, **152**
closed shell, negative elementary, **152**
constraint, **152**
density, average value of, 240
electric moment of, **157**
moment, and electric current moment relation, **86, 516**
Charge, moment, Hertz doublet radiator, **86**
per unit area, **157**
momentum per unit volume, **23**
random motion, **240**
Charge distribution, **240**
arbitrary, in volume elements with respect to polarization, **240–241**
of radiator, often assumed, **361**
Charge effects retarded at VHF's and UHF's, **780**
Chireix-Mesny antenna, 1290
Chu, L. J., spheroidal dipole (prolate spherical radiator), **743**
Ci, $\overline{\text{Ci}}$, and Si formulas, **712, 722**
Ci functions, applied to radiation, **466–469**
asymptotic formulas and applications, **468–469**
available, **468–469**
remarks on waves and tables, **468–469**
Ci and $\log_e$ functions, applied, **563, 566–567**
Ci and $\log_{10}$ functions, **512, 514**
for linear standing-wave radiator, **506**
Ci and Si curves, **665**
Ci and Si formulas and expansions, **665**
Ci and Si functions, applied to linear radiator, **643–648**
maximum and minimum (zero) extreme values, 1265
Ci, Si, and Ei functions, formulas, **643**
Ci, Si, and log functions, integral solutions, linear radiator, **641–648**
Circuit, closed (*see* Closed circuit)
Circular aerials, radiation, **747–759**
Circular antenna radiator, directivity, plane of circle, **749**
Circular aperture radiator, 1136–1153
Circular cross section, guide wavelength, **305**
Circular disk, and vertical feeder, both radiating, **762–765**
and vertical linear radiator combination, directivity pattern, **765**
Circular disk radiator, **759–765**
Circular gate radiator, spherical wave front, 1179
Circular guide, **95, 305–310, 376–379,** 1190–1193, 1212–1215, 1220, 1221, 1227–1232
Bessel and Neumann functions solution, 1231
cross section, **305**
cutoff characteristics, 1193
distribution function, 1212
distributions, 1190–1192, 1221
excitation, 1220
TM modes, **382–383,** 1191–1193, 1199, 1212, 1213, 1215, 1217
Circular and linear half-wave radiator, comparison with factor 60 of linear radiator, **754**
Circular loop, radiation resistance, **784**
Circular plane wave-front radiator, alignment, directivity curves, 1152

Circular polarization, **549–550, 785–788**
explained by Lissajous figures, **549–550**
of incident wave and pickup system, 795
Circular radiator, axial field value, **754**
Bessel, Gamma, and Gauss functions applied, **756–759**
current distributions, **753**
different lengths, axial electric field value, **755**
directivity patterns, Cartesian coordinates, **751**
electric field intensity formula, **749**
maximum radiation effect, **756**
numerical application, **755–759**
polar directivity, plane of radiator, **752**
radiation condition, **748**
two driven by common terminal voltage, **753**
two radiators, three-wavelength distribution, resultant effect, **753**
Circular and rectangular gate radiator, 1173
Circular and rectangular guide, 1221
Circular slot radiator, diffraction, 1182, 1280
impressed voltage, 1182, 1280
Circular wave-front radiator, amplitude directivity, 1141
alignment, computations tabulated, 1151
classic derivation, 1136
curtain, 1148
Fraunhofer diffraction, 1137
inherent advantage, 1172
Circular wave guide (*see* Circular guide)
Circular wire radiator (*see* Radiator, circular wire)
Circulation, **103–107**
and curl actions, **104–108**
current, **156**
electric field, **14, 23, 101–107**
magnetic and electric field, **101–103**
guide, 1192
magnetic field, **139**
magnetic vectors, **14, 23, 101–107, 139**
of vector, enclosing a vanishing area in the limit, **26**
Classical line equations, compared with Maxwell's field concept equations of lines, **97**
Clausius-Mossoti relation, 971, 972
applied to troposphere, 970
Clockwise and counterclockwise space screw wave propagation, **786**
Clockwise curl, **23**
Closed circuit, frequency effect and delayed mutual actions, **777**
radiation effects, **774**
self- and mutual radiation resistance and reactance, **776**
single and coupled, treated with field concepts, **776**
solved with field concepts, **774, 780–784**
Closed current loop, differential and vector relations, **778**
Closed current loop, at low and higher frequencies, **778**
radiation conditions, **776**
relation for radiation effect, **779**
retarded and simultaneous actions along closed path, **778**
Closed-line integral applied to closed circuit with radiation, **777**
Closed- and open-line integral and radiation, **779**
Closed- and open-stub matching, **433**
Closed shell, negative elementary charges, **152**
Closed-stub matching, formulas, **430, 431**
Coaxial bicones, Schelkunoff, **735**
Coaxial line, attenuation computed from field energy transfer, **481**
concentric line, attenuation, **483**
and eccentric coaxial line, characteristic impedance, **403**
guide action, **95,** 1186
inner and outer conductors, watt loss, **482**
and Laplace equation, **475**
and Lecher line, C and L values compared, **484**
optimum Q dimensions, **487**
and optimum ratio, $D/d = 3.6$, total power transfer, **481, 483**
to a parallel-wire conversion, **526**
and parallel-wire line, radiation effects, **491**
principal TEM wave, **406**
Q value, frequency and inner-diameter effect, **487**
sleeve (bazooka), **526**
smallest Q value, **487**
total energy transfer, **481**
watts/meter power loss, **482**
wave conditions, 1230
Coaxial radiators, conditions, **773–774**
directivity and numerical application, **773–774**
numerical example of pattern, **773**
Code transmission, group and phase velocity, **369**
Coefficient of reflection (*see* Reflection coefficient)
Coefficient of refraction (*see* Refraction coefficient)
Coil and linear radiator for causing helical wave propagation, **786**
Collinear antennas, group characteristics and alignment formula, **586–589**
n equal, group characteristic formulas, **587**
Collinear and parallel alignment, curtains of half-wavelength radiators, formulas and numerical applications, **671–684**
Collinear radiators, **9, 661, 676, 677, 681, 682**
equal and natural phasing, formulas, **677**
formulas and numerical applications, **671–684**

Collinear radiators, half-wave dipoles, numerical applications, **588**
horizontal and vertical, **604**
radiation resistance, **681**
Common field factor, **334, 335**
Comparison formulas, electric and magnetic fields, elementary electric and magnetic dipoles, **163**
Complementary and principal waves, **97, 492**
voltage contribution, biconical antenna, **738**
Complementary screens, Babinet principle applied, 1036
Complementary slot and wire radiators, 1172, 1173
Complementary wave action, due to conductor and corresponding field changes, **95**
Complementary wave-front radiator, 1172, 1173
Complementary waves, **74, 76, 94, 97, 494–498**
account for radiation from lines, **97, 492**
biconical line, **736–738**
current and charges, double line, to physical terminals, **492**
not quasi-plane but rapidly attenuated, **492**
satisfy boundary conditions along spherical S surface, biconical antenna, **78**
TE and TM, **92–97**
Complete line equations, principal and complementary wave effects, **97**
Complex characteristic functions, **319**
Complex characteristic impedance, **70, 123**
for metal, **43, 48**
Complex conjugate fields, **618**
Complex current and field ratio, related to propagation constant, **364**
Complex dielectric constant, **5, 17, 36, 40, 43, 48, 70, 126, 132,** 801
Complex field, C vector, **218–221**
Complex field energy, **118**
in definite volume, dissipative medium, **121**
Complex field power, dipole, **655**
Complex Fresnel integral, 1064
Complex impedance and admittance, double line, **407**
Complex index, of reflection, 843
of refraction, **56, 63,** 838
general wave medium, **56**
Complex medium of wave, **3, 56–63**
Complex mirror, **10**
Complex power flow, **118, 121, 124, 125, 210–214**
Complex Poynting vector, **122, 127, 196, 209–214**
numerical examples, **128–133**
real part applied to linear radiator, **505**
Complex propagation constant, **50, 53, 70, 126, 363**
Complex quantity, analyzed, **480**
applied to electromagnetic field, **480**
Complex relative dielectric constant, **5, 46**
Complex scalar potential, **315**
Complex total current, **29**
Complex vector C relations, **315**
Complex vector potential, **315**
Complex watts, **210**
Complex wave function, 1064
Complex wave medium, **3, 4, 12, 45, 117–138,** 840, 845–853
current flow, **28, 29, 140**
Complex wave power flow, **121**
Component curl relations, **27, 86**
Component gradient, **20, 21, 22**
Components, of cross (vector) product, **197**
of Hertz vector in true radiation region, **268**
of propagation constant, **320**
of vector potential, true radiation region, **87**
Concentration or negative divergence of vector, **23**
Concentric cage aerials, **772–774**
Concentric feeder, principal TEM wave, **406**
Concentric line, attenuation formula, **414**
characteristic impedance, **403, 405**
coaxial line, **94**
formulas, **403**
inner and outer conductor, optimum ratio $D/d = 3.6$ and total power transfer, **481**
Q value, frequency and inner diameter effect, **487**
total energy transfer, **481**
watts/meter power loss, **482**
wave-guide action, **95, 494, 737–738,** 967, 1230–1232
Condenser, current and fields, **101**
Conductance, numerical, of line and stub connections, **436**
positive and negative, line measurements, **438**
susceptance, voltage and current distributions, double line, **438**
Conducting medium, wave penetration, **477–480**
wave propagation, **477–480**
Conduction current, **11, 16, 28, 98, 396**
and displacement current, **6, 16**
extreme wave medium cases, **396**
relative magnitudes, **392–401**
and surface currents in guides, 1193, 1207
electric, **11, 12, 16, 28, 29, 43, 48, 49, 50**
magnetic, **11**
wave guide, 1186–1199
Conductivity, **3, 5**
earth crust, **5, 10, 12, 29, 33, 47, 55, 57**
ocean, **5, 6, 48, 54**
Conductor, good, **6**
infinitely long, **456**

Conductor, internal impedance, **11, 96, 712, 713,** 1196–1199
linear, resonance and antiresonance conditions, **456**
standing waves, directivity, **463**
traveling waves, **463**
phase and attenuation constants, same numeric values, **477–478**
standing wave, distributions, n = 1,2,3, electric field, **463**
outgoing, electric field value, **463**
surface resistance, 1198
wave propagation, **16, 42, 43, 45, 48**
Cone, antenna, radiated power, **75**
current, **78**
biconical line, **78, 83**
line, **73–76**
Schelkunoff double line, **78**
Confirmation of electric images, ray theory, 803
Confocal ellipse, **551, 552**
Abraham radiator, **552**
Confocal hyperbolas, **551**
Abraham linear radiator, **552**
Confocal (orthogonal) ellipses and hyperbolas, **551, 556**
Conical antenna, radiation and Poynting vector, **73–76**
Conical dipole, fine, (half-wave); G and F functions and curves, **740–741**
Schelkunoff, **735**
theory, second Hankel function applied, **739**
Conical horn, 1184
Conjugate electric and magnetic fields, applied to formulas, **618**
Conjugate field vector applied to radiator problems, **505, 507**
Conjugate products, exponentials applied, **510**
Conjugate vectors, **117, 118, 124, 209–214**
advantage of, **210**
sum of two, rule, **211**
Conservation, of charge, **230**
of current, **230**
of electric energy, relation for solving equations, **230, 233**
applied for computing radiated power without Poynting vector, **195**
of electricity, **230**
Constant amplitude plane, wavefront, 791, 793
Constant phase plane, wavefront, 791, 793
Constants C and L, coaxial and parallel-wire line, compared, **484**
electromagnetic, **2–5**
Constraint charge, **152**
Constraint electron, **152**
Continuity, condition, wave guide, **357**
energy for Poynting vector and corresponding wavefront surface product, 885
equation, **230**
Continuity, interface of two different wave mediums, **65**
normal magnetic flux density, **65**
tangential electric field, **65**
Contour, of integration, **343**
surface, **21**
of wave interference with group velocity, **387**
Contribution of induction, due to dielectric substance, electric polarization, **196**
due to magnetic substance, magnetization, **196**
Convection, electric current, **4, 23, 152, 223,** 978
magnetizing current, due to circulating electronic charge, **152**
Converter, impedance, quarter-wavelength section, **698**
unbalanced to balanced feeder supply, **525**
Coordinate systems, **18, 20, 27, 144–151, 215**
Cartesian, **18, 20, 145, 146, 215**
curvilinear, **18, 20, 145, 146, 215**
cylindrical, **18, 20, 145, 146, 215**
reference orthogonal, **145, 146, 215**
spherical, **18, 20, 145, 146, 215**
Copper, annealed, conductivity, **5**
Copper plane reflector, penetrating power, normal wave incidence, 899
Copper plate, internal field, **16, 43–45, 477–479,** 898–899, 1196–1199, 1203–1214
penetrating power to incident power ratio, 899
power dissipation, 1196, 1203–1214
Copper wave medium, **45, 477–479,** 898–899, 1196–1199, 1203–1214
field amplitude decay, **477**
Corkscrew wave propagation, caused by coil and linear radiators, **786**
Cornu spiral, 1041, 1043, 1047, 1048, 1054, 1055, 1056, 1057, 1073
applied, to Fresnel diffraction, rectangular wave-front radiator, 1162
to Fresnel patterns, 1160
to wave front, 1045, 1047
and electromagnetic diffraction, 1065
expressing Fresnel integrals, 1041
outstanding factor, 1044
radius of curvature, 1044
solution, 1042, 1043
for finding effect of primary wave front, 1054
for nonobstructed wave region, 1047–1048
for obstructed wave region, 1048
Cosine expression, applied to mutual radiation resistance, **190**
Cosine function, series expansion applied to radiation resistance, **519**
imaginary, explanation, 805, 818, 819, 820
Cosine integral, applied to linear radiator, **506**
function applied to radiation formula, **465**

Cosine series expansion, applied to mutual radiation resistance, **190**
squared time function, **536**
Cosine and sine expansions, applied to radiation formulas, **782**
integral functions, used for radiation resistance formulas, linear radiator, **537**
Cos $\theta = x$ substitution, applied, **341**
Coulomb's law, **215**
Counterclockwise and clockwise space screw wave propagation, **786**
Counterclockwise curl, **23**
Coupled linear radiators, self- and mutual parameters, **656–662**
staggered half-wave, conditions, formulas, **678–679**
Coupling loop, **19,** 1219
Critical angle applied, 964
Critical wave incidence, 805
Cross product, **22, 154, 197,** 1268–1269
and curl nomenclature, **11, 26, 197,** 1270, 1272–1275
identified with curls of magnetic and electric vectors, **119, 121, 197–202,** 1273–1275
a new vector, 1269
in Poynting vector, **37**
in vector analysis, **197**
rule, **197,** 1268–1269
vectors, **11, 198,** 1268–1269, 1273–1275
Cross section, effective, electromagnetic field energy tubes, surface of medium separation, 793
shape of guide, 1217
Cross surface wave, near earth crust, 906
propagations, 907
Crystal detector, with current meter as probe, **421**
Cups and sleeves, quarter wavelength, **694–705**
Curl, **11, 14, 20, 22, 101, 104, 148, 200,** 1268–1275
action, **104–108**
clockwise, **23**
components, **27, 147–151, 199–200,** 1269–1270
applications, **28–35, 150–151**
Cartesian, **148, 199, 200,** 1269–1270
curvilinear orthogonal, **147**
cylindric, **148, 150**
electric and magnetic field vectors, **147–151, 198–200,** 1269–1270
equation simplified, **150,** 901
spherical, **149, 150**
concept of, **22, 24, 101, 104, 314**
definition of, **11, 14, 26, 101, 104, 198,** 1272
derivation of, **104–107**
electric and magnetic fields interlinked, **101–103,** 1218
field vector, **15**
formula, **198**
Curl, meaning of, **22, 101, 104**
nabla operator, **198,** 1271–1272
negative, counterclockwise, **23**
nomenclature, cross product, vector analysis, **151, 198,** 1268–1269, 1271–1275
relations applied to propagation, **374**
resultant, determinant solution, **197,** 1270
rotor or rot identity, **198**
of vector, **22, 198,** 1270, 1272, 1274–1275
physical meaning of, **22**
relation, expressed in vector analysis notation, **617**
vortex motion, rotation, **23**
Curling effects between condenser plates, **97–103**
Current, actual, and reflector effect, parabolic cylinder reflector, 1029
advantage, half-wave pickup antenna, curves, 1008
antenna, received, actual and image for vertical and horizontal polarization, 845–853
and charge, distribution on radiator, **361**
effects, retarded at VHF's and UHF's, **780**
circular and rectangular guides, 1186, 1191, 1194, 1207
circulation of, **156**
elementary, magnetic moments, **157**
collected, receiving antenna array, **556–558**
component, along surface of conductor, **1, 99, 213,** 1185, 1193, 1197
conduction of, **11, 12, 29,** 1185, 1193, 1197
conservation of, **230**
density of, **11, 12, 28, 29**
conduction and displacement, dissipative wave medium, **11, 34**
in definite direction, computed from appropriate curl component of magnetic field vector, **30**
electric, **11–13, 16, 65, 199, 356**
magnetic, **356**
of magnetic and electric current sheets, **356**
resultant, in space element, **300**
total, **28, 29**
vector components, **229**
vector potential relation, **225**
of volume element, **612**
displacement of (*see* Displacement current)
magnetic (*see* Magnetic current)
received over reflectors, formulas, 913
small, circulations summed up, **156**
total, **14, 29**
for variable magnetic field circulation, **26**
voltage, conductance and susceptance distributions, along double line, **438**
and impedance, driven and parasitic half-wave radiators, **652**

Current, and voltage locations, line measurements, reflections, theory, **439**
Current distribution, **91, 166**
on feeder and relative phase, **700**
and half-wave spaced radiation effects, **703**
along Lecher feeder and linear antenna, **74, 89, 116, 191, 698, 699, 702**
linear radiator, higher harmonic, **538**
moment of, 1029
radiator (circular), **753**
short electrical length and equivalent length by means of equal areas, **518**
sinusoidal, general case, linear antenna, **642**
Current effects, along thin linear radiator, **642**
electric (*see* Electric current)
electromagnetic field, **12**
element, path difference, between reference distance and element, **612**
go and return, Lecher wires, found from current function, **489**
Current flow, on conductor next to field, **348**
rectangular guide walls, 1194
wave guide, 1186, 1191, 1194, 1207
Current function, **90, 306–310**
Hertz solution, **270**
and potential, applied to Lecher line, **488**
time derivative of Hertz vector, relation, **282**
Current loops, **160,** 1219
circular, radiation resistance, **784**
closed, differential and vector relations, **778**
low and higher frequencies, 778
relation for radiation effect, **779**
plane of any type, radiation resistance, **784**
treated with field equations (Maxwell), **780–784**
two, radiation conditions, **776**
Current meshes, **155–156**
Current minimum on line, **440**
Current moment, differential radiator, linear, **86**
Current node, linear antenna, **529**
Current penetration, dissipative wave medium, **31, 41, 45, 48**
metal, **6, 43, 45, 48, 477,** 1198
Current probe, for line, **421**
Current radiator, linear differential, **31, 86, 89, 144, 161, 163, 165, 168–187**
Current ratio, and reflection coefficient, relations, **423**
Current relations, in source-to-antenna systems, **451–455**
Current sheets, **143, 348, 353, 356,** 1089, 1093, 1127, 1184
actual, **350**
in advancing wave front, **367**
aperture radiator, 1184
Current sheets, concept, applied to wave-front radiator, **353**
current surfaces, and surface integrals, **356**
electric and corresponding field, **353**
electric and magnetic, boundary conditions, **350–355**
fields, **348–355**
equivalent, **350, 352**
flow density relations, applied, **349**
magnetic and corresponding field, **353**
open wave-guide aperture, 1126–1131
substitution in primary wave front, 1092
total field contribution, applied to parabolic reflector, 1030
Current skin, thickness, guide wall, 1198
outside at opening of guide, 1195
Curtain array, circular wave-front radiators, 1148
of dipoles, **589–592**
horizontal and vertical half-wave radiators, **590**
half-wave inphase dipoles, gap terminations, **687**
half-wave linear radiators, computation of various radiation resistances, **682**
half-wave radiators, numerical data, **599–605**
parallel collinear alignment, formulas and numerical applications, **671–684**
vertical and horizontal beam width, **604**
wave-front radiators, rectangular apertures, 1117
Curvature, of earth, approximate formulas, 886
effect of, is unity, perpendicular wave incidence, 886
equivalent earth, concept, 1002
equivalent value, 997
speculations, 871–872
electromagnetic ray, 997
modification of, 987
upward, 998
radius of, Cornu spiral, 1044
Curved earth crust and line of sight, explanation, 871
Curved electromagnetic path, proving wave propagation possible beyond optical limit, 987
Curved path propagation in troposphere, 970
Curved radio beams, concept of equivalent earth radius, 986
Curves, mutual linear radiator impedance, resistance, and reactance, **691**
stub length and location, matching, **432**
Curvilinear coordinates, **18, 145–147, 151,** 1272
application to Hamiltonian nabla operator, 1271–1272
Curvilinear orthogonal coordinates, **18, 144, 145, 147, 151,** 1272

Curvilinear orthogonal coordinates, system applied to radiators and Maxwell's equations, **144–151,** 1272
Cutoff characteristics, circular wave guide, 1193
Cutoff frequency, **384,** 1187–1232
computations, rectangular and circular guides and modes, 1227
cylindric guide, **377, 379, 380, 383,** 1187–1232
for air and other pure dielectrics, comparison, **379**
and energy transfer, **96**
and wavelength, guide, **96, 308,** 1186–1232
Cutoff wavelength, **308–310,** 1187, 1188, 1190, 1193, 1196, 1207, 1213, 1221, 1222, 1227, 1230, 1232
cavity resonator, 1233
formulas, 1188–1232
longest for TE waves, **305**
Cycles per second, **5**
Cycles in pulse, **360**
Cylinder, metallic and axial slots, directivity, 1036, 1095, 1182
surface, radiation conditions, **766**
Cylindrical cage antenna, **772–774**
relative directivity patterns, **772**
Cylindrical cavity resonator, 1233–1237
Cylindrical coordinates, **18, 20, 145, 146, 215**
Cylindrical dipoles, alignment of several, **729–734**
condition of, accounts for magnitude of radius of cylinder, **718**
current distributions, **728, 730**
driven, **719, 729**
entrance gap current formulas, **721, 724**
gap current, **721, 724**
general self-impedance formula, **712**
hollow, input resistance and reactance, characteristic impedance, **742**
numerical applications, **724–727**
radial displacement current, **744**
radiator, tapered input terminals, **744**
several parallel on circle, **720**
table for integral solutions, **733**
two in parallel, **719**
Cylindrical guide, Bessel derivative, 1213
boundary conditions applied, **378**
cutoff frequency, **377, 379**
distributions, **95, 304, 306, 307, 377,** 1185–1232
excitation, 1220
longest cutoff wavelength, **305**
metal surface, radiation effects, **765–772**
p values, **383**
phase constant, **383**
Poynting vector, 1199
TM modes, **382–383,** 1185–1232
phase velocity, **380,** 1185–1232
$T_{n,m}$ waves, **379**
Cylindrical parabolic antenna, 1182
Cylindrical radiators, **765–774**
center-fed, internal and external resistances and reactances, **715**
factors, Δ and Ω, King theory, **710, 711**
integral equations and method of successive approximations, **709**
integral solutions, **722–723, 725–726, 732–733**
internal ohmic resistance and reactance, **713**
King, Blake, and Harrison calculations and theory, **705**
metal surface, Bessel functions applied to formulas, **767–772**
directivity, computations tabulated, **770, 771**
electric field and directivity formulas, **769**
polar and rectangular plots, relative field amplitude directivity, **771**
models, **709**
Oseen and Hallén theories, **705**
surface, **765–772**
radius effect and directivity, **770, 771**
Cylindrical and rectangular guide relations, **95, 305–307, 374, 377, 378, 381, 383,** 1185–1232
Cylindrical surfaces of field actions, **641**
Cylindrical wave, **247**
Cylindrical wave guide (*see* Cylindrical guide)

D

$D_{\theta_{avg}}{}^2$, average energy directivity, **630**
Δ, Murphy operator, or a factor in King's theory for cylindric surface radiator, respectively, **710**
∇, nabla operator, of vector or a scalar function, 979, 1271
∇^2, additional differentiation of Hamiltonian nabla operator, **313,** 1271
Dalembertian of wave function, **311**
Decay, factor, application, **346**
field amplitude, wave-spread effect, 871, 885–886
Decelerated electrons, **4**
Decelerated field, **4**
Decibel formulas, double line, **414**
Decibel gain, half-wave antenna in front of plane metal reflector, 1005
Decrement, logarithmic, electromagnetic wave in space, space dissipation uniform, **138**
Degree of ray bending, troposphere, 973
Del operator, known as Laplace and Hamiltonian operator, but Δ and ∇, **28, 109, 127, 199, 220,** 979, 1271
Delay, negative phase shift on feeders, **446**
numeric computation, 879
time, **36,** 937

Delay angle, **86, 89, 90, 136**
dealing with many wavelengths of propagation, **453, 454,** 872, 878–880
equivalent, and relative phase condition, 872
Delay lens, metallic, 1241
De Moivre law, applied to radiation, **642**
Density, current, volume element, **612**
dry air, 975
formula, 976
electric charge in field, **22–24**
electric field energy, **13, 36, 111, 131**
electromagnetic field energy, **13, 25, 35, 37, 111, 112, 131**
nonpolar gas, 970
power, average value, radiation field, **629**
watt, wave front, **130**
wattless (reactive), wave front, **130**
Destructive and reinforced wave interference, diffraction, 1038
electromagnetic rays, 926, 927, 930, 949, 951, 956
Detector arrangements, line probe, **427**
Determinant, formula for vector and product of vectors, **197**
Devore, H. B., and H. Iams, lens (electromagnetic), 1241
microwave optics, between parallel conducting sheets, 1241
Diacaustics and catacaustics, **319**
Diamond antenna, Bruce rhombic, **458**
Dielectric bound and constraint charges, **152**
Dielectric constant, **5**
actual value of, compared with equivalent value, **17**
of air, **4, 5**
due to dry air and water-vapor content, 977
of earth crust, **6**
equivalent, dissipative wave medium, **5, 17, 36, 40**
gradient of, causing curved wave front, **371**
of ice, **395**
of ionosphere, 977
of ocean, **5, 6**
relative equivalent, **5, 347**
of earth crust, 900
table for useful substances, **5**
of troposphere, **6,** 970–984, 986–997
unit of, explained, **65**
of vacuum, empty space, **5**
at VHF's and UHF's, **395**
of wave medium, **4–5**
Dielectric displacement current, **12,** 15, **28, 29**
effect of, **16**
Dielectric and dissipative wave mediums, comparison, refraction law, 802
Dielectric guide attenuation, leaky, 1214
Dielectric lens, 1240
Dielectric loss, wave guide, 1217
Dielectric mirror, **10,** 946
wave reflection, 946
Dielectric tube, 1185
Dielectric wave medium, **3, 16,** 791–800, 804–808, 810–816
divergence of Poynting vector, **35**
means for separating horizontal from vertical polarization, 814, 817
perfect, angles of incidence $\theta_1 < \theta_B$ complex reflection coefficient, 819–820
assumed electric and magnetic vector potentials, compared, **358**
phase and group velocity relation, **381**
propagate modulated waves without distortion, **394**
Difference between wave-guide wavelength and corresponding unbounded wave-medium wavelength, **305, 310**
Difference between vertical and horizontal polarization, **17,** 916
Differential, Lecher line section, electric radiation field contribution, **501**
retarded vector potential, applied to radiation, **782**
surface of spherical wave front, **628**
Differential antenna, **8, 31, 86, 161, 163, 165–194, 235, 241, 551**
Differential electric field contributions, numeric values, **555**
Differential equation, Bessel, and solution, **295, 322, 326, 330, 1231**
general wave equation, solution with separation constants, **294**
Legendre (associated) equation, **327**
for $\Phi_1(r)$ function, and derivation of new function, Φ, **329–330**
Differential linear radiator, directivity, **31, 32, 464, 534**
electric field intensity with active and reactive terms, **516**
elementary, **31, 86, 161, 163, 165–194, 235, 241, 551**
field formula applied to, **540**
general space orientation, **29–31, 607**
meridian directivity, **625**
radiation advantage and gain, formulas and application, **624**
radiation resistance, **517**
terms in near field, **553**
Differentiation of products, application of partial operation to radiation, **513–514**
Diffracted beam due to incident primary beam, 1061
Diffraction, antenna, circular, air gap voltage excitation, 1182, 1280
basic concepts, 1018
circular slit radiator, 1280
different sources present, 1019
display, applied to 300- and 1200-Mc waves, 1057
edge, 1063

Diffraction, edge, assumed as a line of a Riemann space, 1065
effects, experimental, mountain ridges, 1058
electromagnetic, 1018
Brewster wave incidence dip on Cornu spiral, 1073
curves and formulas, 1074
field amplitude, Fraunhofer pattern computations, 1083, 1097, 1103, 1104, 1107, 1119–1123, 1137, 1139, 1141–1148
Green function and theorem, 1280–1283
spherical earth crust, 1069
from end of rectangular wave-guide opening, 1124
factor, spherical earth, **345**
field regions, obstructed and unobstructed, 1050
twofold, 1049
formula, electric field, 1066
electromagnetic, Burrows-Gray, 1075
Fraunhofer, field amplitude pattern, circular wave-front radiator, 1143
field amplitude pattern, circular and rectangular wave fronts compared, 1144, 1145
Fresnel, **784**
geometric shadow region, numerical application, 1055, 1056
Green's theorem applied to Kirchhoff solution, 1061
inclination factor, 1061
less for shorter waves, 1021
maxima and minima, 1052
more pronounced for relatively longer waves, 1038
obstacles, 1028
obstructing wedge, above and below, 1039
parabolic cage projector, curves for main beam width, 1035
pattern, parabolic projector, 1032
rectangular slot radiator formula, 1096, 1109
and ray theory concepts, 790
and refraction dependent on operating wavelength, 1018
screen, assumes absorption on side of arriving primary radiation, in electromagnetic case, 1020
sharp edge, formulas, 1050
due to sharp mountain ridge (wedge), in unobstructed and obstructed field regions, 1039
zonal rings, 1040
by slots, **10**
apertures in screen, 1020
spectra, wave trapping, 1240
theory, A. Sommerfeld, 1063
and wave obstruction, 1018–1184
of waves, **318**
into geometric shadow region, **318**
Diffractivity, circular aperture, **1139**, **1140**, 1142
circular and rectangular wave-front radiators, 1140
double-slot radiator, 1113
envelope of resultant amplitude, has shape of single-slot pattern, 1123
formula, rectangular aperture, 1084
N slot radiators, 1114
numerically applied, 1108
tables and curves, 1084–1086, 1095, 1098, 1102, 1105, 1106, 1108, 1119, 1139, 1140, 1142, 1146
Diffractor, parabolic, and wavelet concept, 1028
Dimension of electric field, **16**
Diode probe, line measurement, **427**
Dip, Brewster (*see* Brewster dip)
Dipole, atomic, **152**
center-fed, actual and equivalent network, **680**
charge moment, **152**
complex field power, **655**
curtains, **589–592**
cylindrical (*see* Cylindrical dipoles)
effects, in atoms, **152**
electric (*see* Electric dipole)
electric current moment, **152**
elementary (*see* Elementary electric and magnetic dipole)
fine and conical, capacitance and inductance per unit length, **742**
gap, impedance (mutual), **652**
induced voltage, **651**
terminals, dynamically insulated from ground, quarter-wavelength sleeve, **703**
general, finite length, field formula, general electric length, **533**
half-wave (*see* Half-wave dipole)
hemispherical, **743**
Hertzian, **89**
and image dipoles, rectangular guide, 1182
magnetic (*see* Magnetic dipole)
radiation effects, near obstacles, **194**
radiation resistance, different from half-wavelength current distributions, **663**
rhombic cross section, **743**
special, such as folded half-wave, radiation resistance, **662**
television channel dimensions, 1285–1287
thick spheroidal, **743**
Dipole moment, atomic, **153**
Dipole radiator, analysis of, **530**
cylindric, nominal impedance, **747**
self-impedance, **713**
different forms, formulas, **743**
self-radiation resistance and reactance, **712**
Direct and indirect field components, 930
Direct and indirect ground-reflected wave contributions, 869

Direct ray, **10**
Direction, change of, wave propagation, due to refraction effects of wave medium, **366**
components, **18, 22, 27, 33, 38, 39, 64, 65, 87, 89, 93, 101, 105, 147–150, 161, 163, 169, 172, 176, 184, 197–200, 205, 207**
cosine, **21, 207, 208, 289,** 1269, 1272
of flow of current, **66**
of radio beam or ray, **57, 59, 62**
of wave propagation and wave front, **8**
Direction factor, in receiving antenna array, **447**
of array, geometric progression applied, **447**
Direction finder loop orientation, close to radiator, **20**
Directivity, alignment of several linear radiators, **579–583**
amplitude and power, computation, half-wave radiator, **535**
and antenna gain, **620**
aperture radiator, normal and inclined primary wave front, 1115
Beverage antenna, **457–461**
components, **594**
computations, cylindric metal surface radiator, tabulated, **770, 771**
differential linear radiator, **31**
disk radiator, **761–762**
eight linear radiator array, **634**
electric doublet radiator, **535**
and electric field, formulas, cylindric surface radiator, **769**
value of half-wave radiation sections with partial radiation suppression, **559–562, 564**
and electromagnetic fields of two linear radiators, **569–571**
elementary linear radiator, **31,** 535
equatorial, different spacings and phasings of linear radiators, formulas, **583–584**
two like linear inphase and equal current radiators, patterns, 580
evaluations, linear radiator, **543–545**
factor, variable, **628**
concentric line radiator, partial radiation suppression, **567**
formula, general, applicable to half-wave radiator, **537**
and applications to cylindric cage antenna, **772–774**
four half-wave radiators, **632**
graphical method, average value, 632
group characteristic, **595**
half-wave dipole, **32, 239, 251, 534,** 545
compared with other higher harmonic excitations, **545**
half-wave radiator, alignment, formulas, **585–586**
Directivity, half-wave radiator, compared with elementary point radiator, **533**
Hertz doublet, **31, 32, 535**
horizontal disk and vertical linear radiator combined, **764**
isotropic point-source radiator, **535**
linear conductor, array unequally spaced, **605–609**
for higher harmonic excitation, **538**
for odd and even half-wave distributions, **544**
stationary-wave excitation, **463**
traveling-wave excitation, **463**
zero current value at either end, **625**
magnetic dipole, compared with electric dipole, **86, 161**
matched line, **459**
meridian, **624**
linear radiator, **625**
N circular aperture radiators, 1150
n linear aligned radiators, formula, **640**
in plane of circular wire radiator, **749**
and Poynting vector formulas, harmonic excitations of linear radiator, **623**
radiating slots in cylinder, 1036, 1095, 1182, 1284
space distribution of equal linear radiators, **594**
space field, **631**
(*See also* Amplitude directivity; Power directivity)
space relative, two half-wave vertical radiators, compared with one half-wave radiator, **633**
squared, average value applied, **509**
total, group factor, **593**
two differential linear radiators, **187**
two elementary parallel radiators in equatorial plane, **570**
vector diagram, linear half-wave radiator, evaluation solution, **539**
vertical and horizontal half-wave radiators, 926–927
vertical, linear, and horizontal disk radiators, over a metal reference plane, Cartesian patterns, **763**
Directivity patterns, alignment, equal linear radiators, different spacings and current timing, **581**
calculation, half-wave linear radiators, **632–634**
circular disk and vertical linear radiators, **765**
coaxial radiator, **774**
half-wave, linear elementary, and singlet (point source) radiators, compared, **534**
linear radiator, fundamental and higher harmonic excitation, **545**
in plane of circular wire radiator, Cartesian coordinate patterns, **751**
relative, cylindric cage antenna, **772**

Directivity patterns, relative, linear radiator, odd and even current distribution, **623**
stationary- and traveling-wave excitations of linear conductor, compared, **464**
two linear radiators, equatorial plane, **575–579**
useful types compared, **534**
Disadvantage of radiation, **627**
Discone antenna, **728**
and matching, **728**
Discone radiator, **73–76, 728**
Discontinuity, circuit and radiation, **779**
Kirchhoff equation (diffraction), **311**
mouth of guide, **261**
normal electric field, **65**
sphere of, **77**
tangential magnetic induction field, **65**
wave mediums, **66**
Discontinuous variation, Kirchhoff wave equation, **311**
Discrimination, against reflected waves, **787**
against wave components, due to polarization, **786–787**
Disk and linear radiator combination, directivities, Cartesian plots, **763**
Disk radiator, application of Bessel function, **760–765**
directivity, **761–762**
horizontal over metal reference plane together with vertical linear radiator, directivities, tabulated, **764**
radiation pattern, **762**
theory, **759–765**
and vertical feeder, both radiating, **762–765**
Dispersion, anomalous, **366, 370**
normal, **366**
Dispersive wave medium, **51, 389–401**
cause and effect of, **393–401**
and nondispersive medium, compared, **399**
and velocity of propagation, **389–401**
and wave propagation, **387**
Displacement and conduction current, extreme wave-medium cases, **396**
relative magnitudes, **392–401**
Displacement current, **11, 15, 99, 100, 396**
compared with conduction current, **6, 16, 30, 31, 33, 52**
electric, **98**
longitudinal, wave guide, **1186**
magnetic, **11, 15**
tubes as electric field tubes, **74**
wave guide, 1186
Displacement factor, dissipative wave medium, different frequency, **31**
Dissipation, heat, general wave medium, **29, 43, 45, 46, 51, 117–128**
metal medium, **43, 45**
term d, earth crust near earth surface, 905
Dissipative medium, phase factor, **138**
logarithmic space decrement, **138**
Dissipative wave medium, **4–7, 12–17, 29–31, 36–39, 41–63, 117–143**
behavior, like leaky dielectric, 840
with respect to stiffness (electromagnetic), **43**
Brewster angle and dip in, 861–863
for characteristic wave impedance, attenuation constant, phase constant, $q = \sqrt{1 - (1/Q^2)}$, and $Q = \omega\kappa/\sigma$, **52–56**
complex field energy in a definite volume, **121**
dispersive and nondispersive, formulas compared, **399**
divergence of field energy over an enclosing volume, **122**
dry earth crust, **394**
effect of frequency, **43**
electric and magnetic, scalar potentials compared, **358**
expression for finding relative magnitudes of electric and magnetic fields, **45**
extreme cases, for conduction and displacement currents, **396**
field energy concentrations, **117**
field relations, **97**
formulas, expressed in medium Q value, **5, 52–56, 123, 126–128, 140–143**
frequency effect, **43, 390–401**
gradients, 854
heat loss, **117–133**
leaky dielectric, **5, 16–17, 28–31, 33–36, 40, 42–56, 98, 118–138,** 840
and nondissipative, scalar potentials, **358**
numerical applications, **52–56**
numerical computation of reflection coefficient, 843–845
ocean, **6, 41, 43, 46, 48, 52, 137, 400,** 900, 910
phase angle, characteristic wave impedance, **43**
phase factor and refracted wave, 796–826
power factor, **140**
Poynting vector, real and imaginary parts, **125**
propagation constant, **30, 44, 46, 48, 50, 53, 55,** 58–59, **70, 126–127**
pseudo Brewster angle, formulas, 826–829
reflection, curves, 858
rate of electromagnetic field power increase, **122**
reflections, 845–853
useful concepts on, 853–860
refractions, 821–824
separation of attenuation and phase constants in propagation constant relation, **390**
tabulated values, phase and magnitude of refractive index, 841
use of total electromagnetic field energy content, **130**

Dissipative wave medium, useful and dissipated field power, **140**
useful reflection concepts, 853–860
Distance to field point in Cartesian coordinates, **607**
Distance parameter, vertical and horizontal polarization, 1075
diffraction, vertical and horizontal polarization, 1078
Distant field effects, power directivity, for electric and magnetic radiation vectors, **617**
Distant radiation field, TEM waves and customary line conditions compared, **316**
Distant radiation region, **89**
Distilled water (ideal), index of refraction, **394**
Poynting vector, **41**
Distorted AM effect, Rayleigh wave trains, **388**
Distortion, of fields in concentric and parallel-wire lines and guides, **95**
general, **240**
of phase and amplitude for certain wave propagation conditions, 394
of PM, FM, AM, phase and group velocities, **369**
random motion, **152, 240**
Distortionless double-line condition, **372**
Distribution function, of amplitude, **306–310**
circular guide, 1212
half-wave radiator, **91**
linear radiator, **89, 91**
parallel planes, cylindrical guide, **309**
rectangular guide, 1187
and circular guide, 1190
XY plane, **302, 306, 308**
Distributions, along conductor (experimental with probe), **456**
current, and electric lines, 1186
along Lecher feeder and linear radiator, **698, 699**
equivalent electric currents due to an electromagnetic field content in field surface, **356**
Div $\dot{B}$ and div $\dot{D}$, curvilinear coordinates, **151**
Div $(\dot{\xi} \times \dot{H})$, **25, 121, 201–202,** 205, 1273–1275
dissipative wave medium, **202**
nondissipative (pure dielectric) wave medium, **201**
Div $(\dot{\xi} \times \dot{H}) = \dot{H}$ curl $\dot{\xi} - \dot{\xi}$ curl $\dot{H}$, relation important, dissipative wave medium energy solutions, **121, 201**
Div grad, relation, 1272
Divergence, **20, 22–25, 35, 38, 39, 108, 109, 111, 120–122, 124, 127, 128, 131, 197, 198, 201–204, 233,** 1271
average, **39, 197**
of charge, rate of leaving unit space, **23**
Divergence, concept, **108**
of cross product, **25**
current density, **199**
different notations, **198,** 1271–1275
electromagnetic field energy flux, surface divergence, **38**
is equal to time rate at which electromagnetic density increases within volume, **25**
expression, dissipative wave medium, **128**
formulas, **198, 201–204**
identity, **198**
imaginary, **123**
linear, **109**
magnetic flux always vanishes, **22, 24**
mathematical definition, **198,** 1271–1275
Maxwell's equations, **197**
meaning of, **22**
negative, **23**
nomenclature, **22, 23**
positive, **23**
Poynting vector, **201**
in pure dielectric wave medium, **35**
of a quantity, **23**
real, **123**
relations, Cartesian, cylindric and spherical coordinates, **22, 109, 111, 197–199, 203,** 1271
surface, **38, 109**
two vectors, applied to electromagnetic field, 1273
of a vector, **22, 198,** 781
and dot product (vector operated by nabla), 978
gives strength of source, 980
and vector analysis, notation ∇, **22, 198,** 1271–1275
volume, **38, 109**
Divergent progressive electromagnetic field, **332**
Divergent wave, **332**
amplitude decay, **332**
Bessel and Neumann functions, **332**
Stokes separation constant of, **332**
Diverging cones, Schelkunoff line, **735**
Dominant longitudinal electric wave conditions, **377**
Dominant TE wave, conditions, **374**
Dominant $TE_{1,0}$ wave, dominant mode, **305**
Dominant transverse wave, **43**
Dominant wave in wave guide, **43, 307**
Dot or scalar product, **22, 38, 197,** 1268–1269, 1271–1275
Double-cone lines of different angular spread, **80, 85, 735**
Double-cone radiator, characteristic impedance, compared with double ribbon line, **79**
Schelkunoff, **76–86, 735**
Double integral, applications, radiation, linear radiator, **511–514**
normal wave incidence, 1158–1160

Double integral, solution, primary wave incidence in aperture, 1158
radiation resistance, parallel-wire line, **511–514**
rectangular aperture, 1111
Double layer, **154**
electric, **157**
elementary solid angle, **154**
magnetic, **154, 157**
Double-leaf Riemann surface applied to diffraction, 1065
Double line, approximation formulas, **412**
attenuation and phase constant, **407–408**
beads, characteristic impedance, **405**
db formulas, **414**
different standing-wave ratio, **411**
E_{min}/E_{max} gives measure of load mismatch, **412**
feeder, linear current distribution, equivalent length by means of equal areas, **518**
formulas, **407–408**
attenuation and characteristic impedance, **414**
derived from Maxwell's field relations and from classical transmission-line theory, compared, **68**
reflection effects, **411**
useful for stubs, **415–416**
generalized line length and characteristic impedance formulas for measurements, **410**
guided TEM wave, **67**
high-frequency line, formulas, **412**
impedance loaded, **411**
incident and reflected waves, **68, 78, 410, 417–420, 422, 423, 735–736**
input, admittance and impedance, compared, **415**
impedance, **410**
load impedance and characteristic impedance, **411**
matched, **411**
high-frequency line, **414**
maximum and minimum input impedance, **415**
with no true nodal points, **411**
open-ended, **412**
input impedance, 409
length one-quarter of wavelength, like series resonance, **415**
lines shorter than quarter wavelength, like capacitance, **412**
output current, through load at far end, input voltage has a constant relation (quarter-wave transformer action), **409**
phase and group velocity, **410**
potential, current and phase distributions, **409**
with power absorption in load, partial and total, **411**
pure capacitance load, **412**
Double line, pure inductance load, **412**
Q value, **415, 486–487**
quarter-wavelength section, **409**
radiation resistance, solution, **510**
reactance terminated, **411**
reflection coefficient, and phase, **412–413**
relations, **406–416**
principal and complementary wave terms, **97**
sending-end impedance, entrance impedance, **408**
shielded and unshielded, characteristic impedance formulas, **403, 405**
short-circuited, at far end, input impedance, **409**
lines shorter than quarter wavelength, like inductance, **412**
quarter-wavelength line, like parallel resonance, **415**
standing (stationary) waves, **411**
standing-wave ratio, **411**
and reflection coefficient, **417**
theory, classical Kirchhoff, **491–492**
transfer or driving impedance, **409**
transmission line, equation compared with electromagnetic field theory, **492**
and Maxwell's equations, **68, 492**
traveling and standing waves, fundamentals, **416–420**
voltage and current, at any distance, from input end, **410**
from load end, **408, 410**
at far (load) end, **408**
and impedance at input end, **408**
relations, reflection effects, **411**
with voltage and current distributions, **411**
wave interference, **411**
Double-slot radiator, formula, 1113
Double-stub impedance, matching, **433, 445**
Double stubbing of feeder, 864
Doublet effect, **240**
and elementary linear radiator relations, formulas, **241–249**
formulas, electric and magnetic dipoles, applied, **165–168**
Hertz, **8, 31,** 89, **144, 241**
magnetic, **144, 152, 153, 155, 158–165**
radiator, **31, 86,** 89, **144, 157–163,** 938
Doubly modified electromagnetic path, 998
Downward bending of ray, 974
Downward ray curvature, 996
Drift, random motion, **152**
Driven and parasitic radiators, formulas, **652**
numerical application, **688–694**
Drude, P., fundamental diffraction explanations and procedures, 1034
Dry air density, 975
Dry ground (*see* Wave medium, dry ground)
Duct for waves (*see* Wave duct)
Dyne, 1243

E

Earth, curvature, speculations, 871–872
curved, **346**
distance parameter, **347**
spherical, formula, **347**
radius, actual and equivalent, **347, 348**
formulas, actual and effective values, 1077
surface, curvature effect is unity for perpendicular wave incidence, 886
Earth crust, actual and perfect, radiation patterns, 912–928
attenuation, 909
and phase constants, 907
Brewster angle and dip, curves, 860
conditions and forward tilt of electric field, elliptic polarization, due to actual earth effect, 900
effect, general, **4–7, 10, 12, 16, 28, 30, 34, 42–46, 52–56, 62, 117–133, 135–139, 142**
resultant field, for given ground and fixed radiator elevation, frequency-height product significance, 931–932
rhombic antenna, **458**
electromagnetic waves near, 902
fairly good conductor, 931
flat, propagation conditions, 930
index of refraction (complex), curves, 842
magnitude and phase tabulated, 841
magnitude and phase, reflection coefficient, 851
parabolic curvature applied, 871–872
phase velocity, 909
propagation constant, 904
Q value, **5, 52–56,** 1076
relative equivalent dielectric constant, applied, 900
spherical, curvature, effect, approximate formula, 886
equivalent, 997
expression for increasing divergence of waves, 1074
secondary radiation and Hertz vector, 1069
wavelength, 909
wet, reflection coefficient, tabulated computations, 936, 939, 941
Eccentric coaxial feeder, formulas, 403
Echo, field value, compared with field value at distant reception point, 887
long-time electromagnetic, **368**
Eckart, C., on refraction, 997
Edge diffraction, 1038
Effective cross sections, elementary field energy tubes, surface of medium separation, 793
Effective electric and magnetic field associations, in terms of power directivity, antenna array, **622**
Effective (equivalent) length, half-wave linear radiator, **192**
Effective field, for one and two half-wave radiators, **630**
Effective field values, electric and magnetic, using electric and magnetic radiation vectors, **618**
Effective spherical primary wave cap, 1179–1180
Ei (jx) and Ei ($-jx$) formulas, **658**
Einstein, A., velocity of energy propagation limit, **380**
Elasticity, electromagnetic, vacuum, **391**
Electric axial field value, circular wire radiator, different length, table, **755**
Electric charge, **21**
density, in terms of divergence, **23, 110, 197**
moment, **157**
momentum per unit volume, **23**
in motion, **23**
Electric current, density, general case, **28, 29**
linear, **65, 228–230, 233, 240–241, 299–300**
surface, **65, 228**
volume, **199, 227, 228**
Electric current element, between-field, **163, 168–187**
directivity, **31**
distant radiation field, **163–187**
moment, of, **86, 159, 161,** 1062
aperture radiator, 1062
near field, **163, 168–187**
relation for a space point, **611**
Electric current filament, **161**
Electric current moment, **162, 239**
compared with charge moment, **516**
Electric current sheet, **143, 323, 356,** 1030, 1089, 1093
effect, opening of parabolic reflector, 1029
self-radiation effect, **619**
Electric dipole, applied to linear radiator, **89**
compared with magnetic dipole, **153**
elementary, electric field components, **164**
field, begins with TM wave, while small-loop radiator (magnetic dipole) begins with TE wave, **293**
and magnetic dipole, applied, **156, 162, 187**
general comparison, **144–194**
moment, **153**
neighborhood and between-field region, total field, **168–180**
power flow, **158**
radiated power, **159**
small, explores electric field distribution, **156**
small vertical, **153**
two, **187–191**
Electric displacement, **12, 15, 16, 196**
Electric displacement current, **11, 15**
Electric distance, effect, elementary electric and magnetic dipoles, **171, 182–183**
equivalent, **171**

Electric double layer, **157**
potential, **157**
Electric doublet, **144, 153, 157, 159, 163**
charge moment, **162**
elementary case of linear radiator, **144**
summed up (integrated), **144**
(*See also* Doublet effect)
Electric energy density, **120**
Electric field, **229**
axial, **307**
and characteristic wave impedance, Poynting vector, **36**
circulation, **11, 23, 101, 349**
components, computed from potential gradients, applied, **471–473**
contribution, **35**
and directivity formulas, cylindric metal surface radiator, **769**
earth crust, diffraction, 1066, 1074
energy, **13**
explored by small electric dipole, **156**
formula, parallel with linear radiator, **664**
resultant space distribution, half-wave radiators, applied, **595**
space distribution, half-wave radiators, **593**
forward tilt over ocean surface, 910
front of half-wave radiator, metal plane reflector, formulas, 1004, 1005
general finite dipole, formula, **533**
gliding, **71**
half-wave radiators, one and two, **630**
simple formula for measurements and calibrations, **533**
intensity, and directivity, half-wave radiation sections, partial radiation suppression, **559–562, 564**
and electric potential, flow function used, **302**
electromagnetic diffraction, 1066
formulas, alignment of half-wave radiators, **585–586**
circular radiator, **749**
Hertz doublet, active and reactive terms, **516**
inphase and antiphase linear radiators, formulas, **579**
linear radiator, odd and even half-wave distributions, **544**
longer ranges, graphical solution, 930
n equal collinear antennas, formula, **588**
radiation vector, frequency and distance to field point, formula, **615**
square root of power proportionality and inverse distance effect, free-space radiation, 874
standing-wave distribution, $n = 1,2,3$, of single conductor, **463**
and surface charge, **65–67**
represented by magnetic current sheet, **348**
maxima and minima, locations, 946–949
Electric field, maxima and minima, values, direct and ground-reflected rays, 876
radiated, Lecher wires, **507**
received, over obstructions, 913–949
relation, electric and magnetic vector potentials, **357**
forced electric field, **775**
resultant, large angle of wave incidence, 943
vertical and horizontal polarization, over wet earth crust, 941
vertical polarization, 953
simplification in terms of magnetic and electric vector potentials, **617**
space distribution of equal radiators, **594**
and surface charge relationship, for electromagnetic field, **65**
tubes as displacement current tubes, **74**
value, along axis of circular wire radiator, **754**
half-wave radiator (stationary waves), **463**
resultant, for reflections, 876
single conductor, outgoing traveling wave, **463**
two parallel antiphase elementary radiators, compared with single radiator, **569**
Electric flux, **24, 65**
density, **24, 65, 196**
solenoidal condition, **313**
Electric illumination, in plane wave front, 1028
Electric lines of force, **3, 95**
wave guide, **186**
Electric longitudinal waves, **381**
Electric and magnetic associations (effective) for power directivity of antenna array or Poynting vector, **622**
Electric and magnetic current sheet, **348**
concepts, applied to Huygens wavelet source, 1089
fictitious, **356**
mutual radiation effect, **619**
power directivity, **619**
Electric and magnetic currents, **11, 155, 157**
density distributions, radiated power, formulas, **620**
elements, application, **612**
basic space relation, **611**
Schelkunoff, **356, 361**
Electric and magnetic dipoles, **153**
actions compared, **161**
comparison, **144–194**
elementary, electric and magnetic field components, **163**
features, **180–187**
power flow, **158**
relations, comparisons, **161–165**
shells, **151–161**
(*See also* Electric dipole)
Electric and magnetic doublet, formulas, applied, **165–168**

Electric and magnetic field, boundary, plane of medium separation, 896
computed from electric and magnetic, vector potentials, **229–240**
conditions, comparison of, **314**
gradients, **316**
integrals, and Poynting vector method, **649**
magnitude, **39–45**
plane waves, field associations, plane of medium separation, 793
Poynting vector field, **499**
radiation vector formulas, **615**
rectangular guide, beyond open end, 1126
relations, general, include electric and magnetic vector potentials, **617**
incident, reflected and refracted fields, 793
values, found by equating coefficients of ambiguous sign, **335**
in presence of both electric and magnetic vector potential actions, **617**
vectors, **296**
curl relations, Cartesian, **148**
cylindric, **148**
spherical, **149**
curl and vector analysis identities, **297**
waves, different mediums, 791
Electric and magnetic guide circulations, 1192
Electric and magnetic lines of force, biconical line, TM wave, **737**
cylindric, guide, **377**
and rectangular guide, 1191
Lecher and concentric line, **403**, **474**
Electric and magnetic polarizations vanish in empty space (vacuum), **196**
Electric and magnetic radiation vectors, **609–620**, 1090, 1091
applied, **610**
definition of, **612**
integral formulas, **612**
Electric and magnetic vector potential, applied, **214–218**, 1184
compared, **356**, **358**
dimensions in mks units, **224–225**, 1247
energy, **224–225**
formula, **216**, **613**
method for $\mathcal{E}$ and H, **214**
general wave equation, **492**
relations, applied to electric current elements, **612**
retarded, formulas, **218**, **222–224**, **226**, **227**, **230**, **231**, **235**, **253**, **254**, 257, 258, **290**, **300**, **356**, **358–360**, **612**, 613
Electric path difference, **446**
Electric polarization, **153**, **196**, **221**, 313
contribution over vacuum, **196**
and magnetization potential, combined, **312**
measure of, **153**
of medium, **313**
potential, **90**
Electric potential, electric double layer, **157**
Electric potential gradient, **306**
method for finding electric field effects for slow time variation, **216**
Electric quadrupole, **153**
Electric radiation vector, application, **620**
guide diffraction, formula, 1129
and magnetic radiation vector, **609–620**, 1090–1091
relation, **613**
wave-front radiator, 1089
Electric scalar, and magnetic vector potential, **214**
potential, **244**
and Hertz potential gradient, **282**
Electric shell, **151**, **157**
Electric space charge and assumed magnetic charge concentration compared, **358**
Electric spacing, **445**
Electric surface charge and electric field, **65**
Electric tangential field, interface of two mediums, **65**
Electric type field, relations, **314**
Electric vector, boundary conditions, **65**
waves, 796
found from electric potential, and Hertz vector, **221**
and magnetic vector potential, **359**
longitudinal and transverse, **302**
(*See also* Vector)
Electric vector potential, **214**, **218**, **224**, **307**, **356**
retarded, **164**, **300**, **612**
for solving elementary magnetic dipole fields, **164**
(*See also* Electric and magnetic vector potential)
Electricity conservation, **230**
Electromagnet and keeper compared to magnetic shell, **156**
Electromagnetic aperture, tangential wave front, **261**, 1091, 1097, 1103, 1116, 1117, 1120, 1123, 1126, 1128, 1144
Electromagnetic average field power density, **210**
Electromagnetic boundary conditions, **65**, **200**, **307–309**, **349–351**, **377–379**, 790, 791, 802, 807, 896, 1036, 1184, 1185
diffraction aperture, 1036
wave guide, circular, **307**
general, 1204, 1205
rectangular, **308**, **309**
Electromagnetic catalyzer, 1127
Electromagnetic constants, **4–7**
Electromagnetic density, **13**, **25**, **35**, **112**, **118**, **120**, **122**, **123**, **133**, **134**
Electromagnetic diffraction, 1018–1184
Brewster dip on Cornu spiral, 1073
Cornu spiral, 1073
curves and formulas, 1074
earth crust, spherical, 1069
formula, Burrows-Gray, 1075
Fraunhofer, 1089, 1093, 1094, **1137**, **1148**

Electromagnetic diffraction, Fresnel, 1018–1086, 1093, 1094, 1150–1182
obstacles, 1028
pattern, wave function requirement, 1087
patterns (field amplitude), 1097, 1103, 1104, 1107
sharp mountain-wedge obstruction, 1039, 1051–1060
Electromagnetic discontinuity, radiation, **779**
Electromagnetic energy flux (Poynting), regarding surface divergence, **38**
Electromagnetic field, between-field zone, **163, 168**
concentration, dissipative wave medium, **117–143**
general, **25, 117–143**
medium, **3, 5, 34–35, 39, 117–138**
condenser radiation, **101**
contribution, **35**
and current, **3, 143**
summary, **143**
and directivity, two linear radiators, **569–571**
distant radiation zone, **163, 168–187**
and electric and magnetic dipoles, **144–194**
electric polarization derivation, **313**
ellipsoid of revolution, Abraham solution, **552**
magnetic polarization (magnetization) derivation, **313**
meaning of retarded potentials and vector potentials, **214–218**
in near zone, **163**
power, **210–214**
pure dielectric wave medium, real part yields Poynting vector, **75, 648, 651**
real part, dissipated heat power in dissipative wave medium, **53, 117, 121–125, 130–132, 137, 140, 142**
transfer not possible from denser medium into less dense medium, 804–805, 817
from radiation vectors, **615**
relations, **147–151, 200, 218–229, 249–258**
applied to closed circuit, **775**
vector addition applied, 870
steady-state solutions, 1182
two scalar wave functions, **219**
value, rectangular and circular wave-front radiator, Fresnel diffraction formula, 1170
vectors from electric scalar and magnetic scalar potential, applied to antenna, **229–240**
Electromagnetic field energy, **201–202, 205**
density, **120**
distribution, **133–138**
diverging from unit volume, **201**
instantaneous value, **133–138**
time rate, **201**
Electromagnetic field energy, tubes, applied to regions with wave obstructions, 791
Electromagnetic flux, **25, 35, 64, 110, 123**
density, **25, 35**
divergence, **38, 108–111**
time rate, **25, 35, 37, 112, 122, 133**
Electromagnetic Fraunhofer patterns, circular plane wave-front alignment, 1153
Electromagnetic Fresnel and Fraunhofer patterns, conditions, 1082, 1083, 1089, 1093, 1094, 1137
Electromagnetic horn (*see* Horn, electromagnetic)
Electromagnetic Huygens wavelet radiators, primary wave front, 1089
Electromagnetic index of refraction, **56**
complex, **56, 394,** 802, 803, 817, 821
height gradient, 988, 994
real, 794, 799, 973, 980
Electromagnetic leak, 964
Electromagnetic lens, 1240–1242
Electromagnetic line theory, based on electric and magnetic field concepts, magnetic vector potential and Hertz vector, **493**
Electromagnetic merit (Q value) dissipative wave medium, **5, 52–56, 123, 127, 128,** 1214
Electromagnetic mirror, **10,** 798–824
conductive (metallic), **10,** 855, 863–867, 912–928, 1016
dielectric, **10,** 791, 793, 798–800, 804–808, 811–814, 817, 820
dissipative (general), **10,** 790, 796, 801–803, 823–829, 895
Electromagnetic obstacle (wave) may cause secondary electromagnetic field, **314**
Electromagnetic polarization of electromagnetic waves, **17, 549–552, 785–788,** 794–795, 882–885
Electromagnetic power flowing out of space volume is equal to decrease of electromagnetic field energy in the particular volume, **133**
Electromagnetic Poynting energy flux, unobstructed wave medium, **505**
Electromagnetic properties of any medium, **4–7, 17, 28–63, 70, 117–133, 138–143,** 973–997, 1214
Electromagnetic radiation along spherical earth, **336–346**
Electromagnetic rays and wave obstructions, 789–1017
Electromagnetic rectangular primary wave-front radiator, Fresnel diffraction, 1160
Electromagnetic reflector, 789–1017, 1240–1242
Electromagnetic relations, additional, 1278–1279
fundamental, **11, 144–151, 195–240, 249–261, 267–296, 300–336,** 1275
Electromagnetic theory, methods, **195–361**

Electromagnetic wave, against dissipative dielectric, **56–63,** 789–1184
aperture location, 1080
diffraction, 1065
edge diffraction, 1019
and Fresnel zone, 1022
moving, **63–65**
near ground surface, 902
obstacle, **314**
plane, (*see* Plane electromagnetic wave)
polarization, **17, 549–552, 785–788,** 794–824, 882–885
customary concepts of, **17**
pure dielectric, **64**
Electromagnetic wave medium, conductive, metallic, **43, 45, 46, 48, 477,** 863, 867, 897, 918, 921, 922, 923, 926, 927, 1185, 1196, 1199, 1203
dielectric, **3, 5, 35, 41, 115–117**
imperfect (dissipative), **5, 17, 28, 29, 34–63, 70, 117–133, 138–143,** 1214
properties, **4–7, 17, 28–63, 70, 117–133, 138–143,** 973–997, 1214
Electromagnetic wavelength, diffraction over large curved surface, 1101
Electromagnetic wavelet source, phase factor, 1092
Electron, bound, drift, escape, and free, **152**
in conductor, **152**
general, **152**
potential barrier penetration, 997
spin about an atom, related to elementary magnets, **153**
and magnetic dipole effect, **153**
steady rotation about nucleus, **152**
Elementary aerials and small-loop aerials, **571–573**
Elementary current circulation, magnetic moment, **157**
Elementary electric and magnetic dipole, comparison, **89, 144–194**
curl for computation of current density, **30**
doublet, **157**
potential, electric double layer, **157**
radiation, field contributions, differential Lecher line section, **501**
radiation power, **158–161**
radiators, two, applied to Lecher wire feeders, **191–194**
scalar potential, Hertz doublet, **157**
(*See also* Electric dipole)
Elementary field distributions, parallel-wire line with standing waves, **498**
Elementary function, wave function, spherical coordinates, **322**
Elementary and guide wavelength, 969
Elementary Hertz contribution, **90**
Elementary Hertz vector, contribution, **642**
linear differential radiator, and Hertzian doublet radiator, **90**
Elementary isotropic radiator (singlet or point radiator), **7, 534**
compared with Hertz doublet and half-wave linear radiation pattern shape, **534**
Elementary linear current radiator, electric field intensity, real and reactive terms, **516**
Elementary linear radiator, as equiphase surface, **556**
field formulas applied to finite linear radiator, **540**
terms in near field, **553**
two, excited inphase and antiphase, actions and formulas, **573–575**
Elementary magnetic and electric dipole (*see* Elementary electric and magnetic dipole)
Elementary magnets, **153**
Elementary mesh, circulation, **155–156**
current and finite size current loop, **155**
Elementary radiators, **1, 7, 8, 86–92, 158**
formula, differential linear radiator, **86**
Hertz doublet, **86**
general remarks on, **86–92**
radiation resistance, **517**
resultant length, Cartesian, cylindric and spherical coordinates, **145–147,** 1274
two a certain distance apart, analyzed, **570**
with different spacings, polar patterns, **571**
Elementary solid angle, **154, 626, 628, 640**
and corresponding surface element on spherical wave front, **628**
for double layer, **154**
Elementary space, volume, **215**
volume radiator, **240**
Elementary surface ring, determining radiation content, linear differential radiator, **87**
Elementary surface of spherical wave front, **628**
Elementary wave function, value of q an integer, **333**
Elementary wavelet center, 1088
Elevated refracting wave stratum, 997
Elevations of radiator and pickup antenna systems, curves, 951
Ellipse, confocal, applied, **551**
general, applied to near region of radiator, **555**
of revolution, linear Abraham radiator, **552**
Ellipsoidal circular and linear polarizations, near region, linear radiator, **551**
Ellipsoidal-hyperboloidal coordinates, wavefront application, **551**
Ellipsoidal wave front, **551**
Elliptic, general, circular and linear polarization, explanations, **549–550**

Elliptical polarization, **549-551, 785–788,** 798, 900
arbitrary, vector l concept, **787–788**
cause of, **786**
different earth crust conditions, 900
effect of, 857
half-wave linear radiator, in near field, compared with polarization of linear differential radiator, **551**
reflection area in wave propagation, 1018
Elliptical polarized plane wave, along Z direction of XYZ coordinate system, 794
Emf method, and classic Poynting vector method, field energy, **188–190, 192, 235, 515–608, 648–651**
formulas, **648**
computation, elementary field power, advantage over Poynting vector method, **649**
radiated power, compared with Poynting radiation, **188–190, 192, 235, 515, 516, 608**
input antenna impedance, **649**
physical interpretation, **654**
radiation (useful radiation and interlinked induction field), **188–190, 192, 235, 515–516**
radiation paradox, **235, 515, 649**
useless local interlinked induction field, **648**
Empty space, oscillation constant, **391**
End-fire beaming, **637**
and broadside beaming, **639**
formula for, **584**
line-up effect, 1089
width of beam, **639**
Energy, acceleration, **3**
available, **116**
bound field, **3**
concentration, **115, 117, 118**
broadside, **679**
content, electric field, **11, 36, 120**
electromagnetic field, **11, 35, 63, 120**
magnetic field, **11, 36, 120**
continuity, for Poynting vector and corresponding wave-front surface products, 885
deceleration, **3**
density, **35, 120**
distribution, formulas, **133**
escaping field, **23,** 188–190, **192, 235, 261, 515, 516**
flow, **23**
along guide, 1203
guided TEM wave, **67–74**
moving electromagnetic field, **63–65**
flux in space (wave medium), **8, 11–13, 23, 25, 36–38**
instantaneous, density, **115**
of pulse, **360**
Energy, relations applied to, divergence concept, **108–111**
reflection and refraction, analysis, 792
stream, across one-square-meter area, **37**
at surface, **65**
transfer, in guide and cutoff frequency, **96, 123, 306, 359, 366, 385, 386, 480,** 1199
tubes of electromagnetic field applied to regions with wave obstructions, 791
Entrance, gap impedance, cylindric dipole, **744**
and thin wire dipole, compared, **716**
hollow cylindric dipole, **741–742**
thin wire dipole, **650, 652–654, 656, 661, 663, 670, 680, 682, 683–687, 690–692, 695, 697, 701, 703, 705, 716,** 1009. 1013, 1014
half-wave dipole, gap resistance, collinear alignment, **681**
Envelope, delay, fixed, **365**
time, of modulated space wave, **365**
motion and group velocity, **385**
time delay, **365**
Epsilon expansion, applied to electromagnetic waves, **173**
Epstein, P. S., on refraction, 997
Equal inphase exciter currents, bilateral beaming, normal to alignment, **581**
Equal and natural phasing, linear radiator, **547–549, 686**
Equal-phased linear radiators, in front, and reflector row, **638**
Equality frequency, **50**
dissipative wave medium, **50**
Equation, of continuity, interface of different wave mediums, **65**
of energy balance, **230, 233**
of Maxwell, **11, 147–151, 200**
component, **147–151**
simplified, **150–151**
conditions for boundary, **65, 307, 309, 350–357, 367,** 791–794, 798, 799, 802, 807, 809, 810, 896, 909, 910, 1018, 1022, 1064, 1067, 1081–1082, 1087, 1089, 1090, 1185, 1196
conductor plane, **65, 350,** 1067, 1185, 1196
dielectric interface plane, **351, 352,** 793, 799, 807, 809–810, 896
electric and magnetic current sheets, **353-357,** 1018, 1020, 1029, 1089–1090, 1126
general dissipative wave medium, 802, 896, 909, 910, 1018, 1022
guide application, 791–794, 798, 1196, 1203
reflection and refraction, 791–794, 798, 802–803, 806, 807–808, 809, 817, 822
screen of wave-front aperture, 1020, 1029, 1089, 1090
wave (*see* Wave equation)

Equatorial directivity, **29, 31**
formulas, different spacing and phasing of exciter currents of individual linear radiators in an alignment, **583–584**
linear, elementary radiator, **31**
radiators excited inphase and antiphase, table and formula, **578**
Equiphase surface, **21**
formed by elementary radiator, **556**
Equipotential surface, **21**
Equivalence principle, **356,** 1182
generalization, **356**
Equivalent and actual length of line, compared, **518**
Equivalent conical line, **735**
Equivalent current sheets, **350, 352, 356**
Equivalent currents, **356**
Equivalent curved elementary path, interpretation, 986
Equivalent delay angle and relative phase condition, 872
Equivalent dielectric constant, **5, 17**
dissipative wave medium, frequency effect, **47**
ionosphere, 979
relative, **5,** 851, 853
Equivalent earth, curvature, 997
concept, 1002
radius, 1000
equivalent curvature formulas, 1000
relations to ray curvature and actual earth curvature, 991
tropospheric, refraction, **347,** 348
wave propagation, **347,** 348
Equivalent electric distance effect, elementary electric and magnetic dipole, **171, 182–183**
Equivalent flat earth, 999
and actual spherical earth, rays compared, 998
two kinds of, 998
Equivalent electromagnetic focusing lens, 1083
Equivalent Fraunhofer electromagnetic case, 1082
Equivalent generalized concept, polarized waves, **787–788**
Equivalent generalized length, applications, **788**
Equivalent height, elementary loop, 573
Equivalent length, linear radiator, equal area procedure, **518**
graphical solution, **166**
half-wave, **166, 625**
numerical example, **166,** 874
Equivalent magnetic shell, **156**
Equivalent power directivity compared with actual power directivity, **630**
Equivalent pulse, **360**
Equivalent radio beam, 948
Equivalent ray, curvature, preferred modification, 1001
traces, construction of, 1002
Equivalent spherical earth ray triangle, 999
Euler constant, **465, 512, 717**
Gamma function, 1261
Even half-wave distributions, Lecher radiator, radiated power, **506**
Even integral cosine function, $\overline{\mathrm{Ci}}\,(x)$ explained and defined, **717**
King theory, **713**
Even and odd half-wave distributions, linear radiator, directivity and electric field formulas, **544**
Excitation, half-wave linear radiator, **191**
Expansions, of sine and cosine functions applied to radiation, **782**
of wave impedance, **160, 245–249**
Experimental and mathematical sine curve conditions, correcting probe linearity, **426**
Experimental standing-wave ratio, double line, **440**
Exponential function, and Bessel identity, **749**
series expansion applied to Hertz doublet, **516**
Exponential law, with distance, for solution of wave equation in true radiation field region, **334**
for wave propagation, **334**
Exponential series expansion applied to radiation, **173**
Exponential waves, **320**
Exterior product, or vector product, vector analysis, **197,** 1268–1269
External resistive and reactive components of self-impedance, cylindrical dipole, **714**
Extinction, of reflected wave, 814–815
of reflections of unpolarized wave by two successive reflections, 817

F

F circulation, **104–108, 349**
$F(x,y)$ function, plane wave-front aperture, general case, 1154
Factor Δ, in King theory for cylindric radiators, **710**
Factor Ω, in King theory for cylindric radiators, **710, 711**
Farad per meter, unit explained, **65–67**
Faraday law of induction, **14, 103, 219**
applied to cylindric dipole solution, **744**
Feed, main, for three parallel half-wave radiators, **695**
Feeder, aperiodic, for J antenna, **702**
characteristic impedance, less or more than radiation resistance for half-wave dipole, **449**
well designed, **452**
input resistance, different gap locations on linear radiator, equal and natural phasing, **686**

Feeder, phasing, sending antenna, **191**
shielded and unshielded, characteristic impedance formulas, **403, 405**
shunting half-wave linear radiator gap, matching, **705**
Lecher wires, half-wave linear radiator, **698**
series and parallel, half-wave radiator, **697**
single line (aperiodic), radiation resistance, **466–468**
supply, balanced and unbalanced conversion, **525**
tangential field components, **480**
Fermat's law applied to electromagnetic ray, 983
Ferrell, E. B., on wave ducts, 1238
Ferromagnetic wave medium containing iron deposits, **29**
Fictitious electric and magnetic current sheets, applied to wave-front radiator, 1093
Field, L. M., on traveling-wave tube, **417**
Field, between-region, **163, 168**
complementary wave, only in neighborhood of physical terminals, **494**
complete cancellation of, **10**
complex and current complex ratio related to propagation constant, **364**
dissipative wave medium, **3, 36, 40, 42–56, 117–138**
distant radiation region, **3, 19, 163, 174**
electric (*see* Electric field)
electric doublet, **8, 31, 32, 86, 152, 153, 158–187**
electric type, **229**
gliding, **71**
escape, **3**
half-wave dipole, **32**
magnetic (*see* Magnetic field)
magnetic dipole, **152, 153, 158–187**
magnetic type, **229**
near-field region, **175**
next to radiator surface, **162, 164, 187, 245**
possible within wave guide, **357**
of radio conductor, **3**
resultant, in neighborhood and between-field region of electric and magnetic dipoles, numerical, **168–187**
vertical and horizontal polarization over wet earth crust, 941
for spaces with exciters, **296**
over spherical earth to field over plane earth ratio, **347**
stored, **3, 11, 25, 35, 52–56, 111–117**
total, in neighborhood and between-field region of electric and magnetic dipoles, numerical, **168–180**
transmitted, of a guide, **357**
of two elementary electric dipoles, **187**
of two linear differential radiators, **187**
Field amplitude, decay within a copper wave medium, curves, **477**
and electromagnetic field energy, 1094
pattern, computation, Fraunhofer, 1098
and radiation intensity, distribution, 1085–1086
Field concentration in a preferred direction, **555, 623**
Field conditions, solenoidal, **198,** 1273
Field configurations, $TE_{m,n}$ guide waves, 1187
Field contour, **21**
Field distortion, **95**
Field effects, construction for Fresnel zones, 1045
electric, half-wave radiator, **533**
value, computed from scalar potential and Hertz vector contribution, **91**
electric doublet, **8, 31, 32, 86, 152, 153, 158–187**
electric type, **229**
gliding, **71**
maxima, formulas for vertical and horizontal polarization, 967
Field energy, available, **116**
collision in ionosphere, 979
concentration, **117, 118, 133**
density in joules/m^3, **118**
distribution, **133–138**
several slot aperture radiators, 1125
electric, **11, 13**
electromagnetic, **11, 13**
first Fresnel zone, 1024
fluctuations, due to reinforcements and destructive wave interference, 1038
heat loss (space dissipation) in wave propagation and useful radiation energy, **119**
instantaneous, **133**
magnetic, **11, 13**
in motion, **64**
relations, **25, 35–39, 52–56, 63–65, 67, 71, 101, 103, 108, 111–128, 130–138**
transfer, guide, 1185
and wave front, **10**
traveling and stationary waves, **111–117**
tubes, applied to regions with wave obstructions, 791
Field fluctuation, 1038
and decay, diffraction, 1048
Field formulas, electric and magnetic, TE and TM guided waves, 1200
resultant space wave, earth crust reflection, 962
Field-free sources and sinks, **300**
Field gain, over half-wave radiator when reflector is present, 1004
of radiator, **620**
Field illumination, 1037
Field intensity, **4, 11–12, 37, 39–44, 64, 66, 71, 75, 78, 82, 86, 87, 89, 91, 93, 95, 98, 101–105**
caused by primary wave front, 1023

Field intensity, due to diffraction, **346**
electric, Hertz doublet, active and reactive terms, **516**
elementary spherical zone, 1023
formula for distances over plane earth, 870
free-field value, **10**
linear primary radiator, diffraction, 1178
and radiation resistance, standing- and stationary-wave excitation, along linear conductor, **461–465**
Field magnitudes and relative phases, for dielectric and dissipative wave medium, **39**
Field maxima and minima, 946–949
altitude of reception center for a given fixed radiation center, 950
conditions, 888
formulas for diffraction, 1038
in unobstructed but general field decay in obstructed field region, diffraction, 1050
Field patterns, concentric line, **95**
Fraunhofer, **784**
Fresnel, **784**
in guide, **95, 260**
linear radiator, with partial radiation suppression, notes on, **557**
on reference metal plane, 866–867
linear vertical radiator, on horizontal metal plane, 863–867
parallel wires, Lecher line, **95**
polar (*see* Polar field patterns)
rectilinear and curved, 1003
Field penetration, into radio conductor, **3**
of wave, **16, 45, 477,** 1196–1199
Field point close to parallel-wire radiator, **488**
Field power, advantages in db for antenna array, **621**
density, average value, **210**
gain, antenna array, **620**
maximum available in unit space volume, **37**
Field ratio, for plane metal reflector, 1005
and power ratio, several turnstile bays, **621**
Field reference value at one meter distance, 870
Field relation, for sharp-edge obstruction, 1046
for space with exciters, **296–297**
for stationary waves, **115, 116**
for traveling wave, computed total electromagnetic field concentration and velocity, **112, 113**
Field values received, vertical and horizontal polarizations, 880
Field vector, auxiliary, **222, 312,** 1238–1240, 1248, 1275–1276
common, **312, 315, 334, 335**
complex, **220**
curl, **15**
Filament radiator, **8**
Fine conical dipole, **742**
First Fresnel zone, 1018
Fitzgerald vector, **153, 219, 222, 312**
depends on magnetic polarization, **219, 222, 313,** 1238–1240, 1248, 1275–1276
and Hertz vector combined, **312**
applied to wave-duct theory, 1236–1240
magnetization potential, for electromagnetic solutions, **219–222**
Fixed and variable factor of phase, **612**
Flare, electromagnetic horn, 1184
Flat distribution, **441**
Flat earth crust, propagation conditions, 930
requirement, 872
and spherical earth, compared with respect to wave spread, 887
Flat single feed line and half-wave radiator, matching joint, **466**
Flow density, **104–108, 349**
applied to current sheets, **349**
and curl of vector, **104**
Flow function, **301–302, 306–310**
and electric scalar potential, formula, **302**
for field in planes parallel with the XY plane, **302, 306**
for fixed field in XY plane, **302**
form of, of field in parallel planes, **302**
Φ volt, **306**
Ψ ampere, **306**
Ψ expresses field, **302**
related to current density of Poisson equation, **301**
satisfies wave equation, **302**
voltage and current functions, **104–106, 110**
Flux, electric, **11, 12, 196**
magnetic, **11, 196**
Flux density, **11**
relations applied to boundary between different mediums, **351**
FM and PM, phase and group velocity, **371**
side bands, **399**
FM wave and phase and group velocity, **369**
Focal linear radiator, 1028
Focusing lens and electromagnetic equivalent, 1082, 1083
Folded and half-wave dipole dimensions, 1285–1287
Folding dipole, dimensions for short-wave channel assignment, 1287
gap termination, **662**
Force, electric, **3**
magnetic, **3**
moving charge, **152, 153**
two charges separated, **215**
Form factor, linear radiator, 1012
over metal plane, 1016–1017
reference current dependency, 1016

Formulas, converting curvilinear references into electromagnetic Cartesian, cylindric, and spherical coordinate relations, **146–151**
equatorial directivity, different spacings and phasings of radiator currents in alignment, **583–584**
line propagation, **363**
Forward and backward radiation, **638–639**
Forward beaming and slot separation, wave-front radiators, 1121
Forward electric vector tilt, and polarization (elliptic), curves for different earth crust conditions, 900
Forward factor, angles smaller than four degrees, 1158
diffraction, numeric, 1108, 1122
significance near direct forward direction, 1033
Forward-moving wave, **76**
Forward-thrust factor, in beaming, **601, 603**
linear antenna array, **603**
Forward tilt, 958
of electric field vector, ocean surface, tabulated, 910
Forward-traveling wave, **333, 337**
Forward wavelet effect, 1135
Foster, R. M., antenna arrays, **594**
Fractional order, Bessel function, **322, 323, 332**
Frame antenna, **572**
Frank, P., and R. Mises, "Differenzial Gleichungen der Mechanik und Physik," 1281
Fraunhofer diffractivity, N circular aperture radiators, 1150
Fraunhofer and Fresnel diffraction, rectangular aperture slot, 1110
Fraunhofer patterns, **784**, 1082, 1093
field amplitude, circular wave-front radiator, 1143
and rectangular wave fronts compared, 1144, 1145
field amplitude diffraction, 1083, 1097, 1103, 1104, 1107, 1119–1123, 1137, 1139, 1141–1148
functions, field amplitude and field energy, 1094
general formula, 1120
Free-field intensity, **10**
Free-space equivalence theorem, relations, **357**
Free-space field intensity, **346**, 871
Free-space pattern and polar meridian patterns, 866
Freehafer, J. E., on wave ducts, 1237
Frequency, **19, 49–52, 162**
dependency of wave obstacle, **143**
height product, significance in wave propagation in space, 932, 956
and phase velocity, **394**
resonance, cavity, 1234
Frequency, resonance, slot, same as for linear half-wave radiator, 1036
and wavelength, applied, 789
Frequency effect, **394–401**
closed-circuit and delayed mutual actions, **777**
components of total current density in a definite direction, **30**
dissipative wave medium, **36, 42, 43**
equivalent dielectric constant, **47**
phase velocity, dispersive wave medium, **389**
power loss in guide wall, 1210
resultant field maxima and minima, curves, 951
standing space wave patterns over earth crust, 949
Frequency equality, **50**
operating, wave guide, **384**
spectrum and phase and group velocity, **371**
wobble method, 929
Fresnel diffraction, electromagnetic rectangular primary wave-front radiator, 1160
half- and full-wavelength widths, rectangular aperture, curves, computations, 1167
Fresnel directivity, formula, rectangular wave-front radiator, 1162
Fresnel equations, first and second, 811
Fresnel formula, classic, 814
of optics, 814
for perfect dielectric mediums, 810–812
Fresnel integrals, applied, 1045
$C^2(s)$ and $S^2(s)$, formulas, 1172
complex, 1064
and Cornu spiral procedure, 1041
curves, area procedure, 1044
equations, 1041–1044
Fresnel magnitudes of zonal areas, plane wave front, 1027
Fresnel patterns, 1082, 1083, 1093, 1094, 1150
computations tabulated, 1164
electromagnetic, **784**
and Fraunhofer patterns, 1182
cap (first zone), 1172
$C(s)$ and $S(s)$ functions, formulas, and curves, 1166
Fresnel relations of reflections and refractions applied to radio waves, 790–796
Fresnel theory, assumes plane wave front, 1034
Fresnel wave interference, 1019
explanation, refers to pure wave phenomenon, 1019
Fresnel wavelet summations, effects with respect to amplitude and phase, 1159
Fresnel zones, on advancing wave front, 1022
applied to electromagnetic waves, 1022

Fresnel zones, consecutive effects, **1171**
consecutive radii, 1023
field contribution, 1176
first, field energy, 1024
zonal step, 1045
and half-wavelength step, 1022
resultant effects, 1045
significance, applied to circular electromagnetic wave-front radiator, 1170
square-root numbers for radii, 1024
zonal areas, magnitudes, 1024, 1025
zonal rings, 1026
Friis, H. T., and W. D. Lewis, scanning aberrations, 1241
Function, of position, **18, 19**
of time, **18**
wave (*see* Wave function)
Fundamental concepts of currents and fields, **3–143**
Fundamental methods in electromagnetic theory, **144–361**
Furry, W. H., on wave-duct theory, 1237

G

G and *F* functions, fine conical half-wave dipole, **740–741**
Gain, aerial, for equipartition, **640**
antenna, and directivity, **620**
Bruce rhombic or diamond antenna, **458**
directive antennas, factors affecting, **594**
electromagnetic horn, 1184
absolute, 1184
field of radiator, **620**
formula, radiator systems, application, **627–641**
half-wave dipole with reflector, curves, 1008
measurements and isotropic point-source radiator, **8**
and radiation advantage, **623–624**
differential linear radiator, **624**
Gamma function, **331,** 1256–1264
applied, 1256–1264
curves, 1260, 1262
formulas, 1255–1265
and Gauss function, **331,** 1256–1264
applied, circular radiator, **756–759**
formulas, **331,** 1255–1265
negative arguments, 1262
numerical applications, 1258–1265
positive arguments, 1260
table, 1257, 1261, 1263
Gap impedance, dipole, **652, 653, 657, 663, 664, 670, 690, 691, 692, 698,** 701, 1009, 1013
active resistance, formula, **663, 670,** 684
numeric, **670, 671, 673, 675–677,** 680, **682, 692–693, 695–696, 698,** 1009, 1013
reactive, formula, **663, 670**
numeric, **670**
Gap resistance dipole, also different gap (feeder) locations, numeric values, **670, 671, 673–677, 680–687,** 1008–1014
with reflector, 1008–1014
Gap termination line-up, parallel inphase halfwave dipoles, **687**
and antiphase dipoles, **675**
total radiation resistance, **676**
Gas constant per mole, 974
Gate radiator, 1173
conditions, 1174
Gauss function, **331,** 1255–1265
and Gamma functions, **331,** 1255–1265
applied to circular radiator, **756–759**
formulas, **331,** 1255–1265
Gauss law, **25, 352**
and Gauss theorem, applied to divergence concept, **108–111**
Gauss relation for space charge, **197**
Gauss theorem, **22, 24, 25, 120, 122, 196**
applied, **121**
Gauss transformation, volume into surface integral, **122**
Gauss unit, **7,** 1243, 1252
and cgs units, **7,** 1243, 1252
General Bessel and Neumann functions, **304**
General dissipative wave medium (*see* General wave medium, dissipative)
General ellipse, equation near field, **555**
half-wave radiator, near field, elliptical polarized, **551**
General field relations, **319**
General integral, of general Bessel and Neumann functions, **304**
of $Z_n(x)$ function, **304**
General Maxwell curl equations, reference orthogonal curvilinear coordinates, **147**
General Maxwell electromagnetic field property equations, **151**
General radiation formula, **592–595**
space distribution, linear radiators, **592–595**
Schelkunoff, **357–360, 609**
General wave equation, **311, 318–321, 323, 324, 336**
including electromagnetic refraction, **319**
spherical coordinates, **325**
using Hertz function, **336**
General wave function, compared with wave function of electromagnetic waves, 1176
General wave medium, dispersive and nondispersive formulas compared, **399**
dissipative, **3–7, 12–17, 28–31, 33–63, 117–143**
like leaky space dielectric, 840
orientation of cubic meter of space, **33**
phase factor, refracted wave, 796–826
extreme cases for conduction and displacement currents, **396**
propagation constant, **58**
reflection curves, 858
Generalized curvilinear orthogonal coordinates, **144–147, 151, 215**

Generalized electrical length Ω and characteristic impedance, double line, formulas, **410**
$\Omega = l\Gamma$, by means of open-ended and short-circuited double-line measurements, **410**
Generalized equivalent length, applications, **788**
concept, polarized wave, **787–788**
Generalized line angle, **372**
Generalized refraction, 803
Snell's law, 802, 803
Geometric progression, applied, to antenna array, **447**
to direction factor of arrays, **447**
Geometric shadow limit, 1072
Geometric shadow region, **6, 17, 346**
curved earth crust and line of sight, 871
diffraction, **6, 17, 784,** 1039, 1040, 1048, 1050, 1052–1053, 1055–1060
reached by ray bending, 987
Geometrical attenuation, 886
or wave spread, 886
Geometrical line of sight, 887
Giorgi mks units, **4, 7, 195,** 1243
compared with cgs units, 1252
Gliding electric field, **71**
Good conductor, characteristic wave impedance of conductor wave medium, **43**
Grad, of point function, 1271–1272
of potential, **21,** 1271–1274
of scalar field, 1271–1274
Grad div., nomenclature in vector analysis, **313,** 642, 1272–1273
used in solution, **257,** 1273–1274
Gradient, atmospheric index of refraction, **6, 56–63,** 973–997
constant value, 998
and curvature of radio beam, 976
components, Cartesian, **22,** 1270–1272
cylindric, 1271, 1274
spherical, 1271, 1274
definition of, **21–22**
dielectric constant, troposphere, 969–997
in wave medium causes curved wave path, **370–371**
dissipative wave medium, 854
electric potential, **306**
general, **11, 20, 21, 301,** 1269
humidity and temperature effect, **143,** 969–977
magnetic potential, **306**
tropospheric refractive index, positive or negative, 987
a vector function, **21**
Graphical interpretation of Fresnel integrals, 1043
Graphical method for average directivity, **632**
Graphical solution, for complex coefficient of reflection, 843
for $D_{\theta_{avg}}{}^2$, **630**
for direct and ground reflected rays, 930
Grazing wave incidence, reflection coefficient, 860, 948
Green function, applied to ring-slit circular-aperture diffraction radiator, 1280–1283
Green theorem, applied, **490, 656,** 1087, 1279–1283
to coupled linear radiators, **656**
in Kirchhoff solution for diffraction, 1061
to linear radiator, **656**
to parallel-wire radiation effect, **490**
symmetrical, 1279
various forms, **311,** 1061, 1087, 1279
Ground, actual and perfect, radiation patterns, 912–928
conditions, perfect, 915
earth crust, **4–5, 10, 28, 47, 50**
dry soil, **5, 46**
ocean water, **5, 6, 41, 47–49, 52, 54**
rivers and lakes, **5**
rocky soil, **5, 12, 57, 62**
wet soil, **5, 57, 62, 47**
effect, Brewster angle and dip, 860
on radiation, 899–958
reflection, different earth crusts, 796–832, 834, 835, 842, 843, 845, 848, 849, 851, 852, 855, 858, 860, 868, 870 877, 881, 884, 887, 895, 900, 910, 911, 917, 918, 920, 921, 923, 926–927, 930, 933, 941, 942, 944, 949, 951, 956, 957, 959, 965
reflection coefficient, dry soil, 836
ocean, 836, 852
wet ground, tabulated computations, 833, 834
surface wave, 899–912
Group characteristic, and alignment formulas, collinear antennas, **586–589**
linear radiators, found from resultant chord of graphical solution, **582**
and characteristic of one-slot radiator, 1124
derivation and formula, n equal collinear radiators, **587**
for directivity, **595**
geometrical progression solution, **582**
inphase and antiphase excitations, linear radiators, 579
n-linear radiators aligned, **581**
unequal spaced radiators, **606**
Group factor, total directivity, **593**
Group moved as a whole, **387**
Group and phase velocity, **50, 366–401**
applications to guide modes, **380–385**
curves, wave guide, **384**
details, **380**
formulas applied to cylindrical wave guides, **378–379**
illustrated, **369, 371**
interrelation, wave guides, **384**
relative magnitudes, **366**

Group radiation characteristic, **579, 580, 582, 583, 586, 587, 588, 589, 593,** 1092, 1093, 1094, 1115
Group velocity, **366, 368–379**
cannot always be taken as velocity of wave power transfer, **366–367**
differs from phase velocity only in dispersive mediums, **366**
formula, **366**
no longer applies to single pulse, **389**
paradox, for which c'' may exceed c, **366**
Guide, attenuator, 1193
boundary conditions, **307–309,** 1185
circular and rectangular, formulas, **260–270, 304–310, 374–385,** 1190
(*See also* Circular guide, Rectangular guide)
elementary wavelength, 969
energy flow along, 1203
high-pass feeder, 1193
mode, phase and group velocity, propagation constant and cutoff frequency, **380–385**
power flow along, 1199–1217
radiator, **261,** 1126–1128
formulas, 1126–1136
rectangular (*see* Rectangular guide)
ribbon line as, **68**
slot apertures, 1116
and transmission line, metallic energy absorption, **480**
wave (*see* Wave guide)
Guide action, **95**
dielectric, between boundary planes, 964
missing central conductor portion, concentric line, **95**
near and along earth surface, 959
due to tilted electric field vector, 900
Guide wavelength, along guide, **305, 378,** 1186, 1187
and elementary wavelength compared, 969
rectangular and circular cross sections, **305**
compared with unbounded wavelength of inside guide medium, 305
TE and TM excitations, **305**
Guided radiation, along n parallel conductors, **469**
resistance, **474**
Guided surface wave, 903
conditions, 958
Guided $TE_{m,0}$ wave and zigzag uniform plane wave, 967
Guided TEM wave, **67–73**
Gyration and polarization, **786**

H

H circulation, **14, 139, 349**
H field represented by electric current sheet, **348**
H waves, **212**
longitudinal, **381**
$H_0^{(1)}$ and $H_0^{(2)}$ symbols, **339**
$H_{2,0}$ and $H_{0,2}$ waves, **382**
$H\,dl$ circulations, **139**
H_0 functions, **304, 323, 330**
Half-wave antenna, normal and parallel to metal reflector, 926, 927
Half-wave cylindrical dipole, formulas, gap impedance, King theory and classical dipole theory compared, **716**
Half-wave curtain arrays, driven inphase, different beam width in vertical and horizontal planes, **604**
Half-wave dipole, antiphase excitation method, **576**
array, radiation gain, referred to maximum field value, of a single half-wave radiator, **620**
entrance impedance, Hallén, King, and classical sinusoidal current distributions compared, **727**
excitations regarding current phase, **576**
feeders, characteristic impedance more or less than radiation resistance, **449**
formulas, 1286
inphase, in curtain, gap terminations, **687**
excitation method, **576**
and reflector, optimum gain dimensions, 1287
Half-wave end radiators, partial radiation suppression, **558**
Half-wave filament radiator (thin radiator), conditions, **767**
Half-wave Fresnel zone step, difference of average values, 1025
Half-wave horizontal dipole curtain, **590**
Half-wave inphase radiator sections, concentric line feeder, half-wave internal conductor exposures, **566**
Half-wave Lecher wire radiation, **193–194**
Half-wave linear radiator, **551,** 938
computations, amplitude and power directivity, **535**
directivity, **535**
in front of quasi-perfect reflector, 1003
Lecher wire feeders, **698**
over metal plane, 923
radiation advantage, **629–630**
section, coaxial and parallel-line conversion, **526**
shunt-fed, for matching, **705**
Half-wave radiators, **9, 32**
alignment, collinear, and curtains, formulas and numerical application, **671–684**
directivity and electric field formulas, **585–586**
entrance gap resistances, **681**
alternate mounting, and quarter-wavelength sleeves, **703**
amplitude and power directivity, table, **535**

Half-wave radiators, average value of power directivity, **630**
collinear, natural and equal phasing, formulas, **677**
curtain, computation, various radiation resistances, **682**
numerical application, **599–605**
directivity, **32, 534**
electric, field and directivity formulas, **578**
field formula, **533**
field value, standing waves, **463**
end feed, quarter- and half-wave Lecher line, **698**
equivalent length, **625**
fed by aperiodic feeder, single line, **466**
front and backup alignment and phasing, **602**
inphase and in parallel, radiation resistance, **673–674**
lattice structure, space distribution, **592**
meridian directivity, **625**
mutual effects, computations, **696**
in neighborhood of metal reflector, 1012
orientation effect, **595**
parallel, identical, alternate antiphase excitations, radiation resistance, **675**
power directivity, compared with isotropic radiator, **630**
radiation advantage and gain, **624–625**
radiation resistance, **192, 251**
is $120(D\theta^2)_{avg}$, **538**
unobstructed radiation space, **251**
reflector and front alignments, **602**
series and parallel feed, **697**
single, compared with two radiators, **633**
three, common feeding conditions, **695**
two, mutual radiation effects, resistance and reactance, formulas and table, **670–671**
in parallel, numerical calculations for Ci functions, **669**
vertical, over wet soil, altitude effect, 939
Half-wave reflection jump, 951
Half-wave spaced radiation effects, **703**
Half-wave vertical dipole curtain, **590**
Half-wavelength phase jump, reflection coefficient, 931, 933, 934
Half-wavelength step, Fresnel zones, 1022
Half-wavelength and quarter-wavelength sections and aperiodic feeder, **699**
Hallén distribution, **709**
Hallén and King theory, first and second fundamental relations, **710**
Hallén method, simplified, **718**
Hallén model, field distribution and shape of radiator, **709**
Hallén and Oseen theories, cylindric radiators, **705**
Hamiltonian nable operator, **22, 198,** 1271–1272
Hankel functions, **295, 323, 333, 339, 343**
applied, **479**
boundary conditions, circular guide, 1232
Bessel functions of third kind, **339**
second, applied to dipole cone theory, **739**
spherical, **332**
traveling waves, **333**
zero-order, **339**
Harrison, C. W., polarized field of arbitrary polarization, **787**
Hartree, D. R., on wave duct, 1237
H dl circulations, **139**
Heat loss, coaxial line, **482**
metal plate, computed from surface resistance, 1196–1199
wave guide, dielectric, 1214–1217
metal wall, 1203–1214
Heaviside, O., electromagnetic units, symmetrical forms, **221**
Height effect, antenna over reflector, 922
characteristic functions, vertical and horizontal polarizations, 921
linear antenna, over actual ground, different wave incidences and general polarization, 881–885
Height-frequency product, relation to antenna pattern, 956
significance in space propagation, 928–932
Height-gain, calculations, optical region of electromagnetic waves, 997
factor, vertical and horizontal polarization, curves, 1080
function, wave duct, 1240
Helical polarization of wave, **786**
Helical space propagation, **786**
Henry per meter, unit explained, **65–67**
Hertz doublet, **8, 31, 86, 89, 90, 144, 153, 157–161, 163–165, 168–187, 241, 243**
application of series expansion of exponential function, **516**
and differential linear radiator, formulas, **242**
directivity, **8, 535**
compared with half-wave and point-source (singlet) radiator, **524**
electric field intensity, active and reactive, **516**
elementary, Hertz vector contribution, **90**
electric scalar potential, **157**
and elementary linear radiator, applied to linear antenna and compared, **343**
compared, **243, 245,** 873
field formulas, in inverse distance terms, **244**
and wave resistance, distant radiation region, **241**
field pickup points close to radiator, **245**
wave impedance at any distance, **245–249**
fields and stimulating doublet charges, **89**

Hertz doublet, and Fitzgerald vector, applied to wave duct, 1238
combined, **312,** 1275
independent from each other and separable, **314,** 1275–1276
moment, **179**
radiation, advantage and gain, **624**
resistance, **160–161**
radiator, **8, 89,** 938
derivations and formulas, **86, 516–517**
wave impedance, **160**
Hertz function, a meter-volt concept, **283**
Hertz potential, **90–92, 153, 218**
general wave equation, **492**
and magnetic vector potential interrelated, **290**
spherical coordinates, **273, 336**
wave equation, wave duct, 1238
Hertz radiation from lines, **493**
Hertz solution, elementary space radiator, **273–283**
Hertz vector, **153, 218, 219, 222, 249, 258, 312,** 336–339, **342–345, 642–644, 658,** 1238–1240, 1248, 1275, 1276
application, Kirchhoff wave equation, **258–270**
components, **268**
in space, **268**
computation of electric field of radiator, **657–658**
electric current density, **252**
electric polarization dependency, **313**
electric polarization potential, electromagnetic field solutions, **219**
elementary, **642**
formulas, **249–258**
general wave equation, spherical coordinates, **336**
incident and reflected portions, 1072
magnetic vector potential, **221–222, 252**
method for fields, linear radiator, **235**
$\prod_c$ complex, **312**
primary and secondary portions, applied, **338**
electromagnetic diffraction, earth crust, 1068
solving, elementary space radiator, **273–283**
linear antenna problems, **642**
space point, outside spherical earth surface, **344**
total, **338**
spherical earth, 1068
used in wave equation, **273**
and wave motion, **337**
Heterogenous wave line, different propagation properties from current and charge, **496**
HF line, common assumptions, **412–416**
driving impedance, **409**
matched, formulas for attenuation, **414**
High-angle radiation, **620**
High and low impedance points, Lecher line, **698**
High and low impedance terminations, lines applied, **527**
Higher harmonic excitation, linear radiator, **538**
Hollow cylinder, radiation conditions, **766**
Hollow cylindrical dipole, input resistance and reactance, characteristic impedances, **742**
Hollow guide, displacement currents and electric lines, 1186
Poynting vector, 1199
Homing radio beam, **56**
Homogeneous potential wave line, like current and charge waves, **496**
Horizontal antenna, 917
Horizontal current loop, magnetic dipole, **153**
Horizontal half-wave dipole curtain, **590**
Horizontal linear radiator, quasi-perfect and actual earth crust, 918
Horizontal polarization, **28, 551**
no angle of wave incidence, total refraction into dielectric medium, 815
over wet soil at 100 Mc/sec, tabulated, 954
path triangle, 877
reflection coefficient, actual values, 829–839
wave transmission over wet soil, 936
(*See also* Horizontal and vertical polarization)
Horizontal polarized wave, **28**
Horizontal slot aperture, vertically polarized waves caused by, 1036
Horizontal and vertical linear receiving antennas compared, 793
Horizontal and vertical polarization, 794
actual and image antenna currents, 845–853
actual and perfect earth crust, 912–928
arriving wave, down-coming, due to ground-reflected and direct effects, 797
characteristic functions, 921
comparative derivations, wave reflection and refraction, 798–824
defined, **17,** 796
exact definition (Fig. 220), 796, 798
step 1, 798
height-gain factor, curves, 1080
magnitude and phase, complex reflection coefficient, 843
for different wave incidence, 855
over flat ground, compared, 876–880
phase lag, 860
reflecting plane of medium separation, 797
reflection coefficient, general formulas, 829–830
relative image current curves, 849

Horizontal and vertical width of radio beam, **604**
Horn, conical, 1182–1184
electromagnetic, **31,** 1132–1184
apex of, 1184
Cornu spiral and Fresnel integrals, 1045
effective area, 1184
gain, 1184
guide matching, 1221
mouth, field condition, **784**
optimum, 1184
pyramidal, 1183
radiator and current sheets, **357**
rectangular, 1182–1183
Humid atmosphere, 974
Humidity decrease and temperature increase, 969–977, 981–997
Humidity effect, troposphere, 970
Huygens elementary diffraction radiator, 1089–1091
Huygens elementary radiator, radiation vectors, 1090
Huygens elementary wavelet source, 1092
Huygens factor, 1062, 1089, 1095, 1096, 1102, 1105, 1108, 1113, 1118, 1119, 1122, 1138, 1141, 1142, 1146
forward, effect, 1062
main beaming, 1034
generalized, wave-guide diffraction, 1135
Huygens-Fresnel wavelet effect, 1021
Huygens-Kirchhoff factor, vanishes, 1096
Huygens principle, **17,** 1019
Huygens radiation intensity, 1091
Huygens radiators, 1094
Huygens wavelet, **17,** 1021
center, and wavelets, 1020–1022, 1037, 1040, 1089
method, electromagnetic diffraction (P. S. Epstein), 1066
Hybrid TEM wave, definition, **94**
Hygrometric and barometric tables, 975
Hyperbola, confocal, applied, **551**
Hypergeometric functions, **327**
and Legendre functions, applied to integral equations, potential theory, **327**
$x = \cos\theta$, applied, **328**
Hypergeometric series, **327**
convergence for values smaller than unity, **328**
Hypothetical field reference value, 938
Hypothetical point radiator (singlet), **611**
Hypothetical symmetry of curls of electric and magnetic field vectors, **16**

I

Iams, H., and H. B. Devore, on microwave optics between parallel conducting sheets, 1241
Ice, dielectric constant, **395**
Identity, of curl of cross product electric or magnetic vector, vector analysis notation, **26**
of curl and rot notation, **198**
div $(\dot{\xi} \times \dot{H}) \equiv H \operatorname{curl} \dot{\xi} - \dot{\xi} \operatorname{curl} \dot{H}$, **201–203**
of $q(q+1)$, **338**
in vector analysis and divergence notation, **198**
Image, antenna, 830
effects, 929–930, 933, 944
of aerials, 830
blurred, 822, 850
electric current sheet, **360**
negative and positive, **360**
surface, **360**
magnetic current sheet (surface), **360**
ray, 932
relative antenna current, curves, vertical and horizontal polarization, 849
Image and actual antenna currents, 830
vector addition, 848
vertical and horizontal polarization, 845–853
Imaginary angles, corresponding to amplitude decay in perfect dielectric wave medium, 805
interpreted, **61**
Imaginary currents, aperture mouth, parabolic reflector, 1028
Imaginary reception plane, 1021
Impedance, characteristic (*see* Characteristic impedance)
concept (Schelkunoff), electromagnetic wave, moving in medium, **4, 7, 36, 39–45**
converters, quarter-wavelength type, **698**
current and voltage, driven and parasitic radiator, **652**
determination, magnitude and phase, **421–424**
electromagnetic wave, in atmosphere, **4, 8, 32, 36**
impinging copper plane, normal, 898
input, of double line at far end, **410**
internal, plane conductor, 1196
matching, with quarter wave, line section, **437**
wavelength transformer, **435**
to a feeder, **428**
mutual, linear radiators, **652**
per unit length, double line, **407**
transformation, quarter-wavelength section, **438**
voltage and current, several driven radiators, **652**
(*See also* Wave impedance)
Imperfect dielectric attenuation guide, **123, 124, 128, 136, 138,** 1214
Impressed electric field, **131, 296, 775, 780, 782**
on closed circuit, differential and integral relations, **775**

Impressed field, **296, 356**
and actual field, **357**
Incidence, angle of, and angle of reflection, **57**
generalized Snell's law, **57,** 802
Snell's law, 793
of wave (*see* Wave incidence)
Incident power of radio beam at plane of medium separation, 794
Incident radio wave, polarization distinction, 790
Incident and reflected current, disturbances, **422**
waves, **417**
Incident and reflected field components, at places above ground reflection, 884
Incident, reflected, and refracted rays, planes of constant phase, 792
Incident, reflected, and refracted waves, different mediums, derivation of formulas, vertical and horizontal polarization, 796–826
Incident traveling waves, 895
Incident wave train for homing beam, **56–63**
Inclination factor, wave-front radiator, 1061
Inclined plane wave-front incidence, aperture radiator, 1115
Inclined primary wave-front incidence compared with perpendicular incidence on aperture area, 1158
Inclined slot aperture, 1036
Increase of magnetic displacement of wave front, **367**
Index of refraction, **56,** 929
atmospheric, **6, 56,** 891
changes, wave duct, 993–997, 1236–1240
complex, **56,** 838
curves and solutions, 984
determination, **395**
different dielectric mediums, 793
distilled water, **394**
and earth crust effect on radiation pattern, 917
electromagnetic (*see* Electromagnetic index of refraction)
formula and values, 799, 800–802, 804, 808, 810, 811, 814–817, 821, 822–824, 859
general (dissipative) wave medium, **46, 56, 58, 394,** 821, 859, 917
curves, 842
formula, **58,** 794
when medium behaves electromagnetically like a good conductor, 859
general value, 839–842
gradient, tropospheric conditions, **61,** 998
ionosphere, 977
magnitude and phase, tabulated, dissipative wave medium, 841
modified, **6,** 994, 995, 996, 1239
nonconductive medium, **394**
Index of refraction, ocean water, 859
radio beam over mountains, **56–63**
relation and expressions, angle of incidence and angle of refraction, two dielectrics, **799**
for wave trapping, **6,** 995, 1239
relative, formulas, 794
relative value of medium, **57–63**
smaller and larger than unity, applied to electromagnetic lenses, 1240–1242
special case, perfect dielectric medium, 804
for superrefraction, **6,** 995–996, 1240–1242
troposphere (*see* Tropospheric index of refraction)
Indirect and direct field components, 930
Indirect and direct wave contributions, 869
Indirect ray, **10,** 831, 845, 849, 851, 852, 855, 858, 860, 868, 877, 881, 884, 887, 921, 930, 933, 942, 944, 948, 949, 951, 956, 957, 959, 965
Induced voltage, dipole gap, **651**
method, for computing radiated power, compared with Poynting vector method, **515, 516**
for radiation, **188–190, 192, 235, 515–516, 608**
in radiator, formulas, **651**
Inductance, and capacitance, parallel-wire and coaxial lines, compared, **484**
closed circuit, **776**
external and internal, **714**
Induction field, **3, 7, 173**
of a radiator, **233**
Induction law (Faraday), **219**
Induction theorem, **356,** 1256
Schelkunoff, **356,** 1256
Infinite long-wave components, classic Rayleigh phase and group velocity concepts explained by, **385**
Infinite number of resonance frequencies, cavity resonator, 1185
Infinite parallel-wire line, radiation effects, **488**
Infinitesimal linear radiator, **31, 87, 144, 158–165, 243**
elementary, **31, 161, 243**
Inhomogeneous absorbing wave medium, 997
Inphase and antiphase, excitations, computations, linear radiators, **578**
field contributions, zonal areas, 1024
half-wave radiators, formulas, **672**
Inphase conditions, electric and magnetic fields, **41**
space fields, 946
Inphase excitation, antenna arrays, formulas, **605**
half-wave radiator sections, by means of radiation suppression, **566**
radiator, **10**

Inphase excitation, two parallel half-wavelength radiators, radiation resistance, **667**
Input admittance and impedance, double line, compared, **415**
Input effects, double line, used for stubbing and matching, **416**
Input impedance, biconical antenna, **76**
conical antenna, **73**
double line, **408, 409**
impedance load at far end, **410**
and admittance, **415**
short-circuited far end, **409**
driven and parasitic parallel linear half-wave radiators, **692**
looking into open-ended double line, **409**
open and short-circuited line, **449**
relation, for an impedance-loaded line and matching, **433**
Input voltage to output current ratio, transfer or driving impedance of line, **409**
Instantaneous power, **36**
Insulator of metal, **449–451**
for half-wavelength radiator, **702**
for quarter-wave section, **701**
Integral, Ci (x), **512–514, 537–538, 563–567, 629, 643–648, 658–670, 676–679, 694, 712–714, 722–725, 732–734, 740**
$\overline{\text{Ci}}$ (x), even integral solution, **712–714, 722–726**
cosine and integral logarithm, formulas, **512, 643, 644, 646, 658, 665, 666, 712, 722**
divergence within a volume and integral of vector field strength on enclosing surface volume divergence theorem $\oint \bar{D} \cdot d\bar{S} = \int \nabla \cdot \bar{D}\, d\tau$, (known also as Gauss theorem and Green theorem), **108–110, 119–121, 130–132, 197, 352**
Ei (jx), **644–648, 658–662**
electric field, **15**
equation, solution, cylinder, radiator current distribution, Hallén and King method, successive approximations, **709–734**
linear radiator, sinusoidal current distribution, **91**
vector form, closed current loop, **778**
form, Maxwell equations, **15, 200**
boundary conditions, **65**
Fresnel, 1041–1047, 1064, 1159–1170
curves, Cartesian coordinates, 1166
spirals (Cornu), 1041–1045, 1047, 1048, 1054–1058, 1073, 1159–1162
table, 1042
li (x), **644**
li (e^x), **644**
logarithm, **643**
with purely imaginary argument, **643**
magnetic field, **15**
method of successive approximation, **711, 717–719**
Integral, odd and even wavelength distributions, linear radiator, **506**
by parts, applied to radiation problem, **513, 514**
Si (x), **537–538, 644–648, 658–670, 676–679, 694, 696, 712–714, 722–726, 732–734, 739–741**
sine, formula, **643, 644**
solutions, linear radiator, using Ci, Si, and logarithmic functions, **641–648**
and moduli signs, **647**
radiator cylindric, Ci, $\overline{\text{Ci}}$, and Si functions, and formulas, **712**
transformations leading to Ci and Si functions, **643–648**
radiator application, **532**
Integration, contour, **343**
Intensity, field (*see* Field intensity)
radiation (*see* Radiation intensity)
Interatomic force, **152**
Interface, boundary conditions, **65, 307–309, 353, 367,** 790–791, 798, 802, 809, 814, 1196–1197
two different, air masses, index of refraction, 997
dielectric mediums, 791–794
wave mediums, 798–824
Interference, factor, Lecher line radiator, **504, 505**
Fresnel zones, 1172
wave (*see* Wave interference)
Interior or scalar product, **197**
Interlace of two circular wire radiators, resultant effect, **753**
Internal impedance, plane conductor, 1196
Internal ohmic resistance and reactance, cylindric radiator, **713**
Intrinsic current sheet, **353**
Intrinsic propagation (three-dimensional) constant, **40, 44–46, 48–50, 53–56, 58, 70, 96, 164, 380**
Intrinsic wave impedance, same as characteristic space wave impedance, **7, 17, 36, 40–45**
Invariant vector, **20**
Inverse distance, effect, **87, 91, 158, 163, 171,** 938
taken out of integral, but not phase factor, **91**
function substituted by more flexible function, **707**
Inverse square distance law, field amplitude value, receiver and transmitter antenna heights compared with distance, elongated path triangle, 876
instead of inverse distance law for certain fields, 890
Inversion of temperature, 969, 988, 994–997, 1238–1239
Ion, **152**
Ionic medium, resonance, 979
Ionized medium, **4,** 977–980
selective absorption, 979

Ionosphere, dielectric constant and refraction index, 979
equivalent dielectric constant, 979
field energy due to collisions, 979
group and phase velocity, 979
index of refraction, formula, 979
phase velocity larger than velocity of light, **395,** 979
$I_n(x)$ and $I_q(x)$ functions, **323,** 1267
IRE standard wave-guide nomenclature, **259–262, 305, 307–310, 374, 375, 377–379, 381–384,** 1185–1233
Isotropic elementary radiator, **7, 534, 611, 623, 630**
Isotropic medium, **4–5, 38, 109, 120**
Isotropic point radiator, **7, 534, 611, 623, 630**
Isotropic point source, directivity, compared with half-wave and Hertz doublet radiator, **534, 535**
radiator and gain measurement, **8, 623**
Isotropic properties, **4–5**
Isotropic radiator, watts for reference standard, **626**
Isotropic reference point-source radiator, **7–8**
actual and equivalent power directivity, **630**
applied to, antenna array, **623**
aerial gain, **624**
Isotropic region, homogeneous, **497**

J

J, current density, electric, and displacement current, **11–12, 28, 33–34, 52, 75, 99, 100, 136,** 140, **199, 228**
linear surface and volume current, **199, 215, 217, 228, 350,** 354, **357**
j, imaginary unit and unit vector, **12, 17, 197,** 1246, 1268–1271
J antenna, aperiodic feeder, **702**
$J_{-0.9}(0.1)$, series, **758**
$J_{\frac{1}{2}}(x)$ etc., order $(1/n)$ or $(2n + 1)/2$, **330, 332, 339**
$J_1(0.1)$, series, **756**
$J_1(p)$ circular diffraction radiator, 1138–1146
$[J_1(p)/p]$ circular wave-front alignment, 1150–1151
$J_1(\rho) - J_{-1}(\rho)$, relation, **756**
J_m, magnetic current density, displacement magnetic current in volts, **11,** 16, **306**
linear, **350, 354, 357**
$J_{n+\frac{1}{2}}(x)$, parameter half of odd order, expressions, **339**
$J_n(x)$, Bessel function or cylinder function, of first kind, nth order or parameter n and argument x, **304, 309, 322, 323, 330, 331, 704, 756,** 1255–1256, 1265–1267
Bessel function, positive order or parameter, **331**
$J_n(x)$, formulas and expansions, **331,** 1255–1256, 1265–1267
n an integer or not an integer, **330, 332, 339**
$J_{-n}(x)$ Bessel function, negative order or parameter, **331**
$J_{-n}(x) = (-1)^n J_n(x)$, series expansion and Gauss function, **331,** 1255–1256
$J_n(x)$ and $J_n'(x)$, **307, 309, 310**
$J_n(x) + jN_n(x) = H_n^1(x)$, Hankel function, **497**
$J_n(x)$ and $N_n(x)$ curves, **304**
$J_n(aK)$ and $N_n(aK)$ curves, **304**
$[J_n(aK)]/[N_n(aK)] = [J_n(bK)]/[N_n(bK)]$, coaxial line, 1232
$[J_n(rK)]A + [N_n(rK)]B$ Bessel solution, coaxial guide, 1231
$J_n(rK)$ and $J_n'(rK)$, guides, 1212
$J_n(\rho)$ formula, for $n = 1, 2, 3, 4, 5,$ **757**
applied general unrestricted, $J_{1.1}(0.1)$, numerical expansion (series), **757**
where n is not an integer, **756**
expansion, **756**
$J_n(\rho)$ and $J_0(\rho)$, circular wire radiator, **749**
$J_0(x)$ and $J_1(x)$, functions of the first kind, order null and one, **304, 309, 322–323, 330–331, 496, 704**
$J_0(x) + jN_0(x) = H_0^1(x)$ and $J_0(x) - jN_0(x) = H_0^2(x)$, Bessel functions of third kind, Hankel functions, **339**
$J_0(x)$, $J_1(x)$, and $J_0'(x)$, functions applied, **304, 309, 322–323, 330–331**
$J_0(k)$ curve, numerical scales, significant arguments for vanishing $J_0(k)$ values, applied, **704**
cylindric hollow radiator, **771, 774**
disk radiator, **761, 764**
significant argument x for vanishing Bessel factor, **704**
$J_q(x)$ function, **323**
$J_{\rho+1}(\rho) - J_{\rho-1}(\rho)$, relation, **756**
$AJ_1(x) + BK_n(x)$ for Bessel equation, n an integer, 1, 2, 3, **330**
$AJ_n(x) - BJ_{-n}(x)$ for n not an integer, **330**
standard comparison Bessel equation, **330**
$\{d[J_0(z)]\}/dz$, series, 1137
Jahnke, E., and F. Emde, formulas and tables, **322, 331, 643**
Jeffreys, H., wave duct, 1250
Jordan, E. C., cylindric slot diffraction radiation, 1036, 1095, 1182
Joulean heat loss, **3, 35, 46, 49, 52, 70, 118, 125, 128, 130–131, 133, 135–138, 140, 142,** 1196, 1203

K

K, expression, circular guide, 1193, 1213, 1224
rectangular guide, **382,** 1215
functions, **323, 331,** 1193, 1213, 1224
κ, κ_0 dielectric constant, **5**

$k_1J_n(x) - k_2N_n(x) = Z_n(x)$, Bessel and Neumann functions, cylindric guide, **304**
general Neumann function, **304**
$K_n(x)$, function, **330, 331**
$K_q(x)$, function, **323**
$\kappa_r - 1$, difference, troposphere, 974
relation, humidity present, 976
Kennelly-Heaviside ionic upper atmosphere, **4**, 977–980
Kilogram to standard pound conversion, 976
Kilometer to statute mile conversion, 969, 976
Kinematic rotary action given by curl of vector, 986
King, R., polarized field of arbitrary polarization, **787**
King, Blake, and Harrison, theories and calculations, cylindric radiator, **705**
King cylindric radiator theory, applied to half-wave cylindrical dipole, compared with customary gap impedance formulas, **716**
method, two parallel cylindric dipoles, zeroth order of approximation, and action of dipole on other dipole, **719**
requirement for factor Ω, **711, 724**
zero-order approximation, **717**
Kirchhoff diffraction formula, **311**
Kirchhoff diffraction theory, 1060
Kirchhoff equation, **311**
classic, must satisfy boundary conditions of electric and magnetic field vectors, **319**
general wave, solution, **292–296, 321–346**
Kirchhoff-Huygens forward effect, end-fire line-up of linear radiators compared, 1062, 1089, 1095, 1096, 1102, 1105, 1108, 1113, 1119, 1122, 1138, 1141, 1142, 1146
Kirchhoff-Huygens forward factor, 1062
generalized, guide diffraction, 1135
relation of discontinuity, **311**
restricted relation, diffraction, 1087
theory applied to aperture occupied by electromagnetic wave front, 1080
vanishes, 1096
wave equation, with discontinuous variation, **311**
Kliatzkin, on antenna radiation, **648**
Klystron field accelerations and decelerations, **4**
Kock, W. W., metal lens, 1241

L

λ/2 line section, properties, **191, 428**
λ/4 line section, applied, **450**
characteristics and relation to characteristic impedance, **436**
effect, **436**
λ/4 line section, formulas and properties, impedance matching, **191, 437**
properties, **409, 411, 428, 435, 449, 450**
short-circuited, applied to insulation, **450**
λ/8 line section, properties, **412, 428, 436**
λ/8 open-ended double line, shunted with λ/8 short-circuited double line on feeder, causing antiresonance for fundamental frequency, **450**
λ/12, double line, applied, **450**
open-ended double line, in shunt with λ/6 short-circuited double line on feeder, suppresses fundamental and third harmonic frequency, **450**
3λ/4 line section, properties, **42**
Lamb, H., basic solution, wave-duct modes, normal mode, 1240
Laplace coordinate transformation, **20, 27, 145, 616**
applied to radiation vector, **616**
Laplace equation, **149–151, 299–301, 340,** 1273–1274
applicable to concentric and parallel-wire line, **475**
and Poisson equation compared, **300**
reduced to two dimensions, a means to solve wave-guide problems, **301,** 1200
in terms of potential, **300–301**
two-dimensional, applied to guide, 1200
Laplace expansions, 1274
Laplace operator (*see* Del operator; Hamiltonian nabla)
Laplace and Poisson equations compared, **300**
Lattice, space, normally disposed of, **592, 594**
structure, half-wave radiators in space, **592**
Law, Ampère, **11, 14, 196**
Ampère-Maxwell, **11, 103**
Biot-Savart, **164, 217**
Coulomb, **213**
Faraday induction, **11, 103, 200**
Gauss (Green theorem), **22, 24–25, 108–109, 120, 122, 196**
Green, same as Gauss theorem and Green theorem, **108,** 1279
Snell, 793, 802, 980
Leak, electromagnetic, 964
Leakage, field, wave duct, 959, 964
Lecher feeder, parallel-wire line, self- and mutual radiated power, **192**
Lecher line, characteristic impedance dependent on wire spacing and diameter, and on ratio of medium permeability and dielectric constant, **404**
and coaxial line, C and L values, compared, **484**
conditions, standing waves, **501**
double, standing current distribution, **501**
elementary section, electric radiation field contributions, **501**

Lecher line, embedded in ideal distilled water, characteristic impedance, **404**
low and high impedance points, **698**
standing waves, electric radiation field contribution, for go conductor, **501**
odd and even integer values, standing modes, electric radiation field contribution of go wire, **502**
radiation field (electric) contribution, half-wave section, return wire, **503**
radiator, direction factor, **502–504**
interference factor, **504, 505**
relative phase factors, go and return wires, **502**
total electric radiation field contributions, go and return wires, **501, 502**
Lecher wires, double parallel-wire line, characteristic impedance, **404**
feeder, actions on field point, **499**
half-wave linear radiator, **698**
linear current distribution, equivalent length, by means of equal areas, **518**
formulas, **403**
infinite length, radiation effect, **488**
Laplace equation, **475**
longitudinal field action, **95**
mutual radiation, effect, **192**
resistance, **192–193**
outgoing wire, self-radiation, **192**
parallel wires, proximity effect, **414**
radiation, **191, 193–194**
radiator, directivity of each wire by itself, without mutual radiation contribution, **505**
formulas, effect of spacing between go and return, **508**
interference factor, mutual line effect on radiation, **505**
Poynting vector has constant value for fixed value of spacing, **508–509**
radiation resistance, **510**
self-radiation resistance, **192**
returning wire, self radiation, **192**
total electric radiation field, self- and mutual radiation effects, **505**
solution, classical Kirchhoff theory, **6, 9, 79–80, 97**
Maxwell's field theory, **70, 80, 97, 492–498**
traveling wave, excitation, **521**
radiation effects, **521–524**
Left-handed-screw space wave propagation, **786**
Left- and right-handed polarization, **786**
Left- and right-handed screw rule, vector product, **197**
Legendre equation, **327–332, 338, 340, 341**
second solution, **328**
Legendre function, **322, 327, 328, 341**
P and *Q* polynomials, **328**
zeroth, first, and second order, **340**
Legendre polynomials, **328**
Lens, antenna, 1241
electromagnetic, metal and dielectric, 1240–1242
based on, optical lens refraction, 1241–1242
wave-guide action, 1241–1242
shape and design, 1242
Level lines and surfaces, **21**
Lewis, W. D., and H. T. Friis, scanning abberation, 1241
li function applied to linear radiator, **644**
Limiting angle, 933, 944
Line, arbitrary double, and Schelkunoff antenna, **76–86**
biconical, **76–86**
closed integral and surface integral relations, Stokes's theorem, **25**
coaxial (concentric) (*see* Coaxial line)
condition at voltage maximum and minimum looking toward load end, **699**
conical, against metal plane, **73–76**
double (*see* Double line)
electric force, **3, 68, 74. 80, 85, 95, 101, 102, 230, 349, 351, 353, 367, 374, 377, 403, 735, 737, 744,** 1186, 1187, 1189–1192, 1194, 1219, 1221, 1230, 1233
guided, relations, TEM waves, **68, 69, 77, 81, 285–291, 485**
parallel wire (*see* Parallel-wire line)
plane against cone, **73–76**
propagation formulas, **363**
Q value, **415, 487**
and radiation, **402–528**
relations, review of, **406–416**
ribbon, **67–73**
Line angle, generalized and double, **372**
Line constants, *C*, *L* and Z_0, bicone, Schelkunoff, **78**
coaxial line, **403, 407, 484**
Lecher, parallel wires, **403, 407, 484**
Line impedance (*see* Characteristic impedance, line)
Line integral, **14, 15, 75, 78, 83, 98, 101–103, 105–107**
closed, **13–15, 198, 350, 776–778**
applied to closed circuit with radiation effect, **777**
electric and magnetic field, **219**
definition of, **25**
electric and magnetic force, **13–15**
magnetic force, **101–103, 139, 219, 349–351, 353**
open, **25**
and surface integrals, **104**
of vector, 974
Line measurement, admittance applications and formulas, **438**
positive and negative conductance concepts, **438–439**
standing-wave concepts, **416–435**

Line radiation, based, on differential radiator, **31, 86, 235, 241**
on two linear differential radiators, **187–191**
Lecher wire feeder, **191–194**
power lines and power frequency, **491–498, 519–521**
stationary waves (standing-wave distribution), **456–469, 498–517**
traveling waves, **456–469, 521–525**
Line of sight, **346,** 887
condition checked numerically, 872
and curved earth crust, explanation, 871
Line solution, classical Kirchhoff theory, voltage and current relations, **40, 68, 69**
Maxwell's electric and magnetic field relations, **65, 68, 200, 284–291, 491–498**
Line and space propagation, compared, **284–291, 363**
formulas, **284–289, 363**
Linear antenna, **8–10, 89–91, 166, 529–744, 762–765, 767–768, 773–774**
array, factor determining broadness of vertical directivity, **603**
forward-thrust factor, **603**
current distribution, **531**
current node, **529**
effective (or equivalent) length, applied numerically, **166,** 874
height effect over actual ground and different wave incidence, 881–885
radiation, **89–91, 166, 529–744, 762, 767, 773**
Linear and coil radiators, helical wave propagation, **786**
Linear conductor (*see* Conductor, linear)
Linear coupled radiators, self- and mutual parameters, **656–662**
Linear current, distribution, equivalent length by means of equal areas, **518**
element, field formulas, applied to linear radiator, **540**
Linear curtain radiator, radiation formulas, **595**
Linear differential radiator, **31, 86, 235, 240**
formulas, **86**
Linear dimensions, expressed in operating wavelength, **180, 508**
Linear divergence and gradient, **203**
Linear electric current density, **350**
Linear elementary radiator, excited inphase and antiphase, fields and directivities compared, **573–575**
Linear end-on array, **446**
Linear half-wave dipoles, over metal reflector, radiation resistance, 1010
Linear half-wave filament (thin) radiator conditions, **767**
Linear half-wave radiator, and circular wire radiator, comparison with respect to factor 60 of linear radiator, **754**
parallel and collinear alignments, formulas, **671–684**
Linear half-wave radiator, shunt and series feeding, **697**
Linear polarization, **549–551, 785–788**
Linear radiators, **20, 32, 91, 230**
alignment, group characteristic, graphical and analytical solution, **581**
backed up by perpendicular metal reflector, 1016
Bechmann solution, cylindrical coordinates, **235**
both driven, formulas, **652**
Ci, li, and Si functions, **643–648**
and coil radiators, helical wave propagation, **786**
conditions, **456**
coupled, self- and mutual parameters, **656–662**
directivity, **625**
applications, **543–545**
formula, unhindered radiation space, **546**
patterns, fundamental and higher harmonic excitations, **545**
eight aligned give 8 fold amplitude maximum effect and 64 fold power effect, **634**
electric field formula parallel to radiator, **664**
elementary (*see* Elementary linear radiator)
elementary theory, self- and mutual effects, half-wave current distributions, **662–666**
equal-phased in front and reflector row, **638**
excited in harmonic distribution, **91, 529–547**
harmonic and higher harmonic current distribution, **538**
Hertz vector, electric field computation, **657–658**
solution, **642**
integral solutions, using Ci, Si, and logarithmic functions, **641–648**
isolated, directivity formula, **538**
maximum and minimum conditions for fundamental and higher modes, **546**
mutual impedance, **652**
effect, self-radiation resistance and self-reactance, **653–654**
resistance and reactance curves, **691**
normal to reference metal plane, 863–867
not parallel to other radiator and not collinear, formulas, **607–609**
one driven and other parasitic, formulas, **652**
polarization, **17, 549–552, 785–788,** 796–824
primary source and imaginary secondary radiators, 1028
projection through metal plane reflector, 1015
radiation power, **625**

Linear radiators, relative amplitude directivity, odd and even current distributions, **623**
several in parallel, aligned, directivity, **579–583**
short length, **230**
sinusoidal current distribution, general case, **642**
staggered, **658–661**
standing waves, Ci and $\log_{10}$ functions used, **506**
thin, current distribution, **642**
two, both driven, **652**
radiated power, self- and mutual watts, **666**
vertical and horizontal disk radiator combination, directivity in Cartesian patterns, **763**
over ocean surface, 911
wave front, with aperture, 1036
Linear wave polarization explained by Lissajous, figures, **549–550**
Lines, not matched, reflected and advancing wave actions, **364**
Lissajous figures, giving general elliptic, circular, and linear polarization explanations, **549–550**
Load admittance, numerical, **442**
and its conjugate, **443**
Load impedance determinations, practical hints, **424–427**
Lobes, positive and negative, **765, 771**
of radiation, **640**
secondary radiation, **10**
and side lobes, inphase excitations of two linear radiators, **577**
linear radiator alignment, **581**
linear radiator excited in harmonic distribution, **545–546**
partially suppressed radiation, **565, 568**
two equal linear radiators excited in phase and of equal amplitude, **580**
Location of stub for line measurements, **440**
Log and cosine integral functions applied to linear radiator problems, **506**
$\log_{10}$ and Ci functions, **512, 514**
Logarithmic decrement, of wave in dissipative wave medium, **138**
in wave propagation, general, **138**
Logarithmic space decrement, power factor and phase difference in dissipative wave medium, **138–143**
Lommel functions, 1254
Long-distance wave propagation, atmospheric refraction, **6,** 987, 993, 994–997, 1236–1240
due to diffraction, 1018, 1052–1060
wave duct, superrefraction, 994–997, 1236–1240
Long-time experimental electromagnetic pulse echoes, ionosphere, **368**
Longest cutoff wavelength, cylindric wave guide, about half the inside guide circumference, **305**
TE waves, **305**
Longest natural wave for $TM_{1,1}$ mode, **305**
Longitudinal complementary waves applied, **335**
Longitudinal component of forward-tilted electric vector of electromagnetic wave causes surface wave-guide actions, 900
Longitudinal current, conical surface, biconical line, **738**
Longitudinal displacement current, guide, 1186
Longitudinal electric wave, **92, 377, 381**
along the direction of wave propagation, **93**
electric n, m waves or transverse $TM_{n,m}$ waves, **383**
Longitudinal H wave, 1185
Longitudinal H or TE waves and longitudinal TM waves, compared in table, **335, 381**
Longitudinal $H_{0,1}$ wave, **381**
Longitudinal linear current density, **349, 350, 354, 355**
Longitudinal magnetic wave, along wave propagation direction, **93**
and electric guide waves, **383**
Longitudinal ribbon current, **69**
Longitudinal slots in cylinder, horizontal pattern, 1036
Longitudinal surface wave, 906
Longitudinal and transverse, fields, 1185
magnetic line effects in guides, 969
wave-guide current, 1204
Loop, elementary, equivalent height, **573**
small, and Hertzian doublet radiator, **160**
for mapping magnetic field distributions, **156**
Loop aerial (small), formulas, **571–573**
Loop antenna, **572**
Loop radiator, small magnetic dipole, **153, 156, 161, 163**
Loop and rod exciter, guide, 1219
Lorentz-Lorenz law for molar refraction, 971
Loss, dielectric, wave guide, 1214
Loss angle, in characteristic wave impedance, dissipative wave medium, **42, 43, 46**
earth crust (solid), **42–56, 117–138**
general medium, **46**
leaky dielectric, **42–56, 117–138**
ocean wave medium, **47–56, 117**
in wave propagation constant formula, **46**
Loss current, **140**
Love, A. E. H., diffraction, 1065
equivalence principle, **356**
induction theorem, **356**
generalized (Schelkunoff), **356**
solution for electromagnetic diffraction, 1066

Low frequency and VHF and UHF effect on closed circuit, **774–780**
Low and high impedance terminations, on Lecher line, **698**
on lines applied, **527**
Low-level wave duct, 1236–1240
Low wave-duct and attenuation increase for 3-cm waves, 996
Lower atmosphere, refractive index, 970
gradient conditions, 994
Lower zonal areas (Fresnel) are about equal, 1027
Lowry, L. R., rhombic Bruce antenna, **458**

M

Magnetic charge, **154, 162**
concentration (assumed) and electric charge concentration compared, **358**
Magnetic current, **11, 14**
density, **11, 94, 224**
element, important relations for space point, **611**
moment, **158,** 1062
(*See also* Magnetic and electric current)
Magnetic current sheet, **356**
no experimental evidence, **348, 355**
self-radiation effect, **619**
Magnetic dipole, **144, 153, 159, 161, 163, 180**
array, effect for thin slot aperture, 1036
effect, due to electron spin, **153**
horizontal current loop, **153**
and magnetic potential, **155**
moment, **153, 162**
radiator starts with principal TM wave, **293**
small current loop, radiated power, **159**
starts with longitudinal principal TE wave, **293**
wave impedance, **160**
total field, in neighborhood and between-field region, **168–180**
(*See also* Magnetic and electric dipoles)
Magnetic displacement, current, **11, 14, 15, 115**
vanishes, **272**
increase rate, **367**
per unit area, **367**
Magnetic double layer, **154, 157**
potential, **157**
Magnetic doublet, **144, 153, 154, 158–161, 163–165, 168–187**
elementary case of layer current, loop radiator, **144**
summed up (integrated) for finite current loop, **144**
Magnetic and electric current, density distributions, radiated power formulas, **620**
elements, application, **612**
basic space relation, **611**
Schelkunoff, **356, 361**
Magnetic and electric current, sheet, **348**
concepts, applied to Huygens wavelet source, 1089
mutual radiation effect, **619**
power directivity, formula, **619**
Magnetic and electric dipoles, elementary, electric and magnetic field components, **163–165, 182–183**
compared, **144–194**
features, **180–187**
general comparison, **144–194**
Magnetic and electric (for other entries beginning with this phrase *see* Electric and magnetic)
Magnetic energy density, **120**
Magnetic field, **97**
circulation, **11, 15, 23, 95, 101–105, 349, 351, 353, 377, 403,** 1187, 1190–1192, 1207
per unit area, current sheet, **350**
components, computed from current function, **471–473**
energy flow, **301**
along Z axis in Cartesian and cylindric coordinates, **301**
contribution, **35**
and displacement current and condenser radiation, **97**
of electric current, derived from magnetic vector potential, **487**
and electric field conditions compared, **314**
energy, along double line, two-dimensional Poisson equation, **490**
explored by small loop (small magnetic dipole), **156**
intensity formulas, **614, 615**
relation, in terms of electric and magnetic vector potentials, **357**
represented by electric current sheet, **348**
small circulations summed up (integrated), **139**
and surface current, **65–67**
(*See also* Electric and magnetic field)
Magnetic flux density, **196**
definition and units of, **196**
solenoidal condition, **313**
Magnetic H wave, guide (TE wave), **93**
induction, **196**
Magnetic lines of force, **3, 14, 25, 73, 80, 95, 101, 102, 105, 139, 349, 351, 353, 377,** 1187, 1190–1192, 1207, 1219
Magnetic loop, **95, 101, 105, 107**
Magnetic mass, **154, 162**
Magnetic moment, **155**
elementary current circulation, **157**
per unit volume, **154**
Magnetic polarization, **196, 222**
contribution over vacuum, **196**
as magnetization, **219, 313**
of medium, **196**
potential (magnetization potential), **149, 219, 222**

Magnetic pole, **154**
Magnetic potential, **155, 224**
gradient, **306**
total, of magnetic shell, **155**
Magnetic radiation vector, **614–620,** 1090
guide diffraction radiator at reception locations, formula, 1129
Magnetic reluctivity, **196**
Magnetic retarded vector potential, **775**
applied to closed circuit radiation, **782**
electric current density relation, **612**
radiation vector relation, **613**
Magnetic shell, **151, 154, 156**
a double layer of positive and negative magnetic masses, **154**
magnetic moment, **155**
magnetic potential, **155**
Magnetic space reluctivity, **196**
Magnetic surface density, **155**
Magnetic type, of field, **229**
relations, **314**
of polarization, 796–798
of polarization vector, **219, 222, 313,** 1240, 1248, 1275–1276, 1277
Magnetic vector potential, **87, 214–218, 222–240, 249, 253–259,** 267–268, **290, 356**
and components, **87, 215,** 217–218, **226–240**
and electric scalar potential method, for finding electric and magnetic fields of aerial, **229–240**
and Hertz potential interrelated, **252, 290**
mks dimension, **224**
retarded, **164, 214, 253–258,** 300
a means for accounting for both radiation and near field of lines, 495
for solving elementary electric dipole fields, **164**
used for finding magnetic field of a current, **487**
(*See also* Electric and magnetic vector potential)
Magnetic vectors, of electromagnetic wave in plane of wave incidence, 796
in terms of current density, **252, 290, 350, 354**
Magnetization, **313**
of atom, **153**
axis, **154**
definition of, **196**
and electron spin, **153**
of medium, **313**
vanishes for vacuum, **313**
of volume density, **154**
Magnetization potential, **153**
applied to wave duct, 1238–1240
and electric polarization potential combined, **312**
Magnetized shell, **154**
Magnetized volume, **154**
Magnetizing convection current, **152**
Magnetomotive force, *H* circulation, **349**
Magnitude, complex quantity analyzed, **480**
electric and magnetic field, expressions for, **45**
general index of refraction, 839–842
and phase, determination, impedance, **421**
reflection coefficient, wet soil, above 40 Mc/sec, 834
and time phase, vector plot, reflection coefficient, vertical and horizontal polarization, 855
of vector, **20**
Main beam width, end-fire beaming, **639**
Main feeder of three dipole gaps of half-wave radiators, does not cause equal inphase gap currents, **695**
Mann, C. R., diffraction, 1034
Mannebeck, C., first correct radiation expression for power line, **493**
on traveling-wave radiation controversy, **493**
Map measure, electromagnetic space beams, 998
for path difference of path triangle, 891
Matched single feeder, general tap joint to half-wave radiator, **466**
Matched single-line feeder, radiation resistance, **466–468**
Matching, for capacitive source, **438**
with closed stub, formulas, **430, 431**
with double stub, **445**
guide, 1221
different mode and cross section, 1221
half-wave dipole with quarter-wave section and cup, **449**
for an inductive load, **438**
load impedance, to a feeder, **428**
to a line, single stubbing, **428**
section, guide, 1221
transformer, quarter-wave Lecher and concentric line sections, **701**
Mathematical formulas, **195–361,** 1222–1226, 1232, 1247, 1254–1279
Mathieu function solution applied, 1063
Matter effect for electric and magnetic polarizations, **196**
Maximum available field power in unit space volume, **37**
Maximum directivity, alignment of linear radiators, solution, **636**
Maximum electric field effect, circular radiator, **756**
Maximum field effects, formulas, vertical and horizontal polarization, 967
intensity, longer ranges, graphical solution, 930
reception orientation, loop antenna, **20**
and zero field effects, 897
Maximum and minimum locations on feeder, **427**
Maximum and minimum voltage effects along line, **427**

Maximum power transfer, concentric line with optimum Q value, **481**
load impedance equal to conjugate characteristic impedance of supply, **452**
violation for mismatch, **427**
Maxwell and Ampère, boundary conditions, **65**
curl relations, **11, 147–151, 200**
Maxwell's component equations, basic for wire-guided and unguided wave propagation, **284**
Maxwell's curl equations, Cartesian coordinates, **148**
curvilinear coordinates, **147**
cylindrical coordinates, **148**
reduced and applied to parallel multiple conductor system, **470–471**
simplified, **150–151**
spherical coordinates, **149**
Maxwell's displacement current, **196**
density, **11**
and Faraday's induction law, **196, 316**
Maxwell's equations, **311**
Cartesian coordinates, **146, 148**
curvilinear coordinates, **147, 151**
cylindric coordinates, **146, 148**
elementary, differential forms, **11, 200**
integral from, **15, 200**
space points where fields change continuously, applied to wave obstructions, 790
spherical coordinates, **146, 149**
Maxwell's field concept solution and classical line solution, **291**
Maxwell's field equations, applied to single and coupled closed circuits, **773–774**
applied to transmission line, **68**
and energy quanta taken collectively, 1019
Mean value of difference of electric and magnetic volume field energy content, **120**
Measure of magnetization related to electron spin, **153**
Measurements using standing-wave ratio concepts, **416–435**
Medium, effect on operating wavelength, **49–52, 54**
electromagnetic properties, **5**
metallic, wave properties, **43–45, 349, 476–484, 487,** 1193–1199, 1203–1214
mountain, **56–63**
nondispersive properties, **50, 366**
ocean, **46–52, 136,** 801, 824, 835, 836, 838, 840, 842–845, 852, 858, 860, 900
polarizations, electric and magnetic, **196**
contributions over empty space, **196**
quality (Q value), **5, 52**
rock, **46**
separation surface, obstructed wave propagation, 790
reflected, refracted, and incident waves, 791
Medium, space substance effect causing electric and magnetic polarizations, **196**
vacuum, dielectric constant, **4**
for wave (*see* Wave medium)
Medium constants, dielectrics and conductors, applied, **476**
Medium dissipation, power factor, **140**
to useful field energy ratio, **143**
Mediums, different dielectric materials and wave propagation, 791
Meridian directivity, **624**
half-wave radiator, **239**
linear radiator, **625**
Merit, dissipative wave medium (Q value), **140 142**
double line, **415**
Mesh circulation, elementary, **139, 155–156**
Meshes of current and larger current loop, **155 156**
Mesny-Chireix antenna, 1290
Metal, electromagnetic properties of, **4–7, 43, 45, 65, 154, 476–484, 487,** 789, 830, 854, 863–867, 895, 896, 898, 899, 917, 918 928, 956, 957, 968, 1187, 1193, 1196–1199, 1203–1214
possible dielectric constant of, **6, 16**
Metal cylinder, slit aperture, radiation, 1036, 1095, 1182
Metal lens, 1240–1242
and delay lens, 1241
Metal and open slot radiators, **784,** 1091–1125, 1145, 1160–1170
Metal plane, surface impedance and resistance and skin depth, 1196–1199
Metal reference plate simulating ideal reflector, real value of reflection coefficient, as in optics, 920
Metal reflector, characteristic value, 924
and horizontal half-wave radiator, 923
and linear radiator, 830, 855, 864, 867, 896, 912–928
and perpendicular radiator, radiation resistance, 1016
plane, distance effect from radiator, 1005
effect, radiator and pickup half-wave images, 1006
field curves, 1005
and vertical and horizontal linear radiator, 1012
solid and wire, **787**
Metal screen aperture, wave guide, 1116, 1117, 1173
Metal skin, guide, power loss, 1208
Metal tubes, 1185
Metallic earth crust, action may be approximated as far as reflections are concerned, 855
Metallic electromagnetic mirror, **10, 476–479,** 830, 855, 864, 867, 896, 912–928
Metallic harmonic suppressor, **450**
Metallic insulation and harmonic suppressor, lines, **449–451**

Metallic insulator, for half-wave radiators, **702**
quarter-wavelength section, **701**
Meter · ampere output, **362**
Meter-kilogram-second coulomb (mks) system (*see* Mks units)
Meter · volt and meter · ampere concepts compared for linear radiator, **283**
Microwave optics, 1241
Milazzo, S., on polarization of electromagnetic waves, **787,** 795
Millibar, unit, 989
Millikan, R. A., on diffraction, 1034
Minimum and maximum location on feeder, **427**
Minimum reflection effect, vertical polarization, 849, 851, 852, 855, 858, 860
formulas, 827
Minor lobe, gain, **627**
Mirror, complex, **10, 52,** 797, 801–804, 809–810, 821–825, 831, 834–863, 868, 876, 877, 881–917, 920, 928–958, 965–967
dielectric, **10,** 791, 793, 796, 798, 799, 805–809, 810–816, 817–820
dissipative wave medium and earth crust, **10, 52,** 797, 801–804, 809–810, 821–825, 831, 834–863, 868, 876, 877, 881–917, 920, 928–958, 965–967
metallic, 830, 855, 864, 867, 896, 912–928
Mismatch, power condition in line, **427**
wave impedance at plane of medium separation, 814
Mks units, **7, 195,** 1243–1251
applied to electromagnetic quantities and relations, **195–196**
conversion to classical cgs system of units, 1252
review, **195–196**
tables, 1252
Model aerial measurements, **297**
Modes (*see* Wave guide, modes)
Modified antenna standard, based on maximum power directivity, **627**
Modified deficit duct, 996
Modified electromagnetic path, doubly modified, 998
oblique coordinates, 998
wave paths, equivalent flat earth and oblique coordinates, 997
Modified index, of refraction, low-level duct, 971, 977, 987, 991–997, 1238–1239
short-wave propagation, 994–995
standard condition, modified wave path, 1238–1240, 1253–1254
Modified radio beam, construction of, 988
ray, 990
Modified ray triangle, actual spherical earth, for modified flat earth, 998
Modified standard of radiator, **627**
Modulation, AM, FM, and PM waves, relation to group and phase velocity, **386**
Modulation product resemblance, circular wave-front array, 1148
Moduli signs, integral solution, **647**
Moisture content of troposphere, 971
Molar polarization, 973
Molar refraction, Lorentz-Lorenz law, 971
Moles, number of, per gram molecular weight, 973
Moment, atomic, **152**
charge, compared with current moment, **516**
current distribution, 1029
element, **161**
differential radiator ($i\,dl$ and $q\,dl$), **152**
doublet (Hertz), **152**
electric current element, **152, 161**
electric and magnetic dipole, **153, 161**
elementary magnetic current, elementary current loop, **162**
magnetic current element, **158**
Momentum per unit volume of space charge, **23**
Monochromatic light and slit, 1018
Morse, P. M., and P. Rubenstein, electromagnetic diffraction, 1063
Mosaic, of elementary Huygens radiators, 1094
of radiation centers in space, **592, 594**
Motion, random, **152**
Mountain-refracted beam, **56–63**
Mountain-wedge, electromagnetic diffraction, 1050–1060
Mouth, parabolic radiator and equivalent current sheets, **350, 352**
rectangular guide, diffraction radiator, 1126
Multipath wave propagation, **10,** 791, 793, 796, 797, 831, 834, 845, 849, 851, 852, 855, 858, 860, 868, 877, 881, 884, 887–895, 930–958, 959, 965, 968, 969
Multiple conductor transmission system, **469**
Multiple mode, **738**
Multiple parallel wires, radiation, **469**
Multiple propagation path (*see* Multipath wave propagation)
Multiple reflections, analyzed, 887–895
reception at transmitting center, 887
Multislot electromagnetic diffraction radiators, 1118
computations for several slots, tabulated, 1119
Mutual antenna impedance, effect on self-radiation resistance and self-reactance, linear radiator, **653–654**
Mutual dipole gap impedance, **652**
Mutual effects between half-wave radiators, tabulated computations, **696**
Mutual impedance, and components, two linear parallel radiators, formulas and curves, numerical values, **691**
linear radiator, **652**
resistance and reactance, **691**
Mutual index of refraction, **58**

Mutual power from half-wave radiator on another half-wave radiator, **667**
Mutual radiation effect, electric and magnetic current sheet, **619**
Mutual radiation resistance, current loops, **781–784**
expanded, **519**
and reactance, parallel half-wave radiators, formulas and numerical applications tabulated, **696**
table for half-wave radiators, **672**
of two elementary electric dipoles, **190**
two parallel half-wave radiators on each other, **667**
Mutual and self-effects, dipole, elementary theory and formulas, **662–666**
Mutual and self-impedance, coupled linear dipoles, **650**
formulas, linear radiators, numerical, **666–671**

N

n different doublet effects, **240**
n equal collinear radiators, group characteristic formula, **587**
N parallel conductors, electromagnetic radiation, **469**
N slot radiators, formula, 1114
N_0 and N_1 functions, **304, 322, 323, 330**
$N_q(x)$ function, **323**
Nabla operator, Hamiltonian, **22, 198,** 1271–1272
product, 1271, 1273, 1274
scalar point function, 1271–1272
second differential, 1272
vector, 1272
Narrow aperture, 1019
Natural and equal phasing of linear radiators, **547–549**
Near-field region (or neighborhood induction field region), **163, 171, 174, 175, 177, 185, 186**
electric field, general ellipse equation, **555**
Negative elementary closed-shell charges, **152**
Negative and positive lobes, **765, 771**
Neper, unit, **362**
Neper attenuation, dissipative wave medium, **53**
unit explained, **362**
Neper loss (attenuation), general or dissipative wave medium, **30, 136, 138**
Neumann function, **295,** 304, **309, 329, 330, 332**
general, and Bessel general function, **304**
with no integer parameter, **295, 322, 323**
roots, **304**
Neutralization, reactance and susceptance effects by stubs, **428,** 430, **431, 433, 448**
reactive effects of radiator, **649**
Newton, unit of mks force, **7,** 1243
Node, current on linear antenna, **529**
Node, pseudo, **697**
Nomenclature, wave guide, IRE recommendation, **304–308, 374–379, 381–383,** 1185–1232
Noncircular wave, **307**
Nondispersive wave medium, **50, 399**
and dispersive wave medium compared, **399**
Nonlinear probe indicator, correction, **426**
Nonmagnetic dielectric, characteristic impedance, double line, **403, 405**
Nonpolar gas, density, 970
Nonrectilinear wave propagation, 969
Nonresonant and resonant conductors, **699**
Nonuniform field relation, power transfer in double line, **73**
Normal atmospheric conditions, field escape, **3,** 994
Normal dispersion, **366**
Normal field components at boundary, **352**
Normal primary wave-front and inclined wave-front incidence on aperture radiator compared, 1115
Normal space lattice, **592, 594**
Norton, K. A., and A. C. Omberg, on elliptical ground reflection Fresnel zones, plane earth surface, 1172
on surface waves, 958
Nucleus of atom, steady rotation about, **152**
Numeric computations of delay, 879
Numeric parameter for arbitrary elliptical polarization, **787–788**
Numerical applications, dissipative wave medium, **42, 45–56, 117–138**
field losses, **42, 45, 46, 117–138**
ground, **16–17, 29–31, 33–35, 36, 40, 42–56, 70, 98, 118–138**
ocean medium, **41–44, 46, 47–49, 52, 54, 400,** 823, 824, 835, 836, 838–844, 852, 857, 859, 860, 861, 862
path triangle, direct and ground-reflected ray, 871–874
phase velocity, **29, 44–56, 380, 384, 392–394, 397–400,** 906–912
propagation constant, **30, 44–56,** 906–912
wave propagation, **45–56,** 906–912
wave reflection, at surface of medium separation, 897–899, 903–912, 913–929, 935–958
Numerical conductance, **436**
Numerical load admittance, **442**
and its conjugate, **443**
Numerical susceptance, open-ended and short-circuited stub, **443**
Numerical values, earth crust, electromagnetic properties, **12, 16, 30–31, 34, 36–37, 39, 41–45, 47–52, 54–56, 59–62, 128–130, 136–138,** 833–863, 900

O

Ω, factor, King theory, cylindric radiator, **710**

Obstacle, diffraction, 1028
wave (*see* Wave obstacle)
Obstructed (partially) space radiation, 789–1017
Obstructions (*see* Wave obstruction)
Ocean, condition, quasi-dielectric effects, 837, 947
dissipative wave medium (*see* Medium, ocean)
earth surface, Brewster dip, 852
electromagnetic properties, **47, 49**
reflector, 946
water, dielectric constant, **6**
index of refraction, 859
Q value, **6, 136**
wave medium, **394, 400**
Odd and even half-wave distributions, linear radiator, directivity and electric field formulas, **544**
Odd half-wave distributions, Lecher radiator, radiated power, **505**
Oersted, electromagnetic cgs unit for magnetic field intensity compared with mks unit, 1252
Ohmic resistance, internal, cylindric radiator, **713**
Ohm's law, electromagnetic field, **4**
moving in space, **4**
generalized, wave impedance, dissipative wave medium, **17, 40, 43, 45**
Omnidirectional antenna, **623**
Omnidirectional radiator, equivalent power directivity, **630**
Omnidirectional reference standard antenna, watts for standard, **626**
One meter of wave propagation, **362**
One-to-one impedance line transformer, applied to coaxial and parallel-wire line conversion, **526**
Open- and closed-line integral, **25–26**
and radiation, **779**
from condenser, **101**
Open and closed stub, matching, **432**
Open-ended double line, formulas, **416**
Open-ended linear conductor conditions, **456**
Open-ended quarter-wave line section, double line, **415**
Open-ended and short-circuited double lines, oscillatory variations with length of line or stub, **409**
for stubs, formulas for input admittance and impedance, **416**
Open rectangular wave guide, diffraction radiator, 1124, 1126–1136
Open stub, matching, **431**
Openings, apertures, in wave obstruction, **784**
rectangular guide, diffraction radiator, 1126
Operating frequency, wave guide, **384,** 1188, 1190, 1193, 1213, 1215, 1222–1225
Operating wavelength smaller than cutoff wavelength, 1187
Operation ∇, on a scalar, 1271
on a vector, **23,** 1272
Operator ∇, **197,** 1271–1275
directional derivative of a scalar, **197,** 1272
Optical Fresnel relations, reflection and refraction, applied to radio waves, 790–796
Optical reflector (*see* Mirror)
Optimum electromagnetic horn, formulas, 1184
Optimum gain, half-wave dipole and reflector, 1287
Optimum Q, concentric line, dimension effect, **487**
Optimum range of frequencies, wave duct, 996
Optimum ratio, coaxial line, **483**
Order N of harmonic excitation, linear radiator, **557**
Orientation, effect, of cubical dissipative wave medium, **29–35**
of individual half-wave radiators, **595**
of particular wave medium, **33**
in space of linear differential radiators, **607**
for wave pickup aerials, **29–35**
Orthogonal confocal hyperbolas and orthogonal confocal ellipses, **551, 556**
Orthogonal coordinates and systems, **18, 20, 144–146, 215**
for Maxwell's equations, **144–151**
transformations into other systems, **146–151**
Orthogonal curvilinear coordinates, **145–147**
applied, **215**
Oscillation constant, and characteristic line impedance analogies, **7**
of empty space, **391**
Oseen and Hallén theories, cylindrical radiators, **705**
viewpoints on radiation, **709**
Oseen model, cylindrical radiator, **709**
and Hallén models, potential distribution and current distribution, **710**
Outgoing and reflected electric and magnetic fields, Schelkunoff bicone line, **78**
Outgoing and reflected electromagnetic waves, 895
Outgoing and returning wave functions, **337**

P

P polynomial of Legendre equation, **328**
P and Q functions, **328**
Parabolic cage reflector and linear radiator along focal line, 1028
Parabolic curvature applied to earth crust, 871–872
Parabolic cylindrical antenna, 1182
Parabolic earth curvature, numerical application, 872

Parabolic projector, different openings, beaming, table, 1031
diffraction pattern, 1032
electromagnetic, wavelet concept applied, 1028
main beam width, table, 1034
radiating system, 1028
radiator, **350**
reflector causes Huygens wavelets, 1021
Paraboloid beam width and aperture width, curves, 1035
Paradox of radiation, **649–650**
Parallel conducting sheet, microwave optics, 1241
Parallel half-wave radiators, mutual effects, formulas and numerical applications tabulated, **696**
three, computations, **695**
two, mutual radiation resistance and reactance, formulas and table, **670–671**
Parallel-line to coaxial-line conversion, **526**
Parallel metal planes and electromagnetic power transfer conditions, 968
Parallel and perpendicular polarization, 882
general case, 881
Parallel polarization, analyzed, 884
general case, 881
perfect reflector, analyzed, 965
perpendicular wave incidence, reflection and refraction coefficients, 803–804
reflection coefficient, 798, 800–804, 808, 811, 814
refraction coefficient, 808–809, 812–813, 960
Parallel ribbon line, **68**
and biconical line compared, **79**
relation to characteristic impedance, **73**
Parallel and series feed, half-wave radiator, **697**
several identical inphase half-wave radiators, radiation resistance, **673**
slot radiator array, 1112
possible applications, 1116
Parallel-wire feeder, self- and mutual radiated power, **192**
Parallel-wire field effects analyzed by means of two differential linear antiphase radiators, **499**
Parallel-wire line, and Laplace equation, **475**
Lecher, **95, 97, 191,** 403, **407, 484**
attenuation formula, 414
standing-wave current distribution, **701**
traveling wave, excitation, **521**
radiation, **521–524**
Parallel-wire radiation, application of Green's theorem, **490**
Parallelepiped, **109, 197,** 215
Parasitic antenna, **9, 652,** 654, **688, 692–694**
and driven radiators, **652**
numerical application, **688–694**
Parasitic radiator (*see* Parasitic antenna)
Partial differentiation and partial integration applied to radiation, **513–514**
Partial harmonic radiation suppression, quarter-wave end radiators, **565**
Partial integration, explained and applied, **511–514**
Partial radiation suppression, **548, 557–568**
Pass and attenuation region, wave guide, **374**
Path curvature, modification, 987
Path difference, **10,** 845–849, 864, 867–887, 888–895
between reference distance and current element, **612**
of direct and indirect ray, 933–937
map measure method, 891
electric, **446**
Path triangle, formed by radiation and reception centers, reflection point on earth crust, 868
horizontally polarized waves, 877
spherical earth, diffraction, 1074
of wave in earth crust, **56–63,** 899–912
Pattern, amplitude and power directivity, half-wave radiator, **633**
diffraction of parabolic projector, 1032
directivity (*see* Directivity patterns)
field (*see* Field patterns)
Fraunhofer (*see* Fraunhofer patterns)
Fresnel (*see* Fresnel patterns)
radiation (*see* Radiation patterns)
Pearcy, T., on wave duct, 1237
Pekeris, C. L., on wave duct, 1237
Penetrating field power, copper plane, and cylinder and rectangular tube, 898, 1193, 1196–1199, 1203–1214
Penetration, depth of, into copper medium, **51, 477**
into dissipative wave medium, **51**
of potential barrier by electrons, 997
of wave, into copper plate, **51, 477,** 899
into conductive medium, **48,** 898–899, 1193, 1196–1199, 1203–1214
into dissipative wave medium, **11, 28–31, 33–37, 41–63, 70, 111–133, 135–143,** 895–912
into ocean wave medium, **137**
into partially conductive medium, **45–52**
reference value, **49**
Per meter wave propagation, **362**
Perfect dielectric wave medium, group and phase velocity relation, **381**
Perfect ground conditions, 915
Perfect metallic reflector, reflection coefficient is ± 1, depending on polarization, 855
Perfect reflection, surface of medium separation, definition of, 792
Permeability, nonferromagnetic rock, **29**

Permeability, relative, **5**
unit explained, **65**
wave medium, **4–5**
Perpendicular polarization, and parallel polarization, 798–824
general case, 881
reflection coefficient, 798, 800–808, 811, 814
refraction coefficient, 808–809, 812–813, 960
Perpendicular wave incidence, applied to copper sheet reflector, 899
on copper plane, penetrating field power, 899
parallel polarization, reflection coefficient, 803–804
refraction coefficient, 803–804
perpendicular polarization, reflection coefficient, 803–804
refraction coefficient, 803–804
reflection coefficient, 803, 814
Phase, fixed, surface of, **369**
relative, **9, 16–17, 30**
between electric and magnetic field, conductive wave medium, **43**
dielectric wave medium, **17, 41**
dissipative wave medium, **17, 36, 42, 43, 45, 46**
earth crust, **17, 36, 42–43, 45–46**
Phase advance, and amplitude distortion, certain wave propagation conditions, **394**
injected, **446**
Phase angle, **10, 16, 30**
due to path difference, **10,** 845–850, 875–880, 885, 888–895, 899, 913–920, 930–937, 939–947
general medium, **30**
line impedance (lengthwise) and line admittance (crosswise) per meter, **407**
total, linear antenna alignment, **581**
vertical and horizontal polarization, 945
wavelengths of propagation, **453–454,** 872, 878–880
Phase constant, **362, 365**
in air and feeders compared, **446**
dissipative wave medium, **137**
formula for line, **371**
guide direction, **381**
Phase delay, wavelet, dependent on wave incidence on aperture, 1116
Phase difference, found from phase front definition, **445**
Phase distribution, double line, **437**
Phase factor, 805, 929
applied, 875
cannot be taken out of integral like inverse distance factor, **91**
fixed and variable factor of, **612**
Fresnel diffraction, important, 1157
Phase factor, imaginary angle, 805
impure, 822
real negative exponent, 806
and wave obstacle, 789
Phase and group velocity, **50**
applications, to guide modes, **380–385**
to TE waves, **376–377**
curve, wave guide, **384**
details, **380**
formulas applied, to cylindrical guides, **378–379**
to different systems of propagation, **371–379**
illustrated, **369, 371**
(*See also* Phase velocity)
Phase integral method, T. L. Eckersley, 1066
Phase jump (abrupt) at Brewster angle of wave incidence, pure dielectric wave medium, 854
reflection coefficient, half-wavelength jump, 931, 933–934, 951
Phase lag, **137**
vertical and horizontal polarization, 860
Phase reflection factor, horizontal and vertical polarization, 894
Phase shift, positive and negative, **446**
Phase shifters applied to antenna array, **446**
Phase velocity, **366, 368–379**
conductive wave medium, pronounced, **51**
dissipative wave medium, **54–56**
formula, **29**
earth crust neighborhood, 907
electromagnetic lens, 1240–1242
explanation, curved radio beam, 982
extreme values, **392**
formula, **366**
based on voltage and current concepts, and Maxwell's field concepts compared, **402**
and frequency, **394**
general (dissipative) wave medium, **29**
larger, than group velocity, **386**
than velocity of light, **368**
partially conductive wave medium, **45, 49, 50, 52–56**
rectangular guide, used as diffraction radiator, 1127, 1196
TM modes, cylindrical wave guide, **380**
troposphere, 976–977
vacuum, **7**
to velocity of light, ratio effect on directivity, Beverage single-line wave pickup, **458–461**
(*See also* Group and phase velocity)
Phasing and alignment, consecutive radiators, **593**
equal and natural, and equivalent network for radiation resistance, **686**
of feeders, **412, 427–428, 430, 431, 433, 435–445, 448**

Phasing and alignment, half-wave radiators, front and reflector plane conditions, **502**
transmitting antennas, and reflectors, **448**
by phase distribution along feeder, **700**
and spacing of radiators along a coordinate axis, **593**
by stubs, **412, 427–435, 436–445**
Physical interpretation of mathematical formula, **11–20**
Physical length and equivalent length compared, **518**
Physical meaning, of curl of vector, **22–24**
of divergence of vector, **22–24**
Physical terminals of lines and complementary waves, **492**
Pickup direction finder (loop), orientation at different distances in near- and between-field region, **20**
Pierce, J. R., on traveling-wave tube, **417**
Pistolkors, A. A., radiation resistance, **648**
Pistolkors ring-shaped slit diffraction radiator, 1280
Plane, of constant amplitude, **366**
and plane of constant phase of wave front, 791, 793
of constant phase, **365, 366**
not coinciding with plane of constant amplitude, **366**
for incident, reflected, and refracted rays, 792
of medium separation, 791
obstructed wave media, 790
of reception centers, diffraction, 1082
Plane aperture, exposing primary wave front, general conditions, 1154
Plane conductor, internal impedance, 1196
Plane and curved earth, wave spread, 885–887
Plane earth attenuation factor, 1074
curves, 1076
Plane electromagnetic wave, **4, 119, 317**
power flow per unit area, **64–65**
Poynting vector, **64**
propagation, **64**
along a definite direction, **44**
Plane metal reflector, relative field ratio, 1005
Plane wave, **8, 19, 64, 113, 302**
directional and associated electric and magnetic field gradients, **40**
and electric and magnetic current sheets, **367**
fixed phase for phase velocity concept, **386**
Plane wave front, **8, 113, 509**
concept, **250**
magnitude of Fresnel zonal areas, 1027
polarization, **785**
radiator, any contours, 1146
uniform electric current illumination, 1028
with wavelets, beam width, 1033
Plunger in stub, **428, 430–433, 448**
PM and FM side pairs, **399**
PM wave and phase and group velocity, **369**
Poincaré, H., diffraction theory, 1034
Point charge, **152**
moving, **152**
Point function, **20, 24,** 1272
Point radiator, hypothetical, **611**
Point-source radiator, **7, 611**
Point-source reference radiator, antenna gain, **624**
Point wavelet sources, Huygens principle, 1019
Poisson current density relation regarding flow function, **301**
Poisson equation, **151, 299–301,** 1272
current density and flow function, **301**
for fixed current density, **301**
and Laplace equations compared, **300**
potential and space charge, **300**
two-dimensional, applied, **489–490**
Pol, B. van der, and H. Bremmer, on diffraction, 1065
field intensity formula, **346**
wave diffraction formula, **346–348**
Polar directivity in plane of circular radiator, **752**
Polar field patterns, meridian, linear radiator, reference metal plane, 866–867
in presence of reflections, 913
radiation, vertical and horizontal polarization, 920, 953
rectilinear and propagation with refraction, 1003
two elementary linear radiators, excited in antiphase, different spacings, **571**
Polar and rectangular plots, relative field amplitude directivity, cylindric metal surface radiator, **771**
Polarizability, 971
Polarization, angle of, 940
arbitrary, **786**
atom, **152**
circular, **549–550, 785–788**
of incident wave and pickup system, 795
definition of, customary radio engineering, **17**
distinction, incident radio wave, 790
distribution, uniform, 1184
experimental sharp wedge electromagnetic diffraction, 1051–1060
electric (*see* Electric polarization)
electromagnetic wave (*see* Electromagnetic wave, polarization)
elementary linear radiator, near-field region, compared with finite linear radiator, **551**
elliptical (*see* Elliptical polarization)
general, **17,** 792
generalized equivalent length, **787–788**

Polarization, gyration, **786**
helical, **785–788**
horizontal (*see* Horizontal polarization)
linear, **549–551, 785–788**
magnetic (*see* Magnetic polarization)
molar, 973
parallel (*see* Parallel polarization)
per cubic meter, troposphere, 972
plane wave, perpendicular and parallel compared with horizontal and vertical polarization, 798
potential, **90**
radio wave, 794
resultant, **785–788**
right- and left-handed, **786**
separation, 815
shift, wave guide, 1221
spiral, **785–788**
type of, **785–788**
vertical (*see* Vertical polarization)
volume density of, **239–240**
and wave front, linear radiator, **549–557**
of waves, **28, 785–788**
Polarized field, arbitrary polarization, **787**
Polynomial, Legendre, **328**
Positive and negative lobes, **765, 771**
Positive phase shift compared with negative shift, **446**
Positron, **240**
Possible fields within guide, **357**
Potential, current, and Hertz functions, applied to space radiation, **270–273, 280**
guided and unguided, **284–291**
for Hertz vector, **284, 300**
electric, Cartesian, cylindric, and spherical coordinates, **300**
double layer, **157**
heterogeneous wave, dying off along line, **496**
homogeneous wave, along line, **496**
across magnetic double layer, **157**
relation, retarded volume charge concentration, **300**
retarded, **300**
Power, complex, definition and derivation method for electromagnetic field, **210–214**
dissipated, per cubic meter of dissipative medium, **138**
per meter distance, coaxial line, **482**
field, maximum available in unit space volume, **37**
hump movement, **387**
instantaneous, **134**
flow, **113, 115**
mutual, of two half-wave radiators, **667**
penetrating into copper plate, formulas, 899
phase difference, **138**
radiated (*see* Radiated power)
Power directivity, and amplitude directivity, table, half-wave radiator, **535**
antenna array and radiated power, **621**
aperture radiator, normal and inclined primary wave front, 1115
average, linear radiator, **626**
circular and rectangular wave-front radiators, 1141
in desired direction, **627**
diffraction, 1094
formula, electric and magnetic radiation vectors, **616**
Poynting vector and distance to field point, **616**
half-wave radiator and directivity of isotropic radiator compared, **630**
linear radiator, different harmonic modes, **545**
with and without partial radiation suppression, half-wave end radiators, **565**
maximum undeterminate, solution, 1094
one and two half-wave radiators, **633**
and Poynting vector relation, **619**
radiation intensity, electric and magnetic radiation vectors, distant field effects, **617**
Schelkunoff, electric and equivalent magnetic radiation vectors acting, **617–619**
total, for electric and magnetic current sheets, **619**
in watts per unit solid angle, electric radiation vector and operating frequency, **616**
Power factor, **138**
and phase difference, wave in dissipative medium, **138**
Power and field advantages in db, antenna array, **621**
Power and field gain, antenna array, **620**
Power flow in watts, of electric elementary dipole, **158**
of magnetic elementary dipole, **158**
Power gain, 1183
of two radiators over a single linear radiator, **632**
Power guide, rectangular, 1201
Power line, mutual radiation resistance, **519**
radiated power, **521**
self-radiation resistance, **519**
Power loss ratio, mismatched to matched line, **427**
wave guide, 1204
Power radiation, Lecher wires, with half-wave current distributions, **506**
with odd half-wave current distributions, **505**
Power relation, electromagnetic waves moving in medium, **4, 111–117**
Power transfer, of incident, reflected, and refracted radio beam at plane of medium separation, 794

Power transfer, for a nonuniform field, double line, **73**
by p_z and $p_{x,z}$ concepts, **284**
in radiation system, **451**
ribbon double line, **71**
between two reflectors, angle of wave incidence effect, 968
useful, of a double line, in field region and not in conductors, **71**
Poynting electromagnetic energy flux, for half-wave radiator in unobstructed wave medium, **505**
and surface divergences of enclosed volume, **38**
Poynting radiation, applied to multiple parallel conductors, **470**
vector applied, **71**
Poynting theorem, general, **19, 41, 201, 208, 249**
Poynting vector, **19, 39, 115, 122, 196**
air and distilled water, **41**
applications, **35, 536, 562, 628,** 886
to coaxial line, **480**
to go and return of Lecher line, **506**
to linear radiator, **415, 505**
to wave-spread solution, 886
average value, **629**
classical definition of, **131**
complex, **122, 127, 128, 196, 209–214**
dissipative wave medium, numerical examples, **128–133**
real part applied to coaxial and parallel wire solution, **474**
solution, 1275
components, **35–39, 203–204, 206–209**
conical antenna, **73**
dielectric wave medium, **35**
direction cosine, **208**
directivity, current and inverse distance, **536**
dissipative wave medium, **35, 42**
divergence of, in pure dielectric wave medium, **35**
effective electric and magnetic field formulas, antenna array, **621–622**
expressed in electric field and characteristic wave impedance, certain type of dissipative wave medium, **36**
field components, applied to Lecher line radiation, **499**
field in distant radiation region, **648**
field energies, **35**
field energy contribution of go and return, Lecher line, **507**
formulas, **249–258**
radiation vector components, **615**
for Lecher wires, and fixed value of wire spacing in wavelength, **508–509**
effect of factor, 1-cos δ, **507–509**
effect of spacing, **508**
and linear radiator, amplitude directivity, formulas, **623**
Poynting vector, method and emf method, field energy formulas, **648**
moving electromagnetic field energy, **64**
notes and formulas, **201–209**
power directivity relation, **619**
radiation, conical antenna, **73–76**
radiation vectors, **71, 615**
real and imaginary divergence ratio, **123, 125**
real part, **36, 41, 125**
real value of, **75**
power loss along line and guide, **480**
three-dimensional space direction, **508**
time average, **37, 65, 115, 117, 118, 120, 131–138, 629**
wave-front surface product, related to energy continuity, 885
Primary radiation center, 1021, 1022
Primary radiation source location and current sheets, advancing primary wave front, **367**
Primary and secondary radiation effects, **342**
Primary wave front, fictitious current sheets, electromagnetic diffraction radiation, 1092
Fresnel zones on, 1022
mosaic of Huygens wavelets, 1092
normal and inclined to aperture radiator, formulas, 1115
surface of equal phase, 1020
Principal beam of paraboloid as a function of aperture, 1035
Principal and complementary waves, **97, 491–498**
Principal double-line wave and Laplace equation, **475**
Principal Fraunhofer field amplitude pattern, 2- and 5-shot apertures, general formula, 1120
Principal TEM wave, not limited by cutoff frequency, **96**
Schelkunoff double-cone radiator, **76**
Principal waves, **74, 76, 85, 93, 97, 491–498**
bicones, electric and magnetic fields, transverse voltage and longitudinal current, **735**
within spherical boundary surface, **77**
Probe, **425, 427**
linearity, checked by mathematical and experimental sine curves, **426**
correction, **426**
location for any load impedance, **425**
measurement on line, **421**
Product solution, wave equation by means of separation constant method, **294**
Progression, geometric, applied to antenna array, **447**
Progressive divergent electromagnetic field, **332,** 1279
Progressive wave, **112, 235, 270, 282, 293, 315, 317,** 1279

Progressive wave, compared with advancing and reflected waves, **64, 68, 74, 78, 101, 111–117, 274–283, 288, 289, 304, 320, 337, 364–365, 408, 410, 413, 417–420, 422, 456–469, 498, 505, 735,** 806–807, 895–897, 912, 943, 946–951, 956–957, 1013, 1020, 1022, 1026, 1037, 1039, 1048, 1050, 1052–1053, 1057
Propagation, in arbitrary direction, **787**
atmospheric, **250**
characteristics of, **362–401**
classic and anomalous, **784**
curved path, 970
definite direction, plane wave, **44**
dielectric medium, **46**
direction changed due to refraction, **366**
dissipative wave medium (earth crust), **30, 46, 50, 56–63, 117–133, 135–143, 390–391,** 796–829, 839–863, 895–912
gradient, 969
ocean, **48–56, 136–138,** 900–912
phase delay, **365**
of phase or state, **386**
in quasi conductor, **45, 48**
in quasi dielectric, **46**
ratio, **365**
TEM wave, **70, 74, 77, 80, 81, 92–93, 95, 285–291, 292–296, 402, 406–449**
hybrid, **94**
velocity of, **4, 29, 368–401**
at surface of medium separation, 791
Propagation components, **320**
Propagation constant, **42–46, 48, 50, 53, 56, 58, 59, 70, 262, 291, 293, 302–304, 306, 308, 317, 320–326, 362–365,** 374–378, **381, 390, 408–412, 455**
dissipative wave medium, applied, **30, 44, 52–58, 70, 126, 164, 302,** 801, 813, 821
attenuation and phase constant, **30**
general remarks, **362–364**
formulas, dielectric and dissipative wave medium, reflection, 801
generalized radian/meter, double line, **406**
good conducting medium, applied, 477
along guide, **262, 303–304, 306,** 308–309, **374–375,** 378–**381, 493,** 1215–1217
loss angle of dissipative wave medium, **46**
medium quality (Q value), **53**
near earth crust, 904–912
principal and complementary waves, double line with radiation effects, **97, 491–498**
pure dielectric and dissipative wave medium compared, **46**
rectangular guide, **374, 381**
and circular guide, **262, 376**
semiconductor and dielectric, **50**
solution for real and imaginary part, **390**
three-dimensional, **50, 316, 320, 323, 390**
attenuation and wavelength constant, **30, 53**
wave guide (*see* Wave guide)
Propagation constant, wave medium (*see* Wave medium)
over wet soil, 796–826, 836, 842, 849, 855, 858, 860, 900, 917, 936, 939, 941, 942, 954–957
(*See also* Wave propagation)
Proton, **240**
Proximity effect, parallel wires, Lecher line, **414**
Pryce, M. H. L., on wave duct, 1237
Pseudo Brewster angle, formulas, 826–829
plots (curves), 849–852
of wave incidence, significance, 853–860
Pseudo cutoff frequency, guide, 1216
Pseudo nodes, **697**
Pulse, of any kind, **360**
energy, **360**
equivalent, **360**
ideal, **360**
modulation and pure dielectric wave medium, **394**
number of possible complete cycles, **360**
shape, **360**
sharp, causing wavelike disturbance, **366**
single, and harmonic wave, comparison formulas, **389**
steady-state condition, basic to phase velocity, not holding, **389**
width, **360**
Pulsed radio waves, **360**
Pure dielectric, **3, 15, 35, 41, 65, 68, 70, 94,** 791, 793, 796, 797, 799, 800, 805–808, 811–813, 815, 834, 835
Pure diffraction pattern, 1121
Pure electron discharge, **4**
Pure radiation region, **163, 174, 175**
Pyramidal horn, 1091

Q

Q, figure of merit, Q value, definition of, **5, 52, 142**
general dissipative wave medium, **5, 52, 142**
ground, earth crust, **347**
polynomial of Legendre function, **328**
smallest value of concentric line, **487**
transmission line, parallel wires spaced, **486–487**
$q(q + 1)$ identity, **338**
Q coaxial line, frequency and inner diameter effect, **487**
Q and P functions, **328, 331**
Q value, coaxial line, formula for operating frequency effect, **487**
dissipative wave medium, **52, 140, 142, 393–401,** 1076
guide, 1226
lines, **415, 487**
wave medium, **5, 6, 52, 142**
Quality, of dissipative wave medium and phase velocity effect, **5, 6, 52, 142, 393–401**

Quality, of double line, **415**
electromagnetic, of earth crust, 1076
of ground, formula, **347**
of wave medium, formulas, **52–56**
Quantum theory and wave phenomena, 1019
Quarter- and half-wavelength, exposed radiator and sections, concentric line, radiation resistance, **568**
sections with aperiodic feeder, **699**
Quarter-wave cups, dipole matching, **449**
end radiators, partial harmonic radiation suppression, **565**
impedance converters, **698**
inverted, applied, **527**
as radiators and metal insulators, **701**
Quarter-wave Lecher wire and concentric line section as matching transformer, **701**
Quarter-wave line, **438**
between two impedances, matching, **437**
dipole matching, **449**
matching, for positive and negative reactance, **438**
on feeders, **527**
Quarter-wave line section, applied, **527**
to dipole matching, **449**
inserted between E_{min} and remainder of line, **436**
as metallic insulator, **701**
properties, **409**
Quarter-wave radiator tips, **649**
Quarter-wave sleeve, alternate mounting, spaced half-wave radiators, **703**
applications, **527**
dipole gap terminals dynamically insulated from ground by, **703**
as partial radiator, **694–705**
as radiator and as insulator, **701**
Quarter-wave transformer, dipole matching to feeder, **449**
impedance matching, **435**
Quartz (fused), conductivity, **404**
relative dielectric constant, **404**
Quasi conductor, **50**
Quasi dielectric, **50**
Quasi-dielectric behavior of ocean surface, 837
Quasi-dielectric reflector, ocean, conditions, 947
Quasi-perfect bicones, 82
earth crust reflector, 928
Quasi-resistive wave impedance, **41**

R

Radar, return fields discussed, 887–895
Radial electric field components, **77**
in near region, **553**
Radial field, **87, 89**
differential and Hertz doublet, **161, 163**
wave (outward moving), **497**
Radian, solid, **629**
Radiated aperiodic feeder power and actual antenna radiation power compared, **468**
Radiated power, for array, **626, 627**
cone antenna, **75**
conical radiator with horizontal reference plane, **76**
electric, current distribution, **609**
dipole, **158–159**
even and odd standing-wave distributions, linear radiator, unobstructed wave medium, **506**
formulas, electric and magnetic current density distributions, **620**
half-wave radiator, in front and backed up by metal reflector, 1004
unobstructed wave medium, **505**
interaction of electric and magnetic current distribution, **610**
Lecher feeder (parallel-wire line), self- and mutual power formulas, **192**
Lecher radiator, even half-wave distributions, **506**
odd half-wave distributions, **505**
Lecher wires, for one conductor, and mutual effect, **500**
linear radiator, **536, 625**
full-wave excitation, **506**
magnetic current distribution, **610**
magnetic dipole, **158–161**
power directivity and solid space angle, formulas, **621**
power line, commercial frequency, **519, 521**
Poynting vector and induced voltage method, **188–190, 192, 235, 515–516, 608**
and radiation resistance, different excitations, linear antenna, **537**
for reference standard antenna, **626**
relations, Lecher wires, **500**
on systems with partial radiation suppression, **563**
total, electric and magnetic current distributions, **610**
double line, **71**
trapped, ideal ribbon double line, **71**
two linear radiators, self- and mutual watts, **666**
in unobstructed space, **537**
wave-front surface causing, **628**
Radiating horn and current sheets, **357**
Radiation, action, **3, 19, 101**
circular wire antenna, **747–759**
closed current loop, **779**
condenser, **101**
conductivity, apparent, **3**
cylindric metal surface, **765–772**
db gain, **627**
differential linear radiator, **31**
directivity patterns, higher harmonic excitation, **538**
effects of, condenser at VHF's and UHF's, **100–103**

Radiation, effects of, dipole, near wave obstacles, **194**
equatorial plane, several equal radiators, **581**
linear conductor, **461**
standing and progressive wave, **456–461**
electromagnetic discontinuity, **779**
obstructions, 789–1184
energy density, **4**
half-wave radiator, point source and Hertz doublet compared, 938
infinitely long parallel-wire line, **488**
linear antenna, **529**
lobes, **640**
magnetic dipole, **158–163**
field-to-induction field ratio, holding for magnetic and electric dipoles, **173**
modified in same feeder, **492**
multiple parallel-wire system, **469**
along spherical earth crust, **336**
transmission line, **402 525**
unobstructed, **529–788**
summary of, **784**
Radiation advantage, **627**
aerial system formulas, **624**
corresponding db gain, elementary linear radiator and Hertz doublet, **624**
definition of, **623**
formulas, **629**
half-wave linear radiator, **629–630**
integer half-wave distributions, linear radiator, **629**
radiator, **623**
two radiators over a single linear radiator, **632**
Radiation beam, guidance, **56**
Radiation center, **120, 608,** 929–930, 1019–1022, 1037, 1040, 1089
distributed in space, **592**
mosaic, **592, 594**
secondary, 1020, 1021, 1040
Radiation field, **3, 89, 159, 160, 171–175, 186, 187**
electromagnetic, differential Lecher line section, **501**
limit, **19**
of radiator, **3, 19, 233**
region, **3, 19, 173**
Radiation flux per square meter wave-front surface, **4, 25, 35, 36, 39, 41, 65, 112, 125, 203, 207, 209**
Radiation formula, general, **592–595**
linear curtain radiators, **595**
space lattice, applied, **596–599**
use of sine and cosine expansions, **782**
Radiation gain, array, referred to maximum field value, single half-wave radiator, **620**
Radiation intensity, circular aperture radiators aligned, 1149
formulas, radiation vectors, **616**
and power directivity, 1093
Radiation intensity, Schelkunoff and Poynting vector relation, **619**
Radiation paradox, **649–650**
Radiation patterns, over actual and ideal earth crust, 903–949
comparison, 938
cylindric radiator, **766**
dependent upon height-frequency product, 956
disk radiator, **762**
forward-thrust factor, **603**
free-end quarter-wavelength radiators on concentric line feeder, **568**
over perfect and actual earth crust, 912–928
in plane of circular wire radiator, **750**
vertical, actual earth surface, 952
ideal, and wet soil conditions, vertical and horizontal polarization, 957
Radiation power, linear radiator, formula, **465**
standing-wave excitation, **465**
traveling-wave (outgoing) excitation, **465**
Radiation region, **19, 171, 174, 175, 186**
Radiation resistance, antenna arrays, over metal reflector, 1009
aperiodic feeder, power flow to radiator and radiated power, **468**
for waves, **466–468**
and characteristic impedance, guided TEM wave, **67, 73.**
circular loop, **784**
collinear half-wave radiators, **681**
cone aerial, **76**
conical radiator with perpendicular reference plane, **76**
current antinode reference, **563**
current loop, any shape in a plane, **784**
with a gap for driving voltage, **783**
dipole, different from half-wave current distribution, **663**
double integral solutions, parallel-wire line, **511–514**
double line, solution for, **510**
electric dipole, **160, 166**
electric and magnetic dipole, **159–161**
electric power line, **519**
elementary linear radiator, **517**
from field power and reference effective current, **537**
formula, applied to case with partial radiation suppression, **566**
exposed concentric line section radiators, **567**
flat metal reflector, 1010
graphical integration and evaluation of power directivity pattern, **538**
guided ribbon line interspace, **67, 72**
half-wave dipole, **251**
folded, and other multipoles, **662**
half-wave Lecher feeder, **193**
half-wave radiator formula, **192, 251**

Radiation resistance, half-wave radiator, metal reflector curves, with and without reflector, 1013
metal sheet backup reflector, 1009
is 120 times average power directivity, **538**
individual half-wave radiators over metal plane, 1014
infinitely long conical radiator, **76**
irregular half-wave radiator array and phasing, **683**
Lecher radiator, solution, **510**
linear half-wave radiator, depends on feed location, **684**
unobstructed radiation space, **251**
linear radiator, different excitation of, **537**
$\lambda/20$ long, **626**
perpendicular metal reflector, 1016
sinusoidal current distribution, **536**
magnetic dipole, **161**
small current loop, **159**
magnetic and electric dipole, **159–161**
meaning of, **684**
mutual (*see* Mutual radiation resistance)
open-ended double line, short electrical length, **517**
parallel-wire line, traveling waves, **523–524**
plot, inphase and alternate antiphase excitation of half-wave radiators, **676**
power line, commercial frequency, **520**
quarter-wave and half-wave exposed sections of concentric line, **568**
related to characteristic impedance of ribbon double line, **73**
ribbon-line guided, trapped in between-space, **73**
self- and mutual effects, Lecher wires, **192–194**
several identical inphase half-wave radiators, **673**
solution, formula with Ci and Si functions, **538**
standing-wave excitation, linear radiator, **465**
systems with partial radiation suppression, **563**
total, Lecher feeder line, **192**
trapped guided radiation, **73**
for ideal ribbon double line, **33**
traveling-wave excitation, linear conductor, **465**
two parallel half-wave radiators, inphase and antiphase excitation compared, **667**
for waves, aperiodic single feeder, **466–468**
Radiation vectors, absolute amount, **619**
concept, application with details, **614–617**
electric, **620**
and magnetic, guide diffraction radiator at reception locations, 1129
vector potential formulas, **613**
Radiation vectors, L_x pattern, rectangular guide opening, 1128
and Poynting vector relations, **615**
Schelkunoff, **609–614**
wave-guide diffraction radiator, 1128–1131
Radiator, antiphase current excitation, **10**
aperture, 1184
axial cylindric slit aperture, 1182, 1284
circular aperture slit, 1182, 1280
circular wire, current distributions, **753**
different wire length, axial field value, **755**
directivity pattern, Cartesian coordinates, **751**
driven by common terminal voltage, **753**
electric field intensity formula, **749**
value along perpendicular axis of circle, **754**
and linear half wave, comparison regarding factor 60 of linear radiator, **754**
maximum electric field effect, **756**
numerical applications of formulas, **755–759**
polar directivity, plane of circle, **752**
radiation, **747–759**
coaxial, directivity, **773–774**
collinear (*see* Collinear radiators)
combination horizontal disk and vertical linear radiator, Cartesian patterns, **763**
directivity pattern, **765**
consecutive, phasing, **593**
spacing, **593**
cylindrical (*see* Cylindrical radiators)
diffraction, 1118
discone, **728**
disk (*see* Disk radiators)
driven and parasitic, formulas, **652**
numerical applications, **688–694**
elementary (*see* Elementary radiator)
filament, 986
front row and reflector back row, **638**
half-wave (*see* Half-wave radiators)
hypothetical point, **611**
inphase current excitation, **10**
input reactance term neutralized by tuning, **654**
linear (*see* Linear radiators)
magnitude and phase, current, **9**
multislot aperture, computations tabulated, 1119
mutual effects, **9, 656–666**
odd and even half-wave distributions, directivity and electric field formulas, **544**
parasitic, **9, 652, 688, 692–694**
several parallel linear, alignment, directivity, **579–583**
slot, **17,** 1036, 1091, 1097, 1103, 1107, 1112, 1116, 1117, 1120, 1121

Radiator, space, **10**
staggered and linear, **658–661**
standing-wave distribution, Ci and $\log_{10}$ functions, **506**
system, gain formulas, **627–641**
thin and linear, current distribution, **531**
two circular, three-wavelength distribution, resultant effect, **753**
two linear, directivity in equatorial plane, **575–579**
two parallel, collinear and staggered, formulas, **661**
vertical disk and exposed vertical feeder, radiation condition, **762–765**
wavelet, 1089
Radii, boundaries of Fresnel zones, 1024, 1026
Radio beam, curvature, dependent on height gradient of index of refraction, 976
in troposphere, cause of, 981
equivalent, 948
in mountainous territory, **62**
vertical and horizontal polarization compared, different mediums, 796–826
Radio wave, guide and electromagnetic horn, wavelength comparable with dimension, 1035
incident, polarization distinction, 790
polarization, 794
(*See also* Polarization)
Radius effect, cylindric surface radiator, **770, 771**
Ramo, S., and J. R. Whinnery, on fields and waves, 1288
Random motion of electrons, flow or drift, **152**
Ratio, of attenuation, **365**
D/d = 3.6, coaxial line and total power transfer, **481**
$k = E_{min}/E_{max}$, **412–413**
of propagation, **365**
of short to long axis, elliptical polarization, earth crust effect, plotted against dissipative component of earth crust, 900
Ray, antenna image, 932
bending, equation of, 983
curvature of, **6**, 982
formula, 982, 997
upward, condition, 998
electromagnetic and wave obstructions, 789–1017
modification, 1000
of traces, 992
Ray theory, and diffraction theory, concepts, 790
type of propagation, **318–319**
relations of wave reception over actual earth crust, 867–876
wave propagation, **319**
Rayleigh, L., classical group and phase velocity concepts, **385**
Rayleigh wave, 1240
trains, distorted AM effect of, **388**
Reactance, effect on radiator neutralized by tuning, **654**
internal, cylindric dipole, **713**
neutralization, half-wave radiators, **669**
Reactive antenna field stubbed out or neutralized by shortening linear antenna, **649**
Reactive and real, field power of radiators, **651**
resistive components (internal and external), cylindrical dipole, **713–714**
Real and imaginary divergence ratio of Poynting vector, **123**
Real negative exponent, amplitude decay, 806
Real part, of complex Poynting vector, applied to linear radiator, **505**
of field power is radiation power in nondissipative wave medium, **651**
Received current over reflectors, formulas, 913
Received electric field, curved earth, curvature effect included, 899
and location of pickup aerial over actual ground, 928
Receiving aerial, arbitrary linear polarization, **787**
Receiving antenna, array solution, **447–448**
Receiving half-wave dipole and plane metal reflector, 1006
Reception, over actual earth crust, ray concept relations, 867–876
at transmitter location, 887
Reception center, **20,** 1021, 1022
Rectangular aperture, cross section of guide, 1116
double integral solution, 1111
Fresnel pattern curves, half- and full-wavelength width, curves for computations, 1167
radiator, formula for computing diffraction pattern, 1109
Rectangular and circular gate radiator, 1173
Rectangular guide, **260–262, 305–310, 374, 381–384,** 1186–1232
condition for $TE_{m,0}$ excitations applied to diffraction radiator, 1127–1128
current flow, $TE_{1,0}$ excitations, 1194
diffraction radiator, generalized Kirchoff-Huygens forward factor, 1135
dipoles and image dipoles, 1182
distributions, 1187, 1190
of possible $TE_{m,n}$ waves, **260**
electric field distributions for consecutive TE excitations, guide radiator, 1128
excitation, 1219
feeders, 1189
formulas, guide wavelength, **305**
Hertz vector, derived electric and magnetic fields at opening, **260**

Rectangular guide, longest TE wave, **305**
Poynting vector, 1199
radiation from opening, **260–270,** 1092, 1116–1117, 1126–1136, 1183
radiation vector, L_x pattern, 1128
TE modes, **381**
wave configuration, 1218
Rectangular and polar plots, relative field amplitude directivity, cylindric metal surface radiator, **771**
Rectangular primary wave-front radiator, Fresnel diffraction, 1160
Rectangular resonator, 1233
Rectangular slot radiator, Fraunhofer field amplitude diffraction pattern, 1097
Rectangular wave-front radiator, expansion of cross section function, 1110
formulas, 1161
phase factor and Huygens electromagnetic wavelets, 1092
Rectangular wave guide (*see* Rectangular guide)
Rectangular window aperture, like condenser in parallel with inductance, 1116
Rectilinear propagation deviation, diffraction, factors affecting, 1028
Reduced curl relations applied to propagation, **374**
Reference coordinates, **146–147**
Reference field at one meter distance from source, 870
Reference free-space field values, 870–871
Reference penetration depth of electromagnetic wave, **49**
Reference radiator, **623**
Reference standard for antennas and arrays, **623**
Reflected beam and earth curvature, 948
Reflected fields and transmitted fields, guide, **357**
Reflected and incident current waves, **417**
field components at places above ground reflection, 884
Reflected polarization and discrimination, **787**
Reflected, refracted, and incident rays, planes of constant phase, 792
Reflected traveling wave, 895
Reflected wave, **113**
and advancing wave, computation, **115**
vanishing in pure dielectric for Brewster wave incidence, 814–815
Reflecting plane, metal, radiation conditions, 1003
Reflection, conductive medium, **10,** 855
curves, pseudo Brewster dip, ocean surface, 852
determination on line, with admittance, conductance, and susceptance effects, theory, **439**
dielectric wave medium, **10,** 789–796, 798–800, 804–820, 834–835
Reflection, and direct wave effects, over earth crust, 913–949
dissipative wave medium, **10,** 802–804, 821–829, 836, 841, 842, 845–863, 895–916
concepts of, 853–860
hundred per cent, surface of medium separation, definition of, 792
law, applied, 962
Snell, 792
minimum, vertical polarization, 849–852, 855, 858, 860
multiple, analysis, 887–895
point, tangential plane, 933
propagation constant, dielectric and dissipative wave medium, 801
and refraction effects, simplification, 962
formulas of optics, applied to radio waves, 790–796
radio waves, comparative derivations of formulas, vertical and horizontal polarization, 798–824
total, **61,** 804–805, 964
applied, 964
and total refraction, 820
vector over actual and perfect earth crust, 912–928
wave (*see* Wave reflection)
Reflection coefficient, **10,** 897, 942
actual values, 829–839
at any angle of wave incidence, formulas, 794
complex, analysis of magnitude and phase, 843
dissipative wave medium, numerically applied, 843–845
curves, magnitude and phase, different mediums, 858
definitions of, in literature, 838
for obstructed wave propagation, 794
different earth crust conditions, magnitude and phase, 835
dissipative wave medium, numerical applications, 843
double line, **412–413**
measurements, **417**
formulas, 798–803, 806, 808, 814–815, 818
using impedance, **419**
compared with formula using standing-wave ratio, **420**
grazing-wave incidence, 860
half-wave phase jump, 931–934
line measurement, definition of, **412**
magnitude and phase, **413**
curves for vertical and horizontal polarization, 851
of load impedance of line, **436**
of metal reflector is ± 1, depending on polarization, 855
parallel polarization, perpendicular wave incidence, 803–804
phase of, **10,** 801
and magnitude, 939

Reflection coefficient, spherical earth crust, 1072
standing-wave ratio on double line, **417**
table, **441**
tabulated computations, dry earth crust, 836
ocean surface above 20,000 Mc/sec, 836
wet soil, 833
value and phase, different polarizations and angles of wave incidence, curves, 834
vertical and horizontal polarization, 960
different angles of wave incidence, 855
general formulas, 829–830
magnitude and phase, different wave incidences, vector plot, 855
numerical examples, 837
vertical polarization, dissipative wave medium, pseudo Brewster angle and dip, **861–863**
and time phase, minimum for, 871
waves, actual values, 829–839
wet earth crust, above 40 Mc/sec, magnitude and phase, 834
Reflection factor, effect for advancing and reflected waves, **115**
vertical and horizontal polarization derived, 798
Reflector, backup, 912
linear radiator, 864
complex (dissipative wave medium), **10,** 796, 801–804, 821–829
dielectric mirror, **10,** 946
effect over earth crust, 917
electromagnetic beaming, **590, 599, 602,** 930, 957, 1009, 1012, 1014, 1028–1036
ideal, simulated by metal plate, 920, 1003–1009
Refracted angle, stratum layer, 997
Refracted radio beam, 143
transmitted, plane at medium separation, 793
Refracted ray, not possible for critical angle of wave incidence, 805
Refracting stratum, 997
Refraction, angle of, 804
and diffraction dependent on operating wavelength, 1018
index of (*see* Index of refraction)
law of, applied, 962
Snell's, generalized, 792, 827
molar, 971
and reflection, comparative derivations of formulas, vertical and horizontal polarization, 798–824
formulas of optics applied to radio waves, 790–796
total, Brewster angle of wave incidence, vertical polarization, 814–815
and total reflection, explanation of, 820
upward and downward, **143,** 984, 987, 988, 996
Refraction coefficient, 803, 804, 806, 808, 809, 811–814
parallel polarization, 808–813
and perpendicular polarization, 808–814, 960
perpendicular polarization, perpendicular wave incidence, 803–804
Refractive index (*see* Index of refraction)
Refractor, metallic, **10,** 796–824, 920, 1003–1009, 1029
coefficient of reflection is ± 1, depending upon polarization, 855
refraction coefficient, 807–814
parabolic cage, reflector effect, 1029
perfect, parallel and perpendicular polarization, 965
shape design, 1242
Relations, currents and electromagnetic fields, **3–143**
Relative dielectric constant, **5**
ionosphere, 979
troposphere, curves, 977
dry-air and water-vapor effects, 977
Relative dielectric gradient, troposphere, 971
Relative equivalent dielectric constant, **5**
earth crust, formula applied, 900
Relative equivalent ground dielectric constant, **347**
Relative image antenna current, curves, vertical and horizontal polarization, 849
Relative index of refraction, medium 2 with respect to medium 1, formula, 794
referred to vacuum, formula, 794
Relative permeability, **5**
Relative phase (*see* Phase, relative)
Relative phase angle and path difference of many wavelengths, 872
Relative phase condition, equivalent delay angle, 872
numerical evaluation, 872
Relative time phase, consecutive radiators, **593**
electric and magnetic field, **41–56**
field, **181**
electric and magnetic components in near-field region, **177**
Reluctivity, magnetic, space, **196**
vacuum, **391**
Resistance, effects, voltage maximum and minimum positions of line, looking toward load end, **699**
external and internal, **714**
radiation (*see* Radiation resistance)
surface, plane conductor, 1198
of wall, curves, 1229
(*See also* Radiation resistance)
Resistive and reactive external components, self-impedance, cylindrical dipole, **713–714**
Resonance, of half-wavelength slots, 1036
modes, applied, 1185

Resonance cavity, cutoff wavelength, formula, 1233
frequency, pure dielectric and air, 1234
and wavelength, 1233–1236
Resonant and nonresonant conductors, **699–700**
Resonant slot radiator, 1036
Resultant electric field value, distant radiation region, compared with field value of return echo, 887
Resultant magnetic potential, magnetic shell, **155**
Resultant wave magnitude, two infinitely long wave trains of slightly different carrier frequency, **386**
Retarded current, and charge effects, VHF's and UHF's, **780**
instantaneous, conical antenna, **75**
Retarded scalar potential, electric, space charge density, **253**
and vector potential, derivation for line, **495–496**
Retarded time function, **37**
Retarded time phase, **612**
Retarded vector potential, closed current loop, **778**
electric, **315, 337–359**
magnetic, **221–229, 253–258, 267, 290, 300, 315, 357–359**
components compared with field components, **87**
and electric potential method, **214**
Rhombic antenna, **458**
Ribbon double line, characteristic impedance, **67, 70**
energy flow, **67**
relation to characteristic line impedance, trapped radiation resistance, **67**
Ribbon-guided radiation resistance, field energy trapped in interspace, **73**
Right-handed screw space wave propagation, **786**
Right- and left-handed polarization, **786**
Right- and left-handed screw rule, vector product, **197,** 1268–1269
Ring-shaped slit diffraction pattern, 1282
Rings, zonal, Fresnel, 1026
Rock, electromagnetic properties of, **29, 46**
Rocky ground, **135**
as wave medium, **12, 34, 36, 39, 46, 135**
Rod and loop exciter, guide, 1219
Root of Bessel function and derivative, **304, 307, 309–310**
particular, **310**
wave guide, **310**
Rot, alternate notation of curl, **198**
and curl identity, **198**
of vector, **198**
Rotation, **14**
measure and curl of velocity vector, **23**
Rubenstein, P., and P. M. Morse, electromagnetic diffraction, 1063

S

Savart, F., and J. P. Biot, Biot-Savart law, **164, 217**
Scalar, **20**
components of vector, **21**
or dot product, **197,** 1268
general, **20, 22**
gradient of, 1269–1270
or interior vector product, **197,** 1268–1269
invariant, **20**
point function, **20**
and vector, compared for divergence and curl of vector, **22**
gradient, curl, divergence, **20–22**
Scalar potential, **214, 218, 229**
complex, **315**
dissipative and nondissipative wave medium compared, **358**
electric, **219–229, 244**
and magnetic compared, **358**
magnetic, **219–229**
product, **197,** 1269, 1271, 1272
and vector potential, **315**
product outcome, applied, **210**
relations, review, 1267
Scalar wave functions, **305, 323**
potential V and U, **219–229**
Scanning aberrations, 1241
Schelkunoff, S. A., approximations for Hallén model, **709**
biconical general line, relations, **735**
biconical line theory, **734–742**
critical review of Hallén integral equation, cylindric radiator, **717**
electric and magnetic currents, **361**
electric radiation vector, **614–617, 620**
equivalence principle, 1182
general radiation formulas, **361**
generalized induction theorem, **356**
induction theorem, **356**
magnetic radiation vector, **614–620,** 1128–1129
radiation vectors, **609–614**
theory for radiators of arbitrary shape, **705**
three-dimensional wave impedance concept, **4, 7, 39**
Screen, with aperture, wave penetration, 1037
complementary, 1036
exposing primary wave front, 1061, 1082
Sea water, electromagnetic properties, **4, 6, 7, 49, 54**
Second Euler function, 1260
Secondary electromagnetic field, caused by electromagnetic obstacle, **314**
source, 1089
Secondary Hertz vector, **338, 342**
Secondary and primary wave fronts, 1020, 1037
Secondary radiation, from spherical earth crust, 1069

Secondary radiation centers, causes of diffraction in face of primary wave front, 1021
locations of equal phase on primary wave front, 1020
radiation lobe, **10**
(*See also* Side lobes)
Secondary wavelet window, 1022
Sectorial horn, 1182
Self- and mutual effects, dipoles, elementary theory and formulas, **662–666**
Self- and mutual impedance formulas, of coupled linear dipoles, **650**
linear radiator, numerical application, **666–671**
Self- and mutual radiation resistance, effects from Lecher line, **192–194**
and reactance, closed circuit, **776**
Self-impedance, cylindrical center-fed radiator, table for different cylinder radius in terms of wavelength, **715**
dipole radiator, in terms of factor Ω, **712**
general dipole, **663–664**
Self-radiation effect, electric current sheet, **619**
magnetic current sheet, **619**
Self-radiation resistance, go and return of power line, **519**
and reactance, dipole radiator, **712**
Semiconductor and semidielectric, **17, 136**
Separation constant, may be complex, **327**
for solving general wave equation, method, **302**
procedure, **294**
wave equation, **294, 322–327**
Separation, of polarization, 815
of slot effect, wave-front radiators, 1121
in solution of wave equation with cylindric coordinates, **324**
of variables, procedure with X and Y functions, **303**
wave equation, spherical coordinates, **322**
Series $F(x,y)$ function, aperture radiator, 1154
and parallel feed, half-wave radiator, **697**
Series solution, exponential function applied to Hertz doublet, **516**
75- to 300-ohm termination conversion, **526**
Shadow, geometric limit for diffracted electromagnetic waves, 1072
geometrical region, **6, 17, 784**
universal factor, **346**
Shadow factor curves, 1077
universal, electromagnetic diffraction, 1074
Sharp edge, diffraction, formulas, 1050
obstruction, advancing primary wave front, 1046
Sharp wedge diffraction, curves, 1053
Sheets, current (*see* Current sheets)
Shell, electric, **151, 157**
magnetic (*see* Magnetic shell)
Sherman, J. B., circular wire aerial radiator, **747**
Short-circuited double line, formulas, **416**
stub on main line suppresses f, 2f, 4f, 6f, etc., **450**
Short-circuited grounded far-end single conductor, conditions, **456**
Short-circuited quarter-wave-line section of double line, **415**
Short-circuited stub, **438, 440**
Short cuts based on Schelkunoff general radiation formulas, **361**
Short linear radiator, meridian directivity, **625**
solution with electric scalar and magnetic vector potential, **230**
Shortening half-wave dipole causes reactance neutralization of gap impedance, **654**
Shunt feed matched, conditions, **705**
Shunt feeding and series feeding of half-wave linear radiator, **697**
Shunting stub across line, **439**
Si and Ci, curves, **665**
formulas and expansions, **665**
functions applied to linear radiators, **643–648**
Si, Ci and $\overline{\text{Ci}}$ formulas, **712**
Sichak, W., polarization of electromagnetic waves, **787,** 795
Side lobes, **564**
gain, **627**
and main lobe, parabolic projector, 1032
Side shift of beam, radio course, **60**
Signal energy, intermodulation energy, **588**
Signal strength in wave ducts, 996, 1237–1240
Signal velocity, **368–370, 379**
Significance, consecutive and zero values of Bessel and Neumann functions, **304**
Significant arguments for vanishing Bessel factors, **704**
Significant Bessel roots, **769**
Similitude relations, **297**
mediums of different size, models, **297–299**
Sinclair, G., elliptical polarized waves, **787**
slot radiator, 1285
Sine and cosine expansions applied to radiation formulas, **782**
Sine function, larger than unity value, applied to wave refraction, **61,** 804–805, 817–820
series expansion, applied to radiation resistance formula, **519**
Single-feed line, match to half-wave radiator, **466**
Single pulse and harmonic wave with phase velocity, comparison formulas, **389**
Single stubbing, matching load impedance to line, **428**
Singlet radiator, 938
Sink and source, **35**

Sinusoidal current distribution, linear radiator, general case, **642**
Skilling, H. H., very clear introduction, electric waves, 1288
Skin, metal, of wave guide, power loss, 1208
Skin current, thickness, guide wall, 1198
Skin effect, action, electromagnetic field, **16**
good conducting wave medium, **45, 143,** 1198
on conductors, **143,** 1198
Slater, J. C., dipoles and images, rectangular guides, 1182
microwave transmission, excellent book, 1182, 1288
Sleeves and cups, quarter wavelength, **694–705**
Sliding probe position, slotted line, **425**
Slit aperture, described by K. Schwarzschild, 1063
Slot aperture, 1036
axial, 1036, 1095, 1182
horizontal, cause of vertically polarized waves like vertical wire radiator, 1036
Huygens-Fresnel principle, 1036
interrupting longitudinal currents, 1036
radiators, field energy distribution, 1125
like shunt capacitance, 1116
like shunt inductance, 1116
vertical, cause of horizontally polarized waves, like horizontal wire radiator, 1036
Slots, action of, like complementary dipoles, 1036
half-wave, resonance, 1036
and open-slot radiator, **784**
radiator, **17, 784,** 1036, 1284
characteristic and group characteristic effect, 1124
separation effect of wave-front radiator, curves, 1121
several, wave-front radiator, derivation, 1112
thin, equivalent to array of magnetic dipoles, 1036
and wire radiator, 1036, 1173
Slotted cylinder antenna, 1036, 1095, 1182
Slotted cylindric radiator, directivity, 1284–1285
Slotted line and sliding probe positions, different load conditions, **425**
using standing-wave ratio concept for measuring reflection coefficient, load impedance, etc., **416–435**
Small electric dipole, explores electric fields, **156**
Small loop aerial, formulas, **571–573**
equivalent height, **573**
explores magnetic field distribution, **156**
Smyth, J. B., wave-duct measurement, 1236
and L. G. Trolese, propagation measurements, lower troposphere, 996–997
Snell's law, **57, 58, 61, 62,** 792, 794, 802–804, 808, 810, 811, 815, 821
of reflection, 792
of refraction, applied, 804, 981
to troposphere, 980
dielectric and dissipative mediums, 802
generalized, 802
formula, 827
and reflection applied to waves in different mediums, 792
Snow, C., hypergeometric functions, **327**
Solenoidal conditions, **198**
electric and magnetic flux densities, **313**
field, 1273
or lamellar field vector distribution, **24**
or sourceless field condition, **312**
wave medium, **198**
Solenoidal vector, **24, 198, 312**
Solid angle, **154, 641**
applied to radiated power and power directivity, **621**
elementary, **626, 628, 640**
space angle, **505–506, 621**
Solid radian, **629**
Solid space pattern, 1002
Solid zonal harmonic of qth degree, **340**
Solution, for cylindrical guide, **309**
typical differential equation with flow function, separation of variables, **302–304**
Sommerfeld, A., on diffraction, 1038
diffraction theory, 1063
integral, **496, 498**
for surface current and charges, **496**
on lines, **493**
mathematical space assumption, explaining electromagnetic diffraction, 1065
surface-wave theory, 958
wave propagation, **370**
Source-into-feeder-into-radiator, power transfer relations, **451–455**
Source and sink of field, **35**
in wave medium, **300**
Source strength given by divergence of vector, 1272
Southworth, G. C., radiation formulas of arrays, **594**
Space charge, velocity imparted, **23**
Space current and time phase in terms of Q value of medium, **140**
Space directivity formula, linear elementary radiator, 31
slot radiator, rectangular aperture, 1108
Space dissipation attenuation, **123–128**
Space field, directivity, **631**
large angle of wave incidence, 943
value, transmitter antenna location, numerical data, 932
Space impedance, moving electromagnetic field, **63–65**
Space lattice, of dipoles, **592**
radiation formula applied, **596–599**

Space orientation, linear differential radiators, **607**
Space point outside spherical earth surface, Hertz vector, **344**
Space power directivity pattern, half-wave radiator, **630**
Space radiation, unobstructed, applied, **529–788**
Space radiator, **10**
Space reluctivity, magnetic, **196**
Space screw propagation, **786**
Space substance, polarization contribution over vacuum, **196**
Space volume charge, Gauss relation, **197**
elementary, **215**
Space wave propagation, frequency-height product significance, 932
Spacing, consecutive radiators, **593**
effect of slots, computations tabulated, 1122
Fraunhofer diffraction pattern, 1123
electrical, **445**
and phasing, radiator alignment, **593**
of stub on line, formulas, **436**
and timing, half-wave radiators, **631**
in wavelength and beam width, collinear half-wave radiators, **604**
Spectra, diffraction, wave trapping, 1240
Sphere of discontinuity, **77**
Spherical boundary, **76**
Spherical coordinates, **18, 145–151, 215,** 1268, 1270–1271, 1274
Spherical earth, conducting condition, **337**
crust and electromagnetic diffraction, 1069
relations for electromagnetic radiation, **336**
diffraction factor, **345**
and equivalent flat earth, rays compared, 998
wave spread, 887
expanding wave fronts, 886
surface and paraboloid surface at apex, applied, 871, 997
Spherical Fresnel zones, 1022
areas, formula, 1024
Spherical Hankel function, **332**
Spherical harmonics, **341**
equation, requiring separation, **326**
solution of waves, **328–345**
Spherical primary wave front, 1020, 1022, 1025, 1047, 1154–1156, 1171–1177
Spherical reflection coefficient, 1072
Spherical trigonometric basic formula, relations of space point to electric and magnetic current elements, **611**
Spherical wave, **74**
Spherical wave front, **8, 551**
circular gate radiator, 1179
conical antenna, **74**
elementary solid angle and corresponding wave-front element, **628**
Spherical wave front, and plane, **8,** 1116–1117, 1120, 1121, 1123, 1154–1171, 1174, 1179–1182
primary, 1020, 1022, 1025, 1047, 1154–1156, 1171–1177
surface, accounting only for radiated power, **628**
area of, 1023
of constant amplitude and constant phase, 791, 793
of discontinuity, **354, 355**
surface element, **628**
Spiral, Cornu (*see* Cornu spiral)
Spread, or positive divergence of a vector, **23**
Square-shaped wave-front radiator, Fraunhofer diffraction pattern, 1108
Staggered coupled half-wave radiators, conditions and formulas, **678–679**
Staggered linear radiators, **658–661**
Standard of antennas, modified, based on maximum power directivity, **627**
Standard atmosphere, definition of, 971, 994
ray curvature, application, 990
Standard Bessel equation, **325**
comparison, **330**
form, with solution, $y = \sqrt{x}\, Z_n(\beta x)$, **338**
Standing wave, **111, 116, 288,** 1279
current distribution, double line, **437**
field energy, **111–117**
space wave, conditions, different transmitter frequencies, 949
field values, 896
and traveling waves, **116**
double line, **437**
voltage distribution, double line, **437**
Standing-wave ratio, concepts and line measurements, **416–435**
conditions, customary HF line assumptions, formulas for impedance and admittance, **416**
definition, $k = E_{min}/E_{max}$, **413**
$r = E_{max}/E_{min}$, **416**
double line, **411**
experimental, **431**
impedance matching, **427**
r, related to reflection coefficient on line, **437**
and stub location, applied, **436**
reflection measurement, **440**
reflection coefficient, double line, **417**
table, **441**
reflection factor, **423**
UHF measurement, **420–423**
Standoff beads, effect of, in shielded feeder lines, **405**
Stationary wave (*see* Standing wave)
Statute mile, 943
to one kilometer conversion, 969
Steady rotation about nucleus of atom, **152**
Stiffness, degree of, dissipative wave medium, **43**

Stokes, Bessel, and Neumann functions, divergent waves, **332**
Stokes solution for divergent waves, **332**
Stokes theorem, **15, 25, 332**
Straight-line propagation, rectilinear, refractive index, 933
Stratton, J. A., linear antenna solution, **641**
signal velocity, **370**
spheroidal dipole, prolate spherical radiator, **743**
Stratton, J. A., and L. J. Chu, steady-state solutions, electromagnetic field, 1182
Stratum layer, refracted angle, 997
Stratum waves, and guide action, 959
lower troposphere, 958
Stub, closed, matching, **430**
formulas, **430**
distance, from voltage maximum, **445**
from voltage minimum, **444**
double, matching, **445**
and double line measurements, open-ended and short-circuited tests, **410**
feeder junction relation, **441**
formulas, **415–416**
and curves, **436**
and relations, **443**
insertion, **436**
length, impedance matching, curves, **432**
and location, curves for matching, **432**
used to neutralize susceptance effects, **433**
and line susceptance, stub and line junction, **441**
location, **432, 440**
impedance matching, curves, **432**
line measurements, **440**
open, matching, formulas, **431**
and short-circuited, input impedance, **441**
numerical susceptance, **443**
oscillatory changes with changing line length, **409**
reactance formula, **441**
relations, **445**
short-circuited, **438**
reactance formula, **441**
shunting line, **439**
spacing effect on line, formulas, **436**
two, impedance matching, **433**
Stubbing out, reactance effects of half-wave radiator, **649, 669**
in succession, **435**
Sturmian-type system of equation, **319**
Substandard atmosphere, 995
Substitution $\cos\theta = x$, applied, **328**
Successive approximations, Hallén and King solutions, **709**
Successive stubbing, for better matching, **435**
Superconductor, **157**
Superrefraction, **6,** 969
Supersonic frequency applied, 929
Surface, of constant phase, **369**
Surface, contour, **21**
of earth, curvature (*see* Earth, curvature)
equipotential, **21**
of integration, **648**
Poynting vector method for radiation power, **648**
plane conductor, 1198
sphere of discontinuity, **77**
Surface charge, **65–67**
density, **352**
and flux, **65**
Surface conduction current, **95, 353,** 1186, 1191, 1194, 1197, 1203
density, guide wall, 1207
and displacement current, guide, 1193
Surface current, **65, 95, 353,** 1186, 1191, 1194, 1197, 1203
and current sheet, **348**
flow on skin, **66, 95,** 1186, 1191, 1194, 1197, 1203
and magnetic field, **65–67**
Surface divergence, **38, 39, 203**
Surface element, spherical wave front, **628**
corresponding elementary solid angle, **628**
and volume element, **240**
Surface integral, **15, 25, 108**
and line integral, **15, 26, 101–102,** 1275
and volume integral, **108–123, 130–133,** 1001
Surface level, **21**
of medium separation, effective cross sections, electromagnetic field energy tubes, 793
incidence, refraction and reflection, angles, 793
relative index of refraction, 793
Surface power density, average, radiation field, **629**
Surface radiator, diffraction, 1091
Surface resistance, 1198, 1229
guide wall curves, different metals, 1229
Surface wave, Sommerfeld, Zenneck, standard broadcast field plots, 899, 900, 906
guided, 903
trapping, 959, 995, 1236–1240, 1253–1254
Surface zonal harmonics, **341**
Surge, characteristic impedance, double line, **7, 403**
Susceptance, condition, stub and line junction, **441**
conductance, voltage and current distributions, double line, **438**
numerical, open-ended and short-circuited stub, **442–443**
positive and negative, line measurement, **439**
Sweep of wave front, speed, **367**

T

Tangential field components, feeder, **480**
and normal field components at boundary, **352**

Tangential magnetic field formula, in terms of radius and current, **75**
Tangential plane, earth crust, applied, 948
reflection point, 933
TE (transverse electric) wave, **92, 292–296**
dominant, conditions, **374**
guide, impedance, 1199
Laplace equation applied, 1200
rectangular, action and relations, **374–377**
TE and TM waves, **305–310, 335,** 1185–1232
Bessel roots tabulated, **310**
boundary conditions, **307–309**
formulas, 1212
guide, circular, cutoff characteristics, **305,** 1193
guided power, formulas, 1202
limited by cutoff frequency conditions, **96**
modes, circular and rectangular guides, 1191
wave functions, **305, 306, 310,** 334, **335**
TE, TM, and TEM waves, **67, 69, 70, 74, 76, 78, 92–97, 290, 292–296, 306, 317, 363–364, 403, 406, 492,** 1185–1232
any wave medium, tabulated, **294–295**
compared and analyzed, **92–97**
field components in spherical coordinates, **292–296**
general description, **92**
illustration of formation of, **95**
$TE_{0,1}$ wave, excitation, electromagnetic horn, 1184
$TE_{1,0}$ wave, excitation, rectangular guide, currents and field, 1194
with slot aperture, 1116
mode preferred, 1220
and $TE_{0,1}$ wave, excitations of guide, **382**
$TE_{1,1}$ wave, guide distribution, circular and rectangular, 1190
$TE_{m,n}$ wave, **259–262, 305–310,** 374, **381, 383,** 1116, 1117, 1187–1190, 1194, 1204, 1206, 1207, 1213, 1219, 1221, 1223
formula, 1188
relations for guide, **377–379,** 1185–1232
$TE_{m,0}$ wave, excited by coaxial feeder, 1189
$TE_{n,m}$ wave, **307**
and $TM_{n,m}$ wave, **307**
$TE_{0,0}$ wave, nonexistent, **381**
TEM (transverse electromagnetic) wave, **76, 92**
action, **95, 285–291, 317**
bicones, electric and magnetic fields, transverse voltages, longitudinal currents, **735**
current and voltage relations, and characteristic impedance, **742**
impossible in hollow guide, **357**
double-line guided, **67**
characteristic impedance, **403, 405**
line-guided relations, **485**
on lines, **494**
Temperature inversion, 969, 984, 994, 995–997, 1236–1240
Terminations at gaps, parallel inphase half-wave radiators, **687**
Theorem, Gauss, **22, 24, 25, 108–109, 120, 122, 196**
Green, 1279
symmetrical form, 1279
Stokes, **15, 25**
Thin dipole radiator, analysis, **530**
Thoma, A., partial radiation suppression, **557**
Three-dimensional characteristic wave impedance, **4, 17, 36, 40–45, 50, 53, 55, 316**
Three-dimensional medium propagation constant, **317, 390**
attenuation and wavelength component, **53**
Cartesian components, **320, 323**
Three-dimensional space propagation constant, **30, 44, 46, 48, 50, 55**
Three-dimensional wave attenuation, neper/meter, dissipative medium, **123**
Three-dimensional wave equation, **320**
300- to 75-ohm termination conversion, **526**
Three-wavelength distributions, two interlaced circular wire radiators, resultant effect, **753**
Thrust (forward) factor, linear array, **603**
Tilt, forward, electric field, 958
over actual earth crust, solid and liquid, curves for all conditions, 900
ocean surface, tabulated, 910
of wave front, curved radio beam, 982
Time angle, positive and negative, reflection coefficient, **436**
average, **118, 189**
Time average of $\cos^2(\omega t - \beta r)$ function, **250**
Time delay, 937
dealing with many wavelengths of propagation, **453–454,** 872, 878–880
of envelope, **365**
Time lag, magnetic field against electric field, ocean, **137–138**
Time phase, **41**
angle, total, evaluations, 872
characteristics, radio beam, reflected, dissipative wave medium, 845, 853
electric and magnetic fields, near-field region, **182–187**
and magnitude, plot of reflection coefficient, vertical and horizontal polarization, 855
reflection coefficient on lines, **436**
relative (*see* Relative time phase)
wave impedance, highly dissipative wave medium, **43**
Time rate of decrease, electromagnetic field energy, **201**

Timing and spacing, half-wave radiators, **631**
TM (transverse magnetic) wave, **305**
distributions, wave guide, 1186
excited in concentric line, **95**
first order, biconical line, **737**
guide, longest wave, **308**
modes and roots of Bessel functions, **379**
wave function, **334–335**
wave impedance, 1199
(*See also* TE wave and TM wave)
$TM_{0,1}$ wave, mode, circular symmetrical, 1219
$TM_{1,1}$ wave, longest wavelength, **308**
mode, longest natural wave, **305**
$TM_{n,m}$ wave, **307**
modes in cylindrical guide, **379**
Total capacitance, ribbon double line, **73**
Total current, **98**
content, **26**
density, **28, 29, 199**
Total directivity, $D_\theta \cdot D_\varphi$ product, n equal collinear antennas, **588**
Total Fresnel zones, operative, 1041
Total generalized electrical length $\Omega = l\Gamma$ of double line of actual length l, **408**
Total magnetic flux, **14**
Total phase for vertical and horizontal polarization, 945
Total radiation resistance, power line, **520**
Total reflection (*see* Reflection, total)
Total refraction (*see* Refraction, total)
Total self-induction, ribbon line, **72**
Trade winds and wave duct, 996
Transformation, of impedance with quarter-wave line section, **438**
of integrals in leading to Ci and Si functions, **643–648**
of unbalanced to balanced feeder, **525**
of volume into surface integral, **122**
Transit time effect, **214, 223,** 1274
in tubes and scalar potential and magnetic vector potential, 1273–1274
Transition stratum, 997
Transmission line, field conditions, compared with space field conditions, **285–291**
and guides, metallic energy absorption, **480**
Kirchhoff solution, 40
more than two parallel wires, **469**
and radiation, **402–527**
remarks on, **456**
relations, **406–416**
Transmission-line equation (classical), **68, 94, 97, 289–291, 362–363, 371, 373, 402, 406–451, 484–488,** 492
Transmission-line theory (classical), based on voltage and current concepts, cannot account for radiation, **492**
and Maxwell's field theory, characteristic impedance formulas, **40–41**
Transmission-line theory (classical), satisfies voltage and current at any point of line, **493**
voltage and current, related to Maxwell's field equations, **40**
Transmitted and reflected fields of guide, **357**
Transverse electric wave (*see* TE wave)
Transverse electromagnetic wave (*see* TEM wave)
Transverse and longitudinal fields, 1185
field components, **88**
magnetic line effects, guide, 969
wave-guide current, 1204
Transverse magnetic wave (*see* TM wave)
Transverse voltage, **78, 83**
biconical line, **78, 83**
ribbon double line, **68**
wave configuration, $TE_{1,0}$ wave, 1218
Trapped field energy, double ribbon line interspace, **73**
radiation, ribbon double line, **68–73**
Trapping, of electromagnetic energy, **143,** 994–997, 1236–1240
of waves, in low wave duct, 958–964, 1236–1240
in lower troposphere, 996, 1236–1240
Traveling wave, **111–112, 116**
backward and forward, **333**
currents and electric and magnetic fields compared, **363**
field energy, **111–117**
Lecher wires, **521**
and standing wave, double line, fundamentals, **416–420**
Traveling-wave tube, **417**
Triangle, path formed by radiation and reception centers and reflection point at earth crust, 868
solution of sum and difference effect on the resultant, in the case of advancing and reflected waves, **115**
Trolese, L. G., wave-duct measurements, 1237
Troposphere, **6,** 969–997, 1003, 1236–1240
conditions, refractive index gradient with height, 994
humidity effect, **6,** 969–997
polarization per cubic meter, 972
ray path, 983
in refractive index variation, 980
superrefraction, 994–997, 1236–1240
temperature effect, 969–997
wave-duct action, 994–997, 1236–1240
Tropospheric index of refraction, **6, 56,** 891, 969–997, 1236–1240, 1253
conditions, 998
general remarks, 980–983
numerical values, 988
physical properties, 973
variable or constant, 1000
well mixed, 997

Tropospheric refraction, general wave equation, **319**
gradient, 998
Tropospheric stratum waves, close to earth crust, 958
Tropospheric wave, **6,** 958–964, 969–997, 1236–1240
Tropospheric wave trapping, 994–997, 1236–1240
Tuning condenser, radiation, **101**
shortening length of dipole neutralizes gap reactance, **654**
Turnstile bay, **620**
power supply by aperiodic feeder, **700**
several, field ratio and power ratio, **621**
Turnstile polarization, **785**

U

Unbalanced to balanced feeder supply systems, **525**
Unbalanced coaxial line to balanced coaxial line, **526**
Unbounded inside wave-guide medium, propagation condition, **380**
Unbounded wave medium, propagation, **363**
Unequal spacings, consecutive half-wave radiator alignment, **605**
Uniform current sheet effect, 1029
Uniform dipole distribution, 1029, 1182
Uniform intensity distribution, electromagnetic horn, 1184
Unilateral beaming, **638**
suitable phasing, **596**
broadside, conditions, **599**
end-firing, formula, **584**
Unit, of dielectric constant explained, **67**
of permeability explained, **67**
solid angle, 1093
applied, **616**
vector, **197,** 1246, 1268, 1269, 1272
or line vector per unit length, **22**
Units, mks, **7, 195,** 1243–1251
compared with cgs units, Gaussian units, Heaviside-Lorentz units, 1243, 1253
Universal shadow vector, electromagnetic diffraction, 1074
Unobstructed radiation, **529–788**
Unobstructed region, diffraction, numerical applications, 1056
Unobstructed space radiation, **529–788**
general remarks on, **784**
Unpolarized wave, definition of, **787**
Upward bending electromagnetic ray, 974
Upward ray curvature, 998

V

Vacuum dielectric constant, **4, 5**
Vacuum oscillation constant, **391**
Vacuum permeability, **4, 5**
Vacuum reluctivity, **391**
Valence electron, flow of, **152**
Value and normal gradient of wave function, boundary surface, **311**
Variable directivity factor, **628**
and fixed factor of phase factor, **612**
Variables, separation procedures with X and Y functions, **303**
for cylindric coordinates, **322–325**
for spherical coordinates, **294, 321–327**
Vector, **20**
addition, electromagnetic field relations, 870
analysis, divergence identity, **198**
conjugate, **124, 210**
cross product, **197, 198, 201, 203, 210,** 1268–1269
diagram, linear half-wave radiator, evaluation solutions, **539**
function P in place of scalar wave function w, wave equation, **315**
identity, average divergence, **201**
div $(\xi \times H) = H$ curl $\xi - \xi$ curl H, **119–121**
electromagnetic fields, **119, 121, 198, 201–203,** 1268–1269, 1272, 1275
l concept, arbitrary elliptical polarization, **787–788**
lamellar vector distribution, **24**
magnitude and phase, **20**
multiplication, **11, 22, 23, 25, 197–199, 201–203, 206, 210–211,** 1268–1269, 1273
operator, **23**
also known as nabla operator, 1271–1272
point function, **20,** 1271
particular vector potential, **361**
radiation (*see* Radiation vectors)
solenoidal, **24, 198, 312**
Vector potential, **300, 301–302, 307**
closed current loop circuit, for low frequencies, **778**
complex, **315**
and current density relation, **225**
electric (*see* Electric vector potential)
formulas, **249–258**
magnetic (*see* Magnetic vector potential)
retarded (*see* Retarded vector potential)
and scalar potentials, **223–229**
Vector potential method, **361**
for finding field effects, fast time variations, **217–218**
Vector product, conjugate vectors, **210**
exterior, **197**
Vector relations, rules, **197,** 1274
and scalar field relations, **218–229**
summary, 1274
Velocity, copper wave medium, **51**
dielectric wave medium, **7, 44, 59,** 791, 793, 796, 799, 800, 805, 806
with refraction, 969–997
dissipative wave medium, **29, 49, 54–56, 59, 62,** 900, 907, 909

Velocity, earth crust wave medium, **50, 54–56, 59, 62,** 900, 907, 909
imparted on space charge, **23**
ocean wave medium, **49, 50,** 900, 911
phase and group (*see* Group velocity; Phase velocity)
progressive (traveling) wave, **112**
pronounced conductive wave medium, **50–51**
propagation, air, **4, 6**
conductive medium, **43, 45**
dissipative medium, **6, 17, 30, 40, 43, 45–46, 48**
tropospheric, 969–1003
signal, **369–370**
wave front, **367**
wave propagation, **368–379,** 799
compared with group and signal velocity, **369–370**
ground, **6, 50, 54–56, 59, 62,** 900, 907, 909
ocean, **6, 49, 50,** 900, 911
surface of medium separation, 791
vacuum, **4**
Vertical antenna, 917
diffraction pattern, 1102
Vertical directivity, vertical and horizontal polarization, over wet earth crust and 100 Mc/sec, curves, 956
Vertical electric dipole, **153**
Vertical half-wave dipole curtain, **590**
Vertical and horizontal polarization (*see* Horizontal and vertical polarization)
Vertical and horizontal waves (*see* Horizontal and vertical waves)
Vertical linear radiator, and horizontal disk radiator, conditions, **762–765**
directivity pattern, **765**
over ocean surface, 911
over quasi-perfect and actual earth crust, 918
receiving antenna compared with horizontal antenna, 795
Vertical pattern, horizontal linear radiator, quasi-perfect and actual earth crust, 918
Vertical polarization, **19, 28, 551,** 940
comparison of different wave mediums, derivations and formulas, 796–826
condition over actual ground, 831
diffraction formulas and curves, 1078–1081
earth crust reflection, 913–949
formulas, 963
maximum field effects, formulas, 967
polar radiation patterns, formulas, 953
reflection coefficient, dissipative wave medium, Brewster angle and dip, 861
resultant electric space field, 953
wet earth crust at 100 Mc/sec, tabulated, 955
(*See also* Horizontal and vertical polarization)
Vertical radiation patterns, actual earth surface, 952
ideal, and wet soil conditions, 957
Vertical slot aperture, metal screen, for horizontally polarized wave, 1036
Vertically polarized wave, **28**
and horizontally polarized arriving wave (down-coming), direct and ground-reflected contributions, 797
Voigt theory applied to apertures, 1034
Voltage, and current, any distance from load end, double line, **408**
effective values, any distance from input end, double line, **411**
locations, line with reflections, **439**
current, conductance and susceptance distributions, double line, **438**
function, **306–310**
impedance, for driven and parasitic radiators, **652**
several driven radiators, **652**
induced in radiator, formulas, **651**
maximum on line, **440**
location, standing-wave ratio, **444**
probe for line, **421**
TEM waves, and complementary waves, biconical line, **738**
Schelkunoff biconical line, **736**
transverse, **78, 83**
Volume density, **110, 200**
of magnetization, **154**
of polarization, **239–240**
Volume divergence, **109**
Volume element, various coordinate systems, **144–147**
Volume and surface integral, **108–115, 119–125, 130–135,** 1279
divergence concept, **108–111**
Gauss, Green, and divergence theorem, 1279
relations, **108**
Volume and surface moment, **240**
Vortex motion, velocity vector, **23**

W

Water-vapor content, in tropospheric wave bending, 997 977
Watson, G. N., diffraction of electromagnetic waves around earth surface, 1065
Watts/meter length, heat loss, coaxial line, **482**
Wave, advancing and reflected (*see* Advancing and reflected wave)
attenuation of, **30, 125, 136, 138, 164**
rigorous, **35**
complementary, **78, 94, 97, 492**
component discrimination due to polarization, **786–787**
conditions of, either side of earth crust surface, vertical polarization, 899–912
crests and troughs of, 1020, 1037, 1039

Wave, decay of, **38**
due to wave spread, plane and curved earth, 885–887
diffraction deviation from rectilinear propagation depending on dimension of wave front, 1028
distribution, double line, **421–435**
disturbance instantaneous in Kirchhoff diffraction theory, 1061
down-coming, effect of, due to direct and ground-reflected waves, 797
near earth crust, 902, 906
noncircular, **307**
plane (*see* Plane wave)
power flow, complex, **121**
progressive (*see* Progressive wave)
refracted in dissipative medium, phase factor, 796–826
stationary, standing (*see* Standing wave)
TE and TM (*see* TE wave; TM wave)
traveling (*see* Traveling wave)
tropospheric, **6,** 958–964, 969–997, 1236–1240
unpolarized, definition of, **787**
zigzag, 967
Wave antenna (Beverage), directivity, **457–461**
Wave duct, **319,** 995, 996, 1236–1240, 1253–1254
low level, 1236–1240, 1253–1254
and trade winds, 996
Wave equation, **267, 273, 288, 292–295, 302–304, 311–312, 318, 321–334, 336,** 1060–1064, 1068, 1087
applied, **497,** 1274
Cartesian coordinates, **323,** 1063
cylindrical coordinates, **324**
and separation, **324**
dielectric (nondissipative) wave medium, **293**
electromagnetic boundary conditions, 1067
exponential law (approximation) with distance, true radiation field, 334
general, **294, 311–312, 318–336,** 338–346
solution by separation constant, **294**
spherical harmonics, **311–335**
tropospheric refraction, **319**
Hertz and Fitzgerald vectors, yielding complex vector, **312, 318–326,** 330
Maxwell's equations satisfied, 1063
satisfied by flow function, **302**
separation constant, **302, 324, 326**
solution by J. R. Carson, general form of N parallel conductors, **492**
spherical coordinates, **321, 325, 329,** 336
three-dimensional, **320**
two-dimensional, diffraction theory, 1063
Wave front, **7, 365–368**
advancing (*see* Advancing wave front)
applications, near-field region, linear radiator, **551**
circular, classic derivation, 1136
Wave front, circular, wave function, 1137
definition of, **7, 93**
direction of wave propagation, **8**
expanding, 886
flat (plane), **19**
general remarks, **365–368**
location of equal phase, applied to phase difference, **445**
normal propagation velocities, surface of medium separation, 791
in opening, **784**
plane (*see* Plane wave front)
primary (*see* Primary wave front)
polarization of linear radiators, **549–557**
separation factor, 1115
spherical (*see* Spherical wave front)
tilts for curved or refracted radio beam, 982
velocity, **367**
watt density, **130**
wattless density, **130**
Wave-front radiators, any contour, distant radiation effect, 1156
Huygens-Fresnel principle applied, 1036
due to Huygens wavelet sources, 1019
Kirchhoff-Huygens principle, **784**
seat of electromagnetic field energy, **10–11,** 1089–1091, 1092–1095, 1160–1170
several, in same primary wave front, treated for distant field point with respect to proper phase, 1112
(*See also* Circular wave-front radiators; Rectangular wave-front radiators)
Wave function, alignment of circular aperture radiators, 1149
aperture radiator array, resembling modulation product, 1148
bounding surface and its normal gradient on surface in Kirchhoff wave equation, **311**
circular diffraction radiator, 1137
complex, 1064
concept of group velocity meaningless, **389**
conditions, electromagnetic diffraction pattern, 1087
Dalembertian of, **311**
elementary, with value q an integer, **333**
formulas, **293–295,** 1061, 1064, 1084, 1087, 1111, 1136, 1146, 1148
general, compared with function of electromagnetic wave, 1176
generalized, **498**
longitudinal electric and transverse magnetic waves, **334–335**
$\Phi_1(\rho)\Phi_2(\varphi)\Phi_3(z)$ solution, **497**
with products, **294, 302–303, 322–326, 334–335**
rectangular slot radiator, 1109
relation, 1021
special solution, 1278

Wave function, spherical coordinates and elementary functions, **322**
solution for finite regions including 0, **497**
for great distance, **497**
TE wave, **294–295**
TE and TM waves, **334–335**
TEM waves, **294–295**
TM wave, **294–295**
three Cartesian components, **320, 323**
twofold, electromagnetic waves, 1029
x, y coordinates, 1088
Wave guide, actions, **6, 95**
as attenuator, **381**
as high-pass network, **374**
tropospheric, **6,** 958, 959, 964, 968, 969, 994–997, 1236–1240
amplitude distribution, **308**
application, **303–310**
attenuation, curves, 1229
due to dielectric dissipation, 1217
formulas, 1217
TE and TM waves, 1206
imperfect dielectric, 1214–1217
due to metal wall dissipation, 1203
for pass and no-pass regions, 1215
bending curvature, 1221
Bessel derivative, **307, 309**
boundary conditions, **307–310,** 1185, 1214, 1232
and cavities, 1185–1237
characteristic curves, 1217
characteristic wave impedance, 1199
circular (*see* Circular guide)
coaxial, **95,** 1230–1232
conditions within guide and outside rectangular opening, 1126
cross section effect, 1217
with rectangular apertures, 1116
current flows, $TE_{1,0}$ excitation, 1194
leakage over opening walls, 1195
curves, dependent on wave mode and guide shape, 1226
rectangular and circular guide, computations, 1227, 1228
cutoff frequency, 1187–1188, 1190, 1193, 1213, 1215, 1217–1219, 1222–1225, 1227–1228
cutoff formulas, **95, 260, 262, 306–310, 377, 379,** 1127, 1187–1190, 1192–1193, 1196, 1207–1232
cutoff wavelength and frequency, **308**
cylindrical (*see* Cylindrical guide)
dielectric loss, 1217
displacement current, **95,** 1186, 1191, 1193–1196, 1205–1207
distributions, **95, 260, 374, 377,** 1186–1187, 1189–1194, 1207, 1219, 1221
electromagnetic horn matching, 1221
energy flow along, 1203
field distortion, **95, 260, 306, 308**
field distribution, **95, 260, 262, 306, 308, 374, 377,** 1186–1194, 1207, 1219, 1221, 1230
Wave guide, fields and currents, rectangular guide, 1194
formulas, **260, 262, 305–310, 374–379,** 1188–1233
TE and TM waves, 1227
general, **94–95, 260, 304–310, 374–379,** 1185–1232
guide wavelength, **261, 305, 309–310, 374–375,** 969, 1125–1127, 1186, 1194, 1196, 1199, 1207–1228
J_0 Bessel curve, boundary condition satisfied by, **379**
K formula, **382**
cylindric guide, **383**
longitudinal magnetic and electric wave, p values, **383**
longitudinal and transverse current, 1204
loss, total attenuation, 1226
matching, 1221
metal wall power loss, 1203
modes, **260, 262, 305, 307–310, 374, 377, 379, 383, 737–738,** 967, 1187–1194, 1201, 1207, 1212, 1215, 1219, 1221–1231
attenuation tabulated, 1222–1225
cross section tabulated, 1222–1225
cutoff characteristics tabulated, 1222–1225
cutoff frequency tabulated, 1222–1225
discrimination, 1226
excitation, 1217
fields tabulated, 1222–1225
formulas tabulated, 1222–1225
K values tabulated, 1222–1225
and shape of guide, 1226
$TM_{0,1}$, circular symmetrical, 1219
nomenclature, IRE recommendations, **304–308, 374, 376–383**
phase and group velocity, **376, 378–385,** 1196, 1199, 1226–1227
curves, **384**
power flow along, attenuation losses, 1199–1217
power loss, 1204
in walls and frequency, 1210
power rectangular guide, 1201
Poynting vector, **212–214,** 1199
propagation constant, **261–262, 295, 306–309, 374–381,** 1126–1127, 1215–1217, 1227, 1230, 1231
along rectangular guide, **381**
properties, 1217
radiation, 261, 1226–1236
radiator, **261, 359,** 1126–1136
rectangular, significant formulas, $TE_{m,0}$ waves, 1126
rectangular (*see* Rectangular guide)
relations, **93–96, 260–262, 294–295, 303–310, 359, 374–385**
derived for rectangular guide, **374–377**
shifting of polarization, 1221
solutions, **260, 262, 304–310, 374–379,** 1188, 1196–1232

Wave guide, surface conduction current, **95,** 1186, 1191, 1193–1196, 1198, 1204–1207
surface wall, impedance, 1198
resistance, 1198
$TE_{m,n}$ relations, **377–379**
$TE_{m,n}$ waves, 1218
three-inch copper cylinder, cutoff frequency, **380**
total attenuation, imperfect dielectric, 1226
twist, 1221
wall, surface resistance curves, 1229
wave pass device, **381**
wavelength, unguided, unbounded for air and pure dielectric, **305,** 1126, 1199
circular guide, **305**
rectangular guide, **305**
Wave illumination, geometrical shadow zone, partially due to wave interference, 1019
Wave impedance, **4, 17, 36, 40, 43, 45**
binomial theorem applied to expansion of, **246**
characteristic (*see* Characteristic wave impedance)
complex, general, **17, 36, 40, 42–43, 45, 50, 53, 55, 70**
small current loop and Hertz doublet, **160**
copper plane, perpendicular, 898
dissipative wave medium (*see* complex, general, above)
electromagnetic wave propagation, **63–65**
Hertzian doublet, **160**
incident wave, 814
magnitude and phase, in medium, **17**
mouth of guide, either side, **356–357**
plane of medium separation, 809–810, 814
reflected wave, 814
refracted wave, 814
small current loop radiator, magnetic dipole, **160**
TE and TM waves, 1199
in terms of series for small current loop radiator and Hertzian doublet, **160**
(*See also* Impedance)
Wave incidence, Brewster angle, 829–839
reflection curves, 849–852
grazing, 860, 948
reflection coefficient, 860
larger than critical angle, 805
normal, impedance to waves, 898
perpendicular (*see* Perpendicular wave incidence)
polarization distinction, 790
reflected and refracted, formulas, 806–807, 960
reflection coefficient, magnitude and time phase, vertical and horizontal polarization, 855
Wave interference, **9–10, 385, 417, 504–505, 545, 676,** 917–918, 923, 926–927, 929, 1013, 1019, 1037–1039, 1050–1058, 1172
destructive, 929
and Huygens principle, 1019
diffraction, 1038
earth crust, 913–949
metal reflector, 917, 918, 921, 923, 926–927
possible causes, **9–10**
radiation resistance effect, **676,** 1013
Wave medium, air, properties, **4**
complex, general, **3, 4, 12, 45, 117–138,** 840, 845–853
dielectric (*see* Dielectric wave medium)
different, derivations of formulas for incident, reflected, and refracted beams, vertical and horizontal polarizations compared, 796–826
discontinuity in, **66**
dispersive (*see* Dispersive wave medium)
dissipative (*see* Dissipative wave medium)
dry ground, **394**
attenuation and phase constant, **397**
group velocity, **398**
earth crust, dry, **394**
electromagnetic properties, **4–7**
extreme cases for conduction and displacement currents, **396**
frequency effect, **390–401**
general (*see* General wave medium)
gradient of dielectric constant, causes curved wave path, **371**
highly dissipative, propagation constant, **48**
logarithmic decrement, **138**
nondispersive and dispersive, formulas compared, **399**
ocean, **394, 400**
perfect, 1273
relative magnitudes of electric and magnetic fields, **45**
Snell's refraction laws for dielectric and dissipative wave mediums compared, 802
without ionization, phase velocity smaller than velocity in empty space, **395**
(*See also* Medium)
Wave model theory, similitude relations, **297–299**
Wave obstacle, aperture occupied by spherical primary wave front, 1047
dimensions in terms of wavelength, 1101
frequency dependency, **143**
phase constant, 789
phase factor, 789
and radiation space, boundary conditions, 790
secondary electromagnetic field due to primary field, **314**
size and effect on propagation, **318**
Wave obstruction, and diffraction radiation, 1018–1184

Wave obstruction, and electromagnetic field energy tubes, applied, 791
and ray wave propagation, 789–1017
wet soil, 939–943
Wave package, **389**
Wave path, curved, **6,** 969, 981–983, 986–988, 991, 998, 1003
linear, (rectilinear), 977
modified, 997
rectilinear, **6,** 977
Wave penetration (*see* Penetration, wave)
Wave polarization (*see* Polarization)
Wave potentials (*see* Scalar potential; Vector potential)
Wave propagation, through apertures, 1034
frequency-height product, significance, 932
ideal wave medium, **391**
metallic wave medium, **45**
multipath, **10,** 887–895
nonrectilinear, 969
over obstructions, numerical, 913–949
from parabolic reflector, 1028
space screw polarization, **786**
over wet soil, 936
type, ray theory, diffraction, **318–319**
(*See also* Propagation)
Wave reception, over actual earth crust, ray concept relations, 867–876
at transmitter location, 887
Wave reflection, from elevated layers, horizontal stratified atmosphere, reflection coefficient formula, 997
formula and graphical solution, **115**
horizontal stratified atmospheric layer, 997
in inhomogeneous wave medium, 997
from large surface of earth crust surface, Huygens wavelets, 1018
from metal planes and general medium, formulas, 895–899
at plane of medium separation, numerical, 897–899
and refraction, comparative derivations, vertical and horizontal polarizations, 798–824
Wave spread, into geometrical shadow region, diffraction, 1039
plane and curved earth, 885–887
solution, Poynting vector used, 886
spherical and flat earth, compared with illustrations, 887
Wave train, damped, within copper medium, **477**
Wave trapping, 958–964, 996, 1236–1240
in low wave duct, 958–964, 1236–1240
in troposphere, 996, 1236–1240
Wave tube (traveling-wave tube), **417**
Wavelength, different mediums, **49–52, 54**
diffraction, 1018
earth crust neighborhood, 907
free wavelength effect in wave duct, 996
and frequency, 789
Wavelength, general dissipative wave medium, **54**
along guide, **381–382**
on line, **10**
in mediums, different Q value, **54**
refraction, 1018
Wavelet, concept, **17,** 1019–1022
applied to parabolic electromagnetic projector, 1028
effects, integration, ignoring phase factor, 1157
elementary, center of, 1088
Huygens sources, rectangular wave-front radiator, 1092
interference, 1172
mosaic of secondary wave sources, diffraction, 1092
primary wave-front expansion, 1020
principle (Huygens), 1019
Wavelike disturbance, as forced function and natural wave-medium function, **367**
due to sharp pulses, **366**
Wedge diffraction, zonal rings, 1040
Wedge-shaped mountains, diffraction, unobstructed and in obstructed (shadow) region, numerical, 1052
and short waves, 1049
Wedge-shaped wave obstruction, Cornu spiral solution applied, 1055
Wet earth crust, vertical polarization, 955
Wet soil, reflection coefficient, tabulated computations, 833
table for 100 Mc/sec and horizontal polarization, 954
wave obstruction, 939–943
Weyl surface waves, 958
Whirl, amperian, **154**
rotation, **14**
Width, diffraction beam, plane wave front with wavelets, 1033
Wind effect and wave-duct propagation, 996
Window of parabolic reflector taken as electric current sheet, 1029
Wire reflector and solid metal reflector compared, **787**
Wire and slot radiator compared, 1036, 1279
Wobble (of frequency of carrier), method, 929

X

$x = \cos\theta$ substitution in integral solutions, **341**

Z

$Z_n(x)$ relations, **343**
Z_n and Γ_n refer to double lines with radiation effects, **97**
Zenneck, J., and Sommerfeld, A., surface wave, 958

Zero and maximum field effects, 897
Zero-order approximation in King theory, **717**
  Bessel function, **301, 704**
  Hankel function, **339**
Zigzag uniform plane wave and guided $TE_{m,0}$ wave, 967
Zigzag wave, 959, 964
Zonal areas, difference between consecutive, 1025
Zonal areas, magnitudes, 1024
  for plane wave front, numerical example, 1027
Zonal Fresnel areas, dimensions for plane wave front, 1027
Zonal parameters of Fresnel zones, 1024
Zonal rings, sharp wave obstruction, 1040
  sharp wedge diffraction, 1040
Zonal solid harmonic of qth degree, **340**
Zones, Fresnel (*see* Fresnel zones)

University of Southern California

DISCARDED

DISCARDED

DISCARDED

1 Brnsd Powell's Used $30.00
Short Wave Radiation Phenomena
Hund, August 2221124154534
COMP-ELEC RADIO 906 12/9/2019